GEOCHEMICAL INDICATORS OF PALAEOPRODUCTIVITY AND PALAEOCLIMATE IN EASTERN EQUATORIAL PACIFIC SEDIMENTS

By

ANDREW JOHN PATIENCE

A Thesis submitted for the degree of

DOCTOR OF PHILOSOPHY

At the University of Edinburgh

March, 1992.

"Twixt Land & Sea" (Joseph Conrad)

Between

Geology & *Biology*

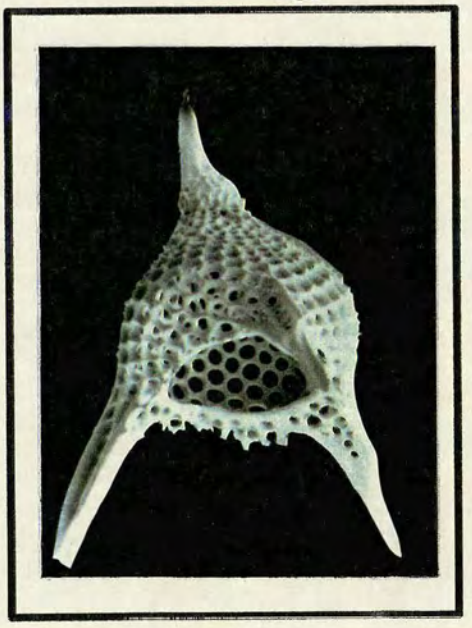

Dedication

To my parents and country.

ACKNOWLEDGEMENTS

I would like to thank my parents without whose love and support this thesis would not have been started let alone finished.

Special thanks must also go to Brian Price and Dick Kroon for their continual enthusiasm and support. Both were always available; ready to listen or make suggestions (academic and otherwise). To Dick especially for knowing when to "take-a-beer".

To Mike Saunders for his invaluable, though occasionally frustrating, help in analytical techniques, and for his knowledge of mountains. To Frances Lindsay for her help in the laboratory and for putting me up. To Geoff Angel for his assistance in XRD, and Godfrey Fiton and Doddie James for their help in XRF analysis.

To Graham Shimmield and Sandy Tudhope for their encouragement and advice, and especially for their reviewing of early drafts of a paper.

To Jim Smith for his expertise in constructing awkward pieces of equipment, and for his contribution towards and aboard the R.R.S. Charles Darwin cruise (38).

To Cliff Ford and Shane Voss for their help in computing problems. To the Departmental secretaries; Helena, Heather, Denise and Nicky for their charming and diverse help. To Mrs Diane Baty and Mrs Yvonne Cooper for their expert instruction in all things photographic.

To a host of people for help in a variety of things: Andy Poole, Gavin McNeill, Ned Pegler, Christine Kay, Tim Brand, George Ritchie and David Whitmarsh. To Steve Mowbray for pointing out the return button and accompanying me round south America.

The skipper and crew of the R.R.S. Charles Darwin on her cruise 38 (Valparaiso-Balboa, April-May, 1989). The Catholic University of Valparaiso for chemicals and hospitality. The funding of N.E.R.C. and the use of their laboratories is gratefully acknowledged.

To Peck and Steedman for their friendship and subtle, though effective, encouragement; and for replenishing important links.

Finally, to Deb's for initially giving me a reason for staying and, very quickly, for enriching all aspects of my life.

ABSTRACT

The chemistry of six sediment cores (1-11m in length), recovered in the eastern equatorial Pacific, has been investigated in an attempt to determine spatial and temporal variations in the biogenic and terrigenous components, and to relate these to local and global changes in palaeoproductivity and palaeoclimate.

Cores P5 and P12 were recovered in the Panama basin during the R.R.S. Shackleton cruise (May, 1976), whereas CD38 cores were recovered during the R.R.S. Charles Darwin cruise (Valparaiso-Balboa, May, 1989). The cores represent a range of sediment composition from a suite of oceanographic environments (eg water depth). The eastern equatorial Pacific is an area of very high biological productivity, lying at the intersection of the equatorial divergence and the continental margin upwelling systems, making it an ideal setting in which to conduct such a study.

Cores were sampled at 2cm (P5 and P12) and 10cm (CD38 cores) intervals and subjected to geochemical (Si, Al, Fe, Mg, Na, K, Mn, P, Ca, Ti, Zn, V, Ni, Cu, Y, Nd, Nb, Ce, Zr, Cr, Sc, Sr, Rb, Ba, I, Br, Mo, U, Pb, Th and La) analysis using XRF; wet chemical techniques (biogenic silica, organic carbon and Cl); preliminary mineralogical analysis using XRD, and stable isotope ($\delta^{18}O$ and $\delta^{13}C$) analysis using mass spectrometry. The $\delta^{18}O$ signals in the carbonate tests of *Neogloboquadrina dutertei* and *Globigerinoides ruber* from cores CD3822, CD3826 and CD3827 provided oxygen isotope chronostratigraphies which were refined by geochemical correlation with well dated nearby cores (AII54-25PC and P6). The sediments are of Pleistocene age and the base of the cores in this study range from 24ka in P5 to 472ka in CD3826.

The sediments divide into two groups: an eastern, hemipelagic set (CD3826, CD3827 and AII54-25PC) which is carbonate-poor but enriched in terrigenous material; and a western, pelagic set (CD3814, CD3822 and P5) which is carbonate-rich but depleted in terrigenous material.

Terrigenous input increases during low sea level stand glacial times (especially stage II), and with decreasing distance from land; consistent with increased input of source material from the shelf, and/or increased wind intensity. The Holocene is a time of rapidly decreasing terrigenous input. Hydrothermal deposits, which have unusually high Si_{terrig}/Al, Fe/Al and K/Al ratios, are present at 13.93ka in core P5 and at the base of core CD3814. Volcanic ash layers "D" (56ka), "L" (234ka) and "K" (328ka), identified by their low Ti/Al and Cr/Al ratios, are present in core CD3826, and were used in age model development. Very high Ti contents in core P5 (especially during stage II) result from increased continental aridity and wind intensity, which promotes increased input of basaltic material from

the Galapagos archipelago. Ti in other cores is derived from central America and the Galapagos archipelago. Cores CD3826 and CD3827, in the eastern part of the Panama basin, contain greater contents of quartz, feldspar and chlorite compared to the other cores; whereas cores P5 and CD3822, recovered in the western part of the basin, have higher contents of opaline silica and barite. Montmorillonite is the most common clay mineral present in these sediments.

The content and mass accumulation rate (MAR) of the biogenic proxies $CaCO_3$ and C-org increase during glacial times suggesting high biological productivity during glacials, sustained by strong upwelling. Biogenic SiO_2 and Ba, however, do not vary with a simple glacials/interglacial cyclicity. Such biogenic tracers suggest that glacial high productivity pulses undergo an evolutionary process, throughout which carbonate communities dominate, but biogenic silica based organisms are relatively more abundant during the initial stages, than towards the end of the pulse when carbonate production reaches a maximum. The peak in the siliceous plankton communities may be linked to water mass redistribution and water chemistry variations which may, ultimately, be the result of solar insolation variations on Milankovitch frequencies. Changes in the ExSr/ExCa ratio illustrate variations in the carbonate plankton community, during the productivity pulse, such as the relative abundances of foraminifera to coccoliths. These changes may, possibly, be related to the intensity of bottom currents, which are more active during interglacial events.

From comparisons between modern productivity estimates and temporal variations in the $CaCO_3$ MARs, it appears that productivity, and not simply preservation, may have an important influence on the $CaCO_3$ signal in this area, at least in supra-lysoclinal sediments (ie CD3822 and especially P5). Ratios of $CaCO_3$ MAR/C-org MAR from core CD3826 indicate a reduction in the potential for net CO_2 transfer to the atmosphere from surface waters, over the last 472ka in this region. Biogenic components indicate that core CD3822 has been subject to very different oceanographic conditions to the eastern cores. Biogenic skeletal (inorganic) P, calculated by two independent methods, shows increases during interglacial episodes in contrast to other biogenic tracers.

I and Br are associated with C-org, and are present in concentrations broadly consistent with oxic conditions. Br is more closely associated with C-org than I. I/C-org and Br/C-org ratios display rapid subsurface decreases resulting from diagenetic alteration which renders them unreliable as proxies of palaeoproductivity. Surface I/C-org ratios are slightly low for normal marine oxic sediments, and they decrease landward, perhaps indicating a terrigenous source of diagenetically inert shelf carbon.

The effects of dilution from shelf material, in determining the final sediment signature, are significant and underestimated.

Redox sensitive Mn and Mo are enriched in surface Mn-Fe oxyhydroxide phases, whereas increases in Mo at depth result mainly from complexation with organic matter. Increases in solid phase Mn at depth (during glacials and interglacials), in core CD3826, mainly result from Mn carbonate precipitation at loci of unusual mineralogies. Mo and U are associated with C-org, especially in core CD3827. This contradicts the hypothesis that increases in C-org dominantly reflect productivity increases. Generally, ExZn and ExNi contents are > ExV and ExCu. None of the metals show any statistical correlation with C-org, although ExZn in core CD3822 broadly parallels the C-org curve. Relatively thick oxide tops encourage preservation of metals in the sediment, and promote the influence of the overlying productivity signal, via scavenging of metals from the water column onto particulates. Cores with shallow redoxclines, however, tend to foster rapid metal recycling with Fe-Mn remobilisation processes dominating the excess metal contents.

LIST OF FIGURES, TABLES AND PLATES

LIST OF FIGURES

Page No.

CHAPTER 1

CHAPTER 2

CHAPTER 3

CHAPTER 5

CHAPTER 6

CHAPTER 7

CHAPTER 8

CHAPTER 9

LIST OF TABLES

CHAPTER 1

CHAPTER 2

CHAPTER 3

CHAPTER 4

CHAPTER 5

CHAPTER 6

LIST OF PLATES

CHAPTER 4

TABLE OF CONTENTS

TEXT **PAGE NO.**

TABLE OF CONTENTS (Contd.)

TABLE OF CONTENTS (Contd.)

TABLE OF CONTENTS (Contd.)

CHAPTER 1

INTRODUCTION

The multi-disciplinary subject of palaeoceanography has long been of interest (Murray and Renard, 1891; Arrhenius, 1952), but detailed study of ocean sediments has recently taken on an urgency as concern for man's effect on the natural environment mushrooms.

Ocean sediments are potentially one of the best tools for studying past climatic variations because they can contain continuous records of low frequency (in the order of 10^3 years) environmental cyclicity and events. This is because the sediment record is a manifestation of the close coupling between the atmosphere, hydrosphere and lithosphere (oceanic and continental). Climatic changes are the result of variations in the earth's orbit around the sun and the tilt of it's axis. These Milankovitch frequencies (Milankovitch, 1941; Berger, 1978) influence, for example, atmospheric humidity, ice volume, sea-level, continental aridity and, perhaps, biological productivity. All these parameters will have some effect on the input to, and chemical signature of, deep ocean sediments. Consequently, ocean sediments should, to some degree, record climatic changes. With such knowledge, one might hope to understand the systems which govern our climate and, perhaps, contribute to the development of the many mathematical, predictive and often widely differing global climatic models being produced today. Such models can have far reaching effects on government policy and spending.

Although some studies (Pedersen, 1979; Shimmield, 1984; Murray, 1987; Lyle et al., 1988) have incorporated many aspects of sediment geochemistry and oceanography in the late Cenozoic records, most previous work has centred on some specific aspect of the complex records. Perhaps realising the pitfalls to such an approach, projects such as the DSDP, ODP, MANOP, JGOFS and CLIMAP have collected a massive database of information on how climatic variation imprints on oceanic proxy records (McIntyre et al., 1976). However, these massive projects have their roots not only in scientific endeavour but in economic exploitation of marine resources. Also although such programmes have produced a wealth of information from which future researchers can draw, the sheer scale of the results has not lent itself towards in-depth consideration of the data.

This study is a further attempt to contribute to our knowledge of ocean sediments and their role in regulating and reacting to climatic variations. Central to the rationale behind this thesis is the quantification of palaeoproductivity, which is believed to result in variations in sediment composition.

Marine sediments essentially consist of terrigenous, biogenic, hydrothermal and authigenic/diagenetic components. Different oceanographic settings, during various palaeoclimatic periods, will result in differing proportions of these main components. For example; increased upwelling of cool, nutrient rich subsurface waters (which is especially prominent along the western continental margins and the equatorial belts), raises the biogenic productivity of the surface waters which, in turn, is thought to leave an imprint on the sediment below. Upwelling failure as a result of the El Ñino southern oscillation event, result in catastrophic biological loses in both ocean and continent.

The cores used in this study, with the exception of CD3813 and CD3814, are located in the Panama basin (figure 1.1). This topographically enclosed miniature oceanic basin provides an excellent opportunity to study sediments derived from different oceanic settings (eg pelagic to hemi-pelagic) in a spatially constrained area. The whole area has exceptionally high euphotic zone primary productivity as a result of strong upwelling. It is for these reasons that the region has received considerable attention over recent years (Pedersen, 1979; Lyle et al., 1988; Murray 1987; Rea et al, 1991, Pedersen et al., 1992). Cores CD3813 and CD3814 at around 10° S are at the southern end of the S-N equatorial transect and which, in some respects, forms part of a quite different oceanographic regime.

Terrigenous/detrital material forms the framework to most marine sediments. Spatial and temporal variations in the input of terrigenous material may alter the degree of dilution of other constituents, whereas compositional changes may change the grain size and diagenetic mobility of elements in the sediment. Such material is derived from erosion of the continental landmass surrounding the oceans and, as a consequence, generally decreases with increased distance from the continental margins. Deposition of terrigenous material is dominantly controlled by turbidity currents, bottom currents, wind intensity, ice volume and sea-level. In most oceanic regions it has been shown (Ruddiman and McIntyre, 1977) that both coarse and fine terrigenous material is deposited mainly during glacial periods which reflects the greater extent and aridity of the continental landmass, and the ice-rafting of glacially eroded debris. Folger (1970) has shown that in north Atlantic sediments, a major constituent of the fine detritus in low latitudes during glacial periods is wind blown aeolian material.

The hydrothermal nature of some sediments from the area is well documented (Lonsdale, 1977; Lupton, 1977; Weiss et al., 1977; Lyle and Dymond, 1978; Corliss et al., 1979, 1986). Little emphasis is placed on this fraction of the sediment except when showing its effects on biogenic components. The considerable input of volcaniclastic debris (ash bands) from central and north-west south America, and the Galapagos archipelago, has allowed the development of a well defined tephrachronology in the region (Ninkovitch and Shackleton, 1975; Ledbetter, 1985). Geochemical identification of these chronostratigraphic markers are used in this thesis to aid correlation between cores, and help develop the age models by increasing the dated control points.

The biogenic component is dominantly the remains of calcareous and siliceous micro-organisms that, during life, inhabited the upper fraction of the water column, only to sink to the ocean floor and become incorporated in the sediment column after death. Thus, biogenic sediments have the potential to record changes, for example, in water temperature, nutrient availability and ocean circulation.

Biogenic material from this region has been extensively studied (Arrhenius, 1952; Moore et al., 1973; Pisias, 1976; Adelseck and Anderson, 1978; Murray, 1987; Lyle et al., 1988; Rea et al., 1991; Pedersen et al., 1992). The area encompasses the Ekman transport driven western continental margin and equatorial divergence, upwelling systems. As a result, surface water productivity is extremely high relative to other oceanic regions. Although the pattern of productivity in the surface waters is complex, with areas of relatively high and relatively low values, it is important to note that all the waters of the area have high productivity compared to, for example, central ocean gyres. Indeed, although ocean margin and equatorial divergence upwelling systems constitute only a small proportion of the surface area of the world's oceans, the sediments which underlie these regions form a major part of the total marine carbon sink due to the intensity of the productivity.

Considerable debate has concentrated on to what degree sediment composition reflects productivity or preservation. Early work centred on the association of the Pleistocene climatic variations, from glacial to interglacial, and the cyclicity in the proxy records of $CaCO_3$ in deep-sea sediments. Arrhenius (1952) endorsed the concept of calcite concentration dominantly reflecting primary productivity.

Many authors (Parkin and Shackleton, 1973; Adelseck and Anderson, 1978; Luz and Shackleton, 1975) reinforce this concept from several different perspectives. However, Berger (1968, 1970, 1973), Broecker (1971) and Thompson and Saito (1974) all claim that dissolution of calcite is the controlling factor in $CaCO_3$ concentration in sediments. Today the importance of both productivity and preservation is accepted, with water depth determining on which factor most emphasis is placed. Comparison of records from cores recovered from different water depths may help clarify the problem.

A similar quantity of argument has centred on organic carbon (C-org) composition in sediments. Pedersen (1979, 1983) shows high levels of C-org during the last glacial maximum (18 ka). The presence of very high concentrations of organic carbon underlying upwelling zones (Muller and Suess, 1979; Krisseck et al., 1980; Calvert and Price, 1983; Lyle et al., 1988) would seem to be evidence of a close association between primary productivity and organic carbon concentration in the sediment. However, hindcasting palaeoproductivity from organic carbon concentrations in the sediment has many problems. Muller and Suess (1979) attempted to quantify palaeoproductivity empirically from the organic carbon concentration. However, it has been suggested that bottom water oxygen concentrations are the limiting factor in C-org content in sediments: high bottom water oxygen resulting in strong degradation of organic matter; low bottom water oxygen favouring preservation of organics (Emerson, 1985; Murray, 1987).

Biogenic silica is intuitively a good indicator of primary productivity because of the high concentration of Diatoms and Radiolaria (both of which have siliceous tests) found in the surface waters of high productivity areas. Pisias, (1976); Heath et al., (1976) and Lyle et al., (1988) use biogenic opal as an indicator of palaeoproductivity. However, both opal and barium, which is believed to be closely associated with biogenic silica (Revelle, 1955; Goldberg and Arrhenius, 1958; Church, 1970, 1979; DeHairs et al., 1980; Bischop, 1988), are themselves prone to dissolution (Calvert and Price, 1983) although perhaps not to such a degree as calcite.

Despite the large amount of work completed, no definitive tracer of palaeoproductivity or climatic variation has been identified. This study evaluates the potential of known biogenic components (SiO_2, Ba, $CaCO_3$, C-org, Sr and P) in recognising such changes. Particular attention is paid to illustrating how the

concentration of each element is dependent not only on its input rate but on the concentration of other sediment components which cause dilution.

The behaviour of some trace metals under different sediment redox conditions were studied. Metals are known to be associated with particulate fluxes to the sediment and in diagenetic recycling (Bonatti et al., 1971; Graybeal and Heath, 1984; Lyle et al., 1984; Fischer et al., 1986; Finney et al., 1988). An evaluation of, the relative importance of the scavenging of metals onto particulate matter by adsorption and, the diagenetic recycling within the sediment, in regulating metal concentrations is undertaken. The importance of Fe-Mn oxyhydroxides in such diagenetic cycling of elements has been extensively studied (Lynn and Bonatti, 1965). This study includes a further examination of how some trace metals behave under changing diagenetic conditions and redox potentials.

The intimate, but differing, association of the Halogens Iodine and Bromine with organic carbon is studied in an attempt to illustrate the nature of the organic matter in the sediments.

Most recent palaeoceanographic investigations have incorporated oxygen isotope age models to date the sediments. Isotopic fractionation in the oceans as a result of temperature and ice volume changes are recorded in the calcareous tests of marine organisms. Therefore the isotopic ratio in the tests of dead calcareous organisms should record past variation in climate. Using this rationale, Emiliani (1955) developed a stratigraphy of the Pleistocene by subdividing the foraminiferal oxygen isotope record into stages and establishing a standard nomenclature; negative isotopic excursions of the interglacial stages were given odd numbers, whereas positive isotopic excursions of the glacial periods were designated by even numbers. However, only later was a direct link forged between the climatic effects on isotopic variations and the orbital changes central to the Milankovitch theory (Emiliani and Shackleton, 1974). Such work has resulted in the SPECMAP age model (Imbrie et al., 1984) and it is against this reference stack, and the age model of core AII54-25PC (see below), that the cores in this thesis are correlated, in development of the age models. For a useful review of the application of oxygen isotope dating techniques to marine sediments and the problems associated with such methods, see Patience and Kroon (1991).

Analytical work presented in this thesis was undertaken on two suites of cores. The gravity cores P5 and P12 (table 1.1) were collected during a cruise of the R.R.S. Shackleton (April 30 - May 25, 1976); and the piston cores CD3813, CD3814, CD3820, CD3822, CD3826 and CD3827 (table 1.1) were recovered during the R.R.S. Charles Darwin cruise 38 (April 14 - May 11, 1989). These cores were chosen to reflect varying oceanographic parameters, particularly water depth (table 1.1), terrigenous and biogenic input and the nature of the productivity regime. The latter suite of cores formed part of a transect (south-north) designed to show sediment compositional variation over the equatorial divergence upwelling zone. Only cores P5, CD3814, CD3822, CD3826 and CD3827 were chosen for more detailed analysis. Geochemical and isotopic data from core AII54-25PC were determined by Dr. Thomas Pedersen and co-workers (University of British Colombia).

Table 1.1 CORE LOCATIONS

CRUISE	CORE	LATITUDE	LONGITUDE	WATER DEPTH(M)
SHP	5	00° 54.57' S	87° 51.08' W	1540
SHP	12	07° 08.66' N	78° 43.92' W	3491
CD38	13	09° 34.76' S	91° 23.74' W	4175
CD38	14+	10° 05.97' S	94° 28.59' W	3550
CD38	20	00° 29.93' N	91° 01.73' W	2412
CD38	22+	03° 31.95' N	88° 47.14' W	2340
CD38	26+	04° 57.63' N	84° 44.37' W	3075
CD38	27+	05° 48.28' N	82° 18.11' W	2725
SHP	*6*	*00° 52.34' N*	*86° 07.73' W*	*2712*
MANOP	*H*	*06° 33.00' N*	*92° 49.00' W*	*3600*
AII54	*25PC*	*04° 16.20' N*	*85° 05.40' W*	*3225*

Station locations fixed by satellite navigation. Cores P5 and P12 recovered by gravity coring; CD38 cores collected by piston core. + Pilot core also sampled. Italised text refers to cores used for comparison (see text).

The location of all the cores are given in figure 1.1. Analytical techniques of core collection, core description and sample preparation are presented in appendix A; results are given in appendix C.

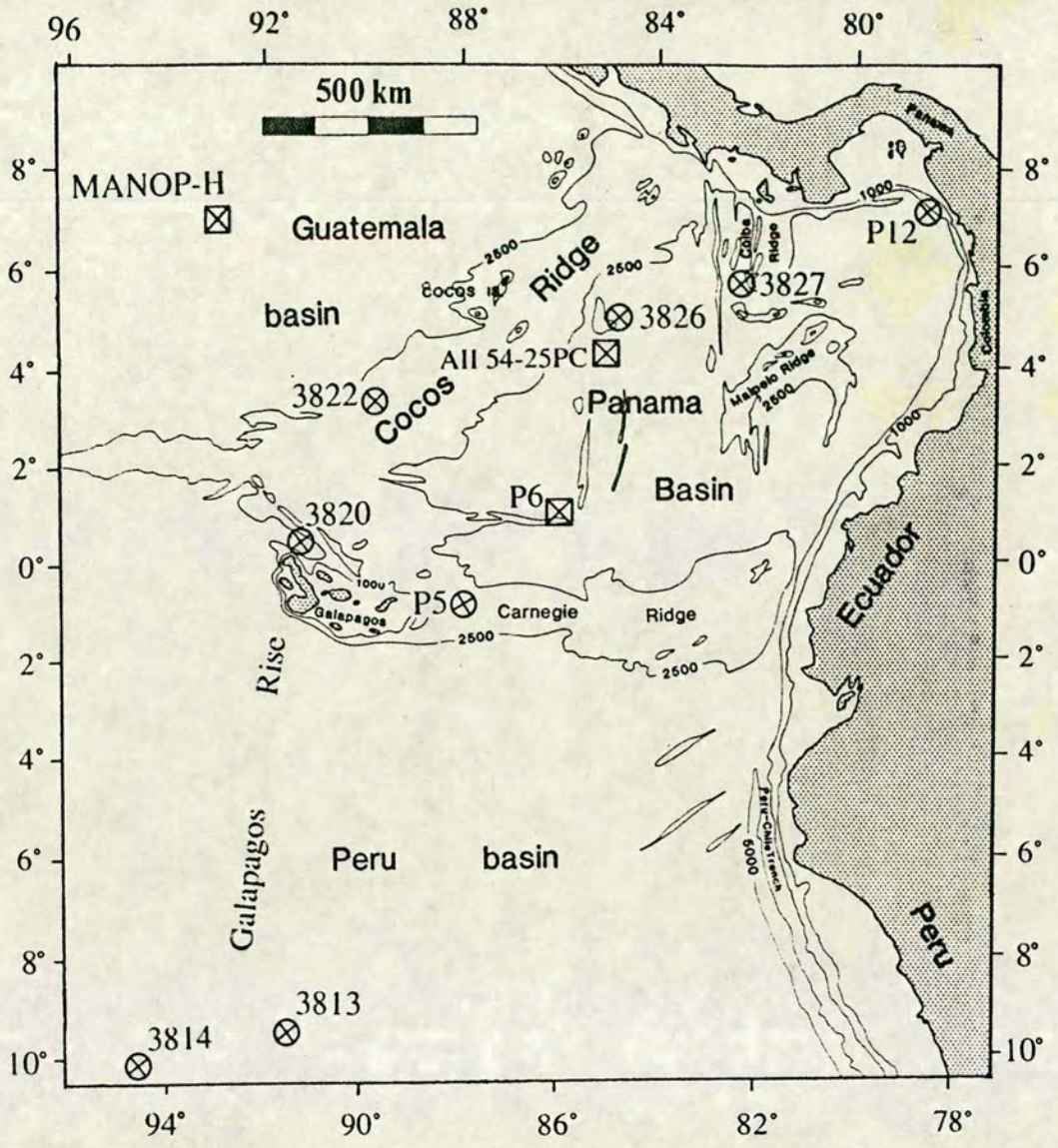

Figure 1.1 Location map of the cores studied in this thesis (circles with cross) and cores used for comparison (squares with cross).

CHAPTER 2

GENERAL GEOLOGICAL, OCEANOGRAPHIC AND ENVIRONMENTAL SETTING

2.1 Geology

The major tectonic features of the study area which lies adjacent to the destructive western continental margin of central and north-western south-America, are summarised in figure 2.1 The Nazca and Cocos oceanic plates are actively subducting beneath the central and south American continental lithosphere. This has resulted in the development of the volcanic (andesitic-rhyolitic) Andean central-south American cordillera which provides a suite of possible source materials to the area.

The Cocos and Nazca plates are presently moving NNE (069°) at 71mm/yr and SE (102°) at 71mm/yr respectively (Hey et al., 1977). This disparity in motion, together with the divergence of the Galapagos spreading centre, has contributed to the Galapagos and Grijalva fracture zones, which are offset by a series of transform faults (eg Ecuador fracture zone, Figure 2.1).

The Galapagos archipelago is at the intersection of the Cocos, Carnegie and Galapagos ridges. This triple point (hot spot) is what has driven most of the tectonism in the area and has produced the volcanic Galapagos archipelago (McBirney, 1969).

According to Van Andel et al., (1971) the Cocos and Carnegie oceanic ridges (spreading centres) are essentially aseismic and Pedersen (1979) suggests that the Coiba and Malpelo ridges are similarly aseismic (see fig 3, Heath and Van Andel, 1973). Seismicity in the Panama basin is confined to very low magnitude earthquakes around the transform faults which divide the Galapagos spreading centre (Macdonald and Mudie 1974).

The physiography of the region is essentially defined by the underlying geology and will be discussed in this section. Three ocean basins lie within the area: the Panama basin, the Peru basin and the Guatemala basin (figure 2.2). The Panama basin is bounded by the continental margins of central and north-western south America to the west and by the Cocos and Carnegie ridges to the north-west and south respectively. The basin is divided into east and west sub-basins by the Coiba fracture zone (figure 2.1): the western sub-basin being rugged and low-lying, whereas the eastern sub-basin is highly fractured with several major troughs, high blocks and irregular intervening ocean floor (Van Andel et al., 1971). The Peru basin is encapsulated by the north

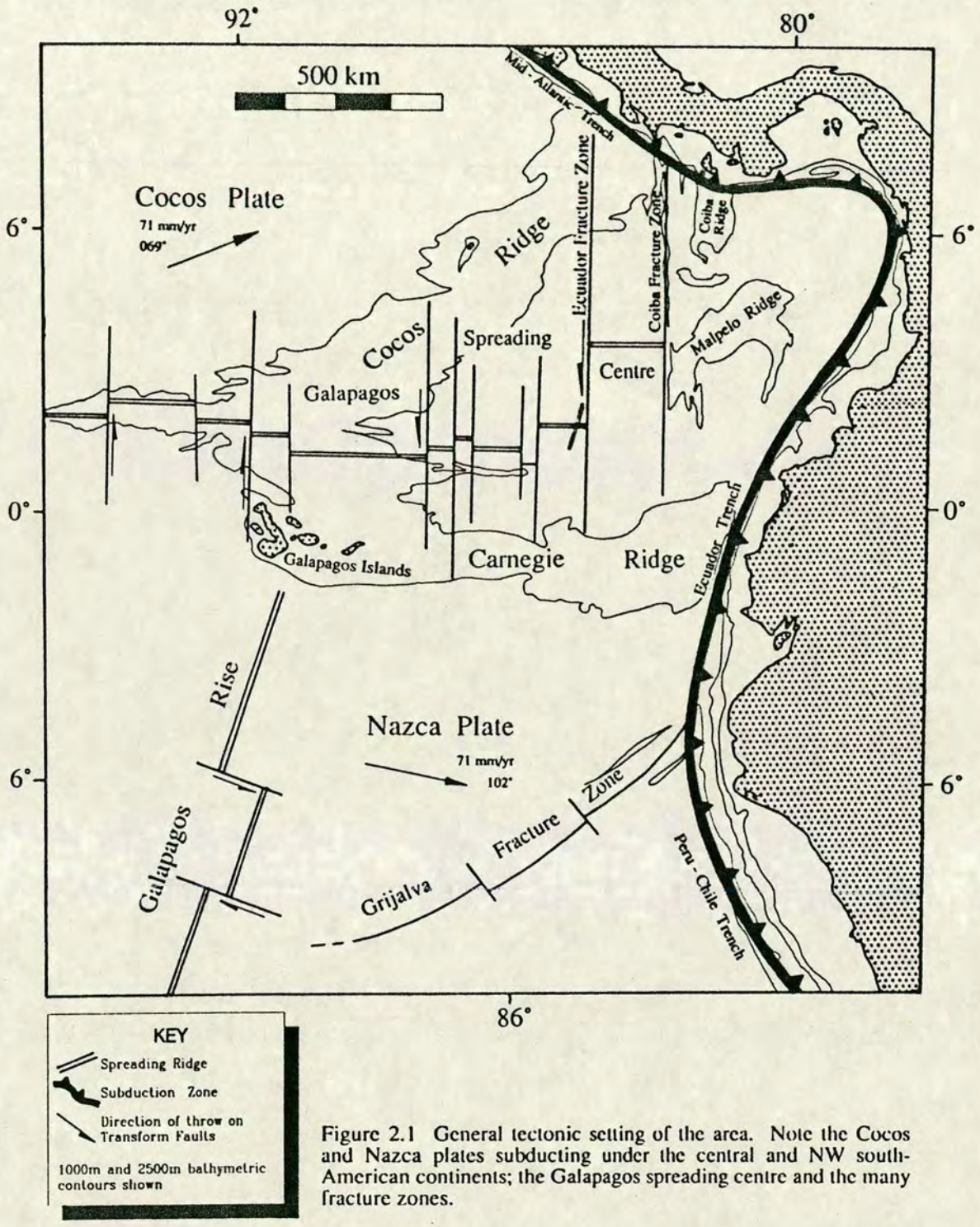

Figure 2.1 General tectonic setting of the area. Note the Cocos and Nazca plates subducting under the central and NW south-American continents; the Galapagos spreading centre and the many fracture zones.

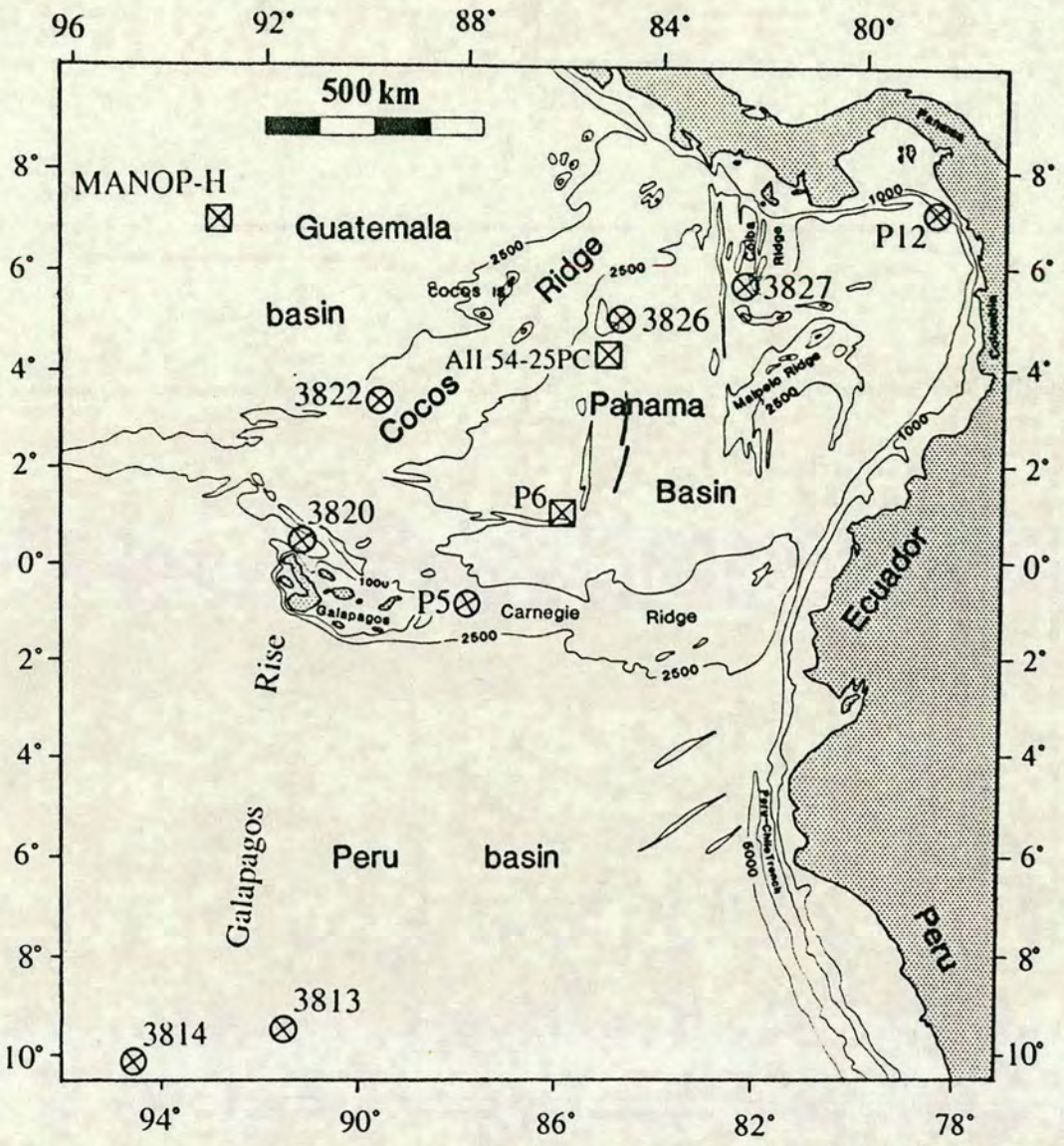

Figure 2.2 Location map of the cores studied in this thesis (circles with cross) and cores used for comparison (squares with cross).

-west south-American continental margin and by the Nazca and east Pacific ridges to the south and west respectively. The Guatemala basin lies to the north west of the Cocos ridge and contains the MANOP-H station which will be discussed in later chapters. The bathymetry of the region (figure 2.2) is mainly controlled by the presence and interaction of the lithospheric plates. The physiography of each of the major ridges is briefly summarised in table 2.1.

2.2 Oceanography

2.2.1 Introduction

The eastern equatorial Pacific lies between two oceanic gyres in the north and south Pacific and incorporates some of the most highly productive waters in the world (figure 2.3). Both the equatorial divergent upwelling and western continental margin upwelling zones are found in the region. These are driven by wind and coriolis forces. As a consequence, many of the underlying sediments generally have very high concentrations of biogenic material. The bathymetric and oceanographic situation is such that considerable differences in, for example; water depth, nutrient availability and terrigenous input occur over relatively small distances and which can be studied from proxy records.

The thermocline which normally lies between 70-100 m (Broecker and Peng, 1982) is found between 25-50 m which is within the euphotic zone. It s depth varies locally and deepens during El Ñino events. It is also generally very well developed which hinders mixing between cool nutrient rich subsurface water with warmer oxygen and nutrient depleted surface water. However the upwelling is generally strong enough to overcome this physical barrier and cool, nutrient-rich, oxygen-replete water does reach the surface and phytoplankton (the lowest trophic level in the food chain) are thus able to extract nutrients directly from the enriched surface waters and flourish. The surface mixed layer in the Panama basin occupies only the top several tens of metres although this can increase locally.

The Panama basin is not stagnant (anoxic) at present and indeed dissolved oxygen concentration increases with depth (see Laird, 1971, figures 5 and 6), therefore its bottom waters must be at least periodically if not continually replenished with oxygen replete water. An idealised diagram of dissolved oxygen and temperature for the

TABLE 2.1 SUMMARY OF THE SUBMARINE RIDGES IN THE AREA

RIDGE	LENGTH(KM)	ORIENTATION	DEPTH RANGE (M)	FEATURES
Cocos	1200	NE-SW	0-2000[A]	four saddles around 2000m[BC], steep sided, level top[D]
Carnegie	1000	E-W	0-2330[C]	one broad saddle at 2330m[C], steep sided, level top[D]
Malpelo	400	NE-SW	0-2000	together with Coiba ridge divides Panama basin into E and W sub-basins
Coiba	200	N-S	0-2000	3600m[E] Coiba gap at S end provides bottom water link between E and W sub-basins[F].
Galapagos	1500	NNE-SSW	0-2000	

Based on data from Chase et al., (1970)[A]; Dowding, (1977)[B]; Lonsdale (1977b)[C]; Van Andel et al. (1971)[D]; Van Andel, (1973)[E] and Pedersen, (1979)[F].

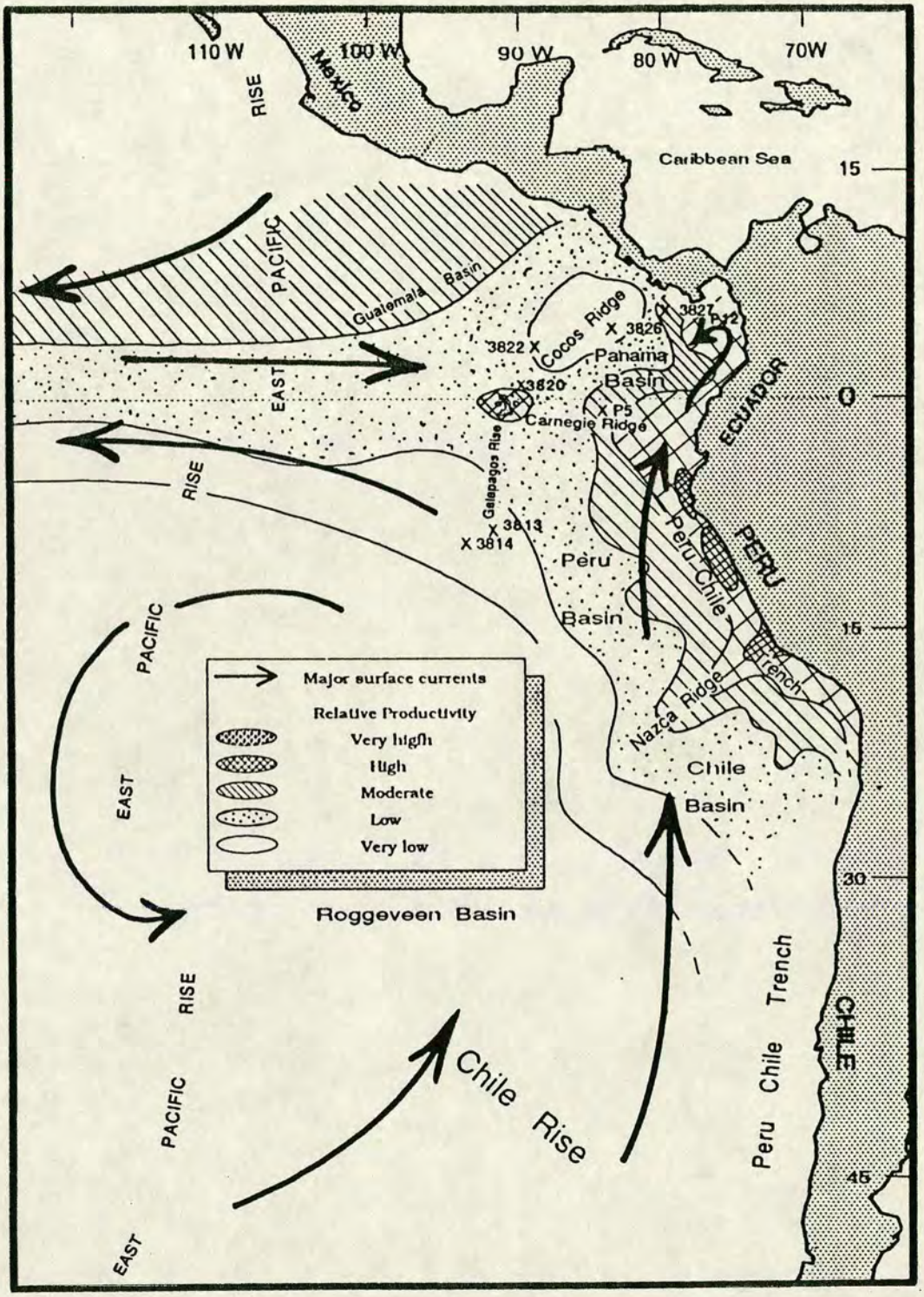

Figure 2.3 Oceanographic overview of the study area showing the major surface circulation and the relative primary productivity in the euphotic zone. Summarised from Moore et al., (1973) and Wefer et al., (1983).

eastern equatorial Pacific is given in figure 2.4 which illustrates the shallow mixed layer and strong thermocline (region of greatest temperature gradient).

2.2.2 Hydrography

Surface circulation

Surface circulation in the World's oceans is dominantly the result of wind velocity; with coriolis forces, landmass distortion and water salinity variations being the primary interfering influences. Surface circulation in the eastern equatorial Pacific is complicated but well documented: Wyrtki (1965, 1966, 1967, 1974); Forsbergh (1969); Stevenson (1970); Dinkelman (1974) and Wyrtki and Kilonsky (1984). Figure 2.5 which is adapted from Wyrtki (1965) summarises the surface circulation of the region and its seasonal migration as a result of variations in trade wind strength and orientation. The doldrums belt and the seasonal migration zone of the trade winds (north-east and south-east) exerts clear influences on the surface circulation of the area (Dinkelman, 1974). The Intertropical Convergence (ITC) where trade winds converge with the buffering zone of the doldrums, migrates seasonally: on or around the equator during the southern maximum of the southern summer (January-March) and 10°-12°N during the southern winter (July-September), (figure 2.5b). The ITC dominates the development of the eastward flowing North Equatorial Counter Current (Wyrtki, 1965). The Counter current is well developed during the southern winter mostly flowing counter clockwise around the upwelling areas of the Costa Rica dome (Molina-Cruz, 1977) (figure 2.5a) and entering the North Equatorial Current, but its penetration into the basin is progressively reduced as the ITC migrates southward and it disappears from the area during the southern summer (Pedersen, 1979).

One of the strongest influences on the area is the cool nutrient rich waters of the Peru current (Figure 2.5) which travels northward parallel to the south-American continent causing considerable Ekman transport driven upwelling in the coastal waters off Peru and northern Chile. When it reaches the equatorial belt it bifurcates: the main stream swinging round to the west eventually contributing to the South Equatorial Current, whilst a weaker flow continues north entering the Panama basin by the Ecuador trench. This weaker stream incorporates some North Equatorial Counter Current water and the great majority of the continental runoff (see section 2.3 and figure 2.6) to form the Colombia current which follows the coastline as far as the Gulf of Panama where it joins the counter-clockwise circulation of the Panama bight (figure

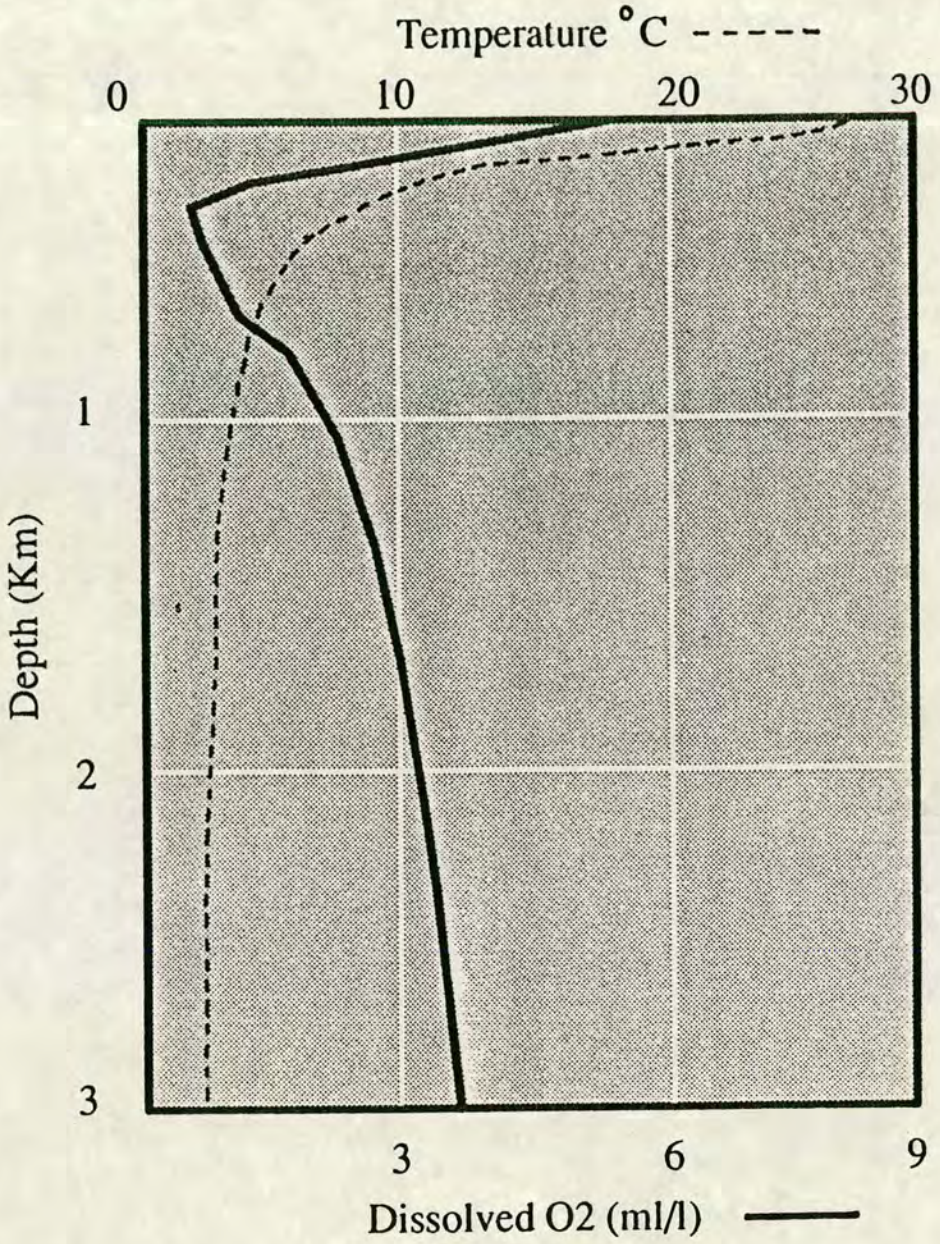

Figure 2.4 Highly diagrammatic illustration of the temperature (°C) and dissolved oxygen (ml/l) content in the equatorial Pacific.

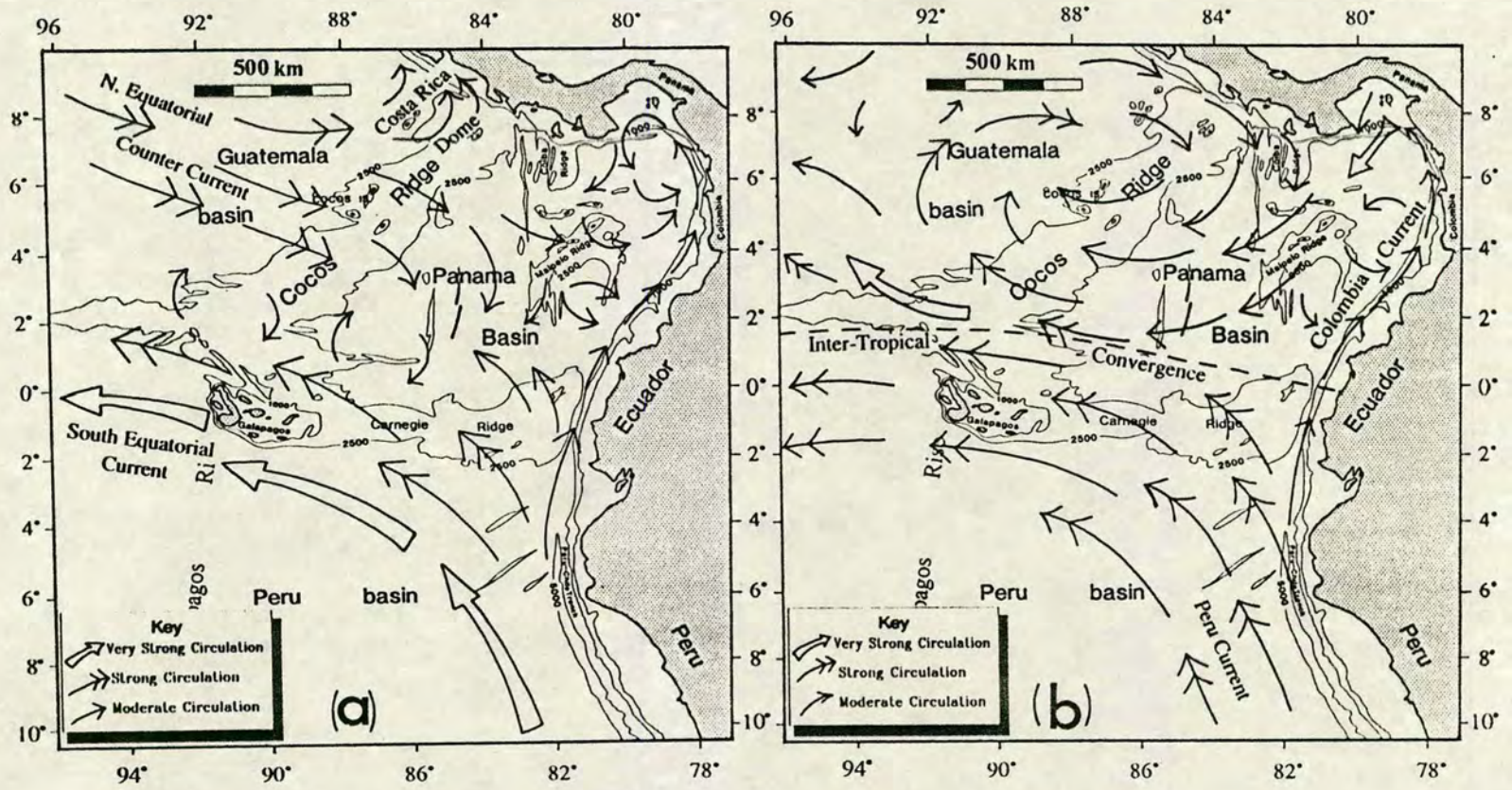

Figure 2.5 Surface circulation in the region during (a) southern winter and, (b) southern summer. Adapted from Wyrtki (1965).

2.5). The Peru current is strongest during the winter months. In contrast, in summer, due to the southward shift of the south-east trades, the circulation in the southern part of the area is dominated by a large, slow moving anticyclonic eddy. As a consequence the Panama bight and Colombia currents are strengthened as a result of being confined to the coastal belt (Pedersen, 1979).

In the central Panama basin surface flow is generally westward in the summer months but is complicated by small clockwise eddies during the winter months when the North Equatorial Counter Current exerts its influence.

Intermediate Water Circulation

Intermediate water circulation is less well documented than surface circulation. The Equatorial Undercurrent or Cromwell current has been studied (Hisard et al. ,1970; Stevenson and Taft, 1971; Pak and Zaneveld, 1973) and is known to flow eastward at about 70-200m depth below the equator with a total width of about 300 km (ie 1.5°N-1.5°S). It is traceable from the Philippines to the Gulf of Panama a distance of some 15000 km. It shallows from its usual 200m depth to surface just west of the Galapagos islands due to the change in bathymetry and sweeps round the north and, to a lesser extent, the south of the islands before rejoining in the Panama basin and continuing east at 100-250m depth towards Ecuador where it dies out around 86° 30' W as a result of intense vertical mixing (Pak and Zaneveld, 1973). A minor southward flowing current at 0-250m depth immediately west of the Colombia current has been reported by Stevenson (1970). Heath et al. (1974) speculate on the existence of a south to southeasterly flowing intermediate water at 300-2000m in the southern Panama basin. The Equatorial Intermediate Current flows to the west at about 500m depth in the west Pacific and does not affect the study area. The only other reasonably well defined intermediate water is Antarctic Intermediate Water (AAIW) which at approximately 1000m depth extends to the southern limit of the area (15°S-10°S) and probably exerts little real influence.

Bottom water circulation

In contrast to surface water currents, bottom water circulation has its driving force in thermohaline gradients and usually has some vertical component of motion. There is no primary source area for deep water in the Pacific, and bottom waters must

originate in other ocean basins entering the south-west Pacific before sweeping up its west side and giving rise to eastward flowing subsidiary bottom currents.

Bottom water circulation in the region is summarised in figure 2.6. Bottom water flow in the area is supplied by a branch of the Antarctic Circumpolar Current that either leaves the Pacific Antarctic Basin through a transform fault trough in the Chile Rise at 41°S (sill depth 3900m) or by eastward spillover across the east Pacific rise (Lonsdale, 1976). This then flows northwards through the Peru basin towards the Panama basin. A well defined 230-300m thick bottom water current enters the Panama basin through the Ecuador Trench (sill depth 2920m) at the eastern terminus of the Carnegie ridge (Laird, 1971; Lonsdale, 1977b). This water mass is somewhat atypical for the south-east Pacific most of whose bottom water generally flows to the east and south (Stommel, 1958). Once into the basin the current bifurcates: one branch continuing north-north-eastwards parallel to the south-American continental slope before sweeping west through the Coiba Gap into the northern part of the western sub-basin; the other branch flowing westwards through the Carnegie-Malpelo pass and on to the south-west part of the basin before escaping into the open Pacific over either of the two saddles (2140m and 2110m) at the south-eastern end of the Cocos ridge.

The central saddle on the Carnegie ridge at 2330m probably experiences a slow, broad inflow which, not being dense enough to sink into the basin floor, generally defines the upper limit of a distinctive basin water (Lonsdale, 1977b). Laird (1971) and Knowsman (1973) suggest outflow of water at this sill which led Pedersen (1979) to postulate that a very broad southerly drift of warmer, less dense basin water occurs just above the slow inflow of Lonsdale (1977b) possibly even balancing the inflow of bottom water.

The driving force behind this renewal is believed to be the geothermal gradients within the basin especially adjacent to the Galapagos spreading centre (Weiss et al., 1977). Lonsdale (1977b) calculates the inflow rate to be 0.35 Ê 10^6 m^3 s^{-1} (0.35 SV), a volume sufficient to fill the Panama basin up to the Carnegie ridge central saddle depth (2330m) in less than 50 years (Pedersen, 1979).

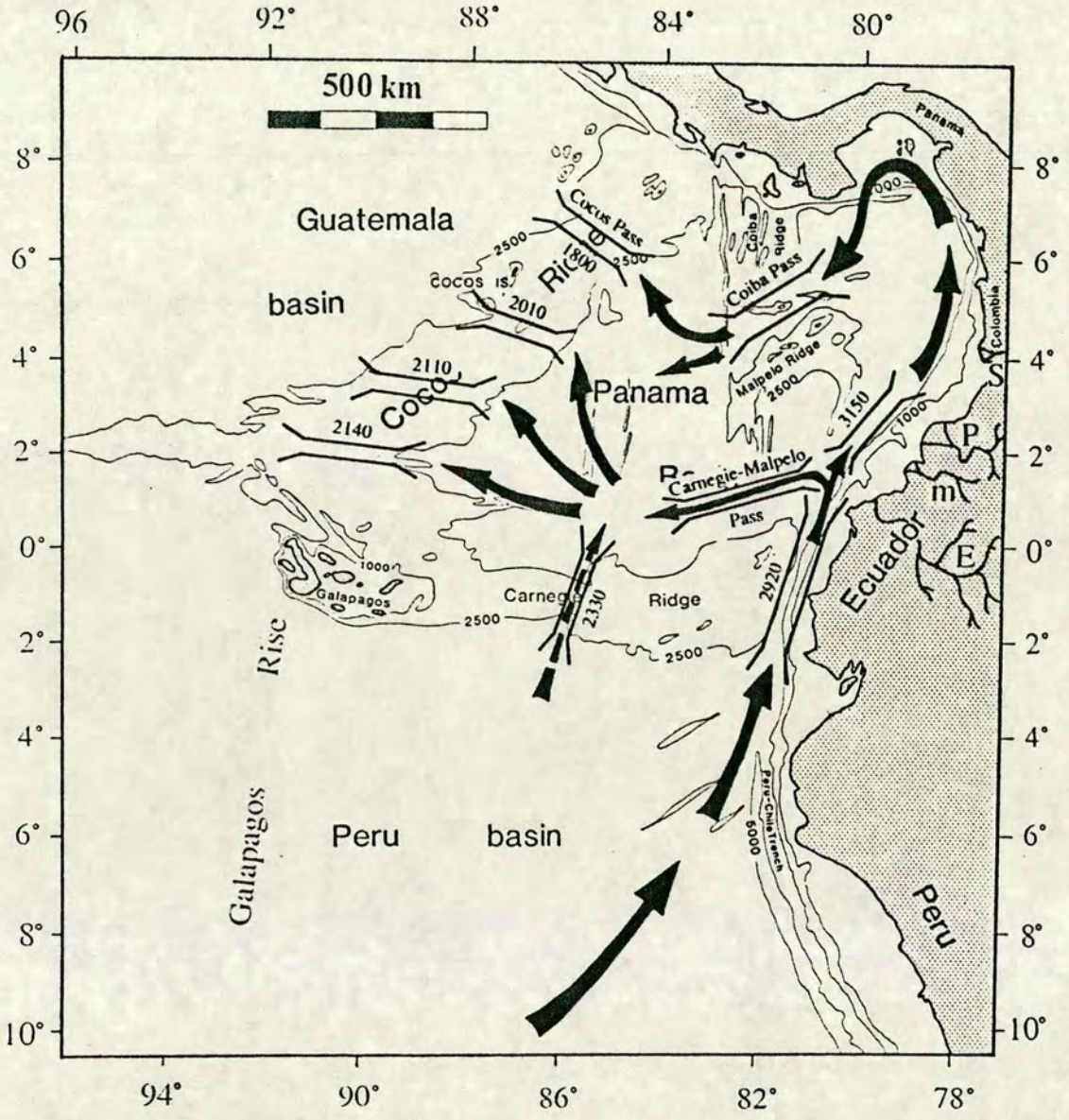

Figure 2.6 Bottom water circulation, deep saddles and riverine (fresh water) input to the area. Depths are in meters; E - Esmereldas; M - Mira; P - Patia; S - San Juan. Adapted from Chase et al., (1970); Heath et al., (1974); Lonsdale, (1977b).

2.3 Oceanic Productivity and Environmental setting

The equatorial Pacific has widespread upwelling especially along the equatorial divergence zone at about 10°N (Wyrtki, 1974; Wyrtki and Kilonsky, 1984) and in the coastal waters off Peru (Figure 2.3 and 2.7). Specific centres of very high production, as summarised by Pedersen et al. (in press), occur: (a) in coastal regions as a consequence of wind driven transport off-shore; (b) in the Galapagos Archipelago area where nutrient rich equatorial undercurrent water is forced surfaceward by the shallow topography; (c) along the southern perimeter of the Panama basin as result of the equatorial divergence and lateral advection of upwelled water in the Peru current; and (d) in the western central area which is influenced by domal upwelling that originates south of Costa Rica (Wyrtki, 1967; Moore et al., 1973; Molina-Cruz, 1977). Such intense productivity led Chavez and Barber (1987) and Feely (1987) to conclude that the equatorial Pacific contributes significantly to the modern global carbon and nitrogen cycles. According to Murray et al. (1990) primary production in the Panama basin area ranges from 335-423mg C m^{-2} day^{-1} (which is considerably less than the values expressed in figure 2.7; from Moore et al., 1973). Despite these levels of productivity there is still an excess of NO_3^- in equatorial Pacific surface waters (Feely et al., 1987) which suggests that primary productivity may be at least partly decoupled from nutrient availability and that iron may be an important limiting factor (Pedersen et al., 1991). This may have important implications for the net transfer of CO_2 between atmosphere and oceans from glacial and interglacial periods.

The distribution of the river systems which provide the area with fresh water and continental lithospheric material are shown in figure 2.5. None of these systems are very large and consequently they are not thought to contribute significant quantities of terrigenous material directly to the Panama basin although they obviously add to the build up of detritus on the shelf which eventually reaches the deep basin by a variety of sedimentary processes.

Today precipitation and riverine input are relatively high compared to past glacial times and aridity is lower, although the coastal regions of north-west south-America are generally desert environments. Also at present there is a net efflux of CO_2 from the oceans to the atmosphere. These subjects will be discussed further in the concluding chapters on Palaeoproductivity and Palaeoclimate.

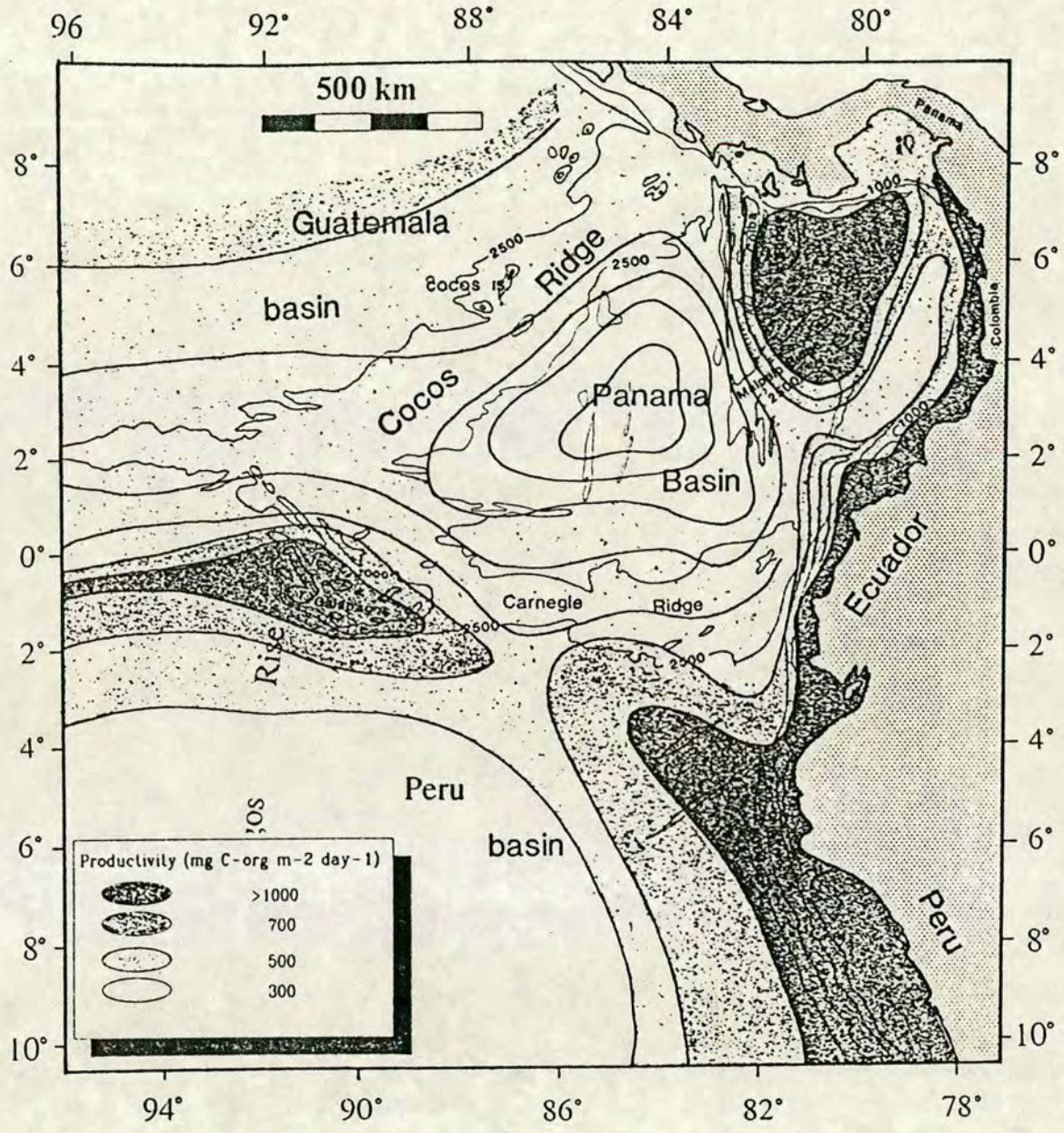

Figure 2.7 Surface water productivity in the euphotic zone. Values are from Moore et al., (1973). Note the areas of especially high primary production in the coastal waters off Peru, Ecuador and Panama, and in the Galapagos platform.

CHAPTER 3
SEDIMENTS AND MINERALOGY

3.1 SEDIMENT DESCRIPTION

Initial assessment of the cores was made from visual and microscopic examination. Descriptions of cores are summarised in table 3.1. From these and subsequent water content and magnetic susceptibility results (chapter 4.2), 6 CD38 cores and 2 Shackleton cores were chosen for further examination. Figures 3.1a and 3.1b are diagrammatic sedimentary logs of the CD38 core used in subsequent chemical analysis. Sediment recovery and sampling techniques are given in appendix A.1

3.2 WATER CONTENTS, DRY BULK DENSITY AND POROSITY

Sediment water content, dry bulk density and porosity result from a combination of sediment composition and the degree of compaction (depth in core). Coarse grained and carbonate rich sediments usually display low porosity values (Pettijohn, 1975), which can have important effects in the cycling of nutrients and chemical species between the sediment surface and overlying water column (Berner, 1975; Martens and Klump, 1980; Reimmens, 1982). Conversely, high clay and organic matter concentrations tend to increase porosity values (Fuchtbauer and Reinech, 1963). Dry bulk density represents the proportion of solids (sediments) relative to voids (interstitial water) and is mainly used for calculation of fluxes (see chapters 5 and 7). Water contents, porosity and dry bulk density were calculated from equations 3.1, 3.2 and 3.3 respectively; results are given in Appendix C.1. It is important to note that the values for cores P5 and P12 may be erroneous because of the dehydration they may have suffered between collection (1976) and sampling (1988). For this reason their water contents, dry bulk densities and porosities will not be discussed in any detail.

Equation 3.1 $$\text{Water Content (\%Wet Wt)} = \frac{\text{Water wt.(g)}}{\text{Total Wet Wt.(g)}} \times 100$$

Equation 3.2* $$\text{Porosity (F)} = \frac{\text{(Water Wt. (g)/1.025)}}{\text{((Water Wt./1.025)+(Dry Wt./2.7))}}$$

* After Berner (1971)

	GENERAL DESCRIPTION	MICROSCOPIC DESCRIPTION
P5	Recovered north flank of Carnegie ridge just east of Galapagos platform. 1cm light brown highly foraminiferal (foram) sediment mantling pale grey-green homogenous foram sand.*	Mainly whole planktonic forams in fine grained matrix of broken carbonate fragments. Occasional rads, very rare micronodules in surface, no .*
P12	Recovered at NE extremity of Panama basin virtually in sight of the Colombian coastline. 4mm brown oxidised top sharply overlying dark green homogenous clay. Intense H_2S generation at base.*	Mainly detrital clay, little coarse detritus. vary rare forams.*
CD3813	Recovered S. end of the east flank of the Galapagos rise. Fragments of Mn nodules (rubbly with mammalian tops, smoother bases) and laminated diatomite found in core catcher. Generally core composed of red clay interspersed with bands of radiolarian (rad) and diatom bearing yelllow-grey-light olive-grey calcareous ooze. Perhaps "hovered" around paleo-CCD (?). Possibly Mn-CO_3 developed.	Not Described
CD3814	Recoverd on the crest of the S. end of the Galapagos rise. Brown oxidised top few cm. Considerable water in top liner suggesting some deformation. Top 3.5m of core greyish-cream or white foram sand. Lower half of core grey-cream nanno-fossil ooze, base interbedded and laminated ash and nanno-foram oozes.	Abundant planktonic forams set in fine grained matrix of nannofossils and foram fragments. Altered basaltic debris at base of core.
CD3820	Recovered N. part of the Galapagos platform. Top 5cm brown oxidised sediment mantling mainly olive-brown laminated and mottled diatom-bearing nanno-fossil ooze. Glauconite rich at top of core.	Not described
CD3822	Recovered from the W. flank of the SW. Cocos ridge just SW of the Medina seamount. 6cm yellow-brown oxic top overlying mainly cream-white foram bearing nanno-fossil ooze with occasional grey-green patches. Base of core contains horizons with black granular mineral. Change around 4.5m. Brown oxide tops on first two sections.	200cm Abundant well preserved planktonic forams, benthics very rare. Some rads, fine carbonate matrix of foram fragments and nannofossil ooze. No obvious shards or heavy minerals.
CD3826	Recovered from the E flank of NE Cocos ridge. Several cm of brown oxic sediment sharply overlying generally homogenous olive-grey foram and rad bearing nanno-fossil ooze with common-abundant irregular black concretions ($MnCO_3$?). Several ash bands obvious (see figure 3.1.). Fragment of wood found at 470cm and a whole pteropod at 770cm.	390cm (180 ka) Mainly fine grained clay and finelt ground carbonate matrix with occasional/rare planktonic forams (whole and fragmented). Rare glass shards; common detrital fragments.
CD3827	Recovered from the SW end of the Coiba ridge NE of the Panama basin. 2cm brown oxic top overlying mainly organic rich green-grey foram-rad bearing nanno-fossil ooze. Laminated foram sand and green-grey nanno-fossil ooze at base.	150cm (20ka) Rads and diatoms abundant. Whole and often fragmented planktonic forams. Rare benthic foram. Fine grained matrix of clay. Some black grains; occasional shards.

* After Pedersen, 1979

Table 3.1 Summary of the general and microscopic descriptions of the sediments from cores studied in this thesis. Cores underlined were chosen for high resolution sampling.

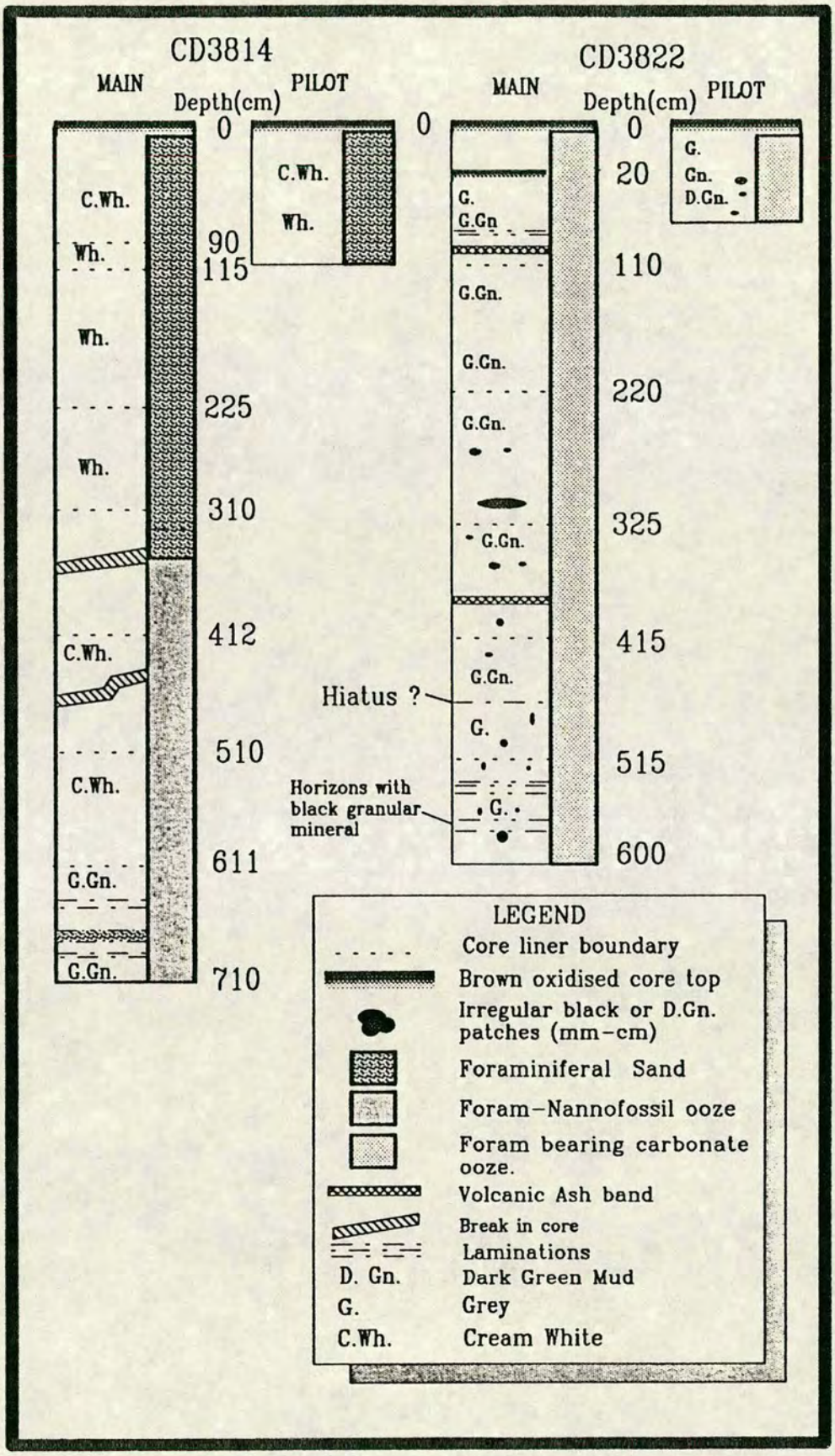

Figure 3.1a Diagrammatic sedimentary logs of cores CD3814 and CD3822.

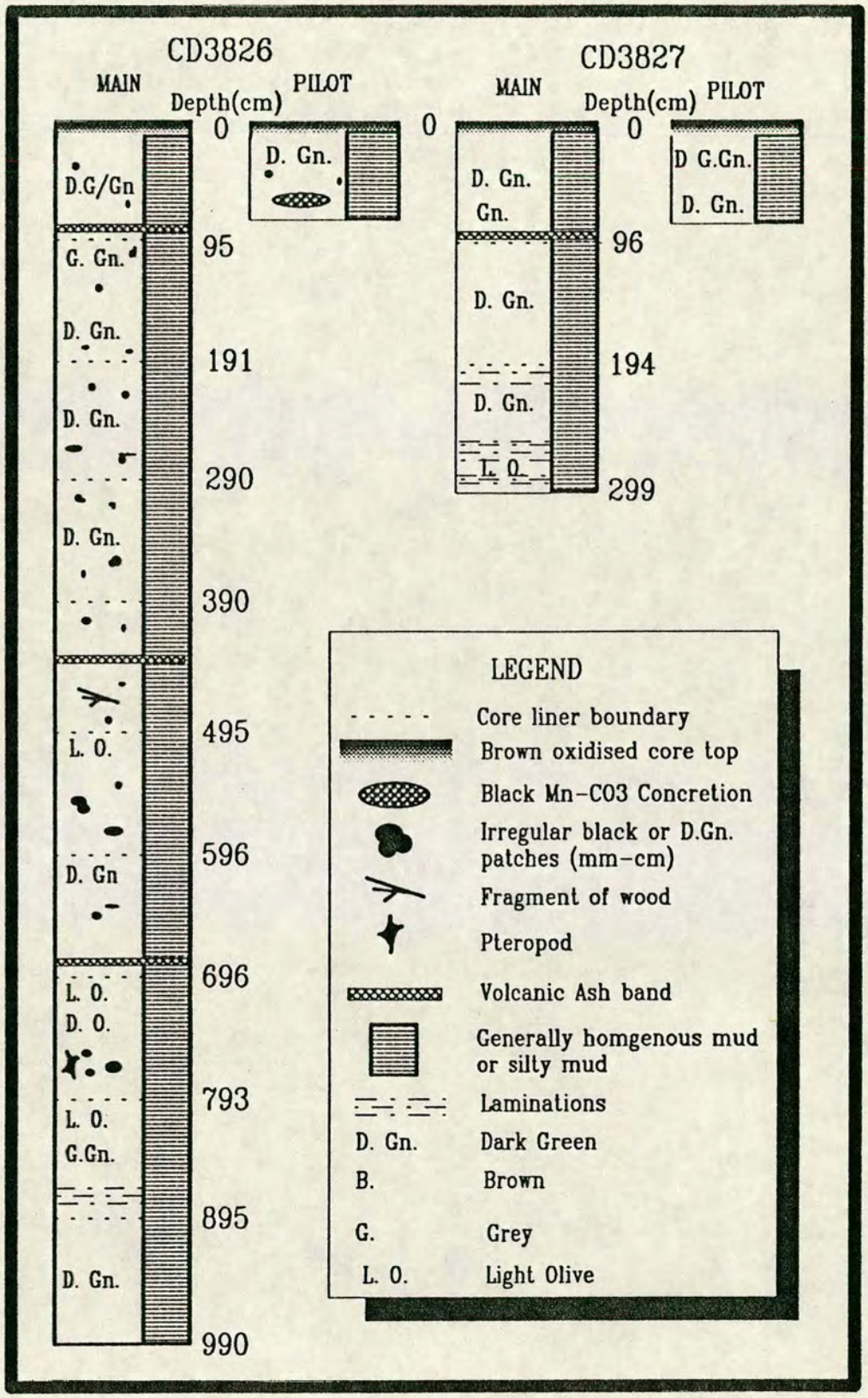

Figure 3.1b Diagrammatic sedimentary logs of cores CD3826 and CD3827.

Equation 3.3 $$\text{Dry Bulk Density } (g/cm^2) = \frac{\text{Dry Wt.(g)}}{((\text{Dry Wt./2.7})+(\text{Water Wt./1.025}))}$$

Where: 1.025 = mean density of water

2.700 = mean sediment density

All cores except P5, CD3813 and, possibly, P12 show a general decrease in water content and porosity downcore (figure 3.2 - 3.4). The topmost sections of cores CD3814 and CD3822 do, however, show slight increases down core. Water contents range from around 30% near the base of CD3820 to approximately 80% for much of CD3813. Although most compaction, and hence water content, occurs in the top half meter of most cores, a general, but smaller, decrease in water content continues to the base of core CD3826 at over 10m (figure 3.2). Pilot core profiles of water content (hollow symbols) overlap the main piston core profiles (filled symbols) in all cores except CD3826 (figure 3.2). This suggests that approximately 10 cm of sediment has been lost from the top of core CD3814 and, approximately 20 cm of sediment has been lost from cores CD3822 and CD3827. Core CD3826 is assumed to have lost 80cm, which is approximately the minimum possible value at just greater than the pilot core length.

Cores that exhibit relatively constant and slowly changing water contents are more likely to have relatively constant sedimentation rates and compositions. Any large fluctuations are likely to be a result of major compositional variation and/or sedimentation breaks (hiatuses). Clear examples of the latter occur in cores CD3820 and CD3822 at around 5m and, in core CD3826 at about 7.5m. The cause of such large changes will be discussed in the following chapters. Graphs of dry bulk density (g/cm^2) and porosity are shown in figures 3.3, 3.4 and 3.5. They display essentially the same features as the water content plots.

3.3 Preliminary Analysis of Mineralogy

3.3.1 Introduction

This section documents some preliminary mineralogical studies using X-ray diffractometry. Semi-quantification of variations in the mineralogy within and between cores was attempted to asses mineralogical inputs in the different areas. A

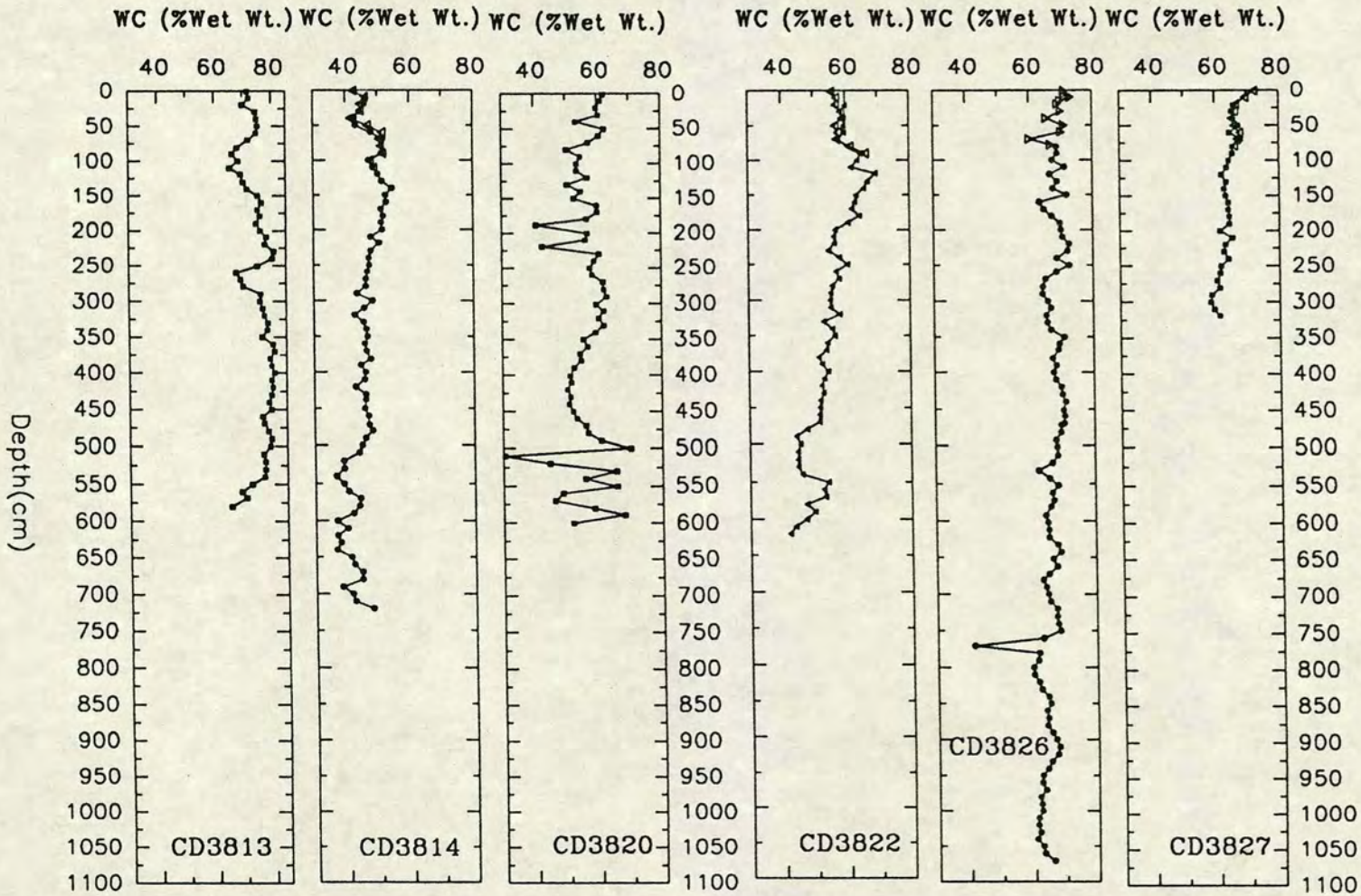

Figure 3.2 Graphs of water content (WC = % Wet Weight) versus depth (cm) from cores CD3813, CD3814, CD3820, CD3822, CD3826 and CD3827. Filled symbols represent values from the main piston core; hollow symbols values from pilot cores.

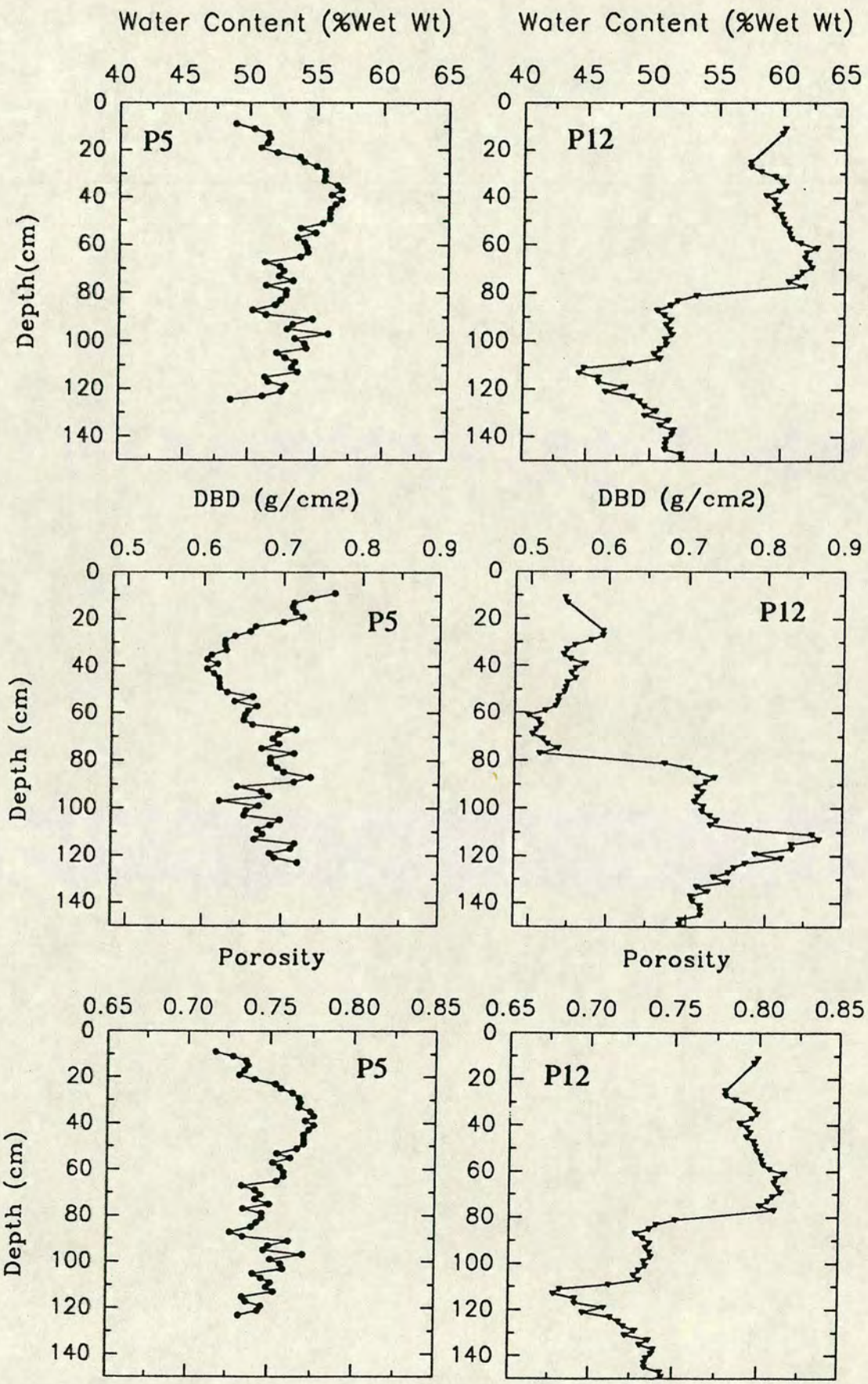

Figure 3.3 Graphs of water content (WC = % wet weight), dry bulk density (g/cm^2) and porosity versus depth (cm) from core P5 (left series of graphs) and P12 (right series of graphs).

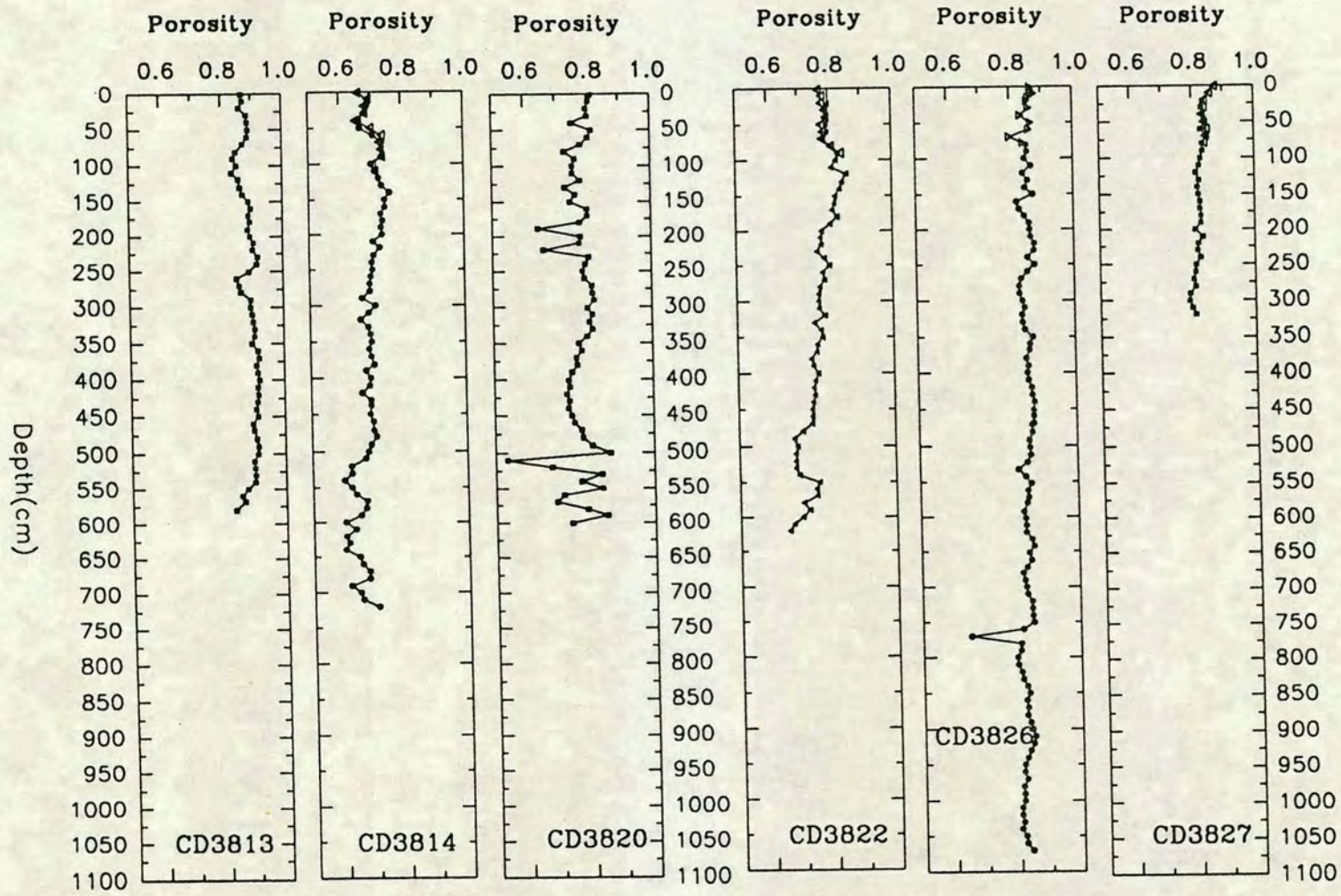

Figure 3.4 Graphs of porosity versus depth (cm) from cores CD3813, CD3814, CD3820, CD3822, CD3826 and CD3827. Filled symbols represent values from the main piston core; hollow symbols values from pilot cores.

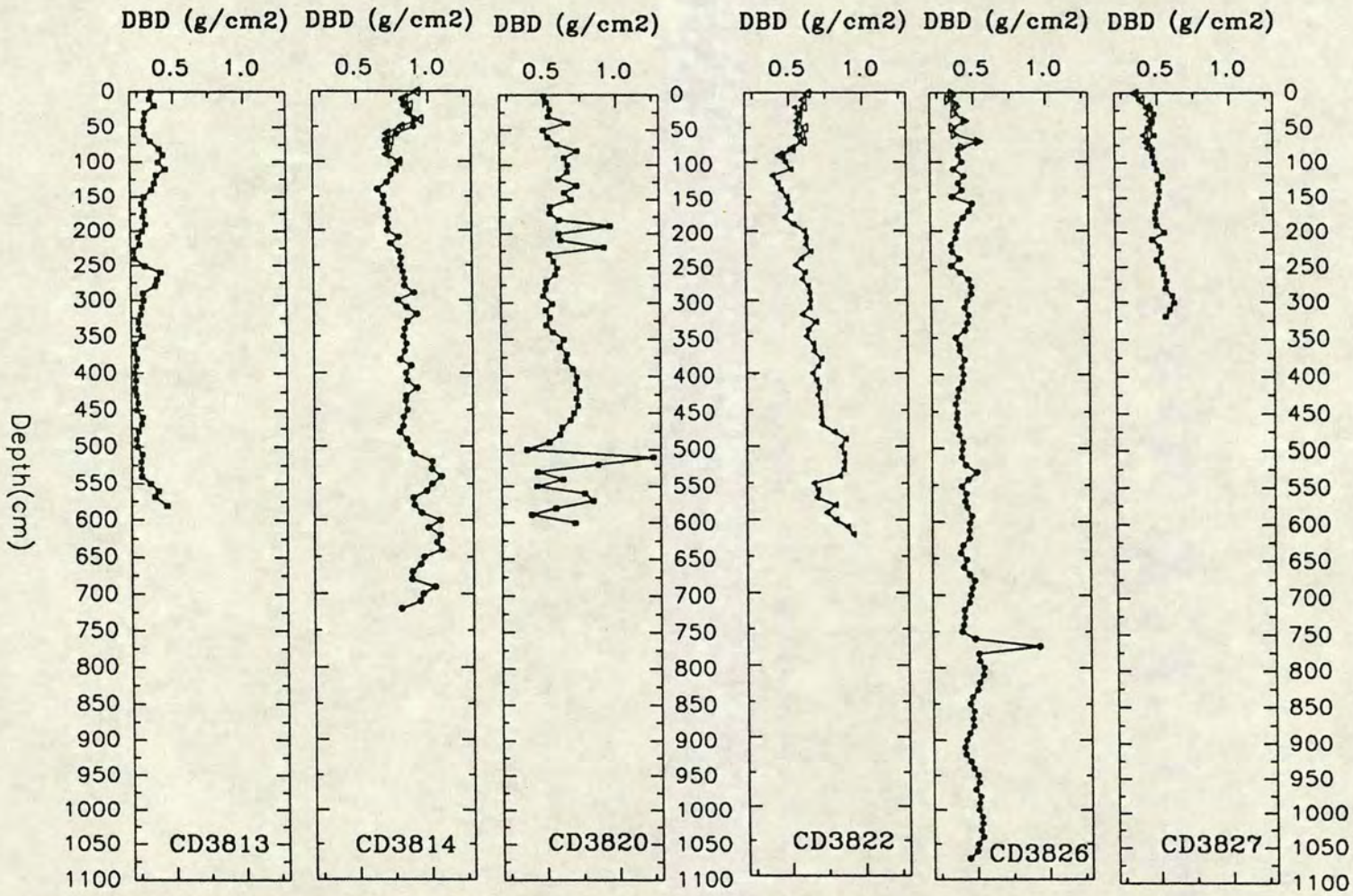

Figure 3.5 Graphs of dry bulk density (g/cm^2) versus depth (cm) from cores CD3813, CD3814, CD3820, CD3822, CD3826 and CD3827. Filled symbols represent values from the main piston core; hollow symbols values from pilot cores.

surface sample and a sample from the last glacial maximum (see chapter 4) from cores CD3822, CD3826 and CD3827 were analysed together with 10 samples from throughout core P5.

The mineralogy of the Panama basin has received some attention (Heath et al.,1974; Pedersen, 1979); work which suggests that, mineralogically, the Panama basin can be divided into an eastern (detritus poor, biogenic rich) province and, a western (detritus rich, biogenic relatively poor) province. According to Heath et al., (1974) the later part contains considerable quantities of authigenic montmorillonite (smectite). Results presented below compliment these earlier, more detailed, studies. Analytical methods are given in appendix A.4.

3.3.2 Mineral Identification

Mineral identification was achieved by correlating peaks at particular 2θ° angles corresponding to minerals from tables completed by Chao (1969). Table 3.2 summarises the minerals identified in this section, together with their associated characteristic 2θ° (and equivalent Å) angles.

Non-clays

Calcite is present in all the sediments from this study (chapter 6) and it s content has been determined using X-ray fluorescence spectrometry. Thus, XRD analysis in this study has concentrated on the mineralogy of carbonate free sediment after it was treated with dilute HCl (appendix A.4).

Quartz and feldspar (see below) are the most abundant non-clay minerals found in these sediments (other than calcite), and quartz (peak intensity at 26.66 2θ°) appears in increase towards land. Thus cores CD3826 and CD3827 seem to contain more quartz than cores CD3822 and P5, as illustrated by the very large (cut off) quartz peak intensity at 26.66 2θ° and the relatively strong "100" quartz peak at 20.85 2θ° (figure 3.6). Feldspar is present in all four cores and appears to be more abundant in cores CD3826 and CD3827 than in cores CD3822 and P5 (c.p. figures 3.6a,b with 3.6c and 3.7). However, the horizon at 13.94 ka in core P5 (figure 3.7) has very high feldspar content which coincides with high K/Al ratios (see chapter 5). This is consistent with the possible increase in the input of basaltic debris at this time. The volcanic ash bands, recognised in chapter 4, have unusually high contents of feldspar

Table 3.2 Summary of the minerals identified in this section and their associated peak names and 2θ° angles derived from Chao (1969).

Mineral	Peak Name	2θ°	equivalent Å	Affected by glycolation	Comments
Calcite*	---	29.40	3.00	NO	
Quartz	100	20.85	4.26	NO	
Quartz	101	26.66	3.34	NO	
Feldspar	---	28.04	3.19	NO	associated with total feldspar[1]
Feldspar	201	21.98	4.04	NO	associated with plagioclase[1]
Halite	---	31.72	---	NO	
Pyrite	---	33.07	---	NO	
Pyrite	---	37.10	---	NO	
Barite	---	25.88	---	NO	
Barite	---	28.79	---	NO	
Chlorite	002	12.40	7.00	NO	
Chlorite	003	25.30	3.54	NO	
Chlorite	---	35.63	---	NO	
Chloritoid	---	30.09	---	NO	
Smectite	---	5-6	---	YES	dominantly montmorillonite

[1] Heath (1969)

* Negligible dolomite (2θ° =30.99) was thought to be present in the sediments studied in this thesis.

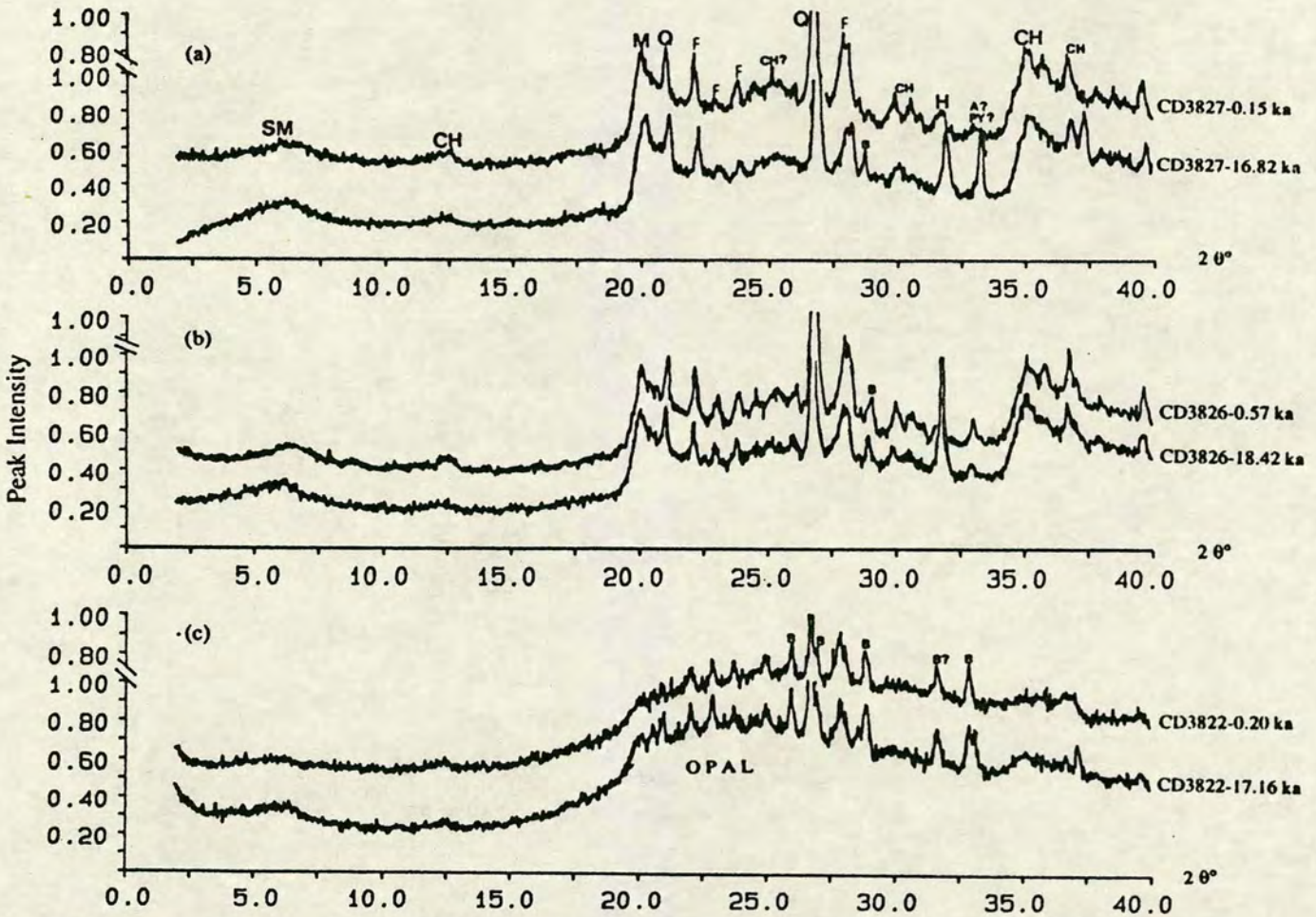

Figure 3.6 Diffractograms illustrating the variations in mineralogy between surficial (latest Holocene) sediments and sediment from the last glacial maximum from cores CD3827 (a), CD3826 (b) and CD3822 (c). All sediment is carbonate free. Note the general similarity of the profiles of all samples from cores CD3826 and CD3827 and how they differ markedly from those in core CD3822. SM = smectite; M = Montmorillonite; Q = quartz; F = feldspar; H = halite (NaCl); CH = Chlorite; A = Hydroxyapatite; PY = Pyrite; B = Barite; Opal = amorphous silica.

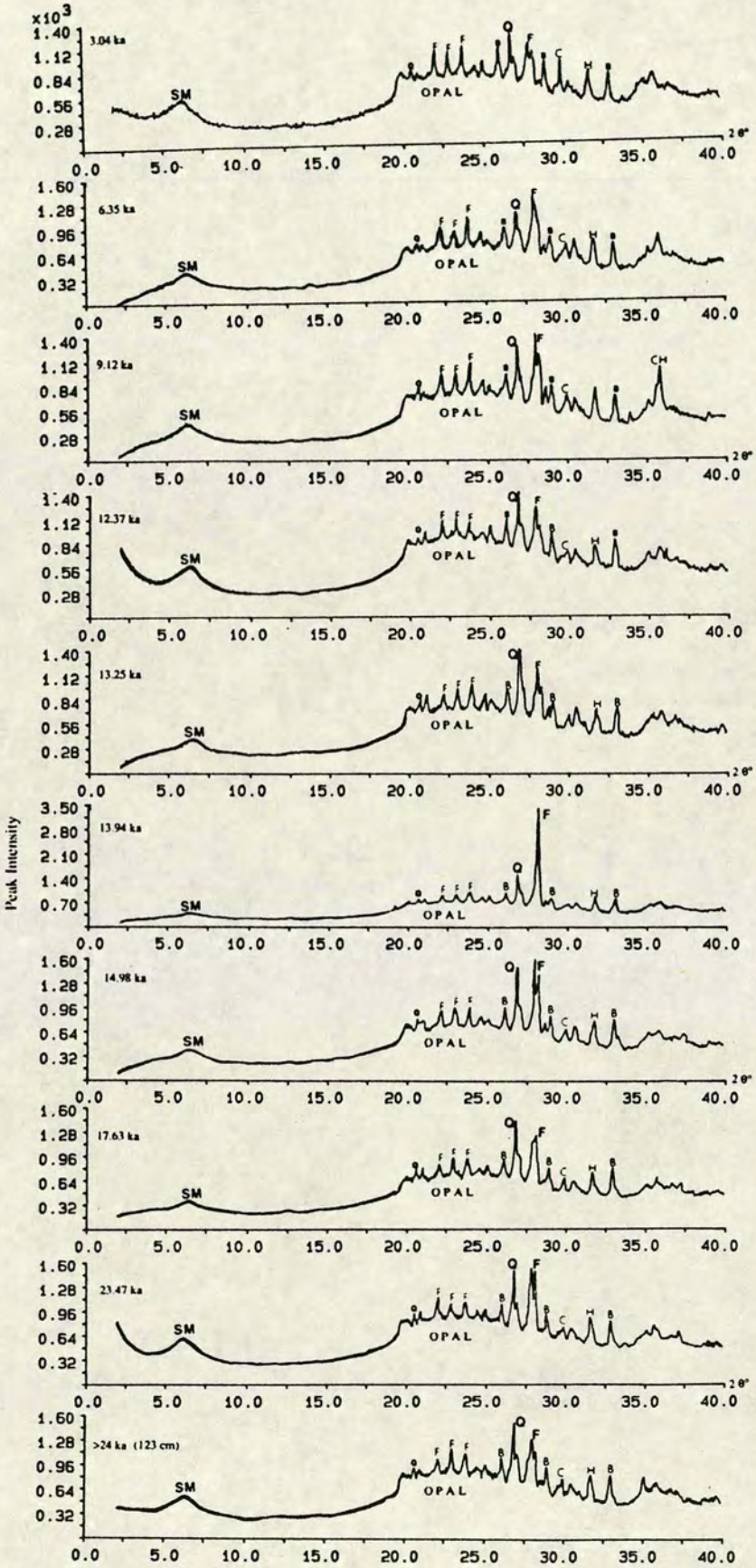

Figure 3.7 Diffractograms illustrating the temporal variations in the mineralogy of carbonate free sediment from core P5. SM = smectite; Q = quartz; F = feldspar; C = Calcite; H = halite (NaCl); CH = Chlorite; B = Barite; Opal = amorphous silica. (see text for details).

compared to normal sediment. Feldspar content (peak intensity) also appears to be lower during the last glacial maximum compared to latest Holocene sediment in cores CD3826, CD3827 and, to a lesser extent, core CD3822 (figure 3.6a-c).

Opal (amorphous silica) is recognised by a very broad hump between 20-30 2θ°. It is present in all cores, but is most obvious in the diffractograms from cores P5 and CD3822 (figures 3.6c and 3.7 respectively). This difference in opal content is quantified and discussed more fully in chapter 6. The volcanic ash layers also have this characteristic broad hump, with differences between cores being not as apparent, with respect to amorphous silica content, as in other parts of the cores. This is consistent with unusually high quantities of volcanic glass in all the tephras.

Barite, which is known to be associated with biogenic silica in the marine environment (Church, 1979; Bishop, 1988), is also present in all the cores, but appears considerably more abundant in cores P5 and CD3822. However, this may be related to mass absorption effects in these carbonate rich cores. The association of Barite ($BaSO_4$) with opal will be discussed more fully in chapter 6.

Pyrite appears to be present in core CD3826 and CD3827 (figures 3.6b and 3.6a respectively) and, more especially, in the ash bands in core CD3826 (figure 3.8a-c). Its peak at 33.07 2θ° is, however, close to the subsidiary barite peak at 32.60 and hydroxyapatite peak at 32.93 2θ°. However, the pyrite peak at 37.10 is clearly identifiable and is most clearly shown in ashes "D" (56 ka) and "L" (234 ka) in core CD3826 (figure 3.8a-b)

Clays

Clay minerals are dominated by smectitic material, identified by its characteristic broad peak between 5-6 2θ° (figures 3.6 and 3.7). The smectite is probably a type of montmorillonite, as this mineral is thought to dominate the clays in the Panama basin (Heath et al., 1974). According to Heath et al., (1974) montmorillonite in the Galapagos platform region is almost exclusively of authigenic origin, with volcanic glass shards being the precursor; whereas in the eastern basin most of the montmorillonite is of terrigenous origin. Smectite content is higher during the last glacial maximum in cores CD38822, CD3826 and CD3827 (c.p. figures 3.6a-c) probably because of increased transport from the continent.

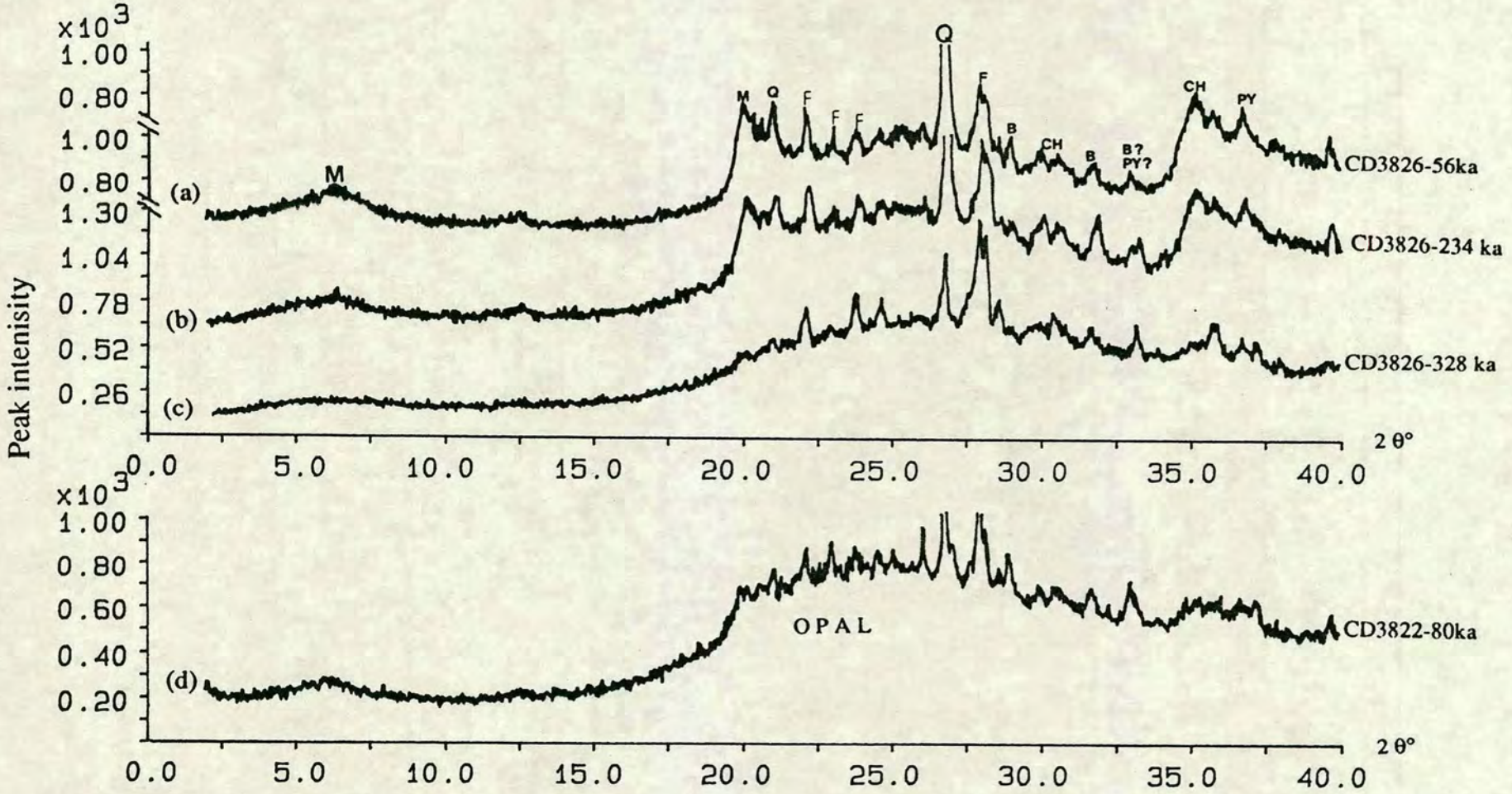

Figure 3.8 Diffractograms illustrating the mineralogy of the volcanic ash horizons in core CD3826 (a-c) and the one ash band in core CD3822 (d). (a) represents ash "D"; (b) represents ash "L"; (c) represents ash "K" and, (d) represents a local ash deposit in core CD3822 not previously recognised (see chapter 4). Abbreviations as in figure 3.6. Note the large broad hump resulting from relatively high contents of amorphous silica in core CD3822.

Samples CD3826-0.57 ka, 18.42 ka, 56 ka and 156 ka and, samples CD3827-0.15 ka and 16.82 ka were analysed twice: initially with no treatment, then after 24 hours in an atmosphere of ethylene glycol which replaces the water in the clay lattice. The result of this expansion of the lattice is that the smectite (montmorillonite) peak is shifted towards smaller 2θ° angles at around 4-5 2θ°. Figure 3.9 illustrates this peak shift for sample CD3826-156 ka, by showing diffractograms of before and after glycolation on the same plot. This plot was shown to be coincident with a synthetic standard of montmorillonite.

Chlorite is present in cores CD3826 and CD3827 (figure 3.6a-b), recognised by several peaks at 14.40, 25.30 and 35.63 2θ°. Chloritoid material also occurs at around 30.09 2θ°. According to Heath et al., (1974) chlorite is the coarsest and densest of the clay minerals in the Panama basin with it s primary source being the San Juan river (see chapter 2). Therefore, one would expect an increase in chlorite with decreasing distance from land, a pattern consistent with the greater quantities of the mineral in cores CD3826 and, especially, CD3827. Illite and kaolinite were not observed in this study.

3.3.3 Temporal variations in the mineralogy of core P5

Ten samples were analysed from core P5 at roughly 20 cm intervals throughout the core. The ages for these horizons were obtained from the age model derived in chapter 4 and, their temporal variations in mineralogy are illustrated in figure 3.7. The removal of calcite from these samples (normally 80-90% $CaCO_3$, see chapter 6), has been almost complete, resulting in weak intensity or absence of the calcite peak. Quartz and feldspar are ubiquitous in these samples, and changes in the intensity of their peaks tend to be quite subtle, except for the horizon at 13.94 ka where the feldspar content increases greatly and, indeed, dominates the whole mineralogy. This correlates with the large increase in K/Al observed at this horizon (see chapter 5) and, as argued in chapter 5, is probably due to the input fragments of weathered basaltic material probably originating in the Galapagos platform during the dry, arid low sea-level stand glacial stage II.

The downcore variations in the quartz/feldspar ratio, calculated from the relative peak heights on the diffractograms, are shown in figure 3.10. This method is, at best, semi-quantitative and could be imprecise, so it s result must be considered tentatively. However, it does illustrate the large increase in feldspar relative to quartz at 13.94 ka and the relatively constant peak ratios of quartz/feldspar elsewhere in the core. The

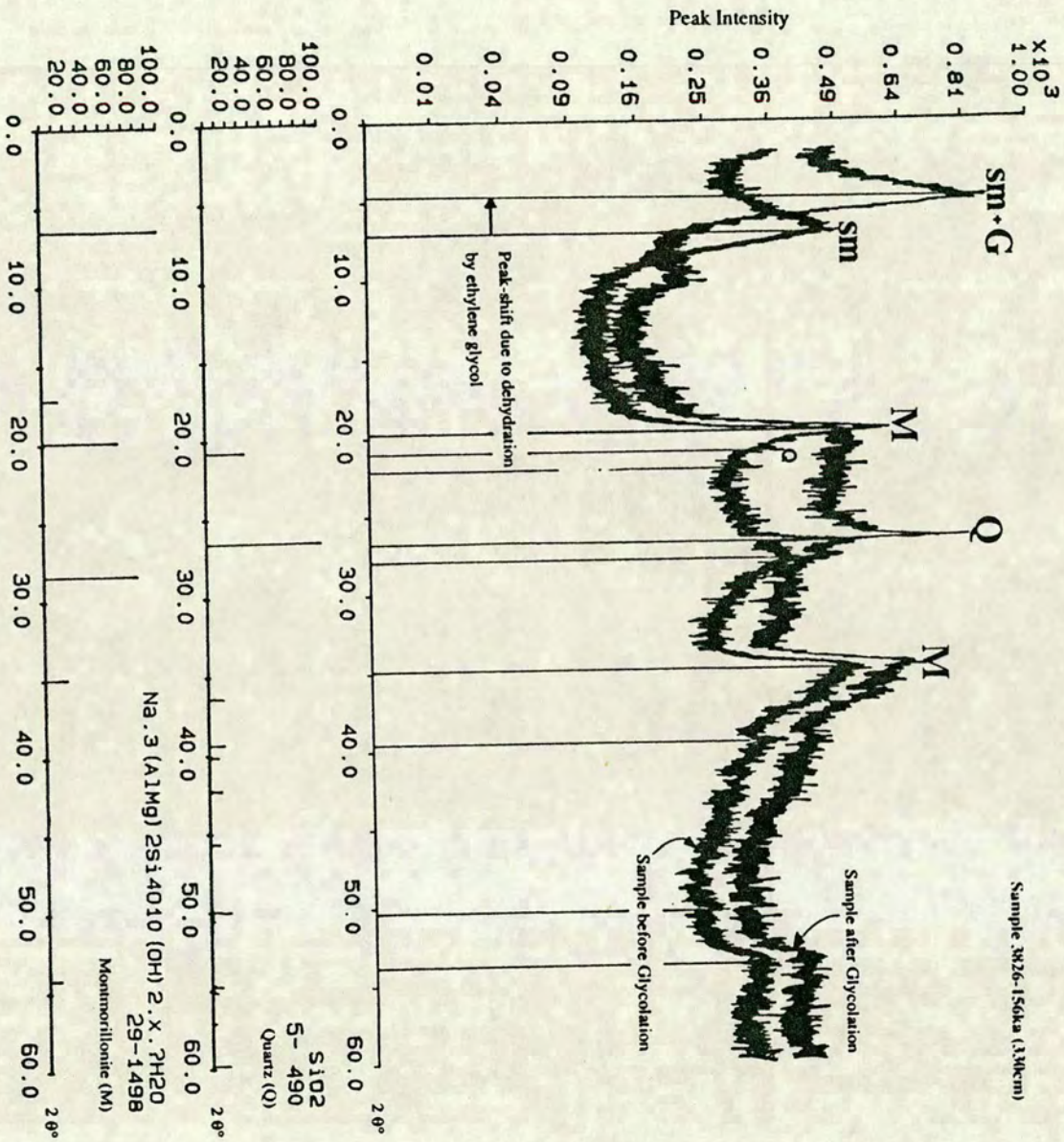

Figure 3.9 Diffractograms illustrating the shift in the broad smectite (mainly montmorillonite) peak from around 5-6 2θ° to around 4-5 2θ° after glycolation (sm+G) in sample CD3826-156 ka. Other smectite and quartz peaks are shown for comparison. G = glycolation; sm = smectite; M = Montmorillonite; Q = quartz.

small variations that do occur suggest that there is a tendency for the quartz/feldspar ratio to be higher during glacial stage II (4 points ≥ 1). Such small changes in quartz/feldspar ratios perhaps suggest a common provenance for these two minerals.

As quartz is almost exclusively an indicator of continental aridity and wind intensity and, feldspar more an indicator of local volcanic activity (Heath, 1969; Heath et al., 1974), the ratio of the two gives an insight into the relative importance of these factors spatially and temporally. Sediments close to a continental source are, perhaps, more likely to reflect variations in terrigenous input than to reflect differences in the local volcanic activity. Conversely, sediments close to the Galapagos platform would tend to reflect changes in the volcanic activity of this active region. The results discussed above are consistent with this hypothesis and that of Heath (1969) who argued for the independence of quartz and feldspar concentrations relative to each other.

Figure 3.10 Graph illustrating the temporal variations in quartz/feldpsar ratio from core P5. Age of oldest point not certain (see chapter 4).

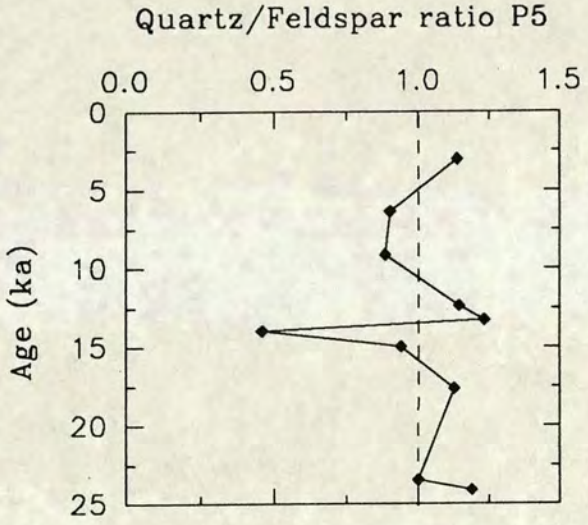

CHAPTER 4

CHRONOSTRATIGRAPHY

4.1 INTRODUCTION

Before sensible interpretation of geochemical data can commence, sediments must be dated so that accumulation rate variations and fluxes can be calculated. Most modern palaeoceanographic investigations employ a combination of oxygen isotope stratigraphy, radiocarbon dating, tephrachronology and biostratigraphy in development of age models. Some of these techniques give a relative stratigraphy, whereas others allow absolute dating, but they all have drawbacks and are best used in conjunction with each other.

The chronostratigraphies for the cores in this thesis are developed from a combination of tephrachronology, biostratigraphy, oxygen isotope stratigraphy, and chemical correlation ("fingerprinting") with nearby dated cores. Each step in the process of age model development and refinement is described, in detail, below as it is considered to be vitally important before any assessment of palaeoclimatic or palaeoproductivity changes can be made. Although cores P5, CD3822, CD3826 and CD3827 allowed production of quite well constrained timescales, the age model for core CD3814 is relatively uncertain. The chapter concludes with a summary of the final age models used as timescales in this thesis.

4.2 PALAEOMAGNETISM AND TEPHRACHRONOLOGY

4.2.1 Palaeomagnetism

Variations in the earth's magnetic field, as recorded by magnetic particles in sediments or rocks, may be employed for chronological development. In deep ocean sediments, volcanic ash deposits (tephra layers) and turbidites exhibit very large magnetic susceptibility intensities relative to other sections of the core (Bradley, 1989). Radhakrishnamurty et al. (1968) illustrate a link between magnetic susceptibility variations and tephra layers, and Robinson (1982) clearly demonstrates an association between remenance magnetisation ratios and microturbidites. Changes in the amount of magnetic material present in sediments can give semi-quantitative estimates of the relative proportions of carbonate to non-carbonate material present: sediments high in carbonate and distal to a lithogenic source will have low magnetic intensity whereas a sediment high in terrigenous material and/or volcanigenic debris will have high magnetic intensity. Clear parallelism between palaeomagnetic parameters and palaeoclimatic indicators has been described by many authors in sediments derived from all the major

ocean basins (Thompson and Oldfield, 1986). Kent (1982) disputes the reality of the palaeomagnetic-palaeoclimatic linkage, whereas Oldfield and Robinson (1985) propose a sedimentological/mineralogical reason for such parallelism. Despite the obvious complexities in the association of palaeomagnetism and palaeoclimatic indicators, the former can be a powerful preliminary tool in analysis of deep ocean sediments, allowing evaluation of their suitability for further analysis and to help develop a basic chronostratigraphy.

Measurement of magnetic properties in marine sediments fall into essentially two categories; natural magnetisation or magnetic susceptibility, and artificially induced magnetisation or remenance magnetisation (SIRM). After preliminary attempts to measure magnetic susceptibility on cores P5 and P12 showed that the readings were to low, SIRM values were determined for all cores. Analytical methods are outlined and results are given in appendices A.2 and C.1 respectively.

Perhaps the most striking feature of the SIRM profiles is the huge variation both within and between cores (figure 4.1 and 4.2). Values range from virtually zero in core CD3822, to over 1000 in core CD3820 (figure 4.1). Cores CD3820 and, to a lesser extent, CD3813 and P12 both have considerably higher values than the other cores. CD3813 was recovered from the eastern flank of the Galapagos rise, and may reflect some periodic hydrothermal or turbiditic input. Core CD3820 however, with its very high values, was recovered from the Galapagos platform and almost certainly reflects the large amount of volcanogenic input to the area through time, from the active Galapagos triple point. That cores CD3813 and CD3814 were collected so close together, and yet display such different SIRM curves, is evidence for the diluting effects of carbonate material and the potential influence of turbidites on magnetic intensity. Cores CD3814, CD3822, CD3826, CD3827 and P5 all exhibit comparatively low SIRM values except for several anomalous horizons at depth (eg 770 cm in CD3826), which have proved to be volcanic ash deposits (see section 4.2.2). Generally, SIRM values increase towards the continent (cp. cores CD3822 and P12), reflecting the reduced diluting effect of carbonate on magnetic material towards the continental landmass. All of the above five cores show a gradual decrease in SIRM values downcore, after an initial sharp decrease at the surface, best illustrated in core CD3827 (figure 4.1). This sharp decrease in magnetic intensity between 30-80 cm, is believed to be the result of selective solution of the magnetic grains driven by organic matter degradation (Karlin and Levi, 1983). This diagenetic effect has never been documented in eastern equatorial Pacific sediments

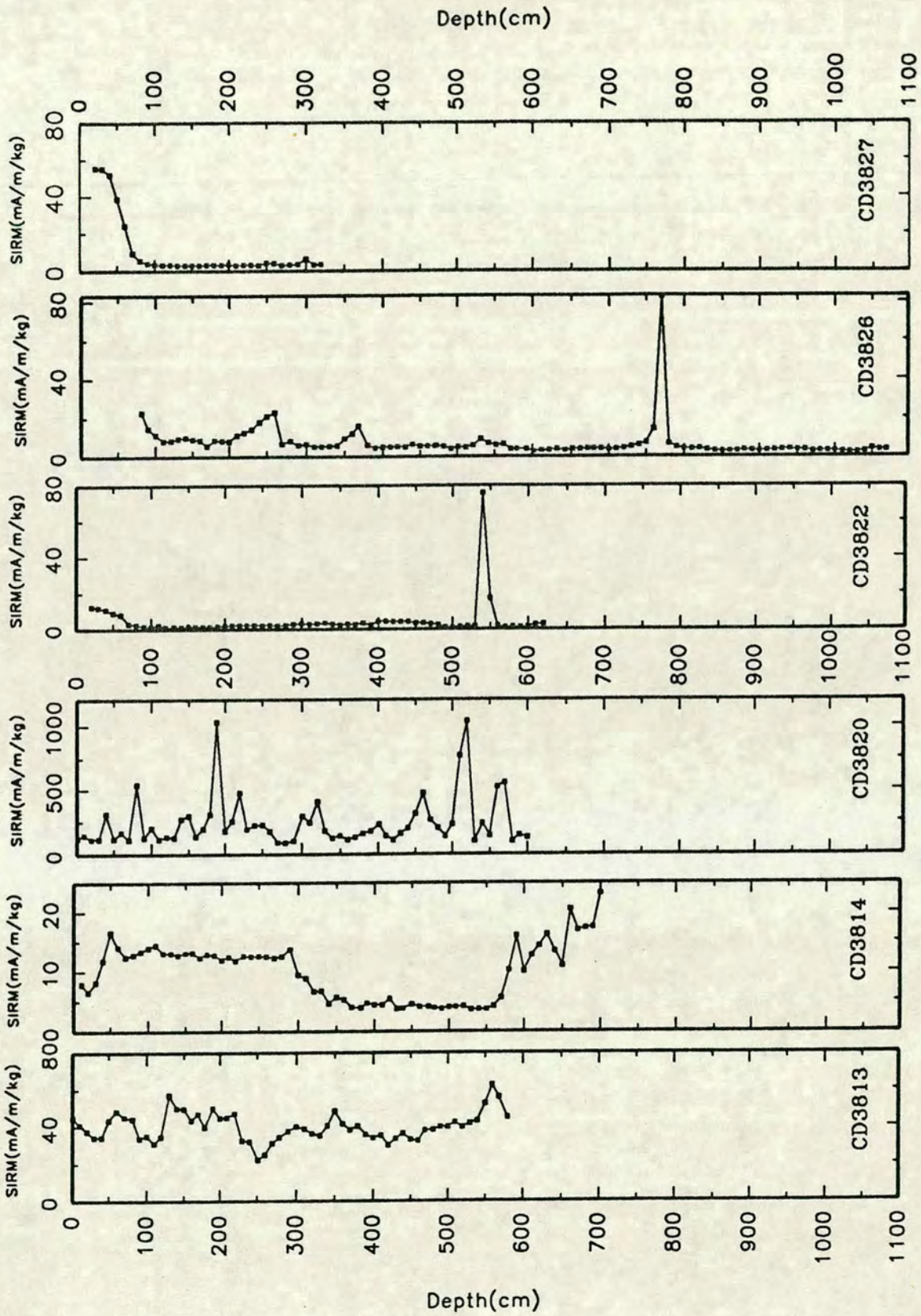

Figure 4.1 Graphs of Remenance magnetisation (mA/m/kg) versus depth (cm) from cores CD3813, CD3814, CD3820, CD3822, CD3826 and CD3827. Note the wide range in scales especially in core CD3820.

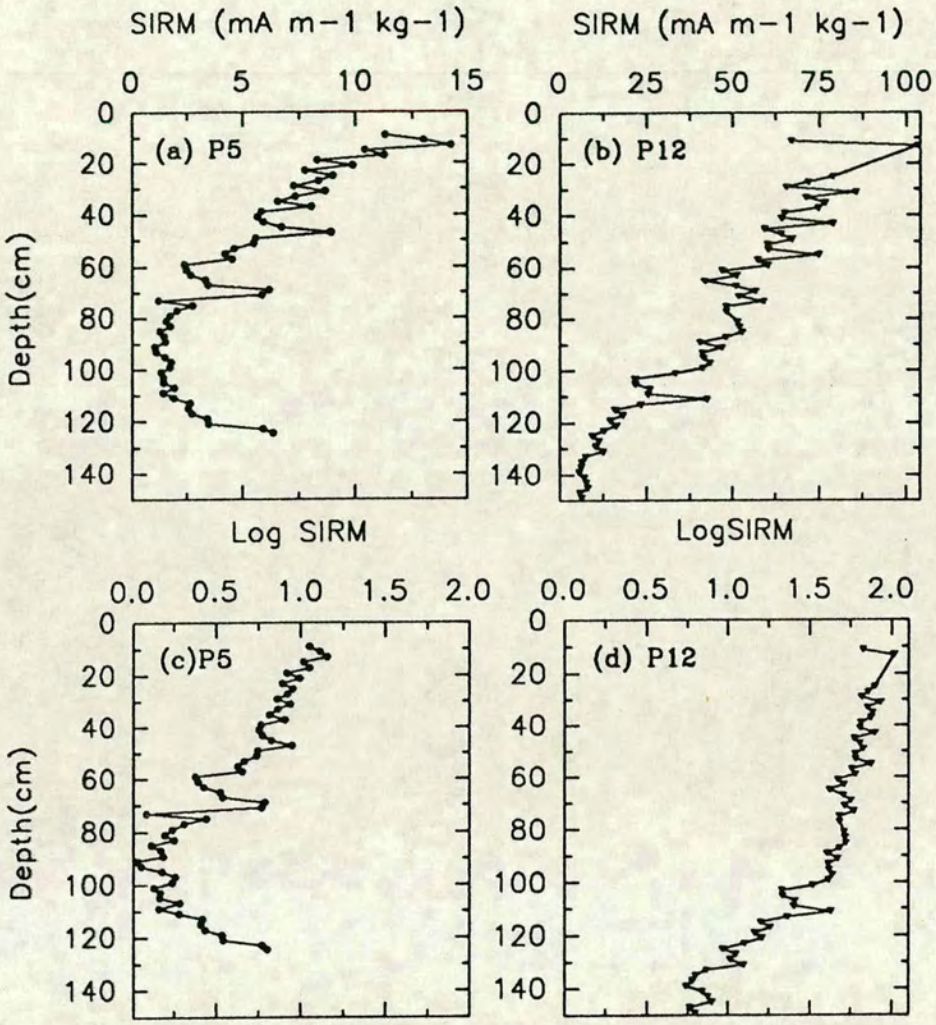

Figure 4.2 Graphs of SIRM (mA m^{-1} kg^{-1}) and Log SIRM versus depth (cm) from cores P5 (a, c) and P12 (b, d).

before this study. Cores CD3822 and CD3826 show a slight decrease in SIRM at around the same depth but do not display anything like the same surface enrichment as CD3827.

As a result of the huge variation in values, natural logarithms of the SIRM results were used in an attempt to enhance variation at the lower end of the scale. Figures 4.2 and 4.3 show LogSIRM curves for all the cores. In most cases there is little difference in the shape of the curves, but cores CD3822 and CD3826 do display indications of cyclicity (eg 400-200cm in CD3826). Section 4.2.2 illustrates how these SIRM profiles were used in the development of basic age models.

4.2.2 Tephrachronology

The tephrachronology of marine volcanic ash deposits adjacent to central America is well documented (Ledbetter, 1982, 1985; Ninkovitch and Shackleton, 1975; Bowles et al., 1973; Drexler et al., 1980). These tephra are the result of andesitic to rhyolitic volcanism associated with plate subduction under the central and N.W. south American continent (Rose et al., 1979; Wright, 1981). Figure 4.4 shows the position of the major Quaternary volcanic centres of central and N.W. south America in relation to the location of cores studied in this thesis. Ash layers in marine sediments are characterised by very low carbonate contents (Ninkovitch and Shackleton, 1975; Pedersen et al., 1991), low Ti/Al ratios (Finney et al., 1988; Pedersen et al., 1991) and, usually, anomalously high magnetic intensity (Bradley, 1989).

As discussed above (section 4.2.1), all the cores contain some anomalous SIRM horizons, but cores CD3820, CD3822 and CD3826 have the most distinct ash layers (figure 4.1). These horizons also tend to have low calcium carbonate concentration and Ti/Al ratios (see chapters 7 and 5 respectively). Comparison with other authors (Ledbetter, 1982, 1985; Ninkovith and Shackleton, 1975; Bowles, 1973; and Drexler, 1980), of the depth in cores to each ash layer, suggests that the three tephras (represented by large magnetic intensity and geochemical variation) were ash layers D, L and K of Ledbetter, (1985). Only core CD3826 contains all three tephra bands, whereas cores CD3822 and CD3827 only contain what is probably ash "D". The ages taken for these ashes are from the timescale of core AII54-25PC (Pedersen et al., 1991), which was developed using dates from Martinson et al. (1987). These ages were chosen in preference to those of previous studies because of the improved resolution of the $\delta^{18}O$ curve (every 3cm), and the U-series re-calibration of the topmost section of core AII54-25PC. Using this improved timescale, the three ash layers were assumed to be at 56 ka (ash "D"), 234 ka (ash "L")

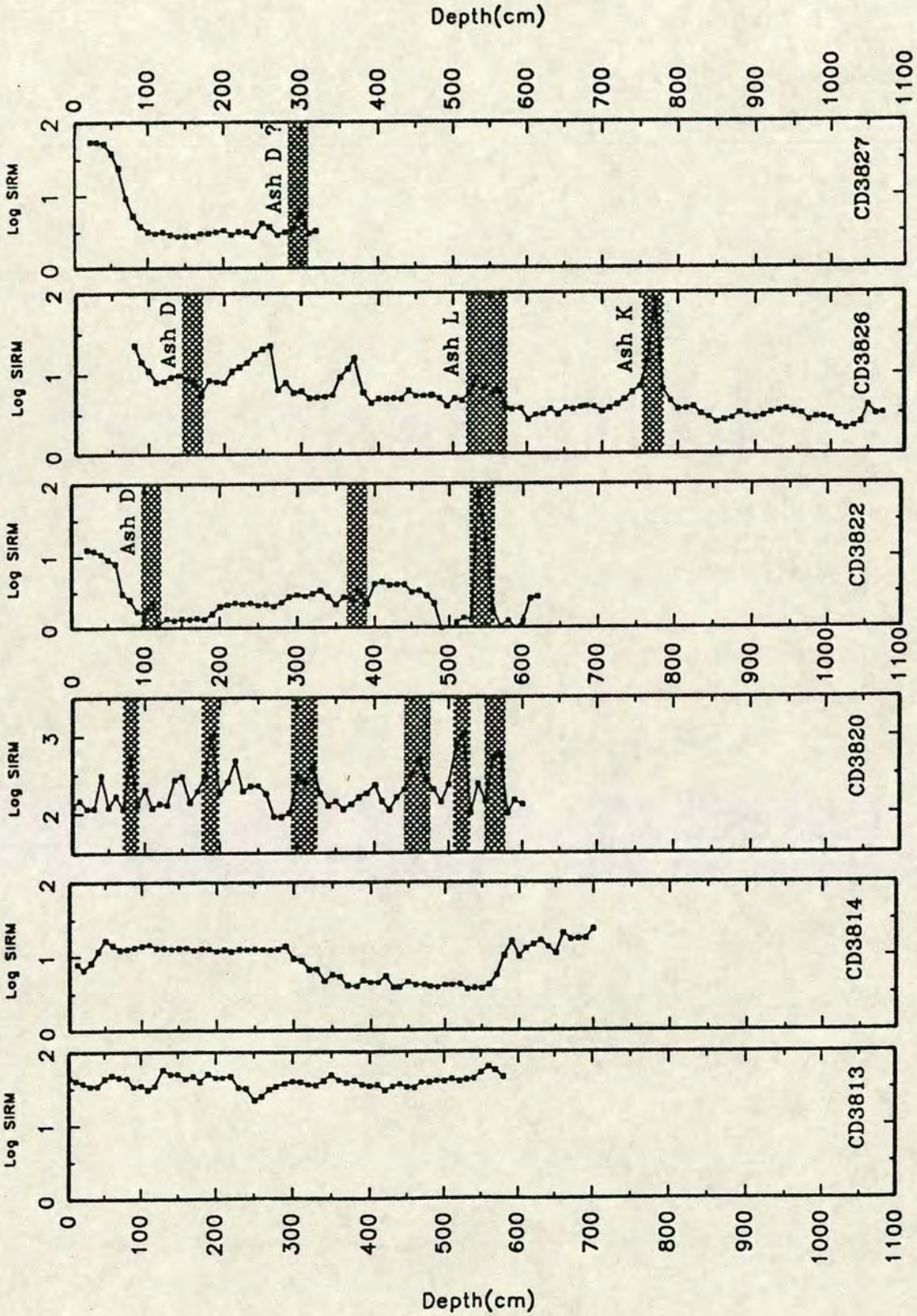

Figure 4.3 Graphs of Log SIRM versus depth (cm) from cores CD3813, CD3814, CD3820, CD3822, CD3826 and CD3827. Note the different scale for core CD3820 and the expansion of variation at the lower end of the scale for all cores. Shaded regions represent ash layers. Local tephras are not lettered; regionally extensive ash bands D (56 ka), K (234 ka) and L (328 ka) are shown (see text for details).

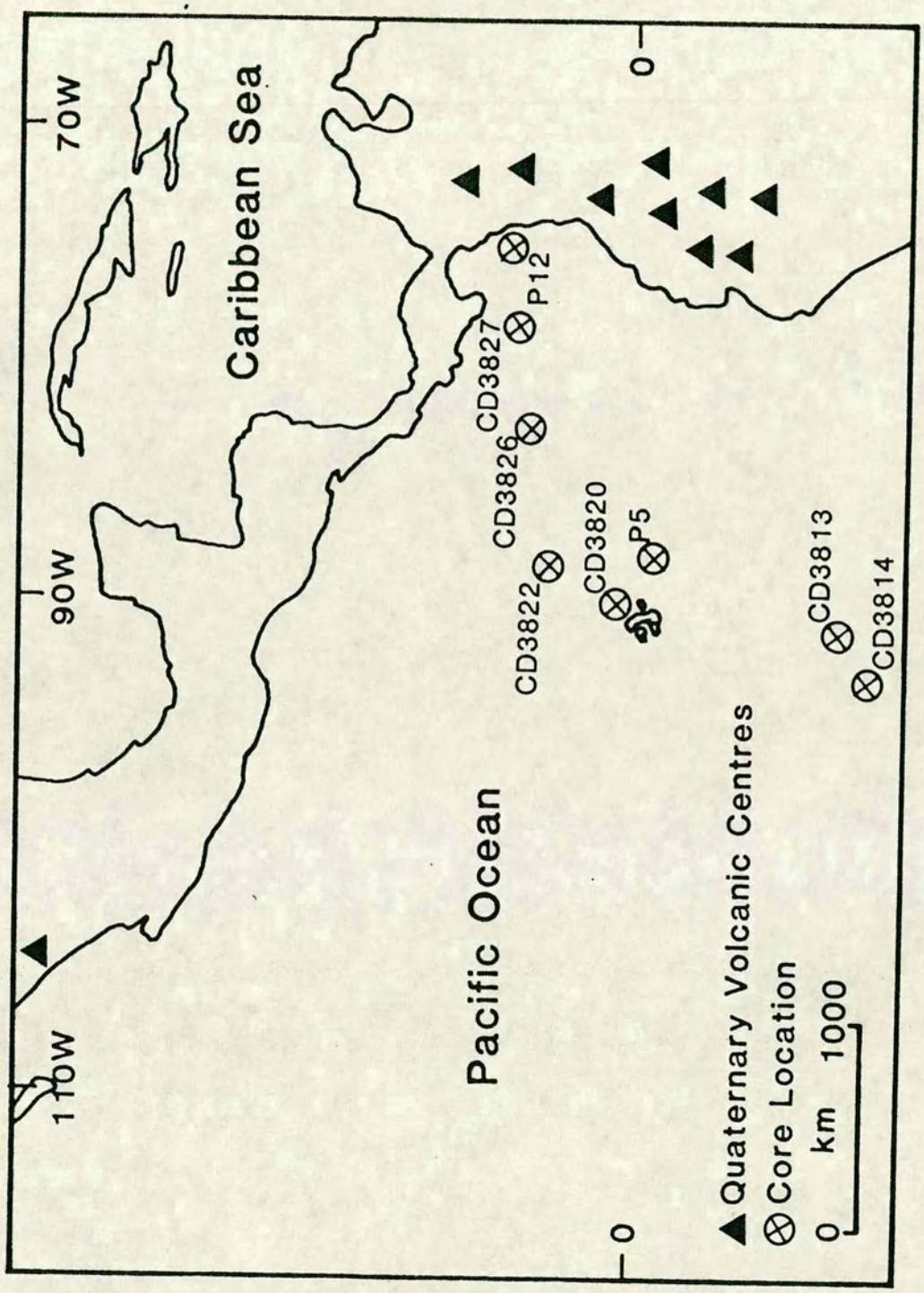

Figure 4.4 Location map of the major Quaternary volcanic centres and cores studied in this thesis.

and 328 ka (ash "K"). Using these dated horizons as control points allowed development of a crude chronostratigraphy for cores CD3822, CD3826 and CD3827 which, it was hoped, would be refined by other dating methods (see below).

4.3 BIOSTRATIGRAPHY AND FAUNAL STUDIES

Biostratigraphy was employed to assign the bottom 1.5 m of core CD3822 to the upper Pliocene (3-3.9 Ma), based on the presence of the planktonic foraminifera *Globoquadrina altispira*, *Sphaeroidinellopsis seminulina* and *Neogloboquadrina humerosa*. All other sediment proved to be of Pleistocene age (D. Kroon, 1991 pers. comm.). In the discussions and illustrations of core CD3822, only the Pleistocene section of the core is used.

The only faunal studies undertaken were made during the picking of foraminifera for stable isotope analysis (see appendix A.3). From these preliminary studies, perhaps the most significant finding was the abundance of planktonic foraminfera and radiolaria species, commonly associated with strong upwelling and productivity, in most cores, but especially in CD3822 and CD3827. Two species were very common to abundant; *N. dutertrei* and *N. pachyderma*, both of which prefer cooler waters and are characteristic of upwelling regimes, although the latter is more usually found in southern ocean waters. The sieved fraction of core CD3827 contained abundant radiolaria of many different species, some of which are shown in plate 4.1. This plate also shows several other common planktonic foraminifera species found in the cores. No quantification of either foraminifera or radiolaria abundances was attempted.

4.4 OXYGEN ISOTOPE STRATIGRAPHY

4.4.1 Introduction

Oxygen isotopic fractionation in the oceans (as a consequence of temperature changes from glacial to interglacial periods) result in the ^{16}O molecule being preferentially evaporated at low latitudes, only to be precipitated at high latitudes and become encorporated into ice sheets. During glacial periods, the oceans become enriched in ^{18}O, which is recorded in the calcareous tests of marine organisms because the $CaCO_3$ is precipitated in approximate isotopic equilibrium with the surrounding sea water. Many

PLATE 4.1

Some common planktonic foraminifera (a and b); a rare benthic foraminifera (c) and several radiolaria spp. (d - f) found in core CD3827:

(a) *Globigerinella aequilateralis;* (b) *Globoquadrina succulifer*; (c) a benthic foraminifera; (d) - (f) Radiolarian spp.

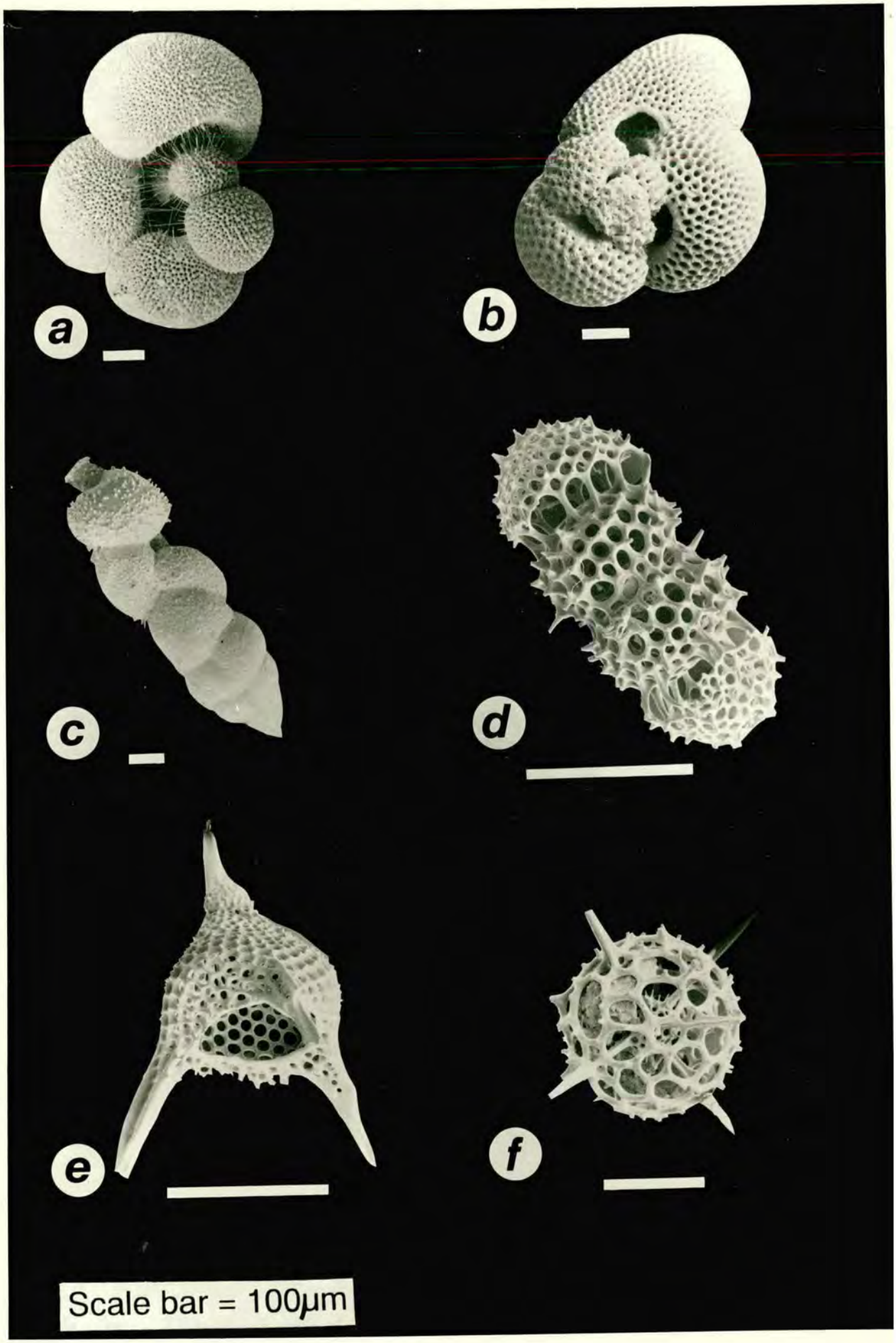
a
b
c
d
e
f
Scale bar = 100μm

factors affect the recorded $\delta^{18}O$ signal and these are well summarised in Patience and Kroon (1991, Appendix D). It is the global synchroneity of the isotopic changes that provides the potential for a high resolution correlative chronology. The isotopic ratio in the tests of dead calcareous creatures should also record past variation in climate.

Using this rationale, Emiliani (1955) developed a stratigraphy of the Pleistocene by subdividing the foraminiferal oxygen isotope record into stages and establishing a standard nomenclature; negative isotopic excursions of the interglacial stages were given odd numbers, whereas positive isotopic excursions of the glacial periods were designated by even numbers. However, only latterly was a direct link forged between the climatic effects on isotopic variations and the orbital changes central to the Milankovitch theory (Emiliani and Shackleton, 1974). Such work has resulted in the SPECMAP age model (Imbrie et al., 1984), and it is against this reference stack and the ages of Martinson et al. (1987) that the $\delta^{18}O$ curve for core AII54-25PC was correlated in development of its age model for the eastern equatorial Pacific (Pedersen et al., 1991) and in this thesis. Hence, the $\delta^{18}O$ profiles from cores studied here are correlated to the AII54-25PC oxygen isotope curve, and ages from the matching $\delta^{18}O$ maxima and minima are taken from its timescale. This approach was favoured, rather than direct correlation with the globally averaged SPECMAP stack, because it was assumed that AII54-25PC more accurately represents the isotope signal of the area with any localised isotopic variation. Also, although the AII54-25PC timescale was itself partly developed by correlation with SPECMAP (Pedersen et al., 1991), so that the distinction between the two methods is perhaps slightly artificial, the author believes that correlating to only one core introduces less potential error than if correlating to AII54-25PC and SPECMAP individually. Analytical methods are outlined, and results given in appendices A.3 and, C.2 and C.3 respectively. The planktonic foraminifera *Neogloboquadrina dutertrei* and *Globorotalia ruber* used in both oxygen isotope and carbon isotope analysis, are shown in Plate 4.2.

4.4.2 The $\delta^{18}O$ Curves

The $\delta^{18}O$ profiles versus depth (cm) for cores CD3814, CD3822, CD3826 and CD3827, together with the oxygen isotope curve of core AII54-25PC and the SPECMAP stack are shown in figure 4.5. Oxygen isotope maxima and minima were correlated from CD38 cores to core AII54-25PC wherever possible because this method is more objective than isotopic stage boundary positioning. However, due to the sometimes poor sample resolution in the cores studied there is as much potential error involved from the possibility of not including the true maximum or minimum horizon, and so the control

PLATE 4.2

Planktonic foraminifera used in stable isotope analysis:
(a) and (b) *Neogloboquarina dutertrei*
(c) - (f) *Globigerinoides ruber*.

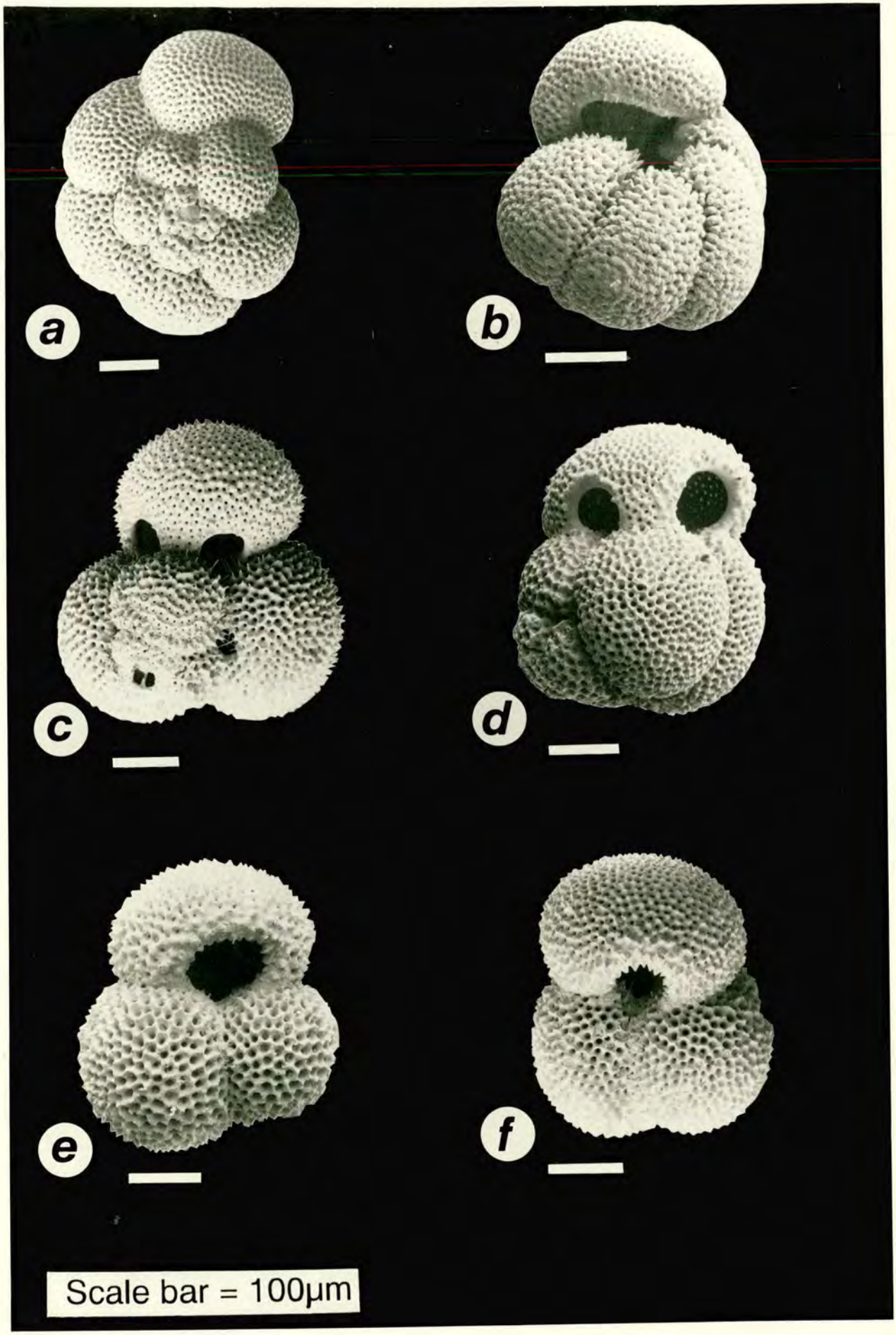
a
b
c
d
e
f
Scale bar = 100µm

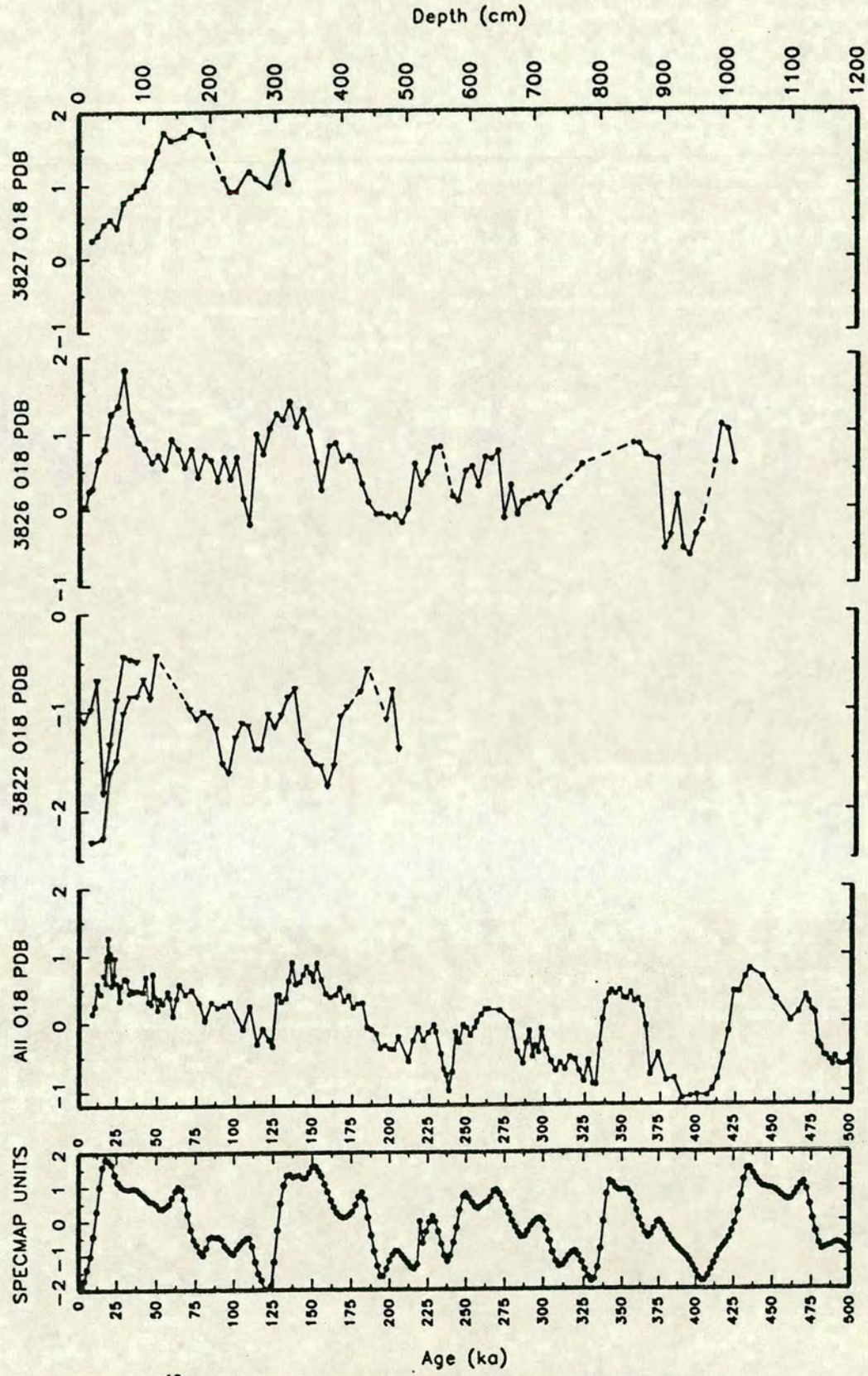

Figure 4.5 $\delta^{18}O$ PDB curves versus depth (cm) for cores CD3822, CD3826 and CD3827 together with the d18O PDB profile of core AII54-25PC and the SPECMAP stack versus age (ka). Hollow symbols in cores CD3822 and CD3826 represent data from pilot cores; filled symbols data from main piston core.

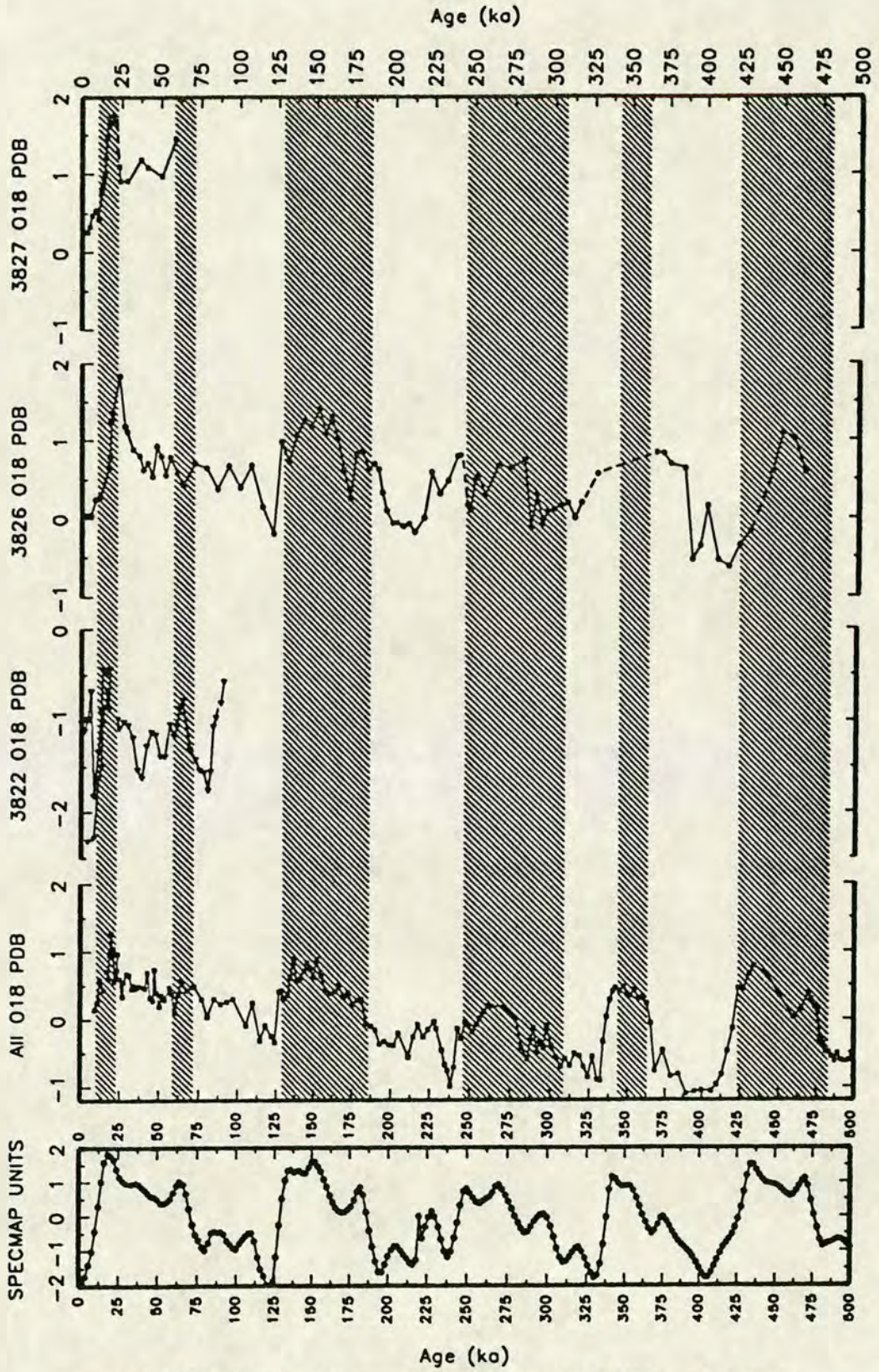

Figure 4.6 $\delta^{18}O$ PDB curves for cores AII54-25PC, CD3822, CD3826 and CD3827 versus age (ka) together with the SPECMAP stack. shaded regions represent glacial stages II, IV, VI, VIII, X and XII. Hollow symbols in cores CD3822 and CD3826 represent data from pilot cores; filled symbols data from main piston core.

points used for the timescale are a combination of isotopic peaks and clear stage boundaries. Dates for these age picks, which were obtained from Pedersen et al. (1991), allowed conversion of CD38 core data from the depth domain to the time domain by assumption of linear accumulation rates between control points. Figure 4.6 shows the $\delta^{18}O$ profiles versus age (ka) for CD38 cores, together with the $\delta^{18}O$ curves of core AII54-25PC and the SPECMAP stack. Tables 4.1-4.3 show the depths (cm) and inferred ages (ka) of the control horizons in cores CD3822, CD3826 and CD3827, achieved by correlation of both oxygen isotope and geochemical data (see section 4.6). This allowed further refinement of the chronostratigraphies with the well dated, nearby, cores P6 (Pedersen, 1979) and AII54-25PC (Pedersen et al., 1991).

In addition to the correlation of isotope curves of cores CD3826 and AII54-25PC and, as a result of their proximity and chemical similarity, stratigraphic correlation of the geochemistries has been employed to achieve a very well constrained timescale for core CD3826 (see section 4.6). Such correlation simply matches maxima and minima in chemical profiles, and ignores any causal implications which are discussed in detail in later chapters. Table 4.1.b shows a summary of the depths (cm) and ages (ka) of all the isotopic and geochemical horizons that were successfully correlated, together with the calculated linear sedimentation rates between these points.

A similar strategy was employed for core CD3827, with the initial oxygen isotope derived timescale being slightly refined by further control points derived from chemical correlation with cores AII54-25PC and P6 (see section 4.6). The depths (cm) and ages (ka) of the control points in core CD3827 are given in table 4.2. This highlights some of the problems associated with age dating of cores by correlation with other cores, especially those which have been dated by different methods, namely; ^{14}C and $\delta^{18}O$ in the case of core P6 and AII54-25PC respectively. Although there is little doubt about the correlation using $CaCO_3$ and C-org between P6 and CD3827, there is the possibility of some error in the ^{14}C dating of core P6, which was done 14 years ago on bulk samples spanning several cm of sediment. However, in the absence of other age data, dates from the correlation of the $\delta^{18}O$ curves between core CD3827 and AII54-25PC are favoured in the development of an age model for CD3827, but ^{14}C dates are used only if they conform with the $\delta^{18}O$ stratigraphy. Thus the 11890 and 12730 yrs B.P. ages at 80cm and 115cm respectively, are excluded from timescale development in core CD3827.

The timescale for core CD3822 was developed using only the $\delta^{18}O$ curve, by correlation with the $\delta^{18}O$ profile in core AII54-25PC . The depths (cm) and ages (ka) to the control

horizons, together with the calculated linear sedimentation rates between the control points are given in table 4.3.

The oxygen and chemical data from core CD3814 are such that no sensible timescale could be achieved. This is probably the result of a combination of the sediment suffering winnowing, washing, periodic mass transport and slumping. Consequently discussion of core CD3814 in subsequent chapters is minimal.

4.5 CARBON ISOTOPE STRATIGRAPHY

4.5.1 Introduction

Carbon isotope determinations on biogenic carbonate were analysed in parallel with oxygen isotope analysis (appendix A.3). Variations in the measured $^{13}C/^{12}C$ ratio ($\delta^{13}C$), relative to a standard, are the result of fractionation of the two isotopes during physical and chemical processes. As with oxygen isotopes, calcareous microfossils will overwhelmingly record the $\delta^{13}C$ signal of the surrounding water in their tests. The factors controlling the enrichment or depletion of either isotope are more complex and varied than with oxygen, but the main ones are summarised below:

1. Global changes in the rates of exchange of the ocean's carbon reservoir with the biosphere, soil and sediments.
2. Global or regional changes in surface water productivity.
3. Internal shifts in water-mass structure and circulation (basin-basin fractionation, oxygen minimum development).
4. Organism specific fractionation ("Vital Effects").
5. Oceanic temperature variations and gradients

Generally, parallel long-period signals for planktonic and benthic data reflect external (global) fractionation, whereas short term variations are usually due to internal influences (water-mass fractionation, surface water productivity), (after Berger and Vincent, 1986).

As a result of the varied, often highly localised effects on the $\delta^{13}C$ signal, carbon isotope stratigraphy is more difficult to interpret than $\delta^{18}O$ for chronostratigraphic development. Despite these problems, $\delta^{13}C$ stratigraphy can be useful in a corroboratory role, especially if there are major shifts in the signal. However, $\delta^{13}C$ is perhaps more

commonly used in the reconstruction of palaeoenvironments and past global carbon budgets especially in relation to productivity changes and atmospheric CO_2.

4.5.2 The $\delta^{13}C$ Curves

The $\delta^{13}C$ curves versus depth (cm) for core CD3822, CD3826 and CD3827, together with the $\delta^{13}C$ profile versus age (ka) for core AII54-25PC, are shown in figure 4.7. The profile of core AII54-25PC shows some distinctive large scale variations (cyclicity), especially towards the base of the core, which are probably due to changes in the global carbon isotope budget. It is difficult to correlate $\delta^{13}C$ excursions of core AII54-25PC with any of the CD38 cores except in the upper parts. The excursion in stage II to lower $\delta^{13}C$ values, observed in core AII54-25PC, is present in cores CD3822 and CD3826, but not in core CD3827. This may be due to the local effects of productivity, water mass fractionation and proximity to a continent (terrigenous carbon source), experienced by core CD3827. Although there is an excursion to lower $\delta^{13}C$ values in the upper part of core CD3827 (50-100cm), it is not believed to be stage II because of the $\delta^{18}O$ profile (discussed above) and the ages derived from geochemical correlation with well dated nearby cores (see section 4.6). As a result of such difficulties in correlation, no control points were obtained by $\delta^{13}C$ stratigraphic correlation. Consequently, the $\delta^{13}C$ profiles versus age (ka) for the CD38 cores (figure 4.8) have timescales developed from the other methods discussed in this chapter.

4.6 CHEMICAL CORRELATION

4.6.1 Introduction

Chemical correlation with well dated, nearby cores P6 and AII54-25PC, was employed either to achieve (in the absence of radiocarbon dates or isotope ages) or refine the age models of the different cores. Both core P6 and AII54-25PC are located in the Panama basin (figure 1.1), the former being collected during the same cruise as core P5 (R.R.S. Shackleton, 1976), and the latter was recovered by the University of British Columbia. Data for P6 was obtained from Pedersen (1979), and for AII54-25PC from Pedersen (1991, pers comm.).

Below is a summary of how each core was correlated, to the nearby dated core, using a technique often described as "geochemical fingerprinting".

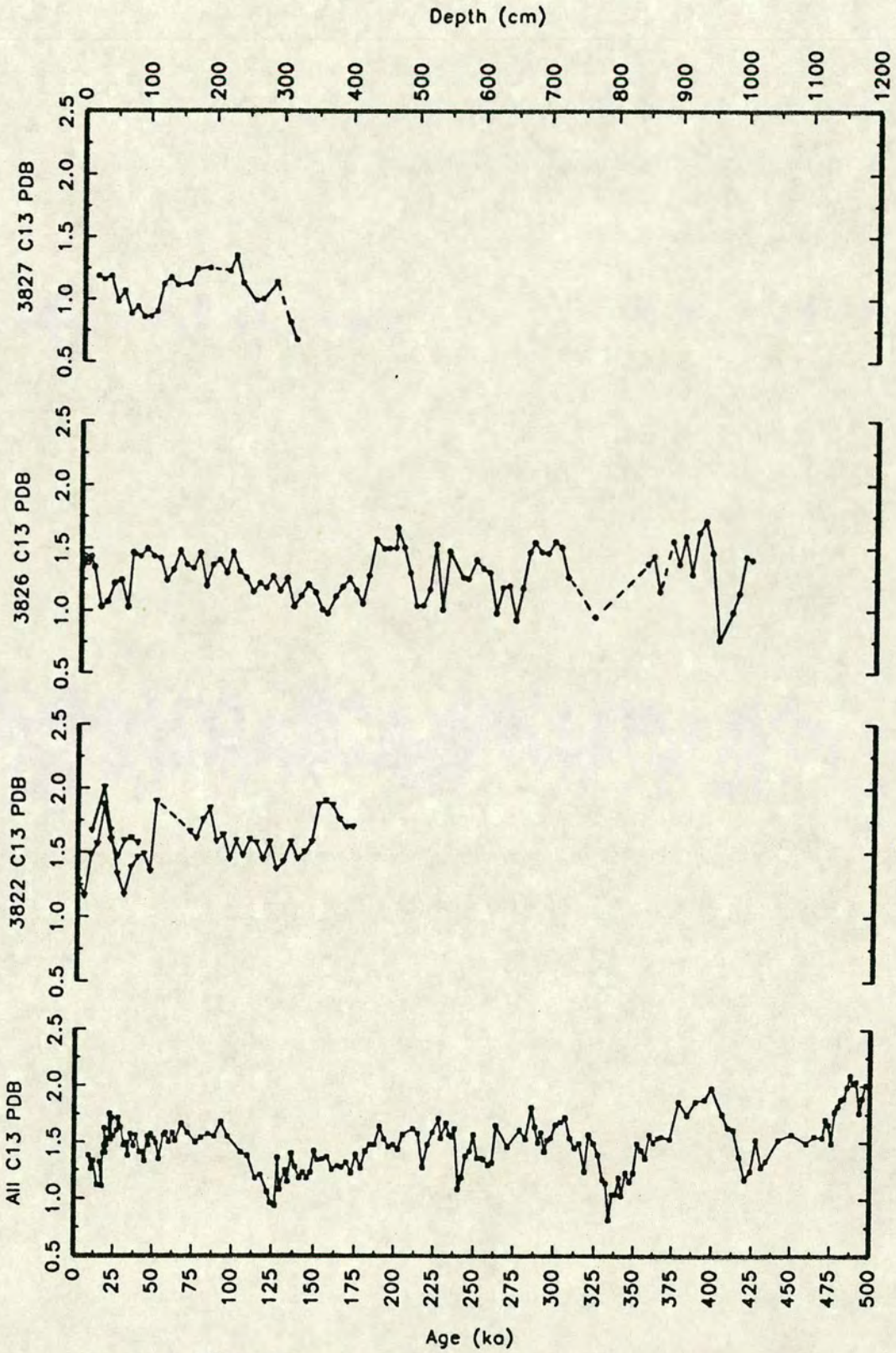

Figure 4.7 $\delta^{13}C$ PDB curves versus depth (cm) for cores CD3822, CD3826 and CD3827 together with the d13C PDB profile of core AII54-25PC versus age (ka). Hollow symbols in cores CD3822 and CD3826 represent data from pilot cores; filled symbols data from main piston core.

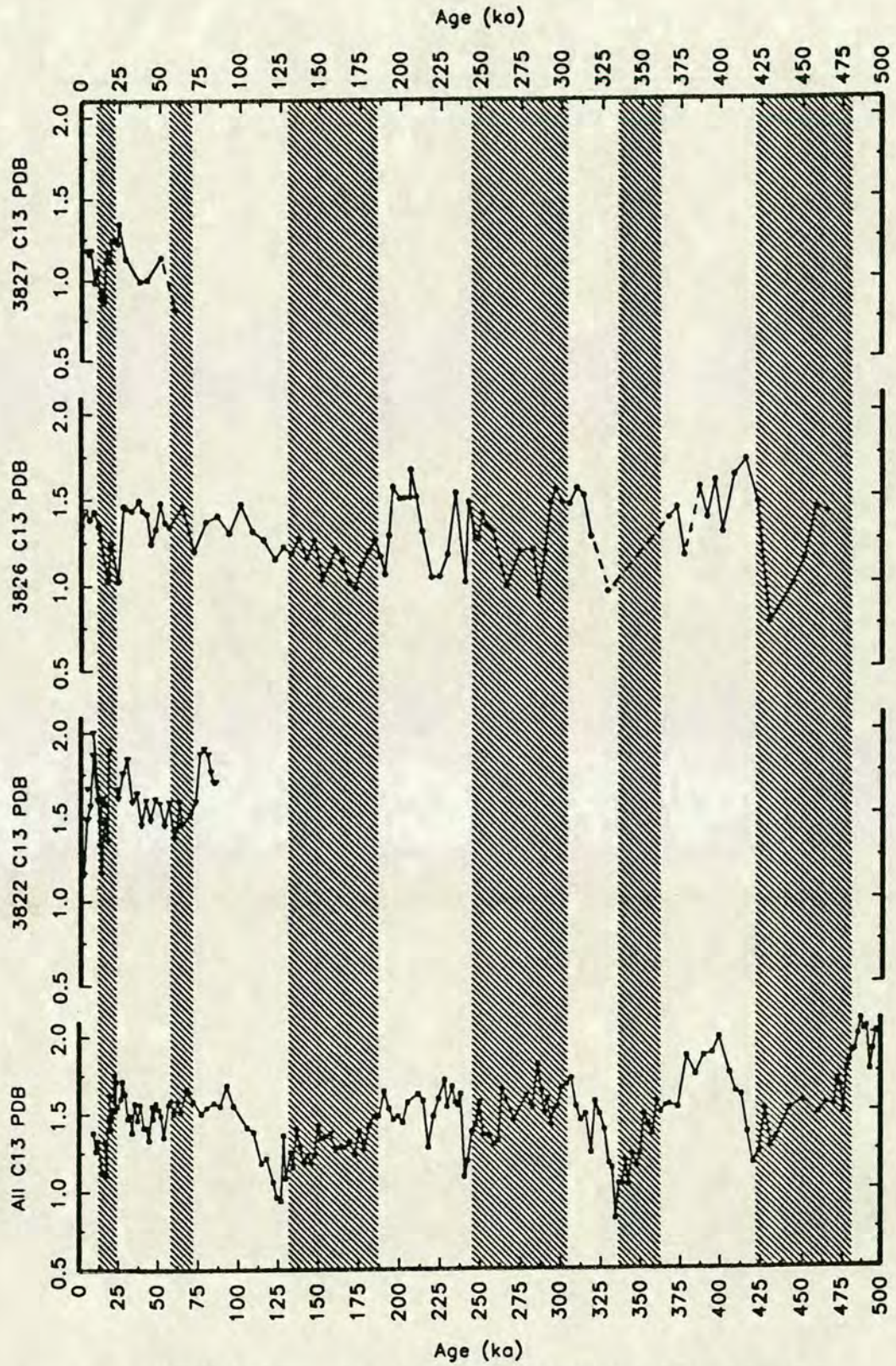

Figure 4.8 $\delta^{13}C$ PDB curves for cores AII54-25PC, CD3822, CD3826 and CD3827 versus age (ka). shaded regions represent glacial stages II, IV, VI, VIII, X and XII. Hollow symbols in cores CD3822 and CD3826 represent data from pilot cores; filled symbols data from main piston core.

4.6.2 Geochemical Fingerprinting

P5 is a short core, recovered less than 200 km south-west of core P6 (figure 4.4) and, although P5 is situated on the Carnegie ridge whilst P6 is in the basin, some elements of their chemistries still match. Figure 4.9 shows $CaCO_3$, C-org, Ti/Al, Si/Al and Fe/Al curves for both cores, together with the radiocarbon dated correlated horizons. The correlation between the two cores using C-org and $CaCO_3$ is quite poor, mainly as a result of the extremely high $CaCO_3$ and low C-org in P5. Consequently, the C-org signal is very noisy and susceptible to influence by slight fluctuations in the $CaCO_3$ which dominates the sediment. However, some correlation has been attempted, and dates are shown on figure 4.9 and in table 4.3. Such problems highlight the difficulties in age model development. The Ti/Al profiles show some degree of correlation and an age of 15500 yrs B.P. has been inferred for the lower spike at around 100cm depth. Fe/Al and Si/Al give by far the best correlation with both elements showing considerable enrichment, relative to Al, at around 45 cm depth. The spike at 11890 yrs B.P. was interpreted by Pedersen (1979) as a hydrothermal pulse, and the fact that Si and Fe correlate in core P5 seems to corroborate this hypothesis. A fourth control point, at 24 ka (121cm), was included to extend the timescale to the base of the core. The position of this horizon, which is to some degree conjectural, is where the $CaCO_3$ record begins to decrease sharply presumed to be the base of glacial stage II, as observed by previous workers (Arrhenius, 1952; Berger, 1973; Adelseck and Andersen, 1978). These three control points allowed the development of a relatively crude timescale (see below) for core P5.

Chemical correlation of CD38 cores were made against cores P6 and AII54-25PC. Using CD3826 as a template for CD38 cores, geochemical maxima and minima in the depth domain from CD3826 were matched to corresponding geochemical maxima and minima in the time domain in AII54-25PC (figure 4.10 and 4.11), which allowed determination of dated control points in CD3826 in addition to the isotopically derived dated control points. Table 4.1a shows that the correlation between the cores was especially good with $CaCO_3$ (with 12 control horizons), and acceptable using Ba/Al, Zn/Al, Ti/Al, Ni/Al and Cu/Al. Linear accumulation rates between control points (age picks) were again assumed, giving sedimentation rates between each dated horizon (table 4.1b), and ages to each 10 cm sample depth throughout the core.

Geochemical correlation of CD3827 was achieved with core P6 and core AII54-25PC using $CaCO_3$ and C-org profiles (figure 4.12). Both these components showed good

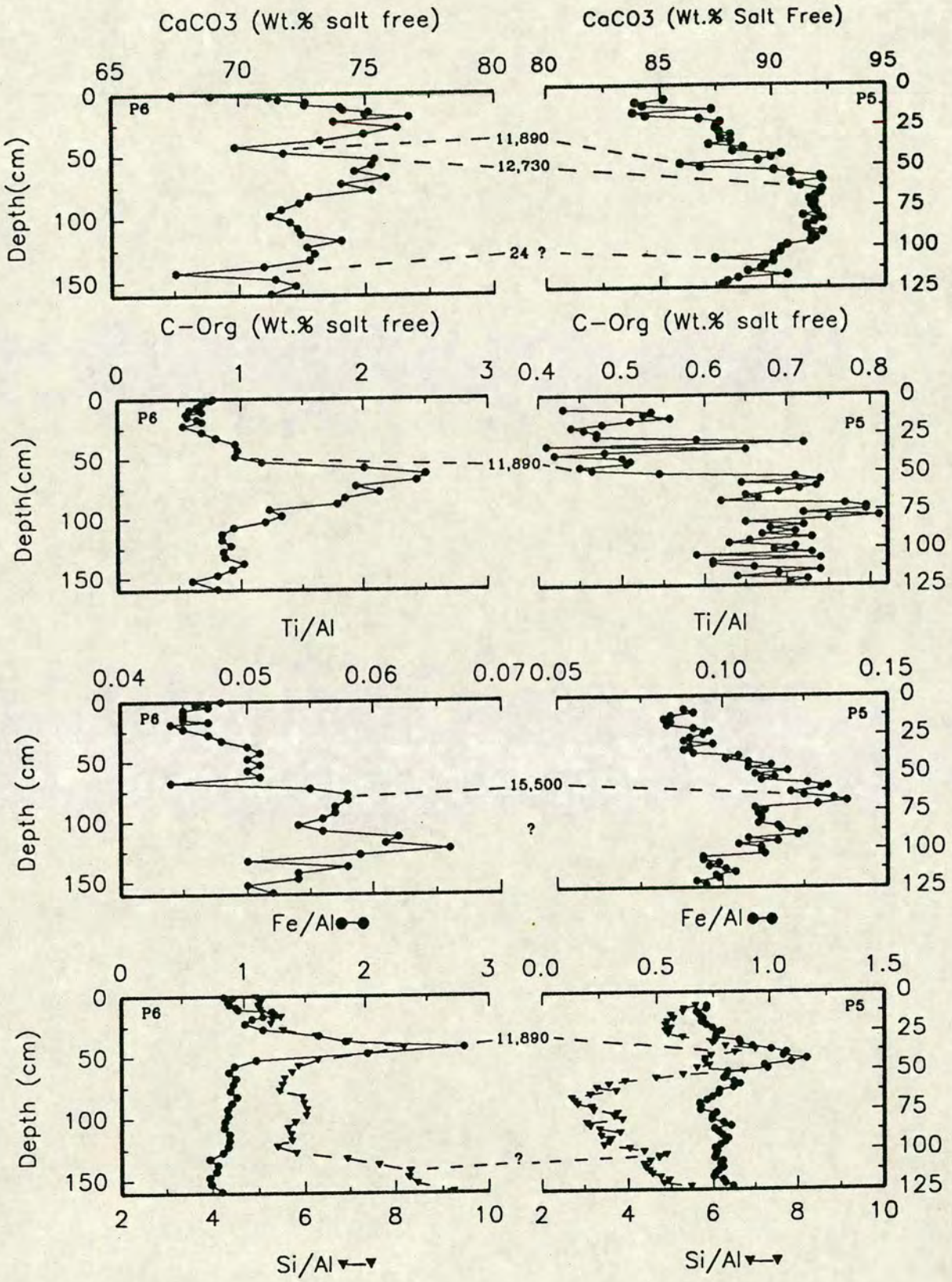

Figure 4.9 Chemical correlation between core P5 (graphs on right) and the radiocarbon dated P6 (graphs on left). Age of correlated horizons are derived from dates in core P6.

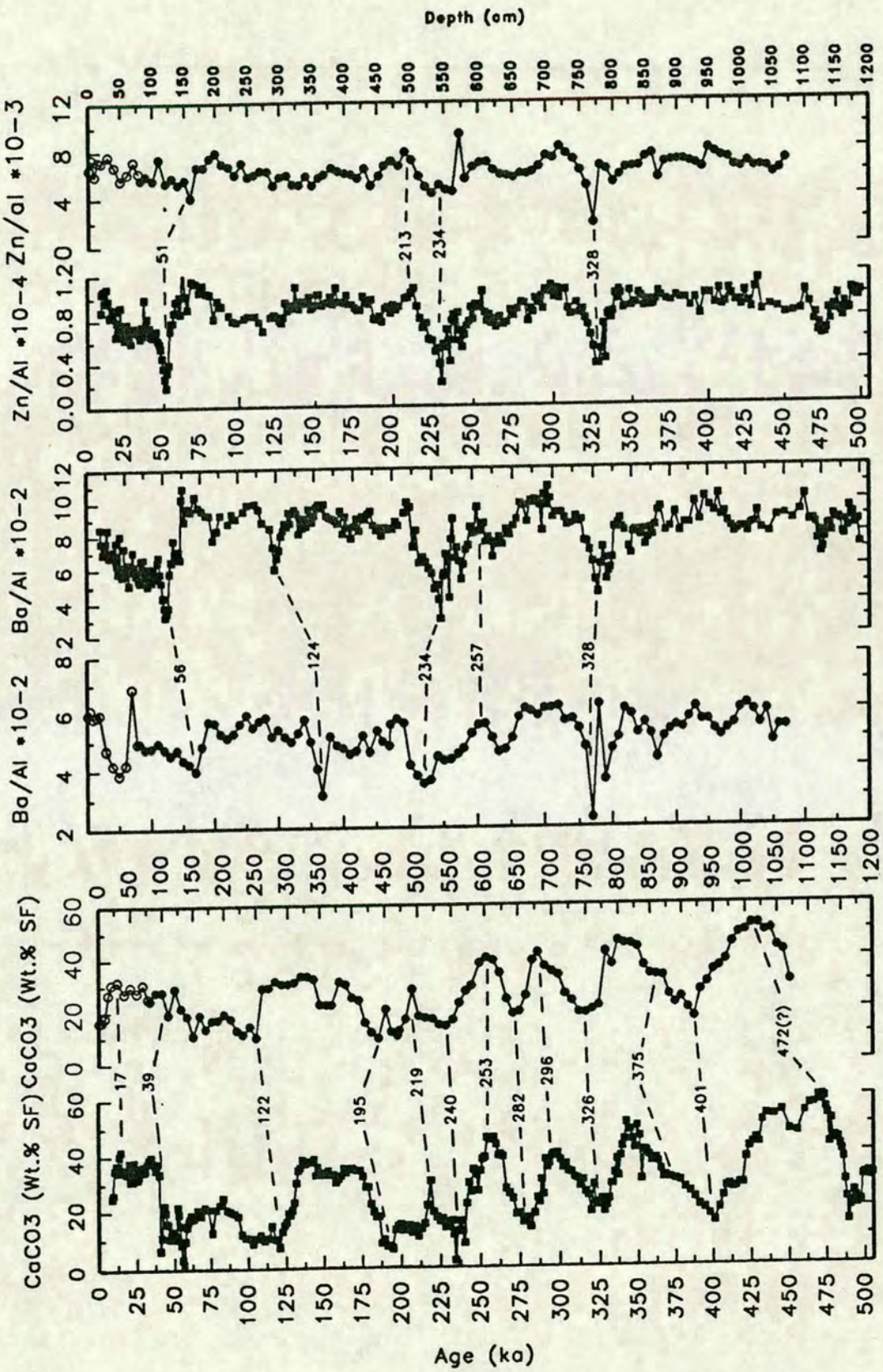

Figure 4.10 Chemical correlation between the $CaCO_3$, Ba/Al × 10^{-2} and Zn/Al × 10^{-4} profiles of cores AII54-25PC and CD3826. Ages of correlated horizons derived from the well constrained age model of AII54-25PC.

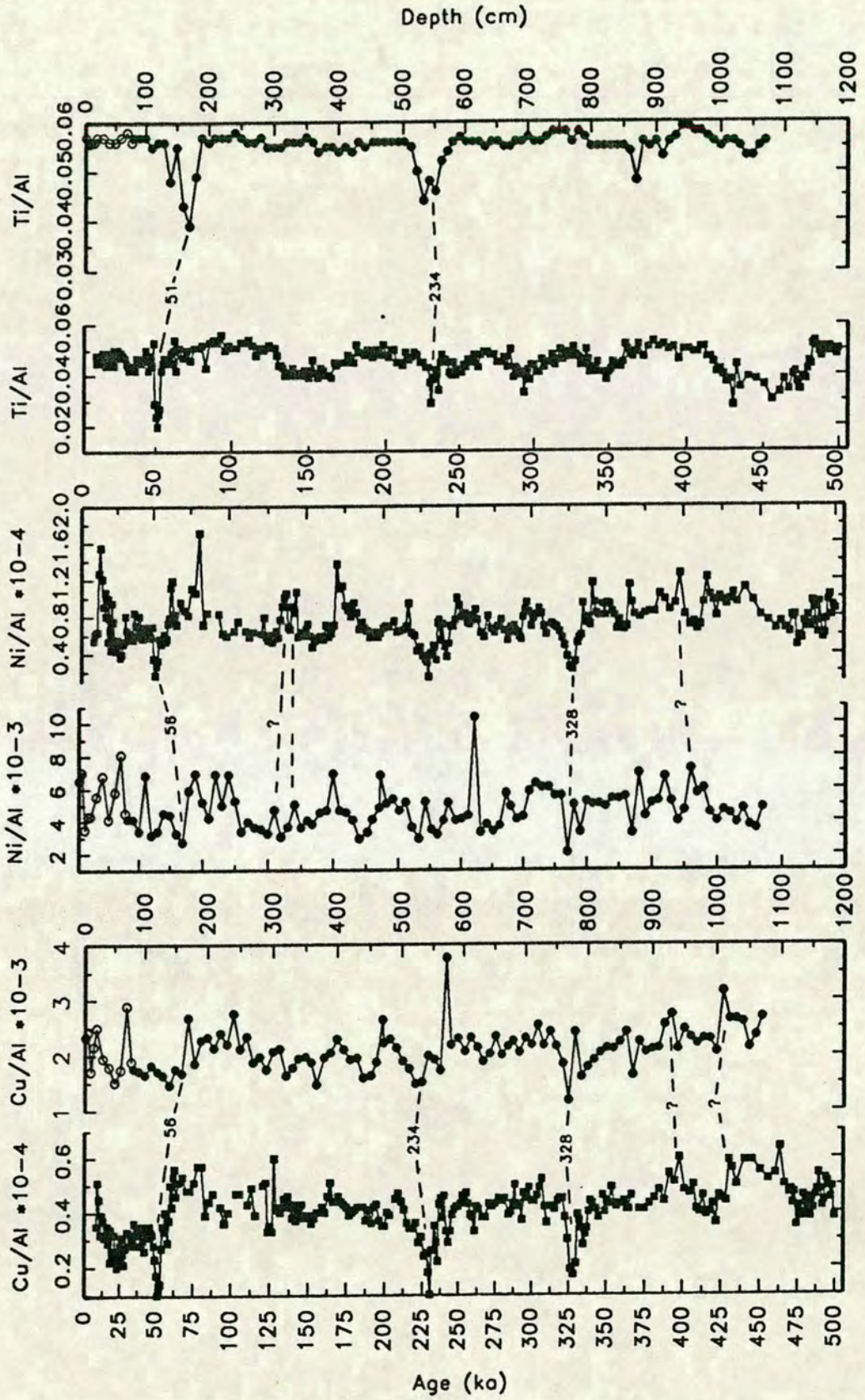

Figure 4.11 Chemical correlation between the Cu/Al x 10^{-4}, Ni/Al x 10^{-3} and Ti/Al profiles of cores AII54-25PC and CD3826. Ages of correlated horizons derived from the well constrained age model of AII54-25PC.

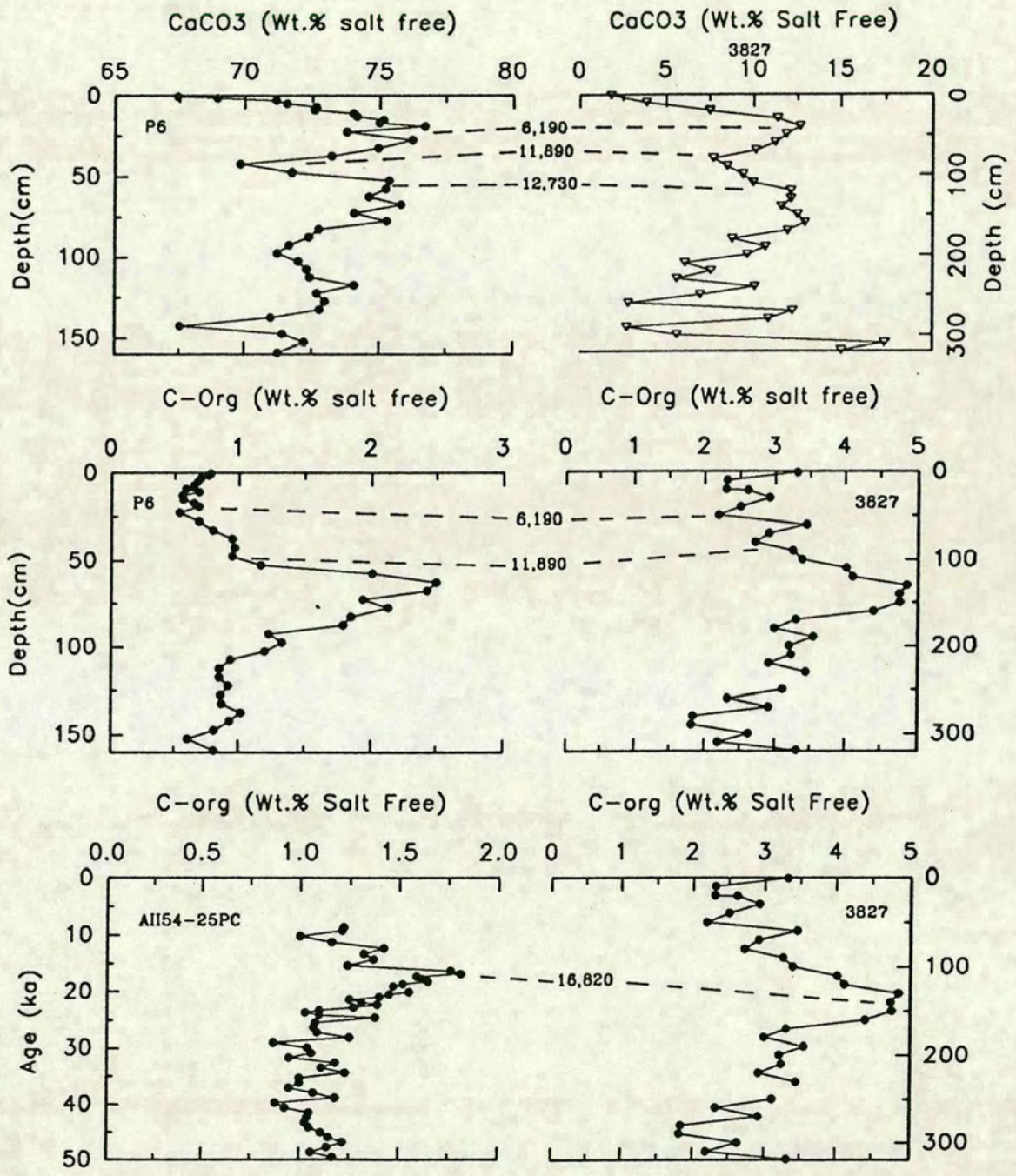

Figure 4.12 Chemical correlation between core P6 and CD3827 (top and middle plots) and, between the last 45 ka of core AII54-25PC and the whole of core CD3827 (bottom plot). Dates derived from radiocarbon ages of P6 and isotope timescale of AII54-25PC.

Table 4.1a. CD3826 Oxygen Isotope stratigraphy and geochemistry versus AII54-25PC isotope chronostratigraphy and geochemistry. Bold text refers to depths and ages derived by comparison of CD3826 and AII54-25PC isotope curves. Numbers in parentheses are uncertain and not used in age model development.

Depth (cm) in CD3826	Estimated age from correlation of $\delta^{18}O_{PDB}$ CD3826 with AII54-25PC $\delta^{18}O$ profile	Estimated age from correlation of CD3826 geochemistry to AII54-25PC geochemistry.					
	$\delta^{18}O$	$CaCO_3$	Ba/Al	Zn/Al	Ti/Al	Ni/Al	Cu/Al
30		17					
65	**19.5**						
110		39					
170			56	(51)	(51)	56	56
180	**64**						
260	**122**	122					
320	**152**						
405	**186**						
442		195					
482			(209)				
492				213			
502		219					
532				234	234		234
532	**234**						
542		240					
567	**245**						
602		253					
612			257				
642		282					
680		296					
750		326					
770			328	328		328	328
860		(375)					
920		401					
1020		472					

Table 4.1b Depths and ages of control points together with sedimentation rates between them in core CD3826. Numbers in parenthesis are uncertain and were not used in the calculation of sedimentation rates or age model development. Bold text refers to correlation using $\delta^{18}O$ horizons.

Depth (cm)	Age Pick (ka)	Sedimentation Rate (cm/kyrs)
		1.76
30	17	
		14.00
65	**19.5**	
		2.31
110	39	
		3.53
170	56	
		0.80
180	**64**	
		1.38
260	**122**	
		2.00
320	**152**	
		2.50
405	**186**	
		4.11
442	195	
(482)	(209)	2.78
492	213	
		1.67
502	219	
		2.00
532	**234**	
		1.67
542	240	
		5.00
567	**245**	
		4.37
602	253	
		2.00
612	257	
		1.20
642	282	
		2.71
680	296	
		2.33
750	326	
		10.00
770	328	
(860)	(375)	2.05
920	401	
(970)	(440)	1.41
1020	472	

Table 4.2 CD3827 Oxygen Isotope Stratigraphy and Geochemistry versus P6 geochemistry and radiocarbon dates and, AII54-25PC geochmistry and stable isotope chronostratigraphy.

Depth(cm) in CD3827	**Estimated Age from $\delta^{18}O_{PDB}$ CD3827 Versus the AII54-25PC $\delta^{18}O$ profile**	*Estimated Age from CD3827 geochemistry Vs. the dated P6* and AII54-25PC geochemistry		
	$\delta^{18}O$	*$CaCO_3$*	*C-org*	C-org
40		*6190*	*6190*	
70	**12**			
(80)		*(11890)*	*(11890)*	
(115)		*(12730)*	*(12730)*	
140				16.82
170	**19.48**			
230	**24**			
310	**59**			

Bold text refers to ages achieved by correlation of $\delta^{18}O$ curves between CD3827 and AII54-25PC: italiced text to ages from geochemical correlation between CD3827 and P6: normal text to ages from correlation of organic carbon (C-org) curves between CD3827 and AII54-25PC. Numbers in parentheses were not used in the development of the age model.

TABLE 4.3 Depths and ages of control points together with sedimentation rates between them in cores CD3822 (a), CD3827 (b) and P5 (c). No. in parentheses not used in age model development.

(a) CD3822

Depth (cm)	Age Pick (ka)	Sedimentation Rate (cm/kyrs)
0	0	
		5.00
40	8	
		3.75
55	12	
		10.67
119	18	
		10.17
180	24	
		3.43
300	59	
		6.00
330	64	
		2.14
345	71	
		3.89
380	80	
		6.00
440	90	

(b) CD3827

0	0	
		6.46
40	6.19	
		5.16
70	12.00	
(80)	(11.89)	
		14.52
(115)	(12.73)	
140	16.82	
		11.28
170	19.48	
		13.27
230	24	
		2.29
310	59	

(c) P5

0	0	
		3.62
43	11.89	
		16.67
57	12.73	
		11.55
89	15.50	
		3.76
121	24	

correlation, allowing the determination of several dated control points (table 4.2). As with core CD3826, linear accumulation rates between dated horizons were assumed to develop the final age model for each 10 cm sample.

4.7 AGE VERSUS DEPTH RELATIONSHIPS

The conversion of data from the depth to time domains result in some sequences being expanded and some being condensed, depending on the rate of sedimentation during that period. This can be seen in figure 4.6 which shows the $\delta^{18}O$ curves versus age (ka) for CD38 cores. The whole of core CD3827 (3 m) represents only approximately 50 ka, whereas stage 5 (57 ka) in core CD3826 is represented by only about 80 cm. The variations in sedimentation rate are most clearly illustrated by age versus depth plots (figure 4.13 and 4.14). Changing sedimentation rates can be identified by variations in the gradient of the graph.

Core CD3826 shows a relatively constant sedimentation rate throughout the core, with the most marked changes occuring at around 70 ka and 250 ka (figure 4.13). The average sedimentation rate throughout the core at 2.16 cm/kyr is close to that of core AII54-25PC at 1.87 cm/kyr.

The depth versus age plot in core CD3827 (figure 4.13) shows similar sedimentation rates during interglacial periods I and III, but shows a marked increase in sedimentation rate during glacial stage II. The average sedimentation rate of core CD3827 at 5.25 cm/kyr is the highest of all the cores.

The age versus depth plot for CD3822 (figure 4.13) shows several changes in sedimentation rate, with glacial stage II again displaying a marked increase. Stage IV however, has a gradient similar to that of the interglacial periods. The mean sedimentation rate of core CD3822 at 4.89 is considerably higher than other cores, with the exception of CD3827.

Core P5 shows a marked increase in sedimentation rate towards the end of glacial stage II, and has an average sedimentation rate of 5.04 cm/kyr (figure 4.14).

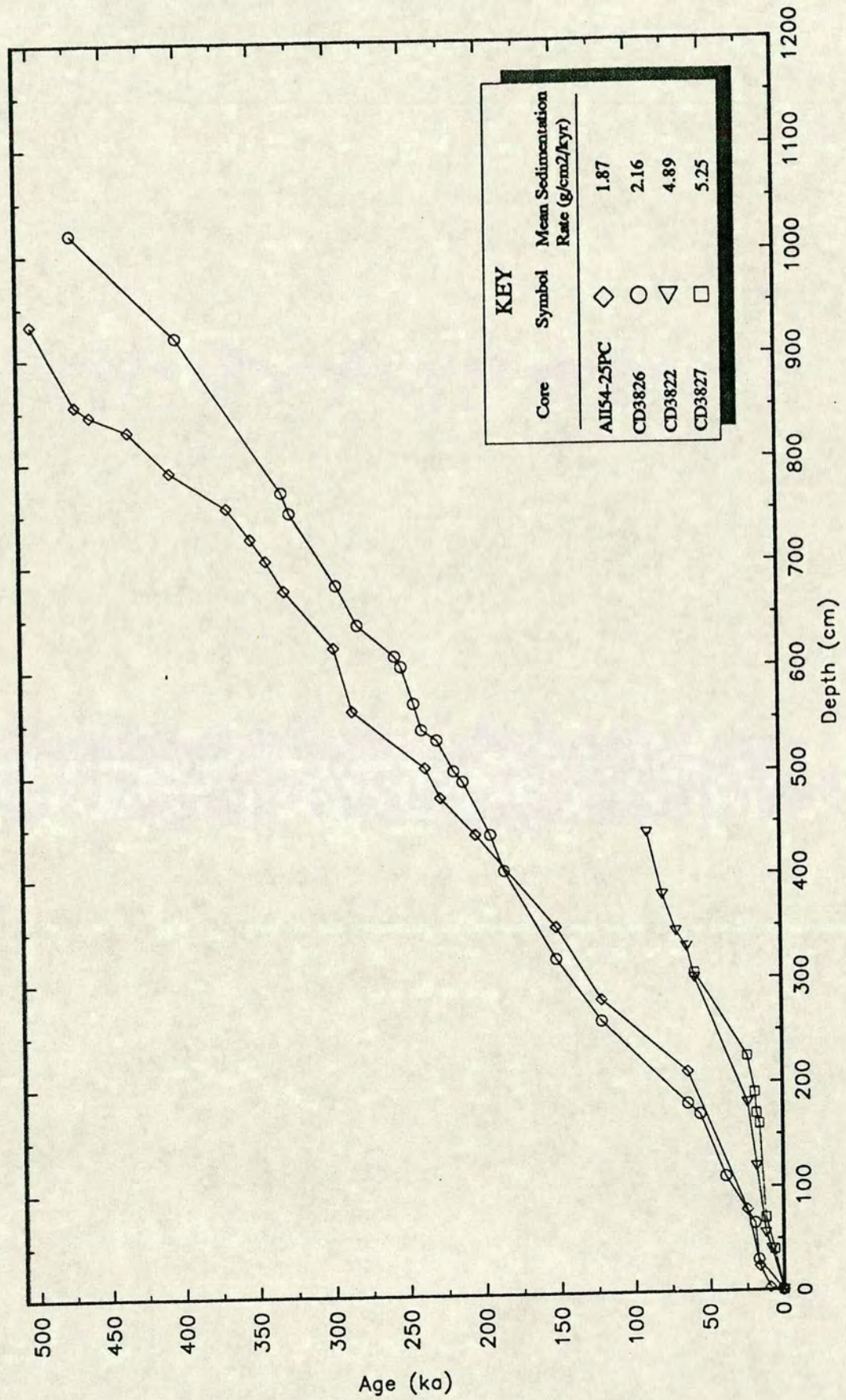

Figure 4.13 Age (ka) versus depth (cm) plot for core CD3822, CD3826, CD3827 and AII54-25PC. The straight lines between control points represents assumed linear sedimentation rates, the magnitude of which is denoted by the gradient of these lines. Mean sedimentation rates for each core are given in the key.

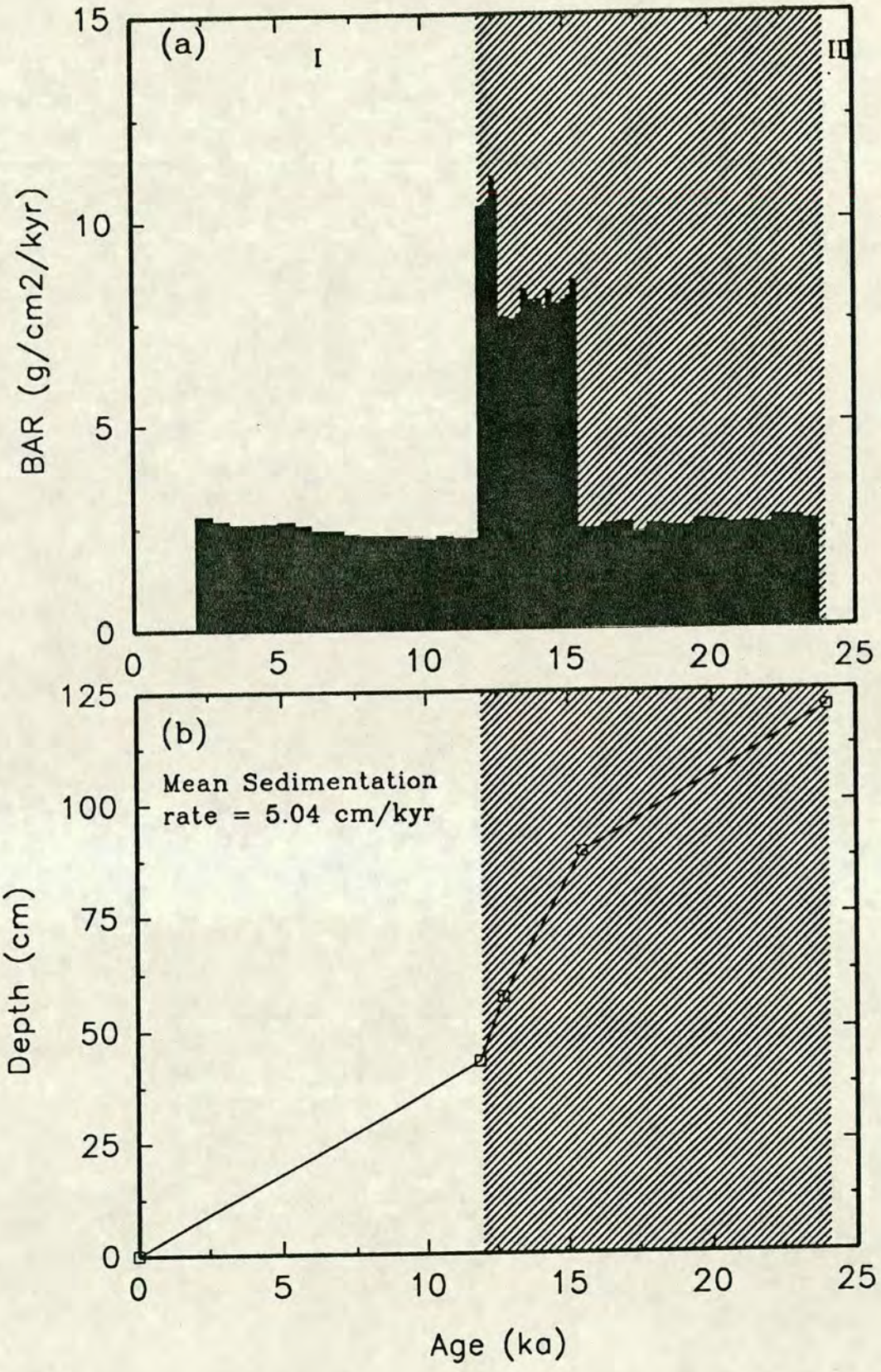

Figure 4.14 Accumulation rate changes in core P5 as illustrated by (a) bulk accumulation rate (g/cm^2/kyr) variations showing the sharp increase during the later part of stage II (shaded region) and, (b) depth (cm) versus age (ka) plot with straight lines representing assumed linear accumulation rates between control points.

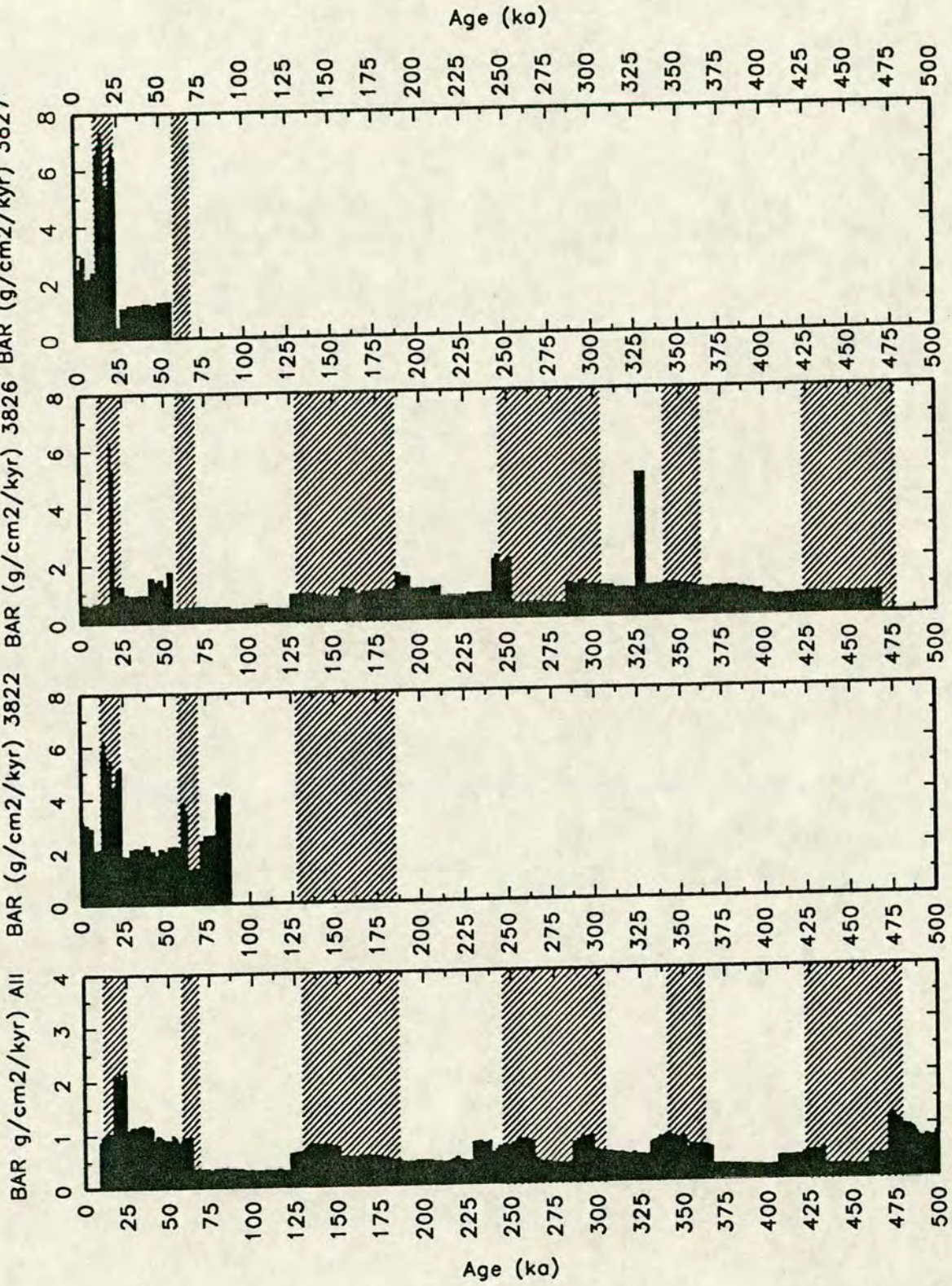

Figure 4.15 Bulk accumlulation rates (g/cm^2/kyr) versus age (ka) for cores AII54-25PC, CD3822, CD3826 and CD3827. Glacial stages are shaded. Note the different scales.

4.8 BULK ACCUMULATION RATES

The age models and sedimentation rates allow calculation of elemental fluxes, which will be discussed in chapters 5 and 7. However, to give a general indication of how bulk sediment accumulation rates have varied over time, rates have been calculated from equation 4.1 (given below), and expressed as bar charts in figures 4.14 and 4.15.

Equation 4.1 Bulk Accumulation Rate ($g/cm^2/kyr$) = DBD × S.R.

DBD = Dry bulk density (g/cm3)

S.R. = sedimentation rate (cm/kyr)

Generally, bulk accumulation rates are higher during glacial periods, with cores CD3822 and CD3827 having similar overall rates of accumulation. Both are considerably higher than in cores CD3826 and AII54-25PC. Core AII54-25PC has much lower overall bulk accumulation rates than the CD38 cores, which is slightly unusual and might be an artifact of different methods of dry bulk density and water content calculation.

CHAPTER 5

THE TERRIGENOUS AND HYDROTHERMAL FRAMEWORK

5.1 Introduction

This chapter illustrates the spatial and temporal variations in the terrigenous and hydrothermal components of the sediment, discusses their influence on other fractions of the sediment and relates them to climatic changes. Terrigenous material originates either from terrestrial sources or from the alterations of oceanic basalts and/or hydrothermal exhalations (McMurty and Yey, 1981; Bonatti, et al., 1983; Shaker, et al., 1987; Nath, et al., 1989). Terrigenous material is transported by a variety of mechanisms: atmospheric aerosols, river systems and ocean currents (see chapter 2 for an outline of these factors in the area). The element which has been shown to be exclusively associated with terrigenous matter is aluminium (Arrhenius, 1952; Bostrom, et al., 1969, Bostrom, 1973; Bischoff, 1979) and, as a result, it has been used as an indicator of clay detritus of terrestrial origin (Finney et al., 1988; Khan, 1989; Shimmield and Mowbray, 1991; Pedersen et al., 1991). Elemental ratios to Al are, therefore, discussed to illuminate changes in the terrigenous component of the sediment, and to corroborate the mineralogical (and grain size) studies of chapter 3. Records of terrigenous elements are often masked by the large variations that occur as a result of volcanic ash deposits as described in chapter 4. For this reason, data from these layers are often omitted to allow the underlying terrigenous trends in the data to emerge.

Correlation matrices are introduced in this chapter and are used throughout this thesis to assign statistical confidence to the correlation between "elements". Principl Component Analysis (PCA) however, is used as statistical proof of the groupings of "elements" into distinct phases. Calculations of confidence limits on the correlation coefficients are shown in appendices A.10 and on the correlation matrices (tables 5.5-5.9). As was mentioned in chapter 4, only the Pleistocene section of core CD3822 is used in diagrams and discussions of this core. However, all the data from core CD3822 is used in the statistical analysis mentioned above.

Analyses were carried out using XRF spectrometry (see appendix A.5) and results are given in Appendix C. Elemental concentrations were corrected for the dilution and contribution effects of residual sea-salt by a method detailed in Appendix A.7. A technique to corroborate the salt correction factors was developed using chloride concentrations (analysed by H.P.L.C.) as the basis of calculating the salt contents (see appendix A.7.2). All data in this thesis are corrected for the effects of sea salt, unless otherwise stated.

5.2 MAJOR ELEMENTS OF THE TERRIGENOUS AND HYDROTHERMAL FRAMEWORK

5.2.1 Silicon

Introduction

Si in marine sediments is composed of varying proportions of aluminosilicates, quartz and biogenic SiO_2 (opal). Cores recovered close to a continental margin, in waters of low biological productivity, tend to be high in terrigenous aluminosilicates, whereas sediments from the open ocean which underlie waters of high biological productivity are often high in biogenic siliceous remains.

The concentration of Si in sediments from the eastern equatorial Pacific varies widely (Arrhenius, 1952; Pisias, 1976; Pedersen, 1979; Murray et al., 1987; Lyle et al., 1988). In upwelling zones (eg off the Peru-Chile coast) siliceous material may constitute up to 60% of the dry weight of the sediment. In contrast, on topographic highs, which are often dominated by $CaCO_3$ material, Si contents may be very low.

Si_{terrig}-Al Relationships

In order to remove the contribution of biogenic silica (opal) from the total Si (Si_{tot}) content of the sediments, biogenic silica concentrations (see chapter 6) were subtracted from Si_{tot} to give a terrigenous Si (Si_{terrig}) value for cores CD3822, CD3826, CD3827 and P5. Biogenic SiO_2 was not determined for core CD3814 since Si_{tot} values in this core are generally less than 1% (appendix C.1.2), making partitioning between the two different Si phases difficult. Thus, the Si values for core CD3814 are Si_{tot} (salt free). No age model for core CD3814 is available (chapter 4), therefore no temporal interpretation was possible. However, one can conclude that much of the aluminosilicate material originally deposited in this core has been subsequently winnowed/washed out by bottom currents. The relationship between Si (terrigenous) and Al in cores studied in this thesis is illustrated in figure 5.1.

According to Turekian and Wedopohl (1961) the world average Si/Al ratio in sedimentary aluminosilicates (deep-sea clay) is around 3.0. A ratio greater than this must represent excess Si in the form of either biogenic SiO_2 or unusual quantities of detrital quartz. It is clear from table 5.1 that only core CD3822 has mean whole core

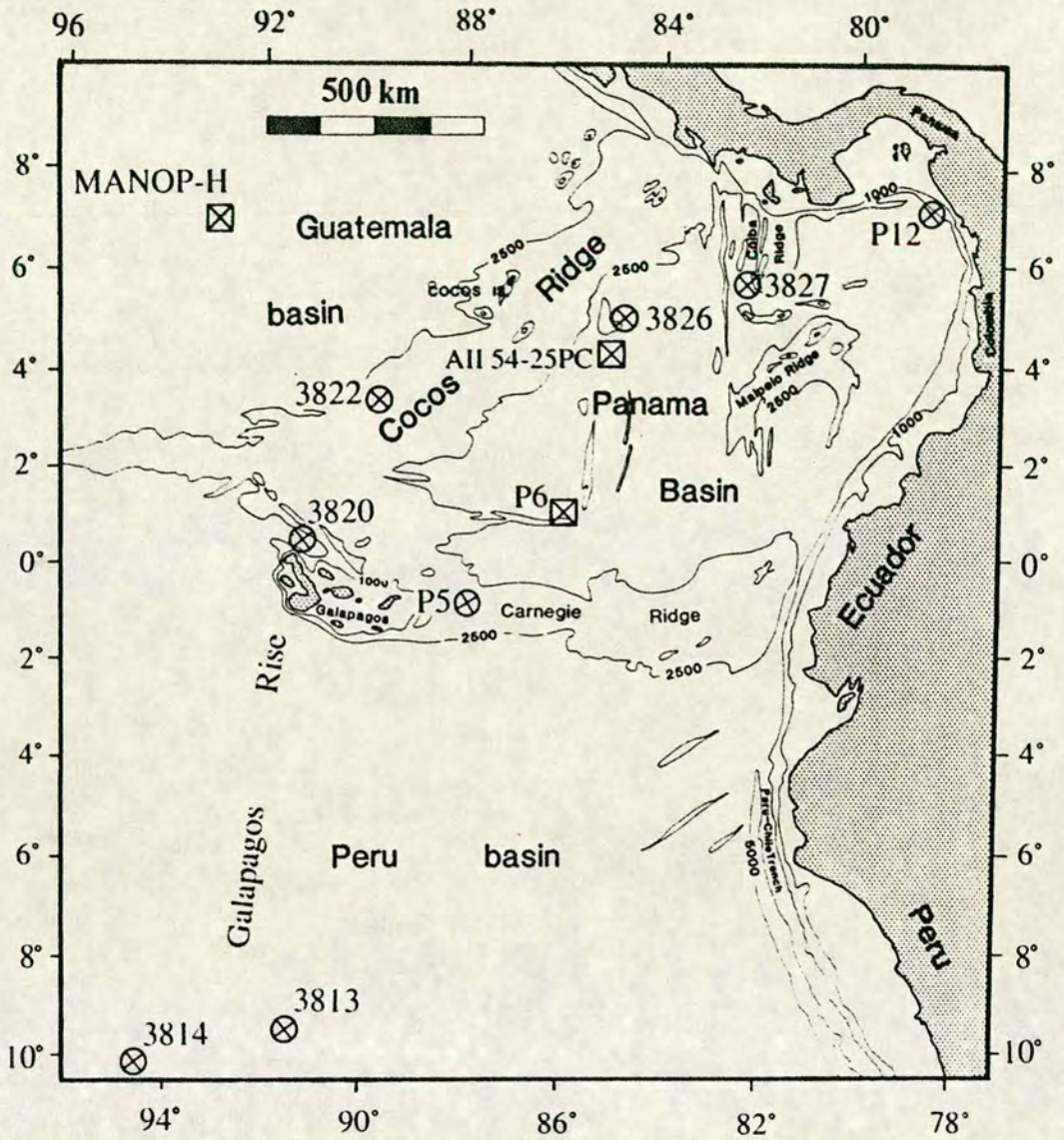

Figure 5.0 Location map of cores studied in this thesis.

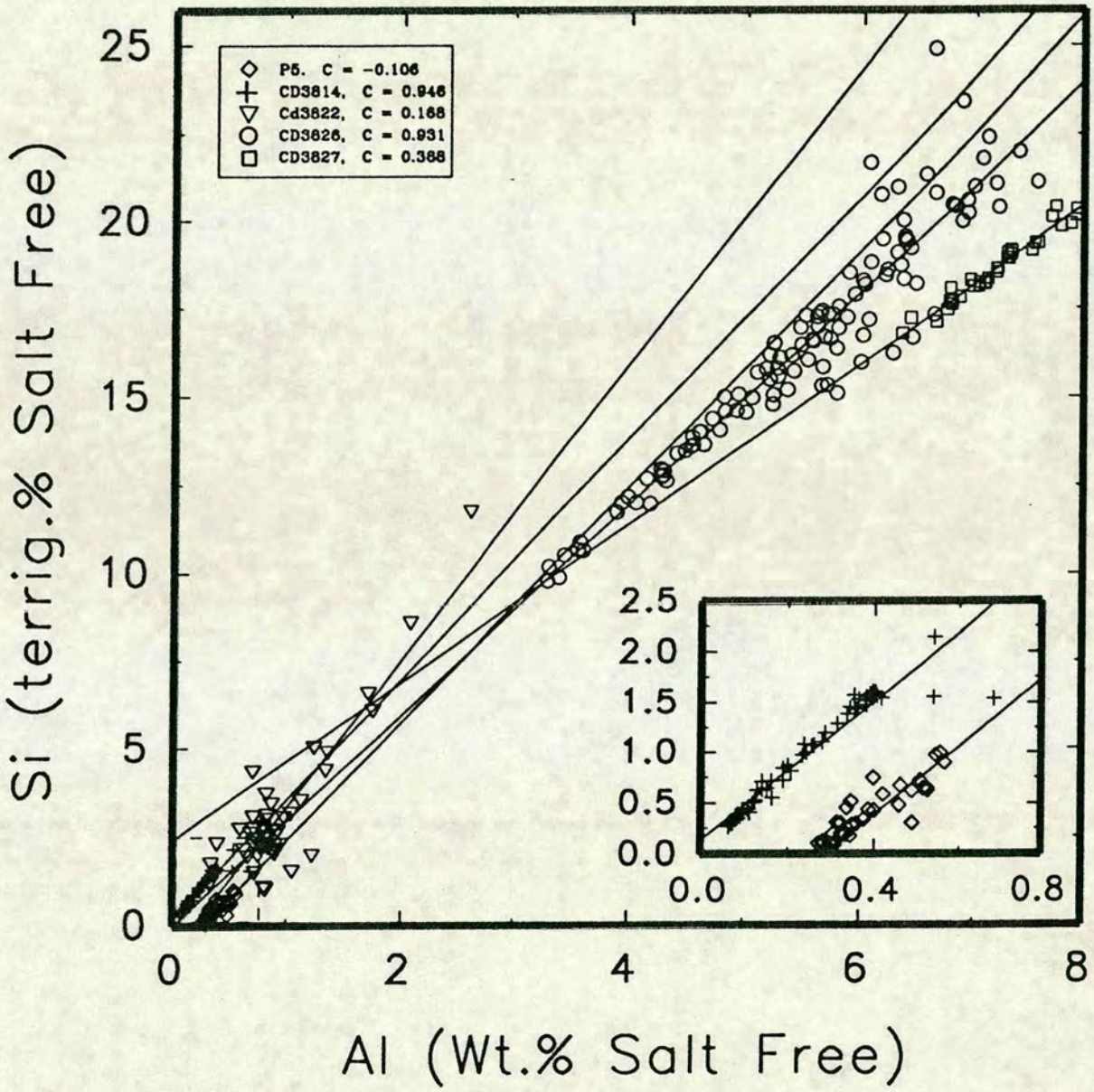

Figure 5.1 Diagram illustrating the relationship between Si_{terrig} and Al from cores studied in this thesis. Inset graph is a detail of the main plot at the lower end of the scale and shows only data from cores CD3814 and P5.

Si_{terrig}/Al values in excess of the world average while the average of all other cores in this study is below the global mean value of Turekian and Wedophol (1961). CD3814 has Si_{tot}/Al values greater than 3.0 but these are meaningless in terms of terrigenous material and are probably the result of repeated washing of the sediment by bottom currents causing loss of the finer grain-sized aluminosilicates. The excess in core CD3822 probably results from several aluminosilicate sources (eg aeolian dust, sorption onto biogenic particles and pluming of shelf sediment into the deep ocean.

Core CD3827 has an intercept on the Si_{terrig} axis (figure 5.1), which may be the result of a high content of Si in aluminosilicates or detrital quartz. One might expect core CD3827 to have the greatest Si/Al ratio due to its position proximal to the continental landmass of Central America (figure 5.0) and for the Si_{terrig}/Al ratio to have decreased with increasing distance from land, but this is clearly not the case (table 5.1). The Si_{terrig} and Al in core CD3826 display a strongly linear relationship (C=0.931) with the regression line intercepting the origin which indicates that there is no Si_{terrig} in excess of that normally bound in deep-sea clays (figure 5.1). Core P5 has a very low concentration of both Si_{terrig} and Al but does show a reasonable regression line intercepting the Al axis at around 0.25% Al. This may be an artifact of the calculation of Si_{terrig} from Si_{tot}-$Si_{biogenic}$ (Opal) as some slightly negative values were produced (Appendix C.4.5.3)

Downcore Variations in Si_{terrig}

Temporal profiles of Si_{terrig}/Al are shown in figure 5.2 and 5.3a. Generally, Si_{terrig}/Al values are close to the world average of 3.0 (Turekian and Wedopohl, 1961; see table 5.1), with cores P5 and CD3827 showing a significant depletion of Si_{terrig} relative to Al and core CD3814 displaying significant enrichment of Si_{tot} relative to Al. Surficial sediments appear to be relatively depleted in Si_{terrig} relative to Al compared to older sediments except in core CD3814. A striking characteristic of the profiles is the wide variation in the degree of change in the Si_{terrig}/Al ratio within and between cores. The Si_{terrig}/Al ratio of core CD3822 varies from around 1 to close to 7; whereas in core CD3827 the ratio only changes by about 0.2 throughout the core.

Core P5 has Si_{terrig}/Al values that are negative which, as suggested above, is probably an artifact of the calculation of Si_{terrig} from Si_{tot}-$Si_{biogenic}$. This is likely

CORE	DEPTH/A	Si/Al	Fe/Al	Mg/Al	K/Al	Ti/Al	Fe/Ti	Cr/Al X10-4	Zr/Al X10-4	Cr/Zr
	9-55	1.11	0.85	0.58	0.17	0.097	8.79	24.18	21.39	1.12
P5	57-101	-0.60	0.77	0.68	0.15	0.119	6.52	33.50	26.05	1.29
	103-123	0.50	0.78	0.71	0.16	0.099	7.97	22.78	23.42	0.97
	WC	0.32	0.81	0.65	0.16	0.106	7.74	27.61	23.62	1.16
	0-2	4.20	1.79	0.78	0.24	0.081	22.17	18.90	50.63	0.37
CD3814	0-310	3.97	1.02	0.44	0.26	0.071	14.63	9.83	49.81	0.20
	320-650	4.12	1.44	0.85	0.28	0.101	15.45	7.94	74.20	0.12
	WC	4.09	1.26	0.66	0.27	0.086	15.06	9.18	58.42	0.20
	0-2	2.42	0.80	0.29	0.17	0.054	18.84	10.28	22.55	0.46
	I	2.52	0.73	0.29	0.19	0.049	15.00	11.11	25.29	0.45
CD3822	II	2.68	0.73	0.33	0.21	0.052	14.22	16.49	23.52	0.71
	III-IV	3.37	0.81	0.34	0.27	0.049	16.55	15.10	22.28	0.68
	WC	3.07	0.73	0.31	0.25	0.048	15.26	14.62	26.40	0.58
	0-2	2.59	0.73	0.27	0.13	0.057	12.84	13.09	12.93	1.01
	I	2.63	0.74	0.27	0.13	0.056	13.14	14.32	13.01	1.10
	II	2.86	0.76	0.36	0.16	0.057	13.36	15.35	13.17	1.17
	III-IV	3.15	0.68	0.29	0.20	0.052	13.09	13.93	12.37	1.12
	V	2.93	0.74	0.33	0.17	0.057	13.04	14.41	12.96	1.11
CD3826	VI	2.99	0.71	0.33	0.18	0.056	12.82	15.50	13.17	1.18
	VII	3.05	0.71	0.30	0.20	0.053	13.27	13.32	13.35	1.01
	VIII	3.01	0.74	0.34	0.18	0.056	13.29	15.40	13.22	1.17
	IX	3.07	0.68	0.32	0.20	0.057	11.88	13.54	16.87	0.92
	X	3.00	0.73	0.32	0.20	0.055	13.18	15.28	14.16	1.08
	XI	2.95	0.74	0.34	0.18	0.055	13.38	14.46	12.52	1.15
	WC	3.00	0.72	0.32	0.19	0.055	13.02	14.51	13.50	1.09
	0-2	2.53	0.69	0.23	0.12	0.062	11.15	14.37	10.81	1.33
	I	2.57	0.67	0.25	0.13	0.062	10.81	16.14	11.07	1.46
CD3827	II	2.59	0.70	0.23	0.15	0.063	11.18	17.36	11.29	1.54
	III	2.62	0.69	0.23	0.15	0.063	11.18	17.06	11.02	1.55
	WC	2.60	0.69	0.24	0.14	0.062	11.10	16.97	11.18	1.52
This study 0-2 Mean		2.51	1.00	0.39	0.17	0.063	15.25	14.16	24.23	0.79
This study WC Mean		2.82	0.84	0.44	0.20	0.071	12.44	16.58	26.62	0.91
Mean Deep Sea Clay*		2.98	0.77	0.25	0.3	0.055	14.13	10.71	17.86	0.6

Table 5.1 Terrigenous elements/Al from this study and world average deep-sea clay (Turekian and Wedopohl, 1961). Depth/age (depth/A) intervals chosen to represent contrasting periods of deposition. WC = whole core; Si/Al is Si_{terrig}/Al (see text) except in core CD3814 which is Si_{total}/Al.

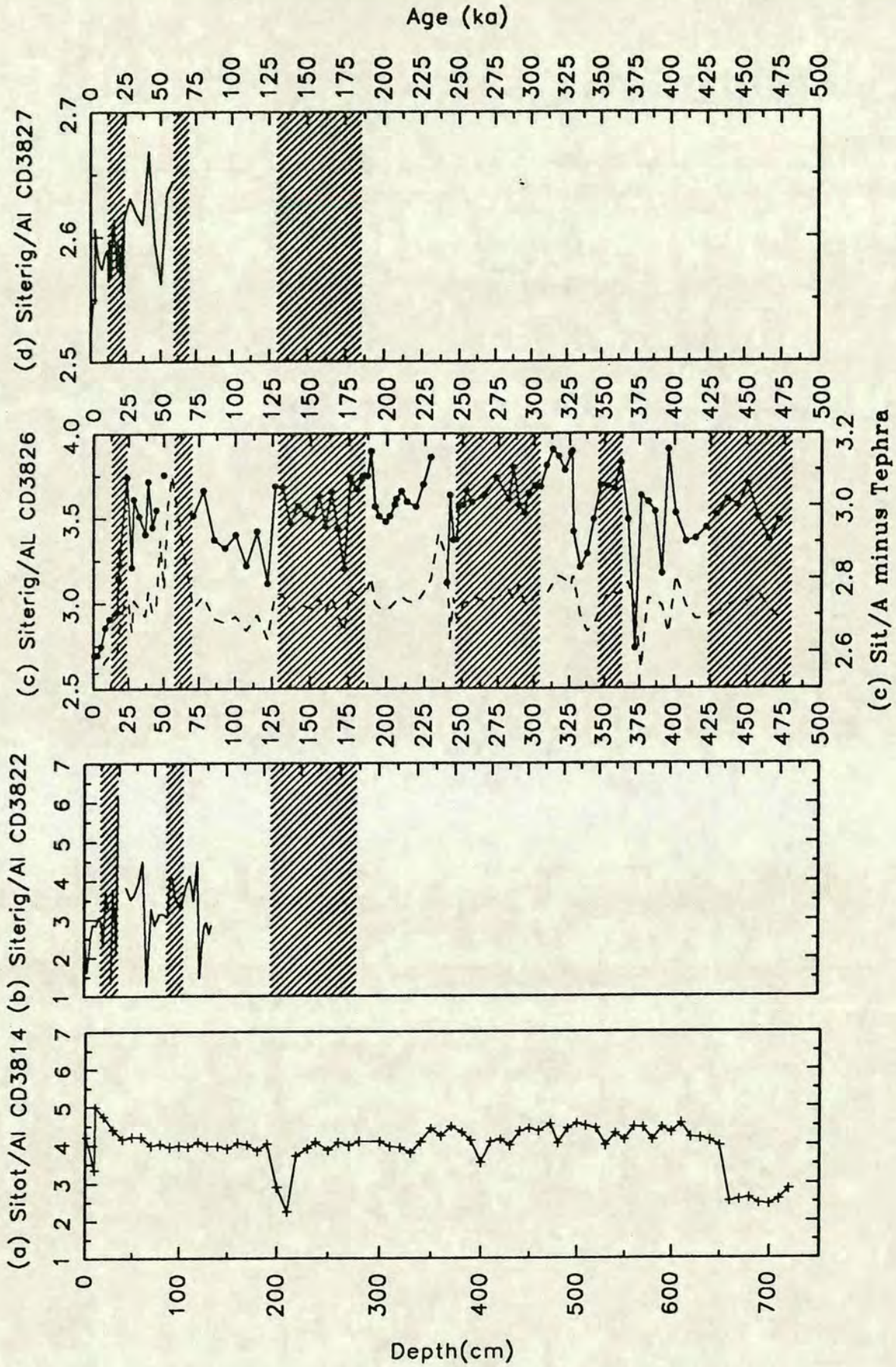

Figure 5.2 Temporal variations in the Si_{terrig}/Al from CD38 cores. Plot with symbols and lines omits tephra horizon data (lower scale) in core CD3826 (c). Shaded regions represent glacial stages II, IV, VI, VIII, X and XII.

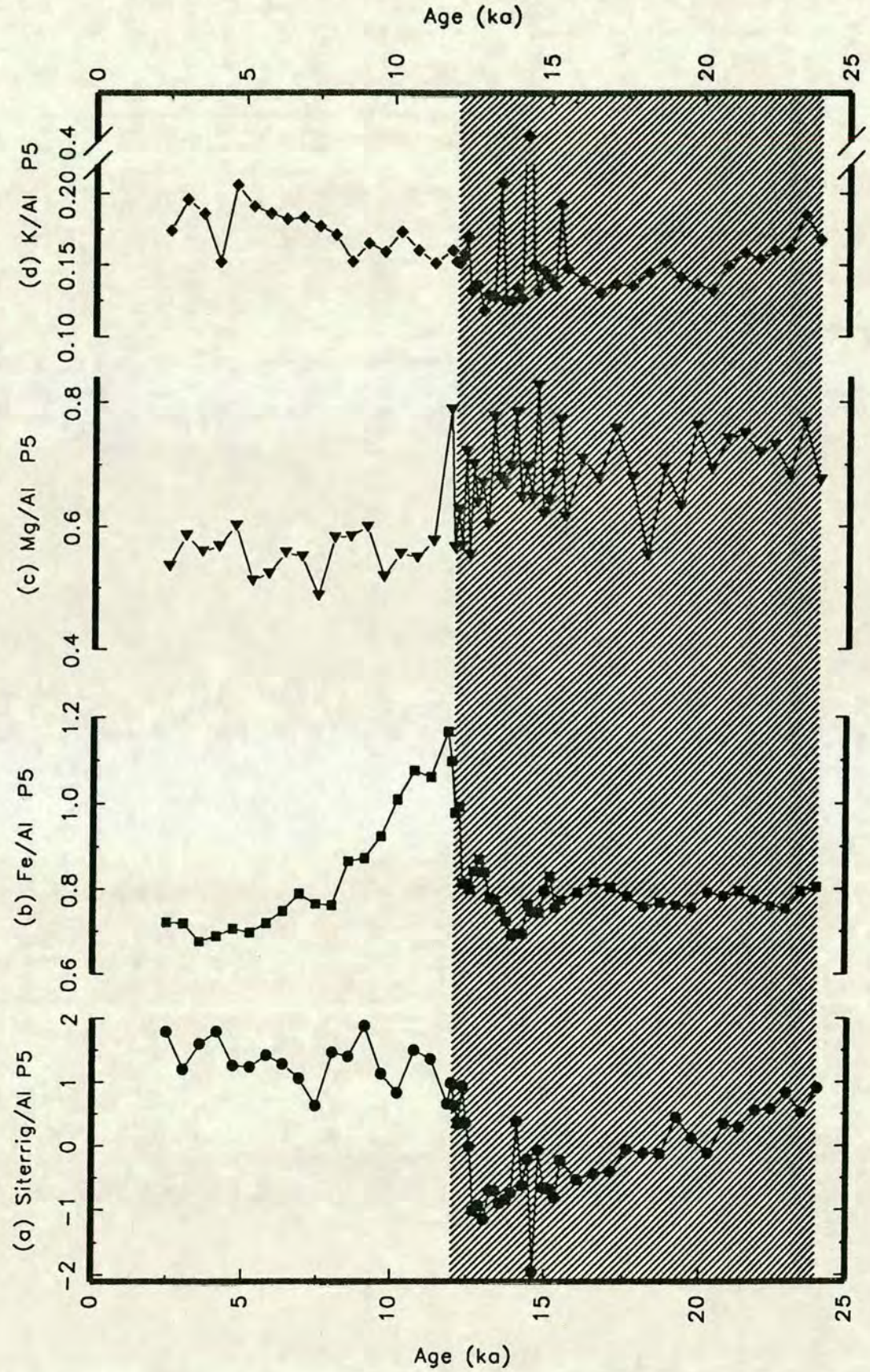

Figure 5.3 Temporal variations in the Si_{terrig}/Al (a), Fe/Al (b), Mg/Al (c) and K/Al (d) from core P5. Note the break in the scale of K/Al. Shaded region represents glacial stage II (12-24 ka).

when Si_{tot} is small as the relative amount of Si_{biog} is high. However, Figure 5.3a shows a single cycle of Si_{terrig}/Al ratio for core P5 with maximum values near the surface decreasing to a minimum at around 14ka only to increase again at the base of the core. If terrigenous material is greater during glacial periods, and almost all Si is from biogenic SiO_2, the decrease in Si_{terrig}/Al during the last glacial maximum may simply be due to dilution by the Al flux to the region.

Core CD3814 shows a virtually constant Si_{tot}/Al ratio of 4 throughout the core except for two strong depletions at 200cm and below 650cm, where values are around 3.5 (figure 5.2a), both almost certainly due to hydrothermal deposits.

Core CD3822 shows the largest scale variation of all the cores together with a strong cyclicity with long and short periods (figure 5.2b). The "sawtooth" pattern is such that maximum and minimum Si_{terrig}/Al values are not synchronous with glacial and interglacial periods, although there is a general tendency for high Si_{terrig}/Al ratios during glacials. This is probably due to volcanic ash deposits.

The Si_{terrig}/Al ratio of core CD3826 is dominated by the spikes caused by tephra layers at 56 ka, 234 ka and 328 ka (figure 5.2c). Values in the sediment where tephra is absent are generally around 3.0 except for a strong decrease during stage I culminating in the core minimum value of 2.6 at the surface (table 5.1). The build up of Si_{terrig}/Al from the surface sediment into stage II is consistent with the concept of greater dust input to the oceans during glacial periods as a result of increased continental aridity and availability of subaerial continental shelf sediments (Hays et al, 1969; Janecek and Rea, 1985) during periods of lowered sea level. Some cyclicity is present downcore which will be discussed further in relation to palaeoclimate tracer fluxes (chapter 7).

Core CD3827 displays the least variation in Si_{terrig}/Al varying from 2.5 at the surface to only 2.68 at the base. Overall, there is a gradual increase in values downcore with a slight enrichment during stage II and into stage IV which again agrees with greater terrigenous input during glacials (figure 5.2d).
The Holocene decrease in Si_{terrig}/Al in cores CD3822, CD3826 and CD3827 is more clearly illustrated in figure 5.4, which shows the record over the last 150 ka, and demonstrates the contrast with the Si_{terrig}/Al profile in core P5 which increases during the Holocene.

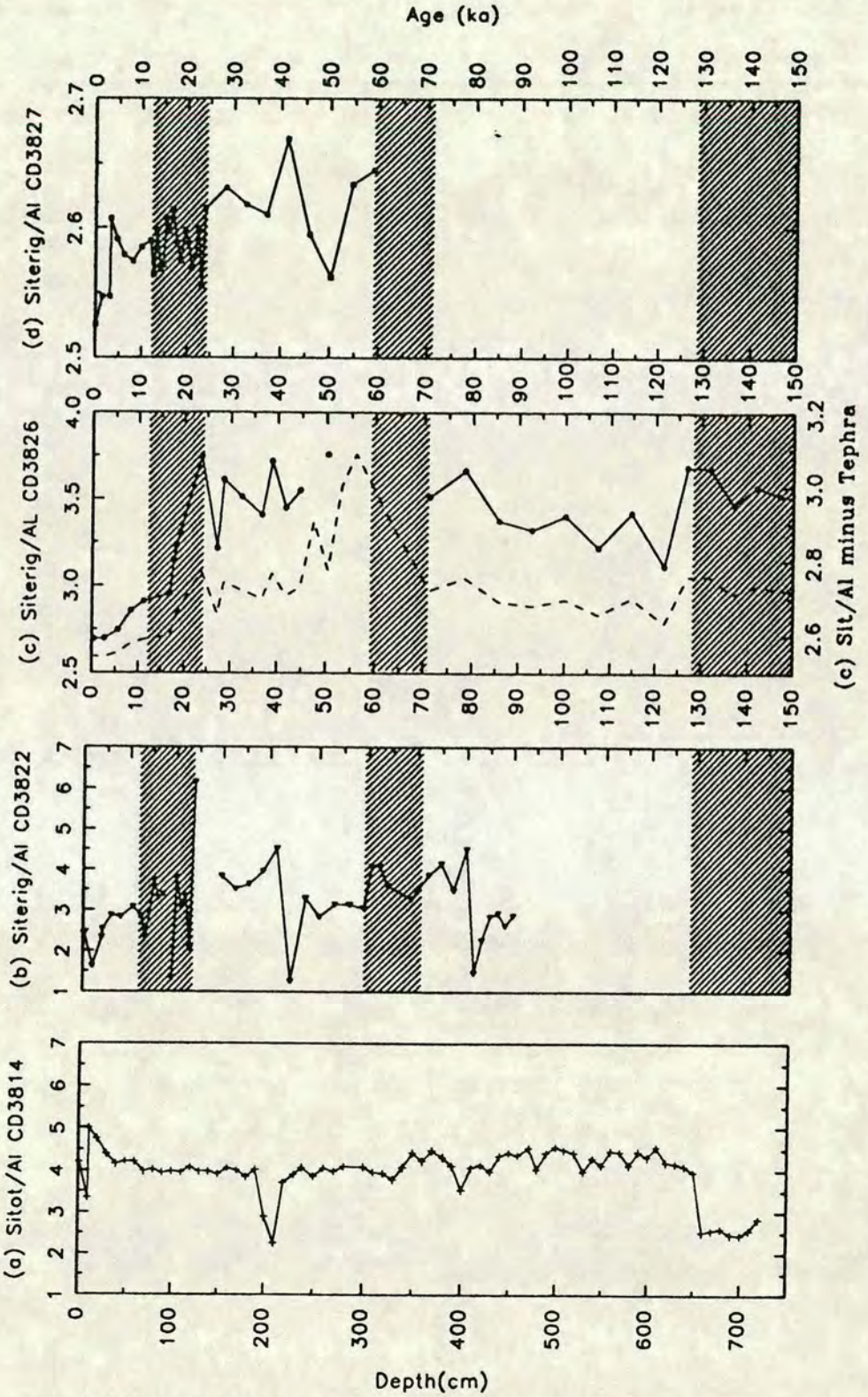

Figure 5.4 Temporal variations in the Si_{terrig}/Al from CD38 cores over the last 150 ka. Plot with dotted line and no symbols is the complete data (upper scale) for the time interval in core CD3826 whereas the plot with symbols and solid lines is from the data omitting tephra horizons (lower scale). Shaded regions represent glacial stages II, IV and the younger part of stage VI.

5.2.2 Iron and Magnesium

Introduction

Iron and Magnesium in the sediments from this study generally covary strongly (Figure 5.3b, 5.3c, 5.7 and 5.8; Tables 5.5-5.9) and, as a result, they will be considered together.

Iron has three possible source pathways to deep-sea sediments. Firstly as minerals such as ilmenite, haematite and magnetite (Goldberg and Griffin, 1964). According to Carrol (1958) Fe may be associated with clay minerals, such as nontronite, in the following ways: (a) as an essential constituent within the crystal lattice; (b) as a minor constituent in the crystal lattice and; (c) as iron oxide coatings on the surface of the clay particles. Secondly through biological mechansims (Revelle, 1944) which according to El Wakeel and Riley (1961) are generally insoluble Fe coatings on the skeletal parts of foraminifera. Finally there is an authigenic removal of Fe from sea water; most not ably in the form of sorption onto oxyhydroxide mineral surfaces. The latter two sources are considered to be quantitatively less important relative to the input of Fe from terrigenous clay minerals.

Magnesium in deep sea sediments is derived from carbonate material or clays (often volcanigenic). Concentrations of MgO in volcanigenic clays may reach 8.34% (El Wakeel and Riley, 1961) especially those containing smectites.

Fe-Al and Mg/Al Relationships

The relationship Fe and Mg with Al in the cores studied in this thesis is illustrated in figure 5.5 and 5.6 respectively. The general linearity of the Fe-Al relationship in all cores except CD3822 (C=0.483) clearly shows that most Fe is held in Fe-aluminosilicate clay minerals. However, all the cores show a positive intercept on the Fe-axis which indicates that there is some Fe present in excess of that held in the terrigenous clay minerals. The intercept in cores P5 and CD3814 is negligible (figure 5.4b), but intercepts of 0.4%, 0.5% and 1.2% Fe for cores CD3822, CD3826 and CD3827 respectively. Although the correlation in CD3822 is not especially strong (C= 0.483), the 0.40% Fe intercept may represent a concentration of residual Fe oxide likely to be an input from or formation of Fe-rich clay minerals.

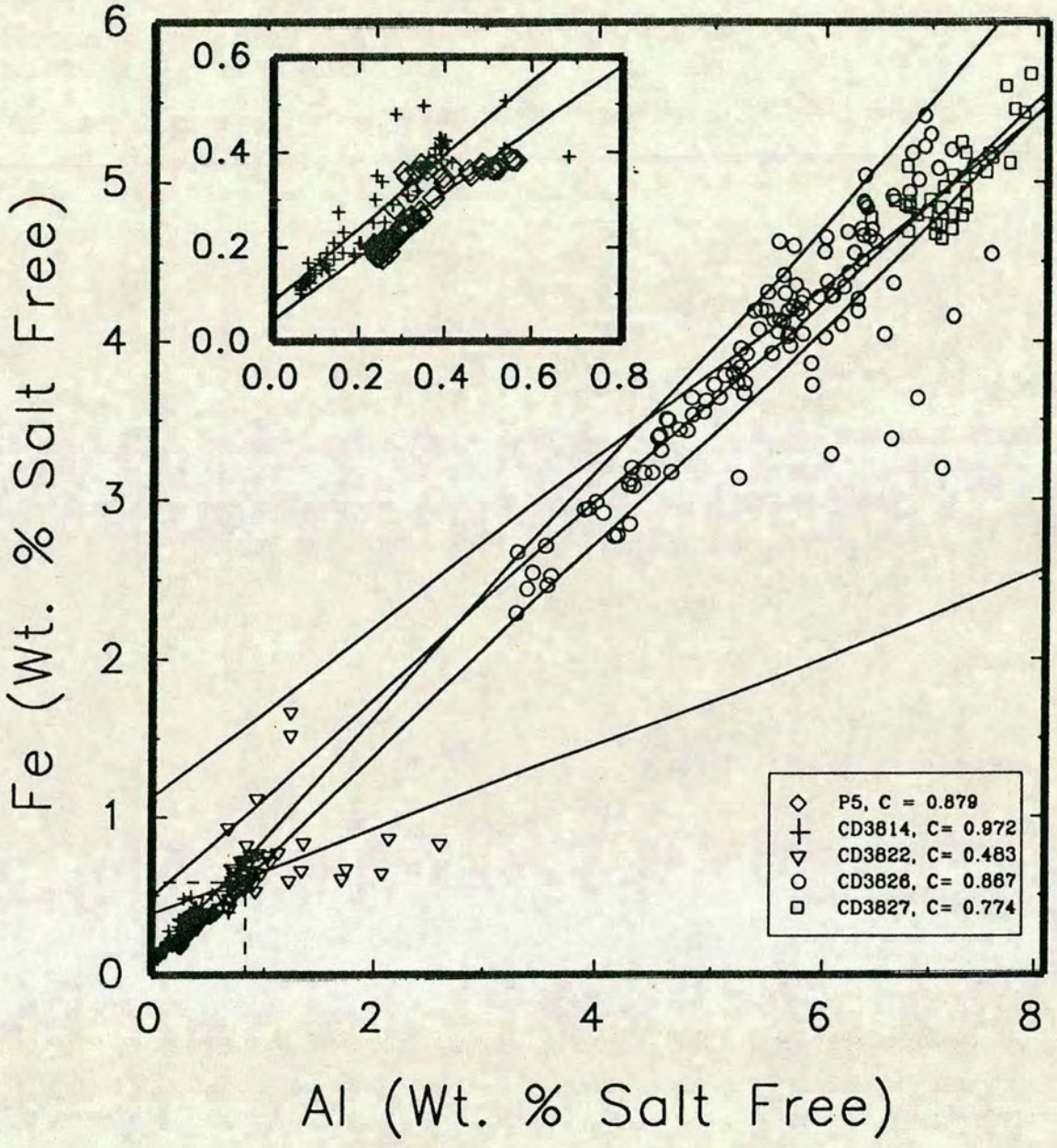

Figure 5.5 Diagram illustrating the relationship between Fe and Al from cores studied in this thesis. Inset graph is a detail of the main plot at the lower end of the scale and shows only data from cores CD3814 and P5. Note the points below the regression line especially in core CD3826 probably associated with feldspathic tephra input (see text for details).

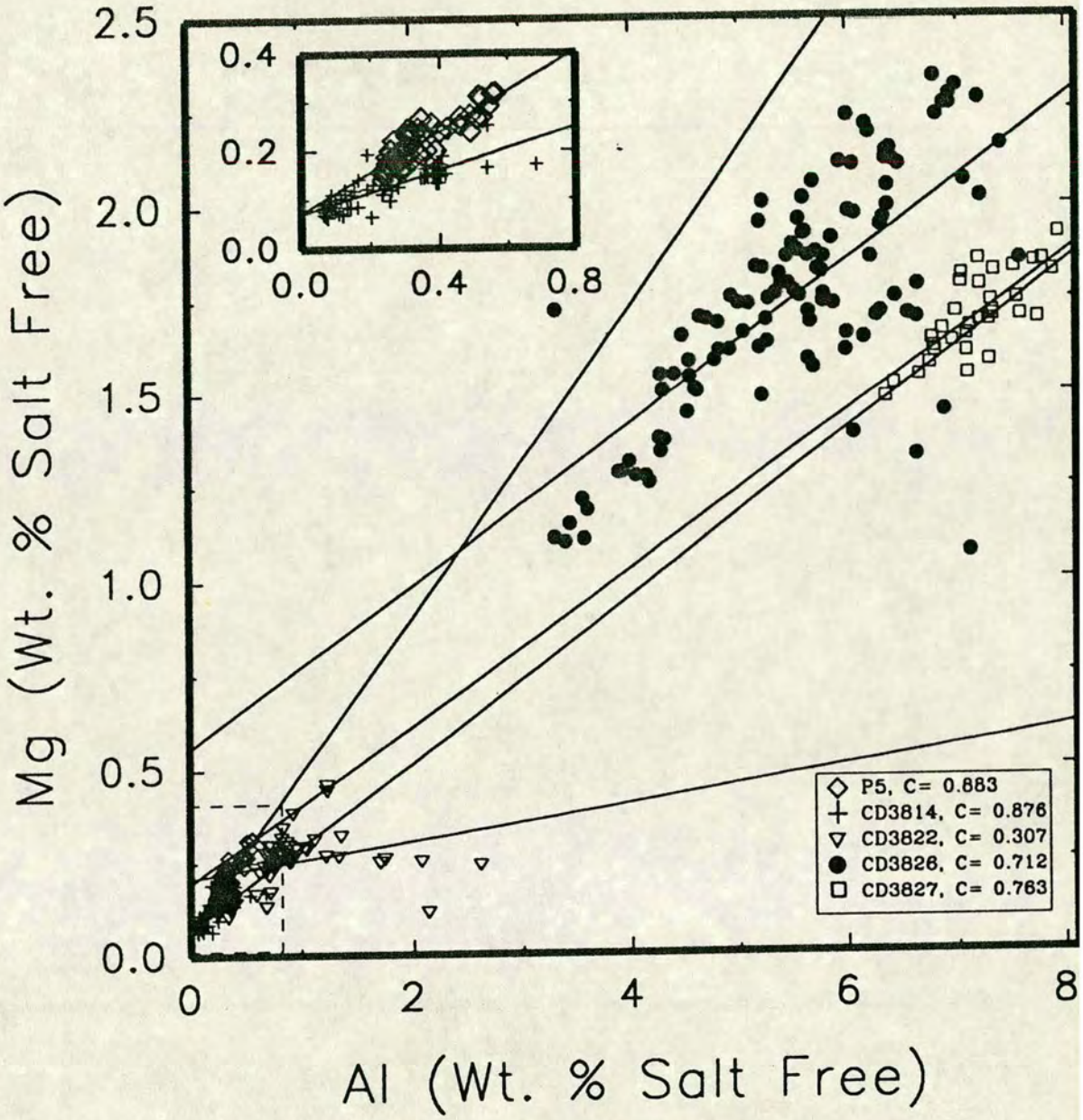

Figure 5.6 Diagram illustrating the relationship between Mg and Al from cores studied in this thesis. Inset graph is a detail of the main plot at the lower end of the scale and shows only data from cores CD3814 and P5. Note the points below the regression line especially in core CD3826 probably associated with feldspathic tephra input (see text for details).

The plots of Mg versus Al (figures 5.6) illustrate that generally all the Mg is held in detrital aluminosilicates occuring mainly as chlorite or smectite. The intercepts on the Mg axis of the regression lines at 0.2, 0.55 and 0.2 for core CD3822, CD3826 and CD3827 respectively show that little, if any, Mg in the sediment is held in biogenic carbonate phases (eg dolomite).

Points below the regression lines especially for cores CD3822 and CD3826 in both Fe and Mg versus Al plots (figure 5.5 and 5.6) probably represent relatively high quantities of feldspar which tend to offset the regression lines causing the observed intercepts.

Downcore Variations in Fe and Mg

Introduction

A strong control on the Fe (,K and Rb) contents of terrigenous material is the illite/chlorite/smectite mineralogy (Boyle, 1983). The downcore variation in Fe/Al and Mg/Al in all the cores studied in this thesis covary weakly in core P5 (figure 5.3b and 5.3c, table 5.9) and strongly in cores CD3814, CD3822, CD3826 and CD3827 (c.p. figures 5.7, 5.8 and tables 5.5-5.8). That Mg is so closely associated with Fe and not with $CaCO_3$, as is the case in most sediments containing considerable concentrations of dolomite (high Mg calcite), suggests that Mg and Fe are held in the same phases. These phases are probably terrigenous clay minerals, and possibly, smectites that may be associated with Fe release and precipitation (eg nontronite) followed by Mg sorption from seawater.

Fe/Al Profiles

The Fe/Al profile for core CD3814 (figure 5.7a) can be divided in half; the upper 3m shows little variation, except in one horizons at 2m depth that is depleted in Fe relative to Al and is probably due to an ash deposit. The top half of the core has an average Fe/Al ratio of approximately 1.0 (table 5.1), which is quite high for marine sediments, and may indicate the presence of some feldspar and/or volcanic ash. Holocene values are strongly enriched in Fe (and Mg) which is almost certainly a consequence of high smectite content. Smectites form by the alteration of volcanic matter and low temperature interaction between amorphous hydroxides (often nontronites) and biogenic SiO_2 (Kastner, 1977). In the lower half of the core Fe/Al

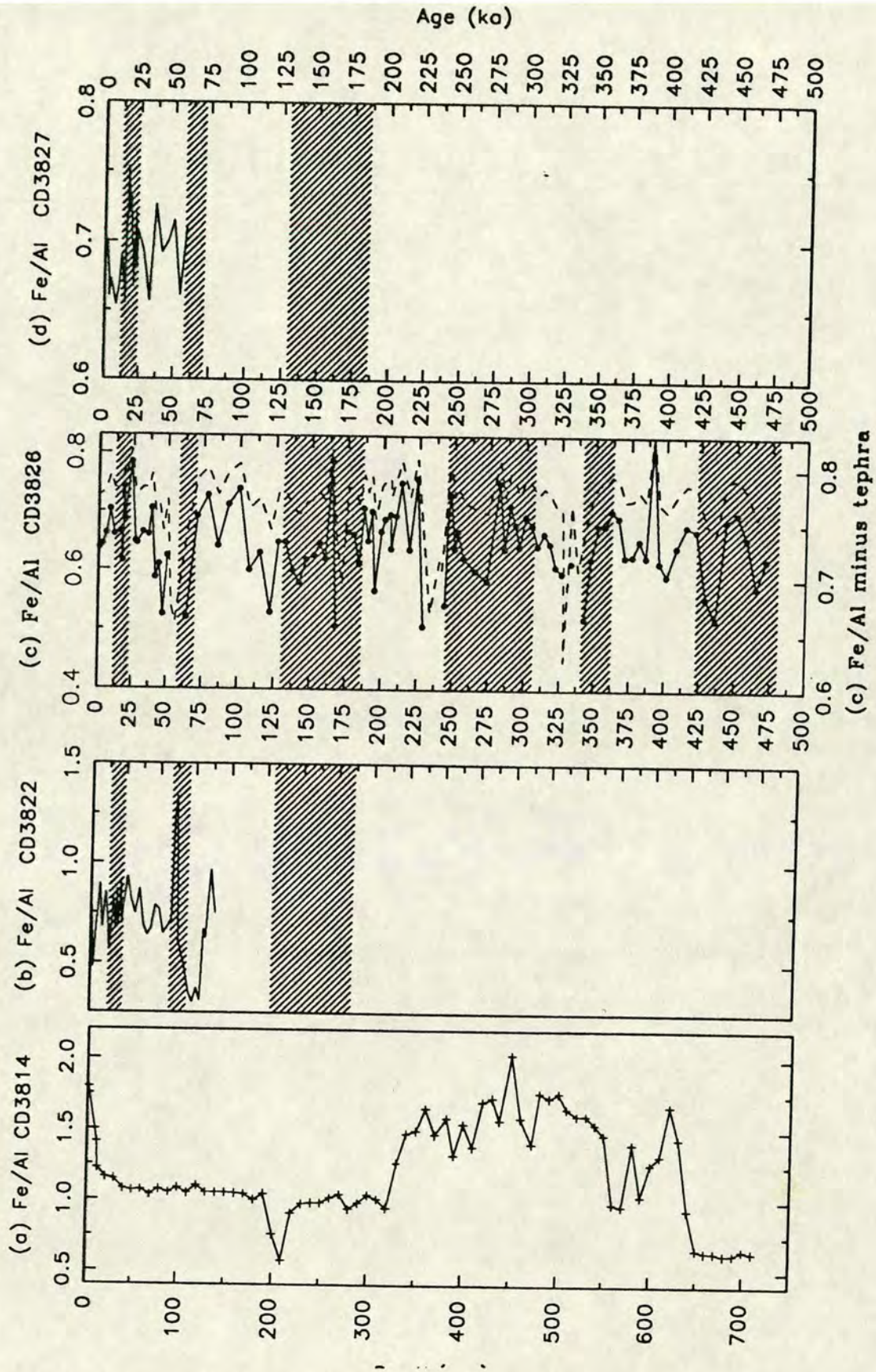

Figure 5.7 Temporal variations in Fe/Al from CD38 cores. Note the different scales and the very high values especially in the lower half of core CD3814 almost certainly the result of hydrothermal deposits. Shaded regions represent glacial stages II, IV, VI, VIII, X and XII.

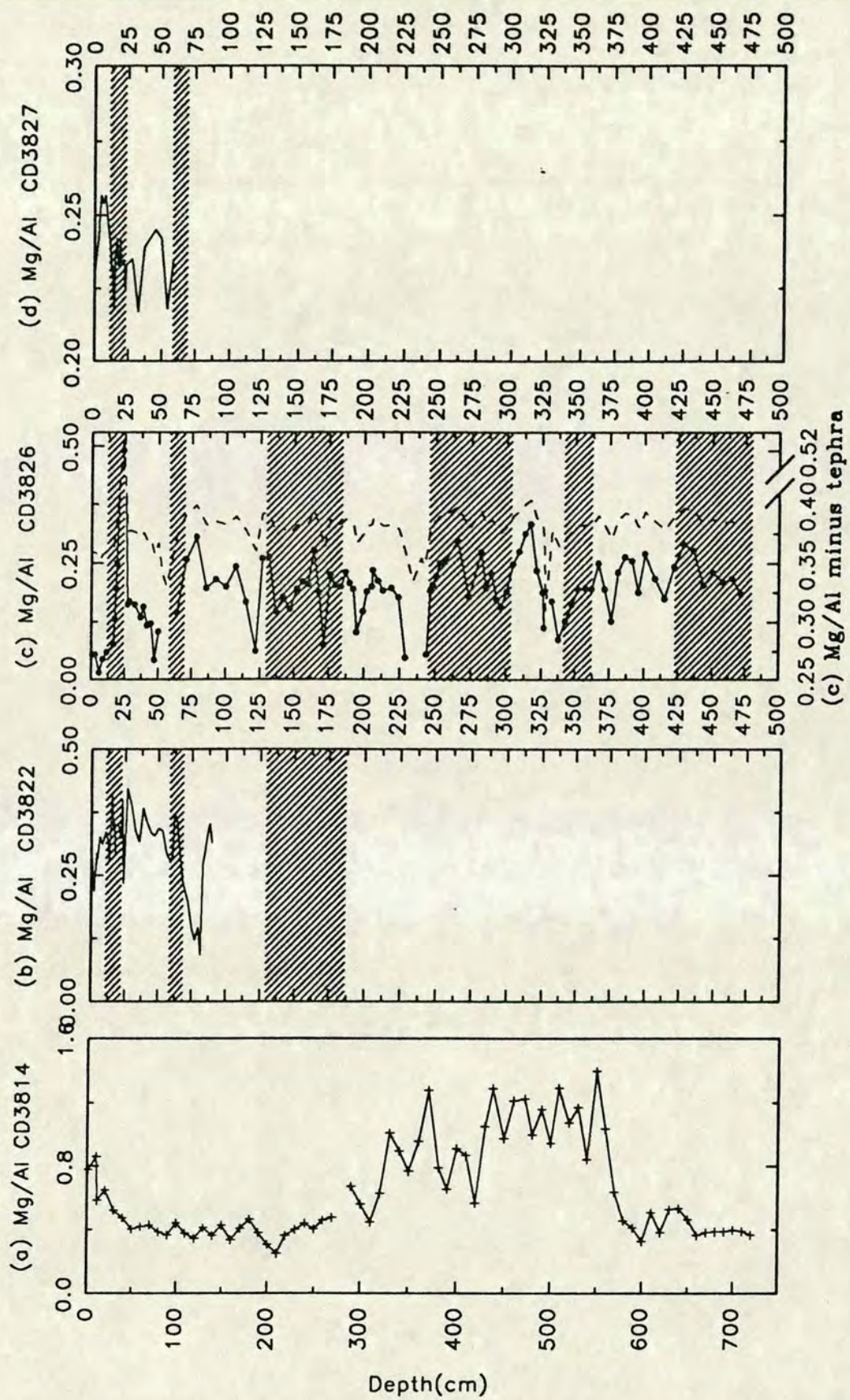

Figure 5.8 Temporal variations in Mg/Al from CD38 cores. Note the different scales and the very high values especially in the lower half of core CD3814 almost certainly associated with sepeolites/nontronites formation and partly the result of hydrothermal activity. Shaded regions represent glacial stages II, IV, VI, VIII, X and XII.

ratios increases to an average value of around 1.4 (table 5.1) which is almost double that of a world average shale (Turekian and Wedopohl, 1961) and is almost certainly the result of a hydrothermal input that has resulted in authigenically formed smectites. Such a hydrothermal-volcaniclastic source for Fe in sediments of the eastern equatorial Pacific has been reported by many authors (Bostrom et al., 1969, 1973; Bender et al., 1971; Sayles et al., 1975; Pedersen, 1979; Dymond et al., 1973). These enrichments are generally believed to be produced by selective precipitation from solution of Fe, Si and other elements which have been leached from recently emplaced basalts by hot, convectively circulating, sea water (Bender et al., 1971; Bischoff and Rosenbauer, 1977; Cann et al., 1977).

Core P5 has the highest Fe/Al (and Ti/Al, figure 5.3) ratio of all the cores in this study situated in the Panama basin. This is probably due to a local input of Fe (and Ti) from the Galapagos archipelago, a topic discussed more fully with respect to Ti/Al ratios (see section 5.3.1). In contrast the considerable enrichment of Fe relative to Al at 11.89 ka in core P5 coincides with a similar spike in a nearby core P6 as described by Pedersen (1979), (see chapter 4.6) and is believed to be hydrothermal. However the Fe enriched region of core P6 has a Fe/Al ratio of around 3.0 which is approximately three times that in P5. This relative depletion in Fe during the hydrothermal spike in P5, compared to P6, is probably due to differences in the hydrothermal input or from dilution by a higher accumulation rate of terrigenous aluminosilicates.

Bostrom (1973) has described the empirical mixing relations of pure metalliferous sediment and terrigenous material with a plot of Fe/Ti (representing metalliferous material) versus Al/Al+Fe+Mn (representing terrigenous material). Pedersen (1979) used an almost identical plot to classify sediments from the Panama basin into varying percentages of metalliferous and non-metalliferous sediment. Figure 5.9 shows just such a plot with a selection of sediments from this study designed to represent the spectrum of sediment compositions encountered together with two samples from core P6 (Pedersen 1979), used for comparison. Table 5.2 shows the elemental values from all the sources used to create this diagram. Of the sample horizons used, most lie close to the empirical mixing curve of Bostrom (1973). Moreover, the majority are grouped around the world average clay and shale compositions of Turekian and Wedopohl (1961) with the only clear exceptions being both P5 horizons (especially P5-18 ka, "non-,metalliferous), sample CD3822-64 ka and sample CD3814-509^{M}. Although the "metalliferous" horizon of P5 (P5-12 ka) is

TABLE 5.2 TERRIGENOUS AND METALLIFEROUS "FACTORS" FROM SEDIMENTS STUDIED IN THIS THESIS AND FROM PREVIOUS WORK

Sample ID	Fe/Ti "Metalliferous factor"	Al/Al+Fe+Mn "Terrigenous factor"	Reference
BD	123.33	0.067	1
EPR^{H}	900.00	0.020	2
EPR^{A}	55.88	0.283	2
DSC	14.17	0.537	3
AS	10.26	0.625	3
$P6\text{-}42.5^{M}$	54.75	0.253	4
$P6\text{-}104.5^{NM}$	15.96	0.510	4
$P5\text{-}12^{M}$	10.804	0.456	5
$P5\text{-}18^{NM}$	6.812	0.556	5
CD3814-110	15.277	0.429	5
$CD3814\text{-}509^{M}$	19.243	0.332	5
CD3822-36	14.134	0.539	5
$CD3822\text{-}64^{M}$	31.254	0.397	5
CD3826-56	13.127	0.645	5
CD3826-195	12.624	0.577	5
CD3827-8	11.775	0.601	5
CD3827-17	10.614	0.568	5

1 = Sayles and Bischoff, (1973); 2 = Bostrom and Peterson (1969); 3 = Turekian and Wedopohl (1961); 4 = Pedersen (1979); 5 = This study.

BD = Bauer Deep Metalliferous sediment from average of core 14 (1); EPR^{H} = East Pacific Rise high heat flow (metalliferous), mean conposition of group (b) sediments (2); EPR^{A} = East Pacific Rise average heat flow (metalliferous), mean of composition of group (a) sediments (2); data from references 2 and 3 are on a salt free basis determined from Cl concentrations (after 4), all other data are on a salt and carbonate free basis; ^{M} = metalliferous type sediment; ^{NM} = non-metallfierous type sediment. Numbers of horizons in cores P5, CD3822, CD3826 and CD3827 are ages in ka, and depth (cm) in core CD3814.

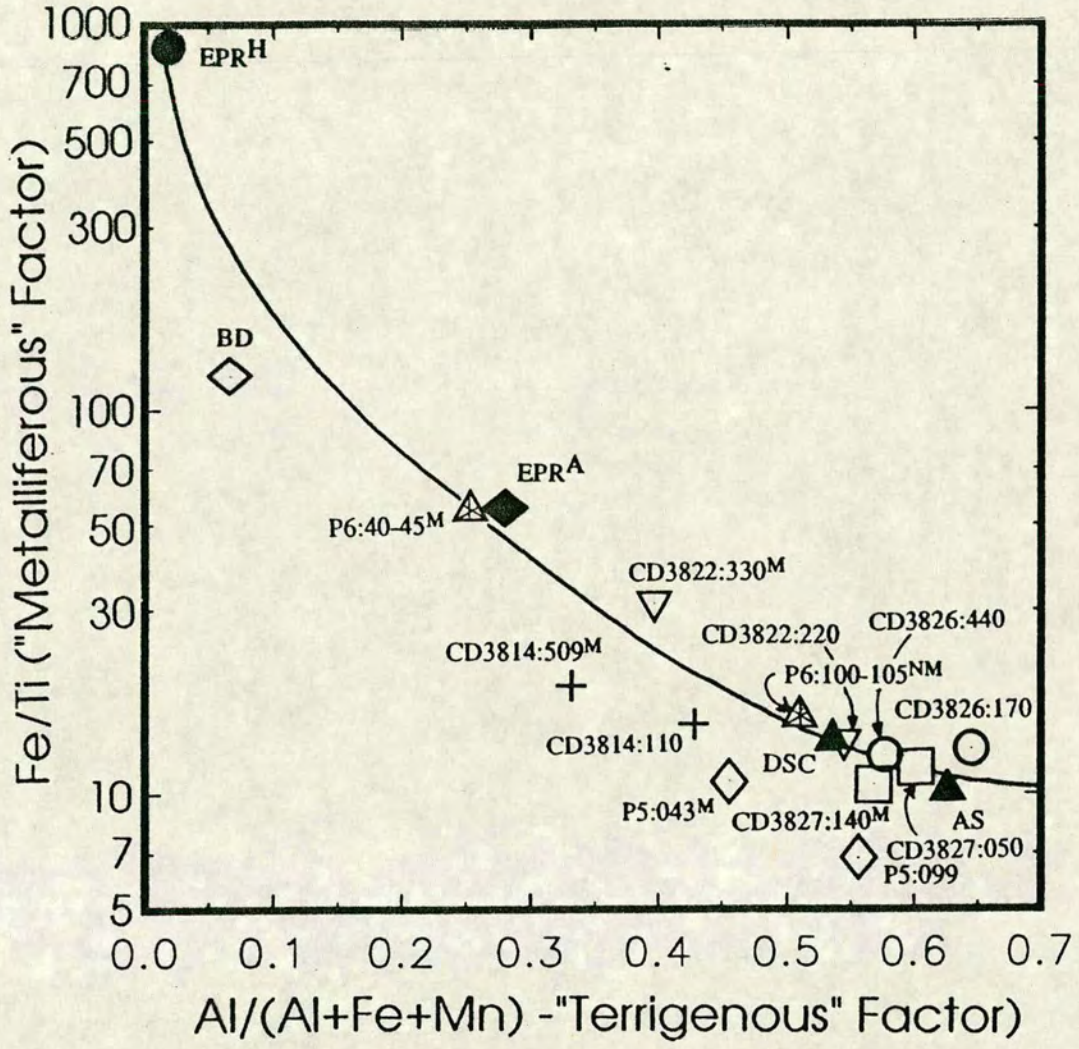

Figure 5.9 Mixing relationships (after Bostrom, 1973) of sediments as defined by the Fe/Ti "Metalliferous Factor" versus the Al/(Al+Fe+MN) "Terrigenous Factor". See table 5.2 for abbreviations.

enriched in Fe relative to the rest of the core, it plots below the mixing curve of Bostrom (1973), (Figure 5.9). This may be due to the strong and unusual Ti enrichment pulling down the Fe/Ti ratio below the mixing curve. However this cannot account for the fact that this "metalliferous" horizon is closer to an average shale composition than the metalliferous horizon in P6 or even the Bauer-deep (hydrothermal) sediment. As P6 is located in the central Panama basin (figure 5.0) and is closer to the Galapagos Spreading Centre, one might expect any hydrothermal event to have a greater effect on P6 than on P5 which is situated some 100 km to the south on the Carnegie Ridge.

That the lower half of core CD3814 has been influenced by hydrothermal deposits appears unrefutable, but both horizons on figure 5.9 plot quite close to the other horizons from other cores studied in this thesis. However, they do contain the lowest and the third lowest terrigenous factor values, and the second and third highest metalliferous factor values of all the cores studied in this thesis, which is further evidence of the hydrothermal nature of the sediment in this part of core CD3814. Sample CD3822-64 ka is quite strongly enriched in Fe and Mn and depleted in Ti and Al which results in it plotting above the mixing curve.

Temporal variations in Fe/Al, in core CD3822 has average Fe/Al values close to the world average shale of Turekian and Wedopohl (1961) at around 0.77 (table 5.1). In the Pleistocene section of the core the main digression from this average occurs in sediments older than stage III. During stage IV there is a large enrichment of Fe relative to Al which is also shown in the Mg/Al profile (see figure 5.8b). The synchroneity of this spike in both Fe/Al and Mg/Al argues in favour of it being the result of a hydrothermal pulse similar to the one at 12 ka in core P5. That this spike cannot be correlated with other cores at the same age must mean that it is a local hydrothermal event. During upper stage V Fe is depleted relative to Al (figure 5.7b) which is interpreted as resulting from an Al rich volcanigenic ash band and causes most other elements (including Ti) to be depleted relative to Al at this point.

Core CD3826 has a relatively constant Fe/Al ratio downcore except for three prominent depletions of Fe relative to Al, which are also interpreted as being feldspar-rich volcanic ash bands (figure 5.7c). Surficial and whole core average values for Fe/Al in CD3826 (0.727 and 0.718 respectively, see table 5.1) are quite close to the world average shale of Turekian and Wedopohl (1961). Again, as in core CD3822, these horizons are depleted in Fe, Mg and, in most cases Ti, which lends

credence to the intepretation of them as feldspar enriched ash bands. Moreover they coincide with the enrichments in Saturation Induced Remenance Magnetisation (chapter 4.2).

The Fe/Al profile in core CD3827 (figure 5.7d) is depleted relative to the world average shale of Turekian and Wedopohl (1961) suggesting a high feldspar content relative to ferro-magnesium minerals at this location. The small increase in the Fe/Al ratio in glacial stage II may be the result of increased ferromagnesium or magnetite material erosion and pluming from the continental shelf or slope to the deep ocean floor during the low sea level stand as was the case with Si_{terrig}.

Mg/Al Profiles

Downcore vaiations in Mg/Al closely resemble those of Fe/Al in all cores except P5 (cp. figures 5.3b, 5.3c, 5.7 and 5.8). The average Mg/Al ratios in core P5 and CD3814 (0.646 and 0.659 respectively, table 5.1) are over twice that for the world average deep-sea clay of 0.25 (Turekian and Wedopohl, 1961) and the variation in the ratios are many times greater than changes in the ratio for other cores studied.

The reason for the strong Mg enrichment and generally noisy signal in core P5 is probably due to sepeolite development. This is backed up by the fact that associated elements (eg Fe) do not follow this trend and sediments from core P5 are not metalliferous according to their position on the mixing curve of figure 5.9. Sepeolite is a hydrous Mg-silicate whose general formula is given in equation 5.1. It is easily precipitated from sea-water and is often associated with biogenic SiO_2 or volcanic glass shards (Kastner, 1977). The enrichment of Mg in core CD3814 especially in the basal half is is also difficult to explain but, as the profile closely matched that for Fe, a hydrothermal source would seem likely.

Equation 5.1 $$Mg_8 Si_{12} O_{13} (OH)_2 (OH_2)_4 . 8 H_2O$$

Cores CD3822, CD3826 and CD3827 also display strong correlation between Fe/Al and Mg/Al, with volcanic ash layers and hydrothermal pulses being the main cause of digression from the average values for each core (table 5.1). The only obvious discordance between the Fe/Al and Mg/Al curves occurs during the Holocene of core CD3827 and at CD3826-24 ka (cp. figures 5.7 and 5.8). In core CD3827 Mg/Al values reach a minimum of 0.218 at around 14 ka and gradually increase to a

maximum of 0.257 in the upper Holocene before dropping off again to a surficial value of around 2.3. The anomalous spike in Mg/Al at CD3826-070 is associated with a $MnCO_3$ phase and is fully discussed in chapter 9.

5.2.3 Potassium

Potassium in marine sediments is dominantly associated with illite and orthoclase/microcline feldspar, therefore variations in the K/Al ratio may reflect changes in illite and feldspar present in the sediments (Boyle, 1983).

Potassium-Aluminum Relationships

The relationship and degree of correlation between K and Al is illustrated in figure 5.10. It shows the regression lines intercepting the origin in all cores except CD3827 which has an intercept of 0.55% K. This suggests that in all cores except CD3827 most of the K is held in terrigenous material as defined by Al. The excess K in core CD3827 most likely originates from higher levels of feldspar relative to illite (chapter 3).

Downcore variations in K/Al

According to Pedersen (1979) smectite is by far the most dominant Al bearing mineral in the area. Therefore, as most K is held in illite, spatial and temporal variations in the K/Al ratio imply changes in the relative proportions of illite to smectite, and in the relative proportions of plagioclase rich tephra to non-tephra material present. Low K/Al ratios in the Galapagos area are possibly the result of locally high Al bearing, K depleted plagioclase and ferromagnesian minerals (Pedersen, 1979). Also, Heath et al. (1974) report the presence of authigenic K-bearing smectite in the region which forms from basaltic debris. Thus the K/Al ratio is a useful tool in the intepretation of mineralogical and textural changes especially when used in conjunction with the Si_{terrig}/Al and Fe/Al curves. K-rich phillipsite is almost certainly absent from the sediment studied in this thesis.

Temporal variations in K/Al broadly parallel the Si_{terrig}/Al profiles and, to some degree, mirror the Fe/Al profiles (cp. Figures 5.2, 5.3, 5.7 and 5.11) with K/Al values ranging from around 0.1 to 0.5. At the upper limit of this range there may be considerable quantities of K-feldspar present in the sediment (eg 80 ka CD3822).

The K/Al ratio in core CD3814 and upper part of core CD3822 are close to the world average of 0.3 whereas cores P5, CD3826 and CD3827 all have average values considerably depleted in K (table 5.1) and possibly illustrates the importance of Fe-Mg smectite in controlling the Al content of the sediment. As with Si_{terrig}/Al, many of the major anomalies are interpreted as being the result of rapid mineralogical changes due to volcanic ash layers. Most cores show lower K/Al ratios during the Holocene (figure 5.12) implying either higher smectite and illite or lower feldspar contents in the recent surficial sediments.

On average, core P5 shows the second most depleted K/Al values of all the cores (table 5.1). The base of the core is relatively high and values decrease to a minimum of around 0.1 at 13ka before increasing towards the surface values of approximately 0.2. Strongly enriched horizons in the core (eg P5-14 ka) are difficult to explain but could be the result of anomalous mineralogy or unusually high input of volcanic feldspar debris. At this point in the core Si/Al, Fe/Al, Mg/Al and K/Al are low whilst Zr/Al and Cr/Al are high (see below) which indicates considerable amounts of Ca-feldspar probably derived from basaltic fragments.

Core CD3814 shows little variation apart from a K depletion at the base of the core coinciding with the volcaniclastic material probably containing feldspar and, a strong double peaked anomaly at 2m which correlates with similar anomalies in most other major elements and whose origin is uncertain (figure 5.11a). The average K/Al ratio is slightly depleted relative to a world average for fine grained sediments and there appears to be no system atic cyclicity downcore.

Core CD3822 is dominated by the K/Al spike coinciding with a tephra layer at 80 ka (figures 5.11b, 5.12a). There are minor increases in K/Al at the begining and towards the end of glacial stage II and during stage IV which are probably the result of variations in volcaniclastic inputs to the sediment.

Core CD3826 displays very constant K/Al ratios which are relatively strongly depleted in K except for the ash bands which have K/Al ratios of around 0.3 (figures 5.11c, 5.12b). If one removes the data points from these ash bands and plots the K/Al variation between 0.1-0.2 the curve looks quite different (solid symbols figure 5.11c). As in core CD3822 and CD3827 there is an increase in the K/Al ratios during glacial periods and the Holocene is a period of decreasing K/Al ratios perhaps indicative of gradually decreasing feldspar or illite input relative to smectite (figure 5.12b).

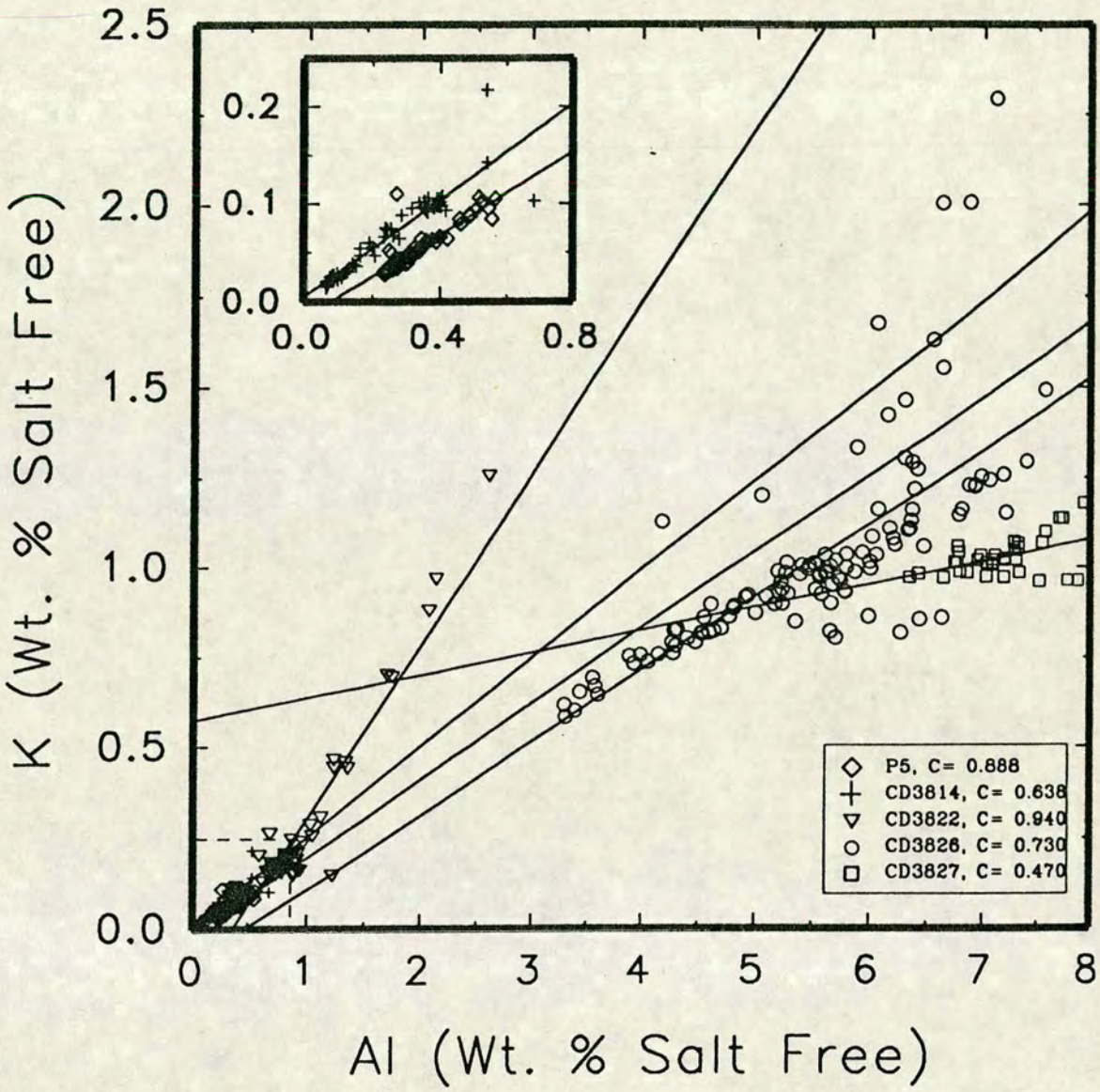

Figure 5.10 Diagram illustrating the relationship between K and Al from cores studied in this thesis. Inset graph is a detail of the main plot at the lower end of the scale and shows only data from cores CD3814 and P5. Points above the regression line especially in core CD3826 represent the feldspathic rich tephra horizons (see text for details).

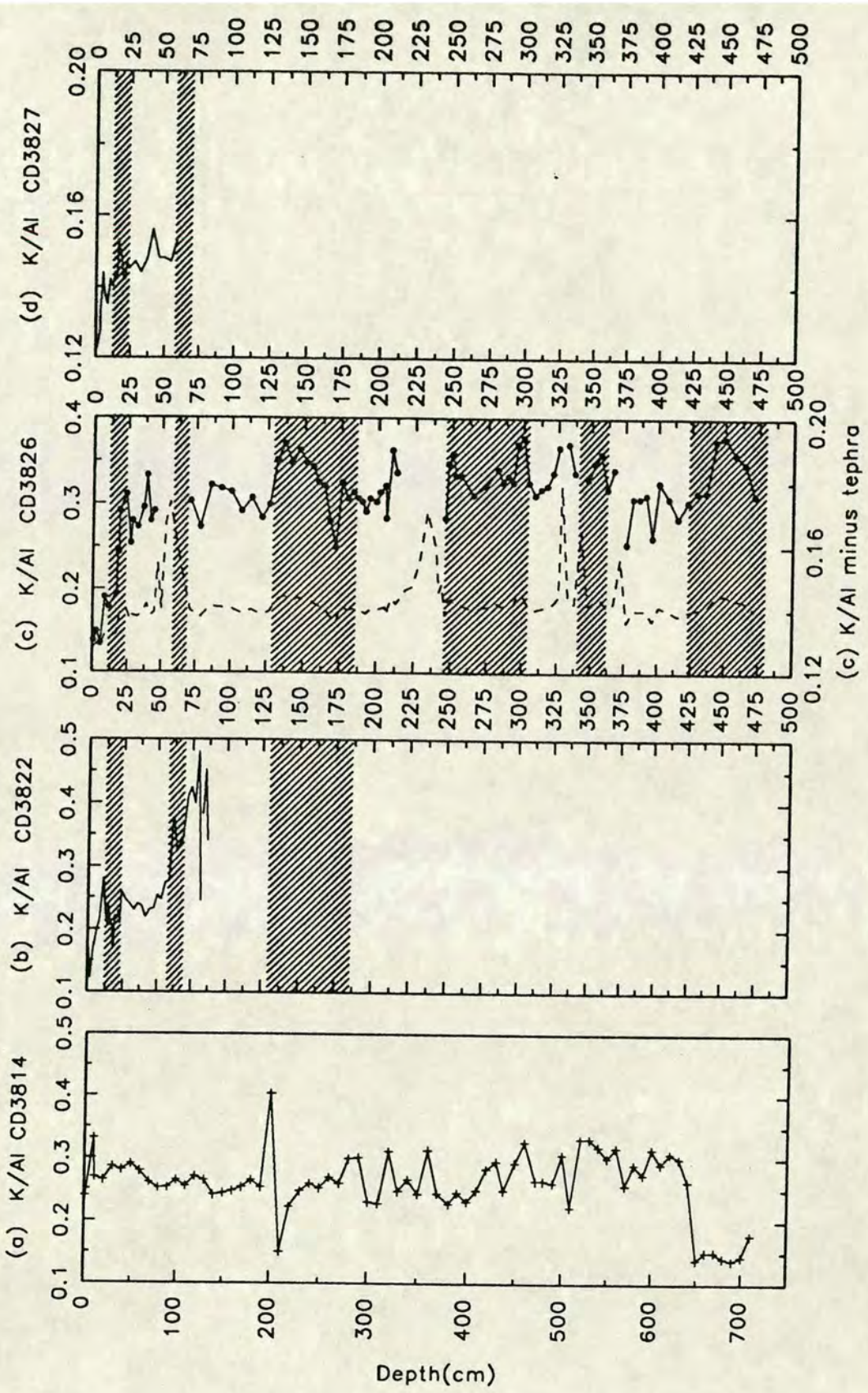

Figure 5.11 Temporal variations in K/Al from CD38 cores. Graph (c) shows a plot for core CD3826 with ash band data included (solid lines + no symbols; upper scale) and with ash band horizons omitted (filled circles + solid lines; lower scale). Shaded regions represent glacial stages II, IV, VI, VIII, X and XII.

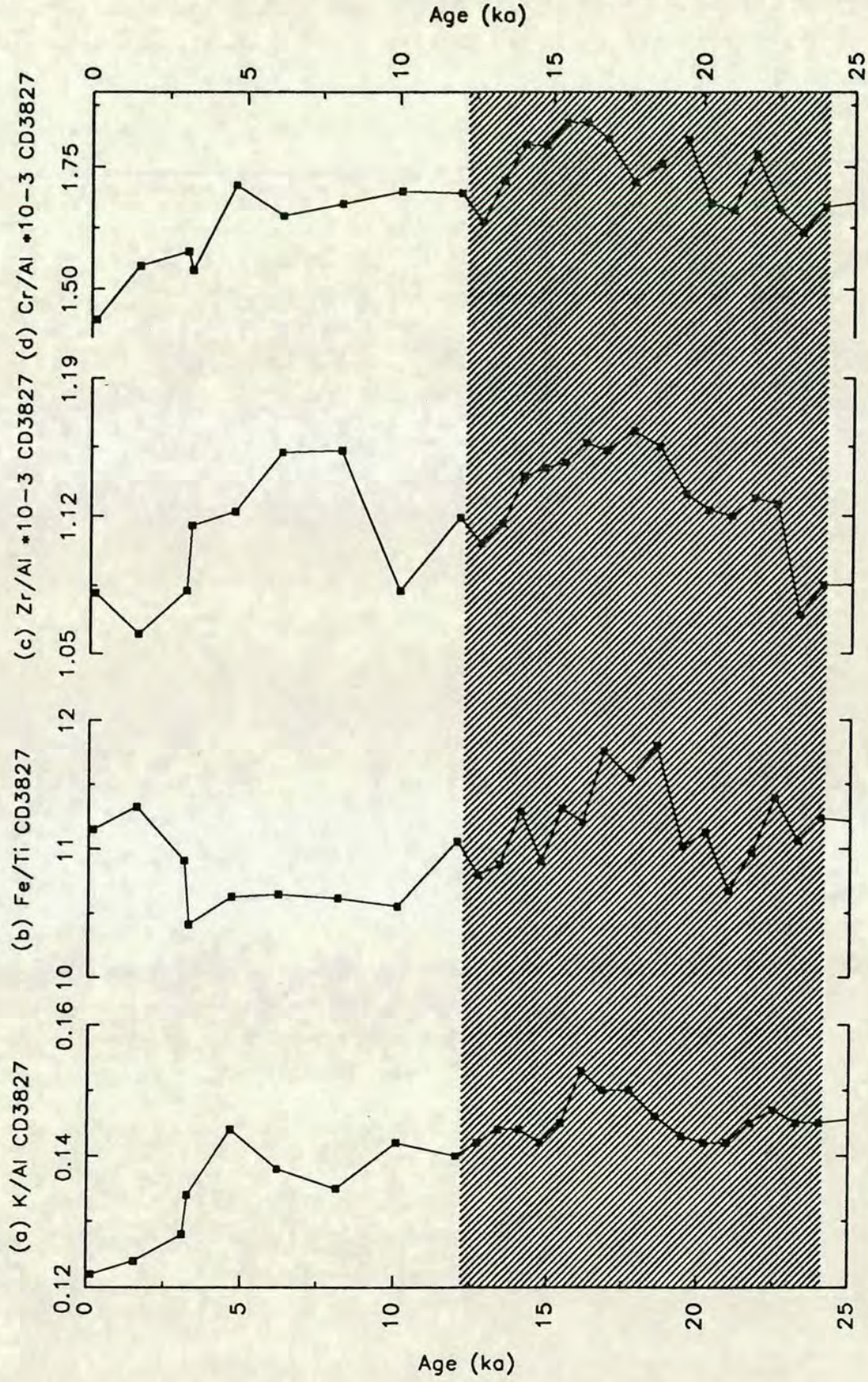

Figure 5.12 Temporal variations in the K/Al (a), Fe/Ti (b), Zr/Al $\times 10^{-3}$ (c) and Cr/Al $\times 10^{-3}$ (d) from core CD3827. Note the Holocene depletion in K/Al and Cr/Al and, the late Holocene decrease in Zr/Al. Shaded region represents glacial stage II (12-24 ka).

Core CD3827 is the most depleted in K relative to Al of all the cores and shows an increase downcore in K/Al ratios (figure 5.11d). Such overall low K/Al ratios would be the result of an impoverished supply of feldspar or illite relative to ferromagnesium minerals such as smectites. The overall decrease in the K/AL values from the base to the surface of the core closely parallels the tephra free plot of K/Al in core CD3826 over the same time period. The increase in K/AL during stage II in core CD3827 is broadly paralleled by enrichments in Fe/Ti, Zr/Al and Cr/Al (figure 5.13). All show a general decrease over the past 25 ka and a distinct enrichment during stage II. This is consistent with increased terrigenous material input during the low sea-level stand last glacial. Fe/Ti, Zr/Al and Cr/Al are discussed more fully below.

All the cores in this study are depleted in K relative to Al compared to the world average of Turekian and Wedopohl, 1961 (table 5.1). The proximity of the Panama basin to the volcanic ash generating igneous landscape of Central and North West South America produces a high aluminosilicate input which tends to depress the K/Al ratio compared with other ocean sediments. This is because of low Si/Al ratios in the volcanic material in the region relative to most sediments. Also, the average K/Al ratio of each core generally increases with increasing distance from land (cp. core CD3827, CD3826 and CD3822; figure 5.0, table 5.1) which is consistent with the seaward increase in K/Al values reported by Pedersen (1979) in the region. This suggests a seaward increase in the illite/feldspar to smectite ratio. In an experiment similar to that of Bostrom (1973), Bischoff and Rosenbauer (1977) analysed a mixed terrigenous and hydrothermal metalliferous sediment from the DOMES area (site C, 14°N 126°W) adjacent to the Clarion Fracture Zone. They report, on a salt included basis, a K/Al ratio of 0.42 as characterising metalliferous sediments, whereas nearby non-metalliferous sediments were shown to have K/Al ratios around 0.33. Sayles and Bischoff (1973) report salt free K/Al ratios of 0.44-0.75 in Bauer deep (metalliferous) sediments while sediments distal to the hydrothermal source have relatively high contents of terrigenous detritus, and have K/Al values ranging from 0.27-0.30. Clearly then, K may be enriched in metalliferous sediments although, as Pedersen (1979) rightly point out, the site(s) in which it resides is uncertain although it may be associated with adsorption from seawater onto interlayer sites in the Fe-smectite (nontronite?) phase or onto hydrogenous oxides. The majority of sediments, except perhaps the one horizon in core P5, appear to belong to the category of non-metalliferous sediments and are much removed from primary sources of hydrothermal output.

5.2.4 Potassium / Rubidium Ratios

The geochemistry of Rb usually parallels that of K due to the diadochous relationship of the two elements: Rb^+ has an ionic radius of 1.47 Å which is sufficiently similar to the 1.33 Å radius of K^+ to permit facile substitution into potassic micas (illite) and feldspar (Pedersen, 1979). Despite the diadochous relationship, K is likely to be enriched relative to Rb in minerals such as clinoptilolite and other zeolites, since the K/Rb ratio in sea water is considerably higher than in the lithosphere (around 3500 and 270 respectively; Riley and Chester, 1971, p64). Rb is thought to be concentrated in the finer grained fraction of the sediment (Calvert, 1976). The parallelism in the two elements is illustrated in the plot of K versus Rb (figure 5.13) which shows strong positive correlation between the two elements in all the cores except CD3827. The variations in the K/Rb ratio in this core are extremely limited and probably produced an erroneous chemical association.

Temporal variations in the K/Rb ratio are presented in figures 5.14 and 5.20d. Cores CD3826 and CD3827 plot close to the world average clay whereas core P5, CD3814 and CD3822 are all depleted in K relative Rb (see also table 5.1). Perhaps these latter three cores are relatively enriched in clinoptilolite type clays compared with the other cores. There is a strong depletion in K/Rb during stage II in cores P5, CD3822, CD3826 and CD3827.

5.3 TRACE ELEMENTS OF THE TERRIGENOUS AND HYDROTHERMAL FRAMEWORK

5.3.1 Titanium

Introduction

Titanium in marine sediments may have several sources including terrigenous material, basaltic debris, authigenic (hydrogenous precipitates) and biological phases. Despite this variety of possible sources, most Ti in deep sea sediments occurs in the continentally derived terrigenous materials such as clays, anatase, rutile and ilmenite (Chester and Aston, 1976). Such resistate minerals as anatase and rutile are generally found in the high density, heavy mineral fraction of detrital sediments (Goldschmidt, 1954). Ti is known to be concentrated in the coarser fraction of the sediment (Spears

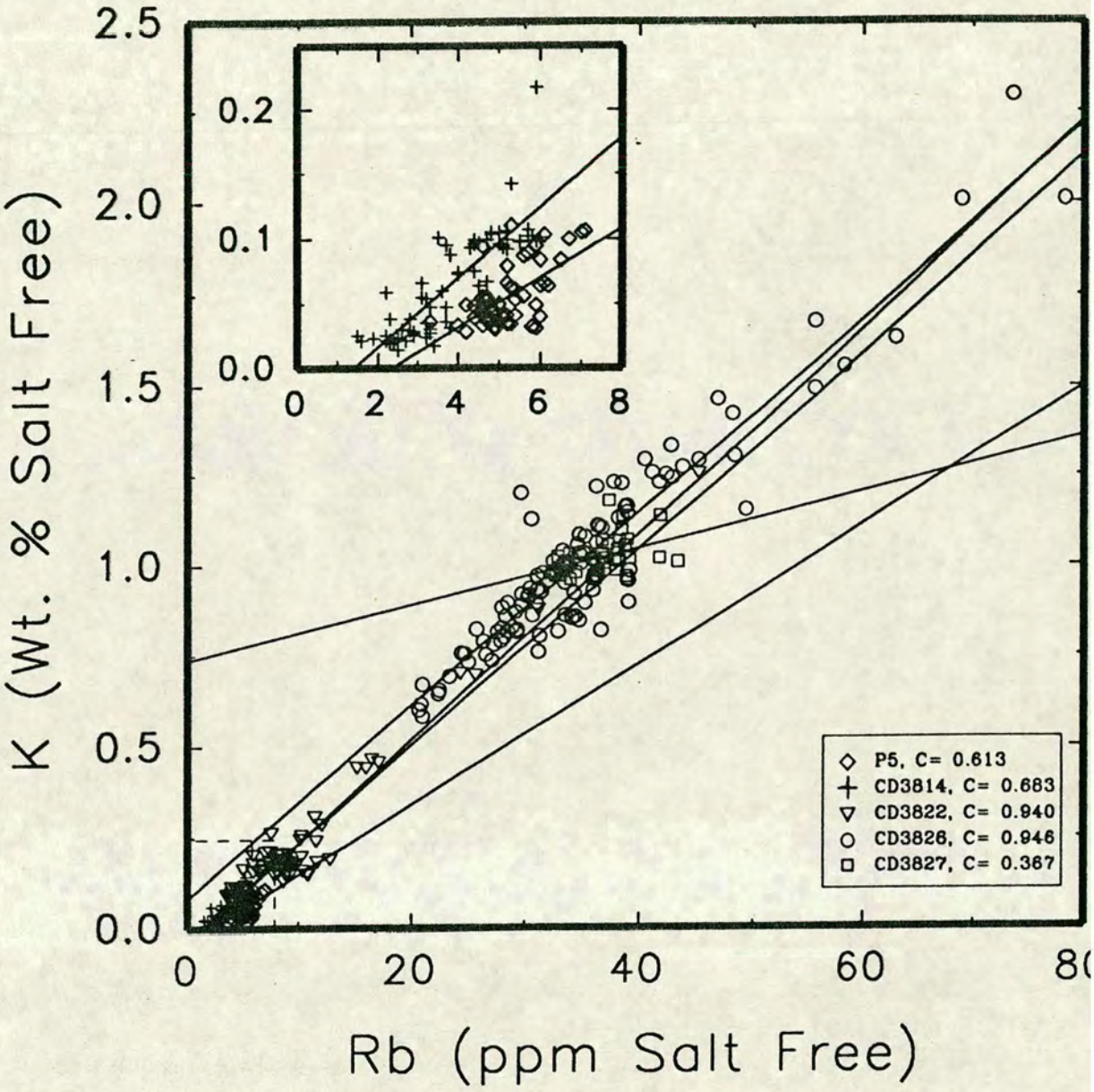

Figure 5.13 Diagram illustrating the relationship between K and Rb from cores studied in this thesis. Inset graph is a detail of the main plot at the lower end of the scale and shows only data from cores CD3814 and P5. Note the high correlation between K and Rb in all cores and that the computer generated regression line of core CD3827 shows an intercept of around 0.75 % on the K axis.

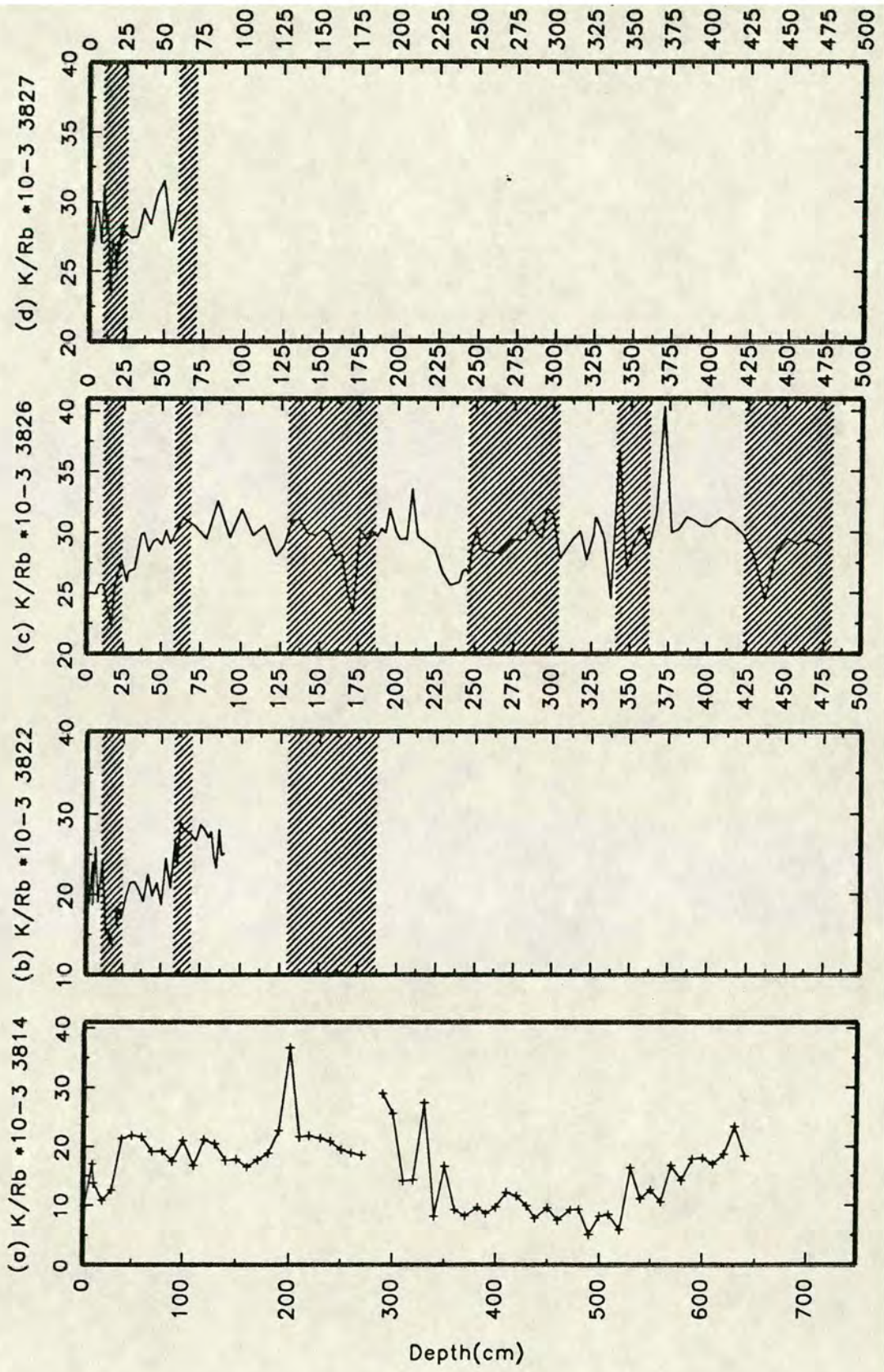

Figure 5.14 Temporal variations in K/Rb × 10^{-3} from CD38 cores. Note the Holocene increase in the ratio in cores CD3822 (b), CD3826 (c) and CD3827 (d). Sharp increases in the profiles probably represent unusually high inputs of feldspar commonly associated with the ash bands. Shaded regions represent glacial stages II, IV, VI, VIII, X and XII.

and Kanario-Sotirou, 1976, Schmitz, 1987). The principal occurrence of Ti in coarse-grained heavy minerals renders the Ti/Al ratio useful as a sensitive indicator of the relative concentration of terrigenous heavy minerals (Pedersen, 1979). Despite this dominant primary source, considerable localised input of Ti from basaltic debris has been reported by Goldberg and Arrhenius (1958) and, more recently, by Bostrom et al. (1973). Ti is present in ferromanganese nodules averaging approximately 0.6% (Chester, 1965) and, according to El Wakeel and Riley (1961) covaries with Fe possibly as a result of scavenging of Ti from sea water by ferric oxides (Goldberg, 1954). According to Bostrom et al. (1974) and Martens and Knauer (1973) Ti occurs in marine organisms such as phytoplankton (≈ 150 ppm) and siliceous frustules (≈ 1000 ppm), however these concentrations are thought to be an indirect manifestation either of injestion of Ti rich particles (Goldberg, 1954) or sorption of Ti onto the surface of organisms or indeed could be the result of aluminosilicate contamination during sample collection. The question of biogenic input of Ti will be discussed further in chapter 6. Boyle (1983) in his work on sediments off Peru was instrumental in developing the Ti/Al ratio as an indicator of climatic change. He proposed that increases in the Ti/Al ratio should occur during glacial periods, as a result of increased intensity of aeolian transport through intensified atmospheric aerosol system and continental aridity.

Boyle (1983) reported the possible interference of Ca on Ti using XRF techniques. This together with the possible interference of the Ba L-α line on the Ti K-α line during XRF spectrometry prompted an investigation to ensure the Ti results were real. The method employed is detailed in appendix A.9. The XRF spectrometer was shown to be capable of resolving the Ba L-α and Ti K-α lines (figure A.9). Further, this experiment also showed the negligible effects of Ca on the Ti determination. Additionally, wet chemical determination of Ti, using a method similar to that of Rigg and Wagenbauer (1961), corroborated the Ti analysis by XRF methods.

Ti-Al Relationships

The linearity of the relationship between Ti and Al in all cores (figure 5.15) demostrates that the majority of Ti is held in aluminosilicate material. Only CD3827 shows any signifcant excess Ti relative to Al which indicates the presence and alteration of Al free titaniferous material, or an authigenic precipitate. Generally, points which lie below the regression line are those horizons associated with volcanigenic ash bands. Cores CD3822 and CD3826 both show some horizons which

lie below the regression lines for each core and indicating unusually low Ti/Al ratios. These horizons will be discussed below.

Ti/Al Profiles

Temporal variations in the Ti/Al ratio are presented in figures 5.16 and 5.17a. The comparison of Ti/Al ratios of surface samples from the Panama basin argues for the existence of two sources of Ti. The first and dominant source is from the continental landmass as Ti/Al ratios increased towards land. The second is the Galapagos platform where high Ti/Al rarios are consistent with an input from the tholeitic and alkali basalts which form the archipelago and which frequently contain considerable titaniferous augite, ilmenite and titaniferous magnetite (McBirney and Williams, 1969). According to Pedersen (1979) the arid climate in the archipelago would foster retardation of weathering of the basalts with the result that most of the Ti enrichment would originate from primary detrital Ti-bearing minerals as opposed to secondary anatase. The distribution of anomalously high Ti/Al values is such that transport of locally derived titaniferous material must be limited to a radius of several hundred kilometers around the archipelago. Core P5, which is strongly enriched in Ti is well within this zone which may be the reason for the anomalously high Ti/Al values in the core. Moreover, the highest values (Ti/Al > 0.13) in core P5 occur during the last glacial maximum during which time the Galapagos archipelago would have had a greater aerial extent and would presumably have been more arid than today. This would have resulted in an increase in the potential titaniferous source material available to weathering and transport mechanisms. The average Ti/Al value for core P5 at 0.106 is unusually high and far in excess of that normally observed in marine sediments (eg Boyle, 1983). The possibility of a biogenic Ti input will be discussed in chapter 6.

None of the other cores studied show any system atic cyclicity in the Ti/Al values and the most characteristic feature of them is the depletion of Ti relative to Al in all the recognised volcanic ash layers. Surficial and average Ti/Al values in the cores studied in this thesis decrease away from the continental margin of central America (c.p. CD3822, CD3826, CD3827). However there is an increase in the Ti/Al ratio towards the Galapagos archipelago (compare CD3822 and P5). Core CD3814 has relatively high Ti/Al ratios, especially in the lower half of the core, which are probably associated with the hydrothermal input to the sediment.

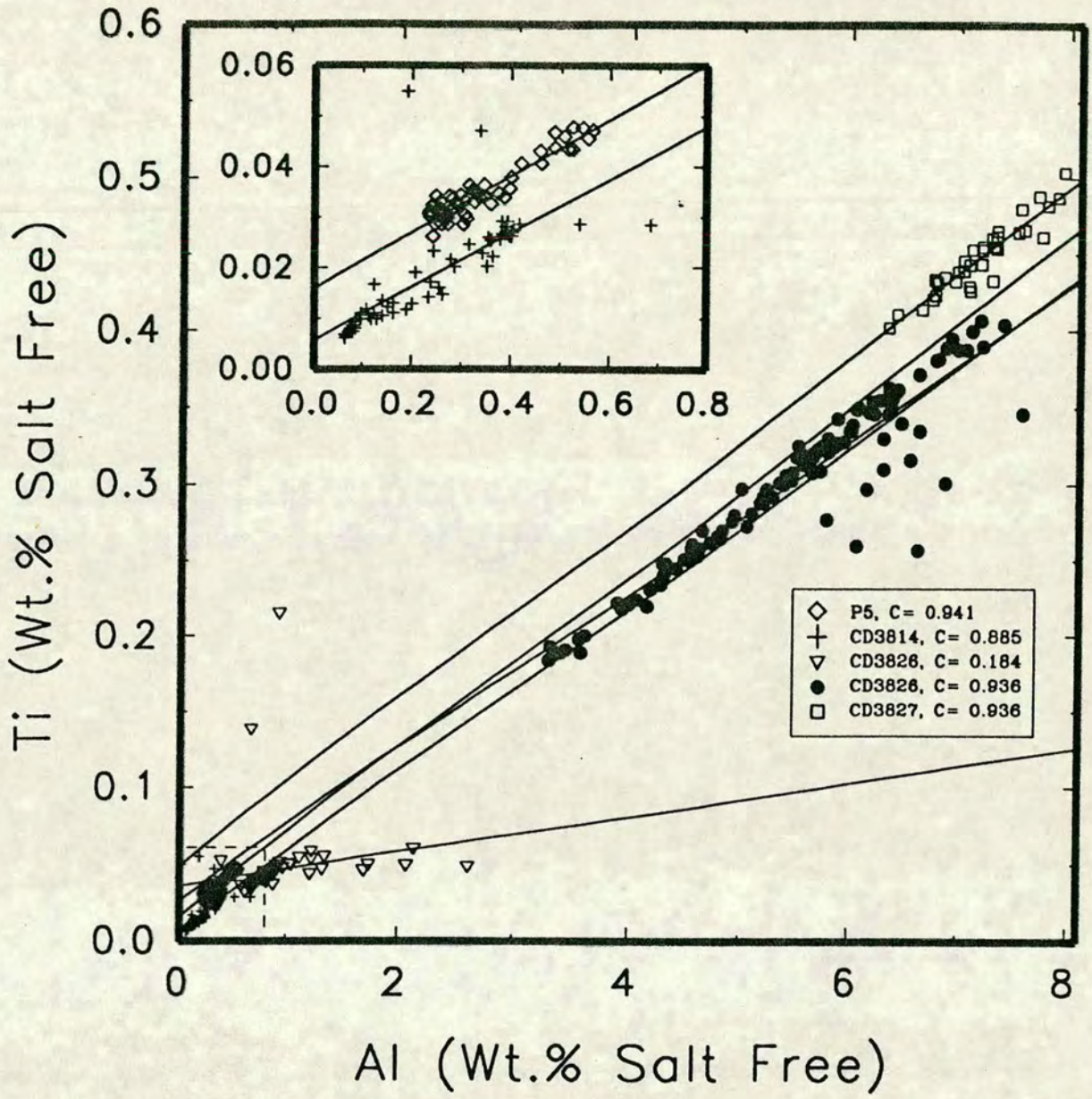

Figure 5.15 Diagram illustrating the relationship between Ti and Al from cores studied in this thesis. Inset graph is a detail of the main plot at the lower end of the scale and shows only data from cores CD3814 and P5. Note the high correlation between Ti and Al in all cores except CD3822. Points below the regression line in core CD3826 (filled circles) represent the ash band horizons that are relatively enriched in feldspar.

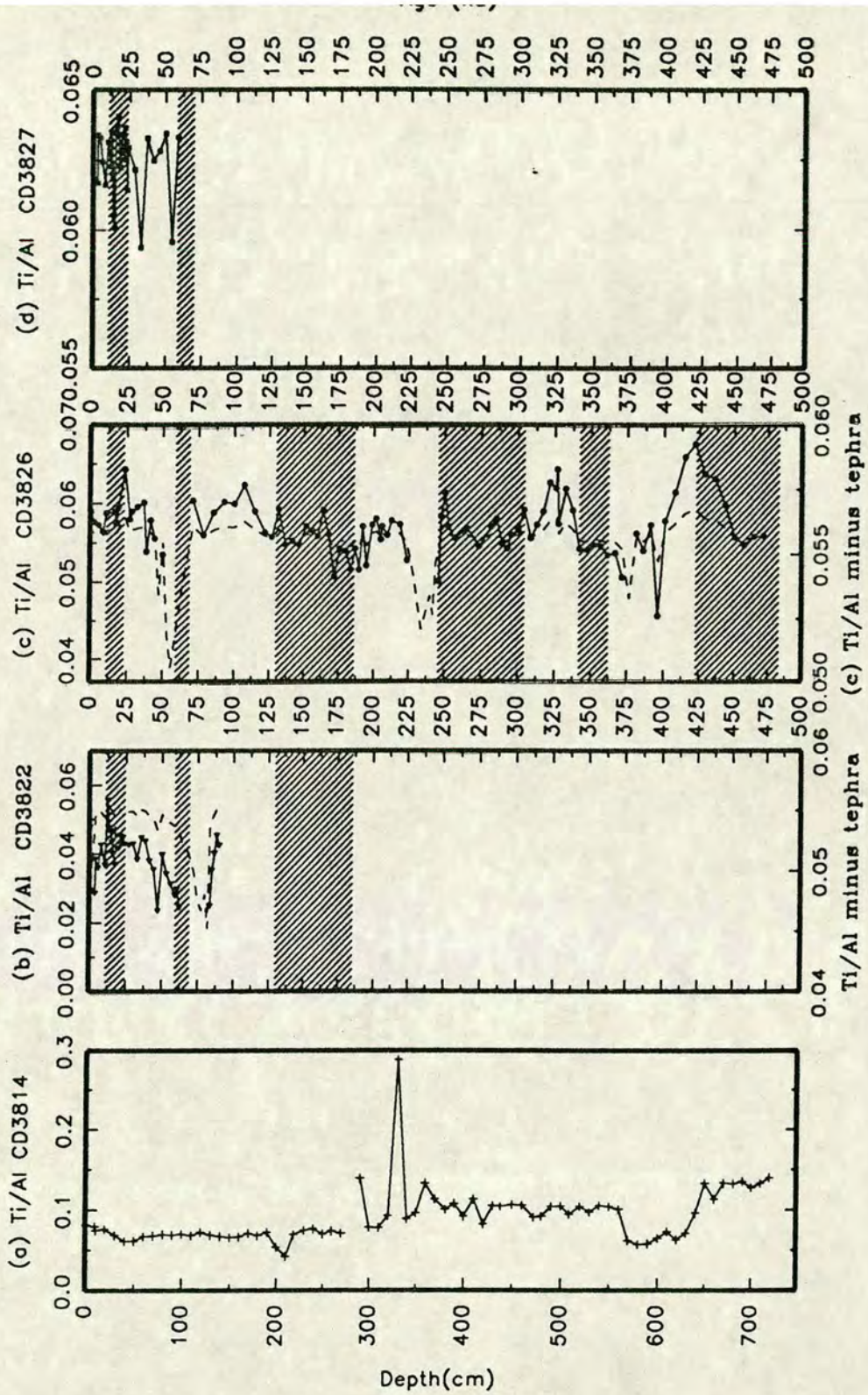

Figure 5.16 Temporal variations in Ti/Al from CD38 cores. In cores CD3822 and CD3826 dotted lines represent plots with tephra horizon data included (upper scale), plots with symbols and solid lines have tephra data omitted (lower scale). Shaded regions represent glacial stages II, IV, VI, VIII, X and XII.

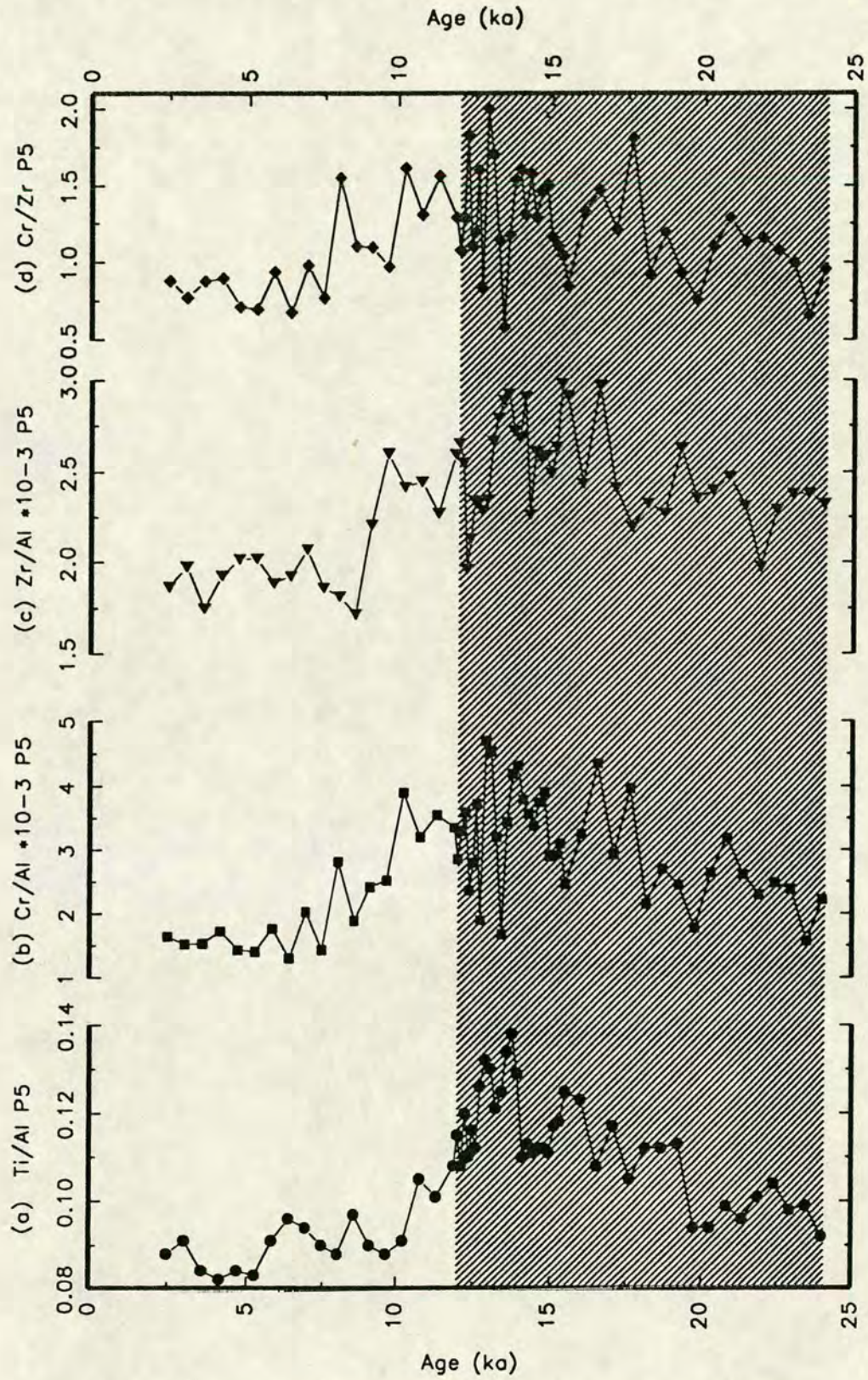

Figure 5.17 Temporal variations in Ti/Al (a), Cr/Al × 10^{-3} (b), Zr/Al × 10^{-3} (c) and Cr/Zr (d) from core P5. Shaded region represents glacial stage II (12-24 ka).

The Ti/Al profile in core AII54-25PC was used for geochemical fingerprinting in development of age models in chapter 4. It shows Ti depleted horizons coinciding with ash bands but it also displays a cylicity where Ti appears to be relatively enriched during interglacial periods (figure 4.11) which is in contrast with the situation in core P5. The Ti/Al ratio in core AII54-25PC tends to move in opposition to $CaCO_3$ (figure 4.11), which might suggest a some effects of dilution except that both Ti and Al are being equally diluted by $CaCO_3$. Hence the cyclicity must reflect a real change in Ti relative to Al. This raises the question of why the Ti/Al ratio mirrors the $CaCO_3$ curve in AII54-25PC, while in core CD3826, whose $CaCO_3$ curve is almost identical to that of AII54-25PC (figure 4.11), there is little sympathetic Ti/Al cyclicity. The effects of Ca as a possible interference on Ti analysis has been shown to be non-existent in this study, however they cannot be ruled out in the analysis for core AII54-25PC.

Ti-Fe Relationships

The linear relationship between Ti and Fe in deep sea sediments reported by El Wakeel and Riley (1961) also holds for the cores studied in this thesis (figure 5.18, tables 5.5-5.9). The varying intercepts on the Ti axis suggests an overall progressive depletion of Ti relative to Fe away from land (cp. figure 5.19 and figure 5.0). Core CD3827 is situated closest to land and shows the greatest intercept of Ti at 0.85% (figure 5.18) is likely to be caused by unusually high contents of coarse grained heavy minerals such as rutile. The large values of Ti in core CD3822 are probably associated with the volcanic ash deposits discussed above. The small Ti intercept in core CD3826 probably indicates a smaller component of rutile in the sediment than in CD3827. Core P5, being quite close to the Galapagos archipelago, probably receives most Ti in the form of titaniferous minerals from the island's basalts. The high Fe/Ti in core CD3814 also suggests some basaltic material into the core although probably from a different source to that in core P5. The lack of excess Ti relative to Fe and the anomalously high Ti/Al ratios in core P5 suggests a proportionately high input of Fe and Ti relative to Al from the Galapagos archipelago.

Downcore variations in Fe/Ti

As discussed above the average Fe/Ti ratios generally increase in a seaward direction (cp. CD3827, CD3826, and CD3822 in table 5.1). Core P5 being strongly enriched in Ti displays the lowest mean Fe/Ti ratio of all the cores and at 7.74 it is just over half

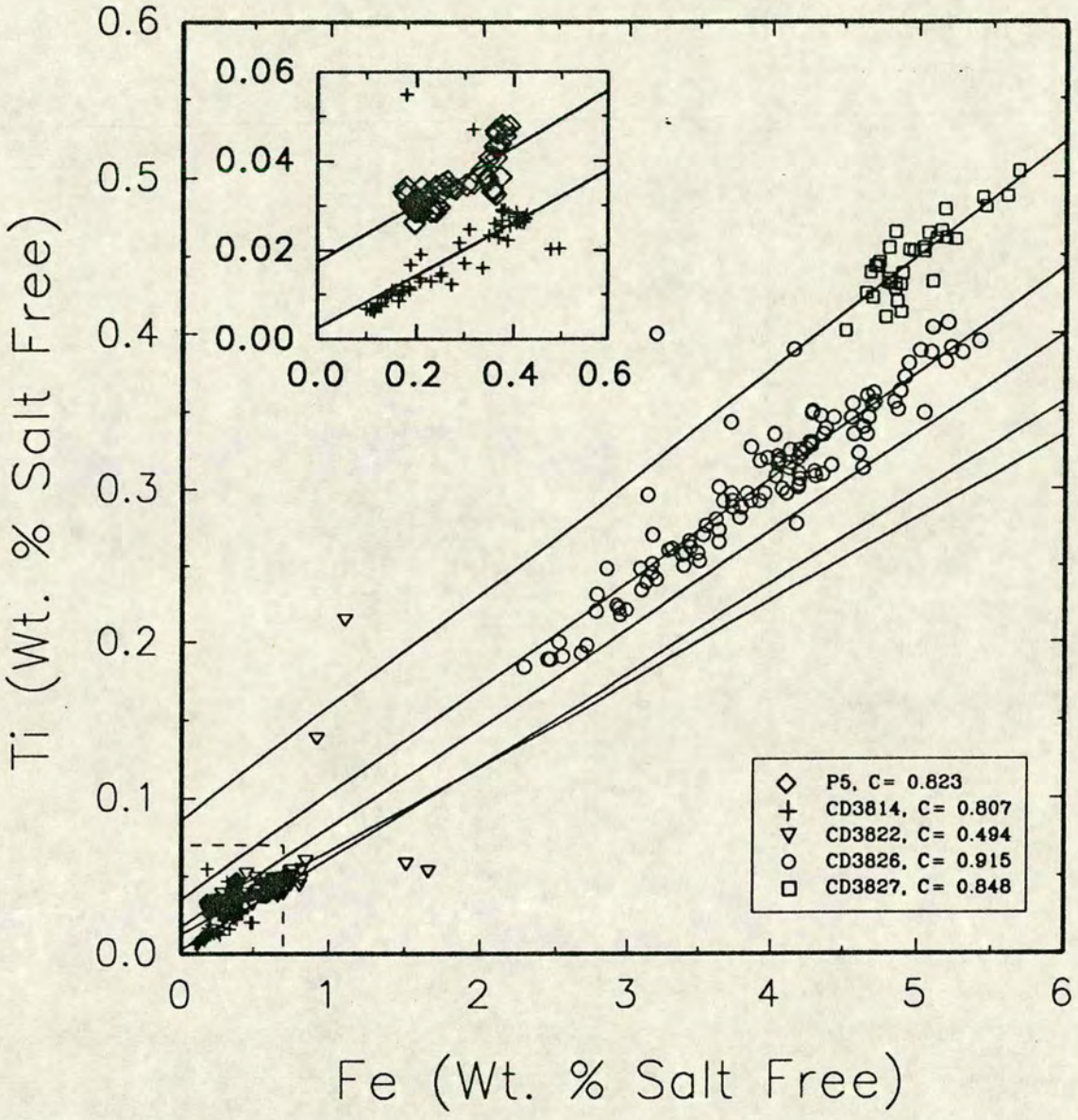

Figure 5.18 Diagram illustrating the relationship between Ti and Fe from cores studied in this thesis. Inset graph is a detail of the main plot at the lower end of the scale and shows only data from cores CD3814 and P5.

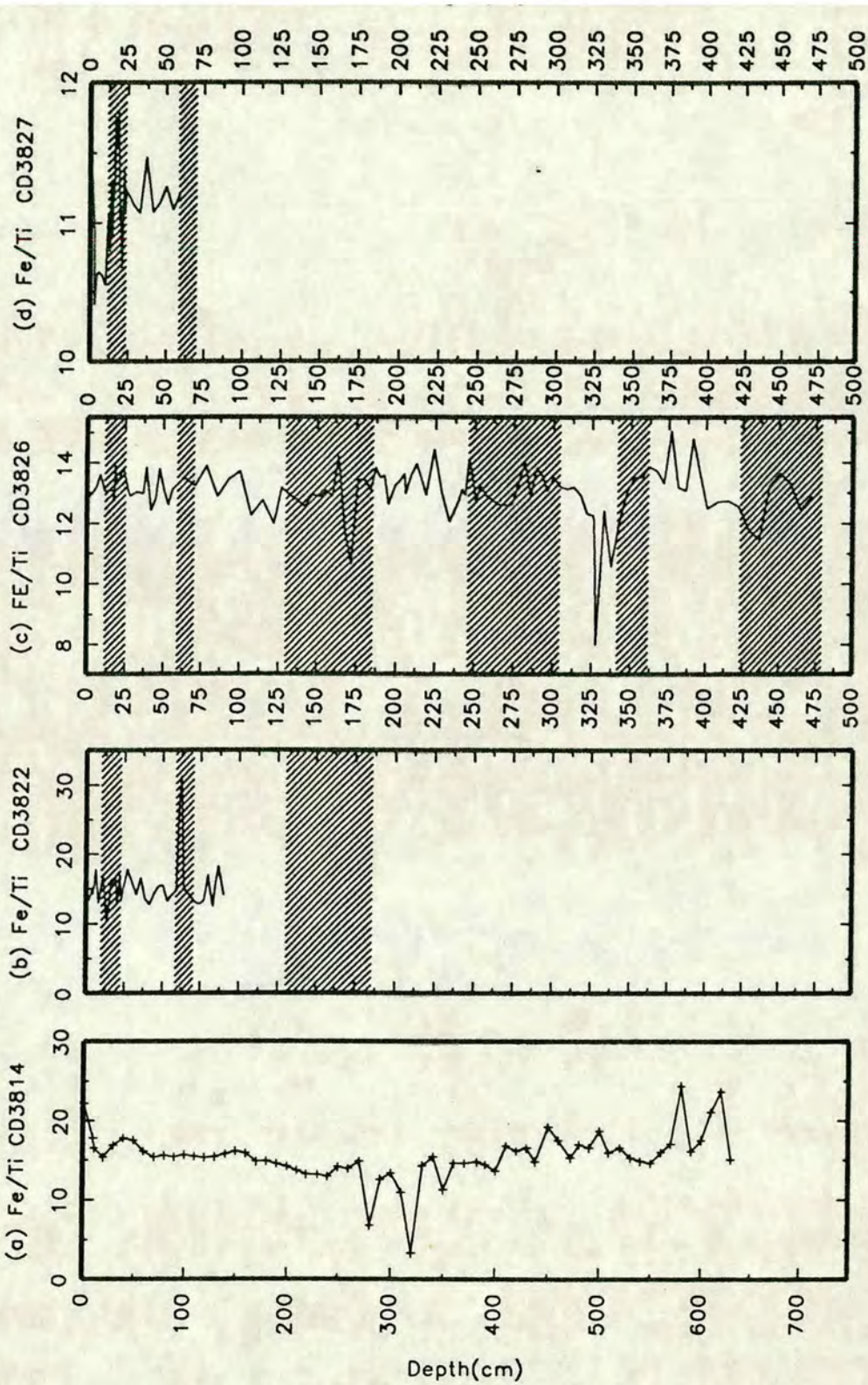

Figure 5.19 Temporal variations in Fe/Ti from CD38 cores. Note the different scales and especially high values in core CD3814 (a) and CD3822 (b). Note also the relatively large increase in values during stage II in core CD3827 (d). Shaded regions represent glacial stages II, IV, VI, VIII, X and XII.

that for the world average of Turekian and Wedopohl (1961). The hydrothermal input of Fe at 12 ka in core P5 also shows up as an increase in the Fe/Ti ratio (figure 5.20a) despite the unusually high Ti contents in this core.

Figure 5.19 shows the downcore varaition in Fe/Ti ratios in CD38 cores which probably results from changes in the terrigenous input or source material dominance. The Fe/Ti curves in cores CD3826 and CD3827 show similarities with Ti/Al profile whereas Fe/Ti curves in cores CD3814 and CD3822 are quite different from other terrigenous indicators (cp. figures 5.16c, 5.16d and, 5.19c, 5.19d). Core CD3827 which probably has the highest terrigenous loading from the continent, displays a strong enrichment of Fe relative to Ti during stage II (figure 5.19d). This spike is also seen in Cr and Zr relative to Al curves (see below) which seems to verify the hypothesis of increased terrigenous input of heavy minerals possibly including magnetite, during the arid, low sea level glacial period mentioned above.

5.3.2 Zirconium

In marine sediments Zr occurs almost exclusively in detrital zircon which is highly resistant to weathering and tends to occur in the coarse grained fraction of the sediments (Hill and Parker, 1970). As a result, any variation in the Zr/Al ratio can be interpreted as representing changes in sediment texture/mineralogy.

Zr-Al Relationships

Only core CD3827 shows excess Zr (30 ppm) relative to Al (figure 5.21) and implies either a different source of aluminosilicate or a relatively small amount of zircon and heavy minerals associated with the aluminosilicates.. Cores P5, CD3814, CD3822 and CD3826 have negligible Zr in excess of that normally held in aluminosilicates.

Relative to the world average clay of Turekian and Wedopohl (1961) cores P5, CD3822 and especially CD3814 are enriched in Zr relative to Al (table 5.1) whereas cores CD3826 and CD3827 are depleted compared to the world average clay (Turekian ad Wedopohl, 1961). As with other terrigenous indicators mentioned above, Zr/Al ratios increases away from land (cp. CD3827, CD3826 and CD3822 in table 5.1) and there is a depletion in Zr relative to Al in the uppermost Holocene in cores CD3822 and CD3827.

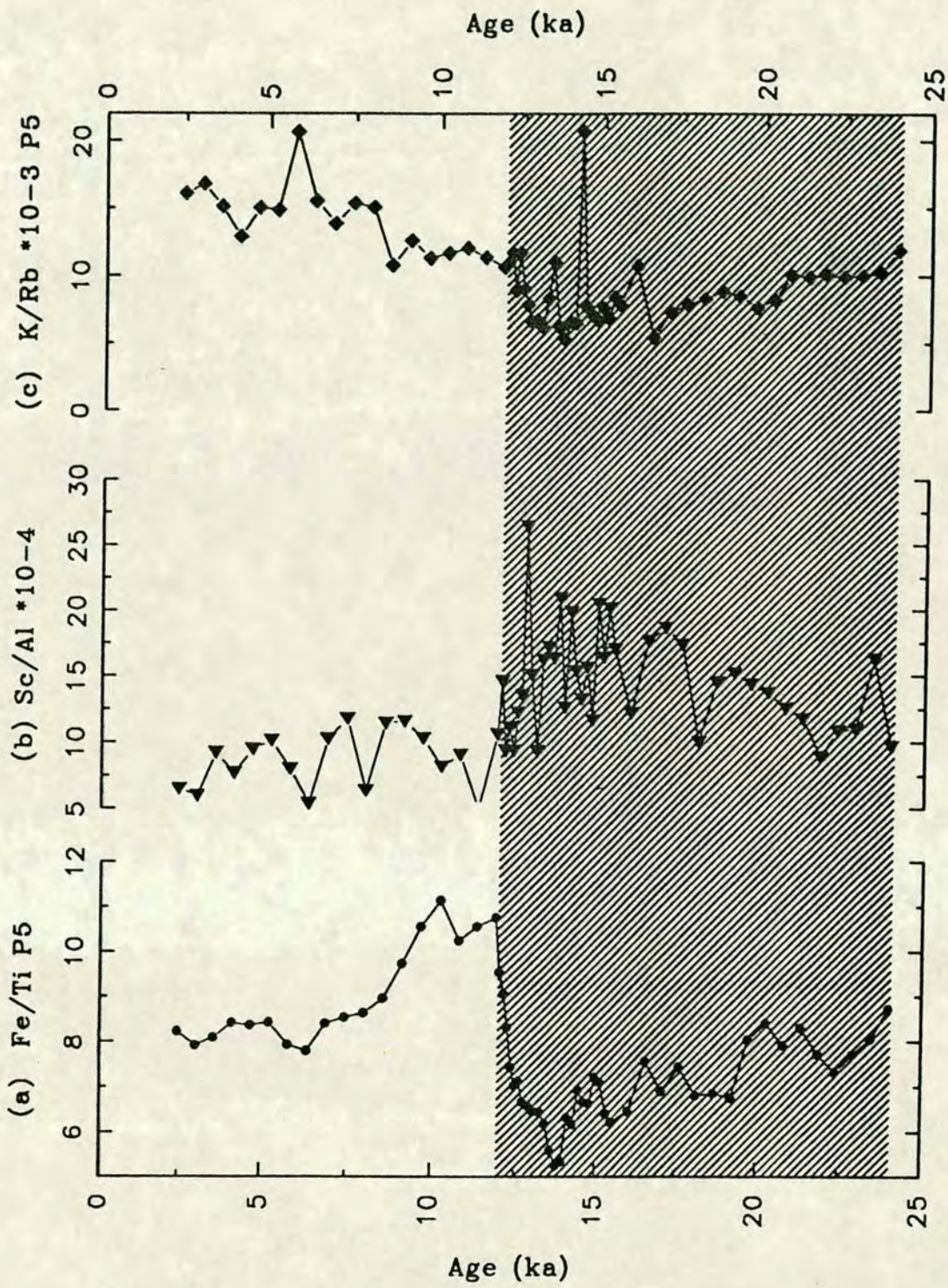

Figure 5.20 Temporal variations in the Fe/Ti (a), Sc/Al $\times 10^{-3}$ (b) and K/Rb $\times 10^{-3}$ (c) from core P5. Shaded region represents glacial stage II (12-24 ka).

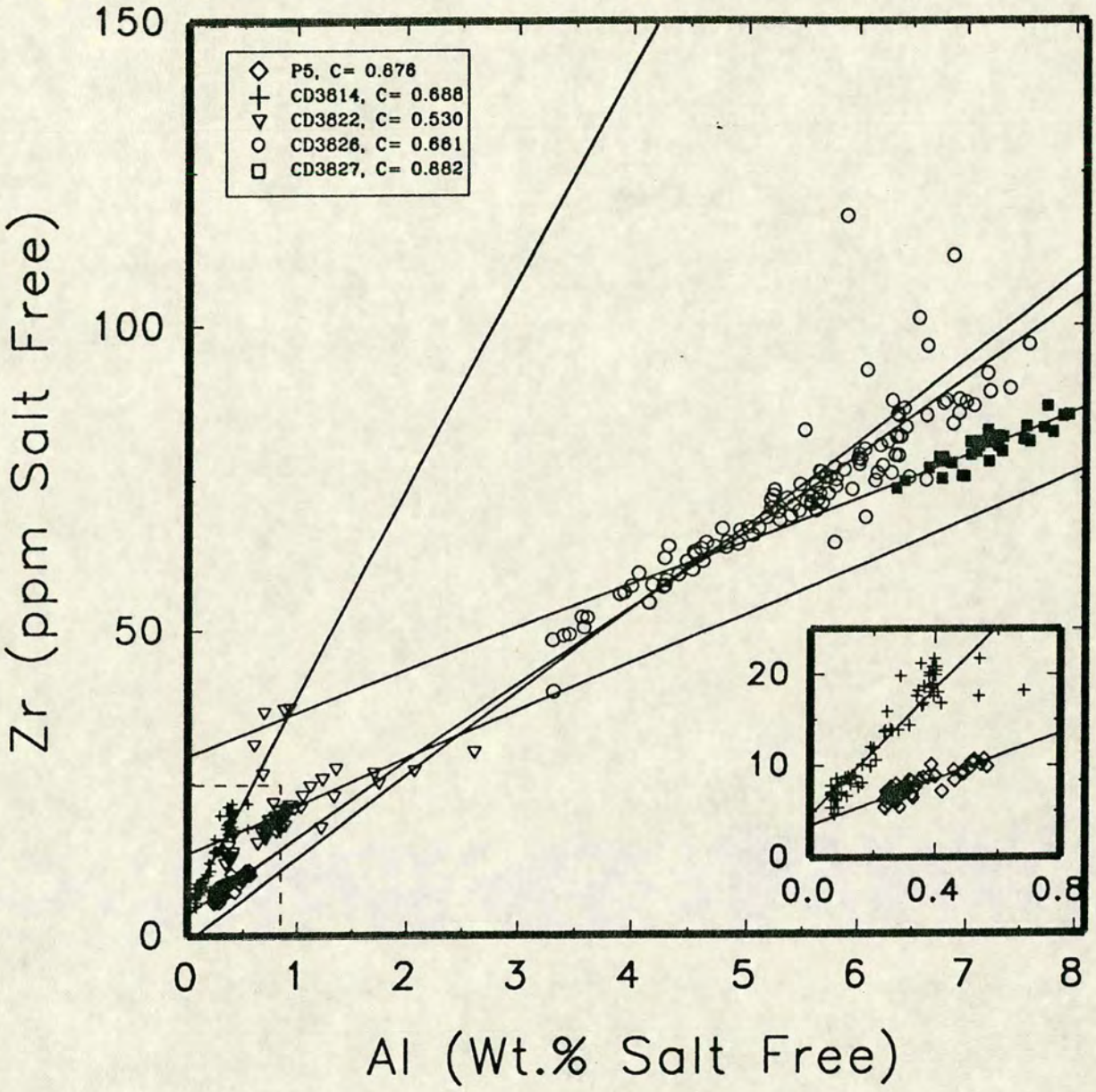

Figure 5.21 Diagram illustrating the relationship between Zr and Al from cores studied in this thesis. Inset graph is a detail of the main plot at the lower end of the scale and shows only data from cores CD3814 and P5. Note the good correlation except in core CD3822 and, the points above the regression line in core CD3826 which are associated with the feldspathic ash bands.

Temporal variations in Zr/Al ratios

Downcore variations in Zr/Al are shown in figure 5.17c and 5.22. The enrichment in Zr/Al in core P5 (figure 5.17c) is greatest during stage II as is Ti/Al. This is probably caused by increased input of Zr bearing basaltic dust from the Galapagos archipelago during the arid glacial periods.

The strong depletion in Zr/Al values in the Holocene section of core CD3822 is immedately preceeded by a large spike at the close of stage II. The enrichment, which is also seen marginally earlier in the Cr/Al record (see below), coincides with the strong negative $\delta^{18}O$ anomaly in the core. The significance of the isotopic signal is not clear but, with respect to the Zr/Al and Cr/Al profiles, it must represent a period of sharply increasing terrigenous material at the switch from glacial to interglacial periods.

Ash layers "L" and "K" in core CD3826 are strongly enriched in Zr relative to Al whereas ash "D" is depleted in Zr relative to Al (figure 5.22c). In sediments containing no ash there is a tendancy for Zr/Al values to be greater during glacials (especially stage II, VI, X and XII). As with other terrigenous elements core CD3827 shows little variation but there is a clear spike in Zr/Al during glaical stage II and in the early part of stage I (figure 5.22d).

5.3.3. Chromium

Chromium in deep sea sediments is usually associated with basaltic pyroclastics (Goldberg and Arrhenius, 1958; El Wakeel and Riley, 1961). According to Goldberg and Arrhenius (1958), a concentration of greater than 100 ppm Cr in deep sea sediments indicates the presence of altered or unaltered basaltic material. They also found that Cr tended to be concentrated in the coarse fraction of the sediment and not in the clay fraction. Cr is not, unlike other transition metals, enriched in ferromanganese nodules (Cronan, 1977). It is, however, often highly concentrated in hydrothermally influenced crestal sediments of the East Pacific Rise (EPR), (Bostrom and Peterson, 1966). According to Pedersen (1979) such a fractionation suggests that the EPR Cr is of hydrothermal origin and implies that the high Cr content in Fe rich band of core P6 resulted from co-precipitation with Fe from hydrothermal solutions. Pedersen (1979) found that ratios of Cr/Al in sediments from all over the Panama

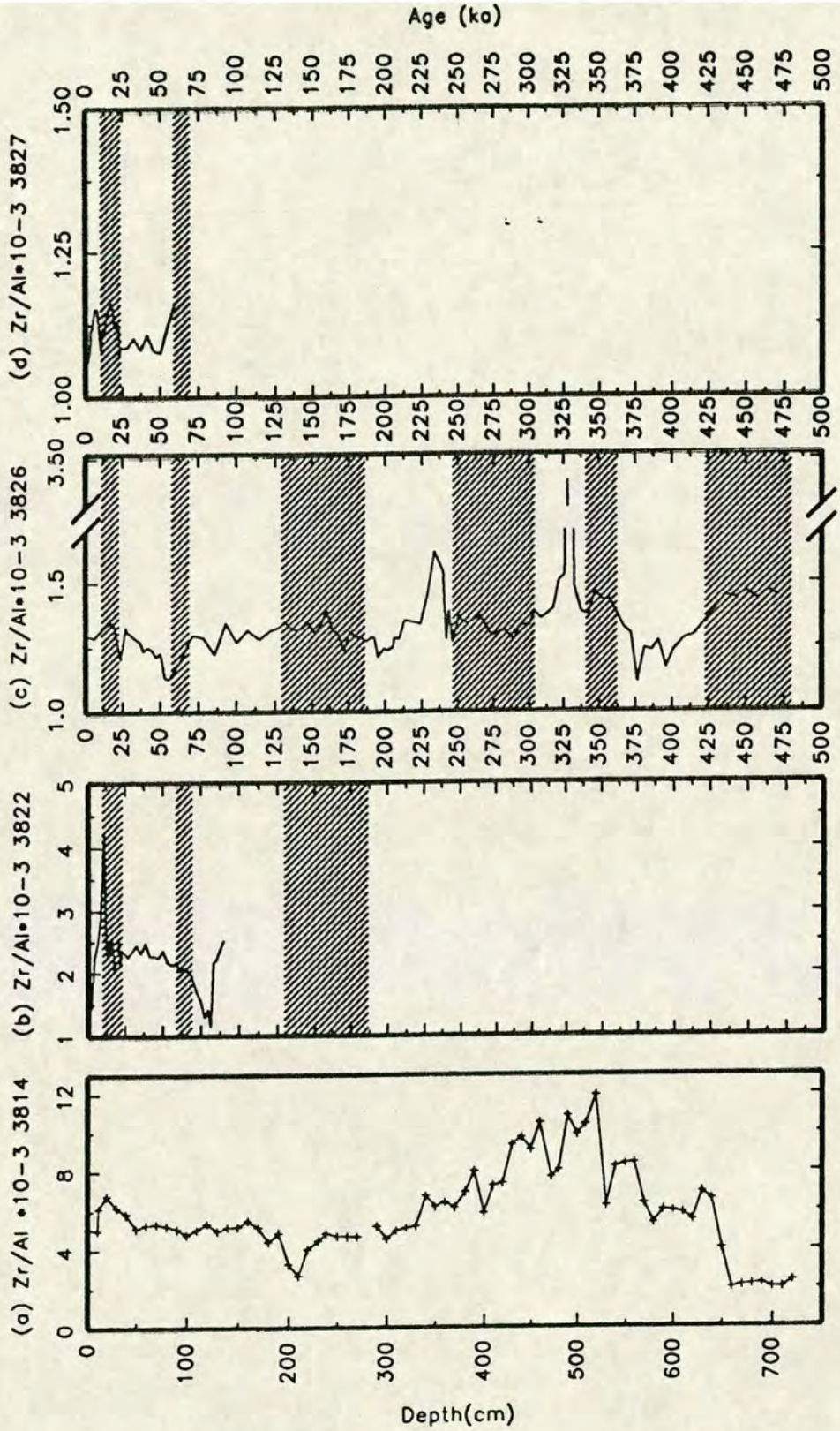

Figure 5.22 Temporal variations in Zr/Al from CD38 cores. Note the very small variation in values in core CD3827 (d), the very large variation in values in core CD3822 (b) and, the very high values in core CD3814 (a). Note also the relatively high values in layers D (56 ka), L (234 ka) and K (328 ka) in core CD3826 (c). Shaded regions represent glacial stages II, IV, VI, VIII, X and XII.

basin did not vary by much except as a result of the hydrothermal pulse in core P6 (see chapter 4.6).

Cr-Al Relationships

The five cores studied show highly variable Cr contents which show a generally linear correlation with Al (Figure 5.23, tables 5.5-5.9). On the whole, core CD3814 has <10 ppm Cr present, which is close to the analytical limit of detection. This resulted in some negative values, which were assumed to be zero. The relationship of Cr to Al is difficult to assess. In cores P5 and CD3822 there is no obvious correlation between Cr and Al, with intercepts of around 10 ppm Cr. Cores CD3826 and CD3827 however, show Cr intercepts of 30 ppm and 91 ppm respectively, which implies a significant amount of Cr is present in the terrigenous fraction of the sediment. This is probably in the form of magnetite of igneous origin. Goldberg and Arrhenius (1958) found that Cr was preferentially associated with the coarse/dense fraction of the sediment which decreases away from land. Their findings are consistent with the decrease in excess Cr seaward observed in this study.

Downcore variations in Cr/Al

Core CD3822 shows clear enrichment of Cr during stage II and a relatively constant ratio down to the base of stage IV (80 ka). At this point the sediment becomes impoverished in Cr, coincident with the ash band, before increasing sharply to around the average value of 1.46×10^{-3} at the base of the Pleistocene section of the core (figure 5.24b). The Pliocene section of the core, which is not shown, displays quite large fluctuations in Cr/Al. The origin of these is not certain because no time fix has been possible during this period.

The Cr/Al profile in core CD3826 (figure 5.24c) is similar to the Ti/Al, Fe/Al and Fe/Ti curves (cp. figures 5.7c, 5.16c and 5.19c) and seems to be generally higher during the glacial periods as is seen in core CD3827 during stage II. If it is assumed that most Cr in the core is derived from the input of terrigenous heavy minerals, then this cyclicity is consistent with increased wind and available source material from the periodically exposed subaerial continental shelves during the low sea level stand glacials. Major decreases in Cr relative to Al, however, are definitely due to volcanic ash bands described above.

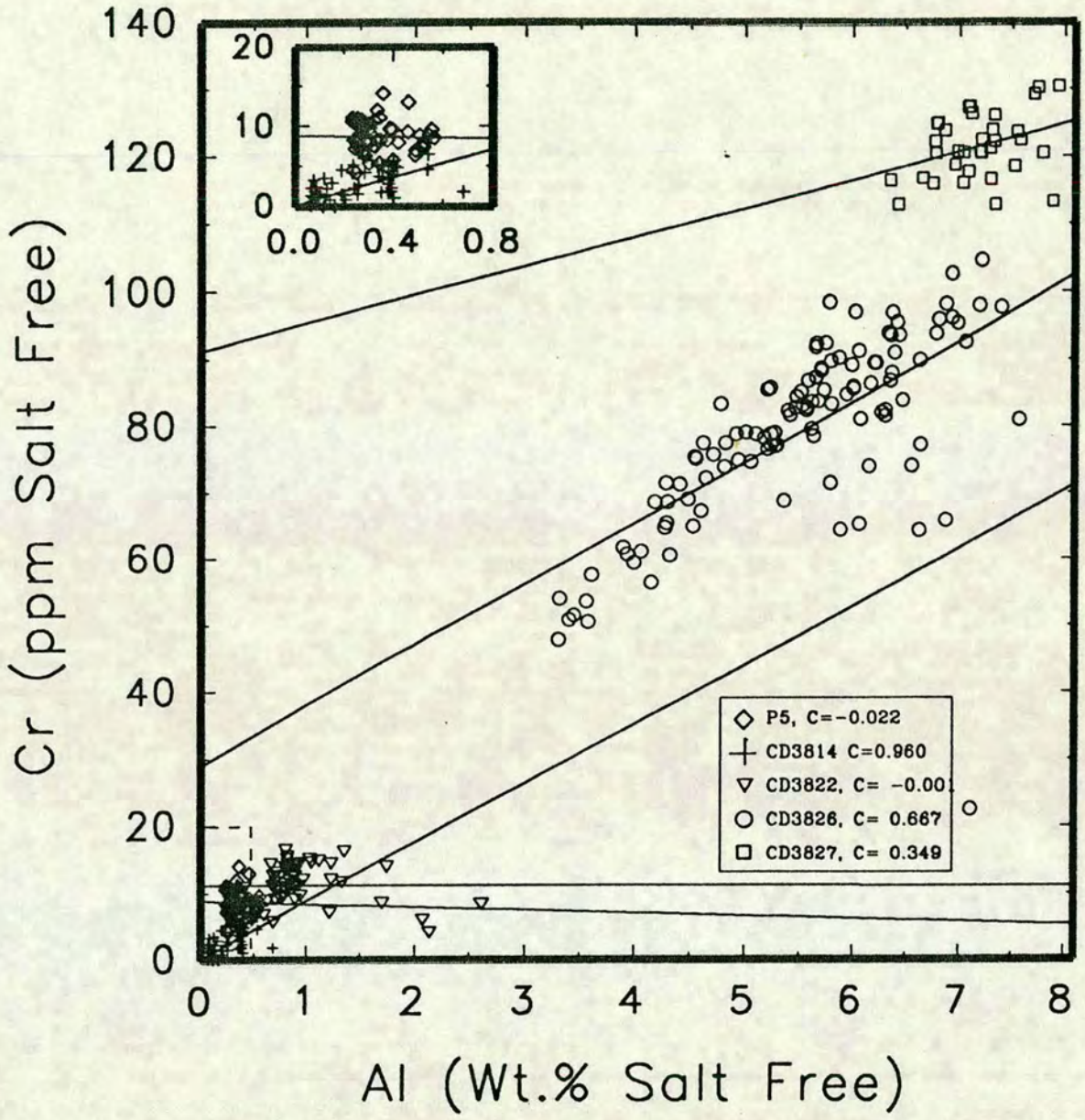

Figure 5.23 Diagram illustrating the relationship between Cr and Al from cores studied in this thesis. Inset graph is a detail of the main plot at the lower end of the scale and shows only data from cores CD3814 and P5. The Cr intercept in core CD3826 is probably due to the points representing the feldsapthic ash bands offsetting the regression line. The large intercept on the Cr axis in core CD3827 may be due to unusually high inputs of magnetite.

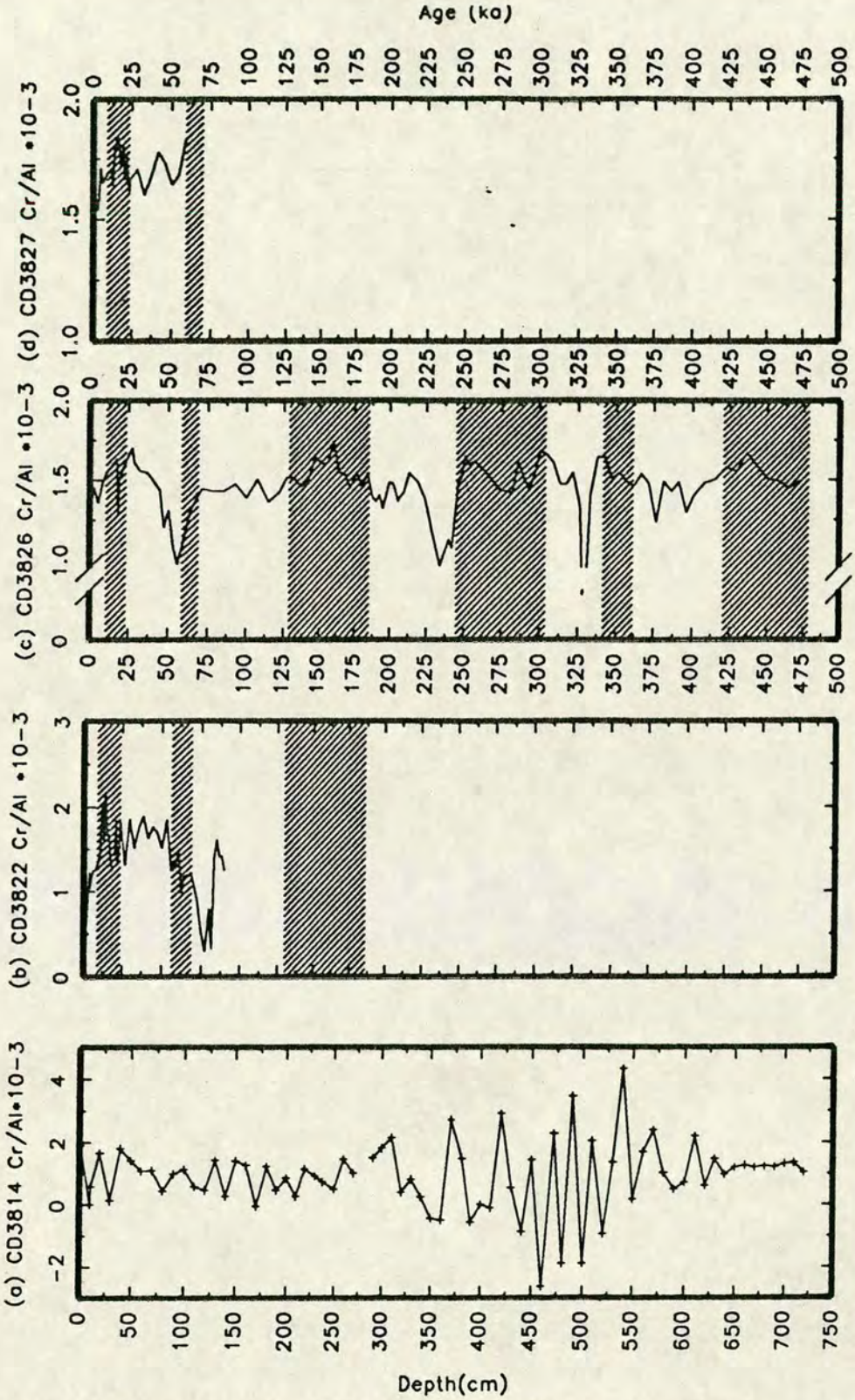

Figure 5.24 Temporal variations in Cr/Al x 10^{-3} from CD38 cores. Note the very small variation in values in core CD3827 (d), the large variations in values and low values of the ash band (80 ka) in core CD3822 (b) and, the relatively low values in layers D (56 ka), L (234 ka) and K (328 ka) in core CD3826 (c). Shaded regions represent glacial stages II, IV, VI, VIII, X and XII.

Core P5 has the highest enrichment of Cr, with Cr/Al ratios ranging between approximately 15 and 45 $\times 10^{-3}$ (table 5.1). Maximum values again occurr during the glacial period (stage II), although the signal is somewhat noisy (figure 5.17b). The general trend of the signal here is of a single cycle which peaks in the glacial. The input of Cr to the sediment, from the hydrothermal pulse at around 12 ka, seems somewhat limited, and suggests that hydrothermal activity as a mojor source for Cr proposed by Pedersen (1979) is somewhat equivocal.

5.3.4 Implications of Cr/Zr fluctuations

Since Cr and Zr are both almost exclusively of terrigenous origin (mainly basaltic detritus), any changes in their ratio between cores must result from some alteration of, or difference in, terrigenous/igneous source rock. Khan (1989), in a study of Arabian sea sediments, described such changes in the ratio of the two elements as being the result of post-depositional mechanical redistribution of Cr.

Temporal changes in the Cr/Zr record for cores studied in this thesis are shown in figures 5.17d and 5.25. Cores CD3822 and CD3826 display Cr/Zr values between 0 and 1, whereas cores P5 and CD3827 are enriched in Cr, which results in Cr/Zr values of around 1.2 and 1.5 respectively. This relative concentration of Cr probably orginates from shelf sediments via pluming and bottom current transport (from the continental margin). The higher Cr/Zr ratios in core P5, CD3822, CD3826 and CD3827 during glacial periods might suggest that the Cr bearing source material is being transported during these times.

5.3.5 Rare Earth Elements

Introduction

Rare earth elements (REEs) in marine sediments are either lithophilic, reflecting clay mineral content and composition, or are associated with phosphatic material. Consequently, clays tend to inherit the REE distribution of the source material (Chaudari and Cullers, 1979), while phosphatic material tends to reflect the REE composition of seawater and pore waters. The low REEs associated with quartz and major silicates (eg feldspars) generally cause a decrease in the REE content of coarse grained sediment (Haskin et al. ,1966). Apatite ($Ca_5(PO_4)_3F$) is an effective

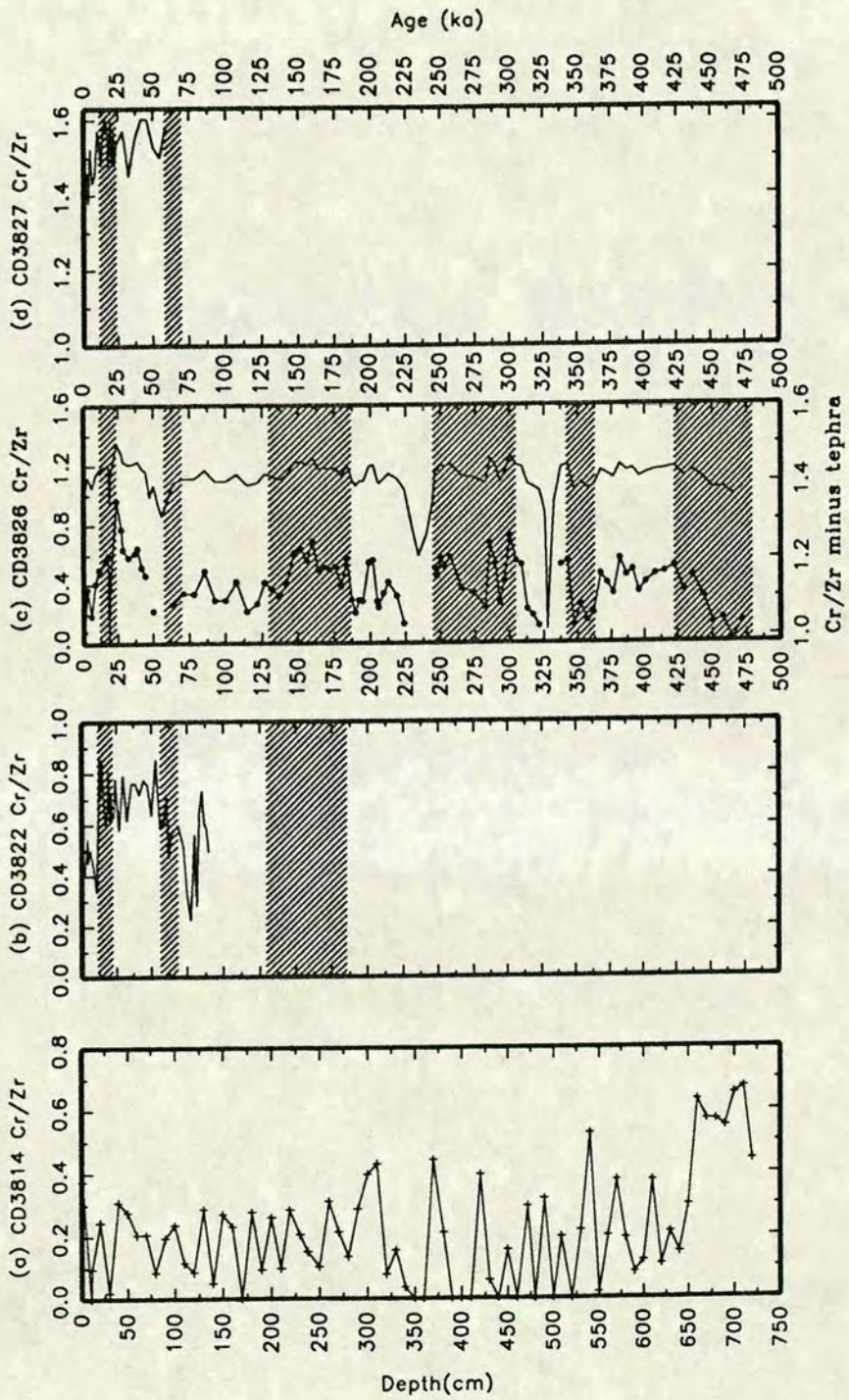

Figure 5.25 Temporal variations in Cr/Zr from CD38 cores. In core CD3826 (c), the solid line without symbols represents the plot with tephra horizon data included (upper scale); the solid line with filled circles represents a plot with tephra data omitted (lower scale). Note the large decrease in the ratio for the ash bands in cores CD3822 (b) and CD3826 (c). Shaded regions represent glacial stages II, IV, VI, VIII, X and XII.

adsorbent of lanthanides and thorium (Chester and Aston, 1976, p.298) and Mn oxides are known to selectively scavenge Ce (dissolved phase) from the water column where Ce^{2+} subsititutes for Mn^{4+}. Surface sediment Mn-oxide may concentrate Ce, however, after burial and a reduction in the release of REE's may result in them being incorporated into diagenetic phosphatic material. Ce, like other REE's, is known to be associated with marine apatite and is influenced by the palaeoredox state at the time of deposition (Wright et al., 1987). Ce, in relation to redox conditions, will be discussed more fully in chapter 9.

This section examines the downcore record of the ratios La/Ce, Nd/Ce, La/Nd and Ce/Nd with respect to possible sediment mineralogy and geochemical changes from glacial to interglacial. The REEs were analysed by XRF (see appendix A.5) and, perhaps as a result of a calibration problem, many of the results produced were negative values especially in the carbonate rich cores. As analytical precis ion is poor, the trends discussed below may not represent a true reflection of mineralogy and source rock changes over time.

Mean REE values and their ratios to Ce and Nd from this study are compared to world averages (Turekian and Wedopohl, 1961) in table 5.3. All the cores are strongly depleted in REEs relative to the world average Deep-Sea Clay.

Downcore profiles of the REE ratios Ce/Nd, La/Ce, La/Nd and Nd/Ce in all cores are shown in figures 5.26-5.30. Only cores CD3826 and CD3827 display any sort of systematic variation. Core CD3826 has several large spikes in all four ratios which are probably caused by some major change in the mineralogy (eg Mn enriched horizon at 24 ka, see chapter 9). Of all the ratios, the Ce/Nd curve appears to be the one that displays the most obvious cyclicity in both cores CD3826 and CD37827 (figure 5.26c, 5.26d). Both cores tend to show generally higher Ce/Nd ratios during the interglacial periods which may be the result of changing proportions of feldspars and clays.

5.3.6 Variations in Scandium

Scandium in marine sediments is almost exclusively held in aluminosilicates. Cores CD3814, CD3822 and P5 are depleted in Sc relative to the world average deep-sea clay of Turekian and Wedopohl (1961). All cores are, however, enriched in Sc

	World Mean REE Values *		Whole core mean REE values				
	Deep-Sea Carbonate	Deep-Sea Clay	CD3814	CD3822	CD3826	CD3827	P5
Nd	14	140	13.19	11.78	19.86	14.71	7.36
Ce	35	45	8.90	10.36	27.27	22.85	3.15
La	10	115	8.41	6.75	15.15	13.88	3.95
Nb	4.6	14	3.82	1.79	4.90	5.49	0.60
La/Ce	0.286	0.333	0.945	0.551	0.556	0.607	1.258
Nd/Ce	0.400	0.406	1.482	1.137	0.728	0.644	2.344
La/Nd	0.714	0.821	0.638	0.573	0.763	0.944	0.537
Ce/Nd	2.500	2.460	0.675	0.879	1.373	1.373	0.427
Y	42	90	21.05	18.09	25.79	15.83	8.49
Y/Al	0.21	10.71	88.64	22.79	4.75	2.21	26.68
Sc	2	19	7.40	5.43	19.93	26.90	3.99
Sc/Al	1.00	2.26	33.04	7.31	3.65	3.75	12.65

Table 5.3 Mean REE values, their ratios to Ce and Nd; mean Y, Y/Al, Sc and Sc/Al and, from Turekain and Wedopohl (1961)*. Ratios to Al are $\times 10^{-4}$

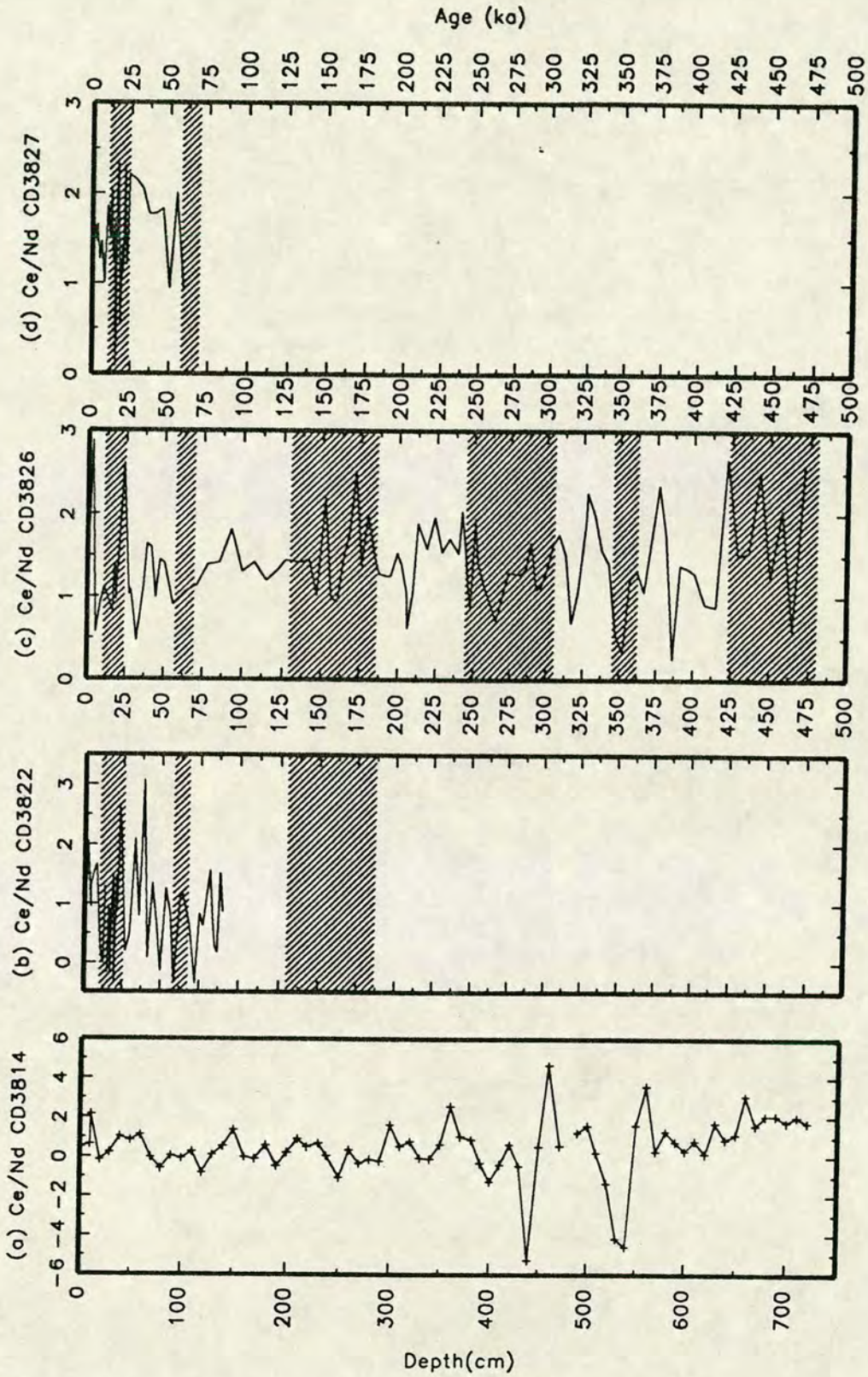

Figure 5.26 Temporal variations in Ce/Nd from CD38 cores. Note the noisy signal in all the cores. Shaded regions represent glacial stages II, IV, VI, VIII, X and XII.

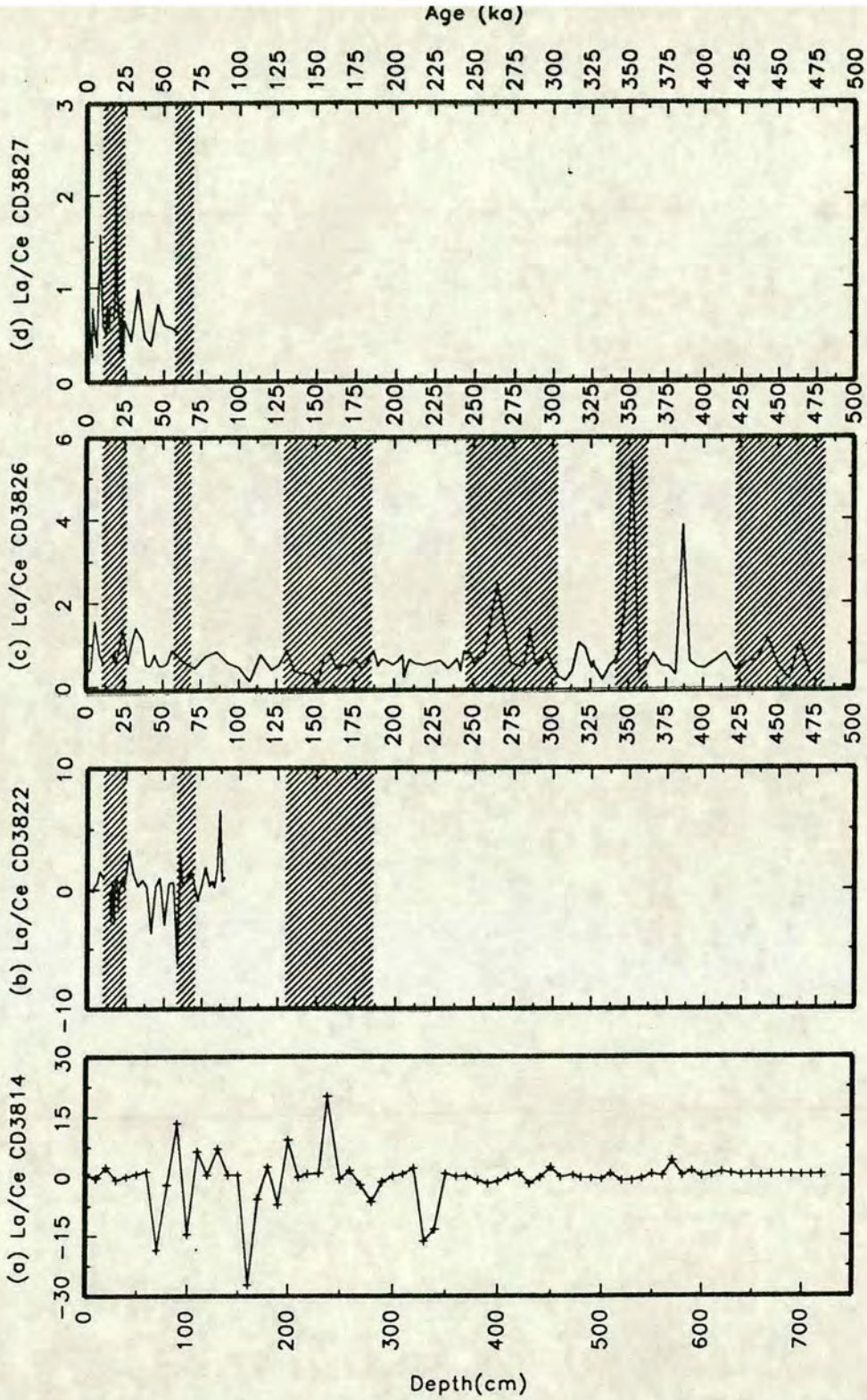

Figure 5.27 Temporal variations in La/Ce from CD38 cores. Note the small variation in values except in horizons associated with the ash bands. Shaded regions represent glacial stages II, IV, VI, VIII, X and XII.

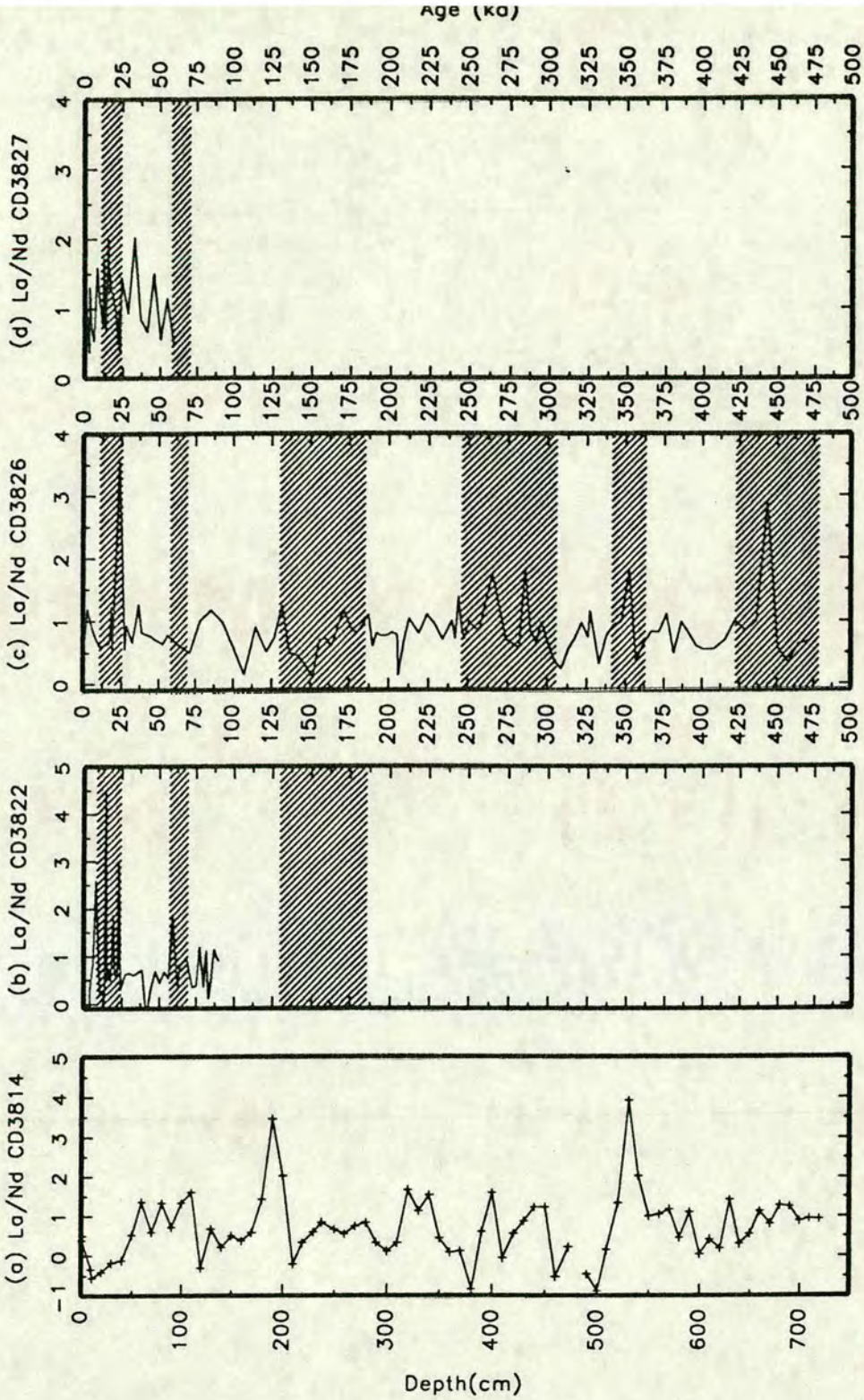

Figure 5.28 Temporal variations in La/Nd from CD38 cores. Note the noisy signal in all the cores. Shaded regions represent glacial stages II, IV, VI, VIII, X and XII.

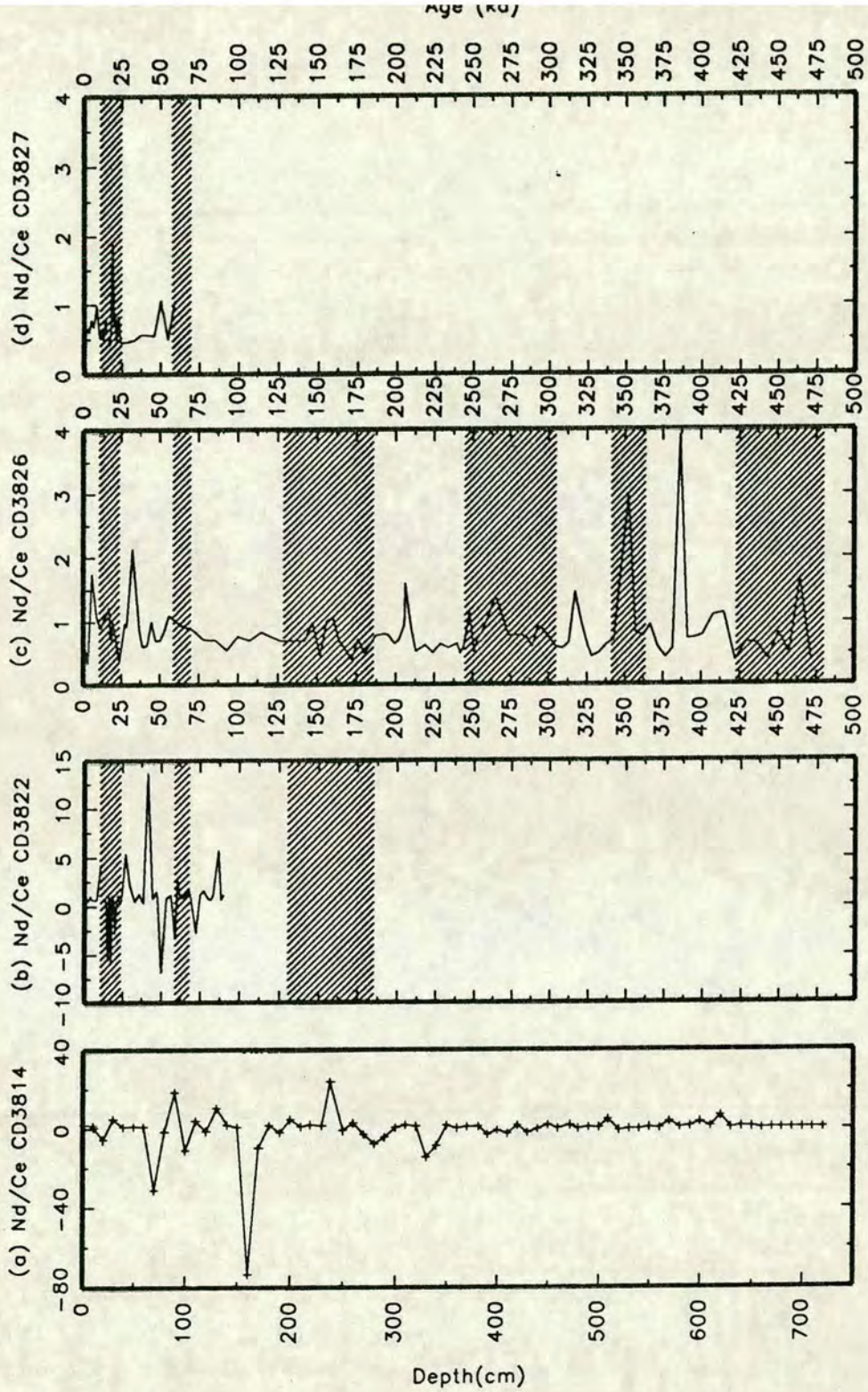

Figure 5.29 Temporal variations in Nd/Ce from CD38 cores. Note the small variation in values except in horizons associated with the ash bands. Shaded regions represent glacial stages II, IV, VI, VIII, X and XII.

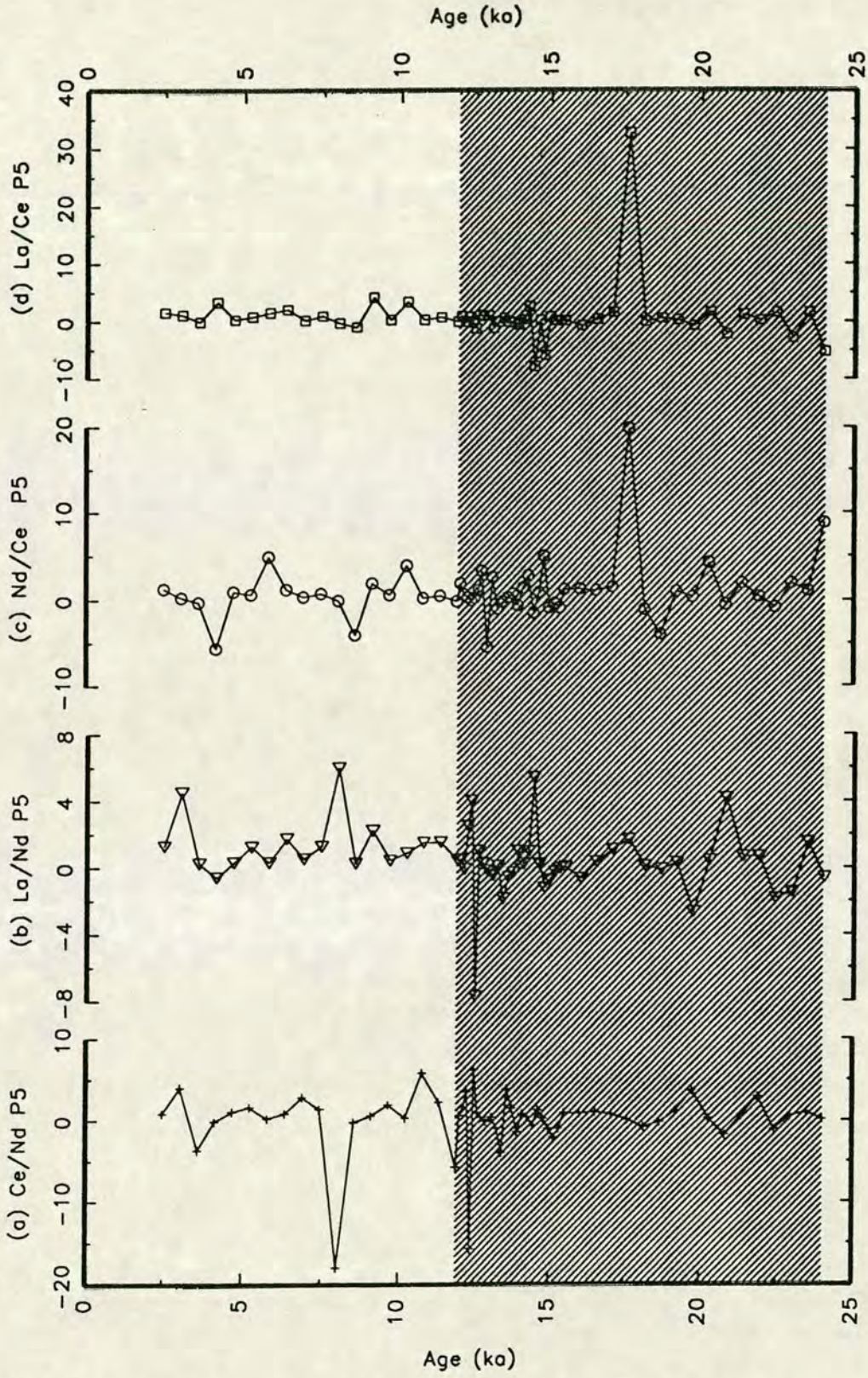

Figure 5.30 Temporal variations in the Ce/Nd (a), La/Nd (b), Nd/Ce (c) and La/Ce (d) from core P5. Note the very small variation in all the ratios except for several isolated large increases. Shaded region represents glacial stage II (12-24 ka).

relative to the world average deep-sea carbonate, whereas cores CD3826 and CD3827 are enriched in Sc even relative to the world average deep-sea clay. In core CD3826, Sc appears to be exclusively associated with Al (figure 5.31). Points which lie below the regression line and are relatively low in Sc, are probably relatively high in feldspar (figure 5.31). Cores P5 and CD3822 show negetive correlations between Sc and Al.

Temporal changes in the Sc/Al ratio are shown in figures 5.20b and 5.32. Core CD3814 shows a strong enrichment of Sc relative to Al in the lower half of the core but there is no obvious cyclicity. Core CD3822 has a relatively constant Sc/Al ratio except for a depletion during stage 5a (around 80 ka). This is probably associated with a Holocene ash band. The Sc/Al ratios in cores CD3826 and CD3827 are an order of magnitude smaller than those of cores CD3814 and CD3822 (figure 5.33). This probably reflects the much lower Al values in the latter two cores than any enrichment of Sc. Core CD3826 is dominated by the depleted Sc/Al ratios in the tephra layers and in some horizons with $MnCO_3$ development (see chapter 9). The Sc/Al ratio does, however, tend to be slightly higher during glacial periods, although there are many exceptions to this. Core CD3827 displays a similar profile to the upper section of core CD3826 although stage III appears to be enriched in Sc relative to Al.

5.4 TERRIGENOUS FLUXES

5.4.1 Introduction

Calculations of the input flux of particular terrigenous elements were made using equation 5.2 and results are given in appendix C.8.

Equation 5.2 **Element Flux (g/cm2/kyr) = Element(%) × DBD × SR**

DBD = Dry Bulk Density (g/cm2)
SR = Sedimentation Rate (cm/kyr)

The very nature of flux calculations renders them susceptible to potentially large errors. They are critically dependent on two factors: (I) the sedimentation rate and, (II) the bulk geochemistry of the sediment. The problems associated with each will now be discussed in some detail before any discussion of elemental fluxes.

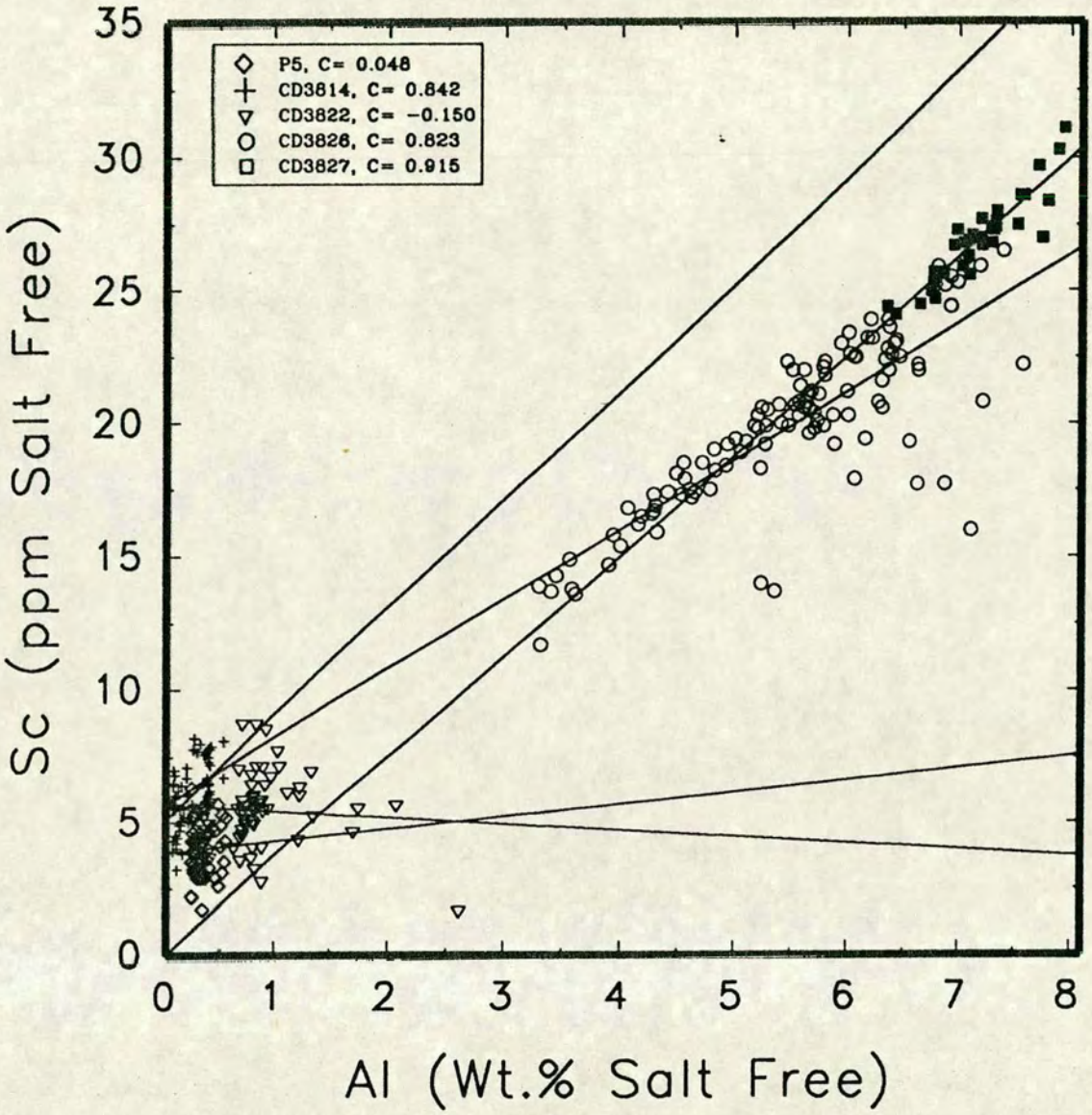

Figure 5.31 Diagram illustrating the relationship between Sc and Al from cores studied in this thesis. Note the good positive correlation in cores CD3814, CD3826 and CD3827 but, the poor positive and negative correlation in core P5 and CD3822 respectively.

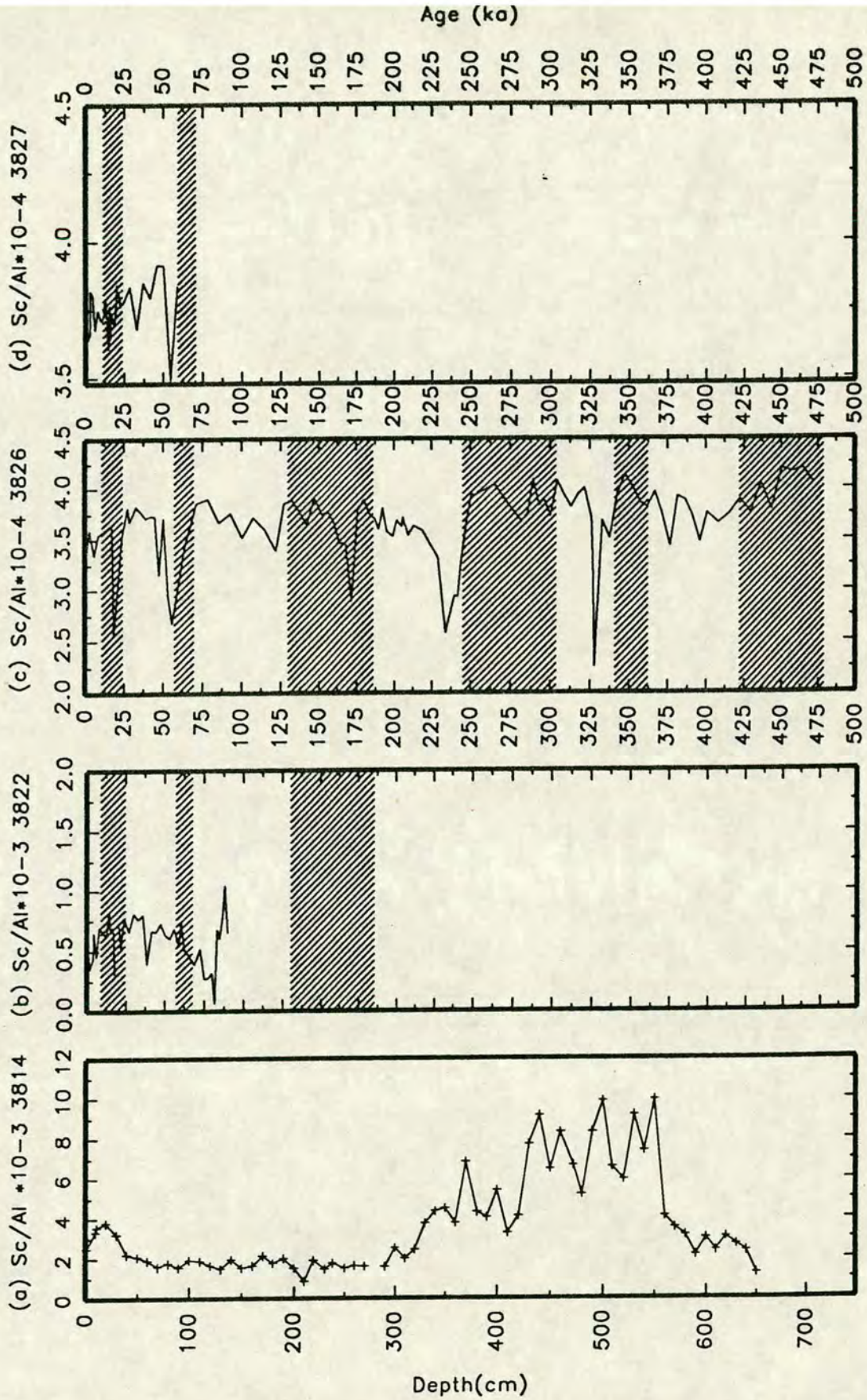

Figure 5.32 Temporal variations in Sc/Al from CD38 cores. Note the different scales, the decrease in the ratio in the ash bands and, the very high values at the base of core CD3814 associated with hydrothermal input to this core (see text). Shaded regions represent glacial stages II, IV, VI, VIII, X and XII.

(I) the sedimentation rate is critically dependent on the accuracy of the age model because any slight error in the identification of a stage boundary could result in a large change in the sedimentation rate above and below control horizons.

(II) The second problem renders flux calculations of sediment composition extremely unreliable. If a sediment is composed of an approximately 50%/50% mixture of two components, then a change in concentration of one component will accurately reflect the flux calculation and will not undu ly affect the flux calculation of the second component. However, if a sediment is composed of a 90%/10% mixture of two components then a small percentage change in the dominant component will greatly affect the concentration and flux of the minor one although the actual input of the minor constituent may not have changed much if at all.

As a result of these problems, ratioing elements against some component (eg Al) has some attractions. This method should, however, be compared to flux calculations in order to illustrate changes in elemental input with time.

5.4.2 Temporal Variations in Terrigenous Fluxes

The components chosen to represent terrigenous input to the region are Al and Si_{terrig}. Together they exemplify the terrigenous material reaching the area from the continental landmass and other sources. In core P5, fluxes of Al, Fe and Ti were used, as Si_{terrig} results were unreliable because of thier excessive dilution from carbonate and of the possibly erroneous calculation of fluxes mentioned above. Figures 5.33 and 5.34 illustrate the temporal variations in the fluxes of Si_{terrig} and Al in core CD3822, CD3826, CD3827 and AII54-25PC. As would be expected, there is a general decrease in the mean accumulation rate of both elements with increasing distance from land; core CD3827 having the highest, and CD3822 the lowest rates (cp. table 5.4 and figure 5.0). This is consistent with the bulk accumulation rates discussed at the end of chapter 4.

Together with this geographic variation there is increased input of both Al and Si_{terrig} during glacial periods and as a result of the rapidly deposited volcanic ash layers. The increase during the glacial periods is best illustrated in stage II in all the cores, although stage III in CD3826 and AII54-25PC is also a period of high input flux of Al and Si_{terrig} (figures 5.33 and 5.34). The fluxes of Al, Fe and Ti in core P5 are shown in figure 5.35. The profiles of all three elements are very similar with a

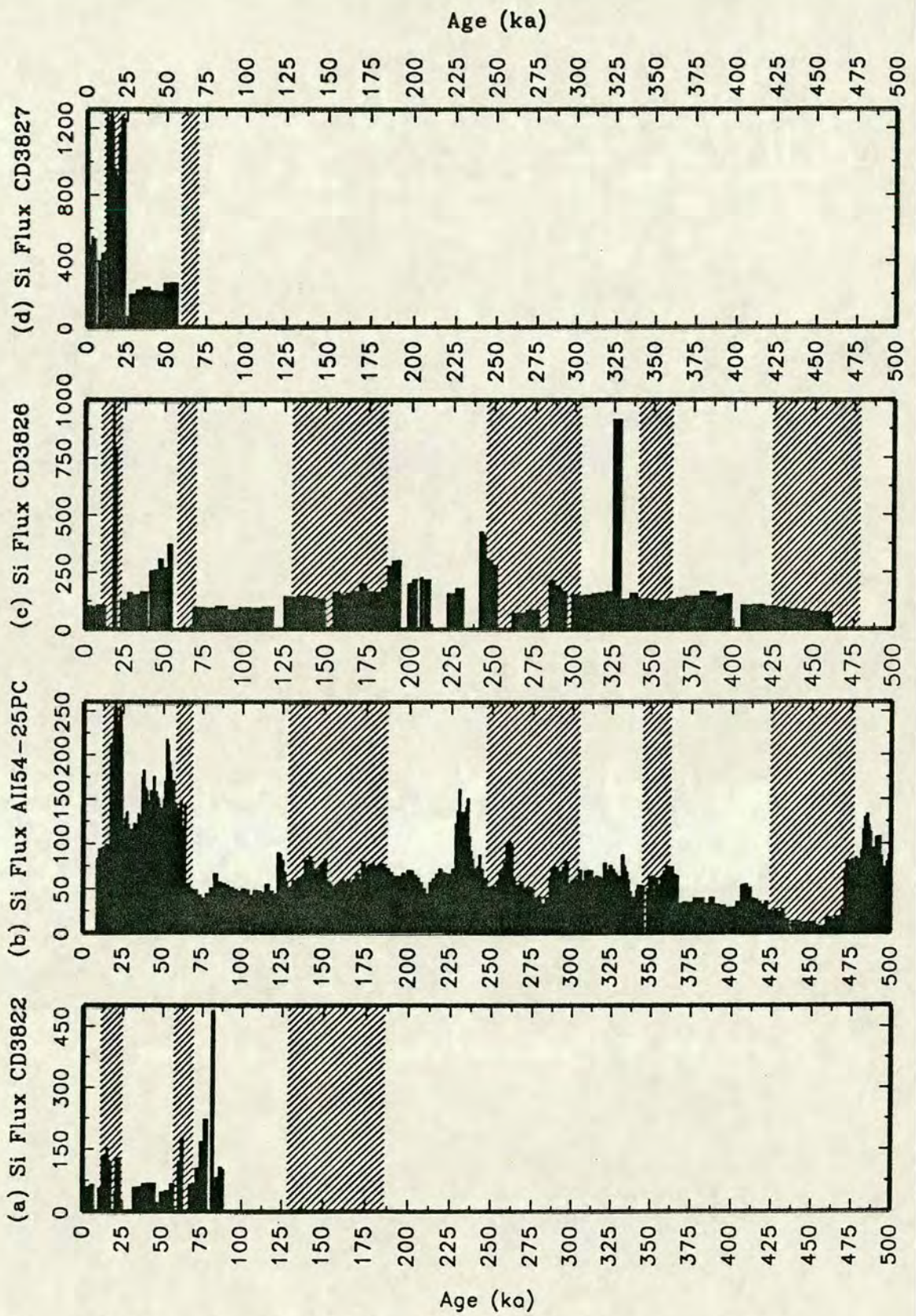

Figure 5.33 Temporal variations in Si_{terrig} flux (mg/cm^2/kyr) from cores CD3822 (a), AII54-25PC (b), CD3826 (c) and CD3827 (d). Si_{terrig} in core AII54-25PC calculated by subtracting the average biogenic SiO_2 of core CD3826 (ie. 4.039 %, see chapter 6) from the total Si in core AII54-25PC. Shaded regions represent glacial stages II, IV, VI, VIII, X and XII.

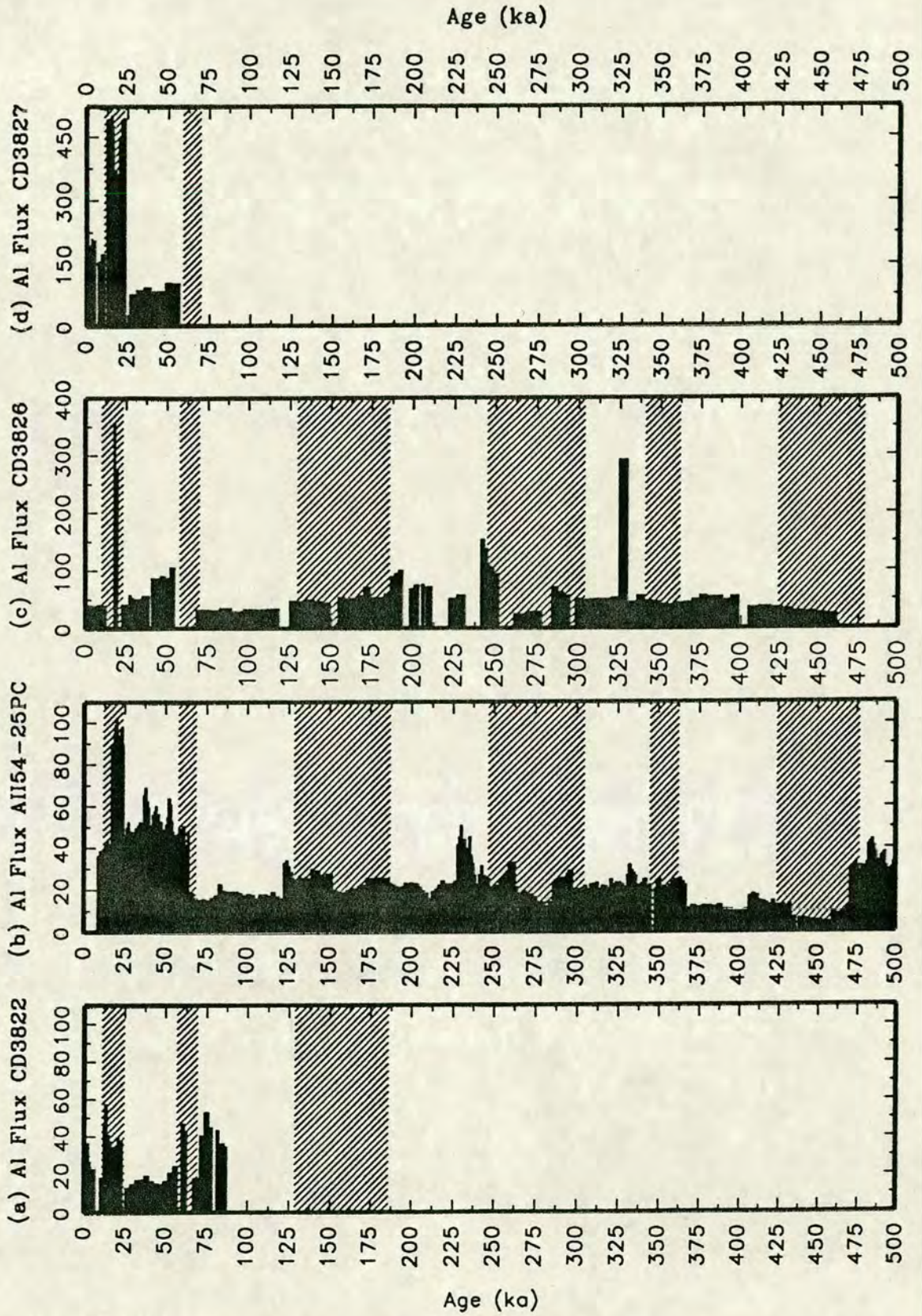

Figure 5.34 Temporal variations in Al flux m(g/cm^2/kyr) from cores CD3822 (a), AII54-25PC (b), CD3826 (c) and CD3827 (d). Shaded regions represent glacial stages II, IV, VI, VIII, X and XII.

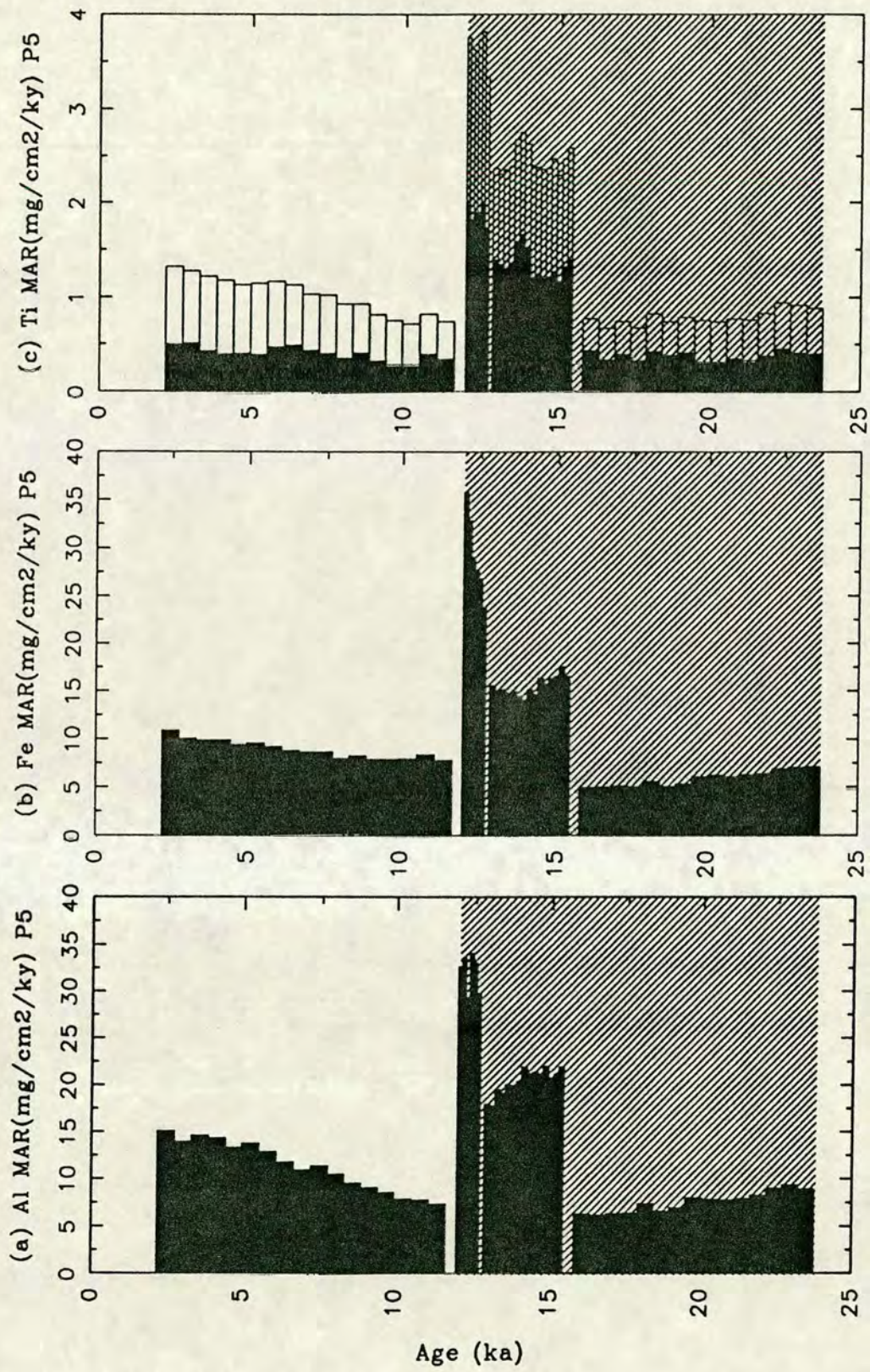

Figure 5.35 Temporal variations in Al (a), Fe (b) and Ti (c) fluxes (mg/cm^2/kyr) from core P5. Ti flux partitioned into total Ti flux (unfilled histograms) and Excess Ti (solid fill in histograms). See text for calculation of excess Ti. Shaded regions represent glacial stages II (12-24 ka).

strong increase during the later part of stage II (15-12 ka). This is consistent with an increased terrigenous input to the region during the last glacial maximum.

Table 5.4 Mean accumulation rates ($mg/cm^2/kyr$) of terrigenous elements.

Core	Mean Al Flux $mg/cm^2/kyr$	Mean Si_{terrig} Flux $mg/cm^2/kyr$
CD3822	30.98	104.63
AII5-25PC	30.98	85.26
CD3826	67.54	200.93
CD3827	292.05	754.00
P5	15.16	*****

5.5 STATISTICAL ANALALYIS OF THE DATASET

5.5.1 Introduction

This section uses statistical analysis in order to assign "elements" to paticular sediment phases, thus justifying the choice of elements used in this chapter as terrigenous, and designating the remaining elements to other sediment constituents especially biogenic phases. Two methods of statistical analysis were performed on all the data from each core: (a) Correlation Matrices and, (b) R-mode Factor analysis (principl component analysis) the results of which are presented in tables 5.5-5.9 and 5.10-5.14 respectively.

Correlation matrices are used throughout this thesis to define the degree of inter-element correlation, "C", in X-Y plots of two elements (eg figure 5.1). Calculation of confidence limits on the correlation coefficient are shown in appendix A.10. Principl component analysis is now described for each core with respect to all the data in an attempt to define certain factors which determine the variance within the dataset; factors which should corroborate the elements chosen to represent the different components in the terrigenous phase and should support the conclusions reached in this (see section 5.6) and later chapters. The results of the principl component analysis are discussed in terms of all the sediment phases, and help to define biogenic and redox sensitive elements, discussed in subsequent chapters.

5.5.2 Principal Component Analysis (PCA)

Introduction

PCA is a data reduction technique for identifying a small set of variables that account for a large proportion of the total variance in the data. The method has been used to statistically define variables by many authors. According to Loring (1978) variables ("elements") may be grouped on the basis of their degree of intercorrelation into factors that are associations of highly correlated variables ("elements"). Li (1982) used factor analysis to establish inter-element relationships in abyssal Pacific ferromanganese nodules and pelagic sediments. Similarly, Gardner et al., (1990) apply factor analysis in their assessment of the inorganic geochemistry of surface sediments from the Mediterranean.

The results of PCA on the data from each core are presented in tables 5.10-5.14. The eigenvalues given in these tables are effectively ratings on the degree of association which a particular element has with that principle component (factor). It is from these eigenvalues that the plots of factors I, II and III against each other are generated (figures 5.36-5.40).

Although PCA can provide good statistical proof that elements are closely associated, one should be cautious in interpreting them, and they should always be checked against some independent evidence. Two possible sources of error can exist; (a) an apparent correlation that could be caused by systematic error in the chemical analysis and, (b) an apparent lack of correlation may also be produced if the uncertainty in the chemical analysis is greater than the natural variability (Li, 1982). For most elements and especially where carbonate dilution is minimal (CD3826, CD3827 and AII54-25PC) such errors are likely to be low (see appendix A.5) but such a source of error may apply especially with the REEs, Pb, Th and U in carbonate rich cores (ie CD3814, CD3822 and P5).

Core CD3826

From table 5.12 it is clear that the first three factors in the PCA account for 64.4% of the total variance of major and trace element data in core CD3826. Obviously these three factors account for the majority of the variance , but it is not until the eleventh factor that over 90% of the total variance is accounted for which illustrates the

Table 5.5 Correlation Matrix of data from core CD3814. n= number of samples; r= coefficient of correlation significant at ≥ 95% confidence limits.

n=	r=		Pb																																				
73	0.654	Th	-0.126	Th																																			
73	0.654	U	0.083	0.212	U																																		
73	0.654	Sc	-0.103	0.738	0.194	Sc																																	
73	0.654	Cr	-0.109	0.568	0.293	0.813	Cr																																
73	0.654	Zr	0.142	0.277	0.281	0.403	0.502	Zr																															
73	0.654	Rb	0.027	0.538	0.388	0.756	0.917	0.751	Rb																														
72	0.655	SiTot	0.000	0.569	0.312	0.758	0.831	0.874	0.938	SiTot																													
72	0.655	Al	-0.088	0.811	0.307	0.842	0.960	0.889	0.961	0.946	Al																												
72	0.655	Fe	-0.020	0.553	0.336	0.766	0.887	0.831	0.962	0.988	0.972	Fe																											
72	0.655	Na	-0.017	0.342	0.264	0.524	0.790	0.724	0.834	0.837	0.836	0.861	Na																										
72	0.655	K	0.160	0.267	0.256	0.420	0.423	0.975	0.883	0.852	0.838	0.783	0.732	K																									
72	0.655	Mn	0.335	0.236	0.158	0.375	0.335	0.427	0.420	0.366	0.320	0.392	0.174	0.382	Mn																								
72	0.655	Mg	-0.154	0.774	0.203	0.971	0.846	0.419	0.777	0.788	0.876	0.795	0.566	0.443	0.271	Mg																							
72	0.655	Ti	-0.156	0.765	0.202	0.966	0.853	0.436	0.789	0.801	0.885	0.807	0.585	0.460	0.231	0.998	Ti																						
73	0.654	La	0.043	0.460	0.299	0.636	0.512	0.388	0.557	0.538	0.541	0.546	0.345	0.356	0.309	0.600	0.595	La																					
73	0.654	Ce	-0.158	0.646	0.186	0.751	0.698	0.392	0.617	0.662	0.717	0.680	0.512	0.364	0.222	0.774	0.773	0.490	Ce																				
73	0.654	Nd	0.076	0.485	0.339	0.513	0.455	0.339	0.499	0.468	0.473	0.467	0.262	0.248	0.483	0.516	0.513	0.531	0.531	Nd																		
73	0.654	Y	0.302	0.321	0.274	0.443	0.347	0.497	0.522	0.488	0.415	0.477	0.213	0.414	0.704	0.360	0.371	0.598	0.276	0.612	Y																
73	0.654	Nb	-0.161	0.766	0.203	0.962	0.846	0.439	0.786	0.801	0.883	0.808	0.585	0.470	0.203	0.997	0.998	0.595	0.770	0.499	0.358	Nb															
72	0.655	P	-0.048	0.758	0.257	0.933	0.840	0.563	0.842	0.852	0.892	0.859	0.616	0.575	0.614	0.947	0.948	0.676	0.768	0.613	0.597	0.943	P													
72	0.655	CaCO3	0.123	-0.755	-0.220	-0.965	-0.861	-0.475	-0.815	-0.823	-0.899	-0.829	-0.602	-0.496	-0.325	-0.994	-0.995	-0.607	-0.770	-0.532	-0.422	-0.993	-0.958	CaCO3												
73	0.654	Sr	0.390	-0.618	0.027	-0.754	-0.677	-0.148	-0.499	-0.536	-0.671	-0.564	-0.476	-0.119	0.560	-0.823	-0.828	-0.329	-0.681	-0.173	0.144	-0.832	-0.662	0.792	Sr											
73	0.654	Ba	0.402	-0.246	0.151	-0.272	-0.277	0.166	-0.081	-0.119	-0.247	-0.122	-0.212	0.147	0.829	-0.366	-0.376	0.100	-0.230	0.224	0.611	-0.383	-0.126	0.319	0.755	Ba										
73	0.654	Cu	0.305	0.229	0.237	0.323	0.257	0.414	0.395	0.364	0.297	0.371	0.161	0.326	0.819	0.240	0.229	0.510	0.294	0.556	0.866	0.221	0.475	-0.286	0.229	0.733	Cu									
73	0.654	Ni	0.074	0.596	0.231	0.765	0.613	0.479	0.663	0.658	0.662	0.666	0.372	0.429	0.898	0.739	0.728	0.616	0.644	0.627	0.727	0.724	0.843	-0.761	-0.359	0.294	0.751	Ni								
73	0.654	Zn	-0.042	0.731	0.273	0.942	0.839	0.556	0.840	0.850	0.892	0.856	0.597	0.571	0.640	0.951	0.949	0.643	0.784	0.612	0.560	0.947	0.974	-0.965	-0.657	-0.112	0.477	0.863	Zn							
73	0.654	V	0.300	-0.242	-0.081	-0.297	-0.395	-0.055	-0.269	-0.290	-0.383	-0.309	-0.379	-0.095	0.327	-0.382	-0.390	0.059	-0.227	0.095	0.339	-0.397	-0.250	0.355	0.594	0.643	0.438	0.044	-0.242	V						
73	0.654	I	0.437	-0.011	0.344	-0.084	-0.081	0.083	0.057	-0.002	-0.063	-0.023	-0.079	0.084	0.405	-0.084	-0.087	-0.089	-0.106	0.192	0.289	-0.086	-0.002	0.072	0.352	0.418	0.248	0.159	0.045	0.081	I					
73	0.654	Br	-0.161	0.477	0.215	0.584	0.638	0.275	0.560	0.547	0.626	0.562	0.510	0.254	0.002	0.823	0.831	0.257	0.576	0.229	0.078	0.825	0.567	-0.821	-0.568	-0.341	0.041	0.389	0.609	-0.428	0.040	Br				
73	0.654	Mo	0.110	-0.150	-0.037	-0.098	0.082	0.027	0.022	0.006	-0.001	-0.002	0.041	-0.017	0.184	-0.080	-0.073	-0.182	-0.074	0.010	-0.055	-0.136	-0.084	0.016	-0.013	0.108	-0.009	0.195	0.068	0.136	0.181	-0.147				

Table 5.6 Correlation Matrix of data from core CD3822. n= number of samples; r= coefficient of correlation significant at ≥ 95% confidence limits.

n	r		Pb																															
63	0.665	Th	0.457	Th																														
63	0.665	U	-0.229	-0.198	U																													
63	0.665	Be	0.144	-0.046	0.032	Be																												
63	0.665	Cr	0.279	-0.170	0.217	0.306	Cr																											
63	0.665	Zr	0.008	0.273	-0.012	-0.125	-0.284	Zr																										
63	0.665	Rb	0.458	0.893	-0.011	-0.254	-0.002	0.318	Rb																									
62	0.666	Siterig	-0.357	0.173	0.058	-0.295	-0.805	0.515	0.191	Siterig																								
62	0.666	Al	0.512	0.850	-0.143	-0.150	-0.001	0.530	0.915	0.168	Al																							
62	0.666	Fe	0.471	0.358	-0.045	0.213	0.301	0.293	0.341	-0.059	0.483	Fe																						
62	0.666	Na	0.383	0.808	-0.102	-0.093	-0.107	0.520	0.627	0.278	0.720	0.577	Na																					
62	0.666	K	0.412	0.723	-0.141	-0.230	-0.156	0.858	0.940	0.373	0.940	0.375	0.709	K																				
62	0.666	Mn	0.450	0.116	-0.304	0.130	0.084	-0.057	0.158	-0.299	0.288	0.329	0.180	0.134	Mn																			
62	0.666	Mg	0.486	0.189	0.041	0.323	0.806	-0.101	0.212	-0.471	0.307	0.802	0.408	0.107	0.348	Mg																		
62	0.666	Ti	0.040	-0.022	0.123	0.368	0.090	0.247	0.034	0.246	0.184	0.494	0.220	0.091	0.010	0.388	Ti																	
63	0.665	La	0.083	0.004	0.021	-0.050	-0.049	0.482	0.214	0.219	0.293	0.243	0.128	0.319	-0.048	0.052	0.086	La																
63	0.665	Ce	0.080	0.040	-0.067	-0.209	-0.161	0.511	0.092	0.203	0.232	0.143	0.117	0.244	0.028	-0.161	-0.016	0.335	Ce															
63	0.665	Nd	0.112	0.082	-0.048	0.033	0.003	0.370	0.049	0.123	0.199	0.184	0.154	0.178	0.157	0.020	0.018	0.282	0.608	Nd														
63	0.665	Y	0.327	0.205	-0.077	0.178	0.220	0.883	0.249	-0.024	0.490	0.543	0.431	0.408	0.283	0.361	0.063	0.472	0.376	0.423	Y													
63	0.665	Nb	-0.102	0.190	0.017	-0.168	-0.311	0.088	0.218	0.543	0.407	0.151	0.406	0.470	-0.121	-0.247	0.108	0.464	0.543	0.382	0.614	Nb												
62	0.666	P	0.240	-0.142	0.120	0.377	0.732	-0.342	-0.091	-0.845	-0.059	0.390	-0.051	-0.228	0.376	0.716	0.010	-0.049	-0.231	0.082	0.298	-0.389	P											
62	0.666	CaCO3	-0.338	-0.823	0.018	0.288	0.170	-0.827	-0.866	-0.458	-0.854	-0.444	-0.830	-0.907	-0.149	-0.140	-0.213	-0.337	-0.202	-0.152	-0.366	-0.436	0.230	CaCO3										
63	0.665	Sr	-0.212	-0.623	-0.131	0.320	0.174	-0.487	-0.863	-0.494	-0.790	-0.311	-0.808	-0.883	0.067	-0.049	-0.147	-0.302	-0.178	-0.080	-0.268	-0.431	0.298	0.908	Sr									
63	0.665	Ba	0.477	0.031	-0.186	0.220	0.582	-0.195	0.152	-0.744	0.274	0.372	0.128	0.034	0.850	0.637	-0.147	0.017	-0.138	0.018	0.388	-0.272	0.647	0.030	0.167	Ba								
47	0.687	B.SiO2	-0.024	0.094	0.312	-0.278	0.022	0.093	0.379	0.293	0.373	0.080	0.180	0.414	0.052	0.096	0.063	0.220	-0.054	-0.107	0.022	0.270	0.064	-0.616	-0.578	-0.168	B.SiO2							
63	0.665	Cu	0.513	0.209	-0.083	0.272	0.458	-0.116	0.249	-0.514	0.305	0.548	0.172	0.165	0.497	0.653	-0.051	0.157	-0.129	0.036	0.428	-0.187	0.674	-0.161	-0.037	0.725	0.168	Cu						
63	0.665	Ni	0.502	0.442	0.001	0.208	0.285	-0.049	0.487	-0.254	0.494	0.473	0.340	0.395	0.584	0.533	0.020	0.040	-0.126	0.058	0.317	-0.145	0.489	-0.409	-0.300	0.543	0.279	0.741	Ni					
63	0.665	Zn	0.507	0.283	0.153	0.087	0.825	-0.045	0.443	-0.389	0.417	0.490	0.277	0.321	0.350	0.625	-0.088	0.087	-0.089	0.124	0.443	-0.095	0.641	-0.371	-0.288	0.552	0.445	0.724	0.891	Zn				
63	0.665	V	0.257	0.083	0.437	0.087	0.492	-0.032	0.252	-0.153	0.217	0.533	0.170	0.138	0.045	0.633	0.321	0.188	-0.112	0.010	0.287	-0.113	0.545	-0.282	-0.251	0.229	0.442	0.393	0.395	0.621	V			
63	0.665	I	-0.026	-0.205	0.518	-0.172	0.400	-0.163	0.030	-0.462	-0.035	-0.030	-0.032	-0.197	0.023	0.273	-0.157	-0.126	-0.185	-0.221	-0.067	-0.169	0.341	0.137	0.010	0.358	0.179	0.195	0.160	0.314	0.297	I		
63	0.665	Br	-0.036	-0.151	0.426	-0.125	0.475	-0.139	0.082	-0.388	-0.002	-0.012	0.017	-0.112	-0.099	0.339	-0.098	-0.133	-0.279	-0.231	-0.017	-0.127	0.443	0.078	-0.080	0.315	0.319	0.250	0.174	0.420	0.392	0.797	Br	
62	0.666	C-org	-0.248	-0.182	0.098	0.014	-0.084	0.039	-0.219	0.045	-0.222	-0.196	-0.037	-0.183	-0.230	-0.196	-0.128	-0.201	-0.120	-0.072	-0.021	0.061	-0.038	0.222	0.128	-0.227	-0.096	-0.067	-0.204	-0.202	-0.292	0.088	0.118	C-org
63	0.665	Mo	-0.280	-0.207	0.388	-0.213	-0.188	0.088	-0.121	0.387	-0.177	-0.039	-0.181	-0.124	0.119	-0.217	0.195	0.088	0.104	0.083	-0.107	0.116	-0.180	-0.161	-0.192	-0.357	0.809	-0.157	0.044	-0.010	0.138	0.103	0.002	-0.098

Table 5.7 Correlation Matrix of data from core CD3826. n= number of samples; r= coefficient of correlation significant at ≥ 95% confidence limits.

n=	r=		Pb																															
111	0.626	Th	-0.013	Th																														
111	0.626	U	-0.265	-0.080	U																													
111	0.626	Sc	0.117	-0.073	-0.080	Sc																												
111	0.626	Cr	0.099	-0.332	0.020	0.844	Cr																											
111	0.626	Zr	0.092	0.716	-0.158	0.346	0.065	Zr																										
111	0.626	Rb	0.095	0.707	-0.049	0.335	0.156	0.738	Rb																									
111	0.626	SiTerig	0.102	0.440	-0.057	0.697	0.517	0.657	0.858	Siterig																								
111	0.626	Al	0.195	0.311	-0.152	0.823	0.667	0.661	0.745	0.931	Al																							
111	0.626	Fe	0.178	-0.048	-0.105	0.905	0.837	0.385	0.383	0.724	0.867	Fe																						
111	0.626	Na	0.220	0.410	-0.198	0.247	0.107	0.623	0.612	0.548	0.554	0.344	Na																					
111	0.626	K	0.039	0.712	0.000	0.376	0.111	0.763	0.946	0.861	0.730	0.388	0.666	K																				
111	0.626	Mn	0.283	0.005	-0.146	-0.145	-0.122	0.033	-0.037	-0.051	-0.055	-0.072	0.107	-0.080	Mn																			
111	0.626	Mg	0.059	-0.172	0.043	0.853	0.821	0.218	0.218	0.615	0.712	0.882	0.201	0.251	0.050	Mg																		
111	0.626	Ti	0.189	0.161	-0.153	0.876	0.755	0.648	0.539	0.805	0.936	0.915	0.468	0.536	-0.018	0.801	Ti																	
111	0.626	La	-0.069	0.510	0.009	0.153	-0.059	0.661	0.478	0.404	0.351	0.180	0.436	0.520	-0.051	0.064	0.335	La																
111	0.626	Ce	-0.011	0.606	-0.035	0.087	-0.150	0.714	0.478	0.346	0.329	0.096	0.433	0.531	-0.014	-0.009	0.306	0.439	Ce															
111	0.626	Nd	-0.023	0.431	-0.058	0.275	0.043	0.614	0.452	0.438	0.412	0.256	0.455	0.518	-0.170	0.150	0.392	0.424	0.675	Nd														
111	0.626	Y	0.083	0.128	-0.052	0.758	0.544	0.481	0.419	0.669	0.736	0.778	0.409	0.487	-0.038	0.744	0.747	0.327	0.270	0.418	Y													
111	0.626	Nb	0.095	0.717	-0.171	0.230	-0.054	0.954	0.679	0.567	0.549	0.256	0.563	0.698	0.040	0.112	0.540	0.641	0.694	0.591	0.374	Nb												
111	0.626	P	0.201	0.103	-0.206	0.239	0.259	0.483	0.143	0.232	0.357	0.364	0.369	0.090	0.540	0.347	0.509	0.278	0.229	0.136	0.281	0.436	P											
111	0.626	CaCO3	-0.219	-0.262	0.120	-0.791	-0.633	-0.602	-0.719	-0.920	-0.944	-0.847	-0.543	-0.716	-0.151	-0.764	-0.882	-0.318	-0.269	-0.384	-0.776	-0.492	-0.382	CaCO3										
111	0.626	Sr	-0.158	-0.214	0.083	-0.738	-0.643	-0.491	-0.685	-0.900	-0.885	-0.802	-0.468	-0.674	-0.214	-0.766	-0.810	-0.284	-0.176	-0.299	-0.723	-0.388	-0.386	0.968	Sr									
111	0.626	Ba	0.236	-0.235	-0.159	0.787	0.689	0.181	0.140	0.465	0.642	0.779	0.226	0.184	0.037	0.717	0.698	-0.041	-0.047	0.176	0.557	0.076	0.200	-0.669	-0.586	Ba								
111	0.626	B.SiO2	0.119	-0.118	-0.095	0.247	0.070	-0.023	-0.138	-0.103	0.074	0.179	-0.014	-0.046	-0.207	0.143	0.090	-0.108	-0.005	0.105	0.305	-0.069	-0.277	-0.100	0.021	0.477	B.SiO2							
111	0.626	Cu	0.197	-0.044	-0.151	0.619	0.527	0.217	0.276	0.495	0.584	0.822	0.285	0.300	0.086	0.615	0.574	0.041	0.042	0.212	0.463	0.149	0.128	-0.611	-0.540	0.698	0.261	Cu						
111	0.626	Ni	0.213	-0.160	0.002	0.535	0.499	0.180	0.159	0.376	0.453	0.550	0.283	0.150	0.246	0.627	0.517	0.058	0.018	0.135	0.451	0.098	0.361	-0.543	-0.497	0.567	0.077	0.550	Ni					
111	0.626	Zn	0.164	-0.197	-0.100	0.762	0.777	0.128	0.220	0.529	0.650	0.776	0.230	0.198	-0.065	0.774	0.684	-0.001	-0.067	0.132	0.545	0.024	0.192	-0.645	-0.597	0.742	0.176	0.797	0.656	Zn				
111	0.626	V	-0.118	-0.184	0.298	0.592	0.700	0.013	0.135	0.391	0.417	0.533	0.078	0.142	-0.167	0.655	0.452	0.031	-0.041	0.066	0.486	-0.074	0.039	-0.422	-0.463	0.402	0.004	0.421	0.376	0.606	V			
111	0.626	I	0.368	-0.301	-0.266	0.021	0.298	-0.075	-0.079	-0.040	0.066	0.191	0.208	-0.252	0.293	0.071	0.156	-0.107	-0.214	-0.116	-0.024	-0.105	0.503	-0.114	-0.151	0.124	-0.200	-0.011	0.247	0.201	-0.006	I		
111	0.626	Br	0.091	-0.296	-0.022	-0.069	0.199	-0.096	-0.125	-0.135	-0.052	0.070	0.201	-0.265	0.102	0.101	0.053	-0.008	-0.175	-0.107	-0.021	-0.107	0.383	0.036	0.020	-0.117	-0.210	-0.066	0.202	0.143	0.097	0.668	Br	
110	0.628	C-org	-0.028	-0.299	0.106	-0.305	-0.040	-0.374	-0.320	-0.353	-0.340	-0.220	-0.142	-0.400	-0.012	-0.148	-0.300	-0.177	-0.312	-0.249	-0.257	-0.301	-0.027	0.329	0.261	-0.273	-0.149	-0.287	-0.083	-0.102	-0.029	0.400	0.444	C-org
111	0.626	Mo	0.402	0.236	0.055	0.084	-0.157	0.271	0.053	0.018	0.059	0.011	0.178	0.144	0.077	0.009	0.065	0.185	0.289	0.117	0.176	0.256	0.091	-0.071	0.017	0.081	0.337	0.132	0.214	0.028	-0.062	-0.123	-0.126	-0.074

Table 5.8 Correlation Matrix of data from core CD3827. n= number of samples; r= coefficient of correlation significant at ≥ 95% confidence limits.

n=	r=		Pb	Th	U	Sc	Cr	Zr	Rb	Siltorig	Al	Fe	Na	K	Mn	Mg	Ti	La	Ce	Nd	Y	Nb	P	CaCO3	Sr	Ba	B.SiO2	Cu	Ni	Zn	V	I	Br	C-org
33	0.719	Th	-0.133																															
33	0.719	U	-0.523	0.083																														
33	0.719	Sc	0.417	0.094	-0.858																													
33	0.719	Cr	-0.251	0.295	0.275	0.285																												
33	0.719	Zr	0.530	-0.023	-0.347	0.731	0.390																											
33	0.719	Rb	-0.093	-0.100	0.247	0.108	0.457	0.417																										
33	0.719	Siltorig	0.312	-0.032	-0.027	0.248	0.279	0.493	0.288																									
33	0.719	Al	0.497	0.043	-0.602	0.915	0.349	0.882	0.256	0.388																								
33	0.719	Fe	0.305	0.019	-0.392	0.790	0.356	0.645	0.253	0.404	0.774																							
33	0.719	Na	0.466	-0.086	-0.863	0.858	-0.037	0.450	-0.121	0.097	0.682	0.577																						
33	0.719	K	0.001,	0.228	0.046	0.479	0.672	0.404	0.367	0.362	0.470	0.525	0.199																					
33	0.719	Mn	0.361	-0.057	-0.592	0.340	-0.102	0.343	-0.226	0.132	0.483	0.329	0.602	-0.210																				
33	0.719	Mg	0.544	0.056	-0.652	0.791	0.165	0.643	-0.251	0.165	0.763	0.583	0.638	0.213	0.545																			
33	0.719	Ti	0.469	0.056	-0.586	0.945	0.333	0.797	0.083	0.369	0.936	0.848	0.682	0.478	0.418	0.845																		
33	0.719	La	0.194	-0.078	-0.123	0.201	-0.095	0.228	0.113	0.015	0.201	0.232	0.144	0.014	0.202	0.160	0.234																	
33	0.719	Ce	0.117	0.224	-0.215	0.201	-0.054	0.069	-0.273	0.197	0.218	0.152	0.211	0.161	0.235	0.244	0.263	-0.083																
33	0.719	Nd	0.096	0.205	-0.280	0.378	0.059	0.227	-0.310	-0.067	0.323	0.278	0.302	0.129	0.255	0.433	0.390	-0.251	0.613															
33	0.719	Y	0.388	-0.038	-0.322	0.299	0.061	0.360	-0.038	0.068	0.322	0.264	0.261	0.048	0.254	0.413	0.303	-0.106	0.072	0.403														
33	0.719	Nb	0.210	0.093	-0.082	0.453	0.377	0.593	0.402	0.256	0.531	0.369	0.371	0.360	0.015	0.298	0.514	0.104	0.124	-0.028	0.077													
33	0.719	P	0.403	-0.273	-0.427	0.289	-0.279	0.458	-0.058	0.036	0.392	0.200	0.349	-0.467	0.528	0.499	0.390	0.241	-0.028	0.125	0.204	0.127												
33	0.719	CaCO3	-0.406	0.023	0.580	-0.872	-0.308	-0.778	-0.406	-0.340	-0.917	-0.855	-0.677	-0.498	-0.379	-0.615	-0.874	-0.272	-0.148	-0.188	-0.264	-0.580	-0.313											
33	0.719	Sr	-0.203	-0.020	0.417	-0.744	-0.329	-0.501	-0.425	-0.245	-0.695	-0.804	-0.567	-0.666	-0.074	-0.361	-0.702	-0.190	-0.160	-0.117	-0.149	-0.517	0.074	0.873										
33	0.719	Ba	0.502	-0.133	-0.606	0.306	-0.371	0.205	-0.536	-0.126	0.298	0.194	0.479	-0.382	0.666	0.696	0.383	0.138	0.182	0.331	0.463	-0.090	0.681	-0.209	0.089									
32	0.722	B.SiO2	0.083	-0.082	0.036	-0.289	-0.330	-0.298	-0.208	0.563	-0.320	-0.112	-0.166	-0.150	-0.016	-0.272	-0.263	-0.163	0.201	-0.149	-0.051	-0.237	-0.184	0.261	0.183	-0.034								
33	0.719	Cu	0.326	-0.274	-0.512	0.442	-0.147	0.238	-0.266	0.125	0.360	0.538	0.528	-0.005	0.339	0.481	0.506	0.036	0.099	0.274	0.551	0.164	0.280	-0.429	-0.392	0.568	0.134							
33	0.719	Ni	0.254	-0.109	-0.106	-0.195	-0.326	-0.075	-0.240	0.626	-0.146	-0.089	-0.074	-0.255	0.235	-0.029	-0.123	-0.094	0.204	-0.093	0.063	-0.224	0.141	0.175	0.297	0.233	0.907	0.150						
33	0.719	Zn	0.519	-0.005	-0.596	0.370	-0.153	0.429	-0.399	0.024	0.464	0.108	0.401	-0.235	0.671	0.746	0.441	0.153	0.167	0.289	0.283	-0.046	0.707	-0.239	0.157	0.808	-0.179	0.206	0.201					
33	0.719	V	0.060	0.186	-0.164	0.578	0.523	0.540	0.302	-0.287	0.596	0.425	0.332	0.397	0.140	0.470	0.558	0.183	-0.089	0.272	0.239	0.435	0.145	-0.543	-0.459	0.059	-0.889	0.048	-0.798	0.184				
33	0.719	I	0.055	-0.400	-0.051	-0.029	-0.274	0.203	0.217	0.064	0.038	0.008	-0.073	-0.577	0.133	0.065	0.041	0.126	-0.234	-0.156	0.041	0.070	0.764	-0.076	0.195	0.311	-0.031	0.172	0.169	0.248	-0.057			
33	0.719	Br	-0.294	-0.364	0.321	-0.221	0.055	-0.035	0.616	-0.333	-0.141	-0.134	-0.249	-0.134	-0.323	-0.387	-0.238	0.181	-0.384	-0.413	-0.217	0.177	0.071	-0.028	-0.061	-0.334	-0.496	-0.230	-0.540	-0.367	0.306	0.455		
32	0.722	C-org	-0.079	-0.287	0.159	-0.439	-0.325	-0.455	-0.038	0.355	-0.467	-0.223	-0.326	-0.199	-0.190	-0.470	-0.428	-0.177	0.107	-0.330	-0.274	-0.245	-0.243	0.336	0.200	-0.195	0.826	-0.037	0.890	-0.352	-0.829	0.055	-0.082	
33	0.719	Mo	-0.505	-0.230	0.724	-0.531	0.105	-0.449	0.373	-0.245	-0.575	-0.163	-0.443	0.063	-0.661	-0.746	-0.516	-0.127	-0.294	-0.295	-0.270	0.014	-0.489	0.338	-0.002	-0.647	-0.484	-0.146	-0.767	-0.888	-0.227	0.000	0.656	0.703

Table 5.9 Correlation Matrix of data from core P5. n= number of samples; r= coefficient of correlation significant at ≥ 95% confidence limits.

n=	r=		Pb																															
57	0.672	Th	-0.024	Th																														
57	0.672	U	-0.138	0.065	U																													
57	0.672	Sc	-0.076	0.156	0.301	Sc																												
57	0.672	Cr	0.052	0.072	0.115	-0.412	Cr																											
57	0.672	Zr	0.089	-0.017	-0.237	0.075	0.013	Zr																										
57	0.672	Rb	-0.233	0.192	0.154	0.343	-0.142	0.608	Rb																									
57	0.672	Siterig	0.018	0.100	-0.009	0.058	0.026	-0.083	-0.028	Siterig																								
57	0.672	Al	0.087	-0.093	-0.306	0.048	-0.022	0.876	0.821	-0.106	Al																							
57	0.672	Fe	0.044	-0.140	-0.279	-0.116	0.147	0.812	0.403	-0.231	0.879	Fe																						
57	0.672	Na	0.078	0.044	-0.212	0.144	-0.318	0.527	0.595	-0.100	0.829	0.372	Na																					
57	0.672	K	0.049	-0.098	-0.213	0.080	-0.062	0.765	0.613	-0.130	0.868	0.749	0.747	K																				
57	0.672	Mn	0.040	-0.021	0.089	0.240	0.016	0.148	0.084	-0.151	0.162	0.182	0.221	0.149	Mn																			
57	0.672	Mg	0.014	-0.019	-0.305	0.057	-0.090	0.773	0.608	-0.099	0.883	0.726	0.684	0.801	0.232	Mg																		
57	0.672	Ti	0.085	-0.010	-0.350	0.002	-0.040	0.800	0.541	-0.091	0.941	0.823	0.568	0.843	0.048	0.790	Ti																	
57	0.672	La	-0.198	-0.186	0.044	-0.024	-0.017	0.135	0.134	-0.107	0.216	0.224	0.169	0.271	0.071	0.153	0.158	La																
57	0.672	Ce	-0.102	0.100	0.067	0.066	0.111	0.225	0.099	-0.258	0.081	0.147	-0.077	0.075	-0.069	-0.035	0.135	-0.009	Ce															
57	0.672	Nd	0.104	-0.025	0.414	0.223	0.092	0.028	0.030	-0.138	-0.032	-0.074	-0.031	0.006	0.014	-0.103	-0.032	-0.088	0.329	Nd														
57	0.672	Y	0.149	0.001	-0.073	0.285	-0.360	0.341	0.294	0.227	0.275	0.002	0.475	0.256	0.126	0.343	0.178	0.122	0.057	0.211	Y													
57	0.672	NB	0.310	0.032	0.067	0.039	-0.040	0.291	0.078	0.061	0.139	0.163	0.123	0.125	0.284	0.221	0.064	-0.144	0.056	0.041	0.122	Nb												
57	0.672	P	0.089	-0.204	-0.026	0.102	0.033	0.686	0.558	0.031	0.778	0.658	0.443	0.705	0.045	0.643	0.743	0.174	0.116	0.191	0.327	0.089	P											
57	0.672	CaCO3	0.019	0.111	0.241	0.082	-0.013	-0.745	-0.540	0.279	-0.874	-0.841	-0.597	-0.786	-0.143	-0.776	-0.803	-0.291	-0.150	0.030	-0.113	-0.087	-0.844	CaCO3										
57	0.672	Sr	0.003	-0.034	0.028	0.199	0.156	0.218	0.138	0.029	0.280	0.249	-0.070	0.274	-0.135	0.087	0.386	0.038	0.222	0.091	-0.252	-0.047	0.355	-0.135	Sr									
57	0.672	Ba	0.089	-0.095	-0.244	0.080	0.016	0.854	0.614	-0.119	0.965	0.850	0.585	0.860	0.119	0.820	0.919	0.255	0.160	0.019	0.271	0.110	0.792	-0.840	0.383	Ba								
57	0.672	B SiO2	0.025	-0.156	-0.266	-0.098	0.061	0.750	0.431	-0.526	0.845	0.915	0.468	0.738	0.229	0.729	0.778	0.260	0.163	-0.026	-0.010	0.098	0.600	-0.880	0.179	0.828	B SiO2							
57	0.672	Cu	0.493	0.088	0.207	-0.141	0.223	-0.149	-0.332	0.015	-0.254	-0.113	-0.252	-0.271	0.108	-0.247	-0.251	-0.081	0.131	0.027	-0.046	0.167	-0.155	0.224	-0.010	-0.179	-0.138	Cu						
57	0.672	Ni	0.240	-0.001	0.001	-0.101	0.230	-0.007	-0.223	-0.304	-0.089	0.093	-0.308	-0.063	0.092	-0.169	-0.012	-0.026	0.172	0.016	-0.386	0.097	-0.100	0.144	0.392	0.002	0.119	0.517	Ni					
57	0.672	Zn	0.114	-0.133	-0.148	-0.134	0.292	0.584	0.212	-0.321	0.640	0.847	0.132	0.554	0.086	0.451	0.645	0.151	0.198	-0.099	-0.270	0.089	0.519	-0.652	0.417	0.695	0.791	0.181	0.445	Zn				
57	0.672	V	0.046	-0.193	-0.074	-0.019	0.173	0.366	0.098	-0.103	0.456	0.585	-0.050	0.319	-0.116	0.295	0.452	0.125	-0.018	-0.012	-0.270	-0.051	0.382	-0.427	0.454	0.459	0.532	-0.046	0.126	0.615	V			
57	0.672	I	0.062	0.115	-0.079	0.141	-0.112	0.405	0.578	0.092	0.469	0.134	0.541	0.464	0.101	0.499	0.456	0.207	-0.033	0.003	0.486	0.049	0.416	-0.334	-0.067	0.444	0.207	-0.188	-0.168	-0.048	-0.148	I		
57	0.672	Br	-0.048	0.093	0.075	0.217	-0.404	-0.043	0.313	0.164	-0.054	-0.399	0.510	0.019	0.089	0.184	-0.132	-0.010	-0.177	0.045	0.631	0.068	-0.091	0.084	-0.472	-0.095	-0.276	-0.177	-0.458	-0.604	-0.542	0.507	Br	
57	0.672	C-org	-0.068	0.023	0.375	0.076	-0.111	-0.561	-0.141	0.154	-0.622	-0.766	-0.264	-0.535	-0.031	-0.463	-0.629	-0.255	-0.242	0.155	0.056	-0.006	-0.455	0.658	-0.230	-0.630	-0.667	0.136	-0.060	-0.680	-0.409	-0.014	0.468	C-org
57	0.672	Mo	-0.079	-0.054	-0.001	-0.056	-0.055	-0.170	-0.152	0.151	-0.209	-0.287	0.011	-0.208	0.006	-0.117	-0.243	0.024	-0.072	0.178	0.414	-0.036	-0.110	0.220	-0.356	-0.244	-0.287	-0.091	-0.338	-0.351	-0.290	0.025	0.395	0.225

Table 5.10 Eigenanalysis of the Correlation Matrix for core CD3814 (table 5.5).

	F-1	F-2	F-3	F-4	F-5	F-6
Eigenvalue	15.907	2.066	1.838	1.698	1.410	1.085
Proportion	0.513	0.067	0.059	0.055	0.045	0.035
Cumulative	0.513	0.580	0.639	0.694	0.739	0.774
	F-7	F-8	F-9	F-10	F-11	F-12
Eigenvalue	1.019	0.838	0.740	0.688	0.606	0.535
Proportion	0.033	0.027	0.024	0.022	0.020	0.017
Cumulative	0.807	0.834	0.858	0.880	0.900	0.917

Weightings of the first six components

Variable	PC1	PC2	PC3	PC4	PC5	PC6
Pb	-0.115	0.079	0.016	-0.249	-0.303	-0.106
Th	-0.057	-0.080	-0.374	0.084	-0.118	0.506
U	-0.055	-0.178	-0.513	0.015	0.204	0.052
Sc	-0.125	0.122	0.170	0.187	0.097	-0.479
Cr	-0.185	-0.043	-0.009	0.044	-0.104	0.069
Zr	-0.243	0.010	0.069	-0.037	0.137	0.041
Rb	-0.221	0.017	-0.088	-0.132	0.167	0.059
Sitotal	-0.244	0.035	-0.025	-0.074	0.072	0.015
Al	-0.229	0.067	-0.064	-0.081	0.053	0.076
Fe	-0.242	-0.016	-0.014	-0.021	0.093	-0.005
Na	-0.051	0.214	-0.115	0.006	-0.587	-0.201
K	-0.229	0.117	-0.028	-0.079	0.006	-0.116
Mn	-0.202	-0.249	0.130	-0.076	-0.014	-0.023
Mg	-0.210	0.253	-0.128	-0.045	-0.157	0.043
Ti	-0.188	0.292	-0.087	-0.049	-0.186	0.089
La	-0.128	0.205	-0.060	0.340	0.208	-0.096
Ce	-0.031	-0.262	0.020	0.508	-0.345	0.013
Nd	-0.156	-0.179	-0.120	0.226	-0.067	0.235
Y	-0.232	0.036	0.015	0.011	0.128	-0.007
Nb	-0.127	0.257	-0.066	-0.002	-0.122	0.037
P	-0.218	0.033	-0.028	0.097	-0.065	0.043
CaCO3	0.196	-0.164	-0.032	0.085	0.131	-0.037
Sr	-0.226	-0.067	-0.109	-0.182	0.154	-0.055
Ba	-0.233	-0.176	0.100	0.006	0.063	-0.046
Cu	-0.226	-0.116	0.106	0.160	-0.005	-0.059
Ni	-0.205	-0.228	0.236	0.073	-0.008	-0.052
Zn	-0.218	-0.224	0.055	0.051	-0.068	-0.124
V	-0.148	0.021	0.255	0.268	0.002	0.243
I	-0.095	-0.358	-0.155	-0.416	-0.089	-0.181
Br	0.040	-0.308	-0.348	0.109	-0.200	-0.372
Mo	0.011	-0.221	0.411	-0.284	-0.257	0.308

Table 5.11 Eigenanalysis of the Correlation Matrix for core CD3822 (table 5.6).

	F-1	F-2	F-3	F-4	F-5	F-6
Eigenvalue	9.651	5.556	3.713	2.482	1.781	1.364
Proportion	0.292	0.168	0.113	0.075	0.054	0.041
Cumulative	0.292	0.461	0.573	0.649	0.703	0.744
	F-7	F-8	F-9	F-10	F-11	F-12
Eigenvalue	1.107	1.067	0.862	0.832	0.673	0.639
Proportion	0.034	0.032	0.026	0.025	0.020	0.019
Cumulative	0.777	0.810	0.836	0.861	0.881	0.901

Weightings on the first six components

Variable	PC1	PC2	PC3	PC4	PC5	PC6
Pb	-0.187	0.017	0.156	-0.020	0.001	-0.121
Th	-0.238	-0.121	0.022	0.087	0.036	-0.056
U	0.047	0.037	-0.384	-0.100	-0.103	0.061
Sc	0.033	0.229	0.129	0.047	-0.061	-0.148
Cr	0.055	0.235	-0.148	0.161	-0.288	0.069
Zr	-0.242	0.001	0.036	0.221	-0.045	0.132
Rb	-0.275	-0.179	-0.100	0.005	-0.016	-0.012
Siterig	-0.276	-0.178	0.011	0.020	-0.077	-0.019
Al	-0.287	-0.137	0.018	0.040	0.057	0.025
Fe	-0.198	0.220	0.047	0.052	-0.068	0.081
Na	-0.245	-0.019	-0.001	0.276	0.155	0.094
K	-0.292	-0.153	-0.017	0.020	-0.028	-0.019
Mn	-0.089	0.133	0.202	-0.204	0.474	0.116
Mg	-0.142	0.296	-0.058	0.147	-0.037	0.042
Ti	-0.218	0.206	0.052	0.143	0.060	0.154
La	-0.063	0.047	0.052	-0.204	-0.355	-0.363
Ce	0.015	-0.035	0.182	-0.302	-0.268	0.408
Nd	-0.033	0.111	0.175	-0.219	-0.198	0.531
Y	-0.108	0.338	0.097	-0.014	-0.133	-0.068
Nb	-0.144	0.017	-0.031	0.159	-0.152	0.275
P	0.002	0.383	-0.131	-0.012	0.008	0.009
CaCO3	0.292	0.114	0.082	0.096	0.007	-0.012
Sr	0.255	0.177	0.167	0.062	0.060	-0.001
Ba	-0.016	0.260	0.184	0.102	0.281	-0.072
BiSiO2	-0.138	-0.035	-0.277	-0.283	0.078	0.036
Cu	-0.138	0.274	0.011	-0.094	0.095	-0.143
Ni	-0.209	0.148	-0.033	-0.152	0.272	-0.065
Zn	-0.181	0.224	-0.219	-0.122	-0.063	-0.005
V	-0.120	0.180	-0.288	-0.124	-0.235	-0.163
I	0.128	-0.017	-0.373	0.060	0.206	0.119
Br	0.082	0.034	-0.420	0.144	0.145	0.009
C-org	0.095	0.037	-0.151	0.305	0.043	0.349
Mo	0.010	0.039	-0.138	-0.500	0.236	0.157

Table 5.12 Eigenanalysis of the Correlation Matrix for core CD3826 (table 5.7).

	F-1	F-2	F-3	F-4	F-5	F-6
Eigenvalue	12.671	5.631	2.949	2.060	1.457	1.212
Proportion	0.384	0.171	0.089	0.062	0.044	0.037
Cumulative	0.384	0.555	0.644	0.706	0.751	0.787
	F-7	F-8	F-9	F-10	F-11	F-12
Eigenvalue	1.137	0.828	0.681	0.622	0.538	0.459
Proportion	0.034	0.025	0.021	0.019	0.016	0.014
Cumulative	0.822	0.847	0.867	0.886	0.903	0.917

Weightings of the first six components

Variable	PC1	PC2	PC3	PC4	PC5	PC6
Pb	-0.054	0.034	0.223	-0.398	-0.113	-0.006
Th	-0.080	-0.356	-0.021	0.020	-0.080	-0.042
U	0.032	0.018	-0.188	0.286	0.257	-0.537
Sc	-0.238	0.151	-0.124	-0.009	0.041	0.050
Cr	-0.187	0.266	-0.017	0.147	0.035	0.066
Zr	-0.191	-0.272	0.082	-0.033	0.105	0.016
Rb	-0.192	-0.226	-0.002	0.149	-0.190	0.061
Siterig	-0.253	-0.079	-0.047	0.153	-0.178	0.021
Al	-0.271	-0.012	-0.009	0.046	-0.088	0.107
FE	-0.248	0.150	-0.016	0.017	0.026	0.084
Na	-0.163	-0.154	0.198	-0.030	0.086	0.123
K	-0.197	-0.244	-0.086	0.097	-0.141	0.005
Mn	-0.010	0.007	0.338	-0.174	-0.325	-0.472
Mg	-0.220	0.204	-0.045	0.059	0.047	-0.146
Ti	-0.265	0.044	0.040	0.017	0.039	0.070
La	-0.114	-0.234	0.048	0.104	0.231	-0.004
Ce	-0.101	-0.286	0.000	-0.068	0.248	-0.084
Nd	-0.134	-0.195	-0.049	-0.029	0.300	0.149
Y	-0.227	0.035	-0.075	-0.030	0.162	-0.013
Nb	-0.159	-0.294	0.093	-0.034	0.102	0.021
P	-0.119	-0.011	0.419	-0.014	0.049	-0.188
CaCO3	0.270	-0.010	-0.021	-0.014	0.145	0.026
Sr	0.252	-0.032	-0.038	-0.106	0.216	0.088
Ba	-0.193	0.201	-0.086	-0.240	-0.035	0.068
BiSiO2	-0.034	0.072	-0.249	-0.440	0.223	0.210
Cu	-0.184	0.131	-0.084	-0.185	-0.072	-0.040
Ni	-0.172	0.158	0.107	-0.112	0.103	-0.246
Zn	-0.198	0.226	-0.032	-0.030	0.043	0.033
V	-0.136	0.187	-0.141	0.252	0.184	-0.219
I	-0.020	0.150	0.469	0.028	0.044	0.210
Br	0.005	0.125	0.391	0.189	0.309	0.149
C-org	0.101	0.114	0.217	0.177	0.280	0.073
Mo	-0.041	-0.092	-0.004	-0.430	0.313	-0.333

Table 5.13 Eigenanalysis of the Correlation Matrix for core CD3827 (table 5.8).

	F-1	F-2	F-3	F-4	F-5	F-6
Eigenvalue	12.003	6.074	3.923	2.398	1.536	1.152
Proportion	0.364	0.184	0.119	0.073	0.047	0.035
Cumulative	0.364	0.548	0.667	0.739	0.786	0.821
	F-7	F-8	F-9	F-10	F-11	F-12
Eigenvalue	0.915	0.824	0.763	0.739	0.667	0.418
Proportion	0.028	0.025	0.023	0.022	0.020	0.013
Cumulative	0.849	0.873	0.897	0.919	0.939	0.952

Weightings on the first six components

Variable	PC1	PC2	PC3	PC4	PC5	PC6
Pb	0.186	0.076	-0.095	0.019	0.091	-0.267
Th	0.010	-0.050	0.308	0.232	0.145	0.138
U	-0.229	-0.133	-0.003	0.158	-0.128	0.049
Sc	0.259	-0.106	0.017	-0.063	0.052	0.026
Cr	0.027	-0.286	0.077	0.285	-0.163	-0.136
Zr	0.220	-0.133	-0.178	0.188	-0.048	-0.056
Rb	-0.028	-0.290	-0.252	0.062	0.009	-0.047
Siterig	0.151	-0.234	-0.161	0.294	-0.032	0.002
Al	0.266	-0.116	-0.067	0.060	0.033	0.036
Fe	0.212	-0.185	-0.049	-0.144	-0.033	0.065
Na	0.220	0.019	0.014	-0.205	0.107	0.057
K	0.085	-0.318	0.168	0.061	0.040	-0.089
Mn	0.184	0.168	-0.048	0.058	0.069	0.070
Mg	0.258	0.077	0.017	0.074	-0.060	-0.051
Ti	0.267	-0.104	-0.030	-0.010	-0.014	0.090
La	0.046	0.000	-0.160	-0.064	0.507	0.109
Ce	0.110	0.010	0.191	0.058	-0.192	0.626
Nd	0.123	0.065	0.242	-0.003	-0.433	0.323
Y	0.129	0.050	0.034	-0.113	-0.434	-0.434
Nb	0.109	-0.207	-0.106	0.013	-0.012	0.138
P	0.127	0.215	-0.316	0.050	-0.058	0.170
CaCO3	-0.238	0.172	0.113	0.115	-0.082	-0.067
Sr	-0.168	0.263	-0.004	0.270	-0.106	-0.066
Ba	0.169	0.290	-0.050	-0.077	-0.107	-0.046
BiSiO2	0.165	0.132	0.191	-0.313	0.196	0.021
Cu	0.166	0.043	-0.042	-0.393	-0.255	-0.129
Ni	0.139	0.217	-0.185	0.338	-0.029	-0.042
Zn	0.177	0.268	-0.055	0.231	0.035	-0.033
V	0.187	-0.221	0.060	0.046	-0.118	-0.097
I	-0.002	0.118	-0.426	-0.017	-0.178	0.186
Br	-0.159	-0.105	-0.353	-0.147	-0.033	0.095
C-org	-0.186	-0.071	-0.305	-0.081	-0.134	0.142
Mo	-0.207	-0.187	-0.056	-0.256	-0.158	0.042

Table 5.14 Eigenanalysis for the Correlation Matrix for core P5 (table 5.9).

	F-1	F-2	F-3	F-4	F-5	F-6
Eigenvalue	10.893	4.634	2.209	1.995	1.582	1.474
Proportion	0.330	0.140	0.067	0.060	0.048	0.045
Cumulative	0.330	0.471	0.537	0.598	0.646	0.691
	F-7	F-8	F-9	F-10	F-11	F-12
Eigenvalue	1.284	1.197	1.109	0.959	0.775	0.744
Proportion	0.039	0.036	0.034	0.029	0.023	0.023
Cumulative	0.729	0.766	0.799	0.828	0.852	0.874

Weightings of the first six components

Variable	PC1	PC2	PC3	PC4	PC5	PC6
Pb	0.014	0.054	-0.263	-0.454	0.215	0.123
Th	-0.029	-0.057	-0.147	0.040	0.192	-0.335
U	-0.084	-0.016	-0.359	0.320	-0.146	0.029
Sc	0.012	-0.158	-0.287	0.314	0.058	-0.248
Cr	0.001	0.228	-0.056	-0.030	0.034	0.235
Zr	0.267	-0.041	-0.095	-0.046	0.052	0.045
Rb	0.187	-0.204	-0.111	0.250	0.043	-0.196
Siterig	-0.062	-0.125	0.050	-0.013	0.586	0.165
Al	0.297	-0.043	0.016	-0.021	0.061	0.024
Fe	0.277	0.128	0.045	-0.060	-0.060	0.035
Na	0.189	-0.266	0.004	-0.108	-0.064	-0.124
K	0.273	-0.074	-0.008	0.009	0.014	-0.021
Mn	0.049	-0.058	-0.211	-0.188	-0.330	-0.243
Mg	0.260	-0.129	0.031	-0.102	0.014	-0.071
Ti	0.282	-0.005	0.027	0.009	0.144	0.011
La	0.080	-0.020	0.134	0.106	-0.275	0.098
Ce	0.046	0.089	-0.257	0.184	-0.179	0.166
Nd	-0.009	-0.035	-0.382	0.223	-0.159	0.407
Y	0.061	-0.346	-0.146	-0.114	0.030	0.276
Nb	0.043	-0.032	-0.298	-0.300	0.036	-0.085
P	0.237	-0.043	-0.103	0.107	0.132	0.249
CaCO3	-0.274	0.003	-0.081	0.014	0.143	-0.016
Sr	0.096	0.203	-0.150	0.306	0.326	-0.024
Ba	0.293	-0.013	-0.041	0.025	0.068	0.050
BiSiO2	0.272	0.099	0.036	-0.051	-0.248	-0.045
Cu	-0.067	0.167	-0.358	-0.323	0.029	0.044
Ni	-0.003	0.297	-0.268	-0.119	-0.028	-0.182
Zn	0.220	0.275	-0.049	-0.045	-0.043	-0.009
V	0.149	0.233	0.077	0.141	0.132	0.091
I	0.127	-0.272	-0.081	-0.030	0.100	-0.041
Br	-0.041	-0.422	-0.036	-0.082	-0.061	-0.039
C-org	-0.210	-0.151	-0.135	0.044	0.018	-0.049
Mo	-0.081	-0.198	0.070	-0.082	-0.149	0.451

chemical complexity of the sediment. The eigenvalues for factors 1-3 for each variable (element) are plotted in figure 5.36. From these graphical representations of the groupings of each variable (element) in 3-D space, it is apparent that the geochemical data roughly define 3 main phase associations: (I) A Carbonate Factor containing $CaCO_3$ and Sr; (II) A Terrigenous Aluminosilicate Factor (TAF) which can be split into two groups, (II-1) containing Th, K, Ce, Nd, La, Nb, Zr and, (II-2) containing Al, Cu, Sc, V, Fe, Mg, Zn, Cr, Ba, V, Ni, Ti, Y, and Si_{terrig}; and, (III) A Redox/Organic Matter Factor containing Mn, I, Br, C-org, Pb, U, Mo and Biogenic SiO_2. The "Elements" Biogenic SiO_2, P, Na, Pb and U all appear to have some weighting in more than one factor.

Core CD3827

Table 5.13 clearly shows that the first three factors in the PCA explains 66.7% of the total variance of major and trace element data in core CD3827. Eigenvalues for factors 1-3 for each variable (element) are plotted in figure 5.37. From these graphical representations it is apparent that the geochemical data roughly define 3 main phase associations: (I) A Terrigenous Aluminosilicate Factor (TAF) which contains all other elements (figure 5.35) except perhaps I and Th and can be separated into two groups: TAF-1 containing Cr, K, Nb, Si_{Terrig}, V, Fe, Zr, Sc, Al, Ti and perhaps Rb; and TAF-2 containing La, Ce, Nd, P, Ni, Zn, Ba, BiSiO2, Pb, Na and Mg; and, (II) An Redox/Organic Matter Factor (OMF) and Carbonate Factor containing C-org, Br, CaCO3, Sr, U and Mo; The elements I, P and Th appear to be distinct and have eigenvalue weightings on the other principle factors.

Core CD3822

Table 5.11 clearly shows that the first three factors in the PCA explains 57.3% of the total variance of major and trace element data in core CD3822. Eigenvalues for factors 1-3 for each variable (element) are plotted in figure 5.38 and from these it is apparent that the geochemical data roughly defines 3 main phase associations: (I) Carbonate Factor containing $CaCO_3$ and Sr; (II) A Organic/Redox Factor containing I, Br, C-org, U, Mo, P (and Biogenic SiO_2); (III) A Terrigenous Aluminosilicate Factor (TAF) which again can be divided into two groups; TAF-1 containing Al, K, Rb, Si_{Terrig} and Th (associated with feldspars); and TAF-2 containing Y, Cu, Sc, Ti, Fe, Mg, Cr, Ni, Mn, Nd, La, Pb, and Nb (associated with smectite). The elements P,

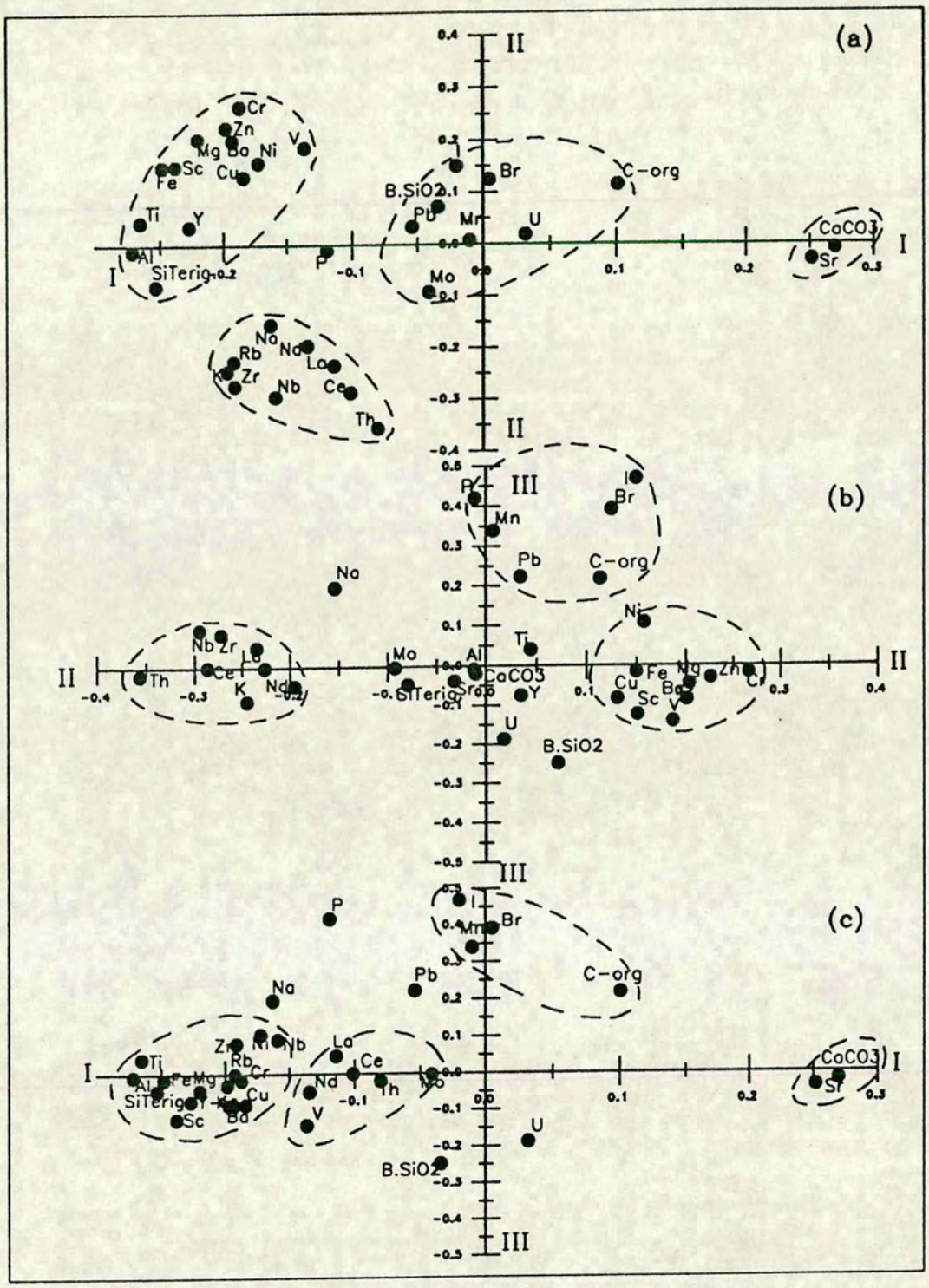

Figure 5.36 Plots of Factor I versus Factor II (a); Factor II versus Factor III (b); and Factor I versus Factor III (c) from principle component analysis of the data from core CD3826.

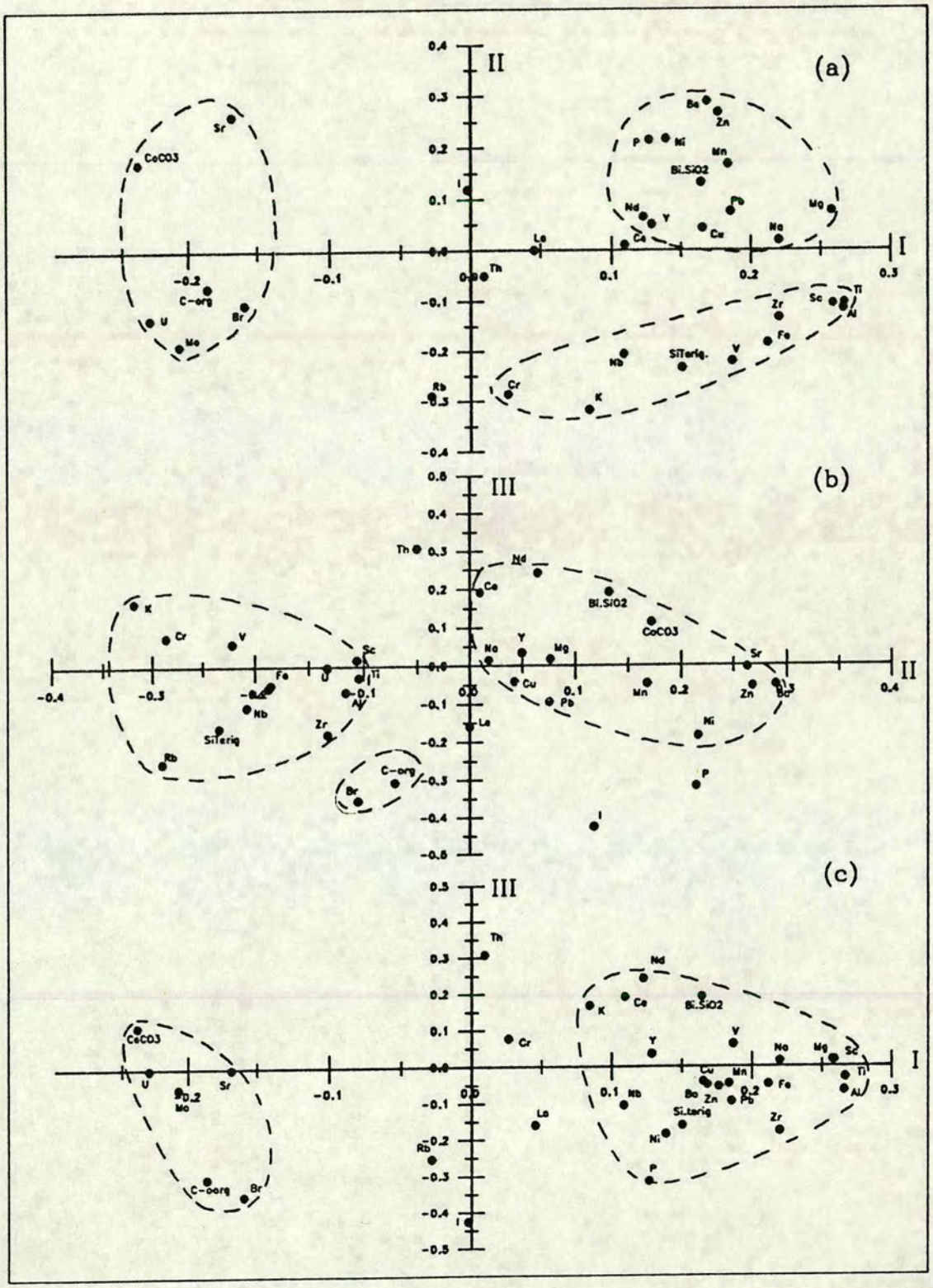

Figure 5.37 Plots of Factor I versus Factor II (a); Factor II versus Factor III (b); and Factor I versus Factor III (c) from principle component analysis of the data from core CD3827.

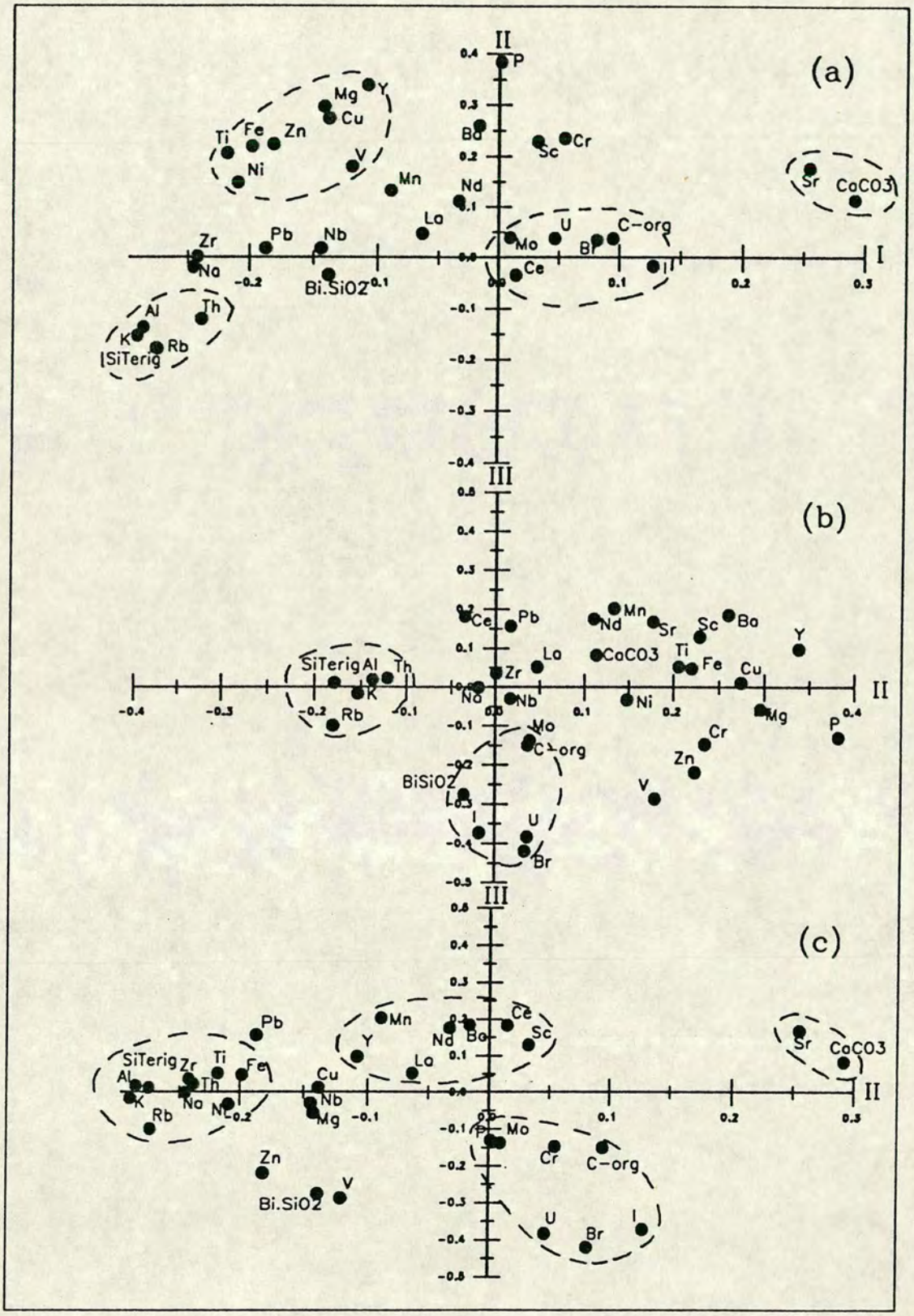

Figure 5.38 Plots of Factor I versus Factor II (a); Factor II versus Factor III (b); and Factor I versus Factor III (c) from principle component analysis of the data from core CD3822.

V, Zn, Biogenic SiO_2, Na and Ce all have eigenvalue weightings towards more than one factor.

Core CD3814

Table 5.10 clearly shows that the first three factors in the PCA account for 63.9% of the total variance in the dataset in core CD3814. From figure 5.39, it is apparent that the geochemical data can be divided into 3 principle phase associations: (I) A Calcium Carbonate Factor containing only $CaCO_3$; (II) A "Non-Carbonate" Factor containing all other elements except Ce, Na and Mo which are all distinct and have very different eigenvalues. The elements Zn, Cu, Ni and Mn may be grouped with the non-carbonate factor, but they have a slight weighting towards the other factors; (III) A Organic Matter/Redox Factor containing Th, U, Br and I.

Core P5

Table 5.14 clearly shows that the first three factors in the PCA explains 53.7% of the total variance of major and trace element data in core CD3822. From figure 5.40, it is apparent that the geochemical data can be divided into 3 principle phase associations: (I) Organic Matter (Productivity) and Carbonate Factor containing $CaCO_3$ and C-org; (II) A Redox Factor containing U, Th and Mo; (III) A Terrigenous Aluminosilicate Factor (TAF) which contains all other elements but which has a core of Al, Fe, Ti, K, Rb, Zr, V, Ni, Sc, Zn, Mn, Mg, P, Ba, Biogenic SiO_2, Pb, Nd, Ce, Nb and Cu. The elements I, Br, Y and SiTeig. are mostly negative values and so are not reliable.

5.5.3 Discussion

Factor (I) versus Factor (II) and Factor (I) versus Factor (III) plots have been shown to be most effective in defining different phase associations although the Factor (I) versus factor (II) plots helps to seperate the factor (II) elements. Although each core often has very different chemical compositions (see chapter 5-8) the PCA enabled some differentiation of the data into several broadly similar Factors or inputs. These factors or inputs are essentially the **biogenic**, **terrigenous** and **authigenic** components, common to most marine sediments. Moreover the relative importance of each factor in each individual core (ie (I) > (II) > (III)) is consistent with the relative dominance of each chemical component as defined by the geochemical

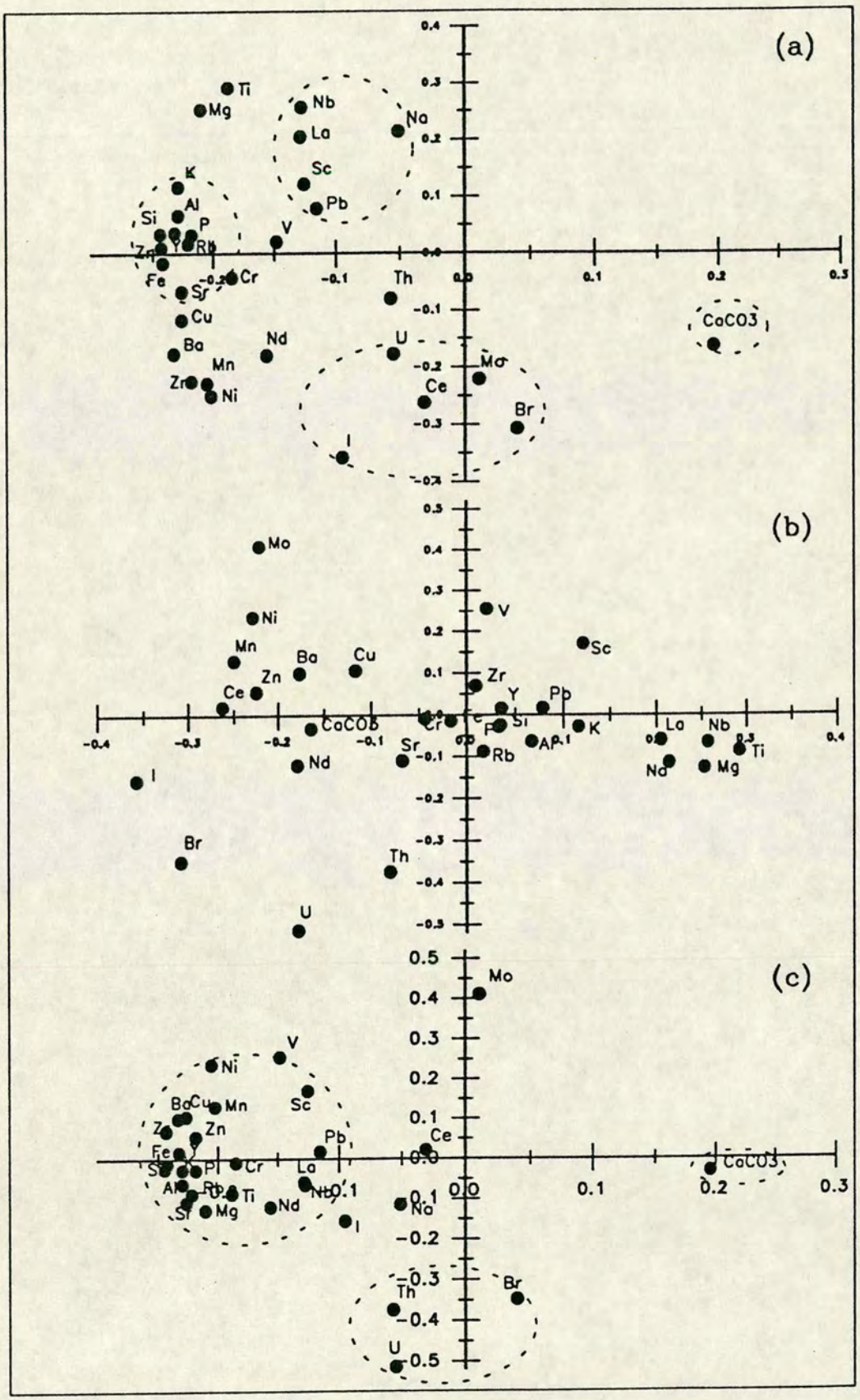

Figure 5.39 Plots of Factor I versus Factor II (a); Factor II versus Factor III (b); and Factor I versus Factor III (c) from principle component analysis of the data from core CD3814.

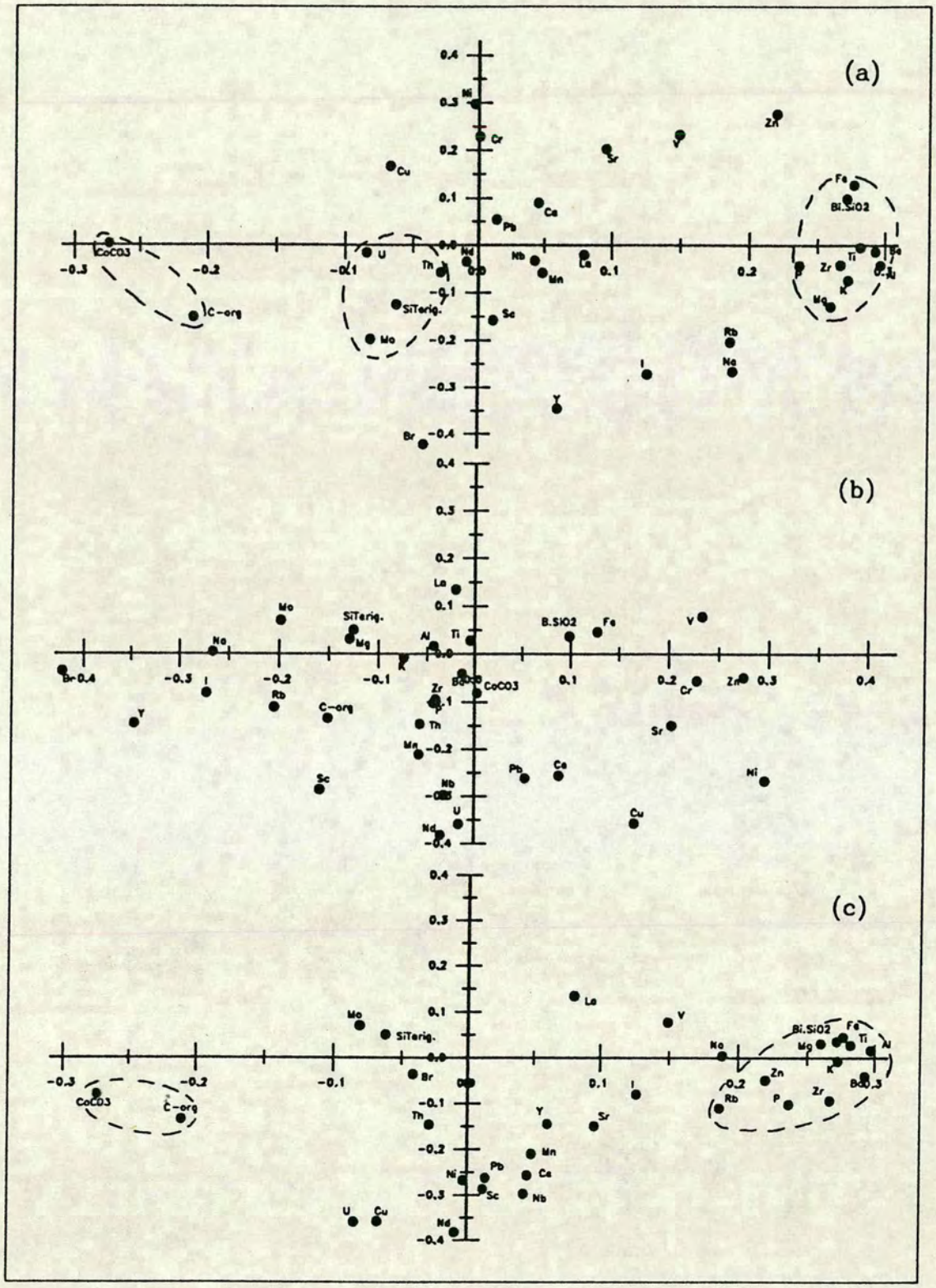

Figure 5.40 Plots of Factor I versus Factor II (a); Factor II versus Factor III (b); and Factor I verus Factor III (c) from principle component analysis of the data from core P5.

analyses of previous chapters. For example, the carbonate rich core CD3814 has $CaCO_3$ as it's factor (I) and, the terrigenous domina ted core CD3827 (situated close to land) has a Terrigenous Aluminosilicate phase as the dominat Factor. This statistical analysis does not conflict with the other geochemical interpretations as discussed above and can be used as a valid tool to aid the interpretion of data.

5.6 CONCLUSIONS AND PALAEOCLIMATIC IMPLICATIONS

Bulk sediment accumulation rates (chapter 4), in all the cores, showed that glacial times were generally periods of high sediment accumulation, especially during stage II. This conclusion has been corroborated by analysis of the terrigenous elements, which show that glacial periods are characterised by high inputs of terrigenous material, which decreases in a seaward direction. Furthermore, the area in the Holocene appears to be a period of rapidly decreasing terrigenous input. These trends are exemplified by the sediment accumulation flux changes and in Si_{terrig}/ Al variations.

For there to be greater terrigenous input to the area, there must be either a greater available source, or a more efficient transport processes carrying material to the deep-ocean, or both. During a low sea level stand sediment on the continental shelf and, possibly on the slope, would become available for erosion and redeposition further offshore. It would therefore contribute to the overall accumulation in ocean basins. Coupled with this, there may be increased biological productivity (see chapter 6) which would also increase sedimentation fluxes. It is likely that there was an increase in global aridity of the continents during the cold, dry glacial periods. Further, an increased wind strength due to the enlarging high latitude ice caps, forcing intensification of the tropical atmospheric pressure cells (Boyle, 1983), would allow more transport of such terrigenous material from the arid continents. The results in this chapter showing higher sediment accumulation rates during glacial times are consistent with these hypotheses.

The ash bands recognised in chapter 4 are commonly rich in feldspathic material and are depleted in Fe, Mg and Ti relative to Al. They are also enriched in K and Si_{terrig} relative to Al. It was shown that although tephra layer D (56 ka) was depleted in Zr relative to Al, the ash bands L (234 ka) and K (328 ka) are enriched in Zr relative to Al whereas all three of these ashes are depleted in Cr relative to Al.

Periodic hydrothermal events are recognised in core P5, CD3814 and CD3822 by their "metalliferous" signature. In core P5 a large increase in Fe relative to Al at 12 ka is attributed to a hydrotheraml deposit. Such hydrothermal deposits are exemplified by the sediments in the lower half of core CD3814 which show unusually high Fe/Al and Mg/Al ratios. These often typify smectite and sepeolite formation. Further evidence for the metalliferous nature of this sediment is the relatively high "metalliferous" Factor (after Bostrom, 1973) determined for the lower half of this core.

Further analysis of sediment composition suggest two sources of Ti, Cr and possibly Zr: (1) the Central American continent and, (2) the Galapagos archipelago. Moreover, Cr is enriched relative to other terrigenous components during glacials and in cores close to either the continent or the Galapagos archipelago. The increase near the continent probably results from a combination of increased terrigenous input from the land and also to some mechanical reworking of shelf sediments.

Principle component analysis has defined three main phases within each core which account for the majority of the variance in the dataset. The three factors are: (i) a biogenic/organic factor; (ii) a terrigenous aluminosilicate factor which may be subdivided into a feldspar and illite component and a Fe-Mg component posssibly associated with smectite/chlorite and, (iii) a diagenetic/authigenic factor. Each core has varying weightings on each factor depending on the dominant sources material.

CHAPTER 6
BIOGENIC TRACERS OF OCEANIC PALAEOPRODUCTIVITY

6.1 Introduction

This chapter documents changes in the biogenic constituents of the sediments in relation to palaeoclimatic variations. It begins with a short review of the current arguments about what are the dominant influences on the contents of biogenic components in the sediment. Results of each tracer are then presented, followed by a discussion that focusses on identifying those biogenic tracers that best document changes in palaeoproductivity through changing global climate and ocean conditions.

Global climate changes are the result of variations in the earth's orbit around the sun and the tilt of it's axis. These Milankovitch frequencies (400ka, 100ka, 41ka, 23ka, 19ka) cause variations in solar radiation which influence oceanic and continental systems. For example, continents become more arid and oceans shrink during glacial times, whereas vegetation cover may increase and wind speeds decrease during interglacial periods. In the eastern equatorial Pacific, glacial stages are thought to have been characterised by lower temperatures and sea level (Emiliani, 1955), and by increased productivity (Arrhenius, 1952; Adelseck and Andersen ,1978; Pedersen , 1979, 1983; Lyle et al., 1988) and eolian input from increased continental erosion and higher wind speeds (Parkin and Shackleton, 1973; Gardner and Hays, 1976; Boyle, 1983; Janecek and Rea, 1984, 1985; Rea et al., 1985; Berger, 1985). The debate as to which biogenic constituents, if any, most accurately reflect palaeoproductivity is still hotly contested.

Initally $CaCO_3$, organic carbon and biogenic opal (SiO_2) were favoured as effective tracers of oceanic palaeoproductivity but, as knowledge of ocean and sediment chemistry increased, additional problems have been recognised that cause confusion, not least dissolution and microbial degradation of organic matter. Most of the arguments centre around whether contents of biogenic components reflect **productivity** or **preservation**. The argument has swings in favour of one and then the other, although currently, for $CaCO_3$ at least, the evidence tends to favour a general dominance of a dissolution (preservation) factor. More recently, Ba and P have been developed as potential tracers, but both have their own particular problems.

Temporal studies are achieved from the age models developed in chapter 4. Analytical methods and tabulated results are presented in appendices A and C respectively. Results are on a salt free basis unless otherwise stated. Data from core AII54-25PC (Pedersen pers. comm.) is included to help corroborate hypotheses.

6.2 Calcium Carbonate

6.2.1 Introduction

Calcium in the marine environment may be derived from terrigenous or biogenic sources, although the former usually contributes only minor quantities to sediments. The biogenic phase in which Ca is most readily held is $CaCO_3$ and, the tests of marine organisms foraminifera and coccolithophorids are almost exclusively composed of this mineral. A relationship between the $CaCO_3$ content of oceanic sediments and climate has long since been established (Murray and Philippi, 1908), although the validity of such a relationship is still strongly disputed.

Arrhenius (1952) claimed that Pleistocene climatic variations caused changes in productivity. He also claimed that $CaCO_3$ cyclicity in sediments is a result of equatorial advance of Polar ice sheets which caused compression of atmospheric subtropical high pressure cells and, in turn, resulted in extreme latitudinal temperature gradients, increased trade winds and upwelling. Such fluctuations in carbonate content and dissolution are reviewed by Volat et al., (1980). The distribution of $CaCO_3$ in the ocean floors and, ultimately, within the sediment column is dependent on 3 main factors:

1. The relative dominance of $CaCO_3$ to SiO_2 faunal community productivity of the overlying water mass.
2. Sedimentation rate which influences the dissolution of the $CaCO_3$ in the water column which is undersaturated with respect to calcite.
3. Dilution by non-carbonate (terrigenous) material.

All these factors act independently, a fact which complicates definitive interpretations.

Primary biological productivity in the surface waters of the eastern equatorial Pacific is generally considered to be some of the highest anywhere in the oceans, with localised areas of extremely high productivity where strong upwelling occurs. The region is situated at the eastern end of a zone of equatorial divergence, and at the northern end of the western continental margin upwelling systems. Being positioned at the crossroads of these two systems results in a relatively complicated pattern of productivity (chapter 2).

Preservation of $CaCO_3$ relates to its saturation in water especially with respect to the activity of the carbonate ion, its rate of input to the sediment and, the temperature and pressure conditions. Dissolution of $CaCO_3$ increases with water depth as a result of the thermodynamic effects of lower temperature and greater hydrostatic pressure which both act to increase the solubility of $CaCO_3$. Superimposed on this bathymetric effect are dissolution patterns which vary according to regional and temporal variations in water mass carbonate chemistry and sediment input (Farrell and Prell, 1991).

Dissolution of $CaCO_3$ increases dramatically below the lysocline (Berger, 1975; Takahashi and Broecker, 1977) which is defined as the depth at which the *in situ* carbonate ion concentration ($[CO_3^{=}]$) equals the saturation $[CO_3^{=}]$, (Broecker and Takahashi, 1978). The majority of all dissolution takes place in the transition zone between the lysocline and the calcite critical depth (the shallowest pelagic depth where the sediments contain $\leq 10\%$ $CaCO_3$), (Lisitzin and Peltelin, 1967). This depth should not be confused with the calcite compensation depth (CCD) at which point sediments contain 0% $CaCO_3$. According to Moore et al. (1973), the CCD lies at approximately 3.4 km in the Panama Basin region, some 1.3 km shallower than in the central equatorial Pacfic and somewhat deeper than in nearshore areas (Kinnet, 1966). The depth to the lysocline is thought to have fluctuated markedly during the Pleistocene climatic cycles while the calcite critical depth has remained relatively constant (Farrell and Prell, 1989). Thus significant changes in the thickness of the transition zone between the lysocline and the calcite critical depth have occured over time (Van Andel et al., 1975; Rea et al., 1991; Farrell and Prell, 1989). Thus, a core situated at a water depth close to the transition zone could suffer temporal fluctuations in preservation, due to sea level changes, and variations in the carbonate ion activity of the deep ocean water. Migration of the sediment position into deeper water as a result of sea floor spreading also has an effect on dissolution, but over a much longer time scale than is being studied in this thesis.

In a recent study from the central equatorial Pacific comparing bottom water sediment trap results with contents of biogenic components in the surface sediments, Murray (1987) concluded that 60-62% of carbonate (89-92% of opal and, 98-99% of organic carbon) exported from the surface waters, is recycled and does not accumulate in the sediment. Swift and Wenkam (1978) also claim that $CaCO_3$ accumulation in the Panama basin is controlled primarily by lateral and vertical variations in dissolution rates.

The debate on the interpretation of $CaCO_3$ contents in ocean sediments has essentially two groups of protagonists: firstly those who advocate productivity as the dominant factor, and who argue that $CaCO_3$ flux from the surface of the ocean (euphotic zone) largely determines the resulting $CaCO_3$ mass accumulation rate (Arrhenius, 1952; Parkin and Shackleton, 1973; Valencia, 1977; Adelseck and Anderson, 1978; Emerson and Bender, 1981; Archer, 1990). The second group however, hold the view expressed by Farrell and Prell (1991) that dissolution is the dominant factor, and that changes in the $CaCO_3$ content of sediments primarily reflect changes in water column carbonate chemistry (essentially bottom water corrosiveness with respect to $CaCO_3$), and that this is most likely linked to circulation variations (Berger, 1968, 1970a, 1970b, 1973; Moore et al., 1973; Thompson and Saito, 1974; Farrell and Prell, 1991). However most authors agree that although dissolution generally dominates, primary production is influential especially in sediments which lie above the lysocline and beneath areas of extreme euphotic zone productivity (as is the case in the Panama basin). Thus productivity and dilution by non-biogenic material (terrigenous) are important and, perhaps, locally are the dominant factors influencing the $CaCO_3$ content. However substantial dissolution can occur in the supra-lysoclinal oxygen minimum zone (Steens et al., 1991).

Terrigenous dilution of carbonate contents is especially important in regions where its input rate changes markedly. However, flux calculations should remove this carbonate dilution problem but they are themselves highly susceptible to slight changes in the age model and sedimentation rates (see chapter 5).

Best estimates for $CaCO_3$ palaeoproductivity are from cores close to the modern lysocline, and indicate that $CaCO_3$ production during glacials was 1.3-1.5 times greater than in interglacial periods (Peng et al., 1977; Adelseck and Anderson, 1978; Schiffelban and Dorman, 1986). Such a change is considerably less than the dynamic range of carbonate contents between glacial to interglacial periods when a 4 fold change is often quite common (eg cores CD3826, AII54-25PC, see below).

6.2.2 Results

Calculations of $CaCO_3$ contents in cores studied in this thesis are shown in appendix B, and range from around 2% to over 90% (table 6.1). On the basis of their $CaCO_3$ contents the cores may be divided into two groups: those rich in carbonate (CD3814,

CD3822 and P5); and those impoverished in carbonate (CD3826, CD3827 and AII54-25PC).

Table 6.1 Mean values and ranges of biogenic tracers from this study.

Cores	P5	CD3822	CD3826	CD3827	AII54-25PC
Water Depth	(1540 m)	(2340 m)	(3075 m)	(2725 m)	(3225 m)
$CaCO_3$	89.5(83.8-92.3)	78.6(51.5-87.4)	22.8(2.4-49.6)	9.4(1.8-17.4)	28.5(1.6-59.5)
Ex.Sr	1141(1119-1161)	1136(730-1236)	460(156-884)	177(72-255)	572(101-1046)
C-org	0.62(0.41-0.62)	1.21(0.43-2.66)	1.41(0.25-2.50)	3.31(1.82-4.85)	0.96(0.23-1.81)
SiO_2	3.04(1.62-4.76)	5.04(2.19-11.74)	4.04(1.28-5.91)	4.40(2.69-6.78)	**********
Ex.Ba	786(543-1116)	2190(1658-2674)	2638(1430-4038)	1179(896-1651)	2084(167-4150)
$Ba/Al*10^{-2}$	26.5(22-31)	25.0(7-34)	5.1(2.3-6.8)	1.9(1.5-2.6)	7.8(3.0-10.9)
SiO_2/ExBa	38.6(23.1-55.9)	23.6(12.2-55.6)	15.6(5.9-24.4)	37.7(22.5-58.7)	**********
$SiO_2/CaCO_3$	0.03(0.02-0.05)	0.07(0.03-0.16)	0.27(0.05-2.2)	0.67(0.22-3.4)	**********

All values are expressed on a weight % salt free basis except AII whose values may not be salt corrected. Figures in Parentheses show the range of values.

Core CD3814 was recovered on the crest of the Galapagos rise in a water depth of 3550 m (the deepest of all the cores), and yet it has the highest mean $CaCO_3$ content, which is evidence that it is not only water depth that determines the content of $CaCO_3$ in sediments. As described in chapter 3, half of the core is foram sand and half nanno-fossil ooze. The aluminosilicate material in this core was shown to be dominated by hydrothermal and volcanigenic debris (chapter 5). Moreover the Galapagos ridge where the core is situated appears to be starved of terrigenous material *sensu stricto*. No cyclicity is present in the core and $CaCO_3$ contents do not vary in any systematic way (Figure 6.1a).

Core CD3822 displays quite a large range in $CaCO_3$ contents from approximately 51% to 87%. However the large decrease in $CaCO_3$ values at around 80 ka is almost certainly due to the diluting effects of a local tephra layer (figure 6.1b). Apart from this, the $CaCO_3$ record does not appear to follow the glacial-interglacial cyclical variation observed in the other cores and in other studies. There is a peak in $CaCO_3$ during stage II, but high carbonate also occurs in upper stage III and V. This apparent decoupling from the normal carbonate profile is difficult to explain.

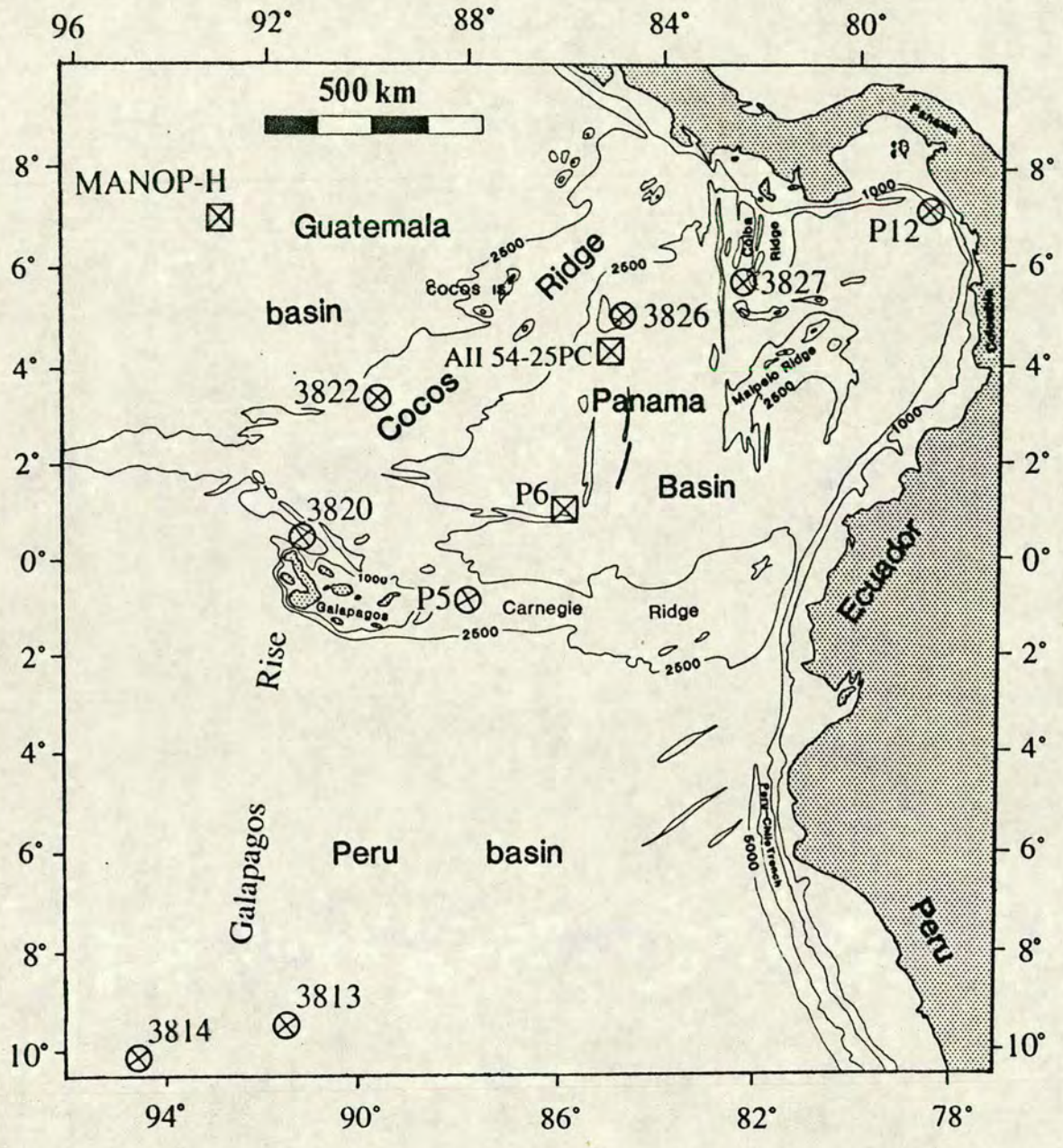

Figure 6.0 Location map of cores studied in this thesis (circles with cross), and of cores used in comparison (squares with cross).

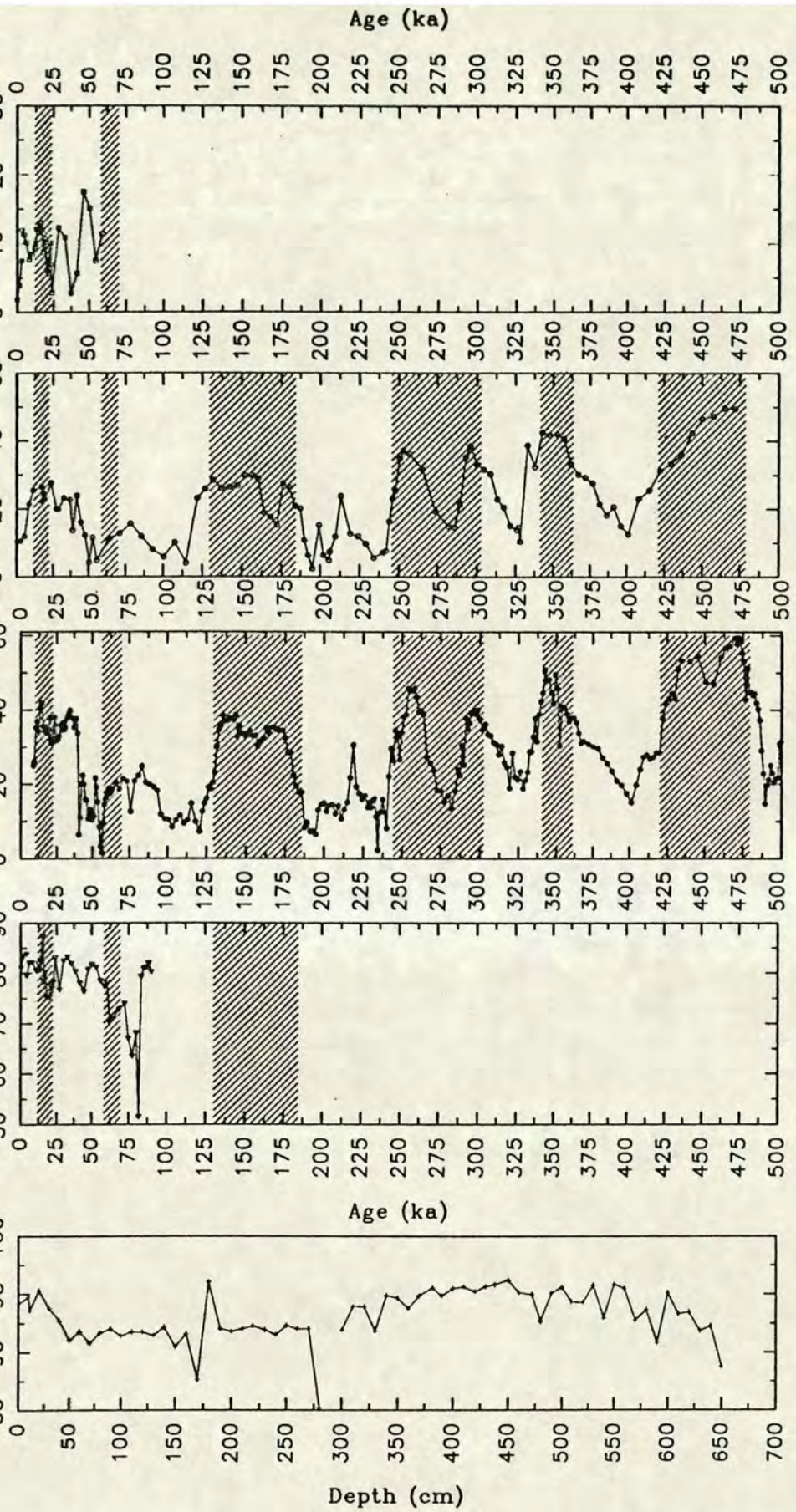

Figure 6.1 Temporal variations in $CaCO_3$ (Wt.% salt free) in CD38 cores and core AII54-25PC. Shaded regions represent glacial stages II, IV, VI, VIII, X and XII. Note: core CD3814 data is expressed in depth domain.

Perhaps core CD3822, which is situated on the north flank of the Cocos ridge, is more a part of the equatorial divergent upwelling system than the western continental margin and Costa Rica Dome upwelling systems in which core CD3826, CD3827 and AII54-25PC are centred. This may result in core CD3822 receiving quite different, and changing, faunal communities compared to cores in the central and eastern Panama basin. Perhaps siliceous communities (eg diatoms) were periodically dominant over carbonate communities; a theory corroborated by the very high biogenic SiO_2 values in the core (see table 6.1). Similar conclusions were reached by Lyle et al. (1988); that of changes in the relative dominance of siliceous and $CaCO_3$ plankton communities. This concept of evolving plankton communities during a productivity event will be discussed futher below especially with respect to $SiO_2/CaCO_3$ and SiO_2/Ex.Ba variations.

Core P5 has the highest average $CaCO_3$ contents of all the cores situated in the Panama basin, and varies from around 84% at the surface to approximately 92% during the Last Glacial Maximum (figure 6.2a). The core was recovered from a water depth of only 1540 m on the crest of the Carnegie ridge some 200 km east of the Galapagos archipelago (figure 6.0). As a result of its bathymetric position, one can assume that virtually no dissolution of the $CaCO_3$, raining down to the sediment surface from the euphotic zone, has occurred and, that the carbonate record in the core is a direct reflection of the combined effects of the overlying productivity and the input of terrigenous material over time. Furthermore, the very high $CaCO_3$ contents rule out significant terrigenous input/dilution. Thus the increase in carbonate content during stage II (figure 6.2a) in core P5 probably reflects increased input of $CaCO_3$ from primary and secondary productivity in the last glacial in the region. Using this carbonate curve as a template for palaeoproductivity variations in carbonate secreting plants and animals, changes of other factors influencing the record such as dissolution and dilution may become apparent in other $CaCO_3$ profiles in other cores.

Downcore variations in cores CD3826, CD3827 and AII54-25PC follow a pattern of high calcium carbonate contents during glacials and low carbonate contents in the interglacial periods (figure 6.1). This cyclicity, which is consistent with previous work in the area (eg Hays et al. ,1969), is especially well developed in cores CD3826 and AII54-25PC which span around 500,000 years each.

Figure 6.2 Temporal variations in $CaCO_3$, SiO_2, organic carbon and Ba in core P5. Shaded region represents glacial stage II. Note the compression of data over the last glacial maximum.

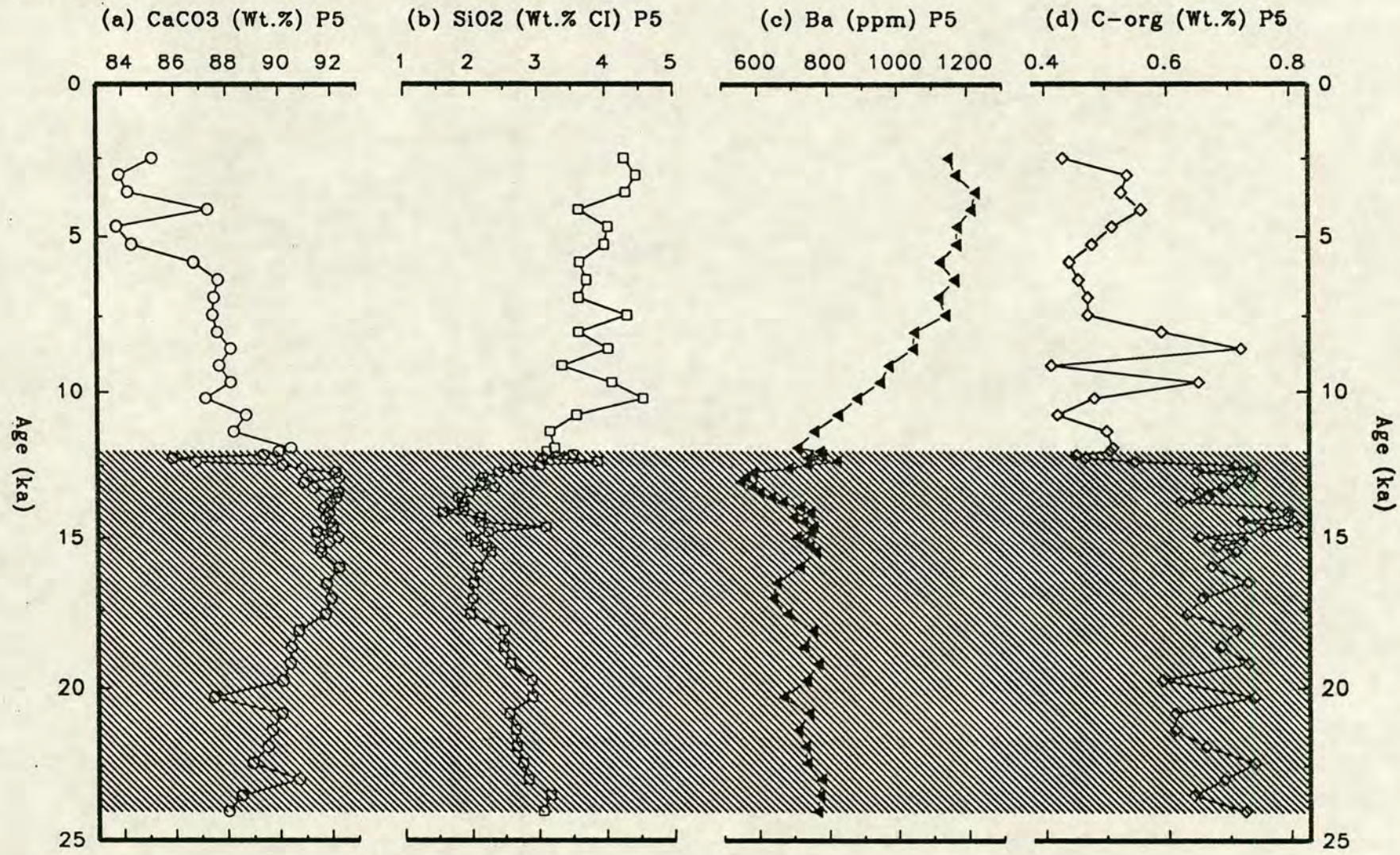

Core CD3827 has a slightly unusual carbonate profile in that there is a double cycle within stages I and II (figure 6.1e). That is to say, the peak during the last glacial maximum is followed by an equivalent increase in stage I at around 10 ka before decreasing almost uniformly to less than 2% $CaCO_3$ in the surface sediments. This doublet in $CaCO_3$ over the past 25 ka has also been observed by Pedersen (1979) in core P6 from the Panama basin (see figure 4.12, this study). The reason for this is uncertain, especially in light of the fact that this doublet is not present in other biogenic or terrigenous tracers. If glacial periods are characterised by higher production and accompanying $CaCO_3$ contents then the increase in $CaCO_3$ at the base of stage I could, conceivably, be due to the "glacial-type" (cooler) conditions that were prevelent during the Younger Dryas Cooling Event at around 10.5 ka (Kennett, 1990). However the duration of this event is thought to be in the order of several hundred to one thousand years (Fairbanks, 1989) and, as the increase in $CaCO_3$ in the Holocene of core CD3827 occured over several thousand years, it seems unlikely that the doublet is due to the Younger Dryas event alone. Thus the origin of a peak in $CaCO_3$ in lower stage I remains ambiguous. It is, perhaps, related to the anomalous negative $\delta^{18}O$ event at approximately the same age in core CD3822 (figure 4.6), although negative $\delta^{18}O$ events usually coincide with periods of low $CaCO_3$ content in sediments.

Generally the dynamic range in $CaCO_3$ values is greater in cores from deeper waters which argues in favour of the dominance, or at least of the strong influence, that dissolution has on the $CaCO_3$ record. The range in $CaCO_3$ values in cores CD3826 and AII54-25PC from full glacial to full interglacial period is around 30 weight % (eg approximately 10-40 Wt.% $CaCO_3$ for stage VII to stage VIII) in both cores; almost a four fold difference. Core CD3827 varies by approximately 10 % from the present Holocene values of approximately 2 Wt.% to the last glacial maximum value of just under 15 Wt.% $CaCO_3$. This difference reflects the dominance of the terrigenous material in core CD3827 throughout its depositional history.

6.2.3 Discussion

Cores CD3826, CD3827 and AII54-25PC were all recovered in the eastern part of the Panama basin which receives the majority of the terrigenous input to the region, whereas cores CD3822 and P5 were recovered from the Cocos and Carnegie ridges respectively, both of which receive relatively low terrigenous inputs (chapter 5). The water depth of cores CD3826, CD3827 and AII54-25PC are similar and all supra-

lysoclinal. Although the lysocline is known to shoal towards the continents (Kinnet, 1966), core CD3827 is still thought to be well above the present surface of accelerated $CaCO_3$ dissolution. Differences in $CaCO_3$ contents of the tops of these three cores are, therefore, the result of differences in the terrigenous input and/or productivity in the eastern Panama basin. Cores CD3826 and AII54-5PC are geographically and geochemically very similar (including $CaCO_3$ contents). That core AII54-25PC was recoverd in slightly deeper water with respectively more dissolution than CD3826, and yet has slightly higher $CaCO_3$ contents, is further evidence that local factors influence $CaCO_3$ content.

Terrigenous dilution will be more important in the eastern Panama basin cores proximal to continental sources (eg CD3827), especially during low sea level stands when a greater amount of terrigenous source material is available for redeposition from the continental shelf. However, cores such as CD3822 and P5 are reasonably distal to terrigenous sources such that changes in detrital input may be less significant than are productivity and dissolution effects on the carbonate content.

Core P5 only extends as far back as the top of stage III (25ka), and there is no guarantee that stage II is typical of the last glacial period or of other glacial episodes. However, if one assumes that stage II in core P5 is reasonably representative of glacials, then one can begin to reconstruct changes in $CaCO_3$ productivity and perhaps ocean chemistry, which are the results of changes in water mass circulation. Deviations from this template of core P5 are therefore the result of either dissolution and/or dilution. Productivity will be discussed more fully with respect to $CaCO_3$ Mass Accumulation Rates (MAR) in chapter 7.

6.2.4 Conclusions

1. The eastern Panama basin has lower $CaCO_3$ contents than the western part caused mainly by dilution from terrigenous material.
2. The exceptionally high $CaCO_3$ contents in core P5 are a result of the shallow water depth that this core was recovered in (ie 1540 m), where dissolution is minimal.
3. $CaCO_3$ contents tend to be higher during the glacial periods in all the cores with several exceptions, most notably in the Holocene of core CD3827 and during stage III in core CD3822. Cores CD3826 and AII54-25PC display the classical glacial-interglacial Pleistocene cyclicity in $CaCO_3$ over 0.5 Ma.

4. The dynamic range of $CaCO_3$ values increases with increasing water depth, and decreases with increasing dominance of terrigenous material.
5. The $CaCO_3$ profile in core CD3814 has probably been affected by winnowing by bottom curents, in addition to the factors common to other cores.

6.3 STRONTIUM

6.3.1 Introduction

Strontium in marine sediments occurs mainly in carbonate, apatite, barite (Church, 1970) and aluminosilicates (El Wakeel and Riley, 1961; Goldberg and Arrhenius, 1958; Hirst, 1962). Sr substition in barite is in the order of 1-5 mole percent, which allows at most a potential Sr contribution of 30-150 ppm Sr to the total Sr. However despite there being several possible sources of Sr, by far the most important is that contributed by carbonate (table 6.2). This fact is reinforced because an average deep-sea clay holds only around 180 ppm Sr and a mean value for marine organisms is 862 ppm Sr (table 6.2). Of the two main carbonate contributors of Sr in deep-sea sediments (foraminifera and coccoliths), foraminifera tend to dominate coccoliths in the cores studied in this thesis, except in the lower half of core CD3814 which is composed of a nannofossil carbonate ooze. Sr in pelagic foraminiferal tests is relatively high at approximately 1600 ppm (Turekian, 1964; Atlantic), compared to Sr contents in coccoliths at approximately 1000 ppm in Cretaceous Chalk (Turekian, 1964). Sr from the celestite ($SrSO_4$) in pteropods tends not to survive burial in sediments of oceanic deposits.

Analytical techniques of Sr determination using X-ray fluoresence spectrometry and results are given in appendices A.5 and C.5 respectively. The contribution of Sr from average deep-sea clay has been removed leaving an Excess Sr (Ex.Sr) value by assuming a Sr/Al ratio for aluminosilicates in deep-sea clay of 0.00214 (Turekian and Wedopohl, 1961). This is quite close to the mean Sr/Al value in core P12 (0.00138), a core that is thought to represent the Sr level of terrigenous input from the continent. The mean Ca/Al of core P12 (0.119) was then used to calculate the terrigenous calcium and substract it from the total Ca in each core, thus leaving a terrigenous free excess Ca (Ex.Ca). The Ex.Sr was then ratioed against the Ex.Ca in an attempt to illustrate temporal changes in foraminiferal/coccolithophorid ratios between cores.

Table 6.2 Mean values of Strontium in the marine environment.

Sediment/Organism Description	Sr (ppm)	Sr/Ca $\times 10^{-3}$	References
Mean Marine organism	862	******	1
Mean deep-sea clay	180	******	2
Mean deep-sea carbonate	2000	******	2
Pure foram# ooze	1600	******	3
Pure Cocolith## ooze	1000	******	3
Pacific *Globigerina* ooze	******	3.3	4
Cocolith ooze	******	2.5-2.6	3
Arabian deep-sea sediment	******	3-4.5	5
This Study: P5	1148.2	3.21*	6
CD3814	1206.8	3.36*	6
CD3822	1150.2	3.62*	6
CD3826	578.4	4.64*	6
CD3827	330.6	3.30*	6
AII54-25PC	646.9	6.38*	6

= Foraminifera; ## = Coccolithoforids; * = Ex.Sr/Ex.Ca $\times 10^{-3}$

References: 1-Martin and Knauer (1973), 2-Turekian and Wedopohl (1961), 3-Turekian (1964), 4-Thompson and Chow (1956), 5-Khan (1989), 6-This Study

6.3.2 Results and Discussion

The Ex.Sr/Ex.Ca ratio in cores from this study varies between approximately 3-6 $\times$ 10^{-3}. The lower end of this range is consistent with values for deep-sea foraminiferal oozes from around the world (table 6.2). However the upper end of this scale, which includes cores CD3826 and AII54-25PC, is considerably higher than would be expected for normal marine sediments.

Downcore variations in the Ex.Sr/Ex.Ca ratio are shown in figure 6.3. There is a strong tendency for the ratios to decrease during glacial periods which may be a

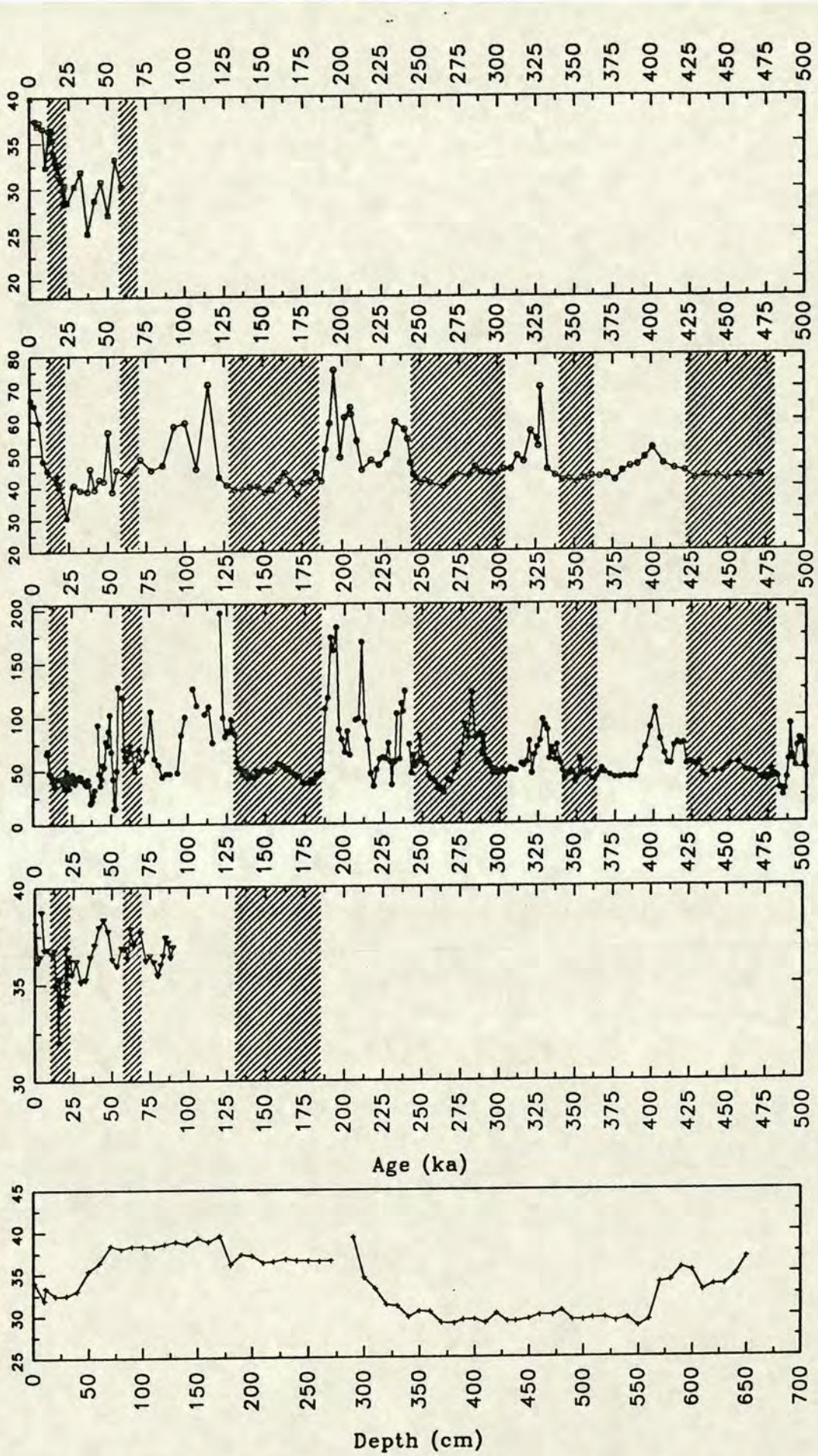

Figure 6.3 Temporal variations in Excess Sr/ Excess Ca $\times 10^{-4}$ in CD38 cores and core AII54-25PC. Shaded regions represents glacial stages II, IV, VI, VIII, X and XII.

reflection of increased terrigenous recrystallised calcite (which may contains 200-600 ppm Sr, N.B. Price, Pers. Comm) as a result of pluming and erosion from the shelf regions during glacial low sea level stands. This lowered Sr content in terrigenous calcite seems to be corroborated by low Ex.Sr/Ex.Ca values in core CD3827 (table 6.2), which was recovered close to the terrigenous source of central America.

Core AII54-25PC, however, has the highest values and a mean (6.38×10^{-3}) that is considerably higher than any of the other cores, although the shape of the Ex.Sr/Ex.Ca profile in cores AII54-25PC and CD3826 are very similar. This is difficult to explain due to its similarity (both geochemically and physically) to core CD3826. Such large values suggest an unusually large input of Sr from barite or apatite because core AII54-25PC, as are all the cores, is corrected for input from terrigenous material by using excess contents. However, even assuming a maximum 5 mole percent substitution of Sr into barite ($BaSO_4$) this only accounts for 150 ppm of the excess Sr and does not account for the very high Ex.Sr/Ex.Ca ratio. Therefore, the large change in Ex.Sr/Ex.Ca observed in core AII54-25PC and, to a lesser extent core CD3826, is most likely due to temporal changes in foraminifera/coccolith production. During interglacials, production may have been domina ted by foraminifera.

The Ex.Sr/Ex.Ca ratio in core P5 decreases during glacial II due to the increase in $CaCO_3$, but its Ex.Sr content varies very little (figure 6.4a). This is probably the result of only very slight changes in the relative proportions of coccoliths to foraminifera in the core.

If dissolution affects foraminifera more than coccoliths (Hay, 1970; Broecker, 1971; Honjo, 1977), then during glacial periods when dissolution is thought to have been lower, there should have been more foraminifera relative to coccoliths. This is consistent with the reduced foraminiferal abundance in glacial stages observed by Prell (1984). It is clear from figure 6.3 and 6.4a that if one assumes the Ex.Sr/Ex.Ca ratio to reflect changes in the foraminifera to coccolith ratio, and that there was indeed decreased dissolution of $CaCO_3$ during glacials, then the curves for cores P5, CD3822, CD3826, CD3827 and AII54-25PC are opposite to what would have been predicted (ie low Ex.Sr/Ex.Ca ratios during the interglacial periods of high dissolution). Thus dissolution is not the cause of the changes in the Ex.Sr/Ex.Ca ratio.

Figure 6.4 Temporal variations in Excess Sr/Ca × 10^{-4}, Ti/Al, Excess Ti (Ex.Ti) and organic carbon (C-org, salt and carbonate free) in core P5. Shaded region represents glacial stage II.

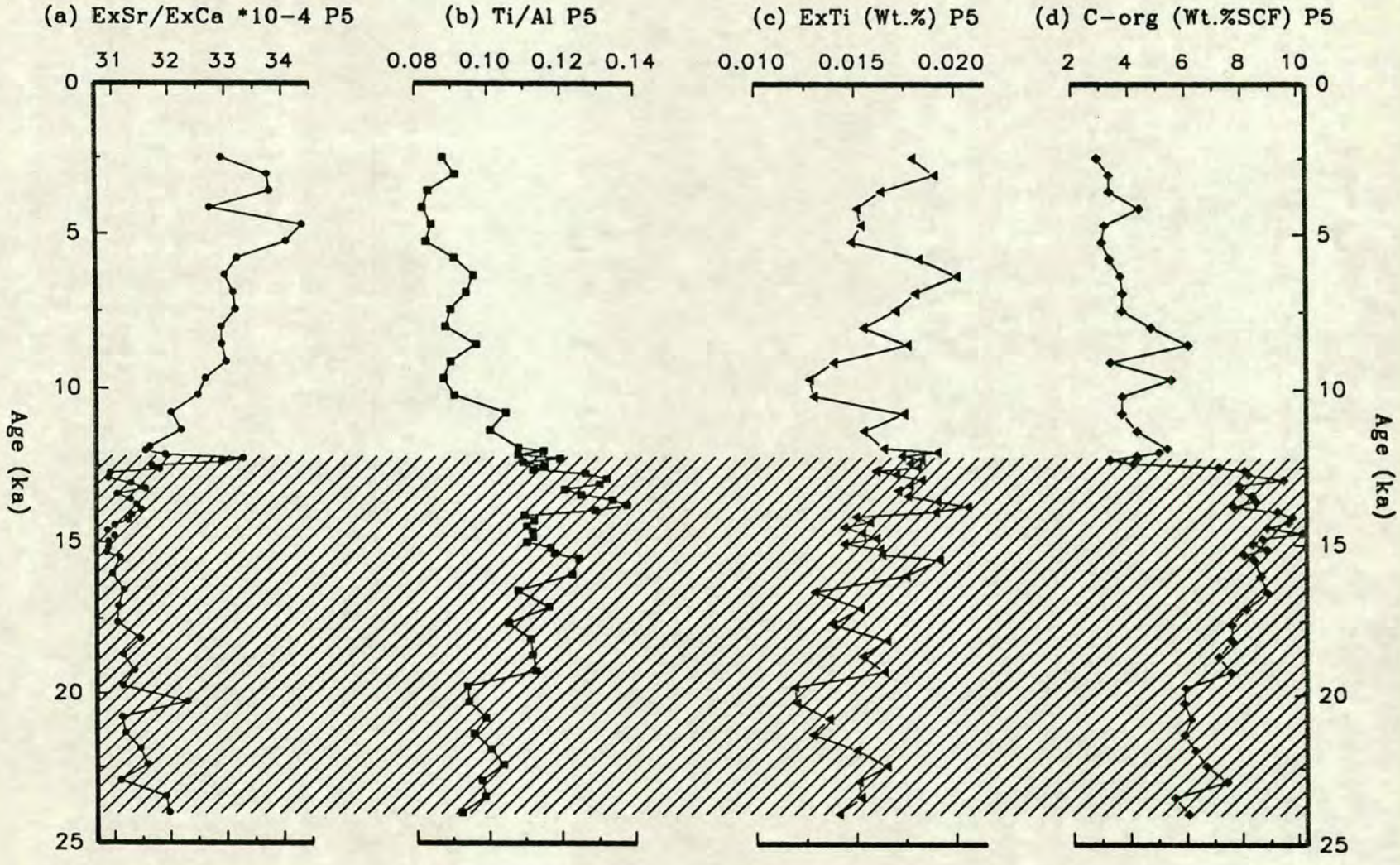

Core CD3814 has relatively low Ex.Sr/Ex.Ca ratios especially in the lower half of the core. The lower section of this core has been shown (chapter 3) to be dominated by carbonate nannofossils (probably mainly coccoliths), whereas the upper section is almost a foraminiferal sand. This distribution argues in favour of the dominance of the foraminifera/coccolith ratio in determining the Ex.Sr/Ex.Ca ratio.

The profiles of Ex.Sr/Ex.Ca in cores P5, CD3814, CD3822, CD3826 and AII54-25PC inversely relate to $CaCO_3$, while in core CD3827 the Ex.Sr/Ex.Ca ratio broadly parallels the trend in $CaCO_3$. This implies some dependancy of Sr on calcite with cores or periods that are highest in calcite exerting the greatest influence. There is an increase in the ratios during the Holocene in all cores except AII54-25PC (which may have the Holocene missing) which implies a high foraminifera content (at least relative to coccoliths) during this period.

6.3.3 Conclusions

1. In high carbonate cores (P5, CD3814 and CD3822) Ex.Sr/Ex.Ca profiles broadly mirror $CaCO_3$ curves indicating a dependancy of Sr on calcite.
2. The variations in the Ex.Sr/Ex.Ca ratio illustrate changes in the relative dominance of coccoliths to foraminifera.
3. The high Ex.Sr/Ex.Ca values for cores AII54-25PC may be partly derived from barite or, more likely, changes in the foraminifera production and/or species abundance.
4. Ex.Sr/Ex.Ca profiles do not reflect differential dissolution of foraminifera relative to coccoliths because the curves are opposite to what would be expected (ie high Ex.Sr/Ex.Ca during the glacials periods of low dissolution).

6.4 Organic Carbon

6.4.1 Introduction

According to Bordovisky (1965a, 1965b), organic matter in marine sediments is composed of a mixture of various pigments (chlorophyll-like compounds and carotinoids), lipid-like substances-bitumens, various carbohydrates and several amino acids. The great majority however is composed of humic acids and residual organic matter.

Marine plankton plays an important role in the biogeochemical cycling of carbon because they are intimately involved in the transfer of carbon between the atmosphere, the ocean and the sea bed. By converting CO_2 into organic tissue and skeletal $CaCO_3$, they transfer CO_2 to the deep ocean and sediment column. Ocean circulation, in turn, transfers nutrients and CO_2 from the abyssal depths to the surface waters of the ocean where it is either utilised as described above or is exported to the atmosphere.

Organic carbon (C-org) in marine sediments is derived from the decaying remains of once living organisms principally phytoplankton, zooplankton, fish debris and, the faecal deposits and molts of still living oganisms. Intuitively, C-org would would appear to be a good indicator of past euphotic zone productivity, and it was Arrhenius (1952) who first used the C-org content in marine sediments as a proxy for productivity variations relating to the Pleistocene climatic cycles. Since this pioneering work, the debate has been similar to that for $CaCO_3$: whether C-org increases result from productivity increases or from preservation events. Four factors define the final C-org content in the sediment:

1. Euphotic zone primary productivity
2. Sediment accumulation rate and bioturbation rate
3. Oxidation state of the bottom waters and degradation rate
4. Dilution from non-organic carbon material ($CaCO_3$ and terrigenous)

Emerson (1985) argues that the increased C-org contents during glacial periods, in low latitude sediments, could be explained by increased preservation, either independently or in addition to increased productivity, because of lowered bottom water oxygen concentrations and increased sedimentation rates during glacials.

Murray (1987) concurs with this suggestion using the somewhat tenuous basis that other biogenic components vary in a different way to C-org, and that 98-99% of C-org leaving the surface waters of the oceans is lost through oxidation and degradation in the water column and sediment-water interface. In contrast to this, the "Productionists" argument refutes the correlation between bottom water oxygen concentration and C-org accumulation rate (Pedersen, 1979, 1983; Pedersen et al. 1988, 1991; Finney, 1988; Lyle, 1988; Lyle et al., 1988; Rea et al., 1991) They favour a dominance of euphotic zone primary productivity on the C-org record,

whilst accepting the reality of organic matter degradation in the water and sediment columns.

Spatial and temporal variations in the C-org content from cores studied in this thesis are presented below. Analytical techniques and tabulated data are given in appendices A.8 and C.9 respectively.

6.4.2 Results and Discussion

Temporal variations in C-org (Wt % salt free) are shown in figures 6.5 and 6.2d. The profiles of C-org on a salt and carbonate free (SCF) basis are shown in figures 6.6 and 6.4d, and do not show significant changes from the salt free curves except in core CD3822 and P5. The C-org (SCF) curve from P5 shows a distinct increase during glacial stage II, whereas in core CD3822 stage IV is somewhat depressed in C-org (SCF) relative to the C-org (SF) profile (figure 6.5a). Values range from virtually zero in the tephra layers to almost 5% in stage II of core CD3827 (table 6.3). Table 6.3 shows a comparison of surficial, Holocene and last glacial maximum C-org contents in sediments from around the world. Glacial periods in all cores from this study are represented by periods of increased C-org content, which most authors interpret as reflecting increased productivity in the eastern equatorial Pacific (Pedersen, 1979, 1983; Pedersen et al. 1988, 1991; Gardner, 1982; Finney, et al., 1988; Lyle, 1988; Lyle et al., 1988; Rea et al., 1991). The spikes in C-org represent approximately a two-fold increase from interglacial values for all the cores, irrespective of the mean interglacial content in each core. In addition to the spikes in C-org, there tends to be a general decrease in C-org values downcore (except in P5), which is the result of organic matter degradation over time. This is best developed on core CD3826 and AII54-25PC because they span almost 0.5 Ma each. This diagenetic decrease in the C-org content is not present in core P5 probably because of the very low values and relative lack of burial of young sediments. The overall pattern of high C-org contents in glacials and reduced values during interglacial periods, is only interrupted by several anomalously low horizons. These correlate with the tephra layers (see chapter 4) and are most obvious in core AII54-25PC (eg. ash "L" at 234 ka). Only ash layer K (328 ka) appears to dilute the C-org record in core CD3826. The relationship between C-org and other biogenic tracers will be discussed further with respect to mass accumulation rates (see chapter 7).

Figure 6.5 Temporal variations in organic carbon (C-org) in CD38 cores and core AII54-25PC. Shaded regions represent glacial stages II, IV, VI, VIII, X and XII.

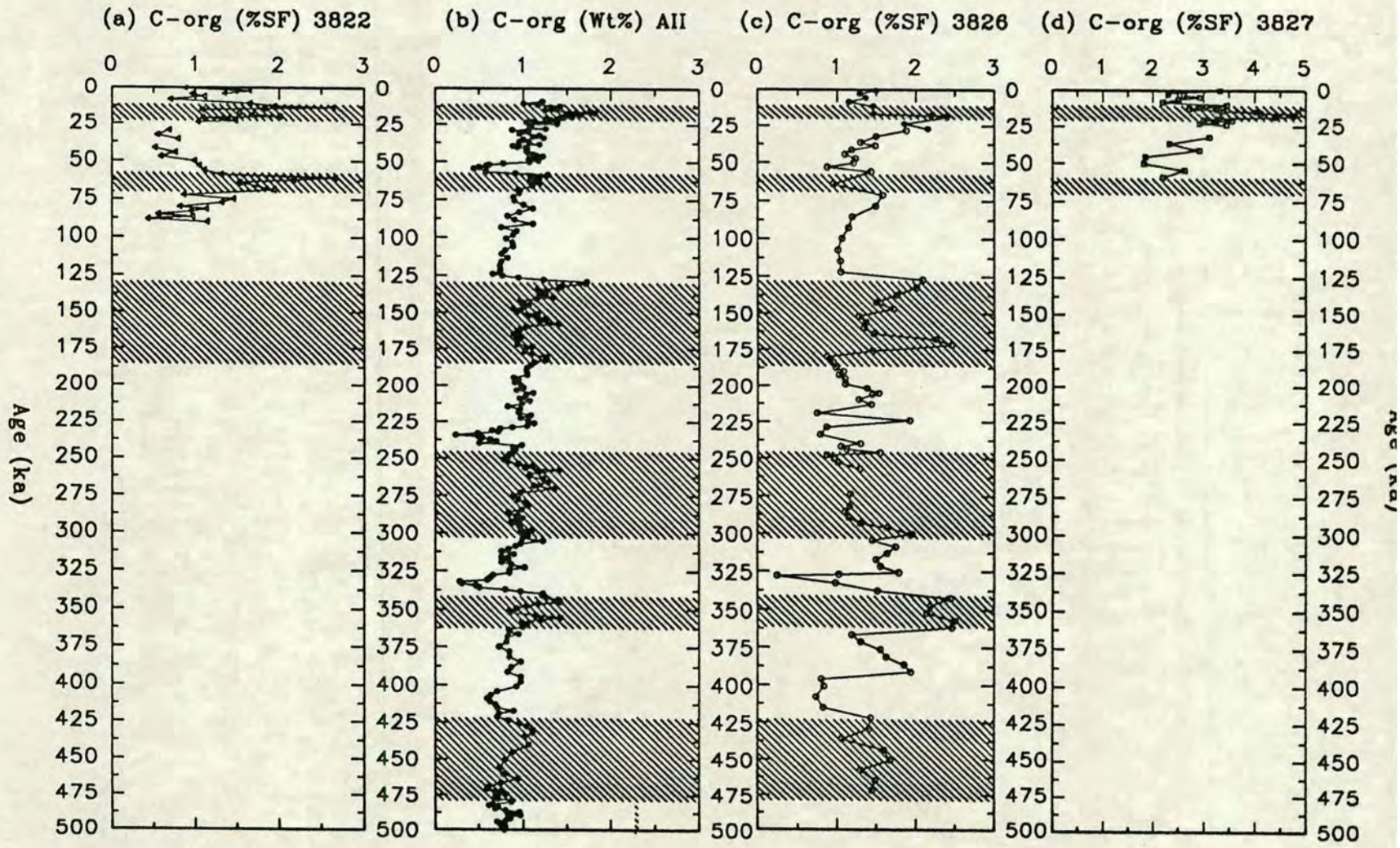

Figure 6.6 Temporal variations in organic carbon (Wt.% salt and carbonate free) in CD38 cores and core AII54-25PC. Shaded regions represent glacial stages II, IV, VI, VIII, X and XII. Note the increased C-org contents during glacial periods in all cores.

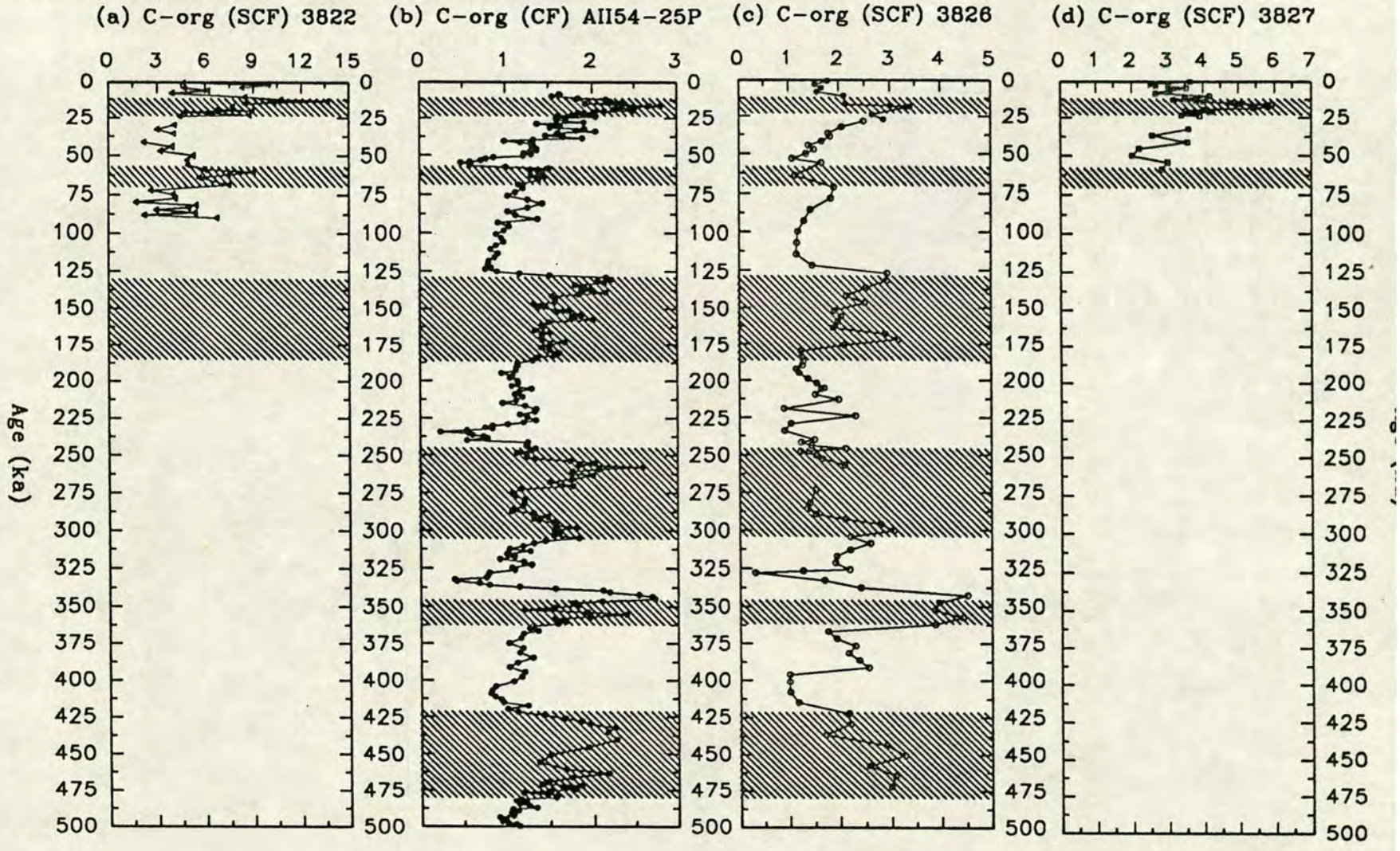

Table 6.3 Comparison of Surficial, Holocene and Last glacial C-org contents in sediments from around the world.

Location of Core	C-org (WT.%)			Reference
	Surface	Holocene	Last Glacial	
SW Africa Continental margin	10	******	*******	1
Peru continental margin	10	******	*******	2
E. Equatorial Atlantic (M12392-1)	******	0.4	2.0-3.0	3
Okhotsk Sea	1.5	******	******	4
Black Sea	2	******	******	5
NW Arabian Sea CD1730	1.5	0.4-1.1	0.4-0.8	6
Panama basin P2 and P6	******	0.4-0.6	1.0-2.5	7
Panama basin AII54-25PC	1.22	1.00-1.22	1.03-1.81	8
Panama basin CD3822	0.88	0.69-1.65	1.07-2.63	9
CD3826	1.49	1.14-1.49	1.45-2.40	9
CD3827	3.32	2.19-3.46	2.72-4.85	9
P5	0.43	0.41-0.72	0.45-0.81	9

References:- 1 = *Calvert and Price (1971)*; 2 = *Reimmers and Suess (1981)*; 3 = *Mueller and Suess (1979)*; 4 = *Listzin (1972)*; 5 = *Degens and Ross (1974)*; 6 = *Khan (1989)*; 7 = *Pedersen (1983)*; 8 = *Pedersen et al., (1991)*; 9 = *This study*.

Core P5 has the lowest C-org values and, partly as a consequence, the signal is very noisy (figure 6.2d). However, there is a definite increase during the Last Glacial Maximum (15 ka), most obvious in the plot of C-org on a carbonate free curve (figure 6.4d). The curve does not, however, collapse at the base of stage II as it does in the other cores (figure 6.5), although this may be caused by the unreliability of the age model at the base of the core P5 (see chapter 4). Although the contents of C-org are

very low (mean = 0.62%), there is still a halving of values from glacial stage II to interglacial stage I.

Core CD3822 displays very well developed spikes of C-org during glacials II and IV, with values increasing by more than a factor of two, from less than 1% during the interglacials to greater than 2.5% in the glacials (figure 6.5a). The shape of the C-org curve, expressed on a carbonate free basis, shows little change from the carbonate included profile except that the spike in stage IV is depressed relative to the stage II peak (cp. figures 6.5a and 6.6a).

Glacial periods in core CD3826 are characterised by an approximate doubling of the C-org contents except in stage IV, VIII and XII (figure 6.5c). Stage VIII is only enriched in C-org relative to stage VII and IX, at around 300 ka. However, stage IX has similar contents as the basal part of stage VIII, except for ash band "k" at 328 ka. Largest increases in C-org occur at 18 ka (stage II), 130 ka (stage VI) and 170 ka (stage VI) and, 350 ka (stage X).

C-org values in core AII54-26PC are slightly lower than in core CD826, but the shape of the curve is remarkably similar (cp. figures 6.5b and 6.5c). As the data for this core was provided by Dr Thomas Pedersen (University of British Colombia), it may be that this difference may be caused by not correcting for the diluting effects of residual sea salt (appendix A.7). Ash layers "D", "L" and "K" in core AII54-26PC seem to exert a greater influence on the C-org record than in core CD3826. The C-org record of this core is described in detail and, in relation to palaeoproductivity and atmospheric CO_2 by Pedersen et al. (1992) and, consequently, will not be discussed here.

Core CD3827 has the highest C-org values of all the cores, ranging from 1.82% to 4.85% (Wt. % salt free). However, the proportionate increase during stage II is approximately the same as in all the other cores. That this core should have higher C-org contents must be due to the combined effects of higher primary productivity and/or greater bulk accumulation rates (see chapter 4), resulting in increased preservation during glacial periods. The higher bulk accumulation rates would preferentially preserve, to a rather limited degree, the organic matter raining down onto the sea floor. It is also conceivable (due to the proximity of the continental landmass, figure 6.0), that a fraction of the total C-org in this core is of terrigenous origin, and diagenetically inert. However, evidence to support the conclusion that the

majority of the C-org in this and the other cores is of marine origin is presented in chapter 8 where C-org is related to halogen contents.

$CaCO_3$ and C-org covary quite strongly (tables 6.4-6.5). That C-org should increase by around two fold and $CaCO_3$ (a potential dilutant) also increase by up to four times during glacials, suggests an intimate relationship between C-org and accumulation rate.

Particle size and sediment texture/mineralogy are known to have an effect on the organic matter content of the sediment (Bordovisky, 1965; Van Andel, 1964; Hunt, 1981). This is thought to be achieved by a preferential winnowing of the organics associated with the fine fraction of the sediment. Elements which indicate sediment texture and mineralogy such as Si_{terrig} and Zr should show an antithetic relationship with organic matter if the grain size of the sediment was a factor. However, only in core P5 is there any obvious anti thetic relationship between the textural indicator Si_{terrig} and C-org (cp. figures 5.2 and 6.5d).

6.4.3 Palaeoproductivity from C-org results

This section attempts to quantify variations in palaeoproductivity by a method incorporating C-org contents as pioneered by Muller and Suess (1979). Most authors agree that C-org contents are critically dependent on the bulk sediment accumulation rate (sedimentation rate × dry bulk density), the overlying productivity of the surface waters and, the oxidation state of the bottom waters. The recognition of these influences led Muller and Suess (1979) to develop an empirical relationship for palaeoproductivity using C-org (%) and the above mentioned factors, which is shown in equation 6.1. Several attempts have been made to refine and expand the equation to incorporate such factors as water depth (eg Samthein et al., 1987). Such requiremnets, which are based on a number of untested factors, do not neccessarily inprove the equation. Palaeoproductivity estimates here are determined using equation 6.1 (after Muller and Suess, 1979); results are presented in appendix C.10.

Equation 6.1

$$R = \frac{C \,.\, fs \,.\, (1-\emptyset)}{0.0030 \,.\, S^{0.30}}$$

R = Palaeoproductivity ($g/m^2/yr$), C = C-org (Wt.% salt free), fs = sediment density (g/cm^2), Ø = sediment porosity (percent water/100), S = sedimentation rate (cm/kyr).

Results and Discussion

Temporal variations in palaeoproductivity (R) are shown in figures 6.7 and 6.8. Values differ considerably, with cores CD3822 and CD3827 displaying similar values ranging from around 20 to almost 130 ($g/m^2/yr$), whereas core P5 varies from only around 10 to approximately 30 ($g/m^2/yr$). Values in core CD3826 vary from around 20 to over 80 ($g/m^2/yr$). Such variations translate into an approximate 2-3 times increase in palaeoproductivity from full interglacial to full glacial period. This is consistent with the magnitudes of increase in the other biogenic tracer fluxes (see chapter 7). However, it is difficult to envisage a scenario whereby the productivity of the eastern equatorial Pacific was 3 times greater than it is at present. This is because present values for productivity in the euphotic zone are generally considered to be close to the maximum possible for any modern marine ecosystem (D. Kroon, pers. comm.). Exceptions to this 2-3 times increase during glacials are in the late Holocene of core P5 which displays increasing palaeoproductivity (figure 6.7a) and, at 225 ka and 380 ka in core CD3826 (figure 6.8), which are all increases during interglacial times. Peaks in productivity tend to occur at the begining or end of a glacial event in core CD3826; at the begining of stage II in core P5 and at the end of the glacials in core CD3822 and CD3827. The values obtained are comparable with those calculated for sediments off the Peru margin (Muller and Suess, 1979), and in the Arabian sea (Khan, 1989).

6.4.4 Conclusions

1. There is a wide range of C-org values both within and between cores.
2. C-org contents approximately double during glacial periods consistent with increased euphotic zone palaeoproductivity and/or preservation due to increased sedimentation rate.
3. There is a possible terrigenous C-org contribution to core CD3827 although the C-org in the core is thought to be dominantly of marine origin (see also chapter 8).
5. The approximate two fold increase in C-org during glacial periods in all the cores broadly matches that for $CaCO_3$ (a potential dilutant), which is further proof in favour of increased productivity during glacial events.
6. Particle size and sediment texture appears to have little effect on the C-org contents in this area.
7. Palaeoproductivity estimates show maxima at the beginning and end of glacial periods in all cores with the exceptions of the late Holocene in core P5 and at 225 ka

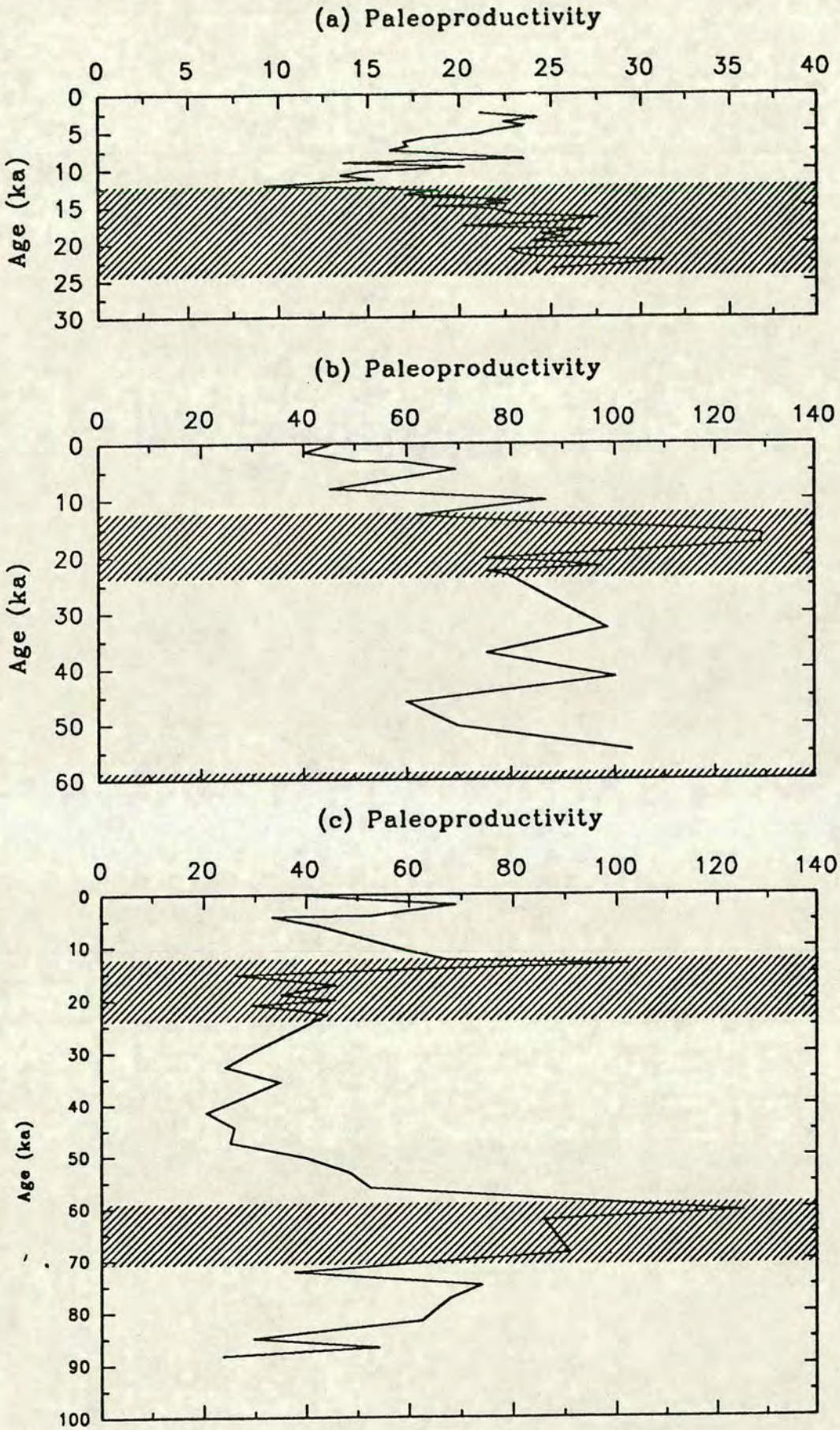

Figure 6.7 Temporal variations in Palaeoproductivity ($g/m^2/yr$) in cores P5 (a), CD3827 (b) and CD3822 (c). Shaded regions represent glacial stages II and IV.

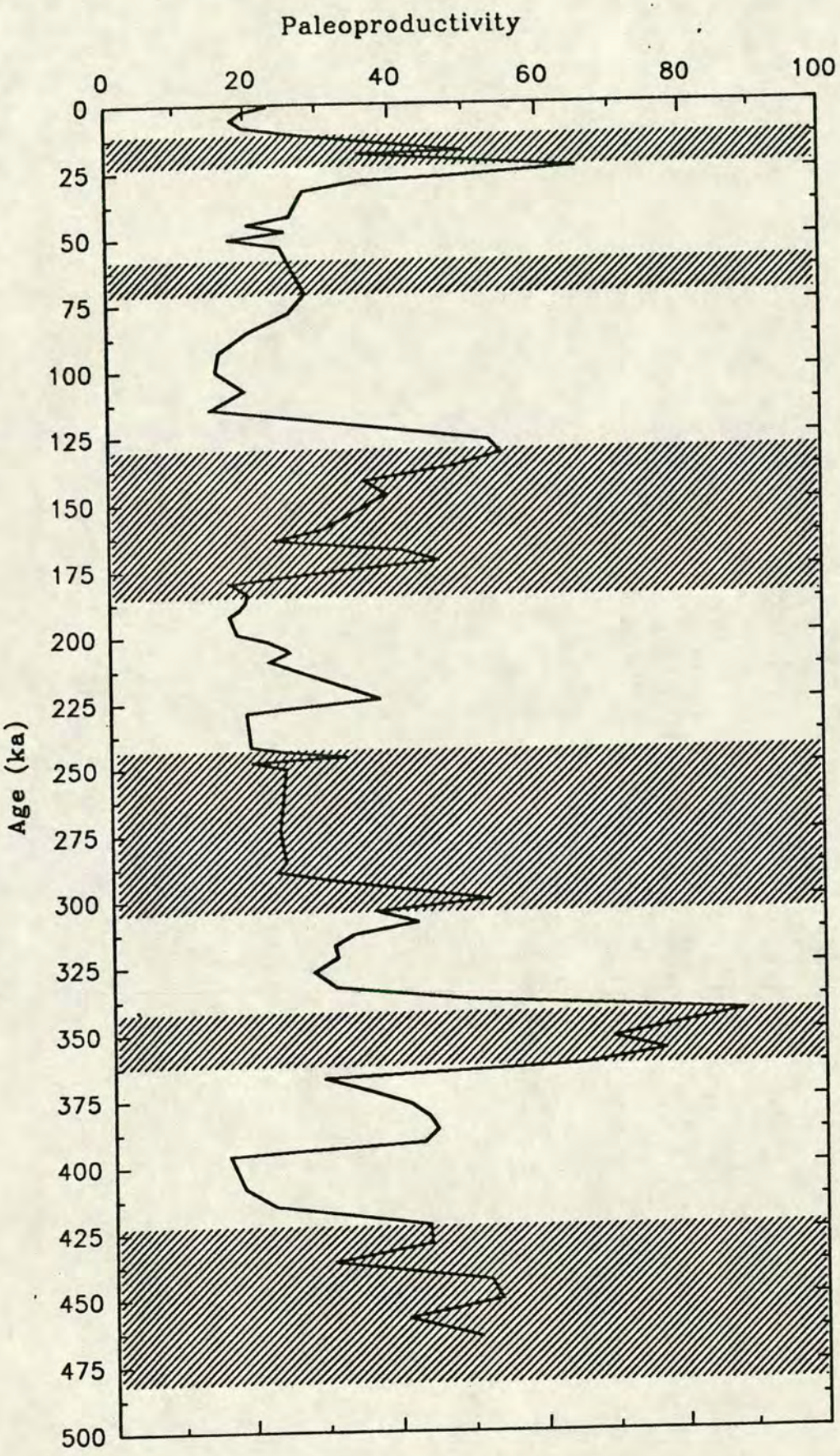

Figure 6.8 Temporal variations in Palaeoproductivity ($g/m^2/yr$) from core CD3826. Shaded regions represent glacial stages II, IV, VI, VIII, X and XII.

and 380 ka in core CD3826. This is consistent with increased biological production during glacials as indicated by other biogenic tracers.

6.5 Biogenic Silica (SiO_2)

6.5.1 Introduction

Amorphous, opaline silica in marine sediments is derived from the skeletal remains of diatoms, radiolaria, silicoflagellates and sponge spicules in approximately that order of abundance. Its content in marine sediments is primarily dependent on 4 factors:

1. Primary productivity in the overlying water column.
2. Faunal/ecological variations.
3. Dissolution in the water and, more importantly, the sediment column.
4. Dilution by non-opaline material and hence the bulk sediment accumulation rate.

Intuitively biogenic silica would appear to be a good indicator of palaeoproductivity, since siliceous plankton are known to be abundant in the surface waters of modern upwelling areas, and sediments underlying these regions have high contents of biogenic silica. Moreover, biogenic silica is less susceptible to differential dissolution in the water column than C-org and, in the deep ocean basins, biogenic $CaCO_3$, despite the oceans never being saturated with respect to SiO_2. According to Wollast (1974) the solubility of amorphous silica at 5°C is 1230 µM/l. The dissolved concentration of silica in the equatorial Pacific is never greater than 200 µM/l (figure 6.9), therefore the siliceous parts of marine organisms will be susceptible to dissolution as soon as they die.

Most opal dissolution occurs in the warm upper parts of the water column (Scharde, 1972) and, as a conseuqence, most of the opal produced in the euphotic zone is recycled (Calvert, 1968; Listzin, 1972; Berger, 1976; Heath, 1976; Van Bennekom and Berger, 1984). Figure 6.10 illustrates the marine geochemical cycle of silica (biogenic, terrigenous and hydrothermal). It shows the recycling of biogenic silica back towards the surface waters from solution of the skeletons of diatoms and radiolarians falling through the water column, especially in its upper parts where temperatures are higher. Murray (1987) estimates that only 8-11% of the biogenic silica exported from the euphotic zone is incorporated in the underlying sediment.

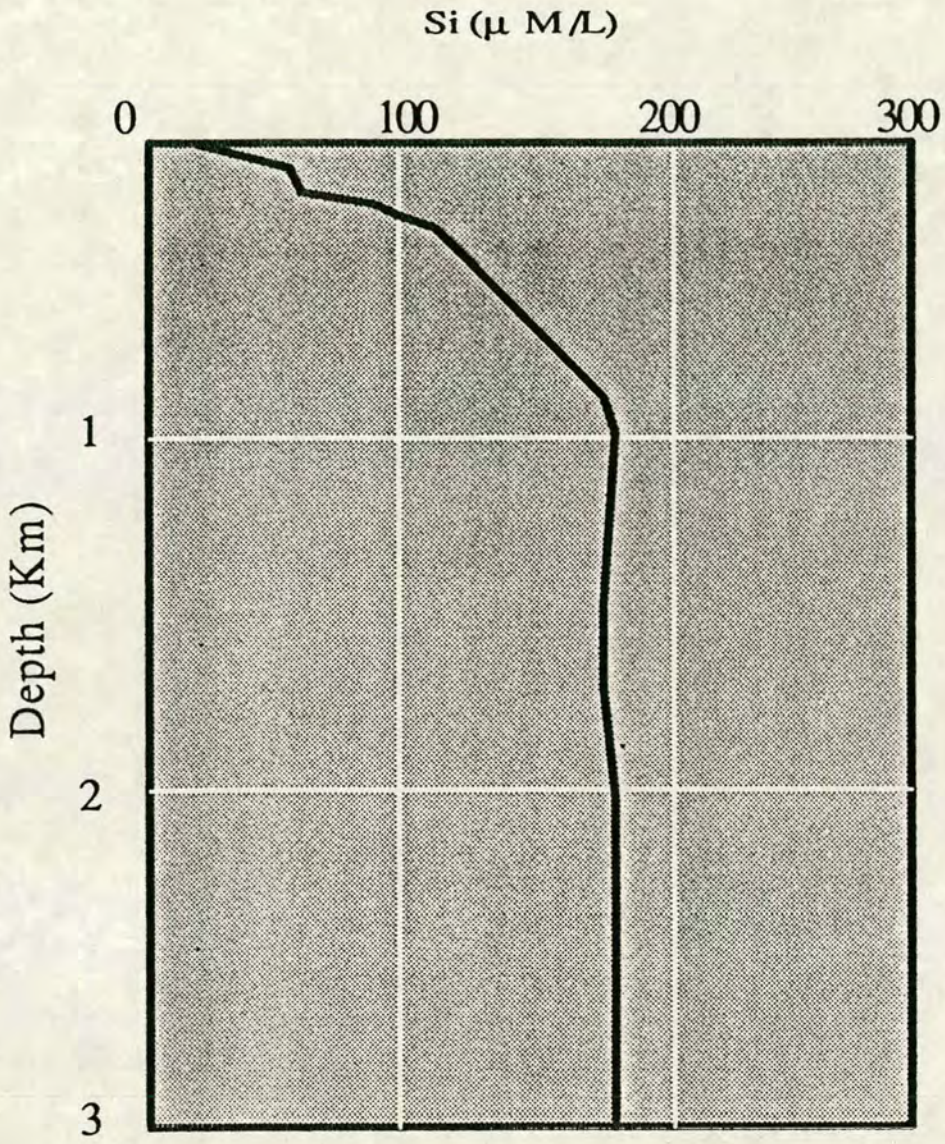

Figure 6.9 Diagrammatic illustration of the dissolved Silica ($Si(OH)_{4(aq)}$) profile in the Pacific ocean.

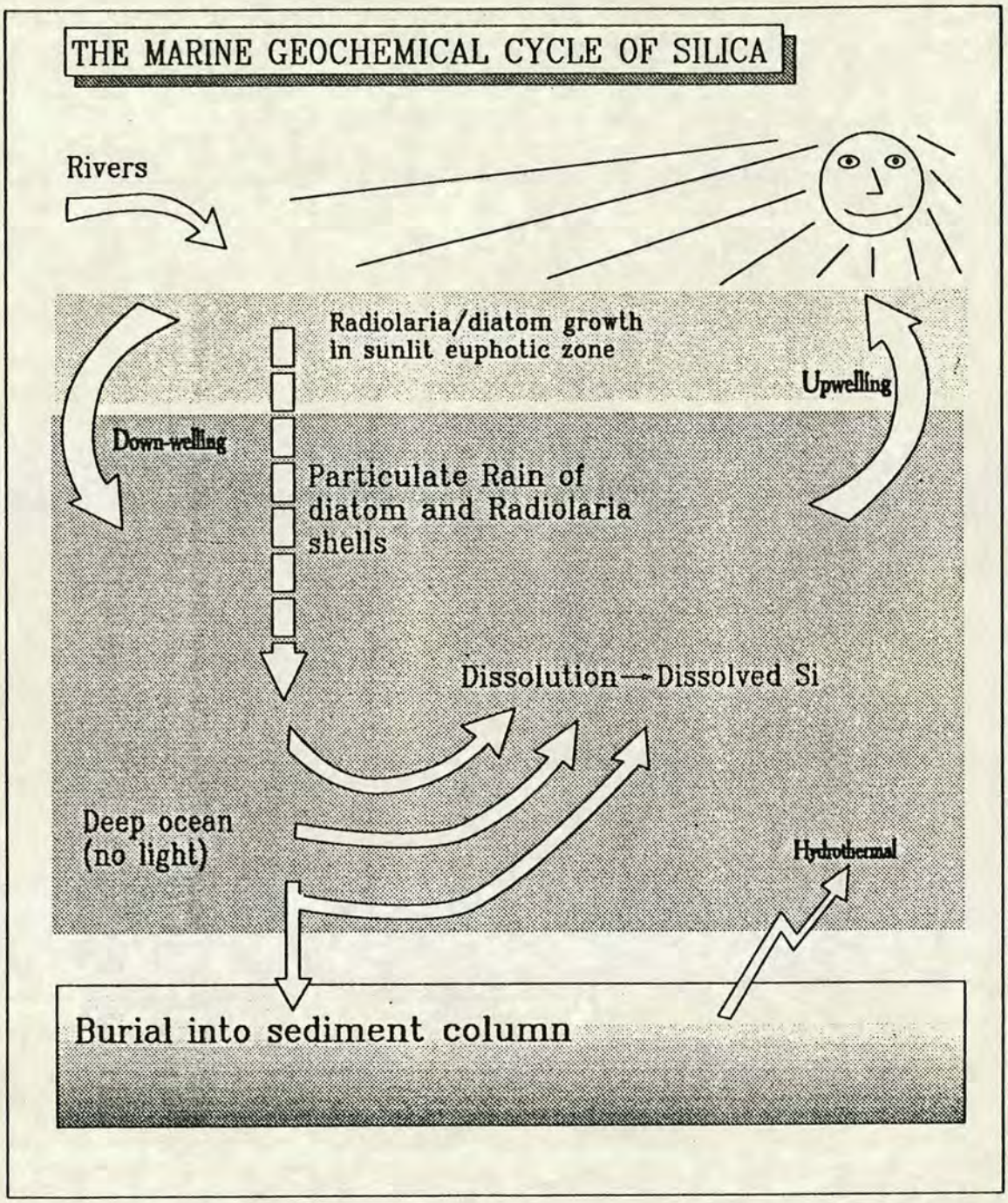

Figure 6.10 Highly idealised model of oceanic circulation and Silica cycles. The top box represents the euphotic zone where primary production occurs; the middle box represents the intermediate and bottom waters of the oceans where no primary producers can survive; the bottom box represents the sediment column where proxies of oceanic processes become encorporated. Note the riverine input; the upwelling and downwelling; the recycling of dissolved silica through dissolution and, the hydrothermal input, all of which help to maintain the balance of silica in the oceans

Nevertheless, opal contents in marine sediments are thought to roughly reflect primary productivity and upwelling (Molina-Cruz and Price, 1977; Broecker and Peng, 1982; Leinen et al., 1986).

Dilution by non-amorphous material reduces the content of SiO_2 but it may also serve to reduce dissolution. As with other biogenic components, the higher the bulk sedimentation rate the greater the preservation and resulting contents of opal will become, given a constant input from productivity. The depositional environment is also crucial to the final content in the sediments. A high energy environment will tend to fragment the fragile siliceous skeletons with the result that a greater surface area will be exposed to the undersaturated waters which, in turn, would cause greater dissolution.

Variations in the abundance and diversity of the siliceous plankton flaura must have a considerable effect on the contents of silica in marine sediments. Some species may be more resistant to solution and fragmentation and, consequently, would tend to produce a much greater content of opal in the sediment. Thus species variation, and their attendant dissolution characteristics may artificially enhance or dampen the productivity signal. Diatoms are likely to dominate the siliceous component of the sediment. The study of species diversity and abundance within and between productivity events is a very complicated subject which involves, for example; ecological, physiological and ontogenetic factors, and is outwith the scope of this study.

Wet chemical analysis of biogenic silica was determined for cores P5, CD3822, CD3826 and CD3827. Analytical methods and tablulated data are presented in appendices A.6 and C.9 respectively.

6.5.2 Results

Biogenic silica is generally inversely correlated to the other main biogenic tracers discussed in this chapter (tables 6.4-6.5). In core P5 strong negative correlations exist between SiO_2 and, $CaCO_3$ and C-org.

Downcore variations in SiO_2 (Wt.% SF) are shown in figures 6.11 and 6.13a. The most identifiable characterstic of biogenic silica in most cores (ie. CD3826, CD3827 and P5) is that they are low in SiO_2 during glacial stage II (12-24 ka). Although core

CD3826 has a strong cyclicity in its signal, it does not alternate on a glacial to interglacial timescale and appears, if anything, to be on a longer periodicity. Core CD3822 shows a very different profile, one that virtually mirrors that of the other cores, and which is high at around 40 ka and during stage II (18 ka).

Salt and carbonate free (SCF) records of biogenic SiO_2, which remove the dilution effects of $CaCO_3$, are shown in figures 6.12 and 6.13c. As a result of core P5 having such high $CaCO_3$ values, the SiO_2 (SCF) profile shows a smaller relative change between stage I and II than the SiO_2 (SF) profile (cp. figures 6.13a and 6.13c). The SiO_2 (SCF) profile is almost constant downcore except for a general increase between 5-13 ka. This may be an artifact of the hydrothermal pulse during this period which is difficult to discriminate analytically from biogenic SiO_2. However, the enrichment in SiO_2 (SCF) begins before the onset of the hydrothermal event as defined by Fe/Al and Si/Al ratios (chapter 5).

Core CD3827 is high in SiO_2 (SCF) during the Holocene and drops to a minimum during upper stage II (16 ka), before increasing during stage III at 26 ka and 40 ka (figure 6.12c).

The SiO_2 (SCF) curve in core CD3826 shows a similar profile to that in core CD3827 during stages I and II (cp. figures 6.12b-6.12c). Below this there is an overall decrease through time (upcore) together with a tendency to be higher in glacial stages, although there are exceptions to this. As in core CD3827, there is an approximate halving of values between the Holocene and the Last Glacial Maximum. Prominent peaks in SiO_2 (SCF) in core CD3826 occur at around 6 ka (I), 137 ka (VI), 190 ka (VII), 290 ka (VIII), 350 ka (X) and 450 ka (XII), most of which are towards the base and tops of glacial stages.

The record of biogenic silica in core CD3822 is unlike any other core in that it is generally considerably higher (see table 6.1), and peaks occur at 13 ka, 18 ka, 40 ka and 80 ka. The highest SiO_2 content (11.74 % salt free) occurs during stage II (18 ka) which is three times of that in the Holocene. Indeed there are several horizons during stage II which represent a doubling of Holocene values. The second spike at around 40 ka in stage III has a similar scale of enrichment (around 2 times).

Figure 6.11 Temporal variations in SiO_2 (Wt.% salt free) in cores CD3822 (a), CD3826 (b) and CD3827 (c). Shaded regions represent glacial stages II, IV, VI, VIII, X and XII.

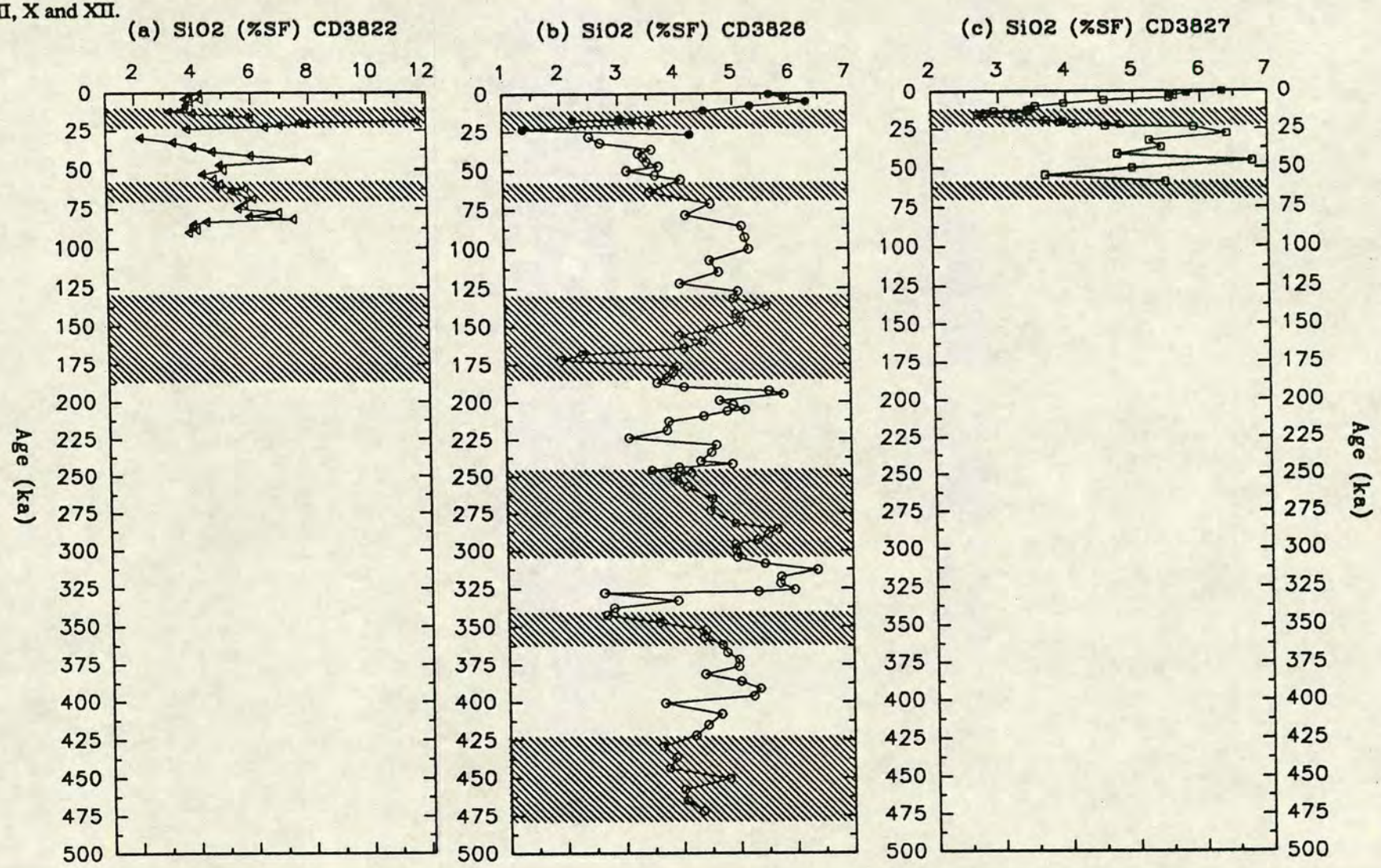

Figure 6.12 Temporal variations in SiO_2 (Wt.% salt and carbonate free) in cores CD3822 (a), CD3826 (b) and CD3827 (c). Shaded regions represent glacial stages II, IV, VI, VIII, X and XII. Note how in cores CD3826 and CD3827 the SiO_2 (SCF) contents decrease during glacials whereas in core CD3822 they increase, at least in stage II.

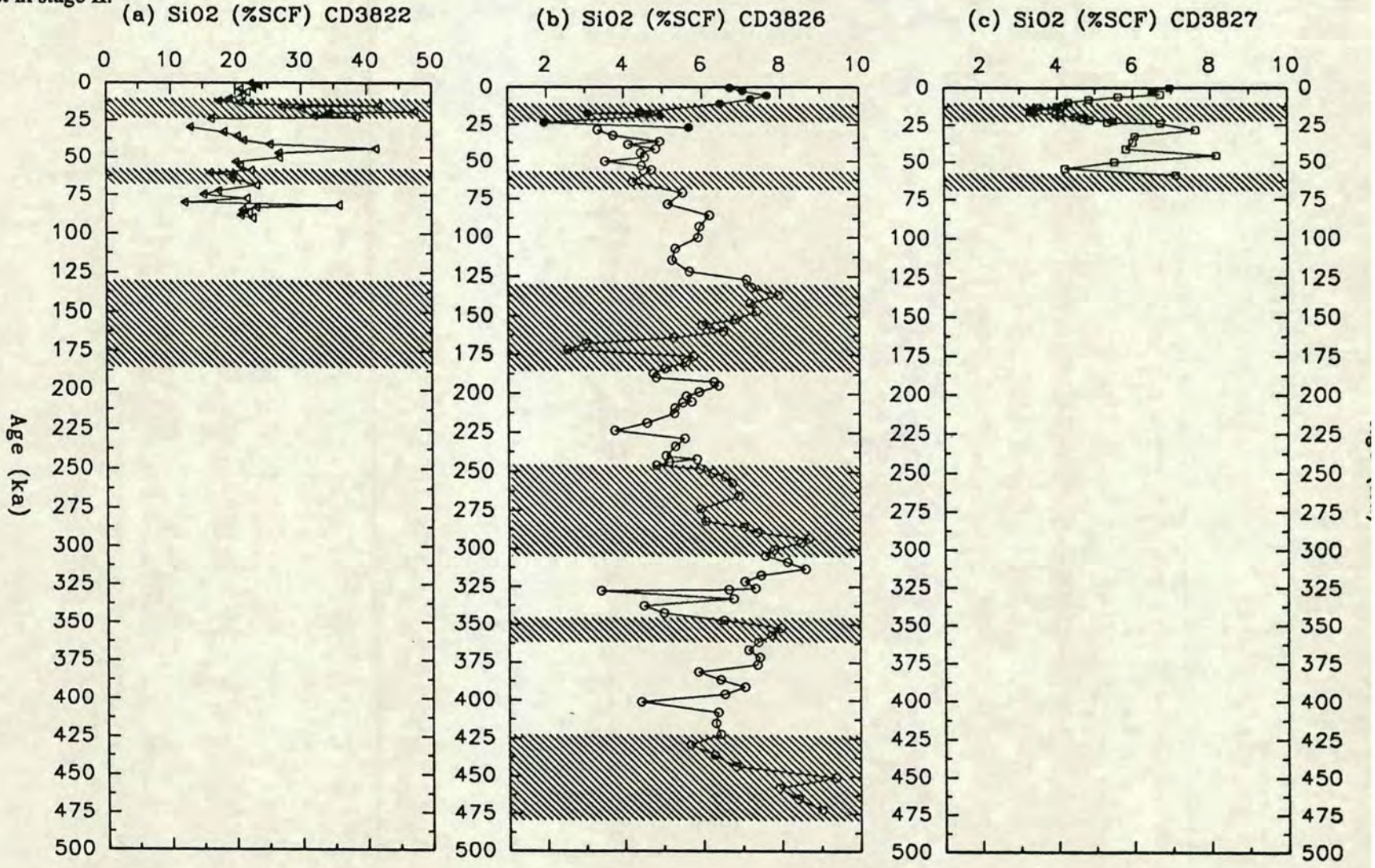

Figure 6.13 Temporal variations in SiO_2, Excess Ba (Ex.Ba), SiO_2 (salt and carbonate free) and Ba/Al × 10^{-2} from core P5. Shaded region represents glacial stage II.

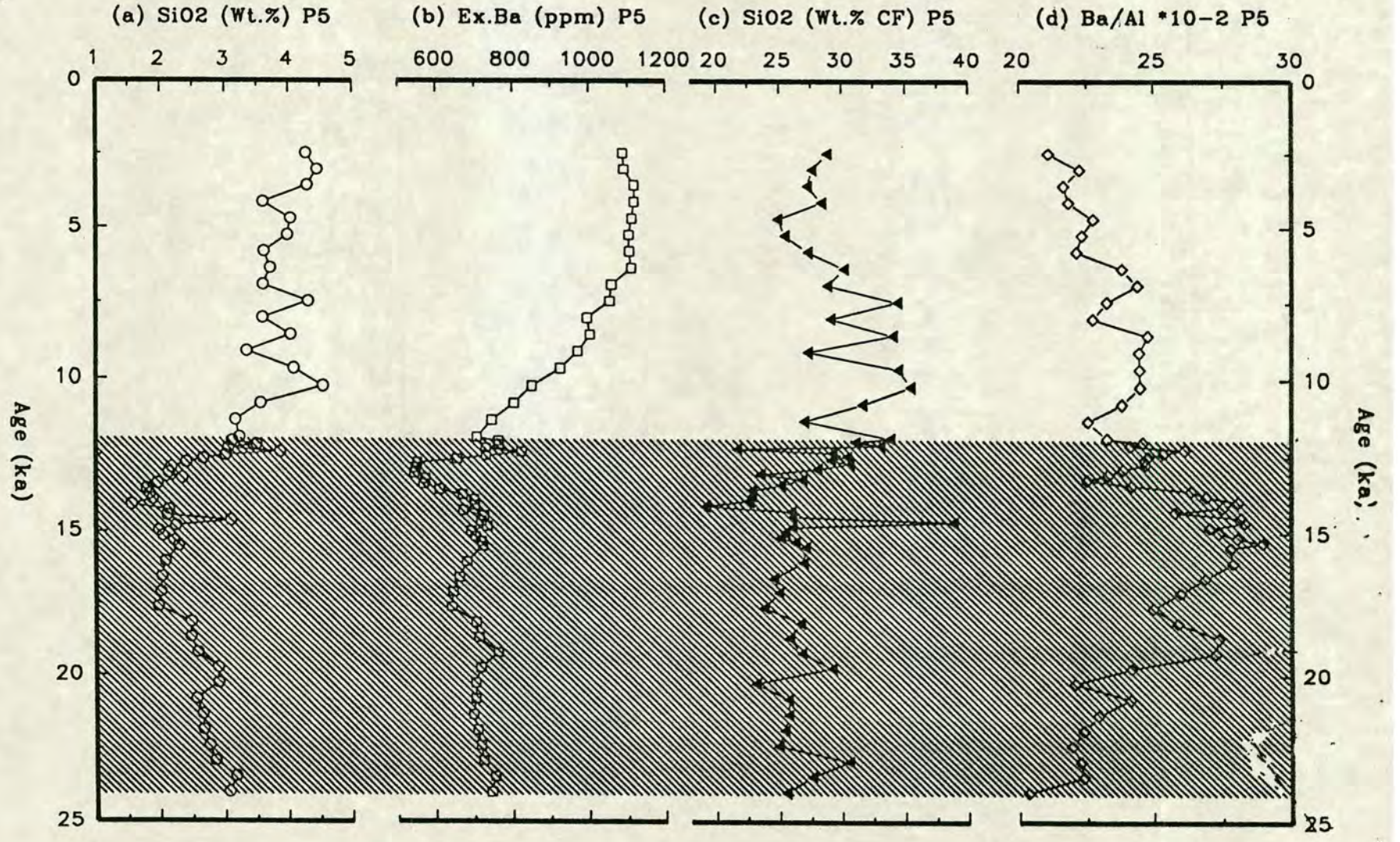

6.5.3 Discussion

Biogenic silica is derived from skeletal remains of siliceous marine plankton, and should therefore provide a reasonably good proxy for palaeoproductivity in the region.

In the carbonate rich cores P5 and CD3822, biogenic SiO_2 represents around 20-30% of the non-carbonate fraction, whereas in cores CD3826 and CD3827 (relatively low in $CaCO_3$) SiO_2 accounts for only about 4-8% of the non-carbonate material. This must be due to the combination of a dilution by terrigenous material and/or greater biogenic SiO_2 production in cores P5 and CD3822, relative to CD3826 and CD3827. A third scenario is possible whereby there is differential solution between carbonate rich and carbonate poor cores.

The suggestion of varying biogenic SiO_2 production is consistent with that of surface sediment biogenic silica variations shown by Moore et al. (1973; figure 8, p467). SiO_2 (salt and carbonate free, SCF) in core CD3827, which has a greater terrigenous input flux than CD3826 (see chapter 5), shows higher SiO_2 (SCF) than in core CD3826. This trend implies that siliceous primary productivity is substantially higher in the region of core CD3827, perhaps as a result of high productivity associated with the Costa Rica Dome upwelling cell. The relatively high values of SiO_2 in core CD3822 (up to almost 50% non-carbonate material) is probably the result of the increased productivity associated with the equatorial divergence system, and the upwelling of cool, nutrient-rich Cromwell Current waters which sweeps round the north (and south) of the Galapagos archipelago causing high biological production.

The position of SiO_2 maxima and minima in core CD3822 clearly demonstrates that it does not follow glacial-interglacial climate trends and, as such, implies that biogenic SiO_2 is dominantly dependent on some other factor(s). This could be availability of a required nutrient or some faunal/ecological factor, which is corroborated by the difference in the SiO_2 records in core CD3822 compared to the other cores.

The records of SiO_2 and C-org, over the last 24 kyrs move in opposition in cores P5, CD3826 and CD3827 and, in parallel in core CD3822. C-org is a reflection of the total organic-C reaching the sediment, which is principally derived from $CaCO_3$ and

SiO_2 secreting plankton. Perhaps a high proportion of the plankton in the area of core CD3822, during glacial stage II at least, was silica bearing compared with other periods in this core, and also higher than in sediments of other sites being investigated in this thesis. In contrast, perhaps in the region of cores CD3826 and CD3827, the dominance of C-org input from $CaCO_3$ based organisms was greater than in core CD3822. Moreover, spatial and temporal variations in the dissolution of $CaCO_3$ do not translate into the sediment record in a way which results in parallel C-org and $CaCO_3$ profiles. Thus it would seem that the input of C-org from siliceous plankton was far greater in core CD3822 than in cores P5, CD3826 and CD3827, at least during the Last Glacial Maximum. In the latter cores, C-org from the other organisms may be the major control on its distribution. Alternating chemical composition of plankton communities (siliceous-$CaCO_3$) has been observed by Dymond and Lyle (1985) and Lyle et al., (1988) in the eastern equatorial Pacific, although no detailed micropalaeontological study has been undertaken.

Generally the distribution of opal on the sea floor is similar to the pattern of productivity in the overlying water, although locally there is a decoupling of this relationship, as is the case in the Panama basin (cp. figures 2.7, 6.12 and 6.13a). The curve in core P5 is difficult to interpret because carbonate values are so high which results in a noisy SiO_2 (SCF) curve (figure 6.13c). SiO_2 (SCF) does not follow $CaCO_3$ or C-org records which is probably a reflection of the overiding dominance of $CaCO_3$ plankton in the region throughout the last 24 ka. Such plankton communities may be composed of varying proportions of coccoliths and foraminifera.

<u>$SiO_2/CaCO_3$ Relationships</u>

Only in core P5 are these two components statistically correlated (C = -0.880). Core CD3822 displays quite strong negative correlation, whereas core CD3827 exhibits a small positive correlation. The ratio of $SiO_2/CaCO_3$ tends to be higher in the interglacial periods in cores P5, CD3826 and CD3827, whereas in core CD3822 increases occur in stage II, and at around 44 ka and 80 ka (figures 6.16 and 6.17). Core CD3826 has one clear exception to this pattern, namely a high at 280 ka which does, however, coincide with the drop in $CaCO_3$ in stage VIII. Values range from around 0.02 in stage II of core P5 to 3.4 at the surface of core CD3827. The results imply the relative dominance of $CaCO_3$ precipitating communities during the glacials in all cores, except CD3822, which is consistent with the above arguments relating to spatial and temporal variations in SiO_2.

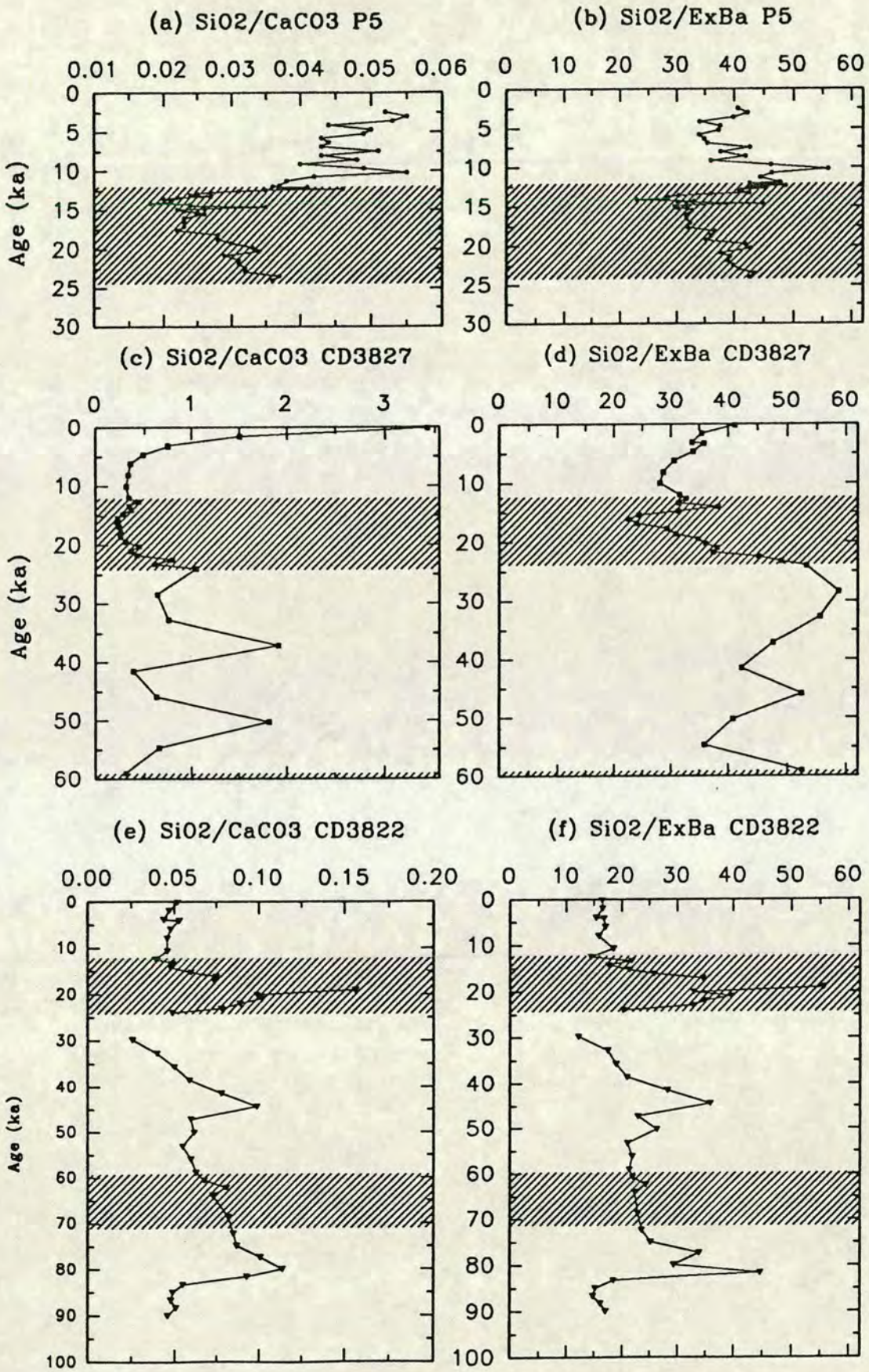

Figure 6.14 Temporal variations in the ratio of $SiO_2/CaCO_3$ (a, c, e) and, SiO_2/Excess Ba $\times 10^{-4}$ (b, d, f) from cores P5 (a, b), CD3827 (c, d) and CD3822 (e, f). Shaded regions represent glacial stages II and IV. Note the wide range in values of the $SiO_2/CaCO_3$ ratio between cores and the similarity of values in the SiO_2/Ex.Ba ratio between cores.

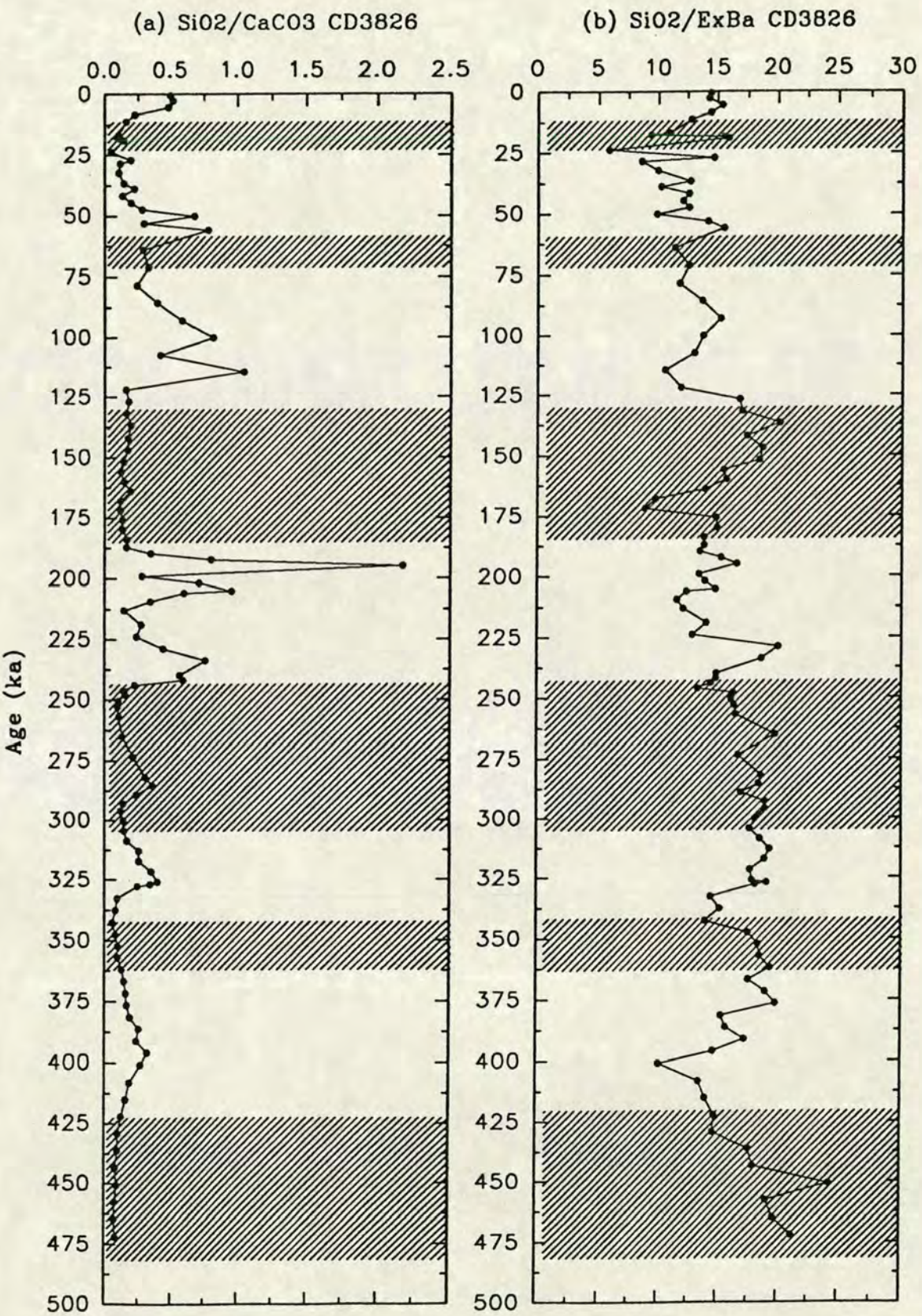

Figure 6.15 Temporal variations in $SiO_2/CaCO_3$ (a) and, SiO_2/Ex.Ba $\times 10^{-4}$ (b) from core CD3826. Shaded regions represent glacial stages II, IV, VI, VIII, X and XII. Note how the glacial-interglacial fluctuations in $CaCO_3$ tend to dominate the $SiO_2/CaCO_3$ signal.

6.5.4 Conclusions

1. All the cores except P5 display an approximate two fold variation in SiO_2 (SCF) from full glacial to full interglacial periods. Although the degree of variation is comparable with C-org and $CaCO_3$, the timing of the variations (maxima and minima) is out of phase.
2. The profiles of biogenic silica (SCF) show distinct cyclicity and are decoupled from the classical glacial-interglacial alternation seen in other palaeoclimatic tracers (eg C-org and $CaCO_3$).
3. The SiO_2 (SCF) contents from core CD3822 increase during the last glacial, whereas SiO_2 (SCF) values in cores CD3826 and CD3827 are depleted during stage II. This is interpreted as resulting from spatial and temporal variations in the species and abundance of siliceous plankton communities.
4. Mean biogenic SiO_2 contents in cores CD3822 and P5 are 24.05% and 28.71% respectively, of the non-carbonate fraction, whereas in cores CD3826 and CD3827 the biogenic SiO_2 contributes only 6.09% and 5.26% respectively to the non-carbonate fraction of the sediment.
5. $CaCO_3$ organisms seem to swamp the siliceous organisms during glacial periods in cores P5, CD3826 and CD3827, whereas in core CD3822 siliceous communities appear to be relatively more dominant than in the other cores, at least in glacial stage II.

In summary, although SiO_2 is potentially a good indicator of palaeoproductivity, it appears that factors which affect the composition of the plankton community with respect to the relative dominance of $CaCO_3$ and SiO_2, tend not to be in phase with normal changes in climatic influences from glacial to interglacial periods. These factors are probably local oceanographic conditions such as nutrient or trace metal availability, which may favour one type of plankton relative to the other. Alternatively, the pulses in productivity as defined by the SiO_2 signal might be a different phase in the evolution of a productivity event. That is to say, perhaps SiO_2 based plankton communities thrive in the early stages of a productivity event when the first cool, nutrient rich waters reach the surface. Subsequently, $CaCO_3$ based plankton may begin to capitalise on the favourable conditions and become even more dominant over siliceous fauna. However such productivity events tend to evolve on a timescale orders of magnitude faster (ie seasonally), than is apparent here. This would tend to favour the importance of water chemistry on floral/faunal variations in species diversity and abundance, as the dominant influence on such biogenic tracers.

6.6 Barium

6.6.1 Introduction

The marine geochemistry of barium has been extensively studied both in the water column (Chan et al., 1976; Boyle and Keigwin, 1982, 1985, 1987; Dehairs et al., 1980; Lea and Boyle, 1990a, 1990b) because of its surrogate role with ^{226}Ra, a radiotracer of ocean circulation (Bishop, 1988), its uptake in corals (Lea and Boyle, 1989) and precipitation in sediments. Ba mainly occurs as barite ($BaSO_4$), which was first recognised in ocean sediments by Murray and Renard (1898). Particulate barite in the oceans seems to be related to the marine biogeochemical cycle. Hypotheses for the production of barite in the water column from the dissolved phase fall into three categories:-

1. Formation of barite in microenvironments (eg. siliceous plankton tests, faecal pellets, marine snow) enriched in sulphate derived from the decay of organic matter (Bishop, 1988).

2. Incorporation of barium into the skeletal remains of siliceous plankton because of the similarities between the dissolved Si and Ba profiles in the oceans (Chan et al., 1976). As an example of this, there is an enrichment of Ba in Black Sea plankton which is dominated by the diatom *Rhizosolenia* (Brongersma-Sanders, 1966). Brongersma-Sanders (1966) suggests that some diatoms (especially Rhizosolenids) tend to concentrate Ba from sea water which ultimately translates Ba to the sediments.

3. Active precipitation of barite by other planktonic organisms. This third possibility is because of the correlation of suspended barite concentration and primary productivity (Church, 1970, 1979; Bostrom et al., 1973; Schmitz, 1987). It is known that planktonic protozoa related to the benthic protozoan *Xenophyophora* precipite at barite (Bishop, 1988).

Barite as dispersed microcrystals in sediments especially those underlying the equatorial divergence upwelling belt in the eastern Pacific, and occasionally the Atlantic, has been observed by Goldberg and Arrhenius (1958). High contents of Barite in the sediments of the equatorial belt decreases westwards but values of biogenic SiO_2 remain unchanged (Bostrom et al., 1973). Church (1970, 1979)

reported a correlation between Ba, $CaCO_3$ and C-org in East Pacific Rise surface sediments. However, the detailed trends of these associations are ambiguous. Increases in the barite content of the sediment from the Arabian Sea are thought to have provided proxy records of marine biogenic productivity (Nair et al., 1989).

6.6.2 Results and Discussion

Results of Ba analysis are expressed in two ways:

1. Ba/Al:- using Al as a terrigenous normalising element.
2. Excess Ba:- Ba in excess of that normally held in marine aluminosilicates.

Both these methods are used to illustrate changes in the biogenic component of Ba. Calculation of the first is obvious, and the formula used to determine the second expression is given in equation 6.2.

The means and ranges of values of Ex.Ba contents and Ba/Al ratios are shown in table 6.1. Values of Ex.Ba range from 541 ppm in core P5 to 4038 ppm in core CD3826. Mean values show > 3 fold variation between cores. Core P5 has the lowest mean Ex.Ba at 805 ppm, and CD3826 the highest at 2638 ppm Ex.Ba. All cores, with reliable chronostratigraphies, show a Holocene enrichment of Ex.Ba, and other interglacial periods also tend to be enriched in Ex.Ba. These trends may be due to carbonate dilution because $CaCO_3$ contents are generally lower during interglacial periods. However, using Al which is diluted by $CaCO_3$ to the same degree as Ba, removes the diluting influence of carbonate.

Equation 6.2 $\mathbf{Excess\ Ba\ (Ex.Ba) = Ba_{total} - (Al_{total} \times Ba/Al_{AS})}$

where:

Ba_{total} and Al_{total} are the total elemental concentrations measured by XRF.

$Ba/Al_{AS} = 0.02738$ which is the mean Ba/Al in deep sea shale from Turekian and Wedopohl (1961).

Ex.Ba reaches a maximum of 1207 ppm at the surface of core P5 and drops gradually to a minimum of 541 ppm at 12 ka, before increasing to around 700 ppm for the remaining part of the core (figure 6.13b). Ba/Al values are low at the surface and at the base of stage II, and reach a maximum during stage II at 15 ka.

The excess Ba and Ba/Al profiles in core CD3814 (figures 6.16a and 6.17a respectively) roughly mirror each other and, as with other elements, show a marked change downcore. A Holocene depletion in Ex.Ba is followed by approximately

Figure 6.16 Temporal variations in Excess Ba (Ex.Ba) in CD38 cores and core AII54-25PC. Shaded regions represent glacial stages II, IV, VI, VIII, X and XII.

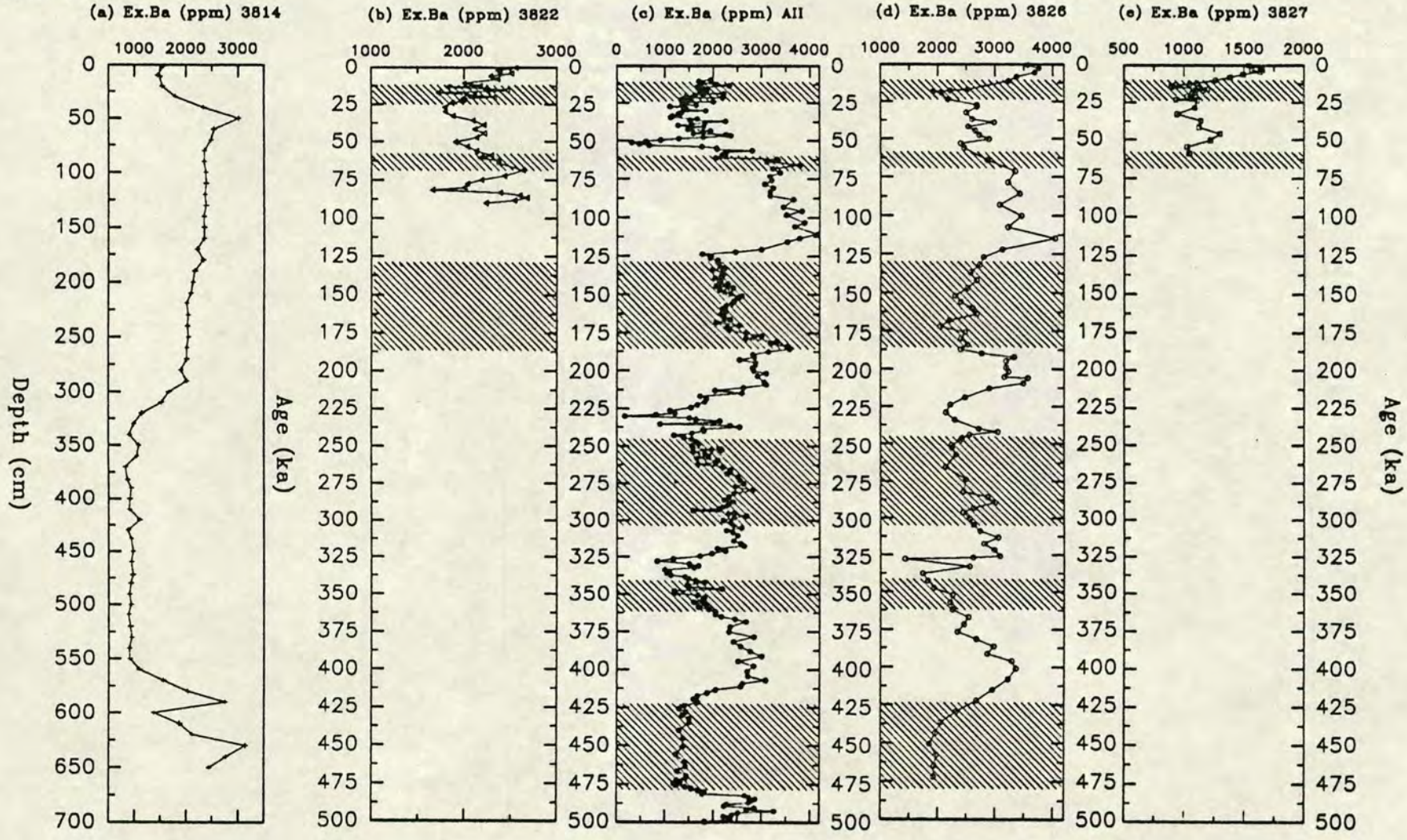

Figure 6.17 Temporal variations in Ba/Al × 10^{-2} in CD38 cores and core AII54-25PC. Shaded regions represent glacial stages II, IV, VI, VIII, X and XII.

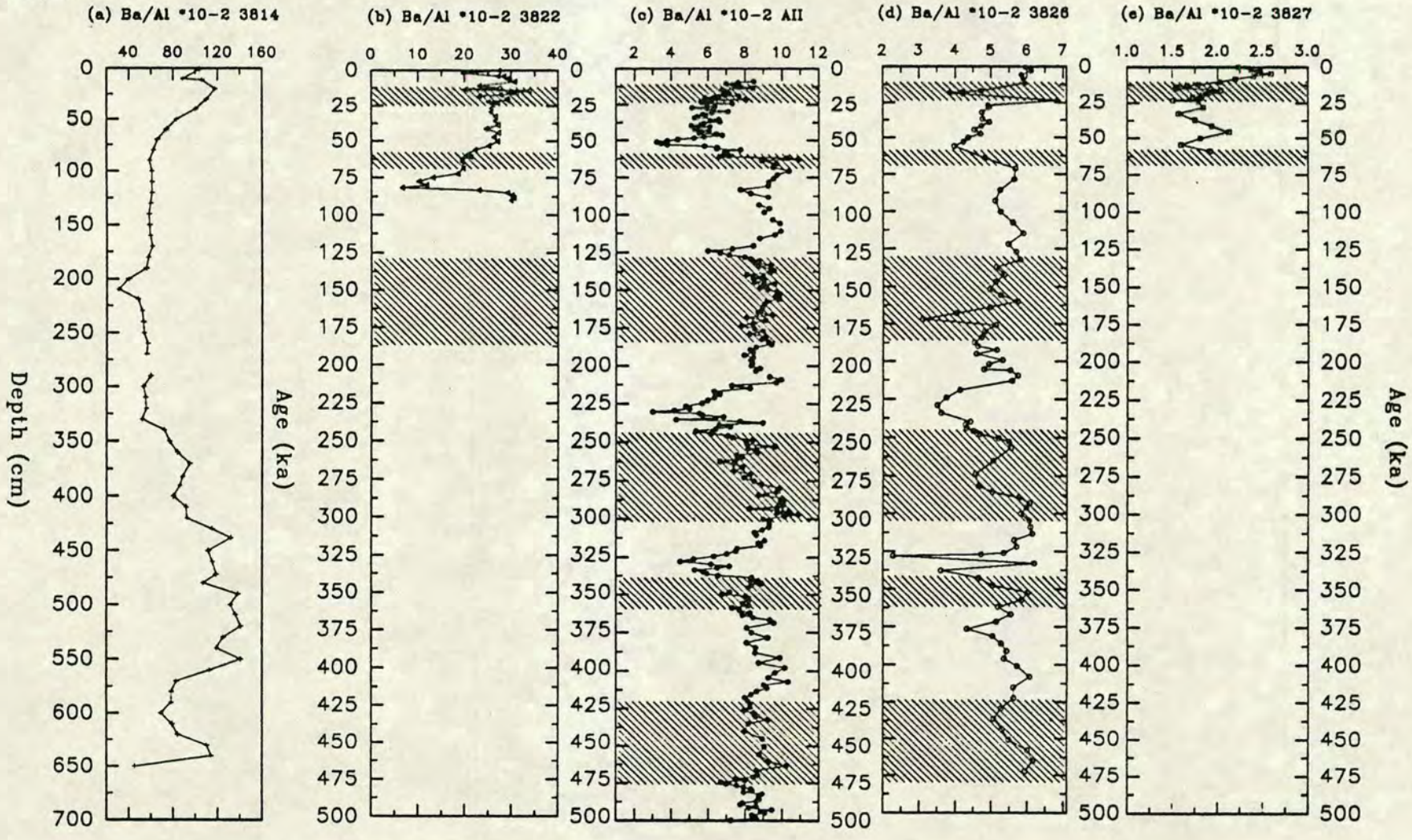

2.5m of relatively constant values at around 2000 ppm, below which Ex.Ba drops to <1000 ppm between 3.5 and 5.5 m depth. At the base of the core there is a further enrichment of values to around 2500 ppm. Such variations are almost certainly due to the change, with time, of the hydrothermal and terrigenous input to this core (chapter 5).

Temporal variations in Ex.Ba from core CD3822 are shown in figure 6.16b. The Holocene enrichment is preceeded by several peaks at around 15 ka, 40 ka, 70 ka and 85 ka. Those at 15 ka and 70 ka coincide with glacial periods, whereas those at 40 ka and 85 ka and in the Holocene occur during interglacial episodes. Comparing this to the Ba/Al ratio profile (figure 6.17b), which is independent of carbonate dilution, increases in the Ba/Al ratio occur during stage II and upper stage V. Clearly neither Ex.Ba or Ba/Al follow conventional glacial-interglacial cyclicity. The $\delta^{18}O$ profile broadly parallels the Ex.Ba curve with increases at 18 ka, 40 ka, and 70 ka (cp. figures 4.6 and 6.16b) which is contrary to what one would expect if the Ex.Ba content was governed solely by carbonate dilution.

The Ex.Ba and Ba/Al plots of core CD3826 are very similar to those of core AII54-25PC (cp. figures 6.16c-d and 6.17c-d). In core CD3826, Ex.Ba values are generally higher during interglacial periods with strong enrichments occuring at 3 ka (stage I), 115 ka (stage V), 206 ka (stage VII), 240 ka (stage VII), 290 ka (stage VIII), 325 ka (stage IX) and, 400 ka (stage XI). The Ex.Ba profile closely mirrors the $\delta^{18}O$ curve (cp. figures 4.6 and 6.16d). The peaks broadly correlate with $CaCO_3$ depleted horizons and are thus the result, at least in part, of carbonate dilution. The profile of Ba/Al is quite different. No systematic cyclicity occurs from glacial to interglacial periods although interglacials (that are not interfered with by tephra layers), have a tendancy to be slightly more enriched in Ba relative to Al (figure 6.17). The $MnCO_3$ horizon at 24 ka (see chapter 9) has an anomalously sharp increase in Ba/Al. The Holocene is a time of increasing Ba/Al values in core CD3826. The lack of variation in Ba/Al ratios over, for example, the stage V/VI boundary in core AII54-25PC and CD3826 is contrary to previous work (eg. Shimmield and Mowbray, 1991; Kroon et al., in press).

In contrast, the Ex.Ba and Ba/Al ratio curves in core CD3827 are very similar which is evidence for the relative interdependence from carbonate dilution and, the dominance of aluminosilicate material in the sediment (figures 6.16e and 6.17e). Enrichments occur in the Holocene and, to lesser extent, during stage III (peaking at

45 ka). Despite stage II containing some of the lowest values in the whole core, a slight increase occurs at the end of the stage before a sharp drop immediately prior to the strong Holocene enrichment. The Ex.Ba profile very broadly mirrors the $\delta^{18}O$ curve as in core CD3826 (cp. figures 4.6 and 6.16e).

6.6.3 Correlation of Ba, biogenic SiO_2 and C-org

Bishop (1988) found a correlation between barite, opal and C-org in oceanic particulate matter from the N.W. Atlantic ocean, and Schmitz (1987) also reports a correlation between SiO_2 and Ba.

From tables 6.4b-d and 6.5, it is clear that there is a positive correlation between Ba and biogenic SiO_2 in cores P5 and CD3826 (0.828 and 0.477 respectively), although only in core P5 is this statistically significant. In cores CD3822 and CD3827 however, the two phases are negatively correlated (-0.168 and -0.034 respectively). However, despite the statistical lack of correlation the shape of the Ex.Ba and biogenic SiO_2 (SCF) curves are similar in cores CD3822, CD3826 and CD3827, although the positions and magnitudes of the peaks are different. Neither Ex.Ba nor Ba/Al curves in core P5 show any similarity with the biogenic SiO_2 (SCF) curve although the SiO_2 (SF) profile tends to parallel the Ex.Ba curve, but broadly mirrors the Ba/Al ratio curve (figure 6.13). In the other carbonate rich core CD3822, the profiles of Ba/Al and biogenic silca (SCF) do not correlate. Only in core CD3827 does a significant positive correlation between C-org and biogenic SiO_2 occur.

<u>SiO_2/Ex.Ba Relationships</u>

If SiO_2 and Ba are associated, as a result of precipitation of barite in the microenvironments of siliceous tests, then their original input ratio should be relatively constant irrespective of geographical/oceanographic setting. The mean values of the SiO_2/Ex.Ba ratio in cores P5, CD3822 and CD3827 are quite similar (figure 6.14 b, d & f) but in core CD3826 the ratios ($\approx 15 \times 10^{-4}$) are approximately half of those in the other cores (figure 6.15b). This could have resulted from a preferential dissolution of SiO_2 in core CD3826 relative to that in the other cores, and/or a relative enrichment in barite in core CD3826. CD3826, which is the only core situated in the main part of the Panama basin (figure 6.0), was recovered from 3075 m water depth. Furthermore, it has the slowest overall accumulation rate. The decreased accumulation rate would tend to preferentially dissolve the biogenic SiO_2 (especially in the surface sediments) relative to the other cores. It would seem likely,

however, that barite may be more resistant to dissolution than SiO_2, and may therefore be less affected by these factors and thus remain relatively enriched in Ex.Ba compared with the other cores.

Assuming this to be true, the more subtle variations in the ratio of the two components should be a sensitive indicator of dissolution changes. Thus, for example, during glacial stage II in core CD3822, accumulation rates increased, dissolution of SiO_2 decreased and, therefore, the SiO_2/Ex.Ba ratio increased. However, if this is the case, the decrease in SiO_2/Ex.Ba curve in core P5 indicates increased dissolution of SiO_2 during the glacial period, a time when $CaCO_3$ is highest due to greater accumulation rate and preservation.

Figure 6.17b shows that there is a gradual decrease in the SiO_2/Ex.Ba ratio over time in core CD3826 which is possibly due to the preferential solution of SiO_2 into the pore waters over time. The pore waters will eventually become saturated with respect to silica, and solution of SiO_2 will cease leaving any remaining silica intact within the sediment. The point at which this is reached is essentially a function of sedimentation rate. It is possible that Ba (as $BaSO_4$) input may be influenced more from C-org and/or S flux to the sediment surface than simply by SiO_2 flux, because barite requires these former two components to form, in whatever environment. However, Ex.Ba and C-org in core P5, whose sediments have suffered minimal dissolution, move antagonistically, whereas Ex.Ba and biogenic SiO_2 vary in parallel. This tends to refute the theory that C-org and S are of primary importance for barite formation, although they do have to be present.

6.6.4 Conclusions

1. Ex.Ba values are high during interglacial periods in core P5, CD3826, CD3827 and AII54-25PC, but tends to increase during glacials in core CD3822.

2. Ba/Al profiles tend to be similar to the Ex.Ba curves except in cores P5 and CD3822 which both show increases in Ba/Al during stage II. However, discrepancies do exist especially with respect to the Holocene enrichment and over the stage V/VI boundary.

3. Ba is broadly associated with biogenic SiO_2 and C-org, although not in core P5, and there are some complications perhaps associated with phase lags between maxima and minima.

4. The Ex.Ba profile mirrors the $\delta^{18}O$ profile in core CD3826 and, to a lesser extent, in core CD3827, but roughly parallels the $\delta^{18}O$ curve in core CD3822.

5. The results confirm that core CD3822 and, to a lesser extent, core P5 must have been subject to quite different oceanographic influences (productivity regime) to cores CD3826, CD3827 and AII54-25PC.

6. From the reduced SiO_2/Ex.Ba ratios in core CD3826, dissolution of SiO_2 appears to have been greater in core CD3826 which has the slowest overall bulk accumulation rate.

6.7 Phosphorus

6.7.1 Introduction

As a result of the importance of phosphorus as a nutrient, considerable effort has been made to quantify its source and sink budgets in the marine environment (Froelich et al., 1982; Ruttenburg, 1990). Phosphorus in marine sediments occurs in four main phases: organic matter, inorganic skeletal debris, detrital apatite and disordered ferriphosphate (Pedersen, 1979). P is an important constituent of organic matter and is potentially an indicator of the palaeoproductivity in the overlying water column. P forms molecules of great physiological importance to organisms, and its release during burial diagenesis by microbial breakdown may be crucial in the formation of diagenetic mineral phases such as apatite (Burnett, 1977; Froelich et al., 1982). Also, P is concentrated in the inorganic skeletal debris of marine organisms (Arrhenius, 1963; Lowenstam, 1974; Suess, 1981), whilst biogenic $CaCO_3$ may contain 300 ± 80ppm of P (El Wakeel and Riley, Froelich et al., 1982). Inorganic phases such as ferriphosphate coatings on grains (Berner, 1973) and detrital apatite also contribute to the total P sink in sediments.

Attempts have been made to partition P into its various phases (Pedersen ,1979; Shimmield, 1984; Murray, 1987) employing a variety of methods and equations. The

two methods used, in this study, to partition P into its different phases are given below. Both rely on some potentially dangerous assumptions.

Method 1. subtracts authigenic P and detrital P from the total P measured by XRF, using equation 6.3. which assumes that the world average P/Al figure is applicable to these sediments The other assumption is that the Y/P ratio in phosphorites (calcium phosphate) remains constant.

Equation 6.3 $$P_{excess} = P_{tot.} - (P_{pt.} + P_{det.})$$

where:

$P_{tot.}$ = Total P measured by XRF

$P_{pt.}$ = Phosphorite/authigenic P derived using equation 6.4 by applying the mean Y/P ratios of phosphorite bands in core CD3810 (26.9×10^{-4}) collected off the Peru margin (G. M cNeil, pers. comm.).

$P_{det.}$ = detrital P derived from average P/Al in world average shale from Turekian and Wedopohl (1961) ie ($0.00875 \times$ Al.). The mean P/Al value in core P12 which is entirely dominated by terrigenous P and lies on the continental slope near N.W. south America (figure 6.0) is 0.00615 which is close to the world average of Turekian and Wedopohl (1961). However, most authors use Turekian and Wedopohl (1961) as the standard, and it is for this reason (to allow comparison with other work), that the world average ratios are used for P and other elements.

Equation 6.4 $$P_{pt.} = (Y_{measured} \times (26.9 \times 10^{-4})).$$

Method 2 subtracts $P_{det.}$ and organic P (P_{org}) from the total P measured from XRF, using equation 7.5 which asssumes a constant average P/Al ratio and C-org:P-org (Redfield) ratio.

Equation 6.5 $$P_{excess} = P_{tot.} - (P_{org} + P_{det.})$$

The P_{excess} includes authigenic ferriphosphate and biogenic skeletal P.
$P_{org.}$ = (C-org/41) from the Redfield ratio of C:N:P = 105:15:1 giving a C:P molecular ratio of 41:1. $P_{det.}$ = as in method 1.

There are several possible sources of error in these calculations, including changes in the C/P ratio for organic matter which is likely to increase with depth during organic

matter diagenesis (Honjo et al., 1982), as a result of the microbial breakdown and release of P from the mostly labile fraction of organic matter (Krom and Berner, 1981). Significant elevations of C/P ratios occur in settling organic matter due to degradation within the water column (after death). Moreover, Froelich et al. (1982) showed, by study of organic matter burial rates that, P_{org} in organic rich sediments is deficient relative to the Redfield ratio in contrast to an excess in organic poor sediments (ie <0.5% C-org). Clearly there are many problems associated with assuming a fixed Redfield ratio.

A further problem may be in the separation of the P_{excess} (**method 2**) into ferriphosphatic and biogenic skeletal material. It is assumed that in cores where the amount of Fe relative to Al is comparable with the world average Fe/Al of Turekian and Wedopohl (1961), authigenic ferriphosphatic material is essentially absent and, P_{excess} is dominated by inorganic skeletal material. This is corroborated by the findings of Pedersen (1979) who, after considerably study, found negligible ferriphosphate in sediments from the Panama basin. Thus in cores CD3822, CD3826 and CD3827 Pexcess (methods 1 and 2) is considered to be almost exclusively inorganic skeletal material and, indeed, indicative of one form of biological production in the oceans.

Suess (1981) showed that P from fish debris dissolution supplied three times as much P to the sediment sink as does organic matter, primarily due to the ability of skeletal debris to survive water column and surface sediment degradation. However, this situation may alter in the somewhat atypical setting of an upwelling system.

Organic (non-skeletal) P in marine sediments is mainly composed of phosphate esters with minor amounts of phosphonates (Ingall et al., 1990). Some components of the organic P are more susceptibly to diagenetic breakdown than others and, Ingan and Van Cappellin (1990) and Froelich et al., (1982) consider the refractory P_{org} to play an important role in the overall marine P budget.

6.7.2 Results and Discussion

The partitioning of P by **methods 1** and 2 in core CD3826 are shown in figure 6.18. Generally, the P_{excess} curves are similar and tend to be higher in the interglacial periods although there are several exeptions to this, most notably at 275 ka (stage VIII) and 65 ka (stage IV). That the two Pexcess's, which were derived

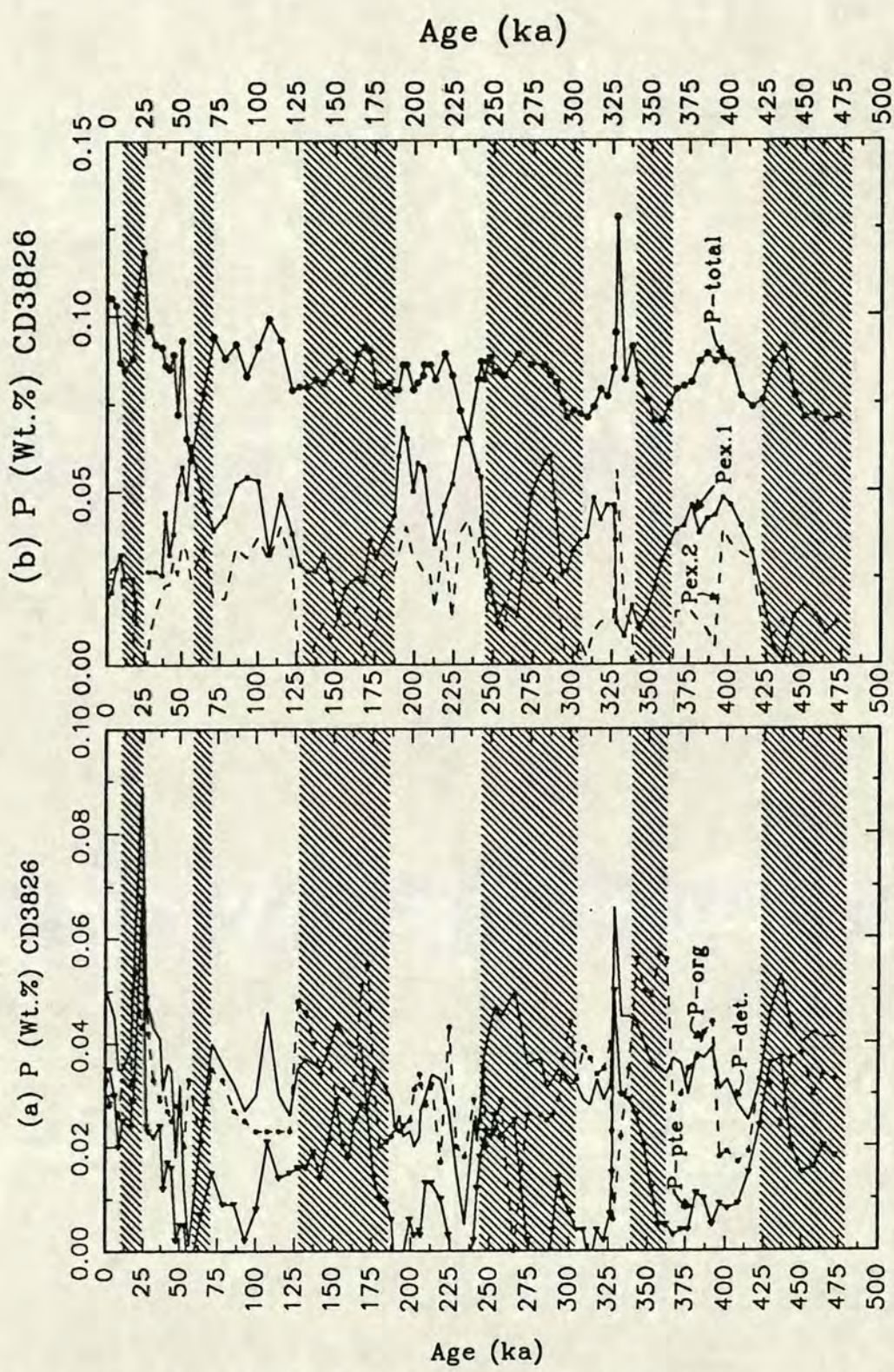

Figure 6.18 Temporal variations in the partitioned phases of P from core CD3826. P-total = total P (solid line, solid circles); P-det = detrital P (solid line, no symbols); P-pte = phosphorite or authigenic P (solid line, solid triangles); P-org = organic P (dashed line, solid circles); Pex.1 = Excess P-1 (solid line, solid squares); Pex.2 = Excess P-2 (dashed line, no symbols). Note the similarity of both excess P curves and how they increase during interglacials. See text for details. Shaded regions represent glacial stages II, IV, VI, VIII, X and XII.

independently, show quite close similarity is evidence for their validity or, that both are dominated by a common factor such as dilution from other constituents in the sediment.

If the modern pattern of euphotic zone primary productivity in the region is correct, then apatitic skelatal P (ie P_{excess} **method 2**) contents which reflects the concentration of fish debris and, ultimately, primary productivity, should record past spatial and temporal changes in primary palaeoproductivity. However, the remains of fish debris in the form of skeletal P will be only a fraction of the original primary productivity because of the loss in volume between each trophic level in the food chain. That is to say, for example, a hundred units of a primary producer material (eg $CaCO_3$) may translate to only one unit of skeletal fish debris.

There are many independent phases of P in marine sediments and dilution by terrigenous or carbonate material is important in determining their contents in the sediment. Thus in the eastern part of the Panama basin (eg core CD3827), where terrigenous input is generally higher than elsewhere (see chapter 5), the skeletal P contents will be higher than, for example, in core CD3822. Also the higher overall accumulation rate in the eastern basin cores will tend to preferentially promote the preservation of organic P (P_{org}).

If the P_{excess} curves are a reflection of biogenic input to the sediment in the form of skeletal apatite, then the results are in direct contradiction to C-org and $CaCO_3$ which tend to be higher during glacial times. Furthermore, when P_{ex} 1 and P_{ex} 2 are normalised against Al to minimise any possible dilution effects, both Pexcess/Al ratio curves show similar increases during interglacial periods (figure 6.19). The fluxes (which remove any dilution effects) of Pexcess are presented in figure 6.20. Clearly the mass accumulation rates of Pexcess 1 and Pexcess 2 both tend to be higher during the interglacial times. This confirms the conclusion of high biogenic productivity of skeletal P during interglacial periods.

Skeletal P is known to concentrate REE's (Arrhenius et al., 1957; Wright et al., 1987; Toyoda et al., 1990), while the sediementation rate and depositional environment are critical in the degree of concentration (Elderfield and Pagett, 1986). As discussed in chapter 5, REE results were generally to low to be reliable but Y did provide reliable data. Figure 6.21 shows the temporal variation in the ratio of Y/P_{total} in core CD3826 and clearly shows that P_{total} is enriched relative to Y during glacial times. If one

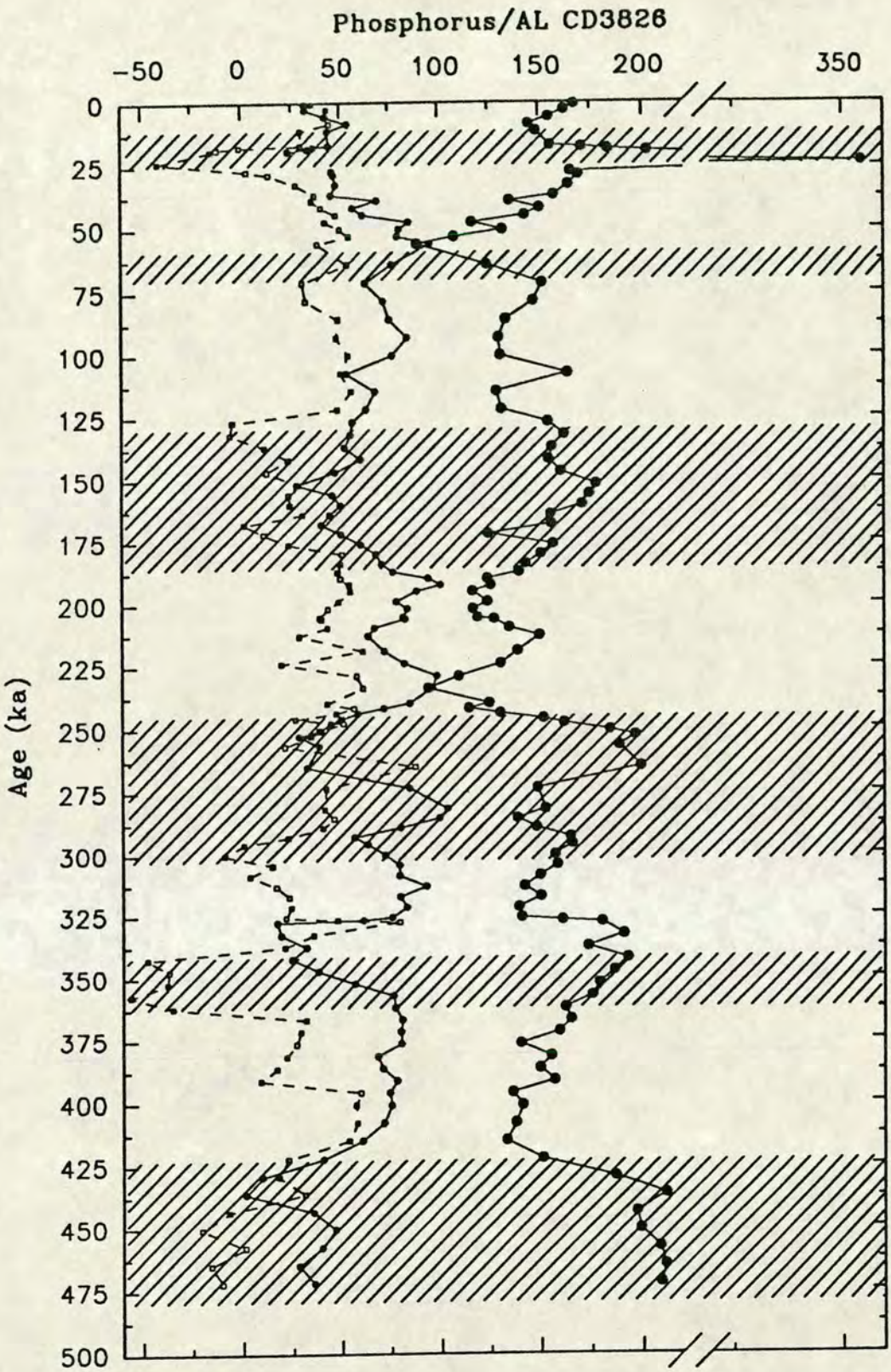

Figure 6.19 Temporal variations in Ptotal/Al (solid line, large solid circles), Pexcess-1/Al (solid line, small solid circles) and Pexcess-2/Al (dashed line, hollow squares) from core CD3826. See text for details. Both excess Pexcess/Al curves show increases during interglacials. Shaded regions represent glacial stages II, IV, VI, VIII, X and XII.

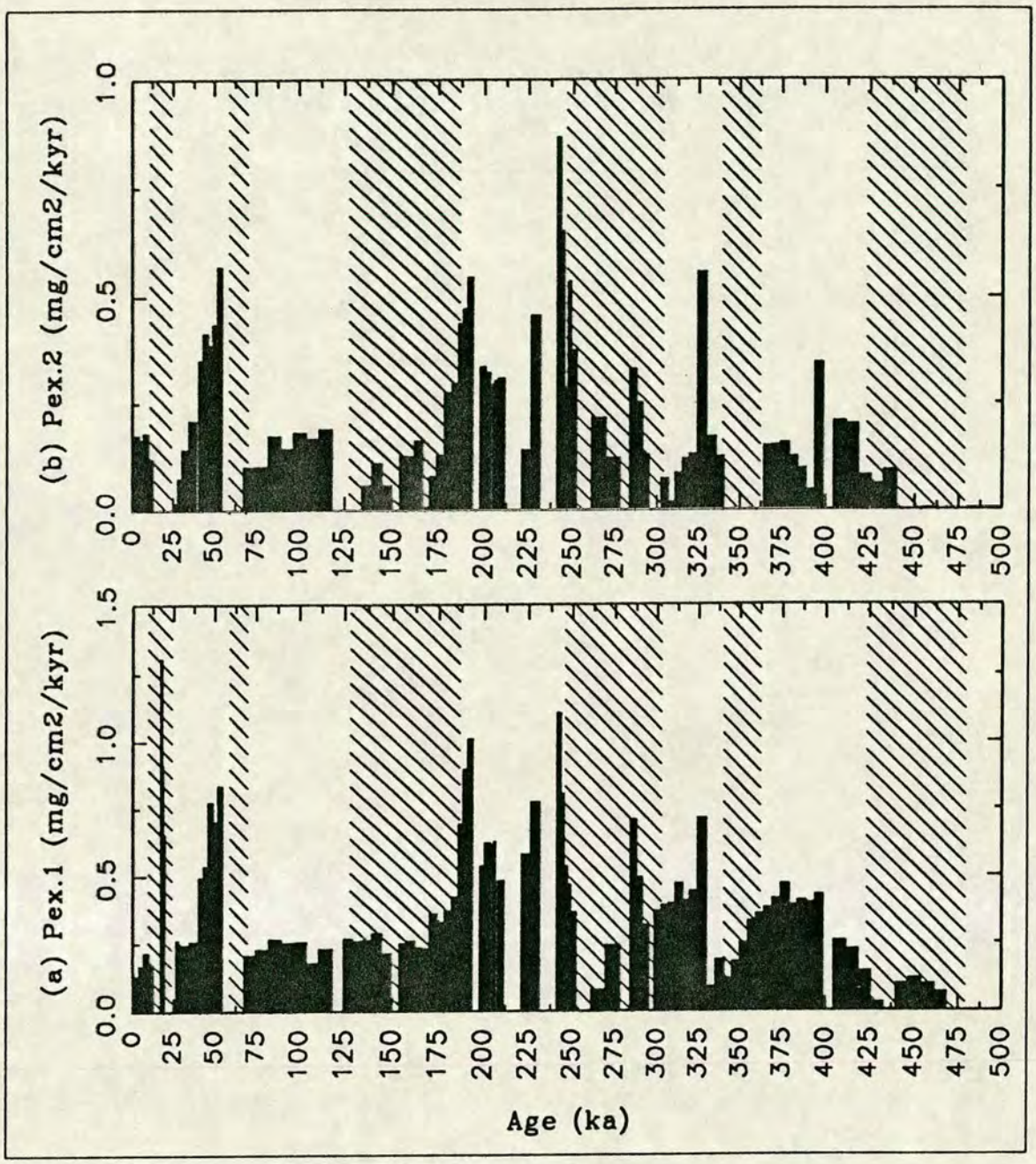

Figure 6.20 Temporal variations in the flux of Pexcess-1 (lower plot) and Pexcess-2 (upper plot) from core CD3826. See text for details. Gaps in the profile represent either negative flux values or the mainifestation of the expanded section of core caused by conversion from the depth to the time domain. Note the increase in flux during interglacials. Shaded regions represent glacial stages II, IV, VI, VIII, X and XII.

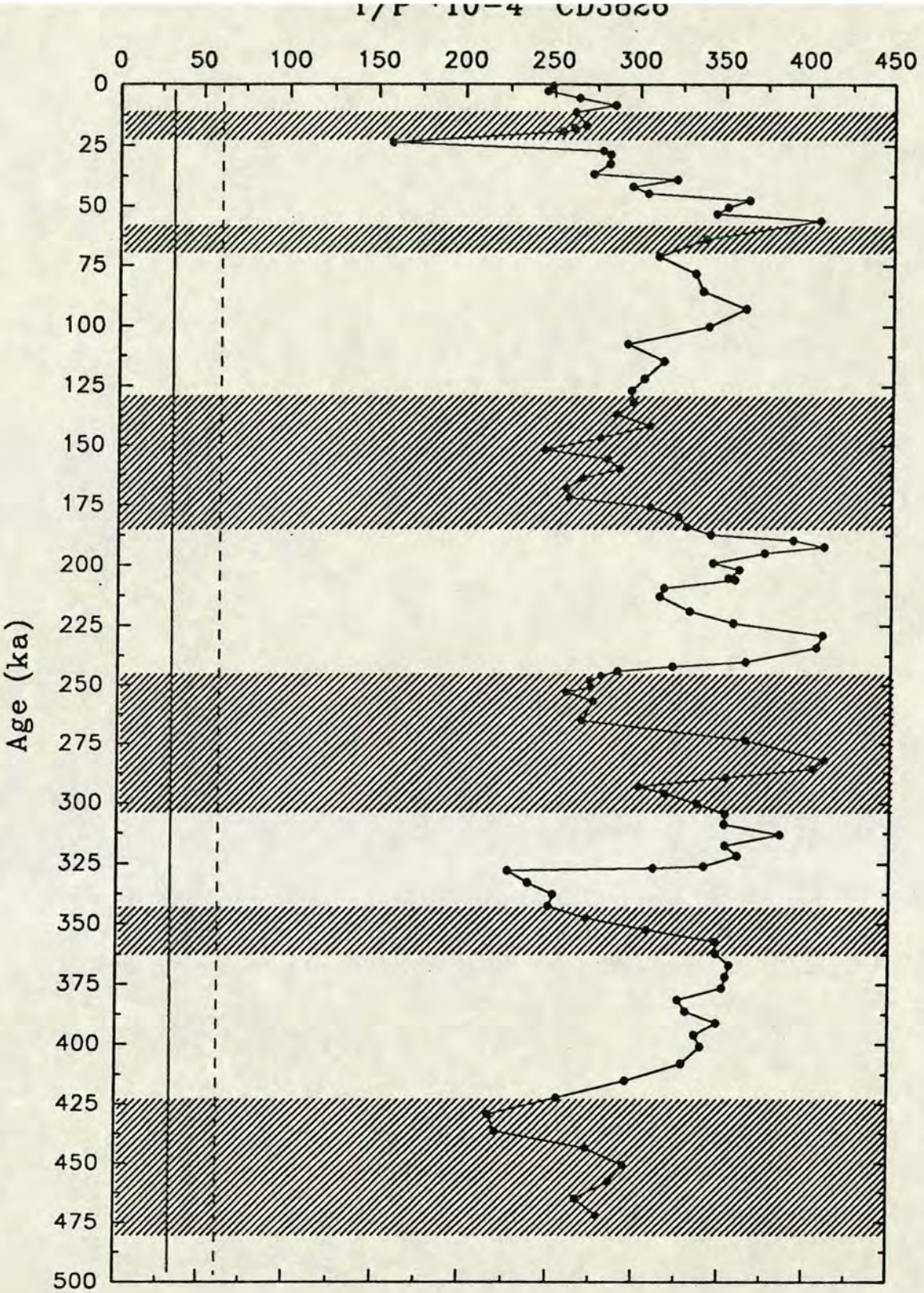

Figure 6.21 Temporal variations in Y/P $\times$ 10^{-4} ratio from core CD3826. Shaded regions represent glacial stages II, IV, VI, VIII, X and XII. The solid vertical line denotes the mean Y/P ratio in the phosphorite bands in core CD3810 and the dotted vertical line the mean Y/P ratio of normal sediment from this core (see text for details). All values are enriched in P relative Y compared to the world average value of Turekian and Wedopohl (1961) of 600.

assumes that the amount of Y associated with the skelatal debris is relatively constant then the excess in P could be due to a sharp increase in phosphatic material, more than large enough to exhaust the available Y.

6.8 Biogenic Titanium !?

The Ti contents in core P5 are anomalously high, and it was suggested (chapter 5) that they may have resulted from the titaniferous basalts found in the Galapagos archipelago or from an extra biogenic source. The low sea level stand and stronger wind systems of the glacial period would promote increased terrigenous material input to the oceans. Particulate scavenging of Ti by biogenic material falling through the water column similar to the other excess metals (chapter 9), would be a possible mechanism by which this extra Ti could enter the system, perhaps originally from increased Ti bearing atmospheric dust. Alternatively, the increased Ti in the glacial may result from a combination of the two processes.

Evidence for the existence of a biogenic source is scarse. It is known that the Pacific ocean has higher Ti concentrations both as a dissolved phase and in its suspended particulates (N.B. Price, pers comm.). The Pacific is effectively the end of the "production" line with respect to nutrient transport and distribution in the world's oceans, and concentrations of dissolved metals are generally higher than in other oceans.

The biogenic component of Ti would not normally be registered because the other sources of Ti (ie. terrigenous) tend to dominate the signal. In core P5 however, which is very high in $CaCO_3$ and the terrigenous input is minimal, the mean Ti/Al ratio is 0.106, with values ranging from 0.0820 to 0.1378. This is far in excess of what is normally found in marine sediments. Boyle (1983) employed high precision Ti analysis of sediments from the eastern equatorial Pacific in an attempt to establish Ti as a proxy for past wind strength and, indirectly, palaeoproductivity. He found that the mean Ti/Al ratio was 0.04450, and values ranged from 0.04326 to 0.04672. Clearly these values are considerably less than Ti/Al values found in core P5. Excess Ti contents were calculated using equation 6.6. Figures 6.4b and 6.4c illustrates the temporal variations in Ti/Al and Ex.Ti in this core.

Equation 6.6 $$Ti_{excess} = Ti_{tot} - (0.05476 \times Al_{tot})$$

where: Ti_{tot} = Ti (Wt. % salt free) measured on XRF

Al_{tot} = Al (Wt. % salt free) measured on XRF; 0.05476 = mean Ti/Al value for marine clays (Turekian and Wedopohl, 1961)

Although the Ti/Al curve shows a maximum during the glacial period, the Excess Ti profile is rather noisy and, if anything, displays a decrease in glacial times. The increased Ti/Al coincides with similar increases in Mg/Al, Fe/Al, Cr/Al and Zr/Al together with a decrease in K/Al. This suggests that the flux of Ti bearing basaltic material, in the form of dust, is increasing relative to the other alumino-sillicates which dominate in the other cores (eg CD3826, CD3827), and which show increases in the K/Al ratio during glacials. Thus, although biogenic particulate scavenging of the Ti bearing dust may concentrate the already increased dust input of Ti, the most important reason for the increased Ti/Al ratios is the relative switch in dominance of the Ti bearing dust derived from Galapagos and the other terrigenous material derived from central America. Therefore, the residual Ti of Murray (1987), could be explained by increased Ti bearing terrigenous material without any need to include a biogenic source which is difficult to verify.

6.9 Conclusions and Palaeoclimatic Implications

$CaCO_3$ contents are higher in the western Panama basin than in the eastern part of the basin, and are higher during glacial times than interglacials in all cores. The range of $CaCO_3$ contents within each core increases with increasing water depth and increasing dominance of terrigenous material.

There is a strong correlation between Excess Sr and Ca. The excess Sr, over that normally held in carbonate organisms, is derived from clay minerals and/or barite. The ratio of Ex.Sr/Ex.Ca tend to be lower during glacial periods as a result of the increased terrigenous input from the continental shelves during the cool arid glacials and/or an increase in the abundance of nannofossils.

Organic carbon contents generally double during glacial periods consistent with increased euphotic zone productivity. A long-term diagenetic decrease in C-org values is observed in core CD3826, whereas the rapid accumulation rate in core

CD3827 appears to have enhanced the preservation of C-org. Particle size and sediment texture appear to have little effect on the C-org profiles. Palaeoproductivity curves show maxima at the beginings and ends of glacial periods in all cores, with the Holocene enrichment observed in core P5 and CD3826 being the exceptions to the rule.

The decoupling of the cyclicity in the SiO_2 profiles from glacial-interglacial alternation is probably because the biogenic SiO_2 is more influenced by local oceanographic factors than global ice volume/temperature variations. Changes in SiO_2 probably reflect spatial and temporal variations in the species and abundance of the siliceous plankton communities. Siliceous communities are relatively more abundant compared to carbonate ones in core CD3822 than in the other cores. Dissolution of SiO_2 is greatest in core CD3826 which has the slowest bulk accumulation rate of all the cores.

Ba is associated with biogenic SiO_2, although there are many exceptions perhaps resulting fom differences in the timing of maxima and minima (ie. phase lags). The excess Ba profiles mirror the $\delta^{18}O$ profile in core CD3826 and CD3827, but roughly parallels the $\delta^{18}O$ curve in core CD3822. Cores CD3822 and P5 have been subject to a very different oceanographic setting to cores CD3826, CD3827 and AII54-25PC.

Excess P (ie biogenic P) in core CD3826, calculated by two independent methods, shows increases during interglacial periods as do Excess P fluxes, which is in direct contrast to the other biogenic tracers discussed in this chapter. Ratios of Pexcess (methods 1 and 2)/Al also show increases during integlacials. However Ptotal/Al ratios tend to be higher during glacials consistent with other biogenic tracers.

Ti/Al ratios are higher during glacial times which is consistent with increased input of Ti bearing basaltic material from the Galapagos archipelago and/or increased wind strength. Ex.Ti values tends to decrease during the glacial. The extra Ti bearing dust observed in P5 is not recognised in most cores because the terrigenous Ti signal is usually so large that it swamps the second terrigenous source, assuming it exists in the other areas.

CD3814 (a)

n=	r=									
72	0.655	P	P							
72	0.655	CaCO3	-0.958	CaCO3						
73	0.654	Sr	-0.862	0.792	Sr					
73	0.654	Ba	-0.126	0.319	0.755	Ba				
73	0.654	Cu	0.475	-0.286	0.229	0.733	Cu			
73	0.654	Ni	0.843	-0.761	-0.359	0.294	0.751	Ni		
73	0.654	Zn	0.974	-0.965	-0.657	-0.112	0.477	0.863	Zn	
73	0.654	V	-0.250	0.355	0.594	0.643	0.438	0.044	-0.242	V

CD3822 (b)

n=	r=										
62	0.666	P	P								
62	0.666	CaCO3	0.230	CaCO3							
63	0.665	Sr	0.296	0.908	Sr						
63	0.665	Ba	0.647	0.030	0.167	Ba					
47	0.687	B.SiO2	0.064	-0.616	-0.578	-0.168	B.SiO2				
63	0.665	Cu	0.674	-0.161	-0.037	0.725	0.168	Cu			
63	0.665	Ni	0.489	-0.409	-0.300	0.543	0.279	0.741	Ni		
63	0.665	Zn	0.641	-0.371	-0.288	0.552	0.445	0.724	0.691	Zn	
63	0.665	V	0.545	-0.282	-0.251	0.229	0.442	0.393	0.395	0.621	V
62	0.666	C-org	-0.036	0.222	0.128	-0.227	-0.096	-0.057	-0.204	-0.202	-0.292	C-org

CD3826 (c)

n=	r=											
111	0.626	P	P									
111	0.626	CaCO3	-0.382	CaCO3								
111	0.626	Sr	-0.386	0.968	Sr							
111	0.626	Ba	0.200	-0.669	-0.586	Ba						
111	0.626	B.SiO2	-0.277	-0.100	0.021	0.477	B.SiO2					
111	0.626	Cu	0.128	-0.611	-0.540	0.698	0.261	Cu				
111	0.626	Ni	0.351	-0.543	-0.497	0.567	0.077	0.550	Ni			
111	0.626	Zn	0.192	-0.645	-0.597	0.742	0.176	0.797	0.656	Zn		
111	0.626	V	0.039	-0.422	-0.463	0.402	0.004	0.421	0.376	0.606	V	
110	0.628	C-org	-0.027	0.329	0.261	-0.273	-0.149	-0.287	-0.083	-0.102	-0.029	C-org

CD3827 (d)

n=	r=											
33	0.719	P	P									
33	0.719	CaCO3	-0.313	CaCO3								
33	0.719	Sr	0.074	0.873	Sr							
33	0.719	Ba	0.681	-0.209	0.089	Ba						
32	0.722	B.SiO2	-0.184	0.261	0.183	-0.034	B.SiO2					
33	0.719	Cu	0.280	-0.429	-0.392	0.588	0.134	Cu				
33	0.719	Ni	0.141	0.175	0.297	0.233	0.907	0.150	Ni			
33	0.719	Zn	0.707	-0.239	0.157	0.808	-0.179	0.206	0.201	Zn		
33	0.719	V	0.145	-0.543	-0.458	0.059	-0.889	0.048	-0.798	0.184	V	
32	0.722	C-org	-0.243	0.336	0.203	-0.195	0.825	-0.037	0.890	-0.352	-0.829	C-org

Table 6.4 Correlation matrix for biogenic tracers and transition metals (see chapter 9) from CD38 cores. n= number of samples used in statistical analysis; r= correlation coefficient at 95 % confidence limit. Coefficients of correlation > r are said to be significant at > 95 % confidence. Coefficients of correlation > 0.5 < r are described in the text as having "strong" correlation.

Correlation Matrix from core P5

n=	r=											
57	0.672	P	P									
57	0.672	CaCO3	-0.644	CaCO3								
57	0.672	Sr	0.355	-0.135	Sr							
57	0.672	Ba	0.792	-0.840	0.383	Ba						
57	0.672	B.SiO2	0.600	-0.880	0.179	0.828	B.SiO2					
57	0.672	Cu	-0.155	0.224	-0.010	-0.179	-0.138	Cu				
57	0.672	Ni	-0.100	0.144	0.392	0.002	0.119	0.517	Ni			
57	0.672	Zn	0.519	-0.652	0.417	0.695	0.791	0.181	0.445	Zn		
57	0.672	V	0.362	-0.427	0.454	0.459	0.532	-0.046	0.126	0.615	V	
57	0.672	C-org	-0.455	0.658	-0.230	-0.630	-0.667	0.136	-0.060	-0.680	-0.409	C-org

Table 6.5 Correlation matrix for biogenic tracers and transition metals from core P5. See table 6.4 for details of abbreviations.

CHAPTER 7
FLUXES OF BIOGENIC TRACERS

7.1 Introduction

This chapter documents the changes in the mass accumulation rates (MARs) of $CaCO_3$, SiO_2, Excess Ba and organic carbon (C-org) from cores P5, CD3822, CD3826 and CD3827, in an attempt to illustrate palaeoproductivity variations over time in the eastern equatorial Pacific. Fluxes of biogenic tracers in the equatorial Pacific have received considerable attention in recent years (Dymond and Lyle, 1985; Murray, 1987; Lyle et al., 1988; Rea et al., 1991; Pedersen et al., 1992). Flux calculations have the advantage that they are essentially independent of dilution processes from other elements, and thus allow quantification of the input of each tracer on a theoretical basis that is independent of other sediment components, which may dominate the sediment chemistry. Therefore, MARs allow comparison of components over time even between cores of vastly differing compositions and accumulation rates.

The problems associated with the calculation of fluxes in sediments has already been discussed in chapter 5. MAR results presented in appendix C.10 are calculated using equation 7.1.

Equation 7.1 **Element (MAR) = Element concentration (%) × SR × DBD**

where **(MAR)** = mass accumulation rate ($g/cm^2/kyr$)

SR = linear sedimentation rate (cm/kyr)

DBD = Dry bulk density (g/cm^2)

7.2 Results

Mean (range) values of MARs of $CaCO_3$, SiO_2, C-org and ExBa are shown in table 7.1. These show division of the cores into two groups, those high in $CaCO_3$ MARs (P5 and CD3822) and those with low $CaCO_3$ MARs (CD3826 and CD3827). The MARs of $CaCO_3$ in cores P5 and CD3822 are generally an order of magnitude greater than in cores CD3826 and CD3827. Such large differences in the MARs of biogenic tracers may be partly, if not entirely, the result of erroneous linear sedimentation rates. Errors in the calculation of the sedimentation rates may result from inaccurate positioning of stage boundaries, using oxygen isotope stratigraphy and geochemical correlation (chapter 4). Thus, the length (cm) of a particular stage may be overestimated, with the res ult that bulk accumulation rates and MARs, over this period, will be spuriously high.

Table 7.1 Mean (range) values of biogenic tracer fluxes (mg/cm^2/kyr) from this study. Ex=Excess.

Core	$CaCO_3$	C-org	SiO_2	ExBa
P5	4447(1906-9973)	31.7(9.3-79.1)	139.5(47.9-422.5)	3.67(1.50-8.67)
CD3822	2699(990-5019)	46.8(10.2-163.7)	183.8(508.8-45.3)	7.43(3.26-12.76)
CD3826	269(19-1396)	18.7(4.7-137.8)	50.3(16.9-263.3)	3.10(1.17-13.98)
CD3827	379(33-890)	142.8(21.9-341.1)	159.8(48.0-296.3)	4.57(1.10-8.39)

Other biogenic tracers do not follow the same amplitude or pattern of change. For example, the highest C-org MAR is found in core CD3827 at 142.8 mg/cm^2/kyr which is approximately three times greater than the C-org MAR of 46.8 mg/cm^2/kyr in core CD3822. The fluxes of SiO_2 and Excess Ba are highest in core CD3822 which reflects the patterns seen in their contents (chapter 6).

7.2.1 Temporal Variations in the Flux of Biogenic Tracers

Temporal variations in the flux of $CaCO_3$, C-org, SiO_2 and Excess Ba are shown in figures 7.1-7.3. All four tracer fluxes show similar profiles which may reflect inaccuracies in the age model and, therefore, MARs. Generally, glacial periods are times of increased input of biogenic tracers, with glacial stage II always exhibiting the greatest increase in all components and cores. These finding are consistent with evidence that there were increases in biological productivity of the surface waters during glacial times (Pedersen, 1979; Murray, 1987; Lyle et al., 1988; Rea et al., 1991; Hovan and Rea, 1991; Pedersen et al., 1992). The temporal record of each tracer suggests that they may be divided into two groups: (1) $CaCO_3$ and organic carbon; and, (2) SiO_2 and Excess Ba, based largely on the shape of the MAR profiles and the degree of statistical correlation between them, which is discussed below.

$CaCO_3$ and Organic Carbon Fluxes

In core P5 the fluxes of these two components are very similar with large increases in values between 16-12 ka (figure 7.1a,b). $CaCO_3$ MAR increases from a background level of around 2,500 mg/cm^2/kyr to almost 10,000 mg/cm^2/kyr and C-org from around 12 mg/cm^2/kyr to approximately 60 mg/cm^2/kyr during this period.

Figure 7.1 Temporal variations in the mass accumulation rates (mg/cm^2/kyr) of $CaCO_3$ (a), C-org (b), SiO_2 (c) and Excess Ba (d) from core P5.

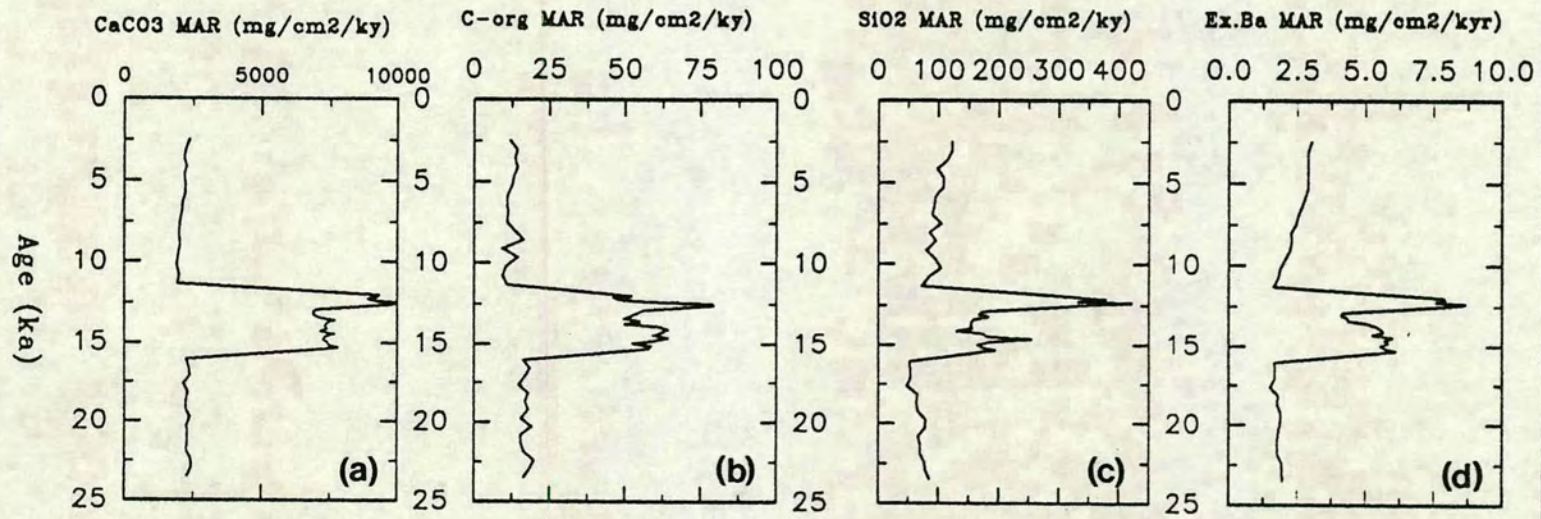

Figure 7.2 Temporal variations in the mass accumulation rates (mg/cm^2/kyr) of $CaCO_3$ (a, e), C-org (b, f), SiO_2 (c, g) and Excess Ba (d, h) from cores CD3822 (upper series of plots) and CD3827 (lower series of plots).

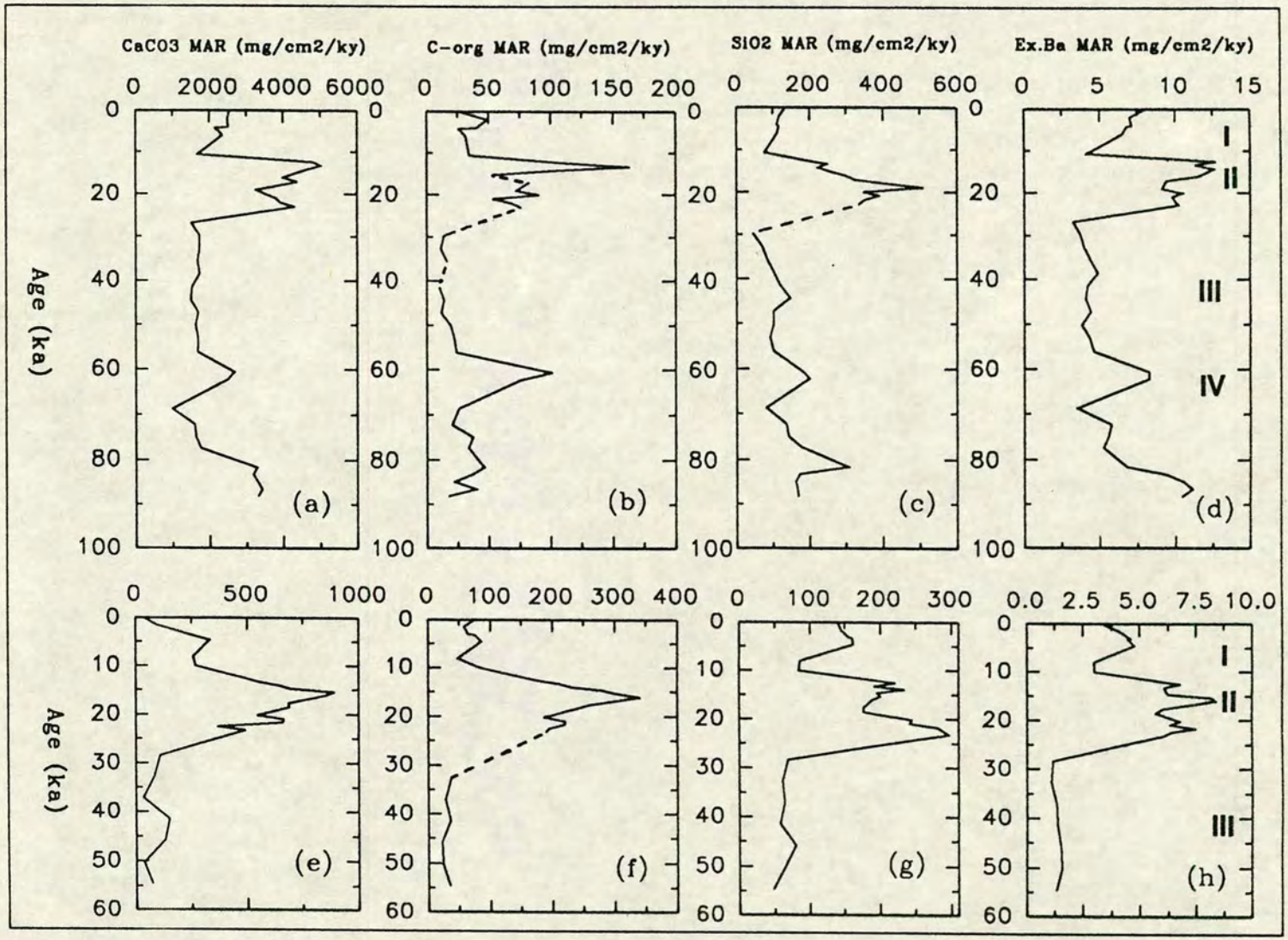

Figure 7.3 Temporal variations in the mass accumulation rates (mg/cm^2/kyr) of $CaCO_3$ (a), C-org (b), SiO_2 (c) and Excess Ba (d) from core CD3826.

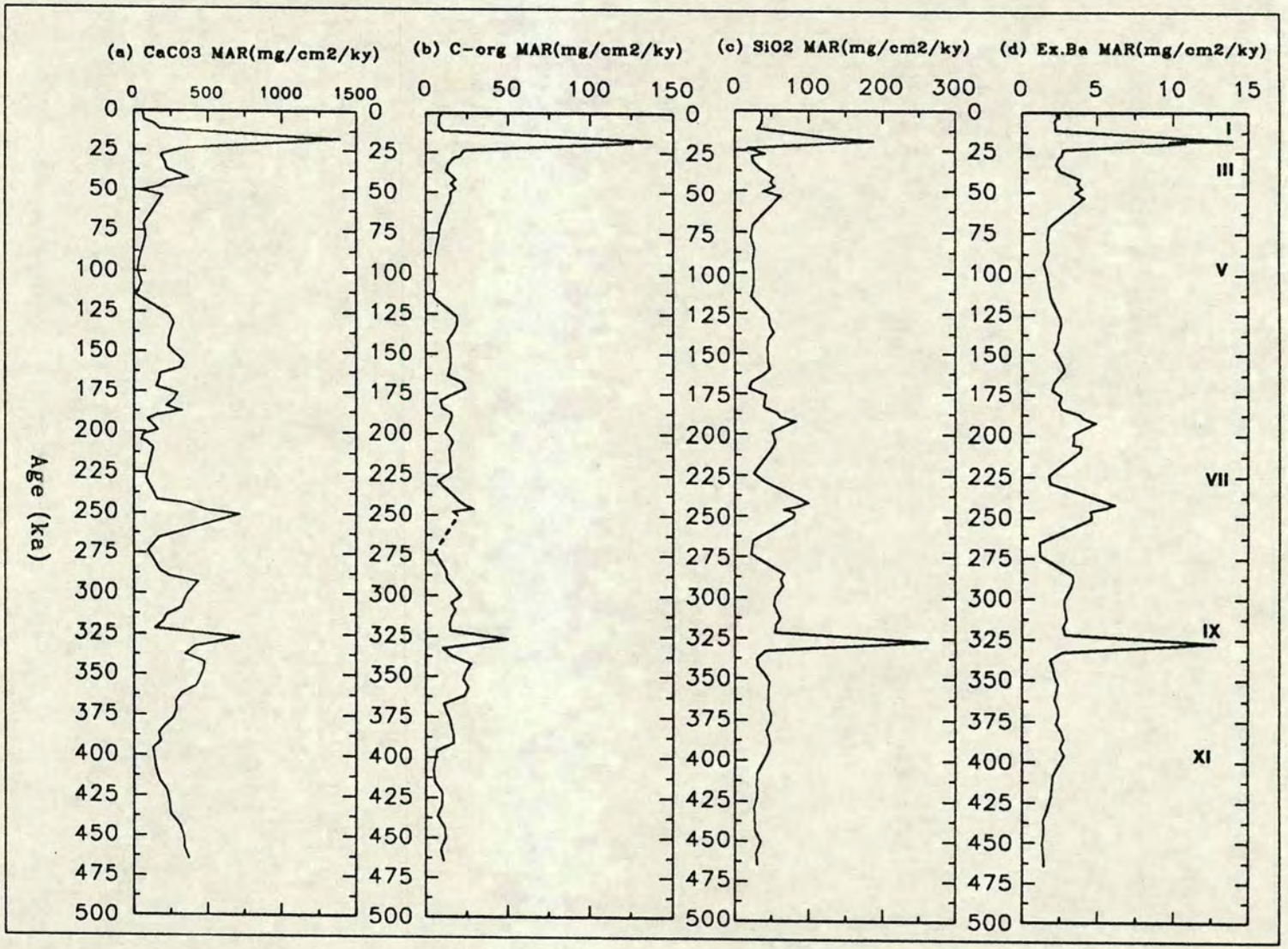

Core CD3822 has the smallest percent change in $CaCO_3$ MARs of all the cores varying from approximately 2,000 mg/cm^2/kyr to approximately 4,000 mg/cm^2/kyr in stage II, and only 3,000 mg/cm^2/kyr during stage IV (figure 7.2a). Organic carbon however shows large increases at 12 ka and 61 ka of approximately 150 mg/cm^2/kyr and approximately 100 mg/cm^2/kyr respectively, in contrast to the background level of close to 25 mg/cm^2/kyr at interglacial times.

The $CaCO_3$ and C-org MARs in core CD3827 (figure 7.2e, f) increase to maxima at 15 ka of 1,300 mg/cm^2/kyr and 350 mg/cm^2/kyr respectively, which are considerably higher than the interglacial levels of approximately 200 mg/cm^2/kyr ($CaCO_3$) and 50 mg/cm^2/kyr (C-org).

Increases in $CaCO_3$ and C-org MARs are present in core CD3826 at 18 ka, 40 ka, 155 ka, 250 ka, 290 ka, 328 ka and 350 ka (figure 7.3a, b). The highest MARs of approximately 1750 mg/cm^2/kyr for $CaCO_3$ and 130 mg/cm^2/kyr for C-org occur during stage II. Background (interglacial) levels of $CaCO_3$ MAR and C-org MAR are approximately 250 mg/cm^2/kyr and 10 mg/cm^2/kyr respectively.

SiO_2 and Excess Ba Fluxes

The SiO_2 and excess Ba fluxes in core P5 show increases between 16 ka and 12 ka with a slight drop in values at 14 ka. The flux of SiO_2 rises from around 100 mg/cm^2/kyr to over 3,000 mg/cm^2/kyr at the beginning of stage II. Similarly, the excess Ba flux increases from approximately 2 mg/cm^2/kyr to over 7 mg/cm^2/kyr at the end of stage II.

SiO_2 and excess Ba fluxes in core CD3822 show increases during stage II and at 82 ka (figure 7.2c,d). However, the maxima are at slightly different times. SiO_2 increases from around 100 mg/cm^2/kyr during interglacials to approximately 500 mg/cm^2/kyr at 20 ka (stage II) and 300 mg/cm^2/kyr at 82 ka (stage VI). Excess Ba rises from a background of roughly 4 mg/cm^2/kyr to around 12 mg/cm^2/kyr at 12 ka (stage I/II), and 10 mg/cm^2/kyr at 85 ka (stage VI).

SiO_2 in core CD3826 has several distinct increases at 18 ka, 55 ka, 140 ka, 190 ka, 240 ka and 328 ka, which are parallelled by the excess Ba MARs (cp. figures 7.3c, d). Except for the 4-5 fold increase in the two constituents during stage II and at 328 ka,

other increases generally represent an approximate doubling of values from background interglacial levels.

7.2.2 Primary Biogenic Tracer Flux Relationships

The relationship between the four biogenic tracers is illustrated using X-Y plots in figure 7.4. Values of R^2 on the regression lines (table 7.2) were used to determine the degree of association between fluxes rather than the correlation matrices used in previous chapters.

Visual inspection of figure 7.4 indicates an especially good linear correlation between $CaCO_3$ and C-org, $CaCO_3$ and Excess Ba and SiO_2 and Excess Ba. This is corroborated by the values of R^2 (table 7.2), with generally high values in all cores for these plots except core CD3822 which shows some scatter (figures 7.4a and 7.4e). Core P5 displays high correlation between $CaCO_3$ and all other tracers, and also between SiO_2 and Excess Ba. What is unusual is that $CaCO_3$ shows a strong correlation with Excess Ba in all cores, a relationship clearly seen in the temporal variations of MARs discussed above. If one can assume that Excess Ba reflects biological productivity of the overlying surface waters, then these results argue in favour of $CaCO_3$ reflecting, to some degree, biological production, and not just preservation events. Alternatively, however, the similarity of the $CaCO_3$ MARs and ExBa MARs may be the result of age model inadequacies.

Table 7.2 Values of R^2 from regression analysis on X-Y plots of biogenic tracers fluxes. Bold numbers refer to correlation ≥ 0.900.

	R^2			
Correlation	**P5**	**CD3822**	**CD3826**	**CD3827**
$CaCO_3$ Vs. C-org	**0.963**	0.779	**0.920**	**0.975**
$CaCO_3$ Vs. SiO_2	**0.963**	0.694	0.766	0.805
$CaCO_3$ Vs. ExBa	**0.956**	**0.939**	0.827	**0.940**
SiO_2 Vs. C-org	0.753	0.574	0.730	0.744
SiO_2 Vs. ExBa	**0.940**	0.636	**0.928**	0.888
C-org Vs. ExBa	0.881	0.701	0.841	**0.911**

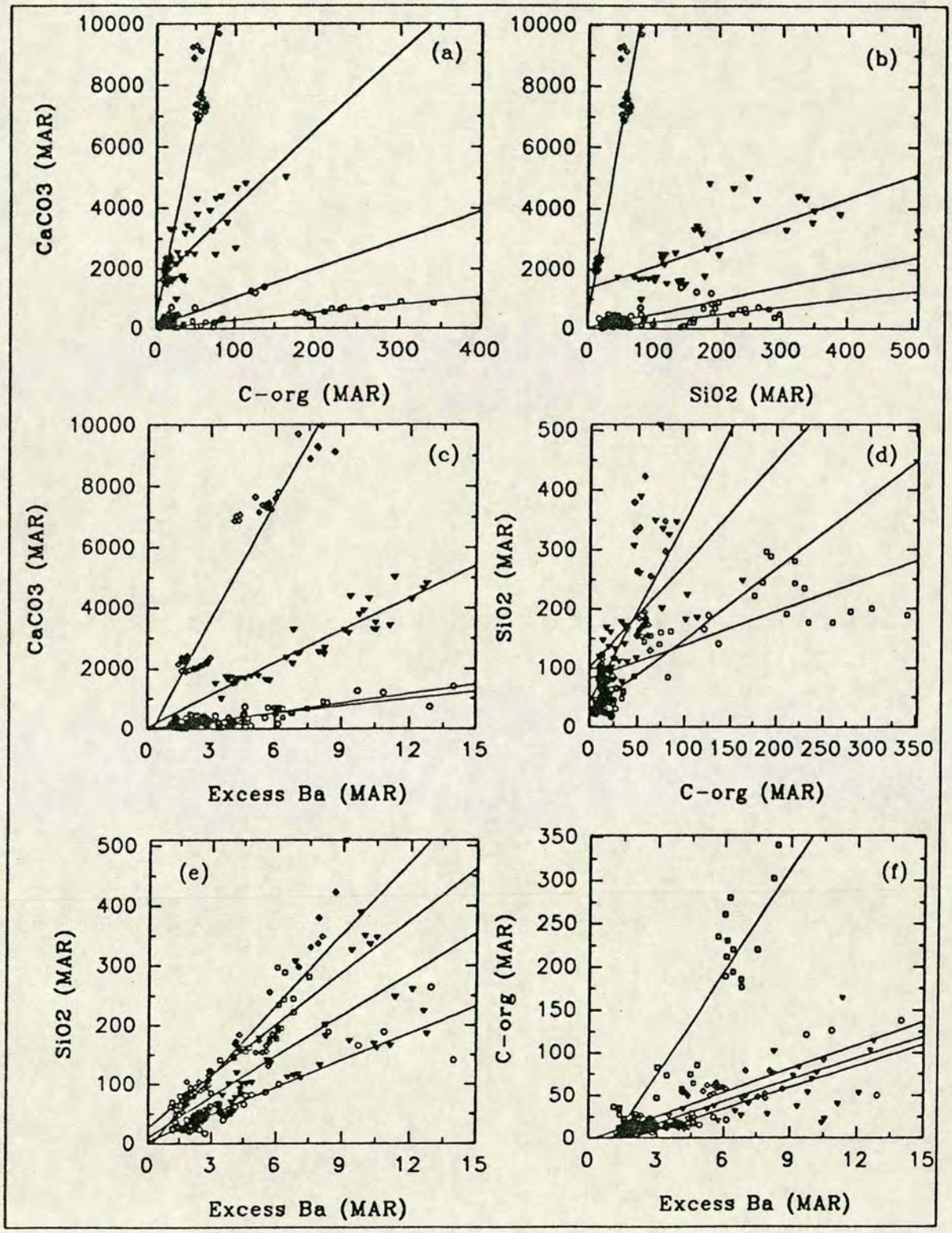

Figure 7.4 Relationship between primary biogenic tracer fluxes from this study. Hollow diamonds refer to data from core P5, hollow triangles to CD3822, hollow squares to CD3827 and hollow circles to CD3826. Values of r^2 for the regression lines are given in table 7.2. Mass accumulation rates (MAR) are given in $mg/cm^2/kyr$.

The gradient of the regression lines on the plots of $CaCO_3$ versus C-org vary considerably (figure 7.4a), with core P5 having a $CaCO_3$ MAR/C-org MAR ratio two orders of magnitude greater than in core CD3827. This has important implications for the global CO_2 budget (discussed below). In contrast, the genetically associated SiO_2 and excess Ba (see chapter 6) display regression line gradients that are very similar in all cores, reflecting a relatively constant ratio between the two tracers.

7.3 Discussion

That the main biogenic components ($CaCO_3$, C-org, SiO_2 and Ba) fall into two groups argues for a structure within productivity events (during glacials), and for the importance of different types of production. Such a dichotomy may suggest that diatom enriched sediments contain relatively less C-org than an equivalent unit of carbonate material. Indeed, much of the C-org in marine sediments probably originates from nannofossil carbonate organisms than from other calcareous organisms (D. Kroon pers. comm.). Thus, during periods of very high diatom accumulation, there may be relatively lower organic carbon (and $CaCO_3$) contents, due to dilution by the SiO_2 communities especially during the early stages of the productivity event. Towards the latter stages of an event, however, these siliceous communities may be replaced by the $CaCO_3$ (C-org rich) communities in the highest productivity periods towards the middle and end of the production episode. However, off south-west Africa diatomaceous oozes have been shown to be rich in organic carbon (Price and Calvert, 1973).

This sequence of changing SiO_2 and $CaCO_3$, and commensurate increases in C-org, has been observed by Rea et al., (1991) who claim that the highest productivity is during the maxima of $CaCO_3$ and C-org, and that the opal tends to decrease during this time. The trends are also consistent with Lyle et al. (1988), and the findings of chapter 6, of the independent behaviour in the production of siliceous and carbonate based organisms.

Support for this hypothesis is most clearly demonstrated in the fluxes from the rapidly accumulating core CD3827 (figure 7.2). Towards the end of interglacial stage III (29 ka), which can tentatively be presumed to be a period of increasing productivity, all four biogenic tracers increase markedly but SiO_2 reaches its maximum at approximately 23 ka (base of stage II), whilst C-org and $CaCO_3$

continue to increase into stage II. Here, the SiO_2 drops to minimum values while $CaCO_3$, C-org and ExBa peak at 15 ka. A second SiO_2 peak occurs at 12 ka. The C-org MAR shows a sharp maximum towards the end of the production event and coincides with peaks in the $CaCO_3$ MAR and ExBa MAR. Although the ExBa reaches its maximum in stage II at the same time as $CaCO_3$ and C-org, it resembles the SiO_2 more closely in overall appearance with peaks at 12 ka and 24 ka.

According to Rea et al., (1991), although production of $CaCO_3$ may also increase at the beginning of a productivity pulse, only later is the $CaCO_3$ MAR sufficiently high to overcome the retardation effects of dissolving C-org in the water column, that the calcite rain eventually exceeds the enhanced dissolution resulting from an increased flux of $CaCO_3$. The point at which this switch from siliceous dominated production to the more $CaCO_3$ and C-org dominated production will vary throughout the oceans and will depend on several other factors. For example, a slowly sedimenting core in a region which is characteristically dominated by the remains of carbonate secreting communities will not necessarily show this evolutionary change in the productivity. No satisfactory explanation has been proposed which accounts for the fact that in some areas of the oceans carbonate communities dominate whilst in other very similar regions siliceous plankton communities flourish. However, the availability of silicate, the intensity of the thermocline and the presence or absence of some trace metals (eg Fe) are probably all important in determining whether siliceous or carbonate communities dominate the plankton.

If preservation dominates the $CaCO_3$ and C-org signals, then the ratio of these two components, which have been shown to be closely associated, would tend to vary in a systematic and relatively gradual way. Temporal variations in the ratio of $CaCO_3$ MAR/C-org MAR from core CD3826 exhibit quite a noisy profile, but displays a definite overall decrease upcore (figure 7.5). Coupled with this is a tendency for glacial times (especially stages VI and VIII) to have higher $CaCO_3$ MAR/C-org MAR ratios. Thus, the distribution of $CaCO_3$ and C-org is not solely controlled by a single preservation factor, but must have other influences probably including surface water productivity as suggested by Pedersen et al., (1992).

7.3.1 Implications of Palaeoproductivity variations for Global CO_2 Budgets

Since the oceans are the largest sink of dissolved (inorganic) carbon on the planet, the marine sedimentary cycles of organic and inorganic carbon have important

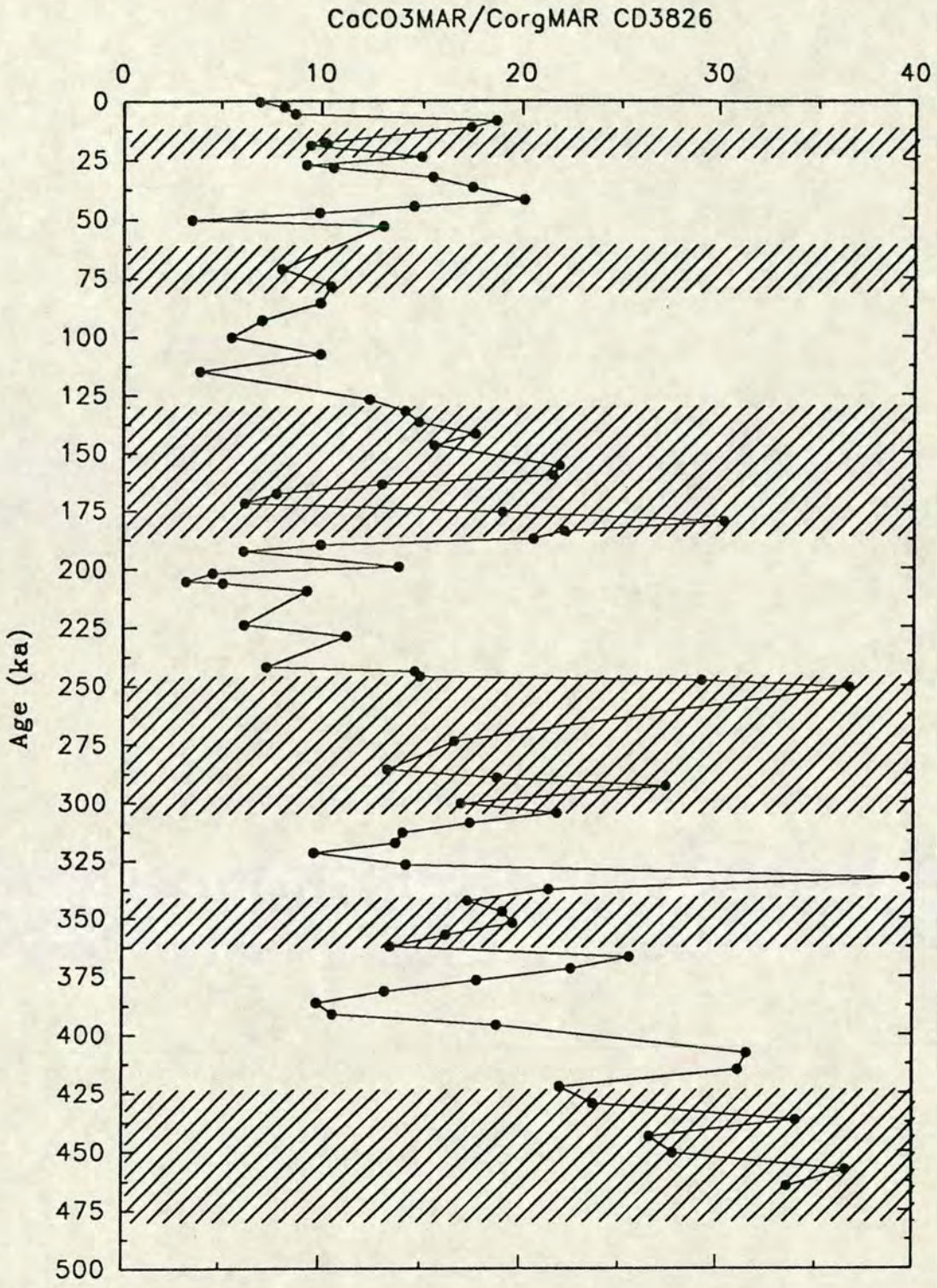

Figure 7.5 Temporal variations in the $CaCO_3$ MAR/C-org MAR ratio from core CD3826. Shaded regions represent glacial stages II, IV, VI, VIII, X and XII.

implications for the transfer and balance of CO_2 between the atmosphere and hydrosphere over time. In this respect the $CaCO_3$/C-org ratio present in the sediment acts as a proxy for long-term CO_2 budgets: high ratios indicating a greater CO_2 availability in the oceans and, potentially, a greater likelihood of net CO_2 transfer from the oceans to the atmosphere (Rea et al., 1991). Thus, the overall decrease in the $CaCO_3$ MAR/C-org MAR ratio observed over the past 472 ka in core CD3826 would indicate that the potential for net CO_2 transfer to the atmosphere from the surface waters of the oceans has decreased in the eastern equatorial Pacific over this time period.

There has been much debate as to what caused the glacial depletions in global atmospheric CO_2 during the Quaternary (Broecker, 1982; Dymond and Lyle, 1985; Sarnthein et al., 1987; Boyle 1988a, 1988b; Lyle and Pisias, 1990; Pedersen et al., 1992). Theories fall into two groups. The first proposes that increased primary productivity during the glacials either enhances; the removal of carbon from the atmosphere to the surface of the oceans and to the sediment column (Flohn, 1982), or promotes nutrient redistribution as a result of increased particulate organic matter flux to deep water (Sarnthein et al., 1987; Boyle, 1988a), or both. The second group propose that changes in primary production are the result, and not the cause of, climatic changes (Lyle, 1988). The results of the $CaCO_3$ MAR/C-org MAR ratio from core CD3826 do not especially favour either argument. The sharp increase at the base of stage VI, and the gradual decrease during this stage, might argue for external climatic forcing of the productivity variations because the drop in atmospheric CO_2 during glacials would promote sequestration of CO_2 into the oceans as a result of increased C-org associated production. In contrast, the increase in the $CaCO_3$ MAR/C-org MAR ratio during glacial stage VIII may reflect the potential increase in atmospheric CO_2 and attendant global temperature until, at the end of the stage, the increased concentration of atmospheric CO_2 forced the climate system to switch to an interglacial-type episode in stage VII. Coupled with this is a tendency for glacial times (especially stages VI and VIII) to have higher $CaCO_3$ MAR/C-org MAR ratios.

Surface water productivity in the Panama basin has been estimated at 335-423 mg C/m^2/day (Murray et al., 1990) and at 164-548 mg C/m^2/day in the central equatorial Pacific (Berger et al.,1987). Murray (1987) showed, from a study of sediments and sediment traps from MANOP site C (1°N 139°W, 4470m), that 40% of the $CaCO_3$ produced in the surface water is preserved in the sediment. This led Rea et al. (1991)

to conclude that modern surface water production must be 2.5 times the surficial mass accumulation rate of $CaCO_3$ in the sediment. Such calculations have many drawbacks, not least the variations in dissolution between cores. However, Holocene $CaCO_3$ MARs in the Panama basin of 137-301 mg/m^2/day (Swift and Wenekam, 1978) are broadly consistent with the surface water production using the above argument.

Thus, assuming that the present day setting is typical of interglacial periods which has low $CaCO_3$ preservation, and applying the figures for recent sediments (Murray, 1987) to the cores studied in this thesis, one can calculate what level of $CaCO_3$ MAR which must be the result of productivity increases and not just preservation events in each core. Using this rationale, $CaCO_3$ MARs greater than 5896 mg/cm^2/kyr, 6339 mg/cm^2/kyr, 255 mg/cm^2/kyr and 496 mg/cm^2/kyr in cores P5, CD3822, CD3826 and CD3827 respectively must have resulted from increased productivity and not just changes in preservation. From figures 7.1-7.3 it is clear that in glacial stages the increase in $CaCO_3$ must be, at least in part, due to productivity increases in cores P5, CD3826 and CD3827, but not in CD3822 where the increase in $CaCO_3$ MAR never exceeds 2.5 times the modern value. However if one takes an early Holocene figure of $CaCO_3$ MAR at around 10 ka, in this core, then the increase during stage II would be greater than 2.5 times the interglacial value and must therefore be due, at least in part, to productivity. In core CD3826, increases above the value assignable to preservation changes of 255 mg/cm^2/kyr occur in all glacial stages except stage IV. There are also spikes above the preservation level at 328 ka in this core, coincident with the rapidly accumulating ash layer L, and during stage III. One must always maintain a healthy respect for the many processes which act to make each core site unique. However, these findings indicate that although dissolution of $CaCO_3$ may be an important, and often the dominant, factor influencing $CaCO_3$ concentration, biological productivity is an important influence during glacial periods. Thus, from these results and from conclusions draw in previous chapters, it is reasonable to assume that the spikes in the fluxes of C-org, SiO_2 and ExBa during glacial times are similarly associated with increases in surface water productivity.

Should productivity be important in controlling $CaCO_3$ concentrations during glacials, what are the implications for carbon cycling between ocean and atmosphere? As discussed above, although the increase in productivity and decrease in atmospheric CO_2 during glacial periods appears irrefutable; which, if either, was the cause and which the result, continues to foster much debate. Pedersen et al., (1992),

in a study of the strength and timing of productivity pulses in the Panama basin using core AII54-25PC, conclude that the potential influence that increased productivity at low latitudes could have on atmospheric CO_2 concentrations has been generally overestimated.

Spectral analysis of the variations in the records of biogenic tracers has been employed to study the relative timing of the changes in each component (Lyle et al., 1988; Rea et al., 1991; Pedersen et al., 1992). However the mathematical programs required for such analysis require large data sets to produce statistical reliability. Core CD3826 is the longest core analysed for this study with 110 data points. Even the most rudimentary spectral analysis program seem to require over 130 data points, of equal depth intervals, in order to provide reliable confidence limits. Thus, spectral analysis in this form is not feasible on the cores analysed for this thesis. However core AII54-25PC has approximately 300 data points (Pedersen et al., 1992). But although cores CD3826 and AII54-25PC have been shown to be geochemically similar, direct comparison of the spectral frequencies is not considered to be viable. Furthermore, spectral analysis is critically dependent on many factors (Patience and Kroon, 1991) which, by their very nature, can make inter-core comparisons very difficult even with large data sets.

7.4 Conclusions

1. Glacial times are periods of increased fluxes of $CaCO_3$, SiO_2, C-org and Excess Ba in all cores except during stage IV in core CD3826.
2. The productivity pulse during the glacial stages undergoes an evolutionary process whereby the SiO_2 and Excess Ba tend to increase at the beginning of the glacial, only to be replaced by $CaCO_3$ towards the end of the stage when productivity is thought to be at a maximum.
3. From comparison of modern productivity values with temporal variations in $CaCO_3$ MARs, it is apparent that euphotic zone productivity, and not just preservation, has an important influence on the $CaCO_3$ signal, at least during glacial times.
4. The records of SiO_2, C-org and Excess Ba MARs are also thought to be strongly influenced by productivity changes.
5. Whether external forcing of climatic change causes, or is enhanced by, productivity variations continues to be ambiguous.

CHAPTER 8

THE CONTRASTING CHEMISTRIES OF THE HALOGENS IODINE AND BROMINE AND THEIR POTENTIAL AS PROXY INDICATORS OF PALAEOPRODUCTIVITY

8.1 Introduction

This chapter seeks to evaluate the potential of Iodine (I) and Bromine (Br) to record variations in palaeoproductivity. Their spatial and temporal distribution is studied together with their intimate association with organic carbon. The diagenetic behaviour with respect to their relationship to organic carbon (C-org) in these sediments will also be assessed.

The halogens iodine and bromine are known to be intimately associated with organic matter in marine oxic sediments; a subject that has received considerable attention from many authors (Gulyayeva and Itkina, 1962; Shishkina and Pavlova, 1965; Bowen, 1966; Bojanowski and Paslawska, 1970; Price et al., 1970; Price and Calvert, 1977; Harvey, 1980; Pedersen and Price, 1980; Wakefield, 1981; Elderfield et al., 1981; Mayer et al., 1981; Ullman and Aller, 1980, 1983, 1985). In the case of I, this association is critically dependent on the redox state of the surface sediments and bottom waters. In oxic surface sediments the concentration of I and Br present is directly proportional to the concentration of organic carbon (C-org) in the sediment (Price and Calvert, 1973; Pedersen and Price, 1980). However, under anoxic conditions the halogen to C-org association breaks down (Wong and Brewer, 1977). Although the I/C-org and Br/C-org ratios in marine surface sediments are relatively constant, diagenesis as a result of organic matter degradation results in a decrease of both halogens relative to C-org as depth in the sediment column increases. This decrease in solid phase I with depth (Price et al., 1970) is matched by a comcomitant increase in total dissolved I in pore waters (Shishkina and Pavlova, 1965; Wakefield and Elderfield, 1985; Kennedy and Elderfield, 1987a), a relationship illustrated in figure 8.1 which shows the interconversion of iodine species (I and IO_3) with depth. Near shore sediments are enriched in both halogens relative to the open marine environment (Kennedy and Elderfield, 1987b).

The relative reactivities of I and Br has been linked to associations with different organic constituents in the sediment. Harvey (1980) proposed that I was associated with nitrogenous organic matter (polypeptides and chitin) as this material has been shown to be more labile during degradation (Gordon, 1971; Suess and Muller, 1980; Grudmanis and Murray, 1982). As Br exists in several chemical forms its mechanism for uptake and removal are thought to be quite different to that of I (Mayer et al., 1981). However, Pedersen and Price (1980) suggest a mechanism for uptake and removal common to both I and Br.

Iodine

Iodine in sediments is present primarily in its electro-positive state as N-iodoamides (Harvey, 1980) whereas in sea-water it is biophilic existing as both iodate (IO_3^-) and iodide (I^-) (Goldschmidt, 1954) although the latter species is more thermodynamically unstable under oxidising conditions (Shishkina and Pavlova, 1965). Equation 8.1 summarises the reversible reaction between the two species:

Equation 8.1 $$IO_3^- + 6H^+ + 6e^- \Rightarrow I^- + 3H_2O$$

(pE = +12.5; pH = 8.1)

after Wong and Brewer, (1977)

I is known to exist in several oxidation states in natural waters and, consequently, its chemistry has been extensively studied (Barkley and Thompson, 1960; Tsunogai, 1971; Trusedale, 1975; Elderfield and Trusedale, 1980). Generally, I parallels nutrient profiles in seawater despite being only slightly depleted in surface waters (Elderfield and Trusedale, 1980; Wong and Brewer, 1974) and the primary source (up to 80%) for I in sediments is not organic matter but seawater from which iodine is sorbed onto degraded organic material at the sediment surface (Price and Calvert, 1973). Plankton seston are believed to be the locus for this process possibly by a mechanism similar to that employed by macroalgae (Shaw, 1959, 1962). The efficiency of this process must then be regulated by the varying environmental conditions under which the sediments were deposited. Any textural/grain size relationship with iodine as suggested by Vinogradov (1939) tend to be masked by the iodine-C-org association.

In marine organisms, I uptake under oxidising conditions may occur as a result of enzymatic processes on cell surfaces, whereas during anoxia a lack of surface enzymatic reactions inhibits iodide sorption and iodine concentration in sediments are little greater than in living materials. Table 8.1 summarised some I contents in the marine environment. In anoxic conditions dissolved iodine is not enriched in pore waters during burial with the result that iodine concentrations at depth are virtually the same as at the surface (Price and Calvert, 1973). According to Francois (1987) surficial enrichment of I in sediments could result from direct reduction of iodate to electropositive iodine species (I_2 or HOI) by sedimentary humic compounds followed by electrophilic substances on organic molecules. Also, the humic-mediated reduction-uptake mechanism has the potential to account for much of the iodine

enrichment in surface sediments and can explain the absence of such enrichment in anoxic sediments (Price and Calvert, 1977). Finally, it has been shown that Fe-oxyhydroxides readily take up iodine species from solution (Music et al., 1980; Ullman and Aller, 1985). Anoxic sediments generally have I/C-org ratios of around 20-30 $\times 10^{-4}$ whereas in oxic open marine conditions the I/C-org ratios are around 250 $\times 10^{-4}$ (Price and Calvert, 1973).

Table 8.1 Iodine in the Marine Environment

Sediment/Organism description	I (ppm)	I/C-org $\times 10^{-4}$	Reference
Sea water	-------	1.0	1
Plankton	-------	1.0-2.8	1
Faecal pellets	-------	1.6-3.1	2
Pacific Red clay	29	106	3
Pacific Grey clay	202	348	3
N.W. Pacific	21-398	70-260	4
Peru Margin	37-610	80-242	4
S.W. Africa organic rich diatom ooze	96-1990	16-252	5
Panama basin hemipelagics	76-801	395	6

1 = Elderfield and Truesdale (1980); 2 = Spencer et al., (1978); 3 = Shishkina and Pavlova (1965); 4 = Pavlova and Shishkina (1973); 5 = Price and Calvret (1973); 6 = Pedersen and Price (1980).

Kennedy and Elderfield (1987a, 1987b) show that iodine is actively and rapidly recycled at, or immediately below, the sediment water interface. Iodine appears to be released initially in surface sediments from decaying, freshly deposited organic matter as thermodynamically unstable iodide (Figure 8.1). In the presence of O_2, this species is oxidised to I_2 and then either reacts with organic matter or is hydrolised to HOI, which is readily sequestered by humic compounds. Subsequent post burial degradation of this organic fraction must must account for the commonly observed decrease in I/C-org ratio with depth and would support an upward flux of dissolved

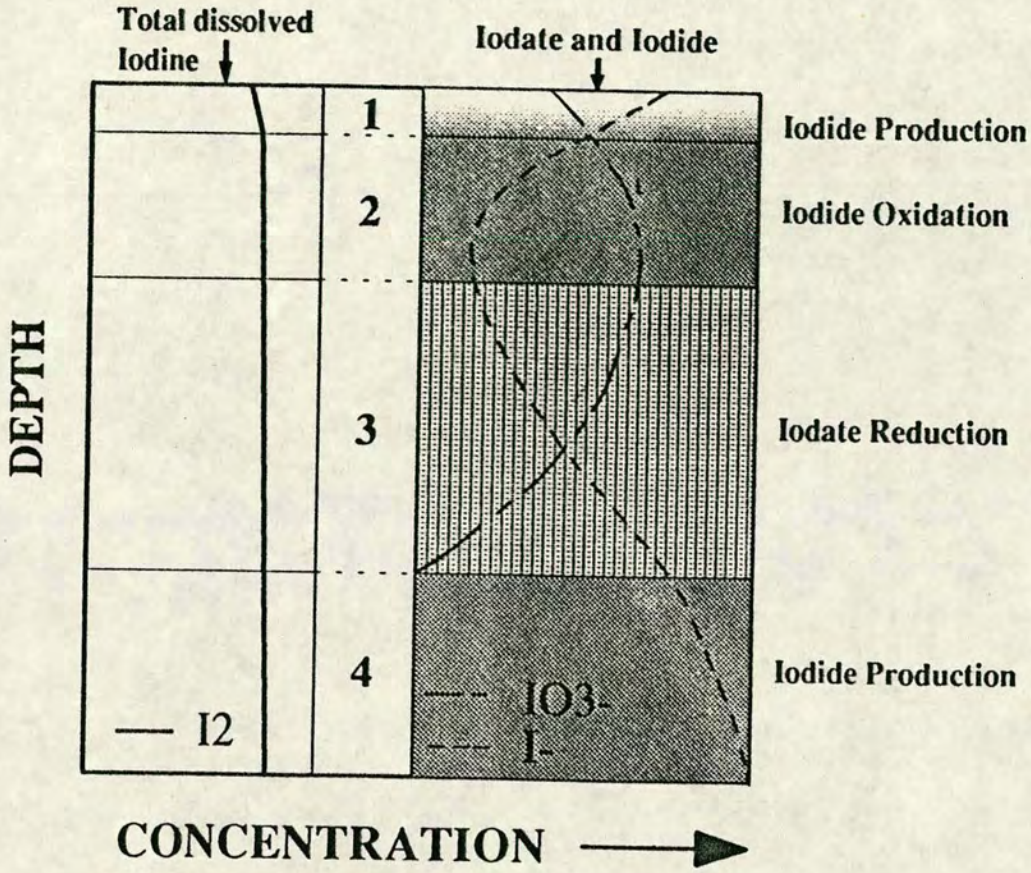

Figure 8.1 Diagrammatic representation of the interconversion of iodine species with depth in the sediment column. Zone 1: iodide production; Zone 2: iodide oxidation; Zone 3: iodate reduction; Zone 4: iodide production. The downward pointing arrows indicate sea-water composition. Adapted from Kennedy and Elderfield, (1987a).

iodine (Shimmield and Pedersen, 1990). Such a recycling mechanism is critically dependent on the C-org accumulation rate and bulk sedimentation rate (Kennedy and Elderfield, 1987a).

Bromine

In contrast to iodine, high levels of bromine may be present in both oxic and anoxic sediments although some of the methods of concentration are thought to be similar to that of iodine enrichment in oxic sediments (Price and Calvert, 1977). However, Mayer et al. (1981) suggest that Br is concentrated by a form of residual enrichment. Unlike iodine, bromine in sediments exists in many different chemical forms (Harvey, 1980). Br is linearly correlated with C-org regardless of the redox state of the overlying water (Price and Calvert, 1977; Mayer et al., 1981; Malcolm and Price, 1984). Kylin (1929) reports high concentrations of Br in many species of Rhodophyta, where the element is sequestered from seawater and used in synthesis of a variety of brominated phenolic compounds that have chemical defense, including antibacterial properties (Fenical, 1975).

Analytical methods are outlined and results given in appendices A.5 and C.7 respectively.

8.2 Results

8.2.1 Iodine

Temporal variations in solid phase I in all cores show the characteristic rapid reduction in I with depth (figure 8.2a and 8.3). All CD38 cores also show an overall relatively gradual decrease in I downcore after an initial sharp drop in the surface sediment. Cores CD3822, CD3826 and CD3827 show marked increases in I content during stage II coincident with increases in C-org and, possibly, palaeoproductivity (chapter 6). Eventual equilibrium is reached in cores at varying ages below which I contents remain relatively constant. Table 8.2 shows the mean, range and surface values for halogens and C-org. Generally I contents covary with organic carbon contents except in core P5 which has mean I and C-org contents of 56.2ppm and 0.625% respectively; compared to core CD3822 which has a mean I of only 21.5ppm but a high mean C-org of 1.25%.

Figure 8.2 Temporal variations in I [(a), ppm salt free], Br [(b), ppm salt free], I/Br (c), I/C-org × 10^{-4} (d) and Br/C-org × 10^{-4} (e) versus age (ka) from core P5. Shaded region represents glacial stage II (24-12 ka).

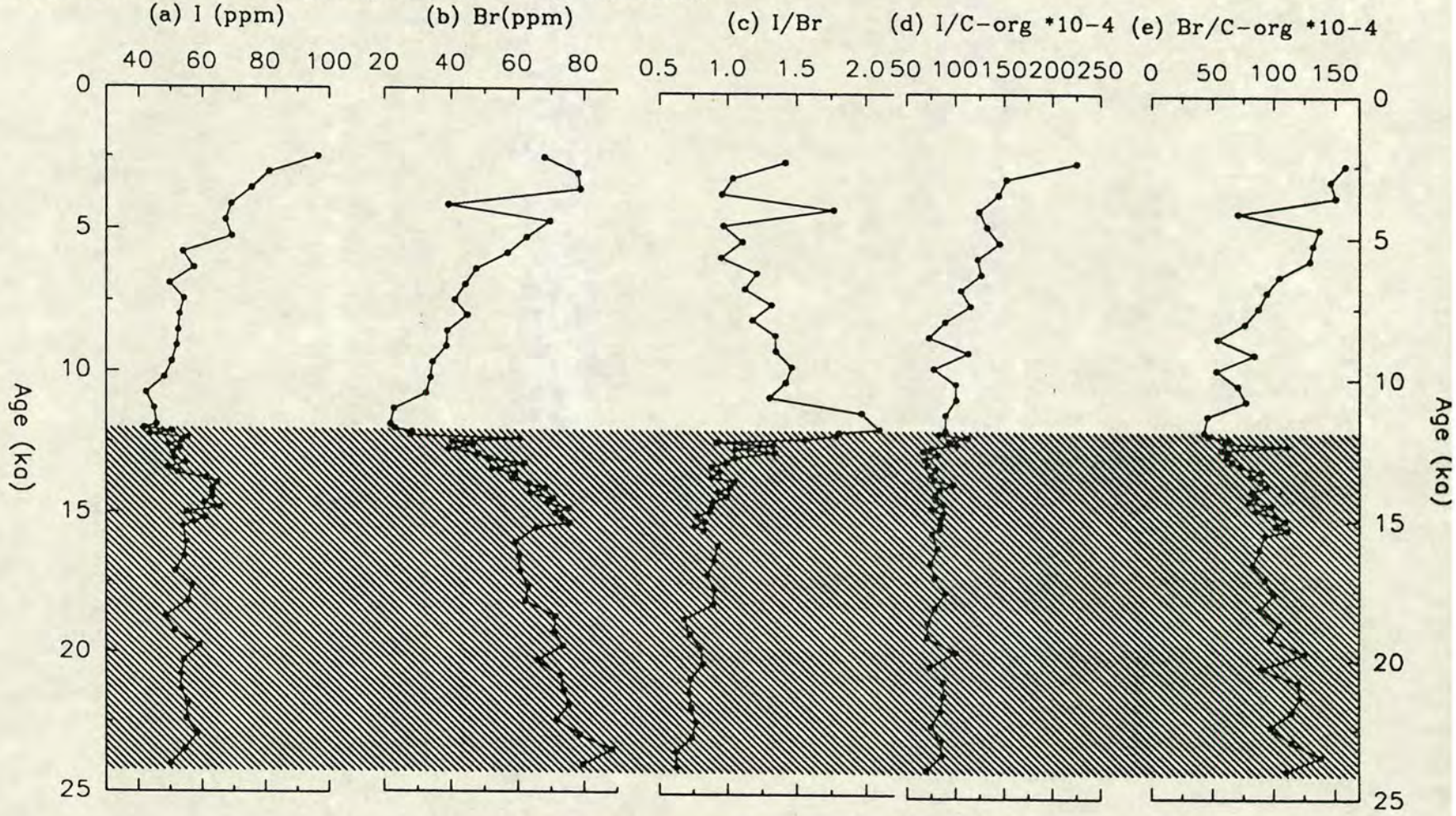

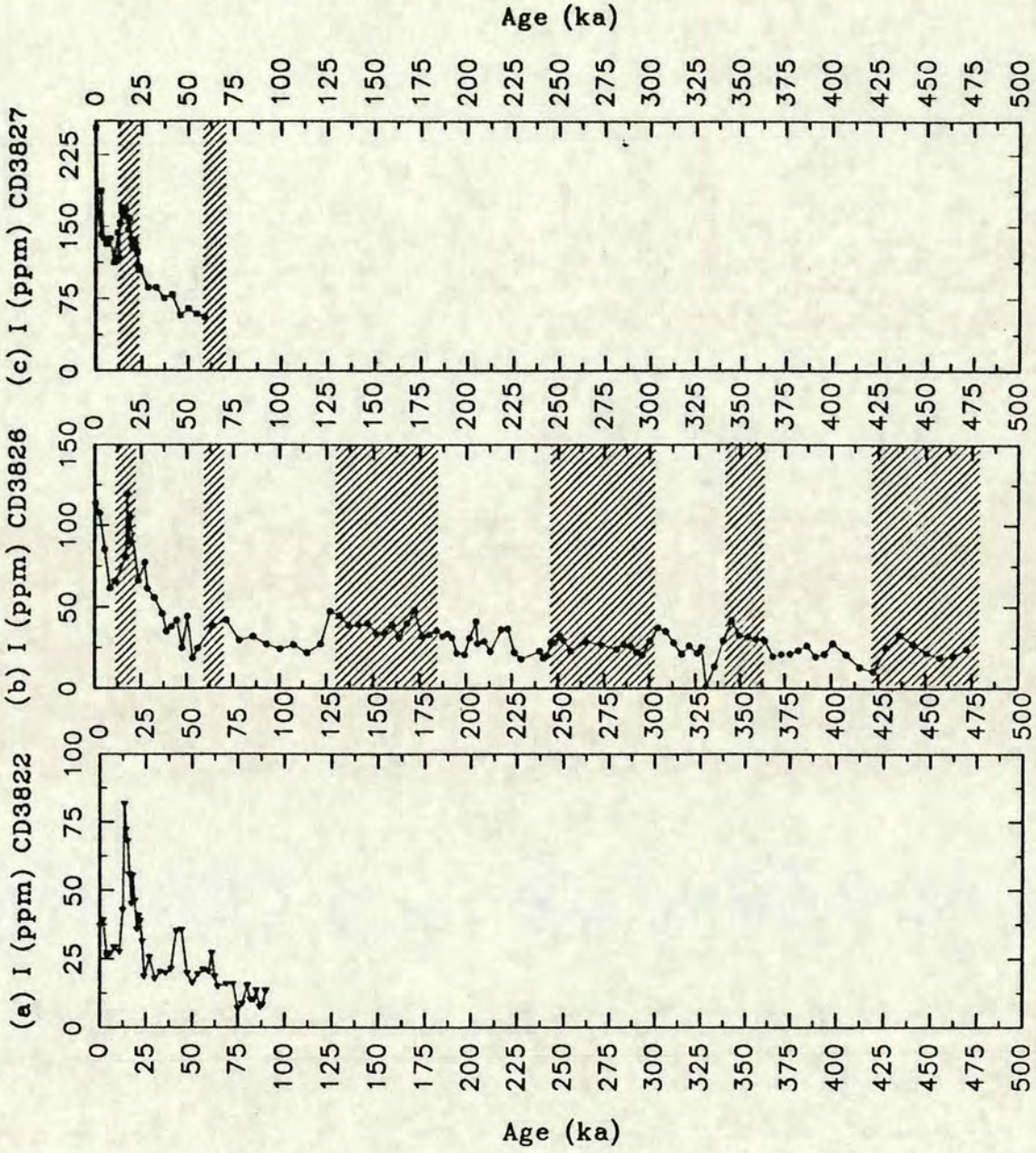

Figure 8.3 Temporal variations in the concentration of I (ppm salt free) in cores CD3822 (a), CD3826 (b) and CD3827 (c). Note the different scales for I. Shaded regions represent glacial stages II, IV, VI, VIII, X and XII.

TABLE 8.2 HALOGEN AND C-ORG AVERAGE AND SURFACE VALUES FROM CORES STUDIED IN THIS THESIS

MEAN

Core	I (ppm)	Br (ppm)	I/Br	C-org (Wt.%)	I/C-org ($*10^{-4}$)	Br/C-org ($*10^{-4}$)
P5	56.2	57.7	1.06	0.625	93.194	92.917
CD3814	2.2	0.0	-----	------	--------	--------
CD3822	21.5	26.3	0.82	1.250	18.702	22.439
CD3826	34.7	60.1	0.63	1.397	24.865	43.661
CD3827	126.4	152.5	0.86	3.048	40.205	46.443

SURFACE SAMPLE

Core	I (ppm)	Br (ppm)	I/Br	C-org (Wt.%)	I/C-org ($*10^{-4}$)	Br/C-org ($*10^{-4}$)
P5(8-10)	96.4	68.0	1.42	0.430	224.186	158.080
CD3814	7.6	1.5	5.12	------	---------	---------
CD3822	37.0	17.3	2.14	0.876	42.237	19.783
CD3826	113.7	93.9	1.21	1.493	76.155	62.871
CD3827	252.7	182.1	1.39	3.319	76.137	54.862

RANGE

Core	I (ppm)**	Br (ppm)**	I/Br	C-org (Wt.%)	I/C-org ($*10^{-4}$)	Br/C-org ($*10^{-4}$)
P5	42-96	22-88	0.6-2.1	0.42-0.81	66.6-224.2	42.7-158.1
CD3814	0-11	0-4	0.0-5.7	--------	---------	----------
CD3822	0-81	0-98	0.0-4.2	0.43-2.66	0.0-63.5	0.0-91.6
CD3826	1-119	11-194	0.1-2.2	0.24-2.50	4.1-84.1	7.84-124.5
CD3827	56-253	77-236	0.4-1.4	1.82-4.85	17.3-76.1	30.6-66.2

** values rounded off to nearest whole number for clarity

From the surficial maximum in core P5, I values reach a minimum around 12 ka before increasing slightly throughout the earlier part of stage II with a notable increase at around 14 ka (Figure 8.2a). I contents in core CD3814 were generally very low with mainy negative values (assumed to be zero). As a result, variations in I content in core CD3814 are not discussed.

The characteristic surface enrichment in I is not well developed in core CD3822 (figure 8.3a), perhaps because some of the surface sediment may have been lost during coring (appendix A.1) although a distinct Mn spike was observed in the surface sediments from this core (Chapter 9) which usually characterises surface sediments. A sharp increase in I content is present during stage II.

Core CD3826 shows a gradual decrease in I contents with depth but is interrupted by slight enrichments during glacial periods VI, X and XII (Figure 8.3b). Core CD3827 contains the highest I contents with a well defined decrease with depth to around 50ppm at 60 ka interrupted by an increase during stage II (figure 8.3c).

8.2.2 Bromine

Bromine occurs in similar contents as iodine (Table 8.2) and the temporal variations (figures 8.2b and 8.4) are similar to those of the I profiles. Br curves tend to parallel C-org profiles. Core CD3822 however, appears to have unusually low Br concentrations for the percentage of C-org (figure 8.4a). Cores P5, CD3826 and CD3827 all show surface enrichments in contrast to core CD3822 where Br values remain relatively constant during the Holocene. Core CD3814 registered mainly negative values after correction for the Br contribution from sea salt (Appendix A.7) and it was assumed that virtually no Br is present in this core.

Br, like I, increases in cores CD3822, CD3826, CD3827 and P5 during glacial stage II, but unlike I, an equilibrium base level for Br is seldom reached. Indeed, cores P5, CD3822, CD3826 and CD3827 all show visible enrichments at depth. Increases in Br in core CD3826 occur during glacial stages II (24ka), VI (130ka, 170ka), X (340ka), XII (435ka) and in interglacial stage VII (figure 8.4b). Between 472-128 ka there is a slight overall increase downcore. In cores CD3822 and CD3827 older peaks occur between 40-50 ka and at 30 ka respectively. No marked change was observed over the Pliocene-Pleistocene boundary at 450cm depth in core CD3822 (see appendix

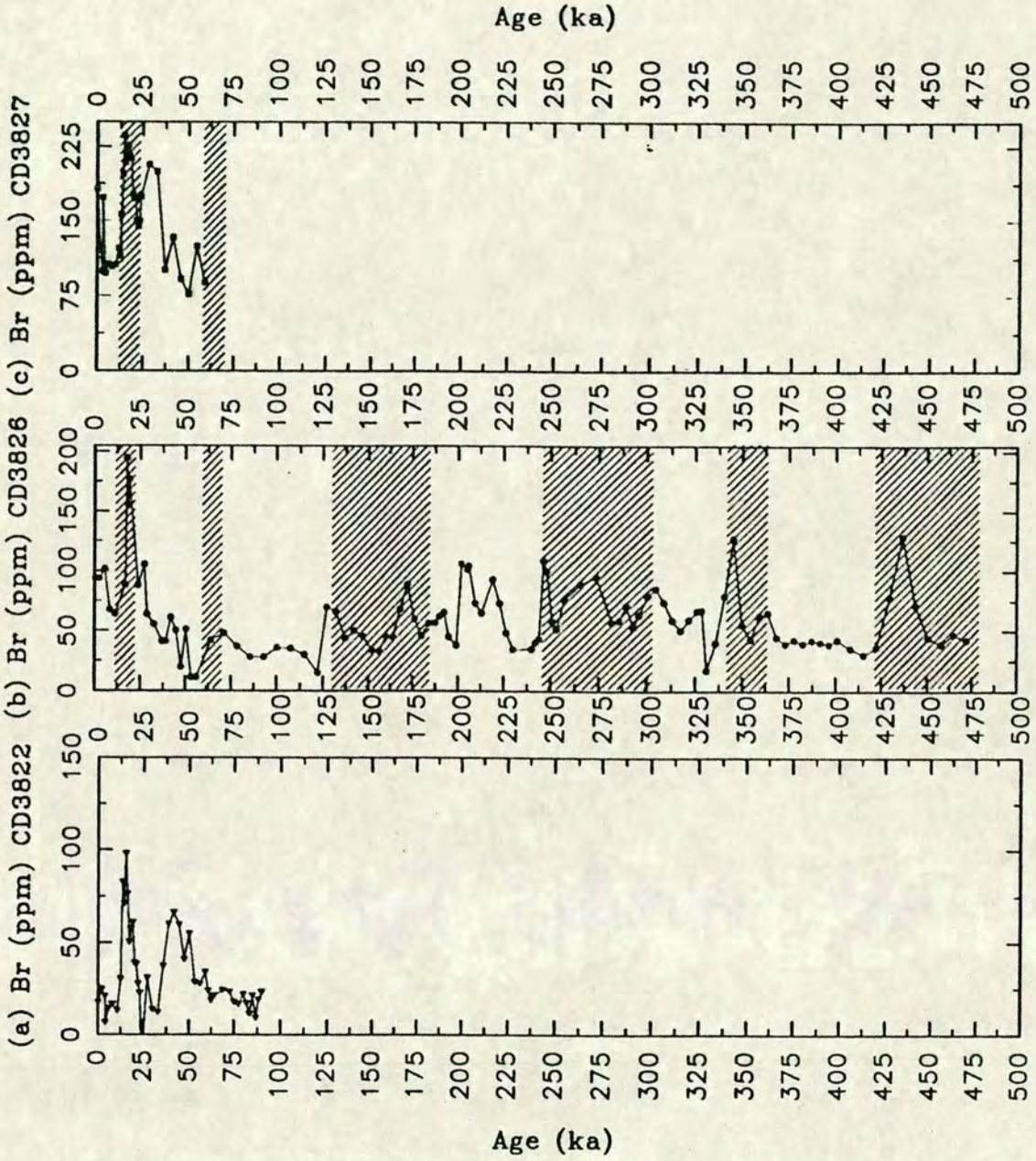

Figure 8.4 Temporal variations in the concentration of Br (ppm salt free) in cores CD3822 (a), CD3826 (b) and CD3827 (c). Note the different scales for Br. Shaded regions represent glacial stages II, IV, VI, VIII, X and XII.

C.7.1). Br contents in core P5 drop from surface levels of around 80ppm to approximately 20ppm at 12 ka before increasing to over 80ppm at 24 ka (figure 8.2b).

I and Br show a statistically positive correlation in cores CD3822 and CD3826 and, a strong positive correlation between cores CD3827 and P5 (table 8.3). Table 8.3 also shows that in cores CD3822, CD3826 and P5, Br is more highly correlated with C-org than I is with C-org. This is in direct contrast with previous authors (eg Price and Calvert, 1973; Pedersen and Price, 1980). The temporal variations in I/Br ratios are shown in figure 8.3c and 8.5. The ratios show little variation which illustrates the chemical similarity of I and Br. A trait common to all the I/Br profiles is a general decrease downcore which indicates that I is being preferentially lost relative to Br from the solid phase during burial diagenesis. This is most pronounced in core CD3827 (figure 8.5c). However, the overall decrease is interrupted by several positive and negative spikes (eg at 55 ka in CD3826) possibly relating to anomalous analysis.

Table 8.3 Statistical analysis of halogen and C-org data. n = number of samples; r = coefficient of correlation that is statistically significant at ≥ 95% confidence limits.

	CD3822				CD3826		
n=63, r=0.665	I			n=111, r=0.626	I		
n=63, r=0.665	0.797	Br		n=111, r=0.626	0.668	Br	
n=62, r=0.666	0.088	0.118	C-org	n=110, r=0.628	0.400	0.444	C-org
	CD3827				P5		
n=33, r=0.719	I			n=57, r=0.672	I		
n=33, r=0.719	0.455	Br		n=57, r=0.672	0.507	Br	
n=32, r=0.722	0.055	-0.082	C-org	n=57, r=0.672	-0.014	0.468	C-org

8.2.3 Variations in the I/C-org and Br/C-org ratios

I/C-org ratios

The I/C-org ratio in core P5 is 224×10^{-4} at the surface and decreases during the Holocene to around 75×10^{-4} during stage II (figure 8.2d) which illustrates the diagenetic pathways of I loss relative to C-org with burial. In cores CD3826 and

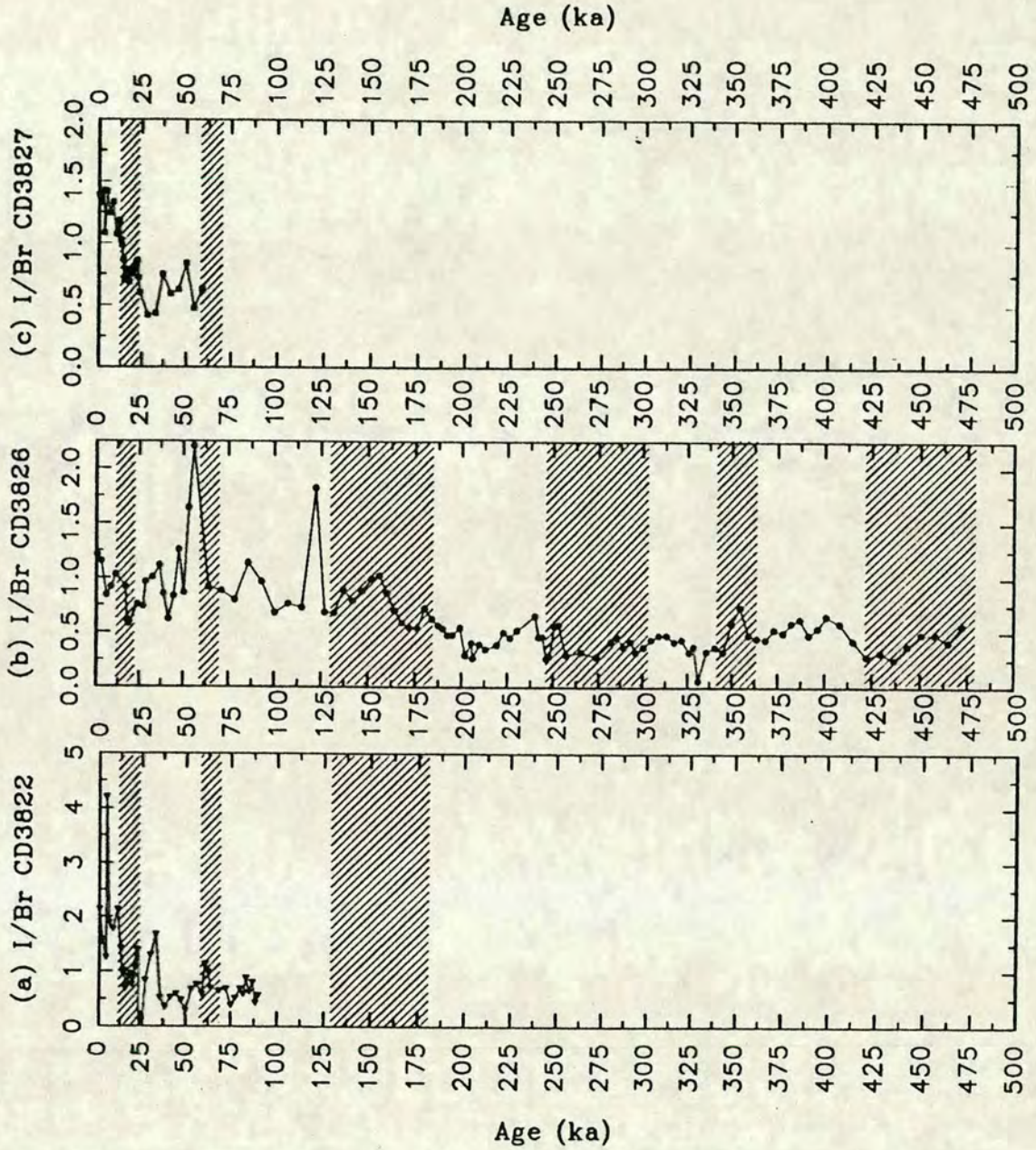

Figure 8.5 Temporal variations in the I/Br ratio in cores CD3822 (a), CD3826 (b) and CD3827 (c). Note the different scales. Shaded regions represent glacial stages II, IV, VI, VIII, X and XII.

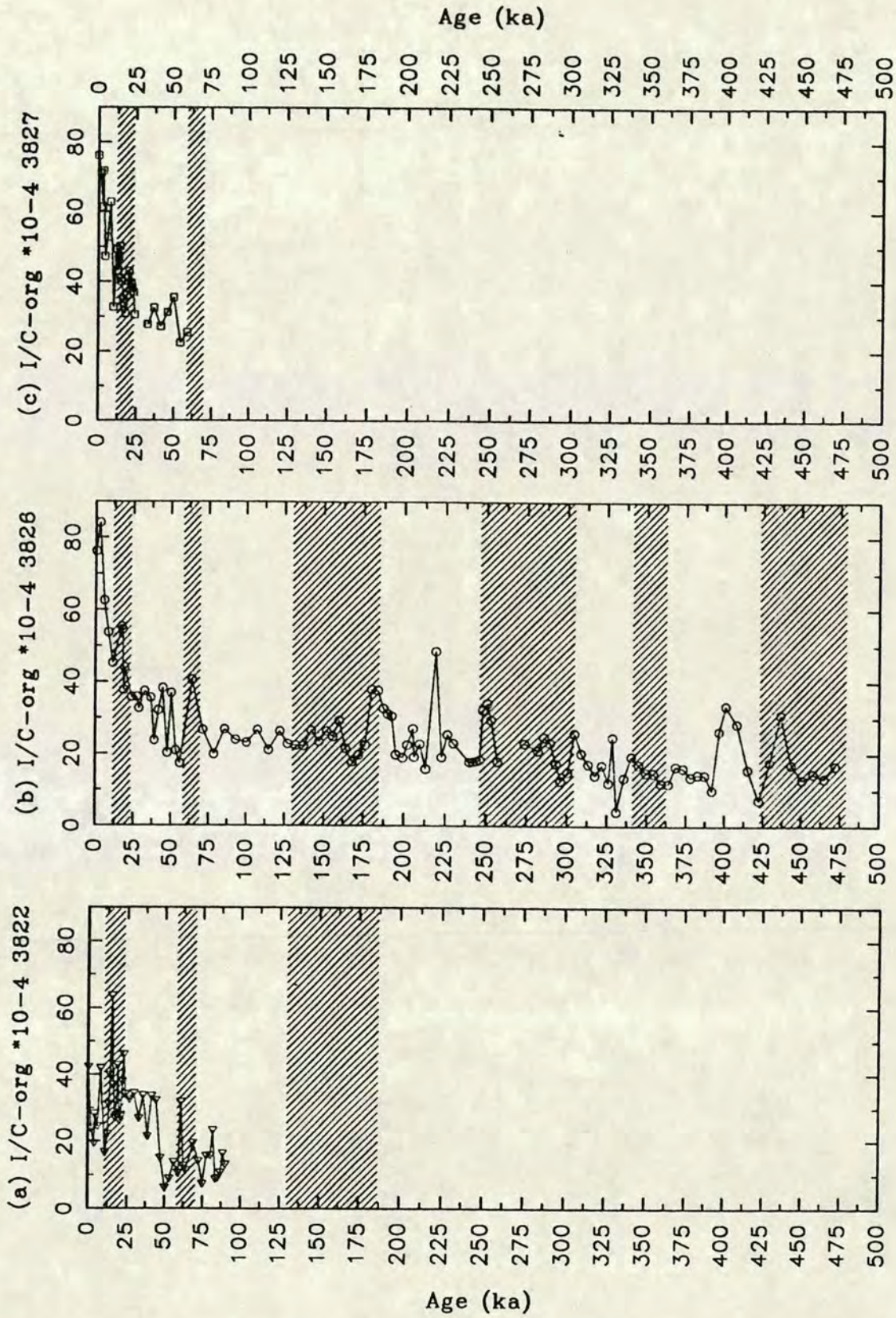

Figure 8.6 Temporal variations in I/C-org x 10^{-4} in cores CD3822 (a), CD3826 (b) and CD3827 (c). Shaded regions represent glacial stages II, IV, VI, VIII, X and XII.

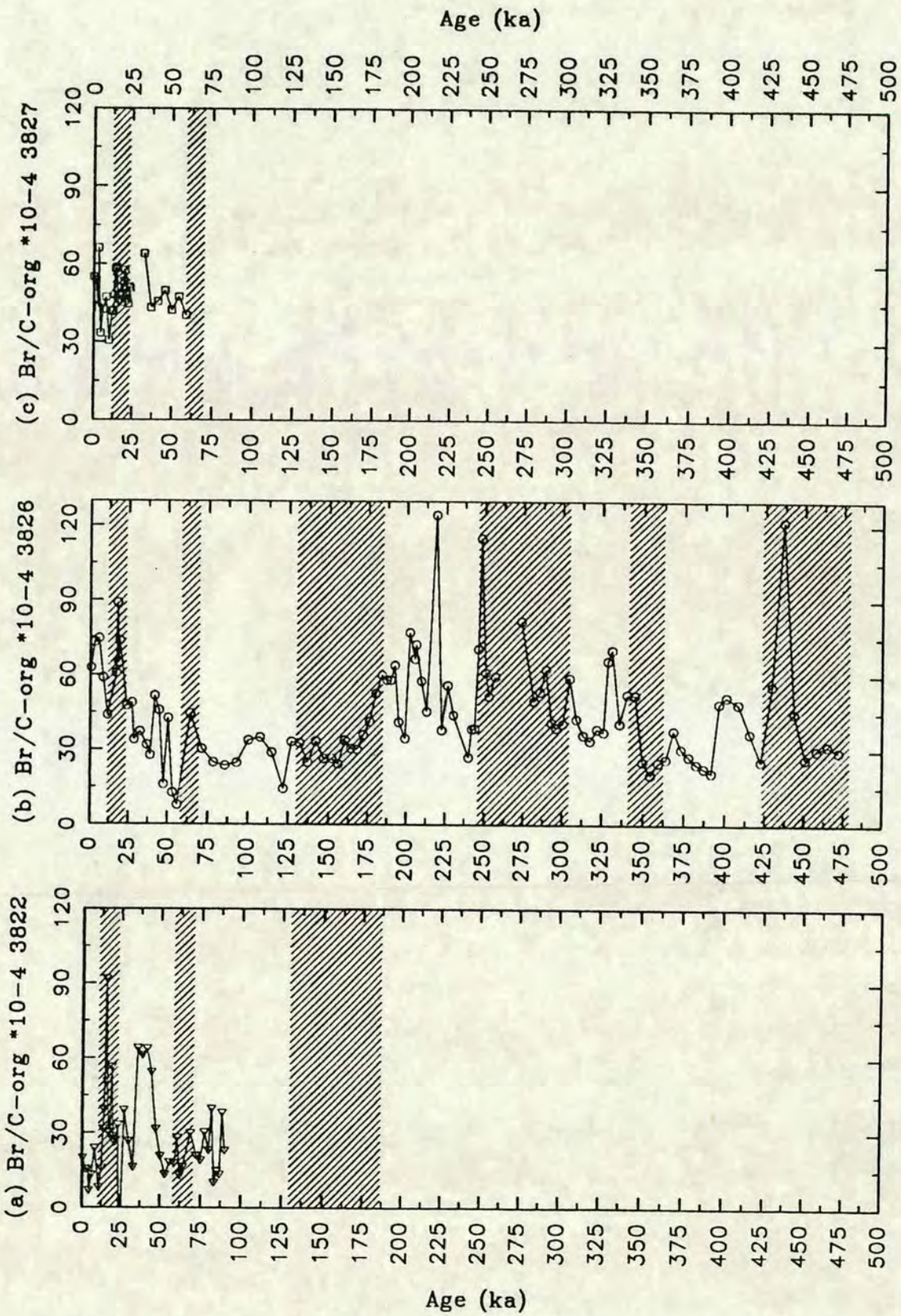

Figure 8.7 Temporal variations in Br/C-org $\times 10^{-4}$ in cores CD3822 (a), CD3826 (b) and CD3827 (c). Shaded regions represent glacial stages II, IV, VI, VIII, X and XII.

CD3827 the I/C-org ratio decreases rapidly during the Holocene and more gradually throughout the rest of the core whilst being punctuated by slight increases during stage II (figure 8.6b, 8.6c). Core CD3822 is anomalous in that there is no Holocene increase and the increase during stage II to around 40, continues into stage III before dropping off to around 10 between 50-90 ka (figure 8.6a).

Br/C-org ratios

The Br/C-org ratio in core P5 is very similar to that of I/C-org with a Holocene increase towards the surface of the core being preceded by a gradual decrease during stage II (8.3e). Core CD3822 shows a Holocene decrease to the minimum values at the surface and an increase during stage II and at 40 ka (figure 8.7a). Cores CD3826 and CD3827 both display Holocene enrichments and spikes during stage II (figure 8.7b and 8.7c respectively). The remainder of core CD3826 shows an overall increases in the Br/C-org ratio which may be due to Br being less labile during diagenesis relative to other organic material (Pedersen and Price, 1980).

8.3 Conclusions and Palaeoclimatic Implications

1. I and Br contents in the surface sediments are consistent with deposition in anoxic environment.
2. I and Br are shown to be closely associated with each other and with organic carbon.
3. I concentrations display the characteristic diagenetic decrease with depth in the sediment column in cores P5, CD3822, CD3826 and CD3827.
4. Br profiles also show decreases in the upper section of the cores but the curves tend to be more noisy and even increase slightly downcore in core CD3826.
5. Both I and Br show increases during glacial times although Br also increases in some interglacial periods.
6. Slight changes in the I/Br ratio illustrate the relative reactivities of the two elements: Br being less labile during diagenesis.
7. Statistical analysis showed that there is generally a stronger correlation between Br and C-org than between I and C-org, in contrast to previous work (eg Pedersen and Price, 1980).
8. I/C-org ratios show the characteristic rapid decrease during the Holocene and more gradual decreases over the past 500 kyr in core CD3826 consistent with the effects of burial diagenesis.

9. Br/C-org ratios are more noisy than the I/C-org ratios and often show increases over time (downcore) consistent with Br being less labile than other organic matter.
10. Although I and Br are closely associated with C-org, their diagenetic mobility renders them unreliable as proxies for palaeoproductivity.

CHAPTER 9

THE GEOCHEMISTRY OF MANGANESE AND OTHER REDOX SENSITIVE ELEMENTS

9.1 Introduction

This chapter documents the distribution of Mn, Mo, U, Ce and, the trace metals Zn, V, Ni, and Cu. It relates these to glacial-interglacial cyclical changes in organic carbon (C-org) content and interprets the results in terms of redox conditions. Finally, it attempts some preliminary palaeoenvironmental reconstruction.

Manganese, together with Fe, forms oxyhydroxide phases in the surface layers of the sediment which are very important in controlling trace metal contents in the marine environment (Finney et al., 1988). Mn has been extensively studied, especially with respect to its behaviour under varying redox conditions (Lynn and Bonatti, 1961; Calvert and Price 1977; Heath and Lyle, 1981; Sawlan and Murray, 1983; Graybeal and Heath, 1984; Thomson et al., 1984, 1986). Such work is reviewed by Shimmield and Pedersen, (1990). Mn (IV) oxide is thought to dissolve upon burial in reducing sediments releasing Mn (II) into the pore waters which slowly migrates upwards, only to become enriched in surficial oxidised sediments by reprecipitation mainly as solid phase Mn (IV). Consequently, a sharp decrease in solid phase Mn oxide with depth in surficial sediments is accompanied by a large increase downcore in the dissolved pore water Mn (II). Such cycling processes have as their driving force, the diagenetic breakdown of organic matter (dominantly carbon), and are potentially the mechanism by which other redox sensitive metals become redistributed and concentrated within the sediment column after burial.

Furthermore, the reliance of Mn on redox states, renders it a potentially sensitive tracer of past redox conditions in the oceans. Large downcore increases in solid phase Mn in the Quaternary have been reported by several authors in the central and eastern equatorial Pacific (Berger et al., 1983; Finney et al., 1988; Mangini, 1988), but the precise mechanism allowing sediments to have high Mn contents continues to be ambiguous.

Analytical methods and tabulated results are presented in appendices A.5 and, C.4 and C.5 respectively.

9.2 Mn distribution

Temporal variations in Mn and C-org in the cores studied in this thesis are shown in figure 9.1-9.3. The mean (and range of) Mn contents from each core are shown in

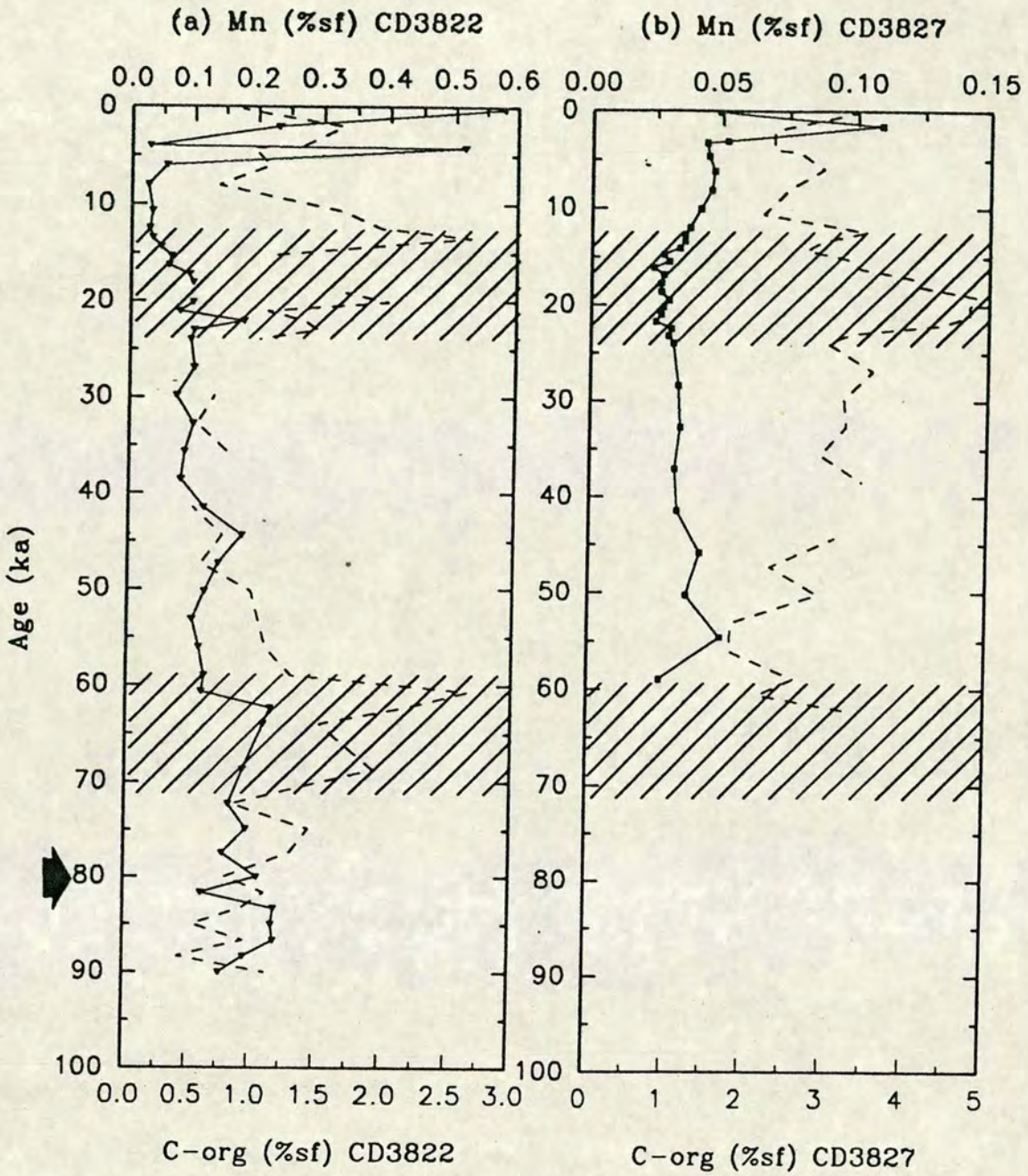

Figure 9.1 Temporal variations in Mn (Wt.% SF; solid symbols, solid line) and C-org (Wt.% SF; dashed line) in, (a) core CD3822 and, (b) core CD3827. Note the surficial enrichment in Mn complicated in core CD3822 by the overlap of the pilot and piston cores. Note also the increase in C-org during stage II in both cores and, in stage IV in core CD3822. These increases are not paralleled by increases in Mn. Shaded regions represent glacial stages II and IV. Arrow indicate the position of a local ash layer (82ka).

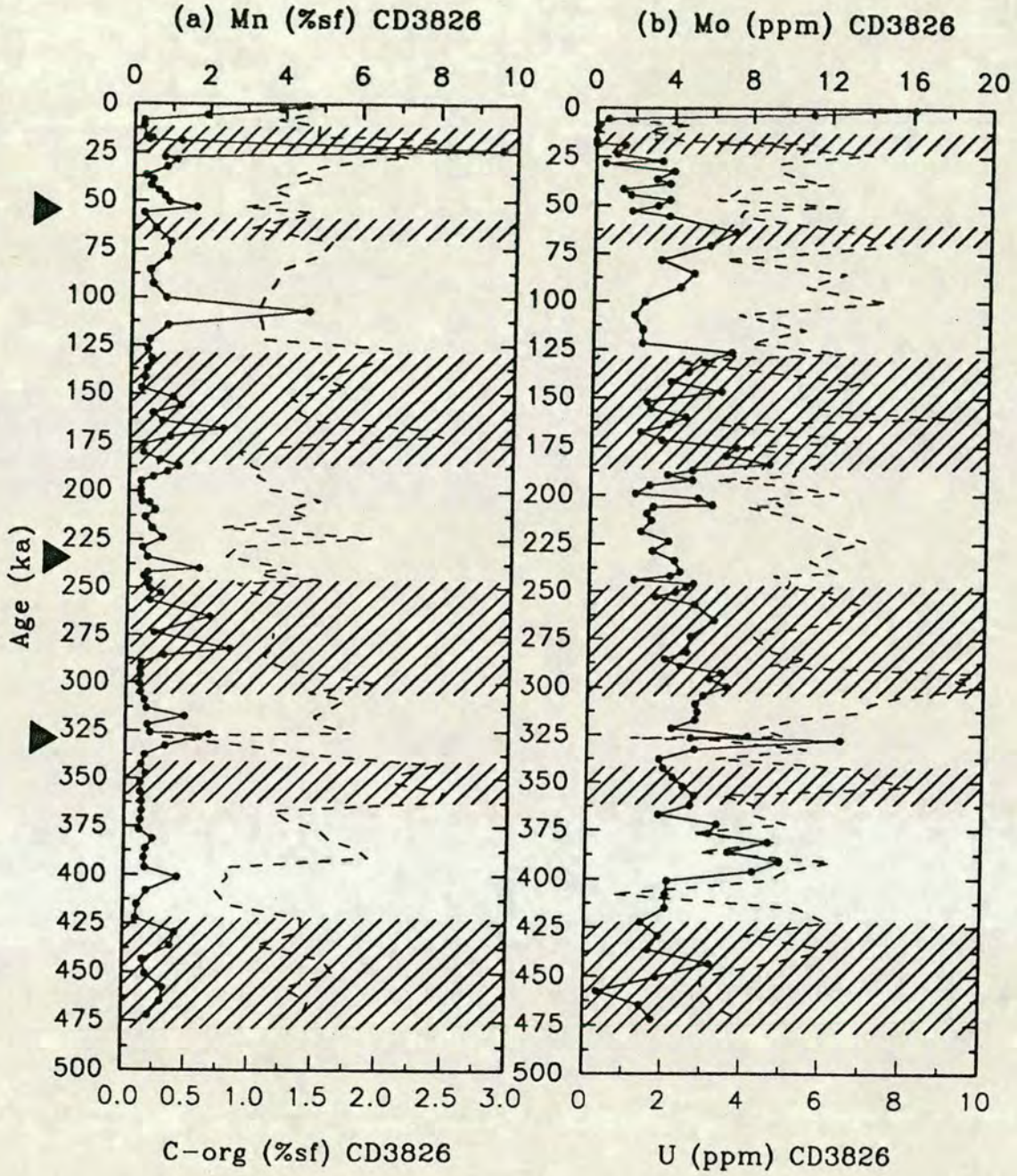

Figure 9.2 Temporal variations in Mn (Wt.% SF), C-org (Wt.% SF), Mo (ppm SF) and U (ppm SF) in core CD3826. (a) Mn (solid circles, solid line) and C-org (no symbols, dashed line). (b) Mo (solid circles, solid line) and U (no symbols, dashed line). Note the surficial enrichment of Mn and Mo; the large subsurface increases in Mn; the slight overall increases in Mo downcore and, the similarity of the C-org and U profiles. Shaded regions represent glacial stages II, IV, VI, VIII, X and XII. Triangles indicate the position of ash layers D (56ka), L (234ka) and K (328ka).

Figure 9.3 Temporal variations in, (a) Mn (Wt.% SF), (b) Mn/Al, (c) U (ppm SF) and, (d) C-org (Wt.% SF) in core P5. Note the lack of surficial enrichment or downcore variation in Mn except for a slight increase at approximately 12 ka. Note also the close similarity of the C-org (d) and U (c) curves. Shaded region represents glacial stage II (12-24 ka).

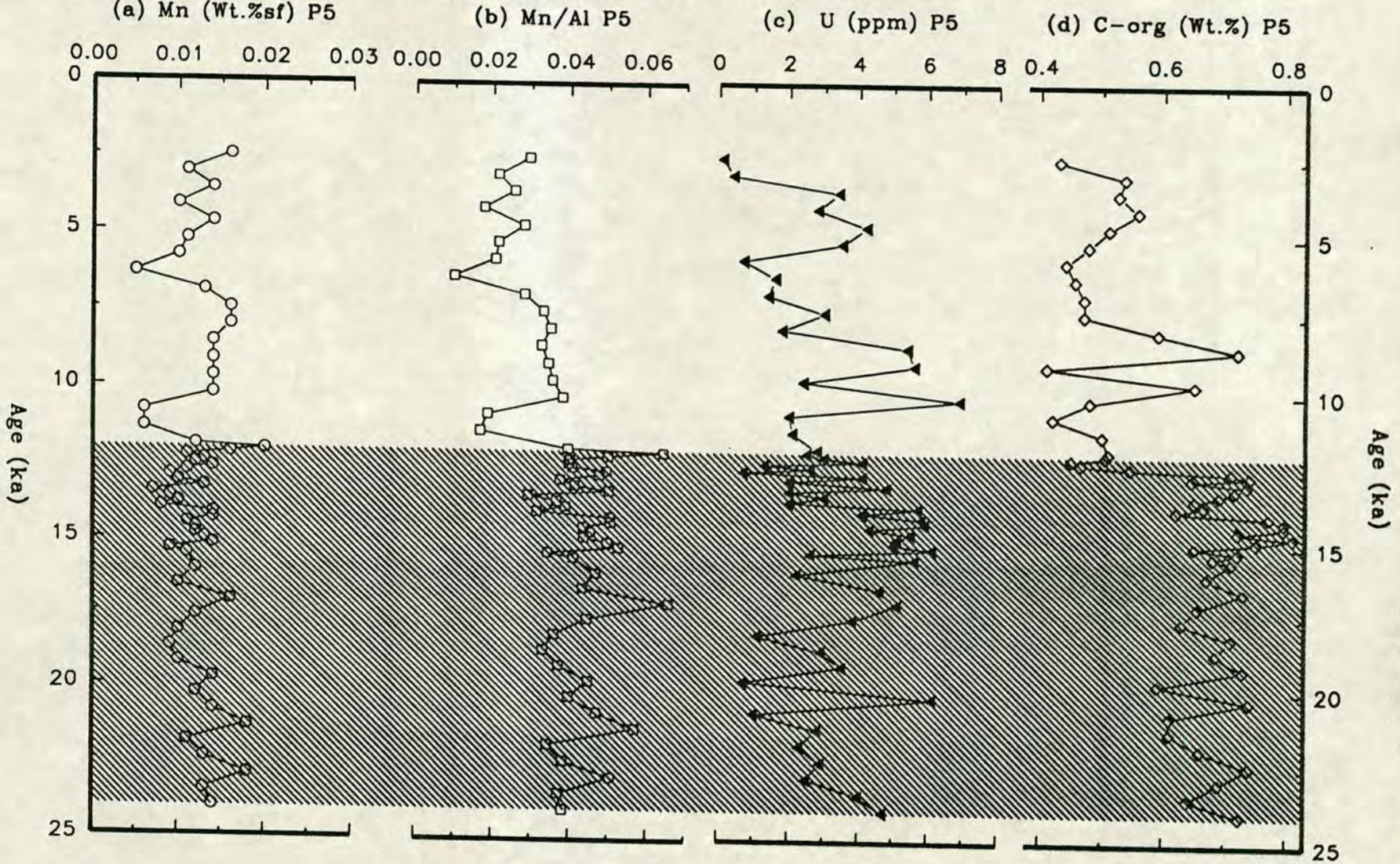

table 9.1. From this table it is clear that core CD3826 has by far the highest mean content of Mn of all the cores studied at 0.941 (Wt.% salt free). This is almost certainly due to the low sedimentation rate in the core which would preferentially promote the formation of Mn-Fe oxyhydroxides, relative to the faster sedimenting cores. Cores P5, CD3822 and CD3827 are relatively low in Mn with mean contents of 0.012, 0.144 and 0.038 respectively. The values for cores P5 and CD3827 are unusually low for normal marine sediments (Turekian and Wedopohl, 1961), probably as the result of their relatively fast sedimentation rates.

Table 9.1 Table showing the mean (and range of) values of Mn, Mo, U and Ce in cores studied in this thesis.

	Mn (Wt.%sf)	Mo(ppm)	U(ppm)	Ce(ppm)
P5	**0.012** (0.005-0.020)	**BDL**	**3.3** (0.1-6.9)	**BDL**
CD3822	**0.144** (0.026-0.578)	**2.1** (0.0-7.8)	**2.4** (0.0-6.4)	**9.74**
CD3826	**0.941** (0.245-9.608)	**4.5** (0.0-16.1)	**5.0** (0.0-10.1)	**27.27**
CD3827	**0.038** (0.024-0.109)	**8.9** (0.0-19.8)	**8.9** (1.2-15.8)	**22.85**

BDL = generally below limit of detection.

Most cores show the characteristic rapid decrease in Mn at depth (figures 9.1-9.3). This enrichment in the surface layers results from the upward diffusion of pore water Mn (II) and precipitation as oxyhydroxide Mn (IV) at, or near, the surface where higher redox potentials prevail. The lack of any Mn enrichment in the surface sediments of core P5 is probably due to the loss of the topmost sediments during gravity coring. The pilot cores of the main piston corers used to recover the CD38 sediments are relatively efficient in preserving the sediment/water interface and, therefore, the Mn oxide top. Pilot core data are used at for all chemical profiles in CD38 cores. Thus, any absence of a surficial enrichment in Mn oxides is probably due to bad coring.

Core CD3822 displays an unusual increase of solid phase Mn downcore punctuated by several highs at 24 ka, 45 ka and 63 ka (figure 9.1a). The reason for this subsurface gradual increase is uncertain, but is probably the result of reprecipitation of Mn (II) from the pore waters back into the solid phase Mn (IV) or the development of Mn carbonate phases.

Although core CD3827 displays a marked decrease on solid phase Mn below a maximum at approximately 2 ka, the surface sample has Mn values close to background levels (figure 9.1b). There is little change at depth except for a slight decrease during stage II to approximately 0.025 % (salt free), and a small increase at the base of stage III (figure 9.1b).

In core CD3826 the content of Mn is generally <1% and does not vary much, except for several large subsurface increases (figure 9.2a). There are several possible causes of these. Firstly, as Mn is highly susceptible to the redox changes, the spikes may be related to changes in the redox state and the diagenetic mineralogy of the sediment. Pedersen and Price (1982) report the existence of a mixed Mn carbonate phase ($(Mn_{48}Ca_{47}Mg_5)CO_3$) in Panama basin sediments, resulting from the precipitation of Mn (II) to Mn (IV) oxide, in a volcanic ash band where porosity and redox potential of the sediment is greater.

In core CD3826 the base level of Mn of around 0.9% increases to greater than 1% Mn at approximately 24 ka, 56 ka, 110 ka, 165 ka, 239 ka, 264 ka, 280 ka, 315 ka, 328 ka and, 400 ka (figure 9.2a). Indeed at 23.93 ka, Mn constitutes almost 10 % of the sediment and calcium also increases in this horizon (chapter 6). Here black coated concretions of several centimetres diameter are surrounded by cream coloured, fine-grained "chalky" material. The mineralogy of both these materials was investigated by X-ray diffractometry using techniques described in chapter 3 and appendix A.4. Figure 9.4 shows diffractograms of the cream coloured and black nodular material from 23.93 ka in core CD3826. The most intense peak, identifying the cream coloured material, occurs between 30.5-31.0 2θ° and represents a composite of mixed Mn carbonate phases of slightly different composition, resulting from the solid solution system between calcite-dolomite-Mn carbonate. Mn carbonate minerals of varying composition have been described in sediments (generally coarse grained) from several areas: in the Guatemala basin (Lynn and Bonatti, 1965), in the Peru trench (Zen, 1959) and in the Panama basin (Pedersen, 1979; Pedersen and Price, 1982). According to Pedersen (1979), Mn carbonate precipitation is encouraged by the decreased supersaturation trends of coarse grained sediment horizons.

The most common Mn carbonate minerals, and those which almost certainly make up the majority of the carbonate found in this horizon are, rhodochrosite and kutnahorite. Formation of such minerals does however require sufficient Mn (II) in the pore waters in order to exceed the solubility product of Mn carbonate minerals such as

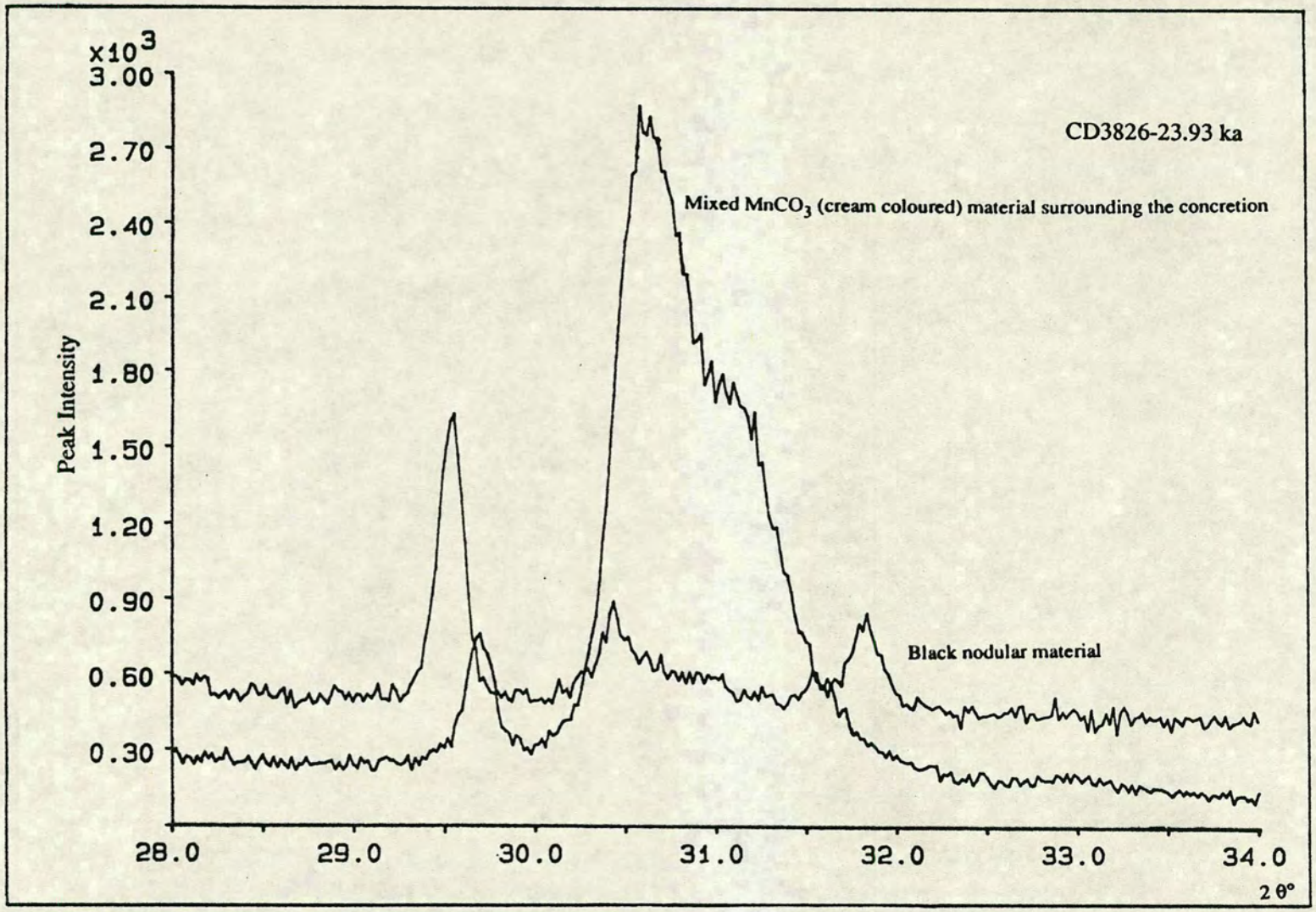

Figure 9.4 Diffractograms showing the mixed Mn carbonate (cream coloured) material that was found surrounding the black nodular material at 23.93 ka in core CD3826. Note the broad peak between 30.5-31.5 2 θ° representing the mixed Mn carbonate phases of slightly differing composition.

rhodochrosite (Johnson, 1982). In the absence of any pore water data this cannot be categorically proved. The black concretionary material and associated Mn carbonate phases are observed at other levels in core CD3826 (chapter 3), but tend not to only coincide with volcanic ash deposits as postulated by Pedersen and Price (1982). However, Mn contents do increase at 56 ka and 328 ka corresponding to the ash layers "D" and "K" respectively (chapter 4).

A second, and less likely, possibility for the large increases in Mn downcore is that they represent the remains of buried Mn nodules. The concretionary material that is high in Mn does resemble small Mn nodules. However it is difficult to envisage a system whereby the Mn oxide nodules do not become reduced at depth and enter the pore waters in the dissolved Mn II state. Perhaps periods of high accumulation rate, coupled with a deepening of the Mn redoxcline in the sediment would have promoted increased preservation of solid phase Mn to the extent that some remnant of the Mn nodule would have remained. However, the sediment accumulation rate in core CD3826 was never very high and there is no evidence that the oxide layer at the surface of the sediment was ever especially thick.

Thirdly, Mangini (1988) proposed that during glacial periods the lowered sea level and relatively stagnant, slowly circulating bottom waters resulted in oceanic suboxic-anoxic conditions which inhibited Mn oxide formation and promoted build up of dissolved Mn in the water column. At the beginning of interglacials however, as circulation begins to increase and the bottom waters become more oxygenated, time-synchronous preferential precipitation of Mn oxides at the surface of the sediment would occur. This would result in a greater likelihood that Mn spikes would be preserved in the sediment column throughout the region. Similar increases in Mn during interglacial stages V, VII and IX are reported by Berger et al. (1983) and Finney et al. (1988). However these authors attribute the preservation of large spikes in Mn not to oceanic circulations patterns but, more directly, to temporal variations in the depth to the redoxcline as resulting from productivity (C-org input) changes.

In core CD3826, spikes in Mn do occur at the base of stage II, III and VII and towards the base of stage V and IX. However, large increases in Mn also occur during the volcanic ash deposits and, indeed, during glacial times. Clearly these increases do not strictly conform to any one model and are, therefore, probably the result of a combination of both unusual mineralogy, forming loci for precipitation of

Mn IV (oxides) and $MnCO_3$ and, changes in the degree of oxygenation of the bottom waters during deposition (caused by water mass and organic carbon flux changes).

9.3 Variations in Mo and U

9.3.1 Introduction

Like Mn, Mo and U are sensitive to the redox conditions in the sediment during deposition and burial (Shimmield and Pedersen, 1990). Organic matter is commonly involved in the precipitation of Mo and U from sea water and may provide the sites for formation and preservation of these elements, in mineral form, in the sediment. Under oxic conditions Mo is known to be associated with Mn oxyhydroxides (Berrang and Grill, 1974), whereas in the reducing environment the Mo is found closely associated with Fe-monosulphides or dissolved organic matter (Shimmield and Pedersen 1990). Anoxic conditions are known to promote Mo contents in the sediment (Bertine and Turekian, 1973; Calvert, 1976), probably during reactions occurring at or near the sediment/water interface (Francois, 1988). Uranium is generally present in very low abundance (around 1-2 ppm) in oxidised marine sediments occurring in aluminosilicates (Turekian and Wedopohl, 1961). However in reducing continental margin sediments, rich in organic matter, solid phase U may reach 10-15 ppm (Veeh, 1967; Yamada and Tsunogai, 1984). The geochemistry of U in anoxic sediments, where it is typically strongly enriched, has been reviewed by Anderson et al. (1989a, 1989b). Contents of either element above such low levels must result from diagenetic/authigenic factors closely linked to the redox potential of the sediment.

Generally, contents of Mo and U increase landward (table 9.1) with cores CD3826 and CD3827 having considerably more Mo and U than in cores CD3822 and P5. As Mo and U are known to commonly form organo-metallic complexes, this distribution is, to a large extent, the result of increased organic carbon contents in cores CD3826 and CD3827. However mean concentrations of C-org in core CD3822 and CD3826 are comparable which suggests that the greater Mo and U contents in core CD3826 must be partly the result of redox differences, influenced by accumulation rate, and not simply the result of organo-metallic complexation.

9.3.2 Temporal variations in Mo and U

Temporal variations in Mo (figures 9.2b, 9.5) tend to show a strong surface enrichment and, especially in core CD3826, a slight downcore increase. The surficial increase is the result of the association with metal-oxyhydroxides. The downcore increase in core CD3826 however, is probably due, at least in part, to a diagenetic coprecipitation of Mo with Fe-monosulphides in the reducing environment at depth in the sediment.

Downcore variations in U in cores studied in this thesis are shown in figures 9.2b, 9.3c and 9.5. Core CD3826 shows little systematic variation in U except for a marked depletion from the base of stage II to the surface of the core and, two large increases at approximately 300 ka and 350 ka. These latter two subsurface enrichments coincide with large increases in organic carbon, which is consistent with the close association of U with organics described above. The surface decrease is probably due to the relatively high redox potentials of surface sediments under which conditions the U would be converted to soluble U (VI) from insoluble U (IV) and enter the pore waters or possibly diffuse into sea-water.

Increases in Mo and U during stage II in core CD3827 correlate strongly with increases in organic carbon from this core (cp. figures 9.1b and 9.5b). Increases in Mo and, to a lesser extent, U correlate with increases in C-org during stage II in core CD3822. However, no comparable increase in Mo and U occurs during stage IV as with C-org (cp. figures 9.1a and 9.5a). These broadly parallel distributions tend to argue in favour of the dominance of organo-metallic complexation in determining the Mo and U contents in cores CD3822 and CD3827. The adsorption of Mo, liberated from Fe sulphides, by organics has been observed by Pilipchuk and Volkov (1968).

The time-synchronous increases in U and Mo with C-org tend to discredit C-org as a palaeoproductivity indicator. If one assumes that large increases in U and Mo relate to conditions of reduced bottom water oxygen contents (ie suboxic - anoxic), then C-org would be preferentially preserved during these periods and its content in the buried sediment would increase without any necessary increase in the euphotic zone productivity. If anoxia occurred in glacial times, it would preserve high contents of C-org and, result in relatively reducing bottom waters with a considerable build up of dissolved Mn. Since there are, in some horizons, high Mn contents during glacial

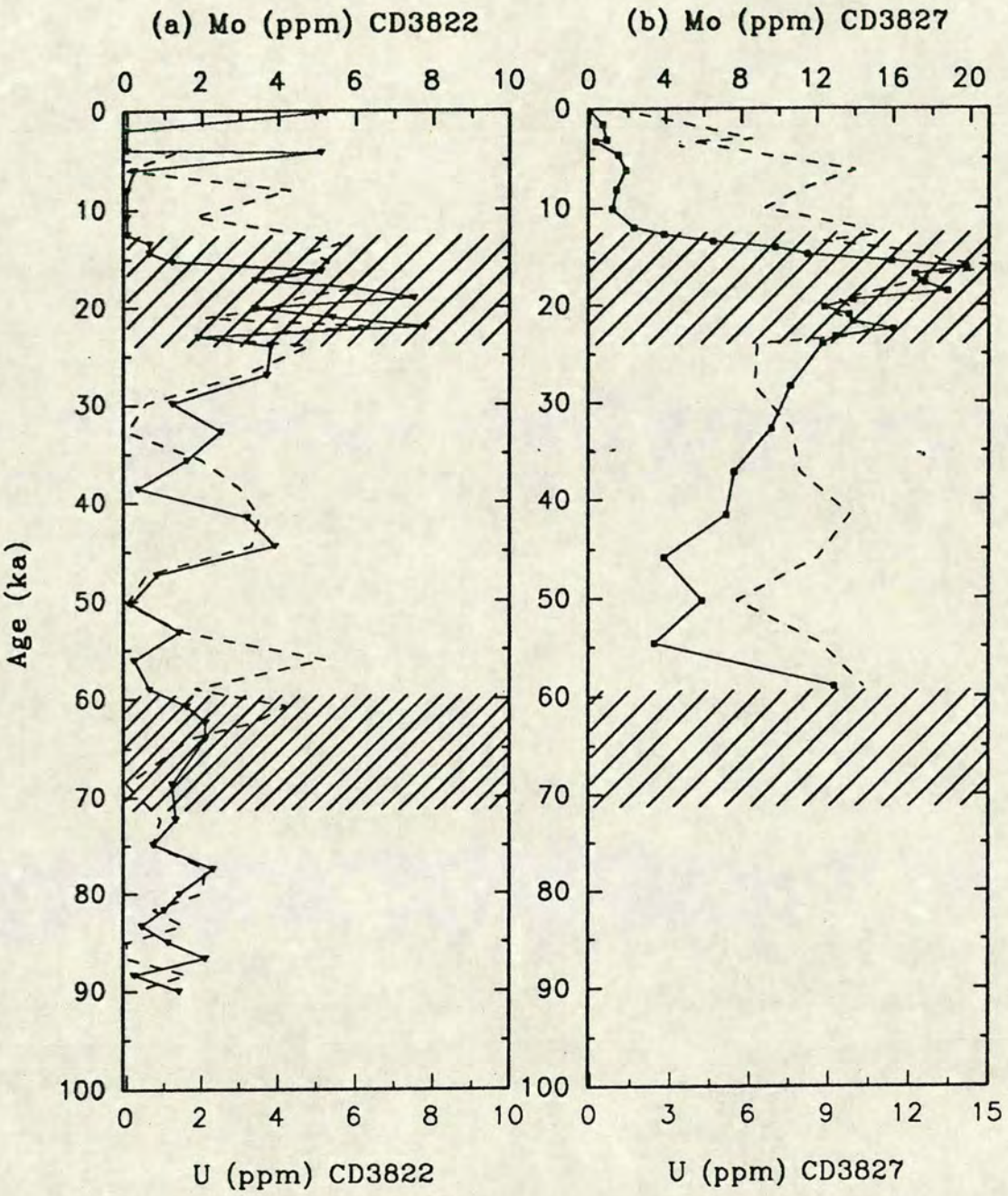

Figure 9.5 Temporal variations in Mo (ppm SF; solid symbols, solid line) and U (ppm SF; dashed line) in core CD3822 (a) and core CD3827 (b). Note the time synchronous increases (especially during stage II) in U and Mo in both cores especially in core CD3827. Shaded regions represent glacial stages II and IV.

episodes, the model of Mangini fails because, increased Mn precipitation should only occur during periods of enhanced bottom water circulation and oxygen content.

The ratio of Mo/U in marine sediments has been used to hindcast the palaeoredox conditions of bottom waters; with values of around unity for anoxic sediments (Bertine and Turekian, 1973) and values of 3-4 for oxic, deep-sea sediments. However, as McNeill and Shimmield (1991) point out, diagenetic processes common in marine sediments can result in highly variable Mo/U ratios and, consequently, anoxic conditions may not necessarily result in ratios close to unity in buried sediments. Consequently the ratio of Mo/U has not been used in this thesis in palaeoredox reconstruction.

9.4 Cerium

Another element that has been employed as a proxy for oceanic palaeoredox conditions is Ce (Elderfield et al., 1981, Elderfield and Greaves, 1982; Wright, et al., 1987). Ce, like other REE's (see chapter 5) is closely associated with phosphatic material which tends to concentrate the REE's from sea water during sedimentation. Wright et al. (1987) have empirically defined a Ce anomaly (Ce_{anom}), changes in which, they claim, record variations in past redox conditions. This is the result of Ce fractionation by co-precipitation with metallic oxides under oxidising conditions. Thus under oxic conditions there is a negative Ce_{anom} in sea water which is reflected in the sediment on the burial of skeletal apatite. The converse happens during reducing (anoxic) conditions. During periods of depleted Ce, the Ce_{anom} values are negative and vice versa.. Thus, in the absence of large variations in La (see chapter 5) a decrease in Ce, as defined by reduced Ce/Nd ratios, should effectively signify a negative Ce_{anom} and, indirectly, reducing (anoxic) conditions.

Figure 9.6 shows the Ce/Nd ratio in cores CD3826 and CD3827. Little systematic variation is clear although stage II in core CD3827 does appear to be enriched in Ce relative to Nd which would indicate a period with relatively stagnant, low oxygen bottom water. In core CD3826, Ce/Nd increases markedly at around 24 ka, 173 ka, 328 ka, 376 ka, 423 ka, and 472 ka. Although some of these horizons correspond to increases in other redox sensitive elements described above and, therefore, corroborate the theory that there were reduced bottom water oxygen concentrations at

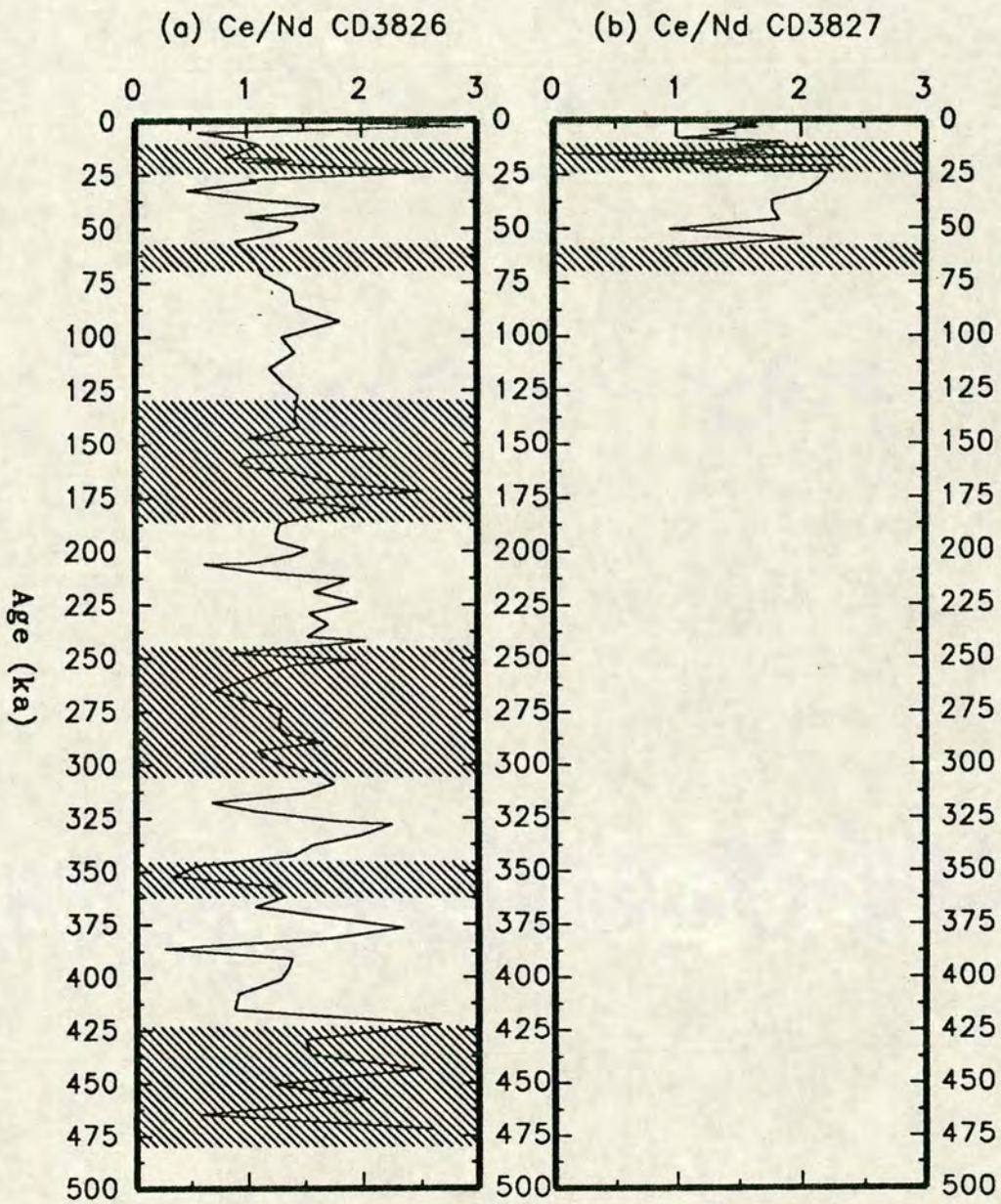

Figure 9.6 Temporal variations in the Ce/Nd ratio in cores CD3826 (a) and CD3827 (b). Note the Holocene increase in both cores and the apparent independence of the ratio from glacial to interglacial stage boundaries. Shaded regions represent glacial stages II, IV, VI, VIII, X and XII.

these times, most Ce enriched horizons do not correlate with anomalies in the other redox sensitive elements.

9.5 Trace Metal Enrichments: Redox Cycling or Productivity Pulses?

9.5.1 Introduction

This section attempts to distinguish between redox cycling driven, and productivity induced, trace metal enrichments.

Anomalously high contents of the trace metals Cu, Ni, Zn (and V), in excess of that normally held in marine aluminosilicates, are known to commonly underlie areas of high surface water productivity and, to be associated with organic matter (Curtis, 1966; Calvert and Price, 1971; Calvert, 1976; Spears and Amin, 1981; Fischer et al., 1986; Balistrieri and Murray, 1986; Finney et al., 1988). Marine plankton commonly contain modest amounts of metals which suggests some association between organic substances and metals. This is corroborated by the positive correlation between C-org and the content of Cu, Zn, Ni, and Mo in shelf sediments of unusually high C-org content (Calvert and Price, 1983). What is ambiguous, however, is the process of metal enrichment. High metal contents are believed to be a consequence of scavenging from the water column by sorption onto particulates (mainly biogenic) on their way to being encorporated in the sediment (Volkov and Famina, 1974; Balistrieri et al., 1981). However, Finney et al. (1988) and, Graybeal and Heath (1984) argue that high levels of some transition metals result from post-depositional recycling from depth in the sediment via sorption onto organic matter (Nissenbaum and Swaine, 1976; Calvert and Morris , 1977); the pump for which is driven by organic matter degradation and Mn-Fe oxyhydroxide remobilisation.

Shimmield (1984), in a study of sediments off Baja, found a reduction in trace metals, relative to Mn, as C-org contents increased probably due to lower metals affinity of the recycled Mn oxyhydroxides. Balistrieri and Murray (1986) compared sediment trace metal content from around the eastern equatorial Pacific and found a metal enrichment hierarchy of Panama basin < MANOP site M < MANOP site H.

Organic matter and metal contents in shelf sediments have also been found to be controlled by the textural characteristics of the sediment (Van Andel, 1964;

Ackerman, 1980; Salomons and Forstner, 1983). However, as no definite association between C-org and characteristic textural indicators was observed for sediments in this study (see chapter 6), textural variations are believed to have little or no effect on the excess metal content.

9.5.2 Results

Excess Metals

Excess (Ex) metal calculations are shown in appendix B and results of ExZn, ExNi, ExCu, and ExV are tabulated in appendix C.3.3 and C.12. Negative values indicate contents of metals that are depleted relative to the world average shale of Turekian and Wedopohl (1961); positive enrichment of values denote enrichment relative to the mean shale. Mean (range) contents of Excess metals (ppm salt free) for all cores are shown in table 9.2a. From this, there appears to be a general hierarchy of enrichment in excess metal contents, with ExZn and ExNi tending to be more abundant than ExCu and ExV. There also appears to be an association between Exmetals content and sediment accumulation rate. Cores CD3826 and AII54-25PC have the slowest bulk accumulation rates (1.21 and 0.74 $g/cm^2/kyr$ respectively), and generally have the highest mean excess metal contents. The low accumulation rates would promote increased C-org preservation and Mn-Fe oxyhydroxide formation which, in turn, would tend to concentrate the metals via recycling processes driven by organic matter degradation. Metals expressed on a carbonate free basis from this study and from MANOP site H sediments (Lyle et al., 1984) are shown in table 9.2b. The general hierarchy of enrichment is similar to that for excess metals. MANOP H sediments are considerably more enriched in Cu, Ni and Zn than the sediments from this study. This is despite having a similar sedimentation rate as core AII54-25PC. These findings are consistent with those of Balistrieri and Murray (1986) who found that Panama basin sediments were depleted in metals relative to MANOP H sediments.

According to Graybeal and Heath (1984), the maximum metal contents in MANOP site H sediments are found at the surface where sediments tend to have a "diagenetic" signature as defined by Bonatti et al., (1972). In a further investigation of MANOP H sediments, Fischer et al., (1986) studied the differences between the primary flux of metals and the accumulation rate. This allowed quantification of the amount of recycled metals as a percentage of the primary input. Table 9.3 shows the results of their calculations. From this, it is clear that 76% and 45% of the Zn and Cu

Table 9.2a Mean (range) contents of Excess metals from this study. Excess metal values expressed as ppm salt free; C-org results as Wt. % salt free.

Core	ExCu (ppm)	ExNi (ppm)	ExZn (ppm)	ExV (ppm)	C-org(Wt.%)
P5	**15.0**(10.8-25.4)	**13.7**(9.1-20.0)	**19.7**(15.0-27.4)	**13.2**(1.5-25.7)	0.62
CD3822	**41.5**(13.5-89.8)	**63.1**(14.1-186.2)	**59.0**(18.6-120.4)	**22.2**(-0.6-40.8)	1.21
CD3826	**82.8**(43.5-183.3)	**212.8**(85.9-424.4)	**276.9**(40.1-465.1)	**106.8**(-29.7-182.6)	1.41
CD3827	**37.6**(31.4-41.8)	**37.1**(17.1-65.9)	**95.2**(69.2-151.2)	**43.3**(29.2-54.7)	3.31
AII54-25PC	**137.7**(-22.1-255.0)	**260.5**(40.6-805.7)	**296.9**(45.0-505.5)	**194.8**(-4.9-394.9)	0.96

Table 9.2b Mean and range of trace metals expressed on a salt and carbonate free (CF) basis. ⊕ sedimentation rate (cm/kyr); [1] Lyle et al., (1984).

Core	Cu(ppmCF)	Ni(ppmCF)	Zn(ppmCF)	V(ppmCF)	C-org(Wt.%)	BAR(g/cm^2/kyr)
P5	**169.2**(85.6-346.8)	**165.7**(92.2-286.1)	**229.7**(165.3-321.1)	**180.7**(63.6-296.2)	0.62	4.85
CD3822	**222.1**(58.1-353.6)	**324.6**(116.0-604.9)	**328.6**(173.2-596.3)	**180.0**(88.9-313.0)	1.21	3.33
CD3826	**146.9**(93.2-279.8)	**337.9**(163.4-676.9)	444.4(139.1-692.0)	**258.0**(98.0-347.4)	1.41	1.21
CD3827	**90.3**(79.4-233.7)	**107.8**(88.2-141.9)	**203.0**(172.3-339.0)	**176.4**(164.7-188.4)	3.31	4.07
AII54-25PC	**227.5**(66.6-361.0)	**418.3**(111.3-1063.8)	**487.9**(133.1-885.8)	**370.6**(107.2-709.8)	0.96	0.74
MANOP-H[1]	**533.4**(450-644)	**722.9**(341-1270)	**524.0**(361-713)	----------	0.94	0.70⊕
Residence Times (yrs)	970	8200	510	45000		

respectively is recycled back to the water column. However, Ni is -6% recycled indicating that this element is undersupplied in the MANOP H sediments.

Table 9.3 Flux ($\mu g/cm^2/yr$), accumulation rate ($\mu g/cm^2/yr$), benthic flux ($\mu g/cm^2/yr$) and % recycled of metals from MANOP site H (adapted from Fischer et al., 1986$^{\oplus}$). AR=accumulation rate; BF=benthic flux.

	Cu	Ni	Zn	Mn
MANOP-H$^{\oplus}$ Flux($\mu g/cm^2/yr$)	0.110	0.048	0.290	0.48
MANOP-H$^{\oplus}$ AR($\mu g/cm^2/yr$)	0.063	0.051	0.066	1.70
MANOP-H$^{\oplus}$ BF($\mu g/cm^2/yr$)	0.050	-0.003	0.220	-1.20
MANOP-H$^{\oplus}$ % Recycled	45	-6	76	-250

Temporal variations in Excess metal concentration.

The profiles of ExZn, ExNi and, to a lesser extent, ExV and ExCu in core CD3822, are all quite similar, with high values occurring during stage II (20 ka), III (42 ka) and IV (60 ka), (figure 9.7). Furthermore, ExZn, ExV and ExNi display a marked depletion during the Holocene. However, all 4 excess metals increase, to a greater or lesser extent, at the surface probably as a result of concentration by Mn-Fe oxyhydroxides. ExCu values are relatively constant and are generally close to the world average shale except for a large decrease at around 80 ka which is consistent with the local tephra layer in this core (chapter 4). The highs in ExCu during stage II, III and IV are much smaller than in the other excess metals. The general downcore increase in ExZn and ExNi in core CD3822 tends to parallel the Mn profile as do the slight increases in all four Ex metals at approximately 40 ka and 62 ka (cp. figures 9.1a and 9.7a-d). From table 6.4, it is clear that a statistical correlation exists between Cu, Ni and Zn (> 95% certain) whereas only relatively weak positive correlation exists between V and these three metals, despite the marked increases in ExV being coincident with smaller increases in the other metals. Although correlation of all the metals (total) with C-org are all weakly negative (table 6.4), excess metal distribution appears to be more closely associated with organic carbon than to Mn oxides.

Statistical analysis of the data from core CD3826 (table 6.4), reveals that only Ni and Zn and, Cu and Zn are statistically correlated ($\geq$ 95% confidence). Excess metal profiles in cores CD3826 and AII54-25PC are very similar (figures 9.8-9.11),

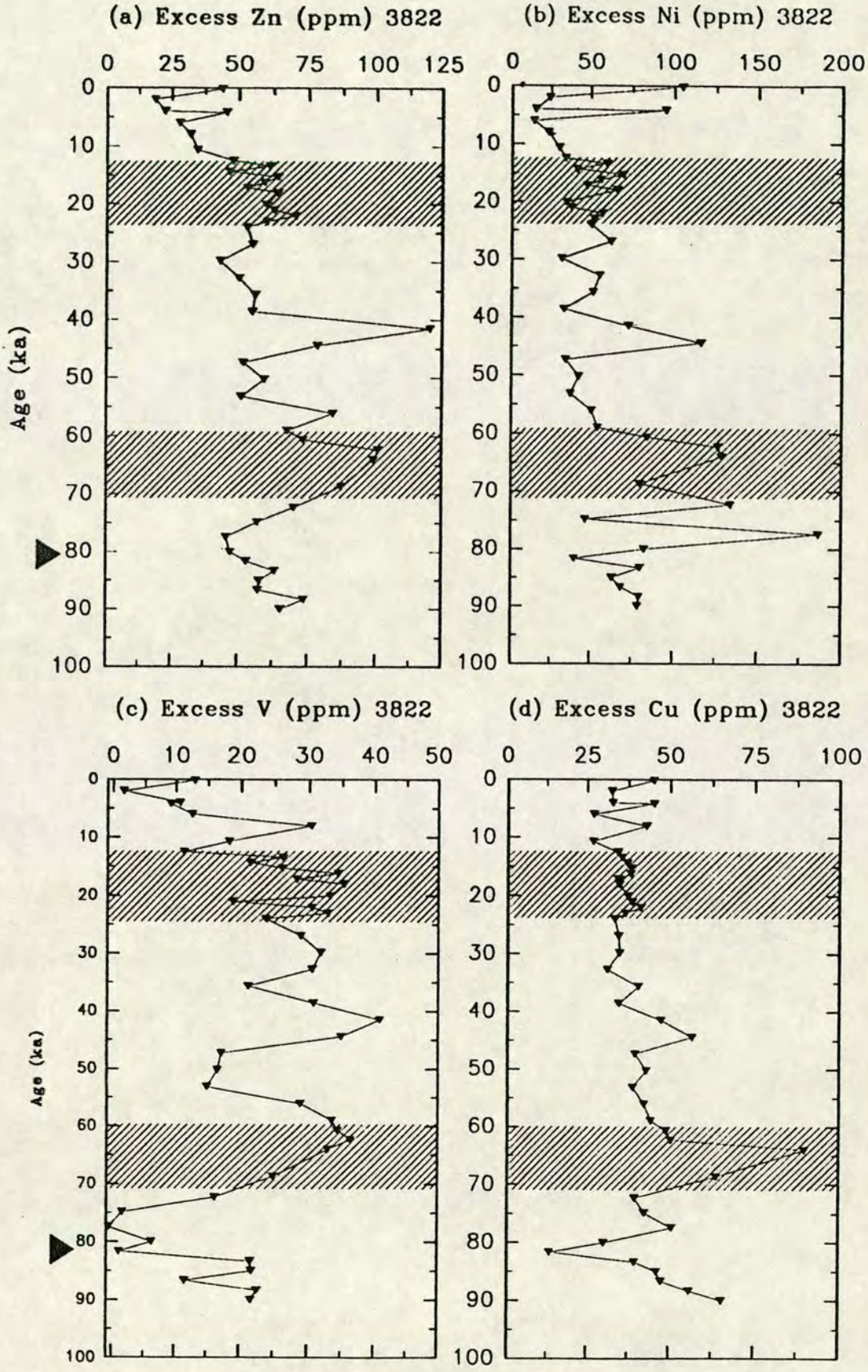

Figure 9.7 Temporal variations in Excess Zn (a), Excess Ni (b), Excess V (c) and Excess Cu (d) from core CD3822. Shaded regions represent glacial stages II and IV. Triangles indicate the position of a local ash layers (82ka).

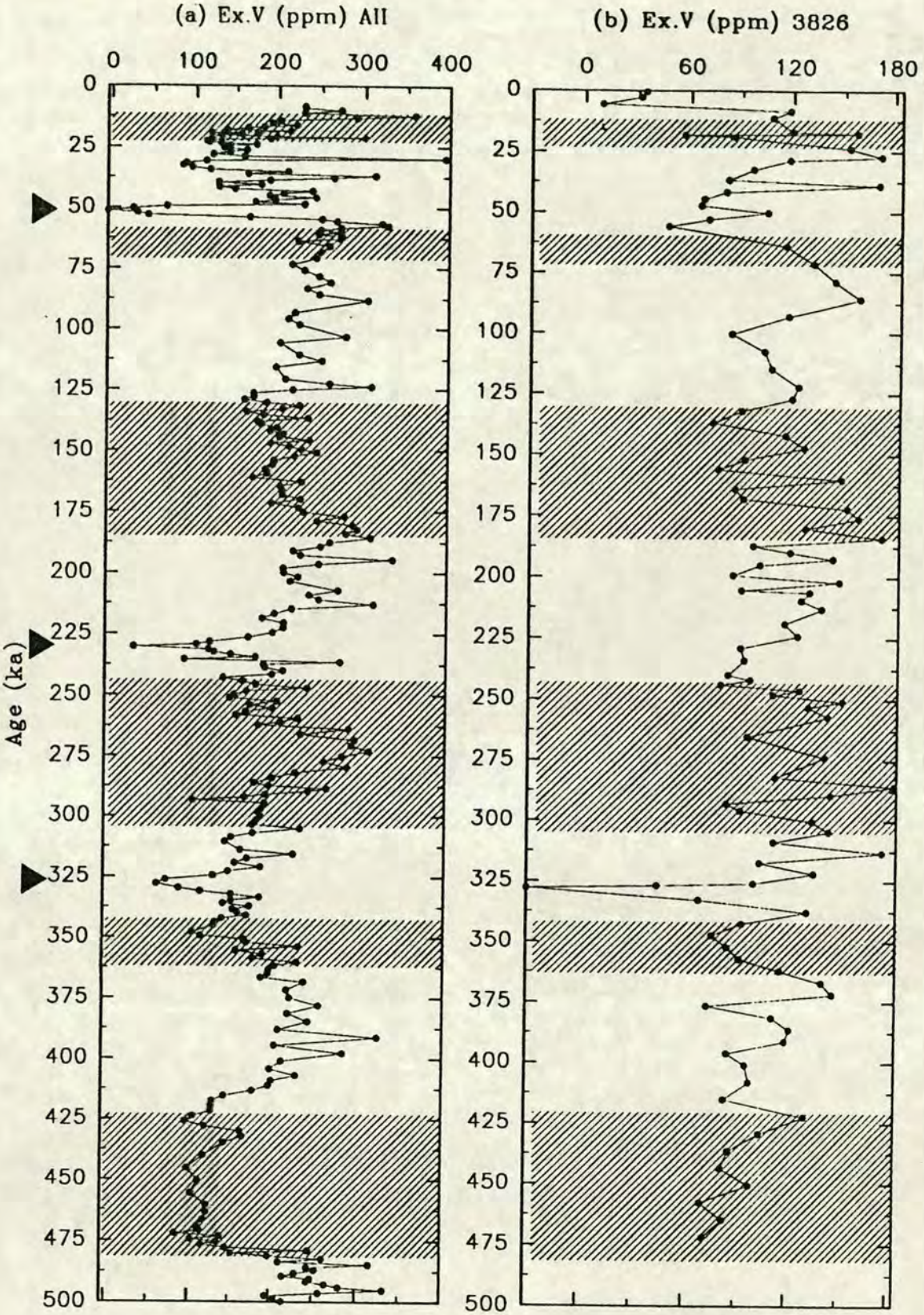

Figure 9.8 Temporal variations in Excess V (Ex.V) from cores AII54-25PC (a) and CD3826 (b). Shaded regions represent glacial stages II, IV, VI, VIII, X and XII. Triangles indicate the position of ash layers D (56ka), L (234ka) and K (328ka).

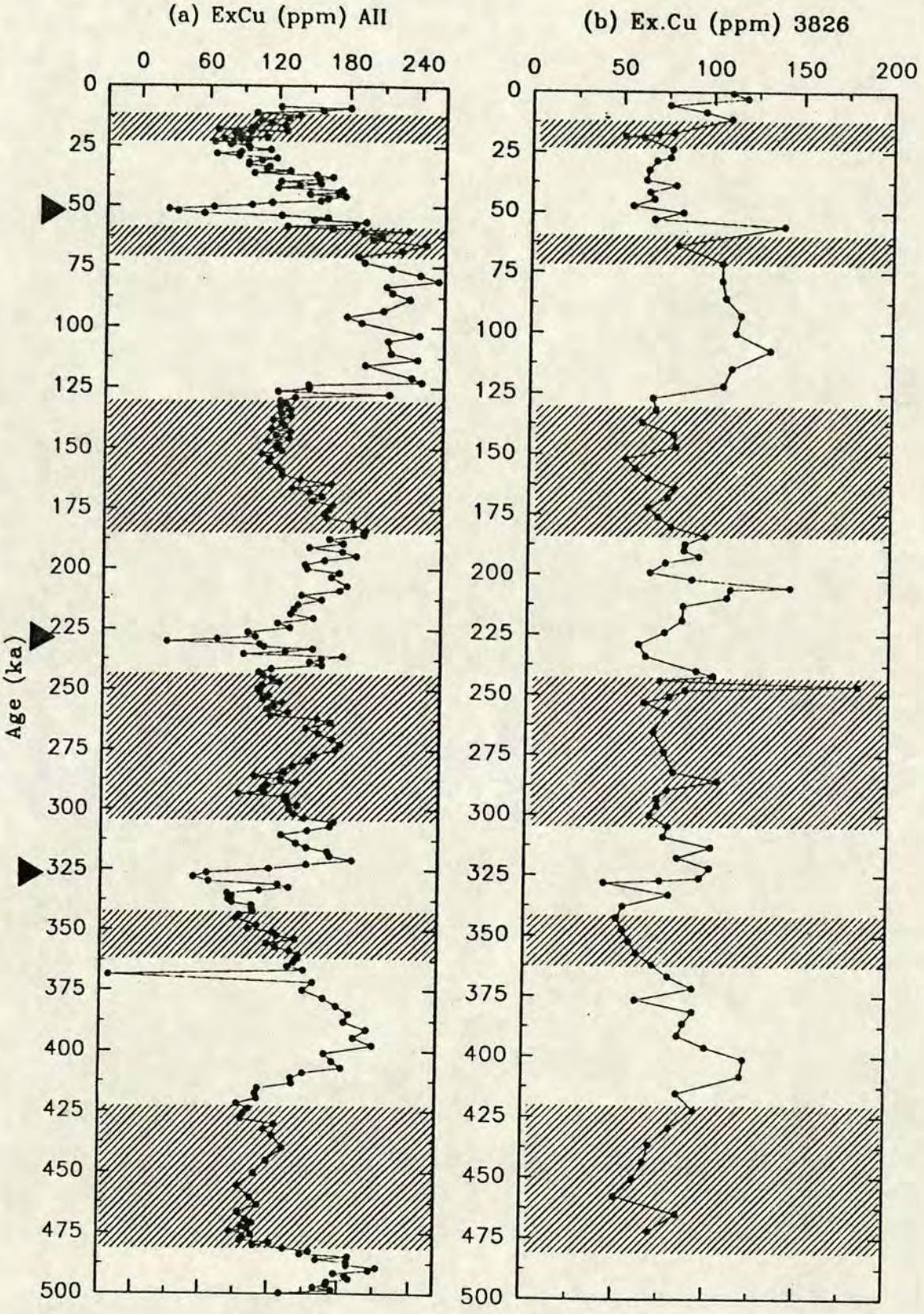

Figure 9.9 Temporal variations in Excess Cu (Ex.Cu) from cores AII54-25PC (a) and CD3826 (b). Shaded regions represent glacial stages II, IV, VI, VIII, X and XII. Triangles indicate the position of ash layers D (56ka), L (234ka) and K (328ka).

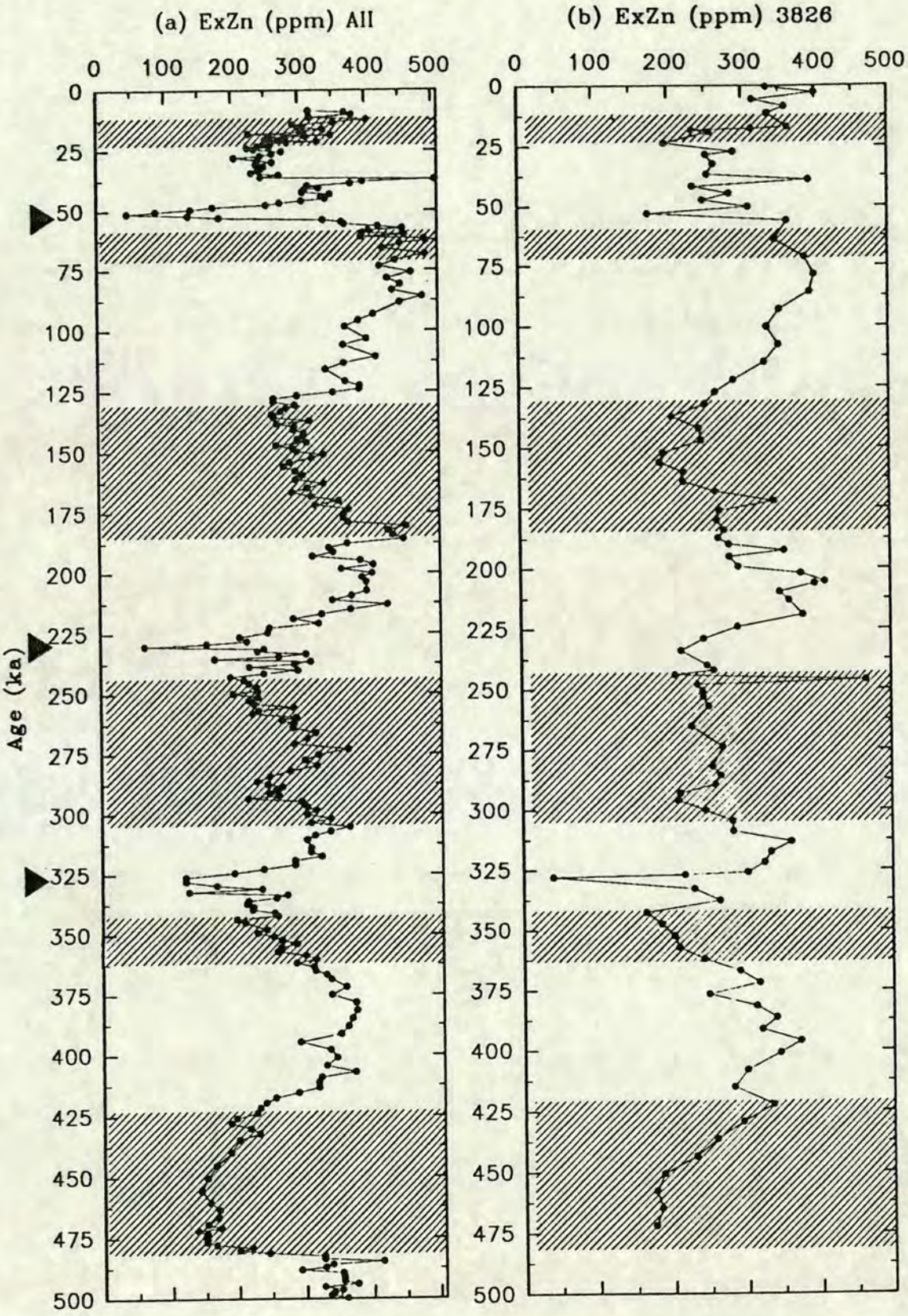

Figure 9.10 Temporal variations in Excess Zn (Ex.Zn) from cores AII54-25PC (a) and CD3826 (b). Shaded regions represent glacial stages II, IV, VI, VIII, X and XII. Triangles indicate the position of ash layers D (56ka), L (234ka) and K (328ka).

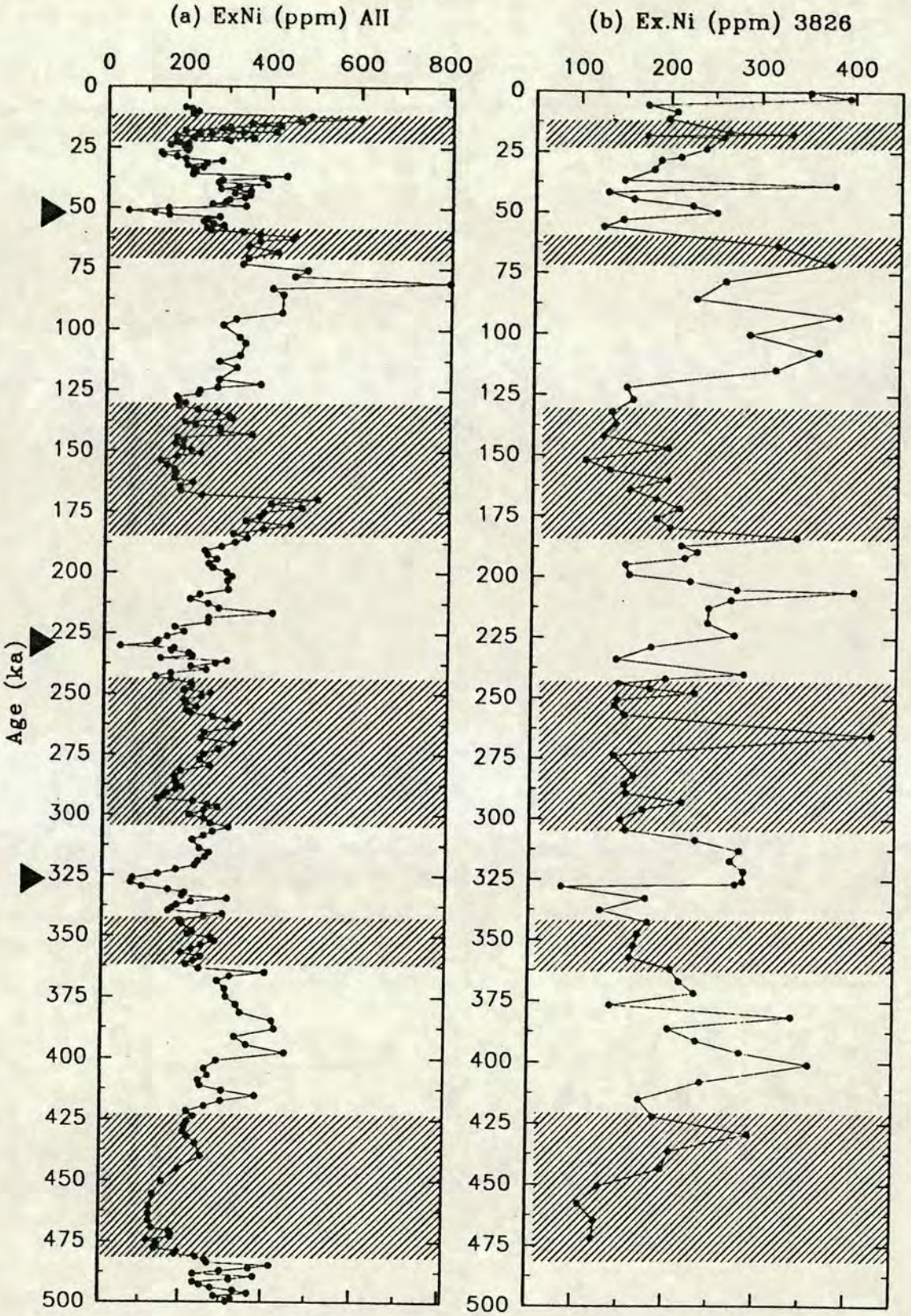

Figure 9.11 Temporal variations in Excess Ni (Ex.Ni) from cores AII54-25PC (a) and CD3826 (b). Shaded regions represent glacial stages II, IV, VI, VIII, X and XII. Triangles indicate the position of ash layers D (56ka), L (234ka) and K (328ka).

although the excess metal contents in core AII54-25PC are considerably higher than in core CD3826. The ExV profile is generally quite noisy and does not exhibit any clear cyclicity (figures 9.8b). There is a distinct increase in ExV at around 85 ka, and a depletion at the surface, but the rest of the core has a relatively constant and noisy signal. Profiles of ExCu, ExZn and ExNi (figures 9.9b, 9.10b and 9.11b respectively) are much smoother and are generally higher during interglacials than glacials. The temporal variations in ExZn seem to show a low frequency cyclicity especially in ExZn. This low frequency cyclicity is also present in ExCu and ExV in core AII54-25PC (figures 9.8a, 9.9a). No positive correlation was observed between the metals and C-org (table 6.4), suggesting that post-depositional concentration of metals was almost exclusively the result of associations with Mn (and Fe ?) oxides.

In core CD3827, a statistically negative correlation exists between Ni and V (table 6.4). Interestingly, a strong positive correlation and a statistically significant negative correlation is observed between Ni and C-org and, V and C-org respectively. This suggests that, in core CD3826, V is more influenced by post-depositional processes, whereas Ni distributions tend to be determined by the C-org content. Temporal variations in excess metals in this core follow essentially two patterns. Firstly, a profile exemplified by ExZn and ExNi, is that of large decreases from maximum levels at approximately 5ka to background levels in stage II and III (figure 9.12a, b). The latest Holocene (surficial) sediments show small decreases in ExZn and ExNi content. This is consistent with Mn oxide recycling mechanism which may promote, retention and reprecipitation of metals in the solid phase at depth in the sediment and, release of metals back into the water column depending on the position of the redoxcline during deposition. The second pattern of excess metal profiles in core CD3827, and that exhibited by ExV and ExCu, is one of decreasing values from the surface, reaching a minimum at the base of the Holocene, before increasing during stage II (figure 9.12c, d). Furthermore, excess metal contents in Stage III tend to be quite high with the result that there is a general decrease upcore especially in ExV. This pattern is complicated by marked increases in ExCu and ExV at around 5 ka, 18 ka, 40 ka, and 59 ka (figure 9.12c, d). These distributions may be summarised in the following way: (1) ExV and ExCu contents, at depth, are dominantly controlled by complexation with organic matter and, (2) ExZn and ExNi contents are mainly controlled by Mn-Fe oxide recycling processes.

The temporal profiles of the excess metals in core P5 may be divided into two groups: 1. ExCu and ExNi and, 2. ExZn and ExV. A strong (but not statistically

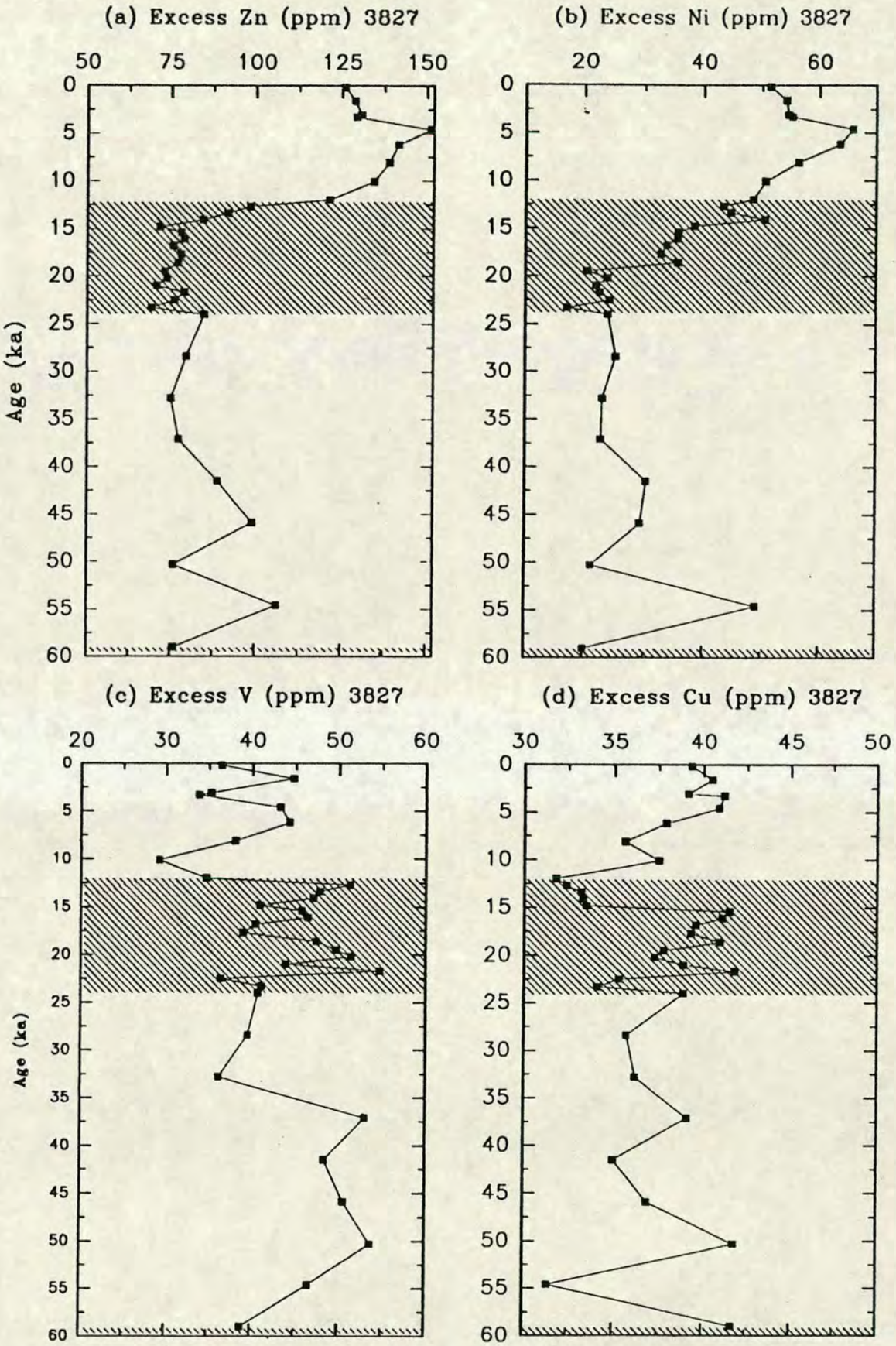

Figure 9.12 Temporal variations in Excess Zn (a), Excess Ni (b), Excess V (c) and Excess Cu (d) from core CD3827. Shaded regions represent glacial stages II and IV.

Figure 9.13 Temporal variations in Excess Cu (a), Excess Ni (b), Excess Zn (c) and Excess V (d) from core P5. Shaded region represents glacial stage II.

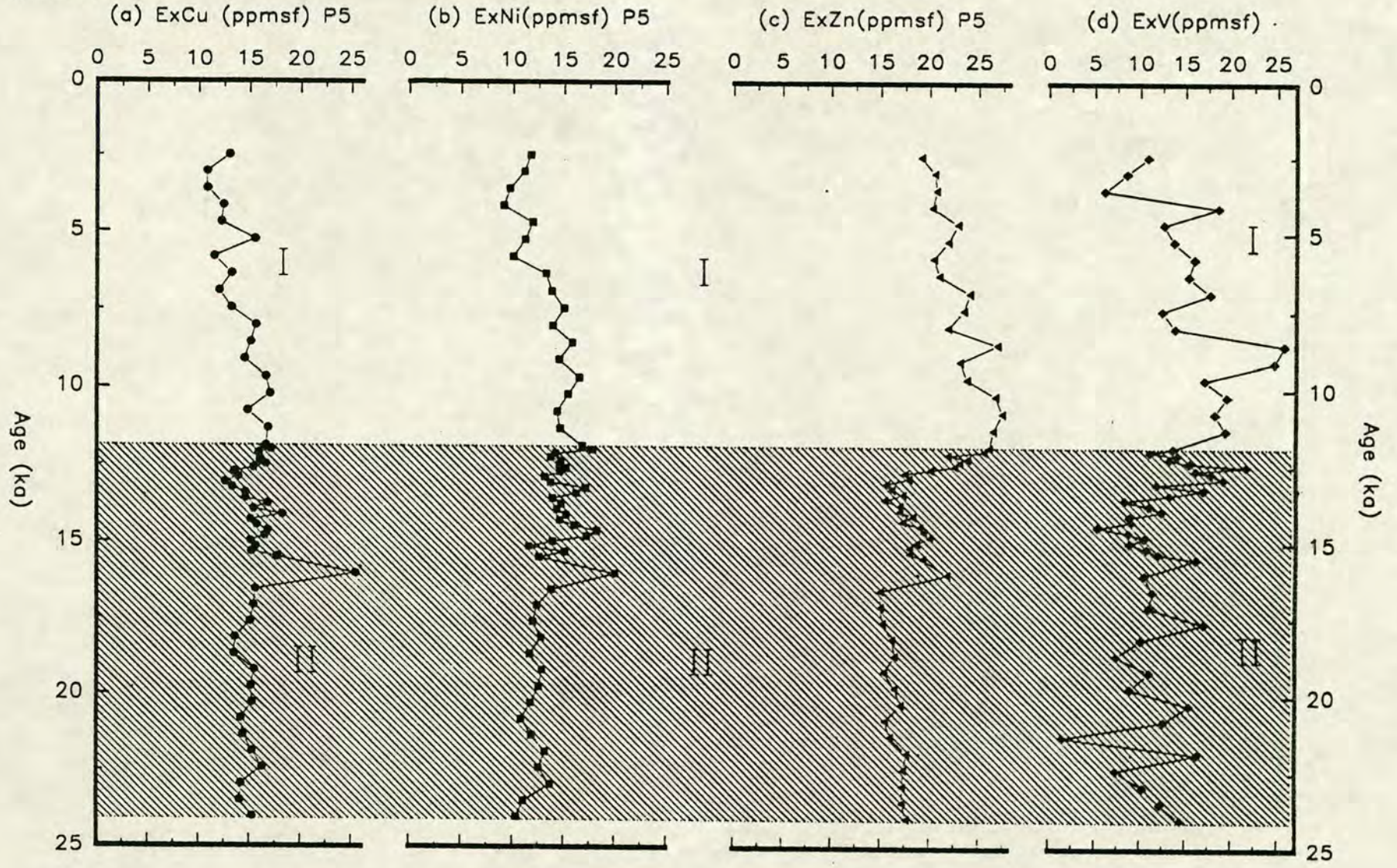

significant) correlation exists between Cu and Ni (table 6.5). The ExCu and ExNi curves look very similar with a slight increase during stage II (which parallels C-org increases), before a slight gradual decrease during the Holocene to the core minimum near the surface (figure 9.13a-b). These profiles are interrupted by a single horizon at around 16 ka that is relatively enriched in both ExCu and ExNi compared to the rest of the core. This may be due to some fragments of basaltic material which have been observed in other parts of the core (chapter 5). ExZn and ExV also have very similar temporal variations and are statistically correlated (figure 9.13c-d, table 6.5). The ExZn curve is relatively constant during stage II (except for a slight increase at 16 ka), before increasing to the core maximum around 11 ka. The Holocene is a period of gradually decreasing ExZn values (figure 9.13c). ExV is more noisy with similar increases at the base of the holocene but does not have the spike at 16 ka (figure 9.13d). Profiles of excess metals in core P5 do not closely parallel either solid phase Mn or C-org trends. The hydrothermal deposit in core P6 (a nearby core) was shown to be, to varying degrees, enriched in Co, Ni, Cu, Zn and Cr (Pedersen, 1979). This deposit is recognised in core P5 at 13.94 ka (chapter 5), but there is no comparable increase in the excess metal contents in this zone. This questions the conclusion of Pedersen (1979) that the trace metal enrichment is of a primary, hydrothermal and not a sorptive source.

Metal / Al Ratios

Metal/Al ratios are shown in figures 9.14-9.19. Profiles are sufficiently similar to the Excess metals curves such that they have no bearing on the argument for or conclusions from, the Excess metal results.

9.5.3 Discussion

There is no doubt that excess metal contents, in all the cores, are generally in excess of that normally held in marine aluminosilicates. The mechanism(s) which has(have) caused this enrichment must be dependant on one or more of the following factors:-

(i) overlying surface water productivity and organic matter flux.
(ii) suitability of particulates (mainly organics) for sorption of metals in the water column.
(iii) redox state of sediment determined mainly by organic matter flux, bulk sedimentation rate and bottom water chemistry.
(iv) water depth available for sorption of metals to take place.

Figure 9.14 Temporal variations in Cu/Al × 10^{-4} (a), Ni/Al × 10^{-4} (b), Zn/Al × 10^{-4} (c) and V/Al × 10^{-4} (d) from core P5. Shaded region represents glacial stage II.

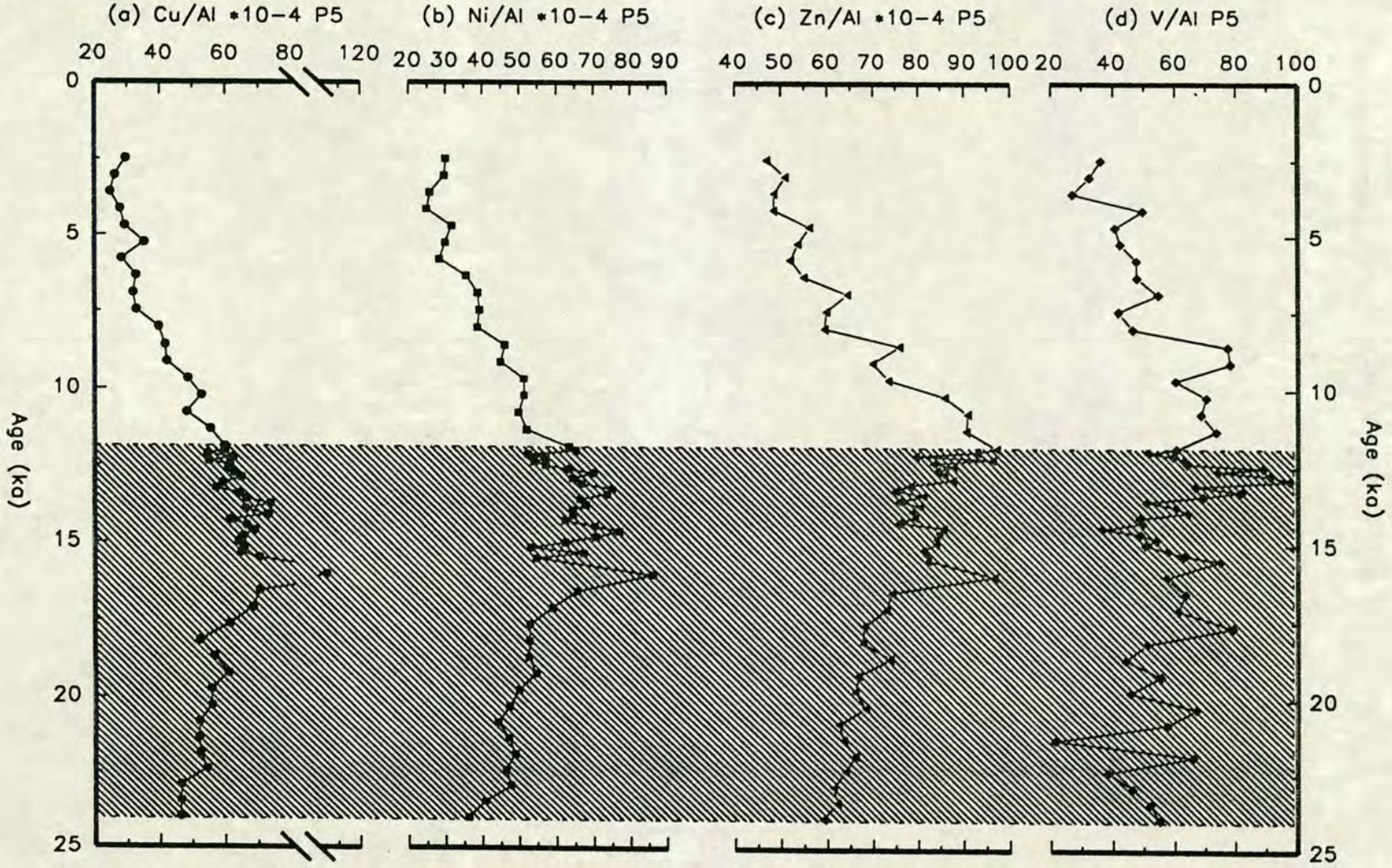

Figure 9.15 Temporal variations in Zn/Al × 10-4 from CD38 cores and core AII54-25PC. Shaded regions represent glacial stage II. IV, VI, VIII, X and XII. Triangles indicate the position of ash layers D (56ka), L (234ka) and K (328ka).

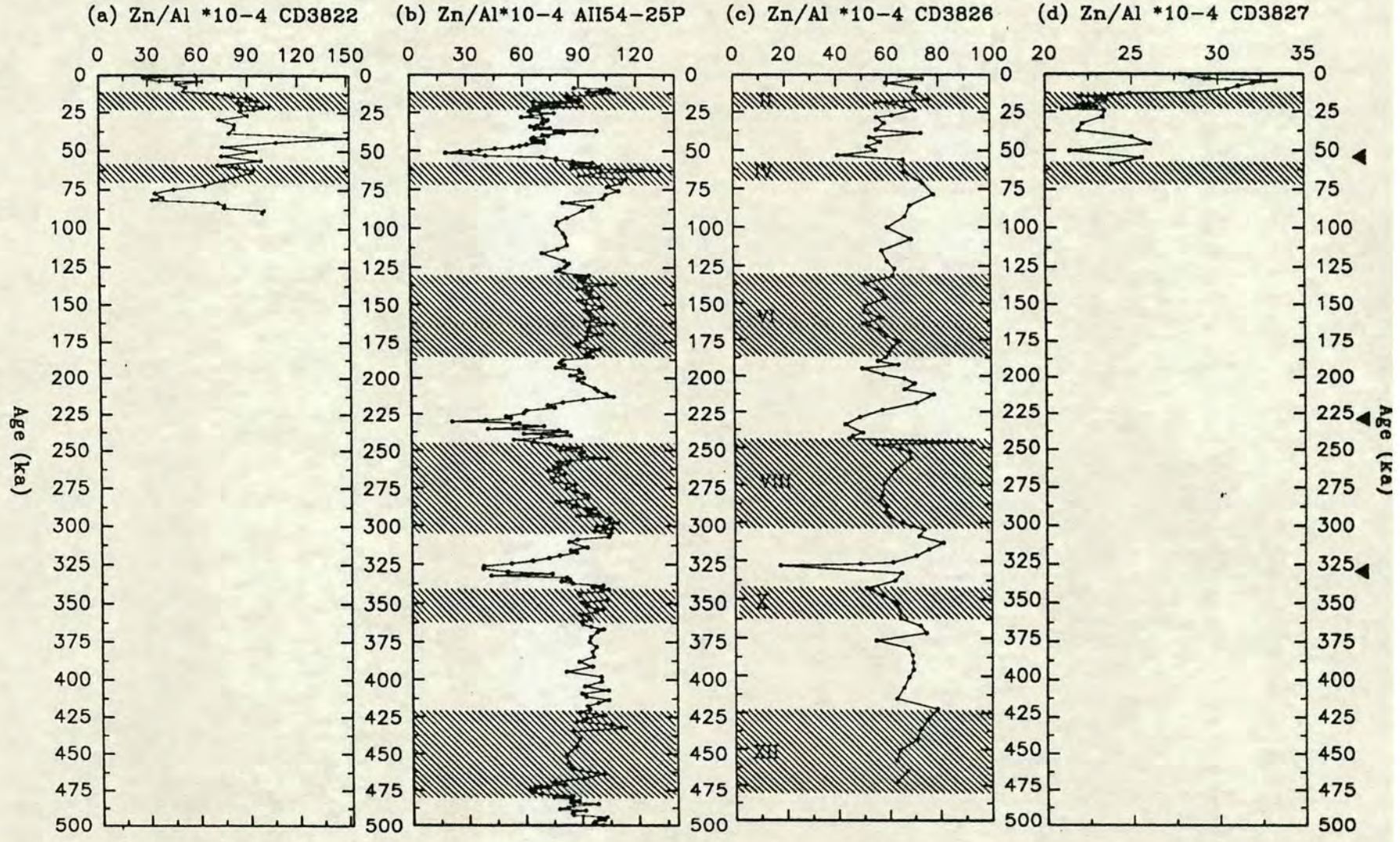

Figure 9.16 Temporal variations in V/Al × 10^{-4} from CD38 cores and core AII54-25PC. Shaded regions represent glacial stage II. IV, VI, VIII, X and XII. Triangles indicate the position of ash layers D (56ka), L (234ka) and K (328ka).

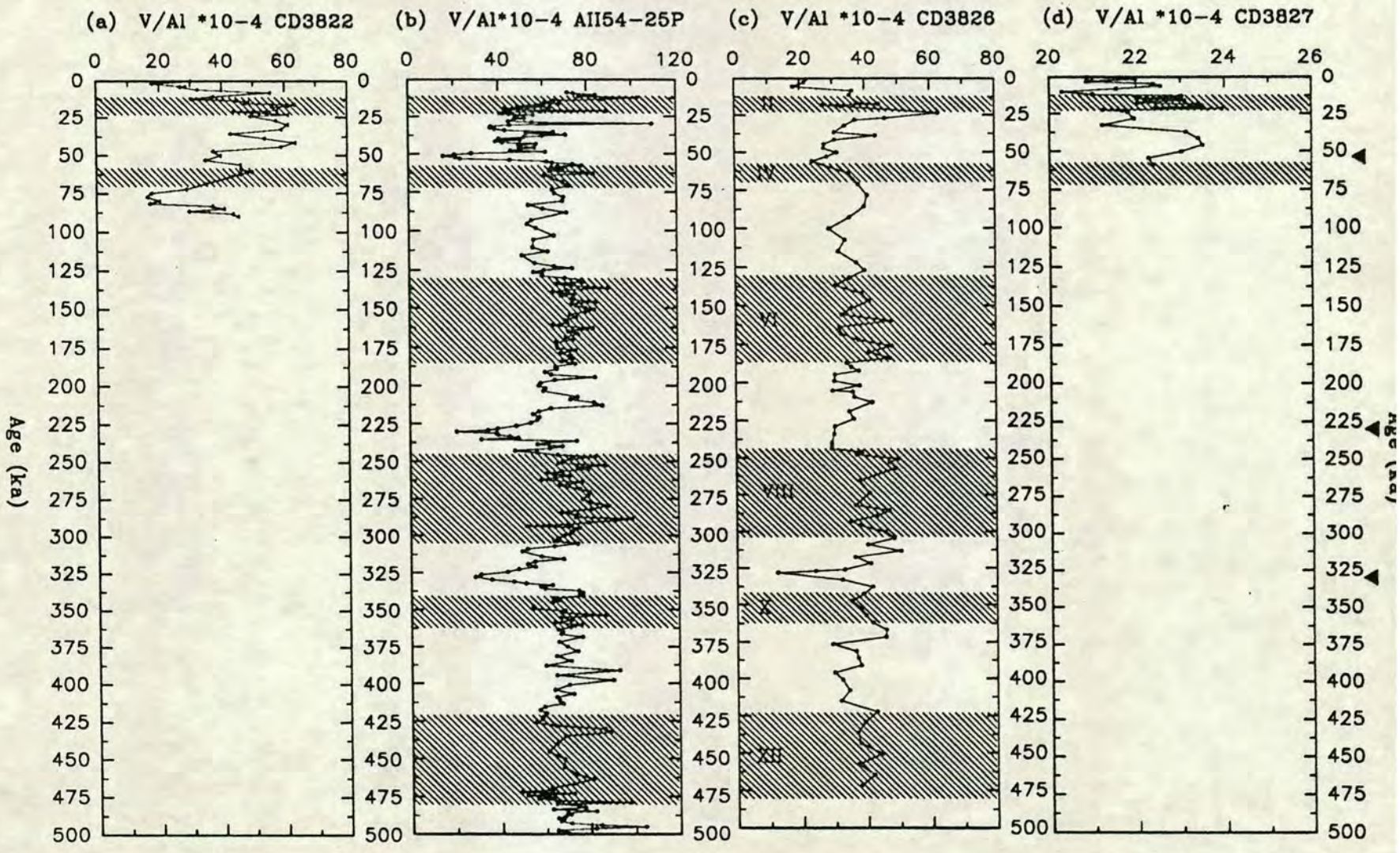

Figure 9.17 Temporal variations in Ni/Al × 10^{-4} from CD38 cores and core AII54-25PC. Shaded regions represent glacial stage II. IV, VI, VIII, X and XII. Triangles indicate the position of ash layers D (56ka), L (234ka) and K (328ka).

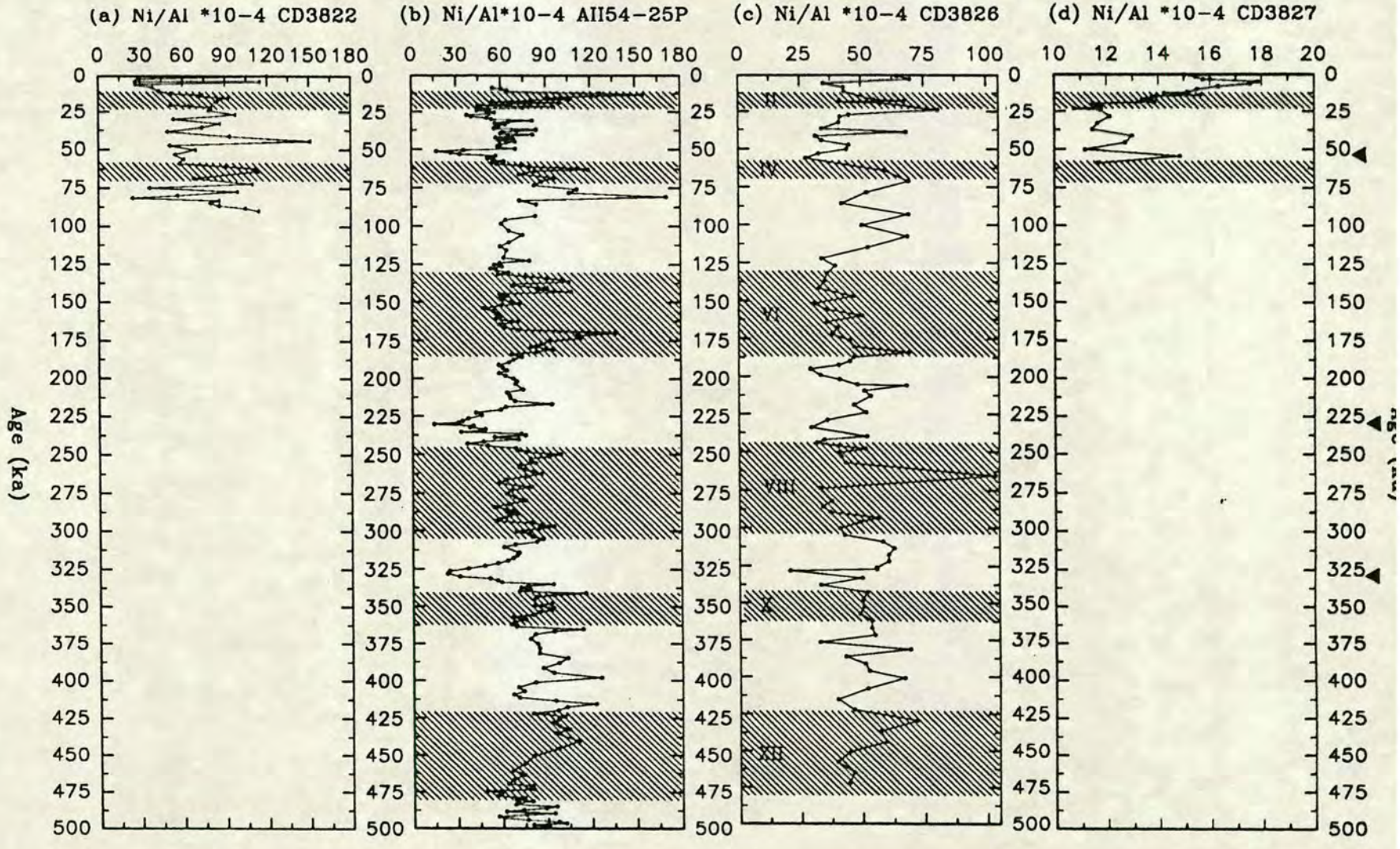

Figure 9.18 Temporal variations in Cu/Al × 10^{-4} from CD38 cores and core AII54-25PC. Shaded regions represent glacial stage II. IV, VI, VIII, X and XII. Triangles indicate the position of ash layers D (56ka), L (234ka) and K (328ka).

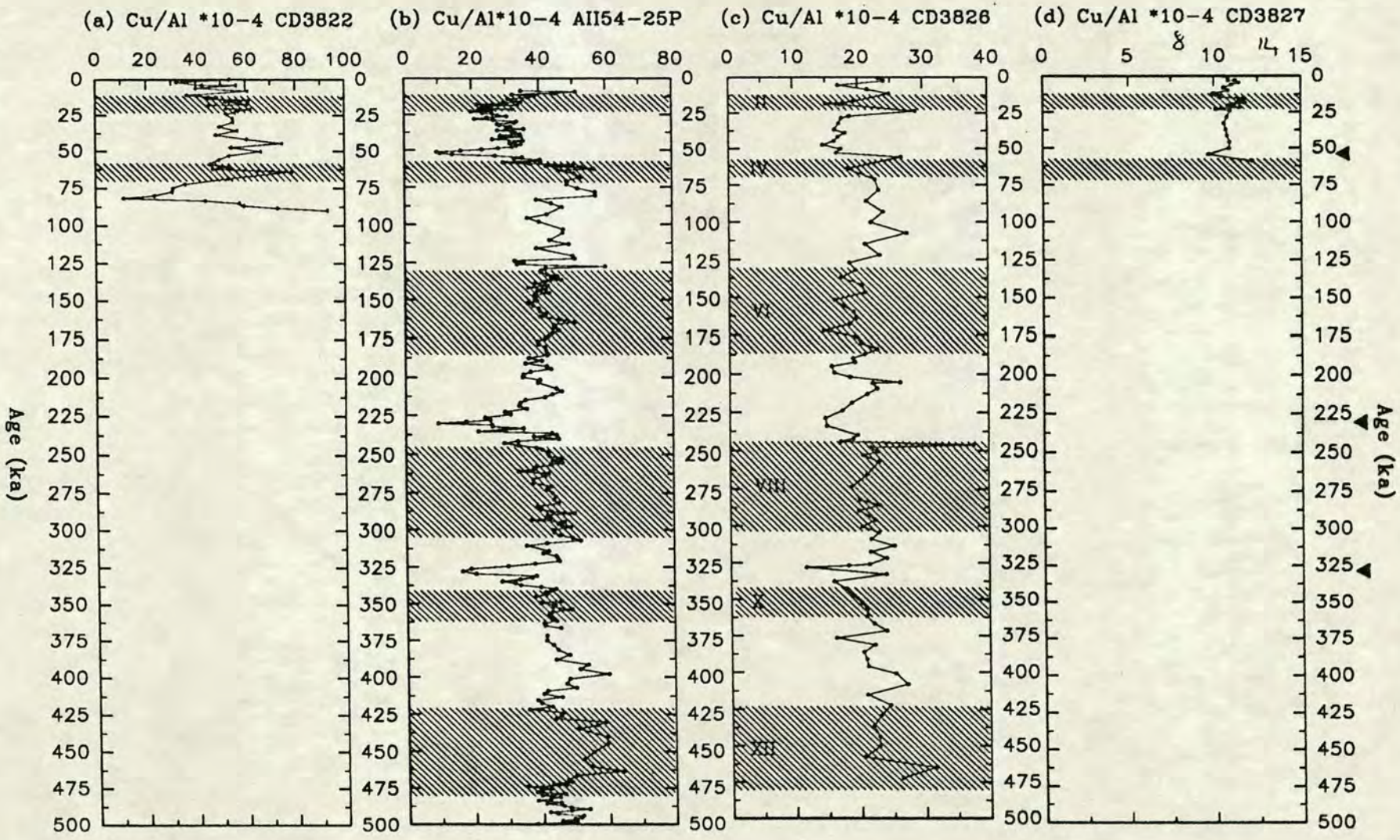

Figure 9.19 tries to summarise the relationships between the primary and secondary processes involved in determining excess metal contents in sediments.

According to Bonatti et al., (1971) the depth to the redoxcline increases westwards in the eastern equatorial Pacific away from the continental landmass. This is mainly because C-org contents tend to increase eastwards and promote shallowing of the redoxcline. From their simple map of thickness of oxide layer (figure 1, p.190, Bonatti et al., 1971), it is clear that cores CD3822 and P5 lie within the zone that commonly contains an oxide top of 8-15cm, in cores CD3826 and AII54-25PC it is between 1-3cm and, core CD3827 lies in the zone which the oxic surface sediments should be < 1cm thick. This is generally consistent with the findings during sedimentary logging of the cores (chapter 3).

In the reducing environment (below the redoxcline) solid phase Mn dissolves and enters the pore fluids. Transition metals will, to varying degrees, follow the Mn into the pore waters and diffuse upwards before being reprecipitated near the sediment surface. Alternatively, they may be recycled back into the bottom water. The mobility of different metals varies; Ni being strongly influenced by Mn remobilisation, whereas Zn and V are rather immobile (Finney et al., 1988). Bonatti et al., (1971) argue for the vertical immobility of Cu whereas Fischer et al. (1986) and Finney et al. (1988) favour a considerable influence of Mn remobilisation on the distribution of Cu.

This contrasting mobility would, at least in part, account for the relative enrichment of ExZn relative to ExCu in most the cores. The shallower the redoxcline the greater the chance of metal remobilisation to the surface sediment and, potentially, back into the water column as a benthic flux. Thus the contrast in Exmetal enrichments is parallelled by geographic differences relating to depth to the redoxcline and remobilisation potential discussed above. In addition to this, however, is the "primary" process of organic matter flux which limits the amount of metal being scavenged from the water column. Scavenging increases fairly uniformly with depth (Brewer et al., 1980; Balistrieri, et al., 1981), as a plentiful supply of dissolved metals increases with depth. However, the limiting factor for scavenging is the surface area of particulates available to dissolved metals in the water column. Therefore, cores with similar overlying productivities, but differing water depths, should have different contents of metals derived from organic particulates. Furthermore, as C-org falls through the water column it is degraded which may affect the surficial bonding

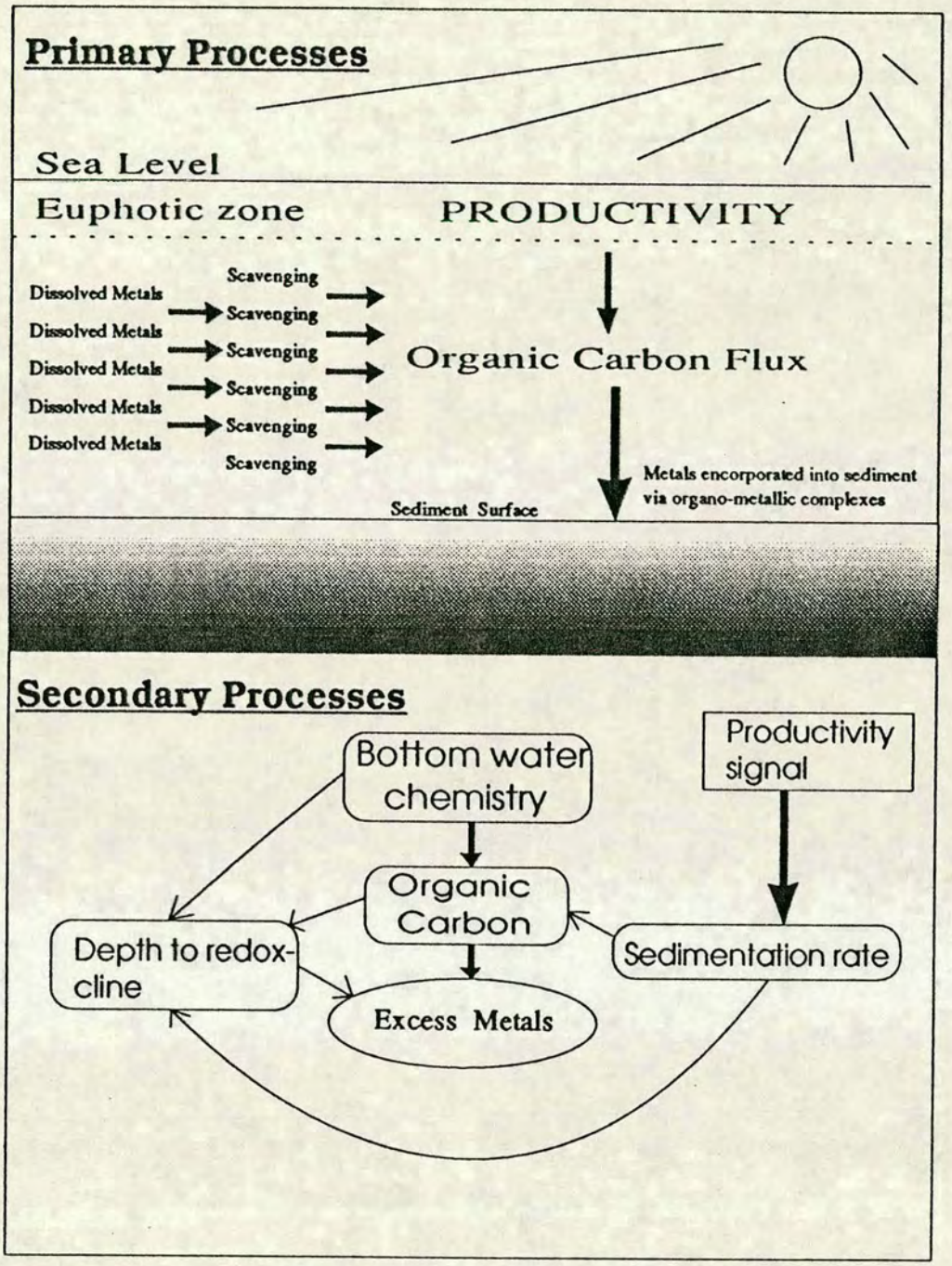

Figure 9.19 Diagrammatic representation of the processes involved in determining the excess metal concentration in marine sediments.

sites of the metals and even cause release of the metals back into the dissolved phase before the organic particulates are incorporated into the sediment.

Cores CD3822 and P5 have similar modern euphotic zone productivity (figure 2.7, this study) and similar (relatively high) overall bulk accumulation rates but, core P5 is from only 1540 m water depth compared to the 2340 m depth in which core CD3822 was recovered. Also, core P5 has, on average, half the C-org content (table 9.2a). Differences in excess metal content should, therefore, reflect differences in water depth and organic matter flux. The C-org MAR in CD3822 is approximately double that of P5, but the excess metal contents in core P5 are < half that of CD3822. Perhaps the differences are due to increases in scavenging of metals onto organic particulates over the extra 800 m water depth to the sediment surface in core CD3822 relative to core P5.

Core CD3827, which has the highest C-org contents and mass accumulation rates, is generally relatively low in excess metals. This may be due to the shallow redoxcline which would inhibit Mn-Fe oxide precipitation and any associated concentration of metals in the sediments. Metal contents in this core may also be influenced by any unusual sedimentation events or clay mineral input from the proximal continental landmass.

V is known to be depleted in the surface oxidised layers where it commonly exists in its fairly soluble $(VO_3)^{3-}$ state, whereas in sub-redoxcline depths V^{5+} should reduce to its lower valence states; being encorporated as insoluble hydroxides or sulphides (Bonatti et al. 1971). There is a surficial ExV depletion in cores P5, CD3822 and CD3826 which is consistent with the above argument. What is surprising is that the mean ExV content in core AII54-25PC is almost double that in core CD3826, despite the two cores being recovered close to each other and in similar water depths. Moreover there is less C-org, on average, in core AII54-25PC which would imply a potentially lower input of scavenged metals from organic matter flux. There is a similar discordance between ExCu values. Unless one assumes analytical differences or some highly localised phenomenon then these differences must remain unresolved.

Cu has been well studied in the water column (Bruland, 1980; Boyle et al., 1981), and is known to be associated with/scavenged by organic phases (Colier and Edmond, 1984; Sawlan and Murray, 1983). ExCu profiles tend to show the least variation of all the metals in all cores, which is in agreement with the work of Bonatti et al.

(1971), who believe that Cu is vertically immobile. However, this contradicts the work of Fischer et al. (1986) and Finney et al. (1988) who argue for considerable Cu mobilisation associated with Mn recycling. Cores P5 and CD3822, which suffer the least influence from recycling processes, both show relatively constant ExCu contents. Cores CD3826 and CD3827, however, are thought to be strongly influenced by Mn-Fe oxyhydroxide remobilisation of metals and both cores show strong depletion in ExCu. This would seem to corroborate the work of Fischer et al, (1986) and Finney et al (1988).

Carbonate free (CF) metal contents (Table 9.2b) follow a similar pattern to the excess metal contents; the slower the mean bulk accumulation rate, the higher the content of metals. Even in cores which have very different bulk chemistries (eg P5 and CD3827), contents of metals (CF) are remarkably similar, especially in Zn, Ni and V. Carbonate free metal contents are influenced by the differential dilution effects of varying aluminosilicate (Al-Si) input. Thus temporal variation in the metal (CF) may be as much a reflection of changes in Al-Si input as changes in the input of metals. If one attributes changes in metal (CF) contents dominantly to changes in the Al-Si input then metal (CF) contents may be used to illuminate relative changes in the temporal input of other tracers by normalising the variations with the metal contents. However, this assumes a relatively constant metal flux and there is little doubt that the actual rain of metals sorbed onto particulates and, the degree of concentration within the buried sediment, must change over time. However, the relationship between metal content and accumulation rate hints at the potential of using metals as indicators of changes in the input of other (eg biogenic) tracers. Zn with its rapid residence time of only approximately 510 years (Broecker and Peng, 1982), and which has been shown to be relatively constant in sediments from MANOP site H (Finney et al., 1988), would seem to have the greatest potential in this respect. There are many problems associated with this reasoning and it should, therefore, be treated cautiously.

The large variations in metal contents in, for example ExZn from core CD3822, which shows large increases during glacial stages II and IV, imply that the increased surface water production of organic carbon during glacial episodes has translated to the sediment a greater amount of scavenged metals (ie ExZn). This is because terrigenous Al-Si diluting material also increases during this time (chapter 5), which would tend to dilute the C-org and metals. Thus ExZn may therefore be tentatively used as a proxy for palaeoproductivity in cores that are not strongly influenced by

diagenetic remobilisation. Quantification of the temporal variations in the diagenetic remobilisation is, however, difficult.

Ni is believed to be the most mobile of the four transition metals studied (Bonatti et al. 1971) and is generally hosted in Mn-Fe species (Goldberg, 1954; Klinkhammer et al., 1982; Sawlan and Murray, 1983). It is perhaps because of this that ExNi curves appear to show no obvious pattern of variation except for an indication of increased values during interglacial periods especially in core AII54-25PC (figure 9.11a).

Cores relatively high in C-org (ie. CD3827 and, during glacials, CD3822) are also probably high in dissolved (pore water) C-org. Thus metals released from particulate biogenic material at the sediment/water interface may tend to become complexed by organic ligands in solution rather than become encorporated into oxide phases (Pedersen, 1979).

9.6 Conclusions

Mn enrichment in surficial sediment in all cores, except P5, is consistent with Mn-Fe oxyhydroxide development. Sub-surface highs in solid phase Mn in core CD3826 are attributed to Mn carbonate precipitation at loci of unusual mineralogy (eg volcanic ash deposits), and probably increased grain size. These Mn highs occur during glacials and interglacials and are, therefore, not related solely to bottom water and surface sediment redox potentials as proposed by Mangini (1988).

Mo and U are associated with organic carbon; the association being especially strong in core CD3827, where all three components are enriched during glacial stage II. This correlation of the redox sensitive elements Mo and U with C-org contents, especially in cores CD3827 and CD3822, discredits the hypothesis that increased C-org solely reflects increased productivity. This is because Mo and U increases during glacials indicate decreased bottom water oxygen concentrations which would tend to preferentially preserve the C-org irrespective of productivity changes. The enrichment of Mo in surface sediments is due to its association with Mn-Fe oxyhydroxides whereas any significant increases in Mo at depth are probably the result of complexation with Fe-monosulphides.

Excess metal can be divided into two groups on the basis of their relative enrichments: group 1- ExZn and ExNi and, group 2- ExV and ExCu. Generally ExZn ≥ ExNi > ExV ≥ ExCu. None of the metals show any statistically positive correlation with C-org, although V and C-org in core CD3827 are negatively correlated. The ExZn in core CD3822 parallels variations in other biogenic tracers. Increases in Excess metal appear to be independent of isotopic stage boundaries, occurring during glacial and interglacial episodes.

In core CD3826 and AII54-25PC; ExCu, ExNi and ExZn trends appear to show low frequency cyclicity. Core CD3827 has marked increases in ExZn, ExNi and ExCu at around 5 ka, which are probably the result of surficial enrichment mechanisms. ExV is depleted in the surface sediments of core CD3826 and CD3822 implying that V is in a soluble ($[VO_3]^{3-}$) oxide state in this region.

In cores that have relatively thick oxide tops, Exmetal contents are mainly influenced by the overlying euphotic zone productivity and particulate scavenging from the water column. However, in cores where the shallow redoxcline fosters rapid metal recycling, Mn-Fe hydroxide remobilisation processes dominate the content of excess metals in the sediment.

These conclusions may be summarised in the following way:

1. In core CD3822, C-org contents are the dominant control in Zn, Ni, V, and Cu distributions.
2. In cores CD3826 and AII54-25PC, Mn contents tend to be the dominant influence on the 4 metal contents.
3. In core CD3827, V and Cu distributions are controlled by C-org contents, Ni and Zn by Mn distributions.
4. In core P5, C-org tends to control Cu and Ni contents; V and Zn distributions show no association with either C-org or Mn contents.

CHAPTER 10

CONCLUDING CONSIDERATIONS

This final chapter attempts to summarise the information presented in previous chapters that is sometimes contradictory, and highlights the many difficulties in a study that attempts to understand the temporal variations in palaeoproductivity during the Quaternary. Most of work undertaken over the last half century in upwelling zones of the equatorial Pacific and other regions, has failed to arrive at a consistent quantification of variations in biological productivity from glacial to interglacial periods.

The sediments from this study divide into two groups: an eastern, essentially hemipelagic set (CD3826, CD3827 and AII54-25PC) which is carbonate poor and, by this definition, enriched in terrigenous material; and, a western, truly pelagic set (CD3814, CD3822 and P5) which is carbonate rich and low in terrigenous material. Mineralogical studies indicate that cores CD3826 and CD3827 contain higher contents of quartz, feldspar and chlorite compared with other cores, whereas CD3822 and P5 are relatively enriched in opaline silica and barite. Montmorillonite is the most common clay mineral in these sediments. Generally, the study of the sediment mineralogy suggests that the input of terrigenous material (eg feldspar) increases during glacial periods, especially towards the continents. These findings are consistent with increased availability of shelf sediment to reworking and redistribution further off-shore, especially during low sea-level stand glacial episodes. Furthermore, the increases in heavy mineral indicators Ti, Cr and Zr near the continents reflects a possibly coarser grained input. This may occur from increases in the mechanical reworking of shelf sediments and which would preferentially concentrate heavy minerals. However, the increased terrigenous content of the sediment during glacials may equally reflect a greater flux of aeolian material, resulting from increased aridity of the continents which could be subject to stronger winds. Increased ice volume is commensurate with an intensification of the tropical atmospheric wind system and increased upwelling (Parkin and Shackleton, 1973; Boyle, 1983; and, Janecek and Rea, 1984). Changes in the southern oscillation of atmospheric pressure systems could also change global wind systems, alter the thickness of the mixed layer and, consequently, alter the intensity of surface water productivity.

Correlation of the $^{18}O/^{16}O$ and $^{13}C/^{12}C$ ratios, from the calcite tests of the planktonic foraminifera *Neogloboquadrina dutertrei* and *Globigerinoides ruber*, with the SPECMAP reference curve, and geochemical correlation with core AII54-25PC and P6, allowed chronostratigraphies to be established for cores CD3822, CD3826,

CD3827 and P5. The tephra layers D (56ka), L (234ka) and K (328ka), are recognised in core CD3826 by their characteristically low Ti/Al, Fe/Al, Mg/Al and Cr/Al ratios, and high feldspathic content. The ages of these ash bands, which originated in the Quaternary volcanic centres of central America and NW south America, helped refine the chronostratigraphy. Although these techniques produced workable age models, only around 1 in 10 sample horizons at best (ie in core CD3826) can be assigned a definite date. The assumption of linear sedimentation rates between these control points (usually at the beginning or end of isotopic stages) has the potential to cause erroneous sedimentation rates and, therefore, inaccurate mass accumulation rates (MARs). This is because elemental flux variations are dominated by changes in the bulk accumulation rates, which are calculated from a mean of a potentially very large fluctuation in the sedimentation rate between each pair of control horizons (ie within each stage). Thus, although MARs can remove dilution effects (see below) by illustrating the input of tracers over time, they are critically dependent on the somewhat inadequate age models. However, in the absence of any better timescale, oxygen isotope stratigraphy and tephrachronology must be used if temporal studies are to be carried out.

The Holocene appears to be a period of rapidly decreasing terrigenous input throughout the region. In the Panama basin sediments, Ti, Cr and possibly, Zr are derived from two sources; central America, and the Galapagos archipelago. Unusually high ExTi values in core P5, which is virtually free of terrigenous input from the central American continent, result from increased input of Ti bearing basaltic material from the Galapagos archipelago. This high Ti material appears absent in the other sediments but it is, in reality, swamped by other terrigenous material from central America.

Hydrothermal deposits, which have unusually high Si_{terrig}/Al, Fe/Al and K/Al ratios, are present in core P5 (at 13.93ka) and at the base core CD3814. The hydrothermal deposit in the nearby core P6 was shown (Pedersen, 1979) to be a locus for trace metal enrichment. The corresponding deposit in core P5 showed no comparable trace metal concentrations. However this deposit does contain very high contents of feldspar which indicates that it may be a small local volcanic ash band, and not a purely hydrothermal deposit.

Temporal records of the contents of the biogenic tracers $CaCO_3$, C-org, SiO_2 and ExBa display two contrasting patterns of variation. $CaCO_3$ and C-org co-vary and

increase 2-3 fold during the glacial periods. However, biogenic SiO_2 and Ba (a proxy for barite), whilst generally co-varying with each other (although not statistically), do not oscillate on a glacial/interglacial cyclicity. Over the stage V/VI boundary (128ka), for example, SiO_2 and Ba (eg figure 6.15, p199), show little change. This penultimate deglaciation is perhaps the most significant global climatic event of the past 150ka which must have caused major changes in the ocean-atmosphere system. If biogenic SiO_2 and ExBa are influenced by changes in global climate systems, then one would expect there to be variation in these tracers over the stage V/VI boundary. That there is little or no change must indicate that SiO_2 and ExBa are more influenced by local oceanographic factors such as water mass distribution and nutrient availability, than by forcing of global climate systems by orbital variations. Dymond and Lyle (1985), Murray (1987), Lyle et al., (1988) and Rea et al. (1991) have observed similar differences between the records of SiO_2 and those of $CaCO_3$ and C-org. They suggest that although dissolution and degradation of $CaCO_3$ and C-org are important, changes in these tracers mainly record variations in surface water productivity. They also attribute the differences in these records, more to the greater sensitivity of biogenic SiO_2 based organisms to local oceanographic conditions and to changes in the composition of the plankton communities, than to the global forcing of oceanic and climatic conditions.

The remains of siliceous plankton communities compose a greater proportion of the non-carbonate fraction in core CD3822 than in any of the other cores. Furthermore, ExBa profiles tend to mirror the $\delta^{18}O$ profiles in cores CD3826 and CD3827, but broadly parallel the $\delta^{18}O$ in core CD3822. These and other factors suggest that core CD3822 has been subject to very different conditions of deposition to those of cores CD3826 and CD3827. Biogenic SiO_2 and barite are known to be susceptible to dissolution, but barite is almost certainly much more resistant than biogenic SiO_2. Furthermore, these two tracers have been shown to be broadly associated (although not statistically) and to reflect, to some degree, productivity. Therefore, variations in the ratio of one to the other should indicate the amount of dissolution of SiO_2 relative to barite. Dissolution of SiO_2 (as indicated by SiO_2/ExBa ratios) appears to have been greatest in core CD3826 which has the slowest mean accumulation rate of all the cores. The association of barite with C-org and $CaCO_3$, observed by Church, 1979, does not exist in the sediments studied here. Barite is one of the few minerals that is not derived from the shelf (terrigenous origin). Thus, the $CaCO_3$/ExBa ratio may illustrate differences in dilution by terrigenous material (see below), at least between cores of similar $CaCO_3$ productivity and water depth.

Long-term changes in the corrosiveness of the oceans to $CaCO_3$ must have a greater effect on sediment composition than the variations in the degree of saturation with respect to silica. These long-term changes in ocean chemistry, which are mainly the result of sea level and ice volume changes on an eccentricity frequency (100kyr), should have a relatively minor effect on the dissolution of SiO_2 which is mainly dependent on water temperature. Therefore, changes in the SiO_2 content should more accurately reflect variations in surface productivity which are, in turn, mainly forced by the intensity of the thermocline and, silicate and nutrient availability.

Core P5, at only 1500m water depth, has suffered negligible dissolution of $CaCO_3$ throughout its history. This core also has very high $CaCO_3$ contents. Although there are variations in the surface water productivity in different parts of the region, if one assumes that the productivity has been comparable throughout the region at any one time, then differences in the $CaCO_3$ content between core P5 and the other cores are the net result of increased dissolution and dilution by terrigenous material.

Variations in the $CaCO_3$ MAR/C-org MAR ratio act as a proxy for long-term CO_2 budgets between the atmosphere and oceans. In core CD3826, there has been a gradual, though noisy, decrease in this ratio indicating a reduced potential for net CO_2 transfer to the atmosphere from the surface waters, over the past 472ka in the region. More detailed examination of the $CaCO_3$ MAR/C-org MAR ratio curve provided evidence for two contrasting hypotheses about what caused the glacial depletions in atmospheric CO_2 during the Quaternary. A marked increase in the $CaCO_3$ MAR/C-org MAR ratio at the base of stage VI, and the gradual decrease during this stage, argues for external forcing of productivity variations, as proposed by Lyle (1988). This is because the drop in atmospheric CO_2 during glacials would promote sequestration of CO_2 into the oceans as a result of increased C-org associated production. In contrast, the increase in $CaCO_3$ MAR/C-org MAR ratio during glacial stage VIII may reflect the increase in atmospheric CO_2 and attendant temperature rise, which forced the climate system to switch to an interglacial-type episode in stage VII. This second scenario is consistent with the hypothesis of Sarnthein et al., (1987).

Murray (1987) claimed that 60% of the $CaCO_3$ produced in the surface waters at MANOP site C is recycled due mainly to dissolution. The assumption of Rea et al., (1991) that this figure could be applied to a different core would seem to be very incautious. However, both MANOP site C (Murray, 1987) and core RC11-210 (Rea

et al., 1991) were recovered from very similar water depths, and would probably have been subject to broadly similar carbonate dissolution histories. Furthermore, Holocene $CaCO_3$ MARs in the Panama basin (Swift and Wenekam, 1978) are broadly consistent with the argument that palaeoproductivity is approximately 2.5 times the surface sediment accumulation rate of $CaCO_3$.

Biogenic tracer MAR relationships showed a huge variation in the ratio between them in different cores. For example, an X-Y plot of $CaCO_3$ MAR versus C-org MAR (figure 7.4, p229) shows that core P5 has a mean ratio of $CaCO_3$ MAR/C-org MAR (as defined by the gradient of the regression line) two orders of magnitude greater than the same ratio in core CD3827. Similar trends are found in the $CaCO_3$ MAR versus SiO_2 MAR, and $CaCO_3$ MAR versus ExBa MAR. It seems unlikely that such large differences may be solely the result of dissolution or production variations between cores, or even a combination of the two. Therefore the problems of age model development and overestimated bulk accumulation rates (as discussed above) may be influencing, if not dominating, these relationships. Similarly, the very marked increases in all the MARs, especially during stage II in all cores, may also be strongly influenced by overestimated sedimentation rates and, therefore, MARs. This is not to say that productivity does not increase during these times, but it is difficult to imagine a scenario wherein productivity rates increase so rapidly and by such large amounts.

Increases in the ExSr/ExCa ratio occur during glacial periods, and possibly reflect a greater abundance of foraminifera relative to coccoliths at these times (ie changes in the carbonate production). These two groups are in mutual opposition, because coccoliths are phytoplankton, whereas foraminifera are zooplankton. Coccoliths tend to be more abundant in stable central ocean gyres (D. Kroon pers. comm.), and it is difficult to explain why they may become relatively more abundant than foraminifera in the unstable upwelling environment at any point in time. Therefore, changes in the abundance of coccoliths may simply reflect the degree of winnowing by bottom currents which would preferentially concentrate coccoliths relative to the foraminifera. This would argue in favour of increased bottom current intensity during interglacials in the Panama basin, which is consistent with rising sea level and increased oceanic circulation, after the relatively stagnant glacials.

Calculation of palaeoproductivity from the empirically derived equation of Muller and Suess (1979), which is very similar to the equation used by Sarnthein et al

(1987), suggests a three fold increase in productivity during the last glacial maximum, compared to present values. As the modern level of euphotic zone productivity in the eastern equatorial Pacific is already extremely high, it is hard to imagine a scenario wherein the relatively confined upwelling region might support three times the present biomass. Thus, calculation of palaeoproductivity, using this method, is thought to be unrealistic. Nevertheless, increases in C-org during glacials, continues to be regarded as a reflection of increases in surface water productivity (Pedersen, 1979, 1992; Lyle et al., 1988; Rea et al., 1991). All agree that the dominant control on C-org content in the sediment is productivity and accumulation rate and, as Muller and Suess (1979) point out, a 10 times increase in accumulation rate will only increase C-org contents two fold. Thus, although accumulation rate, which is dominated by $CaCO_3$ content (Murray, 1987) and, therefore, dissolution cycles (Farrell and Prell, 1991), is undoubtedly important in determining C-org content, it cannot be the sole cause and the dominating influence of the 2-3 times increase in C-org observed in these sediments. Furthermore, increases in $CaCO_3$ preservation, and hence an increase in $CaCO_3$ accumulation rate would, if anything, tend to dilute the C-org contents. Nevertheless, mean C-org contents in core CD3827 are the highest of all the cores and yet this core has been subject to the greatest terrigenous dilution. The C-org spike during glacials in this core, and probably core CD3826, seems to be caused by an increase in preservation resulting from the rapid accumulation, coupled with high primary input of C-org from the intense upwelling and production in this region relatively close to the coast. C-org contents in core P5 are generally very low and show little variation. Terrigenous dilution is negligible in this core and the relatively high accumulation rate, especially during stage II, would promote preservation of both $CaCO_3$ and C-org. Thus, the profile of C-org contents in this core are probably due primarily to the dilution effect of $CaCO_3$.

The problem of dilution by terrigenous material from the shelf, especially during low sea level stand glacial episodes, is a factor that has been largely ignored in previous studies. Al has been used as an indicator of terrigenous material, and ratioed against biogenic components to illustrate variations in these phases. Problems arise when changes in the input of Al are equivalent to, or greater than, the variations in biological productivity. Thus, changes in the ratios of biogenic tracers to Al may be as much a reflection of terrigenous changes, as biogenic productivity variations. Furthermore, with over 100m of possible sea level change from full glacial to full interglacial, variations in Al input must have been significant, and therefore, influential in controlling changes in biogenic elemental ratios to Al.

In addition to the dilution effects of aluminosilicates, there may be inputs of $CaCO_3$ and C-org from the shelf. The contribution from shelf carbonate is very difficult to quantify. However, shelf C-org will always be diagenetically less active and will not have the same association with I or Br, as "normal" marine carbon does. Thus, differences in the halogen to C-org ratios from normal marine values should indicate the relative proportions of non-marine (shelf) to truly marine carbon in the sediment. Surface I/C-org and Br/C-org ratios were slightly low for normal marine sediments deposited in oxidising conditions. Furthermore, they tended to increase towards more normal open marine values, with increasing distance from land (cp. core CD3827 and P5). This probably results from the input of diagenetically less potent, reworked carbon from the shelves with which I and Br would not readily complex. This is not to say that shelf C-org is completely inert and refractory because reworked organic carbon in NE Atlantic distal turbidites has been shown to be diagenetically active, and to have some effect on the oxidation front in the sediment (Thomson et al., 1987). More detailed study of the nature of the organic matter in sediments would illuminate such problems and perhaps help quantify the degree of shelf dilution. Br and especially, I contents tend to increase during glacials. Variations in the I/Br ratio indicate that Br is relatively less labile during diagenesis. The diagenetic mobility of both I and Br possibly renders them unreliable as indicators of palaeoproductivity.

Although fragmentation of foraminifera (and coccoliths) is mainly caused by dissolution (Steens et al., 1991), $CaCO_3$ material on the shelves must be subject to relatively high energy environments resulting in the breakup of the foraminiferal tests. Thus fragmentation indices may hint at the proportion of reworked carbonate in the sediment, especially in supra-lysoclinal cores where dissolution is reduced. During the picking of foraminifera for stable isotope analysis, it was observed that the proportion of foraminifera stained with Fe oxide, to non stained foraminifera, changes spatially and temporally but was not systematically recorded. As the condition of foraminifera must in some way reflect their depositional histories, it is suggested that these stained foraminifera possibly originated from the shelf and are reworked, at least to some degree. The stained foraminifera were observed to be both fragmented and whole.

Biogenic, skeletal P (Pexcess-1 and Pexcess-2) in this study behaves differently to the other biogenic tracers, by increasing during interglacial periods. This finding contrasts with that of Murray (1987) who concluded that P is essentially equally

partitioned between organic phases and calcite tests which increase during glacials. Irrespective of which host P occupies, it is irrefutably a mainly biological indicator (Froelich et al., 1982) and skeletal P is probably less prone to dissolution than other biogenic indicators. Therefore, its increase during interglacial periods could indicate increased biological production. However, the loss in biomass between each trophic level in the food chain must ensure that the input of P from biogenic skeletal production is orders of magnitude less than in primary and secondary production as indicated by other biogenic tracers. That biogenic skeletal P is derived from a very different part food chain to other biogenic tracers may introduce lags in the records of each biomarker, and even account for the anomalous timing of the increases in the P signal.

Interpretation of redox variations in the surface sediments associated with Mn-Fe oxyhydroxides have been hindered by lack of pore water analysis. Large increases in solid phase Mn (IV) at depth in core CD3826, are shown to be the result of Mn carbonate precipitation in horizons of unusual mineralogy (eg volcanic ash layers), and possibly increased grain size. These increases in Mn occur during both glacial and interglacial events. This trend argues against the hypothesis of Mangini (1988), who proposed that Mn precipitation will only occur at the beginning of interglacial periods when oceanic circulation and bottom water oxygen contents were increasing, following a stagnant glacial episode. Cores which have thick Mn-Fe oxide tops (CD3822 and P5), tend to promote the preservation of the primary signal of metal input on particulates. These may have formed as a particulate phase, either directly or indirectly as the result of productivity changes in the overlying water column. Cores CD3826 and CD3827, however, have relatively shallow redoxclines, which foster rapid recycling of the metals within the sediment. This feature, together with the high terrigenous contribution of heavy metals, effectively masks the original production signal of metals sorbed onto particulates. Generally, the hierarchy of metal enrichment is $ExZn \geq ExNi > ExV \geq ExCu$, and none of the metals show a statistical correlation with C-org. Increases in Exmetals are independent of isotopic stage boundaries, occurring during glacial and interglacial episodes. In contrast, solid phase Mo and U tend to be correlated with C-org, especially in core CD3827. Increases in Mo and U at depth may indicate a lowered oxygen environment during burial, which would preferentially allow greater preservation of the C-org. This effectively discredits the hypothesis that C-org contents are solely the result of increased surface water production, and the trend of these two elements favours preservation as an important factor in determining the C-org content of these

sediments. However it should be noted that there may be diffusion of Mo and U from the overlying water column in low redox potential environments.

Principal component analysis defined 3 main sediment phases which account for the majority of the variance in the dataset in each core. These factors are: (i) a biogenic/organic factor; (ii) a terrigenous aluminosilicate factor which may be subdivide into a feldspathic and illite component, and a Fe-Mg component possibly associated with smectite/chlorite; and, (iii) a diagenetic/authigenic factor. Cores P5 and CD3822 have especially strong weightings on factor (i) reflecting the small influence of terrigenous material, whereas cores CD3826 and CD3827 are more dominated by factor (ii), which is as expected given their proximity to the continental landmass.

The difficulties in the study of the multi-component system of sediments are shown. To improve interpretation of the palaeoenvironment of deposition of these sediments, and to further asses the influence that palaeoclimate and palaeoproductivity changes have on their composition, it may be important to conduct detailed faunal studies on the relative abundance and chemical composition of the plankton communities themselves. This may more accurately illustrate the changes in the different types of production over time. Similarly, stable isotope analysis of the different ontogenetic stages in the foraminiferal life-cycle would further illustrate changes in the production cycle. Grain size studies of the terrigenous fraction of the sediment would be especially useful to illuminate variations in the aeolian input. Grain size studies on the bulk sediment may, however, help illustrate variations in the relative abundance of foraminifera to coccoliths, and to corroborate the conclusion that changes in the ExSr/ExCa ratio do not simply reflect bottom current intensity but do, in fact, record changes in the carbonate plankton community.

This study has illustrated spatial and temporal changes in the type of production (siliceous and carbonate), and that these variations can occur within a single production pulse. It also suggests that the dilution effects of shelf material (aluminosilicate, C-org and $CaCO_3$), in determining the final sediment signature, may be significant and have been underestimated in previous studies. Inadequacies inherent in oxygen isotope chronostratigraphy can cause gross overestimation of elemental fluxes and, consequently, will result in erroneous estimates of palaeoproductivity and palaeoclimate variations.

REFERENCES

ACHERMAN, F., (1980) A procedure for correcting the grain size effects of heavy metal analysis of esturine and coastal sediments. *Technol. Lett. 1*, 518-527.

ADELSECK, C.G. JR. AND ANDERSON, T.F., (1978) The late Pliestocene record of productivity fluctations in the eastern equatorial Pacific ocean. *Geology, 6*, 388-391.

ANDERSEN, R.F.; FLEISHER, M.Q.; AND LEHURAY, A.P., (1989B) Concentration, oxidation state, and particulate flux of uranium in the Black sea. *Geochim. et Cosmochim. Acta 53*, 2215-2224.

ANDERSEN, R.F.; LEHURAY, A.P.; FLEISHER, M.Q.; AND MURRAY, J.W., (1989A) Uranium deposition in Saanich Inlet, Vancouver Island. *Geochim. et Cosmochim. Acta 53*, 2205-2213.

ARCHER, D. (1969) *X-ray Analysis of Deep-Sea Sediments.* Unpubld. Ph.D. Thesis, University of Manchester, 108pp.

ARCHER, D.E., (1990) The distribution of calcite in deep-sea sediments: an *in-situ* microelectrode study. Ph.D. Thesis, 300pp. Univ. of Wash., Seattle.

ARRENHIUS, G.O., (1952). "Sediment cores from the east pacific". In *Reports of the Swedish Deep Sea Expedition. (1947-1948). (ed. H.Pettersson) Vol. 5*, 1-227.

ARRHENIUS, G.O.S., (1963) Pelagic sediments. in: *The Sea (ed. M.N. Hill), Vol. 3*, 655-727. Wiley Interscience.

ARRHENIUS, G.O.S., BRAMLETTE, M.N. AND PICIOTTO, E., (1957) Localisation of radioactive and stable heavy nuclides in ocean sediments. *Nature 180*, 85-86.

BALISTRIERI, L., BREWER, P.G. AND MURRAY, J.W., (1981) Scavenging residence times of trace metals and surface chemistries of sinking particles in the deep coean. *Deep Sea Res., 28A*, 101-121.

BARKLEY, R.A. AND THOMPSON, T.G., (1960) The total iodine and iodate content of seawater, *Deep Sea Res., 7*, 24-34.

BARNOLA, J.M.; RAYNAUD, D.; KOROTKEVICH, Y.S. AND LORIUS, C., (1987) Vostok ice core provides 160 000 year record of armospheric CO_2. *Nature 329*, 408-418.

BENDER, M.L.; BROECKER, W.; GORNITZ, V.; LIDDEL, V.; KAY, R.; SUN, S.S. AND BISCAYE, P., (1971) Geochemistry of three cores from the East Pacific Rise. *Earth and Plan. Sci. Lett.* ***12***, 425-433.

BERGER W.H., FISHER, K., LAI, C., AND WU, G. (1987) Ocean productivity and organic carbon flux. Part I. *Overview and maps of primary production and export production, SIO Ref. 97-30*, Univ. of Calif., San Diego.

BERGER, A.L, (1985) Quaternary fluctuations in the northern hemisphere tradewinds and westerlies. *Quat. Res.*, ***24***, 150-163.

BERGER, A.L., (1978) Long-term variations of caloric solar radiation resulting from the earth's orbital elements. *Quaternary Research*, ***9***, 139-167.

BERGER, W.H. AND VINCENT, E., (1986) Deep-sea carbonates: Reading the carbon-isotope signal. *Geologische Rundschau* ***75(1)***, 249-269.

BERGER, W.H., (1968). Planktonic foraminifera: selective solution and paleoclimactic interpretation. *Deep Sea Research*, ***15***, 31-43.

BERGER, W.H., (1970A) Planktonic foraminifera: selective solution and the lysocline. *Marine Geol.*, ***8***, 111-138.

BERGER, W.H., (1970B) Biogenous deep-sea sediments: Fractionation by deep-sea circulation. *Geol. Soc. Amer., Bull.*, ***81***, 1385-1402.

BERGER, W.H., (1973). Deep sea carbonates: Pleistocene dissolution cycles. *J. Foram. Res.*, ***3***, 187-195.

BERGER, W.H., (1975) Deep-sea carbonates: Dissolution profiles from foraminiferal preservation, in: Dissolution of Deep-Sea Carbonates, edited by A.W.H. Bé and W.H. Berger, *Spec. Publ. Cushman Found. Foraminiferal Res.*, ***13***, 82-86.

BERGER, W.H., (1976) Biogenous deep-sea sediments: production, preservation and interpretation. in: J.P. Riley and Chester, R. (eds), *Chemical Oceanography Vol.*, ***5***, 265-374, Academic Press, New York.

BERGER, W.H., FINKEL, R.C., KILLINGLEY AND MARCHIG, V., (1983) Glacial-Holocene transition in deep-sea sediments: manganese spike in the eastern equatorial Pacific. *Nature 303*, 231-233.

BERNER, R.A., (1971). *Priciples of Chemical Sedimentology*. Mcgraw-Hill, New York, 240pp.

BERNER, R.A., (1973) Phosphorite removal from sea water by adsorption on volcanigenic ferric oxides. *Earth Plan. Sci Lett., 18(1)*, 77-86.

BERNER, R.R., (1975). Diagentic models of dissolved species in the interstitial waters of compacting sediments. *Amer. Journ. of Sci. 275*, 88-96.

BERRANG, P.G., AND GRILL, E.V., (1974) The effect of manganese oxide scavenging on molybdenum in Saanich inlet, British Colombia. *Marine Chem., 2*, 125-148.

BERTINE, K.K., AND TUREKIAN, K.K., (1973) Molybdenum in marine deposits. *Geochim. et Cosmochim. Acta 37*, 1415-1434.

BISCHOFF, J.L.; AND ROSENBAUER, R.J., (1977) Recent metalliferous sediments in the North Pacific manganese nodule area. *Earth and Plan. Sci. Lett., 33*, 379-388.

BISCHOFF, J.L.; HEATH, G.R. AND LEINEN, M., (1979) Geochemistry fo deep sea sediments from the pacific manganese nodule province: Domes sites A, B and C. Bischoff and Piper (eds.) in *Marine Geology and Oceanography of the Pacific Manganese Nodule Province*, Plenum New York, 397-473.

BISCHOP, J.K.B., (1988). The Barite-opal-organic carbon association in oceanic particulate matter. *Nature, 332*, 341-343.

BOJANOWSKI, R. AND PASLAWSKA, S., (1970) On the occurrence of iodine in bottom sediments and interstitial waters of the southern Baltic sea, *Acta Geophys. Pol., 18*, 227-.

BONATTI, E.; SIMMONS, E.C.; BERGER, D.; HAMLYN, P.R. AND LAWRENCE, J., (1983) Ultramafic rock/seawater interactions in the oceanic crust. Mg-silicate (sepiolite) deposit from the Indian ocean floor. *Earth and Plan. Sci. Lett., 62*, 229-238.

BONATTI. E., FISHER, D.F., JOENSUU, O. AND RYDELL, H.S., (1972) Post depositional mobility of some transition elements, phosphorus, uranium and thorium in deep-sea sediments. *Geochim. et Cosmochim. Acta, 35*, 189-201.

BORDOVISKY, O.K., (1965A) Transformation and diagenesis of organic matter in sediments. *Marine Geol., 3*, 83-114.

BORDOVISKY, O.K., (1965B) Accumulation of organic matter in bottom sediments. *Marine Geol,, 3*, 33-82.

BOSTROM, K., (1973) The origin and fate of metalliferous active ridge sediments. Stockholm Contribut. *Geol., 27*, 149-243.

BOSTROM, K., JOENSSU, O., MOORE, C., BOSTROM, B., BALZIEL, M., AND HOROWITZ, A., (1973) Geochemistry of barium in pelagic sediments. *Lithos, 6*, 159-174.

BOSTROM, K.; AND PETERSON, M.N.A., (1966) Precipitates from hydrothermal exhalations of the East Pacific Rise, *Econ. Geol. 61*, 1258-1265.

BOSTROM, K.; JONESSU, O.; BROHM, I., (1974) Plankton: its chemical composition and its significance as a source of pelagic sediments. *Chem. Geol. 14*, 255-271.

BOSTROM, K.; PETERSON, M.N.A.; JOESSU, O. AND FISCHER, D.E., (1969) Aluminium-poor ferromangoan sediments on active ocean ridges. *J. Geophys. Res. 74*, 3261-3270.

BOWEN, H.J.M., (1966) *Trace Elements in Biochemistry*, Academic Press, London.

BOWLES, F.A., JACK, R.N. AND CARMICHAEL, I.S.E., (1973). Investigations of deep-sea volcanic ashlayers from equatorial pacific cores. *Geol. Soc. of America Bull, 84* 2371-2388.

BOYLE ET AL., E.A, HUESTED, S.S., AND JONES, S.P., (1981) On the distribution of copper, nickel and cadmium in the surface waters of the north Atlantic and north Pacific oceans. *J. Geophys. Res., 86*, 8048-8066.

BOYLE, E.A., (1983) Chemical accumulation variations under the Peru Current during the past 130,000 years. *J. Geophys. Res., 88*, 7667-7680.

BOYLE, E.A., (1988A) The role of vertical chemical fractionation in controlling Late Quaternary atmospheric carbon dioxide. *J. Geophys. Res., 93*, 15701-15714.

BOYLE, E.A., (1988B) Vertical nutrient fractionation and glacial/interglacial CO_2 cycles. *Nature 331*, 55-56.

BOYLE, E.A., AND KEIGWIN, L.D., (1982) Deep-circulation of the north Atlantic over the last 200,000 years: geochemical evidence. *Science, 218*, 784-787.

BOYLE, E.A., AND KEIGWIN, L.D., (1985) Comparisons of Atlantic and Pacific paleochemical records for the last 215,000 years: changes in deep-ocean circulation and chemical inventories. *Earth Plan. Sci. Lett., 76*, 135-150.

BOYLE, E.A., AND KEIGWIN, L.D., (1987) North Atlantic thermohaline circulation during the past 20,000 years linked to high latitude surface temperature. *Nature, 330*, 35-40.

BRADLEY, R.S., (1989), *Quaternary Paleoclimatology: methods of paleoclimatic reconstruction*, Boston, London, Allen & Unwin, 472pp.

BREWER, G.B., NOZAKI, Y., SPENCER, D.W., AND FLEER, A.P., (1980) Sediment trap experiments in the deep North Atlantic: isotopic and elemental fluxes. *J. Marine Res. 38(4)*,703-.

BROECKER, W.S. (1982) Glacial to interglacial changes in ocean chemistry. *Prog. in Oceanogr. 11*, 151-197.

BROECKER, W.S. AND TAKAHASHI, T., (1978) The relationship between lysocline depth and *in-situ* carbonate ion concentration. *Deep-Sea Res., 27*, 591-613.

BROECKER, W.S., (1971) Calcite accumulation rates and glacial to interglacial changs in oceanic mixing, in *The Late Cenozoic Glaical Ages*, edited by K.K. Turekian, 239-265, Yale Univ. Press, New Haven, Conn.

BROECKER, W.S., AND PENG, T.H., (1982) *Tracers in the Sea*, Eldigio, Palisades, 690pp.

BRONGERSMA-SANDERS, M.K., (1966), *Ned. Akad. Wet. Proc. B70*, 93-99.

BRULAND, K.W., (1980) Oceanographic distribution of Cd, Zn, Ni, and Cu in the North Pacific. *Earth Plan. Sci. Lett. 47*, 177-198.

BURNETT, W.C., (1977) Geochemistry and origin of phosphorite deposits from off Peru and Chile. *Geol. Soc. Amer. Bull, 88(6)*, 813-823.

CALVERT, S.E. AND PRICE, N.B., (1983). Geochemistry of Namibian shelf sediments. Suess, E. and Theide, J. (eds). in: *Coastal upwelling (part A)*, Plenum publishing corporation.

CALVERT, S.E., (1968) Silica balance in the oceans and diagenesis, *Nature, 219*, 919-920.

CALVERT, S.E., (1976) The Mineralogy and Geochemistry of Near Shore Sediments. In: J.P. Riley and R. Chester (eds) *Chemical Oceanography, Vol 6*. 187-280.

CALVERT, S.E., AND MORRIS, A.J., (1977) Geochemical studies of organic rich sediments from the Namibian shelf II Metal-organic associations, in: M. Angel (ed) *A voyage of discovery*, Pergamon Press, London 580-667.

CALVERT, S.E., AND PRICE, N.B., (1971) Recent sediments from the south west Africa shelf, in: F.M. Delany (ed), Geology of the east Atlantic continent SE margin, *Institute of geological Science Report 70/16*, 171-185.

CALVERT, S.E., AND PRICE, N.B., (1977) Geochemical variaiton in ferromanganese nodules and associated sediments from the Pacific. *Marine Chmeistry 5*, 43-74.

CALVERT, S.E., AND PRICE, N.B., (1983) Geochemistry of Namibian shelf sediments, Suess, E., and Thiede, J., (eds) in: *Coastal Upwelling (Part A)*, Plenum publishing corporation.

CANN, J.R., (1969) Spilites from the Carlsberg Ridge, Indian Ocean. *J. Petrology 10*, 1-19.

CARROL, D. AND STARKY, H.C. (1971) reactivity of clay minerals with acids and alkalies. *Clays Clay Minerals 19*, 321-333.

CARROL, D., (1958) Role of clay minerals in the transportation of iron. *Geochim et Cosmochim Acta, 14*, 1-28.

CHAN, L.H., EDMOND, J.M., STALLARD, R.F., BROECKER, W.S., CHUNG, Y.C., WEISS, R.F., AND KU, T.L., (1976) Radium and Barium at GEOSECS stations in the Atlantic and Pacific. *Earth Plan. Sci. Lett., 32*, 258-267.

CHAO, G.Y., (1969) *2θ (Cu) Table for common minerals.* Geological paper 69-2, Carleton University, Ottowa, Canada.

CHASE T.E.; MENARD H.W. AND MAMMERICKX J., (1970) Bathymetry of the north Pacific. *IMR Technical Reports Series TR-15 Institutue of marine resources*, Scripps Institution of Oceanography.

CHAUDARI, S.; AND CULLERS, R.L., (1979) The distribution of rare earth elements in deeply buried Gulf coast sediments, *Chem. Geol., 24*, 327-338.

CHAVEZ F.P. AND BARBER R.T., (1987) An estimate of new production in the equatorial Pacific. *Deep Sea Res. 28*, 323-339.

CHESTER, R. AND ASTON, S.R., (1976) The geochemistry of deep sea sediments. In J.P. Riley and R. Chester (eds) *Chemical Oceanography, Vol 6*, 281-390, Academic Press, London, 414pp.

CHMELIK, F.B. (1967) Electro-Osmotic core cutting. *Marine Chemistry 5*, 321-325.

CHURCH, T.M., (1970). *Marine Barite.* Unpublished Ph.D. thesis, University of California.

CHURCH, T.M., (1979). Marine Barite. Marine minerals, *Min. Soc. Am. Short course Notes Vol 6.*

CLIMAP AUTHORS, (1976) Climate Long Range Investigation Mapping an Prediction. *Geol. Soc. Amer. Mem. 145*, 43-76.

COLIER, R., AND EDMOND, J., (1984) The trace element geochemistry of biogenic particulate matter. *Progr. in Oceanogr., 13*, 113-199.

CORLISS, B.H.; MARTINSON, G.D. AND KEFFER, T., (1986). Late Quaternary deep ocean circulation. *Geol. Soc. Am. Bull. 97*, 1106-1121.

CORLISS, J.B.; DYMOND, J.; GORDON, L.I.; EDMOND, J.M.; VON HERZEN, R.P.; BALLARD, R.D.; GREEN, K.; WILLIAMS, D.; BAINBRIDGE, A.; CRANE, K. AND VAN ANDEL, TJ.H., (1979). Exploration of submarine thermal springs on the Galapagos Rift. *Science, 203*, 1073-1083.

CRONAN, D.S., (1977) Deep Sea Nodules. In, *Marine Manganese Deposits*, ed G.P. Glasby, Elsevier, Amsterdam, 11-44.

CURTIS, C.D., (1966) The incorporation of soluble organic matter into sediments and its effects on trace element assemblages in, G.D. Hobson and M.C. Louis (eds), *Advances in Organic geochemistry*, Pergamon Press, 1-13.

DEHAIRS, F., CHESSELET, R., AND JEDWALS, J., (1980) Discrete suspended particles of barite and the barium cycle in the ocean. *Earth Plan. Sci. Lett.*, ***49***, 528-550.

DINKELMAN M.G., (1974) *Late Quaternary Radiolarian Paleoceanography of the Panama Basin, Eastern Equatorial Pacific.* Unpubl. PhD. thesis Oregon state University, Corvallis, Oregon, 123pp.

DOBBIE, K.E. (1988) *The determination of biogenic silica content of sediments from the Arabian sea off the coast of southern Oman.* Unpubld B.Sc. (Hons) Thesis, University of Edinburgh.

DOUGEN, W.K. AND WILSON, A.L. (1974) The absorptiometric determination of Aluminium in water. *Analyst*. ***99***, 413-430.

DOWDING L.G., (1977) Sediment dispersal within the Cocos Gap, Panama basin. *J. Sediment. Petrology*, ***47***, 1132-1156.

DREXLER, J.W., ROSE, W.I.JR., SPARKS, R.S.J. AND LEDBETTER, M.T., (1980). The Los Chocoyos Ash, Guatemala: A major stratigraphic marker in middle America and in three ocean basins. *Quaternary Res.*, ***13***, 327-345.

DYMOND, J., AND LYLE, M., (1985) Flux comparisons between sediments and sediment traps in the eastern tropical Pacific: Implications for atmospheric CO_2 variations in the Pliestocene. *Limnol. Oceanogr.*, ***30***, 699-712.

DYMOND, J., AND LYLE, M., (1985) Flux comparisons between sediments and sediment traps in the eastern equatorial Pacific: implications for atmospheric CO_2 variations during the Pleistocene. *Limnol. Oceanogr.*, ***30***, 699-712.

DYMOND, J.; CORLISS, J.B.; HEATH, G.R.; FIELD, C.W.; DASCH, E.T. AND VEEH, H.H., (1973) Origin of metalliferous sediments from the Pacific ocean. *Geol. Soc. Amer. Bull.*, ***84***, 3355-3372.

EGGIMAN, D.W.; MNAHEIM, F.T. AND BETZER, P.R. (1980) Dissolution and analysis of amorphous silica in marine sediments. *J. Sed. Petrology 50(1)*, 215-225.

EL WAKEEL, S.K. AND RILEY, J.P., (1961) Chemical and mineralogical studies of Deep-Sea sediments. *Geochim et Cosmochim Acta, 25*, 110-146.

ELDERFIELD, H. AND TRUSEDALE, V., (1980) On the nature of iodine in seawater. *Earth and Plan. Sci. Lett., 50*, 105-114.

ELDERFIELD, H., AND PAGETT, R., (1986) Rare earth elements in ichthyoliths: variations with redox conditions and depositional environment. *Sci. Total Environ. 49*, 175-197.

ELDERFIELD, H.; AND GREAVES, M.J., (1982) The rare earth elements in seawater. *Nature 296*, 214-219.

ELDERFIELD, H.; HAWKESWORTH, C.J.; GREAVES, M.J.; AND CALVERT, S.E., (1981) REE geochemistry of oceanic ferromanganese nodule and associated sediments. *Geochim. et Cosmochim. Acta 45*, 513-528.

ELDERFIELD, H.; MCCAFFREY, R.J.; LUEDKE, W.; BENDER, M.; AND TRUESDALE, V.M., (1981) Chemical diagenesis in Narragasett bay sediments. *Amer. J. Science 281*, 1021-1053.

EMERSON, M., AND BENDER, M., (1981) Carbon fluxes at the sediment-water interface of the deep-sea: calcium carbonate preservation. *J. Marine Res., 39*, 139-162.

EMERSON, S., (1985) Organic carbon preservation in marine sediments, in The carbon cycle and atmospheric CO_2 Natural variations Archean to present. *Geophys. Monogr. Ser., Vol., 32*, 79-89, edited by E.T. Sundquist and W.S. Broecker, AGU, Washigton, D.C.

EMILIANI, C., (1955). Pleistocene Palaeotemperatures. *Journal of Geology, 63(6)*, 539-578.

EMILIANI, C., AND SHACKLETON, N.J., (1974). The Brunhes epoch: Isotope paleotemperatures and geochronology. *Science, 183*, 511-514.

FAIRBANKS, R.G., (1989) A 17,000 year long glacio-eustatic sea-level record: Influence of glacial melting on the Younger Dryas event and deep-ocean circulation. *Nature, 342*, 637-642.

FARRELL, J.W. AND PRELL, W.L., (1989) Climatic change and $CaCO_3$ preservation: An 800,000 year bathymetric reconstruction from the central equatorial Pacific ocean. *Paleoceanography, 4(4)*, 447-466.

FARRELL, J.W. AND PRELL, W.L., (1991) Pacific $CaCO_3$ preservation and $\delta^{18}O$ since 4 Ma: Paleoceanic and Paleoclimatic implications. *Paleoceanography, 6(4)*, 485-498.

FEELY R.A.; GAMMON B.A.; TAFT P.S.; PULLEN L.S.; WATERMAN T.J.G.; CONWAY J.F. AND WISEGARVER D.P., (1978) Distribution of chemical tracers in the eastern equatorial Pacific during and after the 1982-1983 El Ñino/Southern Oscillation event, *J. Geophys. Res., 92*, 6545-6558.

FENICAL, W., (1975) Halogenation in the Rhodophyta, a review, *J. Phycol, 11*, 245-.

FINNEY, B.P.; LYLE, M.W. AND HEATH, G.R., (1988) Sedimentation at MANOP Site H (eastern Equatorial Pacific) over the past 400,000 years: climatically induced redox variations and their effect on transition metal cycling. *Paleoceanography 3(2)*, 169-189.

FISCHER, K., DYMOND, J., AND LYLE, M., (1986) The benthic cycle of copper: evidence from sediment trap experiments in the eastern tropical Pacific ocean. *Geochim. et Cosmochim. Acta, 50*, 1535-1543.

FISCHER, K.; DYMOND, J. AND LYLE, M., (1986). The benthic cycle of copper: evidence from sediment trap experiments in the eastern tropical north pacific ocean. *Geochim. et Cosmochim. Acta., 50*, 1535-1543.

FLOHN, H. (1982) Oceanic upwelling as a key for abrupt climatic change. *J. Meteorol. Soc. Japan 60*, 268-273.

FOLGER, D.W., (1970). Wind transport of land derived minerogenic, biogenic and industrial matter over the north Atlantic. *Deep Sea Res., 17*, 337-352.

FORSBERGH E.D., (1969) On the climatology, oceanography and fisheries of the Panama Bight. *Inter-Am. Tropical Tuna Comm. Bull. 14*, 49-385.

FRANCOIS, R., (1987) The influence of humic substances on the geochemistry of iodine in nearshore and hemipelagic marine sediments, *Geochim Cosmochim. Acta.*, ***51***, 2417-2427.

FRANCOIS, R., (1988) A study on the regulation of the concentration of some trace metals (Rb, Sr, Zn, Pb, Cu, V, Cr, Ni, Mn and Mo) in Saanich inlet sediments, British Columbia, Canada. *Marine Geol.*, ***83***, 285-308.

FROELICH, P.N., BENDER, M.L, LUEDTKE, N.A., HEATH, G.R., AND DEVRIES, T., (1982) The Marine Phosphorus Cycle. *Amer. J. Sci.*, ***282***, 474-511.

FUCHTBAUER, H., AND REINECH, H.E., (1963) Porositt und verdichtung rezenter, mariner sedimente. *Sedimentology* 2, 294-306.

GARDNER, J.V. AND HAYS, J.D., (1976) Reponse of sea-surface temperature and circulation to global climatic change during the past 200,000 years in the eastern equatorial Atlantic ocean. In, Investigation of late Quaternary Paleoceanography and Paleoclimatology (eds. R.M. Cline and J.D. Hays) *Geol. Soc. Amer., Mem.* ***145***, 221-246.

GARDNER, J.V.; DEAN, W.E.; ALONSO, B., (1990) Inorganic geochemistry of surface sediments of the Ebro shelf and slope, north-western Mediterranean. *Marine Geol.*, ***95***, 225-245.

GOLDBERG E.D., (1954) Marine Geochemistry 1. Chemical Scavengers of the Sea. *J. Geol* ***62***, 249-265.

GOLDBERG, E.D. AND ARRHENIUS, G.O.S., (1958). Chemistry of Pacific Pelagic sediments. *Geochim et Cosmochim Acta.*, ***13***, 153-212.

GOLDBERG, E.D. AND GRIFFIN, J.J., (1964) Sedimentation Rates and Mineralogy in the South Atlantic. *J. Geophys. Res.* ***69***, 4293-4304.

GOLDSCHMIDT, V.M., (1954) *Geochemistry*, Oxford Univ. Press. 730pp.

GORDON, D.C., (1971) Distribution of organic carbon and nitrogen at an oceanic station in central Pacific. *Deep-Sea Res.*, ***18***, 1127-1134.

GRAYBEAL, AMY L. AND HEATH, G.R., (1984). Remobilisation of transition metals in surficial pelagic sediments from the eastern pacific. *Geochim. et Cosmochim. Acta,*. ***48***, 965-975.

GRUDMANIS, V. AND MURRAY, J.W., (1982) Aerobic respiration in pelagic marine sediments. *Geochim et Cosmocchim Acta, 46*, 357-361.

GULYAYEVA, L.A. AND ITKINA, E.S., (1962) Halogens in marine and fresh water sediments, *Geochemistry, 6*, 610-.

HARVEY, G., (1980) A study of the chemistry of iodine and bromine in marine sediments, *Marine Chem., 8*, 327-332.

HASKIN, L.A.; WILDEMAN, T.R.; FREY, F.A.; COLLINS, K.A.; KEEDY, C.R.; HASKIN, M.A., (1966) Rare earths in sediments. *J. Geophys. Res., 71*, 6091-6105.

HAY, W.W., (1970) Calcareous nannofossils from cores recovered on leg 4, in Beder et. al., *Initial Reports of the D.S.D.P. IV Washigton, U.S. Govt.* Print Off., 455-501.

HAYS, J.D., SAITO, T., OPDYKE, J.D., AND BURKLE, L.H., (1969) Pliocene-Pleistocene sediments of the equatorial Pacific: their paleomagnetic, biostratigraphic and climatic record. *Geol. Soc. Amer., Bull., 80*, 1481-1514.

HEATH G.R. AND VAN ANDEL TJ.H., (1973) Tectonics and sedimentation in the Panama basin: geologic results of Leg 16, Deep-Sea Drilling Project. *In Initial Reports of the Deep-Sea Drilling Project (ed. A.G. Kaneps), Vol. XVI*, 899-914. U.S. Govt. Printing office, Washington.

HEATH G.R.; MOORE T.C. JR. AND ROBERTS G.L., (1974) Mineralogy of surface sediments from the Panama basin, Eastern Equatorial Pacific. *J. Geol. 82*, 145-160.

HEATH, G.R., (1969) Mineralogy of Cenozoic Deep-Sea Sediments from the Equatorial Pacific Ocean. *Geol. Soc. Amer. Bull., 80*, 1997-2018.

HEATH, G.R., (1976) Dissolved silica in deep-sea sediments. *Soc. Econ. Paleontol. Mineral. Spec. Publ., 20*, 77-93.

HEATH, G.R., AND LYLE, M., (1981) Profiles of solid phase manganese at MANOP sites M and H. *Trans. Am. Geophys. Union (EOS) 62*, 905-.

HEATH, G.R., MOORE, T.C., AND DAUPHIN, J.P., (1976). Late Quaternary accumulation rates of opal, quartz, organic carbon, and calcium carbonate in the Cascadia basin area, northeast Pacific. *Geol. Soc. Amer. Mem., 145*, 393-409.

HEATH, G.R.; THEODORE, C.; MOORE, J.R.; AND ROBERTS, G.L., (1974) Mineralogy of surficial sediments from the Panama basin, eastern equatorial Pacific. *J. Geol. 82*, 145-160.

HEY R., (1977) Tectonic evolution of the Cocos-Nazca spreading centre. *Geol. Soc. Amer. Bull. 88*, 1404-1420.

HEY R., JOHNSON G.L. AND LOWRIE A., (1977) Recent plate motions in the Galapagos area. *Geol. Soc. Amer. Bull. 88*, 1385-1403.

HILL, P.A.; AND PARKER, A., (1970) Tin and Zirconium in sediments around the Brittish Isles: A preliminary reconnaisance. *Econ. Geol. 65*, 409-416.

HIRST, D.M., (1962) The geochemistry of modern sediments from the Gulf of Paria-II. The location and distribution of trace elements. *Geochim. et Cosmochim. Acta, 26*, 1147-1187.

HISARD P.H.; MERLE J. AND VOITURIEZ B., (1970) The Equatorial undercurrent at 170°E in March and April, 1967. *J. Marine Res., 28*, 281-303.

HONJO, S., (1977) Biogenic carbonate particles in the ocean: do they dissolve in the water column? In: Anderson and Malahoff (eds.), The fate of fossil fuel CO_2 in the oceans. *Marine Science, 6*, 269-294, Plunem Press, New York.

HONJO, S., MANGANINI, S.J., AND COLE, J.J., (1982) Sedimentation of biogenic matter in the deep ocean. *Deep-Sea Res. 29*, 609-625.

HORNE, R.A. (1969) Marine Chemistry. Wiley, London. 568pp.

HOVAN, S.A., AND REA, D.K., (1991) Late Pleistocene continental climate and oceanic variability recorded in northwest Pacific sediments. *Paleoceanography 6(3)*, 349-370.

HUNT, C.D., (1981) Regulation of sedimentary cation exchange capacity by organic matter. *Chem. Geol., 34*, 131-149.

IMBRIE, J., SHACKLETON, N.J., PISIAS, N.G., MORLEY, J.J., PRELL, W.L., MARTINSON, D.G., HAYES, J.D., MACINTYRE, A., AND MIX, A.C., (1984). The orbital theory of Pleistocene climate: support from a revised chronology of the marine $\delta^{18}O$ record. In *Milankovitch and climate*, Part 1, (eds Berger A., et al.), Reidel, D., Hingham, Massachusetts, 269-305.

INGALL, E.D., AND VAN CAPPELLIN, P., (1990) Relation between sedimentation rate and burial of organic phosphorus and organic carbon in marine sediments. *Geochim et Cosmochim Acta 54*, 373-386.

INGALL, E.D., SCHROEDER, P.A., AND BERNER, R.A., (1990) The nature of organic phosphorus in marine sediments: New insights from ^{31}P NMR. *Geochim et Cosmochim Acta 54*, 2617-2620.

JANECEK, T.R. AND REA, D.K., (1984) Pleistocene fluctuations in the northern hemisphere tradewinds and westerlies. In *Milankovitch and Climate, Understanding the response to orbital forcing, Part 1*, edited by A.Berger, J.Imbrie, J.Hays, G.Kukla, and B.B.Saltzman, 331-347, D.Reidel, Norwell, Mass.

JANECEK, T.R. AND REA, D.K., (1985) Quaternary fluctuations in the northern hemisphere tradewinds and westerlies. *Quat. Res. 24*, 150-163.

JOHNSON, K.S., (1982) Solubility of rhodochrosite ($MnCO_3$) in water and seawater. *Geochim. et Cosmochim. Acta, 46*, 1805-1809.

KARLIN, R. AND LEVI, S., (1983). Diagenesis of magnetic minerals in recent hemipelagic sediments. *Nature 303*, 327-330.

KASTNER, M., (1977) Authigenic Silicates in Deep-Sea Sediments: Formation and Diagenesis, in *The Sea, Vol 7*, ed., C. Emiliani, 1-72.

KENNEDY, H.A. AND ELDERFIELD, D., (1987a) Iodine diagenesis in pelagic deep-sea sediments, *Geochim. Cosmochim. Acta., 51*, 2489-2504.

KENNEDY, H.A. AND ELDERFIELD, H., (1987b) Iodine diagenesis in non-pelagic deep-sea sediments, *Geochim Cosmochim. Acta., 51*, 2505-2514.

KENNET, J.P., (1990) The Younger Dryas Cooling Event: An Introduction. *Paleoceanography, 5(6)*, 891-895.

KENT, D.V., (1982). Apparent correlation of palaeomagnetic intensity and climatic records in deep sea sediments, *Nature*, ***299***, 538-539.

KHAN, A.A., (1989). *Geochemistry and Palaeoclimate changes in sediments; northern Arabian sea.* Unpublished Ph.D thesis University of Edinburgh, 248pp.

KINNET, J.P., (1966) Foraminiferal evidence of a shallow carbonate solution boundary, Ross Sea, Antarctica. *Science*, ***153***, 191-193.

KLNKHAMMER, G., HEGGIE, D.T., AND GRAHAM, D.W., (1982) Metal diagenesis in oxic marine sediments. *Earth Plan. Sci. Lett.* ***61***, 211-219.

KNOWSMAN R.O., (1973) Coarse components in surface sediments of the Panama basin, eastern equatorial Pacific, *J. Geol.* ***81***, 473-494.

KRISSECK, L.A.; SCHEIDEGGER, K.F. AND KULM, L.D., (1980). Surface sediments of the Peru-Chile continental margin and the Nazca plate. *Geol. Soc. Amer. Bull.*, ***91***, 321-331.

KROM, M.D., AND BERNER, R.A., (1981) The diagenesis of phosphorus in nearshore marine sediments, *Limnology Oceanogr.* ***25***, 797-806.

KYLIN, H., (1929) Uber das Vorkommen von Jodiden, Bromiden ynd Jodidooxydasen bei den Meeresalgen, *Z. Physiol Chem.* ***191***, 50-.

LAIRD N.P., (1971) Panama basin deep water:- properties and circulation, *J. Marine Res.* ***29***, 226-234.

LEA, D., AND BOYLE, E., (1989) Barium content of benthic foraminifera controlled by bottom water composition. *Nature, 388*, 751-753.

LEA, D., AND BOYLE, E., (1990A) A 210,000 year record of Barium variability in the deep northwest Atlantic ocean. *Nature, 347*, 269-272.

LEA, D., AND BOYLE, E., (1990B) Foraminiferal reconstructiuon of barium distribution in water masses of the glacial oceans. *Paleoceanography, 5(5)*, 719-742.

LEDBETTER, M.T., (1982). Tephrachronology at sites 502 and 503, in Prell, W. and Gardner, J.V., and others, *Initial reports of the deep sea drilling project, Volume 68*: Washington D.C., U.S. Government Pirnting office, 403-408.

LEDBETTER, M.T., (1985). Tephrachronology of marine tephra adjacent to central America. *Geol. Soc. Amer. Bull., 96*, 77-82.

LEINEN, M., CWIENK, D., HEATH, G.R., BISCAYE, P.E., KOLLA, V., THIEDE, J., AND DAUPHIN, J.P., (1986) Distribution of biogenic Silica and quartz in recent deep-sea sediments. *Geology, 14(3)*, 199-203.

LI, Y-H., (1982) Inter-element relationships in abyssal Pacific ferromanganese nodules and associated pelagic sediments, *Geochim. et Cosmochim. Acta, 46*, 1053-1066.

LISITZIN, A.P. AND PELTELIN, .V.P., (1967) Features of distribution and modification of $CaCO_3$ in bottom sediments of the Pacific ocean, *Lithol. Miner. Resour. Engl. Transl., 5*, 565-578.

LISITZIN, A.P., (1972) Sedimentation in the world ocean. *Soc. Econ. Paleontol. Mineral. Spec. Publ. No. 17.*, 218pp.

LONSDALE P.F., (1976) Abyssal circulation of the south-eastern Pacific and some geological implications. *J. Geophys. Res. 81*, 1163-1146.

LONSDALE P.F., (1977a) Deep-tow observations at the mounds abyssal hydrothermal field, Galapagos Rift. *Earth and Plan. Sci. Lett. 36*, 92-110.

LONSDALE P.F., (1977b) Inflow of bottom-water to the Panama basin. *Deep-Sea Res. 24*, 1065-1101.

LORING, D.H., (1978) Geochemistry of zinc, copper and lead in the sediments of the eastuary and Gulf of St. Lawrence, *Can. J. Earth Sci. 15*, 757-772.

LOWENSTAM, H.A., (1974) Evolutionary changes in hard part mineralogy of some marine invertebrates. *Goeol Soc. Amer. Abstr., 5(7)*, 719.

LUPTON, J.E.; WEISS, R.F. AND CRAIG, H., (1977). Mantle Helium in hydrothermal plumes in the Galapagos Rift. *Nature, 267*, 600-603.

LUZ B. AND SHACKLETON, N. J., (1975) $CaCO_3$ solution in the Tropical East Pacific during the past 130,000yrs. In *Cushman Found. Foraminiferal Res., Spec. Publ., 13*, 142-150.

LYLE, M. AND DYMOND, J., (1978). The chemistry of hydrothermal mounds near the Galapagos Rift. *Earth and Plan. Sci. Lett., 40*, 12-24.

LYLE, M. AND PISIAS, N.J. (1990) Ocean circulation and atmospheric CO_2 changes: coupled use of models and paleoceanographic data, *Paleoceanography 5*, 15-41.

LYLE, M., (1988) Climatically-forced organic carbon burial in the equatorial Atlantic and Pacific Oceans. *Nature 335*, 529-532.

LYLE, M.; HEATH, G.R. AND ROBBINS, J.M., (1984). Transport and release of transition elements during early diagenesis: sequential leaching of sediments from MANOP site H. Part I, pH 5 acetic acid leach. *Geochim. et Cosmochim. Acta. 48*, 1705-1715.

LYLE, M.; MURRAY, D.W.; FINNEY, B.P.; DYMOND, J.; ROBBINS, J.M.; AND BROSKOFORCE, K., (1988). The record of late Pleistocene biogenic sedimentation in the Eastern Tropical Pacific ocean. *Paleoceanography, 3(1)*, 39-59.

LYNN, D.C., AND BONATTI, E., (1965) Mobility of Manganese in diagenesis of deep-sea sediemnts. *Marine Geology 3*, 457-474.

MACDONALD K.C. AND MUDIE J.D., (1974) Micro-earthquakes on the Galapagos spreading centre and the seismicity of fast spreading ridges. *Geophys. J. Roy. Astr. Soc. 36*, 245-257.

MALCOLM, S.J. AND PRICE, N.B., (1984) The behaviour of iodine and bromine in estuarine surface sediments. *Marine Chemistry, 15*, 263-271.

MANGINI, A., (1988) Ages and growth rates of Mn-nodules and crusts, in P. Halbach; G. Friedrich and U. von Stackelberg (editors): *The Mn-nodule belt of the Pacfic* Ocean, Enke, Stuttgart, 142-150.

MARTENS, G.S. AND KLUMP, J.V., (1980). Biogeochemical cycling in an organic-rich coastal marine basin. I. methane sediments water exchange processes. *Geochim. et Cosmochim. Acta. 44*, 1639-1653.

MARTIN, J.H., AND KNAUER, G.A., (1973) The elemental composition of plankton. *Geochim et Cosmochim Acta 37*, 1639-1653.

MARTINSON, D.G.; PISIAS, W.G.; HAYS, J.D.; IMBIRE, J; MOORE, T.C. AND SHACKLETON, N.J., (1987) Age dating and the orbital theory of the Ice Ages: development of a high resolution 0 to 300 000 year chronostratigraphy. *Quat. Res., 27*, 1-29.

MAYER, L.M.; MACKS, S.A.; MOOKS, W.H.; AND MURRAY, S., (1981) The distribution of bromine in coastal sediments and its use as a source indicator for organic matter. *Organic Geochemistry, 3*, 37-42.

MCBIRNEY, A.R. AND WILLIAMS, H., (1969) Geology and petrology of the Galapagos Islands. *Geol. Soc. Amer. Mem. 118*, 197pp.

MCINTYRE, A.; KIPP, N.G.; BE, A.W.H.; CROWLEY, T.; KELLOG, T.; GARDNER, J.V.; PRELL, W.L.; RUDDIMAN, W.F., (1976). Glacial north Atlantic 18,000 years ago: A CLIMAP reconstruction. *Geol. Soc. Am. Mem., 145*, 43-76.

MCMURTY, G.M. AND YEY, H.W., (1981) Hydrothermal clay mineral formation of the East Pacific Rise and Buaer Basin sediments. *Chem. Geology, 32*, 189-205.

MCNEILL, G., AND SHIMMIELD, G.B., (1991) Diagenetic controls on Uranium, Molybdenum and Vanadium enrichment in orgaic-rich marine shelf sediment. In *Proceedings of Heavy Metals in the Environment.* Editor: J.G. Farmer (EP Consultants Ltd., Edinburgh).

MILANKOVITCH, M., (1941). *Canon of Insulation and the Ice-Age Problem*, Beograd, Koninglich Serbische Akademie, 484pp. (English translation by the Israel program for scientific translation and published for the U.S. department of commerce and the national science foundation).

MOLINA-CRUZ A., (1977) The relation of the southern tradewinds to upwelling processes during the last 75 000 years. *Quat. Res., 8*, 324-338.

MOLINA-CRUZ, A., AND PRICE, P., (1977) Distribution of Opal and Quartz on the ocean floor of the subtropical southern Pacific. *Geology, 5(2)*, 81-84.

MOORE T.C. JR.; HEATH G.R. AND KNOWSMAN R.O., (1973). Biogenic sediments of the Panama basin. *J. Geol. 81*, 458-472.

MULLER, P.J. AND SUESS, E., (1979) Productivity, sedimentation rate, and sedimentary orgainc matter in the oceans, I. Organic carbon preservation. *Deep-Sea Res., 26A*, 1347-1362.

MURRAY J.W.; DOWNS J.N.; STROM S.; WEI C.L. AND JANNASCH H., (1990) Nutrient accumulation, export production and ^{234}Th scavenging in the eastern equatorial Pacific. *Deep Sea Res., 36*, 890-.

MURRAY J.W.; DOWNS, J.N.; STROM, S.; WEI, C.L. AND JANNASCH, H. (1989) Nutrient accumulations, export production and ^{234}Th scavenging in the eastern equatorial Pacific. *Deep Sea Res. 36*, 1471-1489.

MURRAY, D.W., (1987) Spatial and Temporal Variations in Sediment Accumulation in the Central Tropical Pacific. Unpubl. *Ph.D. Thesis*, Oregon State University, 343pp.

MURRAY, J. AND PHILIPPI, E., (1908) Die Grundproben der Deutschen Tiefsee Expidition 1898-1899, *Wiss. Ergeb. Dtsch. Tiefsee. Exped. Valdivia, 10*: 77-206, Vergnaud-Grazzini, C.

MURRAY, J. AND RENARD, A. F., (1891) *Report on deep-sea deposits based on specimens collected during the voyage of H.M.S. Challenger in the years 1872-1876.* H.M.S.O. London. 525pp.

MURRAY, J., AND RENARD, A.F., (1898) *Deep-Sea Deposits, Challenger reports*, Longmans, London, 525pp.

MUSIC, S., SIPALO-ZULJEVIC, J., AND WOLF, R.H.H., (1980) Radiochemical study of the sorption of iodate ions on iron (III) hydroxide precipitate, *Radiochem. Radioanal. Lett., 45*, 235-.

NAIR, R.R., ITTEKOT, V., MANGANINI, S.J., RAMASWAMY, V., HAAKE, B., DEGENS, E.T.DESAI, B.N., AND HONJO, S., (1989) Increased paticulate flux to the deep ocean related to monsoons. *Nature (Lond.) 338(6215)*, 749-751.

NATH, B.G.; RAO, V.P., AND BECKER, K.P., (1989) Geochemical evidence of terrigenous influence in deep-sea sediments up to 8°S in the central Indian ocean. *Marine Geol., 87*, 301-313.

NINKOVITCH, D., AND SHACKLETON, N.J., (1975). Distribution, stratigraphic position and age of ash layer "L", in the Panama basin region. *Earth and Planetary Science Letters, 27*, 20-34.

NISSENBAUM, A., AND SWAINE, D.J., (1976) Organic matter and metal interactions in recent sediments: the role of humic substances. *Geochim. et Cosmochim. Acta. 40*, 809-816.

NORRISH, K. AND HUTTON, J.T. (1969) An Accurate X-ray spectrographic method for the analysis of a wide range of geological samples. *Geochim. Cosmochim. Acta 33*, 431-453.

OLDFIELD, F. AND ROBINSON, S.G., (1985). Geomagnetism and palaeoclimate. In *The Climate Scene*, M.J., Tooley and G Sheil (eds) London: George Allen and Unwin.

PAK H. AND ZANEVELD J.R.V., (1973) The Cromwell current on the east side of the Galapagos Islands. *J. Geophys. Res. 78*, 7845-7859.

PARKIN, D.W. AND SHACKLETON, N.J., (1973). Tradewind and temperature correlation down a deep-sea core off the Sahara coast. *Nature, 245*, 455-457.

PATIENCE, A.J., AND KROON, D., (1991) **Oxygen Isotope Chronostratigraphy**. In: *Quaternary Dating Methods - A User's Guide*, Edited by P.L. Smart and P.D. Frances, *Quaternary Research Association, Technical Guide No.4*, Chapter 10, 199-228, Cambridge. (see appendix D, this thesis).

PAVLOVA, G.A. AND SHISHKINA, D.V., (1973) Accumulation of iodine in interstitial water during metamorphism in relation to the iodine distribution in Pacific sediments, *Geochem. Int., 10*, 804-813.

PEDERSEN, T. F., (1979) *Geochemistry of sediments of the Panama basin, Eastern Equatorial Pacific Ocean.* Unpubl. Ph.D. Thesis University of Edinburgh 235pp.

PEDERSEN, T. F., (1983). Increased productivity in the Eastern Equatorial Pacific during the last glacial maximum (19,000-14,000yrs.b.p.). *Geology, 11*, 16-19.

PEDERSEN, T.F. AND PRICE, N.B., (1980) The geochemistry of iodine and bromine in the sediments of the Panama Basin, *J. Mairne Res., 38*, 397-411.

PEDERSEN, T.F., AND PRICE, N.B., (1982) The geochemistry of manganese carbonate in Panama basin sediments. *Geochim. et Cosmochim. Acta 46*, 59-68.

PEDERSEN, T.F., NIELSEN, B., AND PICKERING, M., (1992) The Timing of late Quaternary Productivity Pulses in the Panama basin and implications for atmospheric CO_2. *Paleoceanography, 6(6)*, 657-677.

PEDERSEN, T.F., PICKERING, M., VOGEL, J.S., SOUTHON, J.N., AND NELSEN, D.E., (1988) The response of benthic foraminifera to productivity cycles in the eastern equatorial Pacific: faunal and geochemical constraints on glacial bottom water oxygen levels. *Paleoceanography, 3*, 157-168.

PENG, T.H., BROECKER, W.S., KIPPHUT,G., AND SHACKLETON,N.J., (1977) Benthic mixing in deep-sea cores as determined by ^{14}C dating and its implications regarding climate stratigraphy and the fate of fossil fuel CO_2. In: *The Fate of Fossil Fuel CO_2 in the Ocenas*, edited by N.R. Anderson and A. Malahoff, 355-371, Plenum, New York.

PETIT J.R.; GRIAT M AND ROYER A., (1981) Ice age aerosol content from east Antarctic ice core samples and past wind strength, *Nature 293*, 391-394.

PETIT, J.R.; MANIER, L.; JOUZEL, J.; KOROTKEVICH, Y.S.; KOTLYAKOV, V.I. AND LORIUS, C., (1990) Palaeoclimatological and Chronological implications of the Vostok core dust record. *Nature 343*, 56-58.

PETTIJOHN, F.J., (1975). *Sedimentary Rocks*. 3rd. Edition, Harper and Rpw, New York, 628pp.

PILIPCHUK, M.F., AND VOLKOV, I.I., (1968) The geochemistry of Molybdenum in the Black sea. *Lith. Miner. Res. 4*, 389-407.

PIPKIN B.W.; GORSLINE D.S.; CASEY R.E. AND HAMMOND D.E., (1977). In *Laboratory exercises in oceanography*, 255pp. W.H. Freeman and Co. San Francisco.

PISIAS, N.G., (1976). Late Quaternary sedimentation rates, periodicities, and controls of carbonate and opal accumulations. *Memoirs Geological Society of America, 145*, 375-391.

PRELL, W.L., (1984) Covariance patterns of foraminiferal $\delta^{18}O$: An evaluation of Pliocene ice volume changes near 3.2 million years ago. *Science 226*, 692-694.

PRICE, N.B. AND CALVERT, S.E., (1973) The geochemistry of iodine in oxidised and reduced recent marine sediments. *Geochim Cosmochim. Acta., 37*, 2149-2158.

PRICE, N.B. AND CALVERT, S.E., (1977) The contrasting geochemical behaviours of iodine and bromine in recent sediments from the Namibian shelf. *Geochim. Cosmochim. Acta., 41*, 1769-1775.

PRICE, N.B.; CALVERT, S.E. AND JONES, P.G.W., (1970) The distribution of iodine and bromine in the southwestern Barents sea, *J. Marine Res.*, **28**, 22-34.

RADHAKRISHNAMURTY, C.; LIKHITE, S.D.; AMIN, B.S.; AND SOMAYAJULA, (1968). Magnetic susceptibility stratigraphy in ocean sediment cores. *Earth and Plan. Sci. Letts.*, **4**, 464-468.

REA, D.K., LEINEN, M., AND JANECEK, T.R., (1985) Geological approach to the long-term history of atmospheric circulation. *Science* **227**, 721-725.

REA, D.K., PISIAS, N.G., AND NEWBURRY, T., (1991) Late Pleistocene Paleoclimatology of the central equatorial Pacific: Flux patterns of biogenic sediments. *Paleoceanography, 6(2)*, 227-244.

REIMMENS, C.E., (1982). Organic matter in anoxic sediments off central Peru: relationship of porosity, microbial decomposition and deformation properties. *Marine Geology* **46**, 175-197.

REIMMER, C.E., AND SUESS, E., (1983) The partioning of organic carbon fluxes and sedimentary oragnic matter decomposition rates in oceans. *Mar. Chem.* **13**, 141-168

REVELLE, R.R., (1944), Carnegie Inst., Washington, *Publ. 556*.

REVELLE, R.R.; BRAMLETTE, M.; ARRHENIUS, G. AND GOLDBERG, E.D., (1955). Pelagic sediments of the Pacific. *Geol. Soc. Am. Spec. Paper*, **62**, 221-236.

RIGG, T. AND WAGENBAUER, H.A. (1961) Spectrophotometric determination of Titanium in Silicate Rocks. *Analytical Chemistry* **33(10)**, 1347-1349.

RILEY, J.P., AND CHESTER, R., (1971) *Introduction to Marine Chemistry*, Academic Press, London, 465pp.

ROBINSON, S.G., (1982). Two applications of mineral-magnetic techniques to deep-sea sediment studies. *Geophys. J. R. Astr. Soc.* **69**, 294.

ROSE, W.I.JR., GRANT, N.K. AND EASTER, J., (1979). Geochemistry of the Los Chocoyos Ash, Quezaltenango valley, Guatemala, in Chapin, C.E. and Elston, W.E., eds, Ash-flow tuffs, *Geol. Soc. America special paper* **180**, 87-99.

RUDDIMAN, W.F. AND MCINTYRE, A., (1977). Late Quaternary surface ocean kinematics and climate change in the high latitude north Atlantic. *J. Geophys. Res., 82*, 3877-3887.

RUTTENBERG, K.C., (1990) Diagenesis and burial of phosphorus in marine sediments, *Ph.D. thesis*, Yale University.

RYAN, B.F., JOINER, B.L., AND RYAN, T.A., (1985) *Minitab Handbook*, 2nd edition, P.W.S. Publ. Boston 379pp.

RYTHER J.H., (1963) Geographical variations in productivity, In *The Sea (ed M.N. Hill), Vol. 2*, 347-380, Wiley, London.

SARNTHEIN, M., AND FENNER, J., (1988) Global wind-induced change of deep-sea sediment budgets, new ocean production and CO_2 reservoirs, *ca* 3.3-2.35 Ma b.p. *Phil. Trans. R. Soc. Lond. B., 318*, 487-504.

SARNTHEIN, M., WINN, K., AND ZAHN, R., (1987) Paleoproductivity of oceanic upwelling and the effects of atmospheric CO_2 and climate change during deglaciation times, In: W.H. Berger and L.D. Labeyrie (eds) *Abrupt climate change*, 311-337, D. Reidel Publ. Co.

SARNTHEIN, M; WINN, K., AND ZAHN, R. (1987) Paleoproductivity of oceanic upwelling and the effect on atmospheric CO_2 and climate change during deglacial times. W.H. Berger and L. Labeyrie (eds) *Abrupt Climatic Change*, 311-337.

SAWLAN, J.J., AND MURRAY, J.W., (1983) Trace metal remobilisation in the interstitial waters of red clay and hemipelagic marine sediments. *Earth and Plan. Sci. Lett. 64*, 213-230.

SAYLES, F.L.; AND BISCHOFF, J.L., (1973) Ferromanganoan sediments in the Equatorial eastern Pacific. *Earth Plan. Sci. Lett. 19*, 330-336.

SAYLES, F.L.; KU, T.L. AND BOWKER, P.C., (1975) Chemistry of Ferromanganoan sediments of the Bauer Deep. Geol. Soc. Amer Bull, 86, 1423-1431.

SCHARDE, H.J., (1972) Kiedelsaure-skelitte in sedimenten des ibro-marokkenischen kontinentalrandes und angrezender. *Tiefsee. Meteor. Forschungsergeb; Reihe C.8*, 10-36.

SCHIFFELBAN, P., AND DORMAN, L., (1986) Spectral effects of time-depth non-linearities in deep-sea sediment records: A demodulation technique for realigning time and depth scales. *J. Geophys. Res., 91*, 3821-3835.

SCHMITZ, B., (1987) Barium, equatorial high productivity, and the northward wandering of the Indian continent. *Paleoceanography 2(1)*, 63-77.

SCHMITZ, B., (1987) The TiO_2/Al_2O_3 ratio in the Cenozoic Bengal abyssal fan sediments and its use as a paleostream energy indicator. *Marine Geology 76*, 195-206.

SHACKLETON N.J.; HALL M.A.; LINE J.; AND SHUXI C., (1983) Carbon isotope data in core V19-30 confirm reduced carbon dioxide concentration in the ice age atmosphere. *Nature 306*, 319-322.

SHAKER, R; SUBBARAO, K.V. AND KOLLA, V., (1987) Geochemical evidence of terrigenous influence in deep sea sediments up to 8ÁS in central Indian basin. *Marine Geol., 87*, 301-313.

SHAW, T.I., (1959) The mechanism of iodine accumulation by brown sea-weed, Laminaria digitata, II Respiration and Iodide uptake, *Proc. R. Soc. London, 152*, 109-.

SHAW, T.I., (1962) Halogens in algae, In *Physiology and Biochemistry of Algae*, Lewin, R.A. ed. Academic Press, London, 247pp.

SHIMMIELD, G. B., (1984) *The geochemistry and mineralogy of Pacific sediments, Baja California.* Unpublished Ph.D. Thesis University of Edinburgh 323pp.

SHIMMIELD, G.B. AND MOWBRAY, S.R., (1991) The inorganic geochemical record of the northwest Arabian sea: A history of Productivity variation over the last 400 ky for sites 722 and 724. *Proceedings of the Ocean Drilling Program Leg 117*, Part B, 409-430.

SHIMMIELD, G.B. AND PEDERSEN, T.F., (1990) The Geochemistry of Reactive Trace Metals and Halogens in Hemipelagic continental margin sediments. In *Reviews in Aquatic sciences, 3(2,3)*, 255-279.

SHISHKINA, D.V. AND PAVLOVA, G.A., (1965) Iodine distribution in marine muds and oceanic muds and in their pore fluids, *Geochem. Int. 2*, 559-565.

SOLOMONS, W., AND FORSTNER, U., (1983) *Metals in the hydrocycle.* Springer, Berlin 348pp.

SPEARS, D.A., AND AMIN, M.A., (1981) Geochemistry and mineralogy of marine and non marine Namurian black shales from the Transley borehole, Derbyshire. *Sedimentology 28*, 407-417.

SPEARS, D.A.; KANARIS-SOLIRIOU, R., (1976) Titanium in some Carboniferous sediments from Great Britain. *Geochim Cosmochim Acta 40*, 345-351.

SPENCER, D.W.; BREWER, P.G.; FLEER, A.; HONJO, S.; KRISHNASWANU, S. AND NOZAKI, Y., (1978) Chemical fluxes from a sediment trap experiment in the deep Sargasso Sea, *J. Marine Res., 36*, 493-523.

STEENS, T.N.F., KROON, D., TEN KATE, W.G., AND SPRENGER, A., (1991) Late Pleistocene periodicities of oxygen isotope ratios, calcium carbonate contents, and magnetic susceptibilities of western Arabian sea margin hole 728A. *Proceedings of the Ocean drilling Program, Scientific Results (Part B), Vol. 117*, 309-320.

STEVENSON M.R. AND TAFT B.A., (1971) New evidence of the equatorial undercurrent east of the Galapagos islands. *J. Marine Res. 29*, 103-115.

STEVENSON M.R., (1970) Circulation in the Panama Bight. *J. Geophys. Res. 75*, 659-672.

STOMMEL H., (1958) A survey of ocean current theory. *Deep Sea Res. 5*, 82-.

SUESS, E. AND MULLER, P.J., (1980) Productivity, Sedimentation rate and Sedimentary organic matter in the oceans II Elemental Fractionation, *Proceedings CRNS Symposium Geophys. Monogr. Series, 29*, 118-129.

SUESS, E., (1981) Phosphate regeneration from sediments of the Peru continental margin by dissolution of fish debris. *Geochim. et Cosmochim. Acta. 45*, 577-588.

SWIFT, A., AND WENKAM, C., (1978) Holocene accumulation rates of calcite in the Panama basin: lateral and vertical variations in calcite dissolution. *Marine Geol. 27*, 67-77.

TAKAHASHI, T., AND BROECKER, W.S., (1977) Mechanisms for clacite dissolution on the sea floor. In *The Fate of fossil fuel CO_2 in the oceans*, edited by N.R. Anderson and A. Malahoff, 455-477, Plenum, New-York.

TERRY R.A., (1956) A geological reconnaissance of Panama. *Calif. Acad. Sci., Occas. Pap. 23*, 91pp.

THEISEN, R. AND VOLLACH, D. (1967) *Tables of X-ray Mass Absorption Coefficients.* Varlag Stahleisen M.B.H; Dusseldorf.

THIRWALL, M.F. (1979) *The Petrochemistry of the British Old Red Sandstone Volcanic province.* Unpubld. Ph.D. Thesis, University of Edinburgh.

THOMPSON, P.R. AND SAITO, T., (1974). Pacific Pleistocene sediments: planktonic foraminifera, dissolution cycles and geochronology. *Geology, 2*, 333-335.

THOMPSON, R. AND OLDFIELD, F., (1986). *Environmental magnetism*, Allen and Unwin, 141-152.

THOMPSON, T.G., AND CHOW, J.J., (1956) The Strontium-calcium atom ratio in carbonate secreting marine organisms. *Pap. Mar. Biol. Oceanogr: Deep-sea Res. Supplement to Vol. 3*, 20-39.

THOMSON, J., CARPENDER, M.S.N., COLLEY, S., AND WILSON, T.R.S., (1984) Metal accumulation rates in northwest Atlantic pelagic seidments. *Geochim. et Cosmochim. Acta 48*, 1935-1948.

THOMSON, J., HIGGS, N.C., JARVIS, I., HYDES, D.J., COLLEY, S., AND WILSON, T.R.S., (1986) The behaviour of manganese in Atlantic carbonate sediments. *Geochim. et Cosmochim. Acta 50*, 1807-1818.

THOMSON, J., COLLEY, S., HIGGS, N.C., HYDES, D.J., WILSON, T.R.S., AND SORENSEN, J., (1987) Geochemical oxidation fronts in NE Atlantic distal turbidites and their effects in the sedimentary record. In *Geological Society Special Publication No. 31, Geology and Geochemistry of Abyssal Plains*, pp167-177, edited by P.P.E. Weaver and J. Thomson. Blackwell Scientific Publ.

TOYODA, K., NAKAMURA, Y., AND MASUDA, A., (1990) Rare earth elements of Pacific pelagic sediments. *Geochim. et Cosmochim. Acta 54(4)*, 1093-1103.

TRUESDALE, V.W., (1975) "Reactive" and "unreactive" iodine in sea water-a possible indication of an organically bound iodine fraction. *Marine Chemistry, 3*, 111-119.

TSUNOGAI, S., (1971) Iodine in the deep water of the ocean, *Deep-Sea Res. 18*, 913-919.

TUREKIAN, K.K. AND WEDOPOHL, K.H., (1961) Distribution of the elements in some major units of the earth's crust. *Bull Geol. Soc. Amer.* ***72***, 175-192.

TUREKIAN, K.K., (1964) The marine geochemistry of Strontium. *Geochim. et Cosmochim. Acta,* ***28***, 1479-1496.

ULLMAN, W.J. AND ALLER, R.C., (1980) Dissolved iodine flux from esturine sediments and implications for enrichment of iodine at the sediment-water interface, *Geochim Cosmochim. Acta.,* ***44***, 1177-1184.

ULLMAN, W.J. AND ALLER, R.C., (1983) Rates of iodine remineralisation in terrigenous near-shore sediments, *Geochim. Cosmochim. Acta.,* ***47***, 1423-1432.

ULLMAN, W.J. AND ALLER, R.C., (1985) The geochemistry of iodine in near-shore carbonate sediments, *Geochim. Cosmochim. Acta.,* ***49***, 967-978.

VALENCIA, M., (1977) Pacific Pleistocene plaeoclimatic stratigraphy: A comparative analysis of results. *Quat. Res.,* ***8***, 339-354.

VAN ANDEL TJ. H., (1973) Texture and dispersal of sediments in the Panama basin. *J. Geol.* ***81***, 434-457.

VAN ANDEL TJ. H.; DEATH G.R.; MALFAIT B.T. HEINRICKS D.F. AND EWING J.I., (1971) Tectonics of the Panama basin, eastern equatorial Pacific, *Geol Soc. Amer. Bull.* ***82***, 1489-1508.

VAN ANDEL, T.H., HEATH, G.R., AND MOORE, T.C., (1975) Cenzoic tectonics, sedimentation and paleoceanography of the central equatorial Pacific. *Mem. Geol. Soc. Amer.,* ***143***, 134pp.

VAN ANDEL, TJ.H., (1964) Recent sediments of the Gulf of California. Van Andel, T.H., and Shar, G.D., (eds.). *J. Amer. Assoc. Petrol. Geol. Mem.,* ***3***, 216-310.

VAN-BENNEKOM,A.J., AND BERGER, G.W., (1984) Hydrology and silica budget of the Angola basin. *Netherlands J. of Sea Research* ***17***, 149-200.

VEEH, H.H., (1967) Deposition of uranium from the ocean. *Earth and Plan. Sci. Lett.,* ***3***, 145-150.

VINOGRADOV, A.P., (1939) Iodine in marine muds. To the problem of the origin of iodine-bromine waters in petroliferous regions, *Yr. Bugeo-Khim, Lab, Akad. Nauk. SSSR.*, *5*, 22-.

VOLAT, J.L., PASTOURET, L., AND VERGNAUD-GRAZZINI, C., (1980) Disssolution and carbonate fluctuations in Pleistocene deep-sea cores: A review. *Marine Geol. 34*, 1-28.

VOLKOV, I.I., FAMINA, L.S., AND VERGNAUD-GRAZZINI, C., (1974) Influence of organic material and processes of sulphide formation of the distribution of trace elements in deep-water sediments of the Black Sea. in: D.A. Ross and E.T. Degens (eds) The Black Sea: Geology, Chemistry and Biology. *Amer. Ass. Petrol. Geol. Mem. 20*, 456-476.

WAKEFIELD, S.J. AND ELDERFIELD, H. (1985) Interstitial water iodine enrichments in sediments from the eastern Pacific, *J. Marine Res.*, *43*, 951-961.

WAKEFIELD, S.J., (1981) *Aspects of geochemistry and early burial diagenesis of metalliferous deep-sea sediments*. Ph.D. thesis University of Leeds, U.K.

WEFER G.; DUNBAR R.B. AND SUESS E., (1983) Stable isotopes of foraminifers off Peru recording high fertility and changes in Upwelling history. In *Coastal Upwelling: Its sediment record Part B: sedimentary records of ancient coastal upwelling (eds) Thiede J. and Suess E.* Plenum Press New York and London.

WEISS, R.F.; LONSDALE, P.; LUPTON, J.E.; BAINBRIDGE, A.E. AND CRAIG, H., (1977). Hydrothermal plumes in the Galapagos Rift. *Nature, 267*, 600-603.

WOLLAST, R., (1974) The Silica problem. In: *The Sea, ed E.D. Goldberg, Vol., 5*, 359-392, Publ. Wiley interscience, New York.

WONG, G.T.F. AND BREWER, P.G., (1974) The determination and distribution of iodine in south Atlantic waters, *J. Marine Res.*, *32*, 25-36.

WONG, G.T.F. AND BREWER, P.G., (1977) The marine geochemistry of iodine in anoxic basins, *Geochim. Cosmochim. Acta.*, *41*, 151-159.

WRIGHT, J.; SCHRADER, H.; AND HOLSER, W.T., (1987) Paleoredox variations in ancient oceans recorded by rare earth elements in fossil apatite. *Geochim. et Cosmochim. acta 51*, 631-644.

WRIGHT, J.V., (1981). The Caliente ignimbrite: Analysis of a compound intraplinian ignimbrite from a major Quaternary Mexican Eruption, *Bulletin Volcanologique*, ***44***, 198-212.

WYRTKI K. AND KILONSKY B., (1984) Mean water and current structure during the Hawaii to Tahiti shuttle experiment. *J. Phys. Oceanogr.* ***14***, 242-254.

WYRTKI K., (1965) Surface circulation of the eastern tropical Pacific Ocean. *Inter-Amer. Tropical Tuna Comm., Bull.* ***9***, 271-304.

WYRTKI K., (1966) Oceanography of the eastern equatorial Pacific Ocean In *Oceanography and Marine Biology Annual review (eds H. Barnes), Vol.* ***4***, 33-68, George Allen and Unwin Ltd., London.

WYRTKI K., (1967) Circulation and water masses in the eastern equatorial Pacific Ocean. *Int. J. Oceanol. and Limnol.*, ***1***, 117-147.

WYRTKI K., (1974) Equatorial currents of the Pacific 1950-1970 and their relations to trade winds. *J. Phys. Oceanogr.* ***4***, 372-380.

YAMADA, M., AND TSUNOGAI, S., (1984) Postdepositional enrichment of uranium in sediments from the Bering sea. *Marine Geol.*, ***54***, 263-276.

ZEN, E.A., (1959) Mineralogy and petrology of marine bottom sediment samples off the coast of Peru and Chile. *J. Sed. Petrology* ***29***, 513-539.

APPENDIX - A

ANALYTICAL METHODS

A.1 SEDIMENT COLLECTION AND SAMPLING

Two gravity cores (table 1.1) collected during a cruise of the R.R.S. Shackleton (April 30 - May 25, 1976) and six piston cores (table 1.1) recovered during the R.R.S. Charles Darwin cruise (April 14 - May 11, 1989) were initially selected and sampled for analysis.

The one metre sections of the piston cores were transported, together with all other material from the latter cruise in a sealed container at 4°C to the University of Edinburgh. The cores from the former cruise were similarly transported in 1976.

The two gravity cores were extruded from their polythene liners using a rubber plug and sectioned every 2cm. This method may result in some compaction of the sediment. The slices of wet sediment were then weighed prior to being dried at 40-50°C for 24-48 hours in order to determine their water contents.

The polythene liners of the sections from the piston cores were halved lengthwise using a circular saw. Subsequently, the sediment cores were sliced in half with a Chromium-Vanadium knife using the principle of electro-osmosis (Chmelik, 1967). One half was used for sampling, the other for archive.

The cores were then sampled using $10cm^3$ polythene plugs (2 cm diameter) at 10cm intervals to the base of each core. Occassionally, as a result of irregularities of the section length, this interval was changed slightly. But, wherever possible, a constant sampling frequency was adhered to even in the presence of anomalous horizons (eg ash bands). The $10cm^3$ plugs of wet sediment were weighed prior to being analysed for magnetic susceptibility (appendix A.2). Subsequently, they were dried at 40-50°C for 24-48 hours to determine the water contents (see Chapter 3).

All dried sediments were ground to a fine powder (<2μm) using a tungsten-carbide lined tema mill for 2-3 minutes; this material being used for XRF, carbon and wet chemical analysis (see below). The sediment from each 2 cm horizon remaining in the core was kept at 4°C and used for XRD and particle size analysis, foraminifera sampling (see appendix A.3) and archive.

As far as possible, plastic utensils were employed to minimise any trace metal contamination. Numbering and identification of the samples is as in the following examples:-

CD3826-090 represents Charles Darwin cruise 38; piston core 26; horizon depth (sample interval) 89-91cm.

CD38P22-070 represents Charles Darwin cruise 38; pilot core 22; horizon depth (smaple interval) 69-71cm.

A.2 Magnetic Susceptibility and Remenance Magnetisation

Methods are consistent with those outlined in Thompson and Oldfield (1986). Initially $10cm^3$ samples from cores P5 and P12 were measured for magnetic susceptibility on a Bartington low field magnetic susceptibility bridge which gave bearly detectable results and, consequently, all samples were magnetised up to 500 mTesla (mT) and measured on a Fluxgate spinner magnetometer, giving Saturation Induced Remenance Magnetisation (SIRM).

A.3 Foraminiferal Sampling and Cleaning for Stable Isotope Analysis using Mass Spectrometry

A.3.1 Preparation

Approximately $10cm^3$ of wet sediment was sampled using a plastic spatula from the same horizons as were used for bulk sediment samples in cores CD3814, CD3822, CD3826 and CD3827. This sediment was then sieved through a 63μm mesh using a fine spray of warm tap water until only foraminifera, radiolaria and other coarse fragments remained. This fraction was subsequently dried at 30-40°C overnight prior to storage ready for picking.

Thirty-five individual intact tests of the species ***Neogloboquadrina dutertrei*** (size fraction 355-425μm) were picked using a fine paintbrush from each datum horizon in cores CD3814 (PP)[1], CD3826 (PP)[1], and CD3827 (PP[1]) and subsequently stored in plastic vials. In core CD3822 (PP)[1] fifty individual tests of the species ***Globigerinoides ruber*** (size fraction 300-355μm) were picked and stored as above.

[1] PP - main piston and pilot core picked for these cores

All foraminifera were sonicated in methanol for approximately one minute, excess alcohol and debris was drained off and the foraminifera left to dry prior to analysis in the isotope ratio mass spectrometer at The Scottish Universities Research and Reactor Centre (S.U.R.R.C.).

A.3.2 Stable Isotope Analysis

Stable isotope determination of foraminifera was carried out on a **VG Isotech PRISM** isotope ratio mass spectrometer under the analytical conditions given in table A.3.1. Between 35-50 individual (depending on the species and size fraction) was required to achieve the optimum weight (~1 mg) for analysis. The standard MBL1 was found to give the best combination of reproducibility and values close to that of the samples. Table A.3.1 also shows typical standard deviation values for MBL1. Results expressed relative to PDB are calculated from equations A.3.2a. and A.3.2b:

Table A.3.1 Analytical conditions for mass spectrometry

Target major ion beam		$6.00\ E^{-09}$ A
Maximum reference ion beam		$1.64\ E^{-08}$ A
Minimum reference ion beam		$2.49\ E^{-09}$ A
Ion Gauge base pressure		$7.60\ E^{-10}$ Torr.
Cold finger Ambient temperature		25°C
	$\delta^{18}O$	$\delta^{13}C$
Typical σ1 for MBL-1	**0.055**	**0.032**

Equation A.3.2a.

$$\delta\ ^{18}O = \frac{^{18}O/^{16}O \text{ sample} - ^{18}O/^{16}O \text{ reference} \times 1000}{^{18}O/^{16}O \text{ reference}}$$

Equation A.3.2b.

$$\delta\ ^{13}C = \frac{^{13}C/^{12}C \text{ sample} - ^{13}C/^{12}C \text{ reference} \times 1000}{^{13}C/^{12}C \text{ reference}}$$

A.4 X-Ray Diffractometry

A.4.1. Preparation

X-ray diffraction was performed on approximately 1g of the ground bulk sediment (see above). As a result of the calcite contents being relatively high in most cores, samples from CD38 were digested by addition of 3M HCl and heating gently until effervescence had ceased. Supernatant acid was decanted off; samples were washed several times with distilled water, the supernatant was decanted off and the resulting carbonate free sediment was dried in an oven at approximately 40°C overnight. Khan (1989) showed that a technique similar to this results in complete removal of calcite whilst leaving the clay minerals essentially intact. Furthermore, HCl is ≈14% (%) acetic acid which was shown by Caroll and Starky (1971) to have negligible effect on clay minerals. Samples were further dissagregated with acetone in a small mortar and pestle before being drawn up in a pipette, dispersed on a glass slide (diameter ≈2cm) and dried at room temperature before being subject to X-ray diffraction. The rapid evaporation of acetone and drying of the sediment slurry is advantageous because, according to Archer (1969), slow drying can result in differential settling which enhances the X-ray response of fine components.

A.4.2. Analysis

A Philips PW 1011/1050 diffractometer was use for mineral identification under the following analytical conditions summarised in table A.4.1:-

Table A.4.1 Summary of the operating conditions used in X-ray diffractometry.

Generator Settings	40kV, 50mA
Cu k-∝1, 2 wavelengths	1.54060, 1.554439
Step size, sample time	0.20°, 3.00secs, 150.00 s/°
Monochromator used	Yes
Divergence slit	Automatic (specimen length: 10.0 mm)
Analyses program No.	8
Peak angle range	2 - 40 2θ°
Range in D-spacing	2.25221 - 44.1372 Å
Crystal Peak Width Range	0 - 2°
Minimum Peak Significant	0.75

A.5 X-Ray Fluorescence Spectrometry

X-ray fluorescence spectrometry was performed on a Phillips PW 1480 sequential automatic x-ray spectrometer and PW1510 sample changer.

A.5.1. Major element Preparation and Analysis

Fused, 45mm glass discs were prepare by a method similar to that of Norrish and Hutton (1969). Around 1.5g of finely ground bulk sediment was dried overnight at 50°C. Approximately 0.8-1.0g of this sediment was subsquently weighed (± 0.0001g) into a platinum crucible. An ultrapure flux, Spectroflux 105 (Johnson-Matthey Chemicals Ltd.), was added in a ratio 5.333:1 (by weight, flux:sample), the crucible was covered (Pt lid) and placed in a muffle furnace at 1100°C for twenty minutes. Batches of four or six crucibles proved practicable.

The flux consists of $Li_2B_4O_2$, La_2O_2 and Li_2CO_3, in which the tetraborate helps to dissolve the sample whilst the La acts as a heavy absorber of the X-rays heping to minimise matrix effects between samples and standards of varying composition. In addition to using La as a heavy absorber, matrix effects for major elements were corrected for by using theoretical absorption coefficients (Theisen and Vollach, 1967) based on a flux:sample ratio of 5.333:1 folowing the correction procedures of Thirlwall (1979).

The crucible was then removed from the furnace, allowed to cool to room temperature on a stainless steel block and reweighed. Any slight weight loss (from H_2O absorbed by the Spectroflux) is made up with additional flux and the sample was refused over a Meker burner. On a hot plate at 220°C a disc-shaped, slightly concave, graphite mould was placed inside a brass sleeve and the moulten glass poured into the centre of the mould. An Aluminium plunger, also at 220°C was used to press the glass into a ≈1 mm thick disc whose upper surface should have a texture resembling "orange-peel". the discs are then allowed to anneal and cool slowly whilst covered by Vitressil cruicibles. The discs are then presented directly to the X-ray tube or stored in a desicator until such time as they could be analysed.

International rock and sediment standards (table A.5.1a.) were used for calibration of the samples as they cover the range in composition of the eastern equatorial pacific sediments. For all elements, the calibration lines are linear over the range of

TABLE A.5.1A. A SELECTION OF THE STANDARDS USED IN XRF CALIBRATION

STANDARDS
Ba-1 (I-III), Ba-2 (I-III), Ba-3 (I-III), Ba-4 (I-III), Ba-5 (I-III), Ba-6 (I-III)
BRIMO-1 (I-III), BRIMO-2 (I-III), BRIMO-3 (I-III), BRIMO-4 (I-III), BRIMO-5 (I-III), BRIMO-6 (I-III), BRIMO-7 (I-III)
MAG-1, BCR-1, AGV-1, GA, BR, GH, SY2, SY3, JB-1, PCC1, SGR-1, GSP-1.

Ba- and BRIMO- standards are a synthetic dilution series made up from the following SPECPURE compounds. $Ba(IO_3)_2$, $KBrO_3$, $(NH_4)Mo_7O_{24}4H_2O$ and $BaCO_3$. Each was prepared using $CaCO_3$ (I), Salisbury Crag DOlomite (II) and Shap Granite (III) matrices which represented a range of possible sediment compositions and mass absorption effects. Calibration lines are periodically revised and some standards are added and some removed, depending on what range of concentrations is required for each element.

compositions investigated. Analytical conditions for XRF major and minor elements are given in table A.5.1b. Precision and Accuracy of the method are given in table A.5.1c.

Although the fusion method provides a very consistent and accurate method of analysis for most rocks and sediments a problem exists with samples containing large quantities of organic matter and/or high carbonate contents, which is manifest in the loss of halogens or alkalies. Pedersen (1979) found that no loss of alkalies occured when samples were immediately fused with Spectroflux. Perhaps the melt eutectic of 700°C for $Li_2O:B_2O_3$ ratio in Spectroflux 105 (Norrish and Hutton, 1969) is sufficiently low to prevent major alkali loss (Shimmield, 1984).

A.5.2. Trace Element Preparation and Analysis

Pressed powder discs, 32mm in diamater, were used for trace element analysis. Approximately 3g of finely ground bulk sediment was placed in a stainless steel sleeve resting on a highly polished tungsten carbide disc. Both the sleeve and cylinder were enclosed within a larger stainless steel cylinder. A "perspex" plunger was inserted inside the sleeve and the sediment was carefully compacted into a semi-competent disc using hand pressure. The "perspex" plunger and the sleeve were removed, excess sediment carefully blown away, and boric acid added sufficient to cover the sediment. A large stainless steel plunger was lowered onto the boric acid powder and a hydraulic press was used to compact the sample at 10 tons for a minute before releasing the pressure slowly for a further half minute. The pressed powder disc was then presented to the X-ray beam after masking down the beam to 28mm or stored in a dessicator until such time as analysis commensed.

The standards used for calibration are given in table A.5.1a including the synthetic dilution series for I, Br, Mo and Ba which were produced. These synthetics were developed with a range of matrices (from carbonate to dolerite) both in an attempt to average out the variations in matrix absorption effects and, to cover the range of expected composition of the sediments.

Table A.5.1B. Analytical conditions for XRF. FL=Flow; SC=Scintilation; FS=flow+scint.

Element	Line	Tube	kV	mA	Crystal	Peak °2θ	+OFF SET °2θ	-OFF SET °2θ	Counter/ Detector	Pulse	Height	Collimator	Sample Prep.	Count Time (secs.)
Al	kα	Rh	40	60	PE	144.955	0.60	0.00	FL	28	76	Coarse	Fusion	50
Ba	Lα	Rh	50	50	Ge220	87.970	1.60	2.70	FL	32	70	Fine	P.D.	100
Br	kα	Rh	80	30	LiF200	29.940	0.00	0.60	FS	27	75	Fine	P.D.	20
Ca	kα	Rh	50	50	LiF200	113.145	0.00	4.00	FL	30	75	Fine	Fusion	20
Ce	Lβ	Rh	50	50	LiF200	71.625	0.00	0.00	FL	32	70	Fine	P.D.	100
Cr	kα	Rh	50	50	LiF200	69.375	1.62	0.88	FL	32	70	Fine	P.D.	40
Cu	kα	Rh	50	50	LiF200	45.040	1.70	0.70	FL	40	70	Fine	P.D.	40
Fe	kα	Rh	50	50	LiF200	57.530	0.00	2.50	FL	18	68	Fine	Fusion	10
I	kα	Rh	80	30	LiF200	12.375	0.50	0.50	SC	25	75	Fine	P.D.	20
K	kα	Rh	50	50	LiF200	136.720	0.00	5.00	FL	32	75	Fine	Fusion	20
La	Lα	Rh	50	50	LiF200	82.950	1.20	1.20	FL	32	70	Fine	P.D.	100
Mg	kα	Rh	40	60	PX1	22.605	3.10	0.00	FL	25	80	Coarse	Fusion	50
Mn	kα	Rh	50	50	LiF200	63.000	2.50	0.00	FL	14	72	Fine	Fusion	10
Mo	kα	Rh	80	30	LiF200	20.300	0.44	0.44	SC	28	70	Fine	P.D.	100
Na	kα	Rh	40	60	PX1	27.275	0.00	0.00	FL	25	75	Coarse	Fusion	50
Ni	kα	Rh	50	50	LiF200	48.685	1.30	0.00	FL	40	70	Fine	P.D.	40
Nb	kα	Rh	80	30	LiF200	21.360	0.40	0.70	FS	20	75	Fine	P.D.	40
Nd	kα	Rh	50	50	LiF200	72.160	2.30	0.00	FL	32	70	Fine	P.D.	100
P	kα	Rh	40	60	Ge111	140.915	3.00	0.00	FL	34	75	Coarse	Fusion	50
Pb	Lβ	Rh	80	30	LiF200	28.245	0.30	0.30	FS	20	75	Fine	P.D.	100
Rb	kα	Rh	80	30	LiF200	26.585	0.54	0.00	FS	20	75	Fine	P.D.	40
Sc	kα	Rh	50	50	LiF200	97.750	0.00	2.00	FL	30	70	Fine	P.D.	40
Si	kα	Rh	40	60	PE	109.070	4.00	0.00	FL	30	75	Coarse	Fusion	50
Sr	kα	Rh	80	30	LiF200	21.110	0.76	0.76	FS	20	75	Fine	P.D.	40
Ti	kα	Rh	50	50	LiF200	86.185	3.50	0.00	FL	28	72	Fine	Fusion	20
Th	Lα	Rh	80	30	LiF200	27.465	0.00	0.30	FS	20	75	Fine	P.D.	100
U	Lα	Rh	80	30	LiF200	26.130	0.00	0.36	FS	20	75	Fine	P.D.	100
V	kα	Rh	50	50	LiF200	123.260	0.00	1.30	FL	32	70	Fine	P.D.	40
Y	kα	Rh	80	30	LiF200	23.760	0.00	0.00	FS	20	75	Fine	P.D.	40
Zn	kα	Rh	50	50	LiF200	41.795	0.66	0.66	FS	22	75	Fine	P.D.	40
Zr	kα	Rh	80	30	LiF200	22.500	0.66	0.76	FS	20	75	Fine	P.D.	40

Table A.5.1c. XRF Analytical Precision and Accuracy for major and minor elements.

Element	Mean (n=10/8*)	σ-1	Total Precision (as % relative σ-1)⊕	Accuracy[1]	Range of concentration
SiO_2	52.137	0.061	**0.117**	0.147	0-74
Al_2O_3	15.619	0.033	**0.211**	0.124	0-30
Fe_2O_3	8.894	0.021	**0.236**	0.157	0-15
MgO	3.407	0.020	**0.582**	0.037	0-44
CaO	1.852	0.010	**0.523**	0.086	0-56
Na_2O	3.111	0.031	**0.996**	0.062	0-11
K_2O	1.439	0.007	**0.486**	0.017	0-13
TiO_2	0.824	0.003	**0.314**	0.017	0-2.6
MnO	0.054	0.002	**4.444**	0.010	0-5
P_2O_5	0.110	0.003	**2.573**	0.014	0-1
Ba	2615.1	11.1	**0.4**	27.66	0-2300
Br	160.1	1.7	**1.1**	2.40	0-370
Ce	26.4	3.5	**13.4**	7.89	0-440
Cr	71.8	1.0	**1.4**	55.48	0-1035
Cu	89.9	0.7	**0.8**	5.69	0-124
I	84.9	3.5	**4.1**	3.70	0-300
La	13.9	2.2	**15.9**	4.30	0-145
Mo	4.4	0.3	**6.4**	0.60	0-10
Nb	3.5	0.2	**6.4**	2.42	0-112
Nd	19.5	2.3	**11.7**	3.14	0-94
Ni	153.4	0.9	**0.6**	4.45	0-2002
Pb	7.0	0.8	**11.4**	2.02	0-870
Rb	26.7	0.2	**0.7**	3.08	0-860
Sc	16.7	1.5	**9.0**	3.19	0-38
Sr	528.2	3.2	**0.6**	8.46	0-1300
Th	0.4	0.4	**100.0**	1.77	0-380
U	10.2	0.9	**9.2**	4.73	0-50
V	198.4	1.2	**0.6**	6.37	0-440
Y	23.7	0.5	**2.3**	1.28	0-180
Zn	285.2	1.2	**0.4**	3.27	0-597
Zr	58.8	0.5	**0.8**	10.49	0-530

⊕Total precision includes counting error, disc reproducibility, error in regression line and error in matrix mass absorption determinations.

[1]Accuracy determined from r.m.s.d. of international standards about the regression line.

Major element concentration in Wt. %, minor elements in ppm. Repeat analysis was performed on sample CD3826-200 for minor elements, and on sample P12-129 for major elements. * Only 8 fused discs could be made with the available bulk sediment sample from a single horizon (P12-129). It is important to note that the R.M.S.D. values are for the calibration line over the total range of concentrations given, and that with the deletion of some high concentration standards, the R.M.S.D. may be significantly reduced (improved). Thus, the R.M.S.D. values quoted are essentially the worst case scenario.

A.6 Biogenic Silica Determination

A.6.1 Introduction and technique summary

The analytical techniques for wet chemical analysis of biogenic silica used in this thesis are consistent with those developed by Dobbie (1988) following the methods of Eggiman et al. (1980). Ground bulk sediment samples (see appendix A.1) were digested in PTFE (Polytetrafluroethylene) bombs in the presence of 2M $NaCO_3$ and the silica determined colorimetrically. The coloring up method relies on the formation of a yellow silicomolybdate acid which is reduced to molybdenum blue, the absorption of which is measured at 812nm in a Perkin-Elmer-550 spectrophotometer.

Approximately 50mg of sample was weighed (to five decimal places) and placed into the PTFE beakers and 20ml of 2M $NaCO_3$ was added. The $NaCO_3$-sediment mixture was swirled to ensure complete wetting of the sediment, the beakers sealed in stainless steel bombs and placed in an oven at 90-100°C for four hours after which the bombs were quenched in water to room temperature (this ensures a consistent period at elevated temperatures). These conditions were shown by Eggiman et al. (1980) and later by Dobbie (1988) to be effective in digesting the amorphous silica and leaving clay minerals essentially intact.

The leachate solutions were quantitatively filtered in vacuum through polycarbonate 0.45µm membrane filters using entirely plastic apparatus. the filtrate and rinsings were transfered to a 100ml volumetric flask and diluted to the mark with deionised water. The solutions were stored in polythene bottles which had been acid and deionised water cleaned prior to being rinsed three times with the filtrate.

Reagent preparation was a described in Dobbie (1988). There now follows a summary of the steps taken to determine the biogenic silica concentrations of the solution (sediments):-

1. 5ml aliquots of sample, reagent blank (deionised water + reagents), $NaCO_3$ blank ($NaCO_3$ + reagents) and a standard containing 2 ml of "silica standard" were acidified using 2.2ml of 50% HCl in a 100ml volumetric flask. This was diluted to 15ml before adding the reagents.

2. 1ml Ammonium molybdate solution was added directly into the 15ml solutions, shaken and left to stand for exactly 10 minutes allowing the complete formation of the silicomolybdate comlex.

3. 5ml of Oxalic acid were added followed immediately by 2ml of strong reducing solution after which the flask was shaken gently. This resulting solution was diluted to the 100ml mark in a volumetric flask with deionised water and left for 1-1.5 hours to allow a stable molybdenum blue color to develop. A $2cm^3$ cell was used in a Perkin-Elmer 550 spectrophotometer at wavelength 812nm to measure the absorbance of silica.

A.6.2 Calculation of Apparent Biogenic Silica

The absorbance readings for the reagent and $NaCO_3$ blanks were subtracted from the standard reading and the standard and sample (unknowns) readings respectively prior to calculation of the apparent biogenic silica content from equation A.6.1:

$$\text{Equation A.6.1 Apparent } SiO_{2biog} = \frac{(R - NaCO_3\ B) \times (2 \times 100 \times 1.00052)}{(S - Reag.B) \times (\text{Sample Weight (mg)}}$$

$$\equiv \text{App. } SiO_{2biog} = \frac{(R - NB)}{(S - RB)} \times \frac{k}{Wt.\ (mg)}$$

Where:

R = Absorption of samples (unknowns)
NB = Absorption of $NaCO_3$ blank
RB = Absorption of Reagent blank
S = Absorption of Standards

$k = 200.104\ (2 \times 100 \times 1.00052)$

Where: 2 ≡ ml standard in 100 ml
100 ≡ %
1.00052≡ g Specpure SiO_2 in standard stock solution

A.6.3 Correction for Non-Amorphous SiO_2

The calculated values are for Apparent biogenic silica because of the possible presence of some non-amorphous silica derived from clays (particularly smectites which are very susceptible to degradation) or quartz. However, according to Eggiman (1980), the SiO_2 contribution from quartz results in a second order effect and so the correction for non-amorphous silica is for the clay derived SiO_2 only. The SiO_2/Al_2O_3 ratio in eastern equatorial pacific sediments is believed to be approximately 3. Using this figure, biogenic silica values in the sediments could be calculated by multiplying the Al_2O_3 contents of the solutions and subtracting this from the the apparent SiO_{2biog} concentration. Thus, equation A.6.2 calculates true biogenic SiO_2:-

Equation A.6.2 True Biogenic SiO_2 = % App. $SiO_{2biog.}$ - (3 × Al_2O_3 %)

The international standard Mag-1 was used as an independent check and has a SiO_2/Al_2O_3 ratio = 3 according to Eggiman (1980) and 3.1 according to a geostandards newsletter (summer, 1989). Table A.6.1 shows repeat analyses of this standard and the standard deviation results.

A.6.4 Determination of Al_2O_3 in solutions

The method used is detailed in Dougen and Wilson (1974) and essentiallly invoves the formation of a catechol violet complex. The procedure is summarised below:-

1. 5ml aliquot of sample (unknowns) solution, $NaCO_3$ blank solution and a standard solution (containing 0.1mg Al_2O_3 / 100ml) were acidified in a 100ml standard flask by addition of 2.45ml of 25% HCl prior to dilution to 35ml with deionised water.

2. The solutions were coloured up in the following way:
1ml of 1:10 Phenolanthroline solution added; flask shaken gently;
2ml of catechol violet solution added; flask shaken gently;
10ml of Hexamine buffer solution added; flask shaken gently; solutions were subsequently diluted to the 100ml mark with deionised water and left for 10 minutes to allow the catechol violet complex (colour) to stabilise.

The absorption of the solution was measured in a $1cm^3$ cell using a Perkin-Elmer 550 spectrophotometer. Equation A.6.3 was then used to calculate the concentration of Al_2O_3.

Table A.6.1 Mag-1 Repeat Analyses

Identification	App. SiO_2 (%)	Al_2O_3 (%)	True SiO_{2biog}	
Mag-1(I)	3.885	0.389	2.820	
Mag-1(II)	3.702	0.338	2.648	
Mag-1(III)	3.603	0.156	2.434	
Mag-1(IV)	3.636	0.155	2.581	
Mag-1(V)	3.980	0.302	3.074	
Mag-1(VI)	4.104	0.050	3.952	
Mag-1(VII)	4.340	0.048	4.196	
				– Mag-1 VI & VII
		Std. Dev.(σ1)	= 0.646	**0.220**
		Mean	= 3.101	2.711
		n	= 7	5

Equation A.6.3 $$Al_2O_3\ \% = \frac{(R - NB)}{(S - NB)} \times \frac{(0.9362 \times 0.02 \times 100)}{\text{sample weight (mg)}}$$

$$\equiv Al_2O_3\ \% = \frac{(R - NB)}{(S - NB)} \times \frac{k}{\text{sample Wt. (mg)}}$$

Where :

R = Absorption reading of sample (unknown)

NB = Absorption reading of $NaCO_3$ blank

S = Absorption reading of standard

k (Factor) = 37.448 ($100 \times 20 \times 0.02 \times 0.9362$): where;

100 = %

20 = ml standard / 100ml

0.02 = ml Al_2O_3 standard

0.9362 = g Al_2O_3 in standard stock solution

A.6.5. Sample Analytical Precision and Accuracy

Table A.6.2 shows results of repeat biogenic SiO_2 analysis of samples CD3822-060 (12.5 ka); CD3826-622 (265 ka) and CD3827-180 (20 ka) together with the mean and standard deviations.

Table A.6.2 Sample repeats from biogenic silica analysis

Sample	n	Mean	σ1
CD3822-060	3	3.111	0.039
CD3826-622	3	3.888	0.087
CD3827-180	3	4.295	0.057

A.7 Correction for the Dilution and Contribution of residual sea salt

Sea salt contains considerable amounts of Na, Mg, Ca, K, S and Br. As a result, correction must be made for the dilution and contribution effects these elements will have on the overall dry bulk sediment composition of marine sediments.

A.7.1 Salt Correction derived from Water Contents

Two steps are necessary; firstly elemental concentrations are corrected for by using the following equations:

$$\text{Wt \% of } Na_{sed.} = \text{total Wt. \% of } Na_{sed.} - (0.306^{1} \times \text{SALT})$$
$$\text{Wt \% of } Mg_{sed.} = \text{total Wt. \% of } Mg_{sed.} - (0.037^{1} \times \text{SALT})$$
$$\text{Wt \% of } Ca_{sed.} = \text{total Wt. \% of } Ca_{sed.} - (0.012^{1} \times \text{SALT})$$
$$\text{Wt \% of } K_{sed.} = \text{total Wt. \% of } K_{sed.} - (0.011^{1} \times \text{SALT})$$

$$\text{PPM } S_{sed} = \text{total } S_{sed} \text{ (ppm)} - (262^{1} \times \text{SALT})$$
$$\text{PPM } Br_{sed} = \text{total } Br_{sed} \text{ (ppm)} - (19^{1} \times \text{SALT})$$

Secondly, all the elemental concentrations were corrected for dilution using the below equation:

$$\text{Element (salt free)} = \text{Element}_{measured} \times (100/(100\text{-SALT}))$$

[1] factors based on composition of elements in sea-water (Horne, 1969; p151).

The salinity of interstitial water is assumed (somewhat tenuously) to be constant and the same as that of normal sea water, at 35 ‰. Water contents are used together with this assumed value to calculate the salt content in sediments from equation A.7.1:

Equation A.7.1

$$\text{Salt} = \frac{3.513 \times W}{100 - W}$$

Where; W = Water Content (% Wet Wt.)

A.7.2 Correction corroboration derived from Chloride analysis of sediments

An independent check was carried out to establish the accuracy of salt concentrations calculated from water contents (see above). It consisted of analysing a representative batch of sediments for Cl^- using High Performance Liquid Chromatography (H.P.L.C.) and calculating the salt (NaCl) concentration stoichiometrically. The method is as follows:

Approximately 1g (±0.00001g) of finely ground bulk sediment was placed in a 500ml volumetric flask and diluted to the mark with deionised water. The flask was shaken vigorously several times over a period of about one hour to dissolve all the salt, after which the solution was quantitatively filtered using a 45µm polycarbonate membrane in vacuum and stored in polythene bottles.

A series of standards was required for calibration. For this, approximately 2g of NaCl was dried in an oven overnight prior to being weighed (±0.00001g) and placed in a 100ml flask where it was dissolved and diluted to the mark with deionised water. From this standard stock of approximately 1000ppm Cl^-, a dilution series was created resulting in six standards ranging from 100ppm Cl^- to 10ppm Cl^- (see table A.7.1). These standards together with the samples (unknowns) were measured under the analytical conditions used given in table A.7.2.

The results from the standards are given in table A.7.1 and the peak area calibration graph (which was shown to be more linear) is shown on figure A.7.2a. From this calibration, the concentration of the Cl^- in the samples was analysed and the salt content of the sediment was calculated (see table A.7.3) using equation A.7.2.

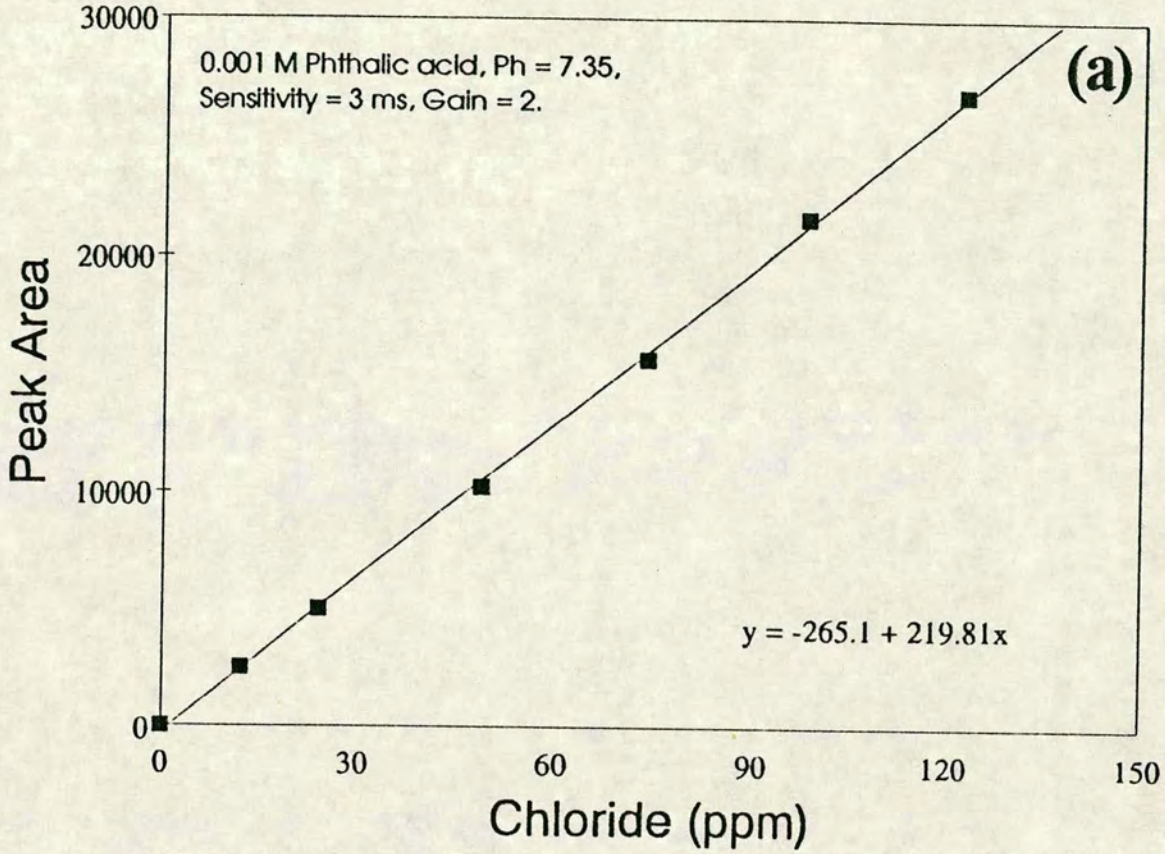

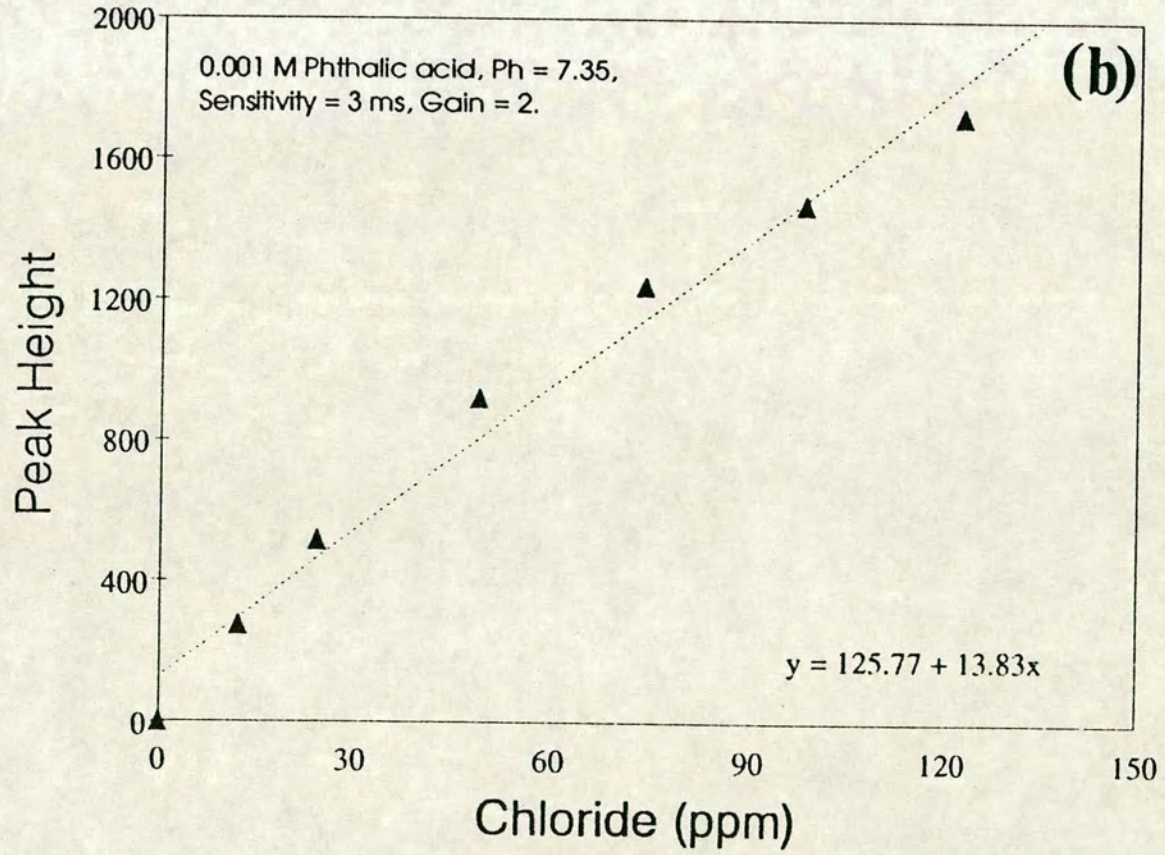

Figure A.7.2 Calibration gragh for Chloride analysis on H.P.L.C.

Table A.7.1 Standard dilution series

Std. ID	PPM Cl	Peak Area	Peak height
0	0	0	0
10	12.28	2529	275
20	24.55	5020	516
40	49.10	10204	920
60	73.77	15644	1240
80	98.21	21598	1471
100	122.76	26825	1724

Y = 216.837 X (forced through origin)

Equation A.7.2 SALT (%) = {[(Cl(ppm) / 2) / (Wt. sample (mg))] / (k × 100)}

Where k = 0.5269 (factor for Cl^- in average sea salt)

This factor (k) may vary slightly depending on the proximity to coasts and the anoxicity of the water. The salt concentrations calculated from both methods compare very well (Mean std. dev.($\sigma 1$ = 0.079, excluding P5 results) except for the samples from P5 which may have lost a considerable amount of moisture before being weighed for water content calculations as a result of being recovered over ten years previously.

Table A.7.2 Analytical conditions for H.P.L.C.

Eluent	= 0.001M Pthalic Acid + "TRIS" buffer; Ph = 7.35
Column type	= Spherical Si
Pump flow rate	= 1 ml / minute
Column temperature	= 25°C
Sample/Std. Vol.	= 10µl
Peak reading	= Area and Height
Sensitivity	= 3µs
Gain	= 2

Table A.7.3 Results of Cl^- analysis of samples

SAMPLE	Peak A	Peak H	Cl(ppm)	SALT[1]	SALT[2]
P5-51†	1039	928	47.9	4.44	3.71
P5-111†	1004	906	46.3	4.34	3.35
CD3814-260	7294	693	33.6	3.04	3.07
CD3814-500	5867	585	27.0	2.52	2.97
CD3822-170	1337	1092	61.6	5.74	5.73
CD3822-570	9523	790	43.9	4.09	3.98
CD3826-270	1027	900	47.4	6.21	6.50
CD3826-980	1334	1094	61.5	5.58	5.61
CD3827-080	1626	1225	75.0	6.84	6.72
CD3827-299	1257	1023	57.9	5.20	4.97
					Mean $\sigma 1$ = 0.079 ⊕

[1]-from equation A.7.2.; [2]-from equation A.7.1; †-water contents unreliable (see text). A=Area; H=Height. ⊕ excluding P5 results.

A.8 Organic Carbon Determination

Marine sediments essentially contain two forms of carbon; carbonate carbon (usually from the $CaCO_3$ of plankton remains) and organic carbon (remains of any lifeform). When analysing for organic carbon (hereafter C-org) one must ensure that all the carbonate carbon is removed whilst still leaving the C-org intact. Furthermore, C-org may be lost by hydrolysis if the sediments are washed following acid removal of carbonate carbon. To avoid this, samples were acid treated in the LECO ceramic cruicibles. As these cruicibles are porous, care was taken to keep the fluid volume to a minimum to reduce any loss of soluble C-org through the cruicible wall.

Organic carbon determination on carbonate-free samples was achieved by combusting in an induction furnace in a stream of CO_2-free oxygen followed by potassium hydroxide absorption of the CO_2 produced. A LECO 521-200 induction furnace equipped with dust-trap, sulphur trap (SO_2 absorption by MnO_2 powder) and catalyst furnace was used for combustion. This was connected to a 572-100 carbon analyser with a glass burette to measure the change in volume which resulted when the O_2-CO_2 mixture from the combustion furnace was flushed through the CO_2-absorbing KOH.

300-500mg (±0.00001g) of dried bulk sediment sample (see appendix A.1) was weighed into LECO ceramic crucibles and placed on Al sheets. Sediments were dampened with distilled water prior to addition of 2 drops (1+1) of 50% HCl. This initial digestion is crucial as extreme care must be exercised to ensure no loss of sample due to the violent efforvescence that ensues especially in carbonate rich samples. The resulting mixture was stirred thoroughly with a glass rod which was washed into the crucibles with distilled water to ensure no sample loss. After evaporation to dryness on a hotplate set at approximately 60°C, samples were allowed to cool before a further 5-8 drops of 50% HCl were added prior to stirring with a glass rod as before. This step was repeated until efforvescence ceased to ensure total removal of the carbonate carbon. Each digestion and drying step took several hours with the samples being left overnight on the hotplate before analysis. A major problem with using HCl can be the formation of strongly deliquescent $CaCl_2$ during digestion and the production of HCl fumes during combustion. The former potential problem was solved by keeping the samples on the hotplate and, for a short period (<30 minutes), in a dessicator until immediately prior to analysis. The latter problem may result in the oxidation of HCl fumes by MnO_2 in the sulphur trap to

chlorine gas which could interfere with the KOH absorption, producing spuriously high results (Pedersen, 1979). This is not considered a serious problem in the sediments analysed in this thesis (because MnO2 values are generally low, <1%). An Fe accelerator and Sn flux were evenly spread over the surface of the sample to ensure compleat combustion in the furnace. Values for organic carbon were calculated from equation A.8.1. Analytical precision was generally quite acceptable; with standard deviations ($\sigma 1$)being 0.010 for ~2% C-org and 0.035 for ~1% C-org.

Equation A.8.1

$$\text{C-org (Wt.\%)} = \frac{(R \times PTC) - SFB}{Wt(g)}$$

Where: R = Reading from LECO
PTC = Pressure/Temperature correction
SFB = Sn-Fe blank correction

A.9 Accuracy of Titanium Analysis by XRF

As a result of the exceptionally high Ti/Al ratios (>0.1) in core P5, an attempt was made to determine whether the Ba Lα line had any interference on the Ti Kα line during analysis. This was achieved in two steps:

1. Testing the resolution of the XRF
2. Wet chemical analysis of Ti

A.9.1 XRF Resolution

Four fused discs were prepared as described in appendix A.5 and scanned in the X-ray spectrometer over the narrow range of 75-90 2θ degrees. The samples (table A.9.1A.) used were chosen to be representative of core material and of extremes of composition. Analytical conditions are as described in section A.5. Figure A.9.1a shows all four disc analysis overlain and, clearly illustrates the positions of the elemental lines on the XRF spectrum and the variation in concentration of Ba between samples. Figure A.9.1B shows sample P5-13 minus the pure $CaCO_3$ profile. This figure clearly shows that the trace drops to almost background values between the Ti Kα and Ba Lα lines. Therefore one must assume that Ti and Ba are resolvable using XRF and that they do not intefere with one another. To make absolutely sure,

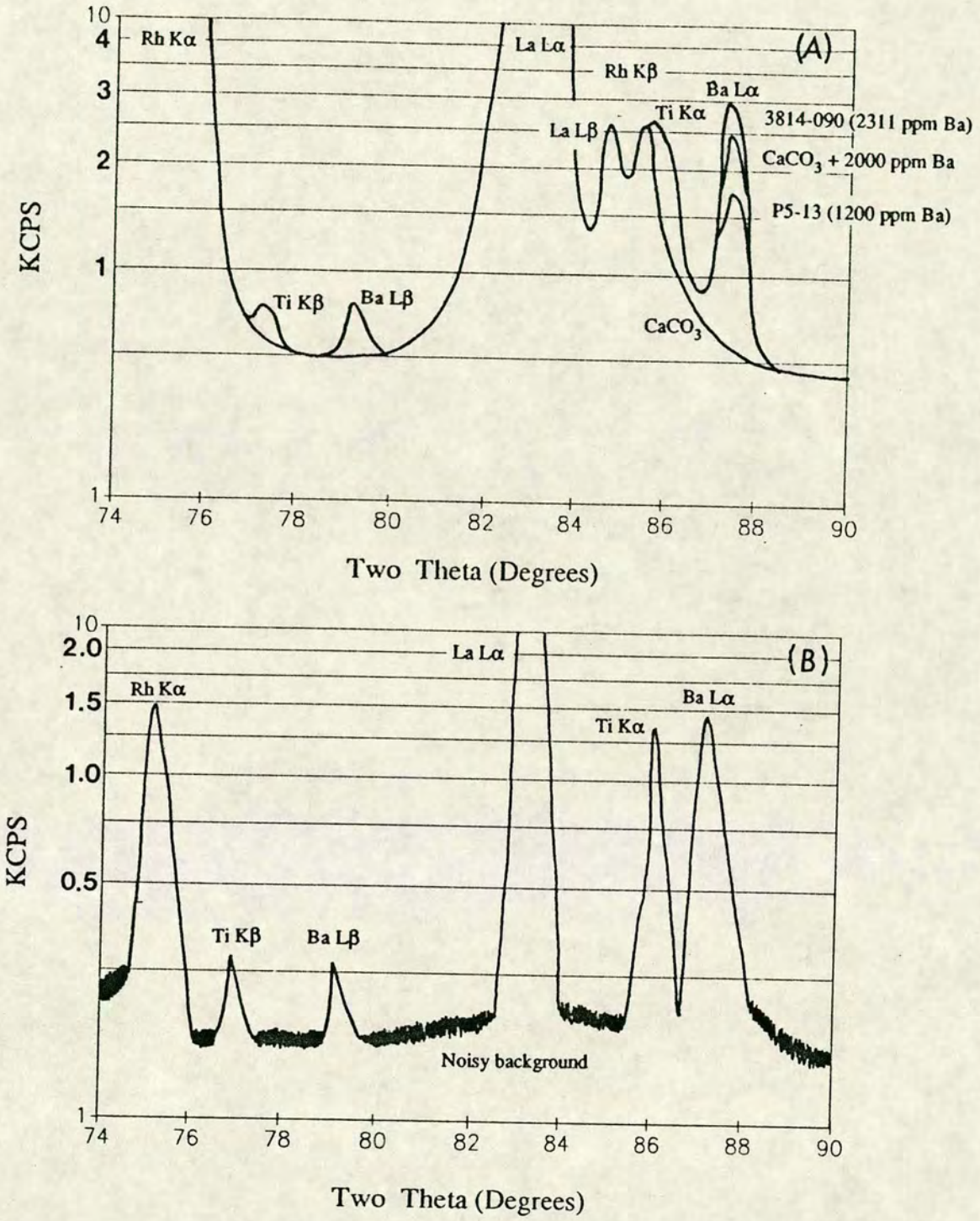

Figure A.9.1. Diagram illustrating the resolution of the XRF spectrometer. (a) Copy of a plot showing the strong La spikes from the heavy absorber flux (see text); the pure $CaCO_3$ with no Ba Lα peak; the Ba Lα line spike in the samples with varying amounts of Ba; and the Ti Kα and Ti Kβ lines. (b) A copy of the plot which subtracts the pure $CaCO_3$ profile from the P5-13 sample in (a). Note the drop to almost background levels between the Ti Kα and Ba Lα lines.

an independent, wet chemical analysis of Titanium was carried out as described below.

A.9.2 Wet Chemical Determination of Titanium

Wet chamical analysis of Ti was determined colorimetrically by a method similar to that of Rigg and Wagenbauer (1961) which measures the absorbance of a yellow titanium complex with disodium 1,2-dihydroxybenzene-3,5-sulphonate at a wavelength of 380mμ and Ph=3.8.

Method

Approximately 0.2g (±0.00001g) sample and 0.1g (±0.00001g) standard (AC-E and synthetic) were dried overnight at 60°C prior to being diigested in platinum crucibles with; 5ml (1+4) concentrated Nitric acid, 1 ml 48% Hydrofluric acid and 2ml (1+1) concentrated sulphuric acid. Samples (unknowns) and standards were evaporated to dryness (subsequent to cesation of white sulphuric acid fumes) and left to "cook" at 60°C overnight (> 12 hours). All solutions were transfered to 50ml volumetric flasks and diluted to the mark with deionised water. From these dilutions the following aliquots were taken:

1. Samples (unknowns)	15ml
2. Standards	0.25ml (diluted to 15ml with deionised water)
3. Blank	15ml

To these aliquots; 25ml buffer, 5ml hydroxybenzene sulphonate reagent and 2ml 20% thioglycolic acid (see Rigg and Wagenbauer, 1961 for reagent preparation) were added before dilution to 50ml with deionised water in a volumetric flask. These solutions were left to stand for at least one hour to allow a stable complex to develop before being measured for absorbance at 380mμ. The Ti concentration in the samples (unknowns) was calculated using equation A.9.1.

Equation A.9.1. $TiO_2\ (\%) = [F \times 100 \times (SP\text{-}RB)] / \text{Sample Wt. (mg)}$

Where $F = [(\text{Wt.(mg) } SiO_2 \text{ Std.})/(ST\text{-}RB)] \times (50/15)$

SP = Sample absorbance reading

ST = Standard absorbance reading

RB = Reagent blank absorbance reading

Results (table A.9.1) compare well with major element analysis of Ti on XRF, wet chemical analysis always being slightly lower (mean difference = -0.00887 % TiO_2). This systematic difference in values, although small, may point to a minor calibration problem (perhaps intercept error) in XRF analysis. However, the variations are very small and do not account for the extremely elevated Ti/Al ratios of core P5.

Table A.9.1 Results of Wet chemical analysis of Ti

Sample	Ti (Wt.%)	Ti (Wt.% XRF)	σ-1
P5-011	0.0384	0.046	0.0038
P5-039	0.0269	0.035	0.0040
P5-061	0.0186	0.029	0.0052
P5-089	0.0209	0.033	0.0060
P5-101	0.0204	0.029	0.0043
P5-123	0.0306	0.037	0.0032

Mean Std. Dev. (σ-1) = **0.0044**

A.10 Statistical Analysis and Confidence Limits

A.10.1 Introduction

Statistical analysis was performed using the MINITAB programme (version 7). Detailed descriptions of the theory and methods behind the technique are given in Ryan et al., (1985) and in the MINITAB manual. Below is a brief summary of the method and calculations of the confidence limits.

A.10.2 Confidence Limits on Correlation Coefficients

The Pearson product moment correlation coefficient was used and only the lower triangle of the matrix is computed in MINITAB. The programme employs "pairwise deletion" of missing values which calculates the correlation coefficients using only the samples that have data from both sets of variables.

In order to achieve a 95% or greater significance to the correlation coefficients, confidence limits are calculated for each core (correlation matrix) using the following method.

Capital letters refer to "population factors"; smallcase letters to "sample factors".

ρ = population correlation of the variables X and Y (taken as r = 0.5).
r = sample correlation coefficient of the variables x and y.
n = sample size (different for each core and some elements).

$$W = 0.5 \log_e \frac{1+\rho}{1-\rho}$$

$$w = 0.5 \log_e \frac{1+r}{1-r}$$

Both w and W are derived from tables taking r = 0.5. The variable w is approximately normally distributed (best when n > 50) with mean = W, and standard deviation = $1 / \sqrt{n-3}$

The standardised normal varable, $z = | w - W | \sqrt{n-3}$.

The null hypothesis, $H_0 \rightarrow r = 0.5$ ie., 25% [$100(0.5)^2$] of the variability of X and Y is explained by a fitted straight line on a graph of X versus Y.

Thus only the limiting coefficient, r remains unknown, and with the appropriate sample size for a 95% confidence limit, the standardised Normal variable (z) = 1.95 (from tables). From the below equation, r is calculated for each core/element and shown in table A.10.1

For example: r = 0.5, W = 0.5493, >95% confidence limits, z = 1.95, n = 57

$\backslash\ | w - W | \sqrt{n-3} = 1.95$
$\backslash\ | w - 0.5493^* | \sqrt{57-3} = 1.95$
$\backslash\ w = (1.95/\sqrt{54}) + 0.5493$
$\backslash\ w = 0.672$
Hence $r^* = 0.815$ (* from tables)

Therefore, when r = 0.5, the limiting correlation coefficient corresponding to a confidence limit of 95% is as shown in table A.10.1. Thus in the correlation matrices (tables 5.5-5.9 and 6.4-6.5) where the correlation coefficient is > the corresponding r value in table A.10.1, one rejects the null hypothesis of r = 0.5 and can conclude that there is statistical correlation (positive or negative) between variables X and Y. Similarly where the coefficient of correlation is < the corresponding r value given in table A.10.1, one must accept the null hypothesis and say that there is no significant correlation.

The sample numbes change for each core and for some elements (eg biogenic SiO_2 and C-org) and, therefore, the confidence limits vary accordingly (as shown in table A.10.1 and on the correlation matrices themselves).

Table A.10.1 Values of n and r for cores studied in this thesis

Core	n	r	Core	n	r	Core	n	r
CD381473		**0.654**	CD3822	63	**0.665**	CD3826	111	**0.626**
CD381472		**0.655**	CD3822	62	**0.666**	CD3826	110	**0.628**
			CD3822	47	**0.687**			
Core	n	r	Core	n	r			
CD382733		**0.719**	P5	57	**0.672**			
CD382732		**0.722**						

The elements to which each r-value applies are given on the correlation matrices throughout this thesis.

APPENDIX B

CALCULATION OF SEDIMENT PARAMETERS

B.1 $Si_{terrigenous}$ (Wt.%) = Si_{total} (Wt% salt free) - $Si_{biogenic}$ (Wt% salt free)

B.2 $CaCO_3$ (Wt%) = Excess Ca × 2.497

Where Excess Ca = $Ca_{meas.}$ - (0.345* × $Al_{meas.}$)

and $element_{meas.}$ = Wt.% element measured using XRF.

B.3 Excess Metals

B.3.1 Excess Ba (ppm salt free) = total $Ba_{meas.}$- ($Al_{meas.}$ × 0.02738*)

B.3.2 Excess Cu (ppm salt free) = total $Cu_{meas.}$- ($Al_{meas.}$ × 0.0005625*)

B.3.3 Excess Ni (ppm salt free) = total $Ni_{meas.}$- ($Al_{meas.}$ × 0.000850*)

B.3.4 Excess Sr (ppm salt free) = total $Sr_{meas.}$- ($Al_{meas.}$ × 0.00214*)

B.3.5 Excess Ti (Wt% salt free) = total $Ti_{meas.}$- ($Al_{meas.}$ × 0.05476*)

B.3.6 Excess V (ppm salt free) = total $V_{meas.}$- ($Al_{meas.}$ × 0.001625*)

B.3.7 Excess Zn (ppm salt free) = total $Zn_{meas.}$- ($Al_{meas.}$ × 0.001187.*)

Where $element_{meas.}$ = element concentration determined using XRF

B.4 Phosphorus partitioning (see chapter 6.7, for details)

B.4.1 Method 1 $P_{excess} = P_{tot.} - (P_{pt.} + P_{det.})$

where: $P_{tot.}$ = Total P measured by XRF

$P_{pt.}$ = Phosphorite/authigenic P derived from Y/P ratios in phosphorite bands incore CD3810. $P_{pt.} = (Y_{measured} \times (26.9 \times 10^{-4}))$.

$P_{det.}$ = detrital P derived from average P/Al in world average shale from Turekian and Wedopohl (1961) ie ($0.00875 \times Al_{meas.}$).

B.4.2 Method 2 $P_{excess} = P_{tot.} - (P_{org} + P_{det.})$

where $P_{org.}$ = (C-org/41) from the Redfield ratio of C:N:P = 105:15:1 giving a C:P molecular ratio of 41:1.; $P_{det.}$ = as in method 1; $P_{tot.}$ = as in method 1

B.5 Terrigenous Fluxes

Element MAR (mg/cm^2/kyr) = element concentration (Wt% salt free) × LSR × DBD

Where **MAR** = Mass accumulation rate (mg/cm^2/kyr), **LSR** = Linear sedimentation rate (cm/kyr)

DBD = Dry bulk density (g/cm^3)

B.6 Biogenic Fluxes (as for terrigenous fluxes above).

B.7 Palaeoproductivity (R)

$$R = \frac{C \,.\, fs \,.\, (1-\emptyset)}{0.0030 \,.\, S^{0.30}}$$

C = C-org (Wt.% salt free), fs = sediment density (g/cm2), Ø = sediment porosity (percent water/100). After Muller and Suess (1979).

* The world mean elemental ratio/Al from Turekian and Wedopohl (1961).

APPENDIX C
TABULATED DATA

CONTENTS Page No.

CONTENTS Page No.

Depth(cm)	WC(%)	DBD	Porosity	SIRM	LogSIRM	SIRM
1	71.783	0.351	0.870	44.75	1.651	8.937
10	72.286	0.343	0.873	41.11	1.614	9.163
20	70.116	0.376	0.861	37.65	1.576	8.242
30	74.623	0.309	0.886	34.40	1.537	10.330
40	75.000	0.303	0.888	34.44	1.537	10.539
50	75.353	0.298	0.890	43.64	1.640	10.740
60	74.900	0.305	0.887	48.43	1.685	10.483
70	72.061	0.346	0.872	45.19	1.655	9.061
81	68.121	0.407	0.849	44.27	1.646	7.507
90	66.545	0.433	0.840	33.86	1.530	6.988
100	68.502	0.401	0.851	35.05	1.545	7.640
110	65.623	0.448	0.834	31.04	1.492	6.706
119	69.411	0.387	0.857	34.56	1.539	7.971
130	70.330	0.373	0.862	57.22	1.758	8.327
140	71.605	0.353	0.869	50.06	1.699	8.859
150	75.315	0.299	0.889	49.76	1.697	10.719
160	76.563	0.281	0.896	43.54	1.639	11.476
170	75.255	0.300	0.889	46.89	1.671	10.684
179	76.019	0.289	0.893	39.94	1.601	11.136
190	74.826	0.306	0.887	49.98	1.699	10.442
200	76.217	0.286	0.894	44.80	1.651	11.258
209	78.331	0.257	0.905	45.09	1.654	12.699
220	77.796	0.264	0.902	47.15	1.673	12.308
230	80.872	0.222	0.918	32.74	1.515	14.853
240	80.395	0.229	0.915	32.19	1.508	14.406
251	75.199	0.300	0.889	22.33	1.349	10.652
260	67.852	0.412	0.848	25.04	1.399	7.415
270	69.346	0.388	0.856	31.26	1.495	7.947
279	70.202	0.375	0.861	34.36	1.536	8.276
290	76.289	0.285	0.894	37.55	1.575	11.303
300	75.962	0.290	0.893	40.09	1.603	11.101
310	76.893	0.276	0.898	38.93	1.590	11.690
320	77.508	0.268	0.901	36.27	1.560	12.106
330	78.583	0.253	0.906	35.44	1.549	12.890
340	78.433	0.255	0.905	40.58	1.608	12.776
350	76.726	0.279	0.897	48.60	1.687	11.581
360	80.314	0.230	0.915	41.62	1.619	14.332
370	80.960	0.221	0.918	38.35	1.584	14.938
380	79.431	0.242	0.910	40.44	1.607	13.566
390	79.934	0.235	0.913	35.96	1.556	13.995
400	80.855	0.223	0.918	34.28	1.535	14.836
410	79.935	0.235	0.913	35.40	1.549	13.995
420	80.293	0.230	0.915	30.11	1.479	14.313
430	79.773	0.237	0.912	33.58	1.526	13.855
440	79.020	0.247	0.908	36.27	1.560	13.232
450	79.640	0.239	0.912	33.23	1.522	13.742
460	76.790	0.278	0.897	32.54	1.512	11.623
469	77.179	0.272	0.899	38.12	1.581	11.881
480	78.645	0.252	0.907	38.36	1.584	12.938
490	79.742	0.237	0.912	39.96	1.602	13.828
500	79.251	0.244	0.910	39.78	1.600	13.418
510	76.905	0.276	0.898	42.36	1.627	11.698
520	77.450	0.269	0.900	39.93	1.601	12.066
530	77.480	0.268	0.901	41.87	1.622	12.086
540	77.141	0.273	0.899	43.06	1.634	11.855
550	72.742	0.336	0.875	52.42	1.719	9.375
560	69.284	0.389	0.856	62.47	1.796	7.924
568	70.859	0.365	0.865	56.00	1.748	8.542
580	65.563	0.449	0.834	45.14	1.655	6.688

Table C.1.1 Water content, Dry bulk density (DBD), Porosity and SIRM (mA/m/Kg) data from core CD3813.

1	42.406	0.919	0.660	*****	*****	2.587
11	46.472	0.821	0.696	7.878	0.896	3.050
20	45.985	0.833	0.692	6.561	0.817	2.991
30	44.551	0.866	0.679	8.169	0.912	2.823
40	42.923	0.906	0.665	11.744	1.070	2.642
50	43.179	0.899	0.667	16.545	1.219	2.670
60	48.105	0.784	0.709	14.047	1.148	3.256
70	51.804	0.705	0.739	12.394	1.093	3.776
80	51.391	0.713	0.736	12.743	1.105	3.714
90	51.348	0.714	0.735	13.286	1.123	3.708
100	47.226	0.804	0.702	13.914	1.143	3.144
110	48.557	0.774	0.713	14.417	1.159	3.316
120	50.093	0.741	0.726	13.051	1.116	3.526
130	51.319	0.715	0.735	12.981	1.113	3.703
140	54.545	0.649	0.760	12.664	1.103	4.216
150	52.463	0.691	0.744	13.048	1.116	3.877
160	52.571	0.689	0.745	13.081	1.117	3.894
170	51.064	0.720	0.733	12.276	1.089	3.666
180	51.601	0.709	0.737	12.823	1.108	3.745
190	50.980	0.722	0.733	12.677	1.103	3.654
200	51.372	0.714	0.736	11.916	1.076	3.711
210	47.710	0.793	0.706	12.369	1.092	3.205
219	50.420	0.734	0.728	11.789	1.071	3.573
230	47.781	0.792	0.707	12.573	1.099	3.214
240	47.113	0.807	0.701	12.490	1.097	3.129
250	47.268	0.803	0.702	12.570	1.099	3.149
260	46.663	0.817	0.697	12.485	1.096	3.073
270	46.168	0.828	0.693	12.234	1.088	3.013
280	46.135	0.829	0.693	12.475	1.096	3.009
290	43.392	0.894	0.669	13.673	1.136	2.693
300	48.165	0.783	0.710	9.377	0.972	3.264
310	45.585	0.842	0.688	8.794	0.944	2.943
320	42.632	0.913	0.662	6.638	0.822	2.611
330	45.427	0.846	0.687	6.706	0.826	2.924
340	46.192	0.828	0.693	4.657	0.668	3.016
350	46.493	0.821	0.696	5.616	0.749	3.052
360	45.659	0.840	0.689	5.291	0.724	2.952
370	46.231	0.827	0.694	4.029	0.605	3.020
382	47.486	0.798	0.704	3.944	0.596	3.177
390	44.431	0.869	0.678	4.690	0.671	2.809
400	45.915	0.834	0.691	4.420	0.645	2.982
410	45.633	0.841	0.689	4.411	0.645	2.949
420	42.770	0.910	0.663	5.400	0.732	2.625
430	45.932	0.834	0.691	3.799	0.580	2.984
438	45.951	0.833	0.691	3.834	0.584	2.987
450	45.567	0.842	0.688	4.502	0.653	2.941
460	46.708	0.816	0.698	4.110	0.614	3.079
472	46.867	0.812	0.699	4.120	0.615	3.099
480	47.897	0.789	0.708	3.918	0.593	3.229
490	45.813	0.837	0.690	3.818	0.582	2.970
500	44.706	0.863	0.680	4.051	0.608	2.840
509	43.636	0.888	0.671	4.064	0.609	2.720
520	38.757	1.012	0.625	4.194	0.623	2.223
530	38.805	1.011	0.626	3.618	0.558	2.228
540	36.345	1.078	0.601	3.706	0.569	2.006
550	38.748	1.013	0.625	3.674	0.565	2.222
560	40.142	0.976	0.639	4.147	0.618	2.356
570	43.862	0.883	0.673	5.587	0.747	2.745
580	43.546	0.891	0.670	10.184	1.008	2.710
590	41.705	0.936	0.653	15.959	1.203	2.513
600	36.548	1.073	0.603	9.977	0.999	2.023
610	39.793	0.985	0.635	12.654	1.102	2.322
620	36.714	1.068	0.604	14.284	1.155	2.038
630	37.584	1.044	0.613	16.206	1.210	2.115
640	36.369	1.078	0.601	13.360	1.126	2.008
650	40.920	0.956	0.646	10.939	1.039	2.433
660	41.873	0.932	0.655	20.473	1.311	2.531
670	44.351	0.871	0.677	16.956	1.229	2.800
680	44.385	0.870	0.678	17.228	1.236	2.804
690	38.079	1.031	0.618	17.441	1.242	2.160
700	41.176	0.949	0.648	23.187	1.365	2.459
710	42.010	0.928	0.656	*****	*****	2.545
720	47.581	0.796	0.705	*****	*****	3.189

Table C.1.2 Water content, Dry bulk density (DBD), Porosity and SIRM (mA/m/Kg) data from core CD3814.

Depth(cm)	WC(%)	DBD	Porosity	SIRM	LogSIRM	SALT
1	62.183	0.506	0.812	126.144	2.101	5.776
10	61.169	0.524	0.806	146.189	2.165	5.534
20	60.041	0.545	0.798	116.107	2.065	5.279
30	60.633	0.534	0.802	116.379	2.066	5.411
40	53.460	0.671	0.752	309.978	2.491	4.035
50	62.431	0.502	0.814	119.306	2.077	5.838
60	60.737	0.532	0.803	167.122	2.223	5.434
70	57.390	0.594	0.780	113.754	2.056	4.732
80	50.467	0.733	0.729	543.773	2.735	3.579
90	54.853	0.643	0.762	129.556	2.112	4.268
100	53.638	0.667	0.753	202.554	2.307	4.064
110	53.752	0.665	0.754	118.052	2.072	4.083
120	57.007	0.601	0.777	134.164	2.128	4.658
130	50.648	0.729	0.730	128.433	2.109	3.605
140	54.881	0.642	0.762	272.188	2.435	4.273
150	52.690	0.686	0.746	298.692	2.475	3.912
160	60.027	0.545	0.798	139.261	2.144	5.275
170	60.205	0.542	0.799	193.805	2.287	5.315
180	56.687	0.607	0.775	306.161	2.486	4.598
189	40.821	0.958	0.645	1030.479	3.013	2.423
200	56.932	0.602	0.777	181.471	2.259	4.644
210	56.349	0.614	0.773	255.726	2.408	4.535
220	42.593	0.914	0.662	477.497	2.679	2.606
230	60.621	0.534	0.802	193.426	2.287	5.408
240	58.993	0.564	0.791	223.983	2.350	5.054
250	57.659	0.589	0.782	225.793	2.354	4.784
260	58.368	0.575	0.787	178.289	2.251	4.925
270	61.779	0.514	0.810	91.385	1.961	5.678
280	62.047	0.509	0.812	90.967	1.959	5.743
290	62.929	0.493	0.817	101.348	2.006	5.963
301	59.632	0.552	0.796	295.301	2.470	5.190
310	62.011	0.509	0.811	244.295	2.388	5.734
320	60.489	0.536	0.801	405.995	2.609	5.378
330	61.938	0.511	0.811	180.769	2.257	5.717
340	59.345	0.557	0.794	125.982	2.100	5.128
350	55.578	0.629	0.767	142.050	2.152	4.395
360	56.824	0.604	0.776	113.334	2.054	4.624
370	54.499	0.650	0.759	131.140	2.118	4.208
380	54.818	0.643	0.762	159.768	2.203	4.262
390	52.489	0.691	0.744	178.227	2.251	3.881
401	51.204	0.717	0.734	228.944	2.360	3.686
410	51.519	0.711	0.737	142.237	2.153	3.733
420	50.374	0.735	0.728	110.937	2.045	3.566
430	51.332	0.715	0.735	158.987	2.201	3.705
440	50.849	0.725	0.732	200.062	2.301	3.634
450	52.070	0.699	0.741	312.179	2.494	3.816
460	53.308	0.674	0.750	474.858	2.677	4.011
470	56.204	0.616	0.772	263.731	2.421	4.508
480	56.829	0.604	0.776	200.951	2.303	4.624
490	60.882	0.529	0.804	139.433	2.144	5.467
500	70.147	0.376	0.861	229.541	2.361	8.255
510	30.643	1.248	0.538	769.772	2.886	1.552
520	44.591	0.865	0.679	1035.464	3.015	2.827
530	65.614	0.448	0.834	101.477	2.006	6.703
540	55.882	0.623	0.769	236.893	2.375	4.450
550	65.808	0.445	0.835	142.549	2.154	6.761
560	48.650	0.772	0.714	521.452	2.717	3.328
570	46.090	0.830	0.692	554.161	2.744	3.003
580	58.565	0.572	0.788	99.343	1.997	4.965
589	68.151	0.407	0.849	144.469	2.160	7.517
600	51.828	0.704	0.739	128.701	2.110	3.780

Table C.1.3 Water content, Dry bulk density (DBD), Porosity and SIRM (mA/m/Kg) data from core CD3820.

Depth(cm)	Age(ka)	WC(%)	DBD	Porosity	SIRM	LogSIRM	SALT
1	0.20	55.732	0.626	0.768	*****	*****	4.423
10	2.00	57.239	0.597	0.779	*****	*****	4.702
21	4.20	60.099	0.544	0.799	12.554	1.099	5.291
30	6.00	58.523	0.572	0.788	12.032	1.080	4.957
40	8.00	59.796	0.549	0.797	10.919	1.038	5.225
50	10.67	59.563	0.553	0.795	9.153	0.962	5.175
60	12.47	59.751	0.550	0.796	8.001	0.903	5.215
70	13.41	57.946	0.583	0.784	3.009	0.478	4.841
80	14.34	60.879	0.530	0.804	2.492	0.396	5.467
90	15.28	64.845	0.461	0.829	1.701	0.231	6.480
100	16.22	63.813	0.478	0.823	1.566	0.195	6.195
110	17.16	61.875	0.512	0.810	2.310	0.364	5.701
119	18.00	69.357	0.388	0.856	1.116	0.048	7.951
130	19.08	66.940	0.426	0.842	1.341	0.128	7.113
140	20.07	65.771	0.445	0.835	1.280	0.107	6.750
150	21.05	63.423	0.485	0.820	1.342	0.128	6.091
160	22.03	62.971	0.493	0.818	1.320	0.121	5.974
170	23.02	61.978	0.510	0.811	1.367	0.136	5.726
180	24.00	64.265	0.471	0.826	1.322	0.121	6.318
190	26.92	60.802	0.531	0.803	1.578	0.198	5.449
200	29.83	56.818	0.605	0.776	1.991	0.299	4.622
210	32.75	56.304	0.614	0.772	2.113	0.325	4.527
220	35.67	56.548	0.610	0.774	2.226	0.347	4.572
230	38.58	54.672	0.646	0.761	2.153	0.333	4.237
240	41.50	58.011	0.582	0.784	2.221	0.347	4.853
250	44.42	60.425	0.538	0.801	2.083	0.319	5.364
260	47.33	56.913	0.603	0.777	2.130	0.328	4.640
270	50.25	57.870	0.585	0.783	2.024	0.306	4.825
280	53.17	55.700	0.626	0.768	2.268	0.356	4.417
290	56.08	55.339	0.633	0.765	2.711	0.433	4.353
300	59.00	55.121	0.638	0.764	2.868	0.458	4.315
310	60.67	55.263	0.635	0.765	2.780	0.444	4.340
320	62.33	57.971	0.583	0.784	2.995	0.476	4.846
330	64.00	53.052	0.679	0.749	3.322	0.521	3.970
340	68.67	55.774	0.625	0.769	2.702	0.432	4.430
350	72.29	56.508	0.611	0.774	2.110	0.324	4.564
360	74.86	54.156	0.657	0.757	2.662	0.425	4.150
370	77.43	53.867	0.662	0.755	2.501	0.398	4.102
380	80.00	51.504	0.711	0.737	3.295	0.518	3.731
390	81.67	52.515	0.690	0.744	2.125	0.327	3.885
400	83.33	54.396	0.652	0.759	4.126	0.616	4.190
410	85.00	53.121	0.678	0.749	4.362	0.640	3.981
420	86.67	52.292	0.695	0.743	3.933	0.595	3.851
430	88.33	52.733	0.685	0.746	4.023	0.605	3.919
440	90.00	51.871	0.703	0.740	4.030	0.605	3.786
450	*****	51.709	0.707	0.738	3.145	0.498	3.762
460	*****	51.627	0.708	0.738	3.310	0.520	3.749
470	*****	51.482	0.711	0.736	2.790	0.446	3.728
480	*****	47.575	0.796	0.705	2.180	0.338	3.188
490	*****	44.279	0.873	0.677	1.000	0.000	2.792
500	*****	45.505	0.844	0.687	0.701	-0.155	2.933
510	*****	44.614	0.865	0.680	1.192	0.076	2.830
520	*****	44.616	0.865	0.680	1.366	0.135	2.830
530	*****	44.746	0.862	0.681	1.315	0.119	2.845
540	*****	45.967	0.833	0.691	75.722	1.879	2.989
550	*****	54.066	0.658	0.756	17.160	1.235	4.135
560	*****	52.686	0.686	0.746	1.753	0.244	3.912
570	*****	53.129	0.677	0.749	1.037	0.016	3.982
580	*****	47.298	0.803	0.703	1.251	0.097	3.153
590	*****	49.813	0.747	0.723	0.982	-0.008	3.487
600	*****	47.088	0.807	0.701	1.219	0.086	3.126
610	*****	43.743	0.886	0.672	2.531	0.403	2.732
620	*****	42.114	0.926	0.657	2.690	0.430	2.556

Table C.1.4 Water content, Dry bulk density (DBD), Porosity and SIRM (mA/m/Kg) data from core CD3822.

Depth(cm)	Age(ka)	WC(%)	DBD	Porosity	SIRM	LogSIRM	SALT
1	0.57	71.236	0.359	0.867	*****	*****	8.700
5	2.83	71.435	0.356	0.868	*****	*****	8.785
10	5.67	73.061	0.332	0.877	*****	*****	9.528
15	8.50	69.991	0.378	0.860	*****	*****	8.194
20	11.33	69.103	0.392	0.855	*****	*****	7.857
30	17.00	70.198	0.375	0.861	*****	*****	8.275
40	17.71	65.567	0.449	0.834	*****	*****	6.689
50	18.42	71.029	0.362	0.866	*****	*****	8.613
60	19.14	70.137	0.376	0.861	*****	*****	8.251
70	23.83	60.198	0.542	0.799	*****	*****	5.313
78	27.29	66.914	0.427	0.842	*****	*****	7.105
81	28.59	68.685	0.398	0.853	22.830	1.359	7.705
90	32.49	68.792	0.397	0.845	14.513	1.162	7.744
100	36.82	67.378	0.419	0.866	11.109	1.046	7.256
110	39.00	71.130	0.360	0.840	8.106	0.909	8.655
120	41.83	66.516	0.433	0.854	8.312	0.920	6.979
130	44.67	68.932	0.394	0.845	9.291	0.968	7.794
140	47.50	67.419	0.419	0.870	9.738	0.988	7.269
150	50.33	71.793	0.350	0.819	8.823	0.946	8.941
160	53.16	63.237	0.488	0.827	8.379	0.923	6.043
170	56.00	64.494	0.467	0.842	5.486	0.739	6.381
180	64.00	66.980	0.426	0.858	8.468	0.928	7.126
190	71.25	69.647	0.383	0.860	8.177	0.913	8.061
200	78.49	69.917	0.379	0.862	7.933	0.899	8.165
210	85.74	70.420	0.371	0.874	10.992	1.041	8.363
220	92.98	72.430	0.341	0.871	12.340	1.091	9.229
230	100.23	71.939	0.348	0.852	14.056	1.148	9.006
240	107.48	68.610	0.400	0.873	17.888	1.253	7.678
250	114.72	72.377	0.342	0.851	20.769	1.317	9.205
260	122.00	68.367	0.403	0.830	22.662	1.355	7.592
270	127.00	64.931	0.459	0.824	6.424	0.808	6.504
280	132.00	64.017	0.475	0.824	7.871	0.896	6.250
290	137.00	63.960	0.476	0.834	5.860	0.768	6.235
300	142.00	65.646	0.448	0.839	6.199	0.792	6.713
310	147.00	66.496	0.434	0.831	5.055	0.704	6.972
320	152.00	65.158	0.456	0.833	5.164	0.713	6.570
330	156.00	65.495	0.450	0.839	5.274	0.722	6.668
340	160.00	66.496	0.434	0.864	5.499	0.740	6.972
350	164.00	70.627	0.368	0.855	9.177	0.963	8.447
360	168.00	69.197	0.390	0.853	11.663	1.067	7.892
368	172.00	68.792	0.397	0.843	15.825	1.199	7.744
380	176.00	67.008	0.425	0.849	5.858	0.768	7.135
390	180.00	68.018	0.409	0.845	4.364	0.640	7.471
400	184.00	67.371	0.419	0.848	4.914	0.691	7.253
410	187.28	67.891	0.411	0.858	4.893	0.690	7.428
420	189.86	69.637	0.383	0.860	4.998	0.699	8.057
430	192.43	69.985	0.378	0.865	4.927	0.693	8.191
440	195.00	70.921	0.364	0.862	6.155	0.789	8.568
452	199.15	70.287	0.373	0.863	5.330	0.727	8.310
460	201.92	70.477	0.370	0.862	5.338	0.727	8.386
470	205.38	70.359	0.372	0.857	5.393	0.732	8.339
472	206.07	69.539	0.385	0.856	5.470	0.738	8.020
482	209.53	69.378	0.387	0.847	5.000	0.699	7.959
492	213.00	67.795	0.413	0.849	3.949	0.597	7.395
502	219.00	68.138	0.407	0.850	4.924	0.692	7.513

Table C.1.5 Water content, Dry bulk density (DBD), Porosity and SIRM (mA/m/Kg) data from core CD3826.

Depth(cm)	Age(ka)	WC(%)	DBD	Porosity	SIRM	LogSIRM	SALT
512	224.00	68.242	0.405	0.840	4.633	0.666	7.549
522	229.00	66.569	0.432	0.811	5.672	0.754	6.995
532	234.00	62.032	0.509	0.834	8.876	0.948	5.740
542	240.00	65.616	0.448	0.850	6.782	0.831	6.704
552	242.00	68.311	0.404	0.839	5.716	0.757	7.573
562	244.00	66.472	0.434	0.841	6.312	0.800	6.965
572	246.14	66.814	0.428	0.836	3.736	0.572	7.073
580	247.97	65.956	0.442	0.825	3.600	0.556	6.806
592	250.72	64.214	0.471	0.830	3.659	0.563	6.304
602	253.00	64.929	0.459	0.832	2.647	0.423	6.504
612	257.00	65.211	0.455	0.831	3.059	0.486	6.585
622	265.33	65.180	0.455	0.848	3.094	0.491	6.576
632	273.67	67.944	0.410	0.854	3.614	0.558	7.446
642	282.00	68.932	0.394	0.839	3.079	0.488	7.794
652	285.69	66.380	0.435	0.846	3.724	0.571	6.936
662	289.38	67.576	0.416	0.831	3.585	0.554	7.321
672	293.07	65.057	0.457	0.819	3.819	0.582	6.540
680	296.00	63.177	0.489	0.824	3.893	0.590	6.027
690	300.29	64.057	0.474	0.829	3.839	0.584	6.261
700	304.58	64.727	0.463	0.832	3.358	0.526	6.446
710	308.87	65.326	0.453	0.846	3.700	0.568	6.618
720	313.17	67.513	0.417	0.845	4.095	0.612	7.301
730	317.46	67.432	0.418	0.847	4.753	0.677	7.274
740	321.75	67.764	0.413	0.851	5.807	0.764	7.385
750	326.00	68.386	0.403	0.817	6.904	0.839	7.599
760	327.00	62.966	0.493	0.652	14.070	1.148	5.973
770	328.00	41.548	0.940	0.809	82.400	1.916	2.497
780	332.87	61.592	0.517	0.807	6.381	0.805	5.634
790	337.73	61.308	0.522	0.797	4.540	0.657	5.566
800	342.60	59.778	0.549	0.798	3.582	0.554	5.221
810	347.47	59.945	0.546	0.808	3.621	0.559	5.257
820	352.33	61.442	0.519	0.813	3.822	0.582	5.598
830	357.20	62.267	0.505	0.826	3.122	0.494	5.797
840	362.07	64.322	0.470	0.831	2.841	0.453	6.333
850	366.93	65.062	0.457	0.822	2.441	0.388	6.542
860	371.80	63.740	0.480	0.825	2.620	0.418	6.175
870	376.67	64.215	0.471	0.824	2.752	0.440	6.304
880	381.53	63.974	0.476	0.833	3.192	0.504	6.238
890	386.40	65.468	0.450	0.840	2.871	0.458	6.660
900	391.27	66.667	0.431	0.847	2.777	0.444	7.026
910	396.13	67.688	0.414	0.843	2.957	0.471	7.359
920	401.00	67.159	0.423	0.831	3.213	0.507	7.184
930	408.09	65.142	0.456	0.823	3.372	0.528	6.565
940	415.18	63.899	0.477	0.813	3.546	0.550	6.218
950	422.28	62.321	0.504	0.812	3.273	0.515	5.810
960	429.37	62.110	0.508	0.819	3.163	0.500	5.759
970	436.46	63.191	0.489	0.808	2.596	0.414	6.031
980	443.55	61.474	0.519	0.810	2.822	0.451	5.606
990	450.64	61.752	0.514	0.811	2.809	0.449	5.672
1000	457.74	62.011	0.509	0.803	2.650	0.423	5.734
1010	464.83	60.806	0.531	0.803	2.180	0.339	5.450
1020	472.00	60.687	0.533	0.807	2.018	0.305	5.423
1030	******	61.293	0.522	0.801	2.166	0.336	5.563
1040	******	60.452	0.537	0.813	2.418	0.383	5.370
1050	******	62.333	0.504	0.816	3.930	0.594	5.813
1060	******	62.718	0.497	0.835	3.091	0.490	5.910
1070	******	65.848	0.444	1.597	3.144	0.497	6.773

Table C.1.5 (Contd.) Water content, Dry bulk density (DBD), Porosity and SIRM (mA/m/Kg) data from core CD3826.

Depth(cm)	Age(ka)	WC(%)	DBD	Porosity	SIRM	LogSIRM	SALT
1	0.15	72.285	0.343	0.873	*****	*****	9.163
10	1.55	69.490	0.386	0.857	*****	*****	8.001
20	3.10	66.667	0.431	0.840	*****	*****	7.026
21	3.25	65.997	0.442	0.836	55.350	1.743	6.818
30	4.64	65.393	0.452	0.833	55.082	1.741	6.638
40	6.19	65.864	0.444	0.836	51.856	1.715	6.778
50	8.13	67.435	0.418	0.845	38.707	1.588	7.275
60	10.06	64.732	0.463	0.829	24.167	1.383	6.448
70	12.00	68.192	0.406	0.850	9.310	0.969	7.531
80	12.69	65.668	0.447	0.834	5.325	0.726	6.720
90	13.38	65.618	0.448	0.834	3.820	0.582	6.705
100	14.07	64.428	0.468	0.827	3.249	0.512	6.363
110	14.75	63.755	0.479	0.822	3.053	0.485	6.179
120	15.44	62.181	0.506	0.812	3.181	0.503	5.776
130	16.13	63.492	0.484	0.821	2.942	0.469	6.110
140	16.82	62.880	0.494	0.817	2.810	0.449	5.951
150	17.71	63.369	0.486	0.820	2.840	0.453	6.077
160	18.59	64.152	0.473	0.825	2.848	0.455	6.287
170	19.48	64.217	0.471	0.825	3.055	0.485	6.305
180	20.23	64.526	0.466	0.827	3.083	0.489	6.390
190	20.99	64.451	0.467	0.827	3.204	0.506	6.369
200	21.74	61.603	0.517	0.809	3.371	0.528	5.636
210	22.49	65.390	0.452	0.833	2.961	0.471	6.637
220	23.25	63.249	0.488	0.819	3.230	0.509	6.046
230	24.00	62.741	0.497	0.816	3.174	0.502	5.916
240	28.38	64.125	0.473	0.825	2.830	0.452	6.279
250	32.75	61.843	0.512	0.810	4.185	0.622	5.694
260	37.13	61.538	0.518	0.808	3.751	0.574	5.621
270	41.50	60.649	0.534	0.802	2.920	0.465	5.414
280	45.88	61.404	0.520	0.807	3.194	0.504	5.589
290	50.25	58.913	0.565	0.791	3.371	0.528	5.037
300	54.63	58.583	0.571	0.788	6.181	0.791	4.969
310	59.00	59.638	0.552	0.796	3.054	0.485	5.191
319	*****	61.290	0.522	0.807	3.279	0.516	5.562

Table C.1.6 Water content, Dry bulk density (DBD), Porosity and SIRM (mA/m/Kg) data from core CD3827.

Depth(cm)	Age(ka)	WC(%)	DBD	Porosity	SIRM	LogSIRM	SALT
9	2.49	48.991	0.765	0.717	11.333	1.054	3.374
11	3.04	50.356	0.735	0.728	13.013	1.114	3.563
13	3.59	51.391	0.713	0.736	14.247	1.154	3.714
15	4.14	51.501	0.711	0.737	10.433	1.018	3.730
17	4.70	51.312	0.715	0.735	11.259	1.051	3.702
19	5.25	50.847	0.725	0.732	8.305	0.919	3.634
21	5.80	52.032	0.700	0.741	9.893	0.995	3.811
23	6.35	53.702	0.666	0.753	7.757	0.890	4.075
25	6.91	53.984	0.660	0.756	8.975	0.953	4.121
27	7.46	54.951	0.641	0.763	8.361	0.922	4.285
29	8.01	55.600	0.628	0.767	7.265	0.861	4.399
31	8.56	55.620	0.628	0.768	8.640	0.937	4.403
33	9.12	55.522	0.630	0.767	7.312	0.864	4.385
35	9.67	56.534	0.610	0.774	6.540	0.816	4.569
37	10.22	56.865	0.604	0.776	8.039	0.905	4.631
39	10.77	56.106	0.618	0.771	5.829	0.766	4.490
41	11.33	56.854	0.604	0.776	5.651	0.752	4.629
43	11.89	56.391	0.613	0.773	5.926	0.773	4.543
45	12.01	56.029	0.620	0.770	6.714	0.827	4.476
47	12.13	55.980	0.621	0.770	8.913	0.950	4.467
49	12.25	55.989	0.621	0.770	5.573	0.746	4.469
51	12.37	55.432	0.631	0.766	5.481	0.739	4.369
53	12.49	53.778	0.664	0.754	4.623	0.665	4.087
55	12.61	54.928	0.641	0.762	4.222	0.626	4.281
57	12.73	53.537	0.669	0.752	4.518	0.655	4.048
59	12.90	54.091	0.658	0.756	2.387	0.378	4.139
61	13.08	54.279	0.654	0.758	2.475	0.394	4.170
63	13.25	54.363	0.653	0.758	2.682	0.428	4.185
65	13.42	53.780	0.664	0.754	3.348	0.525	4.088
67	13.60	51.194	0.717	0.734	3.471	0.540	3.685
69	13.77	52.249	0.695	0.742	6.161	0.790	3.844
71	13.94	52.546	0.689	0.745	5.852	0.767	3.890
73	14.12	52.223	0.696	0.742	1.204	0.081	3.840
75	14.29	53.223	0.675	0.750	2.769	0.442	3.997
77	14.46	51.295	0.715	0.735	2.043	0.310	3.700
79	14.63	52.731	0.686	0.746	1.733	0.239	3.919
81	14.81	52.694	0.686	0.746	1.550	0.190	3.913
83	14.98	52.320	0.694	0.743	1.766	0.247	3.855
85	15.15	51.958	0.702	0.740	1.292	0.111	3.799
87	15.33	50.325	0.736	0.727	1.480	0.170	3.559
89	15.50	51.320	0.715	0.735	1.532	0.185	3.704
91	16.03	54.738	0.645	0.761	1.046	0.020	4.248
93	16.56	53.251	0.675	0.750	1.117	0.048	4.002
95	17.09	52.828	0.684	0.747	1.504	0.177	3.934
97	17.63	55.901	0.622	0.770	1.809	0.257	4.453
99	18.16	53.413	0.672	0.751	1.726	0.237	4.028
101	18.69	54.137	0.657	0.757	1.336	0.126	4.147
103	19.22	54.286	0.654	0.758	1.461	0.165	4.172
105	19.75	52.107	0.698	0.741	1.450	0.161	3.822
107	20.28	52.686	0.686	0.746	1.924	0.284	3.912
109	20.81	53.437	0.671	0.751	1.429	0.155	4.032
111	21.34	53.157	0.677	0.749	1.899	0.279	3.987
113	21.88	53.629	0.667	0.753	2.644	0.422	4.063
115	22.41	51.252	0.716	0.735	2.564	0.409	3.693
117	22.94	51.493	0.711	0.737	2.742	0.438	3.729
119	23.47	52.719	0.686	0.746	3.431	0.535	3.917
121	24.00	52.437	0.692	0.744	3.501	0.544	3.873
123	*****	51.086	0.720	0.733	5.925	0.773	3.669
125	*****	48.746	0.770	0.715	6.352	0.803	3.341

Table C.1.7 Water content, Dry bulk density (DBD), Porosity and SIRM (mA/m/Kg) data from core P5.

Depth(cm)	WC(%)	DBD	Porosity	SIRM	LogSIRM	SALT
11	60.086	0.544	0.799	66.966	1.826	5.288
13	59.897	0.547	0.797	103.232	2.014	5.247
25	57.442	0.593	0.780	78.961	1.897	4.742
27	57.420	0.593	0.780	71.886	1.857	4.737
29	58.218	0.578	0.786	65.567	1.817	4.895
31	59.371	0.557	0.794	85.544	1.932	5.134
33	59.896	0.547	0.797	71.218	1.853	5.247
35	60.135	0.543	0.799	76.760	1.885	5.299
37	59.692	0.551	0.796	74.765	1.874	5.202
39	58.652	0.570	0.789	65.080	1.813	4.983
41	59.301	0.558	0.793	64.235	1.808	5.119
43	59.602	0.553	0.795	78.865	1.897	5.183
45	59.326	0.558	0.793	59.261	1.773	5.124
47	59.841	0.548	0.797	64.129	1.807	5.235
49	59.980	0.546	0.798	67.147	1.827	5.265
51	60.079	0.544	0.799	60.154	1.779	5.287
53	60.439	0.537	0.801	60.315	1.780	5.367
55	60.524	0.536	0.802	74.872	1.874	5.386
57	60.673	0.533	0.803	57.282	1.758	5.420
59	61.398	0.520	0.807	60.217	1.780	5.587
61	62.727	0.497	0.816	46.929	1.671	5.912
63	61.901	0.511	0.811	51.140	1.709	5.708
65	61.780	0.514	0.810	41.936	1.623	5.678
67	62.113	0.508	0.812	50.920	1.707	5.759
69	62.359	0.503	0.814	56.582	1.753	5.820
71	61.582	0.517	0.809	51.620	1.713	5.631
73	61.219	0.523	0.806	59.020	1.771	5.546
75	60.486	0.537	0.801	48.102	1.682	5.377
77	61.785	0.513	0.810	48.147	1.683	5.680
81	53.387	0.672	0.751	51.395	1.711	4.024
83	51.956	0.702	0.740	51.957	1.716	3.799
85	51.447	0.712	0.736	52.768	1.722	3.722
87	50.438	0.734	0.728	48.086	1.682	3.575
89	50.940	0.723	0.732	40.445	1.607	3.648
91	51.468	0.712	0.736	46.883	1.671	3.726
93	51.131	0.719	0.734	41.149	1.614	3.676
95	51.394	0.713	0.736	41.549	1.619	3.714
97	51.579	0.709	0.737	43.427	1.638	3.742
99	51.089	0.720	0.733	41.229	1.615	3.669
101	51.163	0.718	0.734	33.142	1.520	3.680
103	50.681	0.728	0.730	21.500	1.332	3.610
105	50.265	0.737	0.727	21.688	1.336	3.550
107	50.662	0.729	0.730	25.839	1.412	3.607
109	48.412	0.778	0.712	25.269	1.403	3.297
111	44.823	0.860	0.682	42.480	1.628	2.854
113	44.437	0.869	0.678	23.194	1.365	2.809
115	45.970	0.833	0.691	15.883	1.201	2.989
117	45.934	0.834	0.691	18.136	1.259	2.985
119	48.045	0.786	0.709	14.560	1.163	3.249
121	46.519	0.820	0.696	16.177	1.209	3.056
123	48.595	0.774	0.713	12.611	1.101	3.321
125	49.192	0.760	0.718	9.239	0.966	3.401
127	49.540	0.753	0.721	11.172	1.048	3.449
129	50.432	0.734	0.728	10.293	1.013	3.574
131	49.585	0.752	0.722	12.440	1.095	3.455
133	51.386	0.713	0.736	7.336	0.865	3.713
135	50.762	0.727	0.731	6.282	0.798	3.622
137	51.747	0.706	0.739	6.030	0.780	3.767
139	51.663	0.708	0.738	5.492	0.740	3.755
141	51.240	0.717	0.735	6.909	0.839	3.692
143	51.193	0.718	0.734	7.518	0.876	3.685
145	51.156	0.718	0.734	7.930	0.899	3.679
147	52.313	0.694	0.743	5.788	0.763	3.854
149	52.404	0.692	0.744	6.247	0.796	3.868
151	51.289	0.716	0.735	6.821	0.834	3.699

Table C.1.8 Water content, Dry bulk density (DBD), Porosity and SIRM (mA/m/Kg) data from core P12.

Depth(cm)	Age(ka)	Age Pick	LSR (cm/kyr)	BAR (g/cm2/kyr)	DBD (g/cm2)	$\delta^{18}O_{PDB}$	$\delta^{13}C_{PDB}$
1	0.20		5.00	3.13	0.626	-1.022	1.279
10	2.00		5.00	2.98	0.597	-1.105	1.159
20	4.00		5.00	2.99	0.599	-0.981	1.479
21	4.20		5.00	2.72	0.544	-2.319	1.666
30	6.00		5.00	2.86	0.572	-2.972	1.629
40	8.00	8.0		0.00	0.549	-2.283	2.002
50	10.67		3.75	2.07	0.553	-1.626	1.671
55	12.00	12.0					
60	12.47		10.67	5.87	0.550	-1.506	1.330
70	13.41		10.67	6.22	0.583	-1.021	1.166
80	14.34		10.67	5.65	0.530	-0.854	1.381
90	15.28		10.67	4.92	0.461	-0.846	1.461
100	16.22		10.67	5.10	0.478	-0.669	1.485
110	17.16		10.67	5.46	0.512	-0.870	1.352
119	18.00	18.0			0.388	-0.434	1.891
130	19.08		10.17	4.33	0.426	-1.115	1.549
140	20.07		10.17	4.53	0.445	-0.962	1.666
150	21.05		10.17	4.93	0.485	-1.333	1.397
160	22.03		10.17	5.01	0.493	-0.858	1.479
170	23.02		10.17	5.19	0.510	-0.979	1.660
180	24.00	24.0			0.471	-1.081	1.607
190	26.92		3.43	1.82	0.531	-1.011	1.754
200	29.83		3.43	2.07	0.605	-1.048	1.841
210	32.75		3.43	2.11	0.614	-1.183	1.584
220	35.67		3.43	2.09	0.610	-1.537	1.634
230	38.58		3.43	2.22	0.646	-1.629	1.449
240	41.50		3.43	2.00	0.582	-1.276	1.592
250	44.42		3.43	1.84	0.538	-1.127	1.475
260	47.33		3.43	2.07	0.603	-1.154	1.600
270	50.25		3.43	2.00	0.585	-1.388	1.575
280	53.17		3.43	2.15	0.626	-1.392	1.445
290	56.08		3.43	2.17	0.633	-1.038	1.581
300	59.00	59.0			0.638	-1.166	1.371
310	60.67		6.00	3.81	0.635	-1.048	1.430
320	62.33		6.00	3.50	0.583	-0.865	1.583
330	64.00	64.0			0.679	-0.777	1.453
340	68.67		2.14	1.34	0.625	-1.307	1.506
345	71.00	71.0					
350	72.29		3.89	2.37	0.611	-1.421	1.583
360	74.86		3.89	2.55	0.657	-1.542	1.870
370	77.43		3.89	2.58	0.662	-1.563	1.900
380	80.00	80.0			0.711	-1.766	1.867
390	81.67		6.00	4.14	0.690	-1.558	1.761
400	83.33		6.00	3.91	0.652	-1.062	1.700
410	85.00		6.00	4.07	0.678	-0.967	1.702
420	86.67		6.00	4.17	0.695	-1.239	1.743
430	88.33		6.00	4.11	0.685	-0.808	0.425
440	90.00	90.0			0.703	-0.579	1.060
450	*****	*****	*****	*****	0.707	-1.649	1.726
460	*****	*****	*****	*****	0.708	-1.575	1.610
470	*****	*****	*****	*****	0.711	-1.096	0.569
480	*****	*****	*****	*****	0.796	-0.793	1.087
490	*****	*****	*****	*****	0.873	-1.395	1.717
500	*****	*****	*****	*****	0.844	*****	*****
510	*****	*****	*****	*****	0.865	*****	*****
520	*****	*****	*****	*****	0.865	*****	*****
530	*****	*****	*****	*****	0.862	*****	*****
540	*****	*****	*****	*****	0.833	*****	*****
550	*****	*****	*****	*****	0.658	*****	*****
560	*****	*****	*****	*****	0.686	*****	*****
570	*****	*****	*****	*****	0.677	*****	*****
580	*****	*****	*****	*****	0.803	*****	*****
590	*****	*****	*****	*****	0.747	*****	*****
600	*****	*****	*****	*****	0.807	*****	*****
610	*****	*****	*****	*****	0.886	*****	*****
620	*****	*****	*****	*****	0.926	*****	*****

Table C.2.1 Stable Isotope, Sedimentation Rate (LSR) and Bulk Accumulation Rate (BAR) data from core CD3822.

Depth(cm)	Age(ka)	Age Picks (kyr)	LSR (cm/kyr)	BAR (g/cm2/kyr)	DBD (g/cm2)	$\delta^{18}O_{PDB}$	$\delta^{13}C_{PDB}$
1	0.57	0.6	1.76	0.634	0.359	0.026	1.353
5	2.83		1.76	0.628	0.356	0.029	1.433
10	5.67		1.76	0.586	0.332	0.038	1.383
15	8.50		1.76	0.669	0.379	0.238	1.428
20	11.33		1.76	0.692	0.392	0.277	1.348
30	17.00	17.0			0.375	0.655	1.030
40	17.71		14.00	6.300	0.450	0.788	1.071
50	18.42		14.00	5.082	0.363	1.248	1.218
60	19.14		14.00	5.264	0.376	1.354	1.243
	19.50	19.5					
70	23.83		2.31	1.254	0.543	1.824	1.027
78	27.29		2.31	0.986	0.427	1.174	1.460
81	28.59		2.31	0.922	0.399	1.110	1.448
90	32.49		2.31	0.917	0.397	0.883	1.433
100	36.82		2.31	0.970	0.420	0.800	1.492
110	39.00	39.0			0.361	0.622	1.434
120	41.83		3.53	1.532	0.434	0.707	1.417
130	44.67		3.53	1.394	0.395	0.533	1.242
140	47.50		3.53	1.479	0.419	0.923	1.326
150	50.33		3.53	1.239	0.351	0.791	1.477
160	53.16		3.53	1.726	0.489	0.549	1.365
170	56.00	56.0			0.467	0.783	1.339
	62.25		0.80				
180	64.00	64.0			0.426	0.421	1.460
190	71.25		1.38	0.530	0.384	0.701	1.199
200	78.49		1.38	0.524	0.380	0.643	1.367
210	85.74		1.38	0.513	0.372	0.371	1.401
220	92.98		1.38	0.471	0.341	0.668	1.302
230	100.23		1.38	0.482	0.349	0.391	1.468
240	107.48		1.38	0.552	0.400	0.673	1.311
250	114.72		1.38	0.472	0.342	0.137	1.262
260	122.00	122.0			0.404	-0.205	1.151
270	127.00		2.00	0.920	0.460	0.978	1.219
280	132.00		2.00	0.952	0.476	0.716	1.182
290	137.00		2.00	0.954	0.477	1.050	1.271
300	142.00		2.00	0.896	0.448	1.242	1.157
310	147.00		2.00	0.868	0.434	1.166	1.259
320	152.00	152.0			0.456	1.397	1.031
330	156.00		2.50	1.128	0.451	1.077	1.116
340	160.00		2.50	1.085	0.434	1.297	1.213
350	164.00		2.50	0.923	0.369	1.019	1.145
360	168.00		2.50	0.978	0.391	0.615	1.006
368	172.00		2.50	0.993	0.397	0.243	0.976
380	176.00		2.50	1.065	0.426	0.819	1.113
390	180.00		2.50	1.025	0.410	0.853	1.193
400	184.00		2.50	1.050	0.420	0.628	1.257
	186.00	186.0					
410	187.28		3.89	1.603	0.412	0.689	1.163
420	189.86		3.89	1.494	0.384	0.621	1.058
430	192.43		3.89	1.474	0.379	0.319	1.283
440	195.00	195.0			0.364	0.088	1.566
452	199.15		2.89	1.081	0.374	-0.077	1.498
460	201.92		2.89	1.072	0.371	-0.073	1.500
470	205.38		2.89	1.078	0.373	-0.108	1.503
472	206.07		2.89	1.116	0.386	-0.115	1.665
482	209.53		2.89	1.121	0.388	-0.084	1.505
492	213.00	213.0			0.413	-0.190	1.306
	215.99		1.67				
502	219.00	219.0			0.408	-0.007	1.039

Table C.2.2 Stable Isotope, Sedimentation Rate (LSR) and Bulk Accumulation Rate (BAR) data from core CD3826.

Depth(cm)	Age(ka)	Age Picks (kyr)	LSR (cm/kyr)	BAR (g/cm2/kyr)	DBD (g/cm2)	$\delta^{18}O_{PDB}$	$\delta^{13}C_{PDB}$
512	224.00		2.00	0.812	0.406	0.582	1.044
522	229.00		2.00	0.866	0.433	0.309	1.170
532	234.00	234.0			0.510	0.474	1.529
	235.00		1.00				
542	240.00	240.0			0.449	0.785	1.011
552	242.00		5.00	2.025	0.405	0.799	1.477
562	244.00		5.00	2.175	0.435	0.381	1.281
	245.00	245.0					
572	246.14		4.37	1.875	0.429	0.156	1.270
580	247.97		4.37	1.936	0.443	0.096	1.260
592	250.72		4.37	2.063	0.472	0.484	1.410
602	253.00	253.0			0.460	0.543	1.340
	255.50		2.00				
612	257.00	257.0			0.455	0.289	1.310
622	265.33		1.20	0.547	0.456	0.664	0.983
632	273.67		1.20	0.493	0.411	0.643	1.190
642	282.00	282.0			0.395	0.740	1.200
652	285.69		2.71	1.182	0.436	-0.134	0.926
662	289.38		2.71	1.130	0.417	0.295	1.186
672	293.07		2.71	1.241	0.458	-0.090	1.470
680	296.00	296.0			0.490	0.074	1.546
690	300.29		2.33	1.107	0.475	0.107	1.472
700	304.58		2.33	1.081	0.464	0.146	1.462
710	308.87		2.33	1.058	0.454	0.185	1.553
720	313.17		2.33	0.974	0.418	-0.005	1.510
730	317.46		2.33	0.976	0.419	0.190	1.271
740	321.75		2.33	0.965	0.414	*****	*****
750	326.00	326.0			0.404	*****	*****
760	327.00		10.00	4.940	0.494	*****	*****
770	328.00	328.0			0.941	0.562	0.952
780	332.87		2.05	1.064	0.518	*****	*****
790	337.73		2.05	1.075	0.523	-0.177	0.814
800	342.60		2.05	1.130	0.550	0.689	1.182
810	347.47		2.05	1.124	0.547	0.512	1.022
820	352.33		2.05	1.068	0.520	0.550	1.218
830	357.20		2.05	1.040	0.506	0.591	1.161
840	362.07		2.05	0.966	0.470	0.735	1.268
850	366.93		2.05	0.941	0.458	0.832	1.380
860	371.80		2.05	0.986	0.480	0.821	1.440
870	376.67		2.05	0.970	0.472	0.683	1.160
880	381.53		2.05	0.978	0.476	0.310	1.478
890	386.40		2.05	0.927	0.451	0.624	1.557
900	391.27		2.05	0.886	0.431	-0.545	1.379
910	396.13		2.05	0.853	0.415	-0.372	1.596
920	401.00	401.0			0.423	0.144	1.294
930	408.09		1.41	0.644	0.457	-0.548	1.628
940	415.18		1.41	0.674	0.478	-0.637	1.717
950	422.28		1.41	0.712	0.505	-0.360	1.468
960	429.37		1.41	0.718	0.509	-0.187	0.767
970	436.46		1.41	0.691	0.490	0.959	0.806
980	443.55		1.41	0.733	0.520	0.589	0.991
990	450.64		1.41	0.726	0.515	1.081	1.141
1000	457.74		1.41	0.719	0.510	1.016	1.434
1010	464.83		1.41	0.750	0.532	0.577	1.408
1020	472.00	472.0			0.534	0.436	1.308
1030	*****	*****	*****	*****	0.523	1.078	0.629
1040	*****	*****	*****	*****	0.538	0.345	1.686
1050	*****	*****	*****	*****	0.505	*****	*****
1060	*****	*****	*****	*****	0.498	0.237	1.630
1070	*****	*****	*****	*****	0.445	-0.056	1.695

Table C.2.2 (contd.) Stable Isotope, Sedimentation Rate (LSR) and Bulk Accumulation Rate (BAR) data from core CD3826.

Depth(cm)	Age(ka)	Age Pick (kyr)	LSR (cm/kyr)	BAR (g/cm2/kyr)	DBD (g/cm2)	$\delta^{18}O_{PDB}$	$\delta^{13}C_{PDB}$
1	0.15		6.462	2.216	0.343	*****	*****
10	1.55		6.462	2.494	0.386	-0.234	1.255
20	3.10		6.462	2.785	0.431	-0.167	1.406
21	3.25		6.462	2.856	0.442	0.258	1.185
30	4.64		6.462	2.921	0.452	0.328	1.160
40	6.19	6.19			0.444	0.470	1.186
50	8.13		5.164	2.158	0.418	0.533	0.984
60	10.06		5.164	2.391	0.463	0.419	1.063
70	12.00	12.00			0.406	0.769	0.887
80	12.69		14.523	6.492	0.447	0.847	0.942
90	13.38		14.523	6.506	0.448	0.944	0.861
100	14.07		14.523	6.797	0.468	0.994	0.865
110	14.75		14.523	6.956	0.479	1.214	0.903
120	15.44		14.523	7.349	0.506	1.479	1.122
130	16.13		14.523	7.029	0.484	1.723	1.172
140	16.82	16.82			0.494	1.616	1.116
150	17.71		11.278	5.481	0.486	1.399	1.313
160	18.59		11.278	5.335	0.473	1.667	1.120
170	19.48	19.48			0.471	1.761	1.243
180	20.23		13.274	6.186	0.466	*****	*****
190	20.99		13.274	6.199	0.467	1.693	1.249
200	21.74		13.274	6.863	0.517	1.375	1.573
210	22.49		13.274	6.000	0.452	1.077	1.391
220	23.25		13.274	6.478	0.488	1.090	1.225
230	24.00	24.00			0.497	0.907	1.347
240	28.38		2.286	1.081	0.473	0.912	1.129
250	32.75		2.286	1.170	0.512	*****	*****
260	37.13		2.286	1.184	0.518	1.178	0.992
270	41.50		2.286	1.221	0.534	1.083	1.000
280	45.88		2.286	1.189	0.520	0.734	1.180
290	50.25		2.286	1.291	0.565	0.974	1.136
300	54.63		2.286	1.305	0.571	0.161	0.738
310	59.00	59.00			0.552	1.455	0.818
319	*****	*****	*****	*****	0.522	1.010	0.675

Table C.2.3 Stable Isotope, Sedimentation Rate (LSR) and Bulk Accumulation Rate (BAR) data from core CD3827.

Depth(cm)	Age(ka)	Age Picks (ka)	LSR (cm/kyr)	BAR (g/cm2/kyr)	DBD (g/cm2)
9	2.49		3.620	2.769	0.765
11	3.04		3.620	2.661	0.735
13	3.59		3.620	2.581	0.713
15	4.14		3.620	2.574	0.711
17	4.70		3.620	2.588	0.715
19	5.25		3.620	2.625	0.725
21	5.80		3.620	2.534	0.700
23	6.35		3.620	2.411	0.666
25	6.91		3.620	2.389	0.660
27	7.46		3.620	2.320	0.641
29	8.01		3.620	2.273	0.628
31	8.56		3.620	2.273	0.628
33	9.12		3.620	2.281	0.630
35	9.67		3.620	2.208	0.610
37	10.22		3.620	2.186	0.604
39	10.77		3.620	2.237	0.618
41	11.33		3.620	2.186	0.604
43	11.89	11.89			0.613
45	12.01		16.670	10.335	0.620
47	12.13		16.670	10.352	0.621
49	12.25		16.670	10.352	0.621
51	12.37		16.670	10.519	0.631
53	12.49		16.670	11.069	0.664
55	12.61		16.670	10.685	0.641
57	12.73	12.73			0.669
59	12.90		11.552	7.601	0.658
61	13.08		11.552	7.555	0.654
63	13.25		11.552	7.544	0.653
65	13.42		11.552	7.671	0.664
67	13.60		11.552	8.283	0.717
69	13.77		11.552	8.029	0.695
71	13.94		11.552	7.960	0.689
73	14.12		11.552	8.040	0.696
75	14.29		11.552	7.798	0.675
77	14.46		11.552	8.260	0.715
79	14.63		11.552	7.925	0.686
81	14.81		11.552	7.925	0.686
83	14.98		11.552	8.017	0.694
85	15.15		11.552	8.110	0.702
87	15.33		11.552	8.503	0.736
89	15.50	15.50			0.715
91	16.03		3.765	2.428	0.645
93	16.56		3.765	2.541	0.675
95	17.09		3.765	2.575	0.684
97	17.63		3.765	2.342	0.622
99	18.16		3.765	2.530	0.672
101	18.69		3.765	2.473	0.657
103	19.22		3.765	2.462	0.654
105	19.75		3.765	2.628	0.698
107	20.28		3.765	2.583	0.686
109	20.81		3.765	2.526	0.671
111	21.34		3.765	2.549	0.677
113	21.88		3.765	2.511	0.667
115	22.41		3.765	2.696	0.716
117	22.94		3.765	2.677	0.711
119	23.47		3.765	2.583	0.686
121	24.00	24.00			0.692
123	*****	*****	*****	*****	0.720

Table C.2.4 Stable Isotope, Sedimentation Rate (LSR) and Bulk Accumulation Rate (BAR) data from core P5.

Depth(cm)	Age(ka)	Del18OPDB N.dutertrei	Del13CPDB N.dutertrei	SPECMAP Age(ka)	SP. Units	SPECMAP Age(ka)	SP. Units
2.75	9.14	0.15	1.38	0	-2.09	180	0.71
7.00	10.58	0.25	1.26	2	-1.91	182	0.83
12.00	12.28	0.59	1.33	4	-1.74	184	0.62
18.75	14.58	0.44	1.12	6	-1.41	186	0.11
24.00	16.36			8	-1.02	188	-0.42
25.50	16.59	0.71	1.32	10	-0.44	190	-0.88
33.75	17.85	0.60	1.11	12	0.29	192	-1.31
37.75	18.46	0.95	1.40	14	1.01	194	-1.62
41.50	19.03	1.00	1.47	16	1.58	196	-1.62
44.50	19.49	1.27	1.62	18	1.81	198	-1.41
49.75	20.29	0.95	1.40	20	1.78	200	-1.17
53.50	20.86	1.04	1.47	22	1.65	202	-0.99
58.50	21.62	0.56	1.53	24	1.38	204	-0.88
64.50	22.54	0.64	1.75	26	1.14	206	-0.88
70.50	23.46	0.72	1.52	28	1.02	208	-1.00
73.50	23.91	0.97	1.71	30	0.96	210	-1.12
78.00	24.60			32	0.94	212	-1.23
79.50	25.05	0.60	1.55	34	0.94	214	-1.35
85.50	26.83	0.34	1.60	36	0.96	216	-1.40
88.50	27.72	0.56	1.71	38	0.94	218	-1.27
94.50	29.50	0.67	1.63	40	0.85	220	-0.01
100.50	31.28	0.65	1.47	42	0.77	222	-0.64
105.50	32.76	0.45	1.49	44	0.67	224	-0.31
109.50	33.95	0.50	1.38	46	0.59	226	-0.03
114.50	35.43	0.46	1.57	48	0.56	228	0.12
120.50	37.21	0.49	1.46	50	0.50	230	-0.02
126.50	38.99	0.48	1.56	52	0.38	232	-0.31
134.00	41.22	0.46	1.41	54	0.37	234	-0.68
139.50	42.85	0.69	1.41	56	0.41	236	-1.02
145.50	44.63	0.32	1.33	58	0.50	238	-1.18
151.50	46.41	0.28	1.55	60	0.68	240	-1.03
154.50	47.31	0.73	1.47	62	0.89	242	-0.65
159.50	48.79	0.40	1.57	64	1.00	244	-0.20
165.50	50.57	0.20	1.53	66	0.93	246	0.30
170.00	51.91	0.36	1.49	68	0.66	248	0.70
176.50	53.83	0.29	1.35	70	0.22	250	0.78
186.50	56.80	0.47	1.56	72	-0.24	252	0.66
190.50	57.99	0.38	1.58	74	-0.53	254	0.52
197.50	60.07	0.11	1.50	76	-0.69	256	0.40
205.50	62.44	0.37	1.58	78	-0.88	258	0.37
210.75	64.00	0.57	1.51	80	-0.98	260	0.43
215.50	67.95	0.43	1.66	82	-0.77	262	0.50
220.50	72.11	0.49	1.58	84	-0.48	264	0.55
226.25	76.89	0.30	1.50	86	-0.45	266	0.67
230.50	80.42	0.04	1.54	88	-0.47	268	0.85
235.75	84.79	0.30	1.57	90	-0.46	270	0.89
240.50	88.74	0.23	1.55	92	-0.52	272	0.77
245.50	92.90	0.26	1.68	94	-0.71	274	0.60
250.50	97.05	0.30	1.55	96	-0.80	276	0.42
260.50	105.37	-0.09	1.41	98	-0.91	278	0.21
265.50	109.53	0.24	1.38	100	-0.96	280	-0.01
271.50	114.52	-0.31	1.18	102	-0.80	282	-0.19
275.50	117.84	-0.09	1.21	104	-0.69	284	-0.35
280.50	122.00	-0.25	1.06	106	-0.59	286	-0.47
285.50	124.14	-0.34	0.96	108	-0.51	288	-0.46
291.50	126.71	0.41	0.94	110	-0.50	290	-0.31
295.50	128.43	0.42	1.36	112	-0.73	292	-0.15
298.50	129.71	0.31	1.08	114	-1.19	294	-0.05
305.50	132.71	0.36	1.25	116	-1.53	296	0.02
309.50	134.43	0.62	1.15	118	-1.72	298	0.05
314.50	136.57	0.89	1.40	120	-1.98	300	-0.05
319.50	138.71	0.57	1.28	122	-2.12	302	-0.30
325.50	141.29	0.60	1.18	124	-1.89	304	-0.61
330.50	143.43	0.71	1.23	126	-1.19	306	-0.93
335.50	145.57	0.83	1.18	128	-0.26	308	-1.20
340.50	147.71	0.74	1.23	130	0.51	310	-1.34
345.50	149.86	0.62	1.42	132	1.05	312	-1.31
350.50	152.00	0.88	1.34	134	1.33	314	-1.19
355.50	154.94	0.64	1.35	136	1.35	316	-1.06
360.50	157.89	0.43	1.37	138	1.28	318	-0.95
365.50	160.83	0.38	1.26	140	1.32	320	-0.91
371.50	164.37	0.41	1.29	142	1.33	322	-1.03
375.50	166.72	0.51	1.28	144	1.26	324	-1.23
380.50	169.67	0.32	1.32	146	1.26	326	-1.45
385.50	172.61	0.39	1.23	148	1.41	328	-1.65
390.50	175.56	0.22	1.39	150	1.57	330	-1.79
395.50	178.50	0.28	1.27	152	1.58	332	-1.72
400.50	181.44	0.29	1.42	154	1.45	334	-1.40
405.50	184.39	-0.07	1.48	156	1.30	336	-0.84
410.50	187.33	-0.10	1.48	158	1.07	338	-0.04
415.50	190.28	-0.16	1.64	160	0.85	340	0.75
420.50	193.22	-0.37	1.53	162	0.60	342	1.12
425.50	196.17	-0.33	1.46	164	0.40	344	1.07
430.50	199.11	-0.38	1.48	166	0.25	346	0.94
435.50	202.06	-0.39	1.44	168	0.15	348	0.86
440.50	205.00	-0.21	1.57	170	0.11	350	0.86
450.50	211.39	-0.56	1.62	172	0.12	352	0.88
455.50	214.58	-0.26	1.58	174	0.18	354	0.86
460.50	217.78	-0.08	1.28	176	0.27	356	0.74
465.50	220.97	-0.26	1.48	178	0.47	358	0.53

Table C.3.1 Stable Isotope data from core AII54-25PC (Pedersen, pers comm., 1991), and the SPECMAP Stack (0-500 ka; Imbrie et al., 1984).

Depth(cm)	Age(ka)	Del18OPDB N.dutertrei	Del13CPDB N.dutertrei	SPECMAP Age(ka)	SP. Units
470.50	224.17	-0.15	1.59	360	0.28
476.50	228.00	-0.04	1.71	362	0.03
480.50	229.38	-0.14	1.54	364	-0.18
490.50	232.83	-0.46	1.67	366	-0.38
495.50	234.55	-0.68	1.57	368	-0.50
500.75	236.36	-0.76	1.55	370	-0.43
505.50	238.00	-0.99	1.62	372	-0.25
510.50	240.32	-0.72	1.09	374	-0.07
515.25	242.52	-0.14	1.19	376	-0.03
520.50	244.95	-0.29	1.38	378	-0.15
525.50	247.27	-0.04	1.42	380	-0.30
530.50	249.59	-0.08	1.57	382	-0.46
535.50	251.91	-0.19	1.36	384	-0.61
541.50	254.69	-0.08	1.36	386	-0.73
544.50	256.08	0.01	1.35	388	-0.82
550.50	258.86	0.11	1.30	390	-0.90
555.50	261.18	0.19	1.32	392	-0.98
560.50	263.50	0.19	1.65	394	-1.07
570.50	271.00	0.17	1.46	396	-1.19
580.50	278.50	0.01	1.61	398	-1.35
585.50	282.25	-0.43	1.53	400	-1.51
590.50	286.00	-0.60	1.81	402	-1.66
595.50	288.00	-0.31	1.64	404	-1.77
600.50	290.00	-0.13	1.50	406	-1.77
605.50	292.00	-0.50	1.59	408	-1.64
610.50	294.00	-0.34	1.42	410	-1.46
615.50	296.00	-0.44	1.52	412	-1.27
620.50	298.00	-0.10	1.54	414	-1.08
625.50	300.91	-0.40	1.66	416	-0.91
630.50	303.82	-0.57	1.68	418	-0.79
635.50	306.73	-0.71	1.72	420	-0.68
640.50	309.64	-0.59	1.54	422	-0.53
645.50	312.55	-0.69	1.45	424	-0.34
650.50	315.45	-0.52	1.49	426	-0.10
656.25	318.80	-0.55	1.24	428	0.25
660.50	321.27	-0.71	1.57	430	0.69
665.50	324.18	-0.86	1.49	432	1.17
670.50	327.09	-0.56	1.39	434	1.50
675.50	330.00	-0.90	1.17	436	1.49
680.50	332.07	-0.91	1.14	438	1.34
685.50	334.14	-0.34	0.82	440	1.19
690.50	336.21	0.03	1.04	442	1.06
695.50	338.28	0.28	1.04	444	0.97
700.50	340.34	0.41	1.19	446	0.95
704.50	342.00	0.46	1.03	448	0.93
710.25	344.74	0.41	1.23	450	0.91
715.50	347.24	0.47	1.15	452	0.87
720.50	349.62	0.35	1.23	454	0.79
725.50	352.00	0.34	1.49	456	0.71
730.50	354.67	0.43	1.43	458	0.64
735.50	357.33	0.30	1.36	460	0.58
740.50	360.00	0.33	1.57	462	0.61
745.50	362.67	0.23	1.50	464	0.73
750.50	365.33	-0.06	1.54	466	0.87
755.50	368.00	-0.77	1.55	468	1.01
760.50	373.43	-0.47	1.53	470	1.08
765.50	378.86	-0.85	1.86	472	0.88
770.50	384.29	-0.82	1.74	474	0.44
775.50	389.71	-1.11	1.86	476	0.03
780.50	395.14	-1.08	1.88	478	-0.35
784.50	399.49	-1.06	1.98	480	-0.70
790.50	406.00	-1.07	1.75	482	-0.86
795.50	409.57	-0.98	1.63	484	-0.82
800.50	413.14	-0.83	1.61	486	-0.79
805.50	416.71	-0.48	1.37	488	-0.76
810.50	420.29	-0.14	1.17	490	-0.71
815.50	423.86	0.45	1.24	492	-0.68
820.50	427.43	0.44	1.52	494	-0.69
825.50	431.00	0.66	1.28	496	-0.74
830.50	434.00	0.78	1.33	498	-0.82
835.50	442.33	0.66	1.52	500	-0.91
840.50	450.67	0.34	1.57		
845.50	460.00	0.02	1.49		
850.50	465.00	0.14	1.55		
855.50	470.00	0.38	1.54		
860.50	471.92	0.29	1.70		
865.50	473.85	0.17	1.66		
870.50	475.77	0.13	1.49		
875.50	477.69	-0.32	1.77		
880.50	479.62	-0.37	1.82		
885.50	481.54	-0.49	1.88		
890.50	483.46	-0.50	1.89		
895.50	485.38	-0.56	1.99		
900.50	487.31	-0.63	2.09		
905.50	489.23	-0.51	2.02		
910.50	491.15	-0.61	2.04		
915.50	493.08	-0.63	1.76		
920.50	495.00	-0.63	1.89		
925.50	496.92	-0.61	2.01		
930.50	498.85	-0.51	2.00		
933.50	500.00	-0.63	2.01		

Table C.3.1 (Contd.) Stable Isotope data from core AII54-25PC (Pedersen, pers comm., 1991), and the SPECMAP Stack (0-500 ka; Imbrie et al., 1984).

Table C.3.2 Major element and sedimentation rate data from core AII54-25PC (SF=salt free; SCF=salt and carbonate free; MAR=mass accumulation rate).

Depth(cm)	Age(ka)	DBD (g/cm2)	LSR (cm/kyr)	BAR (g/cm2/kyr)	C-org (Wt.%SF)	C-org (Wt.%SCF)	CaCO3 (Wt.%)	Sitotal (Wt.%)	Siterrig. (Wt.%)	Ti (Wt.%)	Al (Wt.%)	Si/Al	Siterrig/Al	Ti/Al	Al(MAR) (mg/cm2/kyr)	Siterig(MAR (mg/cm2/kyr)
0.00	8.65	0.298	2.90	0.863	1.220	1.626	24.97	13.627	9.588	0.20	4.18	3.26	2.294	0.048	36.085	82.770
3.00	9.22	0.301	2.90	0.873	1.210	1.637	26.10	13.572	9.533	0.18	3.98	3.41	2.395	0.045	34.756	83.246
6.00	10.24	0.332	2.90	0.963	1.000	1.543	35.18	13.754	9.715	0.19	4.01	3.43	2.423	0.047	38.601	93.521
9.00	11.26	0.339	2.90	0.982	1.160	1.839	36.93	12.540	8.501	0.17	3.80	3.30	2.237	0.045	37.315	83.478
12.00	12.28	0.329	2.90	0.953	1.420	2.162	34.31	14.027	9.988	0.19	4.15	3.38	2.407	0.046	39.561	95.212
15.00	13.30	0.352	2.90	1.022	1.320	2.211	40.31	13.448	9.409	0.20	4.10	3.28	2.295	0.049	41.889	96.129
18.00	14.32	0.359	2.90	1.040	1.370	2.353	41.78	13.538	9.499	0.19	4.14	3.27	2.294	0.046	43.054	98.784
21.00	15.34	0.333	2.90	0.966	1.240	1.922	35.50	14.091	10.052	0.19	4.27	3.30	2.354	0.044	41.252	97.112
24.00	16.36	0.329			1.760	2.679	34.31	14.372	10.333	0.19	4.29	3.35	2.409	0.044		
27.00	16.82	0.333	6.40	2.132	1.810	2.806	35.50	14.011	9.972	0.19	4.17	3.36	2.391	0.046	88.907	212.614
30.00	17.28	0.332	6.40	2.122	1.590	2.450	35.10	12.864	8.825	0.19	3.91	3.29	2.257	0.049	82.989	187.306
33.00	17.73	0.332	6.40	2.128	1.620	2.504	35.31					3.23				
36.00	18.19	0.326	6.40	2.090	1.650	2.489	33.70	13.968	9.929	0.20	4.22	3.31	2.353	0.047	88.178	207.474
39.00	18.65	0.330	6.40	2.111	1.520	2.324	34.60	14.760	10.721	0.22	4.50	3.28	2.382	0.049	94.976	226.276
42.00	19.11	0.330	6.40	2.113	1.470	2.251	34.71	15.912	11.873	0.23	4.68	3.40	2.537	0.049	98.897	250.899
45.00	19.56		6.40							0.22	4.48		0.000	0.049		
48.00	20.02	0.342	6.40	2.190	1.550	2.494	37.84	15.785	11.746	0.22	4.67	3.38	2.515	0.047	102.274	257.232
51.00	20.48	0.322	6.40	2.058	1.450	2.142	32.31	16.333	12.294	0.22	4.68	3.49	2.627	0.047	96.306	252.993
54.00	20.94	0.318	6.40	2.032	1.400	2.034	31.16	15.146	11.107	0.22	4.39	3.45	2.530	0.050	89.219	225.719
57.00	21.40	0.321	6.40	2.053	1.250	1.840	32.08	14.626	10.587	0.18	4.12	3.55	2.570	0.044	84.570	217.317
60.00	21.85	0.317	6.40	2.030	1.310	1.900	31.05	15.233	11.194	0.21	4.39	3.47	2.550	0.048	89.113	227.234
63.00	22.31	0.318	6.40	2.036	1.390	2.024	31.32	15.719	11.680	0.22	4.53	3.47	2.578	0.049	92.223	237.787
66.00	22.77	0.329	6.40	2.104	1.270	1.934	34.33	16.192	12.153	0.22	4.60	3.52	2.642	0.048	96.794	255.727
69.00	23.23	0.343	6.40	2.195	1.100	1.775	38.03	15.432	11.393	0.22	4.46	3.46	2.554	0.049	97.891	250.054
72.00	23.68	0.335	6.40	2.143	1.030	1.608	35.94	15.572	11.533	0.22	4.54	3.43	2.540	0.048	97.280	247.126
75.00	24.14	0.319	6.40	2.044	1.100	1.610	31.67	14.989	10.950	0.22	4.37	3.43	2.506	0.050	89.303	223.771
78.00	24.60	0.322			1.380	2.042	32.41	15.491	11.452	0.21	4.49	3.45	2.550	0.047		
81.00	25.49	0.320	3.40	1.089	1.080	1.587	31.94	15.003	10.964	0.20	4.25	3.53	2.580	0.047	46.275	119.373
84.00	26.38	0.324	3.40	1.101	1.070	1.596	32.94	15.684	11.645	0.22	4.52	3.47	2.576	0.049	49.756	128.192
87.00	27.27	0.334	3.40	1.137	1.090	1.699	35.83	15.962	11.923	0.22	4.60	3.47	2.592	0.048	52.298	135.553
90.00	28.16	0.329	3.40	1.119	1.250	1.907	34.45	14.878	10.839	0.20	4.30	3.46	2.521	0.047	48.133	121.329
93.00	29.05	0.337	3.40	1.146	0.870	1.371	36.54	14.123	10.084	0.19	4.07	3.47	2.478	0.047	46.648	115.576
96.00	29.94	0.330	3.40	1.122	1.040	1.591	34.63	14.365	10.326	0.19	4.25	3.38	2.430	0.045	47.669	115.819
99.00	30.83	0.332	3.40	1.129	1.060	1.636	35.21	13.192	9.153	0.17	3.88	3.40	2.359	0.044	43.804	103.334
102.00	31.72	0.341	3.40	1.159	0.950	1.520	37.52	14.638	10.599	0.18	4.28	3.42	2.476	0.042	49.611	122.853
105.00	32.61	0.344	3.40	1.169	1.180	1.912	38.27	14.449	10.410	0.18	4.14	3.49	2.514	0.043	48.409	121.719
108.00	33.50	0.347	3.40	1.179	1.110	1.820	39.00	14.319	10.280	0.19	4.30	3.33	2.391	0.044	50.712	121.237
111.00	34.39	0.350	3.40	1.190	1.230	2.042	39.76	15.268	11.229	0.19	4.40	3.47	2.552	0.043	52.360	133.625
114.00	35.28	0.342	3.40	1.163	1.000	1.607	37.79	14.246	10.207	0.18	4.33	3.29	2.357	0.042	50.348	118.681
117.00	36.18	0.342	3.40	1.161	1.000	1.604	37.67	15.366	11.327	0.19	4.48	3.43	2.528	0.042	52.020	131.529
120.00	37.07	0.332	3.40	1.129	0.950	1.466	35.20	19.445	15.406	0.27	5.77	3.37	2.670	0.047	65.134	173.907
123.00	37.96	0.334	3.40	1.136	1.070	1.666	35.77	20.053	16.014	0.27	6.04	3.32	2.651	0.045	68.622	181.938
126.00	38.85	0.341	3.40	1.160	1.180	1.890	37.55	18.043	14.004	0.25	5.37	3.36	2.608	0.047	62.268	162.385
129.00	39.74	0.326	3.40	1.110	0.880	1.327	33.67	18.423	14.384	0.24	5.34	3.45	2.694	0.045	59.258	159.619
132.00	40.63	0.251	3.40	0.852	0.930	0.994	6.43	20.879	16.840	0.24	5.34	3.91	3.154	0.045	45.519	143.549
135.00	41.52	0.261	3.40	0.887	1.050	1.179	10.95	20.743	16.704	0.27	5.73	3.62	2.915	0.047	50.797	148.080
138.00	42.41	0.283	3.40	0.963	1.040	1.300	19.97	20.590	16.551	0.27	5.80	3.55	2.854	0.047	55.880	159.459
141.00	43.30	0.290	3.40	0.985	1.030	1.325	22.26	19.949	15.910	0.29	5.85	3.41	2.720	0.050	57.631	156.731
144.00	44.19	0.283	3.40	0.963	1.050	1.311	19.92	22.214	18.175	0.29	6.24	3.56	2.913	0.046	60.090	175.025
147.00	45.08	0.273	3.40	0.927	1.110	1.319	15.83	19.985	15.946	0.24	5.71	3.50	2.793	0.042	52.905	147.746

Table C.3.2 (Contd.) Major element and sedimentation rate data from core AII54-25PC (SF=salt free; SCF=salt and carbonate free; MAR=mass accumulation rate).

Depth(cm)	Age(ka)	DBD (g/cm2)	LSR (cm/kyr)	BAR (g/cm2/kyr)	C-org (Wt.%SF)	C-org (Wt.%SCF)	CaCO3 (Wt.%)	Sitotal (Wt.%)	Siterrig. (Wt.%)	Ti (Wt.%)	Al (Wt.%)	Si/Al	Siterrig/Al	Ti/Al	Al(MAR) (mg/cm2/kyr)	Siterig(MAR (mg/cm2/kyr)
150.00	45.97	0.272	3.40	0.924	1.150	1.362	15.58	21.158	17.119	0.29	6.08	3.48	2.816	0.048	56.204	158.252
153.00	46.86	0.260	3.40	0.884	1.220	1.365	10.62	21.177	17.138	0.27	5.85	3.62	2.930	0.046	51.710	151.488
156.00	47.75	0.262	3.40	0.892	1.140	1.291	11.70	20.203	16.164	0.26	5.89	3.43	2.744	0.044	52.565	144.251
159.00	48.64	0.266	3.40	0.904	1.060	1.220	13.08	19.418	15.379	0.27	5.11	3.80	3.010	0.053	46.171	138.957
162.00	49.53	0.259	3.40	0.881	1.170	1.304	10.29	19.889	15.850	0.16	5.54	3.59	2.861	0.029	48.828	139.693
165.00	50.42	0.263	3.40	0.894	1.070	1.215	11.94	20.743	16.704	0.14	5.73	3.62	2.915	0.024	51.246	149.389
168.00	51.31	0.262	3.40	0.890	0.770	0.869	11.37	23.124	19.085	0.12	6.15	3.76	3.103	0.020	54.724	169.823
171.00	52.20	0.288	3.40	0.979	0.610	0.778	21.60	26.244	22.205	0.16	6.48	4.05	3.427	0.025	63.426	217.340
174.00	53.09	0.281	3.40	0.956	0.580	0.717	19.12	26.117	22.078	0.17	6.37	4.10	3.466	0.027	60.873	210.983
177.00	53.98	0.271	3.40	0.921	0.500	0.589	15.14	24.912	20.873	0.24	5.74	4.34	3.636	0.042	52.846	192.166
180.00	54.87	0.255	3.40	0.867	0.440	0.480	8.40	25.025	20.986	0.25	5.50	4.55	3.816	0.045	47.682	181.937
183.00	55.76	0.244	3.40	0.830	0.580	0.599	3.23	24.564	20.525	0.26	5.57	4.41	3.685	0.047	46.220	170.315
186.00	56.65	0.241	3.40	0.819	0.580	0.589	1.57	24.876	20.837	0.25	5.59	4.45	3.727	0.045	45.757	170.557
189.00	57.54	0.258	3.40	0.876	0.910	1.007	9.60	20.719	16.680	0.25	5.34	3.88	3.124	0.047	46.781	146.126
192.00	58.44	0.269	3.40	0.916	1.280	1.498	14.53	19.404	15.365	0.25	5.39	3.60	2.851	0.046	49.347	140.671
195.00	59.33	0.274	3.40	0.930	1.080	1.290	16.28	19.025	14.986	0.25	5.27	3.61	2.844	0.047	49.033	139.429
198.00	60.22	0.276	3.40	0.940	1.180	1.428	17.36	18.643	14.604	0.25	5.15	3.62	2.836	0.049	48.402	137.255
201.00	61.11	0.280	3.40	0.953	1.150	1.417	18.82	19.573	15.534	0.24	5.29	3.70	2.936	0.045	50.408	148.023
204.00	62.00	0.277	3.40	0.940	1.160	1.405	17.41	16.437	12.398	0.22	4.41	3.73	2.813	0.050	41.434	116.572
207.00	62.89	0.278	3.40	0.944	1.070	1.302	17.81	15.580	11.541	0.22	4.09	3.81	2.822	0.054	38.595	108.925
210.00	63.78	0.280	3.40	0.952	1.180	1.451	18.67	19.117	15.078	0.21	5.03	3.80	2.997	0.042	47.870	143.473
213.00	65.87	0.285	1.20	0.342	1.100	1.384	20.52	20.413	16.374	0.28	5.44	3.75	3.008	0.051	18.608	55.973
216.00	68.37	0.280	1.20	0.336	0.940	1.155	18.64	18.758	14.719	0.22	4.76	3.94	3.092	0.047	15.985	49.419
219.00	70.86	0.287	1.20	0.345	0.950	1.208	21.34	18.154	14.115	0.22	4.42	4.11	3.196	0.050	15.221	48.639
222.00	73.35	0.285	1.20	0.343	0.890	1.123	20.73	16.638	12.599	0.21	4.53	3.67	2.779	0.046	15.529	43.157
225.00	75.85	0.265	1.20	0.318	0.900	1.030	12.66	16.421	12.382	0.24	4.72	3.48	2.624	0.051	14.991	39.337
228.00	78.34	0.285	1.20	0.342	1.000	1.261	20.71	16.994	12.955	0.24	4.68	3.63	2.767	0.051	16.034	44.369
231.00	80.84	0.290	1.20	0.348	1.110	1.428	22.25	18.697	14.658	0.26	4.97	3.76	2.948	0.052	17.288	50.960
234.00	83.33	0.297	1.20	0.356	0.950	1.262	24.75	22.606	18.567	0.27	6.33	3.57	2.932	0.043	22.569	66.177
237.00	85.83	0.285	1.20	0.341	0.820	1.030	20.39	20.891	16.852	0.30	5.71	3.66	2.952	0.053	19.488	57.535
240.00	88.32	0.283	1.20	0.340	0.900	1.123	19.89	20.449	16.410	0.31	5.62	3.64	2.921	0.054	19.089	55.759
243.00	90.82	0.281	1.20	0.338	1.110	1.374	19.20	20.056	16.017	0.30	5.67	3.54	2.827	0.053	19.123	54.064
246.00	93.31	0.279	1.20	0.335	0.750	0.918	18.27	19.364	15.325	0.32	5.73	3.38	2.675	0.056	19.168	51.273
249.00	95.81	0.263	1.20	0.315	0.920	1.044	11.86	19.587	15.548	0.29	5.83	3.36	2.667	0.050	18.388	49.044
252.00	98.30	0.260	1.20	0.312	0.880	0.985	10.64	19.310	15.271	0.29	5.58	3.46	2.736	0.052	17.414	47.651
255.00	100.80	0.260	1.20	0.311	0.800	0.893	10.44	20.057	16.018	0.29	5.81	3.45	2.755	0.051	18.109	49.894
258.00	103.29	0.255	1.20	0.306	0.870	0.951	8.55	19.990	15.951	0.29	5.76	3.47	2.769	0.051	17.650	48.870
261.00	105.78	0.259	1.20	0.311	0.880	0.981	10.29	17.624	13.585	0.28	5.17	3.41	2.629	0.053	16.077	42.259
264.00	108.28	0.262	1.20	0.315	0.790	0.893	11.57	19.288	15.249	0.30	5.62	3.43	2.712	0.053	17.692	47.975
267.00	110.77	0.257	1.20	0.309	0.750	0.829	9.48	19.561	15.522	0.31	5.79	3.38	2.682	0.054	17.875	47.942
270.00	113.27	0.259	1.20	0.311	0.820	0.915	10.34	18.668	14.629	0.29	5.51	3.39	2.657	0.052	17.138	45.528
273.00	115.76	0.270	1.20	0.324	0.750	0.880	14.80	20.947	16.908	0.28	5.83	3.59	2.898	0.048	18.901	54.770
276.00	118.26	0.258	1.20	0.310	0.730	0.810	9.91	19.346	15.307	0.28	5.48	3.53	2.793	0.051	16.991	47.457
279.00	120.75	0.253	1.20	0.303	0.740	0.798	7.30	18.528	14.489	0.26	5.26	3.52	2.753	0.050	15.954	43.914
282.00	122.64	0.265	2.30	0.609	0.730	0.836	12.70	18.722	14.683	0.28	5.38	3.48	2.729	0.051	32.771	89.441
285.00	123.93	0.270	2.30	0.621	0.650	0.764	14.91	18.216	14.177	0.28	5.45	3.34	2.599	0.052	33.896	88.110
288.00	125.21	0.273	2.30	0.629	0.760	0.906	16.13	16.943	12.904	0.25	4.98	3.40	2.589	0.051	31.320	81.103
291.00	126.50	0.281	2.30	0.647	0.940	1.163	19.18	14.709	10.670	0.22	4.39	3.35	2.430	0.051	28.400	69.015
294.00	127.79	0.280	2.30	0.643	1.230	1.512	18.63	13.043	9.004	0.20	3.99	3.27	2.257	0.051	25.665	57.935
297.00	129.07	0.284	2.30	0.654	1.720	2.158	20.29	11.852	7.813	0.18	3.75	3.16	2.083	0.048	24.520	51.077
300.00	130.36	0.292	2.30	0.672	1.710	2.222	23.04	11.556	7.517	0.16	3.52	3.28	2.134	0.044	23.660	50.482
303.00	131.64	0.314	2.30	0.722	1.440	2.061	30.13	12.259	8.220	0.16	3.69	3.32	2.226	0.044	26.672	59.375
306.00	132.93	0.330	2.30	0.758	1.400	2.139	34.55	11.705	7.666	0.14	3.35	3.49	2.286	0.043	25.425	58.113
309.00	134.21	0.334	2.30	0.767	1.160	1.801	35.60	11.979	7.940	0.13	3.33	3.60	2.386	0.040	25.524	60.904
312.00	135.50	0.345	2.30	0.793	1.170	1.903	38.53	11.845	7.806	0.13	3.29	3.60	2.372	0.040	26.106	61.936

Table C.3.2 (Contd.) Major element and sedimentation rate data from core AII54-25PC (SF=salt free; SCF=salt and carbonate free; MAR=mass accumulation rate).

Depth(cm)	Age(ka)	DBD (g/cm2)	LSR (cm/kyr)	BAR (g/cm2/kyr)	C-org (Wt.%SF)	C-org (Wt.%SCF)	CaCO3 (Wt.%)	Sitotal (Wt.%)	Siterrig. (Wt.%)	Ti (Wt.%)	Al (Wt.%)	Si/Al	Siterrig/Al	Ti/Al	Al(MAR) (mg/cm2/kyr)	Siterig(MAR (mg/cm2/kyr)
315.00	136.79	0.338	2.30	0.778	1.250	1.980	36.88	11.855	7.816	0.13	3.25	3.65	2.406	0.041	25.282	60.840
318.00	138.07	0.339	2.30	0.779	1.180	1.873	36.99	12.410	8.371	0.13	3.27	3.79	2.557	0.040	25.520	65.242
321.00	139.36	0.342	2.30	0.786	1.340	2.153	37.76	14.471	10.432	0.16	3.80	3.81	2.747	0.043	29.866	82.030
324.00	140.64	0.341	2.30	0.784	1.150	1.839	37.47	13.161	9.122	0.14	3.45	3.81	2.641	0.040	27.071	71.488
327.00	141.93	0.340	2.30	0.782	0.960	1.532	37.33	14.976	10.937	0.15	3.73	4.01	2.929	0.040	29.221	85.574
330.00	143.21	0.345	2.30	0.794	0.970	1.579	38.55	14.183	10.144	0.15	3.66	3.88	2.775	0.041	29.009	80.501
333.00	144.50	0.323	2.30	0.743	1.060	1.577	32.77	13.228	9.189	0.14	3.57	3.71	2.577	0.040	26.501	68.297
336.00	145.79	0.334	2.30	0.768	1.010	1.570	35.65	13.353	9.314	0.14	3.52	3.79	2.644	0.041	27.041	71.484
339.00	147.07	0.326	2.30	0.751	0.880	1.327	33.69	13.046	9.007	0.14	3.43	3.80	2.624	0.042	25.778	67.630
342.00	148.36	0.326	2.30	0.750	0.970	1.460	33.57	14.339	10.300	0.15	3.68	3.90	2.801	0.041	27.568	77.231
345.00	149.64	0.323	2.30	0.744	0.920	1.370	32.85	14.622	10.583	0.14	3.66	4.00	2.895	0.039	27.193	78.725
348.00	150.93	0.324	2.30	0.746	1.160	1.735	33.14	15.151	11.112	0.16	3.71	4.08	2.992	0.042	27.714	82.931
351.00	152.29	0.329	1.70	0.559	1.050	1.600	34.36	14.480	10.441	0.16	3.52	4.11	2.964	0.046	19.699	58.379
354.00	154.06	0.324	1.70	0.550	1.260	1.878	32.90	14.156	10.117	0.14	3.54	4.00	2.859	0.041	19.470	55.659
357.00	155.83	0.324	1.70	0.552	1.180	1.765	33.13	13.394	9.355	0.13	3.35	4.00	2.794	0.039	18.469	51.599
360.00	157.59	0.314	1.70	0.534	1.400	2.004	30.13	13.755	9.716	0.15	3.52	3.91	2.762	0.043	18.782	51.873
363.00	159.36	0.318	1.70	0.541	1.030	1.501	31.37	14.310	10.271	0.14	3.46	4.13	2.964	0.042	18.747	55.573
366.00	161.13	0.322	1.70	0.547	0.960	1.420	32.38	15.046	11.007	0.14	3.63	4.14	3.029	0.040	19.880	60.210
369.00	162.89	0.332	1.70	0.565	0.930	1.436	35.22	14.188	10.149	0.14	3.49	4.07	2.911	0.040	19.681	57.298
372.00	164.66	0.326	1.70	0.555	0.890	1.342	33.66	14.976	10.937	0.14	3.73	4.01	2.929	0.039	20.720	60.679
375.00	166.43	0.332	1.70	0.564	0.980	1.512	35.20	13.770	9.731	0.16	3.49	3.95	2.791	0.045	19.676	54.924
378.00	168.19	0.332	1.70	0.564	0.922	1.423	35.20	14.674	10.635	0.17	3.86	3.80	2.754	0.044	21.796	60.028
381.00	169.96	0.330	1.70	0.560	0.930	1.420	34.53	16.037	11.998	0.18	4.00	4.01	3.000	0.045	22.403	67.211
384.00	171.73	0.329	1.70	0.560	0.930	1.419	34.45	14.779	10.740	0.18	3.97	3.72	2.703	0.045	22.235	60.109
387.00	173.49	0.329	1.70	0.559	1.100	1.677	34.39	18.307	14.268	0.20	4.57	4.01	3.125	0.045	25.534	79.801
390.00	175.26	0.322	1.70	0.547	1.020	1.508	32.37	17.371	13.332	0.22	4.64	3.74	2.870	0.048	25.405	72.921
393.00	177.03	0.309	1.70	0.525	1.010	1.412	28.47	18.657	14.618	0.23	4.81	3.88	3.040	0.047	25.227	76.691
396.00	178.79	0.308	1.70	0.524	1.080	1.508	28.39	18.850	14.811	0.22	4.85	3.89	3.056	0.045	25.400	77.634
399.00	180.56	0.290	1.70	0.493	1.260	1.622	22.30	19.208	15.169	0.27	5.21	3.69	2.914	0.052	25.650	74.747
402.00	182.33	0.282	1.70	0.479	1.260	1.565	19.48	19.774	15.735	0.25	5.16	3.83	3.048	0.049	24.755	75.445
405.00	184.09	0.278	1.70	0.472	1.120	1.363	17.82	20.530	16.491	0.26	5.42	3.79	3.044	0.049	25.566	77.832
408.00	185.86	0.278	1.70	0.472	1.080	1.314	17.82	19.647	15.608	0.26	5.35	3.67	2.916	0.048	25.266	73.665
411.00	187.63	0.255	1.70	0.433	1.040	1.135	8.34	20.767	16.728	0.27	5.38	3.86	3.109	0.050	23.308	72.472
414.00	189.39	0.258	1.70	0.438	1.030	1.141	9.70	19.633	15.594	0.25	5.10	3.85	3.058	0.048	22.357	68.366
417.00	191.16	0.252	1.70	0.429	1.040	1.121	7.25	19.026	14.987	0.23	4.99	3.81	3.001	0.047	21.433	64.325
420.00	192.93	0.253	1.70	0.430	1.040	1.123	7.41	18.924	14.885	0.25	4.88	3.88	3.052	0.050	20.962	63.975
423.00	194.69	0.251	1.70	0.427	0.890	0.952	6.55	18.896	14.857	0.25	5.03	3.76	2.956	0.049	21.441	63.385
426.00	196.46	0.266	1.70	0.452	0.940	1.081	13.04	18.948	14.909	0.25	5.16	3.67	2.888	0.048	23.317	67.332
429.00	198.23	0.269	1.70	0.458	0.900	1.052	14.47	18.092	14.053	0.26	4.96	3.65	2.835	0.052	22.678	64.295
432.00	199.99	0.270	1.70	0.459	0.970	1.140	14.93	19.399	15.360	0.25	5.08	3.82	3.025	0.048	23.332	70.573
435.00	201.76	0.265	1.70	0.450	1.000	1.146	12.71	19.531	15.492	0.24	5.10	3.83	3.038	0.047	22.962	69.758
438.00	203.53	0.269	1.70	0.457	0.920	1.073	14.27	18.366	14.327	0.25	5.00	3.67	2.863	0.050	22.854	65.428
441.00	205.32	0.269	1.60	0.431	1.110	1.299	14.58	18.449	14.410	0.25	4.92	3.75	2.929	0.050	21.206	62.111
444.00	207.24	0.263	1.60	0.421	1.020	1.160	12.06	17.748	13.709	0.21	4.63	3.83	2.958	0.045	19.524	57.761
447.00	209.15	0.268	1.60	0.430	0.950	1.107	14.20	15.870	11.831	0.19	4.30	3.69	2.751	0.045	18.474	50.818
450.00	211.07	0.260	1.60	0.416	1.070	1.198	10.66	14.751	10.712	0.17	3.78	3.90	2.832	0.044	15.739	44.575
453.00	212.99	0.266	1.60	0.426	0.980	1.129	13.18	17.405	13.366	0.22	4.49	3.88	2.980	0.049	19.091	56.885
456.00	214.90	0.271	1.60	0.433	0.820	0.966	15.13	18.206	14.167	0.22	4.69	3.88	3.019	0.046	20.327	61.373
459.00	216.82	0.288	1.60	0.461	0.960	1.225	21.65	18.465	14.426	0.23	4.81	3.84	3.000	0.047	22.160	66.480
462.00	218.74	0.315	1.60	0.504	0.940	1.352	30.48	18.323	14.284	0.23	4.77	3.84	2.994	0.049	24.067	72.045
465.00	220.65	0.281	1.60	0.450	1.080	1.337	19.24	19.248	15.209	0.24	5.05	3.81	3.011	0.048	22.745	68.474
468.00	222.57	0.277	1.60	0.443	0.960	1.163	17.47	19.238	15.199	0.23	5.16	3.73	2.947	0.045	22.835	67.293
471.00	224.49	0.273	1.60	0.436	1.050	1.249	15.94	19.253	15.214	0.23	5.23	3.68	2.908	0.045	22.835	66.404
474.00	226.40	0.275	1.60	0.440	1.120	1.348	16.92	20.388	16.349	0.23	5.42	3.76	3.015	0.043	23.883	72.009
477.00	228.17	0.267	2.90	0.776	1.040	1.206	13.80	19.788	15.749	0.23	5.35	3.70	2.945	0.043	41.487	122.170

Table C.3.2 (Contd.) Major element and sedimentation rate data from core AII54-25PC (SF=salt free; SCF=salt and carbonate free; MAR=mass accumulation rate).

Depth(cm)	Age(ka)	DBD (g/cm2)	LSR (cm/kyr)	BAR (g/cm2/kyr)	C-org (Wt.%SF)	C-org (Wt.%SCF)	CaCO3 (Wt.%)	Sitotal (Wt.%)	Siterrig. (Wt.%)	Ti (Wt.%)	Al (Wt.%)	Si/Al	Siterrig/Al	Ti/Al	Al(MAR) (mg/cm2/kyr)	Siterig(MAR (mg/cm2/kyr)
480.00	229.21	0.271	2.90	0.785	0.870	1.025	15.13	21.407	17.368	0.21	5.72	3.74	3.034	0.037	44.943	136.373
483.00	230.24	0.267	2.90	0.776	0.730	0.847	13.78	24.786	20.747	0.19	6.52	3.80	3.181	0.029	50.587	160.906
486.00	231.28	0.272	2.90	0.789	0.640	0.759	15.65	20.484	16.445	0.20	5.39	3.80	3.051	0.038	42.529	129.745
489.00	232.31	0.273	2.90	0.792	0.710	0.847	16.13	21.147	17.108	0.22	5.57	3.80	3.074	0.039	44.102	135.580
492.00	233.34	0.262	2.90	0.758	0.480	0.541	11.28	21.795	17.756	0.22	5.23	4.17	3.397	0.042	39.636	134.651
495.00	234.38	0.242	2.90	0.702	0.230	0.235	2.24	24.181	20.142	0.23	5.53	4.37	3.640	0.041	38.845	141.398
498.00	235.41	0.264	2.90	0.765	0.490	0.558	12.26	23.749	19.710	0.20	5.89	4.03	3.345	0.034	45.083	150.785
501.00	236.45	0.265	2.90	0.767	0.530	0.606	12.60	18.120	14.081	0.21	4.72	3.84	2.984	0.045	36.209	108.049
504.00	237.48	0.273	2.90	0.791	0.620	0.737	15.90	15.600	11.561	0.20	4.09	3.81	2.824	0.048	32.379	91.423
507.00	238.70	0.264	2.20	0.581	0.690	0.788	12.43	18.274	14.235	0.21	4.65	3.93	3.061	0.045	27.027	82.741
510.00	240.09	0.254	2.20	0.560	0.500	0.544	8.17	16.934	12.895	0.19	4.04	4.19	3.191	0.046	22.627	72.193
513.00	241.48	0.289	2.20	0.636	0.980	1.258	22.07	15.795	11.756	0.19	4.27	3.70	2.754	0.045	27.162	74.801
516.00	242.87	0.312	2.20	0.687	0.880	1.250	29.59	16.761	12.722	0.19	4.55	3.68	2.793	0.041	31.290	87.399
519.00	244.26	0.302	2.20	0.664	0.910	1.236	26.38	14.896	10.857	0.16	4.02	3.71	2.704	0.040	26.675	72.131
522.00	245.65	0.329	2.20	0.724	0.880	1.342	34.45	12.320	8.281	0.16	3.58	3.44	2.312	0.045	25.940	59.978
525.00	247.04	0.323	2.20	0.711	0.870	1.293	32.74	12.695	8.656	0.14	3.58	3.55	2.421	0.040	25.415	61.519
528.00	248.43	0.303	2.20	0.666	0.830	1.132	26.65	11.896	7.857	0.13	2.99	3.98	2.629	0.042	19.912	52.342
531.00	249.82	0.327	2.20	0.719	0.820	1.240	33.85	11.155	7.116	0.12	2.92	3.82	2.437	0.041	21.009	51.196
534.00	251.21	0.343	2.20	0.755	0.770	1.244	38.12	11.069	7.030	0.12	2.94	3.77	2.394	0.041	22.175	53.093
537.00	252.60	0.346	2.20	0.760	0.820	1.337	38.68	10.929	6.890	0.13	2.85	3.84	2.421	0.044	21.637	52.379
540.00	254.00	0.377	2.20	0.830	0.940	1.735	45.82	10.814	6.775	0.13	2.91	3.71	2.324	0.043	24.185	56.214
543.00	255.39	0.375	2.20	0.826	1.100	2.016	45.44	12.152	8.113	0.14	3.12	3.90	2.604	0.046	25.728	66.989
546.00	256.78	0.374	2.20	0.822	1.010	1.840	45.10	12.500	8.461	0.14	3.22	3.88	2.626	0.045	26.487	69.562
549.00	258.17	0.377	2.20	0.830	1.400	2.585	45.84	13.596	9.557	0.16	3.46	3.93	2.763	0.045	28.714	79.323
552.00	259.56	0.366	2.20	0.805	1.170	2.067	43.39	16.421	12.382	0.20	4.12	3.99	3.009	0.048	33.119	99.642
555.00	260.95	0.348	2.20	0.767	1.070	1.765	39.39	17.374	13.335	0.20	4.26	4.08	3.132	0.048	32.646	102.234
558.00	262.34	0.350	2.20	0.771	1.060	1.761	39.82	16.967	12.928	0.19	4.30	3.95	3.010	0.043	33.099	99.618
561.00	263.88	0.346	1.30	0.450	1.220	1.996	38.89	17.991	13.952	0.23	4.73	3.80	2.947	0.048	21.322	62.833
564.00	266.13	0.305	1.30	0.396	1.280	1.761	27.33	17.713	13.674	0.23	4.61	3.84	2.964	0.049	18.288	54.212
567.00	268.38	0.300	1.30	0.390	1.120	1.506	25.62	19.002	14.963	0.24	4.94	3.85	3.032	0.049	19.226	58.288
570.00	270.63	0.294	1.30	0.382	1.350	1.769	23.67	17.187	13.148	0.22	4.52	3.80	2.907	0.048	17.276	50.222
573.00	272.88	0.279	1.30	0.362	0.960	1.174	18.22	18.536	14.497	0.23	4.90	3.78	2.956	0.048	17.765	52.521
576.00	275.13	0.279	1.30	0.363	0.880	1.077	18.29	17.800	13.761	0.20	4.58	3.89	3.007	0.045	16.588	49.886
579.00	277.38	0.271	1.30	0.353	0.940	1.110	15.29	15.157	11.118	0.18	4.00	3.79	2.780	0.045	14.097	39.192
582.00	279.63	0.275	1.30	0.358	1.010	1.216	16.94	15.586	11.547	0.19	3.94	3.96	2.934	0.047	14.088	41.330
585.00	281.88	0.267	1.30	0.347	1.050	1.215	13.61	13.673	9.634	0.15	3.47	3.94	2.776	0.043	12.046	33.442
588.00	284.13	0.279	1.30	0.363	0.980	1.199	18.29	15.159	11.120	0.19	3.87	3.92	2.876	0.050	14.018	40.310
591.00	286.20	0.295	2.50	0.737	0.830	1.091	23.95	12.606	8.567	0.12	3.05	4.13	2.807	0.039	22.484	63.107
594.00	287.40	0.290	2.50	0.725	0.830	1.069	22.37	14.175	10.136	0.14	3.38	4.20	3.003	0.043	24.474	73.502
597.00	288.60	0.315	2.50	0.788	0.920	1.323	30.47	13.476	9.437	0.13	3.16	4.26	2.983	0.042	24.928	74.366
600.00	289.80	0.298	2.50	0.745	0.990	1.322	25.14	13.324	9.285	0.13	3.20	4.17	2.906	0.041	23.820	69.217
603.00	291.00	0.342	2.50	0.855	0.920	1.480	37.82	12.680	8.641	0.12	3.00	4.22	2.876	0.040	25.699	73.904
606.00	292.20	0.331	2.50	0.828	0.860	1.322	34.97	12.350	8.311	0.13	3.04	4.06	2.732	0.041	25.182	68.801
609.00	293.40	0.336	2.50	0.841	0.870	1.367	36.35	11.936	7.897	0.10	2.88	4.14	2.739	0.033	24.244	66.406
612.00	294.60	0.347	2.50	0.866	0.940	1.539	38.93	12.568	8.529	0.13	3.19	3.94	2.674	0.040	27.639	73.901
615.00	295.80	0.350	2.50	0.875	0.950	1.578	39.79	13.291	9.252	0.14	3.31	4.02	2.798	0.042	28.940	80.985
618.00	297.00	0.346	2.50	0.866	0.960	1.570	38.87	13.237	9.198	0.13	3.30	4.01	2.786	0.038	28.581	79.639
621.00	298.29	0.351	1.70	0.596	1.090	1.815	39.95	13.152	9.113	0.14	3.28	4.01	2.779	0.044	19.559	54.345
624.00	300.04	0.341	1.70	0.579	0.970	1.552	37.50	14.262	10.223	0.16	3.54	4.03	2.889	0.044	20.506	59.237
627.00	301.78	0.330	1.70	0.561	1.050	1.607	34.65	14.691	10.652	0.15	3.62	4.06	2.944	0.041	20.297	59.749
630.00	303.53	0.336	1.70	0.571	0.990	1.551	36.17	14.664	10.625	0.15	3.67	4.00	2.898	0.041	20.920	60.631
633.00	305.27	0.326	1.70	0.553	1.220	1.833	33.43	16.913	12.874	0.18	3.95	4.28	3.258	0.046	21.867	71.242
636.00	307.02	0.324	1.70	0.551	0.970	1.449	33.07	14.664	10.625	0.16	3.67	4.00	2.898	0.043	20.206	58.563
639.00	308.76	0.318	1.70	0.540	0.910	1.323	31.24	16.862	12.823	0.19	4.17	4.04	3.072	0.045	22.551	69.284
642.00	310.51	0.316	1.70	0.537	0.830	1.199	30.75	17.183	13.144	0.19	4.26	4.03	3.083	0.045	22.916	70.643

Table C.3.2 (Contd.) Major element and sedimentation rate data from core AII54-25PC (SF=salt free; SCF=salt and carbonate free; MAR=mass accumulation rate).

Depth(cm)	Age(ka)	DBD (g/cm2)	LSR (cm/kyr)	BAR (g/cm2/kyr)	C-org (Wt.%SF)	C-org (Wt.%SCF)	CaCO3 (Wt.%)	Sitotal (Wt.%)	Siterrig. (Wt.%)	Ti (Wt.%)	Al (Wt.%)	Si/Al	Siterrig/Al	Ti/Al	Al(MAR) (mg/cm2/kyr)	Siterig(MAR (mg/cm2/kyr)
645.00	312.25	0.307	1.70	0.522	0.750	1.041	27.98	17.481	13.442	0.22	4.46	3.92	3.014	0.048	23.276	70.160
648.00	314.00	0.314	1.70	0.534	0.890	1.276	30.23	15.550	11.511	0.17	3.83	4.06	3.005	0.044	20.470	61.521
651.00	315.75	0.300	1.70	0.510	0.750	1.010	25.77	16.666	12.627	0.20	4.30	3.88	2.940	0.046	21.915	64.424
654.00	317.49	0.297	1.70	0.504	0.830	1.101	24.58	16.553	12.514	0.22	4.32	3.83	2.895	0.050	21.786	63.080
657.00	319.24	0.281	1.70	0.477	0.750	0.925	18.96	16.964	12.925	0.20	4.32	3.93	2.994	0.046	20.594	61.665
660.00	320.98	0.308	1.70	0.524	0.860	1.201	28.41	18.964	14.925	0.23	4.73	4.01	3.156	0.048	24.795	78.252
663.00	322.73	0.289	1.70	0.491	1.010	1.294	21.92	18.426	14.387	0.23	4.62	3.99	3.115	0.049	22.672	70.633
666.00	324.47	0.287	1.70	0.487	0.840	1.066	21.17	19.518	15.479	0.23	4.82	4.05	3.212	0.047	23.486	75.435
669.00	326.22	0.293	1.70	0.498	0.840	1.097	23.43	18.435	14.396	0.24	4.70	3.92	3.061	0.051	23.434	71.736
672.00	327.96	0.280	1.70	0.476	0.650	0.801	18.83	18.152	14.113	0.23	4.78	3.80	2.954	0.048	22.762	67.248
675.00	329.71	0.286	1.70	0.487	0.620	0.786	21.07	17.147	13.108	0.20	4.39	3.91	2.989	0.047	21.351	63.819
678.00	331.03	0.293	2.40	0.702	0.590	0.769	23.27			0.17	3.81			0.044	26.789	
681.00	332.28	0.310	2.40	0.743	0.280	0.393	28.75	15.729	11.690	0.20	4.27	3.68	2.735	0.046	31.750	86.839
684.00	333.52	0.310	2.40	0.743	0.300	0.421	28.77	14.150	10.111	0.17	3.93	3.60	2.572	0.044	29.202	75.120
687.00	334.76	0.323	2.40	0.775	0.460	0.684	32.74	12.863	8.824	0.18	3.61	3.56	2.442	0.050	28.013	68.411
690.00	336.00	0.342	2.40	0.820	0.500	0.802	37.67	11.280	7.241	0.15	3.23	3.49	2.240	0.046	26.492	59.353
693.00	337.24	0.319	2.40	0.765	0.790	1.153	31.50	10.199	6.160	0.12	2.93	3.48	2.102	0.041	22.417	47.117
696.00	338.48	0.346	2.40	0.830	0.960	1.566	38.71	8.141	4.102	0.10	2.51	3.24	1.633	0.041	20.847	34.035
699.00	339.72	0.361	2.40	0.866	1.220	2.113	42.26	8.701	4.662	0.11	2.66	3.27	1.752	0.043	23.036	40.360
702.00	340.97	0.372	2.40	0.892	1.210	2.187	44.68	9.433	5.394	0.11	2.78	3.39	1.938	0.041	24.825	48.121
705.00	342.24	0.402	2.10	0.845	1.250	2.537	50.73	10.431	6.392	0.13	2.95	3.54	2.169	0.045	24.903	54.021
708.00	343.67	0.388	2.10	0.814	1.400	2.691	47.97	10.636	6.597	0.11	2.61	4.07	2.524	0.041	21.284	53.729
711.00	345.10	0.389	2.10	0.817	1.410	2.723	48.21	10.536	6.497	0.11	2.75	3.83	2.362	0.041	22.475	53.079
714.00	346.52	0.372	2.10	0.781	1.160	2.097	44.67			0.16						
717.00	347.95	0.358	2.10	0.752	1.030	1.766	41.68	10.728	6.689	0.10	2.68	4.00	2.494	0.038	20.173	50.313
720.00	349.38	0.396	2.10	0.832	0.920	1.823	49.53	11.621	7.582	0.12	2.96	3.93	2.564	0.041	24.589	63.050
723.00	350.81	0.377	2.10	0.792	0.840	1.551	45.85	12.064	8.025	0.13	3.16	3.82	2.541	0.042	25.023	63.585
726.00	352.27	0.315	1.90	0.598	0.840	1.207	30.40	11.262	7.223	0.15	3.32	3.39	2.174	0.045	19.881	43.225
729.00	353.87	0.355	1.90	0.674	1.140	1.928	40.88	13.231	9.192	0.14	3.24	4.08	2.834	0.043	21.855	61.948
732.00	355.47	0.353	1.90	0.671	1.420	2.386	40.49	12.048	8.009	0.14	3.11	3.88	2.579	0.044	20.830	53.728
735.00	357.07	0.347	1.90	0.659	1.200	1.965	38.94	13.441	9.402	0.14	3.39	3.97	2.777	0.043	22.297	61.919
738.00	358.67	0.338	1.90	0.643	0.980	1.552	36.85	14.844	10.805	0.17	3.69	4.02	2.926	0.045	23.734	69.449
741.00	360.27	0.342	1.90	0.650	1.040	1.673	37.83	15.588	11.549	0.20	3.83	4.07	3.015	0.052	24.898	75.079
744.00	361.87	0.342	1.90	0.650	0.990	1.593	37.85	15.360	11.321	0.19	3.69	4.16	3.066	0.050	24.010	73.617
747.00	363.47	0.337	1.90	0.641	0.830	1.308	36.55	15.636	11.597	0.19	3.99	3.92	2.907	0.048	25.550	74.284
750.00	365.07	0.327	1.90	0.621	0.840	1.268	33.76	14.664	10.625	0.18	3.81	3.85	2.790	0.047	23.643	65.953
753.00	366.67	0.317	1.90	0.602	0.940	1.362	30.98	14.701	10.662	0.18	3.70	3.97	2.879	0.049	22.299	64.203
756.00	368.54	0.319	0.90	0.287	0.820	1.197	31.51	15.840	11.801	0.20	3.93	4.03	3.002	0.052	11.276	33.854
759.00	371.80	0.316	0.90	0.285	0.810	1.171	30.82	16.517	12.478	0.20	4.37	3.78	2.856	0.047	12.442	35.531
762.00	375.06	0.314	0.90	0.283	0.720	1.031	30.14	16.423	12.384	0.21	4.14	3.97	2.994	0.051	11.694	35.008
765.00	378.31	0.312	0.90	0.281	0.840	1.194	29.64	18.046	14.007	0.23	4.38	4.12	3.198	0.053	12.316	39.386
768.00	381.57	0.304	0.90	0.274	0.840	1.152	27.10	18.410	14.371	0.23	4.51	4.08	3.185	0.051	12.355	39.350
771.00	384.83	0.299	0.90	0.269	0.970	1.303	25.54	16.593	12.554	0.23	4.40	3.77	2.852	0.052	11.860	33.829
774.00	388.09	0.293	0.90	0.264	0.860	1.125	23.53	19.261	15.222	0.24	4.76	4.05	3.201	0.050	12.559	40.196
777.00	391.34	0.286	0.90	0.257	0.820	1.037	20.89	16.801	12.762	0.22	4.21	3.99	3.031	0.051	10.835	32.838
780.00	394.60	0.283	0.90	0.254	0.970	1.209	19.75	16.570	12.531	0.19	4.19	3.95	2.987	0.046	10.676	31.890
783.00	397.86	0.277	0.90	0.249	0.970	1.176	17.53	15.698	11.659	0.19	3.82	4.11	3.052	0.050	9.517	29.051
786.00	401.11	0.271	0.90	0.244	0.920	1.084	15.15	15.858	11.819	0.20	3.93	4.04	3.011	0.050	9.567	28.805
789.00	404.37	0.283	0.90	0.255	0.700	0.872	19.77	17.925	13.886	0.20	4.17	4.30	3.331	0.049	10.610	35.344
792.00	407.05	0.295	1.40	0.413	0.630	0.829	24.00	17.086	13.047	0.20	4.07	4.20	3.207	0.049	16.789	53.845
795.00	409.15	0.305	1.40	0.427	0.590	0.812	27.31	16.838	12.799	0.21	4.15	4.06	3.086	0.051	17.703	54.634
798.00	411.25	0.307	1.40	0.429	0.620	0.860	27.88	15.973	11.934	0.20	3.98	4.01	2.996	0.051	17.104	51.244
801.00	413.35	0.304	1.40	0.425	0.680	0.930	26.90	13.360	9.321	0.16	3.47	3.85	2.686	0.047	14.750	39.621
804.00	415.45	0.305	1.40	0.426	0.700	0.962	27.21	13.093	9.054	0.16	3.35	3.91	2.704	0.047	14.279	38.607
807.00	417.55	0.308	1.40	0.432	0.890	1.244	28.43	12.283	8.244	0.14	3.17	3.87	2.597	0.045	13.707	35.604

Table C.3.2 (Contd.) Major element and sedimentation rate data from core AII54-25PC (SF=salt free; SCF=salt and carbonate free; MAR=mass accumulation rate).

Depth(cm)	Age(ka)	DBD (g/cm2)	LSR (cm/kyr)	BAR (g/cm2/kyr)	C-org (Wt.%SF)	C-org (Wt.%SCF)	CaCO3 (Wt.%)	Sitotal (Wt.%)	Siterrig. (Wt.%)	Ti (Wt.%)	Al (Wt.%)	Si/Al	Siterrig/Al	Ti/Al	Al(MAR) (mg/cm2/kyr)	Siterig(MAR (mg/cm2/kyr)
645.00	312.25	0.307	1.70	0.522	0.750	1.041	27.98	17.481	13.442	0.22	4.46	3.92	3.014	0.048	23.276	70.160
648.00	314.00	0.314	1.70	0.534	0.890	1.276	30.23	15.550	11.511	0.17	3.83	4.06	3.005	0.044	20.470	61.521
651.00	315.75	0.300	1.70	0.510	0.750	1.010	25.77	16.666	12.627	0.20	4.30	3.88	2.940	0.046	21.915	64.424
654.00	317.49	0.297	1.70	0.504	0.830	1.101	24.58	16.553	12.514	0.22	4.32	3.83	2.895	0.050	21.786	63.080
657.00	319.24	0.281	1.70	0.477	0.750	0.925	18.96	16.964	12.925	0.20	4.32	3.93	2.994	0.046	20.594	61.665
660.00	320.98	0.308	1.70	0.524	0.860	1.201	28.41	18.964	14.925	0.23	4.73	4.01	3.156	0.048	24.795	78.252
663.00	322.73	0.289	1.70	0.491	1.010	1.294	21.92	18.426	14.387	0.23	4.62	3.99	3.115	0.049	22.672	70.633
666.00	324.47	0.287	1.70	0.487	0.840	1.066	21.17	19.518	15.479	0.23	4.82	4.05	3.212	0.047	23.486	75.435
669.00	326.22	0.293	1.70	0.498	0.840	1.097	23.43	18.435	14.396	0.24	4.70	3.92	3.061	0.051	23.434	71.736
672.00	327.96	0.280	1.70	0.476	0.650	0.801	18.83	18.152	14.113	0.23	4.78	3.80	2.954	0.048	22.762	67.248
675.00	329.71	0.286	1.70	0.487	0.620	0.786	21.07	17.147	13.108	0.20	4.39	3.91	2.989	0.047	21.351	63.819
678.00	331.03	0.293	2.40	0.702	0.590	0.769	23.27			0.17	3.81			0.044	26.789	
681.00	332.28	0.310	2.40	0.743	0.280	0.393	28.75	15.729	11.690	0.20	4.27	3.68	2.735	0.046	31.750	86.839
684.00	333.52	0.310	2.40	0.743	0.300	0.421	28.77	14.150	10.111	0.17	3.93	3.60	2.572	0.044	29.202	75.120
687.00	334.76	0.323	2.40	0.775	0.460	0.684	32.74	12.863	8.824	0.18	3.61	3.56	2.442	0.050	28.013	68.411
690.00	336.00	0.342	2.40	0.820	0.500	0.802	37.67	11.280	7.241	0.15	3.23	3.49	2.240	0.046	26.492	59.353
693.00	337.24	0.319	2.40	0.765	0.790	1.153	31.50	10.199	6.160	0.12	2.93	3.48	2.102	0.041	22.417	47.117
696.00	338.48	0.346	2.40	0.830	0.960	1.566	38.71	8.141	4.102	0.10	2.51	3.24	1.633	0.041	20.847	34.035
699.00	339.72	0.361	2.40	0.866	1.220	2.113	42.26	8.701	4.662	0.11	2.66	3.27	1.752	0.043	23.036	40.360
702.00	340.97	0.372	2.40	0.892	1.210	2.187	44.68	9.433	5.394	0.11	2.78	3.39	1.938	0.041	24.825	48.121
705.00	342.24	0.402	2.10	0.845	1.250	2.537	50.73	10.431	6.392	0.13	2.95	3.54	2.169	0.045	24.903	54.021
708.00	343.67	0.388	2.10	0.814	1.400	2.691	47.97	10.636	6.597	0.11	2.61	4.07	2.524	0.041	21.284	53.729
711.00	345.10	0.389	2.10	0.817	1.410	2.723	48.21	10.536	6.497	0.11	2.75	3.83	2.362	0.041	22.475	53.079
714.00	346.52	0.372	2.10	0.781	1.160	2.097	44.67			0.16						
717.00	347.95	0.358	2.10	0.752	1.030	1.766	41.68	10.728	6.689	0.10	2.68	4.00	2.494	0.038	20.173	50.313
720.00	349.38	0.396	2.10	0.832	0.920	1.823	49.53	11.621	7.582	0.12	2.96	3.93	2.564	0.041	24.589	63.050
723.00	350.81	0.377	2.10	0.792	0.840	1.551	45.85	12.064	8.025	0.13	3.16	3.82	2.541	0.042	25.023	63.585
726.00	352.27	0.315	1.90	0.598	0.840	1.207	30.40	11.262	7.223	0.15	3.32	3.39	2.174	0.045	19.881	43.225
729.00	353.87	0.355	1.90	0.674	1.140	1.928	40.88	13.231	9.192	0.14	3.24	4.08	2.834	0.043	21.855	61.948
732.00	355.47	0.353	1.90	0.671	1.420	2.386	40.49	12.048	8.009	0.14	3.11	3.88	2.579	0.044	20.830	53.728
735.00	357.07	0.347	1.90	0.659	1.200	1.965	38.94	13.441	9.402	0.14	3.39	3.97	2.777	0.043	22.297	61.919
738.00	358.67	0.338	1.90	0.643	0.980	1.552	36.85	14.844	10.805	0.17	3.69	4.02	2.926	0.045	23.734	69.449
741.00	360.27	0.342	1.90	0.650	1.040	1.673	37.83	15.588	11.549	0.20	3.83	4.07	3.015	0.052	24.898	75.079
744.00	361.87	0.342	1.90	0.650	0.990	1.593	37.85	15.360	11.321	0.19	3.69	4.16	3.066	0.050	24.010	73.617
747.00	363.47	0.337	1.90	0.641	0.830	1.308	36.55	15.636	11.597	0.19	3.99	3.92	2.907	0.048	25.550	74.284
750.00	365.07	0.327	1.90	0.621	0.840	1.268	33.76	14.664	10.625	0.18	3.81	3.85	2.790	0.047	23.643	65.953
753.00	366.67	0.317	1.90	0.602	0.940	1.362	30.98	14.701	10.662	0.18	3.70	3.97	2.879	0.049	22.299	64.203
756.00	368.54	0.319	0.90	0.287	0.820	1.197	31.51	15.840	11.801	0.20	3.93	4.03	3.002	0.052	11.276	33.854
759.00	371.80	0.316	0.90	0.285	0.810	1.171	30.82	16.517	12.478	0.20	4.37	3.78	2.856	0.047	12.442	35.531
762.00	375.06	0.314	0.90	0.283	0.720	1.031	30.14	16.423	12.384	0.21	4.14	3.97	2.994	0.051	11.694	35.008
765.00	378.31	0.312	0.90	0.281	0.840	1.194	29.64	18.046	14.007	0.23	4.38	4.12	3.198	0.053	12.316	39.386
768.00	381.57	0.304	0.90	0.274	0.840	1.152	27.10	18.410	14.371	0.23	4.51	4.08	3.185	0.051	12.355	39.350
771.00	384.83	0.299	0.90	0.269	0.970	1.303	25.54	16.593	12.554	0.23	4.40	3.77	2.852	0.052	11.860	33.829
774.00	388.09	0.293	0.90	0.264	0.860	1.125	23.53	19.261	15.222	0.24	4.76	4.05	3.201	0.050	12.559	40.196
777.00	391.34	0.286	0.90	0.257	0.820	1.037	20.89	16.801	12.762	0.22	4.21	3.99	3.031	0.051	10.835	32.838
780.00	394.60	0.283	0.90	0.254	0.970	1.209	19.75	16.570	12.531	0.19	4.19	3.95	2.987	0.046	10.676	31.890
783.00	397.86	0.277	0.90	0.249	0.970	1.176	17.53	15.698	11.659	0.19	3.82	4.11	3.052	0.050	9.517	29.051
786.00	401.11	0.271	0.90	0.244	0.920	1.084	15.15	15.858	11.819	0.20	3.93	4.04	3.011	0.050	9.567	28.805
789.00	404.37	0.283	0.90	0.255	0.700	0.872	19.77	17.925	13.886	0.20	4.17	4.30	3.331	0.049	10.610	35.344
792.00	407.05	0.295	1.40	0.413	0.630	0.829	24.00	17.086	13.047	0.20	4.07	4.20	3.207	0.049	16.789	53.845
795.00	409.15	0.305	1.40	0.427	0.590	0.812	27.31	16.838	12.799	0.21	4.15	4.06	3.086	0.051	17.703	54.634
798.00	411.25	0.307	1.40	0.429	0.620	0.860	27.88	15.973	11.934	0.20	3.98	4.01	2.996	0.051	17.104	51.244
801.00	413.35	0.304	1.40	0.425	0.680	0.930	26.90	13.360	9.321	0.16	3.47	3.85	2.686	0.047	14.750	39.621
804.00	415.45	0.305	1.40	0.426	0.700	0.962	27.21	13.093	9.054	0.16	3.35	3.91	2.704	0.047	14.279	38.607
807.00	417.55	0.308	1.40	0.432	0.890	1.244	28.43	12.283	8.244	0.14	3.17	3.87	2.597	0.045	13.707	35.604

Table C.3.2 (Contd.) Major element and sedimentation rate data from core AII54-25PC (SF=salt free; SCF=salt and carbonate free; MAR=mass accumulation rate).

Depth(cm)	Age(ka)	DBD (g/cm2)	LSR (cm/kyr)	BAR (g/cm2/kyr)	C-org (Wt.%SF)	C-org (Wt.%SCF)	CaCO3 (Wt.%)	Sitotal (Wt.%)	Siterrig. (Wt.%)	Ti (Wt.%)	Al (Wt.%)	Si/Al	Siterrig/Al	Ti/Al	Al(MAR) (mg/cm2/kyr)	Siterig(MAR (mg/cm2/kyr)
810.00	419.65	0.309	1.40	0.432	0.720	1.007	28.49	11.500	7.461	0.12	2.94	3.91	2.537	0.041	12.710	32.242
813.00	421.75	0.342	1.40	0.479	0.700	1.126	37.81	11.529	7.490	0.13	3.03	3.81	2.475	0.042	14.491	35.868
816.00	423.85	0.358	1.40	0.501	0.830	1.423	41.67	9.078	5.039	0.10	2.53	3.59	1.993	0.040	12.678	25.263
819.00	425.95	0.364	1.40	0.510	0.950	1.668	43.05	8.899	4.860	0.09	2.47	3.61	1.972	0.037	12.571	24.784
822.00	428.05	0.371	1.40	0.519	1.030	1.854	44.45	9.253	5.214	0.10	2.51	3.69	2.079	0.038	13.012	27.054
825.00	430.15	0.364	1.40	0.510	1.110	1.949	43.04	8.745	4.706	0.07	2.34	3.74	2.013	0.028	11.922	23.993
828.00	432.25	0.404	1.40	0.566	1.100	2.247	51.05	8.793	4.754	0.10	2.30	3.83	2.071	0.044	12.993	26.905
831.00	434.87	0.416	0.60	0.250	1.010	2.158	53.19	10.446	6.407	0.10	2.76	3.79	2.325	0.035	6.887	16.008
834.00	440.07	0.416	0.60	0.250	1.060	2.260	53.09	9.421	5.382	0.10	2.46	3.83	2.188	0.039	6.138	13.430
837.00	445.27	0.424	0.60	0.254	0.880	1.930	54.41	8.689	4.650	0.08	2.22	3.92	2.098	0.038	5.636	11.822
840.00	450.47	0.386	0.60	0.231	0.790	1.507	47.57	9.459	5.420	0.08	2.18	4.34	2.487	0.036	5.045	12.546
843.00	455.67	0.382	0.60	0.229	0.730	1.375	46.90	7.538	3.499	0.06	2.02	3.73	1.731	0.030	4.637	8.028
846.00	460.50	0.422	1.00	0.422	0.770	1.678	54.11	8.246	4.207	0.07	2.15	3.83	1.954	0.033	9.085	17.752
849.00	463.50	0.438	1.00	0.438	0.940	2.168	56.64	7.577	3.538	0.07	1.90	3.99	1.863	0.038	8.315	15.492
852.00	466.50	0.440	1.00	0.440	0.750	1.745	57.02	8.357	4.318	0.07	2.13	3.93	2.031	0.034	9.363	19.014
855.00	469.50	0.456	1.00	0.456	0.600	1.475	59.33	9.737	5.698	0.10	2.43	4.01	2.347	0.040	11.073	25.984
858.00	470.96	0.445	2.60	1.157	0.590	1.396	57.74	10.062	6.023	0.10	2.50	4.03	2.412	0.041	28.895	69.705
861.00	472.12	0.457	2.60	1.188	0.750	1.850	59.47	10.897	6.858	0.10	2.61	4.17	2.624	0.037	31.053	81.497
864.00	473.27	0.453	2.60	1.179	0.680	1.656	58.94	9.578	5.539	0.08	2.51	3.82	2.209	0.034	29.553	65.289
867.00	474.42	0.429	2.60	1.116	0.800	1.789	55.28	11.277	7.238	0.10	2.97	3.80	2.439	0.034	33.112	80.761
870.00	475.58	0.416	2.60	1.081	0.700	1.491	53.04	11.640	7.601	0.11	2.89	4.03	2.632	0.039	31.209	82.129
873.00	476.73	0.363	2.60	0.944	0.680	1.188	42.77	11.677	7.638	0.11	2.94	3.97	2.597	0.039	27.758	72.081
876.00	477.88	0.405	2.60	1.054	0.710	1.456	51.23	12.062	8.023	0.11	2.98	4.05	2.694	0.038	31.379	84.530
879.00	479.04	0.372	2.60	0.966	0.870	1.572	44.66	11.878	7.839	0.13	3.00	3.96	2.613	0.042	28.982	75.742
882.00	480.19	0.372	2.60	0.968	0.860	1.559	44.82	12.514	8.475	0.14	3.20	3.91	2.648	0.045	30.987	82.054
885.00	481.35	0.368	2.60	0.957	0.650	1.158	43.87	13.648	9.609	0.15	3.41	4.00	2.816	0.044	32.644	91.933
888.00	482.50	0.370	2.60	0.963	0.610	1.097	44.39	16.026	11.987	0.22	4.28	3.74	2.797	0.052	41.263	115.428
891.00	483.65	0.359	2.60	0.933	0.710	1.220	41.81	17.879	13.840	0.24	4.55	3.93	3.042	0.053	42.433	129.090
894.00	484.81	0.352	2.60	0.914	0.680	1.137	40.17	18.548	14.509	0.25	4.79	3.87	3.027	0.051	43.827	132.677
897.00	485.96	0.340	2.60	0.884	0.790	1.259	37.24	17.713	13.674	0.23	4.61	3.84	2.964	0.051	40.757	120.820
900.00	487.12	0.310	2.60	0.807	0.950	1.339	29.05	17.989	13.950	0.23	4.66	3.86	2.993	0.049	37.622	112.617
903.00	488.27	0.291	2.60	0.757	0.820	1.062	22.79	16.644	12.605	0.21	4.44	3.75	2.840	0.047	33.611	95.454
906.00	489.42	0.270	2.60	0.701	0.960	1.126	14.74	17.221	13.182	0.22	4.44	3.88	2.970	0.049	31.133	92.463
909.00	490.58	0.282	2.60	0.734	0.840	1.045	19.59	18.620	14.581	0.25	4.86	3.83	2.999	0.051	35.687	107.031
912.00	491.73	0.287	2.60	0.745	0.850	1.078	21.18	18.291	14.252	0.25	4.90	3.73	2.906	0.051	36.554	106.240
915.00	492.88	0.298	2.60	0.774	0.800	1.067	25.02	17.968	13.929	0.24	4.86	3.70	2.868	0.049	37.605	107.862
918.00	494.04	0.292	2.60	0.759	0.700	0.909	22.96	15.330	11.291	0.21	4.12	3.72	2.740	0.051	31.260	85.648
921.00	495.19	0.284	2.60	0.740	0.780	0.979	20.36	13.767	9.728	0.19	3.77	3.65	2.579	0.049	27.893	71.941
924.00	496.35	0.287	2.60	0.746	0.740	0.940	21.27	13.914	9.875	0.20	3.93	3.54	2.512	0.050	29.324	73.674
927.00	497.50	0.288	2.60	0.749	0.790	1.009	21.68	14.713	10.674	0.20	4.03	3.65	2.648	0.049	30.195	79.956
930.00	498.65	0.316	2.60	0.823	0.760	1.098	30.81	14.636	10.597	0.19	4.01	3.65	2.643	0.048	32.982	87.162
933.00	499.81	0.318	2.60	0.827	0.780	1.136	31.33	15.682	11.643	0.20	4.05	3.87	2.873	0.050	33.517	96.303
936.00	502.12	0.320	2.60	0.832	0.760		31.91					3.74				
939.00	503.27	0.314	2.60	0.818	0.740		30.25					3.73				
942.00	504.42	0.318	2.60	0.826	0.740		31.24					3.67				
945.00	505.57	0.318	2.60	0.828	0.730		31.39					3.68				

Table C.3.3 (Contd.) Minor element data from core AII54-25PC (Ex.=excess).

Depth(cm)	Age(ka)	Ba(ppm)	Sr(ppm)	Cu(ppm)	Ni(ppm)	Zn(ppm)	V(ppm)	Ex.Ba (ppm)	Ex.Sr (ppm)	Ex.Ca (Wt.%)	ExSr/ExCa *10-4	Ex.Cu (ppm)	Ex.Ni (ppm)	Ex.Zn (ppm)	Ex.V (ppm)	Al (Wt.%)	Ba/Al *10-2	Cu/Al *10-4	Ni/Al *10-4	Zn/Al *10-4	V/Al *10-4
630.00	303.53	3407	731	168	299	355	234	2403.3	652.5	15.211	50.669	147.4	267.8	311.5	174.4	3.67	9.294	45.827	81.561	96.837	63.830
633.00	305.27	3663	707	195	346	416	295	2581.0	622.4	15.542	45.506	172.8	312.4	369.1	230.8	3.95	9.270	49.347	87.559	105.273	74.653
636.00	307.02	3270	730	190	305	384	235	2266.3	651.5	15.174	49.978	169.4	273.8	340.5	175.4	3.67	8.920	51.828	83.198	104.747	64.103
639.00	308.76	3549	679	174	287	367	217	2406.2	589.7	15.609	45.923	150.5	251.5	317.4	149.2	4.17	8.503	41.689	68.762	87.929	51.991
642.00	310.51	3668	664	152	261	356	211	2500.6	572.8	14.597	47.768	128.0	224.8	305.4	141.7	4.26	8.603	35.649	61.214	83.495	49.487
648.00	314.00	3464	723	162	274	357	223	2415.4	641.0	13.446	50.094	140.5	241.4	311.5	160.8	3.83	9.044	42.298	71.541	93.212	58.225
651.00	315.75	3742	614	174	302	362	293	2565.9	522.1	14.049	46.448	149.8	265.5	311.0	223.2	4.30	8.711	40.508	70.306	84.275	68.211
654.00	317.49	3812	621	192	292	378	239	2628.7	528.5	12.918	48.184	167.7	255.3	326.7	168.8	4.32	8.820	44.425	67.562	87.461	55.299
657.00	319.24	3259	630	194	275	339	224	2077.1	537.6	12.808	50.872	169.7	238.3	287.7	153.9	4.32	7.550	44.942	63.707	78.533	51.892
660.00	320.98	3540	597	215	271	344	262	2245.1	495.8	12.014	49.081	188.4	230.8	287.8	185.1	4.73	7.485	45.462	57.303	72.739	55.400
663.00	322.73	3231	619	176	224	296	221	1966.5	520.2	11.807	48.508	150.0	184.7	241.2	146.0	4.62	6.996	38.110	48.504	64.095	47.854
666.00	324.47	3035	661	145	180	254	206	1715.5	557.9	10.675		117.9	139.0	196.8	127.7	4.82	6.298	30.088	37.351	52.706	42.746
669.00	326.22	2450	775	90	116	179	146	1162.4	674.4	11.651	55.021	63.5	76.0	123.2	69.6	4.70	5.210	19.137	24.666	38.062	31.045
672.00	327.96	2145	772	79	111	180	136	837.1	669.8	9.809	53.223	52.1	70.4	123.3	58.4	4.78	4.490	16.538	23.237	37.682	28.471
675.00	329.71	2695	813	90	138	222	157	1494.3	719.2	9.330	56.649	65.3	100.7	169.9	85.7	4.39	6.145	20.523	31.468	50.622	35.801
678.00	331.03	2726	852	147	198	284	174	1681.7	770.4	7.079	75.942	125.5	165.6	238.7	112.0	3.81	7.147	38.541	51.913	74.461	45.620
681.00	332.28	2768	742	159	243	179	219	1597.7	650.5	10.815	45.844	135.0	206.7	128.2	149.5	4.27	6.476	37.199	56.851	41.878	51.236
684.00	333.52	2066	851	132	234	323	248	989.8	766.9	8.229	63.212	109.9	200.6	276.3	184.1	3.93	5.256	33.584	59.535	82.178	63.097
687.00	334.76	2065	896	102	341	303	209	1075.7	818.7	7.905	70.574	81.7	310.3	260.1	150.3	3.61	5.715	28.231	94.380	83.862	57.846
690.00	336.00	1914	927	104	250	256	193	1029.0	857.8	8.824	76.427	85.8	222.5	217.6	140.5	3.23	5.922	32.176	77.347	79.203	59.712
693.00	337.24	1913	952	99	213	250	220	1110.6	889.3	6.973	96.058	82.5	188.1	215.2	172.4	2.93	6.528	33.781	72.680	85.305	75.068
696.00	338.48	2097	945	100	198	255	193	1409.0	891.2	7.916	90.845	85.9	176.6	225.2	152.2	2.51	8.345	39.797	78.798	101.482	76.808
699.00	339.72	2210	971	118	190	255	201	1481.5	914.1	8.865	86.898	103.0	167.4	223.4	157.8	2.66	8.306	44.346	71.405	95.833	75.539
702.00	340.97	2387	904	119	323	290	214	1625.1	844.5	11.005	59.111	103.3	299.3	257.0	168.8	2.78	8.578	42.767	116.081	104.221	76.908
705.00	342.24	2615	869	121	279	297	187	1808.2	805.9	11.054	69.376	104.4	254.0	262.0	139.1	2.95	8.875	41.065	94.688	100.797	63.464
708.00	343.67	2174	913	108	217	231	173	1458.5	857.1	12.682	64.556	93.3	194.8	200.0	130.5	2.61	8.319	41.328	83.038	88.395	66.201
711.00	345.10	2242	899	105	224	245	174	1488.8	840.1	14.701	58.350	89.5	200.6	212.3	129.3	2.75	8.150	38.171	81.431	89.065	63.254
714.00	346.52	2175	860	114	225	277	162	2175.0	860.0	12.266	72.498										
717.00	347.95	1920	805	123	249	277	146	1185.7	747.6	15.204	58.620	107.9	226.2	245.2	102.4	2.68	7.159	45.861	92.840	103.280	54.436
720.00	349.38	1998	790	117	241	266	161	1188.3	726.7	16.608	55.038	100.4	215.9	230.9	112.9	2.96	6.757	39.566	81.498	89.953	54.445
723.00	350.81	2540	809	139	298	293	217	1675.3	741.4	17.562	48.083	121.2	271.2	255.5	165.7	3.16	8.043	44.013	94.360	92.776	68.712
726.00	352.27	2721	769	144	310	307	223	1811.4	697.9	19.966	40.366	125.3	281.8	267.5	169.0	3.32	8.191	43.346	93.314	92.411	67.126
729.00	353.87	2655	798	159	275	328	283	1767.1	728.6	18.900	45.348	140.8	247.4	289.5	230.3	3.24	8.187	49.032	84.804	101.148	87.271
732.00	355.47	2440	780	134	251	303	207	1589.8	713.5	18.980	44.265	116.5	224.6	266.1	156.5	3.11	7.858	43.153	80.831	97.577	66.662
735.00	357.07	2777	794	143	228	301	243	1850.0	721.5	17.889	48.073	124.0	199.2	260.8	188.0	3.39	8.202	42.238	67.344	88.906	71.775
738.00	358.67	2693	756	157	279	346	237	1682.0	677.0	16.373	45.661	136.2	247.6	302.2	177.0	3.69	7.293	42.520	75.560	93.705	64.186
741.00	360.27	2949	678	165	262	363	291	1900.4	596.0	19.484	37.298	143.5	229.4	317.5	228.8	3.83	7.700	43.081	68.408	94.779	75.980
744.00	361.87	3050	672	164	244	332	263	2039.0	593.0	17.986	41.221	143.2	212.6	288.2	203.0	3.69	8.260	44.415	66.081	89.914	71.227
747.00	363.47	3130	688	162	277	361	261	2037.9	602.6	11.779	59.249	139.6	243.1	313.6	196.2	3.99	7.847	40.615	69.447	90.507	65.436
750.00	365.07	3202	680	156	434	361	257	2159.2	598.5	15.986	45.578	134.6	401.6	315.8	195.1	3.81	8.407	40.958	113.947	94.781	67.475
753.00	366.67	3456	677	169	350	376	247	2442.1	597.8	15.846	45.030	148.2	318.5	332.0	186.8	3.70	9.333	45.639	94.518	101.539	66.703
756.00	368.54	3746	644		322	386	301	2669.8	559.9	15.192	47.496	-22.1	288.6	339.3	237.1	3.93	9.531	0.000	81.924	98.207	76.581
759.00	371.80	3536	610	181	344	414	288	2339.6	516.5	14.318	47.281	156.4	306.9	362.1	217.0	4.37	8.092	41.423	78.727	94.747	65.911
762.00	375.06	3450	573	171	345	389	288	2317.3	484.5	14.694	40.562	147.7	309.8	339.9	220.8	4.14	8.340	41.336	83.398	94.034	69.619
765.00	378.31	4032	566	190	371	428	326	2832.7	472.3	14.719	40.287	165.4	333.8	376.0	254.8	4.38	9.205	43.378	84.701	97.714	74.427
768.00	381.57	3645	534	202	382	431	292	2409.5	437.4	14.163	42.551	176.6	343.6	377.4	218.7	4.51	8.078	44.766	84.656	95.515	64.711
771.00	384.83	3765	504	212	456	423	314	2559.9	409.8	13.067	45.802	187.2	418.6	370.7	242.5	4.40	8.554	48.168	103.606	96.108	71.343
774.00	388.09	4058	476	210	465	421	285	2755.9	374.2	11.966	49.954	183.2	424.6	364.5	207.7	4.76	8.533	44.157	97.777	88.525	59.928
777.00	391.34	4150	542	226	367	403	392	2997.1	451.9	12.151	46.076	202.3	331.2	353.0	323.6	4.21	9.856	53.671	87.156	95.705	93.093
780.00	394.60	3659	604	215	395	343	272	2510.4	514.2	11.823	43.686	191.4	359.3	293.2	203.8	4.19	8.722	51.252	94.160	81.765	64.840
783.00	397.86	3872	663	229	481	383	345	2826.3	581.3	11.578	41.844	207.5	448.5	337.6	282.9	3.82	10.138	59.957	125.937	100.278	90.329

Table C.3.3 (Contd.) Minor element data from core AII54-25PC (Ex.=excess).

Depth(cm)	Age(ka)	Ba(ppm)	Sr(ppm)	Cu(ppm)	Ni(ppm)	Zn(ppm)	V(ppm)	Ex.Ba (ppm)	Ex.Sr (ppm)	Ex.Ca (Wt.%)	ExSr/ExCa *10-4	Ex.Cu (ppm)	Ex.Ni (ppm)	Ex.Zn (ppm)	Ex.V (ppm)	Al (Wt.%)	Ba/Al *10-2	Cu/Al *10-4	Ni/Al *10-4	Zn/Al *10-4	V/Al *10-4
477.00	228.17	2662	480	134	181	282	208	1197.7	365.5	8.098	46.195	103.9	135.5	218.5	121.1	5.35	4.977	25.055	33.843	52.728	38.892
480.00	229.21	2380	431	103	178	225	198	812.8	308.5	11.639	34.616	70.8	129.3	157.0	105.0	5.72	4.158	17.995	31.098	39.310	34.593
483.00	230.24	1953	308	63	96	142	135	167.1	168.4	7.104	50.096	26.3	40.6	64.5	29.0	6.52	2.994	9.659	14.718	21.771	20.697
486.00	231.28	2971	441	138	222	308	207	1495.1	325.6	6.383	59.948	107.7	176.2	244.0	119.4	5.39	5.512	25.601	41.183	57.137	38.401
489.00	232.31	3154	450	143	216	300	217	1630.3	330.9	5.761	61.280	111.7	168.7	233.9	126.6	5.57	5.667	25.696	38.813	53.908	38.993
492.00	233.34	3559	510	183	257	368	232	2128.0	398.2	6.131	60.344	153.6	212.6	305.9	147.1	5.23	6.810	35.014	49.172	70.410	44.389
495.00	234.38	3524	447	161	268	332	267	2009.0	328.6	4.890	74.751	129.9	221.0	266.3	177.1	5.53	6.369	29.096	48.434	60.000	48.253
498.00	235.41	2509	377	127	193	239	186	895.5	250.9	5.378	57.364	93.9	142.9	169.0	90.2	5.89	4.258	21.551	32.750	40.556	31.563
501.00	236.45	3637	602	205	345	369	352	2345.0	501.0	4.742	35.513	178.5	304.9	313.0	275.3	4.72	7.708	43.444	73.114	78.200	74.597
504.00	237.48	3659	700	184	312	338	253	2537.9	612.4	5.626	57.881	161.0	277.2	289.4	186.5	4.09	8.936	44.939	76.201	82.551	61.791
507.00	238.70	3054	644	177	257	277	264	1780.9	544.5	5.798	57.078	150.8	217.5	221.8	188.4	4.65	6.568	38.065	55.270	59.571	56.775
510.00	240.09	2907	736	184	289	342	275	1800.4	649.5	3.895	102.209	161.3	254.6	294.0	209.3	4.04	7.193	45.527	71.507	84.621	68.043
513.00	241.48	2724	706	142	205	294	266	1555.1	614.6	0.239	1377.092	118.0	168.7	243.3	196.6	4.27	6.381	33.263	48.020	68.868	62.309
516.00	242.87	2423	625	133	168	247	212	1175.9	527.5	4.209	59.613	107.4	129.3	192.9	138.0	4.55	5.320	29.201	36.885	54.230	46.545
519.00	244.26	2480	726	134	203	261	227	1380.7	640.1	4.485	111.722	111.4	168.9	213.3	161.8	4.02	6.177	33.374	50.559	65.004	56.536
522.00	245.65	2532	786	139	249	263	236	1551.4	709.4	5.880	104.139	118.9	218.6	220.5	177.8	3.58	7.070	38.812	69.527	73.436	65.897
525.00	247.04	2616	800	145	251	274	296	1636.9	723.5	4.425	123.059	124.9	220.6	231.5	237.9	3.58	7.315	40.548	70.189	76.621	82.773
528.00	248.43	2514	904	127	227	269	215	1695.7	840.0	2.791	232.718	110.2	201.6	233.5	166.4	2.99	8.411	42.491	75.949	90.001	71.934
531.00	249.82	2345	869	123	291	231	199	1545.5	806.5	8.331	73.781	106.6	266.2	196.3	151.5	2.92	8.031	42.122	99.655	79.107	68.149
534.00	251.21	2376	890	125	269	269	194	1572.1	827.2	11.308	46.650	108.5	244.0	234.1	146.3	2.94	8.093	42.576	91.623	91.623	66.077
537.00	252.60	2738	897	132	226	254	249	1958.8	836.1	10.087	63.456	116.0	201.8	220.2	202.8	2.85	9.620	46.381	79.409	89.247	87.491
540.00	254.00	2379	855	127	232	263	218	1580.9	792.6	13.370	53.055	110.6	207.2	228.4	170.6	2.91	8.162	43.571	79.594	90.229	74.791
543.00	255.39	2679	800	145	258	324	248	1825.9	733.3	12.686	57.028	127.5	231.5	287.0	197.4	3.12	8.598	46.537	82.804	103.986	79.594
546.00	256.78	2783	792	139	234	273	218	1900.9	723.1	10.317	81.422	120.9	206.6	234.7	165.6	3.22	8.639	43.146	72.634	84.740	67.668
549.00	258.17	2600	766	134	249	267	210	1652.7	692.0	13.209	61.059	114.5	219.6	225.9	153.8	3.46	7.515	38.732	71.972	77.175	60.700
552.00	259.56	3216	635	156	307	340	294	2089.1	546.9	14.917	55.452	132.8	272.0	291.1	227.1	4.12	7.814	37.904	74.594	82.612	71.435
555.00	260.95	3209	618	142	343	321	276	2043.0	526.9	15.152	55.181	118.0	306.8	270.4	206.8	4.26	7.536	33.345	80.546	75.380	64.812
558.00	262.34	2849	566	182	372	339	251	1672.9	474.1	18.003	44.027	157.8	335.5	288.0	181.2	4.30	6.633	42.370	86.603	78.920	58.434
561.00	263.88	3494	527	196	362	342	363	2197.7	425.7	17.827	41.135	169.4	321.8	285.8	286.1	4.73	7.380	41.398	76.459	72.235	76.670
564.00	266.13	3617	529	174	291	374	306	2354.0	430.3	17.678	40.901	148.1	251.8	319.2	231.0	4.61	7.841	37.720	63.084	81.077	66.336
567.00	268.38	3636	480	187	286	366	374	2284.6	374.4	17.946	38.557	159.2	244.0	307.4	293.8	4.94	7.367	37.888	57.947	74.156	75.776
570.00	270.63	3740	527	196	362	342	363	2501.6	430.2	16.887	32.387	170.6	323.6	288.3	289.5	4.52	8.269	43.335	80.036	75.614	80.257
573.00	272.88	3888	462	205	327	426	390	2545.3	357.1	15.268	34.508	177.4	285.3	367.8	310.3	4.90	7.928	41.804	66.683	86.871	79.530
576.00	275.13	3876	533	199	290	377	353	2623.1	435.1	15.436	30.712	173.3	251.1	322.7	278.6	4.58	8.471	43.489	63.376	82.389	77.144
579.00	277.38	3545	609	178	275	351	323	2450.0	523.4	15.011	28.357	155.5	241.0	303.5	258.0	4.00	8.864	44.508	68.763	87.767	80.765
582.00	279.63	3885	592	173	299	368	349	2807.4	507.8	10.396	41.389	150.9	265.5	321.3	285.0	3.94	9.871	43.956	75.970	93.502	88.674
585.00	281.88	3369	691	157	225	324	281	2418.8	616.7	9.673	38.704	137.5	195.5	282.8	224.6	3.47	9.708	45.242	64.837	93.365	80.974
588.00	284.13	3377	632	151	212	297	261	2318.2	549.2	8.941	48.116	129.2	179.1	251.1	198.2	3.87	8.733	39.048	54.823	76.804	67.494
591.00	286.20	3053	829	122	207	268	226	2217.3	763.7	6.713	53.187	104.8	181.1	231.8	176.4	3.05	10.002	39.969	67.817	87.802	74.042
594.00	287.40	3334	791	146	213	288	249	2409.9	718.8	6.780	64.168	127.0	184.3	247.9	194.2	3.38	9.878	43.259	63.111	85.333	73.777
597.00	288.60	3187	824	158	223	308	313	2320.9	756.3	5.647	92.682	140.2	196.1	270.4	261.6	3.16	10.075	49.946	70.493	97.363	98.944
600.00	289.80	3160	855	134	209	298	292	2285.2	786.6	6.316	80.398	116.0	181.8	260.1	240.1	3.20	9.890	41.938	65.411	93.266	91.388
603.00	291.00	3016	879	128	188	286	239	2193.3	814.7	5.038	122.427	111.1	162.5	250.3	190.2	3.00	10.038	42.600	62.568	95.184	79.542
606.00	292.20	2957	858	130	178	301	215	2124.2	792.9	6.865	80.011	112.9	152.1	264.9	165.6	3.04	9.721	42.739	58.519	98.956	70.683
609.00	293.40	2366	854	107	161	253	149	1576.6	792.3	9.228	82.754	90.8	136.5	218.8	102.2	2.88	8.207	37.113	55.844	87.754	51.681
612.00	294.60	3305	839	150	253	336	241	2431.6	770.7	8.557	83.997	132.1	225.9	298.1	189.2	3.19	10.361	47.024	79.314	105.333	75.552
615.00	295.80	3213	778	149	288	341	242	2307.7	707.2	11.826	63.951	130.4	259.9	301.7	188.3	3.31	9.718	45.066	87.108	103.138	73.195
618.00	297.00	3585	829	152	313	346	239	2681.2	758.4	9.688	81.197	133.4	284.9	306.8	185.4	3.30	10.860	46.047	94.821	104.818	72.403
621.00	298.29	3319	787	160	279	358	235	2421.0	716.8	14.789	55.090	141.6	251.1	319.1	181.7	3.28	10.120	48.783	85.066	109.153	71.651
624.00	300.04	3178	773	154	247	348	242	2209.0	697.3	13.643	58.119	134.1	216.9	306.0	184.5	3.54	8.980	43.515	69.794	98.333	68.381
627.00	301.78	3351	751	159	283	384	238	2360.3	673.6	14.214	55.739	138.6	252.2	341.0	179.2	3.62	9.261	43.943	78.212	106.125	65.776

Table C.3.3 (Contd.) Minor element data from core AII54-25PC (Ex.=excess).

Depth(cm)	Age(ka)	Ba(ppm)	Sr(ppm)	Cu(ppm)	Ni(ppm)	Zn(ppm)	V(ppm)	Ex.Ba (ppm)	Ex.Sr (ppm)	Ex.Ca (Wt.%)	ExSr/ExCa *10-4	Ex.Cu (ppm)	Ex.Ni (ppm)	Ex.Zn (ppm)	Ex.V (ppm)	Al (Wt.%)	Ba/Al *10-2	Cu/Al *10-4	Ni/Al *10-4	Zn/Al *10-4	V/Al *10-4
321.00	139.36	3071	693	146	256	338	243	2031.0	611.7	13.437	51.738	124.6	223.7	292.9	181.3	3.80	8.085	38.439	67.400	88.989	63.977
324.00	140.64	3101	735	147	314	332	256	2155.2	661.1	13.861	51.207	127.6	284.6	291.0	199.9	3.45	8.977	42.555	90.899	96.110	74.109
327.00	141.93	3140	710	137	316	350	253	2117.4	630.1	15.039	45.986	116.0	284.3	305.6	192.3	3.73	8.408	36.683	84.611	93.715	67.742
330.00	143.21	3297	717	153	391	348	267	2296.2	638.8	14.383	49.050	132.4	359.9	304.6	207.6	3.66	9.020	41.856	106.965	95.202	73.043
333.00	144.50	3032	707	140	210	339	261	2055.8	630.7	14.424	49.565	119.9	179.7	296.7	203.1	3.57	8.504	39.266	58.898	95.079	73.202
336.00	145.79	3369	706	151	226	352	295	2404.4	630.6	14.670	41.698	131.2	196.1	310.2	237.7	3.52	9.562	42.859	64.147	99.911	83.732
339.00	147.07	3070	705	132	205	306	249	2130.0	631.5	14.595	45.295	112.7	175.8	265.2	193.2	3.43	8.942	38.448	59.711	89.129	72.527
342.00	148.36	3227	717	143	225	334	274	2220.4	638.3	14.506	43.437	122.3	193.7	290.3	214.3	3.68	8.777	38.895	61.199	90.846	74.526
345.00	149.64	3357	717	141	245	339	288	2356.2	638.8	15.004	42.575	120.4	213.9	295.6	228.6	3.66	9.184	38.573	67.024	92.740	78.788
348.00	150.93	3596	708	146	269	379	307	2579.2	628.5	12.699	49.663	125.1	237.4	334.9	246.7	3.71	9.683	39.315	72.437	102.058	82.670
351.00	152.29	3478	710	128	211	359	278	2513.4	634.6	13.858	45.505	108.2	181.1	317.2	220.7	3.52	9.872	36.331	59.890	101.898	78.907
354.00	154.06	3401	697	135	169	327	254	2432.0	621.3	13.084	48.269	115.1	138.9	285.0	196.5	3.54	9.610	38.146	47.753	92.399	71.771
357.00	155.83	3295	728	133	183	316	250	2378.2	656.3	13.007	49.077	114.2	154.5	276.2	195.6	3.35	9.840	39.718	54.650	94.369	74.659
360.00	157.59	3219	729	141	203	335	244	2255.8	653.7	12.721	50.215	121.2	173.1	293.2	186.8	3.52	9.150	40.081	57.706	95.229	69.361
363.00	159.36	3124	742	145	207	345	245	2175.3	667.9	12.830	48.989	125.5	177.5	303.9	188.7	3.46	9.016	41.848	59.741	99.569	70.708
366.00	161.13	3253	757	146	204	337	231	2257.9	679.2	13.341	47.567	125.6	173.1	293.8	171.9	3.63	8.951	40.174	56.133	92.729	63.562
369.00	162.89	3096	753	161	248	376	286	2141.5	678.4	12.755	48.709	141.4	218.4	334.6	229.4	3.49	8.881	46.183	71.139	107.857	82.040
372.00	164.66	3241	751	189	219	355	265	2218.4	671.1	12.869	51.000	168.0	187.3	310.6	204.3	3.73	8.678	50.606	58.639	95.053	70.955
375.00	166.43	3296	724	154	219	330	263	2341.5	649.4	11.648	56.123	134.4	189.4	288.6	206.4	3.49	9.455	44.175	62.821	94.661	75.442
378.00	168.19	3114	716	171	274	362	270	2056.7	633.4	12.151	54.964	149.3	241.2	316.1	207.2	3.86	8.064	44.281	70.953	93.741	69.917
381.00	169.96	3637	665	183	546	405	293	2542.0	579.4	12.535	54.186	160.5	512.0	357.5	228.0	4.00	9.094	45.759	136.526	101.269	73.264
384.00	171.73	3347	673	174	440	369	259	2259.3	588.0	13.690	49.554	151.7	406.2	321.8	194.4	3.97	8.425	43.798	110.753	92.882	65.193
387.00	173.49	3563	603	195	516	426	300	2313.0	505.3	13.036	51.480	169.3	477.2	371.8	225.8	4.57	7.805	42.714	113.027	93.313	65.714
390.00	175.26	3940	561	193	429	420	307	2668.3	461.6	13.682	47.463	166.9	389.5	364.8	231.5	4.64	8.483	41.553	92.365	90.427	66.098
393.00	177.03	4312	513	189	420	421	357	2995.4	410.1	13.637	46.443	162.0	379.1	363.9	278.9	4.81	8.967	39.304	87.343	87.551	74.242
396.00	178.79	3991	542	192	388	428	326	2664.3	438.3	13.353	43.393	164.7	346.8	370.5	247.3	4.85	8.236	39.623	80.072	88.327	67.277
399.00	180.56	4739	424	216	496	520	373	3313.8	312.6	13.324	44.130	186.7	451.8	458.2	288.4	5.21	9.104	41.496	95.286	99.897	71.657
402.00	182.33	4592	437	216	434	492	378	3178.4	326.5	13.229	38.196	187.0	390.1	430.7	294.1	5.16	8.894	41.836	84.059	95.293	73.213
405.00	184.09	5004	413	228	363	502	369	3520.8	297.1	12.411	37.194	197.5	317.0	437.7	281.0	5.42	9.238	42.090	67.012	92.672	68.119
408.00	185.86	5037	417	226	396	517	397	3571.2	302.4	10.829	37.869	195.9	350.5	453.4	310.0	5.35	9.409	42.216	73.971	96.573	74.157
411.00	187.63	4608	405	197	368	433	350	3135.0	289.9	10.793	40.610	166.7	322.3	369.1	262.6	5.38	8.565	36.618	68.402	80.484	65.057
414.00	189.39	4208	493	207	333	402	335	2811.7	383.9	8.311	37.612	178.3	289.7	341.4	252.1	5.10	8.252	40.592	65.300	78.830	65.692
417.00	191.16	4208	508	178	291	407	301	2840.7	401.1	7.187	45.431	149.9	248.6	347.7	219.9	4.99	8.427	35.644	58.273	81.502	60.275
420.00	192.93	3873	489	205	297	375	308	2537.6	384.6	6.492	45.761	177.6	255.5	317.1	228.7	4.88	7.941	42.031	60.893	76.886	63.149
423.00	194.69	4244	478	218	321	448	417	2868.0	370.5	6.499	46.532	189.7	278.3	388.3	335.3	5.03	8.445	43.379	63.874	89.145	82.977
426.00	196.46	4275	514	192	302	469	334	2861.4	403.5	2.700	107.367	163.0	258.1	407.7	250.1	5.16	8.280	37.187	58.493	90.838	64.691
429.00	198.23	4160	516	174	311	419	289	2802.8	409.9	3.278	117.111	146.1	268.9	360.1	208.5	4.96	8.393	35.104	62.743	84.532	58.305
432.00	199.99	4219	464	177	345	466	292	2828.5	355.3	2.309	173.709	148.4	301.8	405.7	209.5	5.08	8.308	34.853	67.935	91.761	57.498
435.00	201.76	4484	494	204	359	451	309	3087.7	384.9	2.387	161.123	175.3	315.7	390.4	226.1	5.10	8.793	40.003	70.398	88.439	60.593
438.00	203.53	4278	435	197	347	456	298	2907.8	327.9	2.025	182.930	168.9	304.5	396.6	216.7	5.00	8.549	39.366	69.340	91.121	59.548
444.00	207.24	4315	512	208	346	452	348	3046.2	412.8	4.608	87.570	181.9	306.6	397.0	272.7	4.63	9.312	44.885	74.665	97.539	75.096
447.00	209.15	4269	599	200	274	426	309	3091.4	507.0	5.205	78.755	175.8	237.4	374.9	239.1	4.30	9.926	46.503	63.710	99.052	71.848
450.00	211.07	3654	726	165	247	391	312	2618.4	645.1	5.375	66.108	143.7	214.9	346.1	250.5	3.78	9.661	43.624	65.303	103.375	82.488
453.00	212.99	3258	545	186	296	482	387	2029.8	449.0	4.483	85.846	160.8	257.9	428.7	314.1	4.49	7.263	41.463	65.984	107.447	86.270
456.00	214.90	3871	528	167	324	429	295	2586.3	427.6	5.119	64.053	140.6	284.1	373.3	218.8	4.69	8.250	35.591	69.050	91.428	62.870
459.00	216.82	3036	477	164	452	387	277	1719.4	374.1	5.254		137.0	411.1	329.9	198.9	4.81	6.314	34.105	93.998	80.481	57.605
462.00	218.74	3156	505	161	300	345	262	1849.5	402.9	4.278	96.493	134.2	259.4	288.3	184.5	4.77	6.614	33.741	62.872	72.303	54.908
465.00	220.65	3200	464	182	301	385	292	1816.8	355.9	5.175	97.963	153.6	258.1	325.0	209.9	5.05	6.334	36.026	59.581	76.208	57.799
468.00	222.57	3076	493	152	221	314	293	1663.8	382.6	3.819	168.906	123.0	177.2	252.8	209.2	5.16	5.964	29.470	42.848	60.879	56.808
471.00	224.49	2964	465	163	245	312	282	1531.5	353.0	4.745	94.636	133.6	200.5	249.9	197.0	5.23	5.665	31.156	46.829	59.635	53.901
474.00	226.40	2585	486	128	205	272	256	1100.4	370.0	5.501	77.730	97.5	158.9	207.6	167.9	5.42	4.767	23.606	37.807	50.164	47.213

Table C.3.3 (Contd.) Minor element data from core AII54-25PC (Ex.=excess).

Depth(cm)	Age(ka)	Ba(ppm)	Sr(ppm)	Cu(ppm)	Ni(ppm)	Zn(ppm)	V(ppm)	Ex.Ba (ppm)	Ex.Sr (ppm)	Ex.Ca (Wt.%)	ExSr/ExCa *10-4	Ex.Cu (ppm)	Ex.Ni (ppm)	Ex.Zn (ppm)	Ex.V (ppm)	Al (Wt.%)	Ba/Al *10-2	Cu/Al *10-4	Ni/Al *10-4	Zn/Al *10-4	V/Al *10-4
156.00	47.75	3397	419	189	341	323	268	1784.3	293.0	3.557	77.541	155.9	290.9	253.1	172.3	5.89	5.767	32.088	57.895	54.839	45.501
159.00	48.64	2678	512	143	303	233	313	1278.9	402.6	3.985	73.519	114.3	259.6	172.3	230.0	5.11	5.241	27.984	59.295	45.597	61.252
162.00	49.53	2418	473	128	387	205	155	901.1	354.4	4.630	86.961	96.8	339.9	139.2	65.0	5.54	4.365	23.105	69.856	37.004	27.978
165.00	50.42	2164	400	96	201	155	118	595.1	277.4	3.462	102.391	63.8	152.3	87.0	24.9	5.73	3.777	16.754	35.079	27.051	20.593
168.00	51.31	1983	292	59	104	118	95	299.1	160.4	4.100	67.655	24.4	51.7	45.0	-4.9	6.15	3.224	9.593	16.911	19.187	15.447
171.00	52.20	2235	255	69	172	212	135	460.8	116.3	3.822	41.969	32.6	116.9	135.1	29.7	6.48	3.449	10.648	26.543	32.716	20.833
174.00	53.09	2409	237	91	208	257	146	664.9	100.7	7.879	14.764	55.2	153.9	181.4	42.5	6.37	3.782	14.286	32.653	40.345	22.920
177.00	53.98	3327	392	155	326	405	259	1755.4	269.2	6.899	14.593	122.7	277.2	336.8	165.7	5.74	5.796	27.003	56.794	70.557	45.122
180.00	54.87	3571	465	193	294	430	340	2065.1	347.3	5.380	50.028	162.1	247.3	364.7	250.6	5.50	6.493	35.091	53.455	78.182	61.818
183.00	55.76	3597	489	182	285	435	358	2071.9	369.8	2.710	128.177	150.7	237.7	368.9	267.5	5.57	6.458	32.675	51.167	78.097	64.273
186.00	56.65	4330	489	226	309	486	411	2799.5	369.4	0.631	586.315	194.6	261.5	419.6	320.2	5.59	7.746	40.429	55.277	86.941	73.524
189.00	57.54	3723	495	216	332	519	414	2260.9	380.7			186.0	286.6	455.6	327.2	5.34	6.972	40.449	62.172	97.191	77.528
192.00	58.44	3704	477	158	292	469	360	2228.2	361.7	3.209	118.637	127.7	246.2	405.0	272.4	5.39	6.872	29.314	54.174	87.013	66.790
195.00	59.33	3609	484	196	302	459	335	2166.1	371.2	5.178	69.850	166.4	257.2	396.4	249.4	5.27	6.848	37.192	57.306	87.097	63.567
198.00	60.22	3656	499	259	378	520	355	2245.9	388.8	5.893	62.997	230.0	334.2	458.8	271.3	5.15	7.099	50.291	73.398	100.971	68.932
201.00	61.11	3499	522	223	419	456	333	2050.6	408.8	6.339	61.328	193.2	374.0	393.2	247.0	5.29	6.614	42.155	79.206	86.200	62.949
204.00	62.00	4522	537	232	493	541	345	3315.5	442.7	6.908	59.181	207.2	455.5	488.7	273.4	4.41	10.262	52.649	111.878	122.771	78.292
207.00	62.89	4452	573	231	485	540	338	3332.4	485.5	6.448	68.657	208.0	450.2	491.4	271.6	4.09	10.887	56.491	118.606	132.056	82.657
210.00	63.78	4475	570	229	417	511	305	3097.6	462.3	6.646	73.051	200.7	374.2	451.3	223.2	5.03	8.895	45.520	82.890	101.575	60.627
213.00	65.87	5282	492	275	394	491	348	3791.6	375.5	6.878	67.217	244.4	347.7	426.4	259.5	5.44	9.703	50.520	72.381	90.201	63.931
216.00	68.37	4528	582	251	456	546	327	3224.4	480.1	7.570	49.605	224.2	415.5	489.5	249.6	4.76	9.511	52.720	95.778	114.682	68.683
219.00	70.86	4584	571	213	385	497	316	3374.6	476.5	6.898	69.598	188.2	347.5	444.5	244.2	4.42	10.378	48.221	87.160	112.516	71.539
222.00	73.35	4408	626	219	373	475	290	3166.7	529.0	8.021	59.406	193.5	334.5	421.2	216.3	4.53	9.723	48.307	82.276	104.775	63.968
225.00	75.85	4495	576	243	524	524	307	3203.0	475.0	7.762	68.146	216.5	483.9	468.0	230.3	4.72	9.526	51.497	111.048	111.048	65.061
228.00	78.34	4344	571	266	496	488	324	3062.2	470.8	4.509	105.360	239.7	456.2	432.4	247.9	4.68	9.279	56.818	105.946	104.237	69.206
231.00	80.84	4594	565	283	848	511	342	3232.5	458.6	7.737	60.853	255.0	805.7	452.0	261.2	4.97	9.239	56.912	170.535	102.763	68.777
234.00	83.33	4905	536	248	459	515	337	3171.3	400.5	8.319	55.125	212.4	405.2	439.8	234.1	6.33	7.746	39.165	72.487	81.331	53.221
237.00	85.83	4734	471	249	478	553	341	3171.2	348.9	9.158	43.730	216.9	429.5	485.2	248.2	5.71	8.294	43.624	83.743	96.883	59.742
240.00	88.32	5190	462	263	4438	518	396	3651.8	341.8	7.487	46.597	231.4	4390.2	451.3	304.7	5.62	9.238	46.814	789.964	92.204	70.488
246.00	93.31	5015	439	242	476	479	313	3446.4	316.4	7.297	46.838	209.8	427.3	411.0	219.9	5.73	8.754	42.241	83.085	83.609	54.634
249.00	95.81	5427	461	212	369	458	307	3830.9	336.2	7.015		179.2	319.4	388.8	212.3	5.83	9.309	36.366	63.298	78.565	52.662
252.00	98.30	5035	479	223	336	435	316	3506.9	359.6	6.635	47.686	191.6	288.6	368.7	225.3	5.58	9.022	39.957	60.205	77.944	56.621
258.00	103.29	5463	469	272	377	469	373	3885.7	345.7	4.056	82.902	239.6	328.0	400.6	279.4	5.76	9.483	47.216	65.442	81.412	64.748
261.00	105.78	5097	498	243	386	427	287	3681.9	387.4	3.597	99.964	213.9	342.1	365.6	203.0	5.17	9.862	47.017	74.686	82.619	55.531
	110.77	5735	442	249	379	483	319	4150.4	318.2	3.489		216.4	329.8	414.3	225.0	5.79	9.910	43.026	65.489	83.459	55.121
267.00	113.27	5287	499	269	327	432	341	3779.2	381.2	2.739	126.240	238.0	280.2	366.6	251.5	5.51	9.601	48.848	59.380	78.447	61.922
270.00	115.76	5125	521	228	372	408	293	3527.4	396.1	3.506	110.498	195.2	322.4	338.7	198.2	5.83	8.783	39.075	63.755	69.924	50.215
273.00	120.75	4435	565	263	325	431	295	2993.8	452.4	3.964		233.4	280.3	368.5	209.5	5.26	8.426	49.966	61.745	81.884	56.046
282.00	122.64	3925	555	272	425	454	348	2452.0	439.9	3.108	102.370	241.7	379.3	390.1	260.6	5.38	7.296	50.558	78.997	84.388	64.685
285.00	123.93	3256	551	178	323	454	398	1762.7	434.3	3.486	109.349	147.3	276.6	389.2	309.4	5.45	5.970	32.637	59.223	83.242	72.974
288.00	125.21	3307	615	176	276	409	299	1942.6	508.4	5.233	75.703	148.0	233.6	349.8	218.0	4.98	6.636	35.319	55.386	82.076	60.002
291.00	126.50	3131	704	146	267	349	243	1928.8	610.0	3.317		121.3	229.7	296.9	171.7	4.39	7.131	33.252	60.810	79.486	55.344
294.00	127.79	3180	766	238	211	309	237	2087.9	680.6	2.297	196.923	215.6	177.1	261.6	172.2	3.99	7.973	59.669	52.900	77.470	59.418
297.00	129.07	3104	753	157	214	306	222	2077.1	672.7	4.446	98.938	135.9	182.1	261.5	161.1	3.75	8.276	41.860	57.057	81.587	59.190
300.00	130.36	3074	809	143	229	335	245	2109.4	733.6	5.322	81.600	123.2	199.1	293.2	187.7	3.52	8.725	40.589	64.999	95.086	69.540
303.00	131.64	3140	752	149	214	324	286	2129.0	673.0	5.867	86.651	128.2	182.6	280.2	226.0	3.69	8.504	40.353	57.957	87.747	77.456
306.00	132.93	3148	767	142	257	312	261	2229.7	695.2	7.159	85.216	123.1	228.5	272.2	206.5	3.35	9.386	42.339	76.628	93.027	77.821
309.00	134.21	2894	781	151	304	298	218	1983.0	709.8	6.986	97.425	132.3	275.7	258.5	163.9	3.33	8.697	45.381	91.362	89.559	65.516
312.00	135.50	3085	762	143	332	301	238	2184.1	691.6	7.679	87.602	124.5	304.0	261.9	184.5	3.29	9.376	43.460	100.900	91.479	72.332
315.00	136.79	3100	775	151	342	353	289	2210.7	705.5	8.808	83.290	132.7	314.4	314.4	236.2	3.25	9.544	46.489	105.294	108.680	88.976
318.00	138.07	3052	785	136	226	305	230	2155.4	714.9	11.627	57.881	117.6	198.2	266.1	176.8	3.27	9.320	41.533	69.018	93.144	70.240

Table C.3.3 Minor element data from core AII54-25PC (Ex.=excess).

Depth(cm)	Age(ka)	Ba(ppm)	Sr(ppm)	Cu(ppm)	Ni(ppm)	Zn(ppm)	V(ppm)	Ex.Ba (ppm)	Ex.Sr (ppm)	Ex.Ca (Wt.%)	ExSr/ExCa *10-4	Ex.Cu (ppm)	Ex.Ni (ppm)	Ex.Zn (ppm)	Ex.V (ppm)	Al (Wt.%)	Ba/Al *10-2	Cu/Al *10-4	Ni/Al *10-4	Zn/Al *10-4	V/Al *10-4
0.00	8.65		720	145	228	366	298		630.5	9.503	66.355	121.5	192.5	316.4	230.1	4.18		34.689	54.545	87.560	71.292
3.00	9.22	3039	767	203	241	417	295	1949.3	681.8	9.979	68.327	180.6	207.2	369.7	230.3	3.98	7.636	51.005	60.553	104.774	74.121
6.00	10.24	2798	734	180	258	428	337	1700.1	648.2	13.612	47.620	157.4	223.9	380.4	271.8	4.01	6.978	44.888	64.339	106.733	84.040
9.00	11.26	2811	740	122	243	363	291	1770.6	658.7	14.338	45.941	100.6	210.7	317.9	229.3	3.80	7.397	32.105	63.947	95.526	76.579
12.00	12.28	3172	664	161	525	452	426	2035.7	575.2	13.247	43.422	137.7	489.7	402.7	358.6	4.15	7.643	38.795	126.506	108.916	102.651
15.00	13.30	3452	679	151	635	402	357	2329.4	591.3	15.655	37.767	127.9	600.2	353.3	290.4	4.10	8.420	36.829	154.878	98.049	87.073
18.00	14.32	2802	654	128	502	343	269	1668.5	565.4	16.239	34.817	104.7	466.8	293.8	201.7	4.14	6.768	30.918	121.256	82.850	64.976
21.00	15.34	2970	670	137	390	358	261	1800.9	578.6	13.709	42.208	113.0	353.7	307.3	191.6	4.27	6.956	32.084	91.335	83.841	61.124
24.00	16.36	3039	648	149	457	389	290	1864.4	556.2	13.230	42.040	124.9	420.5	338.1	220.3	4.29	7.084	34.732	106.527	90.676	67.599
27.00	16.82	2851	670	123	336	354	250	1709.3	580.8	13.721	42.327	99.5	300.6	304.5	182.2	4.17	6.837	29.496	80.576	84.892	59.952
30.00	17.28	2799	657	118	316	356	226	1728.4	573.3	13.592	42.182	96.0	282.8	309.6	162.5	3.91	7.159	30.179	80.818	91.049	57.801
36.00	18.19	2911	651	91	228	277	206	1755.6	560.7	14.141		67.3	192.1	226.9	137.4	4.22	6.898	21.564	54.028	65.640	48.815
39.00	18.65	3445	654	152	448	403	286	2212.9	557.7	12.994	43.150	126.7	409.8	349.6	212.9	4.50	7.656	33.778	99.556	89.556	63.556
42.00	19.11	3076	610	122	372	368	250	1794.6	509.8	13.321	41.866	95.7	332.2	312.4	174.0	4.68	6.573	26.068	79.487	78.632	53.419
45.00	19.56	2839	613	110	294	312	192	1612.4	517.1	13.344	38.209	84.8	255.9	258.8	119.2	4.48	6.337	24.554	65.625	69.643	42.857
48.00	20.02	2718	592	108	267	339	231	1439.4	492.1			81.7	227.3	283.5	155.1	4.67	5.820	23.126	57.173	72.591	49.465
51.00	20.48	2728	607	112	210	308	207	1446.6	506.8	14.598	33.706	85.7	170.2	252.4	131.0	4.68	5.829	23.932	44.872	65.812	44.231
54.00	20.94	2627	609	112	250	324	268	1425.0	515.1	12.383	40.932	87.3	212.7	271.9	196.7	4.39	5.984	25.513	56.948	73.804	61.048
57.00	21.40	3314	702	133	393	378	366	2185.9	613.8	11.957	43.077	109.8	358.0	329.1	299.1	4.12	8.044	32.282	95.388	91.748	88.835
60.00	21.85	2720	639	97	329	337	261	1518.0	545.1	12.357	49.674	72.3	291.7	284.9	189.7	4.39	6.196	22.096	74.943	76.765	59.453
63.00	22.31	2707	609	112	339	315	193	1466.7	512.1	11.913	45.755	86.5	300.5	261.2	119.4	4.53	5.976	24.724	74.834	69.536	42.605
66.00	22.77	2587	624	119	209	303	187	1327.5	525.6	12.004	42.657	93.1	169.9	248.4	112.3	4.60	5.624	25.870	45.435	65.870	40.652
69.00	23.23	2681	590	89	216	294	188	1459.9	494.6	13.201	39.812	63.9	178.1	241.0	115.5	4.46	6.011	19.955	48.430	65.919	42.152
72.00	23.68	2578	637	105	238	312	204	1334.9	539.8	14.700	33.644	79.5	199.4	258.1	130.2	4.54	5.678	23.128	52.423	68.722	44.934
75.00	24.14	3195	636	102	193	277	244	1998.5	542.5	13.853	38.969	77.4	155.9	225.1	173.0	4.37	7.311	23.341	44.165	63.387	55.835
78.00	24.60	2669	615	118	227	288	214	1439.6	518.9	12.163	44.600	92.7	188.8	234.7	141.0	4.49	5.944	26.281	50.557	64.143	47.661
81.00	25.49	2520	662	118	238	327	203	1356.4	571.1	12.445	41.696	94.1	201.9	276.5	133.9	4.25	5.929	27.765	56.000	76.941	47.765
84.00	26.38	2881	635	138	237	316	235	1643.4	538.3	12.286	46.481	112.6	198.6	262.3	161.6	4.52	6.374	30.531	52.434	69.912	51.991
87.00	27.27	2360	620	113	172	299	216	1100.5	521.6	12.654	42.538	87.1	132.9	244.4	141.3	4.60	5.130	24.565	37.391	65.000	46.957
90.00	28.16	2559	670	90	174	256	191	1381.7	578.0	13.802	37.789	65.8	137.5	204.9	121.1	4.30	5.951	20.930	40.465	59.535	44.419
93.00	29.05	2554	678	108	206	289	225	1439.6	590.9	13.285	43.507	85.1	171.4	240.7	158.9	4.07	6.275	26.536	50.614	71.007	55.283
96.00	29.94	3004	688	142	229	313	464	1840.4	597.1	14.149	41.762	118.1	192.9	262.5	394.9	4.25	7.068	33.412	53.882	73.647	109.176
99.00	30.83	2404	685	127	315	284	175	1341.7	602.0	13.363	44.680	105.2	282.0	237.9	112.0	3.88	6.196	32.732	81.186	73.196	45.103
102.00	31.72	2444	684	118	281	301	157	1272.1	592.4	13.639	44.135	93.9	244.6	250.2	87.5	4.28	5.710	27.570	65.654	70.327	36.682
105.00	32.61	2431	679	117	233	295	151	1297.5	590.4	14.517	40.809	93.7	197.8	245.8	83.7	4.14	5.872	28.261	56.280	71.256	36.473
108.00	33.50	2323	664	136	272	292	165	1145.7	572.0	14.834	39.801	111.8	235.5	240.9	95.1	4.30	5.402	31.628	63.256	67.907	38.372
111.00	34.39	2315	657	134	251	283	189	1110.3	562.8	15.107	37.862	109.3	213.6	230.8	117.5	4.40	5.261	30.455	57.045	64.318	42.955
114.00	35.28	2848	702	154	254	324	281	1662.4	609.3	15.400	36.549	129.6	217.2	272.6	210.6	4.33	6.577	35.566	58.661	74.827	64.896
117.00	36.18	2731	630	124	249	298	236	1504.4	534.1	14.619	41.682	98.8	210.9	244.8	163.2	4.48	6.096	27.679	55.580	66.518	52.679
120.00	37.07	3826	387	185	484	574	406	2246.2	263.5	14.553	36.702	152.5	435.0	505.5	312.2	5.77	6.631	32.062	83.882	99.480	70.364
123.00	37.96	3477	429	200	430	468	362	1823.2	299.7	13.410	19.651	166.0	378.7	396.3	263.9	6.04	5.757	33.113	71.192	77.483	59.934
126.00	38.85	3014	507	185	329	442	277	1543.7	392.1	13.606	22.030	154.8	283.4	378.2	189.7	5.37	5.613	34.451	61.266	82.309	51.583
129.00	39.74	2726	523	152	319	378	215	1263.9	408.7	14.399	27.230	122.0	273.6	314.6	128.2	5.34	5.105	28.464	59.738	70.787	40.262
132.00	40.63	3259	507	186	435	394	266	1796.9	392.7	12.849	31.810	156.0	389.6	330.6	179.2	5.34	6.103	34.831	81.461	73.783	49.813
135.00	41.52	3093	467	170	372	378	222	1524.1	344.4	1.940	202.474	137.8	323.3	310.0	128.9	5.73	5.398	29.668	64.921	65.969	38.743
138.00	42.41	3054	467	152	329	376	242	1466.0	342.9	3.703	92.990	119.4	279.7	307.1	147.8	5.80	5.266	26.207	56.724	64.828	41.724
141.00	43.30	3537	421	207	401	417	334	1935.3	295.8	7.307	46.922	174.1	351.3	347.5	238.9	5.85	6.046	35.385	68.547	71.282	57.094
144.00	44.19	3492	437	206	366	409	307	1783.5	303.5	8.219	35.993	170.9	313.0	334.9	205.6	6.24	5.596	33.013	58.654	65.545	49.199
147.00	45.08	3140	435	179	398	408	282	1576.6	312.8	7.235	41.944	146.9	349.5	340.2	189.2	5.71	5.499	31.349	69.702	71.454	49.387
150.00	45.97	3922	421	211	388	378	342	2257.3	290.9	5.660	55.265	176.8	336.3	305.8	243.2	6.08	6.451	34.704	63.816	62.171	56.250
153.00	46.86	3953	401	195	350	343	291	2351.3	275.8	5.516	52.736	162.1	300.3	273.5	195.9	5.85	6.757	33.333	59.829	58.632	49.744

Table C.3.3 (Contd.) Minor element data from core AII54-25PC (Ex.=excess).

Depth(cm)	Age(ka)	Ba(ppm)	Sr(ppm)	Cu(ppm)	Ni(ppm)	Zn(ppm)	V(ppm)	Ex.Ba (ppm)	Ex.Sr (ppm)	Ex.Ca (Wt.%)	ExSr/ExCa *10-4	Ex.Cu (ppm)	Ex.Ni (ppm)	Ex.Zn (ppm)	Ex.V (ppm)	Al (Wt.%)	Ba/Al *10-2	Cu/Al *10-4	Ni/Al *10-4	Zn/Al *10-4	V/Al *10-4
786.00	401.11	3770	677	189	322	394	276	2695.3	593.0	11.349	41.613	166.9	288.6	347.4	212.2	3.93	9.605	48.151	82.034	100.378	70.315
789.00	404.37	3852	663	197	294	381	266	2710.7	573.8	10.316	42.403	173.6	258.6	331.5	198.3	4.17	9.241	47.259	70.529	91.399	63.812
792.00	407.05	4193	669	204	302	423	295	3079.2	581.9	9.705	42.229	181.1	267.4	374.7	228.9	4.07	10.307	50.147	74.238	103.982	72.517
795.00	409.15	3732	664	172	279	373	268	2596.5	575.2	8.857	42.250	148.7	243.7	323.8	200.6	4.15	8.998	41.472	67.272	89.937	64.619
798.00	411.25	3651	669	161	283	367	262	2560.4	583.8	7.865	57.456	138.6	249.1	319.7	197.3	3.98	9.166	40.418	71.045	92.133	65.773
801.00	413.35	2988	812	159	331	361	234	2037.8	737.7	7.410	69.394	139.5	301.5	319.8	177.6	3.47	8.610	45.818	95.382	104.027	67.430
804.00	415.45	2782	852	129	410	330	198	1865.2	780.3	6.566	88.528	110.2	381.5	290.2	143.6	3.35	8.308	38.524	122.440	98.550	59.130
807.00	417.55	2530	868	126	327	294	181	1661.0	800.1	5.600	105.890	108.1	300.0	256.3	129.4	3.17	7.971	39.698	103.025	92.628	57.026
810.00	419.65	2390	883	126	285	277	176	1584.7	820.1	7.421	77.316	109.5	260.0	242.1	128.2	2.94	8.126	42.839	96.898	94.178	59.839
813.00	421.75	2501	866	109	243	269	177	1672.5	801.2	9.127	63.758	92.0	217.3	233.1	127.8	3.03	8.265	36.023	80.307	88.900	58.495
816.00	423.85	2091	965	117	256	258	147	1398.7	910.9	10.444	55.081	102.8	234.5	228.0	105.9	2.53	8.269	46.270	101.241	102.032	58.134
819.00	425.95	1962	984	112	239	227	136	1287.0	931.2	10.691	54.601	98.1	218.0	197.7	95.9	2.47	7.959	45.434	96.952	92.084	55.169
822.00	428.05	2119	980	110	234	219	161	1432.5	926.3	10.360	71.210	95.9	212.7	189.2	120.3	2.51	8.451	43.869	93.322	87.339	64.208
825.00	430.15	1994	1009	138	229	246	202	1353.8	959.0	10.499	74.328	124.8	209.1	218.2	164.0	2.34	8.528	59.020	97.939	105.210	86.392
828.00	432.25	2118	963	129	240	259	204	1489.4	913.9	11.008	72.682	116.1	220.5	231.7	166.7	2.30	9.225	56.188	104.536	112.812	88.856
831.00	434.87	2254	936	139	262	234	189	1499.4	877.0	11.060	74.148	123.5	238.6	201.3	144.2	2.76	8.178	50.434	95.062	84.903	68.575
834.00	440.07	1959	1029	146	273	218	159	1285.5	976.4	14.782	54.204	132.2	252.1	188.8	119.0	2.46	7.964	59.353	110.982	88.623	64.638
837.00	445.27	1979	1061	131	216	192	135	1372.1	1013.6	16.387	55.586	118.5	197.2	165.7	99.0	2.22	8.928	59.102	97.450	86.623	60.907
840.00	450.47	1970	1058	120	176	178	148	1373.3	1011.4	16.947	54.949	107.7	157.5	152.1	112.6	2.18	9.039	55.059	80.753	81.671	67.906
843.00	455.67	1769	1066	105	151	167	137	1215.7	1022.8	17.503	52.925	93.6	133.8	143.0	104.2	2.02	8.754	51.960	74.724	82.641	67.796
846.00	460.50	1995	1062	117	144	182	158	1405.5	1015.9	16.958	56.548	104.9	125.7	156.4	123.0	2.15	9.266	54.342	66.882	84.532	73.385
849.00	463.50	1939	1087	122	141	193	154	1419.0	1046.4	20.171	45.305	111.3	124.9	170.4	123.1	1.90	10.210	64.241	74.245	101.627	81.091
852.00	466.50	1830	1080	106	143	194	154	1247.7	1034.5	20.974	41.815	94.0	124.9	168.7	119.4	2.13	8.605	49.845	67.244	91.226	72.417
855.00	469.50	2106	1015	115	154	181	151	1441.2	963.0	20.969	46.562	101.3	133.4	152.2	111.5	2.43	8.673	47.362	63.424	74.544	62.188
858.00	470.96	2109	998	121	199	202	156	1425.4	944.6	21.526	47.085	107.0	177.8	172.3	115.4	2.50	8.447	48.460	79.699	80.901	62.478
861.00	472.12	1955	1001	112	205	169	127	1239.5	945.1	18.792	53.820	97.3	182.8	138.0	84.5	2.61	7.481	42.858	78.446	64.670	48.598
864.00	473.27	2003	1026	117	202	181	181	1316.5	972.3	18.542	55.159	102.9	180.7	151.2	140.3	2.51	7.988	46.661	80.560	72.185	72.185
867.00	474.42	1989	912	104	146	184	152	1176.4	848.5	21.414	47.443	87.3	120.8	148.8	103.8	2.97	6.702	35.044	49.197	62.001	51.218
870.00	475.58	2015	927	122	170	186	183	1224.2	865.2	22.457	46.593	105.8	145.4	151.7	136.1	2.89	6.976	42.239	58.857	64.397	63.358
873.00	476.73	2220	883	115	172	185	165	1414.7	820.1	22.582	45.810	98.5	147.0	150.1	117.2	2.94	7.548	39.099	58.479	62.899	56.099
876.00	477.88	2356	891	113	166	201	195	1540.5	827.3	23.472	41.030	96.2	140.7	165.6	146.6	2.98	7.911	37.941	55.737	67.489	65.474
879.00	479.04	2497	835	139	223	255	294	1675.8	770.8	22.827	41.380	122.1	197.5	219.4	245.3	3.00	8.325	46.342	74.347	85.016	98.019
882.00	480.19	2682	827	126	219	239	206	1805.7	758.5	23.506	40.206	108.0	191.8	201.0	154.0	3.20	8.380	39.369	68.428	74.677	64.366
885.00	481.35	2704	783	153	272	286	254	1769.8	710.0	23.306	41.721	133.8	243.0	245.5	198.6	3.41	7.925	44.841	79.717	83.821	74.442
888.00	482.50	3824	629	180	302	377	331	2650.8	537.3	21.785	38.948	155.9	265.6	326.1	261.4	4.28	8.924	42.008	70.480	87.983	77.248
891.00	483.65	3978	597	174	310	380	285	2732.4	499.6	20.898	41.401	148.4	271.3	326.0	211.1	4.55	8.744	38.247	68.141	83.527	62.646
894.00	484.81	4174	483	216	460	471	394	2861.7	380.4	16.779	48.875	189.0	419.3	414.1	316.1	4.79	8.709	45.068	95.979	98.274	82.208
897.00	485.96	4040	528	188	410	393	319	2777.0	429.3	20.162	41.030	162.1	370.8	338.2	244.0	4.61	8.758	40.755	88.882	85.196	69.154
900.00	487.12	4008	549	214	342	383	329	2732.0	449.3	17.529	43.975	187.8	302.4	327.7	253.3	4.66	8.600	45.918	73.383	82.180	70.593
903.00	488.27	3488	592	213	275	345	302	2272.8	497.0	17.569	43.174	188.0	237.3	292.3	229.9	4.44	7.859	47.991	61.961	77.732	68.044
906.00	489.42	3437	586	238	420	406	288	2221.8	491.0	17.163	41.367	213.0	382.3	353.3	215.9	4.44	7.744	53.624	94.631	91.476	64.890
909.00	490.58	4182	551	234	366	412	327	2850.9	447.0	17.267	31.117	206.7	324.7	354.3	248.0	4.86	8.602	48.133	75.285	84.747	67.263
912.00	491.73	4028	560	205	279	413	324	2685.3	455.1	16.203	30.837	177.4	237.3	354.8	244.3	4.90	8.214	41.804	56.894	84.220	66.071
915.00	492.88	4584	590	214	295	413	344	3254.4	486.1	15.517	24.517	186.7	253.7	355.3	265.1	4.86	9.439	44.067	60.747	85.046	70.837
918.00	494.04	3638	700	213	315	424	348	2509.7	611.8	14.365	29.884	189.8	280.0	375.1	281.0	4.12	8.828	51.688	76.439	102.890	84.447
921.00	495.19	3419	676	193	367	371	394	2386.3	595.3	11.079	40.550	171.8	334.9	326.2	332.7	3.77	9.065	51.170	97.302	98.362	104.460
924.00	496.35	3290	703	193	402	399	322	2213.8	618.9	8.599	57.801	170.9	368.6	352.3	258.1	3.93	8.371	49.104	102.278	101.515	81.924
927.00	497.50	3434	684	183	323	388	261	2330.3	597.7	5.375	91.354	160.3	288.7	340.1	195.5	4.03	8.519	45.398	80.129	96.255	64.749
930.00	498.65	3453	701	198	363	383	271	2355.1	615.2	7.267	61.507	175.4	328.9	335.4	205.8	4.01	8.611	49.379	90.528	95.516	67.584
933.00	499.81	2934	682	154	352	408	281	1824.5	595.3	7.899	57.612	131.2	317.6	359.9	215.2	4.05	7.241	38.005	86.868	100.688	69.346

Depth(cm)	C-org(Wt.%)	CaCO3(Wt.%)	Fe/Al	Si/Al	Ti/Al
0.5	0.78	67.419	0.839	4.923	0.048
1.5	0.76	68.942	0.907	5.007	0.047
3.0	0.70	71.165	0.881	5.063	0.046
5.0	0.68	71.564	0.872	5.028	0.047
7.0	0.65	72.638	0.884	4.978	0.045
9.0	0.59	72.588	0.935	4.986	0.045
11.0	0.69	74.011	0.954	5.023	0.045
13.0	0.56	74.136	1.229	5.061	0.045
15.0	0.57	75.135	1.256	5.302	0.045
17.0	0.65	74.985	1.158	5.475	0.047
19.0	0.69	76.708	1.067	5.291	0.044
22.5	0.54	73.761	1.008	5.256	0.045
27.5	0.69	76.233	1.158	5.518	0.047
32.5	0.80	74.935	1.618	6.245	0.048
37.5	0.95	73.212	1.840	6.968	0.050
42.5	0.97	69.841	2.798	8.180	0.051
47.5	0.95	71.764	2.021	7.412	0.050
52.5	1.17	75.359	1.100	6.290	0.051
57.5	2.01	75.235	0.922	5.853	0.050
62.5	2.50	74.585	0.878	5.714	0.051
67.5	2.43	75.809	0.933	5.548	0.044
72.5	1.94	74.061	0.914	5.505	0.055
77.5	2.13	75.260	0.890	5.440	0.058
82.5	1.85	72.763	0.944	5.935	0.058
87.5	1.79	72.388	0.901	5.973	0.057
92.5	1.23	71.664	0.868	6.044	0.057
97.5	1.33	71.214	0.871	6.024	0.056
102.5	1.20	72.013	0.847	5.790	0.054
107.5	0.94	72.313	0.841	5.627	0.056
112.5	0.85	72.438	0.884	5.694	0.062
117.5	0.85	74.061	0.882	5.714	0.061
122.5	0.92	72.688	0.870	5.397	0.066
127.5	0.86	72.987	0.832	5.808	0.059
132.5	0.87	72.788	0.728	6.939	0.050
137.5	1.02	70.990	0.789	7.633	0.058
142.5	0.93	67.544	0.780	8.312	0.054
147.5	0.81	71.439	0.725	8.284	0.054
152.5	0.61	72.238	0.737	8.465	0.050
159.0	0.81	71.264	0.823	9.240	0.052

Table C.3.4 Geochemical data from core P6 (Pedersen, 1979).

Depth(cm)	Si(Wt.%)	Al(Wt.%)	Fe(Wt.%)	Mg(Wt.%)	Ca(Wt.%)	Na(Wt.%)	K(Wt.%)	Ti(Wt.%)	Mn(Wt.%)	P(Wt.%)
1	0.622	0.148	0.266	0.211	36.758	1.016	0.0639	0.0120	0.0581	0.0319
10	0.533	0.159	0.224	0.247	36.815	1.521	0.0855	0.0126	0.0627	0.0279
11	0.687	0.138	0.168	0.193	36.372	1.031	0.0706	0.0102	0.0511	0.0279
20	0.603	0.127	0.147	0.193	37.066	0.964	0.0664	0.0096	0.0596	0.0262
30	0.696	0.159	0.182	0.187	36.544	0.935	0.0764	0.0108	0.0635	0.0249
40	0.944	0.227	0.245	0.205	36.186	0.927	0.0930	0.0138	0.1007	0.0305
50	1.491	0.354	0.378	0.241	35.507	1.002	0.1320	0.0216	0.1603	0.0423
60	1.402	0.333	0.357	0.259	35.593	1.053	0.1287	0.0222	0.1007	0.0410
70	1.454	0.365	0.378	0.296	35.021	1.224	0.1370	0.0246	0.1247	0.0428
80	1.468	0.365	0.392	0.277	35.385	1.150	0.1328	0.0252	0.0906	0.0428
90	1.524	0.386	0.406	0.277	35.536	1.076	0.1386	0.0264	0.0852	0.0445
100	1.514	0.381	0.413	0.284	35.493	1.046	0.1353	0.0264	0.0860	0.0436
110	1.505	0.381	0.399	0.265	35.571	0.979	0.1337	0.0258	0.1092	0.0436
120	1.528	0.376	0.413	0.259	35.493	1.098	0.1403	0.0270	0.1092	0.0445
130	1.533	0.386	0.406	0.296	35.314	1.202	0.1428	0.0264	0.1278	0.0419
140	1.533	0.386	0.406	0.296	35.407	1.157	0.1395	0.0258	0.0999	0.0428
150	1.510	0.386	0.406	0.308	34.863	1.165	0.1370	0.0252	0.1038	0.0423
160	1.542	0.381	0.399	0.271	35.300	1.128	0.1370	0.0252	0.0914	0.0432
170	1.398	0.349	0.364	0.277	33.848	1.046	0.1287	0.0246	0.0650	0.0393
180	1.505	0.391	0.392	0.320	37.087	1.261	0.1445	0.0264	0.1162	0.0445
190	1.510	0.376	0.392	0.277	35.557	1.016	0.1353	0.0270	0.0743	0.0428
200	1.496	0.518	0.392	0.296	35.443	1.551	0.2499	0.0276	0.0697	0.0428
210	1.486	0.661	0.378	0.284	35.714	1.128	0.1345	0.0276	0.0589	0.0423
219	1.491	0.402	0.364	0.277	35.679	1.016	0.1287	0.0276	0.0666	0.0428
230	1.486	0.381	0.371	0.271	35.679	1.002	0.1295	0.0282	0.0604	0.0432
238	1.505	0.370	0.364	0.277	35.536	1.076	0.1303	0.0282	0.0550	0.0428
250	1.430	0.370	0.364	0.265	35.843	1.039	0.1279	0.0258	0.0480	0.0432
260	1.393	0.344	0.350	0.271	35.757	1.046	0.1262	0.0252	0.0558	0.0415
270	1.388	0.349	0.364	0.277	35.786	1.113	0.1237	0.0246	0.0511	0.0419
280	1.341	0.328	0.308	0.332	33.140	1.180	0.1312	0.0456	0.0356	0.0410
300	1.253	0.307	0.301	0.271	35.850	1.180	0.1220	0.0240	0.0395	0.0428
310	1.066	0.270	0.280	0.241	36.444	0.972	0.0980	0.0210	0.0341	0.0432
320	0.790	0.201	0.203	0.235	36.551	0.927	0.0780	0.0186	0.0302	0.0454
330	0.701	0.185	0.175	0.284	35.850	1.113	0.0863	0.0533	0.0155	0.0406
340	0.495	0.122	0.154	0.217	36.930	0.979	0.0623	0.0108	0.0163	0.0336
350	0.608	0.138	0.203	0.217	36.815	0.994	0.0697	0.0132	0.0201	0.0327
360	0.514	0.122	0.182	0.229	36.444	1.002	0.0631	0.0162	0.0147	0.0240
370	0.379	0.085	0.140	0.217	36.908	1.031	0.0589	0.0096	0.0116	0.0240
381	0.411	0.095	0.140	0.187	37.151	1.024	0.0565	0.0096	0.0108	0.0214
390	0.435	0.106	0.168	0.187	36.815	1.002	0.0589	0.0114	0.0147	0.0214
400	0.393	0.111	0.147	0.205	37.209	0.950	0.0581	0.0102	0.0101	0.0223
410	0.388	0.095	0.147	0.193	37.194	1.009	0.0548	0.0108	0.0132	0.0218
420	0.481	0.116	0.161	0.175	37.051	0.950	0.0614	0.0096	0.0194	0.0227
430	0.294	0.074	0.126	0.175	37.344	1.024	0.0498	0.0078	0.0093	0.0148
440	0.299	0.069	0.119	0.199	37.273	0.979	0.0531	0.0072	0.0124	0.0166
450	0.374	0.085	0.133	0.193	37.416	1.031	0.0540	0.0090	0.0163	0.0201
460	0.346	0.079	0.161	0.205	37.016	1.024	0.0556	0.0084	0.0124	0.0175
472	0.360	0.079	0.126	0.211	36.901	1.061	0.0598	0.0072	0.0163	0.0179
480	0.341	0.085	0.119	0.199	36.007	1.039	0.0565	0.0078	0.0116	0.0157
490	0.280	0.063	0.112	0.193	36.894	1.046	0.0523	0.0066	0.0139	0.0135
500	0.313	0.069	0.119	0.175	37.180	0.913	0.0506	0.0072	0.0155	0.0148
509	0.285	0.063	0.112	0.187	36.751	0.935	0.0506	0.0060	0.0155	0.0144
520	0.280	0.063	0.105	0.169	36.772	0.816	0.0440	0.0066	0.0163	0.0157
530	0.294	0.074	0.119	0.169	37.530	0.868	0.0490	0.0072	0.0170	0.0153
540	0.318	0.074	0.119	0.145	36.436	0.816	0.0490	0.0078	0.0124	0.0118
550	0.262	0.063	0.098	0.163	37.645	0.801	0.0423	0.0066	0.0093	0.0118
560	0.425	0.095	0.140	0.181	37.416	0.824	0.0531	0.0096	0.0093	0.0170
570	0.823	0.185	0.182	0.205	36.308	0.964	0.0847	0.0114	0.0271	0.0314
580	1.047	0.254	0.245	0.217	36.522	0.950	0.0955	0.0144	0.0240	0.0327
590	1.528	0.344	0.483	0.241	35.421	0.942	0.1295	0.0198	0.0217	0.0436
600	0.846	0.196	0.203	0.157	37.173	0.734	0.0814	0.0126	0.0627	0.0380
610	1.061	0.233	0.294	0.193	36.651	0.861	0.0955	0.0168	0.0379	0.0332
620	1.042	0.249	0.329	0.181	36.594	0.809	0.0980	0.0156	0.1107	0.0367
630	1.169	0.280	0.469	0.223	36.065	0.742	0.1088	0.0198	0.1487	0.0659
640	0.977	0.238	0.343	0.205	36.200	0.853	0.0946	0.0228	0.1231	0.0812
650	2.099	0.529	0.497	0.320	34.849	0.964	0.1611	0.0701	0.1224	0.0851
660	8.226	3.275	2.168	1.279	26.398	1.692	0.4823	0.3710	0.1293	0.1178
670	16.915	6.607	4.253	2.612	14.286	2.752	1.0270	0.8799	0.1169	0.1737
680	15.751	6.057	3.882	2.443	15.966	2.649	0.9456	0.8020	0.0968	0.1602
690	21.636	8.797	5.512	3.499	7.858	3.250	1.2793	1.1904	0.1162	0.2108
700	19.902	8.152	5.120	3.312	10.339	3.168	1.1482	1.0388	0.1239	0.1842
710	17.242	6.729	4.428	2.708	14.207	2.671	0.9946	0.8937	0.1092	0.1663
720	11.708	4.131	2.658	1.611	21.614	2.307	0.7654	0.5784	0.0674	0.1318

Table C.4.1-1 Salt included major element data from core CD3814.

Depth(cm)	Si(Wt.%)	Al(Wt.%)	Fe(Wt.%)	Mg(Wt.%)	Ca(Wt.%)	Na(Wt.%)	K(Wt.%)	Ti(Wt.%)	Mn(Wt.%)	P(Wt.%)	SALT
1	0.638	0.152	0.273	0.118	37.702	0.231	0.0364	0.0123	0.0596	0.0327	2.587
10	0.549	0.164	0.231	0.141	37.915	0.623	0.0542	0.0130	0.0647	0.0288	2.994
11	0.709	0.142	0.173	0.083	37.479	0.101	0.0382	0.0105	0.0527	0.0288	3.050
20	0.622	0.131	0.151	0.085	38.171	0.051	0.0346	0.0099	0.0615	0.0270	2.991
30	0.717	0.163	0.187	0.085	37.570	0.073	0.0466	0.0111	0.0653	0.0256	2.823
40	0.970	0.234	0.251	0.110	37.136	0.122	0.0657	0.0142	0.1034	0.0314	2.642
50	1.532	0.364	0.388	0.146	36.448	0.190	0.1055	0.0222	0.1647	0.0435	2.670
60	1.449	0.344	0.369	0.144	36.750	0.059	0.0960	0.0229	0.1041	0.0424	3.256
70	1.511	0.379	0.393	0.162	36.348	0.071	0.0992	0.0255	0.1296	0.0444	3.776
80	1.524	0.379	0.407	0.145	36.704	0.014	0.0955	0.0261	0.0941	0.0444	3.714
90	1.582	0.401	0.421	0.146	36.858	0.000	0.1016	0.0274	0.0885	0.0462	3.708
100	1.564	0.393	0.426	0.173	36.606	0.087	0.1040	0.0272	0.0887	0.0451	3.144
110	1.557	0.394	0.412	0.148	36.750	0.000	0.1005	0.0267	0.1129	0.0451	3.316
120	1.584	0.389	0.428	0.134	36.746	0.020	0.1052	0.0280	0.1132	0.0461	3.526
130	1.592	0.401	0.421	0.165	36.626	0.071	0.1060	0.0274	0.1327	0.0435	3.703
140	1.601	0.403	0.424	0.146	36.912	0.000	0.0972	0.0269	0.1043	0.0446	4.216
150	1.571	0.402	0.422	0.171	36.221	0.000	0.0981	0.0262	0.1080	0.0440	3.877
160	1.605	0.396	0.415	0.133	36.681	0.000	0.0980	0.0262	0.0951	0.0450	3.894
170	1.451	0.362	0.378	0.147	35.090	0.000	0.0917	0.0255	0.0675	0.0408	3.666
180	1.564	0.407	0.407	0.188	38.483	0.120	0.1073	0.0274	0.1207	0.0462	3.745
190	1.567	0.390	0.407	0.148	36.860	0.000	0.0987	0.0280	0.0772	0.0444	3.654
200	1.553	0.538	0.407	0.164	36.762	0.431	0.2171	0.0286	0.0724	0.0444	3.711
210	1.536	0.683	0.390	0.170	36.857	0.152	0.1025	0.0285	0.0608	0.0437	3.205
219	1.546	0.417	0.377	0.151	36.956	0.000	0.0927	0.0286	0.0691	0.0444	3.573
230	1.536	0.394	0.383	0.158	36.824	0.019	0.0973	0.0291	0.0624	0.0446	3.214
238	1.554	0.382	0.375	0.167	36.645	0.122	0.0990	0.0291	0.0568	0.0441	3.129
250	1.477	0.382	0.376	0.154	36.969	0.077	0.0962	0.0266	0.0496	0.0446	3.149
260	1.437	0.355	0.361	0.163	36.853	0.109	0.0953	0.0260	0.0575	0.0428	3.073
270	1.431	0.360	0.375	0.171	36.860	0.197	0.0934	0.0253	0.0527	0.0432	3.013
280	1.383	0.338	0.317	0.227	34.131	0.267	0.1011	0.0470	0.0367	0.0423	3.009
300	1.287	0.315	0.309	0.177	36.809	0.365	0.0950	0.0246	0.0406	0.0440	3.264
310	1.102	0.279	0.289	0.125	37.633	0.000	0.0642	0.0217	0.0352	0.0447	2.943
320	0.814	0.207	0.209	0.130	37.623	0.028	0.0471	0.0191	0.0311	0.0468	2.611
330	0.720	0.190	0.180	0.192	36.779	0.322	0.0592	0.0548	0.0159	0.0417	2.924
340	0.510	0.125	0.159	0.112	38.006	0.087	0.0310	0.0111	0.0168	0.0346	3.016
350	0.627	0.142	0.209	0.109	37.923	0.074	0.0377	0.0136	0.0208	0.0337	3.052
360	0.530	0.126	0.188	0.120	37.553	0.070	0.0304	0.0167	0.0152	0.0248	2.952
370	0.390	0.087	0.144	0.111	37.994	0.132	0.0273	0.0099	0.0120	0.0247	3.020
381	0.424	0.098	0.144	0.078	38.271	0.103	0.0240	0.0099	0.0112	0.0220	3.177
390	0.449	0.109	0.173	0.072	37.984	0.030	0.0248	0.0118	0.0152	0.0221	2.809
400	0.404	0.114	0.151	0.104	38.249	0.093	0.0280	0.0105	0.0104	0.0229	2.982
410	0.400	0.098	0.151	0.085	38.301	0.099	0.0227	0.0111	0.0136	0.0225	2.949
420	0.496	0.120	0.166	0.068	38.141	0.049	0.0299	0.0099	0.0199	0.0234	2.625
430	0.302	0.076	0.129	0.080	38.319	0.226	0.0215	0.0080	0.0095	0.0152	2.984
440	0.308	0.071	0.123	0.091	38.383	0.068	0.0209	0.0074	0.0128	0.0171	2.987
450	0.385	0.087	0.137	0.085	38.531	0.121	0.0218	0.0093	0.0168	0.0207	2.941
460	0.356	0.082	0.166	0.099	38.101	0.128	0.0240	0.0086	0.0128	0.0180	3.079
472	0.371	0.082	0.130	0.100	38.035	0.123	0.0267	0.0074	0.0168	0.0185	3.099
480	0.352	0.087	0.123	0.087	37.120	0.093	0.0231	0.0080	0.0120	0.0162	3.229
490	0.290	0.066	0.116	0.076	38.085	0.060	0.0173	0.0068	0.0144	0.0140	2.970
500	0.323	0.071	0.123	0.067	38.281	0.004	0.0185	0.0074	0.0160	0.0153	2.840
509	0.293	0.065	0.115	0.084	37.790	0.068	0.0200	0.0062	0.0159	0.0148	2.720
520	0.288	0.065	0.108	0.070	37.767	0.000	0.0145	0.0068	0.0167	0.0161	2.223
530	0.301	0.076	0.122	0.089	38.356	0.192	0.0251	0.0074	0.0174	0.0156	2.228
540	0.325	0.076	0.122	0.064	37.239	0.137	0.0250	0.0080	0.0127	0.0121	2.006
550	0.267	0.065	0.100	0.090	38.391	0.191	0.0207	0.0067	0.0095	0.0120	2.222
560	0.435	0.097	0.143	0.101	38.239	0.147	0.0293	0.0098	0.0095	0.0174	2.356
570	0.842	0.190	0.186	0.121	37.155	0.249	0.0602	0.0117	0.0278	0.0322	2.745
580	1.077	0.261	0.252	0.119	37.519	0.113	0.0671	0.0148	0.0247	0.0337	2.710
590	1.571	0.353	0.496	0.145	36.374	0.116	0.1025	0.0203	0.0223	0.0449	2.513
600	0.868	0.201	0.208	0.065	38.100	0.000	0.0551	0.0129	0.0643	0.0389	2.023
610	1.083	0.238	0.300	0.121	37.383	0.246	0.0747	0.0171	0.0387	0.0339	2.322
620	1.067	0.255	0.337	0.097	37.435	0.101	0.0741	0.0160	0.1134	0.0375	2.038
630	1.193	0.286	0.478	0.151	36.790	0.121	0.0881	0.0202	0.1518	0.0673	2.115
640	0.998	0.243	0.350	0.130	36.957	0.210	0.0729	0.0233	0.1258	0.0829	2.008
650	2.142	0.540	0.507	0.250	35.539	0.357	0.1418	0.0716	0.1249	0.0868	2.433
660	8.431	3.356	2.223	1.218	27.026	0.971	0.4669	0.3803	0.1325	0.1208	2.531
670	17.354	6.779	4.363	2.584	14.625	2.029	1.0251	0.9028	0.1200	0.1782	2.800
680	16.205	6.232	3.994	2.407	16.391	1.843	0.9412	0.8251	0.0996	0.1648	2.804
690	22.260	9.051	5.671	3.493	8.050	2.461	1.2845	1.2247	0.1195	0.2169	2.160
700	20.341	8.332	5.233	3.303	10.541	2.562	1.1492	1.0617	0.1266	0.1882	2.459
710	17.677	6.899	4.539	2.683	14.535	1.967	0.9919	0.9162	0.1119	0.1705	2.545
720	12.014	4.239	2.728	1.556	22.148	1.568	0.7567	0.5935	0.0691	0.1352	3.189

Table C.4.1-2 Salt free major element data from core CD3814.

Depth(cm)	Si/Al	Fe/Al	Mg/Al	Ca/Al	Ti/Al	Mn/Al	P/Al	K/Al	Na/Al	Fe/Ti	K/Rb
1	4.197	1.795	0.779	247.955	0.081	0.392	0.215	0.239	1.518	22.173	0.0099
10	3.358	1.410	0.860	231.754	0.079	0.395	0.176	0.331	3.811	17.783	0.0170
11	4.995	1.221	0.583	264.181	0.074	0.372	0.203	0.269	0.712	16.475	0.0137
20	4.749	1.157	0.649	291.664	0.076	0.470	0.206	0.264	0.388	15.317	0.0108
30	4.388	1.146	0.520	230.055	0.068	0.400	0.157	0.286	0.448	16.857	0.0126
40	4.151	1.076	0.472	158.942	0.061	0.443	0.134	0.281	0.523	17.759	0.0213
50	4.207	1.066	0.402	100.090	0.061	0.452	0.119	0.290	0.521	17.505	0.0218
60	4.207	1.070	0.417	106.681	0.067	0.302	0.123	0.279	0.171	16.086	0.0216
70	3.982	1.035	0.427	95.820	0.067	0.342	0.117	0.261	0.188	15.370	0.0191
80	4.021	1.073	0.384	96.821	0.069	0.248	0.117	0.252	0.037	15.560	0.0192
90	3.946	1.051	0.363	91.905	0.068	0.221	0.115	0.253	0.000	15.383	0.0175
100	3.976	1.084	0.439	93.087	0.069	0.226	0.115	0.264	0.221	15.648	0.0210
110	3.951	1.047	0.375	93.288	0.068	0.287	0.115	0.255	0.000	15.470	0.0168
120	4.069	1.099	0.343	94.386	0.072	0.291	0.119	0.270	0.051	15.301	0.0211
130	3.970	1.051	0.411	91.331	0.068	0.331	0.108	0.264	0.178	15.383	0.0204
140	3.970	1.051	0.361	91.556	0.067	0.259	0.111	0.241	0.000	15.741	0.0176
150	3.909	1.051	0.425	90.159	0.065	0.269	0.110	0.244	0.000	16.116	0.0178
160	4.050	1.047	0.334	92.556	0.066	0.240	0.113	0.247	0.000	15.838	0.0165
170	4.003	1.042	0.406	96.821	0.070	0.186	0.112	0.253	0.000	14.801	0.0177
180	3.845	1.001	0.463	94.626	0.067	0.297	0.114	0.264	0.294	14.853	0.0188
190	4.020	1.043	0.379	94.553	0.072	0.198	0.114	0.253	0.000	14.523	0.0227
200	2.885	0.756	0.305	68.281	0.053	0.134	0.082	0.403	0.800	14.207	0.0367
210	2.248	0.571	0.249	53.952	0.042	0.089	0.064	0.150	0.222	13.700	0.0216
219	3.709	0.905	0.361	88.637	0.069	0.166	0.106	0.222	****	13.192	0.0218
230	3.902	0.973	0.400	93.573	0.074	0.159	0.113	0.247	0.047	13.160	0.0214
238	4.064	0.982	0.437	95.863	0.076	0.148	0.115	0.259	0.319	12.911	0.0209
250	3.862	0.982	0.402	96.692	0.070	0.130	0.117	0.252	0.203	14.113	0.0194
260	4.051	1.017	0.459	103.883	0.073	0.162	0.121	0.269	0.307	13.893	0.0189
270	3.976	1.042	0.475	102.393	0.070	0.146	0.120	0.259	0.547	14.801	0.0185
280	4.090	0.938	0.672	100.933	0.139	0.109	0.125	0.299	0.789	6.756	*****
300	4.083	0.980	0.560	116.739	0.078	0.129	0.139	0.301	1.159	12.545	0.0289
310	3.950	1.037	0.447	134.936	0.078	0.126	0.160	0.230	****	13.337	0.0255
320	3.929	1.009	0.629	181.651	0.092	0.150	0.226	0.227	0.134	10.917	0.0142
330	3.787	0.945	1.010	193.458	0.288	0.084	0.219	0.311	1.696	3.278	0.0143
340	4.072	1.265	0.895	303.235	0.089	0.134	0.276	0.247	0.694	14.263	0.0274
350	4.418	1.475	0.768	267.407	0.096	0.146	0.238	0.266	0.519	15.383	0.0081
360	4.226	1.495	0.956	299.227	0.133	0.121	0.197	0.243	0.555	11.238	0.0166
370	4.473	1.653	1.275	435.644	0.113	0.137	0.284	0.313	1.512	14.588	0.0092
381	4.320	1.469	0.790	389.783	0.101	0.114	0.225	0.244	1.046	14.588	0.0083
390	4.109	1.587	0.656	347.611	0.108	0.139	0.202	0.227	0.279	14.741	0.0097
400	3.534	1.322	0.911	334.638	0.092	0.091	0.200	0.245	0.811	14.416	0.0086
410	4.074	1.543	0.868	390.239	0.113	0.138	0.229	0.231	1.012	13.615	0.0097
420	4.137	1.382	0.566	318.061	0.082	0.166	0.195	0.249	0.407	16.776	0.0122
430	3.976	1.700	1.050	503.820	0.105	0.125	0.200	0.283	2.977	16.158	0.0116
440	4.350	1.729	1.289	541.474	0.105	0.180	0.241	0.295	0.961	16.533	0.0099
450	4.418	1.570	0.975	441.636	0.106	0.192	0.237	0.249	1.386	14.782	0.0078
460	4.359	2.028	1.213	466.040	0.106	0.156	0.220	0.293	1.562	19.172	0.0096
472	4.536	1.587	1.225	464.577	0.091	0.205	0.225	0.326	1.496	17.505	0.0075
480	4.031	1.405	0.997	424.979	0.092	0.137	0.186	0.264	1.069	15.261	0.0092
490	4.418	1.763	1.158	580.580	0.104	0.220	0.213	0.264	0.912	16.975	0.0093
500	4.554	1.729	0.946	540.124	0.105	0.225	0.216	0.261	0.054	16.533	0.0051
509	4.491	1.763	1.290	578.401	0.094	0.244	0.227	0.306	1.034	18.672	0.0082
520	4.418	1.653	1.075	578.762	0.104	0.256	0.247	0.222	-0.254	15.914	0.0084
530	3.976	1.606	1.170	506.396	0.097	0.230	0.206	0.331	2.535	16.533	0.0059
540	4.292	1.606	0.842	491.624	0.105	0.167	0.159	0.331	1.815	15.261	0.0164
550	4.123	1.543	1.396	592.638	0.104	0.146	0.186	0.319	2.953	14.853	0.0112
560	4.467	1.469	1.037	392.662	0.101	0.098	0.179	0.301	1.507	14.588	0.0126
570	4.443	0.982	0.637	195.946	0.062	0.146	0.170	0.317	1.316	15.969	0.0106
580	4.123	0.964	0.455	143.704	0.057	0.095	0.129	0.257	0.432	17.019	0.0167
590	4.445	1.404	0.410	102.919	0.058	0.063	0.127	0.290	0.329	24.401	0.0142
600	4.322	1.036	0.326	189.765	0.064	0.320	0.194	0.274	0.000	16.116	0.0178
610	4.558	1.262	0.508	157.358	0.072	0.163	0.142	0.315	1.037	17.505	0.0180
620	4.192	1.322	0.382	147.069	0.063	0.445	0.147	0.291	0.395	21.096	0.0170
630	4.168	1.672	0.527	128.545	0.071	0.530	0.235	0.308	0.422	23.694	0.0186
640	4.104	1.440	0.533	151.964	0.096	0.517	0.341	0.300	0.865	15.048	0.0233
650	3.967	0.939	0.464	65.832	0.133	0.231	0.161	0.263	0.662	7.082	0.0183
660	2.512	0.662	0.363	8.053	0.113	0.039	0.036	0.139	0.289	5.844	0.0266
670	2.560	0.644	0.381	2.158	0.133	0.018	0.026	0.151	0.299	4.833	0.0389
680	2.601	0.641	0.386	2.630	0.132	0.016	0.026	0.151	0.296	4.841	0.0377
690	2.459	0.627	0.386	0.889	0.135	0.013	0.024	0.142	0.272	4.630	0.0396
700	2.441	0.628	0.396	1.265	0.127	0.015	0.023	0.138	0.308	4.929	0.0392
710	2.562	0.658	0.389	2.107	0.133	0.016	0.025	0.144	0.285	4.954	0.0395
720	2.834	0.643	0.367	5.224	0.140	0.016	0.032	0.178	0.370	4.595	0.0408

Table C.4.1-3 Salt free major elements and their ratios in core CD3814.

Depth(cm)	Age(ka)	Si(Wt.%)	Al(Wt.%)	Fe(Wt.%)	Mg(Wt.%)	Ca(Wt.%)	Na(Wt.%)	K(Wt.%)	Ti(Wt.%)	Mn(Wt.%)	P(Wt.%)
1	0.20	4.076	0.905	0.720	0.422	31.031	1.795	0.203	0.0486	0.552	0.0524
10	2.00	3.627	1.164	0.553	0.428	31.846	1.996	0.193	0.0414	0.221	0.0441
20	4.00	3.613	0.846	0.616	0.422	31.896	1.884	0.201	0.0408	0.028	0.0432
21	4.20	4.015	0.846	0.609	0.434	30.223	1.936	0.203	0.0432	0.488	0.0467
30	6.00	3.889	0.751	0.672	0.428	31.288	1.870	0.203	0.0378	0.053	0.0423
40	8.00	3.744	0.735	0.497	0.422	31.267	1.840	0.215	0.0384	0.025	0.0388
50	10.67	4.197	0.831	0.706	0.470	30.638	2.241	0.291	0.0420	0.031	0.0454
60	12.47	3.566	0.762	0.532	0.434	31.145	1.914	0.224	0.0426	0.028	0.0493
70	13.41	3.805	0.873	0.490	0.422	30.802	1.751	0.235	0.0468	0.033	0.0532
80	14.34	3.585	0.630	0.399	0.428	31.217	2.137	0.211	0.0336	0.045	0.0467
90	15.28	5.212	0.778	0.546	0.561	32.797	2.545	0.242	0.0408	0.060	0.0572
100	16.22	4.833	0.688	0.574	0.464	29.530	2.107	0.209	0.0354	0.057	0.0519
110	17.16	4.632	0.592	0.462	0.422	30.373	2.077	0.185	0.0300	0.088	0.0441
119	18.00	5.955	0.815	0.546	0.531	27.842	2.723	0.224	0.0336	0.091	0.0515
140	20.07	6.118	0.751	0.651	0.513	28.157	2.292	0.240	0.0390	0.092	0.0511
150	21.05	5.800	0.645	0.441	0.440	29.236	2.011	0.205	0.0342	0.074	0.0463
160	22.03	5.796	0.756	0.581	0.464	29.065	1.936	0.232	0.0396	0.170	0.0528
170	23.02	5.384	0.693	0.623	0.489	29.594	1.929	0.222	0.0366	0.095	0.0480
180	24.00	4.225	0.677	0.469	0.392	31.274	1.714	0.210	0.0354	0.090	0.0471
190	26.92	5.768	0.667	0.518	0.483	29.108	2.404	0.233	0.0348	0.097	0.0480
200	29.83	3.791	0.677	0.630	0.434	31.539	1.617	0.218	0.0354	0.071	0.0493
210	32.75	3.590	0.682	0.553	0.398	31.868	1.580	0.213	0.0348	0.096	0.0489
220	35.67	4.146	0.762	0.567	0.410	31.353	1.654	0.226	0.0402	0.084	0.0506
230	38.58	4.646	0.788	0.686	0.458	30.859	1.551	0.236	0.0414	0.080	0.0554
240	41.50	5.324	0.825	0.567	0.470	29.808	1.862	0.249	0.0420	0.115	0.0563
250	44.42	6.146	0.778	0.497	0.458	29.000	1.847	0.229	0.0390	0.171	0.0559
260	47.33	4.529	0.783	0.525	0.428	30.881	1.758	0.232	0.0366	0.139	0.0528
270	50.25	4.394	0.677	0.532	0.410	31.188	1.729	0.210	0.0348	0.117	0.0484
280	53.17	4.464	0.783	0.602	0.428	31.124	1.588	0.247	0.0390	0.098	0.0502
290	56.08	4.838	0.931	0.602	0.434	30.130	1.625	0.278	0.0456	0.110	0.0524
300	59.00	5.455	1.074	0.727	0.458	29.715	1.766	0.341	0.0515	0.118	0.0559
310	60.67	5.207	0.989	0.706	0.440	29.966	1.647	0.321	0.0480	0.115	0.0532
320	62.33	6.908	1.174	1.434	0.615	26.827	2.611	0.474	0.0551	0.218	0.0576
330	64.00	7.422	1.185	1.588	0.573	27.284	1.847	0.489	0.0509	0.211	0.0620
340	68.67	7.025	1.296	0.783	0.470	27.921	1.847	0.470	0.0521	0.180	0.0598
350	72.29	6.861	1.275	0.616	0.422	28.328	1.899	0.486	0.0444	0.158	0.0519
360	74.86	8.885	1.635	0.567	0.392	25.776	1.944	0.716	0.0438	0.186	0.0436
370	77.43	10.708	1.989	0.602	0.392	24.424	1.884	0.887	0.0468	0.150	0.0419
380	80.00	8.965	1.682	0.630	0.386	26.305	1.714	0.710	0.0474	0.204	0.0476
390	81.67	13.957	2.507	0.783	0.374	19.856	2.122	1.249	0.0462	0.118	0.0332
400	83.33	4.786	1.005	0.672	0.428	30.466	1.603	0.292	0.0474	0.229	0.0554
410	85.00	3.931	0.862	0.539	0.404	31.181	1.476	0.227	0.0432	0.225	0.0563
420	86.67	4.235	0.862	0.706	0.428	31.281	1.476	0.245	0.0444	0.230	0.0576
430	88.33	4.136	0.804	0.776	0.428	31.582	1.558	0.237	0.0426	0.184	0.0554
440	90.00	3.739	0.725	0.616	0.368	30.967	1.432	0.208	0.0378	0.148	0.0484
450	*****	3.921	0.767	0.574	0.404	32.061	1.476	0.213	0.0408	0.116	0.0476
460	*****	4.291	0.889	0.609	0.392	31.131	1.484	0.243	0.0456	0.110	0.0497
470	*****	3.903	0.809	0.658	0.398	31.946	1.439	0.220	0.0432	0.089	0.0449
480	*****	4.534	0.688	0.448	0.326	32.018	1.335	0.210	0.0378	0.070	0.0471
490	*****	4.674	0.386	0.357	0.253	32.697	1.053	0.145	0.0246	0.074	0.0502
500	*****	4.235	0.344	0.301	0.271	33.169	1.083	0.140	0.0222	0.075	0.0476
510	*****	4.347	0.365	0.301	0.235	32.933	1.068	0.132	0.0246	0.060	0.0463
520	*****	3.646	0.328	0.266	0.259	33.469	1.091	0.121	0.0240	0.052	0.0445
530	*****	4.249	0.370	0.329	0.265	32.876	1.246	0.141	0.0294	0.044	0.0445
540	*****	6.029	0.899	1.070	0.483	30.287	1.439	0.191	0.2080	0.057	0.0506
550	*****	7.525	0.651	0.881	0.416	28.879	1.558	0.196	0.1325	0.045	0.0397
560	*****	7.044	0.386	0.434	0.296	29.723	1.417	0.148	0.0498	0.037	0.0336
570	*****	6.296	0.333	0.273	0.247	29.508	1.239	0.133	0.0372	0.039	0.0367
580	*****	5.646	0.354	0.350	0.235	31.675	1.113	0.134	0.0330	0.039	0.0384
590	*****	6.202	0.397	0.273	0.265	31.903	1.261	0.146	0.0294	0.034	0.0384
600	*****	6.642	0.667	0.392	0.241	30.473	1.358	0.289	0.0324	0.034	0.0367
610	*****	13.213	2.079	0.825	0.211	22.937	1.818	0.971	0.0581	0.043	0.0284
620	*****	4.431	0.582	0.399	0.253	32.640	1.165	0.226	0.0348	0.035	0.0449

Table C.4.2-1 Salt included major element data from core CD3822.

Depth(cm)	Age(ka)	Si(Wt.%)	Al(Wt.%)	Fe(Wt.%)	Mg(Wt.%)	Ca(Wt.%)	Na(Wt.%)	K(Wt.%)	Ti(Wt.%)	Mn(Wt.%)	P(Wt.%)	SALT
1	0.20	4.264	0.946	0.754	0.271	32.411	0.462	0.162	0.0508	0.578	0.0548	4.423
10	2.00	3.806	1.221	0.580	0.267	33.358	0.584	0.148	0.0434	0.232	0.0463	4.702
20	4.00	3.790	0.888	0.646	0.261	33.404	0.474	0.157	0.0428	0.029	0.0453	4.682
21	4.20	4.239	0.894	0.643	0.252	31.845	0.335	0.153	0.0456	0.515	0.0493	5.291
30	6.00	4.092	0.790	0.707	0.258	32.858	0.371	0.156	0.0397	0.056	0.0445	4.957
40	8.00	3.950	0.776	0.524	0.242	32.925	0.254	0.166	0.0405	0.026	0.0410	5.225
50	10.67	4.426	0.876	0.745	0.294	32.244	0.693	0.246	0.0442	0.033	0.0479	5.175
60	12.47	3.762	0.804	0.561	0.255	32.793	0.336	0.176	0.0449	0.029	0.0520	5.215
70	13.41	3.998	0.917	0.515	0.256	32.308	0.283	0.191	0.0491	0.034	0.0559	4.841
80	14.34	3.792	0.666	0.422	0.239	32.953	0.491	0.159	0.0355	0.048	0.0494	5.467
90	15.28	5.573	0.832	0.583	0.343	34.986	0.601	0.183	0.0436	0.064	0.0611	6.480
100	16.22	5.152	0.733	0.611	0.251	31.400	0.225	0.150	0.0377	0.060	0.0554	6.195
110	17.16	4.912	0.628	0.490	0.224	32.137	0.353	0.130	0.0318	0.093	0.0467	5.701
119	18.00	6.469	0.885	0.593	0.257	30.144	0.315	0.148	0.0365	0.099	0.0559	7.951
140	20.07	6.561	0.806	0.698	0.282	30.108	0.243	0.178	0.0418	0.099	0.0548	6.750
150	21.05	6.177	0.687	0.469	0.229	31.055	0.156	0.147	0.0364	0.078	0.0493	6.091
160	22.03	6.164	0.805	0.617	0.259	30.835	0.115	0.177	0.0421	0.181	0.0562	5.974
170	23.02	5.712	0.735	0.660	0.294	31.319	0.187	0.168	0.0388	0.101	0.0509	5.726
180	24.00	4.510	0.723	0.500	0.169	33.302	0.000	0.150	0.0377	0.096	0.0503	6.318
190	26.92	6.100	0.705	0.547	0.297	30.716	0.779	0.183	0.0368	0.102	0.0508	5.449
200	29.83	3.974	0.710	0.660	0.276	33.009	0.213	0.176	0.0371	0.075	0.0517	4.622
210	32.75	3.760	0.715	0.579	0.242	33.322	0.204	0.171	0.0364	0.101	0.0512	4.527
220	35.67	4.344	0.798	0.594	0.253	32.797	0.268	0.184	0.0421	0.088	0.0530	4.572
230	38.58	4.852	0.823	0.716	0.315	32.172	0.265	0.198	0.0432	0.083	0.0579	4.237
240	41.50	5.595	0.867	0.595	0.306	31.268	0.396	0.206	0.0441	0.120	0.0592	4.853
250	44.42	6.495	0.822	0.525	0.275	30.576	0.218	0.180	0.0412	0.181	0.0590	5.364
260	47.33	4.749	0.821	0.550	0.269	32.325	0.355	0.189	0.0383	0.145	0.0554	4.640
270	50.25	4.616	0.711	0.559	0.243	32.709	0.265	0.165	0.0365	0.123	0.0509	4.825
280	53.17	4.670	0.819	0.629	0.277	32.507	0.247	0.208	0.0408	0.103	0.0525	4.417
290	56.08	5.058	0.973	0.629	0.286	31.447	0.306	0.241	0.0476	0.115	0.0548	4.353
300	59.00	5.701	1.122	0.760	0.312	31.001	0.466	0.307	0.0539	0.124	0.0584	4.315
310	60.67	5.443	1.034	0.739	0.292	31.271	0.334	0.286	0.0501	0.120	0.0557	4.340
320	62.33	7.260	1.234	1.507	0.458	28.132	1.186	0.442	0.0580	0.230	0.0605	4.846
330	64.00	7.729	1.234	1.654	0.444	28.363	0.659	0.464	0.0531	0.219	0.0645	3.970
340	68.67	7.351	1.356	0.820	0.321	29.159	0.514	0.441	0.0546	0.188	0.0626	4.430
350	72.29	7.190	1.336	0.645	0.265	29.626	0.527	0.456	0.0465	0.166	0.0544	4.564
360	74.86	9.270	1.705	0.591	0.249	26.840	0.703	0.700	0.0457	0.194	0.0455	4.150
370	77.43	11.166	2.074	0.627	0.251	25.418	0.656	0.878	0.0488	0.157	0.0437	4.102
380	80.00	9.312	1.747	0.654	0.258	27.278	0.594	0.695	0.0492	0.212	0.0494	3.731
390	81.67	14.521	2.609	0.815	0.240	20.610	0.971	1.255	0.0480	0.123	0.0345	3.885
400	83.33	4.996	1.049	0.701	0.285	31.746	0.334	0.257	0.0494	0.239	0.0578	4.190
410	85.00	4.094	0.898	0.561	0.268	32.424	0.269	0.191	0.0449	0.235	0.0586	3.981
420	86.67	4.404	0.897	0.735	0.297	32.486	0.310	0.211	0.0461	0.239	0.0599	3.851
430	88.33	4.305	0.837	0.808	0.295	32.821	0.373	0.202	0.0443	0.192	0.0577	3.919
440	90.00	3.886	0.753	0.640	0.237	32.138	0.284	0.172	0.0392	0.154	0.0503	3.786
450	*****	4.075	0.797	0.596	0.275	33.267	0.338	0.179	0.0424	0.121	0.0494	3.762
460	*****	4.458	0.923	0.632	0.263	32.297	0.350	0.210	0.0473	0.114	0.0517	3.749
470	*****	4.054	0.841	0.683	0.270	33.137	0.310	0.186	0.0448	0.093	0.0467	3.728
480	*****	4.683	0.710	0.462	0.215	33.033	0.372	0.181	0.0390	0.072	0.0487	3.188
490	*****	4.808	0.397	0.367	0.154	33.601	0.205	0.118	0.0253	0.076	0.0516	2.792
500	*****	4.363	0.354	0.310	0.168	34.135	0.191	0.111	0.0228	0.077	0.0490	2.933
510	*****	4.473	0.376	0.310	0.134	33.857	0.208	0.104	0.0253	0.061	0.0476	2.830
520	*****	3.752	0.338	0.274	0.159	34.409	0.231	0.093	0.0247	0.053	0.0458	2.830
530	*****	4.373	0.381	0.338	0.165	33.803	0.387	0.113	0.0302	0.045	0.0458	2.845
540	*****	6.215	0.927	1.103	0.383	31.183	0.541	0.163	0.2144	0.059	0.0522	2.989
550	*****	7.850	0.679	0.919	0.275	30.073	0.305	0.157	0.1382	0.047	0.0414	4.135
560	*****	7.330	0.402	0.451	0.157	30.884	0.229	0.109	0.0518	0.039	0.0350	3.912
570	*****	6.557	0.347	0.284	0.104	30.682	0.021	0.093	0.0387	0.040	0.0382	3.982
580	*****	5.830	0.366	0.361	0.122	32.667	0.153	0.102	0.0340	0.041	0.0397	3.153
590	*****	6.426	0.411	0.283	0.141	33.013	0.201	0.112	0.0304	0.035	0.0398	3.487
600	*****	6.856	0.688	0.404	0.130	31.418	0.414	0.263	0.0334	0.035	0.0378	3.126
610	*****	13.584	2.137	0.849	0.113	23.548	1.009	0.967	0.0598	0.044	0.0292	2.732
620	*****	4.547	0.597	0.409	0.163	33.464	0.393	0.203	0.0357	0.036	0.0461	2.556

Table C.4.2-2 Salt free major element data from core CD3822.

Depth(cm)	Age(ka)	Si/Al	Ca/Al	Fe/Al	Mg/Al	Ti/Al	Mn/Al	P/Al	K/Al	Na/Al	Siterrig/Al	Fe/Ti	K/Rb
1	0.20	4.506	34.245	0.796	0.286	0.0537	0.6104	0.0579	0.171	0.489	2.422	14.840	0.0238
10	2.00	3.117	27.315	0.475	0.219	0.0355	0.1903	0.0379	0.121	0.479	1.619	13.361	0.0188
20	4.00	4.269	37.618	0.727	0.294	0.0482	0.0329	0.0510	0.177	0.534	2.325	15.102	0.0241
21	4.20	4.744	35.633	0.719	0.282	0.0510	0.5764	0.0552	0.172	0.375	2.528	14.101	0.0186
30	6.00	5.177	41.573	0.894	0.326	0.0503	0.0711	0.0564	0.197	0.470	2.870	17.783	0.0260
40	8.00	5.092	42.437	0.675	0.311	0.0522	0.0337	0.0528	0.214	0.328	2.829	12.946	0.0190
50	10.67	5.054	36.815	0.851	0.336	0.0505	0.0373	0.0546	0.281	0.791	3.075	16.838	0.0241
60	12.47	4.682	40.804	0.698	0.317	0.0559	0.0366	0.0647	0.219	0.418	2.846	12.492	0.0185
70	13.41	4.359	35.223	0.561	0.279	0.0536	0.0373	0.0610	0.208	0.309	2.331	10.473	0.0149
80	14.34	5.695	49.485	0.633	0.359	0.0533	0.0713	0.0742	0.239	0.737	2.916	11.878	0.0154
90	15.28	6.702	42.076	0.702	0.413	0.0524	0.0767	0.0735	0.220	0.723	3.734	13.386	0.0157
100	16.22	7.028	42.831	0.834	0.342	0.0514	0.0822	0.0755	0.205	0.307	3.296	16.219	0.0140
110	17.16	7.818	51.149	0.779	0.357	0.0506	0.1477	0.0744	0.207	0.562	3.386	15.404	0.0149
119	18.00	7.309	34.059	0.670	0.290	0.0412	0.1122	0.0632	0.168	0.356	*****	16.255	0.0137
140	20.07	8.145	37.375	0.866	0.350	0.0519	0.1227	0.0680	0.221	0.302	1.333	16.697	0.0180
150	21.05	8.988	45.188	0.683	0.333	0.0529	0.1140	0.0717	0.214	0.227	3.784	12.898	0.0161
160	22.03	7.662	38.327	0.767	0.322	0.0523	0.2252	0.0698	0.220	0.143	3.085	14.676	0.0181
170	23.02	7.770	42.605	0.898	0.399	0.0528	0.1374	0.0693	0.229	0.255	3.337	17.027	0.0180
180	24.00	6.240	46.075	0.692	0.234	0.0522	0.1327	0.0696	0.208	0.000	2.061	13.252	0.0169
190	26.92	8.653	43.572	0.777	0.421	0.0522	0.1452	0.0720	0.260	1.105	6.142	14.889	0.0197
200	29.83	5.598	46.496	0.930	0.389	0.0522	0.1052	0.0728	0.247	0.300	*****	17.802	0.0215
210	32.75	5.260	46.619	0.810	0.338	0.0509	0.1407	0.0716	0.240	0.286	3.831	15.895	0.0215
220	35.67	5.442	41.086	0.744	0.316	0.0527	0.1098	0.0665	0.230	0.335	3.514	14.109	0.0204
230	38.58	5.894	39.087	0.870	0.383	0.0525	0.1012	0.0703	0.240	0.322	3.632	16.575	0.0191
240	41.50	6.451	36.050	0.687	0.353	0.0508	0.1389	0.0682	0.237	0.457	3.952	13.504	0.0225
250	44.42	7.904	37.211	0.639	0.334	0.0501	0.2201	0.0718	0.219	0.265	4.514	12.747	0.0198
260	47.33	5.785	39.372	0.670	0.328	0.0467	0.1771	0.0674	0.231	0.432	1.249	14.348	0.0215
270	50.25	6.489	45.975	0.785	0.342	0.0513	0.1727	0.0715	0.232	0.372	3.285	15.292	0.0187
280	53.17	5.701	39.686	0.768	0.338	0.0498	0.1256	0.0641	0.254	0.301	2.837	15.440	0.0245
290	56.08	5.196	32.306	0.646	0.293	0.0489	0.1181	0.0562	0.247	0.314	3.136	13.206	0.0207
300	59.00	5.079	27.623	0.677	0.278	0.0480	0.1103	0.0520	0.274	0.415	3.135	14.113	0.0267
310	60.67	5.264	30.239	0.714	0.283	0.0485	0.1159	0.0538	0.277	0.323	3.050	14.733	0.0236
320	62.33	5.882	22.794	1.221	0.371	0.0470	0.1860	0.0491	0.358	0.961	4.074	26.004	0.0290
330	64.00	6.264	22.985	1.340	0.360	0.0430	0.1778	0.0523	0.376	0.534	4.086	31.166	0.0282
340	68.67	5.420	21.502	0.604	0.237	0.0402	0.1386	0.0461	0.325	0.379	3.599	15.023	0.0275
350	72.29	5.382	22.177	0.483	0.199	0.0348	0.1239	0.0407	0.342	0.394	3.272	13.878	0.0267
360	74.86	5.436	15.738	0.347	0.146	0.0268	0.1137	0.0267	0.410	0.412	3.865	12.949	0.0287
370	77.43	5.384	12.255	0.302	0.121	0.0235	0.0755	0.0211	0.424	0.316	4.142	12.867	0.0282
380	80.00	5.329	15.610	0.374	0.147	0.0281	0.1215	0.0283	0.398	0.340	3.483	13.295	0.0271
390	81.67	5.566	7.900	0.312	0.092	0.0184	0.0473	0.0132	0.481	0.372	4.510	16.975	0.0278
400	83.33	4.762	30.262	0.668	0.272	0.0471	0.2281	0.0551	0.245	0.319	1.463	14.181	0.0249
410	85.00	4.559	36.106	0.625	0.298	0.0501	0.2613	0.0653	0.213	0.300	2.260	12.480	0.0233
420	86.67	4.911	36.224	0.819	0.331	0.0514	0.2667	0.0668	0.235	0.346	2.844	15.928	0.0281
430	88.33	5.144	39.218	0.966	0.352	0.0529	0.2292	0.0689	0.242	0.446	2.926	18.245	0.0249
440	90.00	5.159	42.666	0.849	0.314	0.0521	0.2041	0.0668	0.229	0.377	2.618	16.301	0.0251
450	*****	5.112	41.738	0.748	0.345	0.0531	0.1514	0.0620	0.224	0.424	*****	14.073	0.0297
460	*****	4.828	34.979	0.685	0.285	0.0513	0.1237	0.0560	0.227	0.379	*****	13.359	0.0297
470	*****	4.822	39.415	0.812	0.321	0.0533	0.1100	0.0555	0.221	0.369	*****	15.236	0.0249
480	*****	6.593	46.502	0.651	0.302	0.0549	0.1013	0.0685	0.254	0.523	*****	11.855	0.0243
490	*****	12.103	84.583	0.924	0.389	0.0636	0.1905	0.1300	0.297	0.516	*****	14.516	0.0220
500	*****	12.315	96.361	0.875	0.474	0.0645	0.2185	0.1383	0.314	0.540	*****	13.562	0.0251
510	*****	11.909	90.132	0.824	0.358	0.0673	0.1634	0.1267	0.276	0.555	*****	12.239	0.0229
520	*****	11.116	101.943	0.810	0.472	0.0731	0.1582	0.1357	0.275	0.685	*****	11.087	0.0237
530	*****	11.474	88.689	0.888	0.432	0.0793	0.1192	0.1202	0.297	1.015	*****	11.194	0.0282
540	*****	6.705	33.639	1.190	0.414	0.2313	0.0637	0.0563	0.176	0.584	*****	5.146	0.0323
550	*****	11.565	44.307	1.355	0.405	0.2036	0.0690	0.0610	0.231	0.450	*****	6.653	0.0235
560	*****	18.240	76.846	1.123	0.391	0.1288	0.0963	0.0870	0.271	0.570	*****	8.717	0.0209
570	*****	18.891	88.398	0.819	0.300	0.1115	0.1162	0.1100	0.267	0.061	*****	7.341	0.0254
580	*****	15.930	89.261	0.987	0.335	0.0930	0.1114	0.1084	0.279	0.418	*****	10.609	0.0198
590	*****	15.633	80.306	0.688	0.344	0.0740	0.0859	0.0968	0.272	0.490	*****	9.288	0.0211
600	*****	9.965	45.662	0.588	0.188	0.0486	0.0511	0.0550	0.382	0.602	*****	12.102	0.0344
610	*****	6.356	11.017	0.397	0.053	0.0280	0.0205	0.0136	0.452	0.472	*****	14.196	0.0485
620	*****	7.615	56.039	0.685	0.273	0.0597	0.0599	0.0772	0.340	0.658	*****	11.469	0.0341

Table C.4.2-3 Salt free major elements and their ratios in core CD3822.

Depth(cm)	Age(ka)	Si(Wt.%)	Al(Wt.%)	Fe(Wt.%)	Mg(Wt.%)	Ca(Wt.%)	Na(Wt.%)	K(Wt.%)	Ti(Wt.%)	Mn(Wt.%)	P(Wt.%)
1	0.57	17.023	5.724	4.162	1.876	5.877	4.036	0.843	0.324	4.183	0.0960
5	2.83	17.504	5.872	4.288	1.924	5.956	3.969	0.876	0.330	3.543	0.0956
10	5.67	18.084	5.999	4.442	1.888	6.485	3.895	0.881	0.337	1.736	0.0930
15	8.50	16.752	5.502	4.190	1.779	9.860	3.665	0.882	0.307	0.236	0.0799
20	11.33	15.910	5.253	3.882	1.731	11.290	3.383	0.828	0.297	0.226	0.0781
30	17.00	15.237	5.184	3.840	1.761	11.626	3.450	0.844	0.294	0.298	0.0807
40	17.71	15.695	5.279	3.777	1.846	10.182	3.650	0.912	0.297	0.435	0.0903
50	18.42	15.162	4.893	3.826	1.930	10.782	3.732	0.868	0.275	0.359	0.0899
60	19.14	15.219	4.803	3.623	1.985	10.096	3.821	0.914	0.273	1.152	0.0973
70	23.83	10.227	3.137	2.525	1.828	11.612	2.530	0.610	0.183	9.098	0.1113
78	27.29	16.920	5.369	3.938	1.954	9.374	3.383	0.944	0.303	0.754	0.0890
81	28.59	16.995	5.301	3.875	1.972	9.281	3.301	0.974	0.300	1.048	0.0899
90	32.49	16.368	5.147	3.812	1.906	10.396	3.116	0.937	0.293	0.808	0.0847
100	36.82	17.144	5.375	3.973	1.900	10.346	2.797	1.005	0.306	0.295	0.0847
110	39.00	19.154	5.819	4.442	2.141	7.107	3.309	1.155	0.321	0.466	0.0790
120	41.83	16.920	5.279	3.693	1.828	10.768	3.005	0.963	0.297	0.418	0.0794
130	44.67	18.523	5.734	4.085	2.003	7.972	3.250	1.065	0.319	0.609	0.0820
140	47.50	20.729	5.708	3.805	1.792	6.578	3.272	1.398	0.276	0.775	0.0668
150	50.33	21.066	6.433	4.631	2.208	3.868	3.569	1.231	0.354	0.865	0.0851
160	53.16	21.860	5.697	3.085	1.526	6.342	3.079	1.642	0.245	1.584	0.0615
170	56.00	24.987	6.205	3.162	1.478	4.040	3.287	1.947	0.241	0.276	0.0554
180	64.00	20.893	5.856	3.889	2.069	6.285	3.390	1.437	0.288	0.567	0.0729
190	71.25	18.766	5.703	4.309	2.310	6.750	3.487	1.081	0.325	0.922	0.0864
200	78.49	18.425	5.517	4.274	2.352	7.729	3.383	1.004	0.307	0.843	0.0812
210	85.74	20.327	6.300	4.596	2.383	6.621	3.531	1.219	0.357	0.425	0.0842
220	92.98	18.640	5.771	4.428	2.280	5.026	3.546	1.127	0.329	0.488	0.0751
230	100.23	20.439	6.306	4.924	2.413	4.404	3.858	1.215	0.359	0.820	0.0825
240	107.48	17.672	5.592	3.952	2.226	5.727	3.257	1.039	0.322	4.330	0.0916
250	114.72	20.935	6.528	4.722	2.407	3.847	3.836	1.244	0.370	0.877	0.0842
260	122.00	17.074	5.549	3.714	1.810	10.553	3.146	1.020	0.310	0.442	0.0729
270	127.00	16.826	4.835	3.546	1.954	11.426	2.856	0.909	0.269	0.413	0.0746
280	132.00	16.167	4.629	3.393	1.876	12.348	2.663	0.932	0.263	0.507	0.0751
290	137.00	16.882	4.946	3.498	1.761	11.569	2.738	1.016	0.274	0.393	0.0772
300	142.00	16.780	4.914	3.421	1.828	11.640	2.760	0.990	0.273	0.366	0.0759
310	147.00	16.471	4.840	3.470	1.761	11.733	2.916	0.996	0.268	0.276	0.0777
320	152.00	15.499	4.597	3.316	1.749	12.763	2.723	0.927	0.258	1.052	0.0816
330	156.00	15.251	4.502	3.295	1.749	12.784	2.738	0.905	0.252	1.257	0.0786
340	160.00	14.868	4.444	3.190	1.731	12.370	2.738	0.878	0.248	0.561	0.0759
350	164.00	17.462	5.221	4.211	2.196	8.852	3.390	1.025	0.296	0.787	0.0812
360	168.00	16.812	5.406	3.553	2.051	8.466	3.064	0.995	0.301	2.281	0.0842
368	172.00	19.598	6.655	3.833	2.147	8.037	3.339	1.149	0.360	0.979	0.0829
380	176.00	16.181	4.735	3.511	1.876	11.941	2.960	0.931	0.261	0.351	0.0742
390	180.00	16.462	4.893	3.623	1.894	11.512	3.034	0.938	0.270	0.338	0.0738
400	184.00	17.682	5.242	3.735	1.997	9.638	3.153	1.010	0.285	0.743	0.0751
410	187.28	17.513	5.211	3.980	2.057	9.345	3.109	0.995	0.288	1.203	0.0729
420	189.86	20.009	5.840	4.288	2.244	6.070	3.428	1.107	0.318	0.929	0.0724
430	192.43	20.935	6.253	4.757	2.352	4.576	3.569	1.158	0.351	0.577	0.0786
440	195.00	22.374	6.766	4.659	2.286	3.332	3.836	1.278	0.369	0.290	0.0790
452	199.15	19.019	5.808	4.316	2.105	7.672	3.457	1.103	0.326	0.296	0.0720
460	201.92	20.799	6.348	4.785	2.383	4.612	3.576	1.219	0.358	0.292	0.0742
470	205.38	21.253	6.406	4.855	2.425	4.111	3.665	1.240	0.356	0.320	0.0764
472	206.07	20.748	6.242	4.540	2.443	4.969	3.576	1.142	0.350	0.494	0.0794
482	209.53	19.631	5.882	4.456	2.268	6.492	3.954	1.208	0.328	0.643	0.0794
492	213.00	16.784	5.068	3.987	1.930	10.668	3.153	1.011	0.285	0.409	0.0759
502	219.00	19.294	5.935	4.309	2.232	6.835	3.316	1.261	0.333	0.574	0.0825

Table C.4.3-1 Salt included major element data from core CD3826.

Depth(cm)	Age(ka)	Si(Wt.%)	Al(Wt.%)	Fe(Wt.%)	Mg(Wt.%)	Ca(Wt.%)	Na(Wt.%)	K(Wt.%)	Ti(Wt.%)	Mn(Wt.%)	P(Wt.%)
512	224.00	19.248	5.888	4.659	2.172	6.542	3.287	1.279	0.322	0.831	0.0768
522	229.00	21.225	6.173	4.057	1.918	5.849	3.361	1.523	0.312	0.346	0.0676
532	234.00	23.959	6.480	3.428	1.574	4.426	3.205	1.955	0.284	0.486	0.0611
542	240.00	21.673	6.115	3.770	1.840	4.876	3.316	1.596	0.295	1.757	0.0764
552	242.00	21.472	6.999	4.204	1.991	5.341	3.561	1.461	0.320	0.485	0.0803
562	244.00	19.378	5.867	3.966	1.852	8.194	3.250	1.290	0.307	0.397	0.0764
572	246.14	16.882	5.322	4.043	2.003	10.468	3.101	0.979	0.287	0.522	0.0807
580	247.97	16.354	5.041	3.910	1.918	11.268	2.982	1.011	0.285	0.484	0.0816
592	250.72	14.368	4.264	3.099	1.677	14.622	2.619	0.874	0.245	0.554	0.0786
602	253.00	13.681	4.020	2.987	1.647	15.401	2.686	0.802	0.225	0.818	0.0790
612	257.00	14.200	4.116	2.959	1.689	15.015	2.752	0.821	0.229	0.565	0.0777
622	265.33	14.447	4.184	2.959	1.785	13.371	2.671	0.810	0.234	2.042	0.0834
632	273.67	18.051	5.364	3.742	1.997	9.123	3.168	1.040	0.297	0.674	0.0799
642	282.00	17.887	5.174	4.071	2.147	7.386	3.264	1.039	0.290	2.508	0.0790
652	285.69	19.205	5.602	4.071	2.099	7.457	3.138	1.085	0.316	0.928	0.0777
662	289.38	17.939	5.063	3.882	1.997	9.774	3.160	1.000	0.281	0.360	0.0751
672	293.07	14.882	4.232	3.169	1.592	14.715	2.656	0.834	0.234	0.344	0.0698
680	296.00	14.055	4.031	2.938	1.484	15.923	2.537	0.841	0.225	0.358	0.0668
690	300.29	15.167	4.327	3.274	1.641	13.993	2.834	0.909	0.242	0.321	0.0681
700	304.58	15.013	4.248	3.183	1.719	13.385	2.760	0.834	0.241	0.358	0.0672
710	308.87	15.644	4.396	3.211	1.828	12.934	2.797	0.846	0.245	0.448	0.0659
720	313.17	17.574	4.824	3.574	2.081	10.275	3.079	0.941	0.271	0.508	0.0685
730	317.46	17.626	4.856	3.553	2.129	9.367	3.153	0.949	0.275	1.454	0.0729
740	321.75	18.308	5.105	3.630	2.027	7.429	3.175	1.015	0.295	0.535	0.0711
750	326.00	19.771	5.613	3.959	2.105	7.136	3.428	1.158	0.323	0.597	0.0790
760	327.00	19.603	5.533	3.498	1.852	7.450	3.183	1.319	0.322	2.072	0.0890
770	328.00	23.033	6.935	3.113	1.134	6.499	2.945	2.263	0.390	1.902	0.1248
780	332.87	13.559	4.073	2.910	1.502	16.080	2.500	0.843	0.234	0.996	0.0777
790	337.73	15.144	4.936	2.959	1.611	14.007	2.389	0.966	0.280	0.486	0.0855
800	342.60	12.494	3.962	2.630	1.387	17.546	3.376	1.127	0.219	0.396	0.0764
810	347.47	12.896	3.846	2.763	1.405	17.232	2.241	0.755	0.212	0.517	0.0716
820	352.33	13.185	3.714	2.777	1.424	17.210	2.367	0.751	0.206	0.382	0.0663
830	357.20	13.298	3.761	2.812	1.454	16.717	2.537	0.775	0.208	0.385	0.0659
840	362.07	15.050	4.306	3.281	1.647	14.014	2.656	0.835	0.237	0.423	0.0698
850	366.93	15.976	4.497	3.400	1.816	12.891	2.871	0.898	0.248	0.429	0.0742
860	371.80	16.088	4.740	3.414	1.785	12.691	3.799	1.195	0.257	0.406	0.0755
870	376.67	16.191	5.422	3.910	1.864	12.291	2.945	0.941	0.260	0.364	0.0759
880	381.53	17.738	5.264	3.868	2.033	9.924	2.841	0.990	0.294	0.704	0.0816
890	386.40	18.733	5.544	3.994	2.214	8.809	3.020	1.044	0.306	0.543	0.0829
900	391.27	17.607	5.179	4.302	2.081	9.538	3.034	0.987	0.291	0.494	0.0812
910	396.13	18.958	5.994	4.288	2.220	7.722	3.264	1.060	0.315	0.517	0.0816
920	401.00	19.556	5.729	4.029	2.316	6.721	3.294	1.108	0.322	1.330	0.0807
930	408.09	17.392	5.200	3.791	1.997	10.475	2.968	0.980	0.299	0.568	0.0716
940	415.18	16.864	5.184	3.875	1.888	11.454	2.782	0.946	0.304	0.342	0.0690
950	422.28	15.462	4.713	3.504	1.852	13.485	2.560	0.884	0.279	0.317	0.0711
960	429.37	14.368	4.375	2.987	1.816	14.150	2.574	0.839	0.254	1.298	0.0816
970	436.46	13.573	4.026	2.672	1.677	14.965	2.500	0.780	0.233	1.190	0.0851
980	443.55	12.653	3.677	2.770	1.424	17.332	2.389	0.773	0.209	0.493	0.0724
990	450.64	12.078	3.359	2.553	1.357	18.769	2.330	0.715	0.187	0.563	0.0668
1000	457.74	11.601	3.248	2.392	1.297	19.019	2.344	0.678	0.180	1.018	0.0676
1010	464.83	10.956	3.121	2.161	1.255	19.934	2.248	0.642	0.174	0.949	0.0659
1020	472.00	11.162	3.216	2.308	1.243	19.898	2.226	0.627	0.179	0.658	0.0672
1030	******	11.947	3.407	2.378	1.327	18.948	2.344	0.669	0.189	0.558	0.0672
1040	******	12.204	3.386	2.329	1.249	19.040	2.315	0.692	0.179	0.592	0.0620
1050	******	13.905	3.909	2.609	1.418	16.502	2.515	0.777	0.207	0.505	0.0642
1060	******	13.989	4.020	2.910	1.514	16.023	2.560	0.809	0.220	0.359	0.0663
1070	******	17.055	5.026	3.798	1.942	11.669	2.938	0.987	0.280	0.340	0.0694

Table C.4.3-1 (Contd.) Salt included major element data from core CD3826.

Depth(cm)	Age(ka)	Si(Wt.%)	Al(Wt.%)	Fe(Wt.%)	Mg(Wt.%)	Ca(Wt.%)	Na(Wt.%)	K(Wt.%)	Ti(Wt.%)	Mn(Wt.%)	P(Wt.%)	SALT
1	0.57	18.645	6.269	4.559	1.702	6.323	1.505	0.818	0.355	4.582	0.1052	8.700
5	2.83	19.190	6.437	4.701	1.753	6.414	1.404	0.854	0.362	3.884	0.1048	8.785
10	5.67	19.988	6.631	4.910	1.697	7.042	1.083	0.858	0.372	1.919	0.1027	9.528
15	8.50	18.247	5.993	4.564	1.608	10.633	1.261	0.862	0.335	0.257	0.0870	8.194
20	11.33	17.267	5.701	4.213	1.563	12.150	1.062	0.804	0.323	0.245	0.0848	7.857
30	17.00	16.612	5.652	4.187	1.586	12.566	1.000	0.821	0.320	0.325	0.0880	8.275
40	17.71	16.820	5.658	4.048	1.713	10.825	1.718	0.899	0.318	0.466	0.0968	6.689
50	18.42	16.591	5.354	4.187	1.763	11.685	1.199	0.847	0.301	0.393	0.0984	8.613
60	19.14	16.587	5.235	3.949	1.830	10.896	1.413	0.897	0.297	1.256	0.1061	8.251
70	23.83	10.801	3.313	2.667	1.723	12.196	0.955	0.583	0.193	9.608	0.1175	5.313
78	27.29	18.214	5.780	4.239	1.821	9.999	1.301	0.932	0.326	0.812	0.0958	7.105
81	28.59	18.413	5.743	4.199	1.828	9.955	1.022	0.963	0.325	1.135	0.0974	7.705
90	32.49	17.742	5.579	4.132	1.756	11.168	0.809	0.924	0.317	0.875	0.0918	7.744
100	36.82	18.486	5.795	4.284	1.759	11.062	0.622	0.998	0.330	0.318	0.0913	7.256
110	39.00	20.969	6.370	4.863	1.994	7.667	0.723	1.160	0.351	0.510	0.0865	8.655
120	41.83	18.189	5.675	3.970	1.687	11.486	0.934	0.953	0.320	0.450	0.0854	6.979
130	44.67	20.089	6.219	4.430	1.859	8.545	0.937	1.062	0.346	0.661	0.0890	7.794
140	47.50	22.354	6.155	4.104	1.642	7.000	1.129	1.421	0.297	0.836	0.0720	7.269
150	50.33	23.134	7.064	5.085	2.061	4.130	0.914	1.244	0.388	0.950	0.0935	8.941
160	53.16	23.266	6.064	3.283	1.386	6.673	1.309	1.677	0.260	1.686	0.0655	6.043
170	56.00	26.690	6.628	3.377	1.326	4.233	1.425	2.005	0.257	0.294	0.0592	6.381
180	64.00	22.496	6.305	4.188	1.944	6.675	1.303	1.463	0.310	0.610	0.0785	7.126
190	71.25	20.411	6.203	4.687	2.188	7.236	1.110	1.079	0.354	1.002	0.0940	8.061
200	78.49	20.063	6.008	4.654	2.233	8.310	0.963	0.995	0.335	0.917	0.0884	8.165
210	85.74	22.182	6.875	5.015	2.262	7.116	1.061	1.230	0.389	0.464	0.0919	8.363
220	92.98	20.535	6.358	4.878	2.136	5.415	0.796	1.130	0.363	0.537	0.0827	9.229
230	100.23	22.462	6.930	5.412	2.285	4.722	1.211	1.227	0.395	0.901	0.0906	9.006
240	107.48	19.142	6.057	4.281	2.103	6.104	0.983	1.033	0.349	4.690	0.0993	7.678
250	114.72	23.057	7.190	5.200	2.276	4.115	1.122	1.258	0.407	0.965	0.0928	9.205
260	122.00	18.477	6.005	4.020	1.654	11.322	0.890	1.014	0.335	0.479	0.0789	7.592
270	127.00	17.997	5.171	3.793	1.833	12.137	0.926	0.896	0.288	0.441	0.0798	6.504
280	132.00	17.245	4.937	3.619	1.754	13.091	0.801	0.921	0.280	0.541	0.0801	6.250
290	137.00	18.005	5.275	3.730	1.632	12.258	0.885	1.011	0.292	0.419	0.0824	6.235
300	142.00	17.987	5.268	3.667	1.693	12.391	0.757	0.982	0.292	0.393	0.0814	6.713
310	147.00	17.706	5.203	3.730	1.616	12.523	0.841	0.988	0.288	0.297	0.0835	6.972
320	152.00	16.589	4.920	3.549	1.612	13.576	0.763	0.914	0.276	1.126	0.0873	6.570
330	156.00	16.341	4.823	3.530	1.610	13.612	0.747	0.891	0.270	1.347	0.0842	6.668
340	160.00	15.982	4.777	3.429	1.584	13.207	0.649	0.862	0.266	0.603	0.0816	6.972
350	164.00	19.073	5.703	4.600	2.057	9.558	0.880	1.018	0.323	0.859	0.0887	8.447
360	168.00	18.253	5.870	3.858	1.910	9.088	0.705	0.986	0.327	2.476	0.0914	7.892
368	172.00	21.243	7.213	4.155	2.017	8.610	1.050	1.153	0.390	1.061	0.0899	7.744
380	176.00	17.425	5.098	3.781	1.736	12.766	0.837	0.918	0.281	0.378	0.0799	7.135
390	180.00	17.791	5.288	3.916	1.748	12.344	0.809	0.925	0.292	0.365	0.0797	7.471
400	184.00	19.065	5.652	4.027	1.863	10.298	1.007	1.002	0.308	0.802	0.0809	7.253
410	187.28	18.919	5.629	4.300	1.925	9.999	0.903	0.986	0.311	1.300	0.0787	7.428
420	189.86	21.763	6.352	4.664	2.116	6.497	1.046	1.108	0.346	1.011	0.0788	8.057
430	192.43	22.803	6.811	5.181	2.232	4.877	1.157	1.163	0.382	0.628	0.0856	8.191
440	195.00	24.471	7.400	5.095	2.154	3.532	1.328	1.294	0.404	0.318	0.0864	8.568
452	199.15	20.742	6.335	4.707	1.961	8.259	0.997	1.103	0.356	0.323	0.0785	8.310
460	201.92	22.703	6.929	5.223	2.262	4.924	1.102	1.230	0.391	0.319	0.0810	8.386
470	205.38	23.186	6.989	5.296	2.309	4.376	1.215	1.253	0.388	0.349	0.0833	8.339
472	206.07	22.557	6.786	4.936	2.333	5.298	1.220	1.146	0.381	0.537	0.0863	8.020
482	209.53	21.328	6.391	4.841	2.144	6.950	1.650	1.217	0.356	0.698	0.0863	7.959
492	213.00	18.125	5.473	4.306	1.789	11.424	0.961	1.004	0.308	0.442	0.0820	7.395
502	219.00	20.862	6.417	4.659	2.113	7.293	1.100	1.274	0.360	0.620	0.0892	7.513

Table C.4.3-2 Salt free major element data from core CD3826.

Depth(cm)	Age(ka)	Si(Wt.%)	Al(Wt.%)	Fe(Wt.%)	Mg(Wt.%)	Ca(Wt.%)	Na(Wt.%)	K(Wt.%)	Ti(Wt.%)	Mn(Wt.%)	P(Wt.%)	SALT
512	224.00	20.819	6.369	5.039	2.047	6.978	1.056	1.293	0.349	0.899	0.0831	7.549
522	229.00	22.821	6.638	4.362	1.784	6.198	1.312	1.554	0.335	0.372	0.0727	6.995
532	234.00	25.418	6.875	3.636	1.445	4.622	1.537	2.007	0.301	0.516	0.0648	5.740
542	240.00	23.231	6.555	4.041	1.706	5.140	1.356	1.632	0.316	1.883	0.0819	6.704
552	242.00	23.232	7.572	4.548	1.851	5.680	1.346	1.491	0.346	0.524	0.0869	7.573
562	244.00	20.829	6.306	4.263	1.713	8.717	1.202	1.304	0.330	0.427	0.0821	6.965
572	246.14	18.167	5.727	4.351	1.873	11.173	1.008	0.970	0.309	0.562	0.0869	7.073
580	247.97	17.549	5.410	4.196	1.788	12.004	0.966	1.005	0.306	0.519	0.0876	6.806
592	250.72	15.334	4.551	3.307	1.541	15.525	0.736	0.859	0.261	0.592	0.0838	6.304
602	253.00	14.632	4.300	3.195	1.504	16.389	0.744	0.781	0.241	0.875	0.0845	6.504
612	257.00	15.201	4.406	3.167	1.547	15.989	0.789	0.801	0.245	0.604	0.0832	6.585
622	265.33	15.464	4.479	3.167	1.651	14.227	0.705	0.790	0.251	2.186	0.0892	6.576
632	273.67	19.503	5.796	4.043	1.860	9.761	0.961	1.035	0.321	0.728	0.0863	7.446
642	282.00	19.399	5.611	4.415	2.016	7.909	0.954	1.034	0.315	2.720	0.0857	7.794
652	285.69	20.637	6.020	4.375	1.980	7.924	1.091	1.084	0.339	0.997	0.0835	6.936
662	289.38	19.356	5.462	4.189	1.862	10.451	0.993	0.993	0.303	0.389	0.0810	7.321
672	293.07	15.923	4.528	3.390	1.445	15.660	0.700	0.816	0.250	0.368	0.0747	6.540
680	296.00	14.956	4.290	3.126	1.342	16.867	0.737	0.824	0.239	0.381	0.0711	6.027
690	300.29	16.180	4.616	3.492	1.503	14.847	0.980	0.896	0.258	0.342	0.0726	6.261
700	304.58	16.047	4.541	3.402	1.583	14.224	0.841	0.815	0.258	0.382	0.0718	6.446
710	308.87	16.753	4.708	3.438	1.695	13.766	0.826	0.828	0.262	0.479	0.0706	6.618
720	313.17	18.958	5.204	3.856	1.954	10.989	0.911	0.928	0.292	0.548	0.0739	7.301
730	317.46	19.008	5.237	3.832	2.006	10.007	1.000	0.937	0.297	1.568	0.0786	7.274
740	321.75	19.768	5.512	3.920	1.893	7.926	0.989	1.009	0.318	0.578	0.0768	7.385
750	326.00	21.397	6.074	4.285	1.974	7.624	1.193	1.163	0.350	0.646	0.0855	7.599
760	327.00	20.848	5.885	3.720	1.734	7.847	1.441	1.333	0.343	2.204	0.0947	5.973
770	328.00	23.623	7.113	3.192	1.068	6.635	2.237	2.293	0.400	1.951	0.1280	2.497
780	332.87	14.369	4.316	3.084	1.371	16.969	0.823	0.827	0.248	1.055	0.0823	5.634
790	337.73	16.036	5.227	3.133	1.487	14.762	0.726	0.958	0.296	0.514	0.0906	5.566
800	342.60	13.182	4.180	2.775	1.260	18.447	1.876	1.128	0.231	0.418	0.0806	5.221
810	347.47	13.611	4.059	2.916	1.278	18.121	0.667	0.736	0.224	0.546	0.0755	5.257
820	352.33	13.967	3.934	2.942	1.289	18.159	0.692	0.731	0.218	0.404	0.0703	5.598
830	357.20	14.116	3.993	2.985	1.315	17.672	0.810	0.755	0.221	0.409	0.0700	5.797
840	362.07	16.068	4.597	3.502	1.508	14.880	0.767	0.817	0.253	0.451	0.0745	6.333
850	366.93	17.094	4.811	3.638	1.684	13.710	0.930	0.884	0.265	0.459	0.0794	6.542
860	371.80	17.147	5.052	3.638	1.659	13.448	2.034	1.201	0.273	0.432	0.0805	6.175
870	376.67	17.280	5.787	4.173	1.740	13.037	1.085	0.931	0.277	0.388	0.0810	6.304
880	381.53	18.918	5.614	4.126	1.922	10.505	0.995	0.983	0.313	0.751	0.0870	6.238
890	386.40	20.070	5.939	4.279	2.108	9.352	1.052	1.040	0.328	0.582	0.0888	6.660
900	391.27	18.938	5.570	4.627	1.959	10.168	0.951	0.979	0.313	0.531	0.0873	7.026
910	396.13	20.464	6.470	4.629	2.102	8.240	1.093	1.057	0.340	0.558	0.0881	7.359
920	401.00	21.070	6.172	4.341	2.209	7.148	1.181	1.109	0.347	1.433	0.0870	7.184
930	408.09	18.614	5.565	4.058	1.877	11.126	1.026	0.971	0.319	0.608	0.0766	6.565
940	415.18	17.982	5.528	4.132	1.768	12.134	0.938	0.936	0.325	0.364	0.0735	6.218
950	422.28	16.415	5.004	3.721	1.738	14.243	0.830	0.871	0.297	0.336	0.0755	5.810
960	429.37	15.246	4.642	3.169	1.700	14.941	0.862	0.823	0.270	1.377	0.0866	5.759
970	436.46	14.444	4.284	2.844	1.547	15.848	0.697	0.760	0.248	1.267	0.0906	6.031
980	443.55	13.404	3.895	2.935	1.288	18.290	0.714	0.753	0.222	0.523	0.0767	5.606
990	450.64	12.804	3.561	2.707	1.216	19.825	0.630	0.692	0.198	0.597	0.0708	5.672
1000	457.74	12.307	3.446	2.538	1.151	20.103	0.626	0.653	0.191	1.080	0.0718	5.734
1010	464.83	11.587	3.301	2.286	1.114	21.014	0.614	0.615	0.184	1.004	0.0697	5.450
1020	472.00	11.802	3.401	2.441	1.102	20.971	0.599	0.600	0.189	0.696	0.0711	5.423
1030	******	12.650	3.607	2.518	1.187	19.993	0.680	0.644	0.200	0.591	0.0712	5.563
1040	******	12.896	3.578	2.462	1.110	20.053	0.710	0.669	0.189	0.625	0.0655	5.370
1050	******	14.763	4.151	2.770	1.277	17.447	0.782	0.757	0.220	0.536	0.0681	5.813
1060	******	14.868	4.273	3.093	1.377	16.954	0.798	0.790	0.234	0.382	0.0705	5.910
1070	******	18.295	5.391	4.074	1.815	12.429	0.928	0.979	0.300	0.365	0.0744	6.773

Table C.4.3-2 (Contd.) Salt free major element data from core CD3826.

Depth(cm)	Age(ka)	Si/Al	Fe/Al	Mg/Al	Ca/Al	Ti/Al	Mn/Al	P/Al	K/Al	Na/Al	Siterrig/Al	Fe/Ti	K/Rb
1	0.57	2.974	0.727	0.272	1.009	0.0567	0.731	0.0168	0.130	0.240	2.590	12.835	0.0249
5	2.83	2.981	0.730	0.272	0.996	0.0562	0.603	0.0163	0.133	0.218	2.591	12.983	0.0251
10	5.67	3.015	0.740	0.256	1.062	0.0562	0.289	0.0155	0.129	0.163	2.614	13.186	0.0250
15	8.50	3.045	0.762	0.268	1.774	0.0559	0.043	0.0145	0.144	0.210	2.666	13.626	0.0257
20	11.33	3.029	0.739	0.274	2.131	0.0566	0.043	0.0149	0.141	0.186	2.690	13.058	0.0257
30	17.00	2.939	0.741	0.281	2.223	0.0567	0.058	0.0156	0.145	0.177	2.710	13.075	0.0224
40	17.71	2.973	0.715	0.303	1.913	0.0562	0.082	0.0171	0.159	0.304	2.801	12.731	0.0230
50	18.42	3.099	0.782	0.329	2.182	0.0562	0.073	0.0184	0.158	0.224	2.839	13.907	0.0243
60	19.14	3.168	0.754	0.350	2.081	0.0568	0.240	0.0203	0.171	0.270	2.875	13.286	0.0254
70	23.83	3.260	0.805	0.520	3.681	0.0583	2.900	0.0355	0.176	0.288	3.080	13.813	0.0277
78	27.29	3.151	0.733	0.315	1.730	0.0564	0.140	0.0166	0.161	0.225	2.832	13.010	0.0259
81	28.59	3.206	0.731	0.318	1.733	0.0567	0.198	0.0170	0.168	0.178	3.018	12.905	0.0268
90	32.49	3.180	0.741	0.315	2.002	0.0568	0.157	0.0164	0.166	0.145	2.972	13.033	0.0270
100	36.82	3.190	0.739	0.304	1.909	0.0570	0.055	0.0158	0.172	0.107	2.923	12.972	0.0299
110	39.00	3.292	0.763	0.313	1.204	0.0551	0.080	0.0136	0.182	0.113	3.068	13.851	0.0299
120	41.83	3.205	0.700	0.297	2.024	0.0563	0.079	0.0150	0.168	0.165	2.942	12.423	0.0284
130	44.67	3.230	0.712	0.299	1.374	0.0556	0.106	0.0143	0.171	0.151	2.989	12.811	0.0292
140	47.50	3.632	0.667	0.267	1.137	0.0483	0.136	0.0117	0.231	0.183	3.371	13.801	0.0295
150	50.33	3.275	0.720	0.292	0.585	0.0550	0.134	0.0132	0.176	0.129	3.086	13.094	0.0290
160	53.16	3.837	0.541	0.229	1.100	0.0429	0.278	0.0108	0.277	0.216	3.574	12.614	0.0302
170	56.00	4.027	0.510	0.200	0.639	0.0388	0.044	0.0089	0.302	0.215	3.758	13.121	0.0290
180	64.00	3.568	0.664	0.308	1.059	0.0492	0.097	0.0124	0.232	0.207	3.325	13.490	0.0312
190	71.25	3.291	0.756	0.353	1.167	0.0571	0.162	0.0152	0.174	0.179	2.973	13.239	0.0305
200	78.49	3.339	0.775	0.372	1.383	0.0557	0.153	0.0147	0.166	0.160	3.043	13.899	0.0295
210	85.74	3.226	0.729	0.329	1.035	0.0566	0.067	0.0134	0.179	0.154	2.907	12.886	0.0326
220	92.98	3.230	0.767	0.336	0.852	0.0570	0.085	0.0130	0.178	0.125	2.884	13.456	0.0296
230	100.23	3.241	0.781	0.330	0.681	0.0569	0.130	0.0131	0.177	0.175	2.920	13.716	0.0319
240	107.48	3.161	0.707	0.347	1.008	0.0577	0.774	0.0164	0.171	0.162	2.835	12.256	0.0297
250	114.72	3.207	0.723	0.317	0.572	0.0567	0.134	0.0129	0.175	0.156	2.929	12.767	0.0305
260	122.00	3.077	0.669	0.275	1.885	0.0558	0.080	0.0131	0.169	0.148	2.787	11.986	0.0280
270	127.00	3.480	0.733	0.354	2.347	0.0557	0.085	0.0154	0.173	0.179	3.054	13.177	0.0289
280	132.00	3.493	0.733	0.355	2.651	0.0567	0.110	0.0162	0.187	0.162	3.052	12.922	0.0310
290	137.00	3.413	0.707	0.309	2.324	0.0554	0.079	0.0156	0.192	0.168	2.954	12.768	0.0311
300	142.00	3.414	0.696	0.321	2.352	0.0555	0.075	0.0155	0.186	0.144	3.000	12.542	0.0299
310	147.00	3.403	0.717	0.311	2.407	0.0554	0.057	0.0160	0.190	0.162	2.978	12.949	0.0298
320	152.00	3.372	0.721	0.328	2.759	0.0561	0.229	0.0178	0.186	0.155	2.967	12.864	0.0302
330	156.00	3.388	0.732	0.334	2.822	0.0559	0.279	0.0174	0.185	0.155	3.026	13.087	0.0299
340	160.00	3.346	0.718	0.332	2.765	0.0557	0.126	0.0171	0.180	0.136	2.943	12.885	0.0280
350	164.00	3.344	0.807	0.361	1.676	0.0567	0.151	0.0155	0.179	0.154	3.038	14.221	0.0283
360	168.00	3.110	0.657	0.325	1.548	0.0558	0.422	0.0156	0.168	0.120	2.938	11.786	0.0251
368	172.00	2.945	0.576	0.280	1.194	0.0541	0.147	0.0125	0.160	0.146	2.827	10.641	0.0233
380	176.00	3.418	0.742	0.340	2.504	0.0552	0.074	0.0157	0.180	0.164	3.079	13.437	0.0302
390	180.00	3.364	0.740	0.331	2.334	0.0551	0.069	0.0151	0.175	0.153	3.046	13.433	0.0294
400	184.00	3.373	0.713	0.330	1.822	0.0544	0.142	0.0143	0.177	0.178	3.083	13.092	0.0301
410	187.28	3.361	0.764	0.342	1.776	0.0552	0.231	0.0140	0.175	0.160	3.083	13.834	0.0296
420	189.86	3.426	0.734	0.333	1.023	0.0544	0.159	0.0124	0.174	0.165	3.150	13.498	0.0303
430	192.43	3.348	0.761	0.328	0.716	0.0561	0.092	0.0126	0.171	0.170	2.998	13.565	0.0299
440	195.00	3.307	0.689	0.291	0.477	0.0546	0.043	0.0117	0.175	0.179	2.971	12.617	0.0320
452	199.15	3.274	0.743	0.309	1.304	0.0561	0.051	0.0124	0.174	0.157	2.956	13.236	0.0300
460	201.92	3.277	0.754	0.326	0.711	0.0564	0.046	0.0117	0.177	0.159	2.971	13.371	0.0294
470	205.38	3.318	0.758	0.330	0.626	0.0556	0.050	0.0119	0.179	0.174	3.003	13.635	0.0295
472	206.07	3.324	0.727	0.344	0.781	0.0561	0.079	0.0127	0.169	0.180	3.018	12.969	0.0294
482	209.53	3.337	0.757	0.335	1.087	0.0557	0.109	0.0135	0.190	0.258	3.040	13.590	0.0335
492	213.00	3.312	0.787	0.327	2.087	0.0563	0.081	0.0150	0.183	0.176	3.010	13.975	0.0297
502	219.00	3.251	0.726	0.329	1.136	0.0561	0.097	0.0139	0.199	0.171	2.997	12.929	0.0291

Table C.4.3-3 Salt free major elements and their ratios in core CD3826.

Depth(cm)	Age(ka)	Si/Al	Fe/Al	Mg/Al	Ca/Al	Ti/Al	Mn/Al	P/Al	K/Al	Na/Al	Siterrig/Al	Fe/Ti	K/Rb
512	224.00	3.269	0.791	0.321	1.096	0.0548	0.141	0.0130	0.203	0.166	3.058	14.447	0.0286
522	229.00	3.438	0.657	0.269	0.934	0.0505	0.056	0.0110	0.234	0.198	3.135	13.017	0.0267
532	234.00	3.697	0.529	0.210	0.672	0.0438	0.075	0.0094	0.292	0.224	3.406	12.064	0.0256
542	240.00	3.544	0.617	0.260	0.784	0.0482	0.287	0.0125	0.249	0.207	3.254	12.785	0.0259
552	242.00	3.068	0.601	0.244	0.750	0.0457	0.069	0.0115	0.197	0.178	2.788	13.134	0.0268
562	244.00	3.303	0.676	0.272	1.382	0.0523	0.068	0.0130	0.207	0.191	3.029	12.924	0.0270
572	246.14	3.172	0.760	0.327	1.951	0.0540	0.098	0.0152	0.169	0.176	2.906	14.082	0.0267
580	247.97	3.244	0.776	0.331	2.219	0.0565	0.096	0.0162	0.186	0.178	2.907	13.734	0.0288
592	250.72	3.370	0.727	0.339	3.412	0.0574	0.130	0.0184	0.189	0.162	2.996	12.671	0.0304
602	253.00	3.403	0.743	0.350	3.811	0.0561	0.203	0.0196	0.182	0.173	3.002	13.253	0.0286
612	257.00	3.450	0.719	0.351	3.629	0.0556	0.137	0.0189	0.182	0.179	3.041	12.923	0.0285
622	265.33	3.453	0.707	0.369	3.176	0.0560	0.488	0.0199	0.176	0.157	3.009	12.625	0.0283
632	273.67	3.365	0.698	0.321	1.684	0.0553	0.126	0.0149	0.179	0.166	3.028	12.613	0.0294
642	282.00	3.457	0.787	0.359	1.410	0.0561	0.485	0.0153	0.184	0.170	3.077	14.033	0.0293
652	285.69	3.428	0.727	0.329	1.316	0.0564	0.166	0.0139	0.180	0.181	3.018	12.888	0.0311
662	289.38	3.543	0.767	0.341	1.913	0.0554	0.071	0.0148	0.182	0.182	3.106	13.839	0.0301
672	293.07	3.517	0.749	0.319	3.458	0.0552	0.081	0.0165	0.180	0.155	3.002	13.555	0.0296
680	296.00	3.487	0.729	0.313	3.932	0.0558	0.089	0.0166	0.192	0.172	2.981	13.070	0.0320
690	300.29	3.505	0.757	0.326	3.216	0.0560	0.074	0.0157	0.194	0.212	3.034	13.519	0.0315
700	304.58	3.534	0.749	0.349	3.133	0.0567	0.084	0.0158	0.180	0.185	3.055	13.209	0.0278
710	308.87	3.559	0.730	0.360	2.924	0.0556	0.102	0.0150	0.176	0.176	3.053	13.129	0.0286
720	313.17	3.643	0.741	0.375	2.112	0.0562	0.105	0.0142	0.178	0.175	3.112	13.193	0.0295
730	317.46	3.630	0.732	0.383	1.911	0.0567	0.299	0.0150	0.179	0.191	3.155	12.916	0.0301
740	321.75	3.586	0.711	0.344	1.438	0.0578	0.105	0.0139	0.183	0.179	3.137	12.310	0.0277
750	326.00	3.523	0.705	0.325	1.255	0.0576	0.106	0.0141	0.191	0.196	3.098	12.255	0.0298
760	327.00	3.543	0.632	0.295	1.333	0.0583	0.375	0.0161	0.227	0.245	3.144	10.846	0.0312
770	328.00	3.321	0.449	0.150	0.933	0.0562	0.274	0.0180	0.322	0.315	3.150	7.989	0.0311
780	332.87	3.329	0.714	0.318	3.931	0.0575	0.244	0.0191	0.192	0.191	2.928	12.416	0.0296
790	337.73	3.068	0.600	0.285	2.824	0.0567	0.098	0.0173	0.183	0.139	2.830	10.570	0.0245
800	342.60	3.153	0.664	0.301	4.413	0.0552	0.100	0.0193	0.270	0.449	2.867	12.022	0.0369
810	347.47	3.353	0.718	0.315	4.464	0.0552	0.135	0.0186	0.181	0.164	2.961	13.022	0.0271
820	352.33	3.551	0.748	0.328	4.616	0.0554	0.103	0.0179	0.186	0.176	3.056	13.507	0.0291
830	357.20	3.535	0.748	0.329	4.426	0.0553	0.102	0.0175	0.189	0.203	3.053	13.520	0.0304
840	362.07	3.495	0.762	0.328	3.237	0.0550	0.098	0.0162	0.178	0.167	3.048	13.856	0.0287
850	366.93	3.553	0.756	0.350	2.850	0.0551	0.095	0.0165	0.184	0.193	3.120	13.733	0.0315
860	371.80	3.394	0.720	0.328	2.662	0.0541	0.086	0.0159	0.238	0.403	2.961	13.306	0.0404
870	376.67	2.986	0.721	0.301	2.253	0.0479	0.067	0.0140	0.161	0.187	2.609	15.066	0.0300
880	381.53	3.370	0.735	0.342	1.871	0.0558	0.134	0.0155	0.175	0.177	3.027	13.170	0.0302
890	386.40	3.379	0.720	0.355	1.574	0.0551	0.098	0.0150	0.175	0.177	3.011	13.066	0.0312
900	391.27	3.400	0.831	0.352	1.825	0.0561	0.095	0.0157	0.176	0.171	2.983	14.798	0.0309
910	396.13	3.163	0.715	0.325	1.274	0.0526	0.086	0.0136	0.163	0.169	2.813	13.600	0.0305
920	401.00	3.413	0.703	0.358	1.158	0.0563	0.232	0.0141	0.180	0.191	3.155	12.494	0.0305
930	408.09	3.345	0.729	0.337	1.999	0.0574	0.109	0.0138	0.175	0.184	2.979	12.701	0.0312
940	415.18	3.253	0.748	0.320	2.195	0.0587	0.066	0.0133	0.169	0.170	2.902	12.727	0.0307
950	422.28	3.280	0.744	0.347	2.846	0.0593	0.067	0.0151	0.174	0.166	2.910	12.547	0.0298
960	429.37	3.284	0.683	0.366	3.219	0.0581	0.297	0.0187	0.177	0.186	2.939	11.753	0.0280
970	436.46	3.372	0.664	0.361	3.699	0.0579	0.296	0.0211	0.177	0.163	2.975	11.460	0.0244
980	443.55	3.441	0.753	0.331	4.696	0.0569	0.134	0.0197	0.193	0.183	3.017	13.242	0.0283
990	450.64	3.595	0.760	0.342	5.567	0.0557	0.168	0.0199	0.194	0.177	3.001	13.652	0.0295
1000	457.74	3.572	0.737	0.334	5.834	0.0554	0.314	0.0208	0.189	0.182	3.059	13.304	0.0290
1010	464.83	3.510	0.693	0.337	6.366	0.0557	0.304	0.0211	0.186	0.186	2.968	12.435	0.0294
1020	472.00	3.470	0.718	0.324	6.166	0.0557	0.205	0.0209	0.176	0.176	2.907	12.880	0.0289
1030	******	3.507	0.698	0.329	5.542	0.0554	0.164	0.0197	0.178	0.189	2.959	12.596	0.0287
1040	******	3.605	0.688	0.310	5.605	0.0528	0.175	0.0183	0.187	0.198	3.047	13.041	0.0318
1050	******	3.557	0.667	0.308	4.203	0.0529	0.129	0.0164	0.182	0.188	3.058	12.617	0.0309
1060	******	3.480	0.724	0.322	3.968	0.0547	0.089	0.0165	0.185	0.187	3.032	13.228	0.0300
1070	******	3.394	0.756	0.337	2.306	0.0557	0.068	0.0138	0.182	0.172	3.001	13.569	0.0302

Table C.4.3-3 (Contd.) Salt free major elements and their ratios in core CD3826.

Depth(cm)	Age(ka)	Si(Wt.%)	Al(Wt.%)	Fe(Wt.%)	Mg(Wt.%)	Ca(Wt.%)	Na(Wt.%)	K(Wt.%)	Ti(Wt.%)	Mn(Wt.%)	P(Wt.%)
1	0.15	20.781	7.163	4.931	1.991	3.253	3.999	0.975	0.442	0.0449	0.0751
10	1.55	20.753	7.168	5.015	1.997	3.990	3.880	0.974	0.443	0.0999	0.0681
20	3.10	20.229	6.993	4.708	1.960	5.291	3.383	0.971	0.432	0.0480	0.0659
21	3.25	20.257	6.835	4.512	1.948	5.234	3.316	0.993	0.433	0.0410	0.0681
30	4.64	19.434	6.570	4.421	1.936	6.592	3.094	1.017	0.416	0.0418	0.0637
40	6.19	18.892	6.554	4.358	1.918	7.064	3.235	0.981	0.409	0.0441	0.0615
50	8.13	18.892	6.671	4.365	1.985	6.785	3.301	0.981	0.411	0.0426	0.0611
60	10.06	18.967	6.739	4.491	1.906	6.607	3.242	1.029	0.426	0.0395	0.0607
70	12.00	19.004	6.755	4.652	1.888	6.163	3.109	1.026	0.421	0.0348	0.0589
80	12.69	19.542	7.041	4.827	1.876	5.384	3.168	1.071	0.447	0.0333	0.0602
90	13.38	19.037	6.835	4.603	1.834	5.606	3.086	1.058	0.423	0.0333	0.0563
100	14.07	18.546	6.634	4.533	1.737	5.877	2.960	1.025	0.402	0.0318	0.0589
110	14.75	18.336	6.655	4.358	1.677	6.113	2.908	1.015	0.400	0.0263	0.0572
120	15.44	17.892	6.401	4.596	1.725	6.850	2.767	0.994	0.406	0.0287	0.0572
130	16.13	17.719	6.369	4.547	1.743	6.828	2.775	1.044	0.406	0.0225	0.0572
140	16.82	17.859	6.364	4.792	1.761	6.628	2.834	1.019	0.408	0.0263	0.0572
150	17.71	17.817	6.337	4.561	1.701	6.957	2.893	1.019	0.395	0.0256	0.0559
160	18.59	17.490	6.232	4.575	1.677	7.079	2.908	0.978	0.388	0.0256	0.0576
170	19.48	18.317	6.427	4.491	1.792	6.771	2.960	0.991	0.408	0.0279	0.0563
180	20.23	19.173	6.739	4.715	1.816	5.691	3.034	1.024	0.424	0.0263	0.0541
190	20.99	18.757	6.634	4.428	1.779	6.371	2.968	1.012	0.415	0.0256	0.0567
200	21.74	19.107	6.713	4.687	1.785	6.020	2.819	1.037	0.427	0.0240	0.0546
210	22.49	19.776	6.803	4.897	1.822	4.698	3.309	1.073	0.430	0.0287	0.0633
220	23.25	20.201	7.120	4.841	1.822	5.377	3.101	1.099	0.438	0.0279	0.0528
230	24.00	20.622	6.893	4.876	1.828	4.569	2.953	1.067	0.434	0.0302	0.0528
240	28.38	19.949	6.517	4.512	1.761	6.099	2.997	1.024	0.405	0.0318	0.0506
250	32.75	20.309	6.877	4.519	1.701	5.069	2.923	1.050	0.408	0.0333	0.0502
260	37.13	21.370	7.274	5.281	1.948	3.647	3.005	1.135	0.460	0.0310	0.0511
270	41.50	19.201	6.406	4.435	1.749	6.907	2.723	1.060	0.400	0.0318	0.0511
280	45.88	20.094	6.591	4.617	1.822	6.449	2.827	1.037	0.414	0.0410	0.0506
290	50.25	21.519	7.538	5.386	2.009	3.704	2.819	1.175	0.478	0.0364	0.0515
300	54.63	21.019	7.358	4.862	1.792	4.740	2.641	1.135	0.438	0.0488	0.0559
310	59.00	18.345	6.020	4.274	1.598	8.766	2.589	0.978	0.381	0.0263	0.0489
319	*****	18.832	6.068	4.512	1.641	7.851	2.678	0.988	0.388	0.0333	0.0506

Table C.4.4-1 Salt included major element data from core CD3827.

Depth(cm)	Age(ka)	Si(Wt.%)	Al(Wt.%)	Fe(Wt.%)	Ti(Wt.%)	Mn(Wt.%)	P(Wt.%)	Na(Wt.%)	K(Wt.%)	Ca(Wt.%)	Mg(Wt.%)	SALT
1	0.15	22.877	7.885	5.429	0.487	0.0494	0.0826	1.316	0.962	3.460	1.818	9.163
10	1.55	22.557	7.791	5.452	0.481	0.1086	0.0740	1.556	0.963	4.232	1.848	8.001
20	3.10	21.758	7.522	5.063	0.464	0.0516	0.0709	1.326	0.961	5.600	1.829	7.026
21	3.25	21.739	7.335	4.842	0.465	0.0440	0.0731	1.320	0.985	5.529	1.820	6.818
30	4.64	20.816	7.037	4.735	0.446	0.0448	0.0682	1.138	1.011	6.976	1.811	6.638
40	6.19	20.266	7.031	4.675	0.439	0.0474	0.0660	1.245	0.973	7.491	1.789	6.778
50	8.13	20.374	7.194	4.707	0.443	0.0459	0.0659	1.160	0.972	7.224	1.850	7.275
60	10.06	20.274	7.204	4.800	0.455	0.0422	0.0648	1.357	1.024	6.979	1.782	6.448
70	12.00	20.552	7.306	5.031	0.455	0.0377	0.0637	0.869	1.020	6.568	1.740	7.531
80	12.69	20.950	7.548	5.174	0.479	0.0357	0.0646	1.192	1.069	5.685	1.745	6.720
90	13.38	20.405	7.326	4.933	0.454	0.0357	0.0603	1.109	1.055	5.922	1.700	6.705
100	14.07	19.807	7.084	4.841	0.429	0.0339	0.0629	1.082	1.020	6.195	1.604	6.363
110	14.75	19.544	7.093	4.645	0.426	0.0281	0.0609	1.084	1.010	6.437	1.544	6.179
120	15.44	18.989	6.793	4.877	0.431	0.0304	0.0607	1.061	0.987	7.196	1.604	5.776
130	16.13	18.872	6.784	4.843	0.432	0.0239	0.0609	0.964	1.041	7.194	1.616	6.110
140	16.82	18.989	6.767	5.095	0.433	0.0280	0.0608	1.077	1.014	6.972	1.639	5.951
150	17.71	18.970	6.747	4.856	0.421	0.0272	0.0595	1.101	1.013	7.329	1.572	6.077
160	18.59	18.663	6.650	4.882	0.414	0.0273	0.0615	1.051	0.970	7.473	1.541	6.287
170	19.48	19.550	6.860	4.793	0.435	0.0298	0.0601	1.100	0.984	7.146	1.663	6.305
180	20.23	20.481	7.200	5.036	0.453	0.0281	0.0578	1.153	1.019	5.998	1.687	6.390
190	20.99	20.033	7.085	4.729	0.443	0.0273	0.0606	1.088	1.006	6.722	1.649	6.369
200	21.74	20.249	7.114	4.967	0.453	0.0254	0.0578	1.160	1.033	6.308	1.671	5.636
210	22.49	21.182	7.287	5.245	0.460	0.0307	0.0678	1.369	1.071	4.946	1.688	6.637
220	23.25	21.501	7.579	5.152	0.466	0.0297	0.0562	1.332	1.099	5.646	1.701	6.046
230	24.00	21.918	7.326	5.182	0.461	0.0321	0.0561	1.214	1.065	4.781	1.710	5.916
240	28.38	21.285	6.954	4.814	0.432	0.0339	0.0540	1.148	1.019	6.427	1.631	6.279
250	32.75	21.535	7.292	4.792	0.433	0.0353	0.0532	1.252	1.047	5.303	1.580	5.694
260	37.13	22.642	7.707	5.596	0.488	0.0328	0.0541	1.361	1.137	3.792	1.844	5.621
270	41.50	20.300	6.773	4.689	0.423	0.0336	0.0540	1.127	1.058	7.234	1.638	5.414
280	45.88	21.283	6.982	4.890	0.439	0.0435	0.0536	1.183	1.033	6.760	1.710	5.589
290	50.25	22.661	7.938	5.672	0.504	0.0383	0.0542	1.346	1.179	3.837	1.919	5.037
300	54.63	22.118	7.743	5.116	0.461	0.0513	0.0588	1.179	1.137	4.926	1.692	4.969
310	59.00	19.350	6.350	4.508	0.402	0.0278	0.0516	1.056	0.971	9.180	1.483	5.191
319	*****	19.941	6.425	4.778	0.411	0.0353	0.0536	1.034	0.981	8.242	1.519	5.562

Table C.4.4-2 Salt free major element data from core CD3827.

Depth(cm)	Age(ka)	Si/Al	Ca/Al	Fe/Al	Mg/Al	Ti/Al	Mn/Al	P/Al	Na/Al	K/Al	Siterrig/Al	Fe/Ti	K/Rb
1	0.15	2.901	0.439	0.688	0.231	0.0618	0.0063	0.0105	0.167	0.122	2.526	11.148	0.0247
10	1.55	2.895	0.543	0.700	0.237	0.0618	0.0139	0.0095	0.200	0.124	2.547	11.323	0.0266
20	3.10	2.893	0.745	0.673	0.243	0.0617	0.0069	0.0094	0.176	0.128	2.547	10.908	0.0283
21	3.25	2.964	0.754	0.660	0.248	0.0634	0.0060	0.0100	0.180	0.134	2.607	10.411	0.0272
30	4.64	2.958	0.991	0.673	0.257	0.0633	0.0064	0.0097	0.162	0.144	2.591	10.627	0.0301
40	6.19	2.882	1.065	0.665	0.254	0.0625	0.0067	0.0094	0.177	0.138	2.579	10.645	0.0293
50	8.13	2.832	1.004	0.654	0.257	0.0616	0.0064	0.0092	0.161	0.135	2.574	10.615	0.0270
60	10.06	2.814	0.969	0.666	0.247	0.0631	0.0059	0.0090	0.188	0.142	2.585	10.552	0.0311
70	12.00	2.813	0.899	0.689	0.238	0.0623	0.0052	0.0087	0.119	0.140	2.590	11.055	0.0277
80	12.69	2.775	0.753	0.685	0.231	0.0635	0.0047	0.0086	0.158	0.142	2.564	10.794	0.0291
90	13.38	2.785	0.808	0.673	0.232	0.0619	0.0049	0.0082	0.151	0.144	2.598	10.877	0.0272
100	14.07	2.796	0.874	0.683	0.226	0.0605	0.0048	0.0089	0.153	0.144	2.568	11.287	0.0244
110	14.75	2.755	0.907	0.655	0.218	0.0601	0.0040	0.0086	0.153	0.142	2.571	10.900	0.0233
120	15.44	2.795	1.059	0.718	0.236	0.0635	0.0045	0.0089	0.156	0.145	2.607	11.309	0.0260
130	16.13	2.782	1.061	0.714	0.238	0.0637	0.0035	0.0090	0.142	0.153	2.597	11.205	0.0273
140	16.82	2.806	1.030	0.753	0.242	0.0640	0.0041	0.0090	0.159	0.150	2.614	11.756	0.0268
150	17.71	2.811	1.086	0.720	0.233	0.0623	0.0040	0.0088	0.163	0.150	2.588	11.546	0.0264
160	18.59	2.807	1.124	0.734	0.232	0.0622	0.0041	0.0092	0.158	0.146	2.574	11.796	0.0249
170	19.48	2.850	1.042	0.699	0.242	0.0634	0.0043	0.0088	0.160	0.143	2.598	11.018	0.0270
180	20.23	2.845	0.833	0.700	0.234	0.0629	0.0039	0.0080	0.160	0.142	2.588	11.125	0.0260
190	20.99	2.828	0.949	0.667	0.233	0.0625	0.0039	0.0086	0.154	0.142	2.569	10.675	0.0272
200	21.74	2.846	0.887	0.698	0.235	0.0637	0.0036	0.0081	0.163	0.145	2.578	10.966	0.0281
210	22.49	2.907	0.679	0.720	0.232	0.0632	0.0042	0.0093	0.188	0.147	2.599	11.393	0.0275
220	23.25	2.837	0.745	0.680	0.224	0.0615	0.0039	0.0074	0.176	0.145	2.555	11.063	0.0285
230	24.00	2.992	0.653	0.707	0.233	0.0630	0.0044	0.0077	0.166	0.145	2.615	11.235	0.0278
240	28.38	3.061	0.924	0.692	0.235	0.0622	0.0049	0.0078	0.165	0.147	2.631	11.135	0.0274
250	32.75	2.953	0.727	0.657	0.217	0.0594	0.0048	0.0073	0.172	0.144	2.618	11.070	0.0274
260	37.13	2.938	0.492	0.726	0.239	0.0633	0.0043	0.0070	0.177	0.148	2.610	11.472	0.0295
270	41.50	2.997	1.068	0.692	0.242	0.0625	0.0050	0.0080	0.166	0.156	2.669	11.076	0.0283
280	45.88	3.048	0.968	0.700	0.245	0.0628	0.0062	0.0077	0.169	0.148	2.595	11.146	0.0305
290	50.25	2.855	0.483	0.715	0.242	0.0635	0.0048	0.0068	0.170	0.148	2.562	11.261	0.0315
300	54.63	2.856	0.636	0.661	0.218	0.0595	0.0066	0.0076	0.152	0.147	2.634	11.095	0.0271
310	59.00	3.047	1.446	0.710	0.234	0.0633	0.0044	0.0081	0.166	0.153	2.645	11.211	0.0297
319	*****	3.104	1.283	0.744	0.236	0.0639	0.0055	0.0083	0.161	0.153	2.682	11.634	0.0284

Table C.4.4-3 Salt free major elements and their ratios in core CD3827.

Depth(cm)	Age(ka)	Si(Wt.%)	Al(Wt.%)	Fe(Wt.%)	Mg(Wt.%)	Ca(Wt.%)	Na(Wt.%)	K(Wt.%)	Ti(Wt.%)	Mn(Wt.%)	P(Wt.%)
9	2.49	2.939	0.526	0.379	0.403	33.026	1.609	0.128	0.046	0.0155	0.0306
11	3.04	2.684	0.507	0.365	0.423	32.481	1.711	0.137	0.046	0.0108	0.0306
13	3.59	2.873	0.544	0.368	0.438	32.554	1.900	0.141	0.046	0.0139	0.0354
15	4.14	2.625	0.526	0.362	0.496	33.157	1.850	0.139	0.043	0.0093	0.0376
17	4.70	2.509	0.497	0.351	0.432	32.385	1.855	0.142	0.042	0.0139	0.0371
19	5.25	2.481	0.506	0.353	0.389	32.636	1.742	0.135	0.042	0.0108	0.0310
21	5.80	2.380	0.489	0.351	0.390	33.518	1.722	0.131	0.044	0.0101	0.0332
23	6.35	2.333	0.468	0.350	0.409	33.757	1.724	0.129	0.045	0.0046	0.0297
25	6.91	2.143	0.440	0.347	0.390	33.696	1.617	0.125	0.041	0.0124	0.0297
27	7.46	2.307	0.468	0.358	0.384	33.600	1.818	0.129	0.042	0.0155	0.0297
29	8.01	2.323	0.441	0.336	0.413	33.666	1.626	0.122	0.039	0.0155	0.0275
31	8.56	2.444	0.403	0.348	0.391	33.863	1.582	0.108	0.039	0.0132	0.0306
33	9.12	2.281	0.381	0.332	0.385	33.692	1.582	0.110	0.034	0.0132	0.0288
35	9.67	2.324	0.369	0.341	0.356	33.778	1.580	0.108	0.032	0.0132	0.0288
37	10.22	2.407	0.344	0.347	0.356	33.406	1.727	0.109	0.031	0.0132	0.0288
39	10.77	2.158	0.331	0.356	0.347	34.003	1.589	0.102	0.035	0.0062	0.0258
41	11.33	1.915	0.322	0.341	0.351	33.819	1.465	0.098	0.032	0.0054	0.0275
43	11.89	1.702	0.293	0.341	0.392	34.698	1.494	0.095	0.032	0.0116	0.0271
45	12.01	1.751	0.302	0.331	0.332	34.516	1.456	0.094	0.035	0.0194	0.0262
47	12.13	1.831	0.310	0.304	0.356	34.299	1.575	0.095	0.034	0.0155	0.0293
49	12.25	1.518	0.270	0.268	0.315	32.956	1.537	0.090	0.032	0.0108	0.0262
51	12.37	2.099	0.312	0.254	0.362	33.511	1.649	0.094	0.034	0.0124	0.0280
53	12.49	1.506	0.285	0.231	0.319	34.564	1.569	0.085	0.033	0.0116	0.0249
55	12.61	1.240	0.267	0.213	0.339	34.936	1.541	0.081	0.030	0.0132	0.0240
57	12.73	0.892	0.227	0.191	0.294	35.474	1.386	0.075	0.029	0.0108	0.0253
59	12.90	0.805	0.226	0.197	0.296	35.549	1.354	0.070	0.030	0.0085	0.0232
61	13.08	0.738	0.225	0.189	0.284	35.004	1.405	0.073	0.029	0.0093	0.0262
63	13.25	0.921	0.248	0.193	0.341	35.138	1.370	0.076	0.030	0.0124	0.0223

Table C.4.5-1 Salt included major element data from core P5.

Depth(cm)	Age(ka)	Si(Wt.%)	Al(Wt.%)	Fe(Wt.%)	Mg(Wt.%)	Ca(Wt.%)	Na(Wt.%)	K(Wt.%)	Ti(Wt.%)	Mn(Wt.%)	P(Wt.%)
65	13.42	0.747	0.239	0.185	0.311	35.497	1.546	0.094	0.030	0.0070	0.0240
67	13.60	0.628	0.233	0.174	0.289	35.614	1.290	0.069	0.031	0.0085	0.0267
69	13.77	0.661	0.239	0.173	0.304	35.496	1.363	0.071	0.033	0.0093	0.0232
71	13.94	0.697	0.246	0.170	0.333	35.367	1.479	0.075	0.032	0.0077	0.0267
73	14.12	0.825	0.261	0.182	0.310	35.446	1.410	0.075	0.029	0.0132	0.0267
75	14.29	0.836	0.261	0.181	0.326	35.363	1.762	0.149	0.029	0.0132	0.0267
77	14.46	0.933	0.249	0.191	0.295	35.520	1.291	0.077	0.028	0.0108	0.0280
79	14.63	0.946	0.257	0.191	0.353	35.494	1.294	0.076	0.029	0.0116	0.0258
81	14.81	1.029	0.267	0.198	0.306	35.255	1.476	0.081	0.030	0.0116	0.0262
83	14.98	0.760	0.249	0.198	0.297	35.611	1.292	0.076	0.028	0.0124	0.0275
85	15.15	0.785	0.251	0.208	0.309	35.474	1.471	0.075	0.029	0.0132	0.0245
87	15.33	0.833	0.249	0.188	0.319	35.452	1.546	0.085	0.029	0.0085	0.0253
89	15.50	1.007	0.264	0.205	0.297	35.389	1.434	0.079	0.033	0.0108	0.0288
91	16.03	0.841	0.249	0.197	0.300	35.750	1.369	0.071	0.031	0.0116	0.0271
93	16.56	0.841	0.233	0.190	0.298	35.403	1.418	0.072	0.025	0.0101	0.0258
95	17.09	0.844	0.236	0.190	0.320	35.464	1.451	0.074	0.028	0.0155	0.0271
97	17.63	0.902	0.261	0.205	0.318	35.384	1.456	0.077	0.028	0.0116	0.0306
99	18.16	1.125	0.279	0.212	0.303	34.917	1.574	0.085	0.031	0.0101	0.0267
101	18.69	1.121	0.257	0.197	0.312	34.948	1.501	0.079	0.029	0.0085	0.0262
103	19.22	1.322	0.270	0.206	0.320	34.789	1.544	0.082	0.031	0.0101	0.0271
105	19.75	1.384	0.293	0.222	0.361	34.789	1.600	0.081	0.028	0.0132	0.0240
107	20.28	1.318	0.292	0.231	0.343	33.744	1.384	0.081	0.028	0.0116	0.0240
109	20.81	1.294	0.296	0.232	0.350	34.836	1.433	0.083	0.029	0.0139	0.0227
111	21.34	1.321	0.300	0.238	0.349	34.752	1.522	0.085	0.029	0.0170	0.0245
113	21.88	1.417	0.316	0.245	0.355	34.658	1.421	0.086	0.032	0.0108	0.0253
115	22.41	1.471	0.323	0.245	0.370	34.375	1.519	0.091	0.034	0.0124	0.0262
117	22.94	1.603	0.337	0.254	0.364	35.055	1.714	0.094	0.033	0.0170	0.0249
119	23.47	1.652	0.333	0.265	0.383	34.267	1.556	0.100	0.033	0.0124	0.0262
121	24.00	1.756	0.363	0.292	0.372	34.081	1.551	0.099	0.034	0.0139	0.0280
123	*****	2.114	0.386	0.323	0.364	33.930	1.612	0.104	0.037	0.0147	0.0302

Table C.4.5-1 (Contd.) Salt included major element data from core P5.

Depth(cm)	Age(ka)	Si(Wt.%)	Al(Wt.%)	Fe(Wt.%)	Mg(Wt.%)	Ca(Wt.%)	Na(Wt.%)	K(Wt.%)	Ti(Wt.%)	Mn(Wt.%)	P(Wt.%)	SALT
9	2.49	3.038	0.544	0.392	0.291	34.103	0.628	0.0949	0.0477	0.0160	0.0316	3.374
11	3.04	2.780	0.525	0.377	0.307	33.594	0.683	0.1027	0.0478	0.0112	0.0317	3.563
13	3.59	2.980	0.565	0.382	0.316	33.729	0.824	0.1052	0.0472	0.0145	0.0367	3.714
15	4.14	2.773	0.555	0.383	0.315	34.962	0.227	0.0843	0.0456	0.0098	0.0397	3.730
17	4.70	2.603	0.515	0.364	0.310	33.554	0.777	0.1060	0.0435	0.0145	0.0385	3.702
19	5.25	2.572	0.524	0.365	0.268	33.784	0.688	0.1001	0.0435	0.0112	0.0322	3.634
21	5.80	2.470	0.507	0.365	0.265	34.742	0.628	0.0944	0.0460	0.0104	0.0345	3.811
23	6.35	2.431	0.488	0.364	0.271	35.117	0.518	0.0889	0.0468	0.0048	0.0310	4.075
25	6.91	2.232	0.458	0.361	0.252	35.053	0.406	0.0838	0.0431	0.0129	0.0310	4.121
27	7.46	2.409	0.489	0.373	0.238	35.032	0.546	0.0866	0.0438	0.0162	0.0310	4.285
29	8.01	2.426	0.461	0.351	0.268	35.101	0.346	0.0788	0.0407	0.0162	0.0287	4.399
31	8.56	2.552	0.421	0.364	0.245	35.306	0.300	0.0641	0.0407	0.0137	0.0319	4.403
33	9.12	2.382	0.398	0.347	0.238	35.128	0.300	0.0658	0.0357	0.0137	0.0301	4.385
35	9.67	2.433	0.387	0.357	0.200	35.303	0.221	0.0614	0.0339	0.0138	0.0302	4.569
37	10.22	2.519	0.360	0.363	0.200	34.915	0.375	0.0623	0.0326	0.0138	0.0302	4.631
39	10.77	2.259	0.347	0.373	0.190	35.539	0.231	0.0554	0.0364	0.0065	0.0270	4.490
41	11.33	2.005	0.337	0.357	0.194	35.347	0.101	0.0510	0.0339	0.0057	0.0288	4.629
43	11.89	1.780	0.306	0.357	0.242	36.221	0.171	0.0489	0.0332	0.0121	0.0283	4.543
45	12.01	1.831	0.315	0.346	0.178	36.032	0.130	0.0480	0.0363	0.0202	0.0274	4.476
47	12.13	1.914	0.324	0.317	0.204	35.804	0.255	0.0489	0.0351	0.0162	0.0306	4.467
49	12.25	1.587	0.283	0.281	0.161	34.400	0.215	0.0437	0.0338	0.0113	0.0274	4.469
51	12.37	2.180	0.324	0.264	0.233	34.755	0.535	0.0551	0.0355	0.0129	0.0290	4.369
53	12.49	1.575	0.298	0.242	0.165	36.082	0.249	0.0394	0.0344	0.0121	0.0260	4.087
55	12.61	1.293	0.278	0.222	0.195	36.385	0.293	0.0376	0.0312	0.0137	0.0251	4.281
57	12.73	0.930	0.237	0.199	0.151	36.906	0.166	0.0319	0.0300	0.0113	0.0264	4.048
59	12.90	0.838	0.236	0.205	0.158	36.945	0.166	0.0279	0.0312	0.0089	0.0241	4.139
61	13.08	0.769	0.235	0.197	0.141	36.415	0.186	0.0302	0.0306	0.0097	0.0273	4.170
63	13.25	0.960	0.258	0.201	0.200	36.555	0.149	0.0327	0.0312	0.0129	0.0232	4.185

Table C.4.5-2 Salt free major element data from core P5.

Depth(cm)	Age(ka)	Si(Wt.%)	Al(Wt.%)	Fe(Wt.%)	Mg(Wt.%)	Ca(Wt.%)	Na(Wt.%)	K(Wt.%)	Ti(Wt.%)	Mn(Wt.%)	P(Wt.%)	SALT
65	13.42	0.779	0.249	0.193	0.169	36.929	0.333	0.0518	0.0312	0.0073	0.0250	4.088
67	13.60	0.652	0.241	0.180	0.162	36.903	0.191	0.0302	0.0323	0.0088	0.0277	3.685
69	13.77	0.686	0.248	0.180	0.173	36.816	0.237	0.0309	0.0342	0.0096	0.0241	3.844
71	13.94	0.724	0.256	0.176	0.200	36.718	0.328	0.0342	0.0330	0.0080	0.0277	3.890
73	14.12	0.858	0.272	0.189	0.176	36.800	0.256	0.0342	0.0299	0.0137	0.0277	3.840
75	14.29	0.870	0.271	0.188	0.189	36.751	0.591	0.1099	0.0305	0.0137	0.0277	3.997
77	14.46	0.968	0.258	0.198	0.167	36.806	0.193	0.0389	0.0286	0.0112	0.0290	3.700
79	14.63	0.983	0.267	0.199	0.220	36.849	0.136	0.0350	0.0299	0.0121	0.0268	3.919
81	14.81	1.070	0.277	0.206	0.172	36.601	0.324	0.0402	0.0311	0.0121	0.0273	3.913
83	14.98	0.789	0.259	0.206	0.166	36.935	0.164	0.0361	0.0286	0.0129	0.0286	3.855
85	15.15	0.815	0.260	0.216	0.178	36.793	0.350	0.0352	0.0305	0.0137	0.0254	3.799
87	15.33	0.863	0.257	0.195	0.199	36.671	0.512	0.0494	0.0304	0.0088	0.0262	3.559
89	15.50	1.045	0.274	0.212	0.169	36.670	0.341	0.0406	0.0342	0.0112	0.0299	3.704
91	16.03	0.870	0.257	0.204	0.182	36.948	0.355	0.0357	0.0316	0.0120	0.0280	4.248
93	16.56	0.874	0.242	0.197	0.164	36.755	0.265	0.0316	0.0262	0.0105	0.0268	4.002
95	17.09	0.877	0.246	0.197	0.186	36.819	0.299	0.0333	0.0286	0.0161	0.0282	3.934
97	17.63	0.938	0.272	0.213	0.185	36.735	0.304	0.0368	0.0286	0.0121	0.0318	4.453
99	18.16	1.172	0.291	0.221	0.161	36.325	0.362	0.0423	0.0324	0.0105	0.0278	4.028
101	18.69	1.163	0.266	0.204	0.185	36.213	0.410	0.0406	0.0298	0.0088	0.0272	4.147
103	19.22	1.377	0.282	0.215	0.178	36.192	0.331	0.0397	0.0318	0.0105	0.0282	4.172
105	19.75	1.437	0.304	0.230	0.232	36.082	0.484	0.0413	0.0286	0.0137	0.0250	3.822
107	20.28	1.370	0.304	0.240	0.210	35.031	0.229	0.0402	0.0286	0.0121	0.0250	3.912
109	20.81	1.341	0.307	0.241	0.227	36.065	0.367	0.0459	0.0304	0.0144	0.0236	4.032
111	21.34	1.367	0.310	0.247	0.233	35.916	0.513	0.0494	0.0297	0.0176	0.0253	3.987
113	21.88	1.468	0.327	0.253	0.236	35.848	0.383	0.0503	0.0329	0.0112	0.0262	4.063
115	22.41	1.527	0.335	0.255	0.245	35.618	0.429	0.0535	0.0348	0.0129	0.0272	3.693
117	22.94	1.663	0.349	0.263	0.239	36.324	0.631	0.0561	0.0342	0.0177	0.0258	3.729
119	23.47	1.711	0.345	0.274	0.265	35.444	0.522	0.0640	0.0341	0.0128	0.0272	3.917
121	24.00	1.819	0.376	0.303	0.254	35.251	0.517	0.0631	0.0347	0.0144	0.0290	3.873
123	*****	2.193	0.400	0.335	0.239	35.157	0.525	0.0664	0.0379	0.0153	0.0313	3.669

Table C.4.5-2 (Contd.) Salt free major element data from core P5.

Depth(cm)	Age(ka)	Si/Al	Fe/Al	Mg/Al	Ca/Al	Ti/Al	Mn/Al	P/Al	K/Al	Na/Al	Ca/ P	Siterrig/Al	Fe/Ti	K/Rb *10-1
9	2.49	5.584	0.721	0.535	62.679	0.0876	0.0294	0.0581	0.174	1.154	1078.36	1.786	8.222	16.094
11	3.04	5.298	0.719	0.585	64.025	0.0910	0.0214	0.0604	0.196	1.302	1060.48	1.194	7.903	16.784
13	3.59	5.278	0.676	0.559	59.729	0.0836	0.0256	0.0650	0.186	1.459	918.46	1.589	8.084	15.112
15	4.14	4.993	0.689	0.567	62.943	0.0820	0.0177	0.0715	0.152	0.408	880.55	1.789	8.403	12.885
17	4.70	5.051	0.706	0.601	65.125	0.0844	0.0281	0.0748	0.206	1.508	870.68	1.254	8.359	15.014
19	5.25	4.908	0.697	0.511	64.462	0.0829	0.0214	0.0614	0.191	1.312	1050.48	1.228	8.409	14.835
21	5.80	4.870	0.719	0.522	68.502	0.0907	0.0206	0.0680	0.186	1.239	1007.89	1.415	7.923	20.646
23	6.35	4.986	0.747	0.557	72.029	0.0960	0.0099	0.0635	0.182	1.062	1134.37	1.273	7.786	15.514
25	6.91	4.871	0.789	0.550	76.489	0.0940	0.0282	0.0676	0.183	0.887	1132.30	1.046	8.396	13.847
27	7.46	4.929	0.764	0.486	71.688	0.0896	0.0331	0.0635	0.177	1.118	1128.99	0.625	8.526	15.350
29	8.01	5.263	0.761	0.581	76.141	0.0882	0.0351	0.0624	0.171	0.751	1221.01	1.456	8.624	15.066
31	8.56	6.068	0.865	0.583	83.943	0.0967	0.0327	0.0759	0.152	0.713	1105.33	1.389	8.948	10.745
33	9.12	5.987	0.872	0.599	88.281	0.0896	0.0345	0.0757	0.165	0.753	1166.40	1.878	9.732	12.583
35	9.67	6.292	0.924	0.517	91.292	0.0876	0.0356	0.0781	0.159	0.572	1169.27	1.123	10.554	11.276
37	10.22	6.997	1.009	0.555	96.964	0.0906	0.0383	0.0839	0.173	1.042	1156.39	0.822	11.140	11.652
39	10.77	6.515	1.075	0.549	102.488	0.1049	0.0187	0.0778	0.160	0.665	1316.73	1.487	10.250	12.016
41	11.33	5.954	1.061	0.576	104.957	0.1005	0.0168	0.0856	0.151	0.299	1226.46	1.351	10.554	11.314
43	11.89	5.808	1.165	0.788	118.208	0.1083	0.0396	0.0924	0.160	0.557	1278.72	0.649	10.753	10.608
45	12.01	5.807	1.097	0.566	114.283	0.1152	0.0642	0.0869	0.152	0.413	1314.42	0.975	9.524	10.924
47	12.13	5.905	0.979	0.628	110.454	0.1082	0.0499	0.0944	0.151	0.787	1169.66	0.619	9.049	11.678
49	12.25	5.616	0.993	0.569	121.729	0.1197	0.0401	0.0970	0.155	0.760	1254.90	0.329	8.300	8.881
51	12.37	6.736	0.814	0.721	107.390	0.1096	0.0398	0.0897	0.170	1.654	1196.61	0.935	7.432	11.702
53	12.49	5.283	0.811	0.554	121.036	0.1155	0.0407	0.0874	0.132	0.835	1385.53	0.346	7.022	8.987
55	12.61	4.650	0.799	0.700	130.861	0.1123	0.0494	0.0902	0.135	1.054	1451.48	-0.026	7.115	7.822
57	12.73	3.924	0.842	0.639	155.808	0.1265	0.0477	0.1115	0.135	0.699	1397.70	-1.020	6.656	6.509
59	12.90	3.559	0.870	0.670	156.875	0.1323	0.0376	0.1023	0.118	0.707	1532.85	-0.934	6.577	6.678
61	13.08	3.279	0.840	0.602	155.185	0.1303	0.0413	0.1164	0.128	0.792	1333.16	-1.150	6.449	6.148
63	13.25	3.722	0.779	0.777	141.771	0.1210	0.0501	0.0900	0.127	0.579	1574.45	-0.697	6.437	8.257

Table C.4.5-3 Salt free major elements and their ratios in core P5.

Table C.4.5-3 (Contd.) Salt free major elements and their ratios in core P5.

Depth(cm)	Age(ka)	Si/Al	Fe/Al	Mg/Al	Ca/Al	Ti/Al	Mn/Al	P/Al	K/Al	Na/Al	Ca/P	Siterrig/Al	Fe/Ti	K/Rb *10-1
65	13.42	3.127	0.774	0.679	148.304	0.1253	0.0292	0.1006	0.208	1.337	1474.89	-0.705	6.179	11.034
67	13.60	2.700	0.747	0.669	152.878	0.1339	0.0366	0.1146	0.125	0.792	1334.37	-0.900	5.581	6.197
69	13.77	2.765	0.724	0.698	148.316	0.1378	0.0389	0.0969	0.125	0.956	1530.67	-0.842	5.256	5.217
71	13.94	2.834	0.690	0.784	143.630	0.1291	0.0315	0.1084	0.134	1.283	1325.04	-0.743	5.344	6.567
73	14.12	3.159	0.695	0.648	135.485	0.1100	0.0504	0.1020	0.126	0.943	1328.01	0.372	6.315	6.442
75	14.29	3.205	0.694	0.697	135.435	0.1126	0.0505	0.1022	0.405	2.177	1324.83	-0.628	6.162	20.691
77	14.46	3.745	0.765	0.647	142.419	0.1106	0.0435	0.1123	0.150	0.746	1268.47	-0.215	6.920	7.636
79	14.63	3.686	0.746	0.827	138.188	0.1121	0.0453	0.1005	0.131	0.509	1374.86	-1.964	6.656	7.011
81	14.81	3.861	0.744	0.621	132.073	0.1123	0.0436	0.0984	0.145	1.170	1342.84	-0.074	6.624	6.661
83	14.98	3.051	0.796	0.643	142.779	0.1106	0.0497	0.1105	0.140	0.634	1291.86	-0.666	7.200	7.545
85	15.15	3.130	0.830	0.685	141.326	0.1171	0.0525	0.0976	0.135	1.344	1447.74	-0.674	7.093	6.780
87	15.33	3.351	0.756	0.772	142.458	0.1181	0.0343	0.1020	0.192	1.990	1397.10	-0.815	6.401	8.357
89	15.50	3.809	0.774	0.616	133.645	0.1246	0.0410	0.1091	0.148	1.242	1225.48	-0.230	6.213	7.814
91	16.03	3.383	0.792	0.709	143.661	0.1229	0.0467	0.1090	0.139	1.379	1318.00	-0.532	6.448	10.683
93	16.56	3.614	0.816	0.678	151.963	0.1081	0.0433	0.1108	0.131	1.094	1371.34	-0.449	7.551	5.413
95	17.09	3.571	0.804	0.757	149.838	0.1166	0.0655	0.1146	0.136	1.215	1307.25	-0.406	6.894	7.271
97	17.63	3.452	0.783	0.680	135.244	0.1055	0.0445	0.1171	0.135	1.120	1155.21	-0.070	7.429	7.804
99	18.16	4.028	0.758	0.553	124.840	0.1115	0.0360	0.0954	0.145	1.245	1308.06	-0.119	6.797	8.277
101	18.69	4.371	0.768	0.694	136.069	0.1121	0.0332	0.1022	0.152	1.541	1331.22	-0.133	6.851	8.839
103	19.22	4.892	0.762	0.634	128.528	0.1130	0.0372	0.1002	0.141	1.174	1282.25	0.441	6.746	8.447
105	19.75	4.722	0.756	0.762	118.546	0.0940	0.0449	0.0820	0.136	1.589	1445.59	0.116	8.039	7.634
107	20.28	4.513	0.792	0.693	115.394	0.0944	0.0398	0.0823	0.132	0.755	1402.06	-0.125	8.396	8.219
109	20.81	4.367	0.783	0.741	117.441	0.0991	0.0470	0.0767	0.149	1.197	1531.16	0.339	7.905	10.004
111	21.34	4.405	0.795	0.750	115.714	0.0958	0.0568	0.0816	0.159	1.653	1418.43	0.278	8.290	9.890
113	21.88	4.486	0.774	0.720	109.588	0.1005	0.0343	0.0802	0.154	1.171	1365.76	0.551	7.706	10.043
115	22.41	4.559	0.760	0.731	106.366	0.1039	0.0384	0.0812	0.160	1.280	1309.37	0.570	7.314	9.907
117	22.94	4.762	0.754	0.683	104.031	0.0979	0.0506	0.0740	0.161	1.808	1405.58	0.822	7.703	9.997
119	23.47	4.956	0.795	0.767	102.666	0.0988	0.0372	0.0787	0.185	1.513	1305.33	0.520	8.043	10.249
121	24.00	4.838	0.805	0.675	93.760	0.0924	0.0384	0.0770	0.168	1.375	1217.09	0.905	8.714	11.901
123	*****	5.479	0.838	0.597	87.826	0.0947	0.0381	0.0781	0.166	1.312	1123.82	1.068	8.844	10.843

Depth(cm)	Si(Wt.%)	Al(Wt.%)	Fe(Wt.%)	Mg(Wt.%)	Ca(Wt.%)	Na(Wt.%)	K(Wt.%)	Ti(Wt.%)	Mn(Wt.%)	P(Wt.%)
11	23.261	8.622	6.398	2.319	0.951	2.942	1.169	0.497	0.0983	0.0629
13	23.311	8.687	6.370	2.270	0.946	2.913	1.196	0.508	0.0689	0.0603
25	23.658	8.861	6.243	2.203	0.996	2.528	1.223	0.519	0.0619	0.0612
27	23.578	8.785	6.191	2.211	1.023	2.626	1.218	0.521	0.0596	0.0603
29	23.558	8.757	6.121	2.227	1.066	2.735	1.219	0.525	0.0588	0.0564
31	23.577	8.726	6.261	2.242	1.032	2.943	1.250	0.516	0.0581	0.0586
33	23.527	8.666	6.254	2.258	1.002	2.791	1.234	0.513	0.0596	0.0594
35	23.532	8.665	6.266	2.251	0.986	2.757	1.225	0.513	0.0612	0.0590
37	23.480	8.623	6.249	2.247	1.004	2.699	1.223	0.506	0.0627	0.0594
39	23.662	8.699	6.226	2.248	0.971	2.693	1.217	0.506	0.0596	0.0581
41	23.614	8.724	6.224	2.261	0.925	2.771	1.239	0.509	0.0619	0.0590
43	23.605	8.739	6.157	2.279	0.942	2.797	1.227	0.510	0.0534	0.0568
45	23.576	8.669	6.099	2.264	1.015	2.735	1.220	0.507	0.0519	0.0568
47	23.446	8.632	6.188	0.561	1.034	2.810	1.210	0.504	0.0581	0.0590
49	23.591	8.635	6.142	2.252	1.036	2.887	1.222	0.503	0.0511	0.0586
51	23.714	8.667	6.119	2.287	1.019	2.935	1.233	0.504	0.0503	0.0607
53	23.652	8.689	6.126	2.289	0.979	2.866	1.221	0.504	0.0557	0.0616
55	23.655	8.734	6.111	2.272	0.942	2.939	1.213	0.503	0.0527	0.0559
57	23.521	8.666	6.050	2.262	0.986	2.888	1.218	0.506	0.0527	0.0590
59	23.505	8.640	6.089	2.238	1.000	2.869	1.217	0.501	0.0557	0.0577
61	23.476	8.629	6.086	2.264	0.976	2.927	1.218	0.503	0.0550	0.0572
63	23.463	8.611	6.127	2.287	0.938	2.884	1.216	0.498	0.0534	0.0559
65	23.504	8.651	6.178	2.256	0.961	2.855	1.226	0.498	0.0527	0.0551
67	23.379	8.626	6.040	2.288	1.074	2.849	1.208	0.495	0.0534	0.0542
69	23.394	8.590	6.041	2.249	1.097	2.969	1.213	0.492	0.0550	0.0529
71	23.414	8.591	5.999	2.256	1.105	2.893	1.215	0.499	0.0542	0.0551
73	23.493	8.626	6.042	2.267	1.063	2.771	1.210	0.499	0.0550	0.0564
75	23.510	8.682	6.066	2.228	1.053	2.863	1.218	0.503	0.0550	0.0524
77	23.465	8.704	6.056	2.259	1.034	2.895	1.168	0.503	0.0550	0.0538
81	23.615	8.682	6.265	2.283	1.031	2.574	1.236	0.509	0.0627	0.0559
83	23.895	8.853	6.348	2.247	1.033	2.256	1.242	0.521	0.0666	0.0546
85	24.144	8.944	6.430	2.253	1.028	2.120	1.240	0.527	0.0705	0.0551
87	24.087	8.900	6.424	2.276	1.031	2.037	1.247	0.524	0.0643	0.0564
89	24.033	8.934	6.421	2.312	1.013	2.183	1.243	0.522	0.0658	0.0577
91	24.146	8.988	6.388	2.233	0.999	2.120	1.252	0.527	0.0588	0.0590
93	24.103	8.947	6.313	2.209	1.044	2.022	1.247	0.524	0.0565	0.0555
95	24.093	8.914	6.305	2.217	1.064	2.118	1.247	0.523	0.0550	0.0586
97	24.249	8.910	6.247	2.194	1.071	2.124	1.259	0.526	0.0596	0.0529
99	24.103	8.824	6.411	2.208	0.991	2.066	1.268	0.522	0.0612	0.0546
101	24.282	8.988	6.291	2.220	1.009	2.170	1.262	0.526	0.0596	0.0568
103	23.988	8.867	6.375	2.202	1.057	2.234	1.228	0.525	0.0604	0.0586
105	24.031	8.868	6.366	2.211	1.034	2.158	1.239	0.527	0.0542	0.0599
107	24.087	8.838	6.238	2.225	1.069	2.120	1.231	0.531	0.0472	0.0572
109	24.537	8.723	6.319	2.183	1.184	2.093	1.255	0.534	0.0449	0.0489
111	25.091	8.564	6.373	2.130	1.171	2.071	1.250	0.540	0.0434	0.0472
113	25.120	8.406	6.329	2.050	1.282	1.985	1.276	0.517	0.0441	0.0454
115	24.624	8.620	6.077	2.015	1.331	2.107	1.241	0.519	0.0372	0.0454
117	24.509	8.627	6.171	2.065	1.401	2.080	1.238	0.515	0.0434	0.0454
119	23.940	8.561	6.282	2.023	1.242	2.216	1.221	0.503	0.0379	0.0450
121	24.394	8.714	6.211	2.024	1.326	2.185	1.228	0.513	0.0403	0.0468
123	24.395	8.514	6.267	2.030	1.287	2.320	1.244	0.497	0.0403	0.0433
125	24.255	8.526	6.193	2.002	1.323	2.276	1.228	0.497	0.0379	0.0459
127	24.308	8.396	6.192	2.006	1.335	2.233	1.214	0.495	0.0441	0.0476
129	24.263	8.368	6.235	2.107	1.339	2.339	1.215	0.493	0.0434	0.0489
131	24.537	8.320	6.265	2.084	1.315	2.339	1.202	0.503	0.0449	0.0463
133	24.051	8.478	6.246	2.091	1.253	2.399	1.228	0.499	0.0434	0.0463
135	24.372	8.490	6.221	2.100	1.192	2.347	1.248	0.496	0.0418	0.0446
137	24.079	8.530	6.205	2.092	1.215	2.317	1.239	0.499	0.0395	0.0454
139	24.134	8.572	6.248	2.131	1.056	2.392	1.258	0.497	0.0434	0.0446
141	24.197	8.566	6.151	2.076	1.064	2.294	1.261	0.502	0.0426	0.0441
143	24.241	8.567	6.243	2.109	1.134	2.312	1.274	0.504	0.0395	0.0463
145	24.141	8.545	6.155	2.152	1.224	2.349	1.270	0.510	0.0418	0.0428
147	24.165	8.671	6.402	2.252	1.162	2.309	1.233	0.518	0.0426	0.0446
149	24.307	8.691	6.237	2.223	1.017	2.329	1.267	0.514	0.0418	0.0481
151	24.465	8.428	6.344	2.246	1.093	2.236	1.259	0.508	0.0472	0.0402

Table C.4.6-1 Salt included major element data from core P12.

Depth(cm)	Si(Wt.%)	Al(Wt.%)	Fe(Wt.%)	Mg(Wt.%)	Ca(Wt.%)	Na(Wt.%)	K(Wt.%)	Ti(Wt.%)	Mn(Wt.%)	P(Wt.%)	SALT
11	24.560	9.103	6.755	2.241	0.938	1.398	1.173	0.525	0.1038	0.0664	5.288
13	24.602	9.168	6.723	2.190	0.932	1.379	1.201	0.536	0.0727	0.0636	5.247
25	24.836	9.302	6.554	2.129	0.986	1.131	1.229	0.545	0.0650	0.0642	4.742
27	24.750	9.222	6.498	2.137	1.014	1.235	1.223	0.546	0.0626	0.0633	4.737
29	24.770	9.208	6.436	2.152	1.060	1.301	1.225	0.552	0.0619	0.0593	4.895
31	24.853	9.198	6.599	2.163	1.023	1.446	1.258	0.544	0.0612	0.0617	5.134
33	24.829	9.146	6.601	2.178	0.991	1.252	1.242	0.541	0.0629	0.0627	5.247
35	24.848	9.150	6.617	2.170	0.974	1.199	1.232	0.541	0.0646	0.0623	5.299
37	24.769	9.096	6.592	2.167	0.993	1.168	1.230	0.534	0.0662	0.0627	5.202
39	24.903	9.156	6.552	2.172	0.959	1.230	1.223	0.532	0.0627	0.0612	4.983
41	24.888	9.195	6.560	2.184	0.910	1.270	1.247	0.537	0.0653	0.0622	5.119
43	24.895	9.216	6.493	2.201	0.928	1.278	1.234	0.538	0.0563	0.0599	5.183
45	24.849	9.137	6.428	2.186	1.005	1.230	1.227	0.534	0.0547	0.0599	5.124
47	24.741	9.109	6.530	0.387	1.025	1.275	1.216	0.532	0.0613	0.0623	5.235
49	24.902	9.115	6.484	2.172	1.027	1.346	1.229	0.530	0.0539	0.0618	5.265
51	25.037	9.150	6.461	2.208	1.008	1.391	1.241	0.533	0.0531	0.0641	5.287
53	24.993	9.182	6.473	2.209	0.966	1.293	1.228	0.532	0.0589	0.0651	5.367
55	25.001	9.231	6.458	2.190	0.927	1.365	1.220	0.532	0.0556	0.0591	5.386
57	24.869	9.162	6.396	2.180	0.973	1.300	1.225	0.535	0.0557	0.0624	5.420
59	24.896	9.151	6.449	2.151	0.988	1.228	1.224	0.531	0.0590	0.0611	5.587
61	24.951	9.172	6.468	2.174	0.962	1.189	1.225	0.534	0.0584	0.0608	5.912
63	24.883	9.133	6.498	2.201	0.922	1.206	1.223	0.529	0.0567	0.0593	5.708
65	24.919	9.172	6.550	2.169	0.947	1.185	1.233	0.528	0.0558	0.0584	5.678
67	24.808	9.153	6.409	2.201	1.066	1.153	1.214	0.526	0.0567	0.0575	5.759
69	24.839	9.121	6.414	2.159	1.091	1.262	1.220	0.523	0.0584	0.0561	5.820
71	24.812	9.103	6.357	2.170	1.099	1.240	1.222	0.529	0.0574	0.0583	5.631
73	24.873	9.132	6.397	2.183	1.055	1.137	1.217	0.528	0.0582	0.0597	5.546
75	24.846	9.175	6.410	2.144	1.045	1.287	1.225	0.532	0.0581	0.0554	5.377
77	24.878	9.228	6.421	2.173	1.024	1.226	1.172	0.533	0.0583	0.0570	5.680
81	24.605	9.046	6.528	2.224	1.024	1.399	1.242	0.530	0.0653	0.0583	4.024
83	24.839	9.203	6.598	2.189	1.026	1.136	1.247	0.542	0.0692	0.0568	3.799
85	25.077	9.290	6.678	2.197	1.021	1.019	1.245	0.547	0.0732	0.0572	3.722
87	24.981	9.230	6.662	2.223	1.025	0.978	1.253	0.543	0.0666	0.0585	3.575
89	24.943	9.272	6.664	2.259	1.006	1.107	1.248	0.542	0.0683	0.0599	3.648
91	25.081	9.336	6.635	2.176	0.992	1.018	1.258	0.547	0.0611	0.0613	3.726
93	25.023	9.288	6.554	2.153	1.038	0.931	1.252	0.544	0.0587	0.0576	3.676
95	25.022	9.257	6.549	2.160	1.058	1.019	1.252	0.543	0.0571	0.0608	3.714
97	25.192	9.257	6.489	2.135	1.066	1.017	1.265	0.546	0.0619	0.0549	3.742
99	25.021	9.160	6.656	2.151	0.984	0.979	1.275	0.542	0.0635	0.0567	3.669
101	25.210	9.331	6.531	2.164	1.002	1.083	1.268	0.546	0.0619	0.0590	3.680
103	24.887	9.200	6.614	2.145	1.052	1.172	1.233	0.545	0.0627	0.0608	3.610
105	24.916	9.194	6.600	2.156	1.028	1.112	1.244	0.546	0.0562	0.0621	3.550
107	24.988	9.169	6.472	2.170	1.064	1.054	1.236	0.551	0.0490	0.0594	3.607
109	25.374	9.021	6.534	2.132	1.183	1.121	1.260	0.552	0.0464	0.0506	3.297
111	25.829	8.815	6.560	2.084	1.171	1.233	1.254	0.556	0.0446	0.0486	2.854
113	25.846	8.649	6.512	2.002	1.285	1.158	1.281	0.532	0.0454	0.0468	2.809
115	25.383	8.886	6.264	1.963	1.336	1.229	1.245	0.535	0.0383	0.0468	2.989
117	25.263	8.892	6.361	2.014	1.408	1.203	1.242	0.531	0.0447	0.0468	2.985
119	24.744	8.849	6.493	1.967	1.244	1.263	1.225	0.520	0.0392	0.0465	3.249
121	25.163	8.988	6.407	1.971	1.330	1.289	1.232	0.529	0.0415	0.0482	3.056
123	25.233	8.807	6.482	1.973	1.290	1.349	1.249	0.514	0.0416	0.0447	3.321
125	25.109	8.826	6.411	1.942	1.327	1.279	1.233	0.515	0.0393	0.0475	3.401
127	25.176	8.696	6.413	1.945	1.340	1.219	1.218	0.512	0.0457	0.0493	3.449
129	25.163	8.678	6.467	2.048	1.344	1.291	1.219	0.511	0.0450	0.0508	3.574
131	25.415	8.618	6.489	2.026	1.319	1.328	1.205	0.521	0.0465	0.0480	3.455
133	24.978	8.805	6.487	2.029	1.255	1.312	1.232	0.518	0.0450	0.0481	3.713
135	25.288	8.809	6.455	2.040	1.192	1.285	1.254	0.515	0.0434	0.0462	3.622
137	25.022	8.864	6.448	2.029	1.216	1.210	1.245	0.518	0.0410	0.0472	3.767
139	25.075	8.906	6.492	2.070	1.050	1.292	1.264	0.516	0.0451	0.0463	3.755
141	25.125	8.895	6.386	2.013	1.059	1.209	1.267	0.521	0.0442	0.0458	3.692
143	25.169	8.895	6.482	2.048	1.131	1.230	1.281	0.523	0.0410	0.0481	3.685
145	25.063	8.872	6.390	2.092	1.224	1.270	1.276	0.530	0.0434	0.0445	3.679
147	25.134	9.018	6.659	2.194	1.161	1.174	1.239	0.539	0.0443	0.0464	3.854
149	25.285	9.041	6.488	2.163	1.010	1.191	1.274	0.535	0.0435	0.0500	3.868
151	25.404	8.751	6.588	2.190	1.089	1.147	1.265	0.527	0.0490	0.0417	3.699

Table C.4.6-2 Salt free major element data from core P12.

Depth(cm)	Si/Al	Fe/AL	Mg/AL	F/Al	Ca/Al	P/Al	Mn/Al	Ti/Al	Na/Al	Fe/Ti
11	2.698	0.742	0.246	0.129	0.103	0.0073	0.0114	0.0577	0.154	12.869
13	2.684	0.733	0.239	0.131	0.102	0.0069	0.0079	0.0585	0.150	12.541
25	2.670	0.705	0.229	0.132	0.106	0.0069	0.0070	0.0586	0.122	12.021
27	2.684	0.705	0.232	0.133	0.110	0.0069	0.0068	0.0593	0.134	11.893
29	2.690	0.699	0.234	0.133	0.115	0.0064	0.0067	0.0600	0.141	11.652
31	2.702	0.717	0.235	0.137	0.111	0.0067	0.0067	0.0591	0.157	12.139
33	2.715	0.722	0.238	0.136	0.108	0.0069	0.0069	0.0592	0.137	12.198
35	2.716	0.723	0.237	0.135	0.107	0.0068	0.0071	0.0592	0.131	12.221
37	2.723	0.725	0.238	0.135	0.109	0.0069	0.0073	0.0587	0.128	12.347
39	2.720	0.716	0.237	0.134	0.105	0.0067	0.0069	0.0581	0.134	12.314
41	2.707	0.713	0.237	0.136	0.099	0.0068	0.0071	0.0584	0.138	12.225
43	2.701	0.705	0.239	0.134	0.101	0.0065	0.0061	0.0583	0.139	12.078
45	2.720	0.704	0.239	0.134	0.110	0.0066	0.0060	0.0585	0.135	12.035
47	2.716	0.717	0.043	0.134	0.113	0.0068	0.0067	0.0584	0.140	12.283
49	2.732	0.711	0.238	0.135	0.113	0.0068	0.0059	0.0582	0.148	12.222
51	2.736	0.706	0.241	0.136	0.110	0.0070	0.0058	0.0582	0.152	12.132
53	2.722	0.705	0.241	0.134	0.105	0.0071	0.0064	0.0580	0.141	12.161
55	2.708	0.700	0.237	0.132	0.100	0.0064	0.0060	0.0576	0.148	12.144
57	2.714	0.698	0.238	0.134	0.106	0.0068	0.0061	0.0584	0.142	11.952
59	2.721	0.705	0.235	0.134	0.108	0.0067	0.0065	0.0580	0.134	12.145
61	2.720	0.705	0.237	0.134	0.105	0.0066	0.0064	0.0582	0.130	12.110
63	2.725	0.712	0.241	0.134	0.101	0.0065	0.0062	0.0579	0.132	12.295
65	2.717	0.714	0.236	0.134	0.103	0.0064	0.0061	0.0576	0.129	12.396
67	2.710	0.700	0.241	0.133	0.116	0.0063	0.0062	0.0574	0.126	12.192
69	2.723	0.703	0.237	0.134	0.120	0.0062	0.0064	0.0573	0.138	12.268
71	2.726	0.698	0.238	0.134	0.121	0.0064	0.0063	0.0581	0.136	12.023
73	2.724	0.700	0.239	0.133	0.116	0.0065	0.0064	0.0578	0.125	12.109
75	2.708	0.699	0.234	0.134	0.114	0.0060	0.0063	0.0580	0.140	12.055
77	2.696	0.696	0.235	0.127	0.111	0.0062	0.0063	0.0577	0.133	12.050
81	2.720	0.722	0.246	0.137	0.113	0.0064	0.0072	0.0586	0.155	12.305
83	2.699	0.717	0.238	0.136	0.112	0.0062	0.0075	0.0589	0.123	12.180
85	2.700	0.719	0.236	0.134	0.110	0.0062	0.0079	0.0589	0.110	12.198
87	2.706	0.722	0.241	0.136	0.111	0.0063	0.0072	0.0588	0.106	12.271
89	2.690	0.719	0.244	0.135	0.108	0.0065	0.0074	0.0585	0.119	12.293
91	2.687	0.711	0.233	0.135	0.106	0.0066	0.0065	0.0586	0.109	12.132
93	2.694	0.706	0.232	0.135	0.112	0.0062	0.0063	0.0586	0.100	12.045
95	2.703	0.707	0.233	0.135	0.114	0.0066	0.0062	0.0587	0.110	12.058
97	2.721	0.701	0.231	0.137	0.115	0.0059	0.0067	0.0590	0.110	11.877
99	2.732	0.727	0.235	0.139	0.107	0.0062	0.0069	0.0592	0.107	12.275
101	2.702	0.700	0.232	0.136	0.107	0.0063	0.0066	0.0585	0.116	11.961
103	2.705	0.719	0.233	0.134	0.114	0.0066	0.0068	0.0592	0.127	12.135
105	2.710	0.718	0.235	0.135	0.112	0.0068	0.0061	0.0594	0.121	12.090
107	2.725	0.706	0.237	0.135	0.116	0.0065	0.0053	0.0600	0.115	11.754
109	2.813	0.724	0.236	0.140	0.131	0.0056	0.0051	0.0612	0.124	11.839
111	2.930	0.744	0.236	0.142	0.133	0.0055	0.0051	0.0630	0.140	11.808
113	2.988	0.753	0.231	0.148	0.149	0.0054	0.0053	0.0615	0.134	12.244
115	2.857	0.705	0.221	0.140	0.150	0.0053	0.0043	0.0602	0.138	11.715
117	2.841	0.715	0.227	0.140	0.158	0.0053	0.0050	0.0597	0.135	11.979
119	2.796	0.734	0.222	0.138	0.141	0.0053	0.0044	0.0588	0.143	12.486
121	2.799	0.713	0.219	0.137	0.148	0.0054	0.0046	0.0588	0.143	12.113
123	2.865	0.736	0.224	0.142	0.146	0.0051	0.0047	0.0584	0.153	12.605
125	2.845	0.726	0.220	0.140	0.150	0.0054	0.0045	0.0583	0.145	12.457
127	2.895	0.738	0.224	0.140	0.154	0.0057	0.0053	0.0589	0.140	12.515
129	2.899	0.745	0.236	0.141	0.155	0.0058	0.0052	0.0589	0.149	12.648
131	2.949	0.753	0.235	0.140	0.153	0.0056	0.0054	0.0604	0.154	12.466
133	2.837	0.737	0.230	0.140	0.143	0.0055	0.0051	0.0589	0.149	12.518
135	2.871	0.733	0.232	0.142	0.135	0.0053	0.0049	0.0584	0.146	12.544
137	2.823	0.727	0.229	0.140	0.137	0.0053	0.0046	0.0585	0.136	12.436
139	2.816	0.729	0.232	0.142	0.118	0.0052	0.0051	0.0579	0.145	12.582
141	2.825	0.718	0.226	0.142	0.119	0.0052	0.0050	0.0586	0.136	12.253
143	2.829	0.729	0.230	0.144	0.127	0.0054	0.0046	0.0588	0.138	12.393
145	2.825	0.720	0.236	0.144	0.138	0.0050	0.0049	0.0597	0.143	12.060
147	2.787	0.738	0.243	0.137	0.129	0.0051	0.0049	0.0598	0.130	12.356
149	2.797	0.718	0.239	0.141	0.112	0.0055	0.0048	0.0591	0.132	12.135
151	2.903	0.753	0.250	0.145	0.124	0.0048	0.0056	0.0603	0.131	12.489

Table C.4.6-3 Salt free major elements and their ratios in core P12.

Depth(cm)	Ba(ppm)	Sc(ppm)	V(ppm)	Ni(ppm)	Cu(ppm)	Zn(ppm)	Sr(ppm)	Nb(ppm)	Cr(ppm)	Zr(ppm)	Pb(ppm)	Th(ppm)	U(ppm)	Rb(ppm)	Mo(ppr
1	1536.6	3.7	0.0	14.5	23.7	9.4	1252.1	0.4	2.8	7.5	2.6	2.0	3.3	3.6	0.0
10	1404.8	5.3	4.2	17.8	20.8	8.4	1177.8	1.1	0.0	7.9	3.9	0.0	0.0	3.1	0.6
11	1456.0	4.9	6.6	16.3	38.4	23.3	1215.0	0.5	0.8	8.4	3.5	0.0	0.0	2.7	0.0
20	1497.4	4.8	1.0	18.4	27.7	12.3	1204.8	0.9	2.1	8.6	4.6	0.0	0.0	3.1	0.4
30	1748.0	5.1	5.0	16.5	22.6	8.8	1189.8	0.8	0.2	9.8	2.2	0.8	0.0	3.6	0.1
40	2278.7	5.0	8.5	29.3	34.1	14.0	1197.4	0.8	4.1	13.3	3.6	0.0	0.0	3.0	1.4
50	2920.9	7.4	10.2	52.6	57.6	18.9	1261.0	1.0	5.0	18.1	4.3	0.0	0.2	4.7	0.8
60	2448.0	6.3	11.2	25.6	38.6	13.8	1298.2	0.8	3.6	17.6	3.8	0.0	0.5	4.3	0.0
70	2399.1	5.8	10.7	30.1	49.0	16.7	1347.9	0.6	4.0	19.4	5.1	0.7	0.0	5.0	0.8
80	2273.1	6.4	14.5	23.8	40.7	16.5	1348.9	0.8	1.6	19.1	4.1	0.0	0.0	4.8	0.4
90	2281.1	6.0	12.5	22.0	39.8	15.6	1366.0	0.9	3.8	19.6	4.4	0.0	0.9	5.6	0.9
100	2310.8	7.3	6.6	23.3	38.4	14.7	1364.9	1.2	4.3	18.2	6.3	0.0	0.8	4.8	0.0
110	2311.9	7.1	12.7	28.3	44.7	16.2	1365.5	1.0	2.2	19.2	7.3	0.0	2.4	5.8	0.6
120	2284.4	6.2	10.4	28.5	40.3	15.6	1373.0	1.3	1.7	20.1	2.8	0.7	0.6	4.8	0.0
130	2291.3	5.7	9.0	29.7	44.5	14.5	1376.7	1.9	5.5	19.2	6.2	0.0	0.0	5.0	0.1
140	2260.2	7.5	13.6	25.2	38.1	13.7	1369.8	1.3	1.0	19.9	6.1	0.8	0.0	5.3	0.0
150	2263.6	5.9	12.2	26.4	41.4	16.6	1374.2	0.8	5.4	20.0	4.3	0.0	1.4	5.3	0.0
160	2269.5	6.2	9.0	26.9	40.9	14.0	1374.6	0.5	4.8	20.9	3.5	0.0	1.0	5.7	0.4
170	2139.2	7.4	10.3	28.4	47.4	15.8	1341.7	0.9	0.0	18.0	4.1	0.0	0.9	5.0	0.0
180	2253.6	6.9	6.4	20.6	38.8	14.1	1344.2	0.9	4.8	17.3	4.2	1.6	1.2	5.5	0.0
190	2093.8	7.5	11.3	21.7	40.9	14.6	1330.3	1.4	1.7	18.2	4.0	0.0	0.0	4.2	0.0
200	2076.8	7.8	7.0	19.6	36.0	13.7	1322.9	1.7	4.4	16.9	4.3	0.0	0.5	5.7	0.0
210	2036.0	5.5	12.3	19.3	34.8	12.3	1306.8	1.2	1.7	17.6	1.9	2.1	0.0	4.6	0.2
219	1955.7	7.6	5.9	21.2	39.1	15.1	1305.3	1.0	4.6	16.2	3.3	0.3	0.0	4.1	0.3
230	1986.7	5.6	13.5	19.0	36.1	13.2	1316.0	1.2	3.5	17.0	3.8	0.0	2.4	4.4	0.0
238	1972.0	6.5	6.2	17.5	40.5	12.4	1304.0	1.7	2.7	17.9	6.1	0.0	0.8	4.6	0.0
250	1988.7	5.6	10.7	19.0	36.7	13.9	1313.6	2.1	1.8	17.4	3.2	0.5	0.0	4.8	0.0
260	1961.4	5.6	7.8	20.4	40.3	12.7	1309.0	1.0	5.0	16.1	1.8	0.0	0.2	4.9	0.0
270	1961.3	5.6	7.1	19.3	39.1	13.9	1311.6	1.1	3.5	16.3	1.6	0.1	0.9	4.9	0.0
280	1847.3	5.0	6.7	16.2	36.3	13.6	1303.7	1.6	2.2	16.2	6.3	0.4	0.0	4.8	0.0
290	1951.7	5.2	11.5	18.4	40.9	13.8	1311.4	1.1	4.9	17.1	3.5	0.0	0.0	3.4	0.0
300	1625.4	7.7	10.0	17.1	34.9	12.0	1235.1	0.3	5.5	13.9	4.8	0.0	0.0	3.6	0.0
310	1491.9	5.4	6.4	13.2	32.9	9.2	1217.0	1.1	5.8	13.5	3.5	0.9	0.0	4.4	0.0
320	1117.4	4.9	2.7	10.7	28.3	8.3	1151.0	1.5	0.8	10.3	2.3	0.0	0.0	3.2	0.0
330	959.0	6.9	8.4	8.3	26.2	7.8	1114.5	1.0	1.5	9.6	3.6	0.0	0.0	2.1	0.0
340	873.3	5.3	6.7	7.8	21.2	5.3	1101.1	0.4	0.3	8.2	4.1	1.2	0.0	3.7	0.0
350	1052.7	6.2	3.2	9.8	24.3	8.0	1123.3	1.0	0.0	8.5	3.9	0.2	0.4	2.2	0.0

Table C.5.1-1 Salt included trace element data from core CD3814.

Depth(cm)	Ba(ppm)	Sc(ppm)	V(ppm)	Ni(ppm)	Cu(ppm)	Zn(ppm)	Sr(ppm)	Nb(ppm)	Cr(ppm)	Zr(ppm)	Pb(ppm)	Th(ppm)	U(ppm)	Rb(ppm)	Mo(p
360	1017.0	4.6	5.1	10.4	20.2	7.4	1110.6	1.4	0.0	7.8	4.4	1.6	0.0	3.2	0.0
370	802.2	5.8	5.7	8.0	17.1	6.6	1074.1	0.0	2.3	5.2	4.4	0.4	0.2	3.2	0.1
381	841.5	4.1	9.1	7.5	15.7	5.6	1077.2	0.2	1.4	6.6	3.4	0.0	0.6	2.4	0.8
390	910.4	4.3	4.8	8.5	16.4	6.3	1090.0	1.3	0.0	8.5	0.5	0.0	0.0	2.8	0.1
400	887.8	6.0	1.6	7.3	15.3	6.2	1097.0	0.7	0.0	6.5	1.9	0.5	0.0	2.8	0.0
410	874.2	3.1	5.8	5.9	18.0	6.5	1082.0	1.1	0.0	6.9	4.5	0.0	0.0	1.8	0.3
420	1070.7	4.8	6.7	9.4	17.8	7.6	1124.0	0.0	3.4	8.6	1.6	0.0	0.0	2.5	0.0
430	846.6	5.7	6.0	9.1	11.5	6.8	1089.6	0.0	0.4	6.9	2.1	0.0	0.0	2.1	0.2
440	907.8	6.3	6.0	7.7	11.7	5.9	1090.7	1.0	0.0	6.7	3.4	0.0	0.0	2.6	0.0
450	941.4	5.5	8.0	9.3	14.5	6.3	1106.0	1.6	1.2	7.7	3.0	0.0	0.0	2.2	0.5
460	911.2	6.6	6.6	10.0	13.9	4.3	1107.9	1.0	0.0	8.3	3.2	0.6	0.0	3.1	0.2
472	938.7	5.3	6.3	9.7	16.3	5.6	1106.4	1.0	1.8	6.1	2.9	0.0	0.0	2.8	0.8
480	904.0	4.4	3.0	8.4	14.3	5.0	1097.9	0.9	0.0	6.8	2.5	0.0	0.0	2.4	0.4
490	879.9	5.3	7.9	8.6	12.2	5.7	1087.5	0.1	2.2	6.9	4.2	0.7	0.0	3.3	0.4
500	903.6	6.8	5.2	8.1	15.4	6.1	1094.9	0.5	0.0	6.8	2.2	0.0	0.0	2.2	0.4
509	866.3	4.2	5.4	8.8	14.1	6.4	1090.2	0.6	1.3	6.6	1.5	0.0	0.0	2.3	0.0
520	898.0	3.8	6.9	8.2	17.6	5.5	1097.5	0.6	0.0	7.6	3.7	0.0	0.0	2.4	0.0
530	926.4	6.8	6.9	7.9	18.3	5.8	1097.7	1.3	1.0	4.6	3.3	0.0	0.0	1.5	0.0
540	878.3	5.5	3.9	6.5	17.2	5.1	1081.6	1.2	3.2	6.1	2.9	0.0	0.0	2.2	0.0
550	888.4	6.3	4.3	4.7	17.7	5.3	1075.8	0.0	0.1	5.3	2.7	0.0	0.0	1.6	0.0
560	1064.0	3.9	4.1	7.2	22.3	5.4	1098.6	1.5	1.6	8.0	3.6	0.0	0.0	2.7	0.0
570	1521.8	6.5	18.6	18.3	51.2	10.9	1225.7	1.6	4.4	11.7	3.7	1.3	0.2	3.5	0.1
580	1984.7	8.0	7.5	22.2	43.0	12.6	1248.5	1.3	2.6	13.5	1.1	0.0	0.0	4.6	0.0
590	2701.7	7.4	11.3	33.6	45.3	17.9	1267.8	1.3	1.7	20.7	4.6	0.0	0.0	5.6	0.2
600	1340.1	5.9	4.0	16.8	35.3	9.8	1319.3	1.0	1.4	11.7	5.4	0.0	0.0	3.0	0.0
610	1831.9	5.5	8.1	11.2	33.3	14.7	1205.9	1.3	5.1	13.6	6.0	1.1	0.7	4.3	0.1
620	2080.6	7.6	5.1	31.3	49.6	13.9	1235.4	0.5	1.5	13.7	4.6	0.4	0.0	3.9	0.1
630	3084.7	7.5	16.0	51.1	71.1	20.0	1214.0	1.2	4.1	19.4	3.0	0.6	0.0	3.7	0.0
640	2702.9	5.6	6.6	39.8	56.9	17.3	1259.3	1.2	2.3	15.6	3.4	0.6	0.0	3.9	0.0
650	2389.1	6.5	12.1	33.3	54.0	20.1	1284.5	2.2	6.3	21.2	5.2	1.5	0.0	5.2	0.3
660	1471.2	12.3	115.0	41.4	52.1	39.0	1021.1	13.2	41.2	65.3	3.5	1.3	1.1	11.7	0.5
670	835.0	20.6	199.0	53.4	48.4	58.7	666.6	32.8	78.7	138.4	2.4	2.2	2.4	26.4	0.8
680	825.7	17.6	173.6	45.3	42.8	53.7	706.9	29.1	74.7	131.4	2.4	1.8	0.9	23.1	1.1
690	404.6	26.2	238.7	67.0	41.9	67.3	463.8	42.7	107.0	195.5	2.7	3.7	0.0	32.1	1.3
700	466.6	25.5	236.0	71.2	42.6	68.1	502.0	38.7	106.8	163.7	2.4	4.0	0.6	28.4	0.9
710	680.2	22.3	213.8	50.6	37.8	55.0	662.9	30.4	90.5	134.5	3.7	1.8	0.3	23.7	2.5
720	896.0	12.5	128.6	29.6	27.1	43.4	854.9	22.0	42.5	96.3	3.9	1.2	1.0	18.3	1.3

Table C.5.1-1 (Contd.) Salt included trace element data from core CD3814.

Depth(cm)	Ba(ppm)	Cu(ppm)	Ni(ppm)	Zn(ppm)	V(ppm)	Sr(ppm)	Sc(ppm)	Cr(ppm)	Zr(ppm)	Rb(ppm)	Nb(ppm)	Pb(ppm)	Th(ppm)	U(ppm)	Mo(ppm)	SALT
1	1577.4	24.3	14.9	9.6	0.0	1285.3	3.8	2.9	7.7	3.7	0.4	2.7	2.1	3.4	0.0	2.587
10	1449.0	21.4	18.3	8.7	4.3	1214.2	5.5	0.0	8.1	3.2	1.1	4.0	0.0	0.0	0.6	2.994
11	1500.9	39.6	16.8	24.0	6.8	1253.2	5.1	0.8	8.7	2.8	0.5	3.6	0.0	0.0	0.0	3.050
20	1540.9	28.6	19.0	12.7	1.0	1241.9	4.9	2.2	8.9	3.2	0.9	4.7	0.0	0.0	0.4	2.991
30	1795.4	23.3	17.0	9.1	5.1	1224.4	5.2	0.2	10.1	3.7	0.8	2.3	0.8	0.0	0.1	2.823
40	2341.2	35.0	30.1	14.4	8.7	1229.9	5.1	4.2	13.7	3.1	0.8	3.7	0.0	0.0	1.4	2.642
50	3019.2	59.2	54.0	19.4	10.5	1295.6	7.6	5.1	18.6	4.8	1.0	4.4	0.0	0.2	0.8	2.670
60	2544.1	39.9	26.5	14.3	11.6	1341.9	6.5	3.7	18.2	4.4	0.8	3.9	0.0	0.5	0.0	3.256
70	2491.6	50.9	31.3	17.4	11.1	1400.8	6.0	4.2	20.2	5.2	0.6	5.3	0.7	0.0	0.8	3.776
80	2360.6	42.3	24.7	17.1	15.1	1400.9	6.6	1.7	19.8	5.0	0.8	4.3	0.0	0.0	0.4	3.714
90	2355.1	41.3	22.8	16.2	13.0	1418.6	6.2	3.9	20.4	5.8	0.9	4.6	0.0	0.9	0.9	3.708
100	2390.1	39.6	24.1	15.2	6.8	1409.2	7.5	4.4	18.8	5.0	1.2	6.5	0.0	0.8	0.0	3.144
110	2396.4	46.2	29.3	16.8	13.1	1412.3	7.3	2.3	19.9	6.0	1.0	7.6	0.0	2.5	0.6	3.316
120	2372.3	41.8	29.5	16.2	10.8	1423.2	6.4	1.8	20.8	5.0	1.3	2.9	0.7	0.6	0.0	3.526
130	2392.1	46.2	30.8	15.1	9.3	1429.6	5.9	5.7	19.9	5.2	2.0	6.4	0.0	0.0	0.1	3.703
140	2351.4	39.8	26.3	14.3	14.2	1430.1	7.8	1.0	20.8	5.5	1.4	6.4	0.8	0.0	0.0	4.216
150	2355.3	43.1	27.5	17.3	12.7	1429.6	6.1	5.6	20.8	5.5	0.8	4.5	0.0	1.5	0.0	3.877
160	2355.9	42.6	28.0	14.6	9.4	1430.3	6.5	5.0	21.7	5.9	0.5	3.6	0.0	1.0	0.4	3.894
170	2222.4	49.2	29.5	16.4	10.7	1392.8	7.7	0.0	18.7	5.2	0.9	4.3	0.0	0.9	0.0	3.666
180	2339.1	40.3	21.4	14.6	6.6	1396.5	7.2	5.0	18.0	5.7	0.9	4.4	1.7	1.2	0.0	3.745
190	2174.5	42.5	22.5	15.2	11.7	1380.7	7.8	1.8	18.9	4.4	1.5	4.2	0.0	0.0	0.0	3.654
200	2145.6	37.4	20.4	14.2	7.3	1373.9	8.1	4.6	17.6	5.9	1.8	4.5	0.0	0.5	0.0	3.711
210	2111.4	36.0	19.9	12.7	12.7	1350.1	5.7	1.8	18.2	4.8	1.2	2.0	2.2	0.0	0.2	3.205
219	2020.7	40.5	22.0	15.7	6.1	1353.7	7.9	4.8	16.8	4.3	1.0	3.4	0.3	0.0	0.3	3.573
230	2050.9	37.3	19.6	13.6	13.9	1359.7	5.8	3.6	17.6	4.5	1.2	3.9	0.0	2.5	0.0	3.214
238	2036.1	41.8	18.1	12.8	6.4	1346.1	6.7	2.8	18.5	4.7	1.8	6.3	0.0	0.8	0.0	3.129
250	2051.8	37.9	19.6	14.4	11.0	1356.3	5.8	1.9	18.0	5.0	2.2	3.3	0.5	0.0	0.0	3.149
260	2022.3	41.6	21.0	13.1	8.0	1350.5	5.8	5.2	16.6	5.1	1.0	1.9	0.0	0.2	0.0	3.073
270	2022.1	40.3	19.9	14.3	7.3	1352.3	5.8	3.6	16.8	5.1	1.1	1.6	0.1	0.9	0.0	3.013
280	1898.4	37.4	16.7	14.0	6.9	1344.1	5.2	2.3	16.7	4.9	1.6	6.5	0.4	0.0	0.0	3.009
290	2017.6	42.0	18.9	14.2	11.8	1347.7	5.3	5.0	17.6	3.5	1.1	3.6	0.0	0.0	0.0	2.693
300	1674.7	36.1	17.7	12.4	10.3	1276.8	8.0	5.7	14.4	3.7	0.3	5.0	0.0	0.0	0.0	3.264
310	1531.9	33.9	13.6	9.5	6.6	1253.9	5.6	6.0	13.9	4.5	1.1	3.6	0.9	0.0	0.0	2.943
320	1151.1	29.1	11.0	8.5	2.8	1181.9	5.0	0.8	10.6	3.3	1.5	2.4	0.0	0.0	0.0	2.611
330	988.8	27.0	8.6	8.0	8.7	1148.1	7.1	1.5	9.9	2.2	1.0	3.7	0.0	0.0	0.0	2.924
340	900.8	21.9	8.0	5.5	6.9	1135.3	5.5	0.3	8.5	3.8	0.4	4.2	1.2	0.0	0.0	3.016
350	1084.7	25.1	10.1	8.3	3.3	1158.7	6.4	0.0	8.8	2.3	1.0	4.0	0.2	0.4	0.0	3.052

Table C.5.1-2 Salt free trace element data from core CD3814.

Depth(cm)	Ba(ppm)	Cu(ppm)	Ni(ppm)	Zn(ppm)	V(ppm)	Sr(ppm)	Sc(ppm)	Cr(ppm)	Zr(ppm)	Rb(ppm)	Nb(ppm)	Pb(ppm)	Th(ppm)	U(ppm)	Mo(ppm)	SALT
360	1048.7	20.8	10.7	7.6	5.3	1144.4	4.7	0.0	8.0	3.3	1.4	4.5	1.6	0.0	0.0	2.952
370	828.5	17.6	8.2	6.8	5.9	1107.6	6.0	2.4	5.4	3.3	0.0	4.5	0.4	0.2	0.1	3.020
381	865.8	16.2	7.7	5.8	9.4	1112.5	4.2	1.4	6.8	2.5	0.2	3.5	0.0	0.6	0.8	3.177
390	938.4	16.9	8.7	6.5	4.9	1121.5	4.4	0.0	8.7	2.9	1.3	0.5	0.0	0.0	0.1	2.809
400	914.8	15.8	7.5	6.4	1.6	1130.7	6.2	0.0	6.7	2.9	0.7	2.0	0.5	0.0	0.0	2.982
410	897.8	18.5	6.1	6.7	6.0	1114.9	3.2	0.0	7.1	1.9	1.1	4.6	0.0	0.0	0.3	2.949
420	1103.6	18.3	9.7	7.8	6.9	1154.3	4.9	3.5	8.8	2.6	0.0	1.6	0.0	0.0	0.0	2.625
430	872.7	11.9	9.4	7.0	6.2	1123.1	5.9	0.4	7.1	2.2	0.0	2.2	0.0	0.0	0.2	2.984
440	935.3	12.1	7.9	6.1	6.2	1124.3	6.5	0.0	6.9	2.7	1.0	3.5	0.0	0.0	0.0	2.987
450	971.3	14.9	9.6	6.5	8.2	1139.5	5.7	1.2	7.9	2.3	1.6	3.1	0.0	0.0	0.5	2.941
460	940.3	14.3	10.3	4.4	6.8	1143.1	6.8	0.0	8.6	3.2	1.0	3.3	0.6	0.0	0.2	3.079
472	970.0	16.8	10.0	5.8	6.5	1141.8	5.5	1.9	6.3	2.9	1.0	3.0	0.0	0.0	0.8	3.099
480	931.7	14.8	8.7	5.2	3.1	1134.5	4.5	0.0	7.0	2.5	0.9	2.6	0.0	0.0	0.4	3.229
490	905.6	12.6	8.9	5.9	8.1	1120.8	5.5	2.3	7.1	3.4	0.1	4.3	0.7	0.0	0.4	2.970
500	928.9	15.9	8.3	6.3	5.4	1126.9	7.0	0.0	7.0	2.3	0.5	2.3	0.0	0.0	0.4	2.840
509	886.0	14.5	9.0	6.6	5.6	1120.7	4.3	1.3	6.8	2.4	0.6	1.5	0.0	0.0	0.0	2.720
520	918.5	18.0	8.4	5.6	7.1	1122.5	3.9	0.0	7.8	2.5	0.6	3.8	0.0	0.0	0.0	2.223
530	945.4	18.7	8.1	5.9	7.1	1122.7	7.0	1.0	4.7	1.5	1.3	3.4	0.0	0.0	0.0	2.228
540	898.3	17.6	6.6	5.2	4.0	1103.7	5.6	3.3	6.2	2.2	1.2	3.0	0.0	0.0	0.0	2.006
550	909.8	18.1	4.8	5.4	4.4	1100.3	6.4	0.1	5.4	1.6	0.0	2.8	0.0	0.0	0.0	2.222
560	1094.0	22.8	7.4	5.5	4.2	1125.1	4.0	1.6	8.2	2.8	1.5	3.7	0.0	0.0	0.0	2.356
570	1564.2	52.6	18.8	11.2	19.1	1260.3	6.7	4.5	12.0	3.6	1.6	3.8	1.3	0.2	0.1	2.745
580	2035.9	44.2	22.8	13.0	7.7	1283.3	8.2	2.7	13.9	4.7	1.3	1.1	0.0	0.0	0.0	2.710
590	2757.5	46.5	34.5	18.4	11.6	1300.5	7.6	1.7	21.2	5.7	1.3	4.7	0.0	0.0	0.2	2.513
600	1372.0	36.0	17.1	10.0	4.1	1346.5	6.0	1.4	11.9	3.1	1.0	5.5	0.0	0.0	0.0	2.023
610	1870.0	34.1	11.5	15.0	8.3	1234.6	5.6	5.2	13.9	4.4	1.3	6.1	1.1	0.7	0.1	2.322
620	2125.6	50.6	32.0	14.2	5.2	1261.1	7.8	1.5	14.0	4.0	0.5	4.7	0.4	0.0	0.1	2.038
630	3147.9	72.6	52.2	20.4	16.3	1240.2	7.7	4.2	19.8	3.8	1.2	3.1	0.6	0.0	0.0	2.115
640	2770.3	58.1	40.6	17.7	6.7	1285.1	5.7	2.3	15.9	4.0	1.2	3.5	0.6	0.0	0.0	2.008
650	2451.1	55.3	34.1	20.6	12.4	1316.5	6.7	6.5	21.7	5.3	2.3	5.3	1.5	0.0	0.3	2.433
660	1513.6	53.5	42.5	40.0	118.0	1047.6	12.6	42.3	67.0	12.0	13.5	3.6	1.3	1.1	0.5	2.531
670	859.1	49.8	54.9	60.4	204.7	685.8	21.2	81.0	142.4	27.2	33.7	2.5	2.3	2.5	0.8	2.800
680	843.9	44.0	46.6	55.2	178.6	727.3	18.1	76.9	135.2	23.8	29.9	2.5	1.9	0.9	1.1	2.804
690	414.8	42.8	68.5	68.8	244.0	474.0	26.8	109.4	199.8	32.8	43.6	2.8	3.8	0.0	1.3	2.160
700	478.8	43.7	73.0	69.8	241.9	514.7	26.1	109.5	167.8	29.1	39.7	2.5	4.1	0.6	0.9	2.459
710	702.6	38.8	51.9	56.4	219.4	680.2	22.9	92.9	138.0	24.3	31.2	3.8	1.8	0.3	2.6	2.545
720	896.0	28.0	30.6	44.8	132.8	883.1	12.9	43.9	99.5	18.9	22.7	4.0	1.2	1.0	1.3	3.189

Table C.5.1-2 (Contd.) Salt free trace element data from core CD3814.

Depth(cm)	Ba/Al *10-2	Cu/Al *10-3	Ni/Al *10-3	Zn/Al *10-3	V/Al *10-3	Sr/Al *10-2	Sc/Al *10-3	Cr/Al *10-3	Zr/Al *10-3	Rb/Al *10-3	Nb/Al *10-4	Pb/Al *10-3	Th/Al *10-4	U/Al *10-4	Cr/Zr
1	103.740	16.000	9.789	6.346	0.000	84.532	2.498	1.890	5.063	2.430	2.701	1.755	13.503	22.279	0.373
10	88.570	13.106	11.216	5.293	2.647	74.216	3.340	0.000	4.978	1.953	6.931	2.457	0.000	0.000	0.000
11	105.796	27.919	11.851	16.941	4.799	88.338	3.563	0.582	6.107	1.963	3.635	2.545	0.000	0.000	0.095
20	117.738	21.818	14.493	9.688	0.788	94.896	3.781	1.654	6.774	2.442	7.089	3.623	0.000	0.000	0.244
30	109.941	14.241	10.397	5.545	3.151	74.972	3.214	0.126	6.175	2.268	5.041	1.386	5.041	0.000	0.020
40	100.204	14.991	12.881	6.155	3.737	52.640	2.198	1.802	5.847	1.319	3.517	1.583	0.000	0.000	0.308
50	82.911	16.251	14.841	5.333	2.878	35.578	2.088	1.411	5.107	1.326	2.821	1.213	0.000	0.564	0.276
60	73.851	11.582	7.681	4.141	3.361	38.953	1.890	1.080	5.281	1.290	2.400	1.140	0.000	1.500	0.205
70	65.685	13.424	8.246	4.575	2.931	36.928	1.589	1.096	5.315	1.370	1.644	1.397	1.918	0.000	0.206
80	62.271	11.150	6.520	4.520	3.972	36.955	1.753	0.438	5.233	1.315	2.192	1.123	0.000	0.000	0.084
90	58.726	10.306	5.697	4.040	3.237	35.373	1.554	0.984	5.075	1.450	2.331	1.139	0.000	2.331	0.194
100	60.778	10.082	6.117	3.859	1.733	35.835	1.917	1.129	4.778	1.260	3.151	1.654	0.000	2.100	0.236
110	60.831	11.736	7.430	4.253	3.334	35.851	1.864	0.578	5.041	1.523	2.625	1.917	0.000	6.301	0.115
120	60.934	10.730	7.588	4.153	2.769	36.556	1.651	0.453	5.352	1.278	3.461	0.745	1.864	1.597	0.085
130	59.651	11.523	7.691	3.755	2.331	35.650	1.476	1.424	4.972	1.295	4.920	1.606	0.000	0.000	0.286
140	58.322	9.866	6.526	3.548	3.522	35.471	1.942	0.259	5.153	1.372	3.366	1.580	2.072	0.000	0.050
150	58.627	10.721	6.836	4.299	3.159	35.585	1.528	1.398	5.179	1.372	2.072	1.113	0.000	3.625	0.270
160	59.445	10.738	7.063	3.676	2.363	36.090	1.628	1.260	5.487	1.497	1.313	0.919	0.000	2.625	0.230
170	61.321	13.576	8.134	4.525	2.950	38.429	2.119	0.000	5.156	1.432	2.578	1.174	0.000	2.578	0.000
180	57.514	9.912	5.262	3.602	1.635	34.338	1.763	1.226	4.419	1.405	2.299	1.073	4.087	3.065	0.277
190	55.780	10.890	5.778	3.887	3.009	35.419	1.997	0.453	4.846	1.118	3.727	1.065	0.000	0.000	0.093
200	39.851	6.944	3.781	2.643	1.350	25.518	1.505	0.849	3.260	1.099	3.279	0.829	0.000	0.964	0.260
210	30.907	5.263	2.919	1.860	1.860	19.763	0.832	0.257	2.662	0.696	1.815	0.287	3.176	0.000	0.097
219	48.464	9.725	5.273	3.756	1.468	32.467	1.890	1.144	4.029	1.020	2.487	0.821	0.746	0.000	0.284
230	52.115	9.478	4.988	3.466	3.544	34.552	1.470	0.919	4.463	1.155	3.151	0.998	0.000	6.301	0.206
238	53.265	10.937	4.726	3.349	1.674	35.215	1.755	0.729	4.834	1.242	4.591	1.647	0.000	2.160	0.151
250	53.663	9.911	5.131	3.754	2.890	35.474	1.512	0.486	4.699	1.296	5.671	0.864	1.350	0.000	0.103
260	57.007	11.720	5.933	3.693	2.268	38.069	1.629	1.454	4.682	1.425	2.908	0.523	0.000	0.582	0.311
270	56.173	11.199	5.528	3.981	2.034	37.567	1.604	1.002	4.669	1.403	3.151	0.458	0.286	2.578	0.215
280	******	******	*****	*****	*****	******	*****	*****	*****	*****	*****	*****	*****	*****	0.136
290	59.664	12.430	5.592	4.194	3.495	39.854	1.580	1.489	5.197	1.033	3.343	1.064	0.000	0.000	0.287
300	53.112	11.442	5.606	3.934	3.278	40.493	2.524	1.803	4.557	1.180	0.984	1.574	0.000	0.000	0.396
310	54.927	12.154	4.876	3.399	2.364	44.960	1.995	2.143	4.987	1.625	4.064	1.293	3.325	0.000	0.430
320	55.576	14.030	5.305	4.115	1.339	57.063	2.429	0.397	5.106	1.586	7.436	1.140	0.000	0.000	0.078
330	52.012	14.196	4.497	4.226	4.552	60.389	3.739	0.813	5.202	1.138	5.418	1.951	0.000	0.000	0.156
340	71.871	17.441	6.417	4.360	5.512	90.584	4.360	0.247	6.746	3.044	3.291	3.373	9.872	0.000	0.037
350	76.487	17.674	7.128	5.819	2.327	81.702	4.509	0.000	6.182	1.600	7.273	2.837	1.455	2.909	0.000

Table C.5.1-3 Salt free trace elements and their ratios to Al in core CD3814.

Depth(cm)	Ba/Al *10-2	Cu/Al *10-3	Ni/Al *10-3	Zn/Al *10-3	V/Al *10-3	Sr/Al *10-2	Sc/Al *10-3	Cr/Al *10-3	Zr/Al *10-3	Rb/Al *10-3	Nb/Al *10-4	Pb/Al *10-3	Th/Al *10-4	U/Al *10-4	Cr/Zr
360	83.559	16.585	8.539	6.076	4.187	91.185	3.777	0.000	6.404	2.627	11.495	3.613	13.137	0.000	0.000
370	94.998	20.218	9.458	7.803	6.739	126.992	6.857	2.719	6.148	3.783	0.000	5.202	4.729	2.365	0.442
381	88.182	16.515	7.889	5.891	9.572	113.310	4.313	1.473	6.942	2.525	2.104	3.576	0.000	6.311	0.212
390	85.877	15.442	8.004	5.932	4.520	102.635	4.049	0.000	8.004	2.636	12.241	0.471	0.000	0.000	0.000
400	80.032	13.797	6.583	5.591	1.443	98.925	5.411	0.000	5.862	2.525	6.312	1.713	4.509	0.000	0.000
410	91.472	18.897	6.194	6.824	6.089	113.592	3.254	0.000	7.244	1.890	11.548	4.724	0.000	0.000	0.000
420	92.034	15.244	8.050	6.509	5.738	96.259	4.111	2.912	7.365	2.141	0.000	1.370	0.000	0.000	0.395
430	114.738	15.585	12.333	9.216	8.132	147.668	7.725	0.542	9.351	2.846	0.000	2.846	0.000	0.000	0.058
440	131.946	17.014	11.197	8.580	8.725	158.605	9.161	0.000	9.743	3.781	14.542	4.944	0.000	0.000	0.000
450	111.330	17.123	10.983	7.440	9.447	130.609	6.495	1.417	9.093	2.598	18.895	3.543	0.000	0.000	0.156
460	115.020	17.542	12.620	5.427	8.329	139.821	8.329	0.000	10.475	3.912	12.620	4.039	7.572	0.000	0.000
472	118.483	20.546	12.227	7.059	7.941	139.461	6.681	2.269	7.689	3.529	12.605	3.655	0.000	0.000	0.295
480	106.664	16.918	9.938	5.915	3.549	129.889	5.206	0.000	8.045	2.839	10.648	2.958	0.000	0.000	0.000
490	138.055	19.167	13.511	8.955	12.412	170.856	8.327	3.456	10.841	5.185	1.571	6.599	10.998	0.000	0.319
500	131.056	22.364	11.763	8.858	7.551	158.999	9.875	0.000	9.875	3.195	7.261	3.195	0.000	0.000	0.000
509	135.607	22.184	13.845	10.069	8.496	171.526	6.608	2.045	10.384	3.619	9.440	2.360	0.000	0.000	0.197
520	140.750	27.584	12.852	8.620	10.814	172.011	5.956	0.000	11.911	3.762	9.404	5.799	0.000	0.000	0.000
530	124.810	24.711	10.668	7.832	9.317	148.225	9.182	1.350	6.211	2.025	17.554	4.456	0.000	0.000	0.217
540	118.587	23.172	8.757	6.871	5.254	145.713	7.410	4.311	8.218	2.964	16.166	3.907	0.000	0.000	0.525
550	140.451	27.945	7.420	8.368	6.789	169.846	9.946	0.158	8.368	2.526	0.000	4.263	0.000	0.000	0.019
560	112.342	23.451	7.572	5.679	4.312	115.533	4.101	1.683	8.413	2.839	15.775	3.786	0.000	0.000	0.200
570	82.492	27.764	9.923	5.911	10.086	66.465	3.525	2.386	6.344	1.898	8.676	2.006	7.049	1.085	0.376
580	77.977	16.928	8.740	4.960	2.953	49.151	3.149	1.024	5.315	1.811	5.118	0.433	0.000	0.000	0.193
590	78.022	13.148	9.752	5.195	3.280	36.796	2.148	0.493	6.008	1.625	3.773	1.335	0.000	0.000	0.082
600	68.333	17.945	8.540	4.982	2.033	67.067	2.999	0.712	5.948	1.525	5.084	2.745	0.000	0.000	0.120
610	78.715	14.350	4.827	6.335	3.491	51.967	2.370	2.198	5.861	1.853	5.602	2.586	4.740	3.017	0.375
620	83.506	19.892	12.553	5.574	2.045	49.544	3.048	0.602	5.494	1.564	2.005	1.845	1.604	0.000	0.109
630	109.989	25.379	18.240	7.139	5.711	43.334	2.677	1.464	6.925	1.321	4.283	1.071	2.142	0.000	0.211
640	113.913	23.876	16.701	7.259	2.769	52.843	2.350	0.965	6.546	1.637	5.035	1.427	2.518	0.000	0.147
650	45.405	10.252	6.322	3.816	2.297	24.388	1.234	1.196	4.025	0.987	4.177	0.987	2.848	0.000	0.297
660	4.510	1.593	1.266	1.192	3.515	3.121	0.376	1.259	1.996	0.358	4.035	0.107	0.397	0.336	0.631
670	1.267	0.735	0.810	0.891	3.020	1.012	0.313	1.194	2.100	0.401	4.978	0.036	0.334	0.364	0.569
680	1.354	0.707	0.748	0.887	2.866	1.167	0.291	1.233	2.169	0.381	4.805	0.040	0.297	0.149	0.568
690	0.458	0.473	0.757	0.760	2.696	0.524	0.296	1.208	2.208	0.362	4.822	0.030	0.418	0.000	0.547
700	0.575	0.524	0.876	0.838	2.904	0.618	0.314	1.314	2.014	0.349	4.762	0.030	0.492	0.074	0.652
710	1.018	0.562	0.753	0.818	3.180	0.986	0.332	1.346	2.001	0.353	4.522	0.055	0.268	0.045	0.673
720	2.114	0.660	0.721	1.057	3.133	2.083	0.305	1.036	2.346	0.446	5.360	0.095	0.292	0.244	0.441

Table C.5.1-3 (Contd.) Salt free trace elements and their ratios to Al in core CD3814.

Depth(cm)	Age(ka)	Ba(ppm)	Sc(ppm)	V(ppm)	Ni(ppm)	Cu(ppm)	Zn(ppm)	Sr(ppm)	Nb(ppm)	Cr(ppm)	Zr(ppm)	Pb(ppm)	Th(ppm)	U(ppm)	Rb(ppm)	Mo(ppm)
1	0.20	2471.6	5.3	27.0	107.9	48.1	52.8	1195.6	0.8	9.3	20.4	4.1	0.0	0.0	6.5	5.2
10	2.00	2276.8	4.1	20.4	33.0	37.4	31.5	1168.4	0.7	6.8	16.8	4.1	0.4	0.0	7.5	0.0
20	4.00	2299.0	3.8	23.9	21.9	35.9	31.4	1174.8	1.4	10.4	19.0	4.3	0.0	0.0	6.2	0.0
21	4.20	2400.9	5.5	22.4	96.9	47.5	53.2	1182.2	1.2	8.7	19.3	6.7	0.0	1.2	7.8	5.1
30	6.00	2191.7	3.4	24.1	19.8	29.9	35.5	1160.4	1.3	9.3	18.5	3.3	0.0	0.0	5.7	0.2
40	8.00	2259.3	5.1	40.7	28.1	44.7	39.2	1160.2	1.6	9.2	20.6	4.3	0.0	4.1	8.3	0.0
50	10.67	1921.5	5.4	30.8	35.5	30.1	42.8	1131.7	2.8	11.8	35.0	4.2	1.9	1.7	9.7	0.0
60	12.47	2082.3	4.7	23.1	38.8	36.8	54.5	1154.1	1.2	15.6	18.1	3.7	0.0	4.4	9.0	0.0
70	13.41	1758.6	6.1	39.1	64.2	38.8	68.6	1086.8	1.3	13.9	19.9	2.9	0.0	5.3	12.2	0.6
80	14.34	2127.3	5.2	30.5	44.6	38.6	51.6	1102.1	0.3	13.6	16.0	2.9	0.7	4.5	9.8	0.6
90	15.28	2324.7	5.1	37.0	71.5	40.3	69.2	1060.9	1.7	12.9	18.0	1.9	0.0	5.0	10.9	1.2
100	16.22	2138.4	4.8	43.4	58.7	39.7	63.7	1051.2	1.1	11.6	17.7	2.9	0.5	4.9	10.1	5.1
110	17.16	1641.1	3.8	36.2	50.1	35.9	57.1	1038.9	0.8	8.5	14.2	4.9	0.9	3.4	8.2	3.4
119	18.00	1888.3	2.5	45.7	67.8	36.6	68.7	1010.7	1.3	10.5	16.6	1.5	0.0	5.6	10.0	5.9
130	19.08	1960.1	4.1	48.1	61.5	47.5	77.4	977.0	2.1	14.8	18.3	3.7	0.0	4.2	10.8	7.5
140	20.07	2184.1	5.5	43.2	38.7	39.1	64.8	1047.7	1.1	10.7	17.6	1.5	0.0	3.5	9.2	3.4
150	21.05	1885.9	4.1	28.1	41.3	39.9	66.5	1031.7	1.7	11.9	16.3	3.4	0.0	2.0	8.6	5.4
160	22.03	1895.6	3.8	41.0	60.3	43.0	75.3	1068.3	1.2	10.0	16.0	3.0	0.0	6.0	9.2	7.8
170	23.02	1875.8	4.6	42.3	55.3	38.5	65.1	1080.6	0.1	10.4	16.4	5.5	0.0	1.8	8.8	1.9
180	24.00	1769.1	5.2	33.2	52.9	35.2	57.7	1118.5	0.9	12.4	15.9	2.9	0.0	4.5	8.3	3.8
190	26.92	1713.1	4.4	38.1	64.6	36.5	60.0	1061.9	0.5	8.7	15.0	2.5	0.0	2.9	8.8	3.7
200	29.83	1733.2	5.5	41.3	36.0	37.1	49.4	1116.9	1.0	12.6	15.9	3.4	1.7	0.5	7.8	1.2
210	32.75	1814.1	5.2	40.2	58.8	33.6	56.1	1132.0	0.8	10.3	16.7	4.4	0.0	0.0	7.6	2.5
220	35.67	2022.4	6.1	32.5	55.7	43.0	62.5	1151.9	0.9	13.4	17.6	5.3	0.2	1.9	8.6	1.6
230	38.58	2140.5	3.1	42.2	38.5	37.7	62.1	1153.5	0.5	14.9	19.6	4.5	0.0	2.9	9.9	0.3
240	41.50	2030.7	5.5	52.2	76.5	49.7	124.4	1142.7	1.5	13.4	18.7	5.1	0.6	3.3	8.7	3.2
250	44.42	2118.0	5.1	45.7	116.9	58.0	83.4	1121.6	1.4	13.7	17.7	3.0	0.2	3.1	8.6	3.9
260	47.33	2056.3	5.7	29.0	39.5	42.2	58.7	1176.4	1.0	13.3	17.6	5.7	0.0	0.5	8.4	0.8
270	50.25	1833.3	4.3	26.7	46.5	44.7	64.6	1140.6	1.9	10.2	16.0	2.2	0.2	0.0	8.4	0.1
280	53.17	1966.7	4.7	27.0	42.5	41.6	58.2	1129.5	2.1	14.5	17.0	4.5	0.0	1.4	8.1	1.4
290	56.08	2067.8	6.4	42.7	56.4	45.7	91.5	1124.7	1.5	11.6	19.8	4.5	0.0	5.0	11.1	0.2
300	59.00	2220.0	5.8	49.5	61.5	48.5	77.5	1111.4	1.5	14.3	23.3	5.9	0.4	1.7	11.0	0.6

Table C.5.2-1 Salt included trace element data from core CD3822.

Depth(cm)	Age(ka)	Ba(ppm)	Sc(ppm)	V(ppm)	Ni(ppm)	Cu(ppm)	Zn(ppm)	Sr(ppm)	Nb(ppm)	Cr(ppm)	Zr(ppm)	Pb(ppm)	Th(ppm)	U(ppm)	Rb(ppm)	Mo(ppm)
310	60.67	2106.3	7.4	49.0	89.3	52.4	82.0	1102.8	1.3	14.5	20.1	5.6	0.1	4.0	11.6	1.6
320	62.33	2279.8	6.0	53.7	130.7	54.7	109.9	1032.6	1.6	11.5	24.3	7.0	2.2	3.2	14.5	2.1
330	64.00	2305.9	5.8	50.9	134.1	92.9	109.2	1028.7	1.7	13.9	24.6	5.7	1.8	1.6	15.8	2.1
340	68.67	2552.0	5.0	44.9	87.6	68.4	98.8	1071.2	2.1	15.6	26.0	3.7	0.0	0.0	15.3	1.2
350	72.29	2356.0	6.6	36.2	139.1	45.0	82.0	1045.2	1.1	11.2	21.7	5.1	1.7	0.9	16.3	1.3
360	74.86	2141.5	4.4	28.1	59.0	50.0	74.1	965.5	1.6	8.2	25.4	6.3	1.7	0.7	23.4	0.7
370	77.43	2006.0	5.4	31.7	195.5	59.9	67.6	915.0	1.3	5.8	25.8	5.2	3.0	2.0	29.9	2.3
380	80.00	1978.1	5.3	33.4	94.1	38.7	65.7	959.5	2.3	13.5	24.0	6.2	2.5	1.9	24.7	1.4
390	81.67	1662.1	1.5	41.8	59.9	27.1	80.8	755.8	2.0	8.1	28.7	6.7	2.6	0.7	43.4	1.0
400	83.33	2314.3	6.8	37.0	85.7	43.6	72.6	1126.1	0.9	14.1	21.8	4.4	1.1	1.4	9.9	0.4
410	85.00	2517.0	5.2	34.9	68.3	49.3	65.8	1178.8	0.6	13.9	18.9	4.5	0.2	0.0	7.9	1.1
420	86.67	2595.1	6.8	25.2	73.5	50.7	65.4	1174.7	1.7	12.1	19.9	3.5	0.0	0.0	7.2	2.1
430	88.33	2458.1	8.4	34.8	83.6	58.3	80.4	1160.4	2.0	11.4	19.5	6.5	0.4	1.5	7.8	0.2
440	90.00	2167.8	4.7	32.7	82.3	67.2	71.6	1152.9	1.5	9.0	18.3	6.1	1.9	0.2	6.6	1.4
450	*****	2279.4	6.5	30.5	40.9	39.7	54.8	1156.0	1.3	10.3	17.7	1.9	0.4	0.6	5.8	0.7
460	*****	2384.7	6.2	28.0	71.5	44.1	52.5	1152.2	1.2	13.7	20.5	3.3	0.0	0.0	6.8	0.5
470	*****	2213.9	6.8	23.1	35.1	39.8	42.4	1129.1	0.5	11.6	16.8	6.0	0.8	0.0	7.2	1.1
480	*****	1948.6	8.4	23.9	21.3	32.9	36.6	1157.8	0.8	11.3	15.7	2.9	1.1	1.9	7.2	0.8
490	*****	1560.6	4.8	24.7	18.3	33.0	27.6	1191.0	1.4	8.1	12.5	1.5	0.0	0.8	5.2	1.2
500	*****	1458.1	4.6	27.6	13.0	22.9	19.9	1200.3	0.8	5.3	12.6	0.4	0.5	0.3	4.3	0.5
510	*****	1433.6	4.2	43.7	14.7	20.8	28.6	1208.7	0.9	9.0	11.9	3.2	0.2	2.9	4.4	1.6
520	*****	1219.9	5.3	23.1	17.7	21.4	30.0	1148.9	1.3	8.5	11.4	3.1	0.6	3.5	3.8	3.1
530	*****	1316.2	4.4	26.3	25.7	20.0	23.0	1158.6	1.2	9.7	12.4	3.0	0.1	2.7	3.9	3.4
540	*****	1199.6	8.2	52.1	23.4	22.0	22.8	1104.9	2.2	10.9	36.0	3.6	0.0	3.2	4.9	3.3
550	*****	1293.0	6.7	40.1	33.4	27.4	28.1	1097.5	1.6	10.7	25.2	1.5	0.0	4.8	6.4	7.5
560	*****	1345.6	3.5	25.7	30.8	22.1	25.6	1105.8	0.0	7.7	13.1	2.2	0.0	0.3	5.0	5.7
570	*****	1393.5	5.0	22.8	29.3	21.8	29.2	1114.7	1.3	5.9	12.5	1.9	0.0	1.6	3.5	3.5
580	*****	1367.6	5.3	17.0	37.1	47.5	29.9	1141.3	1.1	6.3	14.2	2.2	0.4	2.4	5.0	5.9
590	*****	1357.9	5.5	20.8	16.1	23.0	23.5	1135.7	2.2	10.5	15.9	2.0	0.0	4.0	5.1	3.0
600	*****	1292.1	3.4	28.6	25.4	18.3	38.5	1110.2	4.8	5.5	35.3	2.1	0.8	1.0	7.4	3.7
610	*****	1090.9	3.2	16.7	22.1	17.1	68.3	874.0	23.9	4.0	135.6	2.6	1.5	2.3	19.4	5.1
620	*****	1233.9	6.9	26.9	14.6	19.1	32.1	1145.7	2.7	6.6	30.3	2.5	0.0	2.5	5.8	3.8

Table C.5.2-1 (Contd.) Salt included trace element data from core CD3822.

Depth(cm)	Age(ka)	Ba(ppm)	Cu(ppm)	Ni(ppm)	Zn(ppm)	V(ppm)	Sr(ppm)	Sc(ppm)	Cr(ppm)	Zr(ppm)	Rb(ppm)	Nb(ppm)	Pb(ppm)	Th(ppm)	U(ppm)	Mo(ppm)	SALT
1	0.20	2586.0	50.3	112.9	55.2	28.2	1250.9	5.5	9.7	21.3	6.8	0.8	4.3	0.0	0.0	5.5	4.423
10	2.00	2389.1	39.2	34.6	33.1	21.4	1226.1	4.3	7.1	17.6	7.9	0.7	4.3	0.4	0.0	0.0	4.702
20	4.00	2411.9	37.7	23.0	32.9	25.1	1232.5	4.0	10.9	19.9	6.5	1.5	4.5	0.0	0.0	0.0	4.682
21	4.20	2535.0	50.2	102.3	56.2	23.7	1248.2	5.8	9.2	20.4	8.2	1.3	7.1	0.0	1.3	5.4	5.291
30	6.00	2306.0	31.5	20.8	37.4	25.4	1220.9	3.6	9.8	19.5	6.0	1.4	3.5	0.0	0.0	0.2	4.957
40	8.00	2383.9	47.2	29.6	41.4	42.9	1224.2	5.4	9.7	21.7	8.8	1.7	4.5	0.0	4.3	0.0	5.225
50	10.67	2026.4	31.7	37.4	45.1	32.5	1193.5	5.7	12.4	36.9	10.2	3.0	4.4	2.0	1.8	0.0	5.175
60	12.47	2196.9	38.8	40.9	57.5	24.4	1217.6	5.0	16.5	19.1	9.5	1.3	3.9	0.0	4.6	0.0	5.215
70	13.41	1848.1	40.8	67.5	72.1	41.1	1142.1	6.4	14.6	20.9	12.8	1.4	3.0	0.0	5.6	0.6	4.841
80	14.34	2250.3	40.8	47.2	54.6	32.3	1165.8	5.5	14.4	16.9	10.4	0.3	3.1	0.7	4.8	0.6	5.467
90	15.28	2485.8	43.1	76.5	74.0	39.6	1134.4	5.5	13.8	19.2	11.7	1.8	2.0	0.0	5.3	1.3	6.480
100	16.22	2279.6	42.3	62.6	67.9	46.3	1120.6	5.1	12.4	18.9	10.8	1.2	3.1	0.5	5.2	5.5	6.195
110	17.16	1740.3	38.1	53.1	60.6	38.4	1101.7	4.0	9.0	15.1	8.7	0.8	5.2	1.0	3.6	3.6	5.701
119	18.00	2051.4	39.8	73.7	74.6	49.6	1098.0	2.7	11.4	18.0	10.9	1.4	1.6	0.0	6.1	6.3	7.951
130	19.08	2110.2	51.1	66.2	83.3	51.8	1051.8	4.4	15.9	19.7	11.6	2.3	4.0	0.0	4.5	8.0	7.113
140	20.07	2342.2	41.9	41.5	69.5	46.3	1123.5	5.9	11.5	18.9	9.9	1.2	1.6	0.0	3.8	3.6	6.750
150	21.05	2008.2	42.5	44.0	70.8	29.9	1098.6	4.4	12.7	17.4	9.2	1.8	3.6	0.0	2.1	5.8	6.091
160	22.03	2016.0	45.7	64.1	80.1	43.6	1136.2	4.0	10.6	17.0	9.8	1.3	3.2	0.0	6.4	8.2	5.974
170	23.02	1989.7	40.8	58.7	69.1	44.9	1146.2	4.9	11.0	17.4	9.3	0.1	5.8	0.0	1.9	2.0	5.726
180	24.00	1888.4	37.6	56.5	61.6	35.4	1193.9	5.6	13.2	17.0	8.9	1.0	3.1	0.0	4.8	4.0	6.318
190	26.92	1811.8	38.6	68.3	63.5	40.3	1123.1	4.7	9.2	15.9	9.3	0.5	2.6	0.0	3.1	3.9	5.449
200	29.83	1817.2	38.9	37.7	51.8	43.3	1171.0	5.8	13.2	16.7	8.2	1.0	3.6	1.8	0.5	1.3	4.622
210	32.75	1900.1	35.2	61.6	58.8	42.1	1185.7	5.4	10.8	17.5	8.0	0.8	4.6	0.0	0.0	2.6	4.527
220	35.67	2119.3	45.1	58.4	65.5	34.1	1207.1	6.4	14.0	18.4	9.0	0.9	5.6	0.2	2.0	1.7	4.572
230	38.58	2235.2	39.4	40.2	64.8	44.1	1204.5	3.2	15.6	20.5	10.3	0.5	4.7	0.0	3.0	0.3	4.237
240	41.50	2134.3	52.2	80.4	130.7	54.9	1201.0	5.8	14.1	19.7	9.1	1.6	5.4	0.6	3.5	3.4	4.853
250	44.42	2238.0	61.3	123.5	88.1	48.3	1185.2	5.4	14.5	18.7	9.1	1.5	3.2	0.2	3.3	4.1	5.364
260	47.33	2156.4	44.3	41.4	61.6	30.4	1233.6	6.0	13.9	18.5	8.8	1.0	6.0	0.0	0.5	0.8	4.640
270	50.25	1926.2	47.0	48.9	67.9	28.1	1198.4	4.5	10.7	16.8	8.8	2.0	2.3	0.2	0.0	0.1	4.825
280	53.17	2057.6	43.5	44.5	60.9	28.2	1181.7	4.9	15.2	17.8	8.5	2.2	4.7	0.0	1.5	1.5	4.417
290	56.08	2161.9	47.8	59.0	95.7	44.6	1175.9	6.7	12.1	20.7	11.6	1.6	4.7	0.0	5.2	0.2	4.353
300	59.00	2320.1	50.7	64.3	81.0	51.7	1161.5	6.1	14.9	24.4	11.5	1.6	6.2	0.4	1.8	0.6	4.315

Table C.5.2-2 Salt free trace element data from core CD3822.

Depth(cm)	Age(ka)	Ba(ppm)	Cu(ppm)	Ni(ppm)	Zn(ppm)	V(ppm)	Sr(ppm)	Sc(ppm)	Cr(ppm)	Zr(ppm)	Rb(ppm)	Nb(ppm)	Pb(ppm)	Th(ppm)	U(ppm)	Mo(ppm)	SALT
310	60.67	2201.9	54.8	93.4	85.7	51.2	1152.8	7.7	15.2	21.0	12.1	1.4	5.9	0.1	4.2	1.7	4.340
320	62.33	2395.9	57.5	137.4	115.5	56.4	1085.2	6.3	12.1	25.5	15.2	1.7	7.4	2.3	3.4	2.2	4.846
330	64.00	2401.2	96.7	139.6	113.7	53.0	1071.2	6.0	14.5	25.6	16.5	1.8	5.9	1.9	1.7	2.2	3.970
340	68.67	2670.3	71.6	91.7	103.4	47.0	1120.9	5.2	16.3	27.2	16.0	2.2	3.9	0.0	0.0	1.3	4.430
350	72.29	2468.7	47.2	145.8	85.9	37.9	1095.2	6.9	11.7	22.7	17.1	1.2	5.3	1.8	0.9	1.4	4.564
360	74.86	2234.2	52.2	61.6	77.3	29.3	1007.3	4.6	8.6	26.5	24.4	1.7	6.6	1.8	0.7	0.7	4.150
370	77.43	2091.8	62.5	203.9	70.5	33.1	954.1	5.6	6.0	26.9	31.2	1.4	5.4	3.1	2.1	2.4	4.102
380	80.00	2054.8	40.2	97.7	68.2	34.7	996.7	5.5	14.0	24.9	25.7	2.4	6.4	2.6	2.0	1.5	3.731
390	81.67	1729.3	28.2	62.3	84.1	43.5	786.4	1.6	8.4	29.9	45.2	2.1	7.0	2.7	0.7	1.0	3.885
400	83.33	2415.5	45.5	89.4	75.8	38.6	1175.4	7.1	14.7	22.8	10.3	0.9	4.6	1.1	1.5	0.4	4.190
410	85.00	2621.3	51.3	71.1	68.5	36.3	1227.7	5.4	14.5	19.7	8.2	0.6	4.7	0.2	0.0	1.1	3.981
420	86.67	2699.0	52.7	76.4	68.0	26.2	1221.7	7.1	12.6	20.7	7.5	1.8	3.6	0.0	0.0	2.2	3.851
430	88.33	2558.4	60.7	87.0	83.7	36.2	1207.7	8.7	11.9	20.3	8.1	2.1	6.8	0.4	1.6	0.2	3.919
440	90.00	2253.1	69.8	85.5	74.4	34.0	1198.3	4.9	9.4	19.0	6.9	1.6	6.3	2.0	0.2	1.5	3.786
450	*****	2368.5	41.3	42.5	56.9	31.7	1201.2	6.8	10.7	18.4	6.0	1.4	2.0	0.4	0.6	0.7	3.762
460	*****	2477.6	45.8	74.3	54.5	29.1	1197.1	6.4	14.2	21.3	7.1	1.2	3.4	0.0	0.0	0.5	3.749
470	*****	2299.6	41.3	36.5	44.0	24.0	1172.8	7.1	12.0	17.5	7.5	0.5	6.2	0.8	0.0	1.1	3.728
480	*****	2012.8	34.0	22.0	37.8	24.7	1195.9	8.7	11.7	16.2	7.4	0.8	3.0	1.1	2.0	0.8	3.188
490	*****	1605.4	33.9	18.8	28.4	25.4	1225.2	4.9	8.3	12.9	5.3	1.4	1.5	0.0	0.8	1.2	2.792
500	*****	1502.2	23.6	13.4	20.5	28.4	1236.6	4.7	5.5	13.0	4.4	0.8	0.4	0.5	0.3	0.5	2.933
510	*****	1475.3	21.4	15.1	29.4	45.0	1243.9	4.3	9.3	12.2	4.5	0.9	3.3	0.2	3.0	1.6	2.830
520	*****	1255.4	22.0	18.2	30.9	23.8	1182.4	5.5	8.7	11.7	3.9	1.3	3.2	0.6	3.6	3.2	2.830
530	*****	1354.7	20.6	26.5	23.7	27.1	1192.5	4.5	10.0	12.8	4.0	1.2	3.1	0.1	2.8	3.5	2.845
540	*****	1236.6	22.7	24.1	23.5	53.7	1138.9	8.5	11.2	37.1	5.1	2.3	3.7	0.0	3.3	3.4	2.989
550	*****	1348.8	28.6	34.8	29.3	41.8	1144.8	7.0	11.2	26.3	6.7	1.7	1.6	0.0	5.0	7.7	4.135
560	*****	1400.4	23.0	32.1	26.6	26.7	1150.8	3.6	8.0	13.6	5.2	0.0	2.3	0.0	0.3	5.9	3.912
570	*****	1451.3	22.7	30.5	30.4	23.7	1160.9	5.2	6.1	13.0	3.6	1.4	2.0	0.0	1.7	3.6	3.982
580	*****	1412.1	49.0	38.3	30.9	17.6	1178.5	5.5	6.5	14.7	5.2	1.1	2.3	0.4	2.5	6.1	3.153
590	*****	1407.0	23.8	16.7	24.3	21.6	1176.7	5.7	10.9	16.5	5.3	2.3	2.1	0.0	4.1	3.1	3.487
600	*****	1333.8	18.9	26.2	39.7	29.5	1146.0	3.5	5.7	36.4	7.6	5.0	2.2	0.8	1.0	3.7	3.126
610	*****	1121.5	17.6	22.7	70.2	17.2	898.5	3.3	4.1	139.4	19.9	24.6	2.7	1.5	2.4	5.1	2.732
620	*****	1266.3	19.6	15.0	32.9	27.6	1175.8	7.1	6.8	31.1	6.0	2.8	2.6	0.0	2.6	3.8	2.556

Table C.5.2-2 (Contd.) Salt free trace element data from core CD3822.

Depth(cm)	Age(ka)	Ba/Al *10-2	Cu/Al *10-3	Ni/Al *10-3	Zn/Al *10-3	V/Al *10-3	Sr/Al *10-2	Sc/Al *10-3	Cr/Al *10-3	Zr/Al *10-3	Rb/Al *10-3	Nb/Al *10-3	Pb/Al *10-3	Th/Al *10-3	U/Al *10-3	Cr/Zr
1	0.20	27.323	5.317	11.928	5.837	2.985	13.217	0.586	1.028	2.255	0.719	0.088	0.453	0.000	0.000	0.456
10	2.00	19.564	3.214	2.836	2.707	1.753	10.040	0.352	0.584	1.444	0.644	0.060	0.352	0.034	0.000	0.405
20	4.00	27.162	4.241	2.587	3.710	2.824	13.880	0.449	1.229	2.245	0.733	0.165	0.508	0.000	0.000	0.547
21	4.20	28.366	5.612	11.448	6.285	2.647	13.967	0.650	1.028	2.280	0.922	0.142	0.792	0.000	0.142	0.451
30	6.00	29.177	3.980	2.636	4.726	3.208	15.448	0.453	1.238	2.463	0.759	0.173	0.439	0.000	0.000	0.503
40	8.00	30.726	6.079	3.822	5.331	5.535	15.778	0.694	1.251	2.802	1.129	0.218	0.585	0.000	0.558	0.447
50	10.67	23.136	3.624	4.274	5.153	3.708	13.626	0.650	1.421	4.214	1.168	0.337	0.506	0.229	0.205	0.337
60	12.47	27.335	4.831	5.093	7.154	3.032	15.150	0.617	2.048	2.376	1.181	0.158	0.486	0.000	0.578	0.862
70	13.41	20.148	4.445	7.355	7.859	4.480	12.451	0.699	1.592	2.280	1.398	0.149	0.332	0.000	0.607	0.698
80	14.34	33.793	6.132	7.085	8.197	4.845	17.507	0.826	2.160	2.542	1.557	0.048	0.461	0.111	0.715	0.850
90	15.28	29.895	5.182	9.195	8.899	4.758	13.643	0.656	1.659	2.315	1.402	0.219	0.244	0.000	0.643	0.717
100	16.22	31.095	5.773	8.536	9.263	6.311	15.286	0.698	1.687	2.574	1.469	0.160	0.422	0.073	0.713	0.655
110	17.16	27.699	6.059	8.456	9.637	6.110	17.535	0.641	1.435	2.397	1.384	0.135	0.827	0.152	0.574	0.599
119	18.00	23.179	4.493	8.322	8.433	5.610	12.406	0.307	1.289	2.038	1.228	0.160	0.184	0.000	0.687	0.633
130	19.08	******	*****	*****	*****	*****	******	*****	*****	*****	*****	*****	*****	*****	*****	0.809
140	20.07	29.076	5.205	5.152	8.626	5.751	13.947	0.732	1.424	2.343	1.225	0.146	0.200	0.000	0.466	0.608
150	21.05	29.222	6.182	6.399	10.304	4.354	15.986	0.635	1.844	2.526	1.333	0.263	0.527	0.000	0.310	0.730
160	22.03	25.058	5.684	7.971	9.954	5.420	14.122	0.502	1.322	2.115	1.216	0.159	0.397	0.000	0.793	0.625
170	23.02	27.068	5.556	7.980	9.394	6.104	15.593	0.664	1.501	2.367	1.270	0.014	0.794	0.000	0.260	0.634
180	24.00	26.127	5.198	7.813	8.521	4.903	16.518	0.768	1.831	2.348	1.226	0.133	0.428	0.000	0.665	0.780
190	26.92	25.701	5.476	9.692	9.002	5.716	15.932	0.660	1.305	2.250	1.320	0.075	0.375	0.000	0.435	0.580
200	29.83	25.597	5.479	5.317	7.296	6.099	16.495	0.812	1.861	2.348	1.152	0.148	0.502	0.251	0.074	0.792
210	32.75	26.584	4.924	8.617	8.221	5.891	16.588	0.762	1.509	2.447	1.114	0.117	0.645	0.000	0.000	0.617
220	35.67	26.549	5.645	7.312	8.205	4.266	15.122	0.801	1.759	2.310	1.129	0.118	0.696	0.026	0.249	0.761
230	38.58	27.156	4.783	4.884	7.879	5.354	14.634	0.393	1.890	2.487	1.256	0.063	0.571	0.000	0.368	0.760
240	41.50	24.607	6.022	9.270	15.074	6.325	13.847	0.666	1.624	2.266	1.054	0.182	0.618	0.073	0.400	0.717
250	44.42	27.237	7.459	15.033	10.725	5.877	14.423	0.656	1.762	2.276	1.106	0.180	0.386	0.026	0.399	0.774
260	47.33	26.264	5.390	5.045	7.498	3.704	15.026	0.728	1.699	2.248	1.073	0.128	0.728	0.000	0.064	0.756
270	50.25	27.075	6.601	6.867	9.540	3.943	16.845	0.635	1.506	2.363	1.241	0.281	0.325	0.030	0.000	0.638
280	53.17	25.120	5.313	5.428	7.434	3.449	14.427	0.600	1.852	2.171	1.035	0.268	0.575	0.000	0.179	0.853
290	56.08	22.210	4.908	6.058	9.828	4.586	12.080	0.687	1.246	2.127	1.192	0.161	0.483	0.000	0.537	0.586
300	59.00	20.673	4.516	5.727	7.217	4.609	10.349	0.540	1.332	2.170	1.024	0.140	0.549	0.037	0.158	0.614

Table C.5.2-3 Salt free trace elements and their ratios to Al in core CD3822.

Depth(cm)	Age(ka)	Ba/Al *10-2	Cu/Al *10-3	Ni/Al *10-3	Zn/Al *10-3	V/Al *10-3	Sr/Al *10-2	Sc/Al *10-3	Cr/Al *10-3	Zr/Al *10-3	Rb/Al *10-3	Nb/Al *10-3	Pb/Al *10-3	Th/Al *10-3	U/Al *10-3	Cr/Zr
310	60.67	21.292	5.297	9.027	8.289	4.953	11.148	0.748	1.466	2.032	1.173	0.131	0.566	0.010	0.404	0.721
320	62.33	19.413	4.658	11.129	9.358	4.573	8.793	0.511	0.979	2.069	1.235	0.136	0.596	0.187	0.272	0.473
330	64.00	19.460	7.840	11.317	9.216	4.296	8.681	0.489	1.173	2.076	1.333	0.143	0.481	0.152	0.135	0.565
340	68.67	19.691	5.278	6.759	7.623	3.464	8.265	0.386	1.204	2.006	1.181	0.162	0.285	0.000	0.000	0.600
350	72.29	18.480	3.530	10.911	6.432	2.839	8.198	0.518	0.879	1.702	1.279	0.086	0.400	0.133	0.071	0.516
360	74.86	13.101	3.059	3.609	4.533	1.719	5.907	0.269	0.502	1.554	1.432	0.098	0.385	0.104	0.043	0.323
370	77.43	10.085	3.012	9.829	3.399	1.594	4.600	0.271	0.292	1.297	1.503	0.065	0.261	0.151	0.101	0.225
380	80.00	11.759	2.301	5.594	3.906	1.985	5.704	0.315	0.803	1.427	1.468	0.137	0.369	0.149	0.113	0.563
390	81.67	6.629	1.081	2.389	3.222	1.667	3.014	0.060	0.323	1.145	1.731	0.080	0.267	0.104	0.028	0.282
400	83.33	23.026	4.338	8.527	7.223	3.681	11.204	0.677	1.403	2.169	0.985	0.090	0.438	0.109	0.139	0.647
410	85.00	29.190	5.717	7.921	7.631	4.047	13.671	0.603	1.612	2.192	0.916	0.070	0.522	0.023	0.000	0.735
420	86.67	30.096	5.880	8.524	7.585	2.923	13.623	0.789	1.403	2.308	0.835	0.197	0.406	0.000	0.000	0.608
430	88.33	30.570	7.251	10.397	9.999	4.328	14.431	1.045	1.418	2.425	0.970	0.249	0.808	0.050	0.187	0.585
440	90.00	29.912	9.272	11.356	9.880	4.512	15.908	0.649	1.242	2.525	0.911	0.207	0.842	0.262	0.028	0.492
450	*****	29.716	5.176	5.332	7.144	3.976	15.071	0.847	1.343	2.308	0.756	0.169	0.248	0.052	0.078	0.582
460	*****	26.833	4.962	8.045	5.907	3.151	12.965	0.698	1.542	2.307	0.765	0.135	0.371	0.000	0.000	0.668
470	*****	27.353	4.917	4.337	5.239	2.854	13.950	0.840	1.433	2.076	0.890	0.062	0.741	0.099	0.000	0.690
480	*****	28.335	4.784	3.097	5.322	3.475	16.836	1.221	1.643	2.283	1.047	0.116	0.422	0.160	0.276	0.720
490	*****	40.412	8.545	4.739	7.147	6.396	30.841	1.243	2.098	3.237	1.347	0.363	0.388	0.000	0.207	0.648
500	*****	42.405	6.660	3.781	5.787	8.027	34.908	1.338	1.541	3.664	1.251	0.233	0.116	0.145	0.087	0.421
510	*****	39.276	5.698	4.027	7.835	11.972	33.114	1.151	2.466	3.260	1.205	0.247	0.877	0.055	0.794	0.756
520	*****	37.194	6.525	5.397	9.147	7.043	35.030	1.616	2.592	3.476	1.159	0.396	0.945	0.183	1.067	0.746
530	*****	35.544	5.401	6.940	6.211	7.102	31.288	1.188	2.619	3.349	1.053	0.324	0.810	0.027	0.729	0.782
540	*****	13.339	2.446	2.602	2.535	5.793	12.286	0.912	1.212	4.003	0.545	0.245	0.400	0.000	0.356	0.303
550	*****	19.872	4.211	5.133	4.319	6.163	16.867	1.030	1.644	3.873	0.984	0.246	0.231	0.000	0.738	0.425
560	*****	34.845	5.723	7.976	6.629	6.655	28.635	0.906	1.994	3.392	1.295	0.000	0.570	0.000	0.078	0.588
570	*****	41.813	6.541	8.792	8.762	6.841	33.447	1.500	1.770	3.751	1.050	0.390	0.570	0.000	0.480	0.472
580	*****	38.586	13.402	10.468	8.436	4.796	32.201	1.495	1.778	4.006	1.411	0.310	0.621	0.113	0.677	0.444
590	*****	34.226	5.797	4.058	5.923	5.243	28.625	1.386	2.647	4.008	1.285	0.555	0.504	0.000	1.008	0.660
600	*****	19.385	2.746	3.811	5.776	4.291	16.656	0.510	0.825	5.296	1.110	0.720	0.315	0.120	0.150	0.156
610	*****	5.247	0.823	1.063	3.285	0.803	4.204	0.154	0.192	6.522	0.933	1.150	0.125	0.072	0.111	0.029
620	*****	21.205	3.282	2.509	5.516	4.623	19.689	1.186	1.134	5.207	0.997	0.464	0.430	0.000	0.430	0.218

Table C.5.2-3 (Contd.) Salt free trace elements and their ratios to Al in core CD3822.

Table C.5.3-1 Salt included trace element data from core CD3826.

Depth(cm)	Age(ka)	Ba(ppm)	Sc(ppm)	V(ppm)	Ni(ppm)	Cu(ppm)	Zn(ppm)	Sr(ppm)	Y(ppm)	Nb(ppm)	Cr(ppm)	Zr(ppm)	Pb(ppm)	Th(ppm)	U(ppm)	Rb(ppm)	Mo(ppm)
1	0.57	3413.3	19.0	126.0	370.2	132.9	372.7	460.6	23.9	5.2	74.9	74.0	128.8	0.0	0.0	30.0	14.7
5	2.83	3593.7	21.1	125.8	409.3	141.1	434.0	459.1	23.5	3.6	85.4	76.1	10.0	0.0	0.0	31.1	10.1
10	5.67	3505.8	20.1	107.7	208.5	102.0	356.4	466.0	24.6	5.4	81.3	77.2	10.9	0.2	0.0	31.1	0.5
15	8.50	3243.4	19.5	199.1	236.5	118.5	394.4	555.2	22.8	4.7	81.8	71.9	8.5	1.6	2.2	30.8	0.2
20	11.33	3122.3	18.8	186.0	226.7	130.8	371.3	589.2	20.5	4.8	81.6	69.5	6.0	0.0	1.2	28.8	0.0
30	17.00	2450.0	18.9	195.3	286.8	100.3	394.1	564.1	21.7	4.5	84.2	70.0	7.7	0.6	2.0	33.7	0.0
40	17.71	2215.2	18.3	234.0	355.6	94.2	355.5	524.4	23.6	5.2	86.1	71.1	7.1	0.0	5.1	36.5	0.0
50	18.42	1885.3	12.5	132.4	200.4	73.9	272.0	507.6	23.6	4.3	62.8	65.7	7.2	0.0	2.8	31.8	0.0
60	19.14	2023.9	12.8	157.7	278.3	83.2	293.5	490.4	24.8	3.8	72.3	64.5	7.9	0.1	4.1	32.4	1.4
70	23.83	2146.1	11.1	196.4	253.2	90.6	223.4	409.0	17.6	2.0	51.1	37.8	2.3	0.0	6.6	19.9	1.0
78	27.29	2640.0	20.5	248.1	242.0	100.6	332.5	463.1	24.8	5.0	91.4	71.4	8.4	0.0	4.7	33.4	3.2
81	28.59	2622.5	19.5	196.5	219.7	92.8	296.4	461.2	25.4	4.6	85.3	69.6	8.8	0.2	4.3	33.2	0.5
90	32.49	2444.4	19.7	174.1	211.0	88.0	303.5	490.1	23.9	3.7	80.1	66.5	8.2	0.0	4.3	31.6	3.7
100	36.82	2560.5	20.2	164.9	182.9	88.4	299.6	487.2	23.1	4.1	83.2	68.4	8.7	1.0	4.9	31.0	2.9
110	39.00	2878.5	21.6	251.8	396.0	105.1	426.4	412.5	25.4	3.9	88.5	72.0	7.5	1.1	5.4	35.4	3.5
120	41.83	2498.8	19.7	162.3	166.1	89.7	280.8	508.0	23.5	4.7	77.9	66.1	9.8	0.0	3.4	31.2	1.3
130	44.67	2602.9	21.4	157.4	194.9	94.0	329.5	427.7	25.0	5.0	82.5	71.2	10.0	1.6	3.2	33.5	1.7
140	47.50	2683.0	18.0	155.7	257.0	83.5	297.5	365.5	24.3	4.8	68.5	69.3	8.3	0.2	2.9	44.7	3.5
150	50.33	2808.5	23.9	202.0	283.8	111.9	357.7	307.6	29.9	5.3	84.3	79.1	10.2	1.2	5.7	39.1	2.9
160	53.16	2412.6	16.8	160.6	186.5	95.4	231.5	338.0	21.2	5.1	61.3	64.5	10.6	3.1	3.6	52.2	1.8
170	56.00	2469.3	16.6	147.1	170.1	165.7	411.8	278.8	22.5	5.2	60.2	70.0	14.3	5.2	3.5	64.6	3.6
180	64.00	2822.8	20.1	204.7	345.3	108.1	389.4	367.9	24.7	4.7	76.5	70.6	11.3	2.8	6.2	43.6	6.7
190	71.25	3232.0	22.0	215.9	393.8	129.2	421.7	411.3	26.9	4.6	82.3	74.0	8.9	1.6	6.9	32.5	5.4
200	78.49	3111.2	21.5	224.1	287.8	128.0	430.7	433.7	27.0	4.9	78.9	71.1	9.6	2.3	3.0	31.0	3.1
210	85.74	3308.1	23.1	250.2	264.7	134.1	433.8	404.5	28.4	4.9	90.0	77.0	8.5	2.0	5.9	34.6	4.7
220	92.98	2951.6	21.7	202.4	397.8	137.9	386.2	370.1	27.2	5.8	85.0	77.7	9.1	0.0	4.9	34.7	4.0
230	100.23	3316.5	22.2	181.1	316.1	138.6	377.5	345.6	28.1	5.2	87.5	80.0	9.7	0.0	6.7	35.0	2.4
240	107.48	3131.3	20.8	188.1	382.8	153.8	388.2	345.4	26.9	5.3	84.2	73.7	8.2	0.0	3.4	32.1	1.9
250	114.72	3845.5	23.5	206.0	343.1	137.8	376.1	349.9	26.5	5.6	89.0	83.6	10.7	0.0	4.9	37.4	2.3
260	122.00	3038.0	18.8	206.2	188.3	129.7	331.6	539.4	22.1	5.1	79.1	73.0	8.0	0.0	3.7	33.4	2.3
270	127.00	2749.5	18.6	192.4	190.8	90.4	303.2	539.8	22.1	4.6	73.1	64.1	7.8	0.7	6.0	29.0	6.6
280	132.00	2687.3	18.0	161.7	167.1	91.0	287.3	557.4	22.3	4.4	70.1	62.4	6.0	1.4	2.0	27.9	5.3
290	137.00	2544.5	18.7	151.0	174.1	85.9	250.3	533.2	22.2	4.2	72.1	65.3	7.1	1.4	4.1	30.5	4.6
300	142.00	2635.3	17.9	190.1	160.8	101.6	282.7	543.7	23.3	4.4	73.6	64.8	7.8	0.0	6.3	30.6	3.7
310	147.00	2479.1	18.9	198.6	227.5	102.2	284.6	547.6	21.6	4.0	79.5	65.3	8.4	2.3	5.5	30.9	6.1
320	152.00	2280.0	17.2	162.8	140.4	75.4	234.0	562.1	20.1	3.4	73.6	60.0	7.1	2.3	5.1	28.3	2.6
330	156.00	2366.4	17.0	146.6	164.4	79.7	228.4	571.7	22.2	3.5	72.2	60.3	10.4	1.1	5.4	27.8	2.8
340	160.00	2547.3	16.3	212.6	223.9	85.8	257.0	583.6	22.0	3.7	77.5	62.1	6.3	0.0	8.5	28.6	4.5
350	164.00	2591.5	18.1	166.1	188.5	102.7	262.9	472.0	21.8	5.4	80.8	68.9	7.7	2.8	3.0	32.9	3.6
360	168.00	2177.9	18.7	174.2	218.5	100.8	305.8	435.2	21.8	4.4	83.1	70.5	10.2	0.0	4.5	36.1	2.3
368	172.00	2064.2	19.2	251.2	253.3	97.9	394.4	411.2	21.6	6.4	96.5	82.3	10.0	2.9	6.3	45.6	3.3
380	176.00	2426.5	17.9	226.6	214.4	92.7	304.9	565.2	22.8	3.2	73.2	62.0	7.6	1.2	3.4	28.2	6.9
390	180.00	2359.5	19.0	200.0	229.4	100.0	302.4	555.0	23.9	3.7	71.3	63.1	8.8	0.4	5.5	29.1	6.4
400	184.00	2479.3	19.6	247.7	361.6	120.0	315.7	506.7	24.7	3.9	81.0	67.4	6.9	0.7	5.4	30.9	8.4
410	187.28	2363.7	19.3	176.9	243.8	109.2	307.7	470.9	25.0	3.9	72.6	66.3	8.7	3.0	4.8	30.8	4.8
420	189.86	2700.8	21.0	206.8	264.6	111.7	326.3	395.5	28.4	5.1	79.8	75.2	9.2	0.5	4.8	33.6	3.6
430	192.43	3224.1	23.8	236.2	254.7	121.7	399.7	354.8	32.2	5.1	88.0	80.5	8.6	0.0	2.9	35.7	4.8
440	195.00	3103.2	24.2	205.3	197.4	107.2	336.5	327.3	29.6	4.9	89.4	82.0	9.4	0.4	4.6	37.0	2.7
452	199.15	3083.9	20.5	175.2	193.7	94.2	336.7	460.9	24.8	3.8	86.1	72.3	9.5	0.9	5.8	33.7	2.1
460	201.92	3131.3	23.4	241.0	260.9	118.5	420.7	364.3	26.7	5.7	94.0	78.5	9.8	0.9	4.1	38.3	5.0
470	205.38	3075.1	23.2	189.7	308.9	168.9	451.0	344.6	27.0	6.0	87.4	80.2	12.7	0.9	4.5	38.9	5.7
472	206.07	3452.1	23.2	224.1	424.3	138.1	437.5	388.9	28.4	5.2	86.3	80.3	9.7	1.6	3.7	35.9	2.9
482	209.53	3372.1	20.8	213.7	299.9	134.4	390.0	432.5	25.1	4.1	83.8	75.4	10.8	0.0	4.4	33.4	2.7
492	213.00	2823.0	18.4	212.1	271.4	107.9	394.0	558.3	23.8	4.6	78.2	68.6	8.6	0.7	5.0	31.3	2.9
502	219.00	2452.7	21.3	206.4	277.5	112.2	421.4	416.5	27.3	5.0	88.3	80.0	9.4	0.8	5.6	40.5	2.4

Table C.5.3-1 (Contd.) Salt included trace element data from core CD3826.

Depth(cm)	Age(ka)	Ba(ppm)	Sc(ppm)	V(ppm)	Ni(ppm)	Cu(ppm)	Zn(ppm)	Sr(ppm)	Y(ppm)	Nb(ppm)	Cr(ppm)	Zr(ppm)	Pb(ppm)	Th(ppm)	U(ppm)	Rb(ppm)	Mo(ppm)
512	224.00	2213.5	20.3	212.6	304.5	102.9	338.8	393.8	27.4	5.4	81.4	78.9	8.8	2.9	6.5	41.8	3.7
522	229.00	2165.6	20.5	186.7	222.7	91.6	300.7	382.9	27.7	5.9	71.8	89.8	12.7	3.7	5.7	54.2	3.0
532	234.00	2343.1	16.7	195.0	190.5	97.8	278.7	352.3	24.8	6.6	62.0	104.9	13.7	7.8	5.3	73.8	4.1
542	240.00	2701.5	18.0	179.3	318.5	121.4	305.1	363.4	27.8	6.7	69.0	94.4	12.6	5.4	5.9	58.8	4.3
552	242.00	3001.7	20.5	205.2	243.7	134.4	321.6	389.9	25.8	5.8	74.8	89.6	10.4	3.2	4.3	51.4	3.8
562	244.00	2535.0	19.2	171.2	186.4	101.2	260.8	474.7	22.1	5.0	75.8	81.6	11.4	2.7	4.7	45.0	2.1
572	246.14	2398.1	18.7	205.0	214.6	200.3	495.4	540.2	22.6	3.5	79.4	67.5	10.6	1.6	4.7	33.8	4.9
580	247.97	2362.3	18.6	186.3	259.1	109.6	279.2	558.6	22.3	3.9	76.0	65.8	8.7	0.0	4.7	32.5	4.6
592	250.72	2219.7	16.8	212.1	173.0	97.8	277.5	666.8	21.5	3.3	70.4	58.6	6.5	1.5	5.9	26.5	4.1
602	253.00	2210.7	15.8	189.2	167.3	82.9	275.2	704.6	20.5	2.7	64.1	54.3	6.9	0.0	5.7	25.5	3.2
612	257.00	2281.2	16.3	201.3	178.5	95.0	283.1	679.9	21.4	3.8	66.5	55.2	6.8	0.5	6.5	26.3	5.0
622	265.33	2116.2	16.9	158.5	432.1	88.9	261.3	600.3	22.4	3.4	64.5	57.4	6.7	0.8	6.1	26.1	6.0
632	273.67	2452.7	20.6	219.2	177.3	100.5	312.7	480.3	29.1	4.4	77.1	69.3	7.3	0.5	3.9	32.6	4.8
642	282.00	2401.9	19.0	189.1	195.1	104.1	296.8	399.7	32.5	5.0	73.3	68.2	8.3	2.6	4.3	32.5	4.6
652	285.69	2822.5	21.0	262.5	190.6	129.9	314.4	427.5	31.4	5.0	90.3	72.8	8.8	1.4	5.2	32.4	3.6
662	289.38	2920.6	20.7	217.9	187.8	100.9	299.8	509.5	26.5	3.4	76.6	64.6	4.6	0.1	4.3	30.6	4.4
672	293.07	2566.2	16.2	147.9	240.3	91.1	248.0	714.1	21.1	3.1	60.7	56.0	5.0	1.1	9.4	25.8	6.4
680	296.00	2409.1	15.7	152.7	197.8	90.5	243.6	758.3	21.2	3.6	61.5	53.8	6.5	1.1	8.6	24.2	5.8
690	300.29	2517.8	16.1	197.2	177.3	88.2	281.3	682.6	22.9	3.9	72.6	57.6	5.9	0.0	9.4	26.7	6.7
700	304.58	2571.7	17.3	204.8	181.9	97.4	313.7	667.1	23.7	3.5	70.4	58.9	5.5	0.0	7.5	27.4	5.5
710	308.87	2677.5	17.3	176.8	255.7	95.7	316.0	652.2	23.2	3.3	70.7	59.7	7.7	1.5	6.7	27.0	5.1
720	313.17	2962.0	18.4	242.6	302.6	122.1	392.2	575.3	26.4	4.3	70.9	66.4	5.9	0.0	6.4	29.2	5.2
730	317.46	2738.0	19.1	176.0	293.6	105.1	367.0	517.4	25.7	4.5	71.5	67.9	7.1	1.0	4.9	28.9	5.1
740	321.75	2907.0	20.4	209.6	309.1	123.0	361.0	490.1	25.6	5.9	78.8	76.9	7.3	0.1	4.1	33.7	4.0
750	326.00	3001.7	20.8	185.1	311.9	120.5	345.1	466.1	26.9	5.7	74.8	85.7	7.4	1.8	4.6	36.0	7.6
760	327.00	2611.3	18.1	132.9	308.4	101.0	269.5	468.7	27.7	7.8	60.6	110.8	8.1	3.7	1.0	40.2	5.0
770	328.00	1584.2	15.6	85.6	142.7	81.4	121.5	543.2	28.3	21.1	21.9	239.5	6.5	14.2	3.2	71.8	12.6
780	332.87	2523.1	15.0	131.3	203.3	97.9	264.3	786.3	18.5	3.6	57.1	60.3	8.4	1.7	5.3	26.4	5.2
790	337.73	1780.3	17.3	205.6	163.4	78.9	307.8	682.7	21.6	5.1	80.9	68.3	8.4	3.6	3.1	36.9	3.5
800	342.60	1841.4	15.6	153.9	205.7	70.3	202.8	794.2	19.1	3.9	65.0	54.4	6.8	0.1	6.4	29.0	3.7
810	347.47	1940.7	15.9	135.3	193.5	72.8	221.0	782.9	19.5	3.6	57.9	56.3	6.5	0.0	6.7	25.7	4.2
820	352.33	2234.3	14.9	141.2	188.1	75.3	234.7	766.2	20.4	3.5	57.3	53.1	5.1	0.6	7.8	23.7	4.6
830	357.20	2198.3	14.5	148.6	184.2	79.3	241.0	765.3	22.9	3.4	56.0	53.9	5.7	0.0	3.3	23.4	5.2
840	362.07	2235.4	16.4	179.5	230.9	90.3	277.4	667.6	24.3	4.2	62.9	59.5	7.0	1.2	4.0	26.7	5.0
850	366.93	2490.2	17.8	205.4	241.0	99.5	324.7	622.3	26.4	3.3	69.0	59.5	8.1	0.5	3.9	26.2	3.5
860	371.80	2435.3	17.7	216.0	259.8	113.9	353.2	626.1	26.7	3.1	70.0	61.6	6.9	0.7	4.8	27.9	6.3
870	376.67	2346.9	18.6	158.0	177.5	88.1	296.9	598.8	26.7	3.7	66.9	60.3	8.8	2.4	2.5	29.1	5.9
880	381.53	2651.3	20.6	191.4	363.6	117.0	355.3	523.6	26.6	4.9	78.4	65.4	7.3	0.6	4.5	30.5	8.7
890	386.40	2926.6	21.5	205.3	238.7	113.4	382.7	488.5	27.4	4.6	79.1	68.4	7.7	0.7	2.7	31.1	6.8
900	391.27	2807.2	19.3	196.4	263.7	108.3	358.7	521.3	28.3	4.3	77.0	65.8	8.9	1.6	5.9	29.4	9.2
910	396.13	3210.2	20.8	178.0	314.6	126.7	416.0	464.9	27.4	4.5	77.7	69.8	8.7	0.0	4.7	32.1	7.9
920	401.00	3274.3	21.5	183.7	382.1	145.5	387.6	429.0	27.4	5.1	80.2	70.5	8.1	0.8	4.4	33.8	3.9
930	408.09	3152.2	19.0	177.8	270.0	141.6	341.5	567.3	23.5	4.6	77.0	66.5	7.8	0.7	0.7	29.1	3.8
940	415.18	2909.8	19.4	164.1	206.6	108.9	325.6	598.0	20.4	5.4	77.9	66.9	8.9	1.3	5.1	28.6	3.8
950	422.28	2647.6	18.3	201.3	218.8	115.6	371.4	673.2	18.2	4.3	74.4	63.1	6.8	1.0	5.8	27.5	2.7
960	429.37	2308.8	16.4	170.8	314.3	100.9	328.4	665.0	17.7	4.0	68.0	60.8	7.0	0.6	3.9	27.7	3.6
970	436.46	2042.8	16.3	147.7	229.7	88.3	290.4	703.9	18.8	4.2	67.1	58.2	8.3	0.0	5.9	29.3	3.1
980	443.55	1950.1	13.9	138.4	218.7	83.8	260.0	798.7	19.8	3.1	58.2	52.8	8.1	0.4	4.4	25.1	6.0
990	450.64	1843.2	14.1	148.8	150.7	76.5	215.1	838.5	19.7	3.3	50.6	49.1	6.1	1.7	2.8	22.1	3.5
1000	457.74	1950.4	13.5	120.0	129.0	66.5	204.0	864.1	19.4	2.5	48.5	46.5	6.1	1.5	2.8	21.2	0.7
1010	464.83	1921.4	13.1	130.5	145.1	98.3	209.6	891.0	17.6	2.9	45.2	45.8	6.5	0.2	3.1	19.8	2.7
1020	472.00	1909.8	13.0	121.2	143.4	84.6	203.1	905.4	18.8	4.3	48.0	46.4	4.7	0.0	3.8	19.6	3.3
1030	******	1869.4	12.8	129.5	132.8	89.6	216.8	861.9	18.7	3.6	54.4	49.1	6.9	0.4	3.7	21.2	3.4
1040	******	2014.2	13.1	139.4	160.1	87.4	211.7	876.9	18.3	3.3	47.8	47.7	5.2	1.0	3.7	19.9	2.8
1050	******	1903.7	15.3	125.8	145.7	83.1	225.9	776.6	20.8	2.5	53.1	51.3	6.7	1.8	2.8	23.1	2.2
1060	******	2164.2	15.6	161.9	141.7	94.1	244.5	741.7	21.6	3.2	60.9	53.7	4.7	0.7	4.5	24.8	2.8
1070	******	2706.0	19.3	242.8	241.1	134.1	347.6	591.5	23.9	4.1	76.7	64.2	5.2	0.1	4.8	30.2	6.3

Table C.5.3-2 Salt free trace element data from core CD3826.

Depth(cm)	Age(ka)	Ba(ppm)	Cu(ppm)	Ni(ppm)	Zn(ppm)	V(ppm)	Sr(ppm)	Sc(ppm)	Cr(ppm)	Zr(ppm)	Rb(ppm)	Y(ppm)	Nb(ppm)	Pb(ppm)	Th(ppm)	U(ppm)	Mo(ppm)	SALT
1	0.57	3738.6	145.6	405.5	408.2	138.0	504.5	20.8	82.0	81.1	32.9	26.2	5.7	141.1	0.0	0.0	16.1	8.700
5	2.83	3939.8	154.7	448.7	475.8	137.9	503.3	23.1	93.6	83.4	34.1	25.8	3.9	11.0	0.0	0.0	11.1	8.785
10	5.67	3875.0	112.7	230.5	393.9	119.0	515.1	22.2	89.9	85.3	34.4	27.2	6.0	12.0	0.2	0.0	0.6	9.528
15	8.50	3532.9	129.1	257.6	429.6	216.9	604.8	21.2	89.1	78.3	33.5	24.8	5.1	9.3	1.7	2.4	0.2	8.194
20	11.33	3388.5	142.0	246.0	403.0	201.9	639.4	20.4	88.6	75.4	31.3	22.2	5.2	6.5	0.0	1.3	0.0	7.857
30	17.00	2671.0	109.3	312.7	429.7	212.9	615.0	20.6	91.8	76.3	36.7	23.7	4.9	8.4	0.7	2.2	0.0	8.275
40	17.71	2374.0	101.0	381.1	381.0	250.8	562.0	19.6	92.3	76.2	39.1	25.3	5.6	7.6	0.0	5.5	0.0	6.689
50	18.42	2063.0	80.9	219.3	297.6	144.9	555.4	13.7	68.7	71.9	34.8	25.8	4.7	7.9	0.0	3.1	0.0	8.613
60	19.14	2205.9	90.7	303.3	319.9	171.9	534.5	14.0	78.8	70.3	35.3	27.0	4.1	8.6	0.1	4.5	1.5	8.251
70	23.83	2266.5	95.7	267.4	235.9	207.4	432.0	11.7	54.0	39.9	21.0	18.6	2.1	2.4	0.0	7.0	1.1	5.313
78	27.29	2841.9	108.3	260.5	357.9	267.1	498.5	22.1	98.4	76.9	36.0	26.7	5.4	9.0	0.0	5.1	3.4	7.105
81	28.59	2841.4	100.5	238.0	321.1	212.9	499.7	21.1	92.4	75.4	36.0	27.5	5.0	9.5	0.2	4.7	0.5	7.705
90	32.49	2649.6	95.4	228.7	329.0	188.7	531.2	21.4	86.8	72.1	34.3	25.9	4.0	8.9	0.0	4.7	4.0	7.744
100	36.82	2760.8	95.3	197.2	323.0	177.8	525.3	21.8	89.7	73.8	33.4	24.9	4.4	9.4	1.1	5.3	3.1	7.256
110	39.00	3151.3	115.1	433.5	466.8	275.7	451.6	23.6	96.9	78.8	38.8	27.8	4.3	8.2	1.2	5.9	3.8	8.655
120	41.83	2686.3	96.4	178.6	301.9	174.5	546.1	21.2	83.7	71.1	33.5	25.3	5.1	10.5	0.0	3.7	1.4	6.979
130	44.67	2822.9	101.9	211.4	357.4	170.7	463.9	23.2	89.5	77.2	36.3	27.1	5.4	10.8	1.7	3.5	1.8	7.794
140	47.50	2893.3	90.0	277.1	320.8	167.9	394.2	19.4	73.9	74.7	48.2	26.2	5.2	9.0	0.2	3.1	3.8	7.269
150	50.33	3084.3	122.9	311.7	392.8	221.8	337.8	26.2	92.6	86.9	42.9	32.8	5.8	11.2	1.3	6.3	3.2	8.941
160	53.16	2567.8	101.5	198.5	246.4	170.9	359.7	17.9	65.2	68.6	55.6	22.6	5.4	11.3	3.3	3.8	1.9	6.043
170	56.00	2637.6	177.0	181.7	439.9	157.1	297.8	17.7	64.3	74.8	69.0	24.0	5.6	15.3	5.6	3.7	3.8	6.381
180	64.00	3039.4	116.4	371.8	419.3	220.4	396.1	21.6	82.4	76.0	46.9	26.6	5.1	12.2	3.0	6.7	7.2	7.126
190	71.25	3515.4	140.5	428.3	458.7	234.8	447.4	23.9	89.5	80.5	35.3	29.3	5.0	9.7	1.7	7.5	5.9	8.061
200	78.49	3387.8	139.4	313.4	469.0	244.0	472.3	23.4	85.9	77.4	33.8	29.4	5.3	10.5	2.5	3.3	3.4	8.165
210	85.74	3610.0	146.3	288.9	473.4	273.0	441.4	25.2	98.2	84.0	37.8	31.0	5.3	9.3	2.2	6.4	5.1	8.363
220	92.98	3251.7	151.9	438.2	425.5	223.0	407.7	23.9	93.6	85.6	38.2	30.0	6.4	10.0	0.0	5.4	4.4	9.229
230	100.23	3644.8	152.3	347.4	414.9	199.0	379.8	24.4	96.2	87.9	38.5	30.9	5.7	10.7	0.0	7.4	2.6	9.006
240	107.48	3391.7	166.6	414.6	420.5	203.7	374.1	22.5	91.2	79.8	34.8	29.1	5.7	8.9	0.0	3.7	2.1	7.678
250	114.72	4235.4	151.8	377.9	414.2	226.9	385.4	25.9	98.0	92.1	41.2	29.2	6.2	11.8	0.0	5.4	2.5	9.205
260	122.00	3287.6	140.4	203.8	358.8	223.1	583.7	20.3	85.6	79.0	36.1	23.9	5.5	8.7	0.0	4.0	2.5	7.592
270	127.00	2940.8	96.7	204.1	324.3	205.8	577.4	19.9	78.2	68.6	31.0	23.6	4.9	8.3	0.7	6.4	7.1	6.504
280	132.00	2866.5	97.1	178.2	306.5	172.5	594.6	19.2	74.8	66.6	29.8	23.8	4.7	6.4	1.5	2.1	5.7	6.250
290	137.00	2713.7	91.6	185.7	266.9	161.0	568.7	19.9	76.9	69.6	32.5	23.7	4.5	7.6	1.5	4.4	4.9	6.235
300	142.00	2824.9	108.9	172.4	303.0	203.8	582.8	19.2	78.9	69.5	32.8	25.0	4.7	8.4	0.0	6.8	4.0	6.713
310	147.00	2664.9	109.9	244.6	305.9	213.5	588.6	20.3	85.5	70.2	33.2	23.2	4.3	9.0	2.5	5.9	6.6	6.972
320	152.00	2440.3	80.7	150.3	250.5	174.2	601.6	18.4	78.8	64.2	30.3	21.5	3.6	7.6	2.5	5.5	2.8	6.570
330	156.00	2535.5	85.4	176.1	244.7	157.1	612.5	18.2	77.4	64.6	29.8	23.8	3.8	11.1	1.2	5.8	3.0	6.668
340	160.00	2738.2	92.2	240.7	276.3	228.5	627.3	17.5	83.3	66.8	30.7	23.6	4.0	6.8	0.0	9.1	4.8	6.972
350	164.00	2830.6	112.2	205.9	287.2	181.4	515.5	19.8	88.3	75.3	35.9	23.8	5.9	8.4	3.1	3.3	3.9	8.447
360	168.00	2364.5	109.4	237.2	332.0	189.1	472.5	20.3	90.2	76.5	39.2	23.7	4.8	11.1	0.0	4.9	2.5	7.892
368	172.00	2237.5	106.1	274.6	427.5	272.3	445.7	20.8	104.6	89.2	49.4	23.4	6.9	10.8	3.1	6.8	3.6	7.744
380	176.00	2612.9	99.8	230.9	328.3	244.0	608.6	19.3	78.8	66.8	30.4	24.6	3.4	8.2	1.3	3.7	7.4	7.135
390	180.00	2550.0	108.1	247.9	326.8	216.1	599.8	20.5	77.1	68.2	31.4	25.8	4.0	9.5	0.4	5.9	6.9	7.471
400	184.00	2673.2	129.4	389.9	340.4	267.1	546.3	21.1	87.3	72.7	33.3	26.6	4.2	7.4	0.8	5.8	9.1	7.253
410	187.28	2553.4	118.0	263.4	332.4	191.1	508.7	20.8	78.4	71.6	33.3	27.0	4.2	9.4	3.2	5.2	5.2	7.428
420	189.86	2937.5	121.5	287.8	354.9	224.9	430.2	22.8	86.8	81.8	36.5	30.9	5.5	10.0	0.5	5.2	3.9	8.057
430	192.43	3511.8	132.6	277.4	435.4	257.3	386.5	25.9	95.9	87.7	38.9	35.1	5.6	9.4	0.0	3.2	5.2	8.191
440	195.00	3394.0	117.2	215.9	368.0	224.5	358.0	26.5	97.8	89.7	40.5	32.4	5.4	10.3	0.4	5.0	3.0	8.568
452	199.15	3363.4	102.7	211.3	367.2	191.1	502.7	22.4	93.9	78.9	36.8	27.0	4.1	10.4	1.0	6.3	2.3	8.310
460	201.92	3417.9	129.3	284.8	459.2	263.1	397.6	25.5	102.6	85.7	41.8	29.1	6.2	10.7	1.0	4.5	5.5	8.386
470	205.38	3354.9	184.3	337.0	492.0	207.0	375.9	25.3	95.4	87.5	42.4	29.5	6.5	13.9	1.0	4.9	6.2	8.339
472	206.07	3753.1	150.1	461.3	475.6	243.6	422.8	25.2	93.8	87.3	39.0	30.9	5.7	10.5	1.7	4.0	3.2	8.020
482	209.53	3663.7	146.0	325.8	423.7	232.2	469.9	22.6	91.0	81.9	36.3	27.3	4.5	11.7	0.0	4.8	2.9	7.959
492	213.00	3048.4	116.5	293.1	425.5	229.0	602.9	19.9	84.4	74.1	33.8	25.7	5.0	9.3	0.8	5.4	3.1	7.395
502	219.00	2651.9	121.3	300.0	455.6	223.2	450.3	23.0	95.5	86.5	43.8	29.5	5.4	10.2	0.9	6.1	2.6	7.513

Table C.5.3-2 (Contd.) Salt free trace element data from core CD3826.

Depth(cm)	Age(ka)	Ba(ppm)	Cu(ppm)	Ni(ppm)	Zn(ppm)	V(ppm)	Sr(ppm)	Sc(ppm)	Cr(ppm)	Zr(ppm)	Rb(ppm)	Y(ppm)	Nb(ppm)	Pb(ppm)	Th(ppm)	U(ppm)	Mo(ppm)	SALT
512	224.00	2394.2	111.3	329.4	366.5	230.0	426.0	22.0	88.0	85.3	45.2	29.6	5.8	9.5	3.1	7.0	4.0	7.549
522	229.00	2328.5	98.5	239.5	323.3	200.7	411.7	22.0	77.2	96.6	58.3	29.8	6.3	13.7	4.0	6.1	3.2	6.995
532	234.00	2485.8	103.8	202.1	295.7	206.9	373.8	17.7	65.8	111.3	78.3	26.3	7.0	14.5	8.3	5.6	4.3	5.740
542	240.00	2895.6	130.1	341.4	327.0	192.2	389.5	19.3	74.0	101.2	63.0	29.8	7.2	13.5	5.8	6.3	4.6	6.704
552	242.00	3247.6	145.4	263.7	347.9	222.0	421.8	22.2	80.9	96.9	55.6	27.9	6.3	11.3	3.5	4.7	4.1	7.573
562	244.00	2724.8	108.8	200.4	280.3	184.0	510.2	20.6	81.5	87.7	48.4	23.8	5.4	12.3	2.9	5.1	2.3	6.965
572	246.14	2580.6	215.5	230.9	533.1	220.6	581.3	20.1	85.4	72.6	36.4	24.3	3.8	11.4	1.7	5.1	5.3	7.073
580	247.97	2534.8	117.6	278.0	299.6	199.9	599.4	20.0	81.6	70.6	34.9	23.9	4.2	9.3	0.0	5.0	4.9	6.806
592	250.72	2369.0	104.4	184.6	296.2	226.4	711.7	17.9	75.1	62.5	28.3	22.9	3.5	6.9	1.6	6.3	4.4	6.304
602	253.00	2364.5	88.7	178.9	294.3	202.4	753.6	16.9	68.6	58.1	27.3	21.9	2.9	7.4	0.0	6.1	3.4	6.504
612	257.00	2442.0	101.7	191.1	303.1	215.5	727.8	17.4	71.2	59.1	28.2	22.9	4.1	7.3	0.5	7.0	5.4	6.585
622	265.33	2265.2	95.2	462.5	279.7	169.7	642.6	18.1	69.0	61.4	27.9	24.0	3.6	7.2	0.9	6.5	6.4	6.576
632	273.67	2650.0	108.6	191.6	337.9	236.8	518.9	22.3	83.3	74.9	35.2	31.4	4.8	7.9	0.5	4.2	5.2	7.446
642	282.00	2604.9	112.9	211.6	321.9	205.1	433.5	20.6	79.5	74.0	35.2	35.2	5.4	9.0	2.8	4.7	5.0	7.794
652	285.69	3032.9	139.6	204.8	337.8	282.1	459.4	22.6	97.0	78.2	34.8	33.7	5.4	9.5	1.5	5.6	3.9	6.936
662	289.38	3151.3	108.9	202.6	323.5	235.1	549.7	22.3	82.7	69.7	33.0	28.6	3.7	5.0	0.1	4.6	4.7	7.321
672	293.07	2745.8	97.5	257.1	265.4	158.3	764.1	17.3	64.9	59.9	27.6	22.6	3.3	5.3	1.2	10.1	6.8	6.540
680	296.00	2563.6	96.3	210.5	259.2	162.5	806.9	16.7	65.4	57.3	25.8	22.6	3.8	6.9	1.2	9.2	6.2	6.027
690	300.29	2686.0	94.1	189.1	300.1	210.4	728.2	17.2	77.4	61.4	28.5	24.4	4.2	6.3	0.0	10.0	7.1	6.261
700	304.58	2748.9	104.1	194.4	335.3	218.9	713.1	18.5	75.3	63.0	29.3	25.3	3.7	5.9	0.0	8.0	5.9	6.446
710	308.87	2867.3	102.5	273.8	338.4	189.3	698.4	18.5	75.7	63.9	28.9	24.8	3.5	8.2	1.6	7.2	5.5	6.618
720	313.17	3195.3	131.7	326.4	423.1	261.7	620.6	19.8	76.5	71.6	31.5	28.5	4.6	6.4	0.0	6.9	5.6	7.301
730	317.46	2952.8	113.3	316.6	395.8	189.8	558.0	20.6	77.1	73.2	31.2	27.7	4.9	7.7	1.1	5.3	5.5	7.274
740	321.75	3138.8	132.8	333.7	389.8	226.3	529.2	22.0	85.1	83.0	36.4	27.6	6.4	7.9	0.1	4.4	4.3	7.385
750	326.00	3248.6	130.4	337.6	373.5	200.3	504.4	22.5	81.0	92.7	39.0	29.1	6.2	8.0	1.9	5.0	8.2	7.599
760	327.00	2777.2	107.4	328.0	286.6	141.3	498.5	19.2	64.4	117.8	42.8	29.5	8.3	8.6	3.9	1.1	5.3	5.973
770	328.00	1624.8	83.5	146.4	124.6	87.8	557.1	16.0	22.5	245.6	73.6	29.0	21.6	6.7	14.6	3.3	12.9	2.497
780	332.87	2673.7	103.7	215.4	280.1	139.1	833.2	15.9	60.5	63.9	28.0	19.6	3.8	8.9	1.8	5.6	5.5	5.634
790	337.73	1885.2	83.6	173.0	325.9	217.7	722.9	18.3	85.7	72.3	39.1	22.9	5.4	8.9	3.8	3.3	3.7	5.566
800	342.60	1942.8	74.2	217.0	214.0	162.4	837.9	16.5	68.6	57.4	30.6	20.2	4.1	7.2	0.1	6.8	3.9	5.221
810	347.47	2048.4	76.8	204.2	233.3	142.8	826.3	16.8	61.1	59.4	27.1	20.6	3.8	6.9	0.0	7.1	4.4	5.257
820	352.33	2366.8	79.8	199.3	248.6	149.6	811.6	15.8	60.7	56.2	25.1	21.6	3.7	5.4	0.6	8.3	4.9	5.598
830	357.20	2333.6	84.2	195.5	255.8	157.7	812.4	15.4	59.4	57.2	24.8	24.3	3.6	6.1	0.0	3.5	5.5	5.797
840	362.07	2386.5	96.4	246.5	296.2	191.6	712.7	17.5	67.2	63.5	28.5	25.9	4.5	7.5	1.3	4.3	5.3	6.333
850	366.93	2664.5	106.5	257.9	347.4	219.8	665.9	19.0	73.8	63.7	28.0	28.2	3.5	8.7	0.5	4.2	3.7	6.542
860	371.80	2595.6	121.4	276.9	376.4	230.2	667.3	18.9	74.6	65.7	29.7	28.5	3.3	7.4	0.7	5.1	6.7	6.175
870	376.67	2504.8	94.0	189.4	316.9	168.6	639.1	19.9	71.4	64.4	31.1	28.5	3.9	9.4	2.6	2.7	6.3	6.304
880	381.53	2827.7	124.8	387.8	378.9	204.1	558.4	22.0	83.6	69.8	32.5	28.4	5.2	7.8	0.6	4.8	9.3	6.238
890	386.40	3135.4	121.5	255.7	410.0	219.9	523.4	23.0	84.7	73.3	33.3	29.4	4.9	8.2	0.7	2.9	7.3	6.660
900	391.27	3019.3	116.5	283.6	385.8	211.2	560.7	20.8	82.8	70.8	31.6	30.4	4.6	9.6	1.7	6.3	9.9	7.026
910	396.13	3465.2	136.8	339.6	449.0	192.1	501.8	22.5	83.9	75.3	34.6	29.6	4.9	9.4	0.0	5.1	8.5	7.359
920	401.00	3527.7	156.8	411.7	417.6	197.9	462.2	23.2	86.4	76.0	36.4	29.5	5.5	8.7	0.9	4.7	4.2	7.184
930	408.09	3373.7	151.5	289.0	365.5	190.3	607.2	20.3	82.4	71.2	31.1	25.2	4.9	8.3	0.7	0.7	4.1	6.565
940	415.18	3102.7	116.1	220.3	347.2	175.0	637.6	20.7	83.1	71.3	30.5	21.8	5.8	9.5	1.4	5.4	4.1	6.218
950	422.28	2810.9	122.7	232.3	394.3	213.7	714.7	19.4	79.0	67.0	29.2	19.3	4.6	7.2	1.1	6.2	2.9	5.810
960	429.37	2449.9	107.1	333.5	348.5	181.2	705.6	17.4	72.2	64.5	29.4	18.8	4.2	7.4	0.6	4.1	3.8	5.759
970	436.46	2173.9	94.0	244.4	309.0	157.2	749.1	17.3	71.4	61.9	31.2	20.0	4.5	8.8	0.0	6.3	3.3	6.031
980	443.55	2065.9	88.8	231.7	275.4	146.6	846.1	14.7	61.7	55.9	26.6	21.0	3.3	8.6	0.4	4.7	6.4	5.606
990	450.64	1954.0	81.1	159.8	228.0	157.7	888.9	14.9	53.6	52.1	23.4	20.9	3.5	6.5	1.8	3.0	3.7	5.672
1000	457.74	2069.0	70.5	136.8	216.4	127.3	916.7	14.3	51.5	49.3	22.5	20.6	2.7	6.5	1.6	3.0	0.7	5.734
1010	464.83	2032.2	104.0	153.5	221.7	138.0	942.4	13.9	47.8	48.4	20.9	18.6	3.1	6.9	0.2	3.3	2.9	5.450
1020	472.00	2019.3	89.5	151.6	214.7	128.1	957.3	13.7	50.8	49.1	20.7	19.9	4.5	5.0	0.0	4.0	3.5	5.423
1030	******	1979.5	94.9	140.6	229.6	137.1	912.7	13.6	57.6	52.0	22.4	19.8	3.8	7.3	0.4	3.9	3.6	5.563
1040	******	2128.5	92.4	169.2	223.7	147.3	926.7	13.8	50.5	50.4	21.0	19.3	3.5	5.5	1.1	3.9	3.0	5.370
1050	******	2021.2	88.2	154.7	239.8	133.6	824.5	16.2	56.4	54.5	24.5	22.1	2.7	7.1	1.9	3.0	2.3	5.813
1060	******	2300.1	100.0	150.6	259.9	172.1	788.3	16.6	64.7	57.1	26.4	23.0	3.4	5.0	0.7	4.8	3.0	5.910
1070	******	2902.6	143.8	258.6	372.9	260.4	634.5	20.7	82.3	68.9	32.4	25.6	4.4	5.6	0.1	5.1	6.8	6.773

Table C.5.3-3 Salt free trace elements and their ratios to Al in core CD3826.

Depth(cm)	Age(ka)	Ba/Al *10-2	Cu/Al *10-3	Ni/Al *10-3	Zn/Al *10-3	V/Al *10-3	Sr/Al *10-3	Sc/Al *10-4	Cr/Al *10-3	Zr/Al *10-3	Rb/Al *10-4	Y/Al *10-4	Nb/Al *10-4	Pb/Al *10-4	Th/Al *10-4	U/Al *10-4	Cr/Zr
1	0.57	5.963	2.322	6.468	6.511	2.201	8.047	3.319	1.309	1.293	5.241	4.176	0.908	22.503	0.000	0.000	1.012
5	2.83	6.120	2.403	6.971	7.391	2.142	7.819	3.593	1.454	1.296	5.296	4.002	0.613	1.703	0.000	0.000	1.122
10	5.67	5.844	1.700	3.476	5.941	1.795	7.768	3.351	1.355	1.287	5.184	4.101	0.900	1.817	0.033	0.000	1.053
15	8.50	5.895	2.154	4.299	7.169	3.619	10.092	3.544	1.487	1.307	5.598	4.144	0.854	1.545	0.291	0.400	1.138
20	11.33	5.944	2.490	4.316	7.068	3.541	11.217	3.579	1.553	1.323	5.483	3.903	0.914	1.142	0.000	0.228	1.174
30	17.00	4.726	1.935	5.532	7.602	3.767	10.881	3.646	1.624	1.350	6.501	4.186	0.868	1.485	0.116	0.386	1.203
40	17.71	4.196	1.784	6.736	6.734	4.432	9.933	3.466	1.631	1.347	6.914	4.470	0.985	1.345	0.000	0.966	1.211
50	18.42	3.853	1.510	4.095	5.559	2.706	10.373	2.555	1.283	1.343	6.499	4.823	0.879	1.471	0.000	0.572	0.956
60	19.14	4.214	1.732	5.794	6.110	3.283	10.210	2.665	1.505	1.343	6.745	5.163	0.791	1.645	0.021	0.854	1.121
70	23.83	6.841	2.888	8.071	7.122	6.261	13.038	3.538	1.629	1.205	6.344	5.611	0.638	0.733	0.000	2.104	1.352
78	27.29	4.917	1.874	4.507	6.193	4.621	8.625	3.818	1.702	1.330	6.220	4.619	0.931	1.564	0.000	0.875	1.280
81	28.59	4.948	1.751	4.145	5.592	3.707	8.701	3.679	1.609	1.313	6.263	4.792	0.868	1.660	0.038	0.811	1.226
90	32.49	4.749	1.710	4.099	5.896	3.382	9.522	3.827	1.556	1.292	6.139	4.643	0.719	1.593	0.000	0.835	1.205
100	36.82	4.764	1.645	3.403	5.574	3.068	9.065	3.758	1.548	1.273	5.768	4.298	0.763	1.619	0.186	0.912	1.216
110	39.00	4.947	1.806	6.805	7.328	4.327	7.089	3.712	1.521	1.237	6.084	4.365	0.670	1.289	0.189	0.928	1.229
120	41.83	4.733	1.699	3.146	5.319	3.074	9.622	3.731	1.476	1.252	5.910	4.451	0.890	1.856	0.000	0.644	1.179
130	44.67	4.539	1.639	3.399	5.746	2.745	7.459	3.732	1.439	1.242	5.842	4.360	0.872	1.744	0.279	0.558	1.159
140	47.50	4.700	1.463	4.503	5.212	2.728	6.403	3.154	1.200	1.214	7.831	4.257	0.841	1.454	0.035	0.508	0.988
150	50.33	4.366	1.740	4.412	5.561	3.140	4.782	3.715	1.311	1.230	6.078	4.648	0.824	1.586	0.187	0.886	1.066
160	53.16	4.235	1.674	3.273	4.063	2.819	5.933	2.949	1.076	1.132	9.162	3.721	0.895	1.861	0.544	0.632	0.950
170	56.00	3.979	2.670	2.741	6.636	2.371	4.493	2.675	0.970	1.128	10.411	3.626	0.838	2.305	0.838	0.564	0.860
180	64.00	4.820	1.846	5.896	6.650	3.496	6.282	3.432	1.306	1.206	7.445	4.218	0.803	1.930	0.478	1.059	1.084
190	71.25	5.668	2.266	6.906	7.395	3.786	7.212	3.858	1.443	1.298	5.699	4.717	0.807	1.561	0.281	1.210	1.112
200	78.49	5.639	2.320	5.216	7.806	4.062	7.860	3.897	1.430	1.289	5.619	4.894	0.888	1.740	0.417	0.544	1.110
210	85.74	5.251	2.128	4.201	6.885	3.971	6.420	3.666	1.428	1.222	5.492	4.508	0.778	1.349	0.317	0.936	1.169
220	92.98	5.114	2.389	6.893	6.692	3.507	6.413	3.760	1.473	1.346	6.012	4.713	1.005	1.577	0.000	0.849	1.094
230	100.23	5.260	2.198	5.013	5.987	2.872	5.481	3.521	1.388	1.269	5.551	4.456	0.825	1.538	0.000	1.063	1.094
240	107.48	5.600	2.751	6.846	6.943	3.364	6.177	3.720	1.506	1.318	5.741	4.811	0.948	1.467	0.000	0.608	1.142
250	114.72	5.891	2.111	5.256	5.761	3.156	5.360	3.600	1.363	1.281	5.729	4.060	0.858	1.639	0.000	0.751	1.065
260	122.00	5.475	2.337	3.393	5.976	3.716	9.720	3.388	1.425	1.316	6.019	3.983	0.919	1.442	0.000	0.667	1.084
270	127.00	5.687	1.870	3.946	6.271	3.979	11.164	3.847	1.512	1.326	5.998	4.571	0.951	1.613	0.145	1.241	1.140
280	132.00	5.806	1.966	3.610	6.207	3.493	12.042	3.889	1.514	1.348	6.028	4.818	0.951	1.296	0.302	0.432	1.123
290	137.00	5.144	1.737	3.520	5.061	3.053	10.780	3.781	1.458	1.320	6.166	4.488	0.849	1.435	0.283	0.829	1.104
300	142.00	5.362	2.067	3.272	5.752	3.868	11.063	3.642	1.498	1.319	6.227	4.741	0.895	1.587	0.000	1.282	1.136
310	147.00	5.122	2.111	4.700	5.880	4.103	11.313	3.905	1.642	1.349	6.384	4.462	0.826	1.735	0.475	1.136	1.217
320	152.00	4.960	1.640	3.054	5.090	3.541	12.228	3.742	1.601	1.305	6.156	4.372	0.740	1.544	0.500	1.109	1.227
330	156.00	5.257	1.770	3.652	5.074	3.256	12.699	3.776	1.604	1.339	6.175	4.931	0.777	2.310	0.244	1.200	1.197
340	160.00	5.733	1.931	5.039	5.784	4.784	13.133	3.668	1.744	1.398	6.436	4.951	0.833	1.418	0.000	1.913	1.248
350	164.00	4.963	1.967	3.610	5.035	3.181	9.040	3.467	1.548	1.320	6.301	4.175	1.034	1.475	0.536	0.575	1.173
360	168.00	4.028	1.864	4.042	5.656	3.222	8.050	3.459	1.537	1.304	6.677	4.032	0.814	1.887	0.000	0.832	1.179
368	172.00	3.102	1.471	3.806	5.927	3.775	6.179	2.885	1.450	1.237	6.852	3.246	0.962	1.503	0.436	0.947	1.173
380	176.00	5.125	1.958	4.528	6.440	4.786	11.938	3.781	1.546	1.310	5.956	4.816	0.676	1.605	0.253	0.718	1.181
390	180.00	4.822	2.044	4.688	6.180	4.087	11.342	3.883	1.457	1.290	5.947	4.884	0.756	1.798	0.082	1.124	1.130
400	184.00	4.729	2.289	6.898	6.022	4.725	9.665	3.739	1.545	1.286	5.894	4.712	0.744	1.316	0.134	1.030	1.202
410	187.28	4.536	2.096	4.679	5.905	3.395	9.037	3.704	1.393	1.272	5.911	4.798	0.748	1.670	0.576	0.921	1.095
420	189.86	4.625	1.913	4.531	5.587	3.541	6.772	3.596	1.366	1.288	5.753	4.863	0.873	1.575	0.086	0.822	1.061
430	192.43	5.156	1.946	4.073	6.392	3.778	5.674	3.806	1.407	1.287	5.709	5.150	0.816	1.375	0.000	0.464	1.093
440	195.00	4.587	1.584	2.918	4.973	3.034	4.837	3.577	1.321	1.212	5.469	4.375	0.724	1.389	0.059	0.680	1.090
452	199.15	5.309	1.622	3.335	5.797	3.016	7.935	3.529	1.482	1.245	5.802	4.270	0.654	1.636	0.155	0.999	1.191
460	201.92	4.933	1.867	4.110	6.627	3.796	5.739	3.686	1.481	1.237	6.033	4.206	0.898	1.544	0.142	0.646	1.197
470	205.38	4.800	2.637	4.822	7.040	2.961	5.379	3.621	1.364	1.252	6.072	4.215	0.937	1.982	0.140	0.702	1.090
472	206.07	5.530	2.212	6.797	7.009	3.590	6.230	3.717	1.383	1.286	5.751	4.550	0.833	1.554	0.256	0.593	1.075
482	209.53	5.732	2.285	5.098	6.630	3.633	7.352	3.536	1.425	1.282	5.678	4.267	0.697	1.836	0.000	0.748	1.111
492	213.00	5.570	2.129	5.355	7.775	4.185	11.017	3.631	1.543	1.354	6.176	4.696	0.908	1.697	0.138	0.987	1.140
502	219.00	4.132	1.890	4.675	7.100	3.477	7.017	3.589	1.488	1.348	6.823	4.600	0.842	1.584	0.135	0.943	1.104

Table C.5.3-3 (Contd.) Salt free trace elements and their ratios to Al in core CD3826

Depth(cm)	Age(ka)	Ba/Al *10-2	Cu/Al *10-3	Ni/Al *10-3	Zn/Al *10-3	V/Al *10-3	Sr/Al *10-3	Sc/Al *10-4	Cr/Al *10-3	Zr/Al *10-3	Rb/Al *10-4	Y/Al *10-4	Nb/Al *10-4	Pb/Al *10-4	Th/Al *10-4	U/Al *10-4	Cr/Zr
512	224.00	3.759	1.748	5.172	5.754	3.611	6.688	3.448	1.383	1.340	7.099	4.654	0.917	1.495	0.493	1.104	1.032
522	229.00	3.508	1.484	3.607	4.871	3.024	6.202	3.321	1.163	1.455	8.780	4.487	0.956	2.057	0.599	0.923	0.800
532	234.00	3.616	1.509	2.940	4.301	3.009	5.437	2.577	0.957	1.619	11.388	3.827	1.018	2.114	1.204	0.818	0.591
542	240.00	4.418	1.985	5.208	4.989	2.932	5.943	2.943	1.128	1.544	9.615	4.546	1.096	2.060	0.883	0.965	0.731
552	242.00	4.289	1.920	3.482	4.595	2.932	5.571	2.929	1.069	1.280	7.344	3.686	0.829	1.486	0.457	0.614	0.835
562	244.00	4.321	1.725	3.177	4.445	2.918	8.092	3.273	1.292	1.391	7.671	3.767	0.852	1.943	0.460	0.801	0.929
572	246.14	4.506	3.764	4.033	9.309	3.852	10.151	3.514	1.492	1.268	6.351	4.247	0.658	1.992	0.301	0.883	1.176
580	247.97	4.686	2.174	5.139	5.538	3.695	11.080	3.689	1.508	1.305	6.447	4.423	0.774	1.726	0.000	0.932	1.155
592	250.72	5.206	2.294	4.057	6.508	4.975	15.639	3.940	1.651	1.374	6.215	5.043	0.774	1.524	0.352	1.384	1.201
602	253.00	5.499	2.062	4.161	6.845	4.706	17.526	3.930	1.594	1.351	6.343	5.099	0.672	1.716	0.000	1.418	1.180
612	257.00	5.543	2.308	4.337	6.879	4.891	16.520	3.961	1.616	1.341	6.390	5.200	0.923	1.652	0.121	1.579	1.205
622	265.33	5.057	2.125	10.326	6.245	3.788	14.346	4.039	1.541	1.372	6.237	5.353	0.813	1.601	0.191	1.458	1.124
632	273.67	4.572	1.874	3.305	5.830	4.086	8.954	3.840	1.437	1.292	6.077	5.425	0.820	1.361	0.093	0.727	1.113
642	282.00	4.643	2.012	3.771	5.737	3.655	7.726	3.672	1.417	1.318	6.282	6.282	0.966	1.604	0.503	0.831	1.075
652	285.69	5.038	2.319	3.402	5.612	4.686	7.631	3.749	1.612	1.300	5.784	5.605	0.893	1.571	0.250	0.928	1.240
662	289.38	5.769	1.993	3.710	5.922	4.304	10.064	4.089	1.513	1.276	6.044	5.235	0.672	0.909	0.020	0.849	1.186
672	293.07	6.064	2.153	5.678	5.860	3.495	16.874	3.828	1.434	1.323	6.096	4.986	0.733	1.181	0.260	2.221	1.084
680	296.00	5.976	2.245	4.907	6.043	3.788	18.812	3.895	1.526	1.335	6.004	5.259	0.893	1.613	0.273	2.133	1.143
690	300.29	5.819	2.038	4.097	6.501	4.557	15.775	3.721	1.678	1.331	6.170	5.292	0.901	1.363	0.000	2.172	1.260
700	304.58	6.054	2.293	4.282	7.385	4.821	15.704	4.073	1.657	1.387	6.450	5.579	0.824	1.295	0.000	1.766	1.195
710	308.87	6.091	2.177	5.817	7.188	4.022	14.836	3.935	1.608	1.358	6.142	5.278	0.751	1.752	0.341	1.524	1.184
720	313.17	6.140	2.531	6.272	8.129	5.029	11.925	3.814	1.470	1.376	6.052	5.472	0.891	1.223	0.000	1.327	1.068
730	317.46	5.638	2.164	6.046	7.557	3.624	10.654	3.933	1.472	1.398	5.951	5.292	0.927	1.462	0.206	1.009	1.053
740	321.75	5.695	2.409	6.055	7.072	4.106	9.601	3.996	1.544	1.506	6.602	5.015	1.156	1.430	0.020	0.803	1.025
750	326.00	5.348	2.147	5.557	6.149	3.298	8.304	3.706	1.333	1.527	6.414	4.793	1.016	1.318	0.321	0.820	0.873
760	327.00	4.719	1.825	5.573	4.870	2.402	8.470	3.271	1.095	2.002	7.265	5.006	1.410	1.464	0.669	0.181	0.547
770	328.00	2.284	1.174	2.058	1.752	1.234	7.833	2.249	0.316	3.453	10.353	4.081	3.042	0.937	2.048	0.461	0.091
780	332.87	6.194	2.403	4.991	6.489	3.223	19.304	3.683	1.402	1.480	6.481	4.542	0.884	2.062	0.417	1.301	0.947
790	337.73	3.607	1.599	3.311	6.236	4.166	13.832	3.505	1.639	1.384	7.476	4.376	1.033	1.702	0.729	0.628	1.184
800	342.60	4.647	1.774	5.192	5.118	3.884	20.044	3.937	1.640	1.373	7.319	4.821	0.984	1.716	0.025	1.615	1.195
810	347.47	5.046	1.893	5.031	5.746	3.518	20.357	4.134	1.506	1.464	6.683	5.070	0.936	1.690	0.000	1.742	1.028
820	352.33	6.017	2.028	5.065	6.320	3.802	20.632	4.012	1.543	1.430	6.382	5.493	0.942	1.373	0.162	2.100	1.079
830	357.20	5.845	2.108	4.897	6.408	3.951	20.347	3.855	1.489	1.433	6.221	6.088	0.904	1.515	0.000	0.877	1.039
840	362.07	5.191	2.097	5.362	6.442	4.169	15.504	3.809	1.461	1.382	6.201	5.643	0.975	1.626	0.279	0.929	1.057
850	366.93	5.538	2.213	5.360	7.221	4.568	13.840	3.959	1.535	1.323	5.827	5.871	0.734	1.801	0.111	0.867	1.160
860	371.80	5.138	2.403	5.481	7.452	4.557	13.209	3.734	1.477	1.300	5.886	5.633	0.654	1.456	0.148	1.013	1.136
870	376.67	4.328	1.625	3.274	5.476	2.914	11.043	3.430	1.234	1.112	5.367	4.924	0.682	1.623	0.443	0.461	1.109
880	381.53	5.037	2.223	6.908	6.750	3.636	9.948	3.914	1.489	1.243	5.795	5.054	0.931	1.387	0.114	0.855	1.199
890	386.40	5.279	2.045	4.306	6.903	3.703	8.811	3.878	1.427	1.234	5.610	4.942	0.830	1.389	0.126	0.487	1.156
900	391.27	5.420	2.091	5.092	6.926	3.792	10.066	3.727	1.487	1.271	5.677	5.464	0.830	1.719	0.309	1.139	1.170
910	396.13	5.356	2.114	5.249	6.941	2.970	7.757	3.470	1.296	1.165	5.356	4.572	0.751	1.452	0.000	0.784	1.113
920	401.00	5.715	2.540	6.669	6.765	3.206	7.488	3.753	1.400	1.231	5.900	4.783	0.890	1.414	0.140	0.768	1.138
930	408.09	6.062	2.723	5.192	6.567	3.419	10.909	3.654	1.481	1.279	5.596	4.519	0.885	1.500	0.135	0.135	1.158
940	415.18	5.613	2.101	3.985	6.281	3.165	11.535	3.742	1.503	1.290	5.517	3.935	1.042	1.717	0.251	0.984	1.164
950	422.28	5.617	2.453	4.642	7.880	4.271	14.283	3.883	1.578	1.339	5.834	3.861	0.912	1.443	0.212	1.231	1.179
960	429.37	5.277	2.306	7.184	7.507	3.904	15.201	3.749	1.554	1.390	6.332	4.046	0.914	1.600	0.137	0.891	1.118
970	436.46	5.074	2.193	5.706	7.214	3.669	17.485	4.049	1.667	1.446	7.278	4.670	1.043	2.062	0.000	1.466	1.153
980	443.55	5.304	2.279	5.949	7.072	3.764	21.724	3.781	1.583	1.436	6.827	5.385	0.843	2.203	0.109	1.197	1.102
990	450.64	5.487	2.277	4.486	6.403	4.430	24.962	4.197	1.506	1.462	6.579	5.865	0.982	1.816	0.506	0.834	1.031
1000	457.74	6.005	2.047	3.972	6.281	3.695	26.604	4.156	1.493	1.432	6.527	5.973	0.770	1.878	0.462	0.862	1.043
1010	464.83	6.156	3.150	4.649	6.716	4.181	28.548	4.197	1.448	1.467	6.344	5.639	0.929	2.083	0.064	0.993	0.987
1020	472.00	5.938	2.630	4.459	6.315	3.768	28.150	4.042	1.492	1.443	6.094	5.845	1.337	1.461	0.000	1.181	1.034
1030	******	5.487	2.630	3.898	6.364	3.801	25.300	3.757	1.597	1.441	6.223	5.489	1.057	2.025	0.117	1.086	1.108
1040	******	5.949	2.582	4.729	6.253	4.117	25.901	3.869	1.412	1.409	5.878	5.405	0.975	1.536	0.295	1.093	1.002
1050	******	4.870	2.126	3.727	5.779	3.218	19.865	3.914	1.358	1.312	5.909	5.321	0.639	1.714	0.460	0.716	1.035
1060	******	5.383	2.341	3.525	6.081	4.027	18.448	3.880	1.515	1.336	6.169	5.373	0.796	1.169	0.174	1.119	1.134
1070	******	5.385	2.668	4.798	6.917	4.831	11.770	3.840	1.526	1.277	6.009	4.756	0.816	1.035	0.020	0.955	1.195

Depth(cm)	Age(ka)	Ba(ppm)	Sc(ppm)	V(ppm)	Ni(ppm)	Cu(ppm)	Zn(ppm)	Sr(ppm)	Nb(ppm)	Cr(ppm)	Zr(ppm)	Pb(ppm)	Th(ppm)	U(ppm)	Rb(ppm)	Mo(ppm)
1	0.15	1595.3	27.5	149.5	107.6	76.0	199.4	244.7	5.0	102.9	77.4	6.8	0.0	1.1	35.4	0.0
10	1.55	1702.7	26.1	157.6	110.8	77.6	203.6	280.0	5.2	110.9	76.0	5.8	0.0	3.4	33.3	0.6
20	3.10	1726.4	25.6	146.4	110.1	75.7	204.6	327.7	5.1	110.2	75.7	7.0	1.1	5.7	31.6	0.8
21	3.25	1646.1	26.1	142.6	109.5	76.8	201.6	308.7	5.5	105.1	76.2	7.4	0.2	3.5	33.8	0.3
30	4.64	1704.0	25.0	147.1	117.4	75.1	219.2	351.9	4.4	112.5	73.7	6.1	0.0	6.1	31.4	1.4
40	6.19	1571.7	24.1	147.8	115.0	72.2	209.9	371.2	5.3	108.1	75.5	6.7	0.6	9.3	30.9	1.8
50	8.13	1464.8	25.0	143.7	108.9	70.5	208.0	358.9	5.3	111.7	76.9	7.1	0.3	7.4	33.4	1.3
60	10.06	1362.2	25.0	136.8	104.6	73.0	205.9	329.6	4.6	114.6	72.9	5.5	0.0	6.2	30.8	1.1
70	12.00	1206.5	25.2	141.9	102.3	67.4	192.7	336.2	4.4	114.6	75.6	4.8	1.3	9.3	34.0	2.1
80	12.69	1170.3	26.7	162.2	100.3	69.8	175.3	308.0	6.0	115.3	77.9	6.2	1.4	10.2	34.3	3.6
90	13.38	1059.8	25.6	155.7	99.8	69.4	166.8	318.2	5.2	117.6	76.3	4.8	1.6	8.2	36.2	6.1
100	14.07	1024.8	24.6	151.9	103.7	68.5	157.9	324.2	5.2	119.1	75.6	4.1	0.2	10.2	39.1	9.2
110	14.75	1022.5	24.0	146.5	92.6	68.9	146.2	328.0	5.8	119.4	76.1	4.2	0.9	12.0	40.7	10.8
120	15.44	1228.8	24.1	147.1	88.0	75.1	149.5	340.4	4.8	117.7	73.4	4.6	0.0	12.4	35.8	15.0
130	16.13	1294.9	23.2	147.1	87.6	74.4	149.7	334.5	5.6	117.2	73.7	4.7	0.0	14.8	35.8	18.6
140	16.82	1262.6	23.8	141.4	85.9	73.0	146.7	324.2	4.8	114.9	73.4	5.2	0.0	12.3	35.6	16.1
150	17.71	1204.4	23.5	139.6	84.7	72.6	148.5	329.8	4.5	108.9	73.7	4.5	0.0	11.4	36.0	16.5
160	18.59	1173.1	23.0	145.7	86.3	73.5	146.2	337.9	4.6	109.4	72.0	5.9	0.0	10.1	36.5	17.6
170	19.48	1172.3	24.1	151.0	73.7	71.6	144.8	322.4	5.3	116.0	72.7	5.4	0.8	8.8	34.2	13.0
180	20.23	1209.3	25.9	157.6	79.6	72.8	149.1	292.5	4.9	112.9	75.7	7.3	0.0	9.2	36.7	11.6
190	20.99	1143.2	25.2	148.9	76.9	73.7	145.0	306.8	5.5	110.2	74.3	5.4	0.0	8.7	34.6	12.8
200	21.74	1213.0	25.6	160.7	78.3	77.2	154.2	289.9	5.8	119.2	75.8	4.6	0.8	9.4	34.7	13.1
210	22.49	1179.1	25.6	144.5	80.3	71.2	151.7	261.3	5.7	113.2	76.6	5.8	0.0	9.9	36.4	14.9
220	23.25	1072.8	26.9	154.3	76.6	72.1	149.6	279.8	5.2	115.0	76.2	5.8	0.2	9.3	36.2	12.2
230	24.00	1231.7	26.0	150.3	81.1	75.4	161.6	252.3	5.6	115.0	74.8	5.4	0.0	5.9	36.0	11.6
240	28.38	1198.8	25.0	143.0	79.0	70.1	152.0	298.5	5.1	111.2	70.8	5.5	0.0	5.8	34.9	9.9
250	32.75	1077.9	25.3	145.9	80.1	72.8	152.4	280.4	5.5	110.0	75.8	6.1	0.0	7.2	36.0	9.1
260	37.13	1272.4	28.0	168.2	83.3	77.8	159.3	223.8	6.1	121.9	78.6	6.7	2.6	7.5	36.4	7.2
270	41.50	1239.9	24.3	149.9	83.2	69.1	160.1	311.8	4.6	113.9	71.0	4.4	1.8	9.3	35.3	6.8
280	45.88	1402.2	25.8	154.9	83.8	71.9	171.8	313.3	4.5	114.0	71.2	4.8	1.7	8.1	32.0	3.7
290	50.25	1364.3	29.5	173.5	84.2	82.1	161.6	235.9	5.5	123.8	81.1	5.6	0.0	5.2	35.5	5.6
300	54.63	1175.1	25.7	163.9	109.2	71.2	188.3	283.8	5.3	123.7	82.5	7.9	0.8	8.3	39.8	3.2
310	59.00	1153.0	23.1	134.7	70.1	73.4	143.6	370.4	4.5	110.4	69.7	4.4	1.6	9.8	31.0	12.2
319	*****	1236.6	22.8	141.9	75.9	187.5	272.0	354.0	4.5	106.5	70.5	6.1	0.2	9.4	32.6	15.4

Table C.5.4-1 Salt included trace element data from core CD3827.

Depth(cm)	Age(ka)	Ba(ppm)	Cu(ppm)	Ni(ppm)	Zn(ppm)	V(ppm)	Sr(ppm)	Sc(ppm)	Cr(ppm)	Zr(ppm)	Rb(ppm)	Nb(ppm)	Pb(ppm)	Th(ppm)	U(ppm)	Mo(ppm)	SALT
1	0.15	1756.2	83.7	118.5	219.5	164.6	269.4	30.3	113.3	85.2	39.0	5.5	7.5	0.0	1.2	0.0	9.163
10	1.55	1850.8	84.3	120.4	221.3	171.3	304.4	28.4	120.5	82.6	36.2	5.7	6.3	0.0	3.7	0.7	8.001
20	3.10	1856.9	81.4	118.4	220.1	157.5	352.5	27.5	118.5	81.4	34.0	5.5	7.5	1.2	6.1	0.9	7.026
21	3.25	1766.6	82.4	117.5	216.4	153.0	331.3	28.0	112.8	81.8	36.3	5.9	7.9	0.2	3.8	0.3	6.818
30	4.64	1825.2	80.4	125.7	234.8	157.6	376.9	26.8	120.5	78.9	33.6	4.7	6.5	0.0	6.5	1.5	6.638
40	6.19	1686.0	77.4	123.4	225.2	158.5	398.2	25.9	116.0	81.0	33.1	5.7	7.2	0.6	10.0	1.9	6.778
50	8.13	1579.7	76.0	117.4	224.3	155.0	387.1	27.0	120.5	82.9	36.0	5.7	7.7	0.3	8.0	1.4	7.275
60	10.06	1456.1	78.0	111.8	220.1	146.2	352.3	26.7	122.5	77.9	32.9	4.9	5.9	0.0	6.6	1.2	6.448
70	12.00	1304.8	72.9	110.6	208.4	153.5	363.6	27.3	123.9	81.8	36.8	4.8	5.2	1.4	10.1	2.3	7.531
80	12.69	1254.6	74.8	107.5	187.9	173.9	330.2	28.6	123.6	83.5	36.8	6.4	6.6	1.5	10.9	3.9	6.720
90	13.38	1136.0	74.4	107.0	178.8	166.9	341.1	27.4	126.1	81.8	38.8	5.6	5.1	1.7	8.8	6.5	6.705
100	14.07	1094.4	73.2	110.7	168.6	162.2	346.2	26.3	127.2	80.7	41.8	5.6	4.4	0.2	10.9	9.8	6.363
110	14.75	1089.8	73.4	98.7	155.8	156.1	349.6	25.6	127.3	81.1	43.4	6.2	4.5	1.0	12.8	11.5	6.179
120	15.44	1304.1	79.7	93.4	158.7	156.1	361.3	25.6	124.9	77.9	38.0	5.1	4.9	0.0	13.2	15.9	5.776
130	16.13	1379.2	79.2	93.3	159.4	156.7	356.3	24.7	124.8	78.5	38.1	6.0	5.0	0.0	15.8	19.8	6.110
140	16.82	1342.5	77.6	91.3	156.0	150.3	344.7	25.3	122.2	78.0	37.9	5.1	5.5	0.0	13.1	17.1	5.951
150	17.71	1282.3	77.3	90.2	158.1	148.6	351.1	25.0	115.9	78.5	38.3	4.8	4.8	0.0	12.1	17.6	6.077
160	18.59	1251.8	78.4	92.1	156.0	155.5	360.6	24.5	116.7	76.8	38.9	4.9	6.3	0.0	10.8	18.8	6.287
170	19.48	1251.2	76.4	78.7	154.5	161.2	344.1	25.7	123.8	77.6	36.5	5.7	5.8	0.9	9.4	13.9	6.305
180	20.23	1291.8	77.8	85.0	159.3	168.4	312.5	27.7	120.6	80.9	39.2	5.2	7.8	0.0	9.8	12.4	6.390
190	20.99	1221.0	78.7	82.1	154.9	159.0	327.7	26.9	117.7	79.4	37.0	5.9	5.8	0.0	9.3	13.7	6.369
200	21.74	1285.5	81.8	83.0	163.4	170.3	307.2	27.1	126.3	80.3	36.8	6.1	4.9	0.8	10.0	13.9	5.636
210	22.49	1262.9	76.3	86.0	162.5	154.8	279.9	27.4	121.2	82.0	39.0	6.1	6.2	0.0	10.6	16.0	6.637
220	23.25	1141.8	76.7	81.5	159.2	164.2	297.8	28.6	122.4	81.1	38.5	5.5	6.2	0.2	9.9	13.0	6.046
230	24.00	1309.1	80.1	86.2	171.8	159.8	268.2	27.6	122.2	79.5	38.3	6.0	5.7	0.0	6.3	12.3	5.916
240	28.38	1279.1	74.8	84.3	162.2	152.6	318.5	26.7	118.7	75.5	37.2	5.4	5.9	0.0	6.2	10.6	6.279
250	32.75	1143.0	77.2	84.9	161.6	154.7	297.3	26.8	116.6	80.4	38.2	5.8	6.5	0.0	7.6	9.6	5.694
260	37.13	1348.2	82.4	88.3	168.8	178.2	237.1	29.7	129.2	83.3	38.6	6.5	7.1	2.8	7.9	7.6	5.621
270	41.50	1310.9	73.1	88.0	169.3	158.5	329.6	25.7	120.4	75.1	37.3	4.9	4.7	1.9	9.8	7.2	5.414
280	45.88	1485.2	76.2	88.8	182.0	164.1	331.8	27.3	120.7	75.4	33.9	4.8	5.1	1.8	8.6	3.9	5.589
290	50.25	1436.7	86.5	88.7	170.2	182.7	248.4	31.1	130.4	85.4	37.4	5.8	5.9	0.0	5.5	5.9	5.037
300	54.63	1236.5	74.9	114.9	198.1	172.5	298.6	27.0	130.2	86.8	41.9	5.6	8.3	0.8	8.7	3.4	4.969
310	59.00	1216.1	77.4	73.9	151.5	142.1	390.7	24.4	116.4	73.5	32.7	4.7	4.6	1.7	10.3	12.9	5.191
319	*****	1309.4	198.5	80.4	288.0	150.3	374.9	24.1	112.8	74.7	34.5	4.8	6.5	0.2	10.0	16.3	5.562

Table C.5.4-2 Salt free trace element data from core CD3827.

Depth(cm)	Age(ka)	Ba/Al *10-2	Cu/Al *10-3	Ni/Al *10-3	Zn/Al *10-3	V/Al *10-3	Sr/Al *10-3	Sc/Al *10-4	Cr/Al *10-3	Zr/Al *10-3	Rb/Al *10-3	Nb/Al *10-4	Pb/Al *10-4	Th/Al *10-4	U/Al *10-4	Cr/Zr
1	0.15	2.227	1.061	1.502	2.784	2.087	3.416	3.839	1.437	1.081	0.494	0.698	0.949	0.000	0.154	1.329
10	1.55	2.375	1.083	1.546	2.840	2.199	3.906	3.641	1.547	1.060	0.465	0.725	0.809	0.000	0.474	1.459
20	3.10	2.469	1.082	1.574	2.926	2.093	4.686	3.661	1.576	1.082	0.452	0.729	1.001	0.157	0.815	1.456
21	3.25	2.408	1.124	1.602	2.950	2.086	4.517	3.819	1.538	1.115	0.495	0.805	1.083	0.029	0.512	1.379
30	4.64	2.594	1.143	1.787	3.336	2.239	5.356	3.805	1.712	1.122	0.478	0.670	0.928	0.000	0.928	1.526
40	6.19	2.398	1.102	1.755	3.202	2.255	5.663	3.677	1.649	1.152	0.471	0.809	1.022	0.092	1.419	1.432
50	8.13	2.196	1.057	1.633	3.118	2.154	5.380	3.748	1.674	1.153	0.501	0.795	1.064	0.045	1.109	1.453
60	10.06	2.021	1.083	1.552	3.055	2.030	4.891	3.709	1.700	1.082	0.457	0.683	0.816	0.000	0.920	1.572
70	12.00	1.786	0.998	1.514	2.853	2.101	4.977	3.730	1.696	1.119	0.503	0.651	0.711	0.192	1.377	1.516
80	12.69	1.662	0.991	1.425	2.490	2.304	4.374	3.792	1.638	1.106	0.487	0.852	0.881	0.199	1.449	1.480
90	13.38	1.551	1.015	1.460	2.440	2.278	4.656	3.746	1.721	1.116	0.530	0.761	0.702	0.234	1.200	1.541
100	14.07	1.545	1.033	1.563	2.380	2.290	4.887	3.708	1.795	1.140	0.589	0.784	0.618	0.030	1.538	1.575
110	14.75	1.536	1.035	1.391	2.197	2.201	4.929	3.606	1.794	1.144	0.612	0.872	0.631	0.135	1.803	1.569
120	15.44	1.920	1.173	1.375	2.336	2.298	5.318	3.765	1.839	1.147	0.559	0.750	0.719	0.000	1.937	1.604
130	16.13	2.033	1.168	1.375	2.350	2.310	5.252	3.643	1.840	1.157	0.562	0.879	0.738	0.000	2.324	1.590
140	16.82	1.984	1.147	1.350	2.305	2.222	5.094	3.740	1.806	1.153	0.559	0.754	0.817	0.000	1.933	1.565
150	17.71	1.900	1.146	1.337	2.343	2.203	5.204	3.708	1.718	1.163	0.568	0.710	0.710	0.000	1.799	1.478
160	18.59	1.882	1.179	1.385	2.346	2.338	5.422	3.691	1.756	1.155	0.586	0.738	0.947	0.000	1.621	1.519
170	19.48	1.824	1.114	1.147	2.253	2.349	5.016	3.750	1.805	1.131	0.532	0.825	0.840	0.124	1.369	1.596
180	20.23	1.794	1.080	1.181	2.212	2.338	4.340	3.843	1.675	1.123	0.545	0.727	1.083	0.000	1.365	1.491
190	20.99	1.723	1.111	1.159	2.186	2.245	4.625	3.799	1.661	1.120	0.522	0.829	0.814	0.000	1.311	1.483
200	21.74	1.807	1.150	1.166	2.297	2.394	4.318	3.813	1.776	1.129	0.517	0.864	0.685	0.119	1.400	1.573
210	22.49	1.733	1.047	1.180	2.230	2.124	3.841	3.763	1.664	1.126	0.535	0.838	0.853	0.000	1.455	1.478
220	23.25	1.507	1.013	1.076	2.101	2.167	3.930	3.778	1.615	1.070	0.508	0.730	0.815	0.028	1.306	1.509
230	24.00	1.787	1.094	1.177	2.344	2.181	3.660	3.772	1.668	1.085	0.522	0.812	0.783	0.000	0.856	1.537
240	28.38	1.839	1.076	1.212	2.332	2.194	4.580	3.836	1.706	1.086	0.535	0.783	0.844	0.000	0.890	1.571
250	32.75	1.567	1.059	1.165	2.216	2.122	4.077	3.679	1.600	1.102	0.523	0.800	0.887	0.000	1.047	1.451
260	37.13	1.749	1.070	1.145	2.190	2.312	3.077	3.849	1.676	1.081	0.500	0.839	0.921	0.357	1.031	1.551
270	41.50	1.935	1.079	1.299	2.499	2.340	4.867	3.793	1.778	1.108	0.551	0.718	0.687	0.281	1.452	1.604
280	45.88	2.127	1.091	1.271	2.606	2.350	4.753	3.914	1.730	1.080	0.485	0.683	0.728	0.258	1.229	1.601
290	50.25	1.810	1.089	1.117	2.144	2.302	3.129	3.913	1.642	1.076	0.471	0.730	0.743	0.000	0.690	1.527
300	54.63	1.597	0.968	1.484	2.559	2.227	3.857	3.493	1.681	1.121	0.541	0.720	1.074	0.109	1.128	1.499
310	59.00	1.915	1.219	1.164	2.385	2.238	6.153	3.837	1.834	1.158	0.515	0.748	0.731	0.266	1.628	1.584
319	*****	2.038	3.090	1.251	4.483	2.339	5.834	3.758	1.755	1.162	0.537	0.742	1.005	0.033	1.549	1.511

Table C.5.4-3 Salt free trace elements and their ratios to Al in core CD3827.

Table C.5.5-1 Salt included trace element data from core P5.

Depth(cm)	Age(ka)	Ba(ppm)	Sc(ppm)	V(ppm)	Ni(ppm)	Cu(ppm)	Zn(ppm)	Sr(ppm)	Nb(ppm)	Cr(ppm)	Zr(ppm)	Pb(ppm)	Th(ppm)	U(ppm)	Rb(ppm)
9	2.49	1194.2	3.4	19.0	15.8	15.5	24.7	1094.3	0.9	8.6	9.8	4.4	0.3	0.1	5.7
11	3.04	1189.8	3.0	16.4	15.0	13.3	25.8	1101.9	0.8	7.7	10.0	2.0	0.0	0.4	5.9
13	3.59	1223.9	5.0	14.7	14.0	13.5	26.4	1106.6	0.7	8.3	9.5	2.5	0.0	3.3	6.7
15	4.14	1221.3	4.1	26.5	13.3	14.9	25.9	1110.8	1.0	9.2	10.3	2.8	0.0	2.7	6.3
17	4.70	1205.2	4.7	20.2	15.7	14.5	27.9	1118.4	0.6	7.1	10.0	1.0	0.2	4.0	6.8
19	5.25	1201.4	5.1	21.4	15.1	17.8	27.1	1117.8	0.2	7.1	10.2	3.5	0.1	3.4	6.5
21	5.80	1195.9	3.9	23.2	13.8	13.8	25.4	1118.2	0.6	8.6	9.2	2.6	0.0	0.7	4.4
23	6.35	1192.1	2.5	22.3	16.6	15.3	25.7	1119.3	0.2	6.1	9.0	1.4	0.0	1.5	5.5
25	6.91	1134.8	4.5	24.0	17.0	14.0	28.3	1121.3	0.5	8.9	9.1	0.7	0.0	1.3	5.8
27	7.46	1136.3	5.5	19.5	18.3	15.3	28.0	1120.4	0.7	6.7	8.7	3.2	0.1	2.9	5.4
29	8.01	1072.3	2.8	20.4	17.0	17.4	26.2	1112.5	0.2	12.4	8.0	3.5	0.0	1.7	5.0
31	8.56	1068.7	4.6	31.1	18.5	16.7	30.5	1118.5	0.5	7.6	6.9	1.5	0.0	5.2	5.7
33	9.12	1032.0	4.4	29.7	17.1	16.0	26.6	1115.2	1.0	9.2	8.4	3.1	0.0	5.4	5.0
35	9.67	983.3	3.8	22.2	18.9	17.9	27.1	1106.2	1.8	9.3	9.6	3.1	0.0	2.3	5.2
37	10.22	905.0	2.8	24.1	17.6	18.1	29.5	1088.4	0.5	13.4	8.3	2.4	0.0	6.6	5.1
39	10.77	858.4	3.0	22.7	16.5	16.0	30.1	1093.0	0.5	10.6	8.1	1.2	0.1	1.9	4.4
41	11.33	799.3	1.6	23.6	16.7	17.8	29.1	1091.6	0.0	11.4	7.3	1.9	0.0	2.0	4.3
43	11.89	755.1	3.1	17.7	18.5	17.5	28.4	1099.6	1.0	9.8	7.6	2.3	0.3	2.7	4.4
45	12.01	811.9	4.4	15.5	19.6	18.0	28.0	1092.1	1.0	8.6	8.0	2.5	0.0	2.4	4.2
47	12.13	815.4	2.9	18.4	16.2	16.9	24.6	1097.3	0.3	10.2	7.9	1.5	0.0	2.9	4.0
49	12.25	771.8	3.0	17.0	15.4	16.8	26.0	1098.9	0.3	9.7	5.3	0.0	0.0	3.9	4.7
51	12.37	872.6	2.9	19.8	16.7	17.0	25.8	1099.7	0.6	7.3	6.6	2.4	0.0	1.2	4.5
53	12.49	779.4	3.5	25.4	16.3	17.5	25.1	1101.4	0.2	8.0	6.7	2.4	0.3	2.5	4.2
55	12.61	700.7	3.6	19.7	16.8	16.2	22.4	1112.9	0.4	9.9	6.2	2.1	0.0	0.7	4.6
57	12.73	591.5	6.0	20.7	15.9	14.2	19.5	1099.8	0.0	4.3	5.2	2.7	0.0	3.9	4.7
59	12.90	587.1	3.4	22.0	14.5	14.6	19.8	1098.6	0.0	10.6	5.3	1.7	0.0	1.9	4.0
61	13.08	582.3	2.1	15.0	15.0	13.3	17.6	1096.4	0.6	10.2	6.0	2.9	0.0	4.6	4.7
63	13.25	615.9	4.0	20.2	18.5	14.1	18.5	1109.8	0.2	7.9	6.9	1.1	0.0	1.9	3.8
65	13.42	610.0	4.1	16.5	17.6	15.3	19.4	1104.4	1.2	4.0	6.9	2.2	0.0	2.9	4.5
67	13.60	651.8	3.8	11.8	15.4	15.4	17.6	1116.7	0.6	8.0	6.8	1.8	0.2	1.9	4.7
69	13.77	710.1	5.0	14.4	16.2	17.5	19.2	1116.1	0.6	10.0	6.5	2.1	1.8	5.5	5.7
71	13.94	740.0	3.1	15.8	15.8	16.2	19.3	1115.9	0.9	10.6	6.6	1.5	0.0	3.9	5.0
73	14.12	746.8	5.2	12.7	16.8	19.0	20.7	1113.0	0.7	9.9	7.6	0.1	0.0	5.6	5.1
75	14.29	716.2	4.0	12.9	16.2	16.0	19.7	1107.3	0.5	9.3	5.9	1.6	0.0	5.7	5.1
77	14.46	767.0	3.3	9.1	17.5	16.5	21.3	1103.9	0.3	8.4	6.5	0.3	0.0	4.1	4.9
79	14.63	760.1	4.0	12.5	19.7	17.6	21.7	1098.3	0.5	9.6	6.6	1.4	0.0	5.3	4.8
81	14.81	778.4	3.1	14.3	18.8	17.4	22.4	1095.3	0.4	10.4	6.9	2.4	0.0	4.9	5.8
83	14.98	733.7	5.1	12.5	15.5	15.9	20.9	1102.1	0.8	7.2	6.2	2.2	0.0	4.8	4.6
85	15.15	745.6	4.1	14.4	13.3	16.4	20.3	1098.4	0.8	7.3	6.6	1.2	0.0	5.9	5.0
87	15.33	760.4	5.0	15.6	16.7	16.1	20.3	1096.3	0.5	7.7	7.4	3.3	0.6	2.5	5.7
89	15.50	767.7	4.5	19.8	14.4	18.5	21.7	1103.3	0.2	6.5	7.7	3.9	0.0	5.4	5.0
91	16.03	718.8	3.0	14.1	21.2	25.7	23.8	1100.2	1.1	8.0	6.0	11.7	0.0	2.1	3.2
93	16.56	698.6	4.1	14.7	15.2	16.3	17.2	1104.2	0.7	10.1	6.9	2.3	0.2	4.4	5.6
95	17.09	684.4	4.4	14.4	13.9	16.1	17.2	1103.6	0.9	6.9	5.7	1.5	0.0	4.9	4.4
97	17.63	683.9	4.5	20.5	13.7	15.9	17.6	1094.8	0.0	10.3	5.7	1.2	0.0	3.6	4.5
99	18.16	752.0	2.8	14.2	14.7	14.6	18.9	1102.0	0.0	6.0	6.5	2.7	0.0	1.1	4.9
101	18.69	751.7	3.7	11.2	13.4	14.4	18.8	1086.1	0.2	6.9	5.8	3.3	0.0	2.8	4.4
103	19.22	804.0	4.1	14.9	14.7	16.4	18.0	1092.3	0.1	6.6	7.1	0.0	0.0	3.4	4.5
105	19.75	768.5	4.2	13.3	14.6	16.3	19.3	1086.3	0.7	5.2	6.9	0.2	0.0	0.7	5.2
107	20.28	754.9	4.0	19.5	13.8	16.3	19.9	1092.5	0.6	7.7	7.0	1.7	0.0	5.9	4.7
109	20.81	754.8	3.7	16.9	13.0	15.3	18.4	1082.9	0.4	9.4	7.3	4.2	0.0	1.0	4.4
111	21.34	750.2	3.5	6.3	14.0	15.5	18.9	1081.0	1.0	7.8	6.9	2.2	0.3	2.7	4.8
113	21.88	764.4	2.8	20.7	15.3	16.4	20.7	1087.6	0.7	7.2	6.2	0.1	0.0	2.2	4.8
115	22.41	777.6	3.5	12.4	14.9	17.5	20.6	1089.2	0.5	8.0	7.4	0.7	0.9	2.8	5.2
117	22.94	786.8	3.7	15.5	16.0	15.6	20.6	1093.8	0.9	8.0	8.0	1.1	0.5	2.4	5.4
119	23.47	813.6	5.4	17.2	13.5	15.4	20.6	1092.5	0.4	5.2	7.9	0.7	0.0	3.8	6.0
121	24.00	813.2	3.5	19.8	13.1	16.7	21.3	1089.7	2.3	8.0	8.4	5.0	0.0	4.5	5.1
123	*****	848.5	3.2	18.1	14.6	16.0	20.7	1094.8	0.3	5.6	8.6	0.6	0.0	4.0	5.9

Table C.5.5-2 Salt free trace element data from core P5.

Depth(cm)	Age(ka)	Ba(ppm)	Cu(ppm)	Ni(ppm)	Zn(ppm)	V(ppm)	Sr(ppm)	Sc(ppm)	Cr(ppm)	Zr(ppm)	Rb(ppm)	Nb(ppm)	Pb(ppm)	Th(ppm)	U(ppm)	SALT
9	2.49	1235.9	16.0	16.4	25.6	19.7	1132.5	3.5	8.9	10.1	5.9	0.9	4.6	0.3	0.1	3.374
11	3.04	1233.8	13.8	15.6	26.8	17.0	1142.6	3.1	8.0	10.4	6.1	0.8	2.1	0.0	0.4	3.563
13	3.59	1271.1	14.0	14.5	27.4	15.3	1149.3	5.2	8.6	9.9	7.0	0.7	2.6	0.0	3.4	3.714
15	4.14	1268.6	15.5	13.8	26.9	27.5	1153.8	4.3	9.6	10.7	6.5	1.0	2.9	0.0	2.8	3.730
17	4.70	1251.5	15.1	16.3	29.0	21.0	1161.4	4.9	7.4	10.4	7.1	0.6	1.0	0.2	4.2	3.702
19	5.25	1246.7	18.5	15.7	28.1	22.2	1160.0	5.3	7.4	10.6	6.7	0.2	3.6	0.1	3.5	3.634
21	5.80	1243.3	14.3	14.3	26.4	24.1	1162.5	4.1	8.9	9.6	4.6	0.6	2.7	0.0	0.7	3.811
23	6.35	1242.7	15.9	17.3	26.8	23.2	1166.8	2.6	6.4	9.4	5.7	0.2	1.5	0.0	1.6	4.075
25	6.91	1183.6	14.6	17.7	29.5	25.0	1169.5	4.7	9.3	9.5	6.0	0.5	0.7	0.0	1.4	4.121
27	7.46	1187.2	16.0	19.1	29.3	20.4	1170.6	5.7	7.0	9.1	5.6	0.7	3.3	0.1	3.0	4.285
29	8.01	1121.6	18.2	17.8	27.4	21.3	1163.7	2.9	13.0	8.4	5.2	0.2	3.7	0.0	1.8	4.399
31	8.56	1117.9	17.5	19.4	31.9	32.5	1170.0	4.8	8.0	7.2	6.0	0.5	1.6	0.0	5.4	4.403
33	9.12	1079.3	16.7	17.9	27.8	31.1	1166.3	4.6	9.6	8.8	5.2	1.0	3.2	0.0	5.6	4.385
35	9.67	1030.4	18.8	19.8	28.4	23.3	1159.2	4.0	9.7	10.1	5.4	1.9	3.2	0.0	2.4	4.569
37	10.22	948.9	19.0	18.5	30.9	25.3	1141.3	2.9	14.1	8.7	5.3	0.5	2.5	0.0	6.9	4.631
39	10.77	898.8	16.8	17.3	31.5	23.8	1144.4	3.1	11.1	8.5	4.6	0.5	1.3	0.1	2.0	4.490
41	11.33	838.1	18.7	17.5	30.5	24.7	1144.6	1.7	12.0	7.7	4.5	0.0	2.0	0.0	2.1	4.629
43	11.89	791.0	18.3	19.4	29.8	18.5	1151.9	3.2	10.3	8.0	4.6	1.0	2.4	0.3	2.8	4.543
45	12.01	849.9	18.8	20.5	29.3	16.2	1143.3	4.6	9.0	8.4	4.4	1.0	2.6	0.0	2.5	4.476
47	12.13	853.5	17.7	17.0	25.8	19.3	1148.6	3.0	10.7	8.3	4.2	0.3	1.6	0.0	3.0	4.467
49	12.25	807.9	17.6	16.1	27.2	17.8	1150.3	3.1	10.2	5.5	4.9	0.3	0.0	0.0	4.1	4.469
51	12.37	912.5	17.8	17.5	27.0	20.7	1149.9	3.0	7.6	6.9	4.7	0.6	2.5	0.0	1.3	4.369
53	12.49	812.6	18.2	17.0	26.2	26.5	1148.3	3.6	8.3	7.0	4.4	0.2	2.5	0.3	2.6	4.087
55	12.61	732.0	16.9	17.6	23.4	20.6	1162.7	3.8	10.3	6.5	4.8	0.4	2.2	0.0	0.7	4.281
57	12.73	616.5	14.8	16.6	20.3	21.6	1146.2	6.3	4.5	5.4	4.9	0.0	2.8	0.0	4.1	4.048
59	12.90	612.4	15.2	15.1	20.7	22.9	1146.0	3.5	11.1	5.5	4.2	0.0	1.8	0.0	2.0	4.139
61	13.08	607.6	13.9	15.7	18.4	15.7	1144.1	2.2	10.6	6.3	4.9	0.6	3.0	0.0	4.8	4.170
63	13.25	642.8	14.7	19.3	19.3	21.1	1158.3	4.2	8.2	7.2	4.0	0.2	1.1	0.0	2.0	4.185
65	13.42	636.0	16.0	18.4	20.2	17.2	1151.5	4.3	4.2	7.2	4.7	1.3	2.3	0.0	3.0	4.088
67	13.60	676.7	16.0	16.0	18.3	12.3	1159.4	3.9	8.3	7.1	4.9	0.6	1.9	0.2	2.0	3.685
69	13.77	738.5	18.2	16.8	20.0	15.0	1160.7	5.2	10.4	6.8	5.9	0.6	2.2	1.9	5.7	3.844
71	13.94	770.0	16.9	16.4	20.1	16.4	1161.1	3.2	11.0	6.9	5.2	0.9	1.6	0.0	4.1	3.890
73	14.12	776.6	19.8	17.5	21.5	13.2	1157.4	5.4	10.3	7.9	5.3	0.7	0.1	0.0	5.8	3.840
75	14.29	746.0	16.7	16.9	20.5	13.4	1153.4	4.2	9.7	6.1	5.3	0.5	1.7	0.0	5.9	3.997
77	14.46	796.5	17.1	18.2	22.1	9.4	1146.3	3.4	8.7	6.7	5.1	0.3	0.3	0.0	4.3	3.700
79	14.63	791.1	18.3	20.5	22.6	13.0	1143.1	4.2	10.0	6.9	5.0	0.5	1.5	0.0	5.5	3.919
81	14.81	810.1	18.1	19.6	23.3	14.9	1139.9	3.2	10.8	7.2	6.0	0.4	2.5	0.0	5.1	3.913
83	14.98	763.1	16.5	16.1	21.7	13.0	1146.3	5.3	7.5	6.4	4.8	0.8	2.3	0.0	5.0	3.855
85	15.15	775.0	17.0	13.8	21.1	15.0	1141.8	4.3	7.6	6.9	5.2	0.8	1.2	0.0	6.1	3.799
87	15.33	788.5	16.7	17.3	21.0	16.2	1136.8	5.2	8.0	7.7	5.9	0.5	3.4	0.6	2.6	3.559
89	15.50	797.2	19.2	15.0	22.5	20.6	1145.7	4.7	6.8	8.0	5.2	0.2	4.1	0.0	5.6	3.704
91	16.03	750.7	26.8	22.1	24.9	14.7	1149.0	3.1	8.4	6.3	3.3	1.1	12.2	0.0	2.2	4.248
93	16.56	727.7	17.0	15.8	17.9	15.3	1150.2	4.3	10.5	7.2	5.8	0.7	2.4	0.2	4.6	4.002
95	17.09	712.4	16.8	14.5	17.9	15.0	1148.8	4.6	7.2	5.9	4.6	0.9	1.6	0.0	5.1	3.934
97	17.63	715.8	16.6	14.3	18.4	21.5	1145.8	4.7	10.8	6.0	4.7	0.0	1.3	0.0	3.8	4.453
99	18.16	783.6	15.2	15.3	19.7	14.8	1148.3	2.9	6.3	6.8	5.1	0.0	2.8	0.0	1.1	4.028
101	18.69	784.2	15.0	14.0	19.6	11.7	1133.1	3.9	7.2	6.1	4.6	0.2	3.4	0.0	2.9	4.147
103	19.22	839.0	17.1	15.3	18.8	15.5	1139.9	4.3	6.9	7.4	4.7	0.1	0.0	0.0	3.5	4.172
105	19.75	799.0	16.9	15.2	20.1	13.8	1129.5	4.4	5.4	7.2	5.4	0.7	0.2	0.0	0.7	3.822
107	20.28	785.6	17.0	14.4	20.7	20.3	1137.0	4.2	8.0	7.3	4.9	0.6	1.8	0.0	6.1	3.912
109	20.81	786.5	15.9	13.5	19.2	17.6	1128.4	3.9	9.8	7.6	4.6	0.4	4.4	0.0	1.0	4.032
111	21.34	781.4	16.1	14.6	19.7	6.6	1125.9	3.6	8.1	7.2	5.0	1.0	2.3	0.3	2.8	3.987
113	21.88	796.8	17.1	15.9	21.6	21.6	1133.7	2.9	7.5	6.5	5.0	0.7	0.1	0.0	2.3	4.063
115	22.41	807.4	18.2	15.5	21.4	12.9	1131.0	3.6	8.3	7.7	5.4	0.5	0.7	0.9	2.9	3.693
117	22.94	817.3	16.2	16.6	21.4	16.1	1136.2	3.8	8.3	8.3	5.6	0.9	1.1	0.5	2.5	3.729
119	23.47	846.8	16.0	14.1	21.4	17.9	1137.0	5.6	5.4	8.2	6.2	0.4	0.7	0.0	4.0	3.917
121	24.00	846.0	17.4	13.6	22.2	20.6	1133.6	3.6	8.3	8.7	5.3	2.4	5.2	0.0	4.7	3.873
123	*****	880.8	16.6	15.2	21.5	18.8	1136.5	3.3	5.8	8.9	6.1	0.3	0.6	0.0	4.2	3.669

Table C.5.5-3 Salt free trace elements and their ratios to Al in core P5.

Depth(cm)	Age (ka)	Ba/Al *10-2	Cu/Al *10-4	Ni/Al *10-4	Zn/Al *10-4	V/Al *10-4	Sr/Al *10-2	Sc/Al *10-4	Cr/Al *10-4	Zr/Al *10-4	Rb/Al *10-4	Nb/Al *10-4	Pb/Al *10-4	Th/Al *10-4	U/Al *10-4	Cr/Zr
9	2.49	22.715	29.483	30.053	46.982	36.140	20.815	6.467	16.358	18.641	10.842	1.712	8.369	0.571	0.190	0.878
11	3.04	23.513	26.284	29.643	50.987	32.410	21.776	5.929	15.217	19.762	11.660	1.581	3.952	0.000	0.790	0.770
13	3.59	22.509	24.828	25.748	48.553	27.035	20.352	9.196	15.265	17.472	12.322	1.287	4.598	0.000	6.069	0.874
15	4.14	22.840	27.865	24.872	48.436	49.558	20.773	7.667	17.205	19.262	11.782	1.870	5.236	0.000	5.049	0.893
17	4.70	24.291	29.225	31.644	56.233	40.713	22.542	9.473	14.310	20.155	13.706	1.209	2.016	0.403	8.062	0.710
19	5.25	23.788	35.245	29.899	53.659	42.373	22.133	10.098	14.058	20.197	12.870	0.396	6.930	0.198	6.732	0.696
21	5.80	24.514	28.288	28.288	52.066	47.556	22.921	7.994	17.629	18.859	9.019	1.230	5.330	0.000	1.435	0.935
23	6.35	25.490	32.716	35.495	54.954	47.684	23.934	5.346	13.043	19.244	11.761	0.428	2.994	0.000	3.207	0.678
25	6.91	25.827	31.863	38.690	64.408	54.622	25.520	10.242	20.256	20.711	13.200	1.138	1.593	0.000	2.959	0.978
27	7.46	24.294	32.711	39.125	59.864	41.691	23.954	11.759	14.325	18.601	11.545	1.497	6.842	0.214	6.200	0.770
29	8.01	24.331	39.481	38.573	59.449	46.288	25.243	6.353	28.136	18.152	11.345	0.454	7.942	0.000	3.857	1.550
31	8.56	26.579	41.534	46.011	75.856	77.348	27.818	11.441	18.902	17.161	14.176	1.244	3.731	0.000	12.933	1.101
33	9.12	27.125	42.054	44.946	69.916	78.064	29.312	11.565	24.181	22.079	13.142	2.628	8.148	0.000	14.193	1.095
35	9.67	26.645	48.504	51.214	73.434	60.156	29.975	10.297	25.200	26.013	14.091	4.878	8.400	0.000	6.232	0.969
37	10.22	26.354	52.708	51.252	85.905	70.180	31.695	8.154	39.021	24.170	14.851	1.456	6.989	0.000	19.219	1.614
39	10.77	25.918	48.310	49.820	90.884	68.540	33.002	9.058	32.006	24.457	13.285	1.510	3.623	0.302	5.737	1.309
41	11.33	24.886	55.420	51.995	90.602	73.478	33.987	4.982	35.493	22.728	13.388	0.000	5.916	0.000	6.227	1.562
43	11.89	25.816	59.829	63.248	97.095	60.513	37.593	10.598	33.504	25.983	15.043	3.419	7.863	1.026	9.231	1.289
45	12.01	26.958	59.766	65.079	92.970	51.466	36.262	14.610	28.555	26.563	13.946	3.320	8.301	0.000	7.969	1.075
47	12.13	26.331	54.574	52.314	79.439	59.418	35.434	9.365	32.938	25.511	12.917	0.969	4.844	0.000	9.365	1.291
49	12.25	28.589	62.231	57.045	96.309	62.971	40.706	11.113	35.931	19.632	17.410	1.111	0.000	0.000	14.446	1.830
51	12.37	28.194	54.928	53.959	83.362	63.975	35.532	9.370	23.587	21.325	14.540	1.939	7.755	0.000	3.877	1.106
53	12.49	27.259	61.205	57.008	87.786	88.835	38.521	12.241	27.979	23.433	14.689	0.699	8.394	1.049	8.744	1.194
55	12.61	26.329	60.871	63.126	84.167	74.022	41.817	13.527	37.199	23.296	17.284	1.503	7.891	0.000	2.630	1.597
57	12.73	26.026	62.479	69.959	85.798	91.078	48.390	26.400	18.920	22.880	20.680	0.000	11.880	0.000	17.160	0.827
59	12.90	26.006	64.671	64.229	87.705	97.450	48.663	15.060	46.953	23.477	17.718	0.000	7.530	0.000	8.416	2.000
61	13.08	25.895	59.145	66.705	78.267	66.705	48.757	9.339	45.359	26.682	20.901	2.668	12.896	0.000	20.456	1.700
63	13.25	24.930	57.072	74.882	74.882	81.763	44.921	16.191	31.977	27.929	15.381	0.810	4.452	0.000	7.691	1.145
65	13.42	25.541	64.062	73.692	81.228	69.086	46.242	17.167	16.748	28.891	18.842	5.024	9.211	0.000	12.142	0.580
67	13.60	28.035	66.238	66.238	75.700	50.754	48.031	16.344	34.409	29.248	20.215	2.581	7.742	0.860	8.172	1.176
69	13.77	29.750	73.318	67.871	80.440	60.330	46.760	20.948	41.896	27.232	23.881	2.514	8.798	7.541	23.043	1.538
71	13.94	30.118	65.935	64.307	78.552	64.307	45.418	12.617	43.142	26.862	20.350	3.663	6.105	0.000	15.873	1.606
73	14.12	28.592	72.744	64.321	79.253	48.624	42.613	19.909	37.903	29.098	19.526	2.680	0.383	0.000	21.440	1.303
75	14.29	27.492	61.419	62.186	75.622	49.519	42.506	15.355	35.700	22.648	19.577	1.919	6.142	0.000	21.880	1.576
77	14.46	30.819	66.298	70.317	85.585	36.565	44.356	13.260	33.752	26.118	19.689	1.205	1.205	0.000	16.474	1.292
79	14.63	29.667	68.693	76.890	84.696	48.788	42.867	15.612	37.469	25.760	18.735	1.952	5.464	0.000	20.686	1.455
81	14.81	29.232	65.343	70.601	84.120	53.702	41.133	11.642	39.056	25.912	21.781	1.502	9.013	0.000	18.401	1.507
83	14.98	29.500	63.929	62.320	84.032	50.258	44.312	20.505	28.949	24.928	18.495	3.217	8.845	0.000	19.299	1.161
85	15.15	29.771	65.483	53.105	81.055	57.497	43.857	16.371	29.148	26.353	19.964	3.194	4.791	0.000	23.558	1.106
87	15.33	30.630	64.853	67.270	81.771	62.839	44.161	20.141	31.017	29.808	22.960	2.014	13.293	2.417	10.070	1.041
89	15.50	29.055	70.017	54.500	82.129	74.938	41.757	17.031	24.601	29.142	18.924	0.757	14.760	0.000	20.438	0.844
91	16.03	29.188	104.359	86.086	96.643	57.255	44.675	12.182	32.485	24.364	12.994	4.467	47.510	0.000	8.527	1.333
93	16.56	30.088	70.201	65.464	74.078	63.310	47.556	17.658	43.499	29.717	24.118	3.015	9.906	0.861	18.950	1.464
95	17.09	28.993	68.203	58.884	72.863	61.002	46.751	18.639	29.230	24.147	18.639	3.813	6.354	0.000	20.758	1.211
97	17.63	26.352	61.266	52.789	67.816	78.991	42.185	17.339	39.688	21.963	17.339	0.000	4.624	0.000	13.872	1.807
99	18.16	26.929	52.282	52.640	67.680	50.850	39.462	10.027	21.486	23.276	17.547	0.000	9.669	0.000	3.939	0.923
101	18.69	29.467	56.449	52.529	73.697	43.905	42.576	14.504	27.048	22.736	17.248	0.784	12.936	0.000	10.976	1.190
103	19.22	29.795	60.777	54.477	66.706	55.218	40.480	15.194	24.459	26.312	16.677	0.371	0.000	0.000	12.600	0.930
105	19.75	26.252	55.681	49.874	65.929	45.433	37.108	14.347	17.763	23.571	17.763	2.391	0.683	0.000	2.391	0.754
107	20.28	25.879	55.879	47.309	68.221	66.850	37.453	13.713	26.397	23.997	16.112	2.057	5.828	0.000	20.226	1.100
109	20.81	25.612	51.916	44.112	62.435	57.345	36.745	12.555	31.896	24.770	14.930	1.357	14.251	0.000	3.393	1.288
111	21.34	25.174	52.012	46.978	63.421	21.140	36.274	11.745	26.174	23.154	16.107	3.356	7.382	1.007	9.060	1.130
113	21.88	24.357	52.258	48.753	65.959	65.959	34.656	8.922	22.942	19.756	15.295	2.231	0.319	0.000	7.010	1.161
115	22.41	24.112	54.263	46.201	63.876	38.449	33.773	10.853	24.806	22.946	16.124	1.550	2.171	2.791	8.682	1.081
117	22.94	23.407	46.409	47.599	61.283	46.111	32.540	11.007	23.799	23.799	16.065	2.677	3.272	1.487	7.140	1.000
119	23.47	24.527	46.426	40.698	62.103	51.853	32.935	16.279	15.676	23.816	18.088	1.206	2.110	0.000	11.456	0.658
121	24.00	22.501	46.208	36.247	58.936	54.786	30.152	9.684	22.136	23.242	14.112	6.364	13.835	0.000	12.451	0.952
123	*****	22.004	41.492	37.862	53.680	46.938	28.391	8.298	14.522	22.302	15.300	0.778	1.556	0.000	10.373	0.651

Depth(cm)	Y(ppm)	La(ppm)	Ce(ppm)	Nd(ppm)	La/Ce	Nd/Ce	La/Nd	Ce/Nd
1	14.4	5.5	7.1	14.5	0.783	2.043	0.383	0.489
10	13.3	0.0	7.1	11.4	0.000	1.609	0.000	0.622
11	14.2	0.0	32.6	15.3	0.000	0.468	0.000	2.135
20	14.3	0.0	0.0	13.2	2.304	0.000	0.000	0.000
30	15.7	0.0	1.5	7.6	0.000	4.933	0.000	0.203
40	19.7	0.0	17.7	17.3	0.000	0.977	0.000	1.024
50	28.7	7.8	12.5	14.9	0.623	1.189	0.524	0.841
60	25.5	12.9	10.4	9.5	1.238	0.911	1.359	1.098
70	26.2	7.7	0.0	13.0	0.000	0.000	0.592	0.000
80	28.1	4.6	0.0	3.4	0.000	0.000	1.333	0.000
90	27.0	15.3	1.1	21.2	13.364	18.545	0.721	0.054
100	28.1	19.6	0.0	14.8	0.000	0.000	1.329	0.000
110	27.6	13.8	2.2	8.6	6.333	3.952	1.602	0.253
120	27.7	0.0	0.0	13.9	0.369	0.000	0.000	0.000
130	27.0	8.7	1.2	13.1	7.000	10.500	0.667	0.095
140	27.9	4.3	10.6	20.3	0.402	1.902	0.211	0.526
150	27.5	11.0	29.9	22.0	0.369	0.735	0.502	1.360
160	27.8	8.5	0.0	23.0	0.000	0.000	0.371	0.000
170	26.2	8.3	0.0	14.2	0.000	0.000	0.584	0.000
180	26.7	20.3	8.3	14.2	2.438	1.713	1.423	0.584
190	27.0	11.8	0.0	3.4	0.000	0.000	3.455	0.000
200	25.5	22.0	2.4	10.9	9.217	4.565	2.019	0.219
210	26.7	0.0	16.1	18.0	0.000	1.115	0.000	0.897
219	25.9	7.1	11.1	22.1	0.636	1.991	0.319	0.502
230	27.1	13.2	15.6	22.3	0.848	1.430	0.593	0.699
240	27.5	12.4	0.6	14.8	20.000	23.833	0.839	0.042
250	26.0	7.5	0.0	11.4	0.000	0.000	0.664	0.000
260	24.9	5.9	3.8	10.8	1.541	2.838	0.543	0.352
270	26.6	11.4	0.0	15.5	0.000	0.000	0.740	0.000
280	25.7	12.0	0.0	14.4	0.000	0.000	0.829	0.000
290	26.7	6.4	0.0	19.3	0.000	0.000	0.330	0.000
300	25.8	1.3	19.5	12.1	0.069	0.619	0.111	1.615
310	25.8	7.5	12.6	23.5	0.598	1.869	0.320	0.535
320	25.9	20.5	9.7	12.3	2.128	1.277	1.667	0.783
330	23.3	10.1	0.0	9.0	0.000	0.000	1.126	0.000
340	17.9	12.4	0.0	8.0	0.000	0.000	1.538	0.000
350	19.3	5.3	7.4	11.9	0.708	1.597	0.443	0.626
360	15.4	0.5	16.1	6.3	0.032	0.391	0.082	2.557
370	15.2	1.3	11.8	11.4	0.114	0.974	0.117	1.027
382	13.0	0.0	5.6	6.4	0.000	1.148	0.000	0.871
390	13.4	6.2	0.0	10.3	0.000	0.000	0.600	0.000
400	12.1	6.4	0.0	4.0	0.000	0.000	1.590	0.000
410	12.8	0.0	0.0	10.3	0.150	0.000	0.000	0.000
420	14.4	7.0	7.8	12.5	0.895	1.605	0.557	0.623
430	9.9	7.8	0.0	9.0	0.000	0.000	0.874	0.000
438	9.9	2.8	0.0	2.3	0.000	0.000	1.227	0.000
450	11.7	13.2	5.6	10.7	2.370	1.926	1.231	0.519
460	11.1	0.0	11.0	2.4	0.000	0.215	0.000	4.652
472	10.5	1.7	4.3	7.6	0.381	1.762	0.216	0.568
480	10.1	6.5	0.0	0.0	0.000	0.018	0.000	56.250
490	8.7	0.0	18.6	15.3	0.000	0.822	0.000	1.216
500	9.7	0.0	4.2	2.7	0.000	0.634	0.000	1.577
509	9.8	2.0	2.9	13.2	0.679	4.571	0.148	0.219
520	9.4	8.6	0.0	6.4	0.000	0.000	1.333	0.000
530	8.9	10.0	0.0	2.6	0.000	0.000	3.920	0.000
540	8.3	8.9	0.0	4.4	0.000	0.000	2.023	0.000
550	7.8	10.8	17.3	10.8	0.627	0.627	1.000	1.594
560	9.3	7.2	24.6	6.9	0.292	0.279	1.045	3.582
570	19.6	20.2	4.9	17.2	4.083	3.479	1.174	0.287
580	22.1	6.7	18.9	14.6	0.353	0.772	0.458	1.296
590	31.1	17.2	12.1	15.7	1.424	1.297	1.098	0.771
600	20.9	0.6	4.5	15.0	0.136	3.341	0.041	0.299
610	20.1	7.5	14.8	18.2	0.503	1.228	0.410	0.815
620	24.4	2.3	1.9	12.5	1.211	6.421	0.189	0.156
630	30.6	30.2	36.3	21.2	0.834	0.586	1.423	1.707
640	28.8	3.8	11.0	12.7	0.343	1.148	0.298	0.871
650	26.4	9.5	19.9	17.5	0.479	0.881	0.544	1.135
660	26.8	15.6	43.0	14.0	0.363	0.325	1.118	3.081
670	28.5	23.7	46.6	29.4	0.508	0.631	0.804	1.584
680	28.1	23.9	39.0	18.7	0.612	0.480	1.275	2.082
690	33.5	35.6	59.3	28.4	0.600	0.479	1.252	2.086
700	29.9	21.5	43.3	24.5	0.498	0.566	0.879	1.766
710	29.7	19.2	41.6	20.4	0.462	0.491	0.940	2.035
720	24.8	15.2	28.4	16.3	0.535	0.575	0.930	1.741

Table C.6.1 Rare earth elements and thier ratios to Ce and Nd in core CD3814.

Depth(cm)	Age(ka)	Y(ppm)	La(ppm)	Ce(ppm)	Nd(ppm)	La/Ce	Nd/Ce	La/Nd	Ce/Nd
1	0.20	18.1	2.8	8.8	13.3	0.321	1.512	0.213	0.661
10	2.00	15.0	0.0	12.9	6.3	0.000	0.488	0.000	2.050
20	4.00	15.5	0.0	15.5	16.6	0.000	1.068	0.000	0.937
21	4.20	19.0	5.1	20.0	15.1	0.254	0.757	0.336	1.322
30	6.00	15.5	13.7	23.8	15.6	0.575	0.655	0.878	1.527
40	8.00	15.7	17.6	11.3	6.8	1.561	0.598	2.609	1.672
50	10.67	16.8	2.5	2.8	12.2	0.889	4.296	0.207	0.233
60	12.47	15.8	1.6	0.0	5.6	0.000	0.000	0.283	0.000
70	13.41	14.1	0.0	12.4	9.6	0.000	0.771	0.000	1.297
80	14.34	16.1	2.9	0.0	0.6	0.000	0.000	4.500	0.000
90	15.28	16.9	4.6	0.0	9.5	0.000	0.000	0.483	0.000
100	16.22	17.9	8.7	11.3	11.6	0.774	1.028	0.752	0.972
110	17.16	15.2	4.6	0.0	9.4	0.000	0.000	0.483	0.000
119	18.00	17.6	8.7	11.0	12.4	0.792	1.129	0.702	0.886
130	19.08	18.9	12.3	9.9	6.6	1.239	0.663	1.869	1.508
140	20.07	19.5	6.3	0.0	9.3	0.000	0.000	0.678	0.000
150	21.05	17.9	6.7	18.4	12.5	0.364	0.676	0.538	1.479
160	22.03	18.9	8.5	12.9	14.8	0.661	1.149	0.576	0.871
170	23.02	18.5	19.1	16.7	6.4	1.146	0.382	3.000	2.617
180	24.00	17.2	4.5	33.7	15.5	0.133	0.459	0.290	2.179
190	26.92	16.1	8.5	2.5	13.7	3.333	5.417	0.615	0.185
200	29.83	16.4	7.4	5.3	11.6	1.392	2.176	0.640	0.459
210	32.75	17.4	6.6	23.3	11.1	0.284	0.477	0.594	2.094
220	35.67	17.0	6.1	7.3	9.3	0.829	1.271	0.652	0.787
230	38.58	17.8	3.2	14.1	4.6	0.230	0.326	0.705	3.068
240	41.50	18.6	0.0	1.1	14.4	0.000	13.700	0.000	0.073
250	44.42	17.1	4.6	19.7	14.6	0.237	0.742	0.319	1.348
260	47.33	17.0	9.8	9.5	14.3	1.022	1.495	0.684	0.669
270	50.25	15.0	2.8	0.0	6.5	0.000	0.000	0.435	0.000
280	53.17	18.1	13.9	26.1	20.7	0.534	0.795	0.672	1.258
290	56.08	22.6	11.8	18.9	22.7	0.624	1.199	0.521	0.834
300	59.00	27.4	13.1	0.0	7.0	0.000	0.000	1.866	0.000
310	60.67	24.7	15.4	5.1	14.1	3.000	2.755	1.089	0.363
320	62.33	26.6	4.0	14.6	13.1	0.273	0.899	0.304	1.112
330	64.00	26.8	12.7	19.3	16.2	0.659	0.843	0.782	1.186
340	68.67	24.4	11.5	7.5	12.1	1.528	1.611	0.948	0.621
350	72.29	19.9	4.7	0.0	13.6	0.000	0.000	0.346	0.000
360	74.86	17.4	5.6	12.7	15.3	0.443	1.205	0.367	0.830
370	77.43	15.7	12.0	6.3	10.0	1.917	1.600	1.198	0.625
380	80.00	19.3	3.5	12.4	10.2	0.286	0.824	0.347	1.214
390	81.67	14.1	9.4	13.1	8.3	0.714	0.635	1.125	1.575
400	83.33	23.1	2.2	19.0	22.1	0.115	1.165	0.099	0.858
410	85.00	24.9	6.4	3.6	13.0	1.743	3.571	0.488	0.280
420	86.67	23.4	14.4	2.2	12.6	6.571	5.762	1.140	0.174
430	88.33	21.6	6.0	9.1	5.9	0.667	0.655	1.018	1.526
440	90.00	18.0	7.4	7.2	8.3	1.029	1.159	0.888	0.863
450	*****	20.3	4.4	18.6	14.2	0.235	0.765	0.307	1.307
460	*****	23.0	6.9	7.5	11.0	0.917	1.472	0.623	0.679
470	*****	20.0	2.3	19.8	18.5	0.115	0.932	0.124	1.073
480	*****	17.7	6.9	16.9	10.8	0.409	0.640	0.638	1.562
490	*****	13.3	22.2	19.3	16.5	1.149	0.851	1.350	1.175
500	*****	13.8	2.0	0.0	0.0	0.000	0.054	0.000	18.583
510	*****	13.6	0.8	16.2	20.5	0.051	1.268	0.040	0.789
520	*****	13.0	5.8	5.8	13.7	1.000	2.375	0.421	0.421
530	*****	12.9	0.0	24.8	9.6	0.000	0.386	0.000	2.591
540	*****	15.8	7.7	10.0	11.2	0.773	1.124	0.688	0.890
550	*****	11.5	8.4	5.1	9.3	1.653	1.816	0.910	0.551
560	*****	9.6	1.5	4.0	10.4	0.368	2.632	0.140	0.380
570	*****	11.2	4.9	0.0	1.2	0.000	0.000	3.917	0.000
580	*****	12.8	0.0	5.6	9.7	0.000	1.741	0.000	0.574
590	*****	12.2	7.5	2.3	12.8	3.273	5.636	0.581	0.177
600	*****	17.1	4.6	28.0	14.8	0.166	0.528	0.315	1.895
610	*****	41.7	27.0	52.9	26.2	0.511	0.495	1.031	2.020
620	*****	18.3	4.1	3.0	9.7	1.379	3.276	0.421	0.305

Table C.6.2 Rare earth elements and thier ratios to Ce and Nd in core CD3822.

Depth(cm)	Age(ka)	Y(ppm)	La(ppm)	Ce(ppm)	Nd(ppm)	La/Ce	Nd/Ce	La/Nd	Ce/Nd
1	0.57	26.2	8.8	24.5	16.4	0.357	0.670	0.533	1.493
5	2.83	25.8	13.4	32.2	11.2	0.415	0.347	1.196	2.882
10	5.67	27.2	14.5	9.2	16.0	1.578	1.747	0.903	0.572
15	8.50	24.8	20.3	25.8	28.1	0.785	1.089	0.721	0.919
20	11.33	22.2	13.9	26.0	23.3	0.533	0.896	0.595	1.116
30	17.00	23.7	15.4	19.3	23.8	0.797	1.232	0.647	0.812
40	17.71	25.3	17.6	29.1	22.3	0.603	0.765	0.788	1.308
50	18.42	25.8	17.2	19.4	14.0	0.887	0.723	1.227	1.383
60	19.14	27.0	12.2	24.0	25.1	0.509	1.045	0.487	0.957
70	23.83	18.6	11.6	8.6	3.3	1.358	0.383	3.548	2.613
78	27.29	26.7	11.8	22.1	21.5	0.537	0.976	0.550	1.025
81	28.59	27.5	18.5	21.6	19.8	0.859	0.920	0.934	1.087
90	32.49	25.9	12.2	8.7	18.5	1.413	2.138	0.661	0.468
100	36.82	24.9	16.9	15.2	13.4	1.113	0.879	1.266	1.137
110	39.00	27.8	23.1	45.7	27.9	0.506	0.612	0.827	1.635
120	41.83	25.3	15.5	31.7	19.8	0.488	0.624	0.783	1.603
130	44.67	27.1	17.6	22.8	23.0	0.771	1.010	0.764	0.991
140	47.50	26.2	10.7	21.5	14.9	0.497	0.693	0.717	1.442
150	50.33	32.8	16.0	33.4	23.7	0.480	0.711	0.676	1.407
160	53.16	22.6	12.9	23.4	20.1	0.550	0.859	0.640	1.164
170	56.00	24.0	18.5	21.5	23.7	0.861	1.104	0.779	0.905
180	64.00	26.6	16.7	28.6	26.9	0.583	0.940	0.620	1.064
190	71.25	29.3	15.4	35.6	31.2	0.434	0.878	0.495	1.139
200	78.49	29.4	15.4	21.3	15.4	0.719	0.719	1.000	1.390
210	85.74	31.0	19.5	23.6	16.7	0.829	0.708	1.170	1.412
220	92.98	30.0	22.8	41.9	23.1	0.545	0.553	0.986	1.810
230	100.23	30.9	12.7	28.1	21.5	0.453	0.766	0.592	1.306
240	107.48	29.1	4.4	42.0	29.7	0.106	0.706	0.150	1.416
250	114.72	29.2	15.9	20.9	17.5	0.758	0.837	0.906	1.195
260	122.00	23.9	12.1	31.4	23.7	0.386	0.755	0.511	1.324
270	127.00	23.6	12.3	24.4	16.9	0.504	0.693	0.728	1.443
280	132.00	23.8	20.1	23.0	16.1	0.870	0.699	1.245	1.430
290	137.00	23.7	11.4	33.1	23.4	0.345	0.706	0.489	1.416
300	142.00	25.0	8.7	28.1	19.3	0.309	0.687	0.450	1.456
310	147.00	23.2	6.6	22.5	22.1	0.292	0.986	0.296	1.015
320	152.00	21.5	1.6	35.4	16.1	0.045	0.453	0.100	2.207
330	156.00	23.8	14.0	19.9	20.3	0.704	1.016	0.693	0.984
340	160.00	23.6	10.7	14.0	14.8	0.769	1.062	0.725	0.942
350	164.00	23.8	12.6	30.6	21.2	0.411	0.693	0.593	1.443
360	168.00	23.7	13.1	25.3	14.2	0.519	0.562	0.924	1.779
368	172.00	23.4	16.9	36.4	14.4	0.464	0.396	1.173	2.526
380	176.00	24.6	16.0	24.4	17.8	0.656	0.727	0.903	1.376
390	180.00	25.8	11.9	29.8	14.9	0.399	0.500	0.797	2.000
400	184.00	26.6	14.3	23.1	15.0	0.621	0.650	0.957	1.540
410	187.28	27.0	23.8	27.5	21.5	0.863	0.780	1.106	1.281
420	189.86	30.9	17.3	36.5	28.8	0.473	0.789	0.600	1.268
430	192.43	35.1	17.6	27.3	21.9	0.645	0.801	0.806	1.249
440	195.00	32.4	18.4	30.2	24.1	0.609	0.797	0.764	1.255
452	199.15	27.0	19.1	37.7	24.6	0.506	0.653	0.774	1.531
460	201.92	29.1	13.5	23.2	16.6	0.582	0.714	0.816	1.401
470	205.38	29.5	22.5	30.4	28.8	0.738	0.946	0.780	1.057
472	206.07	30.9	3.0	14.2	22.8	0.214	1.603	0.133	0.624
482	209.53	27.3	20.0	30.6	29.1	0.652	0.950	0.687	1.052
492	213.00	25.7	17.1	31.0	16.4	0.551	0.530	1.039	1.888
502	219.00	29.5	17.6	34.8	21.9	0.506	0.630	0.803	1.586

Table C.6.3 Rare earth elements and thier ratios to Ce and Nd in core CD3826.

Depth(cm)	Age(ka)	Y(ppm)	La(ppm)	Ce(ppm)	Nd(ppm)	La/Ce	Nd/Ce	La/Nd	Ce/Nd
512	224.00	29.6	19.5	34.6	17.6	0.563	0.509	1.104	1.963
522	229.00	29.8	19.2	31.3	20.3	0.615	0.649	0.947	1.540
532	234.00	26.3	19.2	46.4	27.2	0.414	0.586	0.707	1.707
542	240.00	29.8	22.7	34.3	22.5	0.663	0.656	1.010	1.524
552	242.00	27.9	16.6	46.6	22.9	0.355	0.492	0.722	2.033
562	244.00	23.8	21.0	24.8	15.0	0.844	0.606	1.393	1.650
572	246.14	24.3	14.5	19.0	16.7	0.763	0.876	0.871	1.142
580	247.97	23.9	9.8	11.9	13.6	0.820	1.144	0.717	0.874
592	250.72	22.9	10.8	21.0	10.8	0.513	0.513	1.000	1.950
602	253.00	21.9	17.0	26.0	18.5	0.654	0.712	0.919	1.405
612	257.00	22.9	17.8	24.0	21.1	0.741	0.879	0.843	1.137
622	265.33	24.0	21.1	8.6	12.0	2.463	1.400	1.759	0.714
632	273.67	31.4	15.2	27.6	21.3	0.553	0.773	0.716	1.294
642	282.00	35.2	13.7	30.3	23.8	0.452	0.785	0.575	1.274
652	285.69	33.7	26.2	19.1	14.3	1.371	0.747	1.835	1.338
662	289.38	28.6	21.0	41.8	25.1	0.504	0.602	0.837	1.661
672	293.07	22.6	12.2	20.1	18.5	0.606	0.920	0.659	1.087
680	296.00	22.6	18.7	21.5	19.0	0.871	0.886	0.983	1.128
690	300.29	24.4	16.5	33.2	25.1	0.498	0.756	0.660	1.323
700	304.58	25.3	7.3	33.7	20.5	0.216	0.610	0.354	1.641
710	308.87	24.8	5.1	37.7	21.5	0.136	0.571	0.239	1.751
720	313.17	28.5	10.0	27.3	18.0	0.368	0.660	0.557	1.515
730	317.46	27.7	17.8	16.9	24.7	1.051	1.459	0.721	0.686
740	321.75	27.6	20.7	22.7	21.4	0.914	0.943	0.970	1.061
750	326.00	29.1	19.5	45.0	26.2	0.433	0.582	0.744	1.719
760	327.00	29.5	27.5	45.4	23.8	0.607	0.525	1.156	1.906
770	328.00	29.0	51.8	112.6	49.9	0.460	0.444	1.037	2.255
780	332.87	19.6	5.6	35.3	17.7	0.159	0.502	0.317	1.994
790	337.73	22.9	14.3	29.5	18.8	0.484	0.638	0.758	1.567
800	342.60	20.2	18.3	27.2	19.4	0.671	0.713	0.940	1.402
810	347.47	20.6	18.9	10.7	19.2	1.772	1.802	0.984	0.555
820	352.33	21.6	21.2	3.9	11.7	5.405	2.973	1.818	0.336
830	357.20	24.3	8.3	27.7	22.8	0.299	0.824	0.363	1.214
840	362.07	25.9	14.7	29.6	22.5	0.498	0.762	0.654	1.313
850	366.93	28.2	18.1	23.1	21.7	0.782	0.940	0.833	1.064
860	371.80	28.5	15.9	32.9	19.3	0.482	0.586	0.823	1.707
870	376.67	28.5	14.6	30.8	13.1	0.474	0.426	1.114	2.350
880	381.53	28.4	9.8	35.4	20.2	0.277	0.569	0.487	1.757
890	386.40	29.4	16.2	4.2	16.4	3.872	3.923	0.987	0.255
900	391.27	30.4	15.7	26.6	19.1	0.591	0.721	0.820	1.388
910	396.13	29.6	12.3	27.3	20.3	0.451	0.743	0.606	1.346
920	401.00	29.5	12.6	29.6	22.9	0.425	0.775	0.549	1.291
930	408.09	25.2	13.8	22.6	24.6	0.611	1.090	0.561	0.917
940	415.18	21.8	10.2	12.9	14.6	0.793	1.132	0.701	0.883
950	422.28	19.3	9.8	26.1	9.8	0.374	0.374	1.000	2.674
960	429.37	18.8	13.5	23.8	15.9	0.567	0.670	0.847	1.493
970	436.46	20.0	16.8	26.2	16.9	0.642	0.646	0.994	1.547
980	443.55	21.0	20.2	17.6	7.0	1.151	0.398	2.894	2.515
990	450.64	20.9	11.6	24.9	20.2	0.464	0.813	0.571	1.230
1000	457.74	20.6	3.5	21.2	10.3	0.165	0.485	0.340	2.062
1010	464.83	18.6	12.3	11.5	19.2	1.064	1.670	0.637	0.599
1020	472.00	19.9	9.2	35.6	13.6	0.258	0.383	0.674	2.612
1030	******	19.8	5.2	27.4	16.3	0.189	0.595	0.318	1.682
1040	******	19.3	12.2	12.8	12.2	0.950	0.950	1.000	1.052
1050	******	22.1	5.8	31.2	22.7	0.187	0.728	0.257	1.374
1060	******	23.0	12.6	38.0	22.3	0.332	0.587	0.567	1.705
1070	******	25.6	17.3	32.0	23.4	0.540	0.732	0.739	1.367

Table C.6.3 (Contd.) Rare earth elements and thier ratios to Ce and Nd in core CD3826.

Depth(cm)	Age(ka)	Y(ppm)	La(ppm)	Ce(ppm)	Nd(ppm)	La/Ce	Nd/Ce	La/Nd	Ce/Nd
1	0.15	16.8	15.1	15.0	12.4	1.007	0.831	1.212	1.204
10	1.55	16.4	17.7	31.7	19.3	0.558	0.610	0.916	1.640
20	3.10	17.5	8.4	33.0	22.6	0.254	0.684	0.371	1.462
21	3.25	16.2	20.0	25.2	15.2	0.791	0.604	1.310	1.655
30	4.64	17.4	14.6	26.5	20.9	0.551	0.789	0.697	1.267
40	6.19	16.2	10.9	30.4	20.6	0.360	0.678	0.531	1.474
50	8.13	16.3	13.3	8.4	8.3	1.577	0.987	1.597	1.013
60	10.06	14.8	12.6	21.3	11.4	0.593	0.538	1.103	1.860
70	12.00	15.0	15.6	31.0	20.8	0.502	0.669	0.750	1.495
80	12.69	14.8	22.0	26.4	12.8	0.833	0.484	1.723	2.067
90	13.38	13.9	11.0	19.1	13.7	0.579	0.719	0.805	1.391
100	14.07	15.7	9.8	17.4	14.0	0.564	0.804	0.702	1.244
110	14.75	16.1	14.2	17.5	10.3	0.811	0.591	1.371	1.691
120	15.44	14.8	15.5	0.6	7.7	24.333	12.167	2.000	0.082
130	16.13	15.6	10.2	16.0	8.2	0.640	0.513	1.247	1.948
140	16.82	15.2	16.7	26.1	11.1	0.641	0.424	1.510	2.356
150	17.71	15.5	19.5	23.7	15.5	0.821	0.655	1.253	1.527
160	18.59	17.1	13.4	5.9	11.1	2.291	1.891	1.212	0.529
170	19.48	16.3	14.7	20.5	14.4	0.719	0.703	1.022	1.422
180	20.23	16.0	15.6	18.4	16.2	0.849	0.884	0.961	1.132
190	20.99	15.9	12.3	37.0	16.0	0.332	0.434	0.767	2.307
200	21.74	16.7	10.6	33.5	21.3	0.316	0.636	0.498	1.572
210	22.49	14.4	15.9	19.3	16.0	0.822	0.828	0.993	1.208
220	23.25	15.4	8.0	29.8	20.5	0.268	0.689	0.389	1.451
230	24.00	14.3	16.0	24.4	11.1	0.657	0.452	1.452	2.212
240	28.38	14.2	11.5	26.9	12.5	0.429	0.464	0.923	2.154
250	32.75	15.9	17.0	17.2	8.4	0.988	0.488	2.025	2.051
260	37.13	16.7	14.0	29.2	16.5	0.478	0.565	0.846	1.769
270	41.50	15.8	10.1	27.0	15.2	0.376	0.565	0.667	1.771
280	45.88	15.6	19.3	23.4	12.8	0.824	0.548	1.504	1.826
290	50.25	18.5	12.1	20.3	21.6	0.596	1.062	0.561	0.941
300	54.63	16.7	15.3	26.6	13.3	0.573	0.498	1.151	2.008
310	59.00	15.1	8.6	16.7	17.5	0.519	1.051	0.494	0.952
319	*****	15.5	10.6	31.6	10.8	0.336	0.342	0.980	2.922

Table C.6.4 Rare earth elements and thier ratios to Ce and Nd in core CD3827.

Depth(cm)	Age(ka)	Y(ppm)	La(ppm)	Ce(ppm)	Nd(ppm)	La/Ce	Nd/Ce	La/Nd	Ce/Nd
9	2.49	10.1	11.2	7.1	8.7	1.565	1.217	1.286	0.821
11	3.04	10.3	14.5	12.9	3.2	1.129	0.250	4.516	4.000
13	3.59	9.6	1.7	0.0	6.5	0.000	0.000	0.254	0.000
15	4.14	9.8	0.0	0.0	4.7	3.375	0.000	0.000	0.000
17	4.70	9.7	4.6	15.7	14.7	0.291	0.940	0.310	1.063
19	5.25	9.5	7.9	10.1	6.3	0.784	0.629	1.246	1.590
21	5.80	10.1	4.5	2.9	14.2	1.536	4.893	0.314	0.204
23	6.35	8.4	12.6	6.2	7.3	2.051	1.186	1.729	0.843
25	6.91	8.2	3.1	17.1	6.0	0.183	0.354	0.517	2.828
27	7.46	8.4	11.6	12.4	9.1	0.933	0.731	1.276	1.368
29	8.01	7.5	1.3	0.0	0.2	0.000	0.000	6.000	0.000
31	8.56	7.1	2.8	0.0	11.3	0.000	0.000	0.250	0.000
33	9.12	7.9	18.7	4.5	8.4	4.163	1.860	2.238	0.538
35	9.67	8.7	4.5	20.0	10.7	0.225	0.534	0.422	1.873
37	10.22	7.0	9.5	2.8	11.0	3.370	3.889	0.867	0.257
39	10.77	7.3	4.2	16.4	2.8	0.255	0.172	1.481	5.815
41	11.33	6.3	5.2	7.7	3.5	0.685	0.452	1.515	2.212
43	11.89	6.2	0.8	0.0	1.9	0.000	0.000	0.444	0.000
45	12.01	7.7	5.4	5.9	10.9	0.929	1.857	0.500	0.538
47	12.13	8.0	0.0	19.7	12.5	0.000	0.633	0.000	1.580
49	12.25	6.2	12.4	17.0	4.9	0.728	0.290	2.511	3.447
51	12.37	6.4	5.0	0.0	1.3	0.000	0.000	4.000	0.000
53	12.49	7.3	12.1	0.0	0.0	0.000	0.161	0.000	6.200
55	12.61	5.7	1.1	1.0	1.1	1.100	1.100	1.000	0.909
57	12.73	6.4	2.2	2.5	8.1	0.875	3.250	0.269	0.308
59	12.90	6.3	0.0	0.0	11.9	1.000	0.000	0.000	0.000
61	13.08	5.7	0.0	4.3	10.9	0.000	2.537	0.000	0.394
63	13.25	7.7	0.6	0.0	6.7	0.000	0.000	0.094	0.000
65	13.42	8.0	0.0	0.0	2.6	0.470	0.000	0.000	0.000
67	13.60	8.8	0.0	19.7	5.2	0.000	0.263	0.000	3.800
69	13.77	7.5	0.0	15.0	10.3	0.000	0.688	0.000	1.455
71	13.94	8.4	7.5	0.0	7.8	0.000	0.000	0.960	0.000
73	14.12	8.7	2.4	8.3	11.0	0.288	1.325	0.217	0.755
75	14.29	8.1	10.7	4.2	11.2	2.575	2.700	0.954	0.370
77	14.46	8.7	24.1	0.0	4.5	0.000	0.000	5.395	0.000
79	14.63	8.8	3.7	20.8	17.1	0.180	0.820	0.220	1.220
81	14.81	7.8	0.0	1.5	7.2	0.000	4.929	0.000	0.203
83	14.98	9.4	0.0	0.0	5.8	0.700	0.000	0.000	0.000
85	15.15	9.0	1.0	8.1	0.0	0.128	0.000	0.000	0.000
87	15.33	9.5	0.0	0.0	4.9	0.060	0.000	0.000	0.000
89	15.50	10.3	0.5	11.8	13.6	0.044	1.149	0.038	0.870
91	16.03	10.0	0.0	7.4	8.8	0.000	1.183	0.000	0.845
93	16.56	8.8	4.6	14.0	14.3	0.328	1.022	0.321	0.978
95	17.09	9.2	6.1	4.1	5.8	1.513	1.436	1.054	0.696
97	17.63	10.8	17.1	0.5	10.4	32.600	19.800	1.646	0.051
99	18.16	10.7	0.6	0.0	10.7	0.000	0.000	0.058	0.000
101	18.69	8.6	0.0	0.0	10.7	0.538	0.000	0.000	0.000
103	19.22	9.4	3.7	14.4	13.4	0.254	0.928	0.273	1.078
105	19.75	8.8	8.1	0.0	0.0	0.000	0.279	0.000	3.586
107	20.28	9.5	6.0	3.6	15.3	1.657	4.200	0.395	0.238
109	20.81	9.8	8.6	0.0	2.1	0.000	0.000	4.150	0.000
111	21.34	9.5	5.4	4.5	8.4	1.209	1.884	0.642	0.531
113	21.88	8.7	2.0	9.0	3.1	0.221	0.349	0.633	2.867
115	22.41	9.1	0.0	0.0	5.0	1.618	0.000	0.000	0.000
117	22.94	9.8	0.0	2.0	3.7	0.000	1.895	0.000	0.528
119	23.47	9.8	12.1	8.0	8.1	1.506	1.013	1.487	0.987
121	24.00	8.5	0.0	1.5	12.8	0.000	8.786	0.000	0.114
123	*****	8.9	13.1	0.0	2.8	0.000	0.000	4.667	0.000

Table C.6.5 Rare earth elements and thier ratios to Ce and Nd in core P5.

Depth(cm)	Age(ka)	I(ppm)	Br(ppm)	I/Br	C-org(%)	I/C-org *10-4	Br/C-org *10-4
1	0.20	37.0	17.3	2.135	0.876	42.237	19.783
10	2.00	39.0	24.6	1.584	1.646	23.694	14.957
20	4.00	25.9	20.7	1.250	1.341	19.314	15.445
21	4.20	26.9	6.4	4.199	0.956	28.138	6.701
30	6.00	26.9	14.2	1.891	1.102	24.410	12.910
40	8.00	29.0	16.4	1.770	0.694	41.787	23.606
50	10.67	27.4	12.8	2.133	1.645	16.657	7.811
60	12.47	42.7	30.1	1.420	1.935	22.067	15.545
70	13.41	81.4	82.7	0.984	2.631	30.939	31.446
80	14.34	72.1	71.0	1.015	1.817	39.681	39.083
90	15.28	67.9	97.9	0.693	1.069	63.517	91.607
100	16.22	55.7	76.3	0.730	1.515	36.766	50.380
110	17.16	45.1	50.1	0.900	1.668	27.038	30.056
119	18.00	55.3	57.3	0.965	1.999	27.664	28.653
130	19.08	46.2	60.8	0.760	1.080	42.778	56.274
140	20.07	35.7	38.9	0.918	1.371	26.039	28.352
150	21.05	40.6	38.1	1.066	1.470	27.619	25.906
160	22.03	38.8	27.6	1.404	1.024	37.891	26.995
170	23.02	31.2	22.4	1.394	0.679	45.950	32.963
180	24.00	18.4	0.0	0.000	0.540	34.074	0.000
190	26.92	25.5	30.6	0.832	0.785	32.484	39.024
200	29.83	17.6	13.6	1.294	0.512	34.375	26.570
210	32.75	20.2	12.0	1.678	0.754	26.790	15.968
220	35.67	19.6	37.2	0.526	0.582	33.677	63.984
230	38.58	21.1	60.0	0.351	0.982	21.487	61.138
240	41.50	34.9	66.2	0.527	1.040	33.558	63.652
250	44.42	35.4	59.7	0.593	1.099	32.211	54.311
260	47.33	19.6	40.8	0.480	1.301	15.065	31.384
270	50.25	16.1	54.9	0.293	2.659	6.055	20.633
280	53.17	19.2	28.3	0.678	2.163	8.877	13.096
290	56.08	20.9	27.4	0.763	1.521	13.741	18.007
300	59.00	20.2	34.0	0.594	1.934	10.445	17.574
310	60.67	27.0	23.8	1.135	0.851	31.727	27.943
320	62.33	18.4	18.5	0.993	1.450	12.690	12.782
330	64.00	14.7	21.1	0.696	1.307	11.247	16.154
340	68.67	15.7	24.1	0.652	0.808	19.431	29.815
350	72.29	15.7	23.1	0.679	1.120	14.018	20.656
360	74.86	6.8	17.7	0.385	0.939	7.242	18.834
370	77.43	8.6	16.5	0.520	0.550	15.636	30.078
380	80.00	15.1	21.9	0.688	0.960	15.729	22.846
390	81.67	10.0	17.0	0.587	0.430	23.256	39.641
400	83.33	9.9	11.3	0.880	1.133	8.738	9.934
410	85.00	13.2	21.1	0.625	1.459	9.047	14.466
420	86.67	7.4	9.2	0.805	0.696	10.632	13.210
430	88.33	8.2	19.0	0.432	0.500	16.400	37.956
440	90.00	13.2	23.0	0.573	1.010	13.069	22.809
450	*****	6.1	23.1	0.264	0.639	9.546	36.147
460	*****	7.2	22.6	0.318	2.153	3.344	10.502
470	*****	6.0	20.0	0.300	1.546	3.881	12.951
480	*****	10.6	15.4	0.687	1.156	9.170	13.338
490	*****	2.0	9.7	0.206	1.222	1.637	7.963
500	*****	0.0	7.7	0.000	1.599	0.000	4.809
510	*****	3.9	10.2	0.381	1.284	3.037	7.962
520	*****	5.0	9.2	0.544	1.912	2.615	4.806
530	*****	1.4	10.3	0.135	2.190	0.639	4.722
540	*****	0.0	10.6	0.000	0.868	0.000	12.251
550	*****	2.7	9.8	0.274	1.049	2.574	9.382
560	*****	11.1	13.9	0.797	1.391	7.980	10.006
570	*****	5.6	3.3	1.712	1.414	3.960	2.314
580	*****	5.5	5.9	0.935	*****	*****	*****
590	*****	5.1	6.6	0.775	0.868	5.876	7.581
600	*****	4.5	8.7	0.519	1.049	4.862	6.273
610	*****	3.3	4.1	0.802	1.391	3.235	6.234
620	*****	2.8	8.7	0.323	1.414	2.334	2.909

Table C.7.1 I and Br data and thier ratios to organic carbon in core CD3822.

Depth(cm)	Age(ka)	I(ppm)	Br(ppm)	I/Br	C-org(%)	I/C-org *10-4	Br/C-org *10-4
1	0.57	113.7	93.9	1.211	1.493	76.155	62.871
5	2.83	107.6	93.5	1.151	1.279	84.128	73.103
10	5.67	85.2	101.5	0.839	1.361	62.601	74.609
15	8.50	61.5	67.3	0.913	1.144	53.759	58.856
20	11.33	65.9	64.0	1.029	1.458	45.199	43.930
30	17.00	80.3	88.1	0.912	1.451	55.341	60.691
40	17.71	119.2	194.4	0.613	2.187	54.504	88.895
50	18.42	90.0	155.0	0.581	2.386	37.720	64.964
60	19.14	105.3	176.5	0.597	2.396	43.948	73.662
70	23.83	66.1	87.9	0.752	1.848	35.768	47.578
78	27.29	77.1	105.0	0.735	2.153	35.810	48.752
81	28.59	61.3	63.8	0.960	1.876	32.676	34.021
90	32.49	55.6	55.5	1.003	1.489	37.340	37.246
100	36.82	45.9	41.2	1.113	1.292	35.526	31.910
110	39.00	35.0	41.1	0.851	1.481	23.633	27.761
120	41.83	37.9	61.0	0.622	1.182	32.064	51.568
130	44.67	41.9	50.3	0.832	1.098	38.160	45.845
140	47.50	24.8	19.7	1.257	1.227	20.212	16.074
150	50.33	44.2	51.2	0.863	1.201	36.803	42.630
160	53.16	18.3	11.2	1.640	0.876	20.890	12.737
170	56.00	24.6	11.2	2.202	1.426	17.251	7.836
180	64.00	38.3	42.0	0.912	0.945	40.529	44.443
190	71.25	42.0	47.8	0.879	1.577	26.633	30.307
200	78.49	29.4	36.9	0.797	1.482	19.838	24.883
210	85.74	31.8	28.0	1.134	1.188	26.768	23.610
220	92.98	27.0	28.0	0.963	1.135	23.789	24.702
230	100.23	24.2	35.6	0.680	1.051	23.026	33.864
240	107.48	26.7	35.1	0.760	1.004	26.594	34.974
250	114.72	21.8	30.0	0.728	1.037	21.022	28.894
260	122.00	27.3	15.0	1.821	1.041	26.225	14.400
270	127.00	47.4	69.3	0.684	2.086	22.723	33.238
280	132.00	44.8	65.9	0.680	2.009	22.300	32.786
290	137.00	38.9	43.8	0.889	1.755	22.165	24.937
300	142.00	39.4	49.9	0.790	1.490	26.443	33.492
310	147.00	40.0	45.5	0.879	1.716	23.310	26.518
320	152.00	33.4	33.7	0.992	1.270	26.299	26.522
330	156.00	33.7	33.0	1.021	1.359	24.798	24.289
340	160.00	39.0	45.2	0.863	1.335	29.213	33.844
350	164.00	31.2	44.5	0.702	1.455	21.443	30.559
360	168.00	39.9	67.9	0.588	2.252	17.718	30.156
368	172.00	48.1	88.4	0.544	2.450	19.633	36.086
380	176.00	32.2	59.7	0.539	1.440	22.361	41.454
390	180.00	32.8	45.6	0.720	0.866	37.875	52.603
400	184.00	35.3	56.4	0.626	0.939	37.593	60.045
410	187.28	31.8	56.6	0.562	0.975	32.615	58.021
420	189.86	33.3	62.1	0.536	1.071	31.092	58.004
430	192.43	31.0	65.0	0.477	1.016	30.512	63.971
440	195.00	21.5	44.9	0.479	1.089	19.743	41.185
450	199.15	20.7	38.0	0.545	1.096	18.887	34.639
460	201.92	30.7	105.7	0.290	1.371	22.392	77.121
470	205.38	41.0	101.2	0.405	1.520	26.974	66.578
472	206.07	27.5	104.0	0.265	1.439	19.110	72.243
482	209.53	28.7	73.0	0.393	1.267	22.652	57.607
492	213.00	22.5	64.8	0.347	1.426	15.778	45.432
502	219.00	36.1	92.7	0.389	0.745	48.456	124.455

Table C.7.2 Halogen data and thier ratios to organic carbon in core CD3826.

Depth(cm)	Age(ka)	I(ppm)	Br(ppm)	I/Br	C-org(%)	I/C-org *10-4	Br/C-org *10-4
512	224.00	36.5	72.8	0.502	1.915	19.060	37.996
522	229.00	21.9	48.3	0.454	0.864	25.347	55.870
532	234.00	17.9	34.4	0.520	0.782	22.890	44.010
542	240.00	22.8	34.9	0.654	1.289	17.688	27.045
552	242.00	18.5	40.2	0.461	1.041	17.771	38.572
562	244.00	20.0	43.1	0.464	1.114	17.953	38.657
572	246.14	28.2	108.6	0.260	1.538	18.336	70.607
580	247.97	27.9	99.8	0.280	0.867	32.180	115.083
592	250.72	32.4	58.1	0.558	0.950	34.105	61.143
602	253.00	29.4	51.5	0.571	0.998	29.459	51.575
612	257.00	22.9	76.2	0.301	1.281	17.877	59.487
622	265.33	28.5	89.1	0.320	*****	*****	*****
632	273.67	26.6	95.0	0.280	1.162	22.892	81.755
642	282.00	24.1	57.3	0.421	1.152	20.920	49.721
652	285.69	27.0	58.6	0.461	1.095	24.658	53.497
662	289.38	26.2	71.0	0.369	1.136	23.063	62.499
672	293.07	22.3	53.0	0.421	1.287	17.327	41.186
680	296.00	20.5	63.4	0.323	1.626	12.608	38.997
690	300.29	29.2	79.1	0.369	1.944	15.021	40.686
700	304.58	37.2	85.1	0.437	1.445	25.744	58.901
710	308.87	35.0	73.7	0.475	1.734	20.185	42.525
720	313.17	27.9	58.8	0.475	1.628	17.138	36.101
730	317.46	21.0	50.4	0.417	1.489	14.103	33.819
740	321.75	26.0	59.5	0.437	1.544	16.839	38.522
750	326.00	21.4	66.5	0.322	1.780	12.022	37.343
760	327.00	25.0	67.0	0.373	1.018	24.558	65.831
770	328.00	1.0	17.2	0.058	0.245	4.082	70.148
780	332.87	13.1	39.8	0.329	0.977	13.408	40.733
790	337.73	29.1	79.0	0.368	1.508	19.297	52.418
800	342.60	41.5	127.0	0.327	2.441	17.001	52.042
810	347.47	32.4	55.4	0.585	2.183	14.842	25.392
820	352.33	31.5	43.0	0.732	2.136	14.747	20.153
830	357.20	30.0	62.5	0.480	2.499	12.005	25.002
840	362.07	29.2	64.9	0.450	2.459	11.875	26.386
850	366.93	19.5	44.6	0.437	1.178	16.553	37.879
860	371.80	20.8	39.4	0.528	1.293	16.087	30.478
870	376.67	21.1	42.4	0.498	1.542	13.684	27.495
880	381.53	23.2	39.5	0.587	1.615	14.365	24.486
890	386.40	26.1	42.0	0.622	1.843	14.162	22.764
900	391.27	19.4	40.4	0.480	1.928	10.062	20.979
910	396.13	21.0	38.8	0.541	0.796	26.382	48.790
920	401.00	27.6	42.5	0.650	0.825	33.455	51.459
930	408.09	20.7	35.4	0.585	0.728	28.434	48.610
940	415.18	12.9	30.2	0.427	0.821	15.713	36.831
950	422.28	10.3	36.3	0.284	1.417	7.269	25.632
960	429.37	24.9	78.3	0.318	1.404	17.735	55.760
970	436.46	32.7	128.7	0.254	1.055	30.995	121.963
980	443.55	27.2	71.5	0.380	1.592	17.085	44.908
990	450.64	21.6	44.5	0.486	1.671	12.926	26.603
1000	457.74	18.9	38.9	0.486	1.292	14.628	30.096
1010	464.83	19.7	47.2	0.417	1.478	13.329	31.951
1020	472.00	24.1	42.5	0.568	1.438	16.759	29.531
1030	*****	26.3	38.5	0.682	1.636	16.076	23.562
1040	*****	21.7	32.4	0.670	1.880	11.543	17.240
1050	*****	25.4	34.9	0.728	1.426	17.812	24.460
1060	*****	20.4	32.9	0.621	0.909	22.442	36.140
1070	*****	20.1	38.2	0.526	1.399	14.367	27.305

Table C.7.2 (Contd.) Halogen data and thier ratios to organic carbon in core CD3826.

Depth(cm)	Age(ka)	I(ppm)	Br(ppm)	I/Br	C-org(%)	I/C-org *10-4	Br/C-org *10-4
1	0.15	252.7	182.1	1.388	3.319	76.137	54.862
10	1.55	164.3	124.2	1.323	2.314	71.003	53.682
20	3.10	141.5	99.2	1.427	2.303	61.442	43.063
21	3.25	187.0	172.8	1.082	2.611	71.620	66.195
30	4.64	137.9	97.3	1.417	2.922	47.194	33.312
40	6.19	131.9	106.4	1.239	2.504	52.676	42.503
50	8.13	137.8	103.6	1.330	2.193	62.836	47.250
60	10.06	112.8	105.6	1.068	3.455	32.648	30.565
70	12.00	143.6	121.7	1.180	2.917	49.229	41.710
80	12.69	117.2	114.1	1.027	2.720	43.088	41.947
90	13.38	153.4	155.8	0.985	3.253	47.156	47.881
100	14.07	169.8	196.6	0.864	3.392	50.059	57.965
110	14.75	164.4	236.0	0.697	4.024	40.855	58.641
120	15.44	164.2	208.7	0.787	4.117	39.883	50.695
130	16.13	169.3	224.9	0.753	4.853	34.886	46.333
140	16.82	159.6	226.0	0.706	4.749	33.607	47.585
150	17.71	146.7	215.2	0.682	4.761	30.813	45.203
160	18.59	158.7	212.5	0.747	4.407	36.011	48.221
170	19.48	136.3	176.2	0.773	3.303	41.266	53.352
180	20.23	128.5	172.0	0.747	2.995	42.905	57.423
190	20.99	135.5	172.3	0.787	3.554	38.126	48.469
200	21.74	126.7	149.3	0.848	3.206	39.520	46.578
210	22.49	123.4	144.2	0.856	3.234	38.157	44.576
220	23.25	107.5	149.4	0.720	2.919	36.828	51.167
230	24.00	105.0	174.0	0.603	3.442	30.506	50.551
240	28.38	86.5	206.7	0.419	*****	******	******
250	32.75	86.0	199.3	0.432	3.114	27.617	63.990
260	37.13	75.4	100.8	0.748	2.328	32.388	43.286
270	41.50	78.8	133.1	0.592	2.917	27.014	45.642
280	45.88	57.3	91.5	0.626	1.841	31.124	49.716
290	50.25	64.3	76.8	0.838	1.820	35.330	42.177
300	54.63	58.9	124.4	0.474	2.630	22.395	47.288
310	59.00	55.5	88.0	0.630	2.193	25.308	40.149
319	*****	57.5	123.1	0.467	3.317	17.335	37.100

Table C.7.3 Halogen data and thier ratios to organic carbon in core CD3827.

Depth(cm)	Age(ka)	I(ppm)	Br(ppm)	I/Br	C-org(%)	I/Corg *10-4	Br/Corg *10-4
9	2.49	96.4	68.0	1.418	0.430	224.186	158.080
11	3.04	81.1	78.2	1.037	0.535	151.589	146.174
13	3.59	75.5	78.8	0.958	0.525	143.810	150.095
15	4.14	69.1	39.1	1.766	0.557	124.057	70.264
17	4.70	67.4	69.7	0.967	0.510	132.157	136.608
19	5.25	69.2	62.7	1.104	0.477	145.073	131.386
21	5.80	53.9	56.8	0.949	0.440	122.500	129.146
23	6.35	57.3	47.4	1.208	0.455	125.934	104.243
25	6.91	49.7	44.2	1.124	0.470	105.745	94.045
27	7.46	54.1	41.0	1.318	0.470	115.106	87.336
29	8.01	52.8	44.8	1.178	0.590	89.492	75.944
31	8.56	52.3	38.9	1.346	0.720	72.639	53.965
33	9.12	51.9	38.5	1.347	0.460	112.826	83.786
35	9.67	50.4	34.4	1.464	0.650	77.538	52.976
37	10.22	48.0	33.8	1.420	0.480	100.000	70.430
39	10.77	42.3	32.4	1.304	0.420	100.714	77.251
41	11.33	44.9	22.8	1.968	0.500	89.800	45.629
43	11.89	45.7	21.8	2.097	0.510	89.608	42.742
45	12.01	41.8	23.2	1.805	0.505	82.772	45.856
47	12.13	50.5	28.3	1.786	0.450	112.222	62.845
49	12.25	43.4	27.8	1.564	0.465	93.333	59.693
51	12.37	55.3	60.4	0.915	0.545	101.468	110.872
53	12.49	53.6	40.4	1.326	0.710	75.493	56.912
55	12.61	49.3	46.6	1.058	0.740	66.622	62.941
57	12.73	53.1	39.5	1.344	0.645	82.326	61.261
59	12.90	50.7	48.1	1.054	0.735	68.980	65.445
61	13.08	51.3	51.7	0.992	0.715	71.748	72.310
63	13.25	54.7	62.1	0.881	0.690	79.275	90.028
65	13.42	48.9	52.3	0.935	0.650	75.231	80.503
67	13.60	52.2	59.1	0.883	0.665	78.496	88.854
69	13.77	61.0	58.2	1.047	0.620	98.387	93.943
71	13.94	64.7	63.6	1.018	0.770	84.026	82.546
73	14.12	63.3	68.1	0.929	0.795	79.623	85.703
75	14.29	63.1	63.6	0.992	0.795	79.371	80.009
77	14.46	63.2	70.6	0.895	0.720	87.778	98.061
79	14.63	60.8	68.8	0.884	0.810	75.062	84.886
81	14.81	65.5	75.4	0.869	0.750	87.333	100.548
83	14.98	55.1	71.2	0.774	0.650	84.769	109.578
85	15.15	61.1	73.1	0.836	0.720	84.861	101.521
87	15.33	57.5	75.6	0.760	0.680	84.559	111.197
89	15.50	53.9	65.6	0.821	0.710	75.915	92.428
91	16.03	55.0	59.3	0.927	0.670	82.090	88.507
93	16.56	54.3	60.3	0.900	0.730	74.384	82.654
95	17.09	51.5	60.6	0.849	0.655	78.626	92.595
97	17.63	56.7	63.0	0.899	0.630	90.000	100.064
99	18.16	55.6	62.4	0.891	0.710	78.310	87.932
101	18.69	48.6	71.3	0.681	0.685	70.949	104.132
103	19.22	51.5	71.1	0.725	0.730	70.548	97.368
105	19.75	59.1	73.6	0.803	0.590	100.169	124.770
107	20.28	54.3	66.0	0.823	0.740	73.378	89.123
109	20.81	53.2	72.7	0.732	0.610	87.213	119.221
111	21.34	53.4	74.0	0.722	0.610	87.541	121.299
113	21.88	55.4	75.4	0.735	0.660	83.939	114.253
115	22.41	55.0	71.7	0.767	0.740	74.324	96.953
117	22.94	58.4	78.9	0.740	0.690	84.638	114.353
119	23.47	54.7	88.5	0.618	0.640	85.469	138.211
121	24.00	50.1	79.8	0.628	0.725	69.103	110.009
123	*****	57.9	70.3	0.824	0.705	82.128	99.706

Table C.7.4 Halogen data and thier ratios to organic carbon in core P5.

Depth(cm)	Age(ka)	LSR (cm/kyr)	DBD (g/cm2)	Al(Wt.%)	Al(MAR) (mg/cm2/kyr)	Siterrig (Wt.%)	Siterrig(MAR) (mg/cm2/kyr)
1	0.20	5.00	0.626	0.946	29.602	2.291	71.668
10	2.00	5.00	0.597	1.221	36.426	1.977	58.960
20	4.00	5.00	0.599	0.888	26.575	2.065	61.797
21	4.20	5.00	0.544	0.894	24.288	2.260	61.407
30	6.00	5.00	0.572	0.790	22.621	2.268	64.912
40	8.00		0.549	0.776		2.195	
50	10.67	3.75	0.553	0.876	18.172	2.693	55.882
55	12.00						
60	12.47	10.67	0.550	0.804	47.135	2.287	134.132
70	13.41	10.67	0.583	0.917	57.061	2.138	133.015
80	14.34	10.67	0.530	0.666	37.611	1.942	109.692
90	15.28	10.67	0.461	0.832	40.875	3.105	152.617
100	16.22	10.67	0.478	0.733	37.402	2.417	123.292
110	17.16	10.67	0.512	0.628	34.303	2.127	116.138
119	18.00		0.388	0.885			
130	19.08	10.17	0.426	0.806	34.913		
140	20.07	10.17	0.445	0.687	31.122	1.074	48.640
150	21.05	10.17	0.485	0.805	39.666	2.600	128.208
160	22.03	10.17	0.493	0.735	36.824	2.482	124.332
170	23.02	10.17	0.510	0.723	37.479	2.453	127.206
180	24.00		0.471	0.705		1.489	
190	26.92	3.43	0.531	0.710	12.922	4.330	78.804
200	29.83	3.43	0.605	0.715	14.816		
210	32.75	3.43	0.614	0.798	16.817	2.738	57.682
220	35.67	3.43	0.610	0.823	17.207	2.805	58.640
230	38.58	3.43	0.646	0.867	19.221	2.989	66.246
240	41.50	3.43	0.582	0.822	16.396	3.428	68.400
250	44.42	3.43	0.538	0.821	15.134	3.709	68.366
260	47.33	3.43	0.603	0.711	14.703	1.025	21.190
270	50.25	3.43	0.585	0.819	16.419	2.337	46.847
280	53.17	3.43	0.626	0.973	20.897	2.324	49.893
290	56.08	3.43	0.633	1.122	24.366	3.052	66.267
300	59.00		0.638	1.034		3.518	
310	60.67	6.00	0.635	1.234	47.001	3.154	120.110
320	62.33	6.00	0.583	1.234	43.144	5.028	175.793
330	64.00		0.679	1.356		5.042	
340	68.67	2.14	0.625	1.336	17.883	4.881	65.341
345	71.00						
350	72.29	3.89	0.611	1.705	40.490	4.371	103.785
360	74.86	3.89	0.657	2.074	52.966	6.592	168.338
370	77.43	3.89	0.662	1.747	45.018	8.592	221.350
380	80.00		0.711	2.609		6.086	
390	81.67	6.00	0.690	1.049	43.430	11.767	487.136
400	83.33	6.00	0.652	0.898	35.123	1.535	60.026
410	85.00	6.00	0.678	0.897	36.458	2.029	82.503
420	86.67	6.00	0.695	0.837	34.877	2.550	106.282
430	88.33	6.00	0.685	0.753		2.449	100.715
440	90.00		0.703	0.797		1.972	

Table C.8.1 Terrigenous Components and their Fluxes in core CD3822. (Ex.=excess; MAR=mass accumulation rate).

Depth(cm)	Age(ka)	LSR (cm/kyr)	DBD (g/cm2)	Al(Wt.%)	Al(MAR) (mg/cm2/kyr)	Siterrig. (Wt.%)	Siterrig(MAR) (mg/cm2/kyr)
1	0.57	1.76	0.359	6.269	39.717	16.240	102.884
5	2.83	1.76	0.356	6.437	40.442	16.679	104.784
10	5.67	1.76	0.332	6.631	38.848	17.330	101.536
15	8.50	1.76	0.379	5.993	40.080	15.975	106.844
20	11.33	1.76	0.392	5.701	39.437	15.335	106.081
30	17.00		0.375	5.652		15.319	
40	17.71	14.00	0.450	5.658	356.446	15.846	998.294
50	18.42	14.00	0.363	5.354	272.112	15.200	772.465
60	19.14	14.00	0.376	5.235	275.585	15.050	792.242
70	23.83	2.31	0.543	3.313	41.556	10.203	127.976
78	27.29	2.31	0.427	5.780	57.012	16.371	161.474
81	28.59	2.31	0.399	5.743	52.934	17.332	159.748
90	32.49	2.31	0.397	5.579	51.165	16.579	152.042
100	36.82	2.31	0.420	5.795	56.224	16.939	164.338
110	39.00		0.361	6.370		19.542	
120	41.83	3.53	0.434	5.675	86.950	16.697	255.801
130	44.67	3.53	0.395	6.219	86.716	18.588	259.175
140	47.50	3.53	0.419	6.155	91.042	20.749	306.896
150	50.33	3.53	0.351	7.064	87.529	21.798	270.081
160	53.16	3.53	0.489	6.064	104.671	21.674	374.122
170	56.00		0.467	6.628		24.906	
180	64.00		0.426	6.305		20.966	
190	71.25	1.38	0.384	6.203	32.869	18.440	97.715
200	78.49	1.38	0.380	6.008	31.506	18.280	95.859
210	85.74	1.38	0.372	6.875	35.296	19.987	102.603
220	92.98	1.38	0.341	6.358	29.920	18.336	86.285
230	100.23	1.38	0.349	6.930	33.375	20.232	97.444
240	107.48	1.38	0.400	6.057	33.432	17.172	94.787
250	114.72	1.38	0.342	7.190	33.932	21.057	99.380
260	122.00		0.404	6.005		16.736	
270	127.00	2.00	0.460	5.171	47.577	15.790	145.271
280	132.00	2.00	0.476	4.937	47.003	15.068	143.449
290	137.00	2.00	0.477	5.275	50.324	15.582	148.649
300	142.00	2.00	0.448	5.268	47.202	15.803	141.593
310	147.00	2.00	0.434	5.203	45.163	15.496	134.501
320	152.00		0.456	4.920		14.598	
330	156.00	2.50	0.451	4.823	54.384	14.594	164.550
340	160.00	2.50	0.434	4.777	51.827	14.059	152.542
350	164.00	2.50	0.369	5.703	52.610	17.324	159.813
360	168.00	2.50	0.391	5.870	57.375	17.244	168.556
368	172.00	2.50	0.397	7.213	71.593	20.392	202.395
380	176.00	2.50	0.426	5.098	54.297	15.698	167.182
390	180.00	2.50	0.410	5.288	54.206	16.107	165.093
400	184.00	2.50	0.420	5.652	59.350	17.428	182.992
410	187.28	3.89	0.412	5.629	90.211	17.356	278.166
420	189.86	3.89	0.384	6.352	94.883	20.010	298.906
430	192.43	3.89	0.379	6.811	100.410	20.416	300.995
440	195.00		0.364	7.400		21.985	
452	199.15	2.89	0.374	6.335	68.471	18.728	202.422
460	201.92	2.89	0.371	6.929	74.293	20.589	220.752
470	205.38	2.89	0.373	6.989	75.339	20.986	226.224
472	206.07	2.89	0.386	6.786	75.706	20.480	228.462
482	209.53	2.89	0.388	6.391	71.665	19.428	217.848
492	213.00		0.413	5.473		16.476	
502	219.00		0.408	6.417		19.229	

Table C.8.2 Terrigenous Components and their Fluxes in core CD3826. (Ex.=excess; MAR=mass accumulation rate).

Depth(cm)	Age(ka)	LSR (cm/kyr)	DBD (g/cm2)	Al(Wt.%)	Al(MAR) (mg/cm2/kyr)	Siterrig. (Wt.%)	Siterrig(MAR) (mg/cm2/kyr)
512	224.00	2.00	0.406	6.369	51.712	19.475	158.134
522	229.00	2.00	0.433	6.638	57.483	20.807	180.189
532	234.00		0.510	6.875		23.414	
542	240.00		0.449	6.555		21.333	
552	242.00	5.00	0.405	7.572	153.335	21.111	427.504
562	244.00	5.00	0.435	6.306	137.151	19.098	415.387
572	246.14	4.37	0.429	5.727	107.362	16.645	312.043
580	247.97	4.37	0.443	5.410	104.724	15.725	304.419
592	250.72	4.37	0.472	4.551	93.862	13.635	281.242
602	253.00		0.460	4.300		12.908	
612	257.00		0.455	4.406		13.401	
622	265.33	1.20	0.456	4.479	24.509	13.477	73.746
632	273.67	1.20	0.411	5.796	28.584	17.548	86.548
642	282.00		0.395	5.611		17.264	
652	285.69	2.71	0.436	6.020	71.126	18.166	214.642
662	289.38	2.71	0.417	5.462	61.730	16.967	191.734
672	293.07	2.71	0.458	4.528	56.203	13.595	168.736
680	296.00		0.490	4.290		12.787	
690	300.29	2.33	0.475	4.616	51.090	14.007	155.023
700	304.58	2.33	0.464	4.541	49.089	13.874	149.991
710	308.87	2.33	0.454	4.708	49.797	14.375	152.066
720	313.17	2.33	0.418	5.204	50.688	16.195	157.732
730	317.46	2.33	0.419	5.237	51.129	16.521	161.289
740	321.75	2.33	0.414	5.512	53.169	17.290	166.785
750	326.00		0.404	6.074		18.817	
760	327.00	10.00	0.494	5.885	290.710	18.505	914.165
770	328.00		0.941	7.113		22.409	
780	332.87	2.05	0.518	4.316	45.944	12.637	134.510
790	337.73	2.05	0.523	5.227	56.167	14.791	158.951
800	342.60	2.05	0.550	4.180	47.245	11.984	135.432
810	347.47	2.05	0.547	4.059	45.625	12.018	135.076
820	352.33	2.05	0.520	3.934	42.032	12.022	128.450
830	357.20	2.05	0.506	3.993	41.513	12.190	126.740
840	362.07	2.05	0.470	4.597	44.398	14.013	135.334
850	366.93	2.05	0.458	4.811	45.278	15.008	141.240
860	371.80	2.05	0.480	5.052	49.826	14.961	147.561
870	376.67	2.05	0.472	5.787	56.127	15.101	146.458
880	381.53	2.05	0.476	5.614	54.907	16.995	166.223
890	386.40	2.05	0.451	5.939	55.042	17.881	165.708
900	391.27	2.05	0.431	5.570	49.331	16.614	147.132
910	396.13	2.05	0.415	6.470	55.170	18.198	155.181
920	401.00		0.423	6.172		19.470	
930	408.09	1.41	0.457	5.565	35.862	16.578	106.823
940	415.18	1.41	0.478	5.528	37.257	16.041	108.116
950	422.28	1.41	0.505	5.004	35.632	14.560	103.675
960	429.37	1.41	0.509	4.642	33.316	13.645	97.927
970	436.46	1.41	0.490	4.284	29.599	12.746	88.059
980	443.55	1.41	0.520	3.895	28.557	11.751	86.157
990	450.64	1.41	0.515	3.561	25.859	10.688	77.611
1000	457.74	1.41	0.510	3.446	24.778	10.542	75.804
1010	464.83	1.41	0.532	3.301		9.797	
1020	472.00		0.534	3.401		9.886	

Table C.8.2 (Contd.) Terrigenous Components and their Fluxes in core CD3826. (Ex.=excess; MAR=mass accumulation rate).

Depth(cm)	Age(ka)	LSR (cm/kyr)	DBD (g/cm2)	Al(Wt.%)	Al(MAR) (mg/cm2/kyr)	Siterrig (Wt.%)	Siterrig(MAR) (mg/cm2/kyr)
1	0.15	6.46	0.343	7.885	174.773	19.916	441.438
10	1.55	6.46	0.386	7.791	194.343	19.846	495.039
20	3.10	6.46	0.431	7.522	209.494	19.155	533.505
21	3.25	6.46	0.442	7.335	209.498	19.118	546.065
30	4.64	6.46	0.452	7.037	205.549	18.230	532.477
40	6.19		0.444	7.031		18.135	
50	8.13	5.16	0.418	7.194	155.272	18.521	399.741
60	10.06	5.16	0.463	7.204	172.225	18.621	445.169
70	12.00		0.406	7.306		18.925	
80	12.69	14.52	0.447	7.548	490.006	19.351	1256.179
90	13.38	14.52	0.448	7.326	476.636	19.034	1238.364
100	14.07	14.52	0.468	7.084	481.506	18.196	1236.721
110	14.75	14.52	0.479	7.093	493.429	18.233	1268.395
120	15.44	14.52	0.506	6.793	499.208	17.713	1301.665
130	16.13	14.52	0.484	6.784	476.823	17.616	1238.271
140	16.82		0.494	6.767		17.691	
150	17.71	11.28	0.486	6.747	369.843	17.465	957.293
160	18.59	11.28	0.473	6.650	354.732	17.119	913.222
170	19.48		0.471	6.860		17.820	
180	20.23	13.27	0.466	7.200	445.350	18.635	1152.747
190	20.99	13.27	0.467	7.085	439.201	18.205	1128.518
200	21.74	13.27	0.517	7.114	488.220	18.339	1258.598
210	22.49	13.27	0.452	7.287	437.195	18.936	1136.183
220	23.25	13.27	0.488	7.579	490.928	19.363	1254.320
230	24.00		0.497	7.326		19.162	
240	28.38	2.29	0.473	6.954	75.182	18.298	197.827
250	32.75	2.29	0.512	7.292	85.340	19.090	223.405
260	37.13	2.29	0.518	7.707	91.250	20.114	238.147
270	41.50	2.29	0.534	6.773	82.668	18.078	220.659
280	45.88	2.29	0.520	6.982	82.980	18.116	215.320
290	50.25	2.29	0.565	7.938	102.515	20.336	262.619
300	54.63	2.29	0.571	7.743	101.059	20.398	266.229
310	59.00		0.552	6.350		16.793	

Table C.8.3 Terrigenous Components and their Fluxes in core CD3827. (Ex.=excess; MAR=mass accumulation rate).

Depth(cm)	Age(ka)	LSR (cm/kyr)	DBD (g/cm2)	Ti(Wt.%)	Ex.Ti (Wt.%)	Ti(MAR) (mg/cm2/kyr)	Ex.Ti(MAR) (mg/cm2/kyr)	Al(Wt.%)	Al(MAR) (mg/cm2/kyr)	Fe(Wt.%)	Fe(MAR) (mg/cm2/kyr)
9	2.49	3.62	0.765	0.0477	0.0179	1.320	0.495	0.544	15.067	0.392	10.858
11	3.04	3.62	0.735	0.0478	0.0190	1.271	0.506	0.525	13.961	0.377	10.044
13	3.59	3.62	0.713	0.0472	0.0163	1.219	0.421	0.565	14.576	0.382	9.855
15	4.14	3.62	0.711	0.0456	0.0151	1.173	0.390	0.555	14.296	0.383	9.855
17	4.70	3.62	0.715	0.0435	0.0153	1.126	0.396	0.515	13.336	0.364	9.412
19	5.25	3.62	0.725	0.0435	0.0148	1.141	0.387	0.524	13.755	0.365	9.592
21	5.80	3.62	0.700	0.0460	0.0182	1.166	0.462	0.507	12.852	0.365	9.237
23	6.35	3.62	0.666	0.0468	0.0201	1.128	0.485	0.488	11.754	0.364	8.786
25	6.91	3.62	0.660	0.0431	0.0180	1.029	0.429	0.458	10.949	0.361	8.637
27	7.46	3.62	0.641	0.0438	0.0170	1.016	0.395	0.489	11.339	0.373	8.662
29	8.01	3.62	0.628	0.0407	0.0154	0.924	0.350	0.461	10.480	0.351	7.971
31	8.56	3.62	0.628	0.0407	0.0176	0.924	0.401	0.421	9.562	0.364	8.270
33	9.12	3.62	0.630	0.0357	0.0139	0.813	0.316	0.398	9.075	0.347	7.913
35	9.67	3.62	0.610	0.0339	0.0127	0.748	0.280	0.387	8.539	0.357	7.892
37	10.22	3.62	0.604	0.0326	0.0129	0.713	0.282	0.360	7.873	0.363	7.942
39	10.77	3.62	0.618	0.0364	0.0174	0.814	0.389	0.347	7.758	0.373	8.340
41	11.33	3.62	0.604	0.0339	0.0154	0.740	0.337	0.337	7.364	0.357	7.814
43	11.89		0.613	0.0332	0.0164			0.306		0.357	
45	12.01	16.67	0.620	0.0363	0.0191	3.754	1.970	0.315	32.586	0.346	35.752
47	12.13	16.67	0.621	0.0351	0.0173	3.630	1.793	0.324	33.556	0.317	32.851
49	12.25	16.67	0.621	0.0338	0.0183	3.501	1.899	0.283	29.254	0.281	29.058
51	12.37	16.67	0.631	0.0355	0.0177	3.730	1.865	0.324	34.042	0.264	27.720
53	12.49	16.67	0.664	0.0344	0.0181	3.812	2.006	0.298	32.997	0.242	26.770
55	12.61	16.67	0.641	0.0312	0.0160	3.338	1.711	0.278	29.710	0.222	23.749
57	12.73		0.669	0.0300	0.0170			0.237		0.199	
59	12.90	11.55	0.658	0.0312	0.0183	2.369	1.389	0.236	17.902	0.205	15.582
61	13.08	11.55	0.654	0.0306	0.0177	2.310	1.339	0.235	17.729	0.197	14.897
63	13.25	11.55	0.653	0.0312	0.0171	2.354	1.289	0.258	19.451	0.201	15.150
65	13.42	11.55	0.664	0.0312	0.0176	2.393	1.347	0.249	19.101	0.193	14.789
67	13.60	11.55	0.717	0.0323	0.0191	2.677	1.582	0.241	19.994	0.180	14.940
69	13.77	11.55	0.695	0.0342	0.0206	2.747	1.656	0.248	19.930	0.180	14.437
71	13.94	11.55	0.689	0.0330	0.0190	2.627	1.513	0.256	20.348	0.176	14.037
73	14.12	11.55	0.696	0.0299	0.0150	2.403	1.207	0.272	21.839	0.189	15.175
75	14.29	11.55	0.675	0.0305	0.0157	2.382	1.223	0.271	21.160	0.188	14.676
77	14.46	11.55	0.715	0.0286	0.0144	2.361	1.192	0.258	21.347	0.198	16.340
79	14.63	11.55	0.686	0.0299	0.0153	2.369	1.211	0.267	21.133	0.199	15.766
81	14.81	11.55	0.686	0.0311	0.0160	2.467	1.265	0.277	21.962	0.206	16.343
83	14.98	11.55	0.694	0.0286	0.0144	2.294	1.158	0.259	20.740	0.206	16.517
85	15.15	11.55	0.702	0.0305	0.0162	2.472	1.316	0.260	21.113	0.216	17.534
87	15.33	11.55	0.736	0.0304	0.0163	2.584	1.386	0.257	21.887	0.195	16.542
89	15.50		0.715	0.0342	0.0192			0.274		0.212	
91	16.03	3.76	0.645	0.0316	0.0175	0.768	0.426	0.257	6.245	0.204	4.949
93	16.56	3.76	0.675	0.0262	0.0129	0.665	0.328	0.242	6.146	0.197	5.018
95	17.09	3.76	0.684	0.0286	0.0152	0.738	0.391	0.246	6.328	0.197	5.085
97	17.63	3.76	0.622	0.0286	0.0138	0.671	0.322	0.272	6.360	0.213	4.983
99	18.16	3.76	0.672	0.0324	0.0165	0.821	0.418	0.291	7.361	0.221	5.579
101	18.69	3.76	0.657	0.0298	0.0153	0.738	0.377	0.266	6.583	0.204	5.055
103	19.22	3.76	0.654	0.0318	0.0164	0.784	0.404	0.282	6.933	0.215	5.286
105	19.75	3.76	0.698	0.0286	0.0119	0.752	0.314	0.304	7.998	0.230	6.045
107	20.28	3.76	0.686	0.0286	0.0120	0.740	0.310	0.304	7.840	0.240	6.210
109	20.81	3.76	0.671	0.0304	0.0136	0.769	0.344	0.307	7.757	0.241	6.075
111	21.34	3.76	0.677	0.0297	0.0128	0.758	0.325	0.310	7.911	0.247	6.285
113	21.88	3.76	0.667	0.0329	0.0150	0.826	0.376	0.327	8.214	0.253	6.362
115	22.41	3.76	0.716	0.0348	0.0165	0.938	0.444	0.335	9.026	0.255	6.861
117	22.94	3.76	0.711	0.0342	0.0151	0.915	0.403	0.349	9.346	0.263	7.047
119	23.47	3.76	0.686	0.0341	0.0152	0.881	0.393	0.345	8.916	0.274	7.087
121	24.00		0.692	0.0347	0.0141			0.376		0.303	
123			0.720	0.0379	0.0160			0.400		0.335	

Table C.8.4 Terrigenous Components and their Fluxes in core P5. (Ex.=excess; MAR=mass accumulation rate).

Depth(cm)	CaCO3 (Wt.%)	ExSr/ExCa *10-4	Excess Ba (ppm)	Depth(cm)	CaCO3 (Wt.%)	ExSr/ExCa *10-4	Excess Ba (ppm)
1	94.143	34.022	1573.2	370	94.872	29.109	826.1
10	94.673	31.947	1444.5	381	95.563	29.024	863.1
11	93.584	33.372	1497.0	390	94.846	29.474	935.4
20	95.314	32.476	1537.3	400	95.508	29.508	911.6
30	93.813	32.512	1791.0	410	95.637	29.062	895.1
40	92.727	33.009	2334.8	420	95.237	30.209	1100.4
50	91.010	35.375	3009.2	430	95.682	29.274	870.6
60	91.766	36.354	2534.6	440	95.841	29.258	933.4
70	90.761	38.363	2481.3	450	96.212	29.533	968.9
80	91.650	37.994	2350.2	460	95.137	29.964	938.1
90	92.033	38.305	2344.2	472	94.974	29.981	967.8
100	91.404	38.316	2379.3	480	92.690	30.522	929.3
110	91.765	38.250	2385.6	490	95.099	29.398	903.8
120	91.755	38.552	2361.6	500	95.588	29.404	926.9
130	91.455	38.850	2381.2	509	94.362	29.624	884.2
140	92.170	38.559	2340.3	520	94.304	29.690	916.7
150	90.444	39.284	2344.3	530	95.776	29.235	943.3
160	91.593	38.811	2345.0	540	92.986	29.603	896.2
170	87.621	39.518	2212.5	550	95.862	28.629	908.1
180	96.093	36.108	2327.9	560	95.483	29.377	1091.4
190	92.039	37.280	2163.8	570	92.775	33.831	1559.0
200	91.796	37.123	2130.8	580	93.685	34.083	2028.7
210	92.032	36.313	2092.7	590	90.826	35.586	2747.8
219	92.279	36.437	2009.2	600	95.136	35.252	1366.5
230	91.948	36.743	2040.1	610	93.345	32.914	1863.5
238	91.502	36.557	2025.7	620	93.475	33.569	2118.6
250	92.312	36.511	2041.3	630	91.864	33.576	3140.1
260	92.022	36.482	2012.6	640	92.281	34.659	2763.6
270	92.040	36.522	2012.3	650	88.740	36.787	2436.3
280	85.225	39.320	1898.4	660	67.484	36.647	1421.7
300	91.912	34.538	1666.1	670	36.520	39.130	673.5
310	93.969	33.190	1524.3	680	40.929	37.952	673.3
320	93.944	31.316	1145.4	690	20.101	40.206	167.0
330	91.837	31.124	983.6	700	26.320	35.223	250.7
340	94.901	29.814	897.4	710	36.294	38.835	513.7
350	94.693	30.487	1080.8	720	55.302	36.609	779.9
360	93.770	30.414	1045.2				

Table C.9.1 Biogenic Components in core CD3814 (SF=salt free; SCF=salt and carbonate free).

Depth(cm)	Age(ka)	CaCO3 (Wt.%)	C-org (Wt.%SF)	C-org (Wt.%SCF)	SiO2 (Wt.%SF)	SiO2 (Wt.%SCF)	Excess Ba (ppm)	ExSr/ExCa *10-4	SiO2/ CaCO3	SiO2/ Ex.Ba
1	0.2	81.070	0.876	4.625	4.220	22.294	2560.1	38.103	0.052	16.485
10	2.0	83.443	1.646	9.940	3.914	23.638	2355.7	36.128	0.047	16.614
20	4.0	83.792	1.341	8.277	3.691	22.772	2387.6	36.443	0.044	15.459
21	4.2	79.516	0.956	4.668	4.236	20.678	2510.6	38.727	0.053	16.871
30	6.0	82.045	1.102	6.137	3.902	21.730	2284.4	36.748	0.048	17.080
40	8.0	82.213	0.694	3.904	3.755	21.113	2362.6	36.780	0.046	15.895
50	10.7	80.514	1.645	8.444	3.708	19.027	2002.4	36.550	0.046	18.516
60	12.5	81.884	1.935	10.684	3.157	17.426	2174.9	36.712	0.039	14.515
70	13.4	80.673	2.631	13.613	3.979	20.590	1822.9	34.860	0.049	21.830
80	14.3	82.283	1.817	10.256	3.958	22.342	2232.1	35.031	0.048	17.734
90	15.3	87.361	1.069	8.459	5.280	41.776	2463.0	32.006	0.060	21.438
100	16.2	78.407			5.852	27.103	2259.5	35.287	0.075	25.901
110	17.2	80.246	1.515	7.671	5.958	30.161	1723.1	33.942	0.074	34.577
119	18.0	75.268					2027.2			
130	19.1	75.18	1.668	6.721	11.740	47.299	2110.2	34.385	0.156	55.633
140	20.1	77.544	1.999	8.903	7.651	34.073	2320.1	36.862	0.099	32.978
150	21.0	76.995	1.080	4.696	7.878	34.244	1989.4	34.995	0.102	39.599
160	22.0	78.202	1.371	6.289	6.971	31.981	1994.0	36.401	0.089	34.961
170	23.0	83.156	1.470	8.729	6.463	38.369	1969.6	36.198	0.078	32.813
180	24.0	76.698	1.024	4.395	3.788	16.256	1868.6	35.478	0.049	20.272
190	26.9	82.423					1792.5	36.172		
200	29.8	83.204	0.679	4.043	2.186	13.016	1797.8	35.106	0.026	12.160
210	32.8	81.895	0.540	2.982	3.294	18.192	1880.5	35.214	0.040	17.515
220	35.7	80.333	0.785	3.993	3.984	20.259	2097.4	36.389	0.050	18.996
230	38.6	78.075			4.637	21.150	2212.7	37.006	0.059	20.957
240	41.5	76.349	0.512	2.163	5.960	25.201	2110.5	37.942	0.078	28.240
250	44.4	80.716	0.754	3.909	7.968	41.318	2215.5	38.309	0.099	35.963
260	47.3	81.674	0.582	3.177	4.876	26.609	2133.9	37.734	0.060	22.852
270	50.3	81.169	0.982	5.216	5.019	26.653	1906.8	36.268	0.062	26.322
280	53.2	78.522	1.040	4.844	4.291	19.977	2035.2	35.921	0.055	21.083
290	56.1	77.41	1.099	4.864	4.669	20.668	2135.3	36.866	0.060	21.866
300	59.0	78.083	1.301	5.937	4.897	22.345	2289.4	36.851	0.063	21.392
310	60.7	70.245	2.659	8.938	4.776	16.050	2173.5	36.301	0.068	21.972
320	62.3	70.822	2.163	7.413	5.748	19.700	2362.1	37.834	0.081	24.335
330	64.0	72.811	1.521	5.595	5.284	19.433	2367.4	37.029	0.073	22.319
340	68.7	73.975	1.934	7.430	6.030	23.169	2633.2	37.652	0.082	22.899
350	72.3	67.019	0.851	2.580	5.729	17.372	2432.1	36.197	0.085	23.558
360	74.9	63.468	1.450	3.970	5.507	15.076	2187.5	36.446	0.087	25.177
370	77.4	68.113	1.307	4.099	6.901	21.643	2035.0	36.143	0.101	33.913
380	80.0	51.462	0.808	1.665	5.892	12.139	2006.9	35.438	0.114	29.358
390	81.7	79.27	1.120	5.402	7.404	35.718	1657.9	35.988	0.093	44.662
400	83.3	80.963	0.939	4.933	4.417	23.201	2386.8	36.460	0.055	18.505
410	85.0	81.117	0.550	2.912	3.967	21.006	2596.8	37.393	0.049	15.275
420	86.7	81.954	0.960	5.321	3.972	22.010	2674.5	37.140	0.048	14.851
430	88.3	80.249	0.430	2.178	4.096	20.738	2535.5	36.362	0.051	16.154
440	90.0	83.067	1.133	6.692	3.824	22.586	2232.5	36.886	0.046	17.131
450		80.646	1.459	7.540	3.878	20.035	2346.7	35.697	0.048	16.524
460		82.742	0.696	4.033	3.991	23.125	2452.3	36.577		
470		82.482	0.500	2.851	3.479	19.858	2276.6	34.956		
480		83.903	1.010	6.272	5.370	33.360	1993.3	35.836		
490		85.235	0.639	4.326			1594.5	36.261		
500		84.541	2.153	13.928			1492.5	36.048		
510		85.919	1.546	10.983			1465.1	36.551		
520		84.407	1.156	7.416			1246.2	34.192		
530		77.865	1.222	5.520			1344.3	35.084		
540		75.092	1.599	6.419			1211.2	36.015		
550		77.117	1.284	5.613			1330.2	37.687		
560		76.613	1.912	8.174			1389.4	37.042		
570		81.568	2.190	11.880			1441.8	37.646		
580		82.432					1402.1	35.883		
590		78.451	0.868	4.028			1395.7	35.431		
600		58.798	1.049	2.546			1315.0	36.102		
610		83.561	1.391	8.462			1063.0	36.612		
620			1.414	1.414			1249.9	34.826		

Table C.9.2 Biogenic Components in core CD3822(SF=salt free; SCF=salt and carbonate free).

Depth(cm)	Age(ka)	CaCO3 (Wt.%)	C-org (Wt.% SF)	C-org (Wt.% SCF)	SiO2 (Wt.% SF)	SiO2 (Wt.% SCF)	Excess Ba (ppm)	ExSr/ExCa *10-4	SiO2/ CaCO3	SiO2/ Ex.Ba
1	0.57	10.388	1.493	1.666	5.146	5.742	3566.9	66.404	0.495	14.427
5	2.83	10.470	1.279	1.429	5.372	6.000	3763.6	64.724	0.513	14.273
10	5.67	11.871	1.361	1.544	5.686	6.452	3693.4	59.684	0.479	15.396
15	8.50	21.388	1.144	1.455	4.861	6.184	3368.8	48.037	0.227	14.431
20	11.33	25.428	1.458	1.955	4.134	5.544	3232.5	45.106	0.163	12.790
30	17.00	26.510	1.451	1.974	2.766	3.764	2516.3	41.537	0.104	10.994
40	17.71	22.157	2.187	2.809	2.084	2.677	2219.1	43.431	0.094	9.392
50	18.42	24.566	2.386	3.163	2.976	3.946	1916.4	39.903	0.121	15.532
60	19.14	22.697	2.396	3.099	3.288	4.254	2062.6	41.125	0.145	15.942
70	23.83	27.599	1.848	2.552	1.280	1.768	2175.8	30.594	0.046	5.882
78	27.29	19.988	2.153	2.691	3.944	4.929	2683.7	40.256	0.197	14.695
81	28.59	19.911	1.876	2.343	2.313	2.888	2684.2	40.639	0.116	8.616
90	32.49	23.080	1.489	1.935	2.488	3.235	2496.8	39.208	0.108	9.966
100	36.82	22.629	1.292	1.670	3.311	4.279	2602.2	38.691	0.146	12.724
110	39.00	13.656	1.481	1.716	3.053	3.535	2976.8	45.632	0.224	10.254
120	41.83	23.791	1.182	1.551	3.192	4.189	2530.9	39.282	0.134	12.614
130	44.67	15.979	1.098	1.307	3.212	3.823	2652.7	42.381	0.201	12.108
140	47.50	12.175	1.227	1.397	3.433	3.908	2724.8	41.874	0.282	12.598
150	50.33	4.227	1.201	1.254	2.859	2.985	2890.9	56.735	0.676	9.891
160	53.16	11.438	0.876	0.989	3.407	3.847	2401.7	38.643	0.298	14.187
170	56.00	4.861	1.426	1.499	3.816	4.011	2456.1	45.278	0.785	15.537
180	64.00	11.236	0.945	1.065	3.273	3.687	2866.7	44.086	0.291	11.416
190	71.25	12.725	1.577	1.808	4.218	4.833	3345.5	48.418	0.331	12.608
200	78.49	15.573	1.482	1.755	3.815	4.519	3223.3	45.254	0.245	11.836
210	85.74	11.845	1.188	1.347	4.697	5.328	3421.8	46.730	0.397	13.725
220	92.98	8.045	1.135	1.234	4.705	5.116	3077.6	58.311	0.585	15.287
230	100.23	5.820	1.051	1.116	4.770	5.065	3455.0	59.408	0.820	13.807
240	107.48	10.023	1.004	1.116	4.216	4.685	3225.9	45.424	0.421	13.068
250	114.72	4.082	1.037	1.082	4.279	4.461	4038.5	71.029	1.048	10.594
260	122.00	23.098	1.041	1.353	3.724	4.843	3123.2	42.915	0.161	11.925
270	127.00	25.851	2.086	2.813	4.721	6.367	2799.2	40.505	0.183	16.865
280	132.00	28.436	2.009	2.807	4.657	6.507	2731.3	39.100	0.164	17.050
290	137.00	26.064	1.755	2.374	5.185	7.013	2569.3	39.188	0.199	20.180
300	142.00	26.403	1.490	2.025	4.673	6.349	2680.7	39.958	0.177	17.431
310	147.00	26.787	1.716	2.343	4.729	6.460	2522.4	40.097	0.177	18.749
320	152.00	29.660	1.270	1.805	4.260	6.057	2305.6	38.208	0.144	18.478
330	156.00	29.834	1.359	1.937	3.737	5.326	2403.4	39.065	0.125	15.548
340	160.00	28.862	1.335	1.876	4.114	5.783	2607.4	41.550	0.143	15.776
350	164.00	18.953	1.455	1.796	3.742	4.617	2674.5	44.319	0.197	13.993
360	168.00	17.637	2.252	2.734	2.160	2.622	2203.8	41.346	0.122	9.801
368	172.00	15.286	2.450	2.892	1.820	2.149	2040.0	37.583	0.119	8.924
380	176.00	27.484	1.440	1.985	3.695	5.095	2473.3	41.082	0.134	14.938
390	180.00	26.267	0.866	1.175	3.604	4.888	2405.2	41.541	0.137	14.986
400	184.00	20.845	0.939	1.187	3.503	4.426	2518.4	44.192	0.168	13.910
410	187.28	20.118	0.975	1.221	3.343	4.184	2399.2	41.616	0.166	13.932
420	189.86	10.751	1.071	1.200	3.750	4.202	2763.6	51.248	0.349	13.569
430	192.43	6.311	1.016	1.084	5.107	5.451	3325.3	59.189	0.809	15.359
440	195.00	2.444	1.089	1.117	5.318	5.451	3191.4	75.295	2.176	16.662
452	199.15	15.164	1.096	1.292	4.309	5.080	3189.9	48.917	0.284	13.509
460	201.92	6.326	1.371	1.464	4.523	4.828	3228.2	60.828	0.715	14.011
470	205.38	4.906	1.520	1.599	4.707	4.950	3163.5	63.871	0.959	14.880
472	206.07	7.383	1.439	1.553	4.444	4.798	3567.3	61.817	0.602	12.457
482	209.53	11.848	1.267	1.437	4.065	4.611	3488.7	53.824	0.343	11.651
492	213.00	23.811	1.426	1.871	3.529	4.631	2898.6	45.093	0.148	12.173
502	219.00	12.683	0.745	0.854	3.493	4.001	2476.2	47.936	0.275	14.107

Table C.9.3 Biogenic Components in core CD3826(SF=salt free; SCF=salt and carbonate free).

Depth(cm)	Age(ka)	CaCO3	C-org	C-org	SiO2	SiO2	Excess Ba	ExSr/ExCa	SiO2/	SiO2/
		(Wt.%)	(Wt.%SF)	(Wt.%SCF)	(Wt.%SF)	(Wt.%SCF)	(ppm)	*10-4	CaCO3	Ex.Ba
512	224.00	11.939	1.915	2.175	2.876	3.266	2219.9	46.566	0.241	12.957
522	229.00	9.759	0.864	0.958	4.309	4.775	2146.7	49.857	0.442	20.071
532	234.00	5.619	0.782	0.829	4.287	4.542	2297.5	59.574	0.763	18.658
542	240.00	7.189	1.289	1.389	4.061	4.376	2716.2	57.160	0.565	14.952
552	242.00	7.661	1.041	1.128	4.537	4.913	3040.3	54.360	0.592	14.921
562	244.00	16.335	1.114	1.331	3.703	4.426	2552.1	47.105	0.227	14.509
572	246.14	22.965	1.538	1.996	3.257	4.228	2423.8	43.727	0.142	13.438
580	247.97	25.313	0.867	1.161	3.903	5.225	2386.7	42.573	0.154	16.351
592	250.72	34.845	0.950	1.458	3.635	5.579	2244.4	40.998	0.104	16.196
602	253.00	37.219	0.998	1.590	3.689	5.876	2246.7	41.669	0.099	16.418
612	257.00	36.129	1.281	2.006	3.852	6.030	2321.4	40.968	0.107	16.591
622	265.33	31.667			4.251	6.221	2142.5	39.922	0.134	19.840
632	273.67	19.380	1.162	1.441	4.182	5.187	2491.3	43.535	0.216	16.785
642	282.00	14.915	1.152	1.354	4.568	5.369	2451.3	43.282	0.306	18.636
652	285.69	14.600	1.095	1.282	5.287	6.191	2868.0	45.861	0.362	18.434
662	289.38	21.391	1.136	1.445	5.112	6.503	3001.8	44.163	0.239	17.030
672	293.07	35.203	1.287	1.986	4.981	7.687	2621.8	44.120	0.141	18.998
680	296.00	38.422	1.626	2.640	4.641	7.536	2446.2	43.721	0.121	18.972
690	300.29	33.096	1.944	2.906	4.649	6.949	2559.6	44.022	0.140	18.164
700	304.58	31.607	1.445	2.113	4.650	6.799	2624.6	45.008	0.147	17.719
710	308.87	30.318	1.734	2.488	5.087	7.300	2738.4	45.259	0.168	18.576
720	313.17	22.957	1.628	2.113	5.911	7.673	3052.8	49.107	0.257	19.363
730	317.46	20.476	1.489	1.872	5.321	6.691	2809.4	47.519	0.260	18.941
740	321.75	15.042	1.544	1.818	5.301	6.240	2987.9	56.568	0.352	17.742
750	326.00	13.804	1.780	2.066	5.519	6.403	3082.3	54.259	0.400	17.905
760	327.00	14.525	1.018	1.191	5.012	5.864	2616.0	52.125	0.345	19.159
770	328.00	10.440	0.245	0.273	2.598	2.901	1430.0	69.947	0.249	18.169
780	332.87	38.652	0.977	1.592	3.705	6.040	2555.5	45.024	0.096	14.500
790	337.73	32.358	1.508	2.229	2.664	3.938	1742.1	43.218	0.082	15.290
800	342.60	42.460	2.441	4.242	2.564	4.456	1828.4	41.701	0.060	14.024
810	347.47	41.751	2.183	3.747	3.409	5.853	1937.2	41.925	0.082	17.599
820	352.33	41.955	2.136	3.680	4.162	7.171	2259.1	41.119	0.099	18.424
830	357.20	40.686	2.499	4.213	4.121	6.949	2224.3	42.273	0.101	18.529
840	362.07	33.196	2.459	3.680	4.396	6.581	2260.7	42.862	0.132	19.447
850	366.93	30.089	1.178	1.685	4.463	6.384	2532.8	42.847	0.148	17.621
860	371.80	29.227	1.293	1.827	4.677	6.608	2457.3	43.530	0.160	19.032
870	376.67	27.568	1.542	2.129	4.662	6.437	2346.4	41.726	0.169	19.871
880	381.53	21.394	1.615	2.054	4.115	5.236	2674.0	44.558	0.192	15.391
890	386.40	18.235	1.843	2.254	4.683	5.728	2972.8	45.836	0.257	15.754
900	391.27	20.591	1.928	2.428	4.973	6.262	2866.8	46.447	0.242	17.346
910	396.13	15.002	0.796	0.937	4.848	5.704	3288.1	48.644	0.323	14.745
920	401.00	12.532	0.825	0.943	3.422	3.912	3358.7	51.469	0.273	10.187
930	408.09	22.988	0.728	0.946	4.356	5.656	3221.3	46.641	0.189	13.521
940	415.18	25.537	0.821	1.102	4.152	5.577	2951.4	45.254	0.163	14.070
950	422.28	31.253	1.417	2.061	3.969	5.773	2673.9	44.525	0.127	14.842
960	429.37	33.309	1.404	2.105	3.426	5.137	2322.8	42.137	0.103	14.750
970	436.46	35.883	1.055	1.645	3.634	5.668	2056.6	42.859	0.101	17.670
980	443.55	42.314	1.592	2.760	3.537	6.131	1959.3	42.790	0.084	18.053
990	450.64	46.436	1.671	3.119	4.527	8.452	1856.5	41.889	0.097	24.386
1000	457.74	47.229	1.292	2.448	3.777	7.157	1974.7	42.804	0.080	19.127
1010	464.83	49.628	1.478	2.935	3.830	7.604	1941.8	42.273	0.077	19.725
1020	472.00	49.434	1.438	2.845	4.099	8.106	1926.2	43.010	0.083	21.280
1030		46.815	1.636	3.077	4.232	7.956	1880.7	42.705	0.090	22.500
1040		46.990	1.880	3.546	4.267	8.050	2030.5	43.312	0.091	21.015
1050		39.989	1.426	2.376	4.428	7.378	1907.6	43.398	0.111	23.212
1060		38.654	0.909	1.481	4.093	6.671	2183.1	42.372	0.106	18.746
1070		26.392	1.399	1.901	4.533	6.159	2755.0	44.038	0.172	16.455

Table C.9.3 (Contd.) Biogenic Components in core CD3826(SF=salt free; SCF=salt and carbonate free).

Table C.9.4 Biogenic Components in core CD3827(SF=salt free; SCF=salt and carbonate free).

Depth(cm)	Age(ka)	CaCO3 (Wt.%)	C-org (Wt.%SF)	C-org (Wt.%SCF)	SiO2 (Wt.%SF)	SiO2 (Wt.%SCF)	Excess Ba (ppm)	ExSr/ExCa *10-4	SiO2/ CaCO3	SiO2/ Ex.Ba
1	0.15	1.848	3.319	3.381	6.334	6.453	1540.3	39.904	3.428	41.122
10	1.55	3.856	2.314	2.407	5.800	6.033	1637.5	41.637	1.504	35.421
20	3.10	7.504	2.303	2.490	5.568	6.019	1650.9	40.700	0.742	33.725
21	3.25	7.487	2.611	2.823	5.607	6.061	1565.7	37.440	0.749	35.814
30	4.64	11.356	2.922	3.296	5.533	6.242	1632.5	36.871	0.487	33.892
40	6.19	12.647	2.504	2.867	4.559	5.219	1493.5	37.231	0.360	30.526
50	8.13	11.840	2.193	2.487	3.966	4.499	1382.7	36.609	0.335	28.683
60	10.06	11.221	3.455	3.891	3.538	3.985	1258.8	32.367	0.315	28.103
70	12.00	10.106	2.917	3.245	3.482	3.873	1104.7	36.370	0.345	31.518
80	12.69	7.694	2.720	2.947	3.421	3.707	1047.9	35.231	0.445	32.649
90	13.38	8.477	3.253	3.554	2.935	3.207	935.4	36.491	0.346	31.376
100	14.07	9.366	3.392	3.743	3.446	3.802	900.5	36.364	0.368	38.271
110	14.75	9.962	4.024	4.469	2.804	3.114	895.6	35.369	0.281	31.303
120	15.44	12.116	4.117	4.685	2.729	3.106	1118.1	33.798	0.225	24.409
130	16.13	12.121	4.853	5.522	2.686	3.057	1193.4	33.050	0.222	22.510
140	16.82	11.579	4.749	5.371	2.778	3.142	1157.2	32.420	0.240	24.006
150	17.71	12.489	4.761	5.440	3.220	3.680	1097.6	31.678	0.258	29.339
160	18.59	12.931	4.407	5.061	3.305	3.795	1069.7	32.667	0.256	30.892
170	19.48	11.934	3.303	3.751	3.702	4.203	1063.4	31.170	0.310	34.810
180	20.23	8.775	2.995	3.283	3.950	4.330	1094.7	30.809	0.450	36.083
190	20.99	10.682	3.554	3.979	3.911	4.379	1027.0	29.945	0.366	38.086
200	21.74	9.623	3.206	3.547	4.085	4.520	1090.7	28.375	0.424	37.452
210	22.49	6.074	3.234	3.443	4.804	5.114	1063.4	30.385	0.791	45.171
220	23.25	7.568	2.919	3.158	4.574	4.948	934.3	28.590	0.604	48.953
230	24.00	5.626	3.442	3.648	5.898	6.250	1108.6	28.495	1.048	53.204
240	28.38	10.058			6.391	7.106	1088.7	30.303	0.635	58.703
250	32.75	6.960	3.114	3.346	5.231	5.622	943.3	31.853	0.752	55.451
260	37.13	2.830	2.328	2.396	5.410	5.567	1137.2	25.112	1.912	47.571
270	41.50	12.228	2.917	3.323	4.753	5.415	1125.4	28.737	0.389	42.233
280	45.88	10.865	1.841	2.066	6.776	7.602	1294.1	30.770	0.624	52.363
290	50.25	2.741	1.820	1.871	4.974	5.114	1219.3	27.158	1.815	40.795
300	54.63	5.629	2.630	2.787	3.679	3.898	1024.5	33.200	0.654	35.909
310	59.00	17.453	2.193	2.657	5.471	6.627	1042.3	30.245	0.313	52.487
319		15.046	3.317	3.905			1133.5	31.741		

Depth(cm)	Age(ka)	CaCO3 (Wt.% SF)	C-org (Wt.% SF)	C-org (Wt.% SCF)	SiO2 (Wt.% SF)	SiO2 (Wt.% SCF)	Excess Ba (ppm)	SiO2/ CaCO3	SiO2/ Ex.Ba
9	2.49	85.155	0.430	2.897	4.420	29.777	1086.9	0.052	40.669
11	3.04	83.885	0.535	3.320	4.607	28.588	1090.1	0.055	42.262
13	3.59	84.222	0.525	3.328	4.457	28.247	1116.5	0.053	39.918
15	4.14	87.299	0.557	4.386	3.807	29.974	1116.5	0.044	34.096
17	4.70	83.784	0.510	3.145	4.185	25.811	1110.5	0.050	37.691
19	5.25	84.357	0.477	3.049	4.126	26.377	1103.2	0.049	37.400
21	5.80	86.751	0.440	3.321	3.750	28.303	1104.4	0.043	33.953
23	6.35	87.687	0.455	3.695	3.873	31.451	1109.3	0.044	34.913
25	6.91	87.527	0.470	3.768	3.750	30.063	1058.1	0.043	35.440
27	7.46	87.474	0.470	3.752	4.499	35.920	1053.4	0.051	42.715
29	8.01	87.647	0.590	4.776	3.755	30.394	995.4	0.043	37.719
31	8.56	88.159	0.720	6.081	4.210	35.553	1002.8	0.048	41.983
33	9.12	87.714	0.410	3.337	3.498	28.469	970.4	0.040	36.045
35	9.67	88.153	0.650	5.486	4.277	36.097	924.5	0.049	46.258
37	10.22	87.182	0.480	3.745	4.757	37.112	850.4	0.055	55.942
39	10.77	88.741	0.420	3.730	3.730	33.127	803.8	0.042	46.402
41	11.33	88.261	0.500	4.259	3.317	28.253	745.9	0.038	44.465
43	11.89	90.444	0.510	5.337	3.382	35.398	707.1	0.037	47.833
45	12.01	89.971	0.505	5.035	3.260	32.501	763.6	0.036	42.687
47	12.13	89.402	0.450	4.246	3.666	34.589	764.8	0.041	47.932
49	12.25	85.896	0.465	3.297	3.196	22.664	730.5	0.037	43.756
51	12.37	86.783	0.545	4.124	4.017	30.391	823.9	0.046	48.755
53	12.49	90.096	0.710	7.169	3.149	31.791	731.0	0.035	43.074
55	12.61	90.852	0.740	8.089	2.782	30.408	655.9	0.031	42.409
57	12.73	92.153	0.645	8.220	2.506	31.932	551.6	0.027	45.424
59	12.90	92.251	0.735	9.485	2.263	29.210	548.0	0.025	41.306
61	13.08	90.929	0.715	7.882	2.223	24.511	543.4	0.024	40.918
63	13.25	91.278	0.690	7.911	2.438	27.951	572.2	0.027	42.604
65	13.42	92.213	0.650	8.347	2.041	26.215	567.8	0.022	35.952
67	13.60	92.148	0.665	8.469	1.859	23.675	610.6	0.020	30.442
69	13.77	91.931	0.620	7.683	1.916	23.741	670.5	0.021	28.571
71	13.94	91.685	0.770	9.260	1.956	23.526	700.0	0.021	27.948
73	14.12	91.891	0.795	9.803	1.620	19.974	702.3	0.018	23.065
75	14.29	91.767	0.795	9.656	2.225	27.027	671.7	0.024	33.128
77	14.46	91.906	0.720	8.895	2.190	27.049	725.7	0.024	30.171
79	14.63	92.013	0.810	10.141	3.224	40.359	718.1	0.035	44.890
81	14.81	91.394	0.750	8.714	2.333	27.110	734.2	0.026	31.777
83	14.98	92.227	0.650	8.362	2.057	26.467	692.3	0.022	29.717
85	15.15	91.871	0.720	8.858	2.119	26.072	703.8	0.023	30.114
87	15.33	91.567	0.680	8.064	2.294	27.208	718.0	0.025	31.956
89	15.50	91.565	0.710	8.417	2.371	28.109	722.1	0.026	32.834
91	16.03	92.260	0.670	8.657	2.154	27.835	680.3	0.023	31.669
93	16.56	91.777	0.730	8.878	2.102	25.569	661.5	0.023	31.783
95	17.09	91.937	0.655	8.123	2.091	25.930	645.1	0.023	32.408
97	17.63	91.727	0.630	7.615	2.047	24.747	641.4	0.022	31.918
99	18.16	90.704	0.710	7.638	2.581	27.770	703.9	0.028	36.675
101	18.69	90.423	0.685	7.153	2.565	26.779	711.4	0.028	36.052
103	19.22	90.371	0.730	7.582	2.681	27.849	761.9	0.030	35.195
105	19.75	90.097	0.590	5.958	3.000	30.289	715.7	0.033	41.910
107	20.28	87.472	0.740	5.907	3.013	24.050	702.5	0.034	42.888
109	20.81	90.053	0.610	6.133	2.646	26.603	702.4	0.029	37.670
111	21.34	89.682	0.610	5.912	2.741	26.562	696.4	0.031	39.357
113	21.88	89.513	0.660	6.294	2.754	26.262	707.2	0.031	38.941
115	22.41	88.939	0.740	6.690	2.858	25.835	715.7	0.032	39.925
117	22.94	90.701	0.690	7.420	2.943	31.650	721.7	0.032	40.782
119	23.47	88.503	0.640	5.567	3.277	28.499	752.2	0.037	43.556
121	24.00	88.021	0.725	6.052	3.164	26.413	743.0	0.036	42.583
123		87.786	0.705	5.772	3.778	30.932	771.2	0.043	48.987

Table C.9.5 Biogenic Components in core P5.

Depth(cm)	Age(ka)	CaCO3MAR (mg/cm2/kyr)	CorgMAR (mg/cm2/kyr)	SiO2MAR (mg/cm2/kyr)	ExBaMAR mg/cm2/kyr)	Palaeoproductivity (g/m2/yr)
1	0.20	2535.59	27.385	131.996	8.007	40.390
10	2.00	2488.90	49.088	116.739	7.027	68.966
20	4.00	2507.74	40.148	110.462	7.146	52.775
21	4.20	2160.99	25.985	115.112	6.823	33.206
30	6.00	2348.25	31.539	111.671	6.538	42.443
40	8.00					
50	10.67	1670.49	34.137	76.924	4.154	59.756
60	12.47	4802.50	113.513	185.147	12.756	67.423
70	13.41	5018.58	163.672	247.555	11.340	102.868
80	14.34	4647.37	102.624	223.571	12.607	58.604
90	15.28	4294.40	52.556	259.553	12.107	26.168
100	16.22	4000.14		298.578	11.528	
110	17.16	4381.19	82.737	325.292	9.408	45.771
119	18.00					
130	19.08	3258.35	72.303	508.802	9.146	34.913
140	20.07	3511.66	90.535	346.505	10.507	45.642
150	21.05	3796.12	53.260	388.403	9.809	29.323
160	22.03	3917.55	68.675	349.224	9.989	38.246
170	23.02	4311.93	76.239	335.127	10.213	44.065
180	24.00					
190	26.92	1500.20			3.263	
200	29.83	1724.66	14.075	45.314	3.726	29.561
210	32.75	1725.28	11.372	69.389	3.962	24.275
220	35.67	1679.41	16.416	83.296	4.385	34.775
230	38.58	1730.25		102.763	4.904	
240	41.50	1523.47	10.210	118.931	4.211	20.663
250	44.42	1487.86	13.893	146.872	4.084	25.922
260	47.33	1687.89	12.034	100.774	4.410	25.153
270	50.25	1627.01	19.689	100.604	3.822	40.056
280	53.17	1685.72	22.337	92.113	4.369	48.542
290	56.08	1680.62	23.855	101.365	4.636	52.507
300	59.00					
310	60.67	2675.09	101.275	181.869	8.277	125.359
320	62.33	2476.24	75.627	200.977	8.259	86.041
330	64.00					
340	68.67	990.28	25.886	80.719	3.525	90.956
350	72.29	1591.21	20.204	136.033	5.774	37.605
360	74.86	1620.76	37.039	140.642	5.586	74.107
370	77.43	1754.75	33.673	177.796	5.243	67.843
380	80.00					
390	81.67	3281.70	46.360	306.530	6.863	62.485
400	83.33	3166.57	36.731	172.746	9.335	46.615
410	85.00	3297.70	22.353	161.255	10.557	29.558
420	86.67	3415.43	40.021	165.531	11.146	54.183
430	88.33	3300.60	17.693	168.462	10.428	23.643
440	90.00					

Table C.10.1 Biogenic fluxes and Productivity data from core CD3822 (MAR=mass accumulation rate).

Depth(cm)	Age(ka)	CaCO3MAR (mg/cm2/kyr)	C-orgMAR (mg/cm2/kyr)	SiO2MAR (mg/cm2/kyr)	ExBaMAR (mg/cm2/kyr)	CaCO3MAR/ CorgMAR	Productivity (g/m2/yr)
1	0.57	65.810	9.458	35.708	2.260	6.958	23.360
5	2.83	65.777	8.037	36.997	2.364	8.184	19.700
10	5.67	69.550	7.973	36.823	2.164	8.723	18.211
15	8.50	143.045	7.648	35.416	2.253	18.703	19.832
20	11.33	175.902	10.086	31.037	2.236	17.440	27.158
30	17.00						
40	17.71	1395.896	137.773	140.713	13.980	10.132	50.196
50	18.42	1248.421	121.238	165.520	9.739	10.297	35.638
60	19.14	1194.760	126.126	188.652	10.857	9.473	38.564
70	23.83	346.181	23.179	16.954	2.729	14.935	65.442
78	27.29	197.153	21.234	41.874	2.647	9.285	47.212
81	28.59	183.518	17.293	23.095	2.474	10.612	35.925
90	32.49	211.661	13.652	24.736	2.290	15.504	28.240
100	36.82	219.542	12.539	34.635	2.525	17.509	27.284
110	39.00						
120	41.83	364.476	18.103	52.577	3.877	20.133	26.275
130	44.67	222.798	15.314	48.570	3.699	14.549	20.277
140	47.50	180.082	18.148	54.750	4.030	9.923	25.577
150	50.33	52.378	14.881	38.905	3.582	3.520	17.539
160	53.16	197.442	15.115	62.599	4.146	13.063	24.823
170	56.00						
180	64.00						
190	71.25	67.434	8.359	24.311	1.773	8.067	28.323
200	78.49	81.667	7.772	21.785	1.690	10.509	25.959
210	85.74	60.807	6.098	26.310	1.757	9.971	20.077
220	92.98	37.859	5.342	24.391	1.448	7.087	16.101
230	100.23	28.030	5.063	25.248	1.664	5.536	15.580
240	107.48	55.329	5.542	25.206	1.781	9.984	19.621
250	114.72	19.263	4.896	22.240	1.906	3.934	14.876
260	122.00						
270	127.00	237.832	19.187	46.453	2.575	12.395	53.129
280	132.00	270.706	19.123	47.288	2.600	14.156	54.823
290	137.00	248.653	16.743	52.752	2.451	14.851	48.002
300	142.00	236.573	13.351	44.881	2.402	17.719	36.179
310	147.00	232.508	14.892	44.126	2.189	15.613	39.137
320	152.00						
330	156.00	336.373	15.328	45.143	2.710	21.945	33.131
340	160.00	313.153	14.480	47.977	2.829	21.627	30.241
350	164.00	174.838	13.427	37.707	2.467	13.022	23.623
360	168.00	172.397	22.013	22.921	2.154	7.832	41.299
368	172.00	151.715	24.319	19.585	2.025	6.238	46.374
380	176.00	292.704	15.333	42.371	2.634	19.089	31.154
390	180.00	269.242	8.881	39.928	2.465	30.318	17.352
400	184.00	218.873	9.863	39.660	2.644	22.192	19.783
410	187.28	322.420	15.627	57.871	3.845	20.633	19.493
420	189.86	160.600	15.999	60.922	4.128	10.038	18.641
430	192.43	93.047	14.979	82.013	4.902	6.212	17.207
440	195.00						
452	199.15	163.904	11.845	50.800	3.448	13.838	18.214
460	201.92	67.829	14.700	52.934	3.461	4.614	22.439
470	205.38	52.889	16.387	55.360	3.410	3.228	25.198
472	206.07	82.355	16.050	53.892	3.979	5.131	25.577
482	209.53	132.854	14.208	49.521	3.912	9.351	22.800
492	213.00						
502	219.00						

Table C.10.2 Biogenic fluxes and Productivity data from core CD3826 (MAR=mass accumulation rate).

Depth(cm)	Age(ka)	CaCO3MAR (mg/cm2/kyr)	C-orgMAR (mg/cm2/kyr)	SiO2MAR (mg/cm2/kyr)	ExBaMAR (mg/cm2/kyr)	CaCO3MAR/ CorgMAR	Productivity (g/m2/yr)
512	224.00	96.944	15.549	25.262	1.803	6.235	37.979
522	229.00	84.514	7.484	40.119	1.859	11.292	19.502
532	234.00						
542	240.00						
552	242.00	155.129	21.088	99.393	6.157	7.356	20.044
562	244.00	355.293	24.227	86.566	5.551	14.665	24.721
572	246.14	430.540	28.826	65.711	4.544	14.936	33.370
580	247.97	490.039	16.780	81.067	4.620	29.204	20.037
592	250.72	718.728	19.592	80.022	4.629	36.685	24.968
602	253.00						
612	257.00						
622	265.33	173.281		24.898	1.172		
632	273.67	95.583	5.730	22.283	1.229	16.682	24.002
642	282.00						
652	285.69	172.509	12.940	67.123	3.389	13.332	24.813
662	289.38	241.738	12.838	62.333	3.392	18.830	23.545
672	293.07	436.937	15.970	66.147	3.254	27.360	32.148
680	296.00						
690	300.29	366.291	21.518	54.891	2.833	17.023	52.710
700	304.58	341.708	15.625	53.741	2.837	21.869	37.186
710	308.87	320.714	18.342	57.624	2.897	17.486	42.884
720	313.17	223.584	15.857	62.106	2.973	14.100	33.978
730	317.46	199.902	14.536	56.024	2.743	13.752	31.350
740	321.75	145.095	14.896	55.213	2.882	9.741	31.711
750	326.00						
760	327.00	717.545	50.293	263.320	12.923	14.267	28.573
770	328.00						
780	332.87	411.409	10.397	41.795	2.720	39.570	31.465
790	337.73	347.734	16.203	30.313	1.872	21.461	49.551
800	342.60	479.853	27.588	30.575	2.066	17.394	88.746
810	347.47	469.275	24.533	40.447	2.177	19.128	78.530
820	352.33	448.290	22.824	47.110	2.414	19.641	69.436
830	357.20	423.027	25.982	45.489	2.313	16.282	76.981
840	362.07	320.592	23.744	45.328	2.183	13.502	65.590
850	366.93	283.164	11.088	44.941	2.384	25.538	29.684
860	371.80	288.263	12.750	49.162	2.424	22.609	36.029
870	376.67	267.373	14.957	48.262	2.276	17.876	41.467
880	381.53	209.252	15.794	42.930	2.615	13.249	44.130
890	386.40	168.982	17.077	46.497	2.755	9.896	45.173
900	391.27	182.361	17.077	47.369	2.539	10.678	43.378
910	396.13	127.929	6.789	44.627	2.804	18.844	16.450
920	401.00						
930	408.09	148.129	4.694	30.038	2.076	31.557	18.521
940	415.18	172.114	5.532	29.842	1.989	31.115	22.861
950	422.28	222.539	10.087	30.002	1.904	22.062	44.048
960	429.37	239.056	10.073	26.092	1.667	23.732	44.223
970	436.46	247.915	7.286	26.719	1.421	34.024	30.795
980	443.55	310.244	11.672	27.473	1.437	26.580	52.336
990	450.64	337.192	12.131	34.852	1.348	27.797	53.824
1000	457.74	339.623	9.288	28.813	1.420	36.566	40.993
1010	464.83	372.273	11.089	30.386	1.457	33.572	51.017
1020	472.00						

Table C.10.2 (Contd.) Biogenic fluxes and Productivity data from core CD3826 (MAR=mass accumulation rate).

Table C.10.3 Biogenic fluxes and Productivity data from core CD3827 (MAR=mass accumulation rate).

Depth(cm)	Age(ka)	CaCO3MAR (mg/cm2/kyr)	C-orgMAR (mg/cm2/kyr)	SiO2MAR (mg/cm2/kyr)	ExBaMAR (mg/cm2/kyr)	Palaeoproductivity (g/m2/yr)
1	0.15	40.955	73.555	140.396	3.414	45.563
10	1.55	96.185	57.720	144.672	4.084	40.259
20	3.10	208.990	64.147	155.068	4.598	50.060
21	3.25	213.850	74.589	160.162	4.472	59.664
30	4.64	331.688	85.345	161.604	4.768	69.517
40	6.19					
50	8.13	255.544	47.328	85.604	2.984	45.082
60	10.06	268.266	82.593	84.576	3.010	86.793
70	12.00					
80	12.69	499.459	176.573	222.109	6.803	62.087
90	13.38	551.519	211.626	190.950	6.086	74.412
100	14.07	636.594	230.556	234.223	6.120	84.487
110	14.75	693.024	279.936	195.030	6.230	105.547
120	15.44	890.374	302.556	200.561	8.217	120.484
130	16.13	851.976	341.124	188.832	8.389	129.340
140	16.82					
150	17.71	684.543	260.936	176.508	6.016	129.086
160	18.59	689.830	235.094	176.285	5.707	113.071
170	19.48					
180	20.23	542.799	185.286	244.343	6.772	74.484
190	20.99	662.213	220.333	242.468	6.366	88.573
200	21.74	660.422	219.993	280.333	7.485	97.638
210	22.49	364.412	194.039	288.217	6.381	75.297
220	23.25	490.269	189.116	296.290	6.053	79.539
230	24.00					
240	28.38	108.742		69.097	1.177	
250	32.75	81.446	36.437	61.215	1.104	98.488
260	37.13	33.506	27.567	64.050	1.346	75.297
270	41.50	149.247	35.603	58.014	1.374	100.286
280	45.88	129.144	21.886	80.539	1.538	60.092
290	50.25	35.403	23.499	64.239	1.575	69.868
300	54.63	73.463	34.332	48.017	1.337	103.542
310	59.00					

Depth(cm)	Age(ka)	CaCO3MAR (mg/cm2/kyr)	C-orgMAR (mg/cm2/kyr)	SiO2MAR (mg/cm2/kyr)	ExBaMAR (mg/cm2/kyr)	Productivity (g/m2/yr)
9	2.486	2358.2	11.91	122.42	3.010	21.095
11	3.039	2231.9	14.23	122.58	2.900	24.237
13	3.591	2173.8	13.55	115.03	2.882	22.393
15	4.144	2246.9	14.34	97.98	2.874	23.602
17	4.696	2168.6	13.20	108.33	2.874	21.897
19	5.249	2214.0	12.52	108.29	2.895	21.002
21	5.801	2198.3	11.15	95.02	2.799	18.077
23	6.354	2114.1	10.97	93.37	2.674	16.961
25	6.906	2091.2	11.23	89.59	2.528	17.151
27	7.459	2029.8	10.91	104.41	2.444	16.180
29	8.011	1992.5	13.41	85.36	2.263	19.563
31	8.564	2004.2	16.37	95.71	2.280	23.771
33	9.116	2000.4	9.35	79.77	2.213	13.638
35	9.669	1946.6	14.35	94.44	2.041	20.306
37	10.221	1906.2	10.50	104.01	1.859	14.716
39	10.773	1985.3	9.40	83.44	1.798	13.469
41	11.326	1929.8	10.93	72.52	1.631	15.329
43	11.890					
45	12.010	9298.8	52.19	336.90	7.892	10.321
47	12.130	9255.0	46.58	379.48	7.917	9.211
49	12.250	8892.0	48.14	330.90	7.563	9.519
51	12.370	9128.5	57.33	422.51	8.666	11.533
53	12.490	9972.6	78.59	348.52	8.091	16.621
55	12.610	9708.0	79.07	297.23	7.009	16.179
57	12.730					
59	12.903	7012.4	55.87	172.05	4.165	18.879
61	13.076	6869.9	54.02	167.99	4.105	18.104
63	13.249	6885.7	52.05	183.90	4.317	17.444
65	13.423	7073.4	49.86	156.59	4.356	16.986
67	13.596	7632.6	55.08	153.98	5.058	20.291
69	13.769	7381.0	49.78	153.81	5.384	17.786
71	13.942	7297.7	61.29	155.71	5.571	21.644
73	14.115	7388.4	63.92	130.24	5.646	22.839
75	14.288	7155.8	61.99	173.52	5.238	21.463
77	14.461	7591.3	59.47	180.85	5.994	21.825
79	14.634	7291.9	64.19	255.46	5.691	22.580
81	14.808	7242.9	59.44	184.90	5.819	20.907
83	14.981	7394.1	52.11	164.94	5.550	18.547
85	15.154	7450.5	58.39	171.87	5.707	21.024
87	15.327	7785.5	57.82	195.08	6.105	21.859
89	15.500					
91	16.031	2240.3	16.27	52.31	1.652	23.131
93	16.563	2332.2	18.55	53.43	1.681	27.588
95	17.094	2367.4	16.87	53.84	1.661	25.385
97	17.625	2147.9	14.75	47.94	1.502	20.185
99	18.156	2294.7	17.96	65.31	1.781	26.606
101	18.688	2236.5	16.94	63.43	1.759	24.492
103	19.219	2225.1	17.97	66.02	1.876	25.875
105	19.750	2367.5	15.50	78.82	1.881	23.887
107	20.281	2259.0	19.11	77.81	1.814	28.877
109	20.813	2274.9	15.41	66.84	1.774	22.825
111	21.344	2285.7	15.55	69.85	1.775	23.214
113	21.875	2247.7	16.57	69.15	1.776	24.352
115	22.406	2397.4	19.95	77.03	1.929	31.445
117	22.938	2427.8	18.47	78.78	1.932	28.896
119	23.469	2285.7	16.53	84.62	1.943	24.975
121	24.000					
123						

Table C.10.4 Biogenic fluxes and Productivity data from core P5 (MAR=mass accumulation rate).

Depth(cm)	Age(ka)	Al (Wt.%)	C-org (Wt.%)	P total (Wt.%)	P detrital (Wt.%)	P phte. (Wt.%)	P-org (Wt.%)	P Ex.-1 (Wt.%)	PEx.1/Al *10-4	P Ex.-2 (Wt.%)	PEx.2/Al *10-4	Ptot./Al	Y/P *10-4	BAR (g/cm2/kyr)	P Ex.1MAR (mg/cm2/kyr)	PEx.2MAR (mg/cm2/kyr)
1	0.57	6.269	1.363	0.105	0.0503	0.0347	0.0332	0.0201	32.088	0.0216	34.469	0.017	248.939	0.634	0.127	0.137
5	2.83	6.437	1.167	0.105	0.0484	0.0355	0.0285	0.0209	32.396	0.0279	43.288	0.016	245.890	0.628	0.131	0.175
10	5.67	6.631	1.231	0.103	0.0447	0.0296	0.0300	0.0284	42.859	0.0280	42.211	0.015	264.648	0.586	0.166	0.164
15	8.50	5.993	1.050	0.087	0.0346	0.0202	0.0256	0.0323	53.820	0.0268	44.770	0.015	285.494	0.669	0.216	0.179
20	11.33	5.701	1.343	0.085	0.0349	0.0249	0.0328	0.0250	43.771	0.0171	30.022	0.015	262.432	0.692	0.173	0.118
30	17.00	5.652	1.331	0.088	0.0386	0.0244	0.0325	0.0251	44.367	0.0170	30.073	0.016	268.784			
40	17.71	5.658	2.041	0.097	0.0473	0.0288	0.0498	0.0207	36.641	-0.0003	-0.466	0.017	261.252	6.300	1.306	-0.017
50	18.42	5.354	2.180	0.098	0.0515	0.0289	0.0532	0.0179	33.518	-0.0063	-11.810	0.018	262.518	5.082	0.912	-0.321
60	19.14	5.235	2.198	0.106	0.0603	0.0334	0.0536	0.0125	23.783	-0.0078	-14.916	0.020	254.835	5.264	0.655	-0.411
70	23.83	3.313	1.750	0.118	0.0885	0.0675	0.0427			-0.0137	-41.317	0.035	158.157	1.254		-0.172
78	27.29	5.780	2.000	0.096	0.0453	0.0240	0.0488	0.0266	45.942	0.0018	3.112	0.017	278.571	0.986	0.262	0.018
81	28.59	5.743	1.732	0.097	0.0472	0.0234	0.0422	0.0269	46.802	0.0080	13.958	0.017	282.541	0.922	0.248	0.074
90	32.49	5.579	1.373	0.092	0.0429	0.0221	0.0335	0.0267	47.924	0.0153	27.461	0.016	282.300	0.917	0.245	0.141
100	36.82	5.795	1.199	0.091	0.0406	0.0243	0.0292	0.0264	45.595	0.0215	37.054	0.016	272.851	0.970	0.256	0.208
110	39.00	6.370	1.353	0.086	0.0307	0.0117	0.0330	0.0441	69.177	0.0227	35.689	0.014	321.566			
120	41.83	5.675	1.099	0.085	0.0357	0.0174	0.0268	0.0322	56.796	0.0229	40.262	0.015	295.877	1.532	0.494	0.350
130	44.67	6.219	1.013	0.089	0.0346	0.0160	0.0247	0.0384	61.703	0.0297	47.784	0.014	304.718	1.394	0.535	0.414
140	47.50	6.155	1.138	0.072	0.0181	0.0015	0.0278	0.0523	85.043	0.0261	42.415	0.012	363.940	1.479	0.774	0.386
150	50.33	7.064	1.094	0.093	0.0316	0.0051	0.0267	0.0567	80.245	0.0351	49.740	0.013	351.360	1.239	0.702	0.435
160	53.16	6.064	0.823	0.065	0.0124	0.0048	0.0201	0.0483	79.594	0.0330	54.408	0.011	344.534	1.726	0.833	0.569
170	56.00	6.628	1.335	0.059	0.0012	-0.0054	0.0326	0.0634	95.722	0.0254	38.379	0.009	405.970			
180	64.00	6.305	0.878	0.078	0.0233	0.0069	0.0214	0.0482	76.510	0.0338	53.538	0.012	338.919			
190	71.25	6.203	1.450	0.094	0.0397	0.0153	0.0354	0.0390	62.869	0.0189	30.469	0.015	311.317	0.530	0.207	0.100
200	78.49	6.008	1.361	0.088	0.0358	0.0093	0.0332	0.0433	72.021	0.0194	32.249	0.015	332.634	0.524	0.227	0.102
210	85.74	6.875	1.089	0.092	0.0318	0.0085	0.0265	0.0516	75.073	0.0336	48.885	0.013	337.191	0.513	0.265	0.173
220	92.98	6.358	1.030	0.083	0.0271	0.0021	0.0251	0.0535	84.220	0.0305	47.975	0.013	362.373	0.471	0.252	0.144
230	100.23	6.930	0.957	0.091	0.0300	0.0076	0.0233	0.0531	76.572	0.0373	53.832	0.013	340.690	0.482	0.256	0.180
240	107.48	6.057	0.927	0.099	0.0463	0.0209	0.0226	0.0321	53.014	0.0304	50.173	0.016	293.527	0.552	0.177	0.168
250	114.72	7.190	0.942	0.093	0.0299	0.0143	0.0230	0.0487	67.677	0.0399	55.546	0.013	314.633	0.472	0.230	0.188
260	122.00	6.005	0.962	0.079	0.0263	0.0145	0.0235	0.0380	63.299	0.0291	48.437	0.013	303.243			
270	127.00	5.171	1.950	0.080	0.0346	0.0162	0.0476	0.0290	56.114	-0.0023	-4.464	0.015	296.150	0.920	0.267	-0.021
280	132.00	4.937	1.883	0.080	0.0369	0.0161	0.0459	0.0271	54.934	-0.0027	-5.527	0.016	297.092	0.952	0.258	-0.026
290	137.00	5.275	1.646	0.082	0.0362	0.0187	0.0401	0.0275	52.069	0.0060	11.410	0.016	287.405	0.954	0.262	0.057
300	142.00	5.268	1.390	0.081	0.0353	0.0142	0.0339	0.0319	60.525	0.0122	23.141	0.015	306.847	0.896	0.286	0.109
310	147.00	5.203	1.596	0.084	0.0380	0.0210	0.0389	0.0245	47.058	0.0066	12.685	0.016	278.067	0.868	0.213	0.057
320	152.00	4.920	1.186	0.087	0.0443	0.0295	0.0289	0.0136	27.596	0.0141	28.696	0.018	246.303			
330	156.00	4.823	1.269	0.084	0.0420	0.0202	0.0309	0.0220	45.663	0.0113	23.340	0.017	282.615	1.128	0.248	0.127
340	160.00	4.777	1.242	0.082	0.0398	0.0180	0.0303	0.0238	49.797	0.0115	24.106	0.017	289.727	1.085	0.258	0.125
350	164.00	5.703	1.333	0.089	0.0388	0.0246	0.0325	0.0253	44.352	0.0174	30.511	0.016	268.571	0.923	0.233	0.161
360	168.00	5.870	2.074	0.091	0.0401	0.0278	0.0506	0.0236	40.180	0.0008	1.308	0.016	258.830	0.978	0.231	0.008
368	172.00	7.213	2.261	0.090	0.0268	0.0269	0.0551	0.0362	50.216	0.0080	11.065	0.012	260.505	0.993	0.360	0.079
380	176.00	5.098	1.337	0.080	0.0353	0.0138	0.0326	0.0308	60.346	0.0120	23.536	0.016	307.327	1.065	0.328	0.128
390	180.00	5.288	0.802	0.080	0.0334	0.0102	0.0196	0.0360	68.166	0.0267	50.526	0.015	324.061	1.025	0.369	0.274
400	184.00	5.652	0.871	0.081	0.0315	0.0093	0.0212	0.0402	71.061	0.0282	49.908	0.014	329.067	1.050	0.422	0.296
410	187.28	5.629	0.903	0.079	0.0295	0.0061	0.0220	0.0432	76.698	0.0272	48.389	0.014	343.035	1.603	0.692	0.437
420	189.86	6.352	0.985	0.079	0.0232	-0.0043	0.0240	0.0599	94.270	0.0316	49.688	0.012	392.036	1.494	0.894	0.471
430	192.43	6.811	0.933	0.086	0.0260	-0.0088	0.0228	0.0684	100.400	0.0368	54.094	0.013	409.920	1.474	1.008	0.543
440	195.00	7.400	0.996	0.086	0.0216	-0.0007	0.0243	0.0654	88.439	0.0405	54.670	0.012	374.739			
452	199.15	6.335	1.005	0.079	0.0231	0.0058	0.0245	0.0497	78.386	0.0309	48.814	0.012	344.416	1.081	0.537	0.334
460	201.92	6.929	1.256	0.081	0.0203	0.0026	0.0306	0.0580	83.774	0.0300	43.288	0.012	359.896	1.072	0.622	0.322
470	205.38	6.989	1.393	0.083	0.0222	0.0041	0.0340	0.0571	81.662	0.0272	38.873	0.012	353.542	1.078	0.615	0.293
472	206.07	6.786	1.323	0.086	0.0270	0.0033	0.0323	0.0561	82.648	0.0271	39.938	0.013	357.571	1.116	0.626	0.302
482	209.53	6.391	1.166	0.086	0.0304	0.0129	0.0284	0.0430	67.261	0.0275	42.994	0.014	316.022	1.121	0.482	0.308
492	213.00	5.473	1.320	0.082	0.0341	0.0129	0.0322	0.0350	63.996	0.0157	28.655	0.015	313.432			
502	219.00	6.417	0.689	0.089	0.0330	0.0098	0.0168	0.0464	72.265	0.0393	61.301	0.014	330.991			

Table C.11 Phosphorus Partitioning in core CD3826 (see chapter 6 for abbreviation datails).

Depth(cm)	Age(ka)	Al (Wt.%)	C-org (Wt.%)	P total (Wt.%)	P detrital (Wt.%)	P phte. (Wt.%)	P-org (Wt.%)	P Ex.-1 (Wt.%)	PEx.1/Al *10-4	P Ex.-2 (Wt.%)	PEx.2/Al *10-4	Ptot./Al	Y/P *10-4	BAR (g/cm2/kyr)	P Ex.1MAR (mg/cm2/kyr)	PEx.2MAR (mg/cm2/kyr)
512	224.00	6.369	1.770	0.083	0.0274	0.0034	0.0432	0.0524	82.234	0.0125	19.699	0.013	356.741	1.108	0.580	0.139
522	229.00	6.638	0.804	0.073	0.0146	-0.0074	0.0196	0.0655	98.630	0.0385	57.966	0.011	409.509	1.182	0.774	0.455
532	234.00	6.875	0.738	0.065	0.0047	-0.0060	0.0180	0.0661	96.166	0.0422	61.332	0.009	405.919			
542	240.00	6.555	1.203	0.082	0.0245	0.0017	0.0293	0.0557	84.903	0.0280	42.736	0.012	364.017			
552	242.00	7.572	0.963	0.087	0.0206	0.0118	0.0235	0.0545	71.932	0.0428	56.497	0.011	321.305	2.025	1.103	0.866
562	244.00	6.306	1.036	0.082	0.0269	0.0182	0.0253	0.0370	58.657	0.0299	47.417	0.013	289.381	2.175	0.804	0.650
572	246.14	5.727	1.429	0.087	0.0368	0.0215	0.0349	0.0287	50.031	0.0153	26.645	0.015	279.932	1.875	0.537	0.286
580	247.97	5.410	0.808	0.088	0.0402	0.0232	0.0197	0.0241	44.615	0.0276	51.079	0.016	273.262	1.936	0.467	0.535
592	250.72	4.551	0.890	0.084	0.0440	0.0221	0.0217	0.0177	38.911	0.0181	39.799	0.018	273.704	2.063	0.365	0.374
602	253.00	4.300	0.933	0.084	0.0469	0.0255	0.0228	0.0121	28.194	0.0149	34.575	0.020	259.532			
612	257.00	4.406	1.197	0.083	0.0446	0.0215	0.0292	0.0170	38.630	0.0094	21.228	0.019	275.492			
622	265.33	4.479		0.089	0.0500	0.0247	0.0000	0.0145	32.303	0.0392	87.500	0.020	268.739	0.547	0.079	0.214
632	273.67	5.796	1.075	0.086	0.0356	0.0017	0.0262	0.0490	84.550	0.0245	42.249	0.015	364.382	0.493	0.242	0.121
642	282.00	5.611	1.062	0.086	0.0366	-0.0091	0.0259	0.0582	103.807	0.0232	41.323	0.015	411.453			
652	285.69	6.020	1.019	0.083	0.0308	-0.0073	0.0249	0.0600	99.615	0.0278	46.205	0.014	404.227	1.182	0.709	0.329
662	289.38	5.462	1.053	0.081	0.0332	0.0041	0.0257	0.0437	80.042	0.0221	40.488	0.015	353.047	1.130	0.494	0.250
672	293.07	4.528	1.203	0.075	0.0351	0.0140	0.0293	0.0256	56.628	0.0103	22.729	0.016	302.188	1.241	0.318	0.128
680	296.00	4.290	1.528	0.071	0.0335	0.0104	0.0373	0.0272	63.334	0.0003	0.628	0.017	317.512			
690	300.29	4.616	1.823	0.073	0.0322	0.0069	0.0445	0.0335	72.531	-0.0041	-8.793	0.016	336.377	1.107	0.371	-0.045
700	304.58	4.541	1.352	0.072	0.0321	0.0037	0.0330	0.0360	79.372	0.0068	14.871	0.016	352.649	1.081	0.390	0.073
710	308.87	4.708	1.619	0.071	0.0294	0.0037	0.0395	0.0375	79.565	0.0017	3.610	0.015	352.068	1.058	0.396	0.018
720	313.17	5.204	1.509	0.074	0.0284	-0.0027	0.0368	0.0482	92.684	0.0087	16.770	0.014	385.318	0.974	0.470	0.085
730	317.46	5.237	1.381	0.079	0.0328	0.0040	0.0337	0.0418	79.787	0.0122	23.203	0.015	352.640	0.976	0.408	0.119
740	321.75	5.512	1.430	0.077	0.0286	0.0025	0.0349	0.0458	83.055	0.0133	24.213	0.014	359.888	0.965	0.442	0.129
750	326.00	6.074	1.645	0.085	0.0323	0.0072	0.0401	0.0460	75.692	0.0130	21.444	0.014	340.556			
760	327.00	5.885	0.957	0.095	0.0432	0.0154	0.0233	0.0361	61.272	0.0281	47.825	0.016	311.146	1.976	0.713	0.556
770	328.00	7.113	0.238	0.128	0.0658	0.0499	0.0058	0.0123	17.302	0.0564	79.325	0.018	226.744			
780	332.87	4.316	0.922	0.082	0.0445	0.0296	0.0225	0.0082	18.970	0.0153	35.415	0.019	238.159	1.109	0.091	0.169
790	337.73	5.227	1.424	0.091	0.0448	0.0290	0.0347	0.0167	31.923	0.0110	21.055	0.017	252.530	1.119	0.187	0.123
800	342.60	4.180	2.314	0.081	0.0440	0.0264	0.0564	0.0102	24.427	-0.0199	-47.486	0.019	250.098	1.177	0.120	-0.234
810	347.47	4.059	2.068	0.076	0.0400	0.0202	0.0504	0.0153	37.798	-0.0149	-36.755	0.019	272.462	1.171	0.180	-0.175
820	352.33	3.934	2.017	0.070	0.0358	0.0121	0.0492	0.0223	56.649	-0.0148	-37.528	0.018	307.540	1.113	0.248	-0.164
830	357.20	3.993	2.354	0.070	0.0350	0.0046	0.0574	0.0304	76.080	-0.0225	-56.304	0.018	347.515	1.083	0.329	-0.243
840	362.07	4.597	2.303	0.075	0.0343	0.0048	0.0562	0.0355	77.149	-0.0159	-34.681	0.016	348.018	1.006	0.357	-0.160
850	366.93	4.811	1.101	0.079	0.0373	0.0034	0.0269	0.0387	80.446	0.0152	31.679	0.016	355.853	0.980	0.379	0.149
860	371.80	5.052	1.213	0.080	0.0363	0.0039	0.0296	0.0403	79.748	0.0146	28.942	0.016	353.656	1.027	0.414	0.150
870	376.67	5.787	1.445	0.081	0.0304	0.0044	0.0352	0.0462	79.919	0.0154	26.599	0.014	351.623	1.010	0.467	0.155
880	381.53	5.614	1.514	0.087	0.0379	0.0107	0.0369	0.0384	68.401	0.0122	21.717	0.016	325.953	1.019	0.391	0.124
890	386.40	5.939	1.720	0.089	0.0369	0.0099	0.0420	0.0421	70.887	0.0100	16.870	0.015	330.455	0.965	0.406	0.097
900	391.27	5.570	1.793	0.087	0.0386	0.0054	0.0437	0.0433	77.762	0.0050	8.998	0.016	348.649	0.922	0.400	0.046
910	396.13	6.470	0.738	0.088	0.0315	0.0085	0.0180	0.0481	74.318	0.0386	59.695	0.014	335.756	0.888	0.427	0.343
920	401.00	6.172	0.766	0.087	0.0330	0.0076	0.0187	0.0464	75.233	0.0353	57.250	0.014	339.386			
930	408.09	5.565	0.681	0.077	0.0279	0.0089	0.0166	0.0398	71.434	0.0321	57.671	0.014	328.352	0.644	0.256	0.207
940	415.18	5.528	0.770	0.074	0.0252	0.0150	0.0188	0.0334	60.350	0.0296	53.539	0.013	295.861	0.674	0.225	0.199
950	422.28	5.004	1.334	0.076	0.0317	0.0235	0.0325	0.0202	40.453	0.0112	22.467	0.015	255.858	0.712	0.144	0.080
960	429.37	4.642	1.323	0.087	0.0460	0.0361	0.0323	0.0045	9.797	0.0084	18.004	0.019	216.894	0.718	0.033	0.060
970	436.46	4.284	0.991	0.091	0.0531	0.0367	0.0242	0.0007	1.736	0.0133	31.079	0.021	220.922	0.691	0.005	0.092
980	443.55	3.895	1.503	0.077	0.0427	0.0203	0.0367	0.0138	35.330	-0.0026	-6.601	0.020	273.321	0.733	0.101	-0.019
990	450.64	3.561	1.576	0.071	0.0396	0.0146	0.0384	0.0166	46.489	-0.0073	-20.426	0.020	295.046	0.726	0.120	-0.053
1000	457.74	3.446	1.218	0.072	0.0416	0.0164	0.0297	0.0138	39.915	0.0005	1.317	0.021	286.804	0.719	0.099	0.003
1010	464.83	3.301	1.398	0.070	0.0408	0.0196	0.0341	0.0093	28.058	-0.0052	-15.771	0.021	267.086	0.750	0.069	-0.039
1020	472.00	3.401	1.360	0.071	0.0413	0.0176	0.0332	0.0122	35.784	-0.0034	-10.066	0.021	279.739			
1030	*****	3.607	1.545	0.071	0.0396	0.0179	0.0377	0.0137	37.885	-0.0061	-16.980	0.020	278.251			
1040	*****	3.578	1.779	0.065	0.0342	0.0135	0.0434	0.0178	49.865	-0.0121	-33.782	0.018	295.310			
1050	*****	4.151	1.343	0.068	0.0318	0.0087	0.0328	0.0276	66.528	0.0036	8.583	0.016	324.236			
1060	*****	4.273		0.070	0.0331	0.0087		0.0286	67.032	0.0374	87.500	0.016	325.631			
1070	*****	5.391	1.304	0.074	0.0273	0.0055	0.0318	0.0417	77.359	0.0154	28.483	0.014	344.442			

Table C.11 (Contd.) Phosphorus Partitioning in core CD3826 (see chapter 6 for abbreviation datails).

Depth(cm)	Age(ka)	Ex.Cu (ppm)	Cu (ppmCF)	Ex.Ni (ppm)	Ni (ppmCF)	Ex.Zn (ppm)	Zn (ppmCF)	Ex.V (ppm)	V (ppmCF)
1	0.20	45.0	265.9	104.8	596.4	44.0	291.8	12.9	149.2
10	2.00	32.4	237.0	24.2	209.1	18.6	199.6	1.6	129.3
20	4.00	32.7	232.4	15.4	141.8	22.4	203.2	10.6	154.7
21	4.20	45.1	244.8	94.7	499.5	45.6	274.2	9.1	115.5
30	6.00	27.0	175.2	14.1	116.0	28.0	208.0	12.5	141.2
40	8.00	42.8	265.2	23.1	166.7	32.1	232.5	30.3	241.4
50	10.67	26.8	162.9	30.0	192.1	34.7	231.6	18.2	166.7
60	12.47	34.3	214.3	34.1	226.0	48.0	317.4	11.3	134.5
70	13.41	35.6	211.0	59.7	349.1	61.2	373.0	26.2	212.6
80	14.34	37.1	230.5	41.5	266.3	46.7	308.1	21.4	182.1
90	15.28	38.4	340.9	69.4	604.9	64.1	585.4	26.1	313.0
100	16.22	38.2	196.0	56.3	289.8	59.2	314.5	34.4	214.3
110	17.16	34.5	192.7	47.8	269.0	53.1	306.5	28.2	194.3
119	18.00	34.8	160.8	66.1	297.8	64.1	301.8	35.3	200.7
140	20.07	37.4	168.9	34.7	167.2	59.9	280.0	33.2	186.7
150	21.05	38.6	189.2	38.1	195.8	62.7	315.3	18.8	133.3
160	22.03	41.2	198.8	57.3	278.8	70.5	348.1	30.5	189.5
170	23.02	36.7	187.3	52.4	269.1	60.3	316.8	32.9	205.8
180	24.00	33.5	223.1	50.3	335.2	53.0	365.7	23.7	210.4
190	26.92	34.6	165.7	62.3	293.2	55.1	272.3	28.8	172.9
200	29.83	34.9	221.3	31.7	214.7	43.4	294.7	31.8	246.4
210	32.75	31.2	209.5	55.5	366.7	50.3	349.8	30.5	250.7
220	35.67	40.6	248.9	51.6	322.4	56.0	361.7	21.1	188.1
230	38.58	34.7	200.2	33.2	204.4	55.1	329.7	30.7	224.1
240	41.50	47.4	238.2	73.0	366.7	120.4	596.3	40.8	250.2
250	44.42	56.7	259.1	116.5	522.3	78.4	372.6	34.9	204.2
260	47.33	39.6	229.5	34.4	214.8	51.8	319.2	17.1	157.7
270	50.25	43.0	256.3	42.8	266.6	59.4	370.4	16.5	153.1
280	53.17	38.9	231.1	37.5	236.1	51.2	323.3	14.9	150.0
290	56.08	42.3	222.5	50.7	274.5	84.1	445.4	28.8	207.9
300	59.00	44.4	224.4	54.7	284.5	67.7	358.5	33.5	229.0
310	60.67	49.0	249.9	84.6	425.9	73.4	391.1	34.4	233.7
320	62.33	50.5	193.2	126.9	461.6	100.8	388.2	36.4	189.7
330	64.00	89.8	331.6	129.2	478.6	99.1	389.7	33.0	181.7
340	68.67	63.9	263.2	80.1	337.1	87.3	380.2	24.9	172.8
350	72.29	39.6	181.2	134.4	560.0	70.1	330.2	16.2	145.7
360	74.86	42.6	158.2	47.1	186.6	57.1	234.4	1.6	88.9
370	77.43	50.8	171.0	186.2	558.0	45.9	193.0	-0.6	90.5
380	80.00	30.4	126.1	82.9	306.5	47.5	214.0	6.3	108.8
390	81.67	13.5	58.1	40.1	128.4	53.1	173.2	1.1	89.6
400	83.33	39.6	219.5	80.5	431.5	63.3	365.5	21.6	186.3
410	85.00	46.3	269.7	63.5	373.6	57.9	360.0	21.8	190.9
420	86.67	47.7	279.2	68.8	404.8	57.4	360.2	11.6	138.8
430	88.33	56.0	336.2	79.9	482.2	73.7	463.7	22.6	200.7
440	90.00	65.6	353.6	79.1	433.1	65.5	376.8	21.7	172.1
450		36.8	243.6	35.7	251.0	47.5	336.3	18.7	187.2
460		40.6	236.7	66.4	383.8	43.6	281.8	14.1	150.3
470		36.6	239.5	29.3	211.3	34.1	255.2	10.3	139.0
480		30.0	194.0	16.0	125.6	29.4	215.8	13.1	140.9
490		31.7	210.9	15.4	117.0	23.7	176.4	19.0	157.9
500		21.6	159.8	10.4	90.7	16.3	138.9	22.7	192.6
510		19.3	138.5	11.9	97.9	25.0	190.4	38.9	290.9
520		20.1	156.4	15.3	129.4	26.9	219.3	18.3	168.8
530		18.4	132.0	23.2	169.6	19.1	151.8	20.9	173.6
540		17.5	102.5	16.2	109.0	12.5	106.2	38.6	242.6
550		24.8	114.7	29.1	139.9	21.3	117.7	30.8	167.9
560		20.7	100.5	28.6	140.1	21.9	116.4	20.2	116.9
570		20.8	97.1	27.6	130.5	26.3	130.0	18.1	101.5
580		47.0	266.1	35.2	207.8	26.5	167.5	11.6	95.2
590		21.5	135.6	13.2	95.0	19.5	138.6	14.9	122.7
600		15.0	87.7	20.4	121.7	31.6	184.4	18.3	137.0
610		5.6	42.7	4.6	55.1	44.8	170.4	-17.6	41.7
620		16.2	119.2	9.9	91.1	25.9	200.4	17.9	167.9

Table C.12.1 Excess metal and carbonate free metal data from core CD3822 (Ex.=excess; CF=salt and carbonate free).

Depth(cm)	Age(ka)	Ex.Cu (ppm)	Cu (ppmCF)	Ex.Ni (ppm)	Ni (ppmCF)	Ex.Zn (ppm)	Zn (ppmCF)	Ex.V (ppm)	V (ppmCF)
1	0.57	110.3	162.4	352.2	452.5	333.8	455.5	34.4	154.0
5	2.83	118.5	172.8	394.0	501.2	399.4	531.4	31.5	154.0
10	5.67	75.4	127.9	174.1	261.5	315.2	447.0	9.5	135.1
15	8.50	95.4	164.2	206.7	327.7	358.4	546.5	117.8	275.9
20	11.33	109.9	190.4	197.6	329.9	335.3	540.4	107.7	270.7
30	17.00	77.6	148.8	264.6	425.5	362.5	584.6	119.5	289.7
40	17.71	69.1	129.7	333.0	489.6	313.8	489.4	157.3	322.2
50	18.42	50.7	107.2	173.8	290.7	234.1	394.6	56.4	192.1
60	19.14	61.2	117.3	258.8	392.4	257.7	413.8	85.4	222.3
70	23.83	77.0	132.2	239.2	369.3	196.6	325.9	152.7	286.5
78	27.29	75.8	135.3	211.4	325.6	289.3	447.3	171.6	333.8
81	28.59	68.2	125.5	189.2	297.2	252.9	401.0	118.0	265.8
90	32.49	64.0	124.0	181.3	297.3	262.7	427.7	96.5	245.3
100	36.82	62.7	123.2	148.0	254.9	254.2	417.5	82.0	229.8
110	39.00	79.2	133.3	379.4	502.1	391.2	540.6	170.4	319.3
120	41.83	64.5	126.5	130.3	234.3	234.5	396.1	80.7	228.9
130	44.67	67.0	121.3	158.5	251.6	283.5	425.3	67.9	203.2
140	47.50	55.4	102.5	224.8	315.6	247.7	365.3	66.2	191.2
150	50.33	83.2	128.3	251.6	325.4	308.9	410.2	105.1	231.6
160	53.16	67.4	114.6	147.0	224.1	174.4	278.2	70.7	193.0
170	56.00	139.7	186.0	125.4	191.0	361.2	462.3	47.6	165.2
180	64.00	80.9	131.1	318.2	418.9	344.4	472.3	116.2	248.3
190	71.25	105.6	161.0	375.6	490.8	385.0	525.6	132.3	269.1
200	78.49	105.6	165.1	262.3	371.2	397.6	555.5	144.7	289.0
210	85.74	107.7	166.0	230.4	327.7	391.7	537.0	159.4	309.7
220	92.98	116.2	165.2	384.2	476.6	350.0	462.7	117.9	242.5
230	100.23	113.3	161.7	288.5	368.9	332.6	440.5	84.5	211.3
240	107.48	132.5	185.1	363.2	460.8	348.6	467.3	103.7	226.4
250	114.72	111.3	158.2	316.8	394.0	328.9	431.9	108.1	236.5
260	122.00	106.6	182.5	152.7	265.0	287.5	466.6	123.9	290.2
270	127.00	67.6	130.4	160.1	275.2	262.9	437.4	120.3	277.5
280	132.00	69.3	135.6	136.3	249.1	247.8	428.2	90.9	241.0
290	137.00	61.9	123.9	140.8	251.1	204.3	361.0	73.9	217.8
300	142.00	79.3	148.0	127.6	234.2	240.5	411.8	116.7	276.9
310	147.00	80.6	150.1	200.3	334.0	244.1	417.9	127.5	291.6
320	152.00	53.0	114.7	108.5	213.6	192.0	356.1	92.9	247.7
330	156.00	58.3	121.7	135.1	251.0	187.4	348.8	77.4	223.9
340	160.00	65.4	129.7	200.1	338.3	219.5	388.3	149.6	321.3
350	164.00	80.1	138.4	157.4	254.0	219.4	354.3	87.2	223.9
360	168.00	76.4	132.9	187.3	288.0	262.3	403.1	92.1	229.6
368	172.00	65.5	125.3	213.2	324.1	341.8	504.6	153.1	321.4
380	176.00	71.1	137.7	187.5	318.4	267.8	452.8	159.8	336.5
390	180.00	78.3	146.6	203.0	336.2	264.0	443.2	128.8	293.2
400	184.00	97.6	163.5	341.8	492.6	273.3	430.0	173.7	337.4
410	187.28	86.3	147.7	215.5	329.7	265.5	416.1	98.1	239.2
420	189.86	85.8	136.1	233.8	322.5	279.5	397.6	120.0	252.0
430	192.43	94.2	141.5	219.5	296.1	354.5	464.7	144.7	274.6
440	195.00	75.6	120.2	153.0	221.3	280.2	377.3	102.3	230.2
452	199.15	67.1	121.1	157.4	249.0	292.0	432.9	86.4	225.2
460	201.92	90.4	138.1	225.9	304.0	376.9	490.2	148.6	280.8
470	205.38	145.0	193.8	277.6	354.4	409.0	517.4	91.5	217.6
472	206.07	112.0	162.1	403.6	498.1	395.1	513.6	131.5	263.1
482	209.53	110.1	165.6	271.5	369.6	347.8	480.7	126.6	263.4
492	213.00	85.7	152.9	246.6	384.7	360.5	558.4	138.6	300.6
502	219.00	85.2	138.9	245.5	343.6	379.4	521.8	117.1	255.6
512	224.00	75.5	126.4	275.2	374.0	290.8	416.1	124.7	261.1

Table C.12.2 Excess metal and carbonate free metal data from core CD3826 (Ex.=excess; CF=salt and carbonate free).

Depth(cm)	Age(ka)	Ex.Cu (ppm)	Cu (ppmCF)	Ex.Ni (ppm)	Ni (ppmCF)	Ex.Zn (ppm)	Zn (ppmCF)	Ex.V (ppm)	V (ppmCF)
522	229.00	61.2	109.1	183.0	265.3	244.5	358.3	91.1	222.5
532	234.00	65.1	109.9	143.7	214.1	214.0	313.3	93.3	219.2
542	240.00	93.3	140.2	285.7	367.8	249.2	352.4	83.9	207.1
552	242.00	102.8	157.5	199.3	285.5	258.0	376.8	96.9	240.4
562	244.00	73.3	130.0	146.8	239.5	205.4	335.1	79.8	219.9
572	246.14	183.3	279.8	182.3	299.8	465.1	692.0	126.0	286.4
580	247.97	87.2	157.5	232.0	372.3	235.4	401.1	110.5	267.7
592	250.72	78.8	160.2	146.0	283.4	242.1	454.6	151.2	347.4
602	253.00	64.5	141.2	142.4	285.0	243.3	468.8	131.3	322.3
612	257.00	76.9	159.2	153.6	299.2	250.7	474.5	142.7	337.4
622	265.33	70.0	139.3	424.4	676.9	226.5	409.3	95.6	248.3
632	273.67	76.0	134.7	142.3	237.6	269.0	419.1	141.1	293.8
642	282.00	81.3	132.7	163.9	248.7	255.3	378.3	112.4	241.0
652	285.69	105.7	163.4	153.6	239.8	266.3	395.6	182.6	330.3
662	289.38	78.1	138.5	156.2	257.8	258.6	411.5	144.8	299.1
672	293.07	72.0	150.4	218.6	396.8	211.6	409.5	83.4	244.2
680	296.00	72.2	156.4	174.0	341.8	208.3	421.0	91.6	263.9
690	300.29	68.1	140.6	149.9	282.7	245.3	448.5	134.1	314.4
700	304.58	78.6	152.2	155.8	284.3	281.4	490.3	143.9	320.1
710	308.87	76.0	147.1	233.8	393.0	282.5	485.6	111.5	271.7
720	313.17	102.4	171.0	282.2	423.7	361.3	549.2	175.7	339.7
730	317.46	83.9	142.5	272.1	398.2	333.6	497.7	103.3	238.7
740	321.75	101.8	156.3	286.9	392.8	324.3	458.8	135.2	266.4
750	326.00	96.2	151.3	285.9	391.6	301.3	433.3	99.9	232.4
760	327.00	74.3	125.7	278.0	383.7	216.7	335.3	44.1	165.4
770	328.00	43.5	93.2	85.9	163.4	40.1	139.1	-29.7	98.0
780	332.87	79.5	169.1	178.7	351.2	228.8	456.5	67.8	226.8
790	337.73	54.2	123.5	128.6	255.8	263.9	481.9	131.4	321.9
800	342.60	50.7	128.9	181.5	377.2	164.3	371.9	93.3	282.2
810	347.47	54.0	131.9	169.7	350.6	185.1	400.5	75.7	245.2
820	352.33	57.6	137.4	165.8	343.3	201.9	428.3	84.6	257.7
830	357.20	61.7	141.9	161.6	329.7	208.4	431.3	91.8	266.0
840	362.07	70.5	144.3	207.4	369.0	241.6	443.3	115.7	286.9
850	366.93	79.4	152.3	217.0	368.9	290.3	497.0	140.3	314.4
860	371.80	93.0	171.5	234.0	391.2	316.5	531.9	146.7	325.3
870	376.67	61.5	129.8	140.3	261.5	248.2	437.5	73.0	232.8
880	381.53	93.2	158.7	340.1	493.3	312.3	482.1	111.4	259.7
890	386.40	88.1	148.6	205.2	312.8	339.5	501.4	121.8	269.0
900	391.27	85.2	146.7	236.3	357.2	319.7	485.9	119.2	266.0
910	396.13	100.4	160.9	284.6	399.5	372.2	528.3	85.2	226.1
920	401.00	122.0	179.2	359.2	470.7	344.3	477.4	95.9	226.3
930	408.09	120.2	196.8	241.7	375.2	299.4	474.6	98.3	247.1
940	415.18	85.0	155.9	173.3	295.8	281.5	466.3	83.6	235.0
950	422.28	94.6	178.5	189.8	337.9	334.9	573.6	131.0	310.9
960	429.37	81.0	160.5	294.0	500.1	293.3	522.5	104.5	271.8
970	436.46	69.9	146.6	208.0	381.2	258.2	482.0	86.4	245.1
980	443.55	66.9	153.9	198.6	401.6	229.2	477.5	82.3	254.2
990	450.64	61.1	151.4	129.5	298.3	185.7	425.7	98.9	294.5
1000	457.74	51.2	133.7	107.6	259.3	175.5	410.1	70.4	241.2
1010	464.83	85.4	206.4	125.4	304.7	182.5	440.1	83.5	274.0
1020	472.00	70.3	176.9	122.7	299.9	174.4	424.7	72.0	253.4
1030		74.6	178.4	110.0	264.4	186.7	431.6	77.5	257.8
1040		72.2	174.2	138.8	319.2	181.2	422.0	88.2	277.9
1050		64.9	147.0	119.4	257.8	190.6	399.7	65.0	222.6
1060		76.0	163.0	114.3	245.5	209.1	423.6	101.5	280.5
1070		113.5	195.4	212.8	351.3	308.8	506.5	171.4	353.8

Table C.12.2 (Contd.) Excess metal and carbonate free metal data from core CD3826 (Ex.=excess; CF=salt and carbonate free).

Age(ka)	Ex.Cu	Cu	Ex.Ni	Ni	Ex.Zn	Zn	Ex.V	V
	(ppm)	(ppmCF)	(ppm)	(ppmCF)	(ppm)	(ppmCF)	(ppm)	(ppmCF)
0.15	39.3	85.2	51.4	120.7	125.9	223.6	36.4	167.7
1.55	40.5	87.7	54.2	125.3	128.8	230.2	44.7	178.2
3.10	39.1	88.0	54.5	128.0	130.7	237.9	35.2	170.2
3.25	41.2	89.1	55.2	127.0	129.3	233.9	33.8	165.4
4.64	40.9	90.7	65.9	141.9	151.2	264.9	43.2	177.7
6.19	37.9	88.7	63.6	141.2	141.7	257.8	44.3	181.5
8.13	35.6	86.2	56.3	133.2	138.9	254.4	38.1	175.8
10.06	37.5	87.9	50.6	125.9	134.5	247.9	29.2	164.7
12.00	31.8	81.1	48.5	123.1	121.6	231.8	34.7	170.7
12.69	32.4	81.1	43.4	116.5	98.3	203.6	51.2	188.4
13.38	33.2	81.3	44.7	116.9	91.8	195.3	47.8	182.3
14.07	33.3	80.7	50.5	122.2	84.5	186.1	47.1	179.0
14.75	33.5	81.6	38.4	109.6	71.6	173.1	40.9	173.4
15.44	41.5	90.7	35.7	106.3	78.0	180.5	45.7	177.6
16.13	41.1	90.2	35.6	106.2	78.9	181.4	46.4	178.3
16.82	39.6	87.8	33.8	103.3	75.6	176.4	40.4	170.0
17.71	39.3	88.3	32.8	103.1	78.0	180.7	39.0	169.8
18.59	41.0	90.1	35.6	105.8	77.0	179.2	47.4	178.6
19.48	37.8	86.8	20.4	89.3	73.1	175.5	49.7	183.0
20.23	37.3	85.2	23.8	93.2	73.8	174.6	51.4	184.6
20.99	38.9	88.1	21.9	92.0	70.7	173.4	43.9	178.0
21.74	41.8	90.5	22.5	91.8	78.9	180.8	54.7	188.4
22.49	35.3	81.2	24.1	91.6	76.0	173.0	36.4	164.8
23.25	34.1	83.0	17.1	88.2	69.2	172.3	41.1	177.7
24.00	38.9	84.9	23.9	91.3	84.8	182.0	40.7	169.3
28.38	35.7	83.2	25.2	93.7	79.6	180.3	39.6	169.6
32.75	36.2	83.0	23.0	91.3	75.0	173.7	36.2	166.3
37.13	39.1	84.8	22.8	90.8	77.3	173.7	53.0	183.4
41.50	35.0	83.2	30.4	100.2	88.8	192.8	48.4	180.6
45.88	36.9	85.4	29.4	99.6	99.1	204.2	50.6	184.1
50.25	41.8	88.9	21.2	91.2	75.9	175.0	53.7	187.9
54.63	31.4	79.4	49.1	121.8	106.2	210.0	46.6	182.8
59.00	41.7	93.8	20.0	89.6	76.1	183.5	38.9	172.1
	162.4	233.7	25.8	94.6	211.7	339.0	45.9	176.9

Table C.12.3 Excess metal and carbonate free metal data from core CD3827 (Ex.=excess; CF=salt and carbonate free).

Depth(cm)	Age(ka)	Ex.Cu (ppm)	Cu (ppmCF)	Ex.Ni (ppm)	Ni (ppmCF)	Ex.Zn (ppm)	Zn (ppmCF)	Ex.V (ppm)	V (ppmCF)
9	2.49	13.0	108.1	11.7	110.1	19.1	172.2	10.8	132.5
11	3.04	10.8	85.6	11.1	96.5	20.5	166.0	8.5	105.5
13	3.59	10.8	88.9	9.7	92.2	20.7	173.8	6.1	96.8
15	4.14	12.4	121.9	9.1	108.8	20.3	211.8	18.5	216.7
17	4.70	12.2	92.9	11.9	100.5	22.9	178.7	12.6	129.4
19	5.25	15.5	118.1	11.2	100.2	21.9	179.8	13.7	142.0
21	5.80	11.5	108.3	10.0	108.3	20.4	199.3	15.9	182.0
23	6.35	13.2	129.5	13.2	140.5	21.0	217.6	15.3	188.8
25	6.91	12.0	117.1	13.8	142.1	24.1	236.6	17.6	200.7
27	7.46	13.2	127.6	15.0	152.6	23.5	233.5	12.4	162.6
29	8.01	15.6	147.3	13.9	143.9	21.9	221.9	13.8	172.7
31	8.56	15.1	147.5	15.8	163.4	26.9	269.4	25.7	274.7
33	9.12	14.5	136.2	14.5	145.6	23.1	226.4	24.6	252.8
35	9.67	16.6	158.3	16.5	167.2	23.8	239.7	17.0	196.4
37	10.22	17.0	148.1	15.4	144.0	26.7	241.3	19.4	197.1
39	10.77	14.8	148.8	14.3	153.4	27.4	279.9	18.1	211.1
41	11.33	16.8	159.0	14.6	149.2	26.5	259.9	19.3	210.8
43	11.89	16.6	191.9	16.8	202.8	26.1	311.4	13.6	194.0
45	12.01	17.1	187.9	17.8	204.6	25.6	292.3	11.1	161.8
47	12.13	15.9	166.9	14.2	160.0	21.9	243.0	14.0	181.7
49	12.25	16.0	124.7	13.7	114.3	23.9	193.0	13.2	126.2
51	12.37	16.0	134.5	14.7	132.1	23.1	204.1	15.4	156.7
53	12.49	16.6	184.2	14.5	171.6	22.6	264.2	21.6	267.4
55	12.61	15.4	185.0	15.2	191.9	20.1	255.8	16.1	225.0
57	12.73	13.5	188.6	14.6	211.2	17.5	259.0	17.7	274.9
59	12.90	13.9	196.5	13.1	195.2	17.9	266.5	19.1	296.2
61	13.08	12.6	153.0	13.7	172.6	15.6	202.5	11.8	172.6
63	13.25	13.3	168.7	17.1	221.4	16.2	221.4	16.9	241.7
65	13.42	14.6	204.9	16.2	235.6	17.3	259.7	13.2	220.9
67	13.60	14.6	203.6	13.9	203.6	15.4	232.7	8.3	156.0
69	13.77	16.8	225.5	14.7	208.8	17.0	247.4	10.9	185.6
71	13.94	15.4	202.7	14.3	197.7	17.0	241.5	12.3	197.7
73	14.12	18.2	243.6	15.2	215.4	18.3	265.4	8.8	162.9
75	14.29	15.1	202.4	14.6	205.0	17.3	249.2	9.0	163.2
77	14.46	15.7	211.7	16.0	224.5	19.0	273.3	5.3	116.7
79	14.63	16.8	229.3	18.2	256.7	19.4	282.8	8.7	162.9
81	14.81	16.5	210.4	17.2	227.3	20.0	270.9	10.4	172.9
83	14.98	15.1	212.8	13.9	207.4	18.7	279.7	8.8	167.3
85	15.15	15.6	209.7	11.6	170.1	18.0	259.6	10.7	184.1
87	15.33	15.2	198.0	15.1	205.3	18.0	249.6	12.0	191.8
89	15.50	17.7	227.8	12.6	177.3	19.3	267.2	16.1	243.8
91	16.03	25.4	346.8	20.0	286.1	21.8	321.1	10.5	190.3
93	16.56	15.6	206.5	13.8	192.6	15.0	217.9	11.4	186.2
95	17.09	15.4	207.8	12.4	179.4	15.0	222.1	11.0	185.9
97	17.63	15.1	201.2	12.0	173.3	15.2	222.7	17.0	259.4
99	18.16	13.6	163.6	12.8	164.8	16.2	211.8	10.1	159.2
101	18.69	13.5	156.9	11.7	146.0	16.5	204.8	7.4	122.0
103	19.22	15.5	177.7	12.9	159.3	15.4	195.1	11.0	161.5
105	19.75	15.2	171.1	12.6	153.3	16.5	202.6	8.9	139.6
107	20.28	15.3	135.4	11.8	114.6	17.1	165.3	15.4	162.0
109	20.81	14.2	160.3	10.9	136.2	15.5	192.8	12.6	177.0
111	21.34	14.4	156.5	11.9	141.3	16.0	190.8	1.5	63.6
113	21.88	15.3	163.0	13.2	152.1	17.7	205.8	16.3	205.8
115	22.41	16.3	164.3	12.6	139.9	17.4	193.4	7.4	116.4
117	22.94	14.2	174.3	13.7	178.7	17.3	230.1	10.4	173.1
119	23.47	14.1	139.4	11.1	122.2	17.3	186.5	12.3	155.7
121	24.00	15.3	145.0	10.4	113.8	17.7	185.0	14.5	171.9
123		14.4	136.0	11.8	124.1	16.7	175.9	12.3	153.8

Table C.12.4 Excess metal and carbonate free metal data from core P5 (Ex.=excess; CF=salt and carbonate free).

APPENDIX D
Recent Publications of the Author

A.J. PATIENCE AND D. KROON

Oxygen Isotope Chronostratigraphy

In: *Quaternary Dating Methods - A User's Guide*

Edited by P.L. Smart[#] and P.D. Frances, Quaternary Research Association, Technical Guide No.4, 1991, Cambridge, Chapter 10, 199-228.

[#] Permission given for inclusion as appendix.

Chapter 10

OXYGEN ISOTOPE CHRONOSTRATIGRAPHY

A.J Patience and D. Kroon

INTRODUCTION

As a result of a dramatic increase in late Cenozoic palaeoclimatic research, a standard method is required to allow global correlation of ocean sediments. Such a standard correlation technique must use variations in a parameter which can be easily recognised and can be applied globally. In 1955 Emiliani suggested that changes in ocean temperature related to the glacial/interglacial cycles caused a change in the stable isotopic composition of the oceans. This would be directly reflected in the oxygen isotopic composition of foraminifera which are preserved in carbonate bearing ocean sediments retrieved by coring. Subsequently Shackleton (1967) suggested that these variations in the isotopic composition of the oceans were due to changes in the volume of global ice-sheets. The synchroneity of these changes throughout the world provides the potential for a high resolution correlative chronology. Only later was a direct link forged between the climatic effects on isotopic variations and the orbital changes central to the Milankovitch theory (Hays et al., 1976).

There has long been an interest in the effects of orbital variations on the Earth's climate (Croll, 1864, Milankovitch, 1941, Veeh and Chappell, 1970, Berger, 1976, 1988, Imbrie and Imbrie, 1980). The variations in the eccentricity of the Earth's orbit around the sun, the obliquity of the ecliptic and the axial precession of the equinoxes (Figure 10.1) cause changes in the solar insolation specific to each latitude of the globe (Berger, 1988, Broecker and Van Donk, 1970), and form the core of the Milankovitch theory of climate change. The main periodicities (Figure 10.2) of 400 ka and 100 ka (eccentricity), 41 ka (obliquity) and 23 ka and 19 ka (precession) have been calculated from astronomical theory (Berger, 1984). These variations in solar radiation at the Earth's surface have the potential to force changes in global and regional climate, which may, in turn, imprint on the geological record. Thus cyclical changes in the factors directly reflecting climate, such as global ice volume, oceanic water mass chemistry and distribution, marine biogenic diversity, and in the distribution of vegetation and production of sediments on the continents will lead to rhythms in marine sediments. These rhythms can be examined using time series techniques, such as spectral analysis, which have demonstrated there is a close relationship between the predicted Milankovitch frequencies and the periodicities

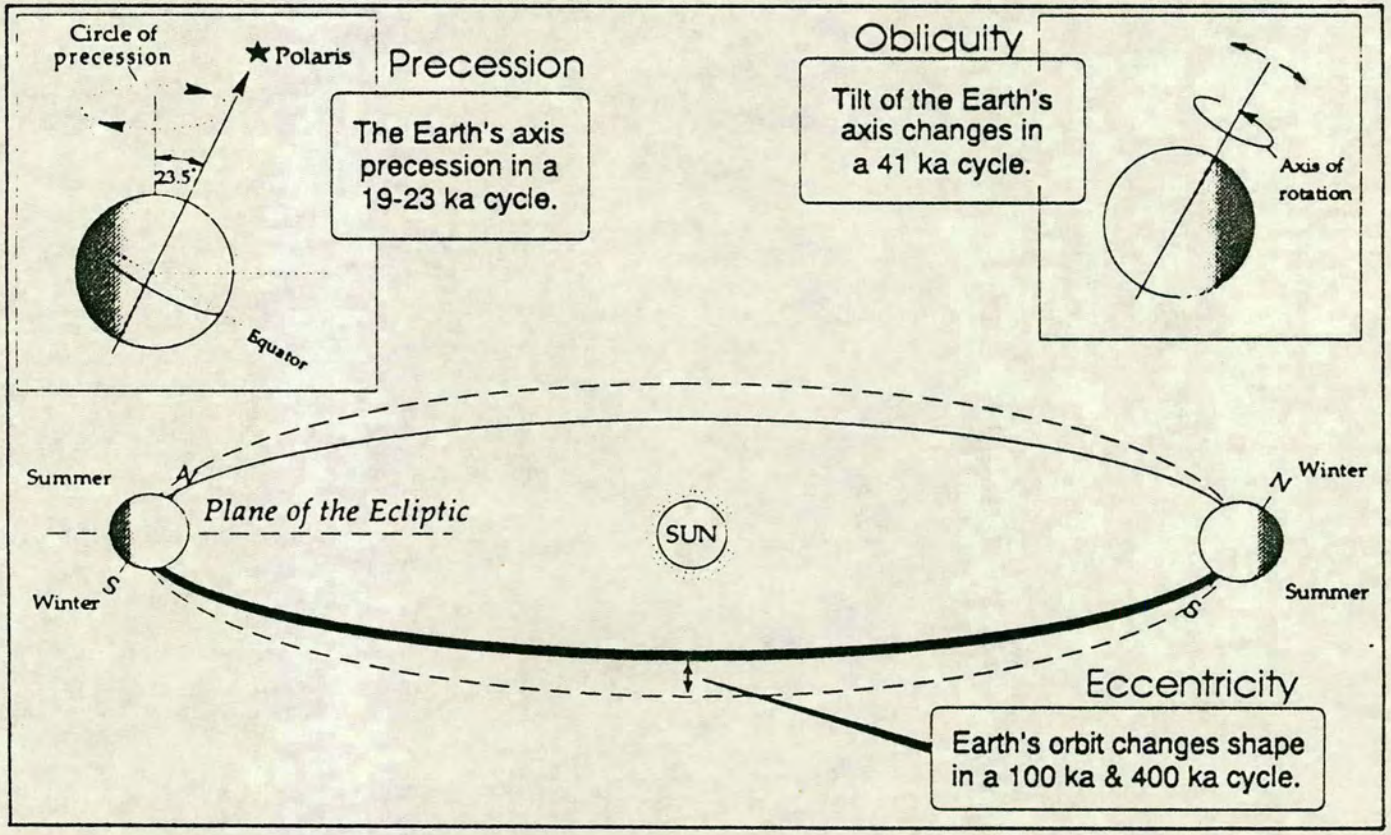

Figure 10.1 *Orbital Eccentricity, Obliquity and Precession; the three astronomical cycles involved in solar input and climate variation.*

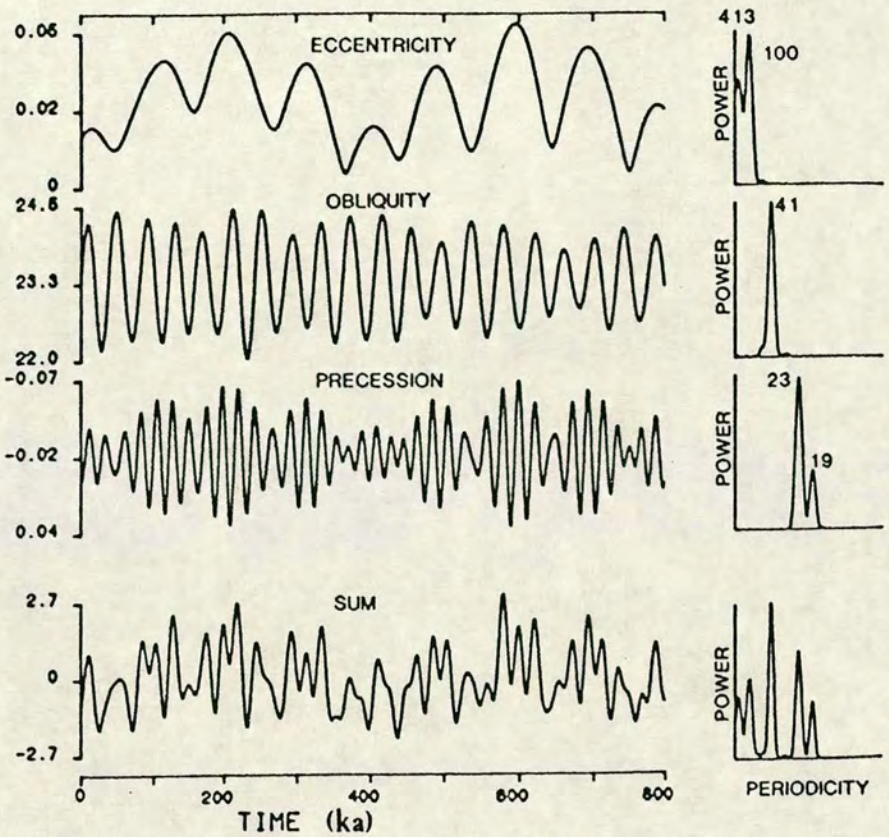

Figure 10.2 *Graphical illustration of the calculated variation in eccentricity, obliquity and precession (0-800 ka). The upper three plots on the left are the result of calculations on solar insolation through the last 800 ka (Berger, 1977). The lower plot is a composite curve called SUM, by Imbrie et al. (1984). Scale for individual cycles in degrees; for SUM, in standard deviation units. Right: variance spectra calculated from these time series, with dominant periods (ka) of conspicuous peaks indicated. (Adapted from Imbrie et al., 1984.)*

dominating the power spectra in ocean sediment cores (Pisias et al., 1973, Pisias, 1976, Hays et al., 1976). The existence of these Milankovitch-driven cycles in sediment cores provides the potential for conversion of cycles of a particular parameter with depth in the sediment to time.

Oxygen isotope curves today form the basis of most detailed correlation in the Pleistocene and late Pliocene marine sedimentary records, because the mixing time of the oceans is relatively short and the palaeoclimate signal is essentially synchronous across the globe. The recognition of the potential of these methods has resulted in the development of the SPECMAP age models (Imbrie et al. 1984), which stack several oxygen isotope curves then smooth, filter and tune the composite curve to the Milankovitch cyclicities. This reference stack can then be used to correlate global isotopic, geochemical and magnetic susceptibility records (Imbrie et al., 1984). Overviews of the development of oxygen isotope dating techniques and their application to chronostratigraphy are presented by Prell et al. (1986), Williams et al. (1988b) and Jansen (1989).

The aim of this review is to critically discuss the problems in the use of oxygen isotopic ratio curves in the development of age models for correlation of late Cenozoic ocean sediments and for mapping climatic variation in space and time. Particular attention will be paid to the difficulties resulting from tuning, stacking, filtering and stretching of profiles, and the problems associated with sampling density and positioning of isotopic stage boundaries.

FACTORS INFLUENCING THE OXYGEN ISOTOPE COMPOSITION OF FORAMINIFERA

There are many factors which contribute to the overall oxygen isotopic signal in the carbonate tests of foraminifera, the most important of which are discussed below.

Ice Volume Effect

The oxygen isotopic composition of the world's oceans is mainly dependent on the balance between low latitude evaporation and high latitude precipitation. This is because the isotopically lighter ^{16}O is preferentially evaporated, while ^{18}O is preferentially condensed. Thus high latitude precipitation is isotopically light ($-30‰$ to $-40‰$; Figure 10.3), and the polar ice sheets are enriched in ^{16}O compared to mean ocean water. If the ice sheets grow as a result of some climatic change, sufficient ^{16}O is removed from the oceans to change the mean oceanic composition (Duplessy, et al., 1970). Conversely, melting of ice sheets will release ^{16}O, decreasing the $^{18}O/^{16}O$ ratio in the oceans. The difference in oceanic oxygen isotopic composition between a full glacial and a full interglacial cycle is estimated to be approximately $1.0‰$ (Berger, 1979). These changes are reflected in the isotopic composition of the tests of foraminifera, which on death fall to the ocean

floor, and accumulate to form a sedimentary record (Shackleton 1967, 1977). Comparable records may also be preserved in other marine organisms, such as corals (Shackleton and Matthews, 1977, Fairbanks and Matthews, 1978), which may be preserved in raised reef terraces, the dating of which has also been of considerable significance in establishing the chronology of deep sea cores (Broecker et al., 1968, Bloom et al., 1974).

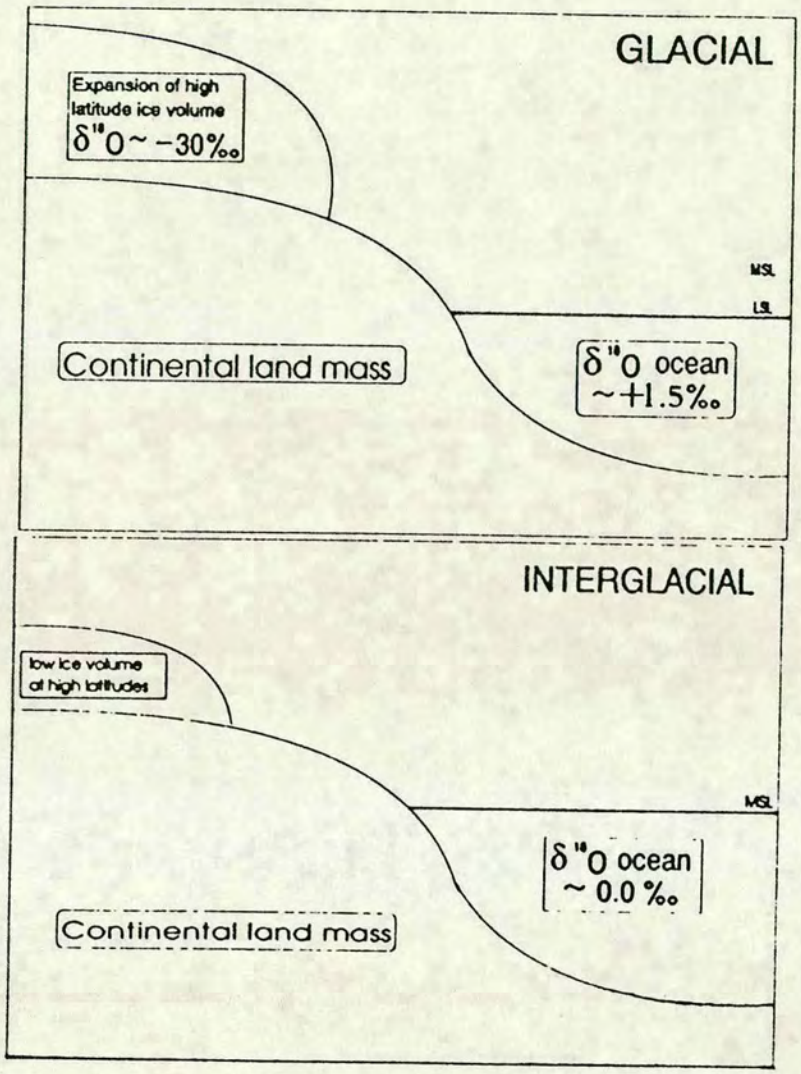

Figure 10.3 *Diagram illustrating the variation in sea level, isotope composition and ice volume between glacial (upper) and interglacial (lower) periods. MSL-Mean Sea Level, LSL-Low Sea Level. During the glacials seawater is depleted in ^{16}O because the lighter isotope has been removed through the meteorological cycle and locked in ice. (After Williams et al., 1988.)*

Temperature Effect

The oxygen isotopic composition of the tests of foraminifera is dependant upon both the isotopic composition of the water from which precipitation occurs, and the temperature. At low temperature there is greater fractionation of ^{18}O relative to ^{16}O, and the tests contain a greater proportion of the heavier istotope than would be the case at higher temperatures (Urey 1948, Shackleton and Opdyke, 1973, Williams et al., 1981). The temperature dependence is about 0.23‰/1°C (Epstein et al., 1953).

The world's oceans are essentially divided into three stratified water regimes which have distinctive temperatures and densities (Figure 10.4):-

1) The upper surface mixed layer varies between 10 m (sheltered coasts in summer) to 200-300 m deep (mid latitudes open oceans) and has a wide seasonal variation in temperature.

2) The permanent thermocline zone usually lies between 70-1000 m and shows limited seasonal variation in temperature.

3) The deep water below 1000 m has a fairly constant temperature which often approaches freezing.

Different foraminiferal species inhabit different parts of the water column: planktonic foraminifera in the surface layers and benthic at the bottom of the oceans. Planktonic species living in the top 50 m of the water column are dominantly *spinose* whereas *non-spinose* forms dominate below this level. However, a single foraminifera species may also migrate in the water column during development. Figure 10.4 illustrates the water mass and temperature regimes inhabited by foraminiferal species that are commonly used in oxygen isotope studies.

Clearly, planktonic foraminifera are subject to much greater temperature and salinity variations (especially near continents where fresh water runoff and upwelling occurs) than are benthic species. For instance, Steens et al. (1990) have measured the isotopic composition of two different planktonic foraminifera through time in a core from the western Arabian sea. The surface dweller *Globigerina bulloides* (d'Orbigny) is on average lighter, and shows both different trends and a greater amplitude of oxygen isotope variation from glacial to interglacial conditions than the deeper dwelling *Neogloboquadrina dutertrei* (Figure 10.5). The latter lives between 50-300 m (Hemleben and Spindler, 1983), and is thus subject to less isotopic variation than the near surface dweller *G. bulloides*. Therefore, *N. dutertrei* should more accurately reflect the global isotopic signal of ice volume. Benthic foraminifera however, receive their isotopic signal from the bottom waters which have a more constant temperature, salinity and chemistry and are often directly derived from the polar regions. They thus more directly reflect ice volume, which may be blurred by local isotopic

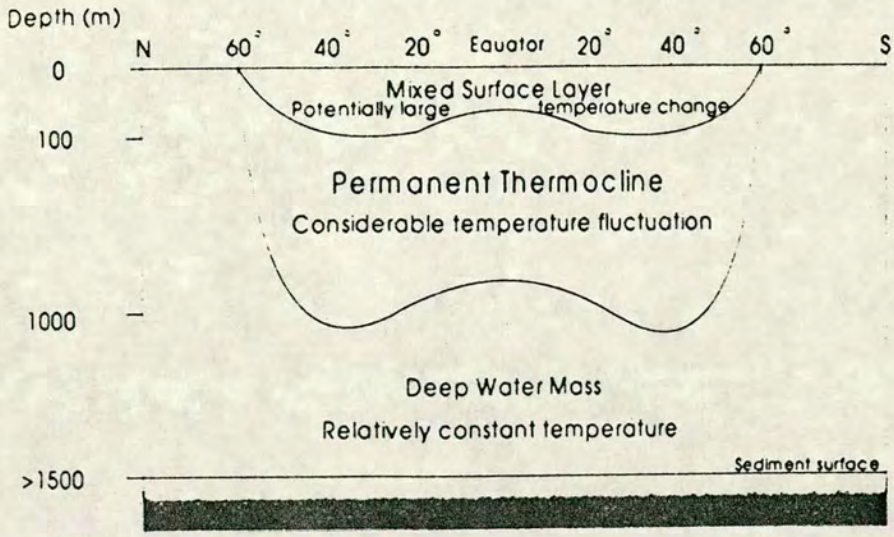

Foraminiferal Species	Approximate Depth Range (m)	Temperature regime/range (°C)
Globigerinoides ruber	0-50	Sub-tropical (20-29)
Globigerinoides sacculifer	0-100	Tropical (15-30)
Globigerina bulloides	0-100	Sub-Arctic/sub-antarctic (0-25)
Globoquadrina pachyderma	50-300	Arctic/Antarctic (2-7)
Neogloboquadrina dutertrei	50-300	Temperate/subtropical (14-25)
Globorotalia crassiformis (LC)	100-300	Sub-tropical (0-25)
Uvigerina spp.	100-2000	(0-20)
Cibicoides spp.	>30	(0-20)

Figure 10.4 *Generalised diagram showing the thermal structure of the oceans, the foraminiferal species most commonly used in oxygen isotope dating and their approximate position in the water column and temperature regimes. LC — left coiling foraminifera. Foraminiferal depth ranges are from Hemleben and Spindler (1983). In general the oxygen isotope profiles generated from benthic foraminifera give the best age models because surface waters experience much greater fluctuation in oxygen isotope ratios.*

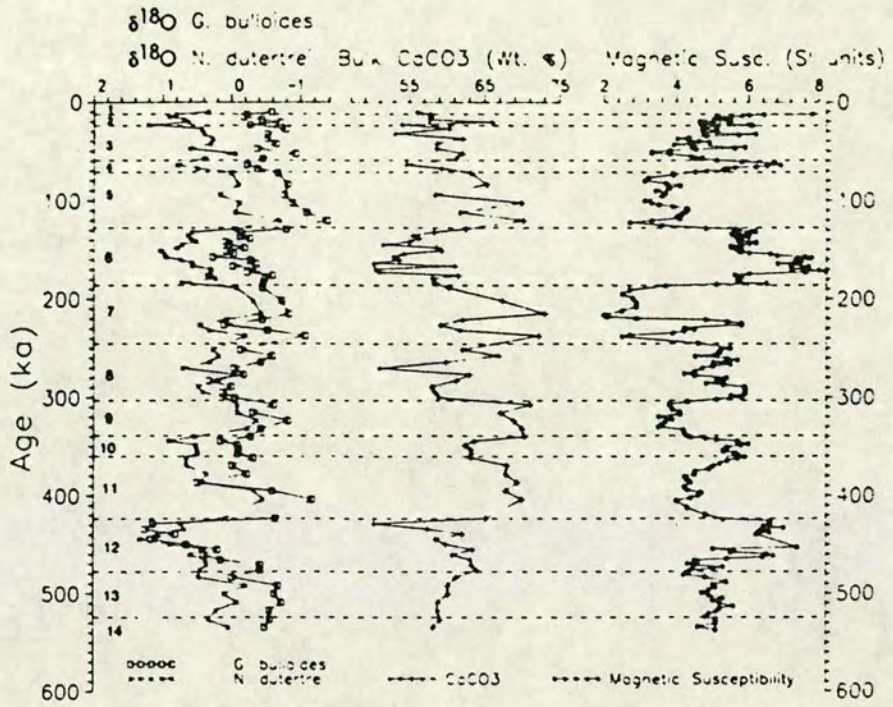

Figure 10.5 *Depth profiles of $\delta^{18}O$ oxygen isotope records from* Globigerina bulloides *(surface dweller) and* Neogloboquadrina dutertrei *(deep dweller), bulk $CaCO_3$ (%) and magnetic susceptibility over the last 600 ka from ODP core 72&A (western Arabian Sea). The oxygen isotope record of* N. dutertrei *has been correlated with the SPECMAP curve to produce this age model. The oxygen isotope record of* N. dutertrei *appeared to be more suitable for dating than that of* G. bulloides, *which is expressed in the power spectra of the two species (see Figure 10.10 e-f). The concentration of variance (power) is more sharply focused in the Milankovitch rhythms in* N. dutertrei *than in the* G. bulloides *record. Figure 10.10 also shows that the magnetic susceptibility and $CaCO_3$ records are consistent with the stable oxygen isotope curve, which illustrates the potential for use of these records for dating. However such a strategy has many drawbacks and is completely unreliable unless a global oxygen isotope curve is available since local differences may have influenced the signal. Figure generated from data in Steens et al. (1990).*

fractionation effects in planktonic records. The benthic signal should therefore always produce a more globally reliable curve for age model development. Indeed, Shackleton and Berger (in press) show by cross spectral analysis of planktonic and benthic $\delta^{18}O$ curves from the same core, that the benthic signal displays greater coherency with the orbital parameters than does the planktonic (Figure 10.6). This diagram also shows the greater amplitude of the $\delta^{18}O$ excursions in the planktonic compared to the benthic record, because the former includes the combined effect of ice volume and temperature fluctuations, whereas the latter predominantly reflects ice volume variations. However, despite this advantage, benthic foraminifera are often scarce in deep sea sediments because of dilution by the large input of planktonic foraminifera and terrigenous material. It is for these reasons that we advocate the use of a combination of species, both benthic and planktonic.

Vital Effects

Foraminifera undergo gametogenetic reproduction and exist in both juvenile and adult stages, which may have significant differences in the extent of oxygen fractionation. Migration of planktonic foraminifera during development is also common, especially in the genus *Globorotalia*, with juvenile stages inhabiting the euphotic surface waters and adult stages existing deeper in the water column. Together, these effects result in variations of oxygen isotope ratio with test size; adult stages (larger tests) having isotope ratios more depleted in ^{16}O than juvenile stages. Furthermore, the degree to which foraminifera precipitate $CaCO_3$ in isotopic equilibrium with the ambient sea water varies, due mainly to physiological differences, resulting in large deviations in oxygen isotope ratios between species. Such combined effects of developmental stage and species variations are termed "Vital Effects", and can give variations up to 1.2‰. They can be compensated for by comparison with extant species whose vital effects have been determined, and by selecting samples of homogeneous size.

Diagenesis and Dissolution

Diagenesis may affect the $\delta^{18}O$ signal by recrystallisation and dissolution (Baker et al., 1982, Elderfield and Gieskes, 1982, Killingly, 1983). The isotopic composition and gradient of pore waters differ between oceans, but in general, the diagenetic effects of these pore waters are assumed to be minor in comparison to the temperature and ice volume induced effects exerted on the planktonic surface dwellers. Generally, as sediment age and depth of burial increases, the diagenetic effect increases.

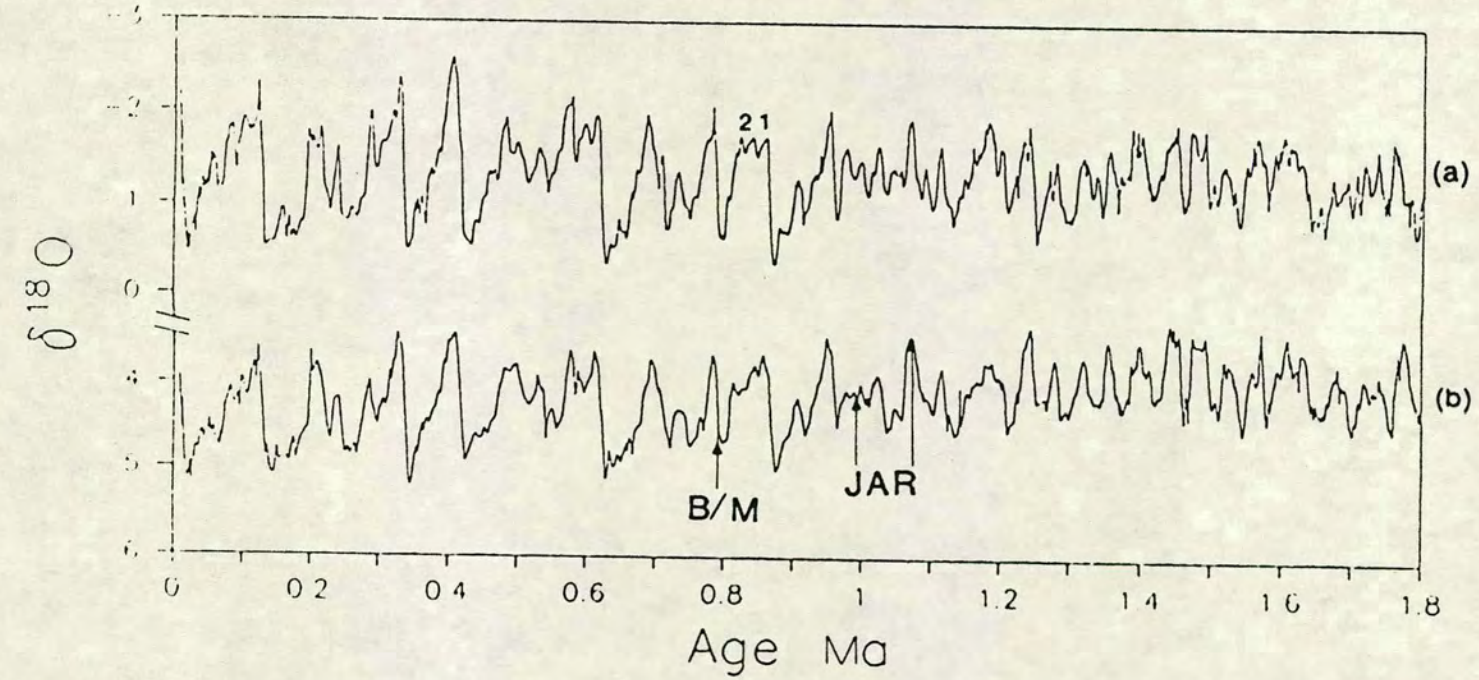

Figure 10.6 *Combined isotope stratigraphy in ODP hole 677.* **A:** *planktonic* (Globigerinoides ruber) *and* **B:** *benthic* (Uvigerina. senticosa). *B — Brunhes; M — Matuyama; JAR — Jaramillo subchron; 21 — isotope stage 21 with its three precessional peaks. Note the enhanced amplitude of the planktonic curve compared to the benthic curve as a result of temperature effects in the surface waters, and that the benthic curve is more positive because of a temperature fractionation effect in the cold bottom waters. Adapted from Shackleton and Berger (in press).*

ANALYTICAL TECHNIQUES

Today, analytical facilities for mass spectrometric determination of stable isotope ratios in $CaCO_3$ samples weighing tenths of milligrams are well established. For a detailed account of such techniques see Williams (1984 and accompanying references).

In summary, the recovered sediment core is cut in half along it's length and approximately 10-20 cm^3 of wet sediment per horizon is sampled. This is subsequently washed using a 63 µm sieve and dried at around 40°C. Foraminifera are then sorted into size fractions (usually between 200-400 µm diameter), which are dependent on the species to be sampled, and 30-50 individuals of each species are hand picked for every sample. Several species may be required to enable $\delta^{18}O$ and $\delta^{13}C$ comparison between planktonic and benthic species.

A homogenised triplicate sample of 0.1-1.0 mg (5-15 foraminifera) is cleaned with alcohol and dried prior to being "roasted" (*in vacuo*) at c 380°C to remove organic contaminants. Purified phosphoric acid at c 60-90°C is then added (*in vacuo*) to dissolve the $CaCO_3$, liberating CO_2.

$$2H_3PO_4 + 3CaCO_3 \rightleftharpoons Ca_3(PO_4)_2 + 3H_2O\ (g) + 3CO_2\ (g) \qquad (10.1)$$

Fractional freezing purifies the liberated CO_2 which is then transferred to an on line isotope ratio mass spectrometer. There it is ionised and separated into it's isotopic constituents (Figure 10.7).

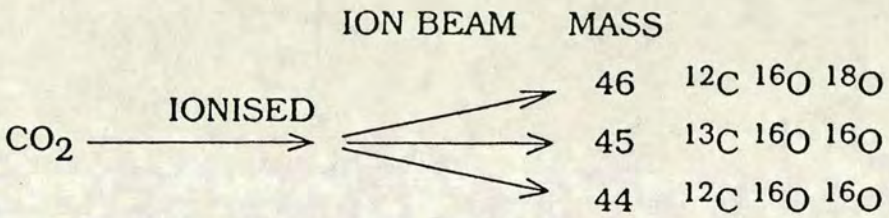

Figure 10.7 *Diagram showing the isotopic separation of liberated CO_2 during mass-spectrometry.*

The mass 46/44 ion beam ratio-intensity gives the $^{18}O/^{16}O$ ratio, and the 45/44 ion beam ratio-intensity produces the $^{13}C/^{12}C$ ratio of the CO_2. These ratios are repeatedly compared to a known CO_2 reference standard. Oxygen isotope ratios are usually expressed as an enrichment or depletion of the minor isotope relative to a standard (commonly the reference carbonate PDB) in parts per thousand (commonly abbreviated δ per mil or ‰). This δ value is calculated using equation 10.2.

$$\delta^{18}O = 1000 * \left[\frac{^{18}O/^{16}O \text{ sample} - {}^{18}O/^{16}O \text{ reference}}{^{18}O/^{16}O \text{ reference}} \right] \qquad (10.2)$$

CONSTRUCTION OF A STANDARD REFERENCE CURVE

To enable correlation of late Cenozoic marine sedimentary records, a standard, globally applicable isotopic template was required. Such a requirement led Imbrie et al. (1984) to generate the "SPECMAP" curve (Figure 10.8a) which encompasses the last 800 ka and is based on averaging (stacking) several low-latitude oxygen isotope profiles derived from shallow-dwelling planktonic foraminifera (*Globigerinoides sacculifer* and *Globigerina bulloides*). They then used the theory of orbital forcing to tune each curve and thus developed an age model. It was hoped that the resulting timescale would act as a type section, against which other curves (e.g. isotopic, geochemical, palaeomagnetic) could be readily compared. Some important points in the methods used in the successful development of such an age model are outlined below.

Critical Reliance on Independent Age Dates

For the SPECMAP reference curve, an initial time scale was achieved by selecting six easily recognisable control points (dated radiometrically) and assuming linear sediment accumulation rates between control points. Stratigraphic inconsistencies in each raw isotopic profile as a result of coring or sedimentation disruption (e.g. stretching, breaks, slumping) were crucial to the selection of such control points, all of which were chosen from undisturbed parts of the selected cores.

Five of the control points were dated using ^{14}C techniques, whereas the Bruhnes-Matuyama magnetic reversal was dated independently by the K-Ar method. Thus, although the overall structure of the SPECMAP curve (Figure 10.8a) may be a good approximation of the global signal, the absolute ages and positions of the stage boundaries may be erroneous because of linear interpolation between the four ^{14}C dated control points (0-35 ka) and the K-Ar dated 730 ka Bruhnes/Matuyama magnetic reversal time control. Furthermore, recent mass spectrometric uranium series ages of ^{14}C dated corals indicate systematic differences greater than 3.5 ka between radiocarbon and true ages for dates older than 20 ka (Bard et al., 1990). After conversion from depth to time, the record must then be further adjusted such that it forms a time series with equally incremented data points.

Nature and Timing of Filtering Process

Subsequent to development of the initial age model, the SPECMAP authors were forced to decide on a tuning strategy which would ultimately determine the accuracy

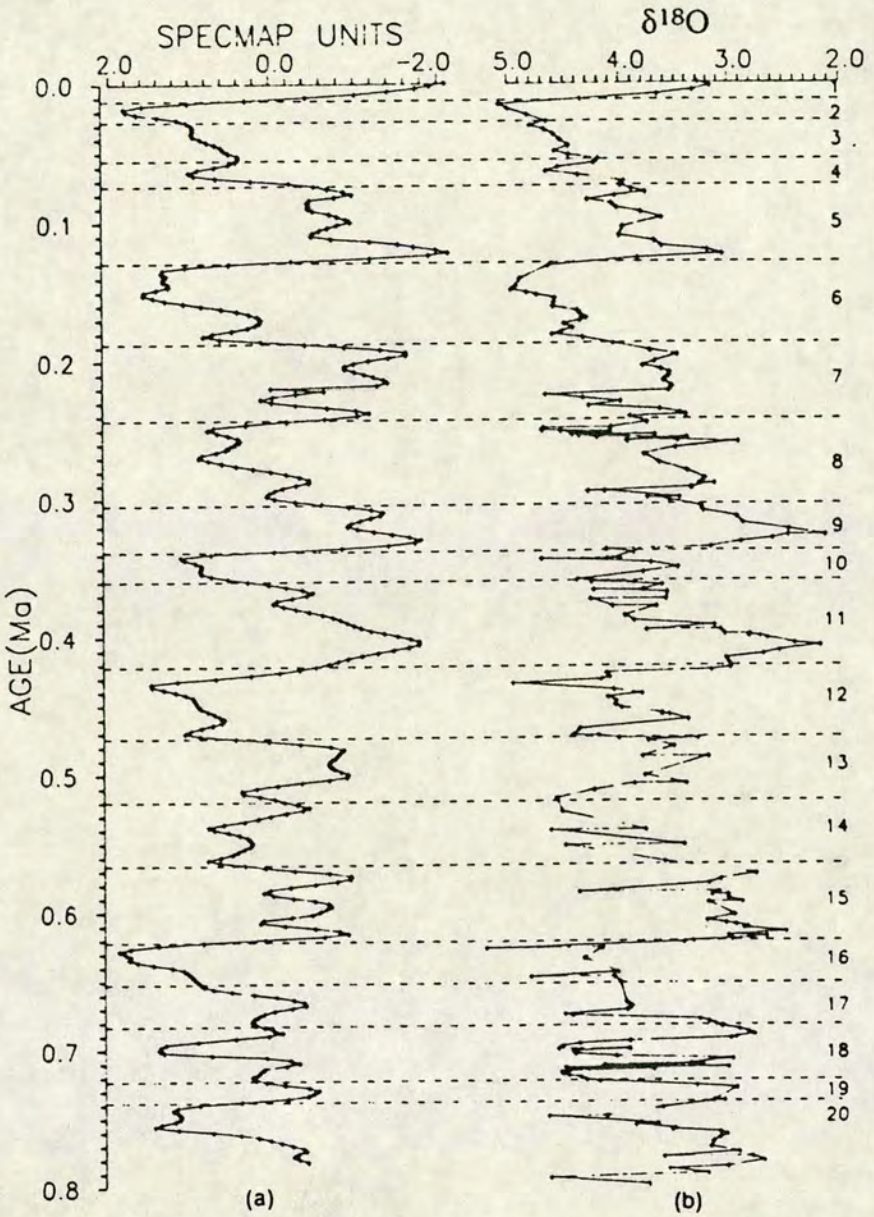

Figure 10.8 *Oxygen isotope curves spanning the last 800 ka. A: the SPECMAP stack generated from data in Imbrie et al. (1983). B: A composite curve generated from uncorrected $\delta^{18}O$ data of two benthic foraminifera species from DSDP hole 607 in Ruddiman et al. (1989). The top 250 ka are from cores V30-97 and CHN82-24-4. Numbers 1-20 indicate oxygen isotope stage stratigraphy. The allocation of oxygen isotope cycles in DSDP hole 607 seems relatively easy for the last 600 ka, but at the base of the Brunhes problems occur (see also Figure 10.12).*

of the final model. They chose the target curve approach of Hays et al. (1976) and Morley and Hays (1981) which matches isotopic observations against the obliquity and precessional rhythms. Least square noise minimisation filters (Wiener filters) were used to remove any high frequency noise from the signal. Then Fourier transform techniques converted the data from the time to the frequency domain. An iterative process (120 steps) was employed to tune the isotopic signal to the orbital frequencies. Control points were moved to attain a maximum phase lock coherency between the orbital frequencies (Figure 10.2) and the isotopic record. As Imbrie et al. (1984) pointed out, the 120 iterations required to achieve the optimum phase lock raises questions as to the validity of the method. Once an optimum correlation between orbital frequencies and the isotope observations had been attained, depth versus age plots were studied for the stacked curve. It was shown that no sharp inflections occurred and the plots were generally smooth which, according to Imbrie et al. (1984), tenuously implies a relatively constant accumulation rate.

There are two schools of thought as to when is the best time to perform the filtering process. Imbrie et al. (1984), and most subsequent authors, filter in the time domain, whereas Shackleton and Berger (in press) advocate a depth domain filtering method. They argue that their depth domain model requires less change in the accumulation rate of reference core V28-238, which is believed to have an exceptionally constant accumulation rate, than do time domain filtered models. Further work to identify the advantages and disadvantages of both methods is needed, but the implication of such models should be considered carefully by users.

Imbrie et al. (1984) used fixed phase lag times for $\delta^{18}O$ events of around 8 ka behind for obliquity forcing and 4-5 ka behind for precessional forcing. These fixed (presumed constant) phase lag times which are based on the ice sheet model of Weertman (1964), have been shown by Pisias et al. (1990) to vary through time. Pisias et al. (1990) also throw doubt on the assumption of a constant response by the climate system to orbital forcing (see below). Finally, the curves were normalised to a zero mean and unit standard deviation before being superimposed and averaged. Suspect data points were removed prior to smoothing with a 9-point Gaussian filter.

CORRELATION OF "NEW" CURVES WITH THE REFERENCE CURVE

A bewildering variety of methods for correlating newly generated curves with the reference type section are employed today. Most attempt to quantify the degree of correlation between at least two signals often from separate locations. The main methods used and their associated problems are outlined below.

Visual Inspection

The human visual system is remarkably efficient at recognising similarity in patterns, enabling a rapid initial approximation as to the correlation of two records. Emiliani

and Shackleton (1974) employed visual analysis to define the isotope stages and substages. Shaw (1964) and Prell et al. (1986) used a graphical correlation method which compares common isotopic events in the "New" curve with those in a reference section.

Stage Boundary Positioning and Tuning

Perhaps the most fundamental weakness in the whole age model development process is the subjectivity of the positioning of isotopic stage boundaries and substages, which are the tielines between any core and SPECMAP. The adoption of the standardised stratigraphic nomenclature of Emiliani (1955) and Shackleton (1969) for stages (numbered from the top of the core with even numbers equivalent to cold stages and odd numbers equivalent to warm) and substages (lettered sequentially,with (a) the highest substage in a given stage) in the curve reduces confusion during correlation. Pisias et. al. (1984) have preferred to use a wholly numerical format for substage and within substage events (e.g. 5.31 for the first event within substage 5.3 which is equivalent to the peak of substage 5e in the Emiliani (1955) scheme) and, although this does not create any great confusion, adoption of a single standard is desirable. There are, however, no standard guidelines which define what is a real positive or negative $\delta^{18}O$ excursion or, indeed, the criteria with which stage boundaries are positioned. Prell et al. (1986) define stage boundaries as being centred on peaks (the events of the Pisias scheme), which is less subjective than placing stage boundaries at the midpoints of anomalies, the scheme utilised by Shackleton and Opdyke (1977). Consequently, errors are almost inevitable in stage boundary positioning and stage numbering, especially in those models which date back millions of years.

Inverse Signal Correlations

Inverse signal correlation (Martinson et al., 1982, 1987) correlates any set (or pair) of isotopic records by defining a continuous non-linear mapping function which maximises the correlation coefficient between data sets being compared. Similarly, semblance methods correlate a reference type section with a "New" data set, and map the coherency as a time difference at any one location against age. The result is a map (Figure 10.9) showing coherency-chrons between the reference and "New" curves (Williams et al., 1988b).

Power Spectral Analysis

There are two common quantitative methods of correlation in the frequency domain; power spectral and cross (power) spectral (or spectral coherency) analysis. Each method plots the amount of spectral power (concentration of variance) present against a harmonic number (1/time window). Power spectral methods thus analyse data sets for the degree of power exhibited by a particular frequency in the frequency domain. Cross spectral analysis quantifies the degree of similarity between two records in

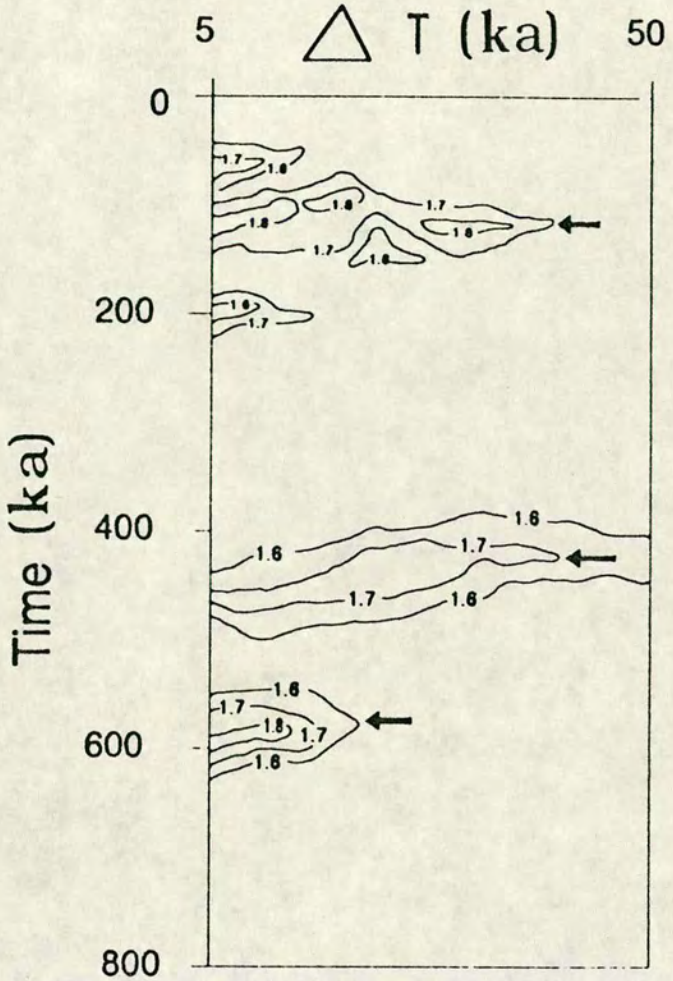

Figure 10.9 *Diagram illustrating the degree of semblance (coherency) between events in a "type" section and any other comparable data set. Contours represent coherency chrons and arrows indicate high coherency events. (Adapted from Williams et al., 1988b.)*

the frequency domain as measured by the spectral coherency measures. A coherency of 1 is indicative of perfect correlation whereas a coherency of zero indicates no correlation. Figure 10.10 presents power spectral analyses of the oxygen isotope composition of planktonic foraminifera, bulk $CaCO_3$ and magnetic susceptibility records from the western Arabian sea ODP hole 728, as previously shown in Figure 10.5.

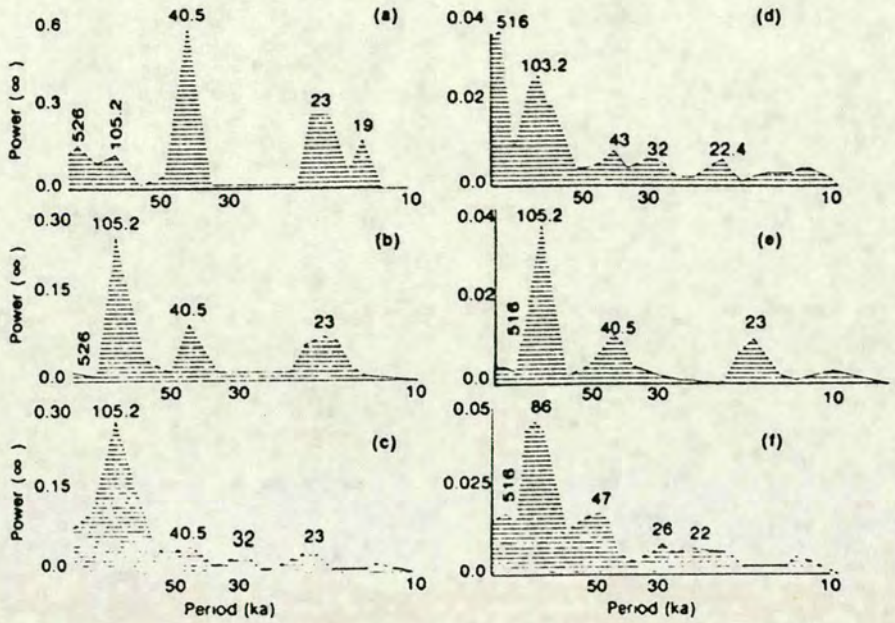

Figure 10.10 *A series of power spectral analyses with period (ka) along the x-axis and power along the y-axis based on a time interval from 12-524 ka and smoothed by a Hanning filter. ODP hole 728A adapted from Steens et al. (1990).* **(a)** *Summed normalised values of orbital parameters calculated at intervals of 2 ka* **(b)** *SPECMAP $\delta^{18}O$ stacked curve calculated at intervals of 2 ka* **(c)** *Magnetic susceptibility sampled with a lag of 2 ka* **(d)** *$\delta^{18}O$ ratios* G. ruber *sampled with a lag of 6 ka* **(e)** *$\delta^{18}O$ ratios* N. dutertrei *sampled with a lag of 6 ka* **(f)** *$\delta^{18}O$ ratios* G. bulloides *sampled with a lag of 6 ka. Power spectra* **(b)** *and* **(c)** *show that there is no direct link between the insolation record and the oxygen isotope records; the eccentricity frequency (100 ka) is much more pronounced in the isotope records. The power spectrum of the magnetic susceptibility record shows the potential for use in dating since all peaks match the Milankovitch rhythms. Nevertheless, one should be very careful in using this kind of parameter, especially where there is no oxygen isotope record available. The power spectra of the different species (d-f) show that the deep dweller* N. dutertrei *rather than the surface dwellers* G. ruber *and* G. bulloides *more accurately document ice volume changes and hence will improve the age model for this core.*

As shown in Figure 10.10, such techniques may be used to quantitatively measure the degree of similarity between two sets of data with respect to the frequencies that are present. Modern computer programmes can vary the time window on which the spectral analysis is performed, which allows comparison of small sections of the record with other parts of the "type" section or theoretical frequency model (e.g. solar input variation, Figure 10.10a). The ability to vary the time window is clearly an advantage but can lead to difficulties when making correlations because any variation in the time window invariably results in subtle or, in some cases, major changes in the structure of the power spectra. Further problems arise as a result of the necessity of spectral analysis programmes to deal only with equally spaced data. That is to say; if, for example, an ash layer or turbidite interrupts normal deposition, and analyses from this horizon are omitted from the data set, the resulting data available to the spectral analysis program will be unevenly spaced. Despite these drawbacks, power spectral analysis does provide a powerful tool to measure quantitatively the degree of similarity in the frequency structure of two records.

Power spectral analysis of curves can also assist in stage boundary positioning and identification because peaks in power should be sharp and well defined if stage boundaries are correctly positioned. However, this process is critically dependent on the time window being analysed and any slight change in this window can affect spectral peaks and boundary positioning. The extensive stretching and condensing of parts of the curve during the tuning process lead one to question to what degree the final timescale actually represents the original data and, indeed, the validity of the timescales.

Sequence Slotting

Sequence slotting is an objective method of comparison which has become possible through the development of computerised dynamic algorithms (Delgoigne and Hansen, 1975). Essentially these combine two records to produce a single "Master" curve which retains the original internal ordering. Problems occur when long blocks (groups) of horizons develop especially in cases of extreme variance. Single or simultaneous multi-core sequence correlations are possible. For an extensive overview of this method see Gordon (1973) and Thompson and Clark (1989).

Bioturbation, Reworking and Accumulation Rate Variation.

Three major potential sources of error in oxygen isotopes stratigraphy are the effects of bioturbation, reworking and accumulation rate variations. Benthic organisms which feed and burrow in the accumulating sediment, cause effective mixing and homogenisation of the upper 1 to 20 cm. This results in a time averaging effect which can be very important, but the extent to which it will blur the global isotopic signal is dependent on the sediment accumulation rate. A rapid accumulation rate renders bioturbation effects almost negligible whereas a slow rate will seriously alter a record. Increasing the sampling density can improve the time resolution, but this cannot

compensate for the bioturbation effect. The bioturbation rate has serious implications for the maximum time resolution (Nyquist frequency) attainable in age models. A high bioturbation rate results in a reduction of the time resolution.

Reworking by, for example, current scouring can result in hiatuses in the record which are often difficult to detect, and which may lead to erroneous estimates of sedimentation rates. Oxygen isotope records can show where these breaks in sedimentation occur and help to counteract the potential errors, but significant variations in accumulation rate can also occur. Ruddiman et al. (1987) outline some of the problems resulting from coring which include variable compression and disturbance.

MORE ANCIENT RECORDS

Following the development of the SPECMAP time scale for the Brunhes chron attempts have been made to extend the $\delta^{18}O$ age models into the upper Pliocene (and older), an objective greatly aided by the immense quantity of core material available from DSDP and ODP legs. Underlying the obvious intrinsic scientific interest were many unanswered questions. Today isotope stage nomenclature is well documented throughout the Pleistocene (Shackleton and Opdyke, 1976, 1977, Williams et al., 1988a) and into the upper Pliocene from many of the world's oceans (Van Donk, 1976, Vergnaud-Grazzini et al., 1983, Prell, 1982, Keigwin, 1979, 1982, 1987 and Thunnell and Williams, 1983, Ruddiman et al., 1989, Raymo et al., 1989, Shackleton and Berger, in press, Sarnthein and Tiedeman, 1989). The most recent of these long term records was obtained from ODP hole 625 (Gulf of Mexico) which gave a high resolution oxygen isotopic record spanning the last 5.35 Ma. (Joyce et al., 1990). These studies have focussed on the nature and timing of variations and transitions in climatic periodicity, their relationships to orbital forcing and the possible existence of other longer term oscillations due to non-orbital forcing (e.g. tectonic), associated with the general evolution of the climate system.

Continuation of isotopic stages back to stage 137 (Sarnthein and Tiedeman, 1989) is regarded with some scepticism because of the ease with which a single excursion may be omitted or misinterpreted, but derivation of such long time scales should nevertheless be encouraged, provided they are treated with caution.

Combining Other Records

Although $\delta^{18}O$ curves potentially produce the most globally consistent signal, other records (e.g. $\delta^{13}C$, geochemistry, magnetic susceptibility, biostratigraphy, tephrochronology) should be used as corroborative evidence and studied in conjunction with the isotope profiles (e.g. Figure 10.5). Of these, perhaps magnetic susceptibility (Ledbetter, 1984a) has the greatest potential. However, tephrochronology (Ledbetter, 1984b, Ninkovitch and Shackleton, 1975) and even

bulk $CaCO_3$ content, which suffers from dissolution and geographic variation, can have some use. If one could demonstrate a linear relationship between isotope ratios and bulk $CaCO_3$ in the Pleistocene, there is potential to extrapolate the isotope record back into much older sediment using the bulk $CaCO_3$ curves which have been determined back in time for many millions of years. One cannot, however, be sure that the linearity persists during the period when an oxygen isotope profile is not available.

In a recent discussion of the SPECMAP age model Imbrie et al. (in press) advocate a combined use of many records (e.g. geochemistry, oxygen isotopes, magnetic susceptibility) each reflecting different parts of the climate system. With such a spectrum of climatic tracers they propose careful examination of the structure of the climatic cycles (whether progressive or stationary oscillations), the spatio-temporal pattern of the 23 ka and 41 ka cycles in relation to forcing by external radiation in order to identify any latitudinal or seasonal Milankovitch pressure points, duration of climate regimes and the identification of monotonic trends especially over the last 400 ka. They go on to question to what degree filtering methods contribute to the wave forms of the observed cycles, the extent to which these oscillations may be accounted for by summation of the various cycles and if any other records (e.g. carbonate cyclicity, see Nelson et al., 1986 or species abundance profiles, see Morley and Shackleton, 1976) fit neatly into the global pattern.

CLIMATE VARIATIONS

Climatic variations are well documented in oxygen isotope profiles during the last 3.5 Ma. Several major isotopic shifts have been identified, one at 2.5 Ma (Shackleton and Cita, 1979, Thunell and Williams, 1983) the other at 3.2-3.0 Ma (Shackleton and Opdyke, 1977). The shift at 2.5 Ma was believed to have resulted from an increase in northern ice-sheet development (Thunell and Williams, 1983); whereas the earlier shift was described as resulting from a cooling of oceanic surface waters (Prell, 1982).

Perhaps one of the clearest examples of climate change is that reported by Ruddiman et al. (1986, 1989) and Raymo et al. (1989) in their analysis of northern hemisphere ice-sheet development. They document the "switch" in dominance from the 100 ka (eccentricity) rhythm in $\delta^{18}O$ during the Brunhes chron (0.735-0 Ma), to the dominance of the 41 ka (obliquity) rhythm during the Matuyama chron (2.47-0.735 Ma). It was as if the climate system had become somewhat unstable and less sensitive to obliquity forcing. Although Figure 10.11 was generated using raw data from Ruddiman et al. (1989), one can clearly see the different periodicities of the $\delta^{18}O$ cycles with Figure 10.11b displaying a marked dominance in the 41 ka rhythm. So how has this transition evolved? Pisias and Moore (1981), Prell (1982) and Maasch (1988) all favour a rapid (several 10^4 years) "switch" around 0.9 Ma.

whereas Imbrie (1985) and Ruddiman et al. (1986, 1989) favour a more gradual transition between 0.78-0.4 Ma, which was accelerated from 0.7-0.6 Ma. Both models agree that by the base of the Brunhes, the 100 ka rhythm was an important feature in climatic variability.

The origin of the 100 ka cycle has long been a contentious issue (Sergin and Sergin, 1976, Pisias and Moore, 1981, Watts and Hayner, 1983, Saltzman, 1987 and Raymo et al., 1989); especially as a direct linear linkage to Milankovitch forcing appears to be very unlikely because insolation spectra (Figure 10.10a) have very low energy in the 100 ka band. However a strong association exists between the 100 ka cycle and the 23 ka cycle envelope (Imbrie et al. in press). It is hypothesised that the 100 ka cycle is internally driven and amplified by climatic instability (Broecker et al., 1985), interactions between climate and forcing mechanisms (Peltier, 1982, Peltier and Hyde, 1984, Saltzman, 1987), and a combination of positive and negative feedback mechanisms within the CO_2-Ice-Ocean system. Computer modelling by Saltzman and Maasch (1988) and Maasch and Saltzman (in press) support the latter idea. Indeed, Saltzman's model results confirm the importance of variations in the amplitude (envelope) of the 23 ka radiation cycle, perhaps in combination with some tectonic forcing (Ruddiman et al., 1989).

As a consequence of variations in the climate system, dating methods which use the Milankovitch theory become less tenable back through time, with the result that discrepancies appear in age estimates. For instance, Black et al. (1988) and Ruddiman et al. (1986, 1989) encountered difficulties when comparing their isotopic record to the SPECMAP stack between 0.8-0.6 Ma especially at the stage 17/16 boundary, despite having used the SPECMAP strategy in developing their age models. This led to tuning problems which forced them to propose that the SPECMAP stage 17/16 boundary date may be 15 ka too young and, although Ruddiman et al. (1989) retain the SPECMAP curve below this point, Black et al. (1988) query the stage 18 boundary age. However, as Ruddiman et al. (1989) point out, a proposed revision of the SPECMAP timescale would not be recommended in light of evidence from a single, potentially atypical, core.

According to Ruddiman et al. (1989), both the 23 ka and 19 ka components of the precessional rhythm increase their amplitude over the Matuyama/Brunhes boundary, especially between 0.8-0.7 Ma, although neither are as prominent as eccentricity or obliquity. Raymo et al. (1989) further extend the $\delta^{18}O$ curve to 2.73 Ma (Figure 10.8b) at stage 116. Between 2.73-1.6 Ma the 41 ka obliquity cycle dominates and only after 2.1 Ma do the 100 ka and 23 ka rhythms show any significant appearance.

The Brunhes/Matuyama boundary appears to be one of climatic disorder with several anomalous rhythms occurring between 0.9-0.6 Ma. Periodicities of 70 ka, 54 ka and 30 ka are reported by Ruddiman et al. (1989) and, of these, only the 54 ka cycle would seem to have the potential to result from orbital forcing as obliquity contains a small insolation component in this band (Berger, 1978). Apart from this minor

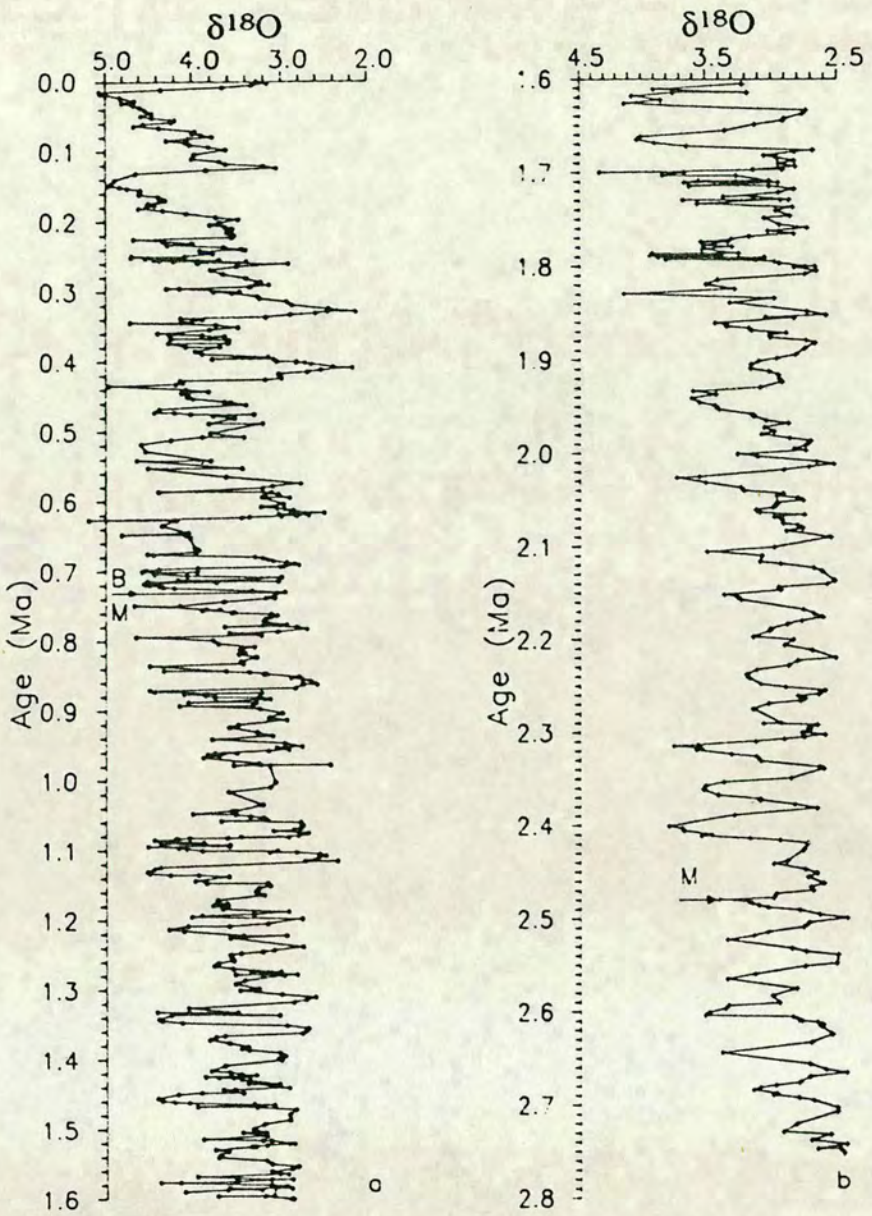

Figure 10.11 *$\delta^{18}O$ curves from 2.8 Ma to present generated from analyses of two benthic species (DSDP hole 607) by Ruddiman et al. (1989) dating from 0-1.6 Ma. Top 250 ka are from cores V30-97 and CHN82-24-4. B/M — Brunhes/Matuyama boundary. Continuation of the record from 1.6 Ma to 2.8 Ma by Raymo et al. (1989). M — base of the Matuyama chron. Note the strong dominance of the obliquity periodicity (41 ka) during the Matuyama which is manifest in the much smoother appearance of the older half of the record.*

association, these anomalous rhythms do tend to suggest that climate tracers such as the oxygen isotope record and the methods of age model development may produce an unknown amount of artefact.

The Brunhes/Matuyama transitory boundary period (0.8-0.6 Ma) has also received attention from Shackleton and Berger (in press), who use planktonic and benthic $\delta^{18}O$ records dating back to the upper Pliocene. Their approach differs from previous models in that they filtered in the depth domain. The net effect of this step is that, in contrast to Imbrie et al. (1984) and Ruddiman et al. (1986), the ages of the magnetic reversals were calculated after tuning and filtering. A good correlation is attained with the models of Imbrie et al. (1984) and Ruddiman et al. (1986, 1989) down to stage 116 (2.73 Ma) but below this point discrepancies appear. The main points on which the revised chronology differs from previous work (e.g. Mankinen and Gromme, 1982), is the inclusion of an extra tilt cycle in the lower Brunhes, allocation of three precessional peaks during stage 21 and the definition of stage 35 as encompassing a single tilt rhythm (Figure 10.6). As a result of these discrepancies, Shackleton and Berger (in press) conclude that currently adopted radiometric dates for the Brunhes/Matuyama boundary and the Jarmillo and Olduvai subchrons underestimate their true astronomical ages by around 6%.

CONCLUDING CONSIDERATIONS

There appears to be a need for a standardisation but not dogmatism in the methods of age model development. Until a more successful method of dating marine sedimentary records is found one must make the most of what is available despite the limitations. The numerous factors which affect the $\delta^{18}O$ signal together with analytical limitations must always be considered carefully.

The great advantage of the SPECMAP curve is that it provides a global reference section to which any core can be compared. The success with which such comparisons have been undertaken is evidence of the validity of applying Milankovitch Theory to age model development and climate research, although many problems remain. For instance, when an unknown record is correlated with the Milankovitch tuned SPECMAP stack, it is not surprising that Milankovitch cyclicities often appear in the unknown profile. The dangers of such circular arguments has led to some speculation regarding the authenticity of the SPECMAP model. Some authors (Pisias et al., 1984, Prell et al., 1986, Ruddiman et al., 1989, Sarnthein and Tiedemann, 1989, Shackleton and Berger, in press) developed their own oxygen isotope-based age models, some of which continue back into the upper Pliocene. Such alternative models rely on essentially the same strategy as SPECMAP but tend to combine planktonic and benthic isotope records and filter raw data in the depth domain rather than in the time domain. This similarity of strategies results in new age models running into essentially the same problems as SPECMAP. The great majority of stack records

using floating time horizons then convert to time with radiometrically defined datum horizons and most then refine the curve by tuning to orbital frequencies.

Although the theoretical basis for isotopic fractionation and orbital variation would seem unequivocal, the degree of coherency between the Milankovitch rhythms and the climate system depends on the degree of linearity of the response to external forcing. Despite the presence of Milankovitch frequencies in the $\delta^{18}O$ record of foraminifera (e.g. Imbrie et al., 1984, Ruddiman et al., 1989) a discordance exists in linearly linking such records to climatic variability. This is manifest in the different spectral composition of the power spectral analysis of the solar input and $\delta^{18}O$ profiles from sediment cores (compare Figures 10.10a and 10.10b-f). Also Pisias et al. (1990) show that any change in phase shifts has serious implications for any age model, as do variations in sensitivity to orbitally induced insolation, which manifests itself in at least two internal feedback mechanisms. One (probably derived from lithospheric movements) enhances the 100 ka rhythm by increasing the rate of climatic change at glacial terminations. The other, which enhances the 41 ka rhythm, accelerates ice sheet growth and slows melting. Such problems can result in discrepancies of several thousand years which are cumulative down core. Thus, linking climate variability to Milankovitch forcing has many problems, some of which may prove to be forever enigmatic. The climate system appears to have varied through time and it is likely that its response to orbital forcing has changed. This has serious implications for age model developmental strategy.

Also, problems are especially acute with respect to the nature and timing of the filtering and tuning processes, and in the positioning of isotopic stage boundaries. The current debate as to the authenticity of the SPECMAP timescale can only be a healthy one. With the knowledge gained from previous attempts, future models are likely to be improvements if they are produced using several lines of corroborative evidence together. Until such models are developed, the SPECMAP curve and other isotope chronologies must be regarded with positive criticism.

More researchers are turning to either a combination of planktonic and benthic (Sarnthein and Tiedemann, 1989, Shackleton and Berger, in press, Zahn and Pederson, in press) or solely benthic curves (Pisias et al. 1984, 1990, Ruddiman et al. 1989, Raymo et al. 1989) to develop their age models. Benthic isotopic signals are less affected by temperature than the planktonic signal. Thus the stacking of benthic curves and their use in conjunction with planktonic stacks can only lead to improvements in timescales.

Oxygen isotopic ratio curves are potentially a powerful tool for dating and correlating ocean sediments through time, but they must be used in conjunction with other corroborative evidence such as carbon isotope ratios, magnetic susceptibility, geochemistry and power spectral analysis to enable the production of a reliable age model. Until a more precise method of dating sediments is found, oxygen isotope stratigraphy must be used and regarded with positive criticism.

REFERENCES

Baker, P., Gieskes, J., and Elderfield, H. 1982. Diagenesis of carbohydrates in deep sea sediments-evidence from Sr/Ca ratios and interstitial dissolved Sr^{2+} data. *Journal of Sedimentary Petrology*, **52**, 71-82.

Bard, E., Hamelin B., Fairbanks, R.G., and Zindler, A. 1990. Calibration of the ^{14}C timescale over the past 30,000 years using mass spectrometric U-Th ages from Barbados corals. *Nature*, **345**, 405-410.

Berger, A.L. 1976. Obliquity and Precession for the last 5 000 000 years. *Astronomy and Astrophysics*, **51**, 127-135.

Berger, A.L. 1977. Support for the astronomical theory of climate change. *Nature*, **269**, 44-45.

Berger, A.L. 1978. Long-term variations of caloric solar radiation resulting from the earth's orbital elements. *Quaternary Research*, **9**, 139-167.

Berger, W.H. 1979. Stable isotopes in foraminifera. In *Foraminiferal Ecology and Paleoecology*, *SEPM Short Course No. 6*, Houston, 156-198.

Berger, A.L. 1984. Accuracy and frequency stability of the earth's orbital elements during the Quaternary. In *Milankovitch and Climate, Part 1*, (ed. Berger, A.L.), Reidel, Hingham, Mass., 3-39.

Berger, A.L. 1988. Milankovitch theory and climate. *Reviews in Geophysics*, **26**, 624-657.

Black, K.P., Nelson, C.S., and Hendy, C.H. 1988. A spectral analysis procedure for dating Quaternary deep-sea cores and it's application to a high-resolution Brunhes record from the southwest Pacific. *Marine Geology*, **83**, 21-30.

Bloom, A.M., Broecker, W.S., Chappell, J.M.A., Matthews, R.K., and Mesolella, K.J. 1974. Quaternary sea level fluctuations on a tectonic coast: New $^{230}U/^{234}Th$ dates from the Huon Peninsula, New Guinea. *Quaternary Research*, **4**, 185-205.

Broecker, W.S., Peteet, D.M., and Rind, D. 1985. Does the ocean-atmosphere system have more than one stable mode of operation? *Nature*, **315**, 21-26.

Broecker, W.S., Thurber, D.L., Goddard, J., Ku, T.L., Matthews, R.K., and Mesolella, K. 1968. Milankovitch hypothesis supported by precise dating of coral reefs and deep-sea sediments. *Science*, **159**, 297-300.

Broecker, W.S. and Van Donk, J. 1970. Insolation changes, ice volumes and the ^{18}O record in deepsea cores. *Reviews of Geophysics and Space Physics*, **8**, 169-191.

Croll, J. 1864. Climate and Time. *Philosophical Magazine*, **28**, 121-137.

Delcoigne, A., and Hansen, P. 1975. Sequence comparison by dynamic programming. *Biometrika*, **62**, 661-664.

Duplessy, J.C., Lalou, C., and Vinot, A.C. 1970. Differential isotopic fractionation in benthic foraminifera and paleotemperatures reassessed. *Science*, **168**, 250-251.

Elderfield, H., and Gieskes, J.M. 1982. Sr isotopes in interstitial waters of marine sediments from Deep Sea Drilling Project Cores. *Nature*, **300**, 493-497.

Emiliani, C. 1955. Pleistocene Paleotemperatures. *Journal of Geology*, **63**, 539-578.

Emiliani, C., and Shackleton, N.J. 1974. The Brunhes epoch: Isotope paleotemperatures and geochronology. *Science*, **183**, 511-514.

Epstein, S., Buchsbaum, R., Lowenstam, H., and Urey, H.C. 1953. Revised carbonate-water temperature scale. *Geological Society of America Bulletin*, **64**, 1315-1325.

Fairbanks, R.G., and Matthews, R.K. 1978. The marine oxygen isotope record in Pleistocene coral, Barbados, West Indies. *Quaternary Research*, **10**, 181-196.

Gordon A.D. 1973. A sequence-comparison statistic and algorithm. *Biometrika*, **60**, 197-200.

Hays, J.D., Imbrie, J., and Shackleton, N.J. 1976. Variations in earth's orbit: Pacemaker of the ice ages. *Science*, **194**, 1121-1132.

Hemleben, C., and Spindler, M. 1983. Recent advances in research on living planktonic foraminifera. In *Reconstruction of Marine Paleoenvironments*, (ed Meulenkamp, J.E.), *Utrecht Micropalaeontlogy Bulletin*, **30**, 141-170.

Imbrie, J. 1985. A theoretical framework for the Pleistocene ice ages, *Quarterly Journal of the Geological Society of London*, **142**, 417-432.

Imbrie, J., Boyle, E., Clemens, S., Farrell, J., Kutzbach, J., MacIntyre, A., Martinson, D., Mix, A., Molfino, B., Pisias, N.G., Prell, W.L., Shackleton, N.J., and Toggweiler, J.R. 1990. Structure of the late Pleistocene climate cycles: major features of the marine record (0-400 ka). *Paleoceanography* (in press).

Imbrie J., and Imbrie, J.Z. 1980. Modelling the climate response to orbital variations. *Science*, **207**, 943-953.

Imbrie, J., Shackleton, N.J., Pisias, N.G., Morley, J.J., Prell, W.L., Martinson, D.G., Hayes, J.D., MacIntyre, A., and Mix, A.C. 1984. The orbital theory of Pleistocene climate: support from a revised chronology of the marine w^{18}O record. In *Milankovitch and Climate, Part 1*, (ed Berger A.), Reidel, Hingham, Massachusetts, 269-305.

Jansen, E. 1989. The use of stable oxygen and carbon isotope stratigraphy as a dating tool. *Quaternary International*, **1**, 151-166.

Joyce, J.E., Tjalsma, L.R.C. and Prutzman, J.M. 1990. High resolution planktic stable isotope record and spectral analysis for the last 5.35 m.y.: Ocean Drilling Program Site 625, Northeast Gulf of Mexico, *Paleoceanography*, **5**, 507-529.

Keigwin, L.D. Jr. 1979. Late Cenozoic stable isotope stratigraphy and paleoceanography of DSDP sites from the east equatorial and central North Pacific ocean. *Earth and Planetary Science Letters*, **45**, 361-381.

Keigwin, L.D. Jr. 1982. Isotopic paleoceanography of the Caribbean and East Pacific: Role of Panama uplift in late Neogene times. *Science*, **217**, 350-353.

Keigwin, L.D. Jr. 1987. Pliocene stable isotope record of DSDP 606: ^{18}O enrichment 2.4, 2.6 and 3.1 My ago. *Initial Reports of the Deep Sea Drilling Project*, **94**, 911-920.

Killingley, J.S. 1983. Effects of diagenetic recrystalisation on ^{18}O ^{16}O values of deep sea sediments. *Nature*, **310**, 504-507.

Ledbetter, M.T. 1984a. Pleistocene magnetostratigraphy. In *Principles of Pleistocene Stratigraphy Applied to the Gulf of Mexico*. (ed Healy-Williams, N.). IHRDC Press, Boston, Massachusetts, 1-24.

Ledbetter, M.T. 1984b. Late Pleistocene tephrochronology in the Gulf of Mexico region. In *Principles of Pleistocene Stratigraphy Applied to the Gulf of Mexico* (ed. Healy-Williams, N.), IHRDC Press, Boston, Massachusetts, 119-148.

Maasch, K.A. 1988. Statistical detection of the mid-Pleistocene transition. *Climate Dynamics*, **2**, 133-143.

Maasch, K.A., and Saltzman, B. (1990). A low-order dynamical model of climatic variability over the full Pleistocene. *Journal of Geophysical Research* (in press).

Mankinen, E.A., and Gromme, C.S. 1982. Paleomagnetic data from the Coso Range, California, and current status of the Cobb Mountain normal geomagnetic polarity event. *Geophysical Research Letters*, **9**, 1279-1282.

Martinson, D.G., Menke, W., and Stoffa, P. 1982. An inverse approach to signal correlation. *Journal of Geophysical Research*, **87**, 4807-4818.

Martinson, D.G., Pisias, N.G., Hays, J.D., Imbrie, J., Moore, T.C., and Shackleton, N.J. 1987. Age dating and the orbital theory of the ice ages: development of a high resolution 0-300 000 year chronostratigraphy. *Quaternary Research*, **27**, 1-29.

Milankovitch, M. 1941. *Canon of Insulation and the Ice-Age Problem*, Koninglich Serbische Akademie, Beograd, pp. 484. (English translation by the Israel program for scientific translation and published for the U.S. department of commerce and the national science foundation).

Morley, J.J., and Hays, J.D. 1981. Towards a high-resolution global, deap sea chronology for the last 750 000 years. *Earth and Planetary Science Letters*, **53**, 279-295.

Morley, J.J., and Shackleton, N.J. 1976. Extension of the radiolarian *Stylatractus universus* as a biostratigraphic datum to the Atlantic ocean. *Geology*, **6**, 309-311.

Nelson, C.S., Hendy, C.H., Cuthbertson, A.M., and Jarret, G.R. 1986. Late Quaternary carbonate and isotope stratigraphy, subantarctic site 594, southwest Pacific. *Initial Reports of the Deep Sea Drilling Project*, **90**, 1425-1436.

Ninkovitch, D., and Shackleton, N.J. 1975. Distribution, stratigraphic position and age of ash layer "L", in the Panama basin region. *Earth and Planetary Science Letters*, **27**, 20-34.

Peltier, W.R. 1982. Dynamics of the ice-age earth. *Advances in Geophysics*, **24**, 2-146.

Peltier, W.R., and Hyde, W. 1984. A model of the ice cycle. In *Milankovitch and Climate, Part II*, (eds Berger, A., Imbrie, J., Hays, J., Kukla, G., and Saltzman, B.). Plenum, New York, 565-580.

Pisias, N.G. 1976. Late Quaternary sediment sedimentation rates, periodicities, and controls of carbonate and opal accumulations. *Memoirs Geological Society of America*, **145**, 375-391.

Pisias, N.G., Dauphin, J.P., and Sancetta, C.S. 1973. Spectral analysis in late Pleistocene-Holocene sediments. *Quaternary Research*, **3**, 3-9.

Pisias, N.G., Martinson, D.G., Moore, T.C. Jr., Shackleton, N.J., Prell, W.L., Hayes, J., and Boden, G. 1984. High resolution statigraphic correlation of benthic oxygen isotope records spanning the last 300,000 years. *Marine Geology*, **56**, 119-136.

Pisias, N.G., Mix, A.C., and Zahn, R. 1990. Non-linear response in the global climate system: evidence from benthic oxygen isotope records in core RC13-110. *Paleoceanography*, **5**, 147-160.

Pisias, N.G., and Moore, T.C. 1981. The evolution of the Pleistocene climate: A time series approach. *Earth and Planetary Science Letters*, **52**, 450-458.

Prell, W.L. 1982. Oxygen and carbon isotope stratigraphy for the Quaternary of hole 502B: Evidence for two modes of isotopic variability. *Initial Reports of the Deep Sea Drilling Project*, **68**, 455-464.

Prell, W.L., Imbrie, J., Martinson, D.G., Morley, J., Pisias, N.G., Shackleton, N.J., and Streeter, H.F. 1986. Graphic correlation of oxygen isotope stratigraphy application to the late Quaternary. *Paleoceanography*, **1**, 137-162.

Raymo, M.E., Ruddiman, W.F., Backman, J., Clement, B.M., and Martinson, D.G. 1989. Late Pleistocene variation in northern hemisphere ice sheets and north Atlantic deep water circulation. *Paleoceanography*, **4**, 413-446.

Ruddiman, W.F., Cameron, D., and Clement, B.M. 1987. Sediment disturbance and correlation of offset holes drilled with the hydraulic piston corer. *Initial Reports of the Deep Sea Drilling Project*, **94**, 615-634.

Ruddiman, W.F., MacIntyre, A., and Raymo, M.E. 1986. Matuyama 41 000-year cycle: north Atlantic ocean and northern hemisphere ice-sheets. *Earth and Planetary Science Letters*, **80**, 117-129.

Ruddiman, W.F., Raymo, M.E., Martinson, D.G., Clement, B.M., and Backman, J. 1989. Pleistocene evolution:northern hemisphere ice sheets and north Atlantic ocean. *Paleoceanography*, **4**, 353-412.

Saltzman, B. 1987. Carbon dioxide and the $\delta^{18}O$ record of late Quaternary climate change: a global model. *Climate Dynamics*, **1**, 77-85.

Saltzman, B. and Maasch, K.A. 1988. Carbon cycle instability as a cause of the late Pleistocene ice age oscillation: modeling the asymmetric response. *Global Biogeochemical Cycles*, **2**, 177-185.

Sarnthein, M. and Tiedemann, R. 1989. Towards a high-resolution stable isotope stratigraphy of the last 3.4 million years:sites 658 and 659 off northwest Africa. In *Proceedings of the Ocean Drilling Program, Scientific Results*, **108**, 167-185.

Sergin, V.Y., and Sergin, S.Y. 1976. Systems analysis of the problem of large scale oscillations of the climate and glaciations of the earth (in Russian). In *Modelirovaine Planetarnoi Sistemy "Ledniti-Okean-Atmosphera"*, (ed Sergin, S.Y.), USSR Academy of Sciences, Moscow, 5-51.

Shackleton N.J. 1967. Oxygen isotope analyses and Pleistocene tempeatures re-assessed. *Nature*, **215**, 15-17.

Shackleton, N.J. 1969. The last interglacial in the marine and terrestrial records. *Proceedings Royal Society London Series B*, **174**, 135-154.

Shackleton N.J. 1977. The oxygen isotope stratigraphic record of the late Pleistocene. *Philosophical Transactions of the Royal Society London*, **280**, 169-182.

Shackleton, N.J., Berger, A. and Peltier, W.A. 1991. An alternative astronomical calibration of the lower Pleistocene timescale based on ODP site 677. *Transactions of the Royal Society of Edinburgh: Earth Sciences*, **81**, 251-262.

Shackleton, N.J., and Cita, M. 1979. Oxygen and carbon isotope stratigraphy of benthic foraminifers at site 397: Detailed history of climatic change during the Neogene. *Initial Reports of the Deep Sea Drilling Project*, **47**, 433-459.

Shackleton, N.J., and Matthews, R.K. 1977. Oxygen isotope stratigraphy of late Pleistocene coral terraces in Barbados. *Nature*, **268**, 618-620.

Shackleton, N.J., and Opdyke, N.D. 1973. Oxygen isotope and paleomagnetic stratigraphy of equatorial Pacific core V28-238: oxygen isotope temperatures and ice volume on a 10^5 and 10^6 year scale. *Quaternary Research*, **3**, 39-55.

Shackleton, N.J., and Opdyke, N.D. 1976. Oxygen isotope and palaeomagnetic statigraphy of Pacific core V28-239 late Pliocene latest Pleistocene. *Memoirs Geological Society America*, **145**, 449-464.

Shackleton, N.J., and Opdyke, N.D. 1977. Oxygen isotope and paleomagnetic evidence for early northern hemisphere glaciation. *Nature*, **270**, 216-219.

Shaw A.B. 1964. *Time in Stratigraphy*, Megraw-Hill, New York, pp. 365.

Steens, T.N.F., Kroon D., Ten Kate, W.G., and Sprenger, A. 1990. Late Pleistocene rhythmicities of oxygen isotope ratios, calcium carbonate contents and magnetic susceptibilities of western Arabian sea margin hole 728A, (ODP leg 117). *Proceedings of the Ocean Drilling Program, Part B: Scientific Results, Leg 117*, (in press).

Thompson, R., and Clark, R.M. 1989. Sequence slotting for stratigraphic correlation between cores: theory and practice. *Journal of Paleolimnology*, **2**, 173-184.

Thunell, R.C., and Williams, D.F. 1983. The stepwise development of Pliocene-Pleistocene paleoclimatic and paleoceanographic conditions in the Mediterranean. *Utrecht Micropaleontological Bulletin*, **30**, 111-127.

Urey, H.C. 1948. Oxygen isotopes in nature and the laboratory. *Science*, **108**, 489-496.

Van Donk, J. 1976. ^{18}O record of the Atlantic ocean for the entire Pleistocene Epoch. *Memoir of the Geological Society America*, **145**, 147-163.

Veeh, H.H and Chappell, J. 1970. Astronomical theory of climatic change: Support from New Guinea. *Science*, **167**, 862-865.

Vergnaud-Grazzini, C., Grably, M., Pujol, C., and Duprat, J. 1983. Oxygen isotope stratigraphy and paleoclimatology of southwestern Atlantic Quaternary sediments (Rio-Grande Rise) at Deep Sea Drilling Project Site 517. *Initial Reports of the Deep Sea Drilling Project*, **72**, 871-884.

Watts, R.G., and Hayner, M.E. 1983. The origin of the 100-kiloyear ice sheet cycle in the Pleistocene. *Journal of Geophysical Research*, **88**, 5163-5166.

Weertman, J. 1964. Rate of growth or shrinkage of non-equilibrium icesheets. *Journal of Glaciology*, **38**, 145-158.

Williams, D.F. 1984. Correlation of marine Pleistocene sediments of the Gulf of Mexico and other basins using oxygen isotope stratigraphy. In *Principles of Pleistocene Stratigraphy Applied to the Gulf of Mexico*, (ed Healy-Williams, N.), IHRDC Press, Boston, Massachusetts, 67-188.

Williams, D.F., Lerche, I., Full, W.E. 1988b. *Isotope Chronostratigraphy: Theory and Methods*, Academic Press, New York, pp. 345.

Williams, D.F., Moore, W.S., and Fillon, R.H. 1981. Role of glacial Arctic ocean ice sheets in Pleistocene oxygen isotope and sea level records. *Earth and Planetary Science Letters*, **56**, 157-166.

Williams, D.F., Thunell, R.C., Tappa, E., Rio, D., and Raffi, I. 1988a. Chronology of the oxygen isotope record, 0-1.88 million years before present. *Palaeogeography, Palaeoclimatology and Palaeoecology*, **64**, 221-240.

Zahn, R., and Pedersen, T.F. 1990. Late Pleistocene evolution of surface and mid-depth hydrography at the Oman margin: Planktonic and benthic records at ODP site 724. *Proceedings of the Ocean Drilling Program, Part B: Scientific results, Leg 117*, (in press).